
ITER

ITER EDA DOCUMENTATION SERIES No. 24

International Thermonuclear Experimental Reactor
(ITER)

Engineering Design Activities
(EDA)

ITER TECHNICAL BASIS

INTERNATIONAL ATOMIC ENERGY AGENCY, VIENNA, 2002

ITER TECHNICAL BASIS
IAEA, VIENNA, 2002
IAEA/ITER EDA/DS/24

Printed by the IAEA in Vienna
January 2002

FOREWORD

Development of nuclear fusion as a practical energy source could provide great benefits. This fact has been widely recognized and fusion research has enjoyed a high level of international co-operation. Since early in its history, the International Atomic Energy Agency has actively promoted the international exchange of fusion information.

In this context, the IAEA responded in 1986 to calls at summit level for expansion of international co-operation in fusion energy development. At the invitation of the Director General there was a series of meetings in Vienna during 1987, at which representatives of the world's four major fusion programmes developed a detailed proposal for co-operation on the International Thermonuclear Experimental Reactor (ITER) Conceptual Design Activities (CDA). The Director General then invited each interested Party to co-operate in the CDA in accordance with the Terms of Reference that had been worked out. All four Parties accepted this invitation.

The ITER CDA, under the auspices of the IAEA, began in April 1988 and were successfully completed in December 1990. The information produced within the CDA has been made available for the ITER Parties and IAEA Member States to use either in their own programmes or as part of an international collaboration.

After completing the CDA, the ITER Parties entered into a series of consultations on how ITER should proceed further, resulting in the signing of the ITER EDA (Engineering Design Activities) Agreement on July 21, 1992 in Washington by representatives of the four Parties. The Agreement entered into force upon signature of the Parties, with the EDA conducted under the auspices of the IAEA.

As the original six-year EDA Agreement approached a successful conclusion, the Parties entered into a series of consultations on how future steps could be taken toward decisions on construction. A provisional understanding was reached that the EDA Agreement should be extended by three years to enable the Parties to complete their preparations for possible construction decisions. By the time of the expiration of the original EDA Agreement, the EU, JA and RF Parties had agreed to extend the Agreement while the US Party, complying with Congressional views, did not participate beyond an orderly close out activity ending in September, 1999.

The ITER Engineering Design Activities were successfully terminated on 21 July 2001.

As part of its support of ITER, the IAEA is pleased to publish the documents summarizing the results of the Engineering Design Activities. Together with the twenty-three previous volumes in the ITER EDA Documentation Series, on:

- ITER EDA Agreement and Protocol 1 (DS/1)
- Relevant Documents Initiating the EDA (DS/2)
- ITER Council Proceedings: 1992 (DS/3)
- ITER Council Proceedings: 1993 (DS/4)
- ITER EDA Agreement and Protocol 2 (DS/5)
- ITER Council Proceedings: 1994 (DS/6)
- Technical Basis for the ITER Interim Design Report, Cost Review and Safety Analysis (DS/7)
- ITER Council Proceedings: 1995 (DS/8)
- ITER Interim Design Report Package and Relevant Documents (DS/9)

- ITER Interim Design Report Package Documents (DS/10)
- ITER Council Proceedings: 1996 (DS/11)
- ITER Council Proceedings:1997 (DS/12)
- Technical Basis for the ITER Detailed Design Report Cost Review and Safety Analysis (DDR) (DS/13)
- ITER Final Design Report, Cost Review and Safety Analysis (FDR) and Relevant Documents (DS/14)
- ITER Council Proceedings: 1998 (DS/15)
- Technical Basis for the ITER Final Design Report, Cost Review and Safety Analysis (FDR) (DS/16)
- ITER Council Proceedings: 1999 (DS/17)
- ITER-FEAT Outline Design Report (DS/18)
- Technical Basis for the ITER-FEAT Outline Design (DS/19)
- ITER Council Proceedings: 2000 (DS/20)
- Final Report of the ITER EDA (DS/21)
- Summary of the ITER Final Design Report (DS/22)
- ITER Council Proceedings: 2001 (DS/23)

this document presents essential information on the evolution of the ITER EDA.

CONTENTS

PLANT DESIGN SPECIFICATION

PLANT DESCRIPTION DOCUMENT

INTRODUCTION

Following on from the Final Report of the EDA (DS/21), and the Summary of the ITER Final Design Report (DS/22), the technical basis gives further details of the design of ITER. It is in two parts. The first, the Plant Design Specification, summarises the main constraints on the plant design and operation from the viewpoint of engineering and physics assumptions, compliance with safety regulations, and siting requirements and assumptions. The second, the Plant Description Document, describes the physics performance and engineering characteristics of the plant design, illustrates the potential operational consequences for the locality of a generic site, gives the construction, commissioning, exploitation and decommissioning schedule, and reports the estimated lifetime costing based on data from the industry of the EDA Parties.

Plant Design Specification

(PDS)

Table of Contents

1 Programmatic Objective

According to the ITER EDA Agreement, "the overall programmatic objective of ITER is to demonstrate the scientific and technological feasibility of fusion energy for peaceful purposes."

2 Technical Objectives and their Interpretation

Following the recommendations of a Special Working Group (SWG) [see verbatim quote from the report in the panel overleaf], the ITER Council asked the Director "to continue efforts with high priority toward establishing, with the assistance of the Joint Central Team (JCT) and Home Teams (HTs), option(s) of minimum cost aimed at a target of approximately 50% of the direct capital cost of the [1998 ITER] design with reduced detailed technical objectives, which would still satisfy the overall programmatic objective of ITER. The work should follow the adopted technical guidelines and make the most cost-effective use of existing design solutions and their associated R&D."

2.1 Interpretation

These technical objectives have been interpreted as follows:

- The existing physics database leads to constraining inductive performance in the following way:
  - H-mode scaling law as recommended by the Confinement Expert Group;
  - normalized beta, $ß_N = ßaB/I < 2.5$ (a = plasma minor radius (m), B = toroidal field at the plasma geometric centre (T), I = plasma current (MA);
  - normalized density, $n/n_{GW} = n\pi a^2/I < 1.0$ (n = electron density, n_{GW} = Greenwald density);
  - safety factor at the 95% flux surface, $q_{95} \sim 3$;
  - impurity factor $Z_{eff} \leq 2.0$;
  - a well controlled, divertor plasma configuration.

- The ITER design shall incorporate features that permit testing to:
  - demonstrate the reliability of nuclear components;
  - furnish data for comparing candidate concepts for nuclear components and to provide a basis of extrapolation;
  - demonstrate tritium breeding;
  - provide fusion materials testing data.

- Maintainability features will be incorporated into the design in such a way as to achieve the mission reliability, operational availability, and scheduled maintenance requirements. In particular, remote handling (RH) features will be designed and qualified that permit timely insertion and removal of in-vessel components, test blanket modules and other test articles.

Plasma Performance

The device should:

- *achieve extended burn in inductively driven plasmas with the ratio of fusion power to auxiliary heating power of at least 10 for a range of operating scenarios and with a duration sufficient to achieve stationary conditions on the timescales characteristic of plasma processes.*
- *aim at demonstrating steady-state operation using non-inductive current drive with the ratio of fusion power to input power for current drive of at least 5.*

In addition, the possibility of controlled ignition should not be precluded.

Engineering Performance and Testing

The device should:

- *demonstrate the availability and integration of technologies essential for a fusion reactor (such as superconducting magnets and remote maintenance);*
- *test components for a future reactor (such as systems to exhaust power and particles from the plasma);*
- *Test tritium breeding module concepts that would lead in a future reactor to tritium self-sufficiency, the extraction of high grade heat, and electricity production.*

Design Requirements

- *Engineering choices and design solutions should be adopted which implement the above performance requirements and make maximum appropriate use of existing R&D database (technology and physics) developed for ITER.*
- *The choice of machine parameters should be consistent with margins that give confidence in achieving the required plasma and engineering performance in accordance with physics design rules documented and agreed upon by the ITER Physics Expert Groups.*
- *The design should be capable of supporting advanced modes of plasma operation under investigation in existing experiments, and should permit a wide operating parameter space to allow for optimising plasma performance.*
- *The design should be confirmed by the scientific and technological database available at the end of the EDA.*
- *In order to satisfy the above plasma performance requirements an inductive flat-top capability during burn of 300 to 500 s, under nominal operating conditions, should be provided.*
- *In order to limit the fatigue of components, operation should be limited to a few 10s of thousands of pulses*
- *In view of the goal of demonstrating steady-state operation using non-inductive current drive in reactor-relevant regimes, the machine design should be able to support equilibria with high bootstrap current fraction and plasma heating dominated by alpha particles.*
- *To carry out nuclear and high heat flux component testing relevant to a future fusion reactor, the engineering requirements are*

  Average neutron flux ≥ 0.5 MW/m^2

  Average neutron fluence ≥ 0.3 MWa/m^2
- *The option for later installation of a tritium breeding blanket on the outboard of the device should not be precluded.*
- *The engineering design choices should be made with the objective of achieving the minimum cost device that meets all the stated requirements.*

Operation Requirements

The operation should address the issues of burning plasma, steady-state operation and improved modes of confinement, and testing of blanket modules.

- *Burning plasma experiments will address confinement, stability, exhaust of helium ash, and impurity control in plasmas dominated by alpha particle heating.*
- *Steady-state experiments will address issues of non-inductive current drive and other means for profile and burn control and for achieving improved modes of confinement and stability.*
- *Operating modes should be determined having sufficient reliability for nuclear testing. Provision should be made for low-fluence functional tests of blanket modules to be conducted early in the experimental programme. Higher fluence nuclear tests will be mainly dedicated to DEMO-relevant blanket modules in the above flux and fluence conditions.*
- *In order to execute this program, the device is anticipated to operate over an approximately 20 year period. Planning for operation must provide for an adequate tritium supply. It is assumed that there will be an adequate supply from external sources throughout the operational life.*

- The mechanical design of the device shall withstand the expected temperatures, pressures, electromagnetic fields, chemical environment, and radiation environment under all projected operating conditions and assumed accident conditions.

- Prior to site selection, structural evaluation shall be in accordance with specific codes and standards which are agreed among the three Parties. If no such codes and standards exist, standards or guidelines established by the JCT shall be surrogated. The design must not preclude readily achievable modifications to incorporate alternate codes and standards, which may be required by the Host Party.

- The design shall facilitate decommissioning, and reduce occupational exposures, by:
  - use of modular components for easy dismantling;
  - segregating radioactive systems or components;
  - designing to avoid contamination or to allow easy decontamination;
  - selection of construction materials to reduce activation products in materials subject to irradiation.

- ITER shall have a waste management program that minimises waste. The treatment systems for radioactive wastes generated in ITER shall be designed to minimize dispersion of radioactive materials during all stages of handling. ITER systems shall be designed to package radioactive waste in accordance with the requirements of the Party that will ship, handle and intern the waste, so that no additional handling or exposure is required by re-packaging.

- Delivery of components, systems and structures will be just in time to fulfil the needs of the experimental programme subject to the following limitations:
  - the initial design and construction must anticipate the requirements for all stages and include those features which are impractical or extremely costly to add at a later time;
  - deferral of a component, system or structure shall not increase the cost of other components, systems or structures greater than the amount of the cost saved by deferral.

- ITER will follow a “staged” approach to maximize the opportunities for deferring cost and reducing the peak demand for funding in any single year. This will also allow early experimental results to better quantify the technical requirements of successively installed equipment. In particular, the ability to study steady state operation will, if necessary, be provided through additional investment.

- ITER operation is divided into four phases. Before achieving full deuterium-tritium (DT) operation, which itself is split into two phases, ITER is expected to go through two operation phases, a hydrogen (H) phase and a deuterium (D) phase, for commissioning of the entire plant.

- The hydrogen phase is a non-nuclear phase, mainly planned for full commissioning of the tokamak system in a non-nuclear environment where full remote handling is not required.

The discharge scenario of the full DT phase reference operation such as plasma current initiation, current ramp-up, formation of a divertor configuration and current ramp-down can be developed or simulated in this phase. The semi-detached divertor operation in DT plasma can be also checked since the peak heat flux onto the divertor target will be of the same order of magnitude as for the full DT phase.

Characteristics of electromagnetic loads due to disruptions or vertical displacement events, and heat loads due to runaway electrons, will be basically the same as those of the DT phase. Studies of the design-basis physics will significantly reduce the uncertainties of the full DT operation. Mitigation of severe disruptions and vertical displacement events (VDEs) or better control of these events in later phases will become possible, leading to a more efficient DT operational phase.

However, some important technical issues will not be fully tested in this phase because of smaller plasma thermal energy content and lack of neutrons and energetic alpha-particles. For example, evaporation of the divertor target surface expected at the thermal quench phase of disruption, effects of neutron irradiation of the in-vessel materials, and alpha-particle heating of the plasma, will not be tested.

The following studies can be carried out to prepare for the full DT phase:

(1) accessibility of the H-mode and other improved confinement modes (confirmation of the adequacy of the heating power);

(2) verification of operational compatibility with plasma density close to the Greenwald limit, beta limit, $q_{95} \sim 3$, semi-detached divertor, low impurity level, and sufficiently good confinement, which is required in the reference high energy multiplication (Q) operation in the full DT phase; studies of high β_N operation by stabilising neoclassical modes with electron cyclotron current drive (ECCD) etc., high plasma density operation by optimized fuelling etc., and further improved confinement modes; assessment of the necessity to improve these capabilities;

(3) steady state operation with a negative or weak central magnetic shear and an internal transport barrier; improvement of the beta limit by stabilising kink modes and resistive wall modes; assessment of the necessity to improve current drive capabilities and stability control.

If the hydrogen phase is substantial, the initial construction cost of ITER could be significantly reduced by delaying the installation of some of the nuclear-related facilities. The actual length of the hydrogen operation phase will depend on the merit of this phase with regard to its impact on the later full DT operation. Operation in this phase is subject to several uncertainties: how high the magnetic field can be without the plasma density exceeding the Greenwald limit, and how high the plasma density needs to be to access the H-mode, avoiding locked modes and beam shine-through, and ensuring adequate divertor operation. EC heating at the 2^{nd} harmonic is expected to help in these respects.

- In the deuterium phase, neutrons will be produced, and tritium will be produced from DD reactions. Part of this tritium will then be burnt in DT reactions. Although the fusion power is low, the activation level inside the vacuum vessel will not allow human access after several deuterium discharges with powerful heating. However, the capacity of the heat transfer system (except for the divertor and heating devices) could be minimal, and demand for the tritium processing system would be very small.

  Characteristics of deuterium plasma behaviour are very similar to those of DT plasma except for the amount of alpha heating. Therefore, the reference DT operational scenarios, i.e., high Q, inductive operation and non-inductive steady state operation, can be simulated in this phase. Since tritium already exists in the plasma, addition of a small amount of tritium from an external source will not significantly change the activation level of the machine. Fusion power production at a significant power level for a short period of time without fully implementing cooling and tritium-recycle systems which would be required in the subsequent full DT phase could therefore also be demonstrated. By using limited amounts of tritium in a deuterium plasma, the integrated commissioning of the device is possible. In particular, the shielding performance can be checked. The major achievements in the D phase should be as follows:
  - replacement of H by D, clean D plasma;
  - confirmation of L-H (mode) threshold power and confinement scalings;
  - establishment of a reference plasma (current, heating power, density, detached/semi-detached divertor, ELMy (edge localised mode) H-mode, etc.);
  - particle control (fuel/ash/impurity/fuelling/pumping);
  - steady-state operation with full heating power;
  - finalisation of nuclear commissioning with a limited amount of tritium;
  - demonstration of high fusion power comparable to the nominal value for the full DT burn, for a short time.

- Following these two phases the ITER plant will have been almost fully commissioned. Most of the plasma operational and control techniques necessary to achieve the technical goals of the DT phase will have been mastered by then. DT operation can be divided into two phases predominantly oriented towards physics and engineering goals respectively

  During the first phase the fusion power and burn pulse length will be gradually increased until the inductive operational goal is reached. Non-inductive, steady-state operation will also be developed. The DEMO-relevant test blanket modules will also be tested whenever significant neutron fluxes are available, and a reference mode of operation for that testing will be established.

  The second phase of full DT operation will emphasise improvement of the overall performance and the testing of components and materials with higher neutron fluences. This phase should address the issues of higher availability of operation and further improved modes of plasma operation. Implementation of this phase should be decided following a review of the results from the preceding three operational phases and assessment of the merits and priorities of programmatic proposals.

- A decision on incorporating tritium breeding during the course of the second DT phase will be decided on the basis of the availability of tritium from external sources, the results of breeder blanket testing, and experience with plasma and machine performance. Such a decision will depend on the R&D completed during the first phase indicating the viability of a tritium-breeding blanket, almost certainly within the same space envelope as the shielding blanket on the outboard side, able to maintain a low tritium inventory with bakeout at 240°C.

- In all operating phases, ITER shall provide facilities for the receipt, storage, processing /recycling and utilisation of hydrogen isotopes for the tokamak. Apart from the H phase, this will include tritium, and the recycling capability shall include the possibility to recover tritium from plasma-facing materials.

- ITER shall have a duty factor[1] capability of about 25%.

- Comprehensive plasma diagnostic information shall allow attainment and monitoring of reliable modes of operation. In the final part of the twenty year operation, pulse reliability[2] shall be greater than 90%. In the final part of the twenty year operation, ITER will also be required to operate at very high availability[3] for periods lasting 1-2 weeks.

[1] the ratio of plasma burn to total pulse length (including both electrical-on and dwell times)

[2] defined as the fraction of pulses for which:
- the necessary subset of data for achieving the goal of a given pulse is successfully acquired and archived, and
- no failure during the pulse which would preclude the initiation of the next pulse.

[3] the ratio of the product of the actual number of pulses and their average duration in an operation plan period in which the device is operational at its acceptable or planned performance level, to the product of the number of pulses and their average duration which could be achieved during that run period in the absence of component failures and software errors.

2.2 Scope of the EDA

The scope of the EDA is described in the adjacent panel from the ITER EDA Agreement.

The Parties shall conduct the following EDA:

(a) to establish the engineering design of ITER including

- *(i) a complete description of the tokamak and its auxiliary systems and facilities,*
- *(ii) detailed designs with specifications, calculations and drawings of the components of ITER with specific regard to their interfaces,*
- *(iii) a planning schedule for the various stages of supply, construction, assembly, tests and commissioning of ITER together with corresponding plan for human and financial resource requirements,*
- *(iv) specifications allowing [timely] calls for tender for the supply of items needed for the start-up of the construction of ITER if and when so decided;*

(b) to establish the site requirements for ITER, and perform the necessary safety, environmental and economic analyses;

(c) to establish both the proposed program and the cost, manpower and schedule estimates for the operation, exploitation and decommissioning of ITER;

(d) to carry out validating research and development work required for performing the activities described above, including development, manufacturing and testing of scalable models to ensure engineering feasibility;

(e) to develop proposals on approaches to joint implementation for decisions by the Parties on future construction, operation, exploitation and decommissioning of ITER.

For the EDA extension this is interpreted as in the following.

- (a) (ii) shall apply only for components critical to the construction decision during the EDA. For the remainder, the design should be scoped to ensure that it can be developed in time within the constraints produced by the detailed design of the critical components.

- Site specific activities shall include design adaptations and their cost estimates, and safety analysis and technical support for the preparation of license applications.

- ITER shall maintain a current estimate of the construction costs, as design progresses. The JCT shall be responsible for developing adaptations of the design and cost estimates to candidate sites which the Parties have proposed. A final cost estimate may be developed for the site selected with the assistance of the site host.

- Project schedules shall be developed by the JCT relevant to the ITER Project and siting decisions reached by the Parties.

- A cost estimate and schedule for deferred components, systems or structures shall be developed so that they may be procured, constructed and commissioned prior to the stage in which they are required.

- The JCT shall maintain current estimates of the R&D costs as the design progresses and shall justify deviations from the construction costs given above.

2.3 Design Principles

Based on all the foregoing, the ITER design during the EDA has adopted the following design principles:

- optimise the design for the objectives of the first phase of active operation and ensure flexibility and capability to accommodate the goals and constraints of following phases;
- within the given resources, maximise the development of the basic tokamak machine and defer that of external systems that can be changed or added later;
- use advanced but proven technologies, but keep the flexibility to introduce new technologies when proven;
- avoid irrevocable choices today if they may be made later when better information is available;
- for systems to be developed and designed later, reserve the maximum space available;
- avoid on-site production and testing as much as possible;
- never compromise safety of the machine operation to improve performance or decrease cost;
- plasma-facing components should be excluded from safety functions;
- emphasise passive safety in the design;
- maximise simplicity, fail-safe and fault-tolerant design, redundancy and diversity (wherever appropriate), independence, and testability.

3 Safety Principles and Criteria

This section provides:

- the safety objectives, principles and criteria that are the high level requirements which should be maintained independently from any design;
- generic elements for the implementation of the safety approach so that each Party can decide how the implementation will satisfy their national laws and regulations; or possibly so that the ITER Parties can agree on a common safety approach for an international realisation of ‘a first of a kind’ machine like ITER.

This section focuses on the safety and environmental issues from the design point of view. Additional aspects would need to be addressed to more fully elaborate the safety principles and generic elements of a safety approach for the operation phase.

In the following, the word 'shall' is used to denote a firm requirement, the word 'should' to denote a desirable option and the word 'may' to denote permission, i.e. neither a requirement nor a desirable option.

3.1 Safety Objectives

A main goal of ITER is to demonstrate the safety and environmental potential of fusion and thereby provide a good precedent for the safety of future fusion power reactors. However, it is necessary to account for the experimental nature of the ITER facility, the related design and material choices, and the fact that not all of them are suited for future fusion power reactors. To accomplish this, ITER safety needs to address the full range of hazards and minimise exposure to these, and to permit siting by any Party.

The following safety objectives are taken into account:

- **General safety**: to protect individuals, society and the environment; to ensure in normal operation that exposure to hazards within the premises and due to release of hazardous material from the premises is **controlled, kept below prescribed limits and minimised;** to prevent accidents with high confidence, to ensure that the consequences of more frequent events, if any, are minor; to ensure that the consequences of accidents are bounded and the likelihood is small.

- **No evacuation**: to demonstrate that the favourable safety characteristics of fusion and appropriate safety approaches limit the **hazards from internal accidents** such that there is, for some countries, **technical justification for not needing evacuation of the public**.

- **Waste reduction**: to reduce radioactive waste hazards and volumes.

ITER shall be developed in such a way that it can be sited by any participant in the ITER EDA Agreement with minor design modifications.

3.2 Safety Principles

The following principles shall be considered in the safety approach. These safety principles not only provide direction to guide the design, but also include on-going, independent review and assessment to ensure the design will meet safety objectives.

3.2.1 'As Low as Reasonably Achievable'

As a basic principle, exposures to hazards shall be kept as low as reasonably achievable (ALARA), economic and social factors being taken into account.

3.2.2 Defence-in-Depth

All activities are subject to overlapping levels of safety provisions so that a failure at one level would be compensated by other provisions. Priority shall be given to **preventing** accidents. **Protection** measures shall be implemented as needed. In addition, measures to

mitigate the consequences of postulated accidents shall be provided, including successive barriers for confinement of hazardous materials.

3.2.3 Passive Safety

Passive safety shall be given special attention. It is based on natural laws, properties of materials, and internally stored energy. Passive features, in particular minimisation of hazardous inventories, help assure ultimate safety margins in addition to fusion's favourable safety characteristics.

3.2.4 Consideration of ITER's Safety Characteristics

The safety approach shall be driven by a deployment of fusion's favourable safety characteristics to the maximum extent feasible. Relevant characteristics are:

- the fuel inventory in the plasma is always below 1 g so that the fusion energy content is small;
- plasma burn is terminated inherently when fuelling is stopped due to the limited confinement by the plasma of energy and particles;
- plasma burn is self-limiting with regard to power excursions, excessive fuelling, and excessive additional heating;
- plasma burn is passively terminated by the ingress of impurities under abnormal conditions (e.g. by evaporation or gas release or by coolant leakage);
- the energy and power densities are low;
- the energy inventories are relatively low;
- large heat transfer surfaces and big masses exist and are available as heat sinks;
- confinement barriers exist and must be leak-tight for operational reasons.

However, the experimental nature of ITER shall also be addressed in the safety approach by the following measures.

- A robust safety envelope will be provided to enable flexible experimental usage. Since ITER is the first experimental fusion device on a reactor scale, it will be equipped with a number of 'experimental components', in particular inside the vacuum vessel. No safety function will be assigned to experimental components. However, experimental components will be designed considering the expected loads from plasma transients, in order to reduce the demands on other systems which do have a safety function.
- Nevertheless, faults in experimental components that can affect safety will be subject to safety assessments. On this basis, related measures will be incorporated in the design as appropriate.

· The experimental programs will be developed in such a way that design modifications will take account of experience from preceding operations and will stay within the safety envelope of the design.

3.2.5 Review and Assessment

Safety assessments shall be an integral part of the design process and results will be available to improve the design and to assist in the preparation of safety documentation for regulatory approval. These analyses shall comprise normal operation, all categories of accidents, and waste characterisation.

An assessment shall be made of potential effluents from the site throughout its lifetime. All effluents (airborne and waterborne) shall be identified and their quantity and characteristics estimated. Effluent assessment shall address normal operation and maintenance. Releases of radioactive materials shall be assessed as part of a demonstration that such effluents are ALARA.

A plant safety assessment shall be made, including a systematic review of the ways in which components might fail and identifying the consequences of such failures. It will also support the Safety Importance classification of components (see 3.4.2). To approach completeness as far as possible, a comprehensive identification procedure shall be applied: Postulated initiating events (PIEs) should be identified by a systematic 'bottom-up' method like the Failure Modes and Effects Analysis (FMEA) as well as by a 'top-down' approach like Global Event Trees or Master Logic Diagrams. A set of reference events shall be selected that encompass the entire spectrum of events. Analysis of reference events shall also address loss of power and aggravating failures in safety systems.

Hypothetical sequences should be used to investigate the ultimate safety margins. The intent is to demonstrate the robustness of the safety case with regard to the project's objectives and radiological requirements.

3.3 Safety and Environmental Criteria

Regulatory approval is required before the construction of ITER and preparations for the future application for approval shall be included in the design process. Before site selection, the design will follow international recommendations, in particular technology-independent ones. Limits on doses to the public and staff from radioactivity and related releases shall be met by design, construction, operation and decommissioning. These project limits shall follow the recommendations by the ICRP (International Commission on Radiation Protection) and the IAEA (International Atomic Energy Agency). Following site selection, Host Country regulations will apply.

An important element of the safety analyses is the assessment of consequences. Doses from releases to the environment will depend on the characteristics of the site, and therefore the project has focussed on limiting the physical releases themselves, rather than the dose. Releases to the environment shall be limited and not exceed the guidelines established by the project in Table 3-1. They should be minimised by design improvement in line with the principle of ALARA.

Table 3-1
Project Release Guidelines

Events or Conditions	Goal	Project Release Guideline
Normal Operation, comprising events and plant conditions planned and required for ITER normal operation, including some faults, events or conditions which can occur as a result of the ITER experimental nature.	Reduce releases to levels as low as reasonably achievable but ensure they do not exceed project release guideline for Normal Operation.	< 1 g T as HT and 0.1 T as HTO and 1 g metal as AP and 5 g metal as ACP per year.
Incidents, or deviations from normal operation, comprising event sequences or plant conditions not planned but likely to occur due to failures one or more times during the life of the plant but not including Normal Operation.	Reduce likelihood and magnitude of releases with the aim to prevent releases, but ensure they do not exceed project release guideline for Incidents.	< 1 g T as HT or 0.1 g T as HTO or 1 g metal as AP or 1 g metal as ACP or combination of these per event.
Accidents, comprising postulated event sequences or conditions not likely to occur during the life of the plant.	Reduce likelihood and magnitude of releases but ensure they do not exceed project release guideline for Accidents.	< 50 g T as HT or 5 g T as HTO or 50 g metal as AP or 50 g metal as ACP or combination of these per event.

HT: elemental tritium (including DT); HTO: tritium oxide (including DTO); AP: divertor or first-wall activation products; ACP: activated corrosion products.

IAEA recommendations are used to interpret the no-evacuation objective: the generic optimised intervention value for temporary evacuation is 50 mSv of avertable dose in a period of no more than 1 week.

ITER shall comply with the ICRP recommendations regarding public and occupational exposures (see Table 3-2 for guidelines established by the project). The radiation protection practices shall be consistent with the IAEA and ICRP recommendations and should make use of best practices. In particular, efforts shall be made to design such that exposures during operation, maintenance, modification and decommissioning are ALARA, economic and social factors being taken into account.

Activated materials are considered long-term waste if criteria for unconditional clearance following IAEA recommendations are not met after a decay period of 100 years.

Table 3-2
Limits and Project Guidelines for Doses from Occupational Exposure

Dose Limits	
ICRP recommended limit for annual individual worker doses	20 mSv/year averaged over 5 years not to exceed 50 mSv/year
Project Guidelines	
Annual individual worker dose	< 5 mSv
Individual dose for any given shift	< 0.5 mSv/shift

3.4 Elements of the Generic Safety Approach

There can be a number of acceptable safety approaches to meet safety objectives. The following sections provide the elements of a generic safety approach implementing the ITER safety principles.

The safety approach shall cover both public and occupational safety for normal operation, incidents, and accidents. The approach shall use a combination of design features and administrative controls to protect the site staff and the public from hazards and to control releases of radionuclides and hazardous materials from the facility. The level of protection required depends on the level of the hazard present in the facility.

3.4.1 Confinement

Confinement of radioactive and toxic materials is a fundamental safety requirement. Confinement is provided by all types of physical and functional barriers which protect against the spread and release of radioactive material. Containment is a special type of confinement when it can accommodate significant pressurisation. Releases would most significantly occur upon breach of barriers, hence confinement barriers shall be protected by appropriate measures such as heat removal, control of energies and monitoring.

The barriers shall be of sufficient number, strength and performance (in terms of leak tightness, retention factors, reliability, etc.) so that releases of radioactive and/or toxic materials during normal operation and for incidents and accidents do not exceed the project release guidelines listed in Table 3-1.

The design of confinement barriers may be graded. Significant, vulnerable, radioactive and/or toxic inventories will require highly reliable barriers, whereas moderate and small inventories may require less reliable barriers.

The design basis for the confinement barriers shall take into account all events, ranging from the initiating events to consequential failures, loads and environmental conditions as identified by the safety assessments taking into account the experimental nature of ITER.

The design of confinement barriers shall implement the principles of redundancy, diversity and independence. Specifically, in the case of multiple barriers, failure of one barrier shall not result in the failure of another barrier.

After pressurisation due to an accident, confinement volumes shall be returned to below atmospheric pressure within a specified period following the accident and a filtered, monitored pathway shall be provided to maintain the pressure inside the volume to below atmospheric pressure.

Measures to protect confinement barriers shall be incorporated as required considering the potential for damage.

Consideration should also be given to the mitigation of consequences from confinement degradation by, failures beyond accidents considered in the design assessment, i.e. by hypothetical sequences.

3.4.2 Component Classification

Systems, structures and components (termed 'components' in the following) important for personnel and public safety (classified as Safety Important, i.e. SIC) shall be identified and

appropriate requirements set. The identification and setting of requirements shall be based on the consequences of failure as determined by safety assessments. The importance to safety of components is not uniform, therefore requirements should be used to develop component-specific safety specifications, taking into account that operational requirements may be more restrictive. The quality level required for components should be commensurate with the required reliability.

3.4.3 Earthquake

Before the ITER site is decided, an assumption for design and safety analysis purposes is to consider three seismic levels (SL-2, SL-1, SL-0) of ground motion. These are specified in Section 4.III.A.5.

Components identified as important to safety (SIC, Section 3.4.2) shall not be damaged as a result of an SL-0/SL-1 earthquake.

Those SIC components that are required to perform a safety function during or after an SL-2 earthquake shall be identified and designed such that the capabilities are maintained. The collapse, falling, dislodgement or any other spatial response of a component as a result of an earthquake shall not jeopardise the functioning of other components providing a safety function. The combination of loads from earthquakes with other loading events shall be considered.

3.4.4 Environmental Qualification

SIC components shall be designed to withstand the environmental conditions created by an accident (such as pressure, temperature, radiation, flooding) under which they are expected to perform their safety function.

3.4.5 Fire

ITER shall be designed to assure that the:

- required safety functions are maintained in case of fire, through a combination of fire prevention, fire detection and suppression, and mitigation of adverse effects on components important to safety (SIC);

- propagation of fire consequences that may impair safety functions are limited by spatial separation, redundancy, diversity, etc.

3.4.6 Decommissioning and Waste

The design shall support decommissioning as appropriate for an experimental device by:

- shielding to reduce induced activation of ex-vessel components during operation;

- use of modular components to simplify dismantling and reduce waste;

- use of remote handling equipment and procedures developed for normal operation.

The design shall reduce the quantities of radioactive liquid waste.

The design shall further incorporate means to reduce the volumes and radiotoxicity of materials which may remain as long-term waste after decommissioning by:

- re-use of components to the extent practical;
- limiting impurities in the materials to allow their clearance as early as practical.

3.4.7 Effluents

The design shall:

- prove that the effluents comply with the project guidelines in Table 3-1;
- reduce radioactivity such that effluents are ALARA;
- monitor the effluents.

3.4.8 Radiation Protection

ITER shall implement design and administrative measures to protect on-site staff against exposure to radiological hazards.

The work to be performed during operation, maintenance, and repair shall be assessed to determine the accessibility and the estimated exposures for activities, against the radiological requirements in Table 3-2 and against recognised limits of exposure to conventional (non-nuclear) hazards.

The design shall provide the means to ensure that the spread of contamination and occupational exposures to radiological hazards are kept ALARA during operation, maintenance and repair. This should include, but not be limited to, access control and zoning, the provision of remote handling, shielding, contamination control, and decontamination equipment as appropriate.

To assure that the radiological requirements are met, through the entire life cycle of ITER, a radiation protection program (RPP) shall be developed and implemented. The scope of the RPP includes programs and processes required for the safety of staff during normal operation and maintenance work. The objectives of the RPP are to:

- prevent acute over-exposures;
- prevent occupational doses over legal limits;
- maintain staff doses ALARA;
- minimise spread of contamination.

Access Control and Zoning

All areas of the ITER plant shall be zoned depending on the anticipated radiological hazard and conditions during short-term maintenance. During activities/events that cause prohibitive radiation levels (e.g. plasma burn phase, in-vessel components moved out of the vacuum vessel, etc.), areas that are otherwise accessible may be designated as 'Restricted' for the duration of the activity, and physical access should be prevented. Such locations shall be returned to accessible only after a formal change control.

Table 3-3 lists the Radiation Access Zones, personnel access limitations, and defines the conditions acceptable in these zones. For contamination control, monitoring is required when crossing from a higher to a lower contamination hazard area, and ventilated air flow shall not move from a higher to a lower contamination hazard area.

Table 3-3
Area Classifications and Radiation Access Zones

Access Zone (Area Classification)	Access Limitations	Airborne / Total Dose Rate / Area Contamination Characteristics
Zone A (Non-Supervised Area)	Unlimited Access.	· No airborne contamination. Dose rate < 0.5 µSv/h; · WHITE contamination control zones only: No surface or airborne contamination and no reasonable possibility of cross-contamination.
Zone B (Supervised Area)	Limited Access for NRW. [(a)] Unlimited Access for RW. [(a)]	· Total dose rate (internal + external) < 10 µSv/h; · GREEN contamination control zones acceptable: No loose contamination tolerated. May be subject to temporary surface or airborne cross-contamination, airborne should not exceed 1 DAC.
Zone C (Controlled Area)	Limited Access for all workers. Access requires planning and an appropriate level of approval for the hazards and the class of personnel requiring access.	· < 100 DAC and < 1 mSv/h; · AMBER contamination control zones acceptable: Airborne and loose surface contamination tolerated but must be identified and controlled. Contamination levels shall be maintained ALARA taking into account the risk of exposure, capability of available protective equipment, possibility of contamination spread, and cost. Airborne contamination in AMBER zones should not exceed 100 DAC.
Zone D (Controlled / Restricted Area)	These are restricted access areas, entry occurs only with a high level of approval from both an operational and a radiological safety view. These areas shall have physical barriers to prevent inadvertent personnel entry.	· Airborne >100 DAC or external dose rate > 1 mSv/h; · RED contamination control zones are only tolerated in Zone D. These areas have permanent or higher than AMBER levels of contamination.

[(a)] Personnel performing work requiring exposure to radiological hazards will be designated as Radiation Workers (RW). All other personnel, including non-designated visitors, will be treated as Non-Radiation Workers (NRW).

Notes: DAC = Derived Air Concentration: unprotected exposure to 1 DAC = 10 µSv/h
1 DAC HTO = 3.1×10^{5} Bq/m^3 = 8.4×10^{-6} Ci/m^3
For internal dose rate, hazard defined in DAC of airborne contamination
For external dose rate, hazard defined as µSv/h

3.4.9 Hazardous Materials

Handling, storage and treatment of hazardous materials (such as intermediately stored radioactive waste, and chemically toxic or reactive materials) shall be designed to:

- limit exposure of site staff during all operations;
- limit the spread of contamination during all operations;
- ensure compatibility with other materials and the surrounding environment;
- prevent chemical reactions during normal operation and accidents.

Beryllium

The project guidelines for beryllium concentrations given in Table 3-4 are one tenth of the occupational exposure limits recognised internationally.

Table 3-4
Project Guidelines for Exposure to Beryllium

Source	Beryllium Concentration
Airborne (Occupational Exposure Limit)	0.2 $\mu g/m^3$
Surface contamination	10 $\mu g/m^2$

3.4.10 Conventional Hazards

Conventional hazards shall be controlled according to appropriate standards. Such hazards include electromagnetic fields, asphyxiation, electrocution, cryogenic materials, vacuum, crane loads, and rotating machinery.

Magnetic Field Hazards

The project guidelines for exposure to magnetic fields are listed in Table 3-5.

Table 3-5
Project Guidelines for Exposure to Magnetic Fields B (T)

Uncontrolled access	B < 10 mT
Daily exposure	B x time ≤ 60 mT-h
Restricted access	B > 100 mT

3.4.11 Security and Proliferation

The design shall provide measures to prevent unauthorised entry to the site and its premises to preclude theft or unauthorised removal of nuclear materials and sabotage.

Design provisions, operational surveillance and administrative measures shall be provided to comply with any international agreements on tritium, lithium-6 and related sensitive technologies with regard to proliferation control.

4 Site Requirements & Assumptions

This following text is reproduced verbatim from the ITER Site Requirements and ITER Site Design Assumptions (N CL RI 3 99-10-19 W 0.2) updated October 1999.

Introduction

The objective of this document is to define a set of requirements that are compulsory for the ITER site, supplemented by assumptions about the ITER site which are used for design and cost estimates until the actual ITER site is known. Part I of this document contains the principles for the development of the site requirements and site design assumptions. Part II of this document contains the compulsory requirements which are derived from the ITER design and the demands it makes on any site. Part III of this document contains site design assumptions which are characteristics of the site assumed to exist so that designers can design buildings, structures and equipment that are site sensitive.

Both the Site Requirements and the Site Design Assumptions are organized in the following categories:

- Land
- Heat Sink
- Energy and Electrical Power
- Transport and Shipping
- External Hazards and Accident Initiators
- Infrastructure
- Regulations and Decommissioning

Each of the categories is subdivided into related elements. Some of the categories are broadly defined. For instance, Infrastructure includes personnel, scientific and engineering resources, manufacturing capacity and materials for construction and operation. Requirements and assumptions for the various elements are justified in the **Bases** statements. These statements explain the rationale for their inclusion and provide a perspective in which they may be used.

I Principles for Site Requirements and Site Design Assumptions

1. The compulsory site requirements are based on the ITER site layout and plant design. These requirements are firm in the sense that reasonable reconfiguration of the plant design will not result in a less demanding set of requirements. Some of the requirements are based in part on how the plant and some of its major components, such as the vacuum vessel and the magnet coils, will be fabricated and installed.

2. This document also addresses the assumptions that have been made to carry out the ITER design until a decision on siting is reached. These site design assumptions form some of the bases for the ITER construction cost estimate and schedule. The assumptions are not compulsory site requirements, but are guidelines for designers to follow until the actual site is known.

3. The requirements for public safety and environmental considerations are, by their nature, site sensitive. Also, the regulatory requirements for siting, constructing, operating and decommissioning ITER are likely to be somewhat different for each potential host country. Therefore, the Safety Contact Persons, designated by each potential Host Country, will help the Project Team to consider any particular requirements that siting in their own country would impose. Until that time, the ITER Plant will be designed to a set of safety and environmental assumptions contained in the ITER Plant Specifications [see 3], which are expected to approximate the actual requirements. Site sensitive considerations during operation such as the shipment of radioactive materials including tritium to the site, the temporary storage of wastes on the site, the shipment of wastes from the site and of the effluents from ITER during normal and off-normal operation, are addressed with the design analysis. Accordingly, a Generic Site Safety Report ("Non-Site-Specific Safety Report") will be available as a firm basis on which the Site Safety Report will later be established to satisfy the licensing authorities of the Host Country.

4. The decommissioning phase of the ITER Plant deserves special attention. In the absence of firm guidance and without prejudice to future negotiations of the Parties, it is assumed that the organization in charge of operating ITER will have a final responsibility to "deactivate" the plant. In this context, "deactivation" is the first phase of decommissioning and includes all actions to shut down the ITER plant and place it in a safe, stable condition. The dismantling phase of decommissioning, which might take place decades after the "deactivation" phase, is assumed to become the responsibility of a new organization within the host country. A technical report on the strategy of deactivation and dismantling will be described inside the design report documentation.

5. In conclusion, the site design assumptions are very important, because without them progress is very limited for the site sensitive designs of buildings, power supplies, site layout and safety/environmental studies. These assumptions were selected so that the design would not be significantly invalidated by actual site deviations from the assumptions. Deviations from the site design assumptions by the actual ITER site may require design and/or construction modifications, but these modifications are expected to be feasible. The modifications may revise the cost estimate and the construction schedule.

II Site Requirements

A. Land

1. Land Area

Requirement The ITER Site shall be up to 40 hectares in area enclosed within a perimeter. All structures and improvements within the perimeter are the responsibility of the ITER project. Land within the perimeter must be committed to ITER use for a period of at least 30 years.

Bases The minimum area for the ITER Site is predicated on sufficient area for the buildings, structures and equipment with allowances for expansion of certain buildings if required for extension of the ITER programme.

The time period is specified to cover the construction (~ 10 years) and operations (~ 20 years) phases. Beyond that, the requirements for any decommissioning will be the responsibility of the Host Country.

2. Geotechnical Characteristics

Requirement The ITER Site shall have foundation soil-bearing capacity adequate for building loads of at least 25 t/m^2 at locations where buildings are to be built. Nevertheless, it is expected that it will be possible to provide at the specific location of the Tokamak Building means to support the average load of 65 t/m^2 at a depth of 25 m. The soil (to a depth of 25 m) shall not have unstable surrounding ground features. The building sites shall not be susceptible to significant subsidence and differential settlement.

Bases The ITER tokamak is composed of large, massive components that must ultimately be supported by the basemat of the structures that house them. Therefore soil-bearing capacity and stability under loads are critical requirements for an acceptable site. The Tokamak Building is composed of three independent halls on separate basemats, but served by the same set of large, overhead bridge cranes. Crane operation would be adversely affected by significant subsidence and differential settlement.

3. Water Supply

Requirement The ITER Site host shall provide a continuous fresh water supply of 0.2 m^3/minute average and 3 m^3/minute peak consumption rates. The average daily consumption is estimated to be about 200 m^3. This water supply shall require no treatment or processing for uses such as potable water and water makeup to the plant de-mineralised water system and other systems with low losses.

Bases The ITER plant and its support facilities will require a reliable source of high quality water. The peak rate of 3 m^3/minute is specified to deal with conditions such as leakage or fires. This water supply is not used for the cooling towers or other uses which may be satisfied by lower quality, "raw" water.

4. Sanitary and Industrial Sewage

Requirement The ITER Site host shall provide sanitary waste capacity for a peak ITER site population of 1000. The host shall also provide industrial sewage capacity for an average of 200 m^3/day.

Bases The ITER project will provide sewer lines to the site perimeter for connection to the sewer service provided by the host. The peak industrial sewage rate is expected to be adequate to deal with conditions such as leaks and drainage of industrial sewage stored in tanks until it can be analyzed for release. Rainwater runoff is not included in industrial sewage.

B. Heat Sink

Requirement The ITER Site shall have the capability to dissipate, on average, 450 MW (thermal) energy to the environment.

Bases ITER and its associated equipment may develop heat loads as high as 1200 MW (thermal) for pulse periods of the order of 500 s. The capability to dissipate 1200 MW should be possible for steady-state operation which is assumed to be continuous full power for one hour. Duty Cycle requirements for the heat sink at peak loads will not exceed 30%. The average heat load would be no more than 450 MW for periods of 3 to 6 days.

C. Energy and Electrical Power

ITER Plant Steady State Electrical Loads

Requirement The ITER Site shall have the capability to draw from the grid 120 MW of continuous electrical power. Power should not be interrupted because of connection maintenance. At least two connections should be provided from the supply grid to the site.

Bases The ITER Plant has a number of systems which require a steady-state supply of electrical power to operate the plant. It is not acceptable to interrupt this power supply for the maintenance of transmission lines, therefore the offsite transmission lines must be arranged such that scheduled line maintenance will not cause interruption of service. This requirement is based on the operational needs of the ITER Plant.

Maintenance loads are considerably lower than the peak value because heavy loads such as the tokamak heat transfer and heat rejection systems will operate only during preparations for and actual pulsed operation of the tokamak.

D. Transport and Shipping

1. Maximum Size of Components to be Shipped

Requirement The ITER Site shall be capable of receiving shipments for components having maximum dimensions (not simultaneously) of about:

- Width - 9 m
- Height - 8 m
- Length - 15 m

Bases In order to fabricate the maximum number of components, such as magnet coils and large transformers, off site, the ITER site must have the capability of receiving large shipments. For the reference case, it is assumed that only the Poloidal Field Coils will be manufactured on site, unless the possibility of transporting and shipping these large coils is proven feasible. For the same reason, it is also assumed that the [Central Solenoid] will be assembled on site

from six modules, unless it proves feasible that the Assembly may be supplied as one large and complete unit. The cryostat will be assembled on site from smaller delivered parts. The width is the most critical maximum dimension and it is set by the Toroidal Field Coils, which are about 9 m wide. The height is the next most critical dimension which is set by the 40° Vacuum Vessel Sector. A length of 15 m is required for the TF coils. The following table shows the largest (~ 100 t or more) ITER components to be shipped:

Largest ITER Components to be Shipped

Component	Pkgs	Width (m)	Length (m)	Height (m)	Weight (t) Each Pkg.
TF Coils	18	9	14.3	3.8	280
Vac. Vessel 40° Sector	9	8	12	8	575
CS Modules	6	4.2	4.2	1.9	100
Large HV Transformer	3	4	12	5	250
Crane Trolley Structure*	2	(14)	(18)	(6)	(600)

* Crane dimensions and weight are preliminary estimates.

PF Coils and CS Assembly**

Component	Pkgs	Width (m)	Length (m)	Height (m)	Weight (t) Each Pkg.
PF1	1	9.5	9.5	2.4	200
PF2	1	18.5	18.5	1.9	200
PF3	1	25.5	25.5	1.2	300
PF4	1	26.0	26.0	1.2	450
PF5	1	18.2	18.2	2.4	350
PF6	1	10.8	10.8	2.4	300
CS Assembly	1	4.2	18.8	4.2	850

** Note that transportation and shipping of the PF Coils and of the CS Assembly are not requirements, but could be considered an advantage.
Note, too, that the PF Coils dimensions are for the coil and connection box envelope, and that for each coil there are vertical protrusions of ~ 1.5 – 1.8 m for the terminals.

2. Maximum Weight of Shipments

Requirement The ITER Site shall be capable of receiving about a dozen components (packages) having a maximum weight of 600 t and approximately 100 packages with weight between 100 and 600 t each.

Bases In order to fabricate the maximum number of components, including magnet coils, off site, the ITER site must have the capability of receiving very heavy shipments. The single heaviest component (Vacuum Vessel Sector) is not expected to exceed 600 t. All other components are expected to weigh less.

E. External Hazards and Accident Initiators

No Compulsory Requirements.

F. Infrastructure

No Compulsory Requirements

G. Regulations and Decommissioning

Details of the regulatory framework for ITER will depend on the Host Country. At a minimum, the Host's regulatory system must provide a practicable licensing framework to permit ITER to be built and to operate, taking into account, in particular, the following off-site matters:

1. the transport of kilograms of tritium during the course of ITER operations;
2. the acceptance and safe storage of activated material in the order of thousands of tonnes, arising from operation and decommissioning.

The agreement with the Host should provide for the issue of the liability for matters beyond the capacity of the project that may arise from ITER construction, operation and decommissioning.

III Site Design Assumptions

The following assumptions have been made concerning the ITER site. These site design assumptions are uniformly applied to all design work until the actual ITER Site is selected.

A. Land

1. Land Area

Assumption During the construction it will be necessary to have temporary use of an additional 30 hectares of land adjacent to or reasonably close to the compulsory land area. It is assumed this land is available for construction laydown, field engineering, pre-assembly, concrete batch plant, excavation spoils and other construction activities.
During operating phases, this land should be available for interim waste storage, heavy equipment storage and activities related to the maintenance or improvement of the ITER Plant.

Bases The assumptions made for the cost and schedule estimates are based on construction experience which uses an additional area of 25 hectares. Only a very limited amount of vehicle parking space (5 hectares) is allocated to the compulsory area, whereas a similar amount will be required to satisfy temporary needs during construction.

2. Topography

Assumption The ITER site is assumed to be a topographically "balanced" site. This means that the volumes of soil cuts and fills are approximately equal over the compulsory land area in Requirement A.1. The maximum elevation change for the "balanced" site is less than 10 m about the mean elevation over the land area in the compulsory requirement.

3. Geotechnical Characteristics

Assumption The soil surface layer at the ITER Site is thick enough not to require removal of underlying hard rock, if present, for building excavations, except in the area under the Tokamak Building itself, at an excavation of about 25 m.

4. Hydrological Characteristics

Assumption Ground water is assumed to be present at 10 m below nominal grade, well above the tokamak building embedment of up to 25 m below nominal grade. This assumption will require engineered ground water control during the construction of the tokamak building pit.

5. Seismic Characteristics

Assumption Using the IAEA seismic classification levels of SL-2, SL-1, and SL-0 and the assumed seismic hazard curves, the following seismic specifications are derived:

IAEA level		Return Period (years)	Peak* Ground Acc.
SL-2	50% tile	10^4	0.2
SL-1	50% tile	10^2	0.05
SL-0		short**	0.05

* Peak Ground Acceleration is for both horizontal and vertical components in units of the gravitational acceleration, g.

** The seismic specifications are not derived probabilistically - local (uniform) building codes are applied to this class. A peak value of 0.05 g is assumed equal to the SL-1 peak value.

Bases Safety assessments of external accident initiators for facilities, particularly when framed in a probabilistic risk approach, may be dominated by seismic events. Assumed seismic hazard curves are used in a probabilistic approach which is consistent with IAEA recommendations for classification as a

function of return period. The selection of the assumed seismic hazard curve is relevant to regions of low to moderate seismic activity. Prior to site selection, specification of the peak horizontal and vertical ground acceleration provide the ITER designers guidelines according to the methodology to be used for seismic analysis, which will rely on a specified Ground Motion Design Response Spectrum and a superposition of modal responses of the structures (according to NRC recommendations). After site selection the actual seismic specifications will be used to adjust the design, in particular by adding seismic isolation, if necessary.

6. Meteorological Characteristics

Assumption A general set of meteorological conditions are assumed for design of buildings, civil structures and outdoor equipment, as follows:

- Maximum Steady, Horizontal Wind ≤ 140 km/h (at 10 m elevation)
- Maximum Air Temperature ≤ 35 °C (24 hr average ≤ 30 °C)
- Minimum Air Temperature ≥ -25 °C (24 hr average ≥ -15 °C)
- Maximum Rel. Humidity (24 hr average) ≤ 95% (corresponding vapour pressure ≤ 22 mbar)
- Maximum Rel. Humidity (30 day average) ≤ 90% (corresponding vapour pressure ≤ 18 mbar)
- Barometric Pressure - Sea Level to 500 m
- Maximum Snow Load - 150 kg/m^2
- Maximum Icing - 10 mm
- Maximum 24 hr Rainfall - 20 cm
- Maximum 1 hr Rainfall - 5 cm
- Heavy Air Pollution (Level 3 according to IEC-71-2[1])

Bases The assumed meteorological data are used as design inputs. These data do not comprise a complete set, but rather the extremes which are likely to define structural or equipment limits. If intermediate meteorological data are required, the designer estimates these data based on the extremes listed above. Steady winds apply a static load on all buildings and outdoor equipment.

B. Heat Sink: Water Supply for the Heat Rejection System

Assumption The JCT has selected forced draft (mechanical) cooling towers as a design solution until the ITER site is selected. At 30% pulse duty cycle (450 MW average heat rejection) the total fresh ("raw") water requirement is about 16 m^3/minute. This water makes up evaporative losses and provides replacement for blowdown used to reduce the accumulation of dissolved and particulate contaminants in the circulating water system. During periods of no pulsing the water requirement would drop to about 5 m^3/minute.
Each blowdown action will lead to a peak industrial sewage rate of 3000 m^3/day.

Bases The actual ITER Site could use a number of different methods to provide the heat sink for ITER, but for the purposes of the site non-specific design, the

[1] Insulation Co-ordination Part 2 Application Guide, Provisional Scale of Natural Pollution Levels

induced draft (mechanical) cooling towers have been assumed. These cooling towers require significant quantities of fresh water ("raw") for their operation. For 450 MW average dissipation, approximately 16 m^3/minute of the water is lost by evaporation and drift of water droplets entrained in the air plume, and by blowdown. This water also supplies make up to the storage tanks for the fire protection system after the initial water inventory is depleted. Cooling towers may not be suitable for an ITER site on a seacoast or near a large, cool body of fresh water. Therefore open cycle cooling will be considered as a design option.

C. Energy and Electrical Power

1. Electrical Power Reliability during Operation

Assumption The grid supply to the Steady State and to the Pulsed switchyards is assumed to have the following characteristics with respect to reliability:

Single Phase Faults - a few tens/year 80%: t < 1 s
- a few / year 20%: 1 s < t < 5 min
where t = duration of fault

Three Phase Faults - a few/year

Bases ITER power supplies have a direct bearing on equipment availability which is required for tokamak operation. If operation of support systems such as the cryoplant, TF coil supplies and other key equipment are interrupted by frequent or extended power outages, the time required to recover to normal operating conditions is so lengthy that availability goals for the tokamak may not be achieved. Emergency power supplies are based on these power reliability and operational assumptions.

2. ITER Plant Pulsed Electrical Supply

Assumption A high voltage line supplies the ITER "pulsed loads". The following table shows the "pulsed load" parameters for the ITER Site:

Characteristic	Values
Peak Active Power*,#	500 MW
Peak Reactive Power	400 Mvar
Power Derivative*	200 MW/s
Power Steps*	60 MW
Fault Level	10-25 GVA
Pulse Repetition time	1800 s
Pulsed Power Duration**	1000 s

from which up to 400 MW is a quasi-steady-state load during the sustained burn phase, while the remaining 80 – 120 MW has essentially pulse character for plasma shape control with a maximum pulse duration of 5 – 10 s and an energy content in the range of 250 – 500 MJ.

* These power parameters are to be considered both positive and negative. Positive refers to power from the grid, while negative refers to power to the grid. Power variations will remain within the limits given above for the maximum power and for the power derivatives.

** The capability to increase the pulse power duration to 3600 s is also assumed, in which case the repetition time would increase accordingly to maintain the same duty factor.

Bases The peak active power, the peak reactive power and the power steps quoted above are evaluated from scenarios under study. Occasional power steps are present in the power waveform. The supply line for pulsed operation will demand a very "stiff" node on the grid to meet the assumption.

D. Transport and Shipping

Bases Several modes of transport and shipping are assumed for ITER because the diversity of these modes provides protection against disruptions for timely delivery of materials and equipment needed by the project. The assumptions for transport and shipping are based on some general considerations which are common for all modes.

When the assumptions describe the site as having "access" to a mode of transport or shipping, it means that the site is not so far away from the transport that the assumed mode would be impractical. Air transport is a good example, because if the airport is not within reasonable commuting time, the time advantage of this mode would be lost (i.e. it would become impractical).

1. Highway Transport

Assumption The ITER Site is accessible by a major highway which connects to major ports of entry and other centers of commerce.

2. Air Transport

Assumption The ITER Site is located within reasonable commuting time from an airport with connections to international air service.

3. Rail and Waterway Transport

Assumption It is assumed the ITER site will have rail and waterway access. The railway is assumed to connect to major manufacturing centres and ports of entry.

E. External Hazards and Accident Initiators

1. External Hazards

Assumption It is assumed the ITER Site is not subject to significant industrial and other man-made hazards.

Bases External hazards, if present at the ITER site, must be recognised in safety, operational and environmental analyses. If these hazards present a significant risk, mitigating actions must be taken to ensure acceptable levels of public safety and financial risk.

2. External (Natural) Accident Initiators

Assumption It is assumed the ITER Site is not subject to horizontal winds greater than 140 km/hr (at an elevation of 10 m) or tornadic winds greater than 200 km/hr. The ITER Site is not subject to flooding from streams, rivers, sea water inundation, or sudden runoff from heavy rainfall or snow/ice melting (flash flood). All other external accident initiators except seismic events are assumed below regulatory consideration.

Bases The wind speeds specified in this requirement are typical of a low to moderate risk site. Tornadic winds apply dynamic loads of short duration to buildings and outdoor equipment by propelling objects at high speeds creating an impact instead of a steady load. The design engineer uses the tornadic wind speed in modeling a design basis projectile which is assumed to be propelled by the tornado. This design basis is important for buildings and structures that must contain hazardous or radioactive materials or must protect equipment with a critical safety function.

ITER is an electrically intensive plant, which would complicate recovery from flooded conditions. This assumption does not address heavy rainfall or water accumulation that can be diverted by typical storm water mitigation systems. For the purposes of this assumption, accidents involving fire, flooding and other initiators originating within the ITER plant or its support facilities are not considered external accident initiators.

F. Infrastructure

Bases The ITER Project is sufficiently large and extended in duration that infrastructure will have a significant impact on the outcome. Industrial, workforce and socioeconomic infrastructure assumptions are not quantitatively stated because there are a variety of ways these needs can be met. The assumptions are fulfilled if the actual ITER site and its surrounding region already meets the infrastructure needs for a plant with similar technical, material and schedule needs as ITER requires.

1. Industrial

Assumption It is assumed the ITER Site has access to the industrial infrastructure that would typically be required to build and operate a large, complex industrial plant. Industrial infrastructure includes scientific and engineering resources, manufacturing capacity and materials for construction. It is assumed the ITER Site location does not adversely impact the construction cost and time period nor does it slow down operation. The following are examples of the specific infrastructure items assumed to be available in the region of the site:

- Unskilled and skilled construction labour

- Facilities or space for temporary construction labour
- Fire Protection Station to supplement on-site fire brigade
- Medical facilities for emergency and health care
- Contractors for site engineering and scientific services
- Bulk concrete materials (cement, sand, aggregate)
- Bulk steel (rebar, beams, trusses)
- Materials for concrete forms
- Construction heavy equipment
- Off-site hazardous waste storage and disposal facilities
- Industrial solid waste disposal facilities
- Off-site laboratories for non-radioactive sample analysis

Bases Efficiency during construction and operation of a large, complex industrial facility varies significantly depending on the relative accessibility of industrial infrastructure. Accessibility to infrastructure can be demonstrated by comparable plants operating in the general region of the site.

2. Workforce

Assumption It is assumed that a competent operating and scientific workforce for the ITER Plant can be recruited from neighbouring communities or the workforce can be recruited elsewhere and relocated to the neighbouring communities.

It is also assumed that ITER has the capability for conducting experiments from remote locations elsewhere in the world. These remote locations would enable "real-time" interaction in the conduct of the experiments, while retaining machine control and safety responsibilities at the ITER Site Control Facility.

Bases The workforce to operate, maintain and support ITER will require several hundred workers. The scientific workforce to conduct the ITER experimental program will also require several hundred scientists and engineers. The assumption that these workers and scientist/engineers come from neighbouring communities is consistent with the site layout plans which have no provisions for on-site dormitories or other housing for plant personnel.

A significant scientific workforce must be located at the ITER Site as indicated in the Assumptions. However, this staff can be greatly augmented and the experimental value of ITER can be significantly enhanced if remote experimental capability is provided. The result of the remote experiment is that scientific staffs around the world could participate in the scientific exploitation of ITER without the necessity of relocation to the ITER Site.
Remote experimental capability is judged to be feasible by the time of ITER operation because of advances in the speed and volume of electronic data transfers that are foreseen in the near future.

3. Socioeconomic Infrastructure

Assumption The ITER Site is assumed to have neighbouring communities which provide socioeconomic infrastructure. Neighbouring communities are assumed to be not greater than 50 km from the site, or one hour travel. Examples of socioeconomic infrastructure are described in the following list:
- Dwellings (Homes, Apartments, Dormitories)
- International Schools from Kindergarten to Secondary School
- Hospitals and Clinics
- Job Opportunities for Spouses and other Relatives of ITER workers
- Cultural life in a cosmopolitan environment

Bases Over the life of the ITER plant, thousands of workers, scientists, engineers and their families will relocate temporarily or permanently to the communities surrounding the ITER site. These people could comprise all the nationalities represented by the Parties. This "world" community will present special challenges and opportunities to the host site communities.

To attract a competent international workforce, international schools should be provided. Teaching should be partially in the mother tongue following programmes which are compatible with schools in each student's country of origin. All parties should assist with the international schools serving these students.

The list of examples is not intended to be complete but it does illustrate the features considered most important. The assumed 50 km distance should maintain reasonable commuting times less than one hour for workers and their relatives.

G. Regulations and Decommissioning

1. General Decommissioning

Assumption During the first phase of decommissioning, the ITER operations organization places the plant in a safe, stable condition. Dismantling may take place decades after the "deactivation" phase. Dismantling of ITER is assumed to be the responsibility of a new organization within the host country. The ITER operations organization will provide the new organization all records, "as-built prints", information and equipment pertinent to decommissioning. Plant characterization will also be provided for dismantling purposes after "deactivation".

Bases Experience and international guidelines (IAEA Safety Series No. 74, 1986, “Safety in Decommissioning of Research Reactors”) stress the importance of good record keeping by the operations organization as a key to decommissioning success.

2. ITER Plant "Deactivation" Scope of Work

Assumption The ITER operations organization will develop a plan to put the plant in a safe, stable condition while it awaits dismantling.

Residual tritium present at the end of ITER operations will be stabilised or recovered to secure storage and/or shipping containers.

Residual mobile activation products and hazardous materials present at the end of ITER operations will be stabilised or recovered to secure storage and/or shipping containers such that they can be shipped to a repository as soon as practical.

ITER deactivation will include the removal of in-vessel components and their packaging in view of long-term storage. This removal from the vacuum vessel will be done by personnel and remote handling tools, trained for maintenance during the previous normal operation.

Liquids used in ITER systems may contain activation products, which must be removed before they can be released to the environment or solidified as waste. It is assumed that all liquids will be rendered to a safe, stable form during the "deactivation" phase, and afterwards no more cooling will be necessary

ITER "deactivation" will provide corrosion protection for components which are vulnerable to corrosion during the storage and dismantling period, if such corrosion would lead to spread of contamination or present unacceptable hazards to the public or workers.

Bases It is recommended (IAEA Safety Series No. 74, 1986) that all radioactive materials be rendered into a safe and stable condition as soon as practical after the cessation of operations**.**

H. Construction Phase

General requirements for the construction phase (except land) are very dependent on local practice. However, water, sewage and power supplies need to be provided at the site for a construction workforce of up to 3000 people.

Plant Description Document

Table of Contents

1 Overview & Summary

1.1 Introduction

1.1.1 Preface

This document presents the technical basis for the ITER Final Design Report foreseen during the current, Engineering Design Activities (EDA), phase of the ITER project. The report presents the results of collaborative design and supporting technical work undertaken by the ITER Joint Central Team (JCT) and the Home Teams (HT) of the Parties to the Agreement on Co-operation in the Engineering Design Activities for ITER[1] (the ITER EDA Agreement).

The overall programmatic objective of ITER, as defined in the ITER EDA Agreement, is "*to demonstrate the scientific and technological feasibility of fusion energy for peaceful purposes*".

The work presented in this report covers the full scope of activities foreseen in Article 2 (a) - (d) of the ITER EDA Agreement, i.e.:

"2 a) to establish the engineering design of ITER including

(i) a complete description of the device and its auxiliary systems and facilities,

(ii) detailed designs with specification, calculations and drawings of the components of ITER with specific regard to their interfaces,

(iii) a planning schedule for the various stages of supply, construction, assembly, tests and commissioning of ITER together with a corresponding plan for human and financial resources requirements, and

(iv) specifications allowing immediate calls for tender for the supply of items needed for the start-up of the construction of ITER if and when so decided,

(b) to establish the site requirements for ITER, and perform the necessary safety, environmental and economic analyses,

(c) to establish both the proposed program and the cost, manpower and schedule estimates for the operation, exploitation and decommissioning of ITER,

(d) to carry out validating research and development work required for performing the activities described above, including development, manufacturing and testing of scalable models to ensure engineering feasibility".

The report is based on detailed supporting technical documentation in all the above areas. In accordance with the terms of the ITER EDA Agreement, this documentation and other information generated in the EDA is available to each of the Parties to use either as part of an international collaborative programme or in its own domestic programme.

[1] ITER EDA Agreement and Protocol 1, ITER EDA Documentation Series No. 1, IAEA, Vienna 1992

The ITER Final Design Report documentation is organised hierarchically as shown in Figure 1.1.1-1. The notion behind this structure is that this documentation arrangement should remain valid also for construction and operation.

The main constituents of the ITER documentation are:

- A top level *Plant Design Specification (PDS)* document, where externally imposed essentially design-independent requirements at the highest level are defined, including safety principles and criteria.

- Design Requirements and Guidelines Level 1 (DRG1) deals with the requirements and specifications above the system level. This includes not only plant-wide requirements but also interfaces or specifications affecting the design of more than one single system. DRG1 identifies the functional and physical interfaces between two systems and refers to any document and drawings defining the interface in more details It effectively includes overall “configuration drawings”. More detailed "Design Background" documents are annexed. These annexes, for example, address in detail Loads Specifications, Quality Assurance, Design Criteria, Design Manuals and Guidelines, Safety Requirements, etc.

- Design Requirements and Guidelines Level 2 (DRG2) defines in one document the boundaries of each system and deals in more detail with the requirements and specifications at the system level. The system division is identical to that of the DDDs.

- Design Description Documents (DDDs) are one per system. They follow a normalized format for the detailed description of the system design and its performance.

- The Plant Description Document (PDD), that is this very document, is the global plant description. It summarises the design based on the details in the DDDs, gives an overview of major plant processes that usually involve more than one system, summarises plant level assessments, and overall planning. The latter items are described in more detail in "Plant Assessment" document annexes. These annexes describe and assess more in detail the entire Plant and processes involving more that one single system. For example: Plant Control, Plasma Performance, Safety Assessment, Assembly Process, Seismic Analysis, Material Assessments, Nuclear Analysis, etc.

- The complete set of Task Reports on detailed design and R&D technology compiled by the Home Teams.

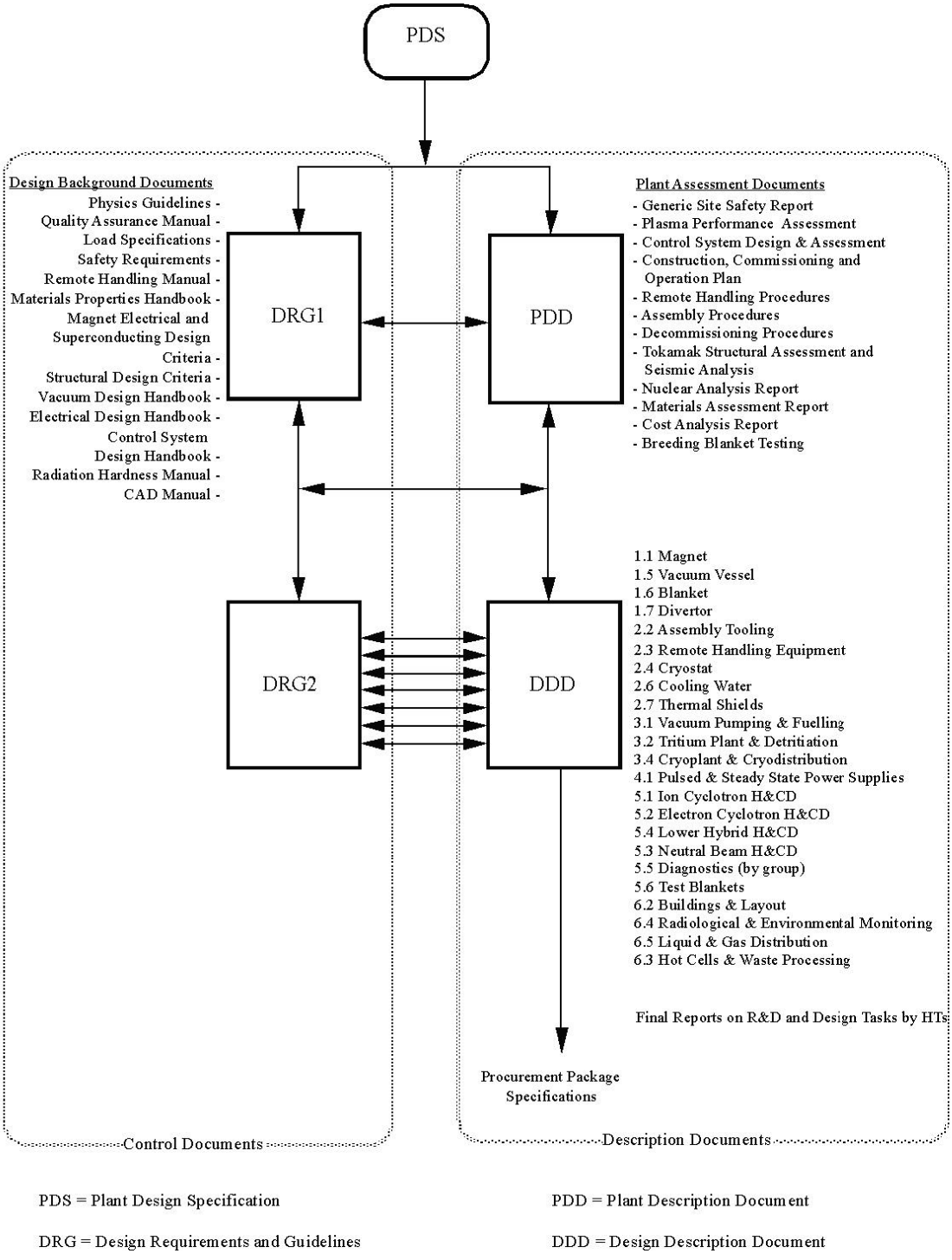

Figure 1.1.1-1 Overall Hierarchy of ITER Documentation

1.1.2 Evolution of the ITER Design

In 1998, at the end of the six years of joint work originally foreseen under the ITER EDA Agreement, a design for ITER had been developed[1] which fulfilled the overall programmatic objectives and complied with the detailed technical objectives, technical approaches, and the cost target adopted by the ITER Parties in 1992 at the start of the EDA.

When they accepted the 1998 report, the ITER Parties, anticipating the Agreement to extend the period of the EDA by three years[2] and recognising the possibility that they might be unable, for financial reasons, to proceed to the construction of the then foreseen device, established a Special Working Group (SWG)[3], and charged it:

- to *propose technical guidelines for possible changes to the detailed technical objectives and overall technical margins, with a view to establishing option(s) of minimum cost still satisfying the overall programmatic objective of the ITER EDA Agreement,* and
- to *provide information on broader concepts as a basis for its rationale for proposed guidelines, and articulate likely impacts on the development path towards fusion energy*.

In reporting on the first task, the SWG[4] proposed revised guidelines for Performance and Testing Requirements, Design Requirements, and Operation Requirements, noting that *"preliminary studies ... suggest that the direct capital costs of ITER can be reduced significantly by targeting the less demanding performance objectives recommended..."* and expressing the view that *"these less demanding performance objectives will satisfy the overall programmatic objectives of the ITER Agreement even though these performance objectives are necessarily less than those that could be achieved with the present* [1998] *design."*

With regard to their second charge, which essentially comes down to a choice between two strategies:

- an ITER-like machine, capable of addressing both scientific and technological issues in an integrated fashion, and
- a number of complementary experiments each of lower cost each of which would specialise on particular scientific or technological issues,

the SWG[5] found that "*the full non-linear interplay between α-particle heating, confinement barriers and pressure and current profile control, and their compatibility with a divertor can be addressed only in an integrated step*" like an ITER-type experiment, capable of providing long burn in conditions in which α−particles are the dominant source of plasma heating. A satisfactory understanding of these physics/plasma/technology interactions is essential to any reactor-oriented fusion development programme. Furthermore, the SWG expressed the unanimous opinion that the world programme is *"scientifically and technically ready to take*

[1] ITER Final Design Report, Cost Review and Safety Analysis, "ITER Council Proceedings: 1998", ITER Documentation Series No 15, IAEA, Vienna, p39

[2] Text of the Agreement extending the EDA Agreement, ibid, p102

[3] SWG Charter, ibid, p108

[4] ITER Special Working Group Report to the ITER Council on Task #1 Results, ibid, p148

[5] ITER Special Working Group Report to the ITER Council on Task #2 Results, "ITER Council Proceedings: 1999", ITER Documentation Series No 17, IAEA, Vienna, p33

the important ITER step." The Parties through the ITER Council subsequently endorsed this viewpoint.[1]

1.1.3 Guidelines and Objectives

The revised performance specifications adopted by the ITER Council in June 1998[2] are set out in full in Table 1.1.3-1; in summary they require ITER:

- to achieve extended burn in inductively-driven deuterium-tritium plasma operation with $Q \geq 10$ (Q is the ratio of fusion power to auxiliary power injected into the plasma), not precluding ignition, with an inductive burn duration between 300 and 500 s;
- to aim at demonstrating steady state operation using non-inductive current drive with $Q \geq 5$.

In terms of engineering performance and testing, the design should:

- demonstrate availability and integration of essential fusion technologies,
- test components for a future reactor, and
- test tritium breeding module concepts; with a 14 MeV-neutron power load on the first wall ≥ 0.5 MW/m^2 and fluence ≥ 0.3 MWa/m^2.

In addition, the device should:

- use as far as possible technical solutions and concepts developed and qualified during the previous period of the EDA, and
- cost about 50% of the direct capital cost of the 1998 ITER Design.

[1]Record of the ITER Meeting, "ITER Council Proceedings: 1999", ITER Documentation Series No 17, IAEA, Vienna, p11

[2]ITER Final Design Report, Cost Review and Safety Analysis, "ITER Council Proceedings: 1998", ITER Documentation Series No 15, IAEA, Vienna, p148

Table 1.1.3-1 ITER Detailed Technical Objectives and Performance Specifications

Plasma Performance

The device should:

- *achieve extended burn in inductively driven plasmas with the ratio of fusion power to auxiliary heating power of at least 10 for a range of operating scenarios and with a duration sufficient to achieve stationary conditions on the timescales characteristic of plasma processes.*
- *aim at demonstrating steady-state operation using non-inductive current drive with the ratio of fusion power to input power for current drive of at least 5.*

In addition, the possibility of controlled ignition should not be precluded.

Engineering Performance and Testing

The device should:

- *demonstrate the availability and integration of technologies essential for a fusion reactor (such as superconducting magnets and remote maintenance);*
- *test components for a future reactor (such as systems to exhaust power and particles from the plasma);*
- *Test tritium breeding module concepts that would lead in a future reactor to tritium self-sufficiency, the extraction of high grade heat, and electricity production.*

Design Requirements

- *Engineering choices and design solutions should be adopted which implement the above performance requirements and make maximum appropriate use of existing R&D database (technology and physics) developed for ITER.*
- *The choice of machine parameters should be consistent with margins that give confidence in achieving the required plasma and engineering performance in accordance with physics design rules documented and agreed upon by the ITER Physics Expert Groups.*
- *The design should be capable of supporting advanced modes of plasma operation under investigation in existing experiments, and should permit a wide operating parameter space to allow for optimising plasma performance.*
- *The design should be confirmed by the scientific and technological database available at the end of the EDA.*
- *In order to satisfy the above plasma performance requirements an inductive flat top capability during burn of 300 to 500 s, under nominal operating conditions, should be provided.*
- *In order to limit the fatigue of components, operation should be limited to a few 10s of thousands of pulses*
- *In view of the goal of demonstrating steady-state operation using non-inductive current drive in reactor-relevant regimes, the machine design should be able to support equilibria with high bootstrap current fraction and plasma heating dominated by alpha particles.*
- *To carry out nuclear and high heat flux component testing relevant to a future fusion reactor, the engineering requirements are*

  Average neutron flux $\geq 0.5\ MW/m^2$

  Average fluence $\geq 0.3\ MWa/m^2$
- *The option for later installation of a tritium breeding blanket on the outboard of the device should not be precluded.*
- *The engineering design choices should be made with the objective of achieving the minimum cost device that meets all the stated requirements.*

Operation Requirements

The operation should address the issues of burning plasma, steady state operation and improved modes of confinement, and testing of blanket modules.

- *Burning plasma experiments will address confinement, stability, exhaust of helium ash, and impurity control in plasmas dominated by alpha particle heating.*
- *Steady state experiments will address issues of non-inductive current drive and other means for profile and burn control and for achieving improved modes of confinement and stability.*
- *Operating modes should be determined having sufficient reliability for nuclear testing. Provision should be made for low-fluence functional tests of blanket modules to be conducted early in the experimental programme. Higher fluence nuclear tests will be mainly dedicated to DEMO-relevant blanket modules in the above flux and fluence conditions.*

In order to execute this program, the device is anticipated to operate over an approximately 20 year period. Planning for operation must provide for an adequate tritium supply. It is assumed that there will be an adequate supply from external sources throughout the operational life.

1.1.4 Modeling of Design Alternatives

To find a set of consistent overall parameters of a tokamak device, a set of non-linear equations are solved, which describe different aspects of the machine performance, both in engineering and in physics. These "system" equations often represent simplifications of much more complex phenomena. The equations that define the physics performance and power balance are often zero dimensional, including the scaling law for energy confinement predictions. Engineering equations, both for plasma and structures, can be very detailed but, with some generally applicable exceptions, must be extracted and qualified by a specific design solution already studied in depth. A costing algorithm completes the suite of procedures, giving the capability to investigate cost trends as a function of dependent variables.

For any given finite Q, four parameters, i.e., the plasma aspect ratio, maximum toroidal field (TF), plasma elongation, and poloidal magnetic flux consumed during the plasma burn phase, are not mutually independent. Allowable elongation, with a given set of plasma vertical position and shape control constraints, is in fact also a function of the aspect ratio. Moreover, for any given burn flux and aspect ratio, the peak field in the TF magnet is automatically determined. There is a limit on plasma triangularity which is strongly interconnected with the divertor geometry, shape control, and issues related to the single null divertor operation, such as the distance separating active and inactive separatrixes (see Figure 1.2.1-5).

On this basis, the system studies indicated a domain of feasible design space, with aspect ratios in the range 2.5 to 3.5 and a major radius around 6 m, able to meet the technical guidelines ad objectives, with a shallow cost minimum across the aspect ratio range. The shallowness of the cost curve and the inevitable approximate nature of the system studies made it clear that no particular choice can be made on the optimal aspect ratio based on estimated costs alone. In addition, there are other important aspects (e.g. plasma access and in-vessel maintenance) for which the cost or performance impact may not be easily factored into a systems optimisation.

1.1.5 Convergence to an Outline Design

To provide a basis for rigorous exploration and quantification of the issues and costing, representative design options that span an appropriate range of aspect ratio and magnetic field were selected for further elaboration and more comprehensive consideration. A task force involving the JCT and the HTs met during 1998 and 1999 to analyse and compare them.

The development of specific representative options provided a more tangible appreciation of the key issues, and a practical framework for the process of convergence was explored and clarified in the joint Task Force. The Task Force recommendations were instrumental in developing consensus on the criteria and rationale for the selection of major parameters and concepts as the precursor to converging and integrating the various considerations into a single coherent outline design which is described in the rest of this report.

In January 2000, the ITER Meeting (Tokyo) *"accepted the ITER-FEAT Outline Design Report, taking note of the TAC Report and recommendations and agreed to transmit the report to the Parties for their consideration and domestic assessment"*. The Parties assessments were overwhelmingly positive in their endorsement of the outline design, and the process of assessment by the Parties offered the opportunity to further tune the design taking

into account their recommendations. The governing body of ITER subsequently approved the design in June 2000 (Moscow ITER Meeting), recognising it as a single mature design for ITER consistent with its revised objectives.

The proposed design is based on:

1. physics understanding: the ITER Physics Basis[1] (IPB) plus new results of "voluntary" physics R&D from Parties;
2. R&D results in technology development since 1992[2], which have provided qualified solutions by testing models after their manufacture: they have demonstrated feasibility through clearly identified manufacturing processes;
3. a consensus across Parties on safety principles and design criteria for limiting the consequences of ITER operation for the environment, and results of analysis on all possible, even hypothetical, accidents with regard to their consequences;
4. a cost target: a cost analysis has been established by industries of all Parties for manufacturing which is probably not yet fully optimised towards a reduced cost; this would be the outcome of "manufacturing R&D", needed anyway to achieve reliable production.

The key requirements to achieve Q >10 in inductive pulsed mode of operation according to the IPB can be summarised as:

1. a plasma current sufficient to provide adequate plasma energy confinement;
2. a large enough plasma density and a plasma energy confinement, good enough to achieve $Q \geq 10$, in high confinement modes of operation (H mode);
3. reliable power exhaust and impurity control in a single-null divertor configuration, while at the same time considering the limits imposed by various instabilities on plasma design parameters such as safety factor, normalised beta, elongation, triangularity, and He ash impurity content after transfer of α-energy to the thermal plasma.

With regard to steady state operation modes, the data presently in hand does not possess the coherence across the present experiments required to develop into the design basis for nominal performance. However, there does not appear to be any crucial conflict regarding designs based on H-mode physics to exploit whatever operational modes future progress will establish, if efficient and flexible current drive systems will be available with an adequate amount of power.

1.1.6 Conclusion

This report marks the achievement of the full technical scope of activities indicated in the ITER EDA Agreement, with a final design which meets the programmatic objective defined in the Agreement and satisfies detailed scientific, technical and costing objectives set by the ITER Council in 1998. With the accompanying body of supporting documentation, the Parties now have at their disposal, in accordance with the purpose of the ITER EDA Agreement, a well founded and robust ITER design that confers a high degree of confidence that it will meet its objectives. While there is still technical work that can be done to finalise

[1] Nuclear Fusion 39 (1999) 2137-2664

[2] Y. Shimomura for the ITER Central Team and Home Teams, ITER Technology R&D, Fusion Engineering and Design 55 (2001), 97 - 358

the details of procurements and to optimise costs, all technical data necessary for future decisions on the construction of ITER is now available. Following the completion of Explorations, the next step is for the Parties negotiators to agree on a preferred site to allow specific site adaptation, and a text for the construction agreement ready to sign.

1.2 Design Overview

1.2.1 Design

ITER is a long pulse tokamak with elongated plasma and single null poloidal divertor (Figure 1.2.1-1 to Figure 1.2.1-5 and Table 1.2.1-1 to Table 1.2.1-3). The nominal inductive operation produces a DT fusion power of 500 MW for a burn length of 400 s, with the injection of 50 MW of auxiliary power.

The major components of the tokamak are the superconducting toroidal and poloidal field coils which magnetically confine, shape and control the plasma inside a toroidal vacuum vessel. The magnet system comprises toroidal field (TF) coils, a central solenoid (CS), external poloidal field (PF) coils, and correction coils (CC). The centring force acting on the D-shaped toroidal magnets is reacted by these coils by wedging in the vault formed by their straight sections. The TF coil windings are enclosed in strong cases used also to support the external PF coils. The vacuum vessel is a double-walled structure also supported on the toroidal field coils. The magnet system together with the vacuum vessel and internals are supported by gravity supports, one beneath each TF coil.

Inside the vacuum vessel, the internal, replaceable components, including blanket modules, divertor cassettes, and port plugs such as the limiter, heating antennae, test blanket modules, and diagnostics modules, absorb the radiated heat as well as most of the neutrons from the plasma and protect the vessel and magnet coils from excessive nuclear radiation. The shielding blanket design does not preclude its later replacement on the outboard side by a tritium-breeding blanket constrained to the same temperature cooling water as the shielding blanket.

The heat deposited in the internal components and in the vessel is rejected to the environment by means of the tokamak cooling water system (comprising individual heat transfer systems) designed to exclude releases of tritium and activated corrosion products to the environment. Some elements of these heat transfer systems are also employed to bake and consequently clean the plasma-facing surfaces inside the vessel by releasing trapped impurities. The entire tokamak is enclosed in a cryostat, with thermal shields between the hot components and the cryogenically cooled magnets.

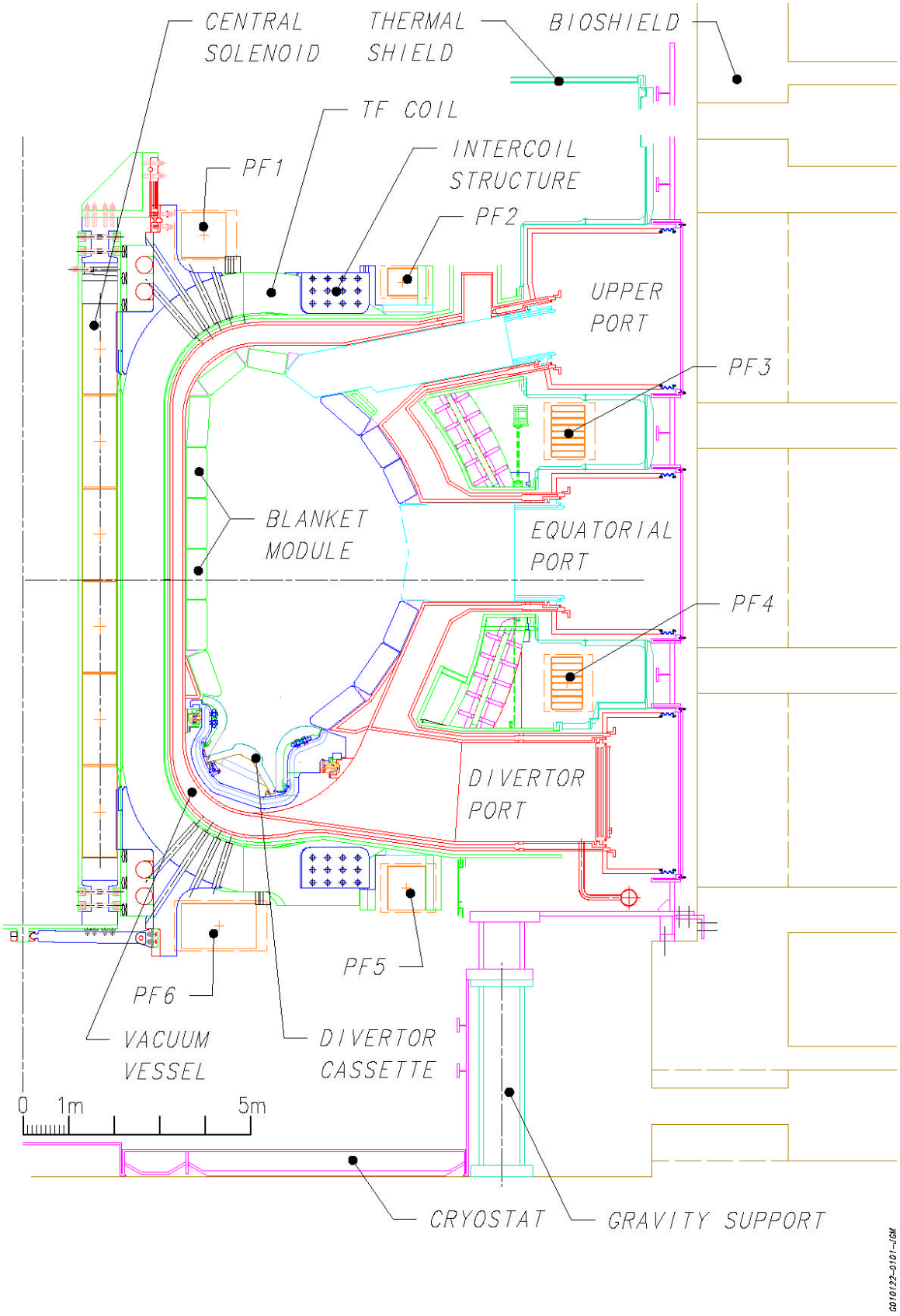

Figure 1.2.1-1 ITER Tokamak Cross-section

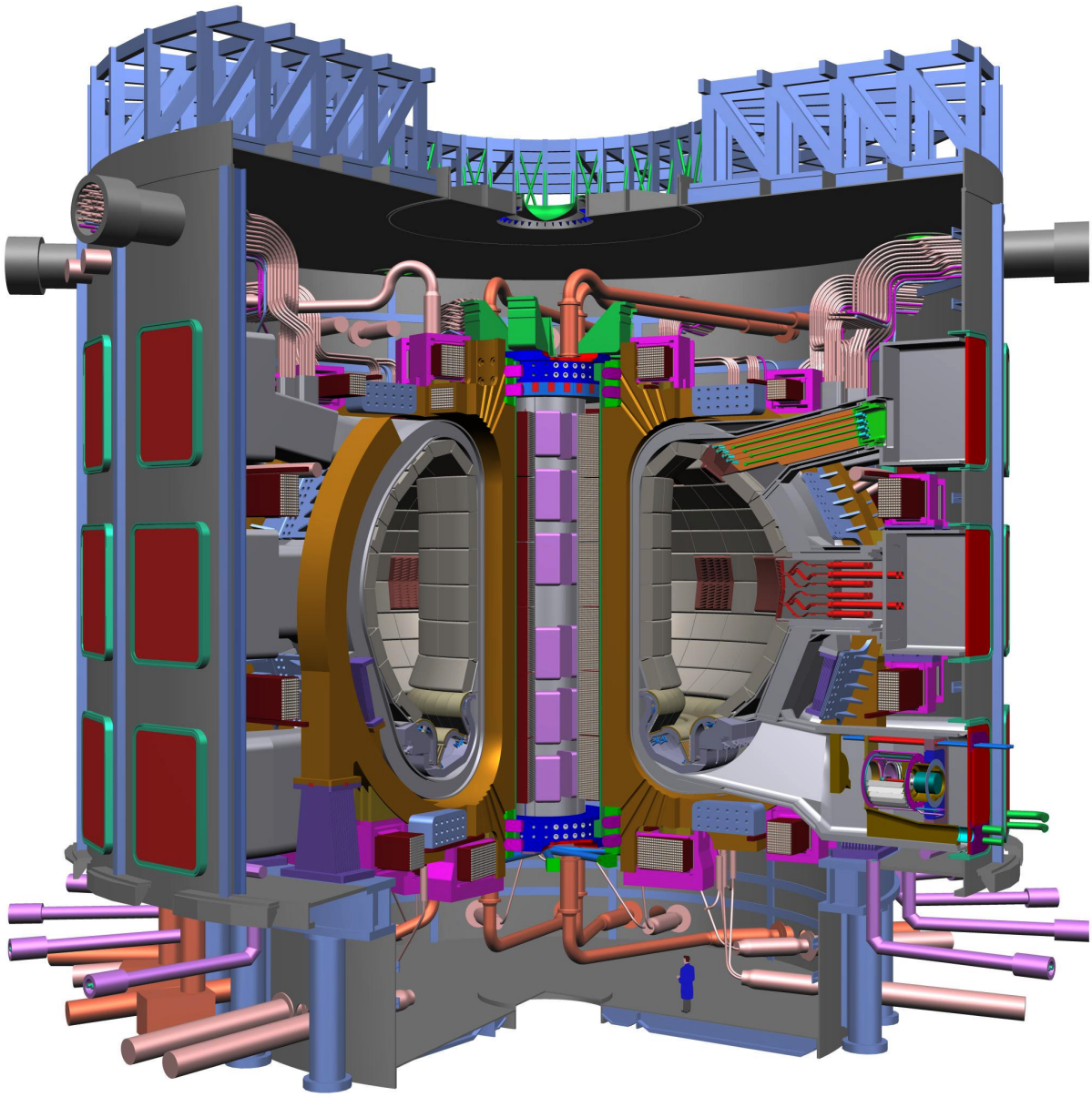

Figure 1.2.1-2 ITER Tokamak Cutaway

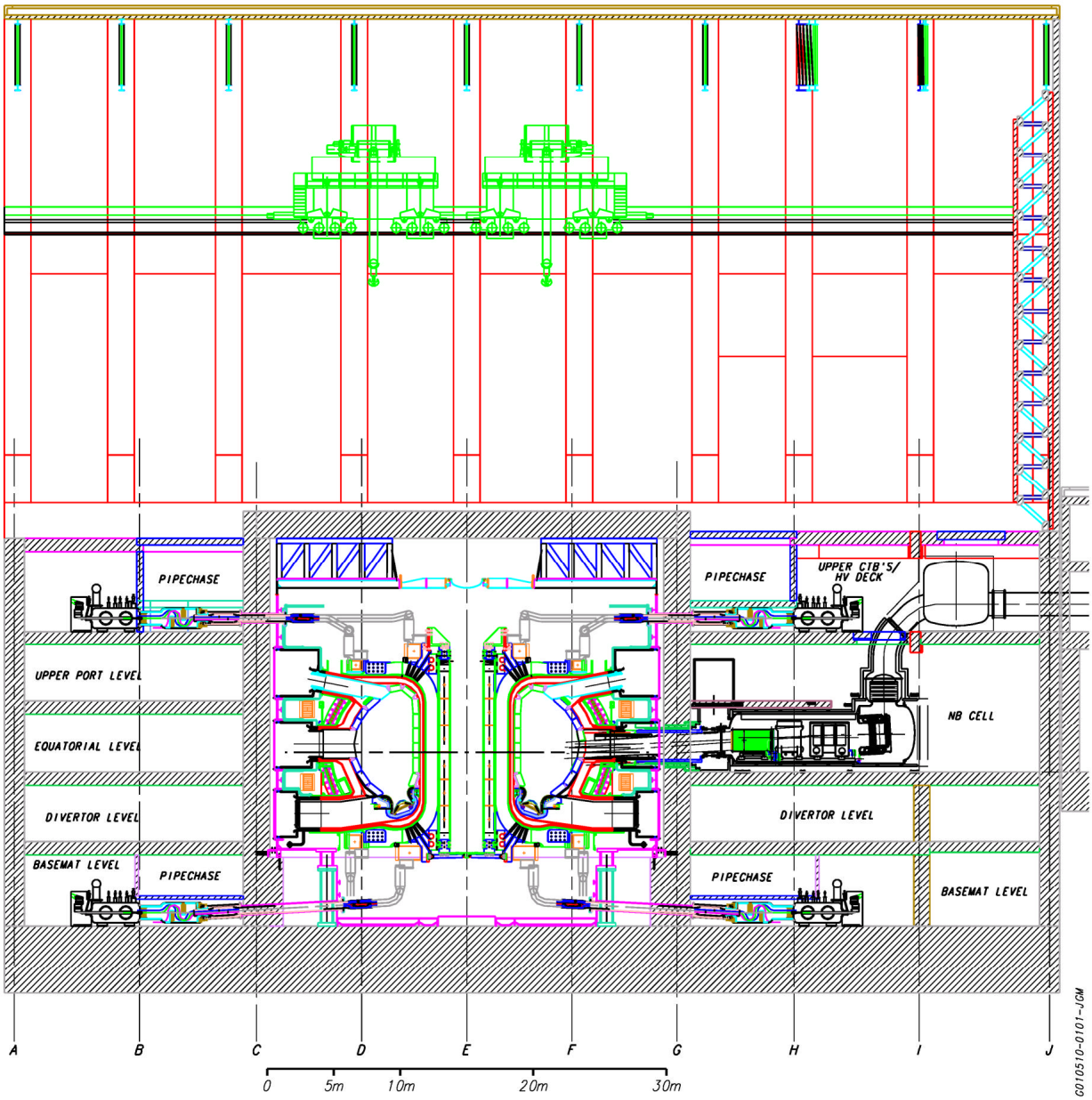

Figure 1.2.1-3 Cross-section NS Through the Tokamak Building

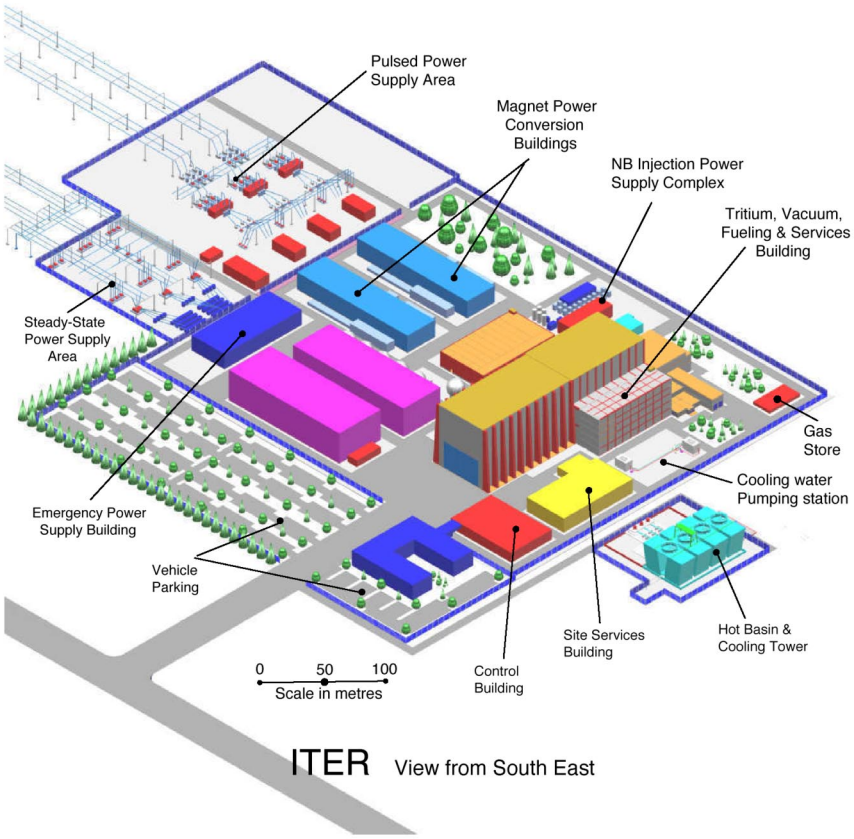

Figure 1.2.1-4 Generic ITER Site View

Figure 1.2.1-5
ITER Nominal Plasma Configuration

(The upper and lower X-points are on different magnetic surfaces, defining two separatrices, the active one within the inactive one.)

(The g1, … g6 refer to gaps whose sizes are control variables for plasma stability.)

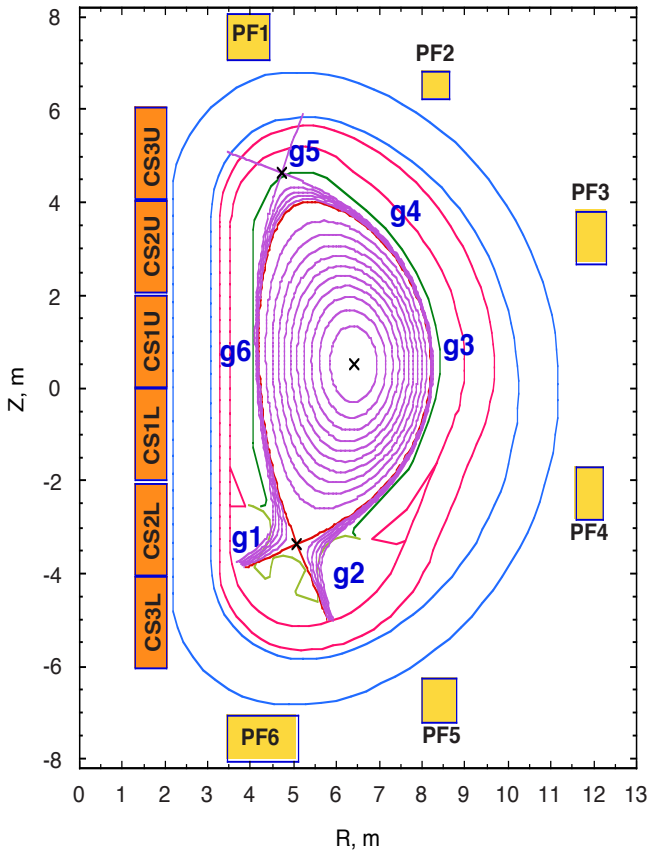

The tokamak fuelling system is designed to inject gas and solid hydrogen pellets. During plasma start-up, low-density gaseous fuel will be introduced into the vacuum vessel chamber by the gas injection system. The plasma will progress from electron-cyclotron-heating-assisted initiation, in a circular configuration touching the outboard limiter, to an elongated divertor configuration as the plasma current is ramped up. Once the current flat top value (nominally 15 MA for inductive operation) is reached, subsequent plasma fuelling (gas or pellets) together with additional heating for ~ 100 s leads to a high Q DT burn with a fusion power of about 500 MW. With non-inductive current drive from the heating systems, the burn duration is envisaged to be extended to 1 hour. In inductive scenarios, before the inductive flux available has been fully used, reducing the fuelling rate so as to slowly ramp-down the fusion power terminates the burn. This phase is followed by plasma current ramp-down and finally by plasma termination. The inductively driven pulse has a nominal burn duration of 400 s, with a pulse repetition period as short as 1800 s. The integrated plasma control is provided by the PF system, and the pumping, fuelling (D, T and impurities such as N_2, Ar) and heating systems all based on feedback from diagnostic sensors.

With regard to safety and licensing issues, the current design focuses on confinement as the overriding safety function, other functions being recognised as being required to protect confinement. Design requirements have been derived from safety principles and release guidelines adopted by the project by identifying the systems, structures, components and procedural measures that can prevent or mitigate releases, and by allocating performance targets (both capability and reliability) to these. Successive barriers are provided for tritium (and activated dust). These include the vacuum vessel, the cryostat, active air conditioning systems, with de-tritiation and filtering capability in the building confinement. Effluents are filtered and detritiated, in such a way that their release to the environment is as low as reasonably achievable (ALARA).

Table 1.2.1-1 Main Plasma Parameters and Dimensions

Total Fusion Power	500 MW *(700 MW)*
Q — fusion power/additional heating power	≥ 10
Average 14MeV neutron wall loading	0.57 MW/m^2 *(0.8 MW/m^2)*
Plasma inductive burn time	≥ 400 s
Plasma major radius (R)	6.2 m
Plasma minor radius (a)	2.0 m
Plasma current (I_p)	15 MA *(17 MA [(1)])*
Vertical elongation @95% flux surface/separatrix (κ_{95})	1.70/1.85
Triangularity @95% flux surface/separatrix (δ_{95})	0.33/0.49
Safety factor @95% flux surface (q_{95})	3.0
Toroidal field @6.2 m radius (B_T)	5.3 T
Plasma volume	837 m^3
Plasma surface	678 m^2
Installed auxiliary heating/current drive power	73 MW [(2)]

(1) The machine is capable of a plasma current up to 17 MA, with the parameters shown in parentheses) within some limitations over some other parameters (e.g., pulse length).

(2) A total plasma heating power up to 110 MW may be installed in subsequent operation phases.

Table 1.2.1-2 Main Engineering Features of ITER

Superconducting Toroidal Field Coils (18 coils)	
Superconductor	Nb_3Sn in circular stainless steel (SS) jacket
Structure	in grooved radial plates Pancake wound, in welded SS case, wind, react and transfer technology
Superconducting Central Solenoid (CS)	
Superconductor	Nb_3Sn in square Incoloy jacket, or in circular Ti/SS jacket inside SS U-channels
Structure	Six modules of 5 hexa- and 1 quad-pancake, wind react and transfer technology
Superconducting Poloidal Field Coils (PF 1-6)	
Superconductor	NbTi in square SS conduit
Structure	Double pancakes
Vacuum Vessel (9 sectors)	
Structure	Double-wall, welded ribbed shell, with internal shield plates and ferromagnetic inserts for TF ripple reduction
Material	SS 316 LN structure, SS 304 with 2% boron shield, SS 430 inserts
First Wall/Blanket (421 modules)	(Initial DT Phase)
Structure	Single curvature faceted separate FW attached to shielding block which is fixed to vessel
Materials	Be armour, Cu-alloy heat sink, SS 316 LN str.
Divertor (54 cassettes)	
Configuration	Single null, modular cassettes with separable high heat flux components
Materials	W alloy and C plasma facing components Copper alloy heat sink, SS 316 LN structure
Cryostat	
Structure	Reinforced cylinder with flat ends
Maximum inner dimensions	28 m diameter, 24 m height
Material	SS 304L
Tokamak Cooling Water System	
Heat released in the tokamak during nominal pulsed operation	750 MW at 3 and 4.2 MPa water pressure, ~ 120°C
Cryoplant	
Nominal average He refrig. /liquefac. rate for magnets & divertor cryopumps (4.5K)	55 kW / 0.13 kg⁄s
Nominal cooling capacity of the thermal shields at 80 K	660 kW
Additional Heating and Current Drive	
Total injected power	73 MW initially, up to 110 MW maximum
Candidate systems	Electron Cyclotron, Ion Cyclotron, Lower Hybrid, Negative Ion Neutral Beam
Electrical Power Supply	
Total pulsed active/reactive power from grid	500 MW / 400 Mvar
Total steady state active/reactive power	110 MW/ 78 Mvar

Table 1.2.1-3 Heating and Current Drive Systems

	NB (1MeV)	EC (170 GHz)	IC (~ 50 MHz)	LH (5 GHz)
Power injected per unit equatorial port (MW)	16.5	20	20	20
Number of units for the first phase	2	1	1	0
Total power (MW) for the first phase	33	20	20	0
The 20 MW of EC module power will be used either i) in up to 3 upper ports to control neoclassical tearing modes at the q = 3/2 and q = 2 magnetic surfaces, or ii) in one equatorial port for H&CD mainly in the plasma centre.				

1.2.2 Operation Scenarios and Phases

As an experimental device, ITER is required to be able to cope with various operation scenarios and configurations. Variants of the nominal scenario are therefore considered for extended duration plasma operation, and/or steady state modes with a lower plasma current operation, with H, D, DT (and He) plasmas, potential operating regimes for different confinement modes, and different fuelling and particle control modes. Flexible plasma control should allow the accommodation of "advanced" plasma operation based on active control of plasma profiles by current drive or other non-inductive means.

Four reference scenarios are identified for design purposes. Three alternative scenarios are specified for assessment purposes to investigate how plasma operations will be possible within the envelope of the machine operational capability assuming a reduction of other concurrent requirements (e.g. pulse length).

Design scenarios

1. Inductive operation I: P_{fus}=500 MW, Q=10, I_p=15 MA, with heating during current ramp-up
2. Inductive operation II: P_{fus}=400 MW, Q=10, I_p=15 MA, without heating during current ramp-up
3. Hybrid operation (i.e., plasma current driven simultaneously by inductive and non-inductive means)
4. Non-inductive operation type I: weak negative shear (WNS) operation

Assessed scenarios

5. Inductive operation III: P_{fus}=700 MW, I_p=17 MA, with heating during current ramp-up
6. Non-inductive operation type II: strong negative shear (SNS) operation
7. Non-inductive operation type III: weak positive shear (WPS) operation

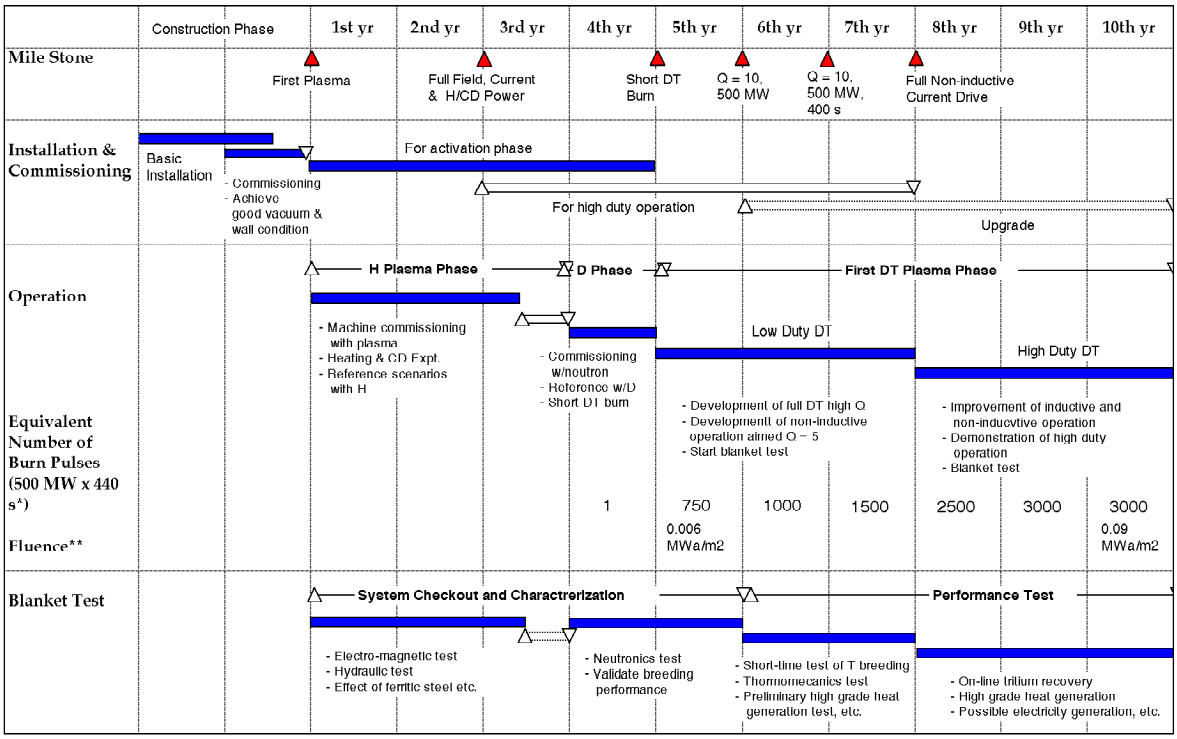

* The burn time of 440 s includes 400 s flat top plus 40 s of full power neutron flux to allow for contributions during ramp-up and ramp-down
** Average fluence at first wall (neutron wall load is 0.56 MW/m^2 on average and 0.77 MW/m^2 at outboard equator)

Figure 1.2.2-1 Initial Operation Plan

During its lifetime, ITER will be operated in successive phases.

H Phase
This is a non-nuclear phase using only hydrogen or helium plasmas, planned mainly for complete commissioning of the tokamak system in a non-nuclear environment where remote handling maintenance is not mandatory. The discharge scenario of the full DT phase reference operation can be developed or simulated in this phase. The peak heat flux onto the divertor target will be of the same order of magnitude as for the full DT phase. Characteristics of electromagnetic loads due to disruptions or vertical displacement events, and heat loads due to runaway electrons, will be basically the same as those of the DT phase.

Some important technical issues cannot be fully tested in this phase because of smaller plasma thermal energy content and lack of neutrons and energetic alpha particles.

The actual length of the hydrogen operation phase will depend on the merit of this phase with regard to its impact on the later full DT operation, in particular on the ability to achieve good H mode confinement with a suitably high plasma density.

D Phase
The characteristics of deuterium plasma are very similar to those of DT plasma except for the amount of alpha heating. Therefore, the reference DT operational scenarios, i.e., high Q, inductive operation and non-inductive steady state operation, can be simulated further. Since some tritium will be generated in the plasma, fusion power production for short periods of time without fully implementing the cooling and tritium-recycle systems could therefore also be demonstrated. By using limited amounts of tritium in a deuterium plasma, the integrated

nuclear commissioning of the device will be possible. In particular, the shielding performance will be tested.

DT Phases
During the first phase of DT operation the fusion power and burn pulse length will be gradually increased until the inductive operational goal is reached. Non-inductive, steady state operation will also be developed. DEMO reactor relevant test blanket modules will also be tested whenever significant neutron fluxes will be available, and a reference mode of operation for that testing will be established.

The second phase of full DT operation, beginning after a total of about ten years of previous operation, will emphasise improvement of the overall performance and the testing of components and materials with a higher neutron fluence. This phase will address the issues of higher availability and further improved modes of plasma operation. The implementation and the programme for this phase will be decided following a review of the results from the preceding three operational phases and an assessment of the merits and priorities of programmatic proposals.

A decision on incorporating in the vessel a tritium breeding blanket during the course of the second DT phase will be taken on the basis of the availability of this fuel from external sources, its relative cost, the results of breeder blanket module testing, and acquired experience with plasma and machine performance.

1.3 Plasma Performance

According to the conclusions of the ITER Physics Basis, obtained from broadly based experimental and modelling activities within the fusion programmes of the ITER Parties, the regime assumed for nominal inductive operation of ITER is the ELMy H-mode confinement regime in the presence of edge localized modes (ELMs).

In this regime, plasma turbulent heat conduction across the magnetic surfaces drops dramatically in a thin transport barrier layer just inside the magnetic separatrix. This layer is commonly observed to undergo successive relaxations called ELMs. The interest in ELMy H-modes follows from experimental observations that show that this mode reduces transport throughout the whole plasma. The standard working hypothesis, supported by many observations, is that H-mode occurs when the power transported across the separatrix (P_{loss}), which must be compensated for by internal and external heating, exceeds a threshold value ($P_{L\text{-}H}$).

From the statistical analysis of confinement results obtained in all tokamak devices, an expression of the energy confinement time has been established as a function of plasma parameters, verified in time through three orders of magnitude, and expressed as

$$\tau_{E,th}^{IPB98(y,2)} = 0.0562 H_H I_p^{0.93} B_T^{0.15} P^{-0.69} n_e^{0.41} M^{0.19} R^{1.97} \varepsilon^{0.58} \kappa_x^{0.78} \qquad \text{(rms err. 0.13)}$$

Where the units are s, MA, T, 10^{19}m^{-3}, MW, m and amu, where ε=a/R and P is the total (from internal and external sources) power crossing the separatrix as P_{loss}, and where H_H is a scalar which can be used to represent either how close the actual value observed in one experiment is from the average, or a level of inaccuracy. This expression will only be valid in H-mode, that is when $P_{loss} > P_{L\text{-}H}$, with

$$P_{L\text{-}H} = 2.84 M^{-1} B_T^{0.82} \bar{n}_e^{0.58} R^{1.00} a^{0.81} \qquad \text{(rms err. 0.27)}$$

Where the units are MW, amu, T, $10^{20}m^{-3}$, m. No statistical uncertainty factor is included in the second equation, so all uncertainties can be handled by assumed variations in H_H.

1.3.1 ITER Plasma Current and Size

Assuming $P_{loss} > P_{L\text{-}H}$, and using the previous expressions for τ_E and $P_{L\text{-}H}$, one can derive the relationship between the plasma parameters and the capability to achieve a given value of $Q = P_{fusion}/P_{add}$, which can be formulated approximately as

$$\left[\frac{H_H I_p \frac{R}{a}}{X}\right]^3 = \frac{Q}{Q+5}$$

With X ~ 50-60, a slowly varying function of parameters. This relation provides the basis for $I_P = 15MA$, R/a = 3.1 if Q = 10, X = 55 and $H_H = 1$.

Expressing now $I_p \cdot R/a = 5 \cdot B_T \cdot a/q \cdot f$, where f is a function of aspect ratio, increasing with triangularity, δ, and mostly with plasma elongation κ, it is obviously important to increase the value of f, decrease the value of q, and compromise between B_T and size.

However, there are limiting values for f and q: too large an elongation provides a condition where the vertical stability of plasma position cannot be assured practically; additionally q below 3 is limited by the occurrence in a large volume near the plasma axis of "sawtooth relaxation" (an instability which periodically destroys the confinement in this volume) and there is an increasing susceptibility to instability as q=2 is approached.

A large aspect ratio allows a larger value of B_T at the expense of a smaller plasma volume, a poorer access to the plasma for heating and maintenance as well as a more difficult plasma shape control. A compromise amongst these and other more detailed considerations leads the choice to the present value.

1.3.2 Plasma Confinement Extrapolation

Experiments have shown that once an ideally stable equilibrium is assured by externally applied shaping fields, the plasma response to auxiliary heating and fuelling is governed by the spontaneous appearance of a fine scale turbulence.

Profiles of plasma parameters, shown for example in Figure 1.3.2-1, are the consequence of transport properties which are governed mainly by turbulence, the characteristic scale of which is much smaller than the device size. The physical processes prevailing depend on dimensionless variables, built from density, temperature and magnetic field values, mainly ρ^* = ion gyration radius/minor plasma radius, β = plasma pressure/magnetic pressure and ν^* = collisionality.

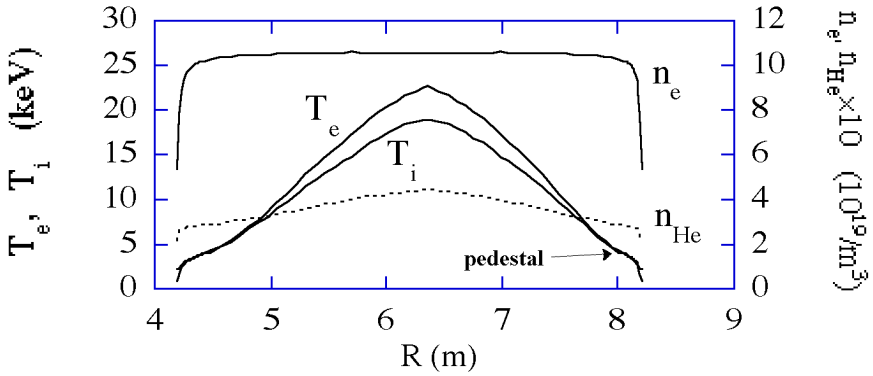

Figure 1.3.2-1 Profiles of Electron Temperature (T_e), Ion Temperature (T_i), Electron Density (n_e), Helium Density (n_{He})

In this respect, experiments having identical non-dimensional parameters, but differing magnetic field, density and temperature, have been shown to have the same non-dimensional energy confinement time defined by $\Omega_{ci}.\tau_E$, (where Ω_{ci} is the plasma ion cyclotron frequency). Therefore, present experiments have been used to simulate ITER discharges, which reduces the problem of extrapolation to that of a single parameter ρ^*.

Accordingly, simulation codes have been written to model plasma evolution. These programs take into account the magnetic configuration in detail, assuming constant density and temperature on a magnetic surface, adjusting the thermal diffusivity in such a manner that the global energy confinement time computed by the code is constrained to be equal to the global scaling relation, and adapting its spatial profile to provide temperature profiles close to those observed in ITER demonstration discharges.

1.3.3 H-mode Pedestal and ELMs

The transport barrier that occurs just inside the magnetic separatrix in H-mode provides a thin layer where the pressure increases sharply (a large radial gradient is established). At its inner edge a pedestal is formed where density and temperature values serve as boundary conditions for the core profiles. Pedestal temperatures can be very important if the core temperature gradient is constrained (a fact not always observed in present experiments) to lie near a marginal upper value. Even if this is not the case, the energy content of the pedestal is generally not negligible compared to the remaining core energy content (in fact about one third). Moreover it has a scaling that differs from the core global scaling, and is not definitely agreed yet.

ELMs appear as a pseudo-periodic relaxation of the pressure gradient in the plasma boundary region, due to an instability that depends on the detailed shape of the magnetic surface near the separatrix (under the global influence of the separatrix curvature variation, triangularity, and magnetic shear). As the ELMs' frequency becomes smaller, their amplitude increases and the energy removed from the pedestal by each ELM becomes larger and, as it is deposited onto the divertor targets, leads to rather strong erosion. The physical phenomena involved are not understood in quantitative terms at present.

1.3.4 Internal Confinement Barrier

In some conditions (not completely understood or controlled until now), a confinement barrier might occur inside the core, and limit even more the turbulent heat conduction across the plasma. For its existence this barrier again appears to require a threshold in the power crossing it. The barrier provides a steep pressure gradient and occurs usually in a region where the magnetic shear is very weak (as at a minimum of q). This internal barrier, if its existence and stability can be controlled on a long time scale, will lead to better confinement performance, which can be the more interesting the larger can be its minor radius. In addition, because a toroidal current is driven by the pressure gradient (the so called "boot-strap" current), this internal barrier is considered an important feature for possible steady-state tokamak operation, where the toroidal current, driven by non-inductive drive methods from auxiliary power, has to be minimised.

1.3.5 Non-axisymmetric Perturbations, Islands, and β Limits

Because fusion power production scales as $\beta^2 B^4$, there is motivation to operate at the highest value of β allowed by plasma stability. For simple, monotonic q profiles, characteristic of inductive operation, the MHD stability limits $\beta_N = \beta/(I/aB)$ to values $< 4\ l_i \simeq 3.5$ (where l_i is the plasma internal inductance).

However, numerous experiments have shown the appearance of modes, no longer rigorously axisymmetric, which change the topology of the magnetic field in the vicinity of low order rational magnetic surfaces (q = 1.5, 2). These modes lead to magnetic "islands" which grow from a small seed width to a much larger dimension as β_N reaches values considerably lower than 3.5. The observed limit in present experiments is around 2.5 but it may decrease with ρ^* (which decreases with increase in the size of the device) by a factor ~ 3. Nevertheless, the stabilisation of these "neoclassical tearing modes" (NTMs) has been achieved by a localised plasma current addition, driven by electron cyclotron waves on the specific magnetic surfaces, a method that will be employed in ITER.

Moreover, the existence of small-amplitude non-axisymmetric "error" fields produced by residual asymmetries in the magnetic coil positions or in ferromagnetic material distributions, can lead to the development of large magnetic islands, again on low order rational magnetic surfaces, and subsequently to disruptions. These error fields should be eliminated by appropriate currents in the correction coils system producing a controlled small amplitude helical field.

Disruptions are abrupt uncontrolled events, involving a rapid cooling of the plasma. Growing, large amplitude, islands overlap and lead to complete chaotic ergodisation of the magnetic field lines, subsequently a large heat flow occurs along field lines to the boundary walls, cooling the plasma and leading to an influx of impurities. This is followed by a rapid decrease of the plasma current. Simultaneously, electrons can be accelerated to large energies by the electric field associated with the decrease in current in these low temperature plasmas, and lead to significant fast electron "runaway" currents, if the confinement of energetic electrons is not limited by the magnetic fluctuations which may remain from the previous field ergodisation phase. These effects, if repeated often at the same location, can lead to sufficient damage that a refit of the components will become necessary, and they are therefore to be avoided whenever possible.

1.3.6 Divertor and Power Exhaust

The magnetic field configuration in Figure 1.2.1-5 shows closed nested magnetic surfaces with increasing internal volumes from the plasma magnetic axis until a separatrix occurs, outside of which magnetic surfaces are open. The particles travel along largely toroidal field lines which slowly rotate poloidally around these surfaces, but they can diffuse outwards due to collisions. The particles diffusing out of the plasma through the separatrix flow along the field lines until they hit a "target". Thus the plasma contact with the wall is located at a large distance from the plasma along field lines (a few times the torus major circumference).

Along these field lines, the power flow is very high and if it were not for the possibility to induce power losses, the power density on the target (even taking into account its inclined position and the flux expansion due to a smaller poloidal field B_p) would be too large for the capability of heat removal and the surface material temperature. This power should remain below 10 MW/m^2 on average. With no power losses, the temperature gradient along the field lines remains small, the pressure constant, and the plasma temperature at the target very high: this is the so-called "attached" plasma divertor operation.

Alternatively, if the plasma density is large enough at the separatrix, the possibility of radiation losses from impurities, and from ionisation of a large neutral density built in front of the target, provides a new more favourable condition, the so-called "detached" plasma. Towards the divertor target, the pressure along field lines decreases, the plasma density increases significantly and the plasma temperature at the target becomes very low (a few eV): the power crossing the separatrix becomes distributed by radiation (and charge exchange neutrals) onto the much larger surface of the divertor side walls, and the power density to the divertor target can remain inside reasonable limits.

In the latter conditions, the impurities removed from the target by erosion and ionised by the plasma contribute to the radiation losses, and thus to the decrease of the plasma temperature. Because this erosion increases with the particle energy impinging on the target, the process in itself may be self-regulating, as modelled in the case of a carbon target material. Moreover, these impurities are mostly stopped from flowing upwards along the field lines and entering the plasma by the hydrogen flow towards the target. This highlights one of the main functions of the divertor: to protect the main plasma from impurities originating from plasma-wall interactions.

Another important function of the divertor is the control of plasma density, and in particular the removal of the helium reaction product, the density of which should remain as small as possible (a few % of the electron density) in order not to dilute the reacting ions D and T.

These helium particles are born in DT fusion reactions with an energy of 3.5 MeV. They quickly become thermalised in the plasma at some keV, and provide, mostly by interaction with the plasma electrons, the heat source needed (in addition to the auxiliary heating power) to keep the plasma temperature constant by compensating for its power losses. This helium "ash" should therefore not be lost to the boundary at high energy, through the action of specific instabilities or because of a large ion gyration radius and too large a magnetic field ripple (along field lines) due to the discreteness of the TF coils. This last source is minimised in ITER by ferromagnetic inserts, installed in the shadow of each TF coil, while the first one appears not to be detrimental in ITER according to the present understanding (with the expected values of alpha pressure and its gradient).

Due to the small-scale turbulence present in the core (and flat density profile), the helium ions created in the plasma volume are driven to the boundary, and then flow into the divertor, where the high neutral particle density allows an easier pumping at high pressure ($\simeq$ 1 Pa).

Together with He, also the outward flow of D and T is pumped at the edge. The plasma density is the result of this outward flow against the gas fuelling near the separatrix and/or solid (D or T) pellet periodic injection (a few tens of mm^3 at a few Hz). The objective with pellets is to push them as far as possible toward the plasma core, well inside the H-mode barrier. With this type of deep fuelling a density gradient will be present leading to an even more favourable plasma performance.

It is generally observed that the plasma density is experimentally limited on average across the plasma width by the so-called Greenwald density ($n_G = I_p/\pi a^2$ x $10^{20}/m^3$). The fusion power being quadratic with the density, it is important, if possible, to provide a peaked density profile, for a given average.

1.3.7 Plasma Performance

The rules and methodologies for projection of plasma performance to the ITER scale are those established in the ITER Physics Basis, which has been developed from broadly-based experimental and modelling activities within the magnetic fusion programmes of the ITER Parties.

Key limiting factors for inductive operation are normalised beta (β_N), density in relation to the Greenwald density (n_G), and the L-H mode transition power threshold (P_{LH}). A view can be formed of the range of possible plasma parameters at which Q = 10 by analysing, by means of transport codes, with flat density profile across the plasma, possible operational domains in relation to the above limiting factors, for given values of plasma current and confinement enhancement factor as illustrated in Figure 1.3.7-1.

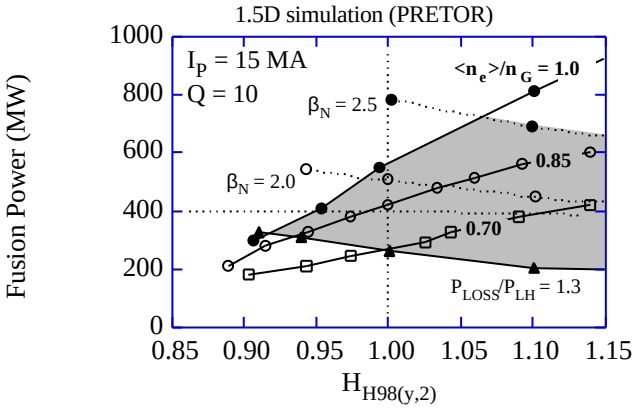

Figure 1.3.7-1 Q = 10 domain (shaded) for I_p = 15 MA (q_{95} = 3.0)

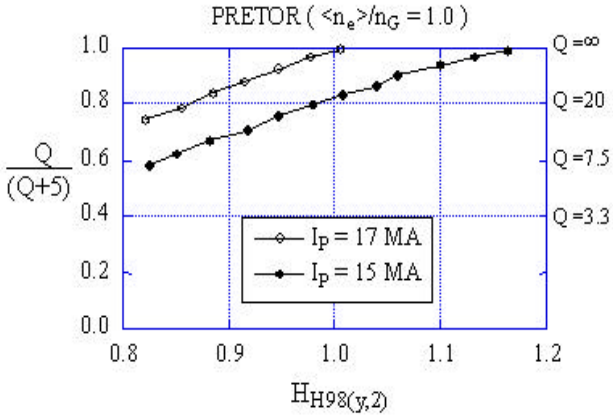

Figure 1.3.7-2 Self-heating Rate versus H_H for I_P=15 and 17 MA

It is evident from Figure 1.3.7-1 , that:

- for operation at a safety factor at the 95% flux surface, q_{95} = 3 the fusion output power from the new ITER design is in the region of 200-600 MW (at $H_{H98(y,2)}$ = 1),

corresponding to a 14MeV neutron flux at the outboard first wall of 0.31-0.92 MWm^{-2}, so that the device retains a significant capability for technology studies, such as tests of tritium breeding blanket modules;

- the margin in H-mode threshold power (at $H_{H98(y,2)} = 1$) is significantly greater than the predicted uncertainty derived from the scaling;
- the device has a capability for Q = 10 operation at $n/n_{GW} \sim 0.7$ and $\beta_N \sim 1.5$ (when $H_{H98(y,2)} = 1$).

The flexibility of the design gives a wide range of operation points not only at Q = 10. For example, different operating points can be obtained by fixing the plasma current and density assumptions and changing the confinement enhancement or the auxiliary power level. These operating points are shown in Figure 1.3.7-2 for I_P=15 and 17MA and for $n=n_G$ and in Figure 1.3.7-3 with $n/n_G = 0.7\text{-}1.0$ and $H_H = 1$. For all these points, power reaching the edge pedestal exceeds by 1.3 times the L-H transition power. A large fusion gain (Q>20) can be obtained at 15MA with H_H=1. The same conditions would imply ignition (Q=∞) at I_P = 17MA while ignition at I_P = 15MA would be also possible at $H_{H98(y,2)} \sim 1.15$.

The inductive burn pulse length at 15MA and Q=10 is 400s-500s being limited by the available magnetic flux. For this reason the burn time can be increased as the plasma current is reduced and the non-inductive drive power is increased. Figure 1.3.7-4 shows how the burn time and Q change versus plasma current. A pulse length of more than 1000s, for blanket testing, may be easily achieved with Q=5.

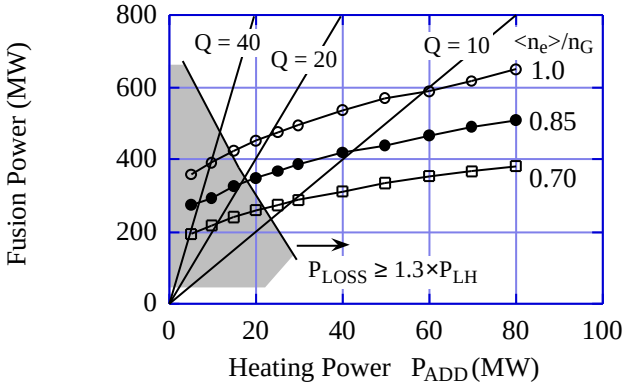

Figure 1.3.7-3
Fusion Gain Q at various Additional Heating Powers and Plasma Densities
I_P = 15 MA, $H_{H98(y,2)} = 1.0$, $\tau_{He}^*/\tau_E = 5$

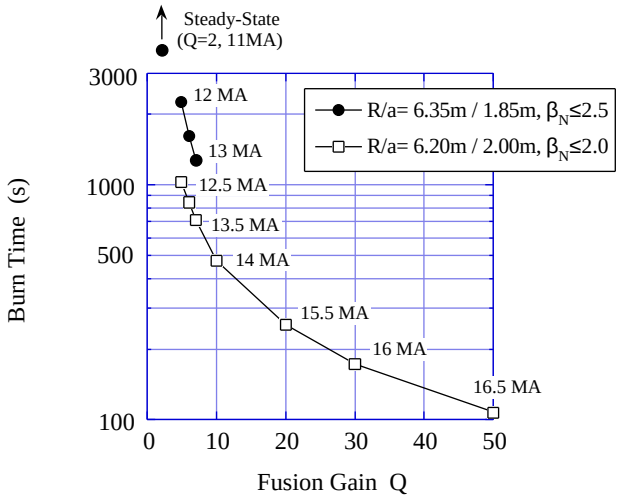

Figure 1.3.7-4
Pulse Length versus Fusion Gain Q
Each plasma current given in the figure is the minimum value for the corresponding Q value with H_H=1.0 $n_e/n_G = 0.85$, $\beta_N \leq 2.0$ or 2.5, $P_{loss}/P_{LH} \geq 1.3$ and $\tau^*_{He}/\tau_E = 5$. The fusion power is in the range 400- 700 MW.

1.4 Functional Role of Systems

The preceding tokamak physics issues are linked with the hardware systems necessary to be installed in ITER, and with their functional requirements and implementation. Figure 1.4.1-1 shows a functional diagram with the basic plant system configuration introducing all systems.

1.4.1 Magnets

The plasma is confined and shaped by a combination of magnetic fields from three main origins: toroidal field coils, poloidal field coils and plasma currents. The nested magnetic surfaces are able to confine a plasma pressure equivalent to a few atmospheres, with a density 10^6 times smaller than in the atmosphere ($n = 10^{20}/m^3$, $T \approx 10$ keV). Aiming in ITER at steady-state operation, all the coils are superconducting: copper coils would require too large an electric power to be acceptable for ITER as well as for a future reactor.

1.4.1.1 Toroidal Field Coils

The toroidal magnetic field value on the plasma axis is 5.3T, which leads to a maximum field on the conductor ≤ 12 T. Because of this high field value, Nb_3Sn is used as superconducting material, cooled at 4.5K by a flow of supercritical helium at ~ 0.6 MPa. The total magnetic energy in the toroidal field is around 40 GJ, the confinement of which leads to significant forces on each coil restrained by a thick steel case to resist circumferential tension (≈ 100 MN) and by constructing a vault with the inboard legs of all 18 coils (the large centripetal forces are due to the 1/R variation of the toroidal field). The compressive stress levels inside this vault are large, and therefore the side surfaces of each coil should match one another as perfectly as possible.

The coils are connected together (Figure 1.4.1-2) by bolted structures, and by two compression rings made of unidirectional glass fibres, that provide an initial inward radial force on each coil (2 x 30 MN).

This very robust assembly is provided mainly to resist the toroidal forces induced by interaction of the TF coil current with the transverse poloidal field from plasma and poloidal field coils. These forces produce a distribution of torque around the TF coil proportional to the magnetic flux crossing unit length (the net torque is thus 0). These local forces are pulsed, and therefore mechanical fatigue is a concern for the highly stressed structural steel of the coils. These forces, due to the highly shaped plasma, are largest across the inboard coil legs (in particular at their lower curved region) where they are resisted by the friction between coil sides (under high compression) and by specific keys.

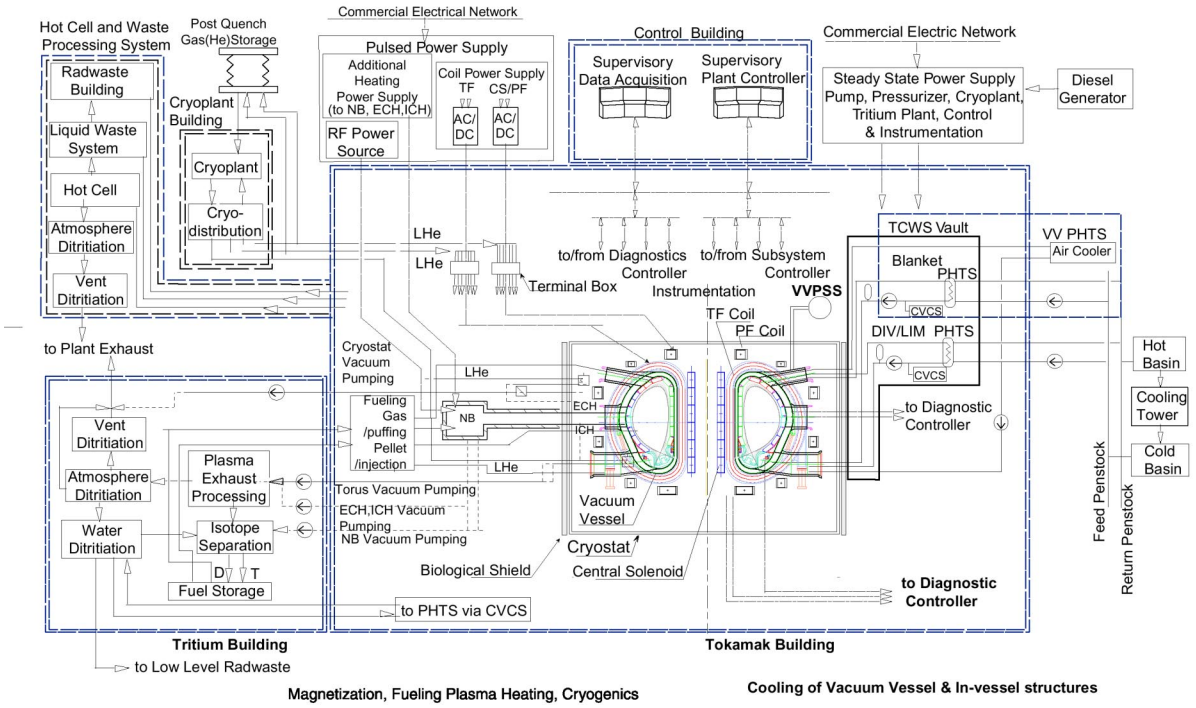

Figure 1.4.1-1 Basic Plant System Configuration

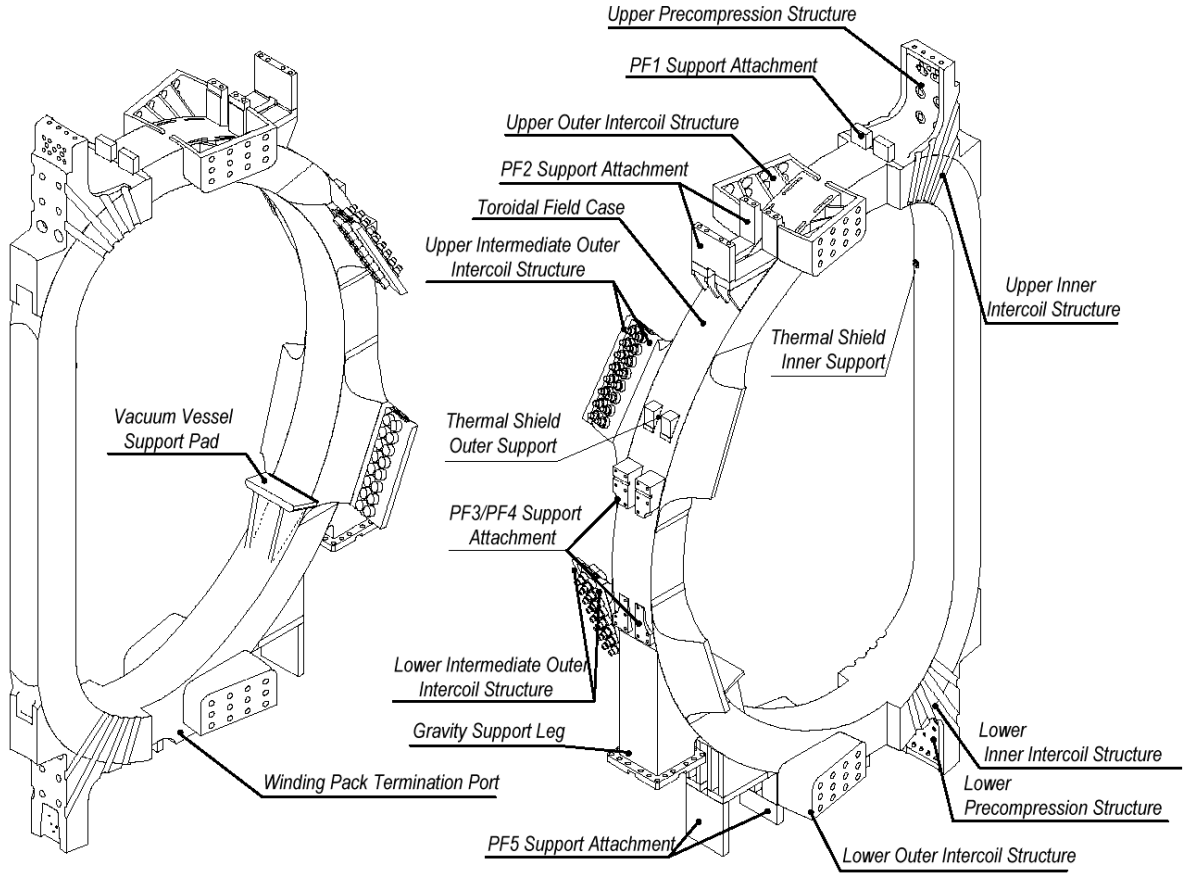

Figure 1.4.1-2 TF Coil Structure

1.4.1.2 Poloidal Field Coils

The plasma shape is controlled by the currents distributed inside the six modules of the central solenoid (CS) and the six large PF coils placed outside the TF coils. All these axis-symmetric coils use superconductors cooled by a flow of supercritical helium at 4.5K and 0.6 MPa. Nb_3Sn is used in the CS modules whereas NbTi can be used in the PF coils since the maximum field value is lower than 6 T. Redundant turns are built into the trapped coils to allow for failures.

The magnetic configuration provided by these currents is such that the plasma toroidal current will experience a vertical force as soon as its centre is displaced vertically, and this force will increase with the displacement: the plasma with its elongated shape is in a vertically unstable equilibrium.

Stabilisation of the plasma vertical position can be achieved in the following way. First, any plasma movement, associated with small changes of its energy content, induces eddy currents in any axisymmetric conducting surface surrounding the plasma, i.e. the double walled vacuum vessel, which passively reacts to slow down the plasma motion. These conducting surfaces are shaped in order that the current distribution can provide a neutral equilibrium position, near the plasma centre of gravity, for most of the expected plasma energy changes, so as to minimise the sources of instabilities.

Second, using an active feedback position control system, the currents in the largest 4 PF coils will be changed through a special power supply feeding them in an anti-symmetric way, across the plasma equatorial plane. These changes provide an additional radial magnetic field leading to the required vertical restoring force on the plasma towards its controlled position.

Moreover, the plasma shape can be similarly feedback-controlled, by an appropriate action on each coil voltage by its own distinct power supply. The “gaps” (Figure 1.2.1-5) between the plasma boundary and the walls are measured at six critical positions, and brought back to a prescribed value after an excursion due to a plasma internal disturbance (e.g. loss of or change in current distribution/internal inductance or loss of plasma thermal energy).

In the inductive scenario, the plasma current is generated by the change in magnetic flux linked with the plasma torus (this is 277 Vs in the nominal 15 MA inductive scenario). This flux swing is largely realised by the CS coil, which will see a complete inversion of field from +13.5 T to - 12 T in the central modules. The external PF coils contribute to make sure that as little poloidal field as possible is present in the plasma region during initiation. Providing a few MW of plasma heating through electromagnetic waves will minimize the flux consumption during plasma initiation and current increase. This method will help securing a robust start-up as well as a sufficient flux variation available (37 Vs) to sustain the current flat top during at least 400 s at a plasma current of 15 MA.

Additionally, after the plasma current is set up inductively, a non-inductive scenario may follow. In this type of scenario the plasma current flat top is extended towards steady state by driving the current non-inductively by means of a set of high energy (l MeV) beams of neutral D tangentially injected at a small angle to field lines. Current drive may also be achieved by toroidally propagating electromagnetic waves (at ion and electron cyclotron frequencies, or at the lower hybrid frequency), in addition to the “bootstrap” current linked to

the plasma radial pressure gradients. The preceding sources of different radial current distributions deposit large amounts of power at specific locations in the plasma, and this has to be done in a way compatible with the necessary plasma pressure profiles and their allowable rates of change. A complete scenario for steady state operation in ITER with Q=5 is yet to be consistently developed. Nevertheless, the non-inductive current drive systems provided in ITER should be able to accommodate the steady state operational requirements (for over 2000 s).

1.4.1.3 Error Field Correction Coils

As mentioned previously, the need to correct imperfections in the magnetic field symmetry, due to the imperfect positioning of the TF, CS and PF coil currents, requires the use of "correction coils", able to provide a helical field of a few 10^{-5} times the TF value. The Fourier components of toroidal and poloidal modes are n = 1 in the toroidal direction, and a distribution between m = 1, 2 and 3 in the poloidal direction. These coils (Figure 1.4.1-3) are composed of 3 sets of six saddle coils, around the torus located between PF and TF coils. The same coils can be used to stabilise possible resistive-wall modes, which happen to have the same geometry as the error fields to be corrected, but a much faster time variation. These coils counteract the MHD instabilities that are not stabilised by the conductive walls, on the longer time scale associated with the wall resistance.

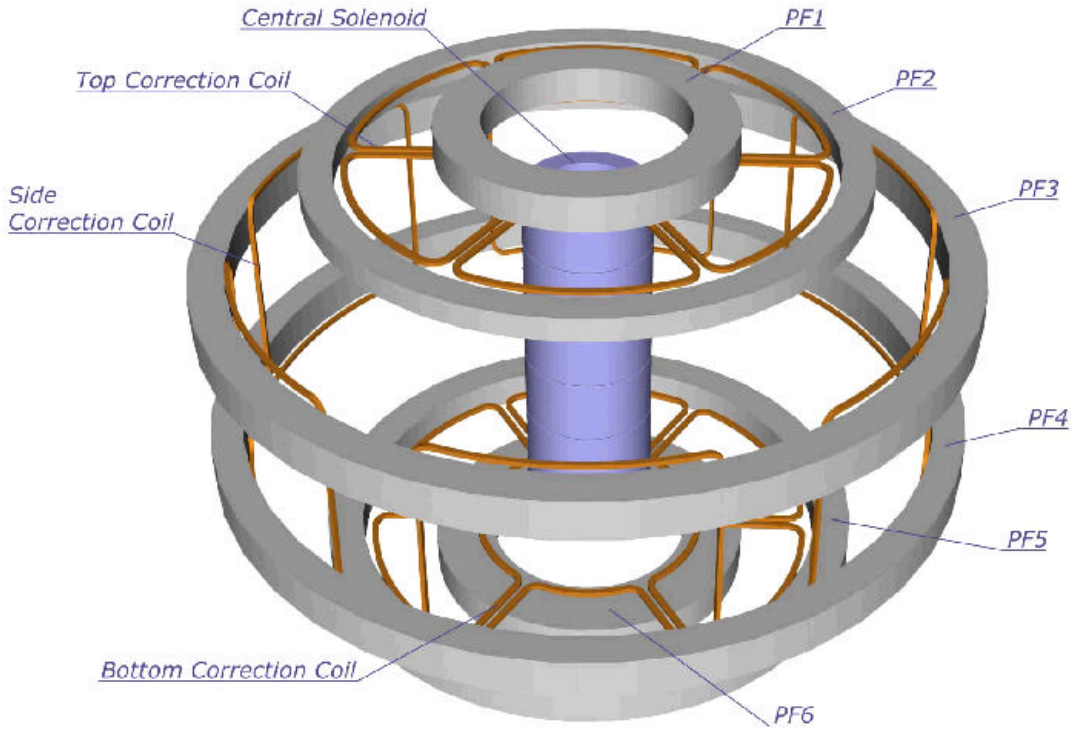

Figure 1.4.1-3 ITER Poloidal Field Coils and Error Field Correction Coils

1.4.1.4 Superconducting Coil Protection

The superconductor of all coils is protected against local overheating, should the coil current continue to flow after a local transition from superconducting to normal conducting state due to an off-normal local energy dump. In this case, after identification of a resistive voltage across the coil terminals increasing with time, an external resistor is switched in, dumping

rapidly a large part of the coil magnetic energy. The time constant of this fast emergency discharge is small enough to minimise the energy dissipated into the coil and to limit its local temperature increase. However there is a minimum value for this time constant due to the maximum voltage through the coil terminals and the induced current (and related forces) in conducting material magnetically coupled with the coil. One example of this limit comes from the forces applied to the vacuum vessel due to the large poloidal current induced in the vessel shells by the fast discharge of all TF coils. A compromise value of 11s has therefore been chosen for the time constant.

In addition, all these coils must be protected against the heat coming from their surroundings. Therefore, a large cryostat vessel places all the coils in a vacuum good enough to limit convective heat transfers. Additionally a thermal shield (VVTS), cooled at about 80K by a flow of helium, is provided between the coils and hot parts to shield against radiative heat transfer. The geometry of this thermal shield is evidently rather complex, but the avoidance of radiation hot spots is necessary to limit the already significant amount of power to be removed from the coils at 4.5K. This permanent heat load (~15 kW) due to nuclear radiation, and conduction through supports, adds to the non-ideal efficiency of the circulation pumps feeding the supercritical helium in each coil.

1.4.1.5 Superconducting Coil Cryogenic Cooling

On top of the steady state cryogenic heat load there is a significant pulsed heat load on the coils from two separate sources: the neutron flux produced by the fusion reaction and attenuated by the blanket and vessel shields, and eddy currents induced by any field change in the coil superconductor and steel cases during the operational scenario of the plasma pulse (or even more during a plasma disruption). Being the cryogenic plant essentially a steady state system, between the coils and the cryogenic plant, an energy storage is present to cushion the pulsed loads.

In effect, this energy storage is mainly provided by the large steel mass of the TF coil cases, and by the temperature variation of the liquid helium bath that cools the supercritical helium flow through heat exchangers. The extra energy dumped into the coils at 4.5K during a nominal pulse amounts to 19 MJ, and a plasma disruption can add a further 14 MJ. Due to the assumed duty cycle, the time average load on the cryogenic plant (all users) amounts to about 55 kW.

1.4.2 Vessel and In-vessel Systems

1.4.2.1 Neutron Shielding

The 14 MeV neutrons, i.e. 80% of the fusion energy produced, transfer energy to the water coolant, and subsequently to the environment, by colliding with the materials present around the plasma (mostly steel and water) in the blanket modules and in the vacuum vessel. The small neutron energy, not absorbed in these two shields, is released in the cold TF coil structure, and should be absolutely minimised. Typical maximum nuclear heating in the design is ~ 15 kW.

In addition to inelastic collisions, the neutrons will be absorbed by some nuclei, which will become activated and later radiate energetic γ rays according to their specific properties. Neutrons, not absorbed in the radial thickness of the blanket, VV and magnets, or leaking

through gaps, will be absorbed outside and induce activation in the cryostat, a process which should be limited as far as possible so as to allow human access, in case of any need for repair. As a result, the shielding thickness (and attenuation efficiency by optimising the volume ratio between steel and water) has been carefully chosen, and its variation along the poloidal length optimised, to match the above two goals while minimizing the shielding envelope requirement.

The radial thickness distribution between blanket and vessel mainly derives from the requirement of reweldability of the vessel inner shell until the ITER end of life. This involves a low enough (around 1 appm) helium content (due to n, α reactions) in the vessel steel material. Accordingly, the blanket thickness is set at 45 cm, and gaps maintained as small as practicable.

1.4.2.2 Blanket Modules

The shielding blanket is divided into two parts: a front part that may be separated from a back one (Figure 1.4.2-1). The back part with a radial thickness of around 30 cm is a pure shield made of steel and water. The front part, the "first wall", includes diverse materials: l cm thick beryllium armour protection, l cm thick copper to diffuse the heat load as much as possible, and around 10 cm of steel structure. This component will become the most activated and tritium-contaminated in the entire ITER device. It could be in contact with the plasma in off-normal conditions, and thus can suffer damage from the large heat locally deposited, and may have to be repaired or possibly changed.

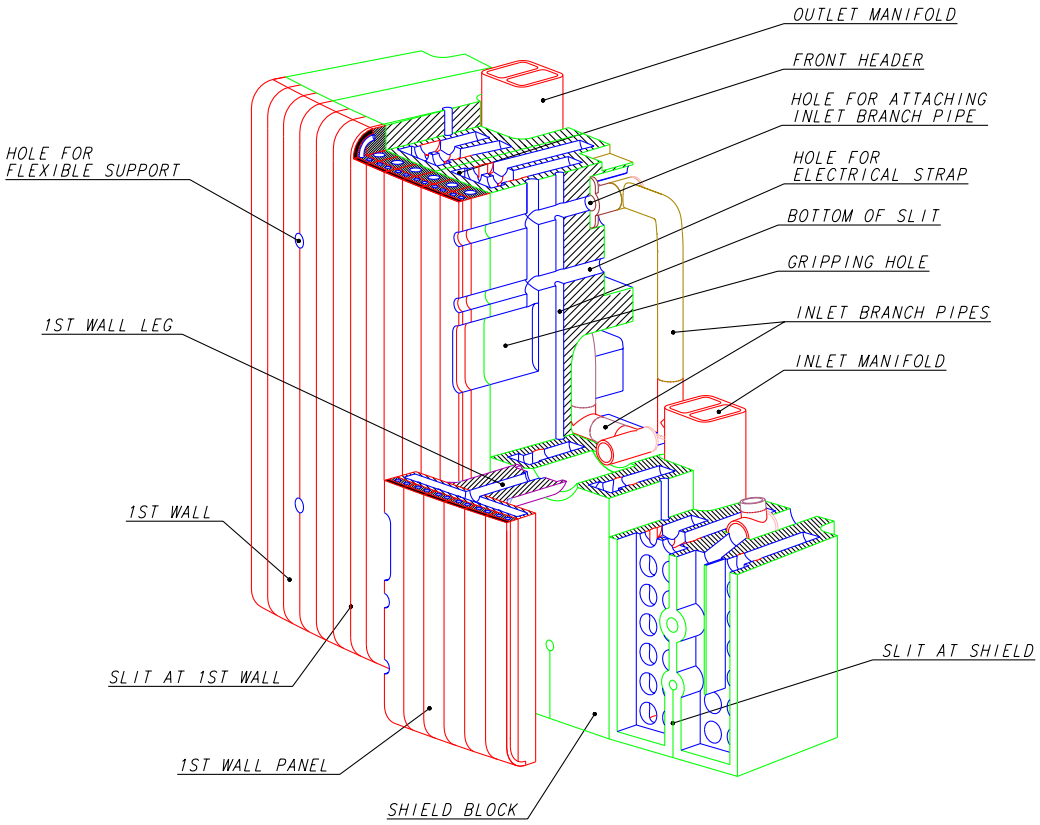

Figure 1.4.2-1 Blanket Module

In order to allow a practical method of maintenance, the blanket wall is modular (~ 420 in total) with a maximum weight of 4.5 t (and about 1.5 m^2 facing the plasma) and moreover the front part of each module is divided in 4-6 first wall panels. Each module is attached to the vessel by 4 flexible links, radially stiff but pliant against toroidal or poloidal motions. This flexibility is required because, across the blanket thickness, the absorbed power density decreases sharply and, whilst the water cooling redistributes the heat progressively toward a uniform temperature, at the end of the pulse the front part becomes necessarily the colder part. Thus the blanket module suffers an alternating thermal expansion together with a "bowing" effect during each plasma pulse. The toroidal and poloidal external forces (i.e. during a disruption) acting on the module are therefore reacted by additional mechanical keys provided with sufficiently large compliance clearances.

1.4.2.3 Blanket maintenance

The maintenance and repair of a blanket module is performed by first removing it from the vessel. For this purpose, a vehicle, equipped with an end gripper, is positioned along a toroidal rail deployed along the vessel torus centreline. The end gripper is engineered to cut the connection to the water pipe feeders and to unbolt the module, and to bring it to an equatorial maintenance door. At this location it will be transferred into a cask, and subsequently to the hot cell for repair or replacement. The cask operates by docking and undocking to the ports of the vessel and of the hot cell, avoiding contamination to the environment. Similar casks are used for removal of any equipment installed in any equatorial or upper port of the vessel, i.e. heating launcher, diagnostics, or tritium breeding test blanket.

1.4.2.4 Divertor

The divertor shares with the blanket a similar modular philosophy and maintenance procedure. The cassettes (54 in total) are removed from the vessel at three lower access ports, to which they are beforehand conveyed by a toroidal mover mounted on annular rails attached to the vessel floor. These rails also act as the mounting point of the cassettes during operation.

Besides providing shielding of the vessel, the modular cassettes (Figure 1.4.2-2) support the divertor target plates, a set of particularly high heat flux components, built with high conductivity armour of carbon fibre composite (CFC) and tungsten.

These materials can be eroded by the plasma particles, mostly during short pulses of high heat loads, associated with ELMs or plasma disruptions. This erosion process not only will call for replacement from time to time of the worn out divertor targets, but also may create dust, and in particular tritiated carbon dust. Studies are going on to define the best way for removal of this dust, mostly to limit the tritium inventory inside the vessel, and to limit the possibility of metallic dust (Be, W) reaction with hot water during an accidental in-vessel water leak, which could lead to hydrogen formation.

1.4.2.5 In-vessel Component Water Cooling

Each divertor cassette is separately cooled by water, with feeder pipes connecting to the manifold outside the vessel and cryostat. Groups of two or three blanket modules are similarly fed by separate pipes installed on the plasma side of the inner shell of the vacuum vessel. This arrangement leads to handling a large number of small size pipes, but (e.g. by

"spiking" specific coolant channels with tracer elements) allows the identification of possible modules or cassettes leaking water, from tests outside the cryostat, a crucial procedure to be able to rapidly localise the leaks in vacuum.

The pressurised coolant water input is continuously maintained around 100°C whereas the output coolant temperature during a pulse at nominal fusion power will be around 150°C. At the end of a pulse, control valves allow the large heat exchanger to the heat rejection system to be short circuited so as not to cool these in-vessel components below 100°C. During standby, the coolant flow is reduced, using a different pump, to 10% of the flow during the pulse, and the flow in the heat rejection system reduced to 25% of its normal value. Subsequent to maintenance periods, the pressurisation will be increased, and the water coolant used to heat and to bake the in-vessel components to 240°C.

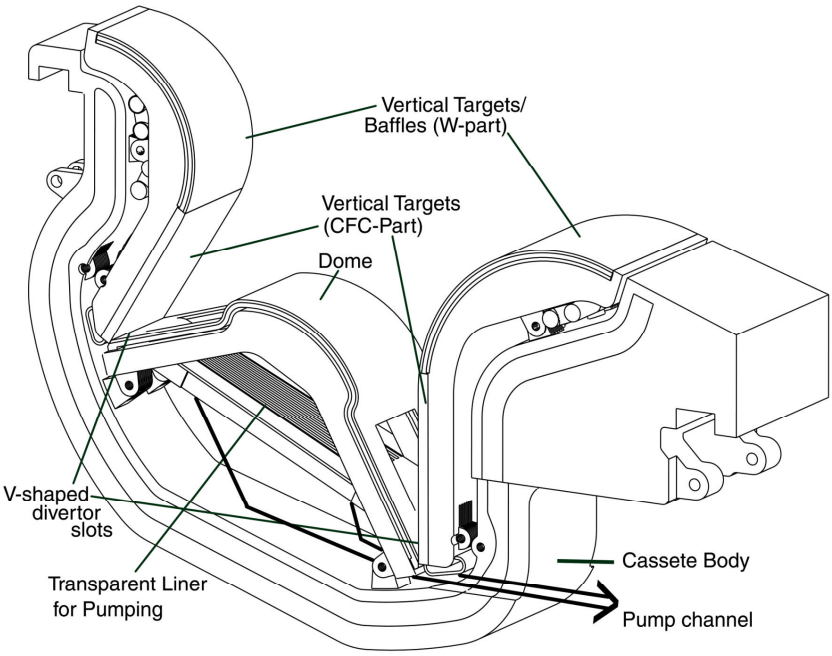

Figure 1.4.2-2
Divertor Cassette

1.4.2.6 Cryogenic Pumps

Well recessed and shielded from neutrons but inside the divertor port are the torus cryogenic pumps operating at 4.5K. These have the capacity to pump hydrogenic atoms as well as helium by adsorption and condensation. The pumping performance can be varied and the condensed gases can be removed by heating the pumping panels to 80K and pumping away the gas released using a roughing pump after a shutter towards the vacuum chamber has been closed. For long plasma pulses, this procedure may be carried out on-line sequentially through all the installed cryogenic pumps in order to limit the amount of hydrogen in each pump below its deflagration level in case of an accidental ingress of oxygen. This limiting amount of hydrogen corresponds to pumping 200 Pam^3s^{-1} of DT for 450 s, with six pumps.

1.4.2.7 Vacuum Vessel

The vacuum vessel is a component with multiple functions, namely it:

- provides a boundary consistent with the generation and maintenance of a high quality vacuum, necessary for limiting impurity influx into the plasma;

- supports the in-vessel components and their resultant mechanical loads;
- participates in shielding against neutrons, and in removing the corresponding power during a pulse, and moreover in removing the decay heat of all in-vessel components in case of there being no other coolant available;
- provides a continuous conductive shell for plasma MHD stabilisation with a toroidal one turn resistance of ~8μΩ;
- provides all access to the plasma through ports, for diagnostics, heating systems, pumping, water piping, etc.;
- provides the first confinement barrier for tritium and activated dust with a very high reliability.

All these functions are central to the operation of ITER and thus require a very robust mechanical design analysed for stresses in all possible normal and off-normal conditions. The vessel is built with two shells linked by ribs and fitted with nuclear radiation shielding material, and ferromagnetic inserts in the shadow of the TF coils to reduce the TF ripple value.

To ensure reliable water cooling, two independent loops are used. These can remove by natural convection the decay heat from all in-vessel components (if they are not cooled directly). The vessel water temperature is maintained at 100°C (at 200°C during baking of the in-vessel components), limiting to ~50°C its difference with the in-vessel component cooling temperature.

1.4.2.8 Vacuum Vessel Pressure Suppression System

In the case of a water pipe rupture inside the vessel, the subsequent chamber pressure will be limited below 0.2 MPa by the opening of rupture disks and communication with a large container located above the tokamak vacuum vessel and half-filled with water, in which the steam will be condensed (the vacuum vessel pressure suppression system - VVPSS). Simultaneously, liquid water condensed in of flowing into the vessel will be driven into drain tanks located at the bottom of the tokamak building.

1.4.3 Mechanical Loads and Machine Supports/Attachments

Part of the technical challenge of the ITER design is due to the large mechanical loads that are applied to the various components.

The mechanical loads acting on ITER fall into four categories:

- inertial loads due to gravitational and seismic accelerations,
- kinetic loads due to coolant and atmospheric pressures,
- thermal loads,
- electromagnetic loads, usually a strong design driver, either static (as in TF coils) or dynamic, acting on the magnet and on all conducting structures nearby due to fast or slow transient phenomena such as plasma disruptions and Vertical Displacement Events (VDEs).

The chosen ITER support hierarchy is schematically drawn in Figure 1.4.3-1 where all core components of the machine are attached to the TF coil cases. Generally speaking, the support scheme of tokamak components must be designed to minimise the reaction of each support to

loads on the component. In interconnecting components, a proper load path must be chosen to maximise the stiffness associated with the load path itself.

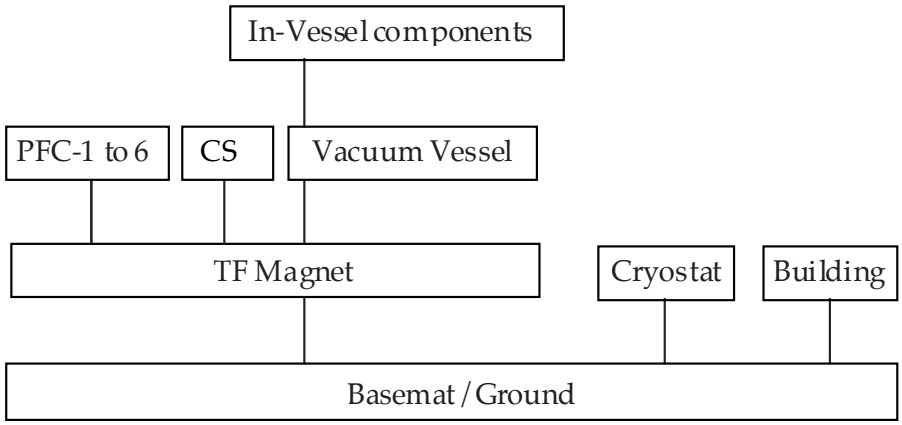

Figure 1.4.3-1 Schematic of Supports Hierarchy

In addition the support methods for the magnet and the vacuum vessel must allow for their changes in temperature from the time of assembly to operation, i.e. the radial shrinkage of the magnet and radial growth of the vessel, and provide adequate resistance to seismic and disruption forces. As a consequence all supports of the machine core are flexible in the radial direction and stiff in all others.

1.4.3.1 Seismic Loads

Earthquakes simultaneously produce vertical and horizontal random ground motions that are typically statistically independent, the horizontal ones having the most important impact on the design. Even if the ground peak horizontal acceleration is a fraction of gravity, a seismic event is, in many cases, one of the most demanding loading conditions, in particular for the interface structures (e.g. supports). Under horizontal excitations with a relatively broadband spectral content in the range 1-10 Hz, resonances occur in component motions. The tokamak global structure exhibits then oscillatory modes that involve horizontal shearing as well as rocking motions

As an additional design constraint, the relative distance between components must be maintained limited in particular in the inboard radial build region where the indirect design "cost" of clearances is large (between vessel, TF coils, thermal shield etc…). Normalised seismic conditions of 0.2 g ground acceleration (at high frequency, 33 Hz) have been applied to ITER for the design of all components and their support leading to a configuration with some margin. In case of the selection of a site with significantly larger seismic loads, the use of horizontal seismic isolators below the building basemat has been shown to be effective at lowering the peak acceleration to acceptable values.

1.4.3.2 Electromagnetic loads

Beyond the TF coil loads, either static in-plane from the toroidal field itself, or out-of-plane cyclic due to their interaction with the poloidal field, as well as the consequence of a emergency TF energy fast discharge on the VV stress level, other important electromagnetic loads are associated with transient phenomena that are consequences of changes in plasma current, internal energy or position. They act on the PF coils and all conductive structures close to the plasma (blanket modules, divertor cassettes, vacuum vessel).

For slow transients (time scales longer than those which induce significant currents in these structures), there is no net force on the PF/CS magnet assembly as a whole. In each PF and CS coil, vertical forces are reacted through the TF coil structure (the shortest path) and radial ones by the development of a toroidal hoop stress inside each coil.

In the case of fast transients, such as plasma disruption or loss of vertical position control (VDE), large currents are induced in conducting structures, and their interaction with the toroidal or poloidal magnetic field develops significant forces and stresses.

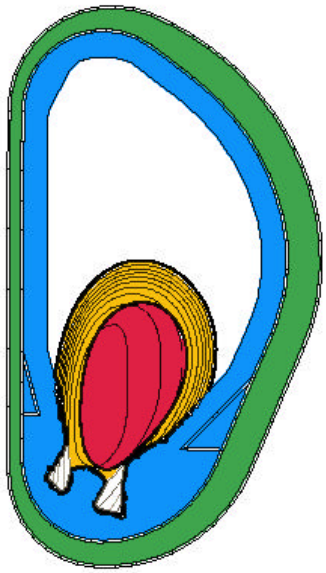

Figure 1.4.3-2 Plasma Current Density during a Downward VDE

In the case of a disruption, the load severity is larger the shorter is the current quench duration (lowest plasma temperature after the thermal quench). In the case of a VDE, load severity will depend on how large is the plasma displacement across the destabilising poloidal field, without a decrease of the plasma current. Again, in all these cases the forces developed between the coils and the vessel are restrained through the stiffest path through the TF coil structure, taking advantage of the direct link between these components.

Detailed numerical studies, under conservative assumptions, of all these important events, have led to the following conclusions:

- the plasma control system will be capable of maintaining the plasma vertical position for all nominal plasma disturbances including minor disruptions: as a result, VDEs should occur only during a major disruption or a failure of the control system;
- during a major disruption, the plasma will move inward and upward as a consequence of the direct inductive coupling between plasma and passive structure, but vertical forces will be much smaller than for a full downward VDE (Figure 1.4.3-2), where loads up to 80 MN may develop and which could occur only in the absence of control; to react to this latter event a “killer pellet” may be used to trigger the plasma quench early during its downward motion, and thus limit the arising vertical loads.

For a conservative design, in ITER these types of events have been often combined with, for example, earthquakes and/or TF coil fast discharge.

1.4.4 Fuel Cycle

The tritium used in ITER will be supplied by external sources. During plasma operation, in order to generate 500 MW of total fusion power, about 0.1 g of tritium will be burnt every

100 s. However, considering the divertor/plasma-purity operational conditions that call for maximum pumping speed and un-burnt fuel recalculation, more than 25 g of tritium will be injected into and pumped from the vessel during the same 100 s.

The need is obvious to process the pumped gases on line, to remove impurities and separate the tritium, and to store it for recycling. A schematic of this fuel cycle is shown in Figure 1.4.4-1. It includes first a permeator to separate impurities from hydrogen in line with the pumping exhaust. After that, the impurity flow is processed before final exhaust, with an ALARA (as low as reasonably achievable) content of tritium. The hydrogen flow is processed to separate the different isotopic masses, by isotope separation through cryogenic distillation. This part of the plant is optimised to minimise the tritium inventory as far as possible, compatible with the isotope separation ratio required (not very high) and the global throughput. For nominal pulses (< 450 s), the fuel cycle does not operate as a steady state, online system. The outlet stream of hydrogen isotopes from the permeator feeds a buffer storage tank, before being processed on a longer timescale by the isotope separation system. For longer pulses, on the contrary, steady state operation could be reached using a direct feed from the permeator output stream.

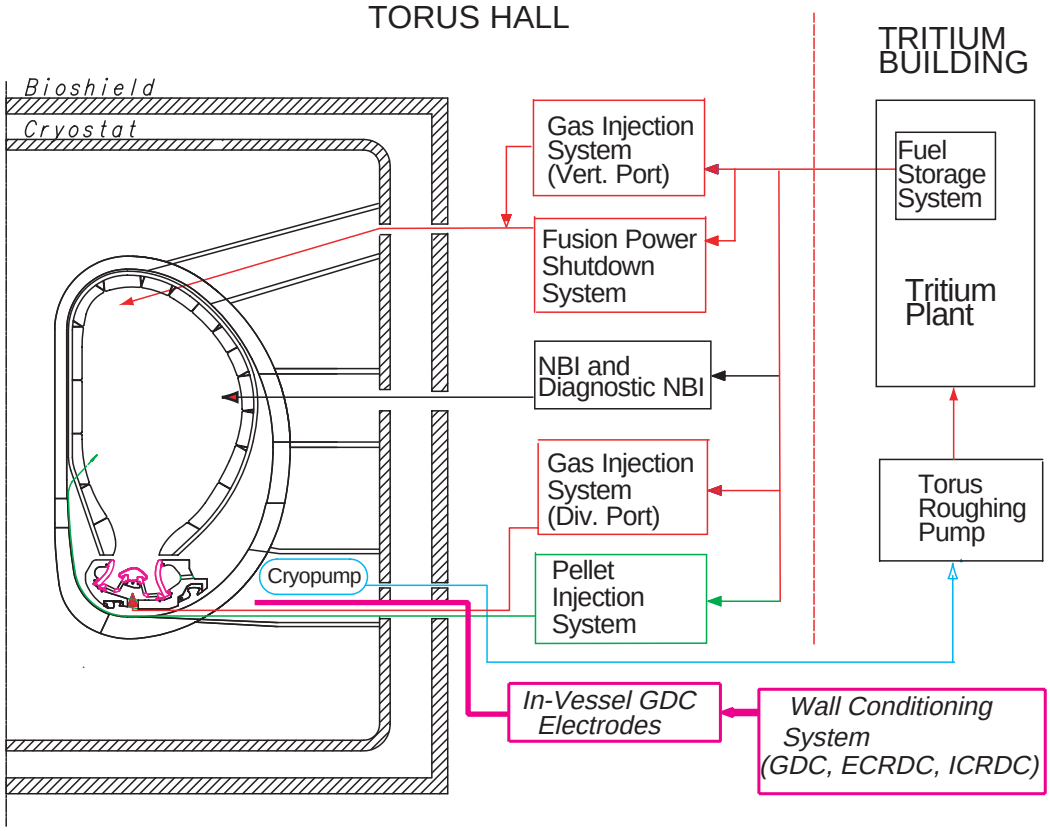

Figure 1.4.4-1 Block Diagram of Fuel Cycle

Segregation of tritium-containing equipment in separated structures, with limitation of the local inventory and robust confinement barriers, is appropriate for safety reasons. The storage of D_2, DT and T_2 is achieved in many parallel canisters, and adsorbed on ZrCo beds, which can deliver rapidly the required flow for plasma fuelling. Their tritium content is measured by calorimetry with around 1% accuracy.

Tritium accountability in the entire fuel cycle is an important issue in particular because a part of the tritium injected in the plasma may remain in the vessel trapped by co-deposition with carbon dust, and it is important to know how much since, if it can be mobilised, there may be a limit placed on operation.

In addition, a small amount of tritium, adsorbed on all in-vessel surfaces, will be progressively desorbed, and recovered, partially in oxidised form, from detritiation systems installed to limit the tritium content in the in-vessel atmosphere during maintenance, or in the hot cell atmosphere during component repair. The resulting tritiated water will be processed to re-inject the tritium into the fuel cycle.

1.4.5 Tokamak Building

The buildings should provide the volumes and controlled atmosphere required for ITER assembly and operation. In addition, the tokamak building is important for its contribution to safety, by the following means.

- A biological shield of borated concrete is provided around the cryostat to limit the radiation levels outside the pit to values insignificant for the activation of components, even if human presence will not be allowed during plasma pulses.

- Part of the building are essential as a further confinement barrier (even containment in this case), forming two concrete leak tight vaults around the neutral beam injectors and the water cooling system, or even as a third confinement barrier in the case of the tritium building (the metallic equipment inside glove boxes provide the first and second barriers in this case).

- A differential pressure (Figure 1.4.5-1) is maintained in the different zones around the tokamak, according to the risk of being contaminated by an accidental release of tritium or activated material during operation or maintenance. In this way, the atmosphere will move only from lower to higher contamination levels. These differential pressures are maintained by the air conditioning system. The design arrangement of a separate cell around each vessel port access allows the atmosphere of each cell to be maintained through a venting system capable of detritiation and filtering. This is especially justified during the maintenance procedure when removing components from the vessel occurs.

- The concrete walls provide appropriate shielding against emission from activated components, during their automatic transport via cask from one vessel port to the hot cell (and back) through the galleries.

The very robust structure of the tokamak and tritium buildings is based on the existence of a common stiff basemat designed to react seismic conditions. Should the actual site have much more severe conditions than the generic site used in the design, the common basemat will be put on isolators and the acceleration amplification suffered by the components above will be maintained below the accepted design level.

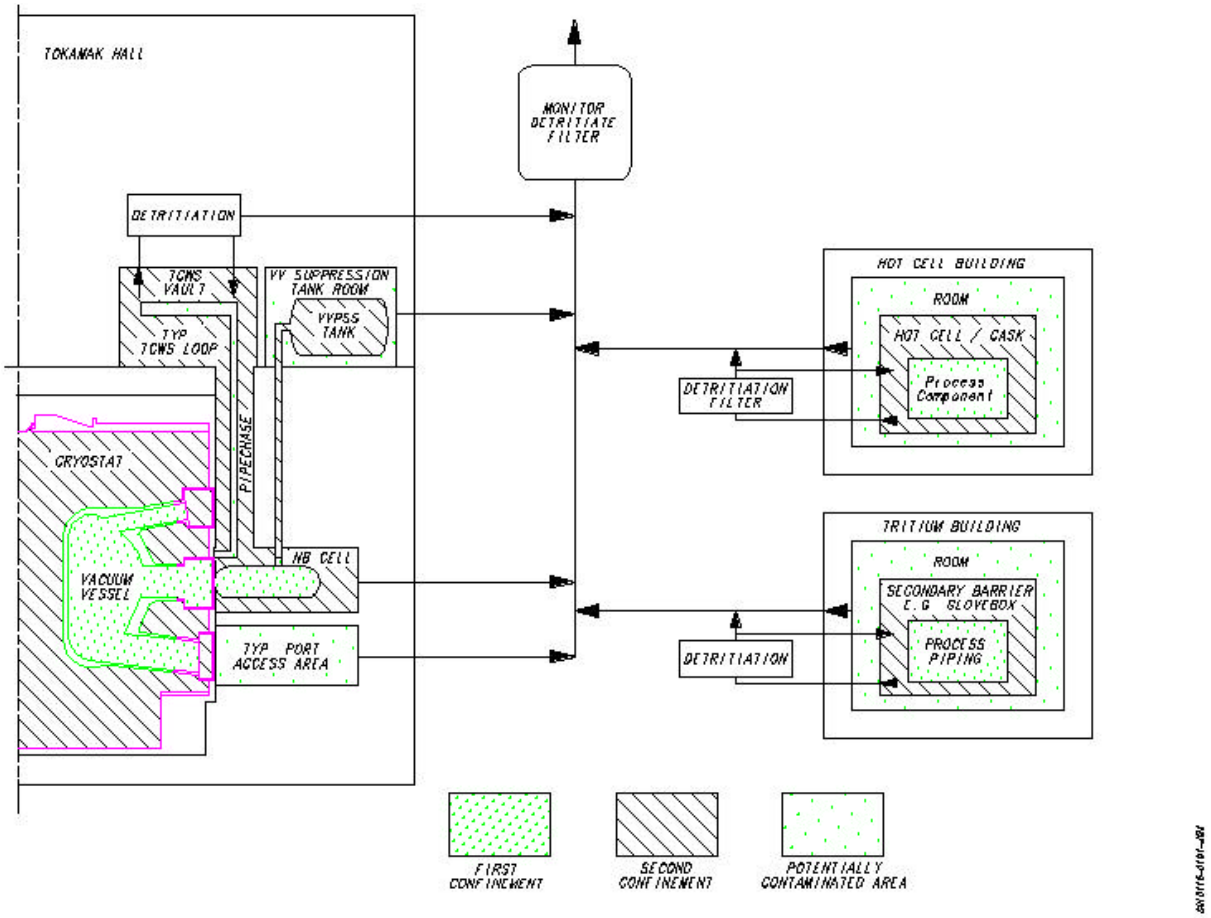

Figure 1.4.5-1 Schematic of Confinement Approach illustrating Successive Confinement Barriers that are Available

1.4.6 ITER Plant Operation and Control

Compared to today's experiments, the need for ITER to operate with a burning plasma under stationary conditions for more than 400 s, while handling about 0.5 GJ of plasma thermal and magnetic energy, poses quite challenging and new constraints in the design of hardware that controls plasma operation. The typical waveforms of a standard driven burn plasma pulse are shown in Figure 1.4.6-1.

One of the most important objectives of plasma operation and control in ITER is the protection of tokamak systems against the normal and off-normal operating conditions. Reliable control of the fusion burn conditions and provision for its rapid termination under off-normal conditions are thus crucial.

To support plasma operation, all plant systems must be efficiently and reliably controlled. In particular, the fuel cycle needs special attention in order to manage and control the tritium inventory within the system. In the water-cooling system, the control of activated corrosion products and tritium content is very important.

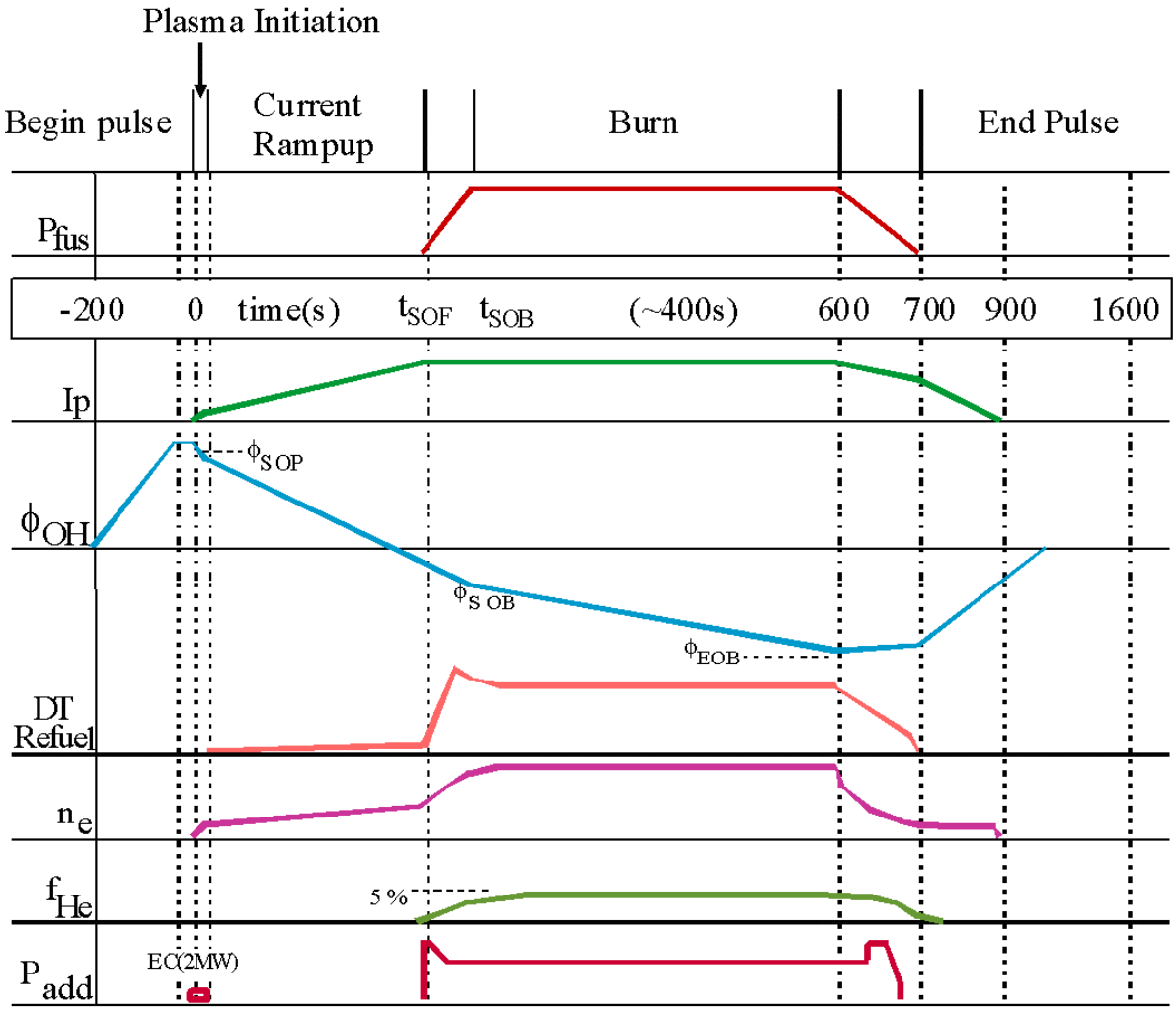

Figure 1.4.6-1 Waveforms for Standard Driven-burn Operation Scenario

The ITER plasma control system comprises four major elements: control of scenario sequencing, plasma magnetic control, kinetic and divertor control, and fast plasma termination by impurity injection.

Control of plasma parameters can be characterised by three basic attributes of closed loop control systems – diagnostics, control algorithms and actuators. The control algorithm is typically a proportional/ integral/derivative (PIDS) feedback scheme. There are, however, alternate algorithms designed with more sophisticated optimisation procedures.

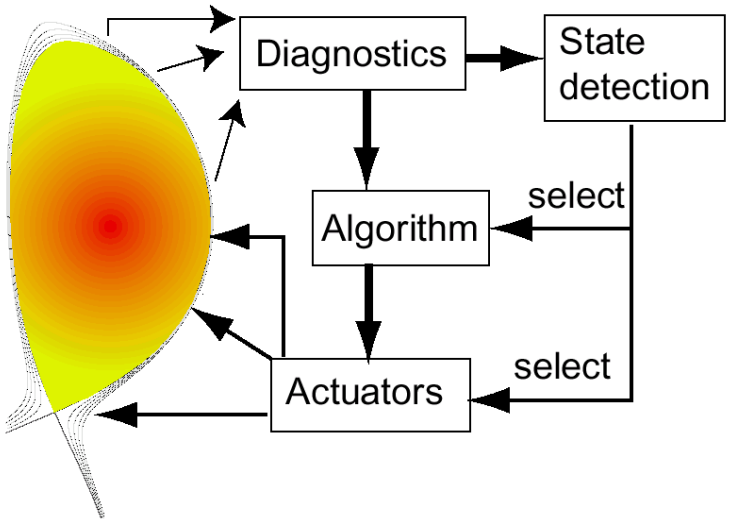

Figure 1.4.6-2 Plasma Feedback Control

Figure 1.4.6-2 introduces the concept of plasma state cognisance, and state-dependent control actions. Here the change of the plasma state can dynamically modify the control algorithms and choice of control actuators so as to more optimally control the overall plasma response. The implementation of state-cognisant control gives the control system a certain degree of autonomy. It will ultimately lead to a highly dynamic and state- and scenario-phase dependent 'expert system'. A plasma control matrix for ITER to relate control actions or actuators and controllable parameters is shown in Figure 1.4.6-3.The vertical organization of the matrix reflects the division of the plasma control system into the four hierarchical categories mentioned above, namely scenario, magnetics, kinetics and fast shutdown.

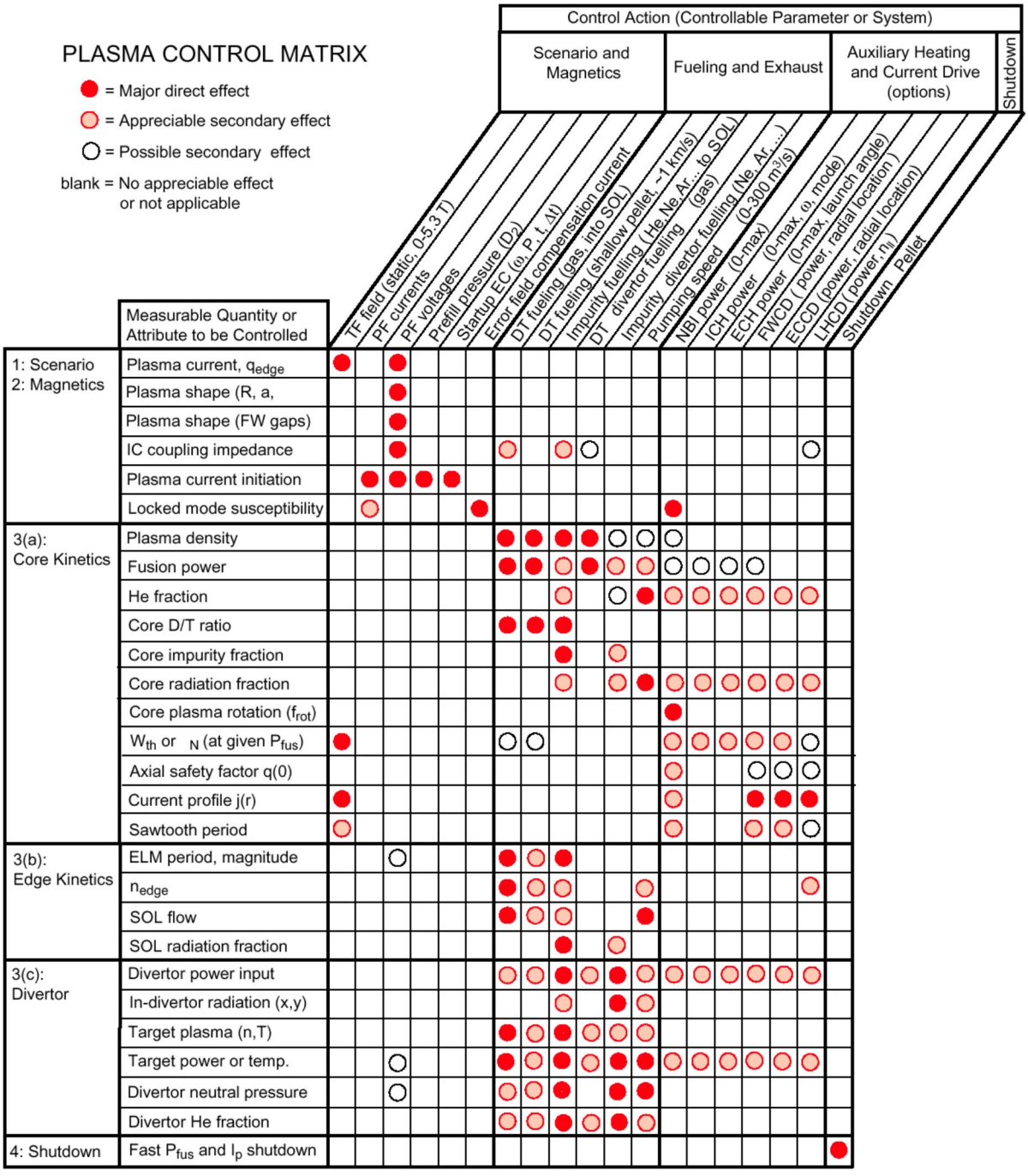

Figure 1.4.6-3 ITER Plasma Control Matrix

The ITER plant operation is controlled and monitored by the "Command Control and Data Acquisition and Communication" (CODAC) system. The CODAC system consists of a centrally positioned supervisory control system (SCS) and sub-control systems dedicated to each plant subsystem under the supervision of the SCS. A conceptual schematic of the ITER plant control system is schematically shown in Figure 1.4.6-4.

In order to achieve integrated control of the entire plant, the SCS provides high level commands to plant subsystems while monitoring their operation. An interlock system, largely independent of the CODAC system, ensures plant-wide machine protection, as well as personnel protection. In so doing, it monitors operational events of the plant and performs preventative and protective actions to maintain the system components in a safe operating condition. The interlock system is also hierarchically structured and has individual interlock elements dedicated to each plant subsystem under the central supervisory interlock system.

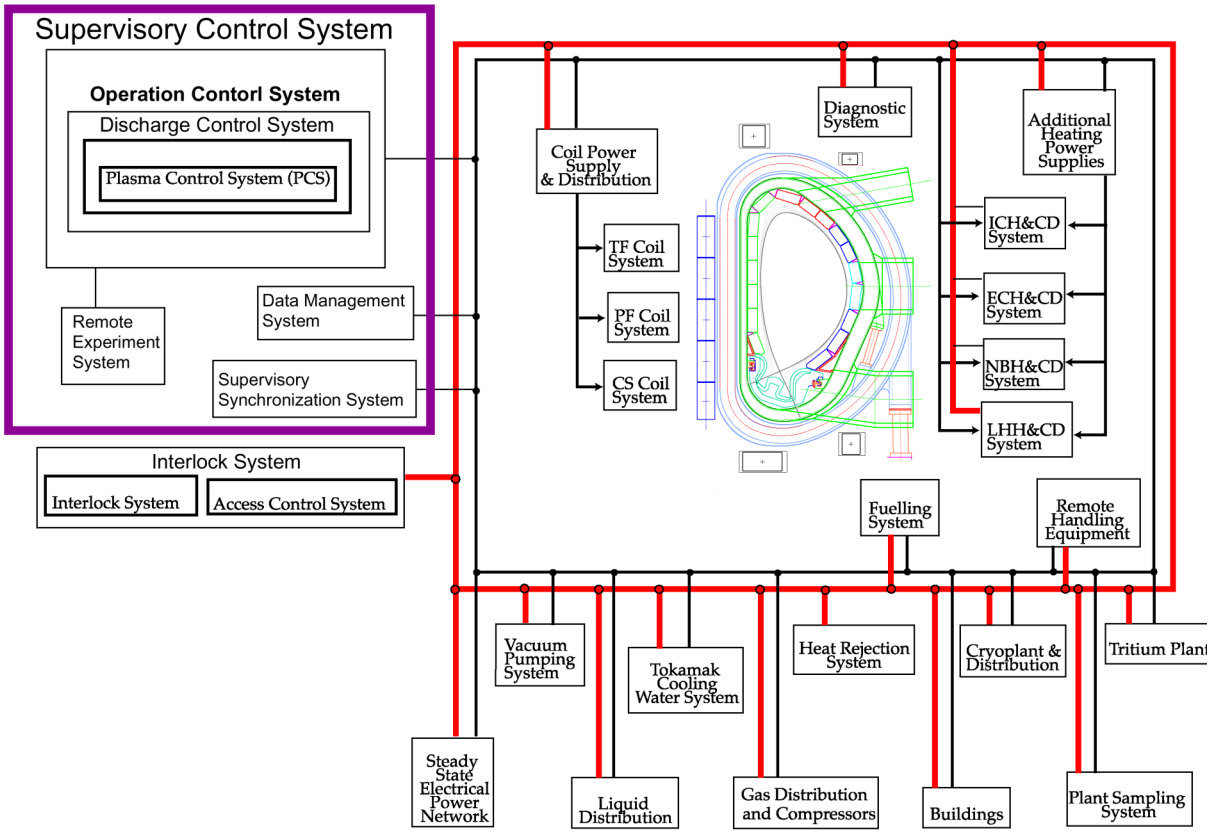

Figure 1.4.6-4 ITER Plant Control System

1.5 R&D Overview

1.5.1 Introduction

The overall philosophy for the ITER design has been to use established approaches through detailed analysis and to validate their application to ITER through technology R&D, including fabrication and testing of full scale or scalable models of key components. Seven large projects were established to confirm the industrial fabrication processes and quality assurance for major key components of the basic machine and their maintenance scheme, namely,

- central solenoid model coil (CS MC) and toroidal field model coil (TF MC) projects,
- vacuum vessel sector, blanket module, and divertor cassette projects,
- blanket and divertor remote handling projects.

Other R&D concerning safety related issues, auxiliary systems including heating and current drive systems, fuelling and pumping system, tritium process system, power supplies and diagnostics are also critical areas. All the key technical issues required for ITER construction have been identified and Home Teams have carried out the associated R&D with a total resource of about 660 kIUA (1 kIUA = 1 M$ in 1989) during the nine years of collaboration (the US contributed up to July 1999). R&D resources were distributed to the various technical areas as shown in Table 1.5.1-1 with three-fourths of the resources devoted to the seven large R&D projects.

Table 1.5.1-1 Percentage of Resources Devoted to the Different R&D Areas

R&D Area	%
Magnets (incl. L-1 & L-2 Projects)	27.9
Vacuum Vessel (incl. L-3 Project)	5.3
Blanket and First Wall including Materials (incl. L-4 Project)	16.3
Divertor & PFC including Materials (incl. L-5 Project)	15.1
In-vessel Remote Handling (incl. L-6 & L-7 Projects)	11.3
Subtotal	75.8%
Fuelling & Pumping	1.9
Tritium System	3.4
Power Supply	1.8
IC H&CD	1.1
EC H&CD	3.7
NB H&CD	3.1
Diagnostics	2.5
Safety Related R&D	3.4
Miscellaneous (incl. Standard Component Development)	3.3
Total	100.0

The technical output from the R&D confirms the manufacturing techniques and quality assurance incorporated in the ITER design, and supports the manufacturing cost estimates for important key cost drivers. The testing of models is continuing to demonstrate their performance margins and/or to optimise their operational performance. During the EDA, the successful progress in R&D has provided valuable and relevant experience in the management of industrial scale, cross-party ventures, offering important insights and

experience for a possible future collaborative construction activity in a joint implementation of ITER.

1.5.2 CS Model Coil and TF Model Coil

These two projects are working towards developing the superconducting magnet technology to a level that will allow the various ITER magnets to be built with confidence. The model coil projects are intended to drive the development of the ITER full-scale conductor, including the manufacturing of strand, cable, conduit and terminations, and the conductor R&D in relation to AC losses, stability and joint performance. These model coil projects also integrate the supporting R&D programmes on coil manufacturing technologies, including electrical insulation, winding processes (wind, react, and transfer) and quality assurance. 29 t of Nb_3Sn strand, from seven different suppliers throughout the four Parties, have been produced and qualified. This reliable production expanded and demonstrated the industrial manufacturing capability for the eventual production of the 480 t of high performance Nb_3Sn strand as required for ITER-FEAT.

The CS model coil is the largest, high field, pulse super conducting magnet in the world. By using approximately 25 t of the strand, the inner module (US), the outer module (JA), and the insert coil (JA) were fabricated (Figure 1.5.2-1) and assembled in the ITER dedicated test facility at JAERI. In April 2000, the maximum field of 13 T with a cable current of 46 kA has been successfully achieved. The stored energy of 640 MJ at 13 T has been safely dumped with a time constant as short as 6 s (11 s in the ITER CS). This model coil is similar in size and characteristics to one of the six modules of the ITER Central Solenoid. The SC insert coil was successfully tested with 10,000 cycles by August 2000 to simulate ITER operation (0 to 40 kA cycles in a steady 13 T background field of the CS model coil.

Figure 1.5.2-1 CS Model Coil
The outer module being placed outside the inner module which has already been installed in the vacuum chamber.

The TF model coil is fabricated (Figure 1.5.2-2) and fully assembled in the EU. It uses a cable similar to the one used in the full-size TF coil. The diameter of the TF model coil is smaller but the cross section is comparable in size to that of the ITER TF coil.

The coil will be tested in summer 2001 in the TOSKA facility at FZK Karlsruhe with a field of 9.7 T at 80 kA (instead of 11.8 T and 68 kA in ITER). In addition, at the same time, a TF insert coil with a single layer will be tested inside the bore of the CS model coil test facility at JAERI at a field up to 13 T.

For the development of the manufacture of the TF coil case, large forged and cast pieces (about 30 t and 20 t respectively) have been produced in the EU. Investigation of the material

properties at 4.5K has revealed values adequate for their use at different locations in the coil. Different welding processes have been qualified.

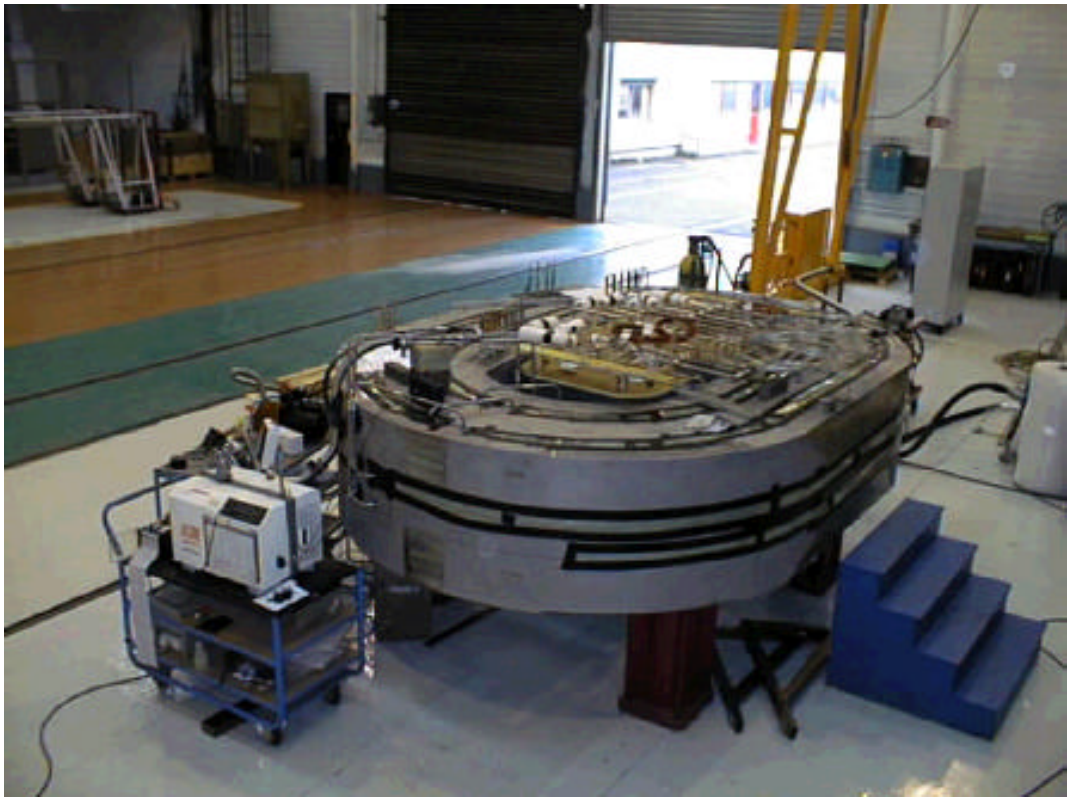

Figure 1.5.2-2 TF Model Coil undergoing Vacuum Tests

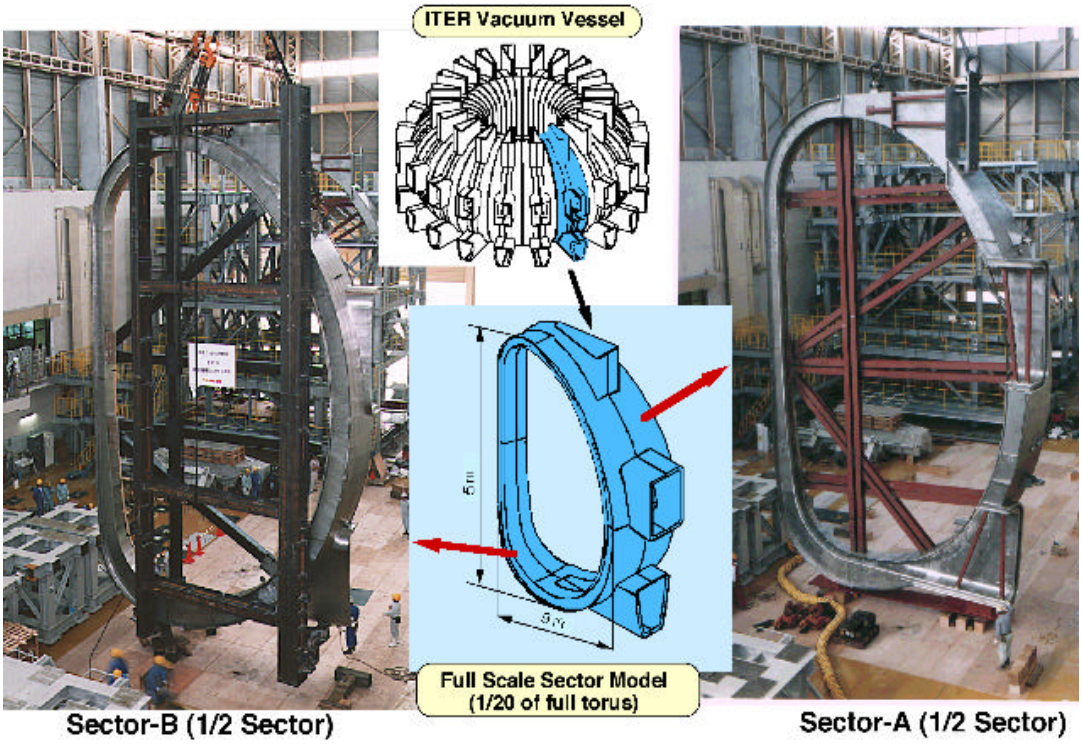

Figure 1.5.3-1 Full Scale Vacuum Vessel Sector R&D

1.5.3 Vacuum Vessel Sector

Two full-scale vacuum vessel segments (half-sectors) have been completed by JA industrial firms, using a range of welding techniques, within the required tolerances. At JAERI, they were welded to each other and the equatorial port fabricated by the RF was attached to the vessel to simulate the field joint (Figure 1.5.3-1) which will be done at the ITER site during the assembly of the machine. Remote welding and cutting systems prepared by the US were also tested and applied.

1.5.4 Blanket Module

The blanket module project aims at producing and testing full-scale modules of the first wall elements and full-scale, partial prototypes of mechanical and hydraulic attachments.

Material interfaces such as Be-Cu and Cu-stainless steel have been successfully bonded by using hot isostatic pressing (HIP) and other advanced techniques. Full-size shield block has been completed by using powder HIP (EU) and other techniques (JA) like forging, drilling, and welding. The mechanical attachments made of titanium alloy have been developed and tested in the RF (Figure 1.5.4-1).

Figure 1.5.4-1 Flexible Mechanical Attachments made of Ti-Alloy (RF)

In parallel with these fabrications, heat cycle and irradiation tests have been performed for the base materials and the bonded structures, and have demonstrated that the performance is well within the required level.

1.5.5 Divertor Cassette

The divertor cassette project aims at demonstrating that a divertor can be built within tolerances and withstand the high thermal and mechanical loads.

A full-scale prototype of a half cassette has been built by the four Parties. Plasma-facing components (PFCs) shipped from the JA and the RF were installed on the inner divertor cassette body fabricated in the US, and hydraulic flux and mechanical tests were performed at Sandia National Laboratory. Other PFC mock-ups fabricated by the EU and the RF were also installed on the outer divertor cassette body fabricated by the EU (Figure 1.5.5-1).

Various high heat flux components were fabricated and tested in the four Parties. High heat cycle tests show that carbon fibre composite (CFC) monoblock survives 20 MW/m^2 x 2000 cycles (EU) and tungsten (W) armours survive 15 MW/m^2 x 1000 cycles (EU / RF). A large divertor target mockup with CFC attached to dispersion-strengthened copper (DSCu) through oxygen-free copper (OFCu) has been successfully tested with 20 MW/m^2 x 1000 cycles from a large hydrogen ion beam with a diameter of 40 cm (JA).

Figure 1.5.5-1 Integrated Outer Divertor Cassette (EU)

Irradiation tests have been also performed. For example, CFC brazed on Cu survived 20 MW/m^2 x 1000 cycles after 0.3 dpa irradiation at 320°C. Tests with pulse heat deposition simulating the thermal load due to disruptions have demonstrated erosion but no disruptive failure of CFC armours even with 0.4 dpa irradiation. (The average neutron fluence of 0.3 MWa/m^2 at the first wall gives 0.38 – 0.59 dpa on the CFC divertor target.)

1.5.6 Blanket and Divertor Remote Handling Systems

The last two of the large projects focus on ensuring the availability of appropriate remote handling technologies which allow intervention in contaminated and activated conditions on reasonable timescales, in particular to replace damaged blanket or divertor modules remotely. In this area, full-scale tools and facilities have been developed. Their testing will be extended over a long period of time, including the ITER operation phase, to optimise their use in detail, minimise any intervention time, and allow training of operators.

The blanket module remote handling project makes use of a transport vehicle on a monorail inside the vacuum vessel for the installation and removal of blanket modules, brought to or from a vacuum vessel port by a docked transfer cask. After successful operation of a 1/4 scale model, the fabrication of a blanket test platform with full-scale equipment and tools, such as a 180° rail, a vehicle with telescopic type manipulator, and a welding/cutting/inspection tool, have been completed in JA (Figure 1.5.6-1). The simulation of installation and removal of a simplified, dummy shield blanket module of 4 t has been successfully performed by using a teach-and-repeat procedure with only 0.25 mm of clearance in positioning.

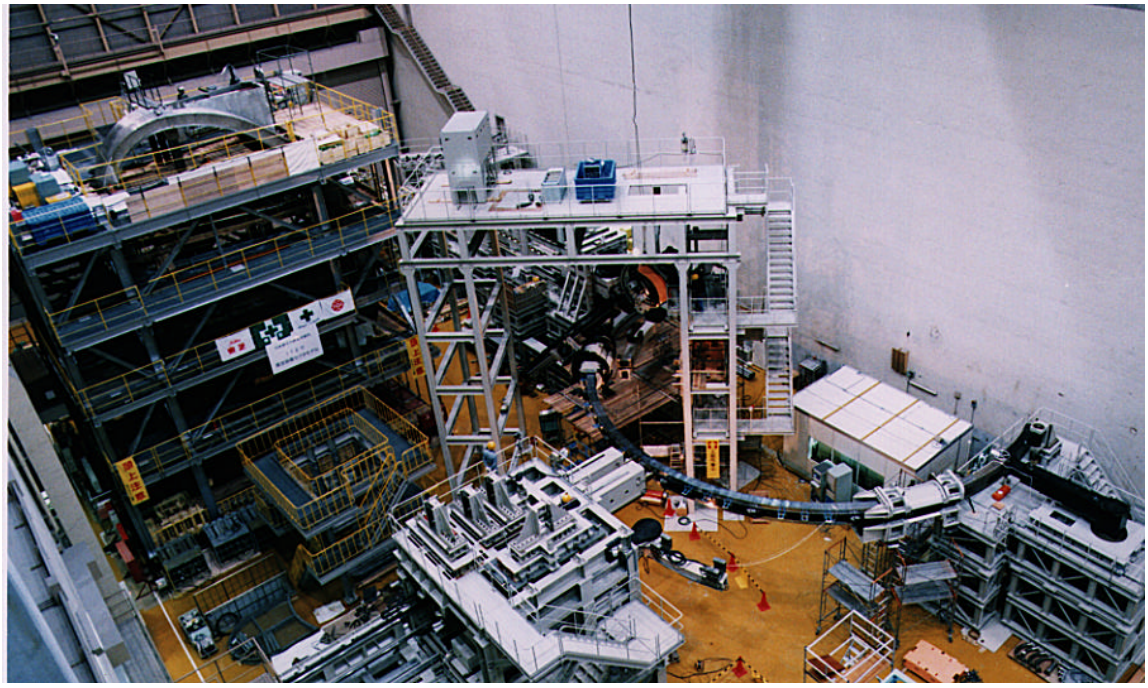

Figure 1.5.6-1 Blanket Maintenance Test Platform at JAERI (JA)

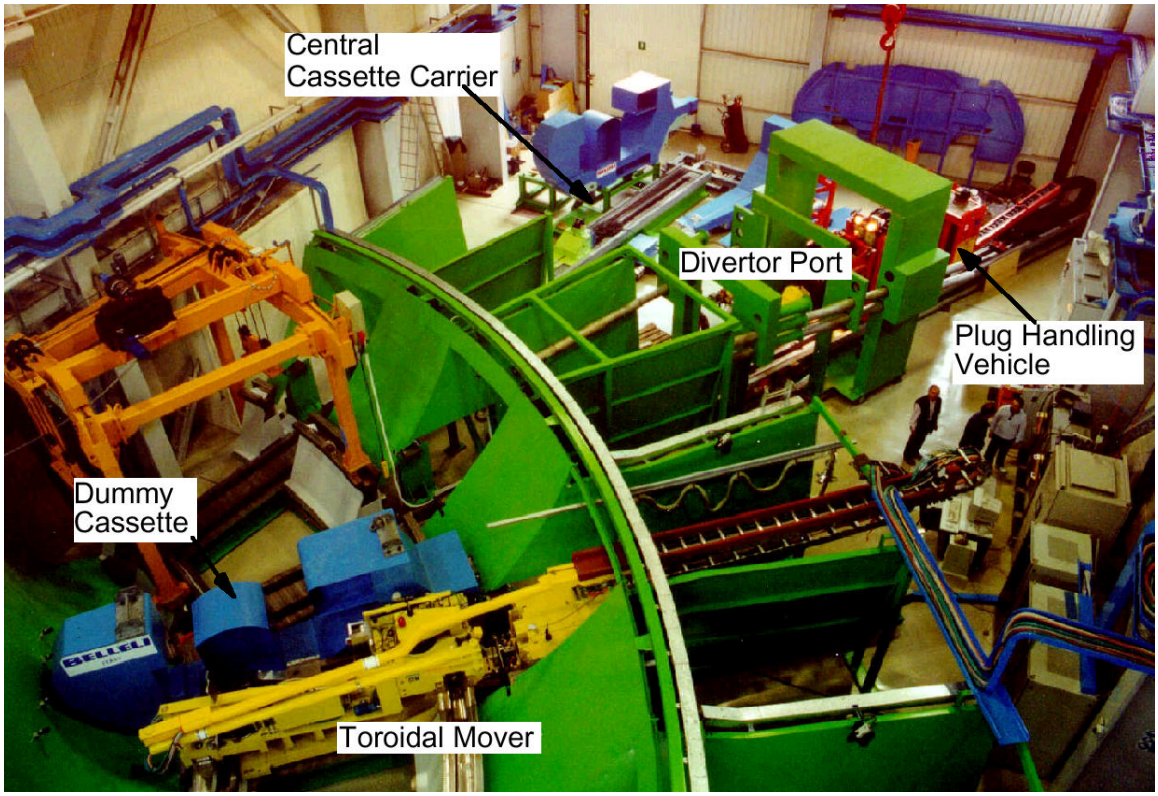

Figure 1.5.6-2 Divertor Maintenance Test Platform at Brasimone (EU)

The divertor remote handling project has involved the design and manufacture of full-scale prototype remote handling equipment and tools, and their successful testing in a divertor test platform (Figure 1.5.6-2) to simulate a portion of the divertor area of the tokamak and in a divertor refurbishment platform to simulate the refurbishment facility. The system is based on a toroidal transporter that moves a cassette in front of a remote handling port from where

the cassette is extracted with a radial mover that is deployed from a transfer cask docked to the port. The real in-vessel operation will be done in a gamma field of 10^4 Gy / h. Key elements such as motor, position sensor, wire/cable, glass lens, electrical insulator, periscope and strain gauge have shown to survive tests at 10^6 –10^7 Gy.

1.5.7 Other R&D

A 50%-scale cryogenic pump for DT, He and impurities has been completed and is under testing in the EU (Figure 1.5.7-1).

A tritium pellet injector (DT and T_2) has been tested in the US ejecting a large pellet (10 mm) from an 80 cm radius curved guide tube at 285 m/s. Further tritium pellet injector development is continued in the RF.

Figure 1.5.7-1 50% Scale Cryogenic Pump (EU)

Gyrotrons at 170 GHz are being developed in all Parties aiming at longer pulses towards steady state (0.5 MW x 8 s in JA, and at 1 MW x 1 s in RF).

Key components for the ICRF (ion cyclotron range of frequencies) plasma heating antenna and the transmission line have been developed and tested at a higher voltage than the expected operational voltage, waiting for the test of a high power density antenna in a present day machine (JET, EU).

Almost full-size negative ion sources and high voltage technology (1 MeV) have been developed for the neutron beam plasma heating in JA (Figure 1.5.7-2) and in EU, but present performance has to be increased to meet the requirements.

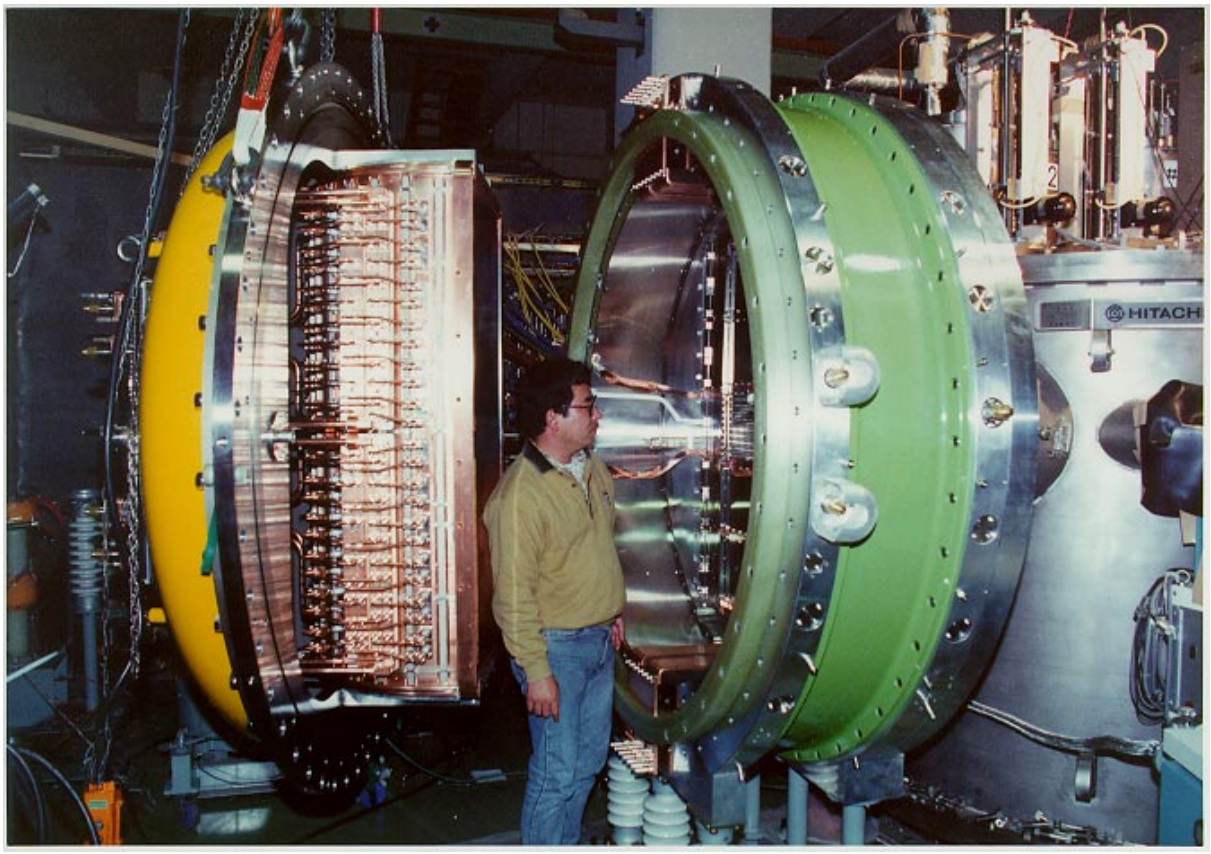

Figure 1.5.7-2 Prototype of Negative Ion Source at JAERI (JA)

Mechanical bypass switches and fast-make switches have been developed and successfully tested at 66 kA as well as explosively actuated circuit breakers at 66 kA at Efremov Institute (RF) for the magnet system power supplies.

Irradiation tests of key components of plasma diagnostics have provided the values required for shielding of components. Lifetime of mirrors positioned near the plasma will be limited by deposition/sputtering and are under investigation

A tritium processing system using about 100 g tritium was successfully operated for 12 weeks in the US.

Safety-related R&D, such as the characterization of dust in tokamaks, tritium co-deposited with carbon, and experiments on steam-material reactions, has provided inputs for key phenomena and data for safety assessments, and the current R&D emphasis is on verification and validation of data, models and computer codes. Neutron shielding tests using 14 MeV neutron sources in Japan and the EU demonstrate that the accuracy of shielding calculations is within 10 %.

1.6 Safety and Environmental Assessment

1.6.1 Objectives and Approach

It is one of the foremost goals of ITER to demonstrate the safety and environmental potential of fusion power. Extensive design and assessment activities are undertaken to ensure the safety and environmental acceptability of ITER and to ensure that ITER can be sited in the territory of any of the Parties with only minor changes to accommodate or take advantage of site-specific features.

A consensus across the Parties on safety principles and criteria for limiting the consequences to the public and the environment from ITER operation has been reached based on internationally recognised safety criteria and radiological limits following ICRP and IAEA recommendations, and in particular on the concept of defence-in-depth and the As-Low-As-Reasonably-Achievable (ALARA) principle. Safety-related design requirements have been established, and assessments have been or are being made to evaluate the success in meeting these requirements in the facility, system and component designs.

Comprehensive safety and environmental assessments of the ITER design and operation have been completed for a generic site with the involvement of Home Team safety experts. These assessments include:

1. estimation of the environmental impact of ITER during normal operation including waste management and decommissioning,
2. evaluation of operating personnel safety,
3. in the case of postulated off-normal and even hypothetical events, estimates of environmental consequences and public safety.

1.6.2 Environmental Impact

The ITER design incorporates many features to ensure that the environmental impact during normal operation will be insignificant, including confinement barriers to prevent releases as well as air/water detritiation and filtration systems to treat releases. The facility can be operated to satisfy the restrictive safety and environmental guidelines that have been established by the project for the design. In addition to meeting prescribed host country limits, the ALARA principle is recommended by international nuclear safety experts and incorporated in national regulations of many countries. The International Basic Safety Standards explain ALARA as the objective to keep all exposures to values such that further expenditures for design, construction, and operation would not be warranted by the corresponding reduction in radiation exposure. For ITER this process involves systematically reviewing systems, activities and pathways with a release potential, estimating releases, and examining ways to reduce the main contributors.

In a comprehensive analysis, sources of potential releases have been identified, release pathways determined, and design features and release control systems assessed. Conservative assumptions have been also made so as not to underestimate potential releases.

Potential doses to members of the public (i.e. the most exposed individual) during normal operation, for a 'generic' or 'average' site, are less than 1% of the natural background level.

The continued application of the process to implement the ALARA principle may further reduce the estimated normal releases.

1.6.3 Waste and Decommissioning

In the frame of ITER's safety objectives, the control of radioactive materials, decommissioning and waste is carefully considered. All activities associated with radioactive materials and waste will comply with the host country regulations and practices. The management will be co-ordinated between the ITER project and the host country. In the absence of an actual host country for ITER, the ultimate waste amounts have been estimated provisionally on the basis of 'clearance'. According to this IAEA concept, by this process, activated materials of known composition can be released from regulatory control if their activation levels are less than the specified clearance level, and used unrestrictedly in the future.

The radioactive materials arising during operation and remaining after final shutdown include activated materials (due to fusion neutrons) and contaminated materials (due to activated tokamak dust, activated corrosion products and tritium) and mixtures thereof. Decay and decontamination will reduce the radioactivity with time after final shutdown. Therefore, a significant fraction of activated material has the potential to be cleared. Since this fraction increases with time at present the ITER project provisionally assumes that radioactive material not allowing for clearance after a decay time of up to 100 years is 'waste' requiring disposal in a repository. Estimated material masses are shown in Table 1.6.3-1.

The experimental nature of the ITER project often calls for frequent replacements of plasma facing components. For this reason the design approach has included practices to reduce the quantities and hazards of radioactive materials, such as modular components, choice of materials, control of impurities, shielding, and re-useable components. About 750 t of such waste is expected during operation which can be stored on-site in the hot cell while low-level contaminated materials (e.g. filters) would be shipped to an off-site storage facility. Moreover, to ensure that ITER can be safely dismantled at the end of its useful operating life, decommissioning plans have been developed, as described in 1.8.5.

Table 1.6.3-1 Masses of Radioactive Materials

Total radioactive material at shutdown	~ 30,000 [t]
Material remaining as waste after a decay time up to 100 years	~ 6,000 [t]

1.6.4 Worker Safety

ITER has established a program for personnel protection against hazards anticipated during construction, operation and maintenance activities. The program addresses radiation protection and conventional hazards. The objective of this work is to ensure that occupational safety is considered in the design of systems and components and, mainly through maintenance procedures, thereby to gain confidence that a high level of worker safety will be achievable.

Assessment of all major system maintenance demonstrates that ITER will maintain occupational exposures below the project guidelines. The project's commitment to ALARA ensures the continuing review, analysis, and improvement of design and maintenance

procedures to ensure that exposures and radiological risks are not only below the guidelines, but also maintained as low as reasonably achievable.

1.6.5 Safety Analysis

During full DT operation ITER will contain radioactive materials that require careful management. Table 1.6.5-1 shows values of tritium assumed for assessment purposes in ITER (the "assessment value"). For the neutrons from the fusion reactions activating surrounding materials, the majority of activation products will be bound in solid metal structures of the in-vessel components. The most relevant source of mobilizable activation products is activated dust originating from plasma facing materials. Of all plasma facing materials envisaged for use in ITER it is tungsten that has by far the largest radiological hazard potential. The assessment value for tungsten dust in the vacuum vessel is 350 kg. Compared to the assessment values, smaller project guidelines are set for tritium and dust to cover uncertainties.

Table 1.6.5-1 Tritium Inventories for ITER: Assessment Values

Type of inventory	**[g]**
In-vessel mobilizable (in plasma facing components, dust, co-deposited etc.)	1000
Fuel cycle circulating inventory	700
Total site inventory	**< 3000**

A comprehensive analysis of off-normal events has been performed to assess the effectiveness of the implementation of the safety requirements and functions in the ITER design. Failures and combinations of failures have been postulated to critically verify that the design is tolerant to such failures and to ensure a robust safe operating envelope for the experimental programme.

The analyses included conservative assumptions of initial facility operating and off-normal conditions and thoroughly examined possible ways for tritium, activated corrosion products in coolants, and neutron-activated tokamak dust, to be released to the environment. Results show that radioactive releases for all of these reference events are well below the project release guidelines that would lead to doses (to the most exposed individual) comparable to the average annual natural background exposure for a generic site. The assessments provide confidence that the operation of ITER will result in no significant risk to the general public from postulated accidents.

In the course of the ITER design, the systematic identification of possible accidents has always been part of the safety assessment. In this process, different approaches were chosen to treat the problem of completeness methodically. One method investigated all possible failures on a system-by-system basis. A complementary method started with postulating a large environmental release of radioactivity and identifying the associated failures in the plant that could lead to it. Another approach systematically identified the energy sources in the plant that may drive accidents. All these methods have been employed during the design process of ITER and have led to similar lists of important accidents. These are discussed below together with the design features in ITER to prevent and mitigate environmental releases of radioactivity.

A fundamental safety principle of ITER is that uncertainties in plasma physics will not have an effect on public safety. The maximum possible fusion power transient is limited by the beta- and density limit to a level below 2 GW. The energy content and fuel in the plasma is limited such that only local melting of plasma facing components could occur. No safety credit is given to experimental in-vessel components. As a consequence of this approach ITER is designed to safely accommodate multiple first wall or divertor cooling channel failures. These postulated failures bound all possible damage to the in-vessel components due to unexpected plasma behaviour.

The first safety-relevant barrier for the plasma and in-vessel components is the vacuum vessel and its extensions (such as equipment in ports, and particularly the neutral beam injection lines). A second safety-relevant barrier is the cryostat and its extensions (such as vaults around the neutral beam injectors and cooling circuits of the heat transfer systems). For the tritium systems the process equipment forms the first barrier and secondary enclosures such as glove boxes or secondary piping are provided to deal with leaks in the primary confinement. Rooms that may receive leakage of radioactivity are equipped with HVAC systems that keep the pressure sub-atmospheric and provide a capability to filter dust and tritium in the exhaust if needed. Any uncontrolled flow of radioactivity is “inwards”, because the internal confinement areas are either evacuated (vacuum vessel and cryostat) or kept at sub-atmospheric pressure. Thus small leaks are excluded from leading to uncontrolled releases of radioactivity.

One very favourable safety feature of ITER is that the decay heat is limited to 11 MW at shutdown and very quickly decreases to only 0.6 MW just one day after shutdown. In case of loss of in-vessel cooling the decay heat will be passively transported by thermal radiation to the vacuum vessel. Even if active vessel cooling pumps fail, the vacuum vessel cooling system will remove the decay heat passively by natural circulation of the water coolant to an air-heat exchanger.

Figure 1.6.5-1 shows the resulting temperature history of the in-vessel components. A maximum temperature of 360ºC is reached 9 hours after plasma shutdown.

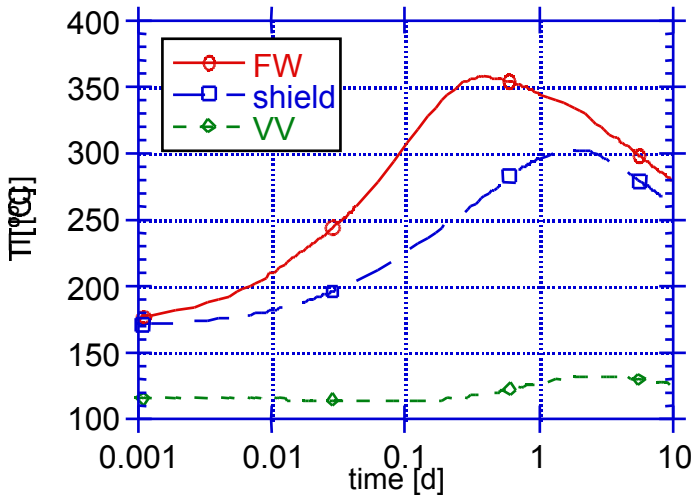

Figure 1.6.5-1
Decay Heat Driven Temperature Transient in ITER in case of Loss of In-vessel Cooling and Failure of the Active Vessel Cooling.
The heat sink is the VV cooling system that removes the decay heat passively by natural circulation to an air heat exchanger.

The vacuum vessel is equipped with a pressure suppression system which consists of a large container of cold water to condense steam which will be formed inside the vacuum vessel

during coolant leakage. For small leaks (equivalent to a break of 1 to 10 cooling channels) the maximum steam pressure inside the vacuum vessel would be less than one atmosphere and the pressure suppression system will not need to be connected. Postulating a multiple FW failure of two toroidal rings (one inboard, one outboard) as a bounding event leads to fast pressurization of the vacuum vessel and rupture of disks to allow connection to the pressure suppression system. The moderate coolant temperatures (100ºC inlet, 150ºC outlet) combined with large connecting ducts between the vacuum vessel and the pressure suppression system limit the maximum pressure in the vacuum vessel to 1.8 bar throughout this event, a value which gives rise to extremely small stress levels in the thick vessel shell.

Ex-vessel pipe failures are investigated as plausible incidents occurring in the heat transport system. The plasma burn is actively terminated on a cooling pressure drop signal to avoid large temperatures in the blanket due to a continued plasma burn without cooling. For a pipe rupture during plasma operation, the maximum absolute pressure inside the tokamak cooling water system (TCWS) vault is 1.5 bar which is below its design pressure of 2 bar. Should the divertor cooling loop be affected by an ex-vessel loss of coolant, failure of the plasma facing components is likely as a result of the high surface heat loads during plasma operation and the expected disruption loads at plasma termination. This would cause pressurization of the vacuum vessel, mobilization of tritium and dust and subsequent transport into the vault through the divertor cooling pipes. The subsequent environmental releases due to leakage from the vault are about one order of magnitude below the project release guidelines for accidents.

Another class of incidents with the potential for environmental releases are bypass events of the first two confinement barriers. In these events it is postulated that the leak tightness of both barriers in one of the many hundred penetrations into the vacuum vessel would fail. Such a penetration could be a heating system waveguide or a diagnostic line. Also in this case the ITER design feature to limit vacuum vessel pressurization to below two atmospheres has the advantage that such a confinement bypass event can be excluded as a consequential failure after a small in-vessel loss of cooling event**.** In any case, the amount of gas released from this failed penetration tightness will be confined in the separate cell around the relevant vacuum vessel port and the atmosphere there will be detritiated and filtered before exhaust to the environment.

Another postulated event analysed to bound structural failures is a full terminal short of a toroidal field (TF) coil, which is a highly unlikely event that requires two independent types of faults. The maximum current induced in a shorted TF coil during a fast discharge is limited by inductive coupling with the other coils during the fast discharge and by quench as the conductor is driven to critical conditions. Some local plastic deformation may be expected to occur in TF coil structures but gross structural failure is prevented.

As bounding events in the fuel cycle, failures in both the fuelling line and secondary confinement piping are investigated. The room will be isolated from normal ventilation and connected by valves to the standby vent detritiation system. The total expected tritium release is more than one order of magnitude below the project release guideline for accidents.

The extensive analysis of a comprehensive range of postulated failures using pessimistic or limiting conditions demonstrates that the modest safety requirements for ITER are adequate, and that releases, if any, would be a small fraction of the project release guidelines. This

contributes to the demonstration that operation of ITER will result in no significant risk to the public.

1.6.6 Study on Ultimate Safety Margin

Ultimate safety margins of the facility are examined, through a sensitivity study, by analysis of hypothetical events by arbitrarily assuming that more and more failures occur. In some countries ITER has the goal to demonstrate the achievement of the "no evacuation" objective according to the IAEA established guideline for evacuation which is 50 mSv of avertable dose. Even under the worst imaginable sequence of events from internal or identified external origins, the design and operation of the facility protects the public to such a degree so that there is no technical justification for dependence on public evacuation as a backup.

For example, one hypothetical event is the postulation of failure of all cooling systems in ITER (including vessel coolant natural circulation) when removing decay heat. Even for this extreme situation the first wall only heats up to a maximum temperature of about 650ºC. This temperature does not induce any significant structural failure and does not degrade the confinement functions.

Another extreme situation postulates common cause failure damage of both the vacuum vessel and cryostat boundaries by some unidentified magnet energy release. This event would not lead to large environmental releases because the cryogenic surfaces would effectively capture most of the mobilized source term and the atmosphere detritiation and filtering would control the building exhaust.

The analysis shows that the design is tolerant to failures, that there is no single component whose failure leads to very large consequences, that there is no single event that can simultaneously damage the multiple confinement barriers, and hence that the ITER design provides a high level of public protection.

1.6.7 Safety Assessment Conclusions

The following conclusions can be drawn from the comprehensive accident analysis: ITER is 'safe' with little dependence on engineered, dedicated 'safety systems' for public protection because of the inherent, fail-safe nature of the fusion energy reaction, limited mobilizable radioactive inventories, multiple layers of confinement, and passive means for decay heat removal. As a result of the safety characteristics of fusion, and engineered design features, it requires an almost inconceivable combination of failures to lead to a significant release of radioactive material.

In summary, the assessments documented in the GSSR shows that ITER can be constructed and operated without undue risk to health and safety and without significant environmental impact. The analyses and assessments completed with the involvement of the Home Teams experts offer a well-developed technical basis for regulatory applications in potential host countries.

1.7 Quality Assurance Program

The central objective of the ITER quality assurance (QA) program is to ensure that the level of quality necessary to achieve ITER objectives, in performance and safety, is specified and

implemented. For this reason the ITER QA program covers all items or activities important to the safety and performance of ITER throughout its life. This has meant the adoption by ITER, in line with organisations qualified to ISO 9000, of:

- a quality policy,
- defined organisation structure, responsibilities, and interfaces,
- personnel qualifications and training,
- quality requirements for contracting organisations,
- documentation,
- defined processes and management systems to achieve these.

In particular, during the design/construction phase of the project the assurance of quality implies the following practices.

- Management. A proper organization of the project management is central in the successful implementation of the project itself. This includes the definition of responsibilities to ensure authority over all actions described below.
- Design. The design of components follows standard practices defined in many international standards (such as ANSI N45.2.11). These practices involve the use of interface control, definition of requirements, design verification, design reviews, configuration management, control of design documents.
- Procurement. This will be controlled to the extent necessary to ensure conformance of ITER procurement specifications with the ITER design. Items or services to be purchased will be specified in writing. Such documents will be reviewed, approved "for procurement" and controlled. Procurement contracts shall be placed with qualified suppliers whose previous performance has been assessed and recorded.
- Manufacture. This activity will be controlled to the extent necessary to ensure items conform with ITER procurement specifications. This implies that work will have to be carried out in well-controlled conditions using approved drawings, procedures, standards and other documents, according to approved pre-established checklists of operations. Approved procurement documents and records shall be maintained to reflect the actual specifications. Item or services status and relevant documentation shall be reviewed and formally accepted by ITER prior to delivery. Manufacturing documents and records shall be maintained to reflect the actual configuration of the item, and approved "as built" on item completion.
- Assembly. Installation is clearly to be controlled to the extent necessary to ensure that the installation of a particular item will not compromise the integrity of the item to be installed, or of the ITER plant.
- Inspection. Inspection and test equipment will also have to be controlled to ensure that equipment used for process monitoring, data collection, inspection and tests are of the proper range, type, accuracy and precision.

1.8 Construction, Commissioning and Decommissioning Plans

1.8.1 Introduction

The planning schedule for procurement, construction/assembly, commissioning and decommissioning set out below depends on a number of assumptions detailed in the following. As the negotiations toward the joint implementation of ITER progress, decisions reached by the Parties may confirm or alter the assumptions that have led to its present status. The actual plan will therefore depend on the licensing procedure, as well as the organization and arrangements that will be put in place for the procurement/construction commissioning.

The ITER Joint Implementation Agreement is expected to be signed at the end of 2002 or the beginning of 2003 following formal negotiations. The ITER legal entity (ILE) will be established after ratification of the agreement within each Party. This organisation will start the formal regulatory procedure and procurement process for the long lead-time items. The regulatory approval process, however, will remain speculative until a site is formally selected.
Furthermore, the following assumptions pertain at T = 0.

- Informal dialogue with regulatory authorities should be established and should orient the technical preparation toward a licence application with a view to solving the major technical issues prior to establishment of the ILE.
- Procurement specification of equipment/material for the longest lead-time items and critical buildings are assumed to be finalized during the co-ordinated technical activities (CTA).
- Procurement sharing is assumed to be agreed among the Parties during the CTA so as to permit the placing of contracts at the appropriate time.
- The construction site work starts immediately at T = 0. It is assumed that site preparation has been started sufficiently early by the host Party so as not to place constraints on the start of construction.

1.8.2 Overall and Summary Schedule

The overall schedule that leads up to the first hydrogen plasma operation is shown in Figure 1.8.3-1. It represents a reference scenario for the schedule of procurement, construction, assembly and commissioning of ITER.

1.8.3 Construction and Procurements

1.8.3.1 Procurement Assumptions

The lead-times for the different components of ITER vary widely. For the purpose of evolving this schedule, procurement is assumed to occur such that systems/components are delivered just in time, i.e. at the latest time, on the critical path, for assembly and installation/construction, in accordance with the construction logic. In a second evolution of this plan, some items should be moved earlier in the schedule to gain some margins, which would remove some items from the critical path line. However if cash flow peaks caused by critical items are too high, only an extension of the overall schedule is possible as a solution.

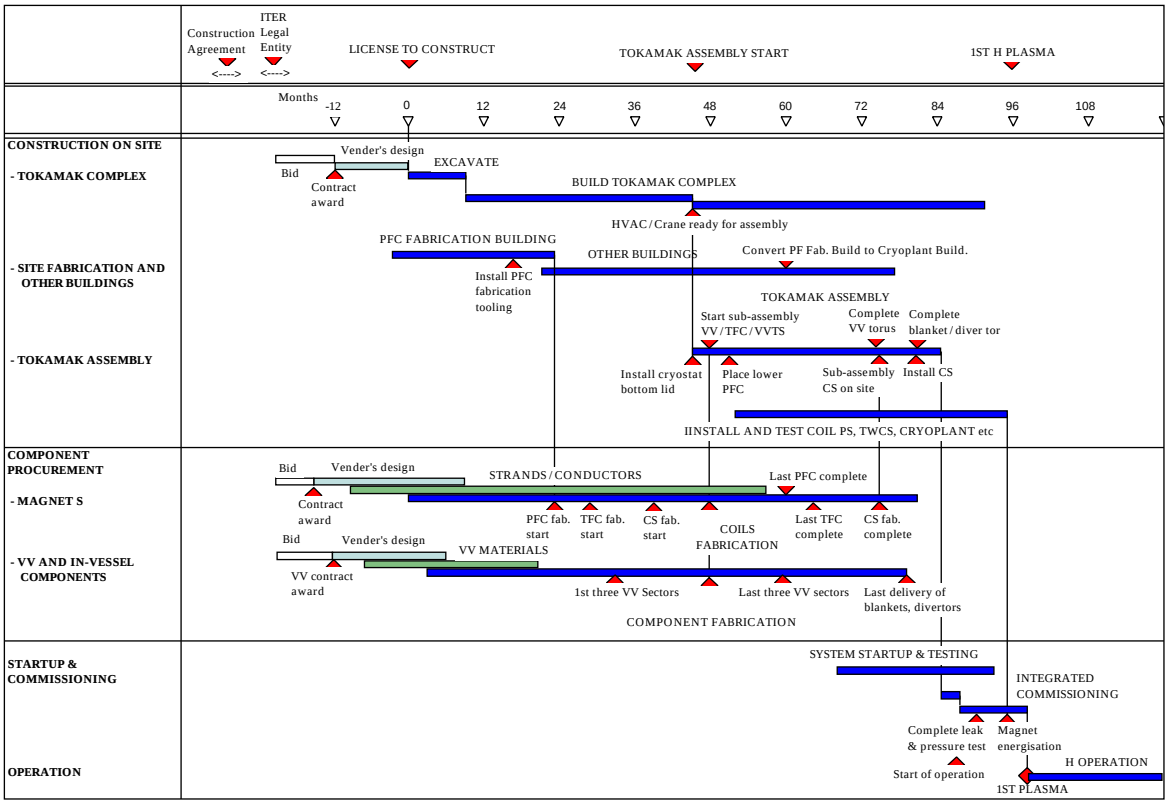

Figure 1.8.3-1 Overall Schedule up to First Plasma

Another important assumption is that the bidding process preceding placing of purchase orders will start only on the establishment of the ILE, before the licence to construct is awarded (T = 0), in order to allow vendor's design and tooling preparation for the critical lead-time components and buildings. In reality, for non-safety-related items (e.g. magnets), manufacturing can even be started before the granting of a construction licence, provided it is clear one will eventually be granted. For safety-related items, however, construction can only start after the license to construct is issued.

1.8.3.2 Buildings and License to Construct

The critical path of the plan starts with the regulatory licensing procedure and the construction of the tokamak buildings. In order to start excavation immediately at T = 0, the manufacturing design of the complex must be complete by then. The contract for the vendor's preparation of the complex thus has to be awarded at least twelve months before. Considering a period for the procurement bid process, the tender documents have to be released 18 to 24 months before T = 0. After the establishment of the ILE, if the license process can be completed in less than 24 months, the construction period defined from the establishment of the ILE to first hydrogen plasma discharge is minimal, equal to ten years. If the regulatory process takes more than two years from establishment of the ILE, the construction period becomes correspondingly longer.

1.8.3.3 Procurement of Long Lead-Time Items

The tokamak building is ready for machine assembly at month 46. In order to start the pre-assembly of TF coils and vacuum vessel sectors in the assembly hall, the first two TF coils at least must be delivered by month 45 and the last two by month 62. Two parallel manufacturing lines are necessary for the procurement of TF coils inside the planned schedule. Most of the PF coils are too large to consider their transfer from the factory to the site (unless both factory and ITER site have deep water access). Thus, fabrication on site is likely to be unavoidable. Nine (40º) vessel sectors are shipped to the construction site and pre-assembled with the TF coils and vacuum vessel thermal shield (VVTS) in the assembly hall before being installed into the pit. Three parallel fabrication lines are necessary for the vacuum vessel procurement to fit into the schedule. The last sector should be accepted at month 62.

1.8.4 Commissioning Plan

Testing of each individual plant subsystem has to start immediately when permitted by their delivery and by the corresponding assembly work. Subsystems not needed in an early phase will be commissioned in parallel with operation.

There will be the need, for about one year, for adequate testing of controls and interfaces between subsystems. CODAC is designed to permit testing of the complete system in the absence of one or more of the sub-subsystems. This one year of integrated testing requires that all the key subsystems have been successful in their individual tests, and the complete Operations Team is assembled and trained on site. This is the first year of ITER operation. After the first plasma there will be further integrated commissioning over about four years leading to full operation in DT. The first 2.5 years of operation without DT is defined as a "pre-nuclear commissioning phase" and "nuclear commissioning" (about one year) will be done by using DD discharges with limited amounts of tritium.

1.8.5 Decommissioning Plan

It is assumed that the ITER organization at the end of operation will be responsible for starting the machine decommissioning through a de-activation (1st phase) period after which the facility will be handed over to a new organization inside the ITER host country. During the first phase, the machine will, immediately after shutdown, be de-activated and cleaned by removing tritium from the in-vessel components and any removable dust. De-activation will include the removal and safe disposal of all the in-vessel components and, possibly, the ex-vessel components. At the end of this phase, the ITER facility will be handed over to the organization inside the host country that will be responsible for the subsequent phase of decommissioning after a dormant period for radioactive decay.

1.9 Cost Estimates

1.9.1 Resources Required for ITER Construction

Although the details of arrangements for implementing ITER remain to be agreed, the items to be purchased are likely to be divided into three categories.

A. Those that can only sensibly be purchased by the host country.

B. Those which are of minor technical interest or size, and whose cost burden must therefore be shared by all Parties. For these items a centrally administered fund can be established.

C. Items of interest to all the Parties due primarily to their high technology content. To ensure each Party obtains its fair share of these items, the Parties must agree beforehand which ones each will contribute. To do this, all Parties must agree on their value to the project. This requires an agreed valuation of items, as described below. Each Party will contribute its agreed items "in kind", using the purchasing procedures and funding arrangements it prefers. Thus the actual costs to each Party (i.e., their share of A+B+C) may not correspond to the project valuation - it may differ due to competitive tendering as well as different unit costs.

The main objective of ITER cost estimates is to provide a realistic and sufficient basis for ITER Parties to make their decisions on the scope of their involvement and to select the desirable systems for them to manufacture. The estimates have been developed from the engineering designs following a “bottom-up” approach which emphasises physical estimates (such as labour hours, material quantities, physical processes, etc.) so as to ensure that the data are comprehensive and coherent and provide a basis for evaluating results from different Parties.

To arrive at an evaluated cost, or valuation, of ITER, about 85 “procurement packages” were developed for the elements of the project work breakdown structure (WBS). Each package comprises comprehensive information, including the functional requirements, detailed designs, specifications, interfaces and other relevant data that would be needed by potential suppliers in order to prepare for contract quotations.

Industrial companies or large laboratories with relevant experience were invited, through the Home Teams, to generate, from the procurement packages, their quantification of the stages in the manufacturing process, and their best estimates of the likely current costs of supply. The information thus generated offers a comprehensive database for cost analysis, comparison and evaluation.

The Joint Central Team analysed the results of the procurement package studies in consultation with Home Teams concerned. Financial data were converted from current costs to the established reference date for ITER cost estimates of Jan 1989, using standard inflation factors for each Party. It is not assumed that the 1989 exchange rates between currencies is better than those at any other date. In particular, exchange rates between any two currencies and interest/inflation rates in any two countries most often do not vary in any coherent way.

Physical quantities (e.g. man-hours, material quantities) were then assessed starting from the industrial estimates, and multiplied by a single set of labour rates (depending on the speciality and type of labour) and material unit costs across all packages, independent of the Party. World market prices have been used where they exist.

The final result is an evaluated cost estimate for building ITER, expressed in IUA [1 IUA = $ 1000 (Jan 1989 value)], which is robust to currency fluctuations and domestic escalation rates and which can be used by the Parties jointly and individually in reviewing their options and the possible budgetary effects of participating in ITER construction.

The evaluated cost estimate for ITER construction is presented in Table 1.9.1-1.

Taking account of the previous assumptions, the total value of the capital investment for ITER amounts to 2,755 kIUA. In addition the cost of spares and items needed only a few years after start of operation (for full DT operation) amounts to 258 kIUA. The present investment cost is about 50 % of the previous estimate for the ITER 1998 design, which amounted to 5603 kIUA and 302 kIUA deferred.

The procurement of the machine core (about 1500 kIUA) could be possibly split into about 40 different contracts of 40 kIUA in average. The procurement of Auxiliaries and Heating and CD systems, excluding the Concrete Building (about 800 kIUA) could be split into about 40 different contracts of 20 kIUA on average.

Table 1.9.1-1 Summary ITER Direct Capital Cost

	Direct Capital Cost (kIUA)	Percentage of Total	Deferred Investment (kIUA)
Magnet Systems	762.1	28%	40.2
Vacuum Vessel	230.0	8%	0.0
Blanket System	165.2	6%	8.6
Divertor	76.0	3%	6.9
Machine Assembly	92.7	3%	0.0
Cryostat	75.8	3%	0.0
Thermal Shields	28.8	1%	0.0
Vacuum Pumping & Fueling System	34.2	1%	6.8
Machine Core, subtotal	**1464.8**	**53%**	**62.5**
R/H Equipment	61.1	2%	52.3
Cooling Water Systems	131.5	5%	16.8
Tritium Plant	36.6	1%	45.2
Cryoplant & Distribution	88.9	3%	7.9
Power Supplies & Distribution	214.7	8%	3.5
Buildings	380.3	14%	12.0
Waste Treatment and Storage	2.1	0%	7.0
Radiological Protection	1.0	0%	3.2
Auxiliaries, subtotal	**916.2**	**33%**	**147.9**
IC H&CD	32.2	1%	2.0
EC H&CD	77.5	3%	3.0
NB H&CD	96.0	3%	0.2
Heating and CD, subtotal	**205.7**	**7%**	**5.2**
Diagnostics	118.0	4%	42.3
CODAC	50.0	2%	0.0
Grand Total	**2754.7**	100%	**257.9**

The ITER construction plan requires a specific schedule for the procurement of each system and therefore appropriate profiles of commitments and payments, the total of which will amount to the JCT estimated capital investment. The most important to consider is the profiles of payments and therefore the necessary cash flow. This important issue is discussed in detail later in Chapter 7 where ,under some assumptions, the peak annual payment reaches about 350 kIUA in the second year after T=0 and continues at this level until the seventh year so that most of the direct capital cost is paid in nine years.

1.9.2 Construction Management and Engineering Support

An estimate of the cost of construction management and support cannot be done without assumptions on the future organisation to execute the construction and the manner of contracting and managing contracts for procurement.

For this purpose, it is assumed that the ITER Legal Entity (ILE), which will be responsible for the management of ITER during its whole life, will provide a direct and effective line of accountability by incorporating all actors in a single management entity, including:

- an International Team at the ITER site that will have the overall responsibility to meet the project objectives and to ensure the design continuity and coherence;

- National Teams, as part of the ILE in each Party, which will manage and follow up the technical content of the procurement contributed by each Party, when the financial and legal contents of the relevant contracts are being taken care of by a Domestic Agency.

With these assumptions it is clear that the size of the International Team can be deduced approximately from its functions, but the size of each Party's National Team will depend on the level of the Party's contribution to ITER construction, on these specific packages in its contribution, and on the specific national practices in contract management.

To exercise its responsibilities, the International Team will probably include a core management group and a few technical groups, in charge of physics, safety, engineering, assembly, etc. These groups should be able to ensure technical continuity with the EDA and CTA, and, as construction approaches its end, these groups, suitably increased by personnel from the National Teams who have followed procurements, will eventually be involved in the integrated commissioning and start up of operation of the facilities.

The global man-years for the International Team during construction amounts to 840 PPY and a similar number for support personnel. The global estimate of professionals and support personnel (clerical, technicians and CAD) for the different National Teams to follow up all procurement contracts in all Parties amounts to about 960 PPY and twice this number for support personnel. Assuming the annual cost of one professional and one support staff member to be 150 IUA and 75 IUA respectively, the cost estimate for the International Team during construction until the start of ITER operation (integrated commissioning of the whole machine) amounts to 189 kIUA and the global estimate for all the National Teams during the same period amounts about 288 kIUA. Excluded from the above numbers are those relevant to diagnostic procurement that should be the responsibility of the Parties Laboratories (estimated resources of 220 professional person years needed) which will afterwards participate in ITER operations.

In addition to personnel costs, a certain amount of R&D during construction will still be necessary. Although the EDA has provided the principle qualification of design solutions to be implemented in ITER, during the manufacturing of components, proposed process improvements and design changes or unexpected difficulties could require new tests. It is therefore prudent to expect a spending in R&D of 60-80 kIUA during ITER construction.

1.9.3 Resources for ITER Operation

Manpower costs of permanent staff on site are costed assuming an average level of 200 professionals and 400 support staff (clerical, technicians and CAD), at 150 IUA and 75 IUA respectively per year; thus the annual personnel cost is about 60 kIUA. The permanent professional and support staff above are expected to operate and maintain the facility, and support the experimental programme.

Electric power costs, which not only include the power required for pulse operation, but also must cover energy consumption during various levels of standby/maintenance of the machine, depend on aspects of the load time profile and on the characteristics of the national electricity network of the host site. With some typical scenario and a unit cost of 0.05 IUA/MWh the estimated cost is about 30kIUA/year.

The ITER plant must be operated, taking into account the available tritium externally supplied. The net tritium consumption is 0.4 g/plasma pulse at 500 MW burn with a flat top of 400 s. Fuel costs include tritium burnt during operation, plus that lost by decay of the inventory (taken as 2 kg) during plant operation. There is no market for tritium for the quantities required, and thus tritium may have little or no monetary value. Nevertheless, a largely hypothetical 10 kIUA/kg for tritium purchase is used. The total tritium received on site during the first 10 years of operation, amounts to 6.7 kg. whereas the total consumption of tritium during the plant life time may be up to 16 kg to provide a fluence of 0.3 MWa/m^2 in average on the first wall. This corresponds, due to tritium decay, to a purchase of about 17.5 kg of tritium. This will be well within, for instance, the available Canadian reserves. Therefore the fuel costs are in average 6.7 kIUA per year during the first ten years, and probably 11.5 kIUA per year after.

In summary, the ITER average annual operation costs amount to about 60 kIUA for the personnel permanently on site, 30 kIUA for the energy consumption, 8 kIUA for the tritium purchase and 90 kIUA for spare parts, maintenance and improvements, i.e. a total average per year of 188 kIUA. Again this value will depend on the ITER site, mostly through the electricity cost (assumed to be 0.05 IUA/MWh), and on the specific arrangement between the Parties on how to support the personnel cost.

1.9.4 Decommissioning Costs

The ITER facility, because of the remote maintenance implemented during operation, offers initially most of the tools, procedures, and even trained staff, to accomplish the decommissioning operations. This capacity is an essential element in keeping the cost down. The estimated cost for decommissioning amounts to 250 kIUA for manpower costs and 85 kIUA for possible hardware costs.

1.9.5 Summary

A summary of the cost estimates for all phases of ITER plant life is set out in Table 1.9.5-1.

Table 1.9.5-1 Summary of ITER Cost Estimates

	Cost (kIUA)
Construction costs	
Direct capital cost	2755
Management and support	477
R&D during construction	60-80
Operation costs (average/year)	
Permanent personnel	60
Energy	~ 30
Fuel	~ 8
Maintenance/improvements	~ 90
Total	188
Decommissioning cost	335

1.10 Conclusions

The ITER project has its origins in the common recognition by the world's leading fusion programmes world-wide of :

- the potential of fusion as a practical long-term energy source, with acceptable environmental characteristics,

- the need for the next step on the path towards realising fusion energy to be the construction and operation of a burning plasma experiment allowing, in one device, full exploration of the physics issues as well as proof of principle, testing of key technological features of possible fusion power stations and demonstration of their safety and environmental characteristics, and

- the attractions of preparing to take such a step in an international collaborative framework which would allow participants to share costs and pool scientific and technological expertise towards a common goal.

After Conceptual Design Activities (CDA) between 1988-1990, the Engineering Design Activities (EDA) began in 1992 and are now completed with the ITER design as summarized in this report. Following the choice of site and the commitment by the ITER Parties of suitable funds, the construction phase (about 10 years) may start. This would be followed by an exploitation phase lasting roughly 20 years.

Nine years of intensive joint work by the ITER Joint Central Team and Home Teams of the four Parties (three after 1999) under the auspices of the IAEA have yielded a mature design supported by a body of validating physics and technology R&D, safety and environmental analyses and industrial costing studies. The ITER design meets all detailed objectives set by the ITER Parties, with margins in physics and technology to allow for uncertainties, whilst satisfying a cost target that makes possible for participants to benefit from the sharing of costs and the pooling of expertise that joint implementation allows.

The demanding technical challenges of the project and its international collaborative nature have led to the breaking of new technical ground in fusion science and engineering. In addition to the technical results, the project has demanded and enabled new modes of closer programmatic collaboration, among:

- physicists, in co-ordinating and collating experiments and results world-wide,
- technologists, in pursuing large, multi-Party projects on the key technological aspects of ITER design, and
- safety and environmental specialists, in pursuing a global approach to the specific safety and environmental characteristics of fusion as an energy source.

These advances provide assurance of the practicality of prospective joint implementation.

The ITER co-operation, in combination with the continuing general progress in fusion research, has brought its Parties and the world fusion development programme to the point at which they are technically ready and able to proceed to construction, thus bringing to successful fruition the Parties' efforts, investments and aspirations to date. By enabling, in a single device, full exploration of the physics issues as well as proof of principle and testing of key technological features of possible fusion power stations, ITER will provide the integration step necessary to establish scientific and technical feasibility of fusion as an energy source.

2 Plant Description: Tokamak System Design and Assessment

2.1 Magnets

2.1.1 Magnet System General Description

2.1.1.1 System Description and Main Parameters

The magnet system for ITER consists of 18 toroidal field (TF) coils, a central solenoid (CS), six poloidal field (PF) coils and 18 correction coils (CCs). The magnet system elevation is shown on Figure 2.1.1-1.

The TF coil cases, which enclose the TF coil winding packs, form the main structural component of the magnet system. The TF coil inboard legs are wedged all along their side walls in operation, with friction playing an important role in supporting the out-of-plane magnetic forces. In the curved regions above and below the inboard leg, the out-of-plane loads are supported by four upper and four lower poloidal shear keys arranged normal to the coil centreline. In these regions, the coils are linked by means of two upper and two lower

pre-compression rings which provide a radial centripetal force and improve the operation of the shear keys. In the outboard region, the out-of-plane support is provided by four sets of outer intercoil structures (OISs) integrated with the TF coil cases and positioned around the perimeter within the constraints provided by the access ducts to the vacuum vessel. The OISs are structures acting as shear panels in combination with the TF coil cases. There is low voltage electrical insulation between TF coils in the inboard leg wedged region and between the OIS connecting elements in order to avoid the circulation of eddy currents.

N 10 GR 1 00-12-07 W 0.1

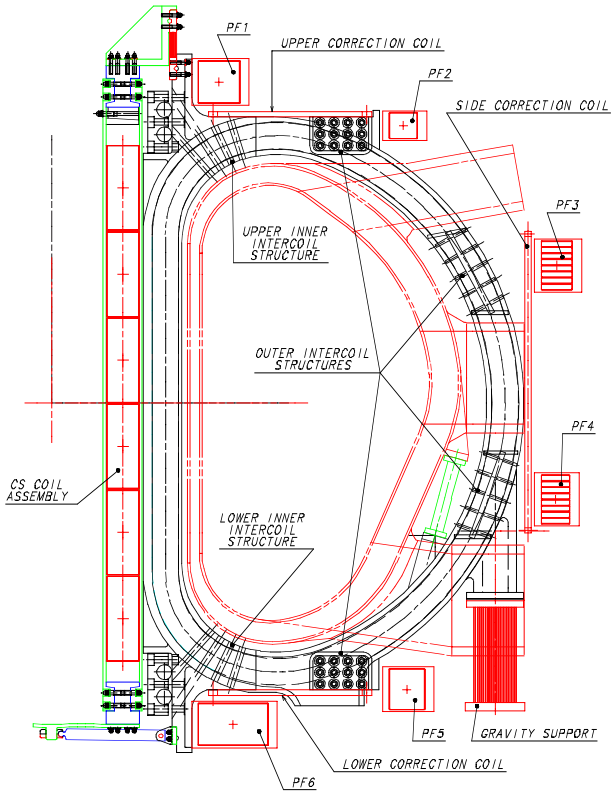

Figure 2.1.1-1 Magnet System Elevation

The CS consists of a vertical stack of six independent winding pack modules. The stack is hung from the top of the TF coils through flexible supports and is provided at the bottom with a locating mechanism which acts as a support against dynamic horizontal forces. The CS pre-load structure, which consists of a set of tie-plates located outside and inside the coil stack, provides axial pressure on the stack. The number of CS modules has been selected to satisfy the plasma equilibrium requirements. The CS coil stack is self-supporting against the coil radial forces and most of the vertical forces, with the support to the TF coils reacting only the weight and net vertical components resulting from up-down asymmetry of the poloidal field configuration.

The six PF coils (PF1 to PF6) are attached to the TF coil cases through supports which include flexible plates or sliding interfaces allowing radial displacements. The PF coils provide suitable magnetic fields for the plasma equilibrium and control and their position and size have been optimized accordingly, within the constraints imposed by the access to the in-vessel components.

Outside the PF coils are located three independent sets of correction coils (CCs), each consisting of six coils arranged around the toroidal circumference above, at and below the equator. These coils are used to correct non-axisymmetrical error fields arising from errors in the position of the TF coils, CS and PF coils and from the NB injection magnetic field correction system, and to stabilise plasma resistive wall modes.

Both CS and TF coils operate at high field and use Nb_3Sn-type superconductor. The PF coils and CCs use NbTi superconductor. All coils are cooled with supercritical helium in the range 4.4 - 4.7K. The conductor type for the TF coils, CS and PF coils is a circular cable-in-conduit multistage cable with about 1,000 strands cabled around a small central cooling spiral tube. The operating currents are 40 - 46 kA for the CS and PF coils and 68 kA for the TF coils. The CCs use a reduced size conductor (about 300 strands) without the central cooling channel.

The coil turn and ground electrical insulation consists typically of multiple layers of kapton-glass impregnated with epoxy resin. Epoxy-glass is used extensively to fill tolerance gaps. The CS and PF coils are pancake wound with a conductor that has a square outer section. The TF coils use a conductor with a circular outer section that is contained in grooves in so-called “radial plates”. There is one radial plate for each double pancake and the conductor is contained in grooves on each side.

Gravity supports, composed of pedestals and flexible elements (one under each TF coil), support the whole magnet system. Each TF coil is electrically insulated from its own support to avoid the circulation of eddy currents between TF coils. The TF coil case also supports the vacuum vessel (VV) and in-vessel component weight and operational loads.

All TF coils, the CS and the upper and outer PF coils (PF1 to PF4) are designed to be removable from the machine in case of a major fault. Individual double pancakes of the PF coils may be disconnected and by-passed in situ in case of fault, since the PF coils have accessible joints located on their external side. In addition, the cryostat design allows the lower (trapped) PF coils (PF5 and PF6) to be rewound in situ under the machine.

In Tables 2.1.1-1, 2 and 3 the main magnet parameters are listed.

Table 2.1.1-1 Overall Magnet System Parameters

Number of TF coils	18
Magnetic energy in TF coils (GJ)	~ 41
Maximum field in TF coils (T)	11.8
Centring force per TF coil (MN)	403
Vertical force per half TF coil (MN)	205
TF electrical discharge time constant (s)	11
CS peak field (T)	13.5
Total weight of magnet system (t)	10,130

Table 2.1.1-2 Parameters for TF Coils and CS

	TF Coil	CS *
		Modules CS 1, 2, 3
Overall weight (including structures) (t)	312x18	925
Coil current (MA)	9.13	24.2 at EOB (12.8 T)
Number of turns per TF coil / CS module: Radial Toroidal / Vertical Total	 11 14 134	 14 38 522
Conductor unit length (m)	760 (double pancakes)	881 (for 6 pancakes) 579 (for 4 pancakes)
Turn voltage (V)	26.5 (discharge)	20 (IM)
Ground/Terminal voltage (kV) in normal operation	3.55 / 3.55 ** (2 coils in series)	5 / 10
Number of current lead pairs	9	6 ***

* CS parameters are for the design option using an Incoloy square jacket.

** A voltage surge (of a few ms) caused by the jitter of the switches may reach about 5 kV.

*** The current leads for CS modules 1 (upper and lower) are connected in series outside the machine and the power supplies and discharge units are interleaved to limit the ground voltage to 5 kV in normal operation.

Table 2.1.1-3 Parameters for PF Coils

	PF1	PF2	PF3	PF4	PF5	PF6
Winding weight (t)	145	129	385	353	255	263
Max. coil current capacity (MA)	11.34	4.39	8.46	7.74	9.90	19.26
Number of turns per coil: Radial Vertical Total	 16 16 252	 11 10 107	 12 16 118	 11 16 172	 14 16 220	 27 16 428
Conductor unit length (m) (double pancake, two-in-hand)	392	560	884	807	727	723
Maximum Turn voltage (V)*	625	1750	875	1000	875	714
Ground/Terminal voltage (kV)*	5/10	7/14	7/14	7/14	7/14	5/10

* Turn voltages are for a two-in hand winding configuration. For PF2 to PF5, a vertical stabilisation voltage of 9 kV (on-load voltage) is assumed, allowing 3 kV above the present 6 kV converter design for possible upgrades.

2.1.1.2 Physical and Functional Interfaces

The magnets are located within the cryostat which provides the thermal insulation for the 4.5K superconducting coils from the ambient heat load. This is done by a vacuum within the cryostat to eliminate the convective heat loads, and by the use of intermediate thermal shields at 80K to intercept the bulk of the thermal radiation and conduction from the cryostat and the vacuum vessel.

Feeders to the coils include the superconducting busbars, cryogen service lines, and instrumentation cables. These feeders run from individual coil terminals inside the cryostat, through cryostat feedthroughs (CF) and into coil terminal boxes (CTBs) or structure cooling valve boxes (SCVBs). These boxes are located outside the cryostat and bioshield, in the tokamak galleries which are accessible for hands-on maintenance. The interfaces between the magnet system and the power supplies and the cryoplant are at these boxes.

Power Supplies

The interface between power supplies and the magnets occurs at the CTBs where the transition is made from superconducting busbars to room temperature (water-cooled aluminium) busbars.

The power supplies have two physical interfaces to the magnets.

i) The current supplies and discharge circuits for the coils. These consist of one supply for the 18 TF coils plus 9 discharge resistors connected between each coil pair. Each PF and CS coil module has its own supply and discharge resistor.

ii) The magnet structure grounding scheme. The magnet structures are all connected to ground through the busbar containment pipes to the cryostat wall. The connection of the cryostat into the overall machine grounding scheme is part of the power supplies.

Cryoplant

The boundary between the cryoplant system and the magnet helium manifolding occurs at the CTBs and SCVBs. These boxes contain the adjustable valves that allow the proper distribution of the helium flow into the magnet components.

In operation, the cryoplant provides supercritical helium to the four sets of coils (TF, CS, PF and CCs), their superconducting busbars, and the magnet structures. The coils, busbars and structure cooling systems are subdivided into a number of closed loops where supercritical helium is circulated by a pump and recooled through a primary heat exchanger located in the auxiliary cold boxes of the cryoplant. For the coils, the supercritical helium is supplied in the temperature range of 4.4 - 4.7K. The cryoplant also supplies liquid helium to the current leads and receives back gaseous helium at room temperature from these current leads.

For the cooldown of the magnet system, the primary heat exchanger is bypassed and cold gaseous helium is passed directly from the cryoplant compressors through the magnets and structures. In this phase, the maximum temperature difference between coil/structure inlet and outlet flows is 50K to limit thermal stresses, and the cooldown rate is about 0.5K/hr. Once the magnet temperature reaches 80K, helium at about 5K can be supplied by the cryoplant and gaseous helium returned from the coils. Once the coils reach the operating temperature, the pump and primary heat exchanger are put back into the circuit.

In the case of a TF coil quench (including the TF coil quench which occurs after a fast discharge), the primary circuit is vented initially to a cold holding tank at 80K and then to tanks at 300K if the capacity of the cold storage is exceeded. The vent opening pressure in the primary loop is 1.8 MPa.

2.1.1.3 Heat Loads

During operation, heat from external sources and from the magnets themselves is deposited in the magnet system. Thermal radiation from the 80K cryostat thermal shield is deposited on the outer surface of the TF coil cases and structures and the PF coils. Thermal radiation from the vacuum vessel shield is deposited on the TF coil case inner surfaces. Heat is conducted from the machine gravity supports, the vacuum vessel supports and the vacuum vessel thermal shield supports.

Nuclear heat is the dominant heat load for the TF coils and is essentially deposited along the inner surface of the inboard legs. Table 2.1.1-4 shows the distribution of the nuclear heat in the TF coil cases and winding pack. The values shown are used for the assessment of the coil performance and may not reflect the latest details of shielding design. Nuclear heat is also deposited in the PF coils in the vicinity of the vessel ports. There is also heat from gamma radiation due to the activation (^{16}N) of the cooling water of in-vessel components. This heat load is small and is deposited essentially in PF coils and feeders in the vicinity of the heat transfer system pipes. All external heat loads are summarized in Table 2.1.1-5, which also shows the internal heat loads due to the operation of the magnets. These include AC losses in conductors, eddy current losses in structures, and resistive losses in joints. The table also includes the losses associated with the magnet feeders and the liquid helium requirements to cool the current leads where the transition is made from superconducting busbars to room temperature busbars.

Table 2.1.1-4 Nuclear Heating in the TF Coils (kW) for the 15 MA Reference Scenario with a Total Fusion Power of 500 MW

	Inboard Leg	Behind Divertor	^{16}N	Around Ports	Total
Coil Case	4.82	1.50	0.4	1.56	8.28
Winding Pack	5.11	0.31			5.42
Total	9.93	1.81	0.4	1.56	13.70

Table 2.1.1-5 Heat Loads in the Magnets and Liquid Helium Requirements for Current Leads (15 MA Reference Scenario with a Total Fusion Power of 500 MW)

Heat loads	TF cases & structures	TF winding	PF & corr. coils	CS & CS structure	Total**
Nuclear heating	8.28 kW during burn	5.42 kW during burn	0.40 kW during burn	0	Average value 3.13 kW
AC & eddy current losses	5.50 MJ	1.36 MJ*	0.78 MJ*	5.28 MJ*	Average value 7.17 kW
Joints	0.0	1.00 kW	0.08 kW average	0.05 kW average	1.13 kW average
Thermal radiation Cryostat Vacuum vessel	5.20 kW 0.28 kW	0	0.11 kW	0.01	5.60 kW
Thermal conduction Gravity supports VV supports Thermal shield	2.0 kW 1.7 kW 0.1 kW	0	0	0	3.8 kW
He feeders, SC bus bars and CTBs	0.77 kW		0.66 kW	0.37 kW	1.8 kW
Helium flow rates for current leads	0.0	61.2 g/s	19.1 g/s	16.1 g/s	96.4 g/s

* A coupling loss time constant of 50 ms is assumed.
** The average values are for a 400 s burn with a 1800 s pulse repetition.

2.1.2 Magnet Structures

2.1.2.1 Description

The TF magnet is subjected to two main force systems. The in-plane loads are generated by the interaction of the current in the TF coils with the toroidal field. The out-of-plane loads are generated by the interaction of the current in the TF coils with the poloidal field. The TF coil cases are the main structural component of the magnet system and they provide support against the TF coil in-plane as well as out-of-plane loads. The PF coils, CS and vacuum vessel are attached to the TF coil cases through supports which are rigid in the vertical and toroidal directions but flexible in the radial direction. In this way, the TF coil cases connect all the PF coils and the CS with the vacuum vessel, and balance all the electromagnetic forces within the magnet assembly. This arrangement results in a compact design without load transmission to structures external to the TF coil cases. Figure 2.1.2-1 shows a TF coil case with all attachments.

N 11 GR 645 01-05-30 W 0.1

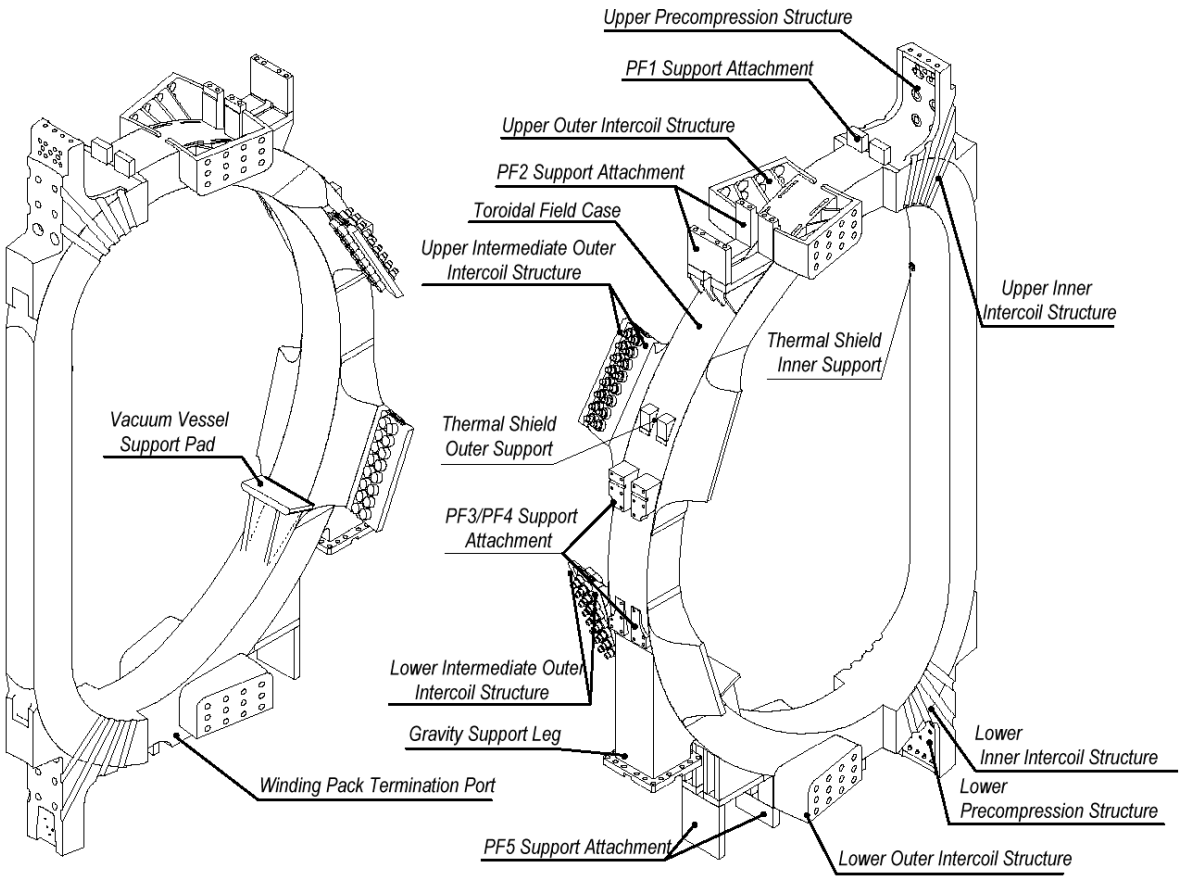

Figure 2.1.2-1 TF Coil Case

Inboard Region

The centring force on each TF coil is reacted by toroidal hoop pressure in the central vault formed by the straight inboard legs of the coils. The front part or "nose" of each coil case is thickened for this purpose. All along their inboard legs, the coil cases are wedged over their full radial thickness. About 40% of the centring force is reacted through the winding pack of the coil and 60% is reacted by the case. The wedging surfaces must be accurately matched to achieve the required magnetic alignment and reduce stress peaks under the large toroidal wedging pressure of about 590 MPa at the "nose" of the coil cases. Machining of the wedging surfaces will ensure that deviations from flatness have only long wavelength and do not result in localised peak stress. Systematic errors, in particular on the wedge angle, could result in significant stress intensification and must be kept within tolerable limits. Analysis has shown that a local assembly gap of 0.4 to 0.6 mm between adjacent wedging surfaces is acceptable, even if all coils have the same error. For each coil, the flatness tolerance band is therefore 0.2 to 0.3 mm and this is considered achievable by precision machining.

Insulation is required between coils to avoid eddy current flow from coil to coil. The insulation will consist of a thin layer of epoxy-glass or ceramic coating which must resist the essentially static compressive load of 590 MPa. R&D activities have been initiated to cover this requirement. A high friction factor is required as friction transmits a significant fraction of the overturning moments. The minimum acceptable friction factor is about 0.2 and it is desirable to achieve higher values.

Inner Intercoil Structures

The inner intercoil structures (IISs) are situated at the inboard curved regions, immediately above and below the inboard straight leg of the TF coils (Figure 2.1.2-2). These regions are particularly critical because this is where the out-of-plane loads are highest and the space available for structures is restricted between the TF coils. At each IIS, the cyclic out-of-plane loads are resisted by a set of four shear keys between the coils. The keys run normal to the coil centreline in key slots machined in the coil case, which is locally thickened. The keys prevent the development of torsion in the cases, which can make a large contribution to the case tensile stresses. At the same time, the relative flexibility of the case in bending gives an almost uniform poloidal distribution of load on the four keys. The shear load per key is in the range of 15 to 19 MN.

N 11 GR 646 01-05-30 W 0.1

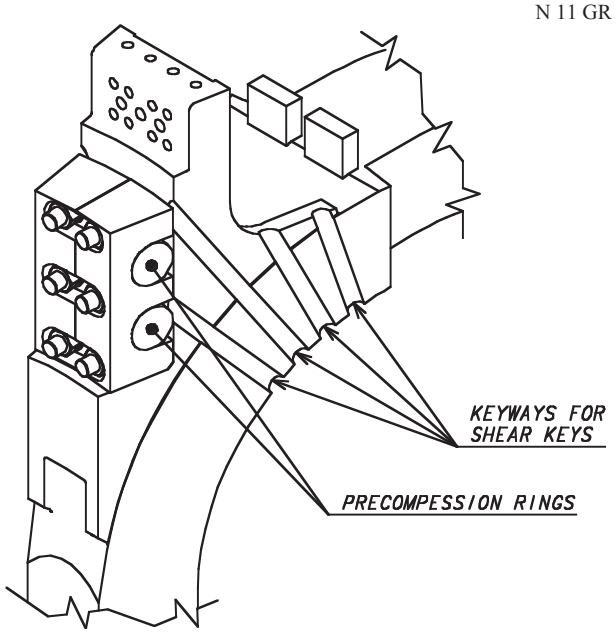

Figure 2.1.2-2 Inner Intercoil Structure

In the inboard curved region, the radial expansion of the coils during energisation results in the opening of toroidal gaps between adjacent cases. Although small, the radial movement is sufficient to create a toroidal gap of about 0.35 mm between key and key slot. During plasma operation, the shear loads acting on the keys tend to increase this gap to more than 1 mm. In order to suppress this undesirable effect, and ensure that the keys do not become loose in their slots, the TF coils are put under a centripetal pre-load at assembly. This pre-load is provided by two pre-compression rings at the top and bottom of the TF coil inboard legs. The rings are tensioned at assembly and the load is transmitted to the TF coils by bolts oriented in the radial direction. The TF coils are therefore put into toroidal compression. Analysis shows that with a radial centripetal pre-load of 60 - 70 MN per TF coil, the toroidal separation in the key region is almost completely eliminated. To be effective, these pre-compression rings need to have a significantly lower elastic modulus than that of the case, so that the pre-compression is not sensitive to assembly tolerances. In view of the limited space available, the rings require a high strength material. Finally, the rings should have a high electrical resistance to avoid the circulation of excessive eddy currents. A material satisfying these requirements is a unidirectional glass fibre-epoxy composite which can be made using a wet glass fibre (S-glass) filament winding technique. The stresses in the rings are limited by pre-

tensioning at room temperature since the material is stronger at 4K. There are no significant extra stresses due to the out-of-plane movements of the TF coils. Table 2.1.2-1 summarises the main requirements for the rings. R&D activities to establish the allowable stress and creep behaviour of unidirectional glass fibre composites are under discussion.

Table 2.1.2-1 Mechanical Parameters for Pre-compression Rings

Material	Peak tensile stress at room temperature (MPa)	Cross-sectional area of two rings (m^2)	Radial displacement to apply pre-compression (mm)
Fibreglass	587	0.22	~ 23

The pre-compression rings increase the overall stiffness of the IIS and contribute to lowering stresses in this region, thus increasing the fatigue life of the TF coil case.

Outer Intercoil Structures

There are four OISs. The upper and lower OISs are located respectively above the upper ports and below the divertor ports of the vacuum vessel. The upper and lower intermediate OISs are located respectively above and below the equatorial ports.

The OISs directly above and below the equator are required to support the out-of-plane forces on the outboard part of the coil. There is a large shear force (in the vertical direction) of about 20 MN acting on each of these two OISs. There is also a toroidal tensile load due to the radial expansion of the coil outboard leg. The pre-load provided by the pre-compression rings significantly reduces this toroidal tension to values of about 8 MN per OIS.

The poloidal extent of the two equatorial OISs belts is limited by the vertical size of the vacuum vessel ports and, due to this limitation, relatively high cyclic stresses occur at the re-entrant corners where the OISs connect to the TF coil cases. Local structural reinforcements and smooth transitions are required to keep stresses within allowable limits. In the current design, the OISs consist of shear panels, with a thickness of about 130 mm, protruding from the side walls of the case. Shear load transmission is provided by multiple-finger friction joints which are welded to the two adjacent shear panels after survey at assembly. The joints are pre-loaded by two rows of insulated bolts acting on the fingers separated by insulated washers. With this multi-finger arrangement, the friction surfaces and the shear capability of each bolt is multiplied by 5. The cross section of a friction joint is shown in Figure 2.1.2-3. Access to the vacuum vessel supports is required during the tokamak assembly and is available before welding of the multi-finger joint.

N 11 GR 557 00-12-07 W 0.1

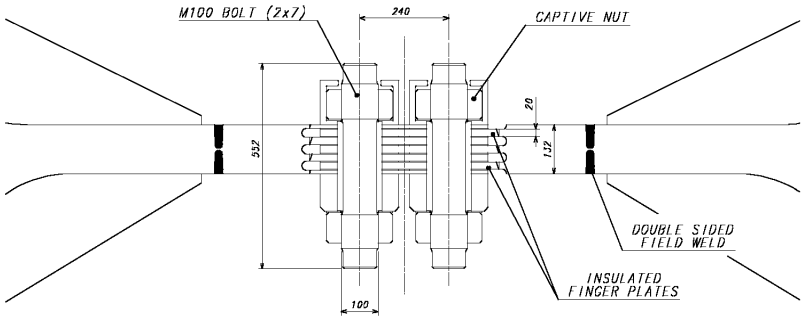

Figure 2.1.2-3 Cross Section of Friction Joint

As an alternative to this friction joint design, a box structure integral to the case has been developed (Figure 2.1.2-4). In this design, shear load transmission is accomplished by insulated bolts and shear keys. This box structure includes a removable central part which is required to gain access to the vacuum vessel supports during assembly. The box structure has been analysed and found to provide adequate out-of-plane support. Its advantage, as compared to the friction joint, is to eliminate in-situ welding. It requires, however, precision machining of the keyways. The final choice between these two design options will be made taking manufacturing aspects and cost into consideration.

N 11 GR 647 01-05-30 W 0.1

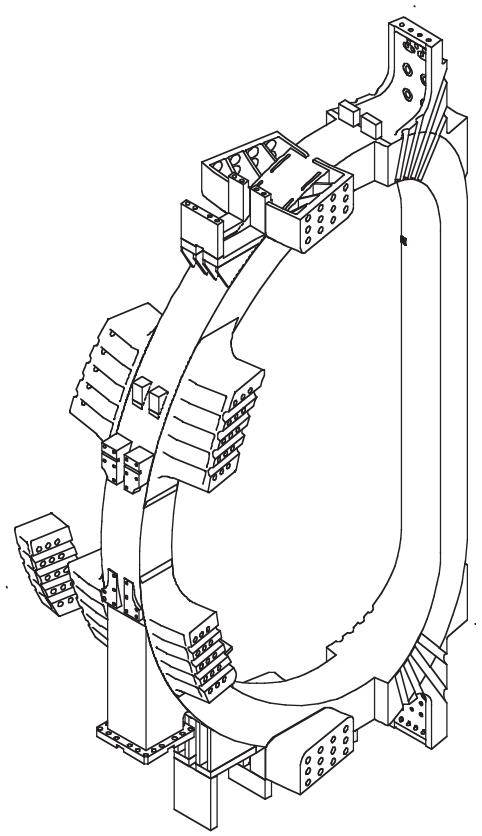

Figure 2.1.2-4 Coil Case showing the Alternative OIS Box Design

Vacuum Vessel Supports

The vacuum vessel supports are attached to the TF coils at a poloidal location just below the equatorial port level, thus minimizing the distance from the TF coil gravity support pedestals. This reduces the toroidal rotation of the whole vessel during machine pulses. These supports are of laminated construction to allow differential radial displacements between the TF coils and the vacuum vessel while providing toroidal registration. The supports are designed to resist gravity, seismic and all electromagnetic loads on the vacuum vessel. The supports must also transmit bending moments caused by vacuum vessel deformations and by TF coil tilting motions.

The thermal load from the hot vessel to the TF coil cases is reduced by a thermal "anchor" consisting of cooling channels for 80K helium gas, half way up the support.

Gravity Supports

The gravity supports for the machine are shown on Figure 2.1.2-5. They are placed under the outer curved region of each TF coil between the PF4 and PF5 coils. Electrical insulation is placed between each TF coil and the top surface of the support pedestal to avoid eddy currents. The machine gravity support pedestals are equipped with flexible plates, so that they can deflect in the radial direction to allow thermal contraction or expansion of the magnet system, but they are rigid against out-of-plane bending caused by TF coil out-of-plane displacement or seismic motion. The pedestals are connected, at their lower ends, to a rigid supporting ring, which is an integral part of the cryostat structure. This ring resists the bending moments transmitted by the pedestals but transfers horizontal seismic loads to the building through horizontal tie plates. The gravity load is transferred to the building through 18 cylindrical support columns (Figure 2.1.2-5).

N 11 GR 559 00-12-07 W 0.1

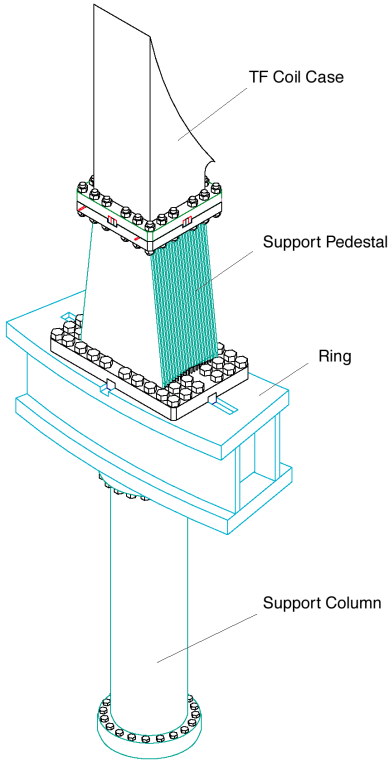

Figure 2.1.2-5 Gravity Support

Thermal conduction from the room temperature supporting ring to the TF coils is reduced by a thermal anchor consisting of cooling channels for 80K helium gas, at a distance of about 600 mm below the top flange of the support pedestals.

Analysis of the gravity supports has been carried out under a number of load combinations which include gravity loads, seismic loads and imposed displacements or moments associated with the motion of the magnets due to thermal contraction and electromagnetic loads. The design meets all requirements for both room and operating temperature conditions.

PF Coil Supports

Each of the PF coils is self-supporting with regard to the radial magnetic loads, and the supports for these coils have been designed to allow for free radial expansion of the coils by using flexible plates or sliding supports. The vertical and lateral loads on each PF coil are transmitted through these supports to the TF coil cases. There are also bending moments due to the tilting motion of the TF coils which is transmitted from the TF coils to the PF coils.

The PF2 to PF5 coils have 18 supports while, because of their smaller diameter, the PF1 and PF6 coils have only 9 supports around their toroidal circumference. A typical support is shown on Figure 2.1.2-6. At each PF coil support, the winding pack is clamped between a pair of plates linked by tie-rods. For the PF2 to PF5 coils, there are flexible plates which provide the link between the TF coil case and one of the clamping plates. For the PF1 and PF6 coils, sliding supports have been provided due to space limitations. For these sliding supports, a low friction material (fibreslip) is placed directly between the clamping plates and the TF coil case surfaces.

N 12 GR 31 00-12-07 W 0.1

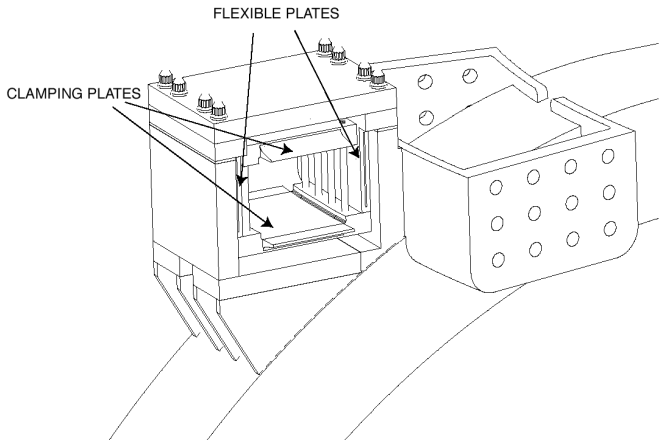

Figure 2.1.2-6 PF2 Coil Clamp (winding pack not shown)

2.1.2.2 TF Magnet Structural Assessment

Structural Design Criteria

The stresses are assessed in terms of plasticity (static limit), fast fracture and fatigue behaviour.

The static stress limit is dependent on the material and the static stress system it has to support. Following the ITER structural design criteria for materials at cryogenic temperatures, operation up to 2/3 of the yield stress is allowed for primary membrane stress systems and up to 30% above this for primary membrane plus bending stresses. For welds, these values are decreased by factors specified in the design criteria. The material is assumed to be one of the family of strengthened austenitic steels defined in ITER materials specifications that have been developed for cryogenic applications.

The fatigue assessment method, which is applied to the TF coil cases, uses a crack growth analysis based on linear elastic fracture mechanics (LEFM). In this type of analysis, the growth of an initial defect is calculated until the defect either penetrates the whole wall thickness of the component or the stress intensity factor reaches the critical value (K_{IC}). To cover uncertainties in the analysis, three safety factors are applied: a) a factor of 2 on the initial defect area that can be detected; b) a factor of 2 on the number of fatigue life cycles; c) a factor of 1.5 (for normal operation conditions), on the value of K_{IC}.

In-plane Loads at the Inboard Leg

A 2D model of the TF coil at the inboard leg has been used for the analysis**.** This model includes details of the conductor and conductor insulation, the radial plates, the ground insulation and the case. The loads applied are the Lorentz forces acting on each conductor, and the poloidal tensile strains on the case and winding pack. These strains have been calculated with the global model described below. The Lorentz forces are reacted by the toroidal wedging pressure. Table 2.1.2-2 summarizes the main results of this analysis and, in particular, how the poloidal tensile and toroidal compressive forces are shared between the case and the winding pack. Figure 2.1.2-7 shows the stress intensity (Tresca) in the TF-coil casing and radial plates**.** All stresses are found to be within allowables.

Table 2.1.2-2 Force and Stress at TF Inboard Leg

Vertical force: - Winding pack - Case	(MN)	 40 60	
Toroidal force: - Winding pack - Case	(MN/m)	 - 60 - 82	
Maximum stresses in:	Stress Type	Stress Value (MPa)	Allowables (MPa)
Case nose (at wedging surface)	S_I S_{tor} P_m P_m+P_b	665 594 520 670	 667 867
Radial plates	P_m+P_b	701	867
Insulation (average shear)	S_{xy}	30	42*

S_I: Tresca stress; S_{tor}: toroidal stress; P_m: primary membrane stress; P_b: bending stress; S_{xy}: shear stress; *: shear stress allowable with > 36 MPa compression.

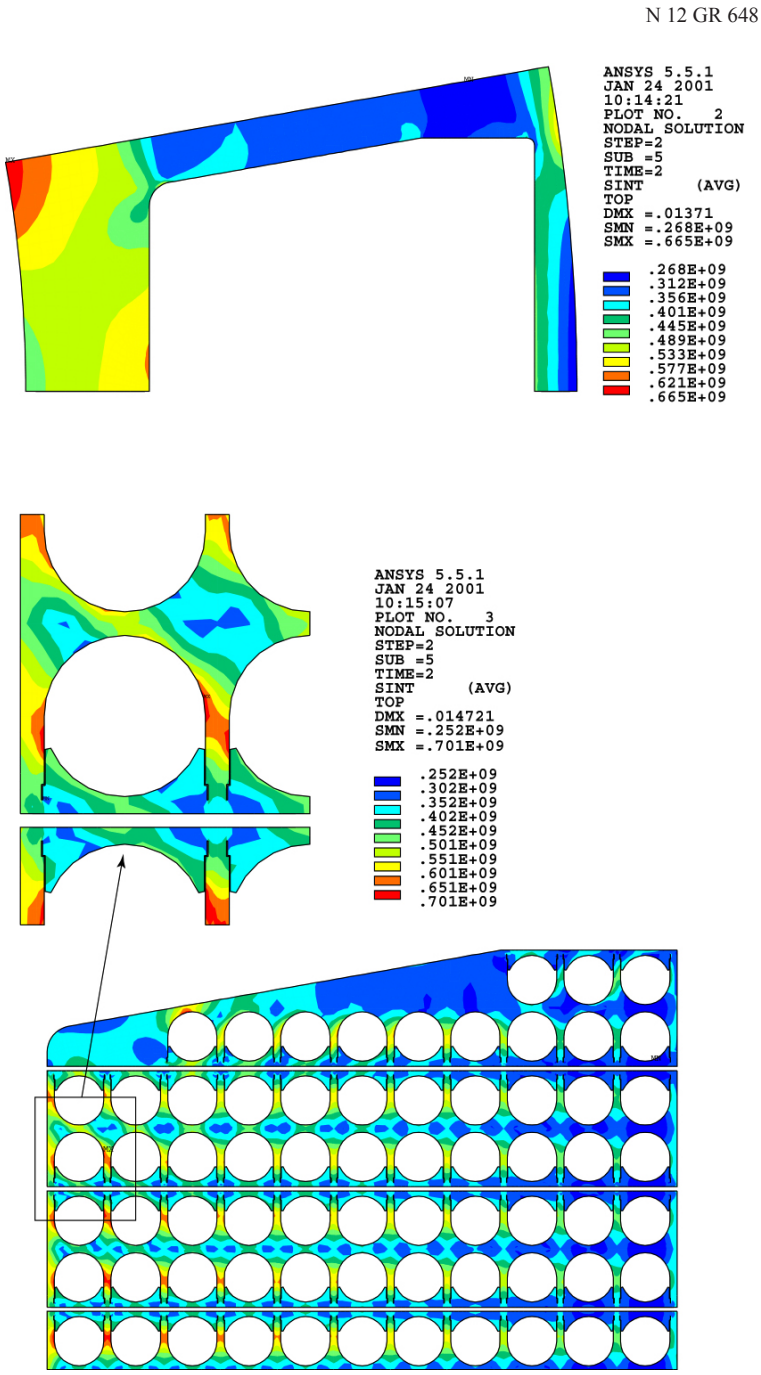

Figure 2.1.2-7 Stress Intensity (Pa) in TF Coil Casing and Winding Pack Radial Plates in Inboard Region

Global Stress Analysis of the TF Coils

The global finite element model of the TF coils and structures is shown on Figure 2.1.2-8. The model incorporates the out-of-plane support structures and gravity supports. The pre-compression rings are not included but their effect has been simulated by local radial forces. The TF coil winding pack is represented by smeared material elastic properties. The model incorporates both in-plane and out-of-plane loads and the load cases considered include loading of the pre-compression rings at room temperature, TF magnet cool-down, TF magnet energisation, initial CS magnetization (IM) defined as the state when the CS is fully

energised just before plasma initiation, and end of burn (EOB). The scenarios considered are the reference 15 MA plasma scenario and a number of other scenarios including in particular the 17 MA plasma scenario.

N 11 GR 560 00-12-07 W 0.1

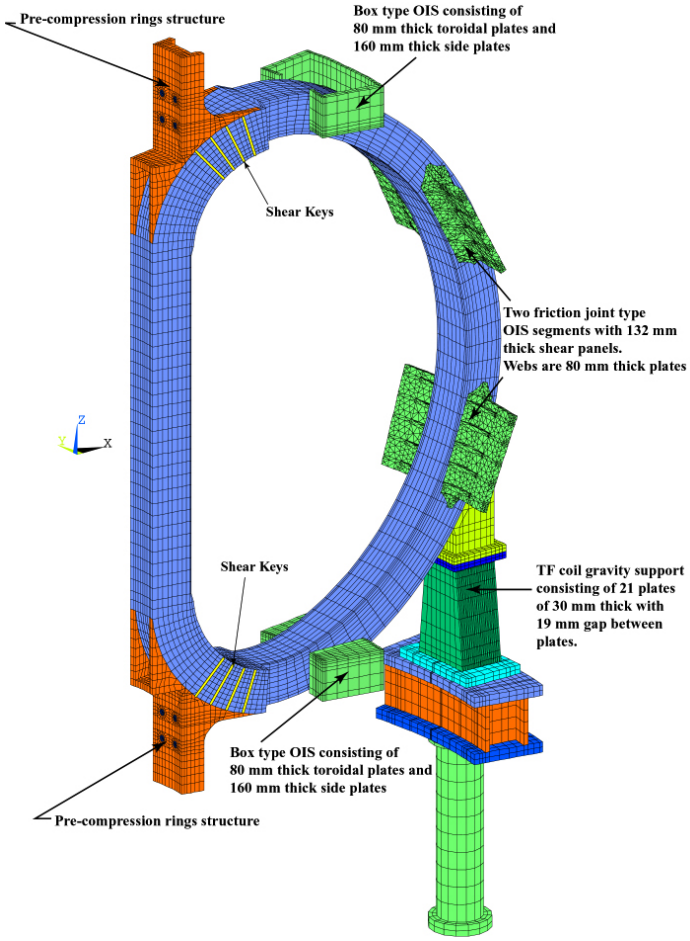

Figure 2.1.2-8 Finite Element Model for TF Coil Analysis

Critical regions have been identified at the upper and lower inboard curved regions where the coils are no longer wedged and behave as unsupported curved beams. In these regions, the out-of-plane forces peak and reverse direction (due to the presence of the PF1 and PF6 coils). These curved regions of the coil case have stress peaks located at the side walls at the end of the straight leg and in front of the shear keys.

Other critical regions are at the outboard legs in the vicinity of the intermediate OISs. Table 2.1.2-3 shows that the two intermediate OISs carry the bulk of the outboard leg shear loads associated with the TF coil overturning moment.

Table 2.1.2-3 Shear Loads (MN) on OIS (15 MA, End of Burn)

	Radial shear	Vertical shear
Upper OIS segment	1.1	1.55
Lower OIS Segment	0.73	1.83
	Maximum shear	
Upper intermediate OIS segment	22.7	
Lower Intermediate OIS segment	25.6	

These large shear loads generate bending moments and local stress in the case and OISs. Stress peaking occurs at the re-entrant corners where the OISs connect to the TF coil cases. These stress peaks have been mitigated by the use of large (500 mm) corner radii and local thickening of the structures. Such design features are compatible with a production of these parts by casting.

The fatigue analysis has been carried out assuming initial defects which are typical of the material and type of production (forgings and castings). A certain level of manufacturing residual stress has also been taken into account for forged sections and welds. Results are shown in Table 2.1.2-4 for the most critical locations. The allowable number of cycles shown in the table exceeds the required number of 60,000 (30,000 tokamak cycles with a safety factor of 2).

Table 2.1.2-4 Fatigue Life in the TF Coil Case and OIS (15 MA Scenario)

Location	Type and area (mm^2) of postulated initial defect	Allowable number of stress cycles
Bottom of inboard leg, side wall	Sub-surface defect in forged base metal, 10 mm^2	256,000
Bottom of inboard leg, side wall	Sub-surface defect in weld, 20 mm^2	99,000
OIS panel (at attachment to case wall)	Sub-surface defect in cast base metal, 30 mm^2	156,000

The results above are for a 15 MA plasma scenario. Analysis of the 17 MA scenario shows that the cyclic stresses tend to increase in proportion to the plasma current. The conclusion is that operation at 17 MA is possible but not for the full fatigue life (30,000 cycles) of the machine.

2.1.3 Conductor Design

2.1.3.1 Conductor Design Criteria

The conductor design is governed by the three criteria of temperature margin, stability and hot spot temperature.

Temperature Margin

For Nb_3Sn, the temperature margin, from the maximum predicted temperature at any point to the local (i.e. based on local peak field on the cable) current sharing temperature must be > 1K during plasma operation. In steady operation without plasma (i.e. in stand-by mode or

after a plasma disruption), the temperature margin must be > 0.5K. For NbTi, the temperature margin must be > 1.5K.

Heat Transfer to Helium and Stability

The well-cooled, ill-cooled criterion, based on empirical assessments of coil performance, is used as a basis for the design with a heat transfer coefficient (which includes safety factors) of 1,000 W/m^{2}K in Nb_3Sn and 600 W/m^{2}K in NbTi.

Hot Spot

The maximum temperature that may be reached locally inside the conductor in the event of a quench has been determined by the differential expansion between conductor materials. Below 150K, materials have a low thermal expansion and 150K is therefore selected as the maximum temperature that may be reached by the conductor jacket. The cable inside the jacket may reach up to 250K on a transient basis as it is much more flexible than the jacket.

2.1.3.2 TF Conductor

The conductor is a circular Nb_3Sn cable-in-conduit with a central cooling channel, cooled by supercritical helium. The TF conductor is almost identical to the conductor used for the TF model coil. As a result, the TF model coil development programme and manufacturing experience[1] are fully applicable, and have been used to establish the reference strand parameters (Table 2.1.3-1).

The conductor parameters are shown in Table 2.1.3-2 and the conductor design in Figure 2.1.3-1. The conductor current of 68 kA is determined by the geometrical fit of the conductors into the winding pack at the inboard leg, and the maximum allowable value of 70 kA.

N 11 GR 561 00-12-07 W 0.1

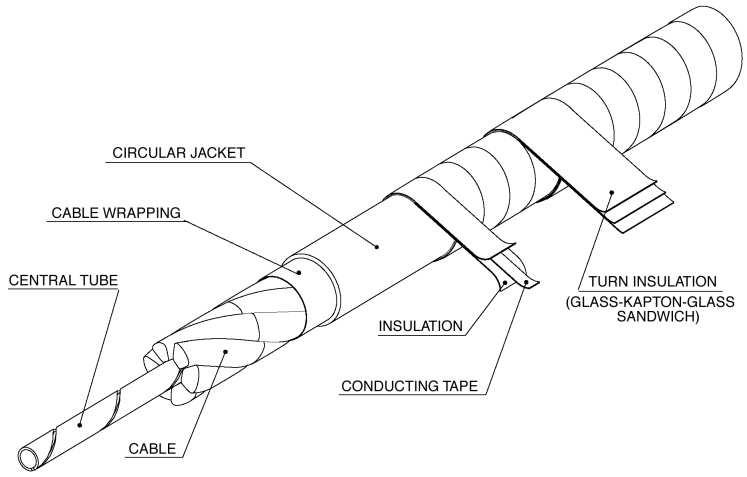

Figure 2.1.3-1 TF Coil Conductor Design

[1] K. Okuno, et al., "Key Features of ITER-FEAT Magnet System," 21st Symposium on Fusion Technology, Madrid, Spain, 11 - 15 September, 2000.

Table 2.1.3-1 Nb_3Sn Strand Properties for TF Coils and CS (Properties for a Superconductor Strain ε = - 0.25%)

J_c non copper at 12 T, 4.2K	650 A/mm^2
B_{com}	28 T
T_{com}	18K
T_c at 12 T	11.7K
Hysteresis loss (± 3 T cycle)	400 mJ/cm^3 of non-copper

Table 2.1.3-2 TF Conductor Parameters

Coolant inlet temperature	≤ 4.6K
Operating current (kA)	68.00
Nominal peak field (T)	11.8
Operating temperature (K)	5.0
Operating strain (%)	- 0.5
Equivalent discharge time constant (s) hot spot	15
Current sharing temperature (K)	6.03
$I_{operation}/I_{critical}$ at 5.0K	0.765
Cable diameter (mm)	40.2
Central spiral outer diameter x inner diameter (mm)	8x6
Conductor outer diameter (mm)	43.4
Jacket material	steel

The strands, about 0.7 mm in diameter, are cabled to a 5 stage cable with the final 6 fifth-stage subunits cabled around a central cooling spiral. The local cable space void fraction is about 34%, to give an acceptable level of transverse conductivity. The cable incorporates pure copper strands to build up the copper section necessary for quench protection, and the final substage has a 50% wrap of Inconel foil (0.1 mm thick) to control AC losses. The final cable is jacketed by the pull-through method with a circular stainless steel tube. The use of stainless steel matches the thermal contraction of the radial plate and avoids delamination of the radial plate insulation layer that occurs over the cover of the conductor groove if a jacket having a significantly different thermal contraction coefficient is used.

The size of the central channel and cooling flow rate (8 g/s per channel) are essentially determined by the nuclear heat. With the reference strand and cable configurations (the cable coupling time constant is assumed to be 50 ms), AC losses in the winding pack during plasma operation are low compared to the nuclear heating and do not represent a design constraint, as shown in Table 2.1.1-5. Although experimental results from the CS model coil programme[1] indicate that coupling losses could be higher, with a coupling time constant of 100 - 200 ms, this would not require a modification of the TF coil conductor design.

The cooling inlets to each pancake are located at the inner surface of the coil. The cold helium then reaches the high field region and, after passing through the pancake, exits on the

[1] H. Tsuji, et al., "Progress of the ITER Central Solenoid Model Coil Program," 18th IAEA Fusion Energy Conference, Sorrento, Italy, 4 - 10 October, 2000.

outer surface of the coil on the outside. The conductor design point of maximum field and maximum temperature occurs towards the end of the TF coil inboard leg, where the helium in the first turn reaches the maximum temperature due, essentially, to the nuclear heat at the inboard leg (where the shielding is thinnest).

2.1.3.3 CS Conductor

The superconductor for the CS is a Nb_3Sn cable-in-conduit type, almost identical to the conductor used for the CS model coil[1] and, therefore, the CS model coil development programme and manufacturing experience are fully applicable. Several design options are being considered for the CS conductor (see 2.1.5.1). In this section, only the design with an extruded square jacket is described.

The conductor current is chosen to be in the range 40 - 46 kA as a compromise between structural issues (the larger the conductor, the larger the stress concentration factors on the jacket), and cable current density (the larger the current, the lower the amount of copper required for thermal protection). The conductor jacket is thick, with a square outer section, and is made of Incoloy 908 or stainless steel, to provide the main structural support for the CS.

The conductor parameters for the Incoloy and steel options are summarised in Table 2.1.3-3 for each of the 6 modules forming the CS stack. The conductor has two design conditions. At IM, the CS modules are all energised with a similar current to a peak field of 13.5 T. This field is achieved with a conductor current of 41.8 kA. At EOB, the current is concentrated in the central CS modules, and the plasma and PF coils act to reduce the overall field. The result is that the peak field is set lower, at 12.8 T, but also that a higher current, 46 kA, is required to reach this. The conductor design is a compromise between these two operating conditions. The cable configuration is similar to that used for the TF coil conductor, with 6 sub-cables arranged around a central cooling space.

The modules are wound as hexa-pancakes and quad-pancakes (see 2.1.5.2) with the helium inlet at the inner diameter in the cross-over regions and the outlet at the cross-over regions at the outer diameter. The high field region is therefore cooled by the coldest helium.

[1] H. Tsuji, et al., “Progress of the ITER Central Solenoid Model Coil Program,” 18th IAEA Fusion Energy Conference, Sorrento, Italy, 4 - 10 October, 2000.

Table 2.1.3-3 CS Conductor Parameters (Incoloy or Steel Square Jacket)

	Incoloy Square Jacket	**Steel Square jacket**
Coolant	Inlet ≤ 4.65K	Inlet ≤ 4.65K
Type of strand	Nb_3Sn	Nb_3Sn
Operating current (kA) IM/EOB	41.8 / 46.0	41.8 / 46.0
Nominal peak field (T) IM/EOB	13.5 / 12.8	13.5 / 12.8
Operating temperature (K)	4.7	4.7
Operating strain (%)	- 0.15	- 0.50
Equivalent discharge time constant (s)	11.5	11.5
Tcs (Current sharing temperature) (K) @ 13.5 T	5.8	
Iop/Ic (Operating current/critical current) IM	0.774	0.735
Cable diameter (mm)	31.8	33.2
Central spiral outer x inner diameter (mm)	8x6	8x6
Conductor outer dimensions (mm)	49.5x49.5	49.5x49.5
Jacket material	Incoloy 908	Stainless steel

2.1.3.4 PF Conductor

The PF coils use NbTi superconductor, cooled by supercritical helium. This gives a substantial cost saving compared to Nb_3Sn, and the elimination of a reaction heat treatment greatly simplifies the insulation of such large diameter coils.

The conductor design criteria (1.5K, 600 W/m^2K and 150K) are slightly different to Nb_3Sn (the temperature margin is higher) because of the lower critical temperature of NbTi. The reference strand parameters are given in Table 2.1.3-4.

Table 2.1.3-4 NbTi Strand Parameters

J_c non-copper at 5 T, 4.2K	2,900 A/mm^2
T_c at 5 T	7.17K
Filament diameter	5 μm
Strand layout	no CuNi internal barriers, Nickel surface coating

The cable configuration is similar to that used with Nb_3Sn with 6 sub-cables arranged around a central cooling space. The conductor current is chosen in the range 40 - 45 kA because of the similarity with the CS conductor and the R&D database. No advantage has been found in using higher current conductors, as the copper fraction is limited by stability. The conductor design is shown in Figure 2.1.3-2.

N 12 GR 32 00-12-07 W 0.1

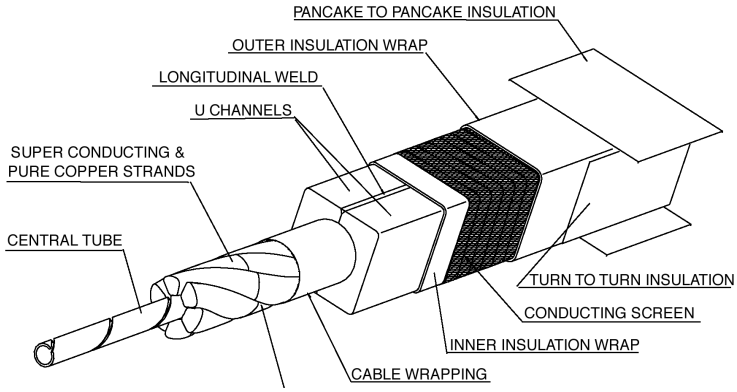

Figure 2.1.3-2 PF Coil Conductor Design

Non-uniform current distribution can be a more sensitive issue with NbTi cables than with Nb_3Sn cables because of the lower value of the critical temperature T_c. To ensure a uniform current distribution in each sub-cable while maintaining AC losses at an acceptable level, the transverse resistivity within the cable must be controlled. A coating (nickel is the reference candidate) is used on the strands. Coupling currents are controlled by the Inconel wrap on each sub-cable to limit the coupling time constant to about 50 ms and the joint layout must provide a uniform contact to each of these sub-cables.

The PF conductors are designed with the capability to operate at a higher current to compensate for the loss of one double-pancake, while still maintaining the same total current capacity in each coil. This mode of operation is referred to as 'backup mode' in 2.1.6.1. In such a case, not only the conductor current increases but also the peak field. Three different conductor designs corresponding to three field values have been selected for the PF conductor design. For the PF2, 3 and 4 coils, the field is up to 4 T, for the PF5 coil, up to 5 T and for the PF1 and 6 coils, up to 6 T. These conductors are shown in Table 2.1.3-5. Both normal mode and backup mode operations can be achieved within the field limits for the 2 lower grades, while the operating field upper limit of the high grade is increased up to 6.4 T in backup mode and requires an operating temperature of 4.7K instead of 5K (sub-cooling is required with the coil He inlet at 4.4K instead of 4.7K).

Table 2.1.3-5 Types of PF Conductor

Coils	**Design Current (kA), Peak Field (T), Operating Temperature (K)**	
	Normal mode	Backup mode
PF1 & PF6	45.0 kA, 6.0 T, 5.0K	52.0 kA, 6.4 T, 4.7K
PF2, 3 & PF4	45.0 kA, 4.0 T, 5.0K	52.0 kA, 4.0 T, 5.0K
PF5	45.0 kA, 5.0 T, 5.0K	52.0 kA, 5.0 T, 5.0K

The conductor parameters are shown in Table 2.1.3-6. The selected operating temperatures include a 0.3K temperature increase (due mainly to AC losses) at the maximum field within the coil, and assumes an inlet temperature of less than 4.7K, allowing a cryoplant window of 4.4 - 4.7K for the PF coils. The helium mass flow per channel is 10 g/s.

Table 2.1.3-6 PF Conductor Parameters

Parameters	PF1 & 6	PF2, 3 & 4	PF5
Coolant inlet temperature (normal/backup)	4.7K /4.4K	4.7K	4.7K
Operating current (kA) (normal/backup)	45 / 52	45 / 52	45 / 52
Nominal peak field (T) (normal/backup)	6.0 / 6.4	4.0	5.0
Operating temperature (K) (normal / backup)	5.0 / 4.7	5.0	5.0
Equivalent discharge time constant (s) hot spot	18	18	18
Current sharing temperature (K) (normal/backup)	6.5 / 6.27	6.65 / 6.51	6.60 / 6.51
$I_{operation}$ / $I_{critical}$ (normal/backup)	0.127 / 0.144	0.365 / 0.422	0.264 / 0.305
Cable diameter (mm)	38.2	34.5	35.4
Central spiral outer x inner diameters (mm)	12x10	12x10	12x10
Conductor outer dimensions (mm)	53.8x53.8	52.3x52.3	51.9x51.9

The conductors use a heavy-walled, stainless steel jacket. Two jacket options are being considered:

i) the reference option: extruded circle-in-square steel conductor;

ii) the alternative option: thin steel circular jacket with external steel U-channels.

In each case, the cable is placed in the jacket by a pull-through, roll-down procedure, as with the TF and CS coils. The U-channels are welded around the circular jacket before spooling. The external shape of these two conductor options is the same and the choice has no impact on the PF coil manufacture, except for the preparation of helium inlet pipes and conductor joints and terminations.

2.1.3.5 CC Conductor

The CCs use a 10.0 kA cable-in-conduit conductor using NbTi superconductor. This CC cable is conservatively designed to operate up to 6 T and 5K. It is formed square with a square outer jacket. The main parameters are summarised in Table 2.1.3-7.

Table 2.1.3-7 Conductor Parameters for the Correction Coils

Operating current (kA)	10.0
Nominal peak field (T)	6.0
Operating temperature (K)	5.0
Jacket material	Cold-worked 316LN

2.1.4 TF Coils Manufacture

The 18 TF coils are each D-shaped and consist of a winding pack contained in a thick steel case. The winding pack is a bonded structure of radial plates (which contain the conductor) with an outer ground insulation.

2.1.4.1 TF Coil Winding Pack

The winding pack design is based on the use of circular conductors supported by radial plates, as shown in Figure 2.1.4-1. This design has advantages in terms of the conductor insulation, long-term quality, and reliability.

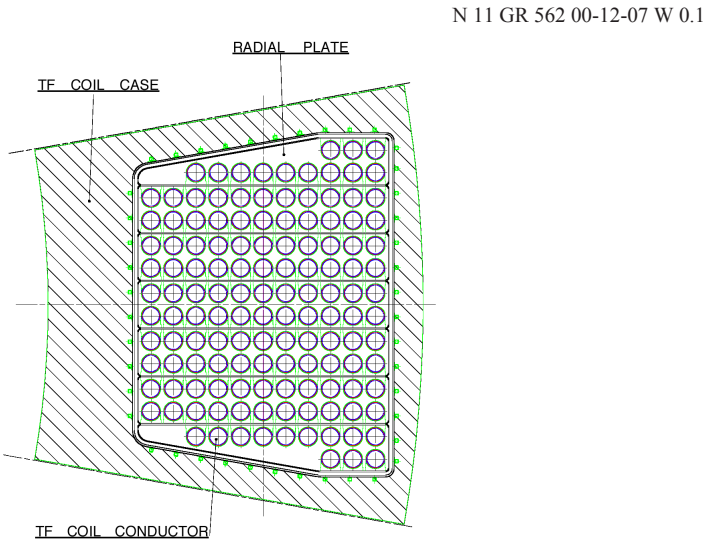

Figure 2.1.4-1 Cross Section of TF Coil at Inboard Leg

- A circular outer cross section of the jacket is the optimum shape for applying insulation tapes, resulting in a robust turn insulation. The turn insulation is not subject to the stress concentration effects which are always present at corners of square conductors.
- During the magnet operation, the Lorentz forces acting on each conductor are transferred to the plate, without accumulation of forces on the conductor and its insulation. As a result, almost no primary load is applied to the conductor insulation and there is no degradation leading to damage due to mechanical cycling.
- With circular conductors in radial plates, delamination between the conductor insulation and the radial plate is of no consequence and has no impact on the mechanical or electrical behaviour of the winding pack.

Additional advantages of the radial plate configuration are that it provides a “double insulation” with two physically independent barriers (the turn and the ground insulation) and it gives the capability of detecting impending faults by monitoring the resistance between conductor and radial plate.

The considerations above indicate that with the radial plate configuration, faults leading to a TF coil short are essentially avoided by design. The radial plate concept has already been demonstrated in the TF model coil project. The main drawback, however, is the relatively high manufacturing cost of the radial plates. R&D activities have been initiated to investigate potentially cheaper manufacturing routes.

The winding uses one-in-hand conductor (about 800 m long) with a double pancake configuration. The conductors are wound and heat treated (about 650°C for 200 hrs) in a vacuum furnace. After heat treatment, the turn insulation is applied. The insulation consists

of a polyimide/glass-fibre mix with epoxy resin filler. The insulated TF conductors are then placed in grooves on each side of a radial plate. Each conductor is contained in its groove by means of a cover plate that is welded in place.

Seven double pancakes are assembled together to form the winding pack of one TF coil. The ground wrap has a minimum thickness of 6 mm and includes multiple wraps of polyimide tape interleaved with glass, vacuum impregnated with epoxy resin. The joints are placed outside the main winding (in a "praying hands" configuration). The coil terminals project out of the case on the lower curved part of the case.

2.1.4.2 TF Coil Cases

The TF coil cases are composed of two half-cases made up of about 7 poloidal sections. These sections are joined by butt welds which have been located, as far as possible, outside the peak stress regions (in particular the upper and lower inner curved regions). The final weld to close the half cases around the winding pack (which cannot be inspected from both sides) is located on the coil midplane where the cyclic stress component is a minimum (Figure 2.1.4-2).

N 11 GR 563 00-12-07 W 0.1

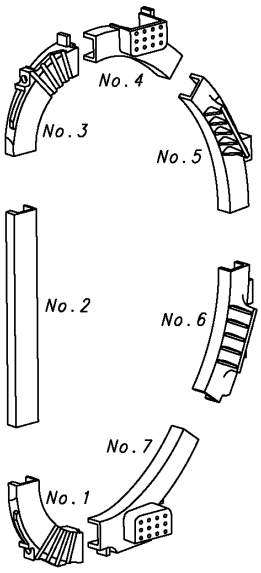

Figure 2.1.4-2 Proposed Segmentation of the TF Coil Case for Manufacture

The high stress sections of the case (the inboard leg and upper and lower inboard curved regions) can be made from high strength forged 316LN (modified) steel. This can be forged avoiding any intermediate welds to build the half case section. On the outboard part of the coil, cast sections have lower stress limits but greatly reduce the amount of welding and appear the most attractive design solution. Butt welds between poloidal sections are expected to be a combination of electron beam welding for the first pass followed by multiple passes of submerged arc welding for the remainder.

The cases are equipped with a set of cooling channels to intercept nuclear and eddy current heat loads before they reach the superconductor in the winding pack. These channels are placed on the inner surface of the case and run poloidally around the circumference (Figure 2.1.4-1).

2.1.5 Central Solenoid Manufacture

2.1.5.1 Flux Generation and Conductor Jacket Options

The solenoid is free-standing and supports the magnetic loads through structural material within the winding. The main load is the magnetic hoop force, which creates tension in the structural material. Because of its central position in the tokamak, the CS has a major role in driving the radial build while itself forming a fairly minor fraction of the total magnet cost (about 12%). Global optimisation studies have shown that in order to minimize the total cost of the machine, it is preferable to adopt the most compact, high field design option, even if it is not the lowest cost choice for the CS itself. As illustrated in Figure 2.1.5-1, the flux generation in the solenoid is improved by the choice of a high field and the use of the highest allowable tensile stresses in the jacket material. For ITER, a peak field of 13.5 T and a tensile peak stress of about 410 MPa have been selected to meet the flux generation requirements.

N 13 GR 27 00-12-07 W 0.1

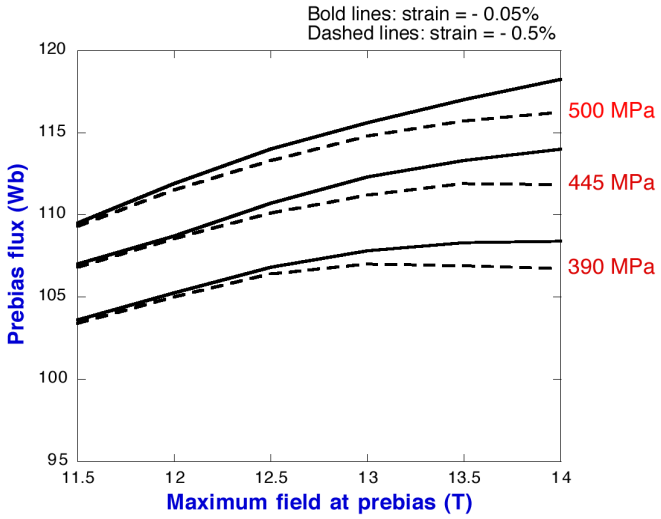

Figure 2.1.5-1 Pre-bias Flux Available from an Optimised CS as a Function of Field, Showing Variation with Allowable Peak Tension and Superconductor Strain

The requirements for the CS conductor jacket material are, therefore, primarily a high fatigue resistance to stress cycling.

There are two basic design options for the CS jacket, as shown in Figure 2.1.5-2, both of which are expected to provide the same flux capability.

i) An extruded jacket with a square outer section. The jacket material is subjected to the Nb_3Sn heat treatment. The possible jacket materials are Incoloy 908, as developed for the CS Model Coil, or a stainless steel, once such a steel has been developed to meet the fatigue life requirements after heat treatment.

ii) A double jacket including an inner titanium circular jacket, which undergoes the Nb_3Sn heat treatment, and an outer stainless steel jacket made up of two U-channels which are applied around the inner jacket after the heat treatment.

N 13 GR 32 01-05-30 W 0.1

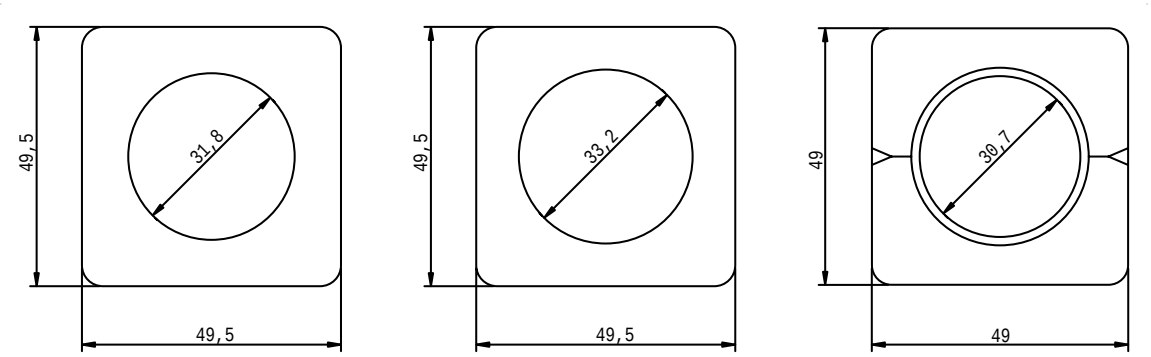

Figure 2.1.5-2 CS Conductor Jacket Options
Incoloy 908 (left), Stainless Steel (centre), Double Jacket (Ti-SS) (right)

Incoloy 908 has significant advantages in terms of its very high fatigue resistance and its thermal contraction which matches that of Nb_3Sn. The use of Incoloy has been successfully demonstrated in the CS model coil. Incoloy 908 is, however, sensitive to stress-accelerated grain boundary oxidation (SAGBO) during the Nb_3Sn heat treatment, and requires strict control of the heat treatment atmosphere ($O_2 < 0.1$ ppm).

There has been recently significant progress in the development of stainless steel as a jacket material for the CS. Solution annealing has been shown to improve the fatigue behaviour (crack growth rate) of those steels. At the time of writing this report, the improvement in property is, however, not quite sufficient to meet the ITER CS fatigue life requirements. It is concluded that the use of steel will become possible only if further improvements of the fatigue behaviour can be achieved or if the detection sensitivity of certain defects (sub-surface defects) can be improved. The planned R&D programme includes the study of vacuum-refined materials and this may result in further improvements.

The double jacket option does not require such strict control procedures for the reaction treatment. For this option, JK2 is proposed as the material of the outer jacket. This material is a cryogenic steel developed in Japan and has a coefficient of thermal contraction close to that of Nb_3Sn between room temperature and 4K. However, JK2 in extruded sections is not fully characterised at cryogenic temperature, especially for fatigue properties. R&D activities are underway to demonstrate the manufacture of U-channels and to establish the fatigue properties of JK2. Some additional work on the use and joining of titanium is also probably required. The main drawback of the double jacket option is the relative complexity of the assembly of the U-channels on the reacted conductor. R&D would be required to fully establish the assembly procedures.

Incoloy 908 is maintained, at present, as the provisional reference solution. The possibility to use stainless steel is very attractive and will be kept under review as new R&D results become available. The Ti-JK2 option remains as alternative solution but requires additional R&D. The final choice will be based on the R&D results.

2.1.5.2 CS Winding Pack

The CS stack consists of 6 electrically independent modules. The modules are each made up of 5 “hexa-pancake” and 2 “quad-pancake” windings (a “hexa-pancake” and a “quad-pancake” use a single conductor length for the winding of 6 pancakes and 4 pancakes

respectively). The electrical joints between hexa or quad pancakes are located at the CS outer diameter and are embedded in the winding pack. Each module weighs about 107 t.

A previous CS jacket design used a smaller extruded section with a co-wound reinforcing strip. The main advantage of this design was to reduce the cross sectional area of the butt welds joining the jacket lengths. However, the co-wound strip complicates the winding process and either requires a longitudinal weld to the square jacket or, if not welded, requires additional insulation which reduces the current density. The single square section is therefore preferred.

Insulation is applied after the conductor is reacted. The turn insulation is applied to the conductor and the strip and consists of overlapping glass and polyimide tapes. Additional insulating shims (1.5 mm thick) are inserted between turns and between pancakes to compensate dimensional deviations of the conductor. To make the joints between the hexa-pancakes, the conductor ends are pulled into an helical shape to provide access to the joint area between two adjacent hexa-pancakes. After stacking all hexa-pancakes, the ground insulation (10 mm thick of overlapping glass and polyimide tapes) is applied. The whole CS module is then subjected to a final vacuum pressure impregnation (VPI) process with epoxy resin.

2.1.5.3 CS Preload Structure

The field curvature at the ends of the CS stack creates vertical forces on the modules. At IM (initial magnetization), these forces are towards the mid-plane of the stack, whereas at EOB (end of burn), the end modules carry opposite currents to the central ones and are repelled with a force up to 75 MN. This means that a vertical support structure is required. This structure applies axial pre-compression to the coil stack so that the modules remain in contact during all operating conditions (Figure 2.1.5-3).

N 13 GR 29 00-12-07 W 0.1

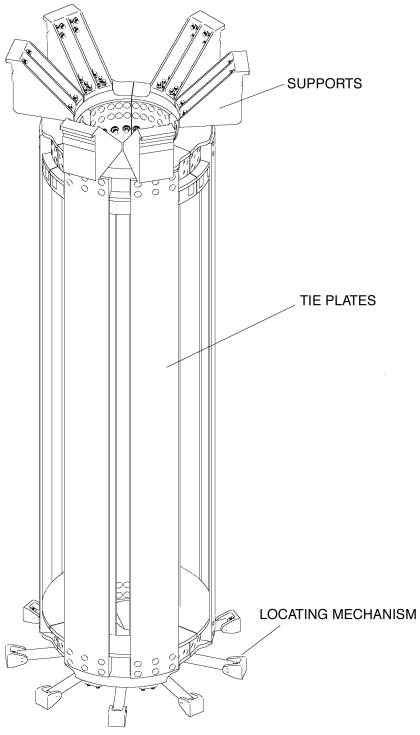

Figure 2.1.5-3 CS Supports and Pre-load Structure

To obtain uniform compression, tie plates running axially along the CS are provided at both inside and outside diameters and connect to rigid flanges at top and bottom. This structure is designed so that it can restrain the maximum vertical separating load. The required axial tension in the structure is achieved partly by pre-tensioning at room temperature and partly by differential contraction during cooldown. This approach relies, therefore, on the use of a jacket material with a thermal contraction coefficient lower than that of the tie-plates. The combination of Incoloy as a jacket material and stainless steel for the tie-plates provides the required differential contraction. If the case of a stainless steel jacket material, preliminary analysis has shown that aluminium tie-plates can provide the required vertical pressure. A full design and analysis of aluminium tie-plates remains, however, to be performed.

The CS pre-load structure consists of the lower flange, the upper flange, buffer plates, a set of 12 tie-plates together with wedges and connecting bolts. The flanges are split into 12 sectors linked by electrically insulated bolted joints to reduce AC losses during pulsing of the machine. The tie plate region needs to have at least 30% open space in the toroidal direction for the current lead and helium pipe arrangement.

The CS assembly is hung from the top of the TF coils through its pre-load structure by supports which resist the net vertical forces but are flexible in the radial direction. At the bottom of the CS, there is a locating mechanism to support the stack against dynamic horizontal forces.

2.1.5.4 CS Joints and Helium Pipe Inlets

The CS joints between hexa-pancakes are located at the outer diameter. Two types of joints are being considered: the overlap type and the butt type. The overlap type of joint uses a cable compacted into a long (typically 500 mm) tube or box with a copper wall to achieve low contact resistance. Contact is achieved by clamping together the two conductor tubes or boxes. In the butt joint, the cable is highly compacted into a copper tube and cut normal to the conductor axis to allow a sintered joint to be made between the two conductor ends. These two joint concepts have been used in the CS model coil and the choice will be made when all experimental data on joint performance has been analysed.

For both types of joint, a structural element, composed of an extension of the reinforcing strip, is provided to transfer the operating hoop load on the conductor around the joint region.

On the top and bottom modules, the joints are exposed to a significant transverse (i.e. radial) field component during plasma operation. This field variation is unfavourable for the "overlap" type of joint since it drives eddy currents in a loop through the joint contact surface. Testing of overlap joints in this configuration is required.

Helium inlets are at the CS inner diameter where tensile stresses are highest. The helium inlet region requires, therefore, a local reinforcement to allow the opening in the conductor jacket without excessive stress intensification. The inlet must also provide a good distribution of helium in the 6 sub-cables of the conductor. These requirements are achieved by cutting locally the jacket and welding specially shaped L-shaped pieces, which include the helium inlet channel, together with the required structural reinforcements and interspace to distribute the helium flow.

2.1.5.5 CS Structural Assessment

The main loads are the magnetic hoop force, which creates hoop tension in the structural material, and the vertical pressure towards the equatorial plane from the outer modules, which creates vertical compression. Analysis of the CS includes global and detailed analysis. Global analysis has been carried out to investigate the behaviour of the CS stack and pre-load structure during the operation scenario. This type of analysis uses models where the CS windings are represented by smeared material elastic properties. A 2D axisymmetric model and a 3D model to look at non-axisymmetric aspects of the windings and structures have been used. Detailed analysis of the CS winding structure has been carried out to evaluate the detailed stress distribution in the conductor and its insulation. This analysis has been carried out with 2D axisymmetric models.

The key parameter is the fatigue strength, which determines the allowable peak tensile stress in the jacket. The highest stresses occur at the inner diameter of the CS. The stress pattern depends on the geometrical configuration of the conductors. The worst configuration is where conductors in neighbouring pancakes are vertically staggered due to turn to turn transitions within pancakes. In this worst configuration, peak tensile stress occurs in the horizontal wall of the conductor jacket. This peaking is due partly to bending of the conductor wall (under the axial pressure) and partly to differential Poisson effects. Table 2.1.5-1 summarizes the main results of the stress analysis and fatigue assessment. For the CS, each plasma cycle includes two stress cycles: one full stress cycle at IM and a cycle at reduced stress at EOB. For the stainless steel option, the stress level is about 10% higher than for the Incoloy option due to the higher differential contraction which reduces strand performance and requires, therefore, a larger cable cross section. A certain level of manufacturing residual stress in the jacket has also been taken into account in the fatigue assessment. The maximum allowable initial defect areas are shown in the table. For the Incoloy option, the defect size is within the sensitivity of non-destructive testing techniques. For the stainless steel option, the defect size is smaller and may be outside the detection capability of non-destructive testing techniques.

Table 2.1.5-1 Tensile Stress in the CS Conductor Jacket and Acceptable Defect Size for the Incoloy and Stainless Steel Square Jacket Options

Conductor option	Peak tensile stress in the jacket (MPa) IM / EOB	Maximum allowable initial defect* area (mm^2) to achieve 60,000 plasma cycles
Incoloy	429/401	0.65
Stainless steel**	470/440	0.28

* A sub-surface defect is assumed.

** The material is a solution heat treated, unaged 316LN steel.

The conductor turn insulation is subject to some shear stress and tensile stress normal to the insulation layer. These stresses are due to bending deformations of the conductor jacket under the axial pressure. Analysis shows that these shear stresses are acceptable but tensile stresses exceed locally the allowable limits. This effect, which was already present in the 1998 CS design, has been investigated experimentally by the US Home Team. A beam representing a section of the winding pack was tested under cyclic compressive load. Local delamination of the insulation near the corners of the conductors was observed, as expected, but without any adverse consequence for the integrity of the electrical barrier of the conductor insulation.

2.1.6 PF Coils Manufacture

2.1.6.1 PF Winding Packs

The PF coils are pancake wound with NbTi superconductors in square jackets. Because of the operational reliability requirements, especially for the electrical insulation, and the difficulty in replacing a coil, the conductor is provided with double turn insulation. The double turn insulation consists of two insulation layers with a thin metal screen in between. Double pancakes are wound two-in-hand. This arrangement allows detection of an incipient short, before it develops into a full short resulting in significant damage to the coil and, as a consequence, the need for a major coil repair or replacement. In the event of the detection of an incipient short in a double pancake, the faulty double pancake must be disconnected and by-passed using busbar links. This work is to be carried out hands-on and requires access to the joint regions at the outer diameter of the coils. Following the by-pass of a double pancake, plasma operation can continue at full performance by using the remaining double pancakes at higher current (backup mode).

The use of double turn insulation and the ability to continue operation with a by-passed double pancake should make a major coil repair or replacement unnecessary throughout the life of ITER-FEAT.

Should, however, such major repair be required, the following strategy could be followed:

- the upper coils, PF1 and PF2, can be relatively easily removed from the cryostat - for them, major repair work, or rewinding, should be carried out outside the cryostat;
- for the lower coils, PF5 and PF6, major repair work, including rewinding, should be carried out under the machine inside the cryostat;
- the PF3 and PF4 coils are trapped by the vacuum vessel ports and are the most difficult to access and repair; for this reason, their resistance to faults has been enhanced by using double pancakes with individual ground insulation and steel separator plates between double pancakes to limit damage propagation in the event of a fault.

Figure 2.1.6-1 shows typical PF coil cross sections. In the PF1, 2, 5 and 6 coils, the outer surfaces of the whole coil are covered with ground insulation with a thickness of 8 mm. The insulation is composed of overlapping glass and polyimide film (barrier) and is vacuum pressure impregnated with epoxy resin. In the PF3 and 4 coils, the outer surface of each double-pancake is covered with ground insulation with a thickness of 8 mm. A steel separator plate is placed between two double pancakes. The plate is formed from a steel strip with a spiral shape so as to form a flat pancake to reduce eddy currents.

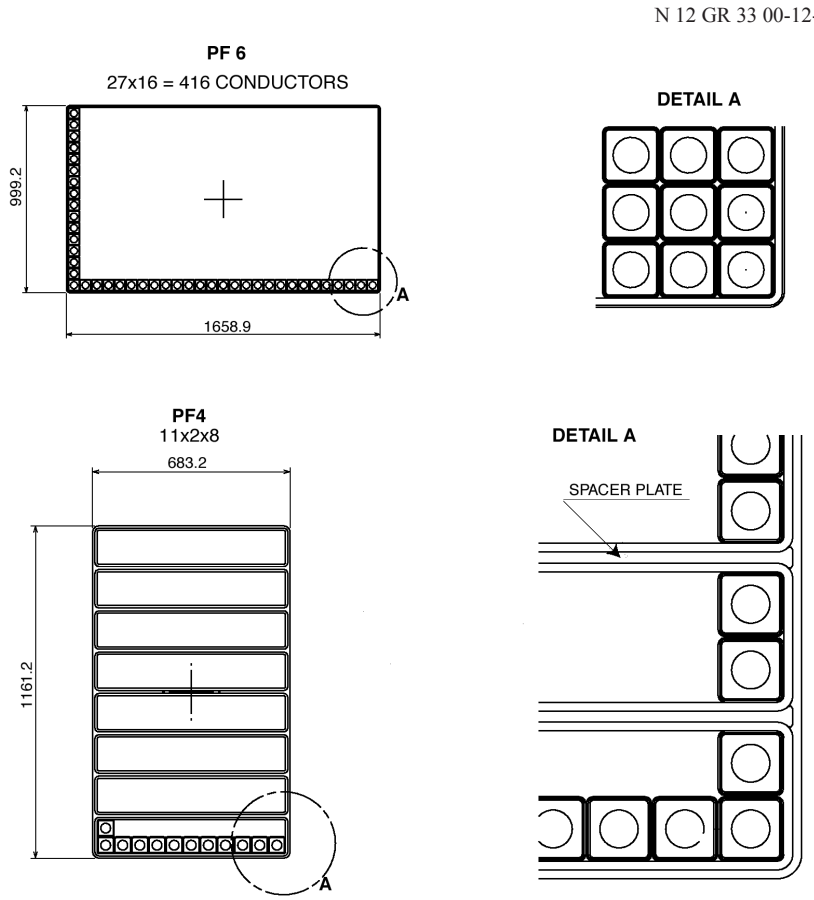

Figure 2.1.6-1 PF Coil Typical Cross Sections

2.1.6.2 PF Joints and Helium Pipe Inlets

The conductors at the ends of each double pancake are brought out of the winding at the outer diameter of the coil. The lap joint is made in the toroidal direction and a structural element is provided to transfer the operating hoop load on the conductor around the joint area. Each double pancake is to be supplied with supercritical helium at the inner diameter of the coil through a coolant inlet pipe located at the cross-over region of each of the two conductors.

2.1.7 Correction Coils Manufacture

Eighteen multi-turn correction coils (CCs) are used to compensate field errors arising from misalignment of the coils and winding deviations from the nominal shape as a result of fabrication tolerances, joints, leads, busbars and assembly tolerances. There are 6 top CCs, 6 bottom CCs, and 6 side CCs, arranged toroidally around the machine inside the PF coils. Pairs of diametrically opposite CCs are connected in series inside the cryostat.

The top and bottom coil sets are essentially planar while the side coils lie on a cylindrical surface. Each coil consists of a bonded winding pack enclosed in a 20 mm thick steel case. The vertical sections of each coil are placed to coincide with a TF coil leg and the coils are supported by clamps attached to the TF coil cases. The layout and geometry of the CCs is shown in Figure 2.1.7-1.

N 12 GR 34 00-12-11 W 0.1

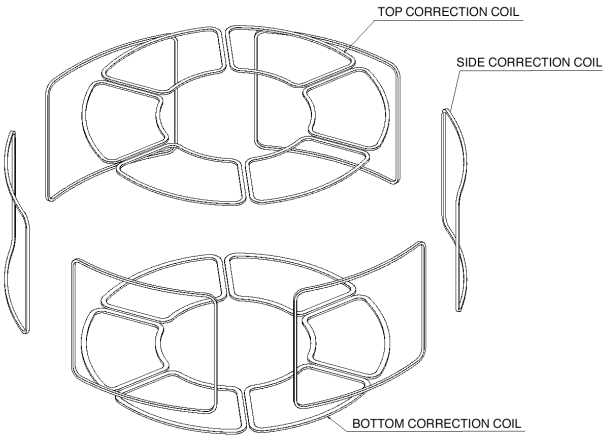

Figure 2.1.7-1 Correction Coils Layout

The current capacity of the CCs is shown in Table 2.1.7-1.

Table 2.1.7-1 Operating Condition of the Correction Coils

Parameters	Top coil	Side coil	Bottom coil
Max. operating current (kA)	10.0	10.0	10.0
Max. current capacity per coil (kA)	140	200	180
Max. total field (T)	< 6	< 6	< 6

2.1.8 Auxiliary Systems

Magnet feeders include the in-cryostat feeders, the cryostat feedthroughs, and the coil terminal boxes or structure cooling valve boxes.

2.1.8.1 In-cryostat Feeders

Each in-cryostat feeder is a subassembly that connects a coil or structure to the end of a cryostat feedthrough (CF) located at the cryostat wall. For a coil, it consists of a steel conduit containing the feed and return busbars (using NbTi superconductor), the return and supply helium lines and high and low voltage instrumentation lines. Figure 2.1.8-1 illustrates, as an example, the layout of magnet feeders at the lower part of the cryostat. The figure shows the feeders from their respective coil terminals inside the cryostat to the coil terminal boxes in the gallery of the tokamak building.

N 11 GR 565 00-12-07 W 0.1

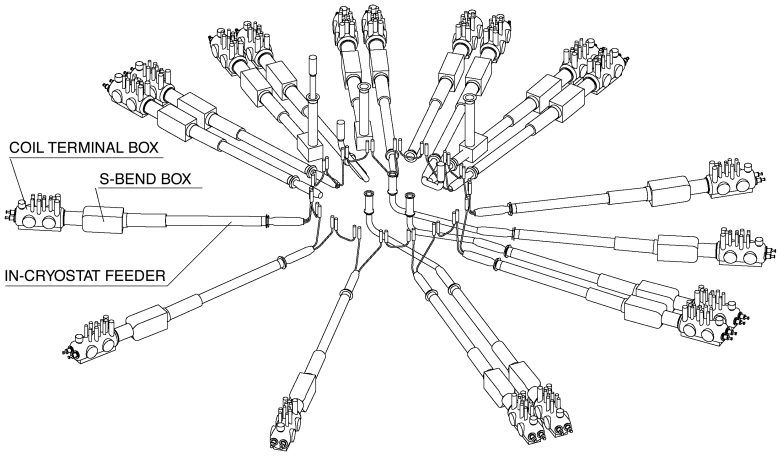

Figure 2.1.8-1 Layout of Feeders at the Lower Part of the Cryostat

Each busbar has a double insulation system that will allow detection of a developing busbar-to-ground short circuit and allow operation to be stopped before the short occurs, providing protection against further damage. Additionally, an over-wrap of steel tape will be applied to serve as an extra protection screen against a short circuit between coil terminals. In each feeder, the pair of superconducting busbars is separated by a steel plate acting as an additional robust protection against damage propagation between busbars. Figure 2.1.8-2 shows the typical design of a feeder and the details of the joints between a coil terminal and the feeder.

N 11 GR 566 00-12-07 W 0.1

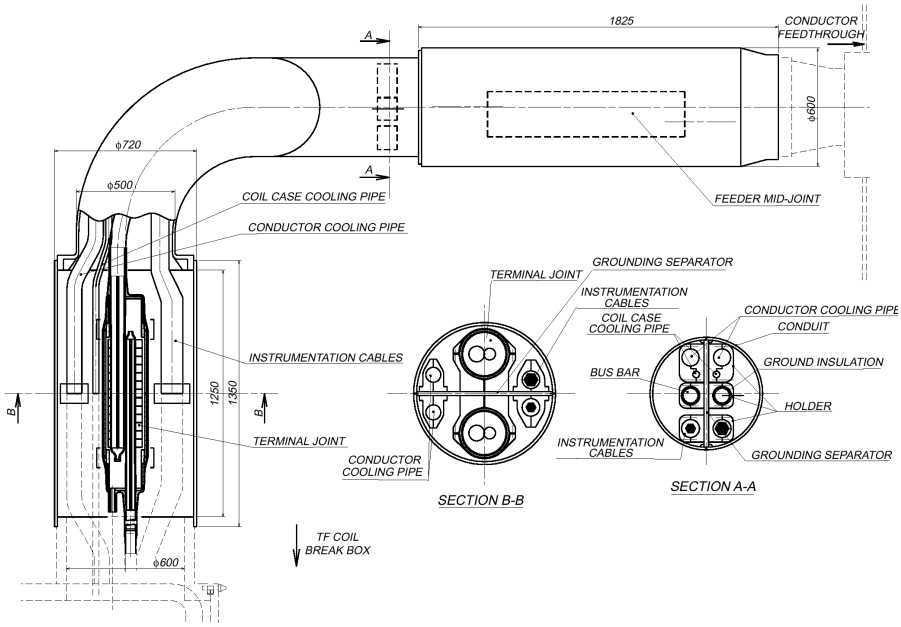

Figure 2.1.8-2 Typical Terminal Joint and Feeder Cross Section

The superconducting cable for the busbars is designed to have more thermal protection than the coils, so that the coils can still be properly discharged in the event of a busbar quench. The time constant of the current decay is taken as 26 s, approximately twice that of the coils. The operating current is taken as 68 kA for all coils, which provides some over-capacity for the CS and PF coils busbars. This has a negligible cost impact and allows a standard cable design. Table 2.1.8-1 shows some of the busbar conductor specifications.

Table 2.1.8-1 Superconducting Conductor for TF, CS and PF Coil Busbars

Type of strand	NbTi
Operating current (kA)	68
Nominal peak field (T)	4
Operating temperature (K)	5.0
Equivalent discharge time constant (s) hot spot	26
Cable diameter (mm)	41
Central spiral od x id (mm)	8x6
Conductor OD (mm)	47
Jacket	steel

2.1.8.2 Cryostat Feedthrough

The cryostat feedthrough (CF) includes the penetration through the cryostat wall and a straight length from the cryostat wall to an S-bend box. The S-bend box is also part of the CF and contains S-shaped bends in the busbars and the cooling lines so as to accommodate the movements of the in-cryostat feeders and the coils, relative to the S-bend boxes which are fixed to the building.

The S-bend box connects to a coil terminal box (CTB). The vacuum barrier at the flange connecting the CF to the CTB is also a feedthrough, which allows the busbars, cooling lines and instrumentation lines to pass from the cryostat vacuum into the CTB vacuum.

2.1.8.3 Coil Terminal Box and Structure Cooling Valve Boxes

The CTBs provide the housing for interconnection of the magnet systems with the cryoplant, the power supplies, and the data acquisition system, and they also house the local cryogenic control components. Valves in the CTBs control the mass flow rate of helium for each coil and each structural element. These valves are also used during cool-down and warm-up operations to control thermal gradients.

All CTBs contain one pair of current leads making the transition from the superconducting helium cooled busbars inside the CTB to the room temperature busbars from the power supply. The number and capacity of the current leads are shown in Table 2.1.8-2. Type F and V current leads, as shown in the Table, are optimized for constant and variable current, respectively.

Table 2.1.8-2 Number and Capacity of Current Leads

Coils	Number of pairs	Maximum Current (kA)	Type	Maximum Voltage (kV)
TF Coil	9	68	F	10
PF Coil	6	45	V	14
Correction Coil	9	8	V	3
CS Coil	6	45	V	10

The Structure Cooling Valve Boxes (SCVBs) contain the remotely controlled helium valves for each structural system. The structure cooling for 18 TF coils and PF coil supports includes two SCVBs. The structure cooling for the CS coil system includes one SCVB.

2.1.8.4 Instrumentation

The functions of the instrumentation system are:
- to detect superconductor quench, electrical insulation faults and other abnormal conditions, and trigger protective energy discharge through the interlock system,
- to monitor coil, feeder and current lead parameters as part of normal machine operation and, if set points are exceeded, notify the operator through the alarm system,
- to measure the cooling and thermo-hydraulic parameters and calculate the required mass flow rates.

The function of the control system is to operate the CTB and SCVB coolant valves to provide the required mass flows to the coils, current leads and structures.

The magnet system contains many different sensors. Each sensor measures a specific physical parameter of the magnet system (voltage, helium mass flow, pressure, temperature, strain, displacements, etc.). For quench detection, redundant quench detection sensors (voltage and mass flow) and wiring are used inside the cryostat for reliability. To limit the possibility of short circuits and ground faults, only voltage taps (no sensors) are connected to the conductors, and each voltage tap has a current-limiting resistor in series to prevent short circuits through the instrumentation wire.

The magnet instrumentation and control systems consist of the following items.

i) Magnet local panels
The magnet local panels condition the analog signals from the sensors, and perform analog-digital signal conversions to interface with the computers including the magnet controller. The panels also detect quenching of the superconductors, receive signals from the power supplies and, through hard-wired interlocks, can trigger a fast protective discharge of the coil energy. The panels are placed close to the CTBs, in the galleries which are accessible for hands-on maintenance.

ii) The magnet controller
The magnet controller is used for the interface to the supervisory control system of CODAC. It summarises data from the local panels for central monitoring.

2.1.9 Magnet Safety

Magnet safety has received particular attention because of the large energy inventory and therefore the potential albeit hypothetical influence of magnet failures on other components, especially those associated with nuclear confinement. Magnet faults (whether or not they involve external components) can have a severe effect on the overall machine availability, and the repair is difficult, so there are multiple monitoring and protection systems built into the design. These include inherent features, detection/monitoring systems (that operate continuously while the coils are charged), and testing systems (that are applied periodically when plasma pulsing is interrupted or when the magnets are discharged). Particular attention is paid to reducing the probability of potential cascade sequences, where the existence of an initial fault increases the probability of others (for example, heat from a short degrades a protection barrier or increases local voltages), and common mode faults where several components (due, for example, to a common design or manufacturing error) have the same initial fault.

All initial faults have some form of protection, either active or inherent in the design, that prevents them leading to events that can cause damage to the magnets or surrounding components. Only a series of faults can lead to damage. As the final result of a safety-related event sequence, various primary 'damage mechanisms' have been identified for the magnets. It is found that all potential damage mechanisms which can affect the nuclear components (either the cryostat, the vacuum vessel or the pipework and ducting within the cryostat) are associated with molten material produced by arcing.

Arcing between conductors and structures within the cryostat is prevented by the use of a hard ground system for the structures and the cryostat walls, and by ensuring that all live conductors are within a robust grounded containment.

Contrary to general expectations, shorts that develop inside coils do not lead to significant arcing and the damage can be confined to the coil. However, external shorts on the CS and PF busbars (superconducting or normal) can potentially lead to molten material generation in the coils themselves (not significantly in the busbars) due to the coupling of extra energy into the coil, followed by a quench that cannot be discharged. Due to the thin confinement cases on these coils, a substantial fraction of this molten material could enter the main cryostat (1,000 kg would be a conservative estimate). Due to the location of the PF coils, most of it would be deposited onto the thermal shields and the vacuum vessel, although distributed over several square metres in the toroidal direction. The vacuum vessel is sufficiently robust to withstand this form of distributed heating (most arc accidents will, however, be associated with helium leakage from the affected coil into the cryostat, and with failure of the feedthroughs in the cryostat wall).

2.1.10 Supporting R&D and General Assessment

The model coil projects were launched to drive the development of the ITER full scale conductor, including the manufacturing of strand, cable, conduit and termination, and the conductor R&D in relation to AC losses, stability and joint performance. These projects also drive the supporting R&D programmes on coil manufacturing technologies, including the entire winding process (wind, react, and transfer), electrical insulation and quality assurance.

Strand for the Model Coil Programme

The total planned production of 29 t of Nb_3Sn strand, from seven different suppliers throughout the four original ITER Parties, has been completed and qualified. This reliable production expanded and demonstrated the industrial manufacturing capability which will be required for the production of 480 t of high performance Nb_3Sn strand for ITER.

CS Conductor and Coil Manufacture

The size of the CS model coil (3.6 m in diameter and 2 m in height) is almost the same as the size of a ITER CS module (4 m in diameter and 2 m in height) and the maximum field and coil current are also the same.

The manufacture of the inner module (USA), the outer module (Japan), and the CS type insert coil (Japan) were completed during 1999. This manufacture has allowed to establish the cabling, jacketing and winding techniques with a conductor very similar in size to the full size CS conductor. The heat treatment, to react the superconducting alloy without degrading the mechanical properties of the Incoloy 908 jacket, is a critical step which has also been successfully completed. The assembly of the two coil modules and the CS type insert coil was completed before the end of 1999 (Figure 2.1.10-1). In April 2000, the maximum field of 13 T and stored energy of 640 MJ, at a maximum current of 46 kA, have been achieved in the ITER dedicated test facility at JAERI-Naka (Figure 2.1.10-2). This full charge has been followed by a comprehensive test programme including current-sharing temperature measurements, AC loss measurements, fast ramp-up and fast discharges, and current and field cycles simulating the ITER CS operation. Although the analysis of the data is not complete, it is already clear that the performance of the CS model coil is broadly according to expectations and meets the full size CS operation conditions. A 10,000 cycles fatigue test of a Nb_3Sn insert coil (JAHT) has also been completed and results are under evaluation.

N 13 GR 30 00-12-07 W 0.1

Figure 2.1.10-1 CS Model Coil and CS Insert Installed in the Vacuum Chamber at the Test Facility in JAERI Naka

N 13 GR 31 00-12-07 W 0.1

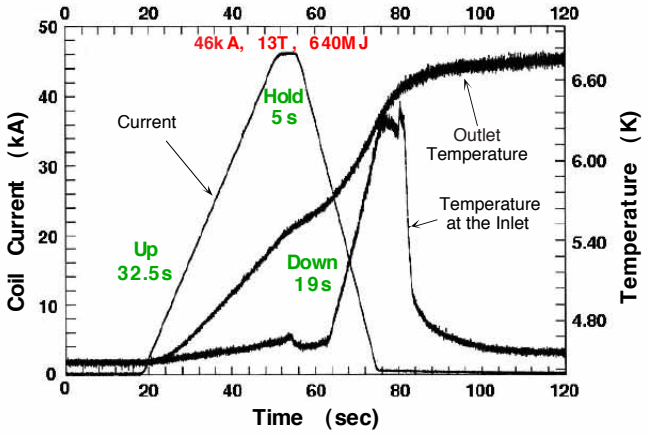

Figure 2.1.10-2 Ramp-up to 46 kA, 13 T, Flattop of 5 s, followed by Ramp-down to Zero

TF Conductor and Coil Manufacture

The model coil uses a cable similar to the full size TF coil cable and the cross section of the TF model coil is smaller but comparable in design (use of radial plates) to that of the ITER TF coil.

The manufacture of the TF model coil was completed by the beginning of 2001. This manufacture has allowed the techniques which will be used for the manufacture of the full size coils to be established:

- forging and machining of the radial plates (Figure 2.1.10-3);
- cabling, jacketing, winding, reaction treatment, and transfer of the conductor on the radial plates;
- impregnation of the double pancakes and winding pack, insertion of the winding pack in the case, closure weld of the case and final impregnation.

All this work has been performed in the EU. The coil testing is expected to start in June - July 2001. The model coil will be tested first on its own and later in conjunction with the LCT coil in the TOSKA facility at FzK (Germany). With the LCT coil, a field of 9.7 T at 80 kA will be achieved. By comparison, the peak field and the operating current are 11.8 T and 68 kA in ITER.

N 11 GR 567 00-12-07 W 0.1

Figure 2.1.10-3 Winding TF Model Coil Conductor into Mould

A test up to 13 T of the TF type insert coil with a single layer of conductor will be performed in the CS model coil test facility at JAERI. The manufacture of this insert coil has been completed in the Russian Federation and the insert was delivered to the JAERI test facility in May 2001. Testing will take place during the 2nd half of 2001. A 1 km jacketing test, which exceeds the ITER requirements, has been separately demonstrated in the Russian Federation.

TF Coil Cases

For the development of the manufacture of the TF coil case, large forged (Figure 2.1.10-4) and cast pieces (about 30 t and 20 t respectively) have been produced in the EU. The use of forgings and castings is attractive since it is expected to result in significant cost reductions as compared to a manufacture based on welded plates. Investigation of the properties of the forging has revealed values exceeding the requirements of 1,000 MPa yield stress and 200 $MPam^{1/2}$ fracture toughness, with low fatigue crack growth rates. The casting also shows properties adequate for the low stress regions of the case (yield stress about 750 MPa). Welding trials have demonstrated successful welding of the cast to forged sections, and have established welding procedures for the case sections and the final closure weld of the half cases.

N 11 GR 568 00-12-07 W 0.1

Figure 2.1.10-4 Forging of Inner Leg Curved Section of TF Coil Case as Hollow Tube

New R&D Activities

New R&D requirements have been identified to improve the database, allow cost reductions and address technology needs specific to the ITER design. As already indicated, they cover the insulation materials and shear keys, the pre-compression rings of the TF coil structure, the radial plate manufacture, the materials and manufacturing technology database for the jacket of the CS conductor, and the CS pancake joint performance.

An R&D programme on NbTi conductors and joints for the PF coils has been launched. Results have already been obtained on investigations of strand coatings for AC loss control. Testing of conductor and joint samples are planned. The manufacture of a NbTi insert coil is an essential part of this programme. The design of this NbTi insert coil is underway and manufacture is planned to take place in 2002. The testing of the insert will take place at the JAERI test facility in 2003.

General Assessment

The ITER magnet design is well advanced, and design solutions have been identified. The R&D programme launched in 1993 is near its completion. This programme has confirmed the manufacturing feasibility of the conductor and the magnets. The experimental results achieved with the CS model coil and CS insert are excellent and confirm the adequacy of the conductor to meet the ITER CS operation conditions. New R&D activities have been launched to facilitate cost reductions and address certain specific technology needs.

2.2 Vacuum Vessel

2.2.1 Function and Main Components

The primary functions of the vacuum vessel (VV) are to provide a high quality vacuum for the plasma, as well as the first confinement barrier of radioactive materials and a second barrier (after the cryostat) for the separation of air from potential sources of in-vessel hydrogen generation. The decay heat of all the in-vessel components can be removed by the water in the VV primary heat transfer system (PHTS) system, even in conditions when the other PHTSs are not functioning. The vessel supports in-vessel components and their loads during normal and off-normal operation. In addition, a tight fitting configuration of the VV to the plasma aids the plasma vertical stability, and the ferromagnetic material in the VV reduces the toroidal field ripple. Along with other in-vessel components, the VV provides adequate radiation shielding, in particular for the magnets and to allow access to the cryostat and port connections two weeks after shutdown.

The main components that make up the VV are the main vessel and the port structures.

The VV is a permanent machine component (RH class 3) and is safety classified (SIC).

2.2.2 Vacuum Vessel Design

2.2.2.1 Overall Arrangement

The VV is a torus-shaped, double wall structure with shielding and cooling water between the shells. The VV is located inside the cryostat and supported by the vessel gravity supports from the toroidal field (TF) coil case (see Figure 2.2-1); these are provided as part of the magnet system.

The blanket and divertor are mounted on the vessel interior and all loads are transferred to the vessel. The blanket modules are supported directly by the VV and the blanket cooling channels are routed over its plasma-side surface (see 2.3). The basic configuration and poloidal cross-section of the VV are shown in Figures 2.2-2 and -3, respectively. Detailed parameters are summarized in Table 2.2-1.

The VV has upper, equatorial, and lower port structures used for equipment installation, utility feedthroughs, cryo-vacuum pumping, and access inside the vessel for maintenance. Most of the port components are also of double wall construction with stiffening ribs between the walls.

The VV components need to be designed and manufactured consistent with an accepted code or standard. In addition, the design, materials and manufacturing of the VV components need to be consistent with providing a high quality vacuum.

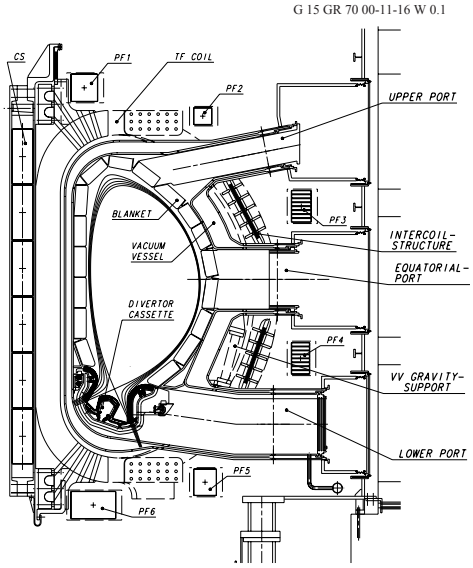

Figure 2.2-1
Tokamak Poloidal Cross-Section

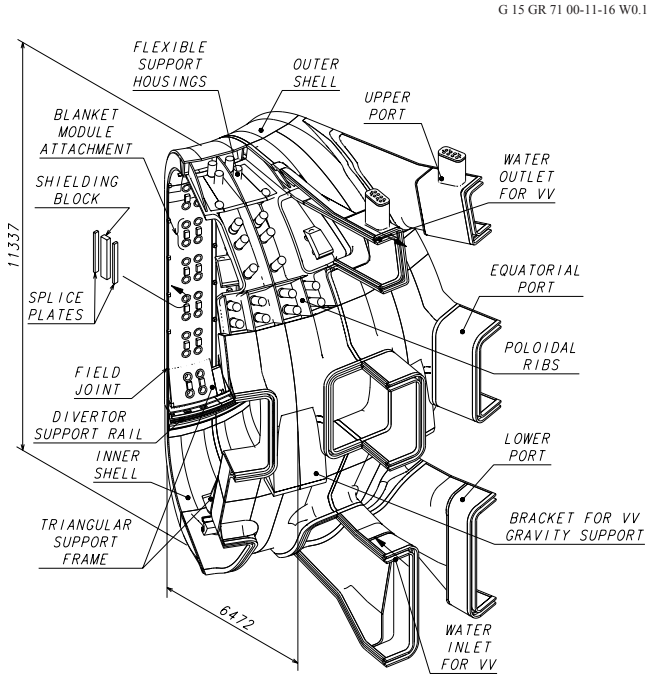

Figure 2.2-2
Vacuum Vessel Overall Arrangement

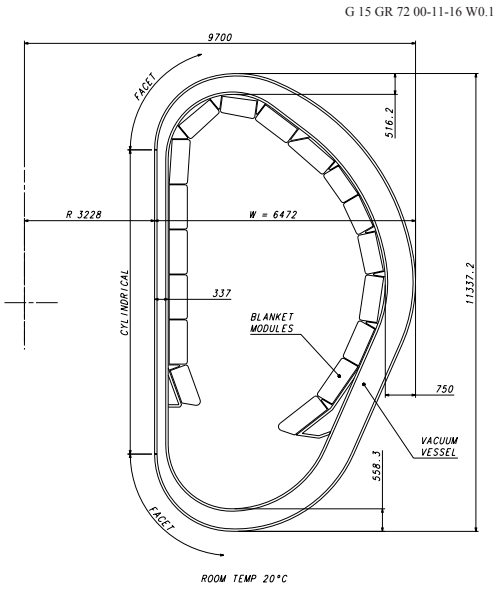

Figure 2.2-3
Vacuum Vessel Cross-Section

Table 2.2-1 Main VV Parameters

Size	
- Toroidal Extent of Sector	40°
- Shell Thickness	60 mm
- Rib Thickness	40 mm
Structure	
- Inboard Straight Region	Cylindrical
- Inboard Top/Bottom	Faceted
- Outboard Region	Faceted
Resistance	
- Toroidal	7.9 μΩ
- Poloidal	4.1 μΩ
Required Leak Rate	1×10^{-8} Pam^{-3}/s
Surface Area / Volume	
- Interior Surface Area	939 m^2
- Interior Volume	1,598 m^3
- Structural Volume (cooling channel)	639 m^3
Materials	
- Main Vessel and Port Structures	SS 316L(N)-IG
- Primary Shielding	SS 30467
- Ferromagnetic Insert Shielding	SS 430
- Connecting Ducts	SS 304
Mass (without water)	
- Main Vessel (without shielding)	2,542 t
- Shielding	2,889 t
- Port Structures	1,967 t
- Connecting Ducts	1,050 t
- Total	8,448 t

2.2.2.2 Materials

The choice of the materials used for the VV has a significant influence on costs, performance, maintainability, licensing, detailed design parameters, and waste disposal. The primary reason for the choice of materials shown in Table 2.2-1 is their high mechanical strength at operating temperatures, water chemistry properties, excellent fabrication characteristics, and low cost relative to other candidates.

The space between the double wall will be filled with shield structures mainly made of an austenitic stainless steel containing 2 weight % boron. The addition of boron to SS 304 was adopted to improve neutron shielding efficiency. A ferritic stainless steel is used as the shielding material under the TF coils in the outboard area to reduce toroidal field ripple. This steel has a high saturated magnetization at ~ 1.7 T. Both the materials have high corrosion resistance in water and excellent fabrication characteristics.

2.2.3 Vacuum Vessel Component Description

2.2.3.1 Main Vessel

The main vessel consists of inner and outer shells, ribs, shield structures, splice plates, shielding structures for field joints, and mechanical structures on the inner and outer shells to support in-vessel components and to support the vessel weight (see Figure 2.2-2).

The double wall structure has stiffening ribs between the shells to give the required mechanical strength and separate the shells. The number of ribs is minimized to simplify the vessel design and to reduce the cost. The basic vessel design is an all-welded structure. The inner and outer shells and stiffening ribs are joined by welding. The inner and outer shells are both 60 mm plates and the stiffening ribs mainly 40 mm plate. The shells and ribs form the flow passages for the vessel cooling water (see 2.2.4). The space between the shells will be filled with shielding.

The heavy steel structure of the VV provides a reliable first confinement barrier. Although the VV is a double wall structure, the inner shell serves as the first confinement barrier.

The VV is divided toroidally into 9 sectors joined by field welding using splice plates at the central vertical plane of alternate ports. The structure of the sector field joint will allow two sector replacement cycles and accommodate a mismatch between adjacent vessel sectors. Each sector includes a full set of port stubs and stub extensions at the toroidal centre of the sector and a set of half port stubs (split on the port centre) on each side. The straight sections of the inboard form a cylinder, and transitions are made to a four-facet per sector design at the top and bottom of this cylindrical section.

The VV is supported by VV gravity supports which minimize the tangential toroidal displacement of VV ports during each pulse (see 2.1).

A "tight fitting" configuration of the VV to the plasma has been employed to position the plasma-facing surface of the blanket modules in the correct position. The tight fitting vessel, together with the toroidally continuous triangular support frames for the lower blanket modules, also aids plasma vertical stability (Figure 2.2-2). The triangular support frames are needed also to provide the structural integrity of the VV.

Each blanket module is attached directly to the VV (or the triangular support frame) by a set of four flexible supports located symmetrically with respect to the module centre (see 2.3). The flexible supports are mounted in housings that are recessed into the VV (Figure 2.2-4). Where flexible support housings occur in the VV double wall structure, stiffening ribs between the shells are partially replaced by housings, which are connected between the inner and outer shells. The double wall structure continues around the housing to maintain the inner shell as the first confinement barrier (Figure 2.2-4). In addition, the module support structures include centring-keys and shear-keys for the inboard, and stub-keys for the outboard modules (see 2.3). The direct attachment of the modules to the VV produces local stresses due to poloidal/radial forces and moments, mainly generated in the modules by plasma disruptions and vertical displacement events (VDEs). To withstand these forces and moments, the vessel shells need to be locally reinforced by toroidal and poloidal ribs in the inboard region where the forces and moments are largest. Poloidal reinforcement ribs are locally connected between the support housings and to the inner shell, while toroidal reinforcement ribs are also used between the housings but they are not connected to the shells so as not to disturb the water flow. The poloidal reinforcement ribs strengthen the inner shell also against the forces from the shear-keys.

The blanket cooling manifolds (see 2.3) are supported on the VV by brackets that are welded to the vessel inner shell by a set of supports which distribute the reaction force from the manifolds to a wide surface, minimizing the local shear stress in the vessel shell.

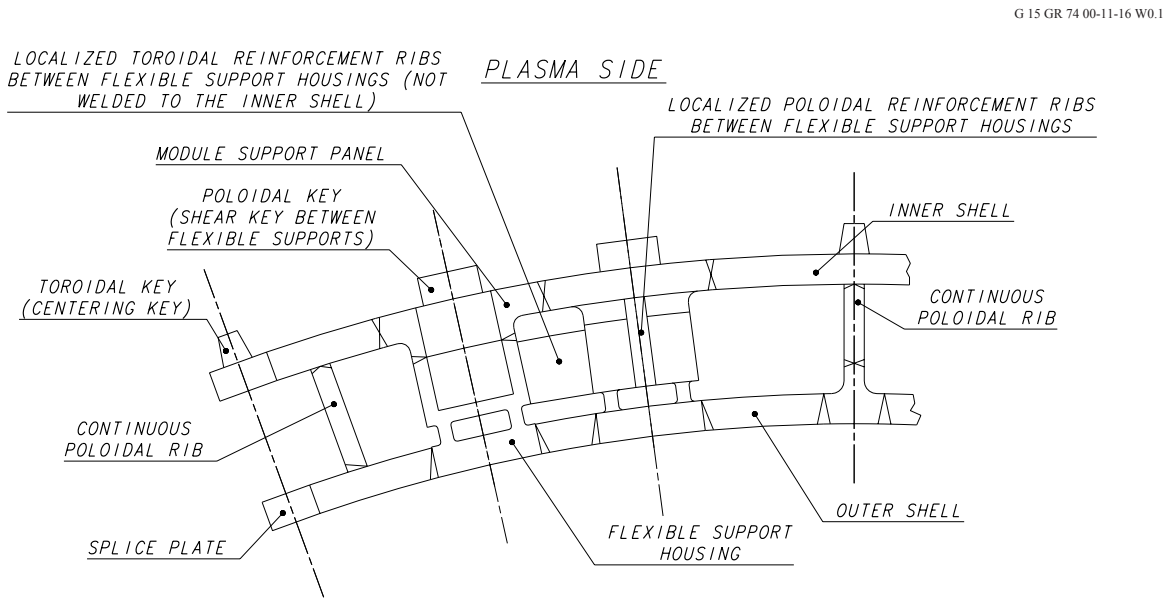

Figure 2.2-4 Typical Toroidal Cross-Section at Inboard Region

In addition to the blanket modules, divertor cassettes are supported by the VV (Figures 2.2-1 and 2) on toroidal rails at the inboard and outboard regions and by radial rails for the three divertor remote handling ports during remote maintenance (see 2.4 and 2.9). Because of the required precise alignment of the cassettes, these rails are installed after the VV is completed in the pit.

To provide adequate neutron shielding, the space between the vessel shells is filled, up to 60%, with steel plates (Figures 2.2-5 to 7). Where ferromagnetic steel is used as the shielding material under the TF coil in the outboard area (12 o'clock to 5 o'clock except the equatorial port region), these plates fill up to 80% of the volume between the shells to reduce toroidal field ripple by about a factor of 2. 40 mm thick plates will be used. Individual shielding plates are bolted together to form shields (Figure 2.2-7). The shields are fixed by bolts and pins to the ribs or module support housings to withstand the mechanical forces. The gaps between the shields and between the shields and the ribs are minimized to avoid excess neutron streaming. The shields for the field joints must be assembled on site and removed if replacement of the TF coil and vessel sector is required. The structure is a three-part shield that can be totally disassembled and removed from the field joint area, maximizing space available for welding, cutting, and inspection equipment.

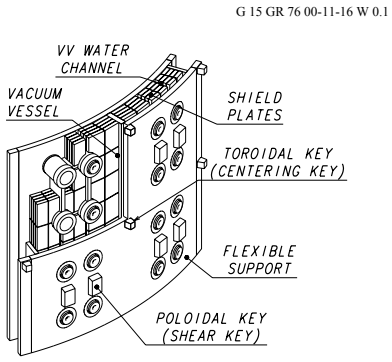

Figure 2.2-5
Arrangement of Shields

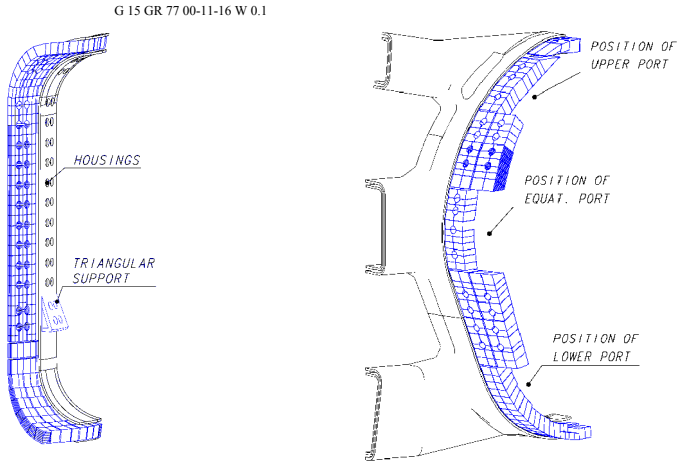

Inboard Region Outboard Region

Figure 2.2-6 Layout of Shields

The vessel is a passive component. There will however be instrumentation to monitor vessel and cooling water temperature, water pressure, local vessel stress/strain, and dynamic movement using thermocouples, pressure gauges, strain gauges and acceleration sensors (see 2.2.6).

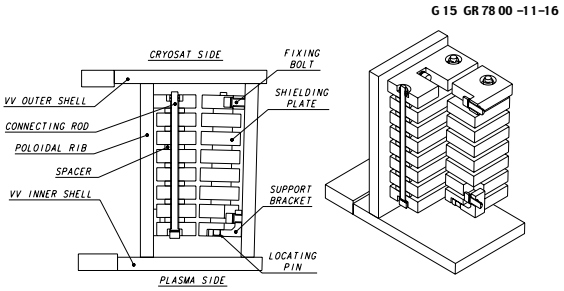

Figure 2.2-7 Structure of Shields

2.2.3.2 Port Structures

The vacuum vessel has upper, equatorial, and lower port structures that will be used for equipment installation, utility feedthroughs, cryo-vacuum pumping, and access inside the vessel for maintenance. A typical port structure includes a port stub and a port extension. The port extensions are normally equipped with the closure plates (on the extension end), which provide the primary vacuum boundary. The port stub is welded to the main vessel at the machine assembly station and the port extension is welded to the port stub in the pit. The port extensions are connected to the cryostat by connecting ducts that are a part of the secondary vacuum boundary. The basic port arrangement is shown in Figure 2.2-8. A summary of the port usage and inside dimensions is given in Table 2.2-2.

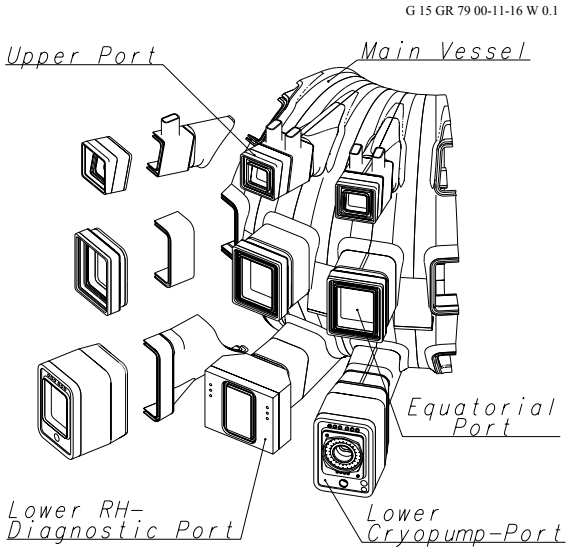

Figure 2.2-8 Port Arrangement

Table 2.2-2 Summary of Port Arrangement

Port Type	Number of Ports	Inside Dimensions (m)
Upper		
- Diagnostics, EC Systems, VV/Blanket Water Piping	18	0.835 to 1.154 (width) x 1.16 (height)
Equatorial		
- Regular (RH/Port Limiter, RF Heating Systems, Diagnostics, Test Blanket Modules)	14*	1.748 (width) x 2.2 (height)
- Heating Neutral Beam	2	0.582 (width) x 1.256 (min. height)
- Heating/Diagnostic Neutral Beam	1	0.582 (width) x 1.256 (min. height) 0.404 (width) x 0.438 (min. height)
Lower		
- RH/Diagnostics, VV/Divertor Piping	5	0.728 to 1.39 (width) x 2.175 (height)
- Cryopumps, IVV Systems, VV/Divertor Piping	13	0.728 to 1.39 (width) x 2.175 (height)

* There is no standard equatorial port next to the first NB port due to limited access for the RH equipment in this area.

The upper ports are inclined upwards and have a trapezoidal cross-section in the area between the TF coils, that is transformed to a rectangular cross-section beyond the coils. The pipes for the VV water outlet are welded to the port outer surface. The blanket pipes run along the port inner surface and exit the port through chimneys located at the port top before the closure plate. Feedthroughs for the helium purge pipes for the breeding blanket also follow this routing.

For the upper ports, the in-port components and the closure plate are integrated into one subassembly. The in-port component, which occupies the space delimited by the blanket pipes, is supported as a cantilever from the end portion of the port extension through the VV closure flange. There are tangential keys to withstand torque moments and the bolted flange joint to withstand all other loads (Figure 2.2-9). The tangential keys are located at the corners of the flange (4-8 keys in total). The keys are adjustable to compensate fabrication/assembly tolerances. The vacuum/pressure seal is made with a lip-welded joint which is incorporated into the bolted flange. The lip seal structure allows repeated cutting/rewelding for the in-port component replacement.

The equatorial ports include regular ports and neutral beam (NB) ports. The regular ports are radial and have a rectangular cross-section. As in the upper port, the in-port components and the port closure plate are integrated. The NB ports provide an angled access for the neutral beams for plasma heating and current drive. The NB ports are situated in three adjacent sectors of the machine and comprise two heating ports and a combined heating/diagnostic beam port. The port structure extends to the interface points with the cryostat and the NB system. The NB port has inner liners located along it, cooled by the blanket cooling water, to cope with the nuclear heating and the radiation of the plasma and the beam. A massive shield is integrated with the port or main vessel walls to enhance local shielding. Additional but similar structures are required for the plasma diagnostic neutral beam.

The lower ports are inclined downwards and have a trapezoidal cross-section in the area between the TF coils, which transforms to a rectangular cross-section beyond the coils. Each of the three RH/diagnostic ports is equipped with a removable closure plate and has a rectangular-box structure at the end to accommodate diagnostic waveguides. The closure plate of these ports is bolted to the port extension with a lip seal joint as in the upper port.

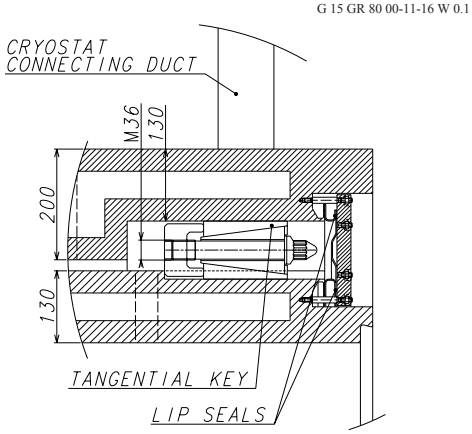

Figure 2.2-9
Support Structure of Port Flange

For the cryopump port, the cryopump and the closure plate are integrated into one subassembly. The port end plate has a large opening for the cryopump closure plate and a small opening at the bottom for the in-vessel viewing access. The cryopump closure plate is either bolted to the port end plate with a lip seal joint or welded to the end plate with a thick weld.

All lower ports are equipped with pipe stubs for the VV cooling water inlet connections and draining pipes. In addition, the divertor coolant pipe feedthroughs penetrate the port end plate.

The port stubs, extensions, and liners are of double wall structure with stiffening ribs between the walls. The connecting ducts have a single-wall construction. The double wall port components are cooled or baked by the VV water flowing between the shells. The total thickness of the port stubs and extensions is normally 200 mm (130 mm as the minimum) and the shell thickness is 60 mm or 40 mm. The NB port components generally require a thicker wall to enhance the port shielding properties. Steel plates may be incorporated between the walls of some ports to enhance local shielding.

2.2.4 Cooling and Baking

Performance differences between the VV and blanket require the use of separate cooling water circuits. Heat deposited in the vacuum vessel during normal and off-normal operations will be removed by cooling water that is supplied by the VV primary heat transfer system (see 3.3). Two independent water loops with the same cooling capability are used in each of the 9 sectors, feeding all sectors in parallel. Table 2.2-3 summarizes the VV cooling and baking conditions.

During normal operation, the design value of the total heat deposition in the VV is mainly due to nuclear heating. The heat is non-uniformly deposited in the VV. In addition, high heat deposition is also expected in the neutron-streaming regions, such as between blanket modules. The non-uniformly distributed heat in the VV is to be removed without any local overheating of the VV. During an off-normal event, e.g., a multiple cooling pump trip in the

blanket cooling system, the main heat load to be considered is thermal radiation from the blanket/divertor.

The water flow velocity and mass flow rate for normal operation need to cope with the nuclear heating rate in the VV in such a way that will keep thermal stresses in the VV structure at acceptable levels. The required water flow condition for normal and baking operation is forced turbulent flow. In order to maintain stresses at acceptable levels for the blanket manifold, the VV cooling water inlet temperature difference with respect to the blanket cooling water inlet temperature has to remain limited (~50˚) for normal and baking operations. During off-normal operation, the decay heat of both the VV and blanket would be removed by the water that is circulated by thermo-gravitational convection due to the heat flux from the vessel wall to the water (i.e., natural convection).

Table 2.2-3 Cooling and Baking Conditions of the Vacuum Vessel

Parameters	Value
Maximum Heating Power	
- Normal Operation (MW)	10
- Off-normal Operation (Decay Heat) (MW)	0.83
Number of Loops of VV PHTS	2
Normal Operation	
- Cooling Mode	Forced Convection (mainly)
- Water Mass Flow Rate for Two Loops (kg/s)	950
- Water Inlet Temperature (°C)	100
- Temperature Rise (°C)	2.5
- Water Inlet Pressure (MPa)	1.1
Off-normal Operation*	
- Cooling Mode	Natural Convection
- Water Mass Flow Rate for Two Loops (kg/s)	40
- Temperature Rise (°C)	5
Baking Operation	
- Water Inlet Temperature (°C)	200
- Water Inlet Pressure (MPa)	2.4

* assuming two loops are in operation to remove the decay heat of 0.83 MW.

The basic flow arrangement for the vessel is shown in Figure 2.2-10. The cooling water is supplied and flows through the lower ports and is routed to an internal supply manifold structure at the bottom of each sector. This manifold distributes the water to channels on both the inboard and outboard sides of the vessel to provide a uniform flow rate in the channels. The water flows up and is collected in an internal manifold at the top of the vessel and is routed through a channel in the upper port wall to an exit point. This configuration was selected to provide a system with maximum natural convection cooling to remove decay heat during off-normal operation. Water is also supplied from the main vessel to the triangular support structure.

Figure 2.2-11 shows water flow passages for the inboard region. Since about 70% of the heat is deposited in the inner shell and the first shield plate during normal operation, the flow route is designed to allow the water to flow mainly through the gap between them. The heat deposited in this region is removed by forced convection of the water which provides sufficient heat removal capability (more than 500 $W/m^2/K$ of heat transfer coefficient). However, the heat deposited in the triangular support structures will be removed mainly by natural convection.

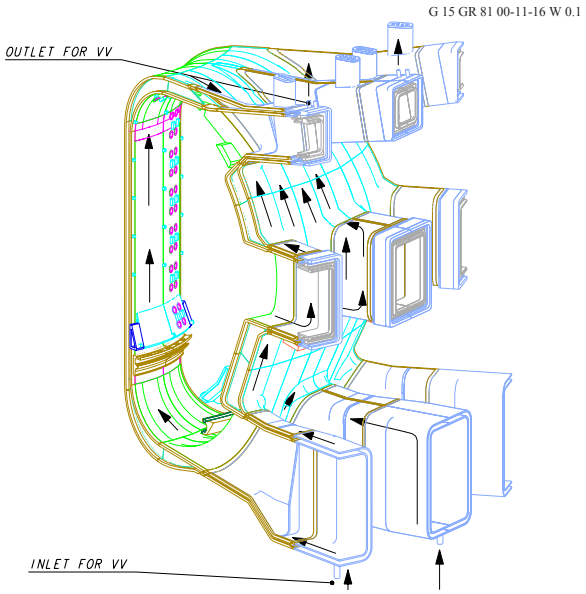

Figure 2.2-10
VV Water Routing

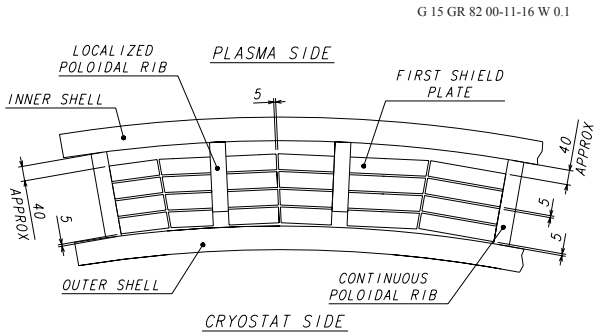

Figure 2.2-11
Water Flow Passage for
Inboard Region (Toroidal section)

2.2.5 Fabrication

To minimize the final assembly time on site, and to deliver a vessel structure with a high quality, the VV is to be fabricated in the factory as 9 sectors each spanning 40°. The practicality of transporting such a large sector from the factory to the site is an important factor in the manufacture of the vessel and must be assessed after the site is selected. The port stubs on the lateral sides of the sector are not installed in the factory. This allows the TF coils to be installed in the assembly area (discussed in 2.2.6).

The shields are installed at the factory before shipment to the site for all circuits except in the area of the field joints. In addition, most of the instrumentation and devices for coolant distribution for blanket modules are installed and experimentally examined at the factory.

Two concepts have mainly been considered for the sector fabrication scheme (Figure 2.2-12). One is to complete the inner shell first because it forms the first confinement boundary. Butt weld joints can be fully applied to the inner shell and inspection can be easily performed. Next, all ribs and support housings would be welded to the inner shell. After shields have been installed, parts of the outer shell would be welded (access is from the rib side and through the open space). The remaining parts of the outer shell would be welded (with a one-sided weld). Another concept is to utilize poloidal segments of a double wall structure, which are fabricated first then welded together to form a sector. This scheme was employed for the full-scale vessel sector fabrication in the L-3 R&D project[1]. In addition to the two schemes, an alternative scheme based on the mixture of the two schemes can be considered. Poloidal segments of a vessel without the outer shells are to be completed first. After the segments are welded together to form a poloidally closed shape, the outer shells will be welded.

[1] K. Koizumi, et al., “Design and Development of the ITER Vacuum Vessel", Fusion Engineering and Design, 41 (1998) 299-304, and K. Koizumi, et al., “Development of double-walled vacuum vessel for ITER,” Proc. 16th IAEA Fusion Energy Conference, Montreal, Canada, October 1996, Vol.3, pp.845-852.

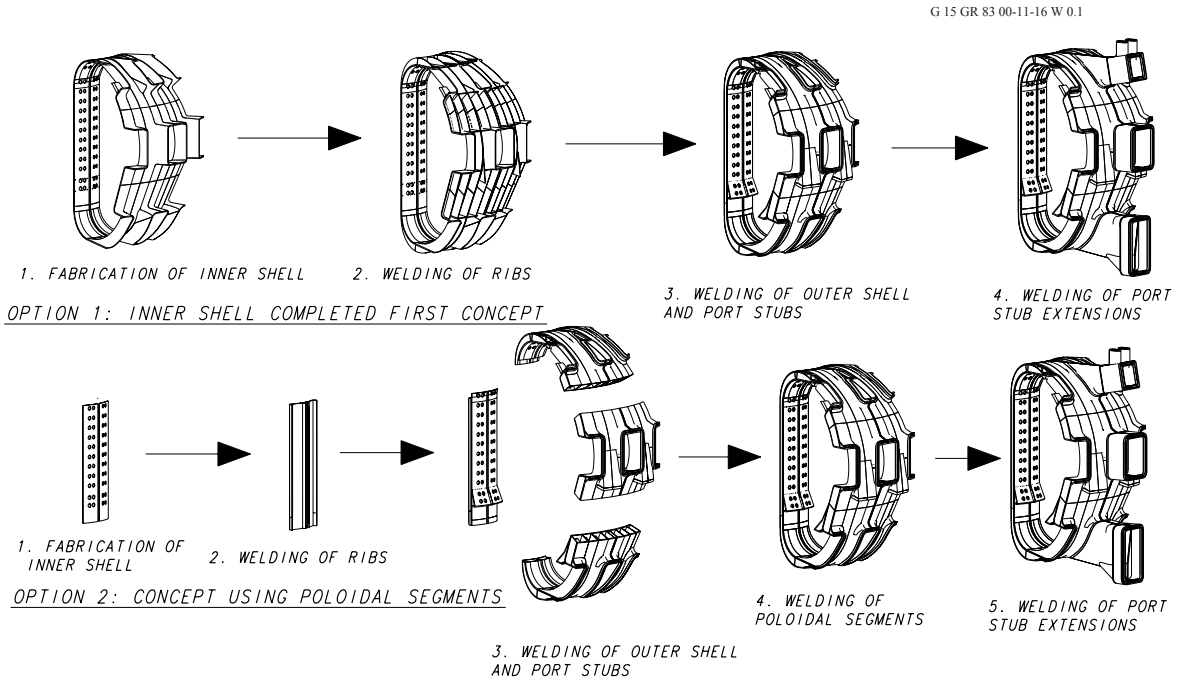

Figure 2.2-12 Options for Fabrication of a VV Sector

Figures 2.2-4 and -13 show an example of the inboard region including the weld joint configurations and the inboard assembly procedure. Most weld joints have conventional configurations and can be radiographically inspected to assure 100% weld efficiency. It is considered that they could be easily code/standard qualified. However, the one-sided weld joints between the outer shell and the ribs and the field joints will be inspected mainly by UT (ultrasonic testing).

Some fabrication and inspection aspects of the vessel are not consistent with the rules of the applied code, and exceptions (called code cases) must be developed and approved. The currently considered code cases for the VV are: (1) the one-sided weld joint design of the outer shell to the stiffening ribs, (2) the one-sided field weld joint design of the vessel sector to the splice plates, (3) the special stainless steel 316L(N)-IG to be used as the fabrication material, and (4) the wish not to use dye penetrant at cut edges, welds, and peripheral base metal surfaces on the vacuum side. Qualification of the VV fabrication/inspection and the code cases depends on the ITER host country and the applied codes/standards.

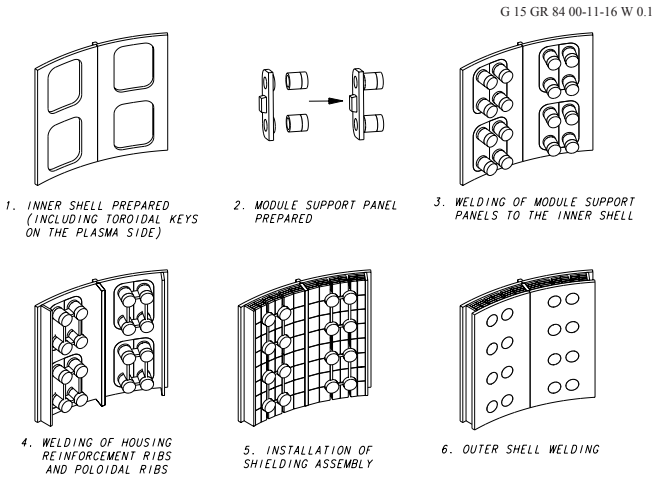

Figure 2.2-13
Fabrication Procedure of VV Inboard Region

To reduce the VV fabrication cost, a forged and/or cast structure has been investigated. For example, the region of the VV gravity support is a highly-stressed region, requiring numerous

reinforcements. Instead of an all-welded shell structure, a forged structure would reduce the fabrication cost and improve the fabrication tolerances. Currently, a thick outer shell made by forging is considered in the region between the equatorial ports where the VV gravity support is mounted. In addition, the large number of housings in the VV for the blanket module support that have a relatively small and simple structure can be manufactured by precision casting for cost saving. Powder HIPing is also being considered for further cost reduction.

The most important VV R&D performed during the EDA was associated with the fabrication of a sector and demonstration of remote welding, cutting and NDT systems. The full scale sector model, fabricated and tested as a part of the L-3 project, provided critical information related to fabrication technology required to produce a high quality sector, and the magnitude of welding distortions and achievable tolerances. Since the basic design of the ITER VV is the same as the fabricated sector model (i.e., the material, the basic torus shape, and the double wall structure with shielding and cooling water between the shells), this R&D also validated the fundamental feasibility of the ITER double wall design. Additional R&D, such as the fabrication of a partial VV sector model, may be required to confirm the improved fabrication technology and associated tolerances, as a first step to be done by the industrial firm chosen for manufacturing the vacuum vessel.

2.2.6 Initial Assembly, Commissioning, and Maintenance

At the ITER site, each sector is mated to two TF coils (and thermal shield) and assembled. Sector/coil mating involves moving a TF coil over each end of the sector. The lateral port stub halves are then welded in place. After the sector/coils are lowered into and positioned in the pit, 9 field joints (located on the centre of the lateral ports) are TIG-welded using splice plates to compensate for the size differences of the sectors. The final machine assembly sequence involves a sequential attachment of adjacent sectors until the resulting 160° and 200° segments are finally joined (see 2.10). Before VV commissioning is complete, the pressure boundary must be pressure tested as required by the code.

The advantages of the proposed VV sector geometry, versus one relying on one shop-manufactured sector per TF coil, result from the reduction in operations and associated requirements. The three most important benefits of assembling this larger sector are (1) the reduction of assembly cost by reducing the number of field joints, (2) improved dimensional stability due to the reduction in field joint welding, and (3) the capability to install in shop all additional piping, etc. inside the VV. In addition, the proposed VV sector geometry provides simple water routings for the VV and blanket modules in the VV structure, and full port structures at the toroidal centre of the sector.

An in-service inspection (ISI) program is not required by design codes, which signify only code-compliant construction. In particular, monitoring the vacuum pressure and mass spectrum in the VV and in the cryostat is expected to satisfy the objective of ISI. Very small leaks through the VV structure, which do not affect the VV structural integrity, can be detected and may also degrade plasma performance. In addition, there will be instrumentation to monitor the VV system status, particularly the vessel and cooling water temperature, water pressure, local vessel stresses/strains, and dynamic movement. As a further measure of investment protection, temperature, pressure stresses/strains or accelerations deviating from set point values will terminate plasma operation.

2.2.7 Design Criteria, Loads and Analyses

2.2.7.1 Design Criteria for the VV

The VV loading events and combinations have been classified into categories (see 2.12). These events are further classified into different service levels A, B, C or D which relate to the damage limits (A: negligible damage, functional; B: negligible damage, maintenance may be needed; C: local distortion possible, repair or replacement may be needed; D large non-local distortion possible, but minimum safety function maintained, and replacement may be needed; these are usually abbreviated to normal, upset, emergency, and faulted, respectively). The VV has been designed in accordance with ASME VIII div.2 for the normal operational design loads (category I and II events). For the events of category III and IV, not covered by ASME VIII, rules and safety factors as specified in ASME III have been used. Table 2.2-4 summarizes the service levels and the stress intensity "k" factors which are used to define the allowable stress.

Table 2.2-4 Design Criteria for Vacuum Vessel

Loading Event Category	Service Level	Damage Limit	Stress Intensity "k" Factor
I Operational	A	Normal	1.0
II Likely	A	Normal	1.0
III Unlikely	C	Emergency	1.2
IV Extremely unlikely	D	Faulted	2.0 (1)

Note:
1. As given in Table ASME III Subsection NC-3217-1 Note 4 the stress limit of Appendix F (fault conditions) may be applied, allowing a "k" value of 2.4.

The allowable stresses for the various types of stress (primary, membrane, bending, etc.) as defined by ASME VIII div.2 appendix 4 are computed as follows:

General Primary Membrane	$< 1.0\ k\ S_m$
Local Primary Membrane	$< 1.5\ k\ S_m$
Primary Membrane + Bending	$< 1.5\ k\ S_m$
Primary + Secondary	$< 3.0\ k\ S_m$ (only for Category I and II)

2.2.7.2 Load Description and Values

The VV must withstand many individual and combined loading conditions during both normal and off-normal operation.

Table 2.2-5 reports the list of the operating states to be considered for the design of the VV. Table 2.2-6 reports the list of the load case combination and the category and the Service Limit Levels. The ICEs have to be combined with disruptions and VDEs, but the time scale evolution of the over-pressure and over-temperature caused by the ingress of water is much longer than the time scale evolution of the EM loads and does not occur at the same time.

Different types of VDEs are considered based on the speed of the plasma current quench (slow=S and fast=F) and on the direction of the plasma movement (downward=D or upward=U). These VDEs are named VDE/S-D, VDE/S-U, VDE/F-D, and VDE/F-U.

Table 2.2-5 VV Design Load Events and Categories

Operating State	ITER Load Category	Service Limit Level (per ASME Code)
1) Construction	I	A
2) Testing		
2a) Pressure Test 1 (Coolant Pressure)	Test	Test
2b) Pressure Test 1 (VV Internal Pressure)	Test	Test
2c) Pressure Test 1 (VV External Pressure)	Test	Test
3) Off State	I	A
4) Baking State	I	A
5) Normal Plasma Operating State		
5a) Centre Disruption (CD) I (54 ms)	I	A
5b) Centre Disruption (CD) II (27 ms)	II	A
5c) Vertical Displacement Event (VDE) I	I	A
5d) Vertical Displacement Event (VDE) II	II	A
6) Ingress of Coolant Event (ICE) II	II	A
7) Toroidal Field Coil Fast Discharge (TFCFD)	I	A
8) Maintenance State	I	A
9) Seismic SL-1	II	A
10) Vertical Displacement Event (VDE) III	III	C
11)Overpressure States		
11a) ICE III (Pressure Pulse in-vessel breach < 0.1 m^2)	III	C
11b) ICE IV (Pressure Pulse in-vessel breach < 0.6 m^2)	IV	C
11c) Cryostat Air Ingress	III	C
11d) Cryostat Water Ingress	IV	C
12) Over-temperature states		
12a) VV loss of (forced) flow (one loop) + VV ex-vessel coolant leak (one loop)	IV	D
13) Seismic SL-2	IV	D
14) Toroidal Field Coil Short	IV	D

Table 2.2-6 VV Design Load Case Combinations and Categories

Operating State	ITER Load Category	Service Limit Level (per ASME Code)
1) Baking State + Seismic (SL-1)	II	A
2) TFCFD + VDE I	I	A
3) TFCFD + CD I	I	A
4) Seismic (SL-1) + CD I	II	A
5) Seismic (SL-1) + VDE I	II	A
6) Seismic (SL-1) + TFCFD	III	C
7) Seismic (SL-1) + CD II	III	C
8) Seismic (SL-1) + VDE II	III	C
9) Seismic (SL-1) + TFCFD + CD II	III	C
10) Seismic (SL-1) + TFCFD + VDE II	III	C
11) Seismic (SL-2) + CD I	IV	D
12) Seismic (SL-2) + VDE I	IV	D

For normal operating conditions (category I and II events), the most severe loads are caused by the coolant pressure, VV and in-vessel component weights, seismic events, plasma

disruptions and VDEs, and the TF coil fast discharge (TFCFD). The loads that mainly drive the design are due to a centred disruption (CD), VDE, and a TFCFD. The maximum vertical and horizontal forces on the VV are reported in 2.12. Seismic loads on the VV are reported in 2.15. The main electromagnetic load conditions estimated for the VV are reported in Table 2.2-7. In the tables, M_r, M_p, F_r, and F_p represent the maximum radial and poloidal moments and forces on modules, respectively. Figure 2.2-14 shows the sign convention for forces and moments. Normal operation coolant pressure is 1.1 ± 0.2 MPa. Maximum internal and external VV pressure in off-normal events is 0.2 MPa. Component weights are defined in Table 2.2-1.

Table 2.2-7 Main Electromagnetic Load Conditions for VV

Event	Load Cat.	Max. EM Pressure on VV		Max. EM Loads on Blanket Module			
		P_r (MPa) due to Eddy Currents+++	P_r (MPa) due to Halo Currents	M_r (MNm)	M_p (MNm)	F_r (MN)	F_p (MN)
TFCFD	I	-1.6	-	-	-	-	-
CD II	II	0.1 ~ 1.2	-0.66	-0.71	0.57	-0.15	-0.39
VDE/S-D II	II	0.1 ~ 1.2	-2.9	-	-	0.20	0.67
VDE/S-U II	II	0.1 ~ 1.2	-1.1	-	-	-0.14	-0.28
VDE/F-D II	II	0.1 ~ 1.2	-1.7	-0.54	0.41	0.12	0.38
VDE/F-U II	II	0.1 ~ 1.2	-0.60	-0.55	-0.41	-0.08	-0.16
TFCFD + VDE/S-D I+	II	-1.6	-2.2	-	-	0.15	0.51
VDE/S-D III	III	0.1 ~ 1.2	-3.9	-	-	0.27	0.90
VDE/S-U III	III	0.1 ~ 1.2	-1.4	-	-	-0.18	-0.37
VDE/F-D III	III	0.1 ~ 1.2	-2.2	-0.72	0.54	0.15	0.50
VDE/F-U III	III	0.1 ~ 1.2	-0.81	-0.73	-0.54	-0.10	-0.21
TFCFD +VDE/S-D II++	III	-1.6	-2.8	-	-	0.19	0.64

\+ I_{halo}/I_{plasma} x TPF (toroidal peaking factor) = 0.348 (60% of the VDE III). B_{tor} is assumed to be $0.95B_{tor}(0)$ at the time of max. EM pressure due to TFCFD.

++ I_{halo}/I_{plasma} x TPF = 0.435 (75% of the VDE III). B_{tor} = $0.95B_{tor}(0)$.

+++ Pressure due to the eddy current induced by a CD has the opposite direction to the pressure due to halo current and TFCFD, and should be neglected in load case combinations.

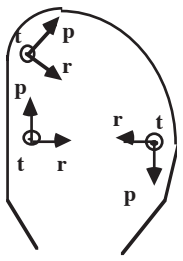

Figure 2.2-14
Local Coordinates

The upper and the equatorial ports are the most loaded constructions since the highest electromagnetic loads affect their in-port components during plasma events. The main loading conditions for these ports are summarized in Table 2.2-8. The data are given for the most loaded in-port components, namely for the EC-launcher for the upper port and the test blanket module for the equatorial port.

Table 2.2-8 Main Load Conditions for the Upper/Equatorial In-Port Components

Loading case/ port structure		Electromagnetic loads					Seismic loads			In-vessel pressure, MPa
		M_r, MNm	M_t, MNm	M_p, MNm	F_r, MN	F_p, MN	a_r, m/s^2	a_t, m/s^2	a_v, m/s^2	
EM I[1] + SL-1	Upper	1.2	1.3	0.26	-	-0.07	2.81	2.58	5.72	
	Equat.	8.6	-	-0.4	0.6	-	2.4	2.24	1.72	-
EM II[2] + ICE II	Upper	1.6	1.6	0.33	-	-0.09	-	-	-	
	Equat.	10.0	-	-0.5	0.7	-	-	-	-	0.2
EM II + SL-1	Upper	1.6	1.6	0.33	-	-0.09	2.81	2.58	5.72	
	Equat.	10.0	-	-0.5	0.7	-	2.4	2.24	1.72	-
EM II[3] + ICE III	Upper	2.1	2.2	0.43	-	-0.12	-	-	-	
	Equat.	9.0	-	-0.7	0.6	-	-	-	-	0.2
EM I + SL-2	Upper	1.2	1.3	0.26	-	-0.07	8.26	7.59	16.81	
	Equat.	8.6	-	-0.4	0.6	-	7.07	6.6	5.06	-

1. Maximum electromagnetic loads enveloping the Category I events
2. Maximum electromagnetic loads enveloping the Category II events
3. Maximum electromagnetic loads enveloping the Category III events

2.2.7.3 Structural Analyses of Main Vessel

2.2.7.3.1 Primary Stresses

The global FE model static analyses of the VV have been performed using two different models (see Figure.2.2-15): model A and model B. Both models have been developed using the ANSYS code. Each model provides, other than the results of the global analysis, boundary conditions for carrying out different specific local detailed analyses (see Section 2.2.7.3.2).

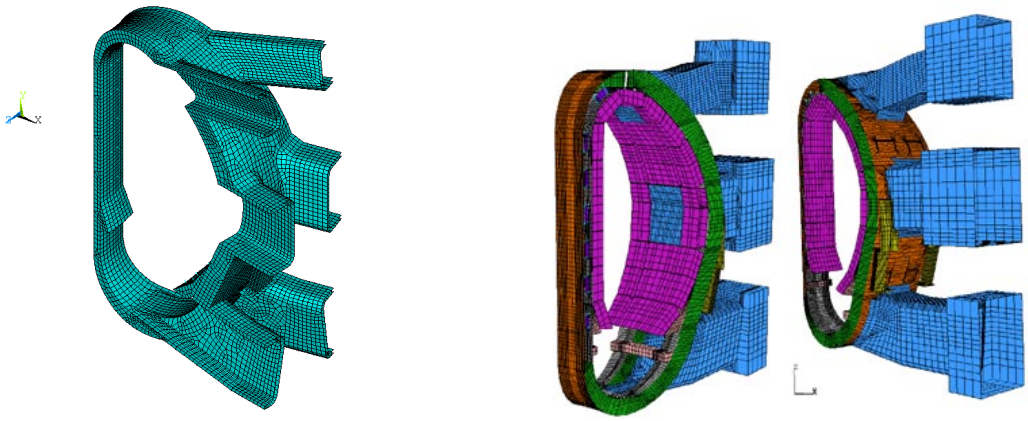

Model A **Model B**

Figure 2.2-15 Global FE Models Used for the Global Analyses of the VV

Table 2.2-9 reports a list of the analyses performed by the two models.

Table 2.2-9 List of the Global VV Analyses Performed by Two Different FE Models

	Model A	Model B
Global Vessel Analyses: Primary Loads		
Gravity (DW)	X	X
Operating Coolant Pressure (CP)		X
Baking Coolant Pressure (BCP)		X
Centre Disruption II (CD II)		X
Toroidal Field Coils Fast Discharge (TFCFD)	X	X
VDE III [1]	X	X
Seismic load (SL-1 and SL-2)	X	X
Internal VV Pressure 0.2 MPa		X
External VV Pressure 0.2 MPa		X
VDE II [1] + DW	X	
TFCFD + VDE I + DW + CP		X
VDE III [1] + DW	X	
SL-1 + VDE II +TFCFD	X	X [2]
SL-1 + CD II + TFCFD + CP		X

Notes:
1. VDE cases include slow, fast, upward and downward events.
2. Includes also coolant pressure.

The definition of the worst case and load case combination depends on the VV region of interest. The CD I and CD II events generate loads on the blanket modules that are generally smaller or similar to those caused by the fast VDE I and VDE II. In addition, CD events have halo current pressures that are smaller than those caused by the fast VDEs. For these reasons, the load case combinations TFCFD+VDE I and TFCFD+VDE II generally cause, in the main VV, larger stress than the combinations TFCFD + CD I and TFCFD + CD II. A typical exception is the support structures of some blanket modules (i.e. the shear keys) that experience larger loads in the CD II events. For these regions the TFCFD+CD II event has to be considered as one of the worst load case.

The load case combinations SL-1+TFCFD, SL-1+VDE II, SL-1+TFCFD+VDE I, and SL-1+TFCFD+VDE II are all classified as category III (load service level C). The load case combination SL-1+TFCFD+VDE II is the one among these that generates the maximum stress in the VV.

As reported in Section 2.2.7.2, ICEs have to be combined with disruptions and VDEs. The VV internal pressure caused by the ICE occurs several seconds after the start of the leak. The disruption and VDE time scale is much shorter (less than a second), therefore, even if the ICE and plasma events are correlated, the associated loads never occur simultaneously and can be analyzed separately.

Among the events that are classified as category IV, the worst load case is represented by the combination SL-2+VDE I. This events generates larger stress than the combination SL-2+CD I, because, as stated previously, the halo current pressures in VDE I are larger than in CD I.

The load case combination SL-1+TFCFD+VDE II is characterized by larger EM loads than the combination SL2+VDE I and, in general, generates larger stress in the VV.

The SL-2 event generates large stress mainly in the VV support. The combination SL-1+TFCFD+VDE II, because it is classified as category III, has stress values that are closer to the allowable than the combination SL-2+VDE I, which is a category IV event.

In conclusion, the load case combinations that mainly drive the design of the VV are:

- TFCFD + VDE I
- SL-1 + TFCFD + VDE II.

Seismic and EM loads have been combined applying equivalent static loads that take into account the dynamic effects (see Sections 2.2.7.3.3 and 2.2.7.3.4).

One of the most critical regions of the VV is the inboard wall because of the high toroidal field, which causes high EM forces. For this region the most severe loading conditions are the TFCFD and its load combination with EM loads due to a VDE, which cause high compressive stresses in the VV inboard wall and increase the risk of buckling.

An analysis of the VV structure performed to calculate the primary membrane and membrane plus bending stresses neglecting stress concentrations around discontinuities has given the results shown in Table 2.2-10. In the table P_m and P_m+P_b represent the membrane and the membrane + bending stress intensity. The most stressed region is the outer shell of the VV inboard wall.

Table 2.2-10 Primary Stress Intensity in the VV Inboard Wall

Event [1]	Load Cat	P_m (MPa)	Limit [2] (MPa)	$P_m + P_b$ (MPa)	Limit [2] (MPa)
TFCFD	I	72	147	78	220
TFCFD+VDEI	I	129	147	180	220
SL-1 +TFCFD+VDEII	III	150	176	207	265

Notes:
1 Loads due to gravity and coolant pressure are included.
2 Limit for AISI 316 L(N) IG @ 150 °C. In the welds a smaller limit value has to be assumed if the joint efficiency is lower than 1.

2.2.7.3.2 Detailed Local Stress Analysis

The VV structure has several geometrical discontinuities that cause localized stresses.

The structural analyses performed on the 3D global models have provided the boundary conditions for local detailed models. Several local detailed analyses have been performed to estimate the maximum local bending and peak stresses at these locations. The regions that have been analyzed in detail are:

- inboard wall : region around the support housings;
- lower and upper parts of the inboard wall region;
- inboard wall triangular support frame for the lower inboard blanket module;
- outboard wall region between the equatorial port and the lower port;
- VV support region.

Figures 2.2-16 and -17 report some of the local detailed models used for the local analyses. The results of these local analyses show that the primary membrane and bending stresses are below the allowable values. The values of the estimated peak stresses do not indicate any risk of fatigue failure.

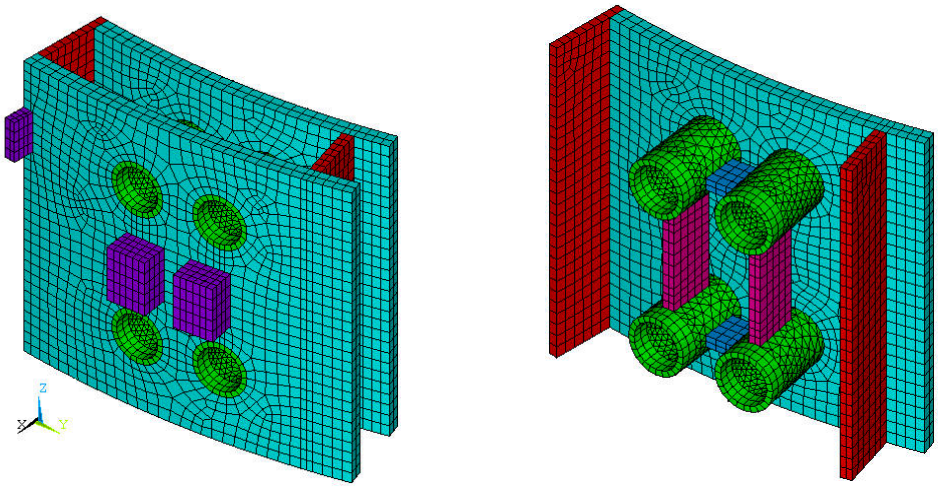

Figure 2.2-16 Sub-Models Used for the Structural Analyses of the VV Inboard Wall

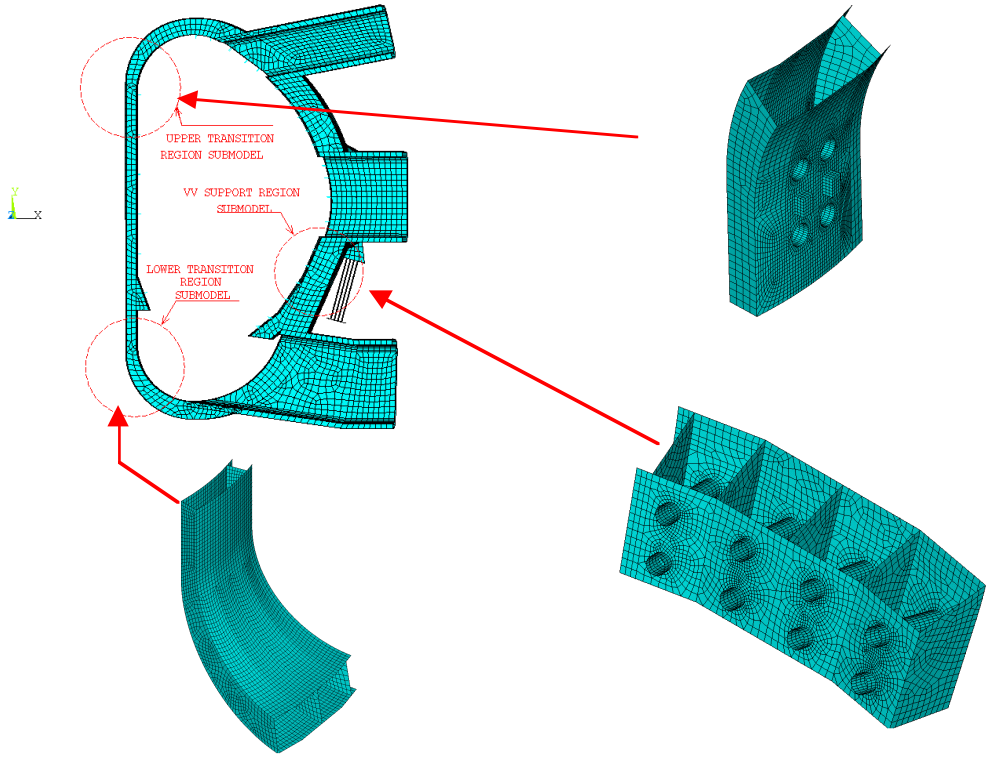

Figure 2.2-17 Sub-Models used for the Structural Analyses of the Upper and Lower Cylindrical/Facet regions and the Outboard Region Below the Equatorial Port

2.2.7.3.3 Dynamic analysis

Due to the impulsive nature of the EM loads on the VV and in-vessel components in disruptions and VDEs, a dynamic analysis of the structure is required to understand the dynamic behavior of the VV and the dynamic amplification of the structure response for

different loading conditions. Different FE models have been developed for the dynamic analysis. The most important models and their main purposes are:

- Model A: a 20° sector model for the dynamic time-history analysis of the symmetric VDE and disruption cases;
- Model B: a 90° sector model for the modal analysis;
- Model C: a 180° sector model for the dynamic time history analysis of the asymmetric VDE cases.

All models have been developed using the ANSYS code. Figure 2.2-18 shows models A and C. Model B is derived from model A reflecting the model from 20° to 90°. Model A and B include the VV inner and outer shells, the poloidal and toroidal ribs, the ports, the cantilever plugs, the connecting ducts to the cryostat, the blanket modules and the VV supports. Divertor structure and other in-vessel components are modelled as "non-structural masses". Model C is a more simplified model with the main VV body (inner and outer shells, poloidal and toroidal ribs) modelled with an equivalent single layer shell.

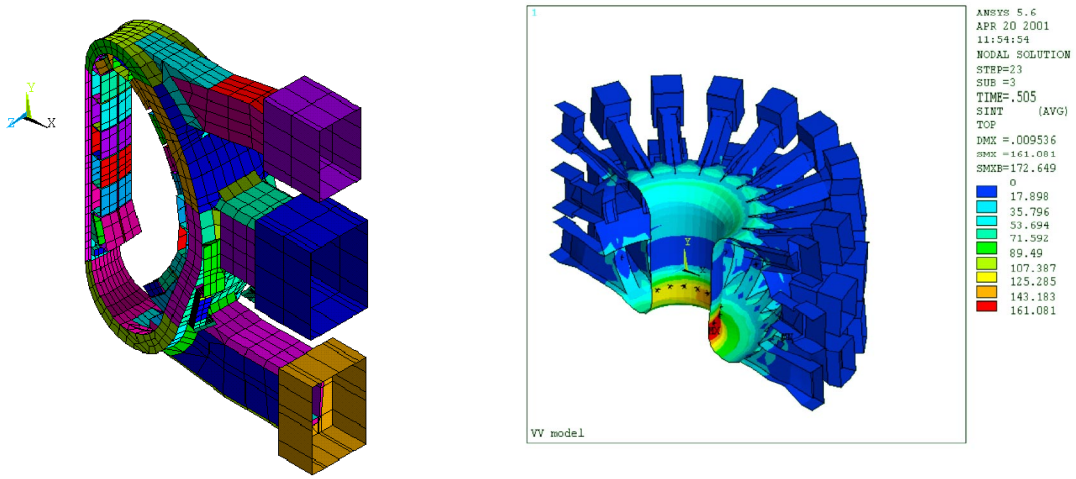

20° Sector Model **180° Sector Model with Stress Intensity (MPa)**

Figure 2.2-18 20° Sector Model and 180° Sector Model with Stress Intensity Contour Plot at Asymmetric VDE/S-D III Obtained at Time 505 s

Considering the results of the dynamic analyses performed on the 20° and the 180° models, the maximum expected vertical and horizontal forces in a VDE/S-D III on a single VV support are 6.0 MN and 4 MN respectively, which indicate that the vertical and horizontal forces on the supports in VDEs are dynamically amplified by factors equal to 1.2 and 1.4 respectively.

The largest displacement of the VV main body and ports have been obtained from the 180° model which includes the effects of the net horizontal force on the VV. Maximum values occur in a VDE/S-D III. The maximum displacements of the upper port plug occur in the VDE/F-U III. The VDE/F-U III has also given the maximum relative displacements of the port plugs with respect to the VV.

Table 2.2-11 reports a summary of the maximum displacements at different locations.

Table 2.2-11 Summary of the Results of the Dynamic Analysis: Maximum Absolute and Relative Displacements in VDE III [1]

Location	Displacements (mm)		
	Radial	Vertical	Toroidal
Top of VV	3.0	6.1	2.1
Inboard Wall	3.6	8.0	2.7
Bottom of VV	3.0	7.2	2.1
Outboard Wall	2.4	0.62	1.6
End of Port Duct of Upper Port	4.7	5.0	2.2
End of Port Duct of Equat. Port	2.5	2.4	1.4
End of Port Duct of Lower port	3.5	4.1	1.1
Upper Port Plug (or Antenna)	2.6	4.8	7.9
Equat. Port Plug (or Antenna)	1.8	0.35	1.4
Relative Displacement Upper Port Plug/VV	1.9	2.7	7.6
Relative Displacement Equatorial Port Plug/VV	0.6	0.7	0.64

[1]. Maximum values do not occur at the same toroidal location and for the same type of VDE

The maximum membrane stress in the VV shell occurs at the inboard wall in the VDE/S-D III. The results of the dynamic analysis show that the amplification factor for this value is equal to 1, which means that the detailed stress analysis of this region (see Section 2.2.7.3.1) can be performed by a static analysis applying the EM loads without any dynamic amplification.

2.2.7.3.4 Seismic analysis

Two independent seismic analyses have been performed with different aims:

- analysis A is orientated at getting results for the whole tokamak machine;
- analysis B is oriented at getting more accurate results for the VV.

The FE model used in the analysis A represents the VV using a single layer shell having a stiffness equivalent to the double shell wall with ribs. The analysis A is described in Section 2.15. The FE model used in the analysis B has a more accurate representation of the inner and outer shells and the poloidal and toroidal ribs.

The FE models used for the seismic analyses have been developed at different stages of the ITER design and for that reason each analysis is somewhat different. Results comparisons and parametric studies showed that it is very important to represent correctly the local stiffness especially at the connections between components. For some tokamak components, most of the flexibility is concentrated at these locations. An incorrect modelling of these connections can cause inaccuracy of the results.

The natural frequencies have been determined as a part of both analyses. The modes making the largest contribution in the horizontal and vertical directions are summarized in Table 2.2-12. The results are in relatively good agreement.

Table 2.2-12 Tokamak Natural Frequencies (1,2)

	Natural frequency (Hz)			
	Analysis A		Analysis B	
	Horiz.	Vertical	Horiz.	Vertical
First natural frequency of the tokamak	2.8	8.3	2.4	8.8
First natural frequency of the VV and in-vessel components	6.4	9.7	4.8 (3)	11.1

1. The VV natural frequencies have been obtained excluding the magnets from the model (VV vertical and horizontal supports at the attachments to the TF coils are restrained in all directions).
2. Vertical modes are obtained applying symmetry constraints to the nodes of the VV on the vertical boundary planes. Horizontal (toroidal) modes are obtained applying anti-symmetry constraints to the nodes of the VV on the vertical boundary planes.
3. A value of 5.5 Hz has been obtained assuming a more rigid connection between the VV support flanges.

The two seismic analyses give the maximum vertical and toroidal forces on the VV supports in the SL-2 case as shown in Table 2.2-13. These values are used for the structural analysis of the VV supports performed using more detailed models and including loads from other sources (see load combinations list in Table 2.2-6).

Table 2.2-13 Maximum Reaction Forces on a Single VV Support for a SL-2 Load

Analysis A		Analysis B	
Toroidal Force (MN)	Axial Force [1] (MN)	Toroidal Force (MN)	Axial Force [1] (MN)
9.2	4.6	8.5	3.5

1. The axial direction corresponds to the axis of the VV support plate, which is inclined with respect to the vertical axis of the machine by 15°

The results for an SL-1 earthquake can be obtained from the SL-2 results scaling the values by a factor 0.34. This factor comes from the consideration that SL-2 has a ground peak acceleration of 0.2g, while the SL-1 value is 1/4 of it (0.05g). In addition SL-2 has a larger damping.

Seismic loads generate relatively small stress in the main VV body, apart from the support regions. The stress analysis of the VV (see section 2.2.7.3.1) for the seismic load is performed applying an equivalent static load (a static load that generates the same stress as expected in the seismic event). This method allows:

- a more detailed FE model for the stress analysis
- the combination of the seismic loads with other applied loads (as listed in table 2.2-6 and 2.2-9).

2.2.7.3.5 Buckling Analyses

In the case of a TFCFD, the induced poloidal currents in the VV interact with the toroidal magnetic field causing compressive stress in the VV inboard wall. Elastic buckling analysis has shown that the critical elastic buckling pressure is much larger than the pressure that causes a stress level above the yield. An assessment of the inelastic buckling has given a minimum load for buckling of 6.6 MPa for the VV in the case of the TFCFD load distribution. The VV geometrical imperfections that have minimum critical inelastic pressure are the radial misalignment of adjacent sectors (the mismatch ±5 mm is compensated by the splice plate) and the imperfection congruent with the first elastic buckling mode (mode m = 6). A sensitivity study on the effect of the increase of the initial

imperfection of the VV geometry from ± 5 mm to ± 10 mm has given a reduction of the critical pressure of ~ 4%. It is assumed that the load factor (ratio between the buckling load and the applied load) is higher than 2.5 for categories I and II[1]. The maximum EM pressure during a TFCFD is 1.6 MPa, which gives a load factor of 4.1.

The inelastic buckling analyses performed for the load case combinations TFCFD + VDE I has given a load factor (LF) equal to 2.5, which is the minimum allowable.

As a consequence, to prevent the structural buckling of the VV inboard wall and to keep the primary stresses below the allowable values, the support frame for the modules in the inboard-bottom region needs to be a toroidally continuous structure.

An assessment of the effect of the support housings and the geometrical discontinuities caused by the module direct attachment to the VV has shown that the support housings do not reduce the buckling inelastic strength of the VV inboard wall. This conclusion has been obtained comparing the results from two FE models: one which includes the support housings and one without the support housings.

2.2.7.3.6 Thermal Stress due to Nuclear Heat Load

The thermal stress in normal operation is generated mainly by the nuclear heating. The nuclear heat load on the surface of the inner shell of the VV on the plasma side is equal to 0.1 W/cm^3 in locations behind the blanket modules (module thickness = 450 mm). The installation and handling procedure of the blanket modules requires the presence of gaps between modules. In the current design, these gaps are filled by the manifolds of the blanket coolant which provide a partial shielding and reduce the nuclear peak load to an estimated value of 0.4 W/cm^3 (see Table 2.2-14). A study on the effect of the heat transfer coefficient (HTC) between the VV coolant and the VV shell in steady state has shown that the thermal stress increases considerably if this coefficient is lower than 500 W/m^{2}K (see Figure 2.2-19). Assuming this value for the HTC, the highest temperature of the vessel structure is about 161˚C (water coolant temperature = 100˚C; nuclear heating rate = 0.4 W/cm^3) and the thermal stress is 175 MPa. Assuming that the maximum primary stress for category I and II events is 180 MPa (see Table 2.2-10), the maximum stress range obtained by the combination of the thermal and the primary stress is not expected to exceed the allowable ($3S_m$ = 441 MPa). The thermo-hydraulic analysis (see 2.2.7.6) has shown that the HTC is > 500 W/m^{2}K even in natural convection (no forced flow) in the inboard and outboard wall (see Figure 2.2-20 – "0-degree" curve) where the nuclear heating is maximum (see Table 2.2-14).

High thermal stress can be generated even in relatively small structures attached to the VV inner shell (i.e. shear and stub keys, divertor support rails) if not actively cooled or properly shielded.

[1] RCC-MR, "Design and Construction Rules for Mechanical Components of FBR Nuclear Islands."

Table 2.2-14 Nuclear Heating Rate on VV Interior Surface

Location	Average (MW/m^3)	Peak (MW/m^3)
Inboard wall	0.1	0.3
Top of the VV	0.083	0.25
Outboard wall	0.15	0.4
Bottom of the VV	0.045	-

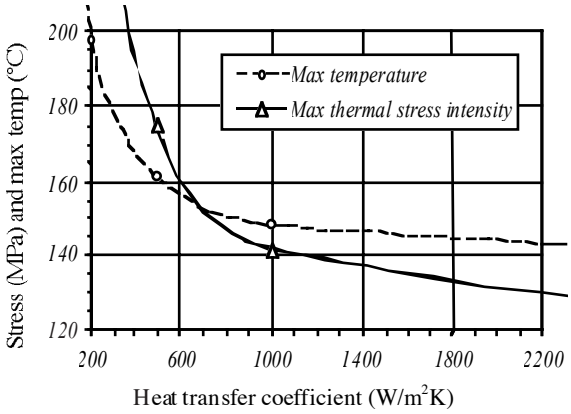

Figure 2.2-19 Effect of Cooling Capability on VV Thermal Stress

2.2.7.4 Structural Analyses of Port Structures

Several static structural analyses have been performed to calculate the stresses/strains for the port structures. The stresses and displacements for the upper and the equatorial ports are summarized in Table 2.2-15 for the worst loading conditions taken from the Table 2.2-8.

Table 2.2-15 Maximum Stresses and Displacements for Equatorial Port Structure

Location		Primary Membrane Stress (MPa)		Primary Membrane plus Bending Stress (MPa)		Maximum Displacement (mm)	
		Upper Port	Equatorial Port	Upper Port	Equatorial Port	Upper Port	Equatorial Port
In-port component	Inner shell	70	70	95	92	0.7	0.8
	Outer shell	100	70	155	97	0.8	0.9
	Ribs	60	70	85	91	0.7	0.8
Port extension	Inner shell	80	85	115	122	0.7	0.5
	Outer shell	35	40	50	62	0.8	0.5
	Ribs	70	45	86	63	0.7	0.5

The maximum primary membrane stresses are 85 MPa and 100 MPa for the port extension and the in-port component, respectively (the stress limit is 147 MPa), and the maximum membrane plus bending stresses are 122 MPa and 155 MPa (the stress limit is 221 MPa). These stresses occur in the areas near to tangential keys, and the stresses in all other areas are much lower. The maximum average contact stress in the key is about 65 MPa for the upper port (maximum stress intensity is 140 MPa), and 230 MPa for the equatorial port (maximum stress intensity is 362 MPa). The maximum stresses are generally below the stress limits. To increase the safety margins, the keys may be manufactured from a stronger material than SS 316 L(N) (e.g., a stainless steel A-286 (AISI 660) that is about twice as strong as SS 316 L(N)).

The static analyses of the ports performed on detailed models, which include the ports and in-port components (attachment points to the VV are assumed fixed) have given maximum displacements of the in-port component ends in the front portion equal to 5.3 mm for the upper port and about 1.4 mm for the equatorial port. These rather small displacements

confirm the feasibility of the cantilever concept. At the back of the port structure, the maximum relative displacement between the port and the in-port component is about 0.1 mm for the upper port and about 0.4 mm for the equatorial port. The latter displacement causes a deformation of the lip-welded joint but resulting stresses are well below the stress limit.

A structural response to the dynamic character of the electromagnetic load application has been also assessed. For this assessment, the maximum accelerations calculated as a result of the VV dynamic analysis (namely, a radial acceleration of 0.3g, a vertical acceleration of 0.6g, and a toroidal acceleration of 4.5g) were applied to the upper port model. The maximum primary membrane stresses are 105 MPa and 110 MPa for the port extension and the in-port component, respectively, and the maximum membrane plus bending stresses are 148 MPa and 163 MPa. The maximum average contact stress in the key is about 45 MPa (the maximum stress intensity is 175 MPa). These values are below the allowables.

2.2.7.5 Operation at 17 MA Plasma Current

The increase of the electromagnetic loads due to an increase of plasma current from 15 MA to 17 MA reduces the stress safety factor for primary loads to values very close to 1. If a joint weld efficiency of 1 is not achieved for some joints (e.g. the one-sided field joint) the primary stress might exceed the allowable values at few locations.

Preliminary buckling analysis has shown that for the present VV design the buckling safety factor is 2.3 for the load case combination TFCFD + VDE I in case of 17 MA operation, which is slightly smaller than the allowable value (following the RCC-MR code[1] the allowable value is 2.5). Therefore, before operating at 17 MA, plasma conditions have to be experimentally ascertained to modify the currently considered conservative assumptions (so that less conservative assumptions can be used for the VV structural analyses).

2.2.7.6 Thermal and Hydraulic Analysis

A series of thermal and hydraulic analyses of the VV have been conducted to clarify the heat balance without any peaked heat in the VV and heat removal capability both during normal (forced convection cooling mode) and off-normal (natural convection cooling mode) operations. As discussed in 2.2.7.3.4, it is expected that the maximum nuclear heating caused by direct neutron streaming between the modules will be approximately four times higher than the average heating rate (~ 0.1 W/cm^3) of the VV inner shell. In order to keep the thermal stress of the VV below the allowable, a sufficient heat removal capability, such as ~ 500 W/m^{2}K of heat transfer coefficient on the wall surfaces, is required for the VV cooling (see 2.2.7.3.4). Such a heat removal capability can be achieved if forced flow cooling with a flow velocity > 0.05 m/s is used. However, the overall water mass flow rate needs to be minimized to keep the required heat transfer system as small as possible.

Since the flow velocity of the water is not so high even for normal operation, it is expected that natural thermo-gravitational convection due to the heat flux from the vessel wall to the water will enhance the heat transfer characteristics (i.e., the forced convection heat transfer). Figure 2.2-20[2] shows an example of the calculated heat transfer coefficient as a function of

[1] RCC-MR, "Design and Construction Rules for Mechanical Components of FBR Nuclear Islands."
[2] M. Onozuka, et al., "Design and Thermal/Hydraulic Characteristics of the ITER-FEAT Vacuum Vessel," in Proc. 21st Symposium on Fusion Technology, Madrid, Spain, September 11-15, 2000.

the flow velocity, where “degrees” indicates inclination angle to the vertical for mixed convection flow. It was assumed that the water temperature is 100˚C and the heat generation is 0.1 W/cm^3. An enhanced heat transfer capability due to natural convection is expected for a flow velocity lower than 0.06 m/s. To confirm the effect of the natural convection on the thermal and hydraulic characteristics of the VV and to reduce the overall water mass flow rate, experimental investigation will be required.

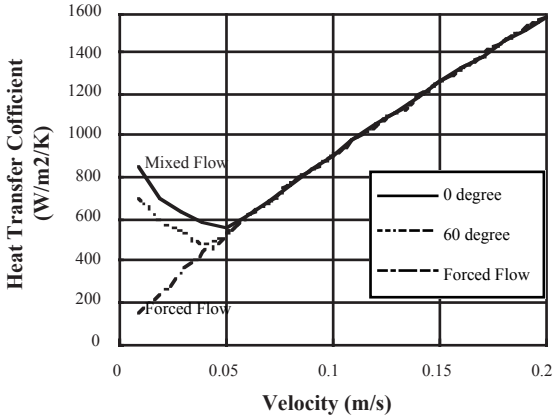

Figure 2.2-20 Heat Transfer Characteristics for VV Coolant Channel

2.2.8 Vacuum Vessel Overall Assessment

The VV must withstand many individual and combined loading conditions during both normal and off-normal operation. Analyses done to date are those considered to be the most severe loading cases, which will drive the basic design of the VV structure. Although further analyses are required for numerous loading conditions to confirm the structural integrity of the VV, based on the analyses performed to date, the VV appears structurally capable of withstanding the expected loads.

The main emphasis of the continued design development up to the procurement will be to refine the procurement specification used for the cost estimation in the detail necessary for procurement tendering to be launched at the start of the construction phase. This will include the development of any necessary technical justification to allow the design to be licensed in any of the potential ITER host countries including the code qualification of vessel features which are not fully covered by or comply with existing codes.

2.3 Blanket

2.3.1 Blanket Function and Main Components

The basic function of the blanket system is to provide the main thermal and nuclear shielding to the vessel and external machine components. The blanket system is also designed to make possible the planned partial conversion (outboard area only) of the shielding blanket to the breeding blanket in a later stage of operation (if justifiable).

The basic concept of the blanket system is a modular configuration with a mechanical attachment system. The blanket modules (BMs) are attached directly to the vacuum vessel. Manifolds that supply cooling water to the modules are mounted on the vacuum vessel behind the modules.

The ITER-FEAT blanket module design is aimed of minimising, (a) the module cost, (b) the radioactive waste, and (c) electromagnetic (EM) loads due to disruptions/VDEs (vertical displacement events). The module configuration consists of a shield block to which separate first wall (FW) panels are mounted. The use of multiple flat panels for the FW provides a simple unit design and reduces the associated machining costs. A deeply slitted configuration minimises induced eddy currents and EM loads in the module. The main shield blanket parameters are given in Table 2.3.1-1.

Table 2.3.1-1 Shield Blanket Parameters for 500 MW Fusion Power Operation

Parameters	Unit	Value
Total blanket thermal power	MW	690
Heat flux on first wall (FW), average/max.	MW/m^2	0.25 / 0.5
Heat flux on limiter, average/max.	MW/m^2	~ 3 / ~ 8
Neutron wall loading, average/max.	MW/m^2	0.56 / 0.78
Number of modules, total/NB port modules		421 / 17
First wall surface area	m^2	680
Weight of modules	t	1,530
Weight limit for module	t/mod.	4.5
Typical blanket module dimension (Inboard equator)	mm	1415x 1095x450

2.3.2 Overall Configuration

2.3.2.1 Shield Blanket Module Arrangement

The 17-fold segmentation of the shield modules in the poloidal direction is established by taking into account the weight limit of 4.5 t per module imposed by the remote maintenance equipment, and the desire to minimise the number of modules for cost reduction. The module toroidal length varies from 1.25 to 1.96 m and the poloidal length from 0.85 to 1.24 m except for modules in the NB port region. The arrangement of shielding blanket modules is shown in Figures 2.3.2-1 and 2.

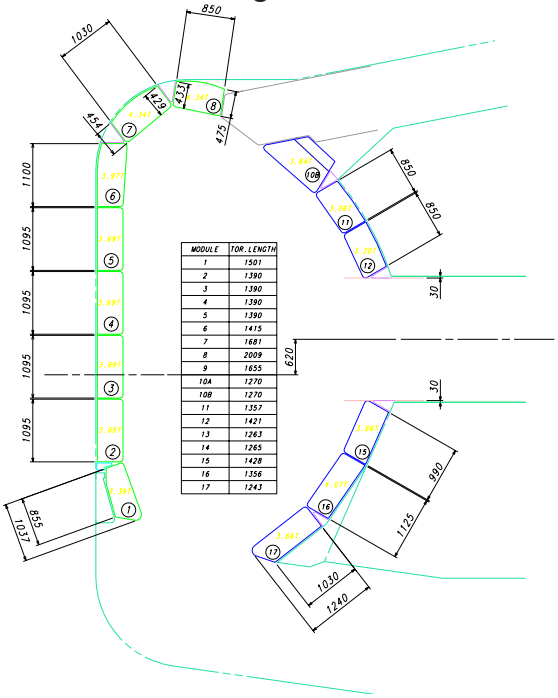

G 16 GR 18 00-12-08 W0.1

Figure 2.3.2-1 Shield Blanket Module Segmentation
(poloidal cross-section through a port)

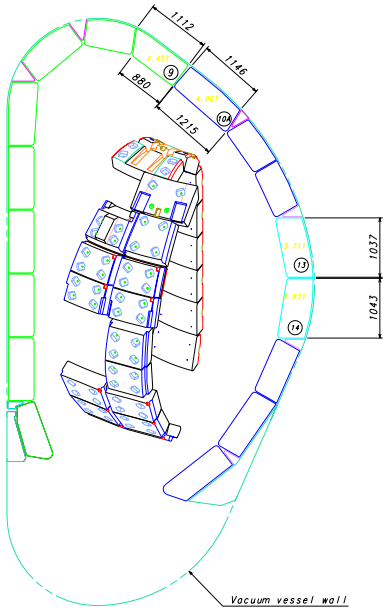

G 16 GR 19 00-12-08 W0.1

Figure 2.3.2-2 Shield Blanket Module Segmentation
(poloidal cross-section in TF coil mid-plane)

The FW/shield modules have a toroidal segmentation of 20º (18 modules) on the inboard, and 10º (36 modules) on the outboard. In the region of the upper ports there are 18 modules between the upper port plugs. In the 13 positions between the 14 normal equatorial ports a polodal segmentation of 2 is used. A different segmentation is used in the region of the NB ports; 17 special modules are used to cover the area between port 3 and port 8.

2.3.2.2 Materials

Materials used for the primary modules and port limiter are shown in Tables 2.3.2-1 and 2, which also show the operating temperatures deduced from the thermal analysis and the estimated neutron damage for a local 14 MeV fluence at the first wall of 0.5 MWa/m^2.

Table 2.3.2-1 Primary Module Materials

Component	Material	Max. temp. (°C)	Neutron damage (dpa)
First wall			
- plasma-facing material	Be (S-65C or DShG-200)	700	1.6
- heat sink	DS Cu Al25-IG or CuCrZr-IG)	400	5.3
- tube and structure	SS 316L(N)-IG	160	2.7
Shield block	SS 316L(N)-IG	340	2.3
Flexible support			
- cartridge	Ti-6Al-4V with ceramic coating	200	0.03
- bolt/collar	Inconel 718/DS Cu Al60 with ceramic	210	0.15
Key structure / pad	SS 316L(N)-IG/bronze with ceramic insulation and MoS_2 coating	260	0.09
Electrical connection			
- bent sheets/support block	CuCrZr-IG/SS 316L(N)-IG	220	0.05
- bolt	Inconel 718	300	0.05
Hydraulic connection/manifold	SS 316L(N)-IG	150	0.05

Remarks: DS - dispersion strengthened, SS - stainless steel, IG - ITER Grade

Table 2.3.2-2 Port Limiter System Materials

Component	Material	Max. temp. (°C)	Neutron damage (dpa)
Limiter module			
- plasma facing material	Be (S-65C or DShG-200)	740	1.6
- heat sink	DS Cu Al25-IG or CuCrZr-IG)	450	5.3
- structure	SS 316L(N)-IG	160	3.4
Main structural and shield part and alignment system bellows	SS 316L(N)-IG	150	0.02
Flexible pivot	Ti-6Al-4V with ceramic coating	200	0.02
High strength bolt	Inconel 718	200	0.02

2.3.2.3 Cooling and Baking

The heat deposited in the blanket modules is cooled by the three independent loops of the primary first wall/blanket (PFW/BLK) primary heat transfer system (PHTS, see also 3.3). Each loop has the same coolant capacity, and feeds three 40º sectors. Adjacent 40º-sectors are cooled by different loops as a safety feature. The maximum heat load for the blanket modules is 690 MW, including the front part of the port plugs except for the port limiters. Table 2.3.2-3 shows the coolant flow condition for the blanket modules. The PFW/BLK PHTS loops cool the 421 blanket modules and the 18 in-port components in the upper ports. At the equatorial level, 12 in-port components and 3 NB liners are cooled by PFW/BLK PHTS loops, 2 port limiters are cooled by the divertor/limiter cooling loop (DIV/LIM PHTS) while the obscured port (port 7) has no port plug.

Table 2.3.2-3 Coolant Flow Condition for Blanket Modules

Maximum Heating Power (MW)	690
Number of PHTS loops	3
Cooling Operation	
- Coolant Inlet Temperature (°C)	100
- Temperature Rise (°C)	48
- Coolant Mass Flow Rate (kg/s)	3,378
- Coolant Inlet Pressure (MPa)	3.0
- Pressure Drop* (MPa)	≤ 1.0
Baking Operation	
- Coolant Inlet Temperature (°C)	240
- Coolant Inlet Pressure (MPa)	4.3

* in the in-vessel part of the blanket cooling system

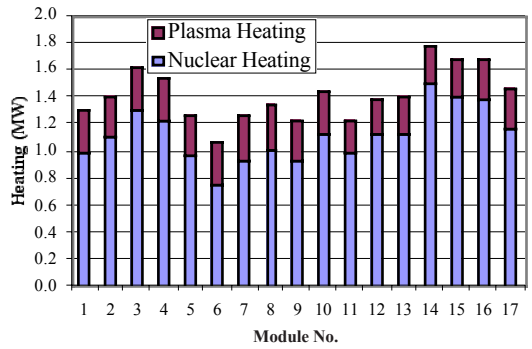

Figure 2.3.2-3 Heat Deposited in Each Module
(see Figure 2.3.2-1 for module no.)

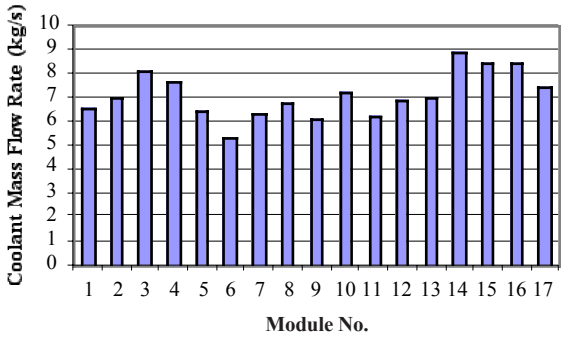

Figure 2.3.2-4 Required Coolant Mass Flow Rate for Each Module

The heat deposited in each module consists of nuclear heating and plasma heating as shown in Figure 2.3.2-3. The nuclear heating for each module is estimated based on the latest nuclear analysis and conforms with the nominal total nuclear heating of 554 MW. The plasma heating for each module is estimated assuming a uniform heat flux with nominal total value of 136 MW. The total surface area of the first wall is 680 m^2, so the average heat flux due to plasma heating is 0.2 MW/m^2. Figure 2.3.2-4 shows the required coolant mass flow

rate for each module. This required flow rate will be achieved using two kinds of orifices. One is installed inside the branch pipes of the blanket modules, providing the flow balance between blanket modules connected in parallel to the manifold. The other is installed inside the pipes around the interface point between the blanket system and the coolant loop to distribute the required mass flow to each manifold from the header of the PHTS.

2.3.3 Primary Modules

2.3.3.1 General

The module configuration consists of a shield body to which a separable first wall (FW) is mounted. The separable first wall has a facet geometry consisting of multiple flat panels, where 3-D machining will not be required. This produces a simple unit design with low associated machining costs. Several FW panels can be produced in each hot isostatic pressing (HIP) cycle. The use of small separate FW panels eases the Be tile HIP joint and will minimise the scrap rate. The separation of the FW from the shield body allows manufacturing process costs to be minimised, and solid HIP will be used only for the FW panel fabrication. The use of multiple panels also makes possible the replacement of individual damaged units, reducing nuclear waste volume, and it simplifies the repair and replacement methods in the hot cell. A configuration with deep slits minimises the induced eddy currents and EM loads.

The blanket module has four or six separate FW panels depending on the option chosen for FW attachment. Two attachment methods are being considered: one is based on a central beam attachment, which is connected to a shield block at its rear side (option B, Figure 2.3.3-1), and the other is an attachment with bolts and small shear ribs to support EM loads and to prevent sliding due to thermal expansion (option A, Figure 2.3.3-2). The shield block has radial cooling channels for both options. For hydraulic connection, two option are under consideration, i.e. separate connectors to use simple water pipes, and a co-axial connector to minimise the number of seal welds (Figure 2.3.3-3). In the following section, the option B primary module with separate connectors will be described in detail.

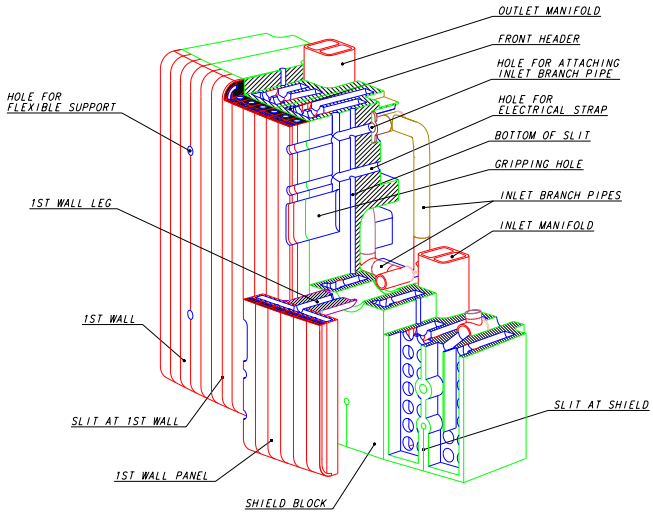

G 16 GR 22 00-12-08 W0.1

Figure 2.3.3-1
FW Panel/Shield Block with Central Beam Attachment

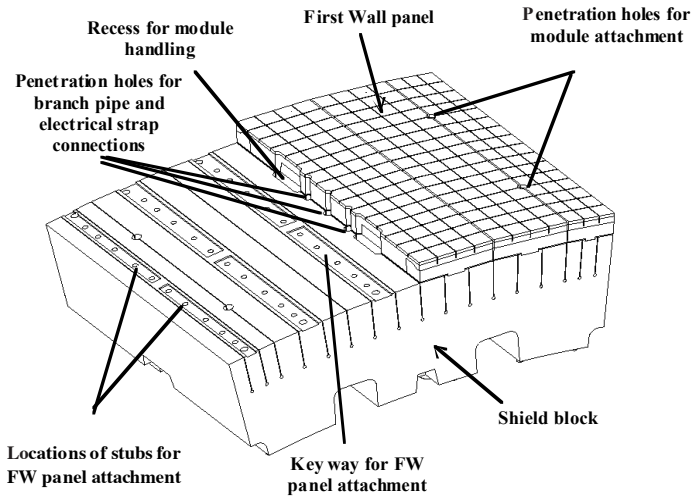

G 16 GR 23 00-12-08 W0.1

Figure 2.3.3-2 FW Panel/ Shield Block Attached with Bolts and Shear Ribs

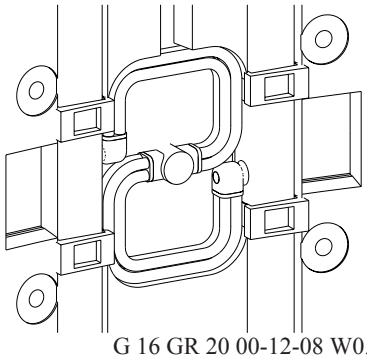

G 16 GR 20 00-12-08 W0.1

Figure 2.3.3-3 Layout of Co-axial Hydraulic Connection for the Inboard Blanket Module

2.3.3.2 First Wall

The FW is composed of flat panels and attachments to the shield block. Each FW panel consists of beryllium armour in the form of tiles attached to a Cu-alloy heat sink plate internally cooled by SS cooling tubes. The Cu-alloy plate is attached to a ~ 50 mm thick steel backing plate that has a structural plus shielding function. A simple straight poloidal cooling channel layout is used. The FW panel will be manufactured using solid HIP as the reference method, with powder HIP also considered as an alternate method if fabrication is possible within acceptable dimensional accuracy.

The FW with central beam attachment (option B) consists of four individual, 81 mm thick, flat panels, as shown in Figures 2.3.3-4 to 6. The panel is provided with narrow (2 mm) poloidal slots, between every other FW cooling channel. The slots are continuous in the heat sink but are discontinued half way through the SS backing, where the toroidal inlet/outlet collectors are located. Front access penetrations (diameter 30 mm) are made in the poloidal slots. They are used to access the blanket module support, hydraulic, and electrical connections, for remote handling. On either side of the penetrations the cooling tubes are displaced inside the Cu-alloy heat sink to provide space for the holes.

The central beam is welded to the rear side of the FW panel at one end and is attached to the shield by welding (or by a bolted connection) on the other. The supporting beam is inserted inside a suitable penetration in the shield block. Its mounting and dismounting is made from the rear of the module. A weld thickness of about 12 mm is needed if the beam is supported at its end as a cantilever. The main advantages of the attachment system are the free thermal expansion of the FW panel, and the location of all the attachment fixtures on the back of module, where the volumetric heating and the irradiation damage is lowest.

The FW coolant inlet and outlet supply channels are routed inside the supporting beam. The inlet is connected to the main blanket supply lines, the outlet to the shield block headers.

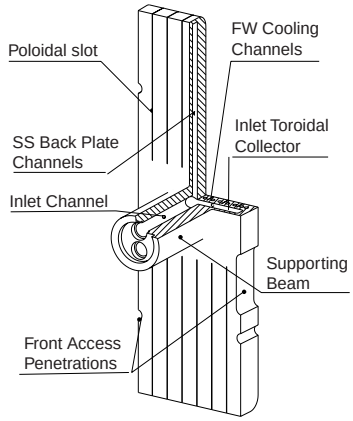

G 16 GR 24 00-12-08 W0.1

Fig. 2.3.3-4 FW Panel Rear Side View

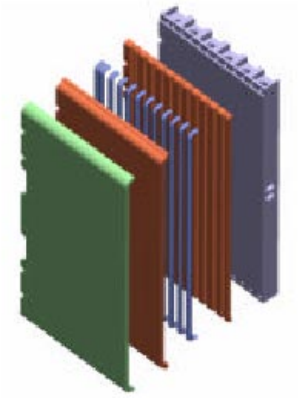

G 16 GR 25 00-12-08 W0.1

Fig. 2.3.3-5 FW Panel before Assembly

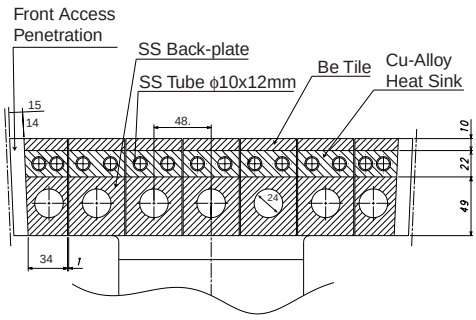

G 16 GR 26 00-12-08 W0.1

Figure 2.3.3-6 FW Panel Cross-section

2.3.3.3 Shield Block

The shield block cooling scheme consists of water headers that distribute the coolant in radial channels. The coolant flow is complicated by the presence of cut-outs in the rear part, radial access holes, and penetration holes for FW legs. Different schemes of cooling layout have been investigated: (a) one header in the front of the module and radial flow though co-axial channels, (b) front and rear headers, (c) a header in the middle of the module with co-axial flow. The layout with one front header has been preferred as in the rear part of the shield block there are many cut-outs and high stressed regions near the supports and keyways.

The shield block has a radial thickness of 0.37 m. It consists of four flat forged blocks electron beam (EB) partially welded together at the rear side (see Figure 2.3.3-7). Three poloidal slits of 0.17 and 0.19 m depths are retained on the front side between forged blocks and four slits 0.16 m deep are also cut from the top and from the bottom to reduce EM loads. Four penetration holes with 170 mm diameter allow the installation of the FW central beam. Eight 30 mm diameter access holes through the inboard FW/shield block provide front access to the bolts used for the flexible and electrical connectors and for laser-seal welding of the branch pipes. In the outboard module, 2 additional 30 mm diameter access holes in the mid-plane of the module (with 570 mm poloidal span) are provided for the temporary attachment of the module onto the VV during maintenance.

G 16 GR 27 00-12-08 W0.1

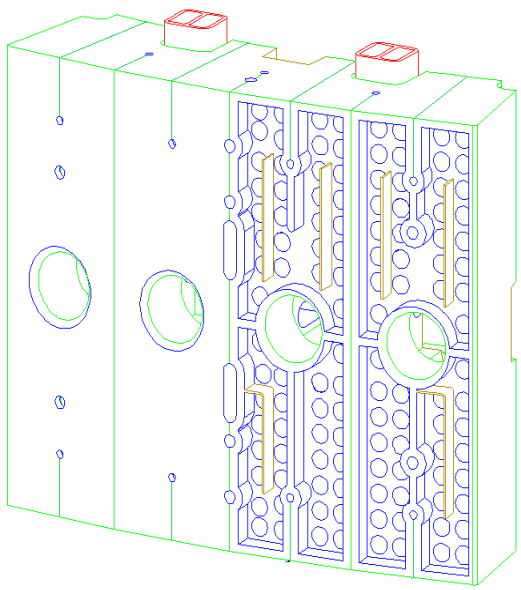

Figure 2.3.3-7 Front Headers and Radial Coolant Holes for Inboard Shield Blocks

The inboard and outboard modules have different arrangements of the support structure to resist the EM moments. Shear keys are used in the inboard (see Figure 2.3.4-2), whilst stub keys are used for the outboard modules (Figure 2.3.4-3). The rear surface of the inboard blocks is highly grooved to provide cut-outs for 3 keyways, 2 electrical straps and coolant branch pipes, coolant connections to FW panels, and cooling manifolds. In the outboard

blocks, there are 4 cut-outs for the keyways, while there are no recesses for the cooling manifolds as they are in between modules.

The shield block can be fabricated by conventional drilling/plugging and machining/welding of flat forged blocks. Power HIP can also be applied to the shield block fabrication with different header configurations, such as the option b) described above.

2.3.4 Module Attachments

The mechanical attachment of the blanket module to the VV provides accurate positioning, movement allowances and load capability. It transfers radial loads while allowing toroidal/poloidal movements of 1 mm due to the different structural rigidities and thermal responses of the modules and the VV. The hydraulic and electrical connection have a similar compliance. The mechanical attachment includes four radial supports and three keys in the poloidal/toroidal directions. Electrical insulation in the mechanical attachment prevents the electrical current flowing through the supports and helps to reduce the EM forces. The hydraulic connection is metallic without any electric break, is compact, and is located in the centre of the module, in between two copper straps handling the large plasma halo current.

2.3.4.1 Flexible Support

The flexible supports react to the module loads in the radial direction while being compliant to the other directions. This feature is provided by a tubular cartridge with axial slits in the tube wall (Figure 2.3.4-1). One end of the cartridge is threaded outside M150 and connected to the VV. The other end is closed by an internal flange, which is used for bolting to the module. The supports are recessed in the VV wall in a shielded position where the low nuclear heating can be removed by thermal conduction. The flexible supports are installed, with the bolts in parking position, in the vessel recesses after the complete welded vessel assembly. The tolerances of the vacuum vessel are compensated by custom machining the large threaded end of the cartridge. A margin of ± 10 mm is available in the axial direction and ± 5 mm transversely. These adjustments allow accurate positioning of the first wall.

The electrical insulation consists of a ceramic coat applied to the flange of the cartridge and to the collar-washer of the bolt. The supports hold the modules by M45 bolts which are driven through the 30 mm access holes. The tool engages the bolt from the tip but does not need a large torque, because the elongation for the preload is achieved using differential thermal expansion provided by a heater in the 10 mm axial bore. The flexible cartridges are made from Ti-alloy (Ti-6Al-4V) due to its high strength, low Young's modulus and adequate toughness after irradiation. The high strength bolts are made of Inconel 718 (ASTM B637) precipitation hardened. The bolt preload (650 kN) is maintained under nuclear heating, and the number of cycles is within fatigue limits.

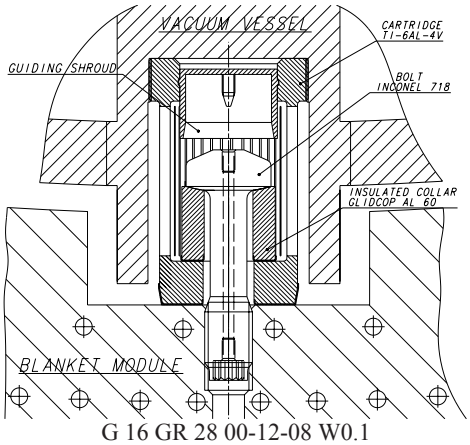

G 16 GR 28 00-12-08 W0.1

Figure 2.3.4-1 Cross-section of a Flexible Support inside a Stub Key

2.3.4.2 Key

Each inboard module has three keys to react the radial torque, the poloidal forces and the smaller toroidal forces (Figure 2.3.4-2). The keys are fitted with bronze pads sliding against the key-ways of the modules during relative thermal expansion. Friction is reduced by coating the exposed surface of the pad with MoS_2 (dry deposition). The electrical insulation is made by ceramic coating of the hidden surface of the pad, which is fixed on the steel keys by insulated screws. The pads are sized for an average compressive stress of 100 MPa, to exclude the yielding of the bronze, the only condition which may damage the ceramic coat. In the inboard blanket the loads are about twice as large as in the outboard and there is less space because of the cooling manifolds. Two large poloidal keys for 1 MN load are built in between the flexible supports and a smaller toroidal key is located in the midplane.

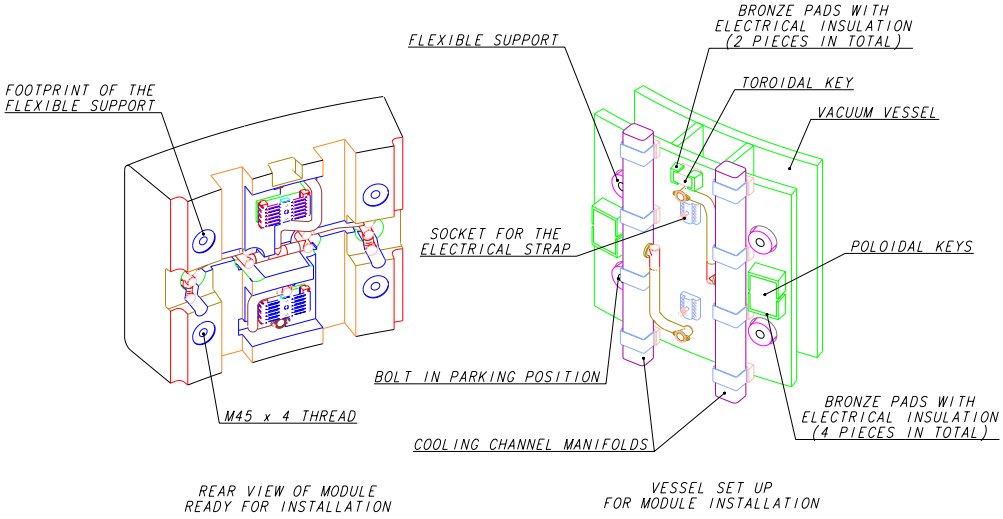

G 16 GR 29 00-12-08 W0.1

Figure 2.3.4-2 Inboard Module Attachment with Poloidal and Toroidal Keys

In the outboard blanket the keys are built as stubs concentric with the flexible support where they extend from the VV (Figure 2.3.4-3). The flexible support is connected to the module at the bottom of the keyway, where the nuclear heating is high but still manageable. Bronze contact pads work as in the inboard blanket and are fixed by insulated screws. The pads are tapered to improve the assembly of the module, leaving a nominal clearance of 0.25 mm for each side.

G 16 GR 31 00-12-08 W0.1

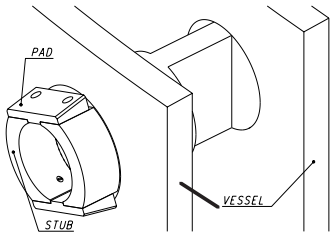

Figure 2.3.4-3 Stub Key and Back View of a Typical Outboard Module

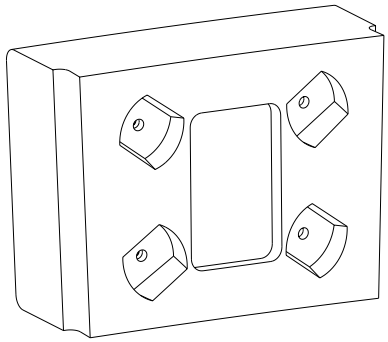

G 16 GR 32 00-12-08 W0.1

Only three stubs per modules are fitted with pads. The fourth remains loose in the module keyway to avoid over constraint during the assembly, and non-uniform thermal expansion. This configuration is used for modules 8 to 16. Module 17 and modules around the neutral

beam penetrations have a combination of 2 stub keys with a shear key, owing to the particular space constraints.

2.3.4.3 Electrical Connection

During a slow VDE, the electrical connections discharge to the vessel up to 280 kA halo currents delivered to the modules by the plasma, and shield the metallic hydraulic connections. The strap withstands the EM forces generated by the large magnetic field, and accommodates displacements of 1 mm resulting from thermal expansion and the clearance of the keys.

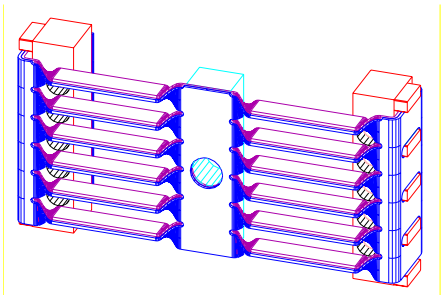

G 16 GR 33 00-12-08 W0.1

Figure 2.3.4-4 One Strap of the Electrical Connection

The electrical connection includes two identical straps (see Figure 2.3.4-4) formed by two overlapped sheets of CuCrZr alloy, a material which provides low electrical resistance, good strength at high temperatures and after irradiation. The useful cross section is 12.8 cm^2. The sheets are bent 90° and louvered to achieve flexibility in all 3 directions. Two SS support blocks resist EM forces from the largest toroidal magnetic field component on the short sides. The blocks link the ends of the strap to the module through 5 M8 screws. The centre of the strap is connected to the vessel by a single M20 bolt. An intermediate SS socket is foreseen to spread the current on the wall and to accommodate the vessel tolerance. The socket is fixed to the wall by 8 M8 screws, or by welded studs.

2.3.4.4 Hydraulic Connection

The hydraulic connection is located in the centre of the module where the thermal displacements are the lowest. It includes flexible branches and a connector, which is kept as compact as possible to reduce the current loops between the vessel and the module. Two separate connectors to the modules are used to deliver the coolant to the first wall panels, whilst the return is from the shield block (see Figure 2.3.4-5). The branches are single pipes 48.6 mm OD routed above and below the electrical straps. The branches routed from the manifolds are remotely connected with the branches from the module at the points above and below the electrical straps.

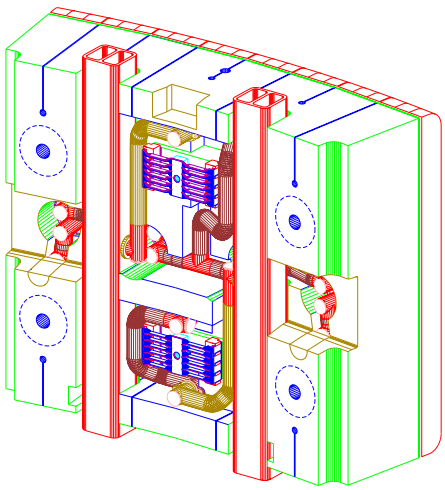

G 16 GR 34 00-12-08 W0.1

Figure 2.3.4-5 Two Separate Hydraulic Connection for Inboard Module

2.3.5 Port Limiter System

There are two limiters in ITER and they are installed in the equatorial ports number 8 and 17. Each port limiter consists of a limiter module, a supporting and alignment system, and a port limiter shield. The location inside ports eases the maintenance, which is important for this high heat flux component. The limiter cooling system is in common with that of the divertor,

because water is in contact with Cu-alloy tubes in both systems and they share the same water chemistry, as well as the same hydraulic parameters (pressure, subcooling, etc.).

2.3.5.1 Port Limiter Module

As shown in Figures 2.3.5-1 and -2, the limiter module is 2,100 high, 1,652 mm long and 458 mm thick and consists of an assembly of 36 mm thick vertical plates attached together at their rear section by welding or by bolting. The rear section of the plates forms a strong continuous backing and the ~ 1 mm gap between plates is insulated with alumina to prevent arcing. The vertical slots significantly reduce the electromagnetic loads due to plasma disruptions. The ability of the plates to independently expand also reduces the thermal stresses. Each plate is formed (Figure 2.3.5-3) by a FW part attached to a shield part. The FW consists of beryllium armour in the form of small tiles (~ 6x6x4 mm) attached to a Cu-alloy heat sink plate internally cooled by Cu-alloy cooling tubes. The FW tubes are provided with swirl tapes to enhance the heat transfer and the margin to the critical heat flux. The shield part consists of a steel plate internally cooled by a SS serpentine tube. The FW tubes are connected to a common inlet manifold on one end and to the serpentine tube at the other end. A common outlet manifold is connected to the serpentine outlet. The FW can alternatively be fabricated separately and attached to the shield part of the plates e.g. by laser welding.

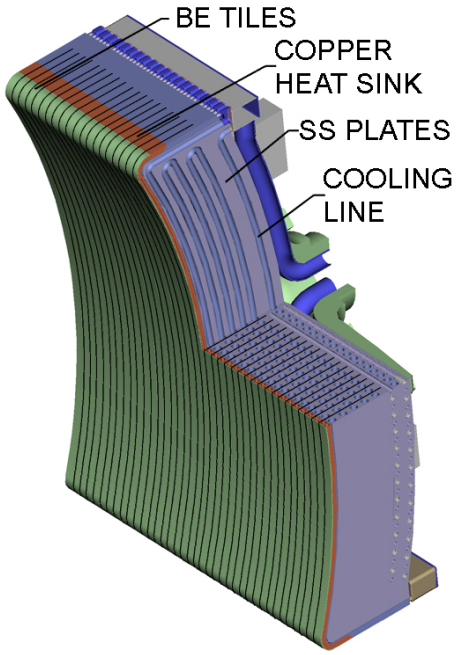

G 16 GR 35 00-12-08 W0.1

Figure 2.3.5-1 Limiter Module Front View

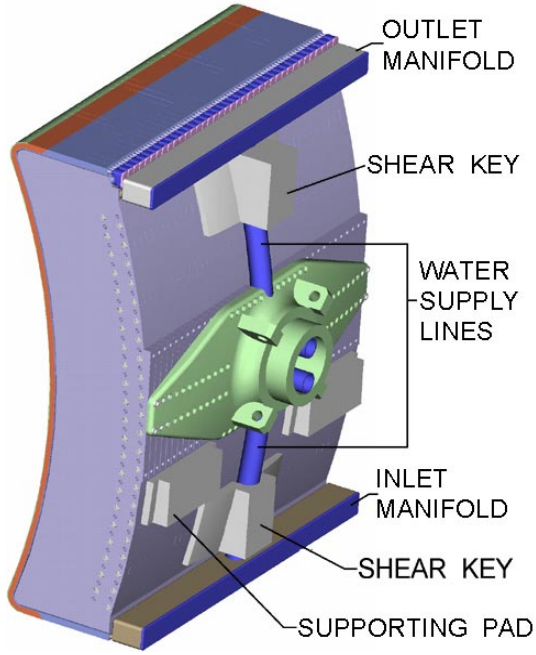

G 16 GR 36 00-12-08 W0.1

Figure 2.3.5-2 Limiter Module Rear View

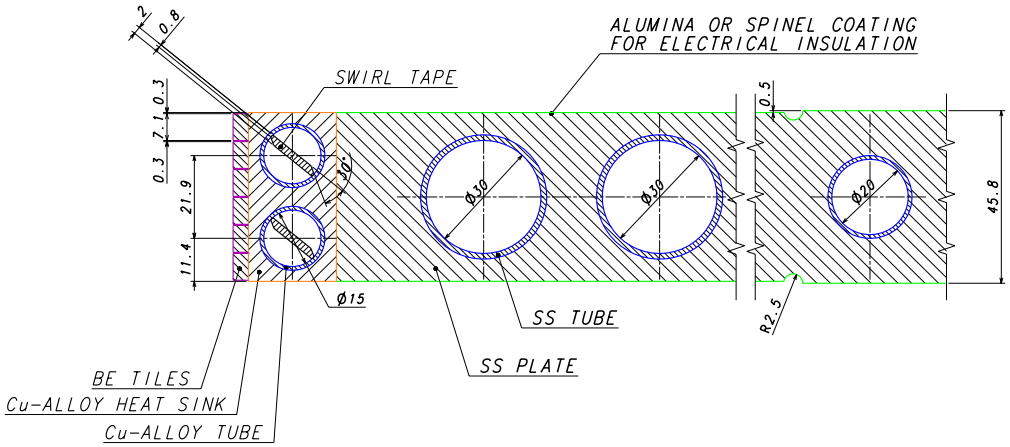

G 16 GR 37 00-12-08 W0.1

Figure 2.3.5-3 Limiter Plate with Integrated FW

2.3.5.2 Plug Body with Supporting and Alignment System for the Limiter Module

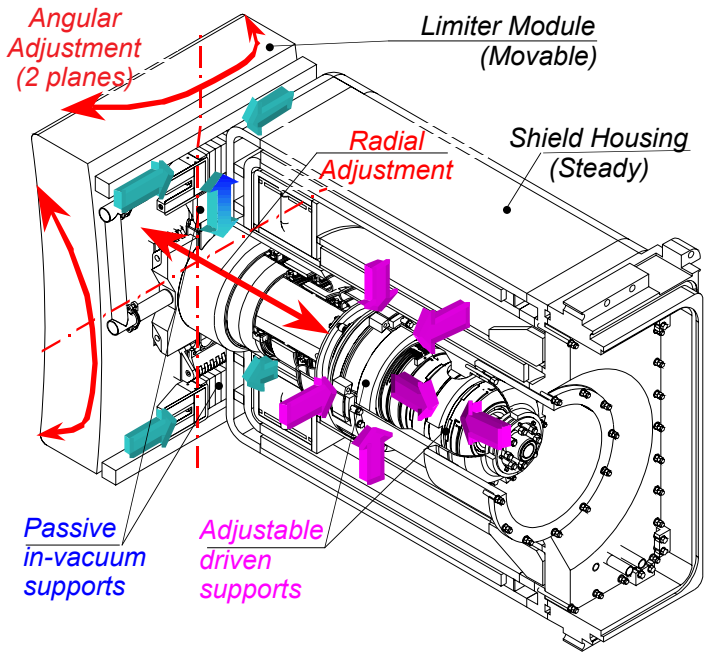

G 16 GR 39 00-12-08 W0.1

Figure 2.3.5-4
Plug Body with Supporting and Alignment System for the Limiter Module

The supporting and alignment system, mounted on and inside the shield housing, supports a limiter module under the EM loads during disruptions, seismic loads and dead weight, providing it with all connections, including hydraulic (Figure 2.3.5-4). This remotely-operated system adjusts the radial position of the limiter module. It also permits small rotations around poloidal and toroidal axes through a pivot point located near the centre of gravity in order to precisely align the front surface of the limiter module to the field surfaces. The adjustable driven supports are doubly sealed, thereby avoiding the need to operate under vacuum, and are powered by hydraulic stepping motors.

The shield housing is a massive welded structure, with internal water channels, providing structural support and nuclear shielding. The shield housing consists of two parts: inner frame and outer frame.

2.3.6 Cooling Manifold and Filler Shield

The coolant is delivered and returned to the blanket modules by a set of manifolds mounted inside the VV chamber aligned with the poloidal rows of modules from the upper port downwards. At the outboard the manifolds occupy the triangular voids between the modules and at the inboard they are located behind them (see Figure 2.3.6-1).

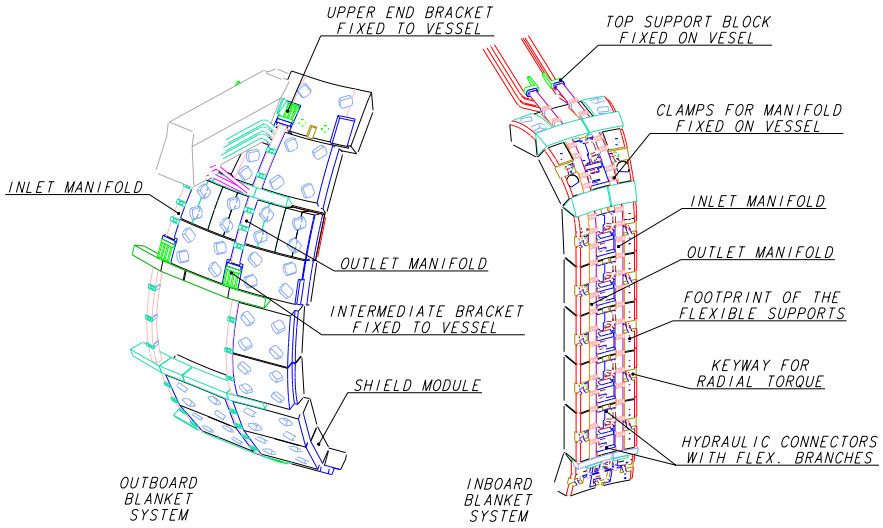

G 16 GR 40 00-12-08 W0.1

Figure 2.3.6-1 Inboard and Outboard Blanket Manifold Overview with Modules

The manifolds include multiple channels feeding groups of 2-4 modules which are separated from the others as far as the tokamak cooling water system (TCWS) vault, where they can be isolated to improve the identification of a leak. The manifold size decreases downwards as the single channels reach the last module of their group.

All manifolds end near the upper port and are fed by eight pipes with ~ 60 mm inner diameter, arranged in two ranks on the side walls (Figure 2.3.6-2). The pipes do not pass through the flange of the VV port but are channelled upwards from the port duct through special twin chimneys built symmetrically either side of the split field joint. The chimneys end with a bulkhead occupied by the pipe feed-throughs. This pipe layout avoid interactions with the EC antennas and the diagnostic plugs.

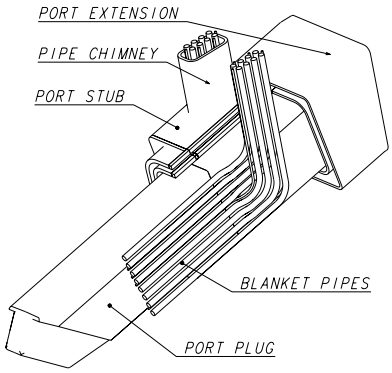

G 16 GR 42 00-12-08 W0.1

Figure 2.3.6-2 Blanket Pipes in Upper Port

The manifolds incorporate triangular filler shields in gaps between the blanket modules, between modules 1 and 2 and between modules 6, 7 and 8 in the inboard region, and also between modules 10 and 11, 13 and 14, 14 and 15, 16 and 17 in the outboard region. The filler shields are cooled with the water in the manifolds.

The flow cross section of the manifold is sized for a coolant speed of 6 m/s, giving a distributed pressure drop of 2.5 kPa/m. The highest manifold reliability has been pursued by adopting a 10 mm wall thickness, which is well above the size of any usual defect of the plates. The stainless steel plates and shaped profiles forming the cross-section of the manifolds are joined by triple pass filler metal welds, which can be fully non-destructively inspected. Any manifold failure will be repaired inside the VV, because the manifolds are too long for an easy replacement. Since the welds have higher failure probability than the base material, they have been concentrated on the accessible faces of the manifolds.

The longitudinal thermal expansion of the manifolds with respect to the VV is restrained to avoid the need for sliding supports, relying on low friction under vacuum. However, the transverse thermal expansion, in the toroidal and radial planes, is small and is unconstrained. The longitudinal end support of the manifolds is a strong flange bolted on a bracket welded on the VV wall (Figure 2.3.6-3). A similar restraint is used above the equatorial port, where the manifold reduces the cross section from 5 (see Figure 2.3.6-4) to 3 channels and changes the poloidal compressive force. The toroidal-radial supports handle lower forces and include an indented socket and a retention clamp fixed by thin welds. There are no lateral loads in the straight portion due to temperature differences (excluding some buckling stabilisation). The supports, spaced at 30-50 cm, are designed to withstand the radial forces directed towards the plasma and the smaller toroidal forces caused by a plasma disruption (thermal quench). They also restrain the radial movement of the manifold when it is colder than the VV (failure in the PHTS control system).

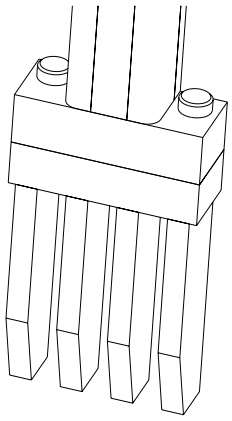

G 16 GR 43 00-12-08 W0.1

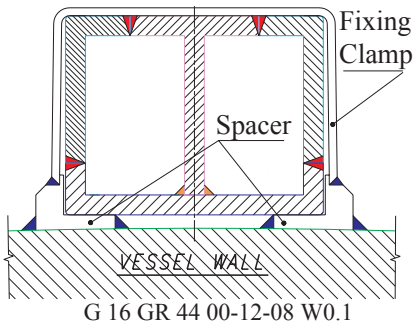

G 16 GR 44 00-12-08 W0.1

Figure 2.3.6-3
Bolted End Support and Welded Intermediate Support for 2 Channel Inboard Manifold

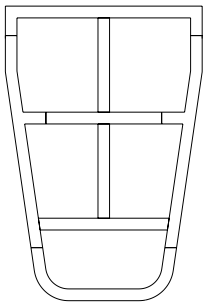

G 16 GR 45 00-12-08 W0.1

Figure 2.3.6-4
Cross Section of Outboard Manifolds with 5 Channels

In the case of a vacuum leak, a cooling group of 2-4 modules is identified by tracer elements injected progressively in the three separate cooling circuits of the blanket. Inside each circuit the feeders of the 48 module loops are closed by ice plugs and progressively opened while watching the mass spectrometers of the VV pumps. The identification of the faulty module inside the leaking group requires a He leak test. Water is removed from the loop of the leaking group by a high speed nitrogen stream, which entrains the liquid upwards and dries the surfaces. The loop is evacuated and connected to the mass spectrometer. The VV is opened and the RH vehicle scans the leaking group of modules with a He puff. After the first wall, where the damage is most likely, the hydraulic connectors are checked because the field weld is the weakest part of the module.

The manifolds are fabricated and tested individually, then shipped to the VV production factory and installed on the 40° sectors. Here the supports are adjusted as required, tightened or welded. But the 9 outboard manifolds with filler shields over the field joint of the VV are only bolted, because they must be removed on site and then finally installed with the welds. The pipes going through the upper ports located in the middle of the 40° VV sectors are also installed and leak tested. The pipes in the 9 ports split by the field joint of the VV are installed in the laydown and assembly hall after the TF coils are in place. On one side of the VV field joints, the pipes are connected to the manifolds in the assembly hall. On the other side the pipes are welded to the manifold across the VV field joint in the pit, after the vessel field joint is done.

2.3.7 Design Features to Accommodate Breeder Blanket

The breeding blanket modules are designed to make possible the partial conversion of the outboard areas for breeding, under the same dimensional, installation, supports, coolant branch pipes and maintenance constraints as the outboard shield blanket modules. Therefore, the conversions should be done in the same way as the replacement of outboard shield blanket modules. Based on work carried out for the 1998 ITER design, the breeder candidate materials are lithium zirconate, lithium titanate and lithium silicate, used in a ceramic pebble bed. Beryllium pebbles are used for the neutron multiplication, and water for heat removal. SS 316L(N)-IG is used as structural material and Be armour is directly attached to the stainless steel without a copper heat sink. The first wall for the breeding blanket module will be integrated with the SS 316L(N)-IG box structure for breeding and cooling. Slits in the radial and poloidal directions to decrease electromagnetic loads will be useful also for the breeding blanket modules. The only additional feature required to allow the later option of breeding blanket installation is the helium purge gas lines for tritium removal. Those can be installed together with the shield blanket system during the initial construction phase. Each purge gas line will feed typically 3 outboard modules. A set of lines are mounted inside the VV chamber, and will have an entrance at the upper port. Layout of the purge gas lines is similar to the blanket cooling water manifolds, and consists of 12 mm OD purge gas manifolds (pipes) and 5 mm OD purge gas tubes. The purge gas tubes, which have one part attached to the breeding blanket module and the other attached to the purge gas manifolds, are able to connected by the remote handling system through the 30 mm front access holes.

2.3.8 Blanket Fabrication

2.3.8.1 Primary Module

The FW panel will be manufactured using solid HIP, the shield block from flat forged blocks, and the coolant channels produced simply by drilling and plugging. Powder HIP can also be used for the shield block or FW panel fabrication, and casting for the shield block.

FW

The main fabrication steps for option B with central mechanical attachment, schematically shown in Figure 2.3.8-1, are as follows:

- produce the Cu-alloy and SS plates by rolling;
- groove the Cu-alloy plates to fit the SS coolant tubes;
- machine the headers and drill the coolant channels;
- assemble and seal welds before HIPing;
- HIP the assembly at T = 1,050°C, p = ~ 150 MPa, t = ~ 2 h;
- attach the Be armour by HIP (e.g. with Ti interlayer at 800°C, 2 h, 120 MPa, or with Cu interlayer at 620°C, 140 MPa for 2 h);
- machine the poloidal slots;
- weld the support legs to the FW panels before drilling the coolant channels;
- weld headers and plug the channels before final surface machining.

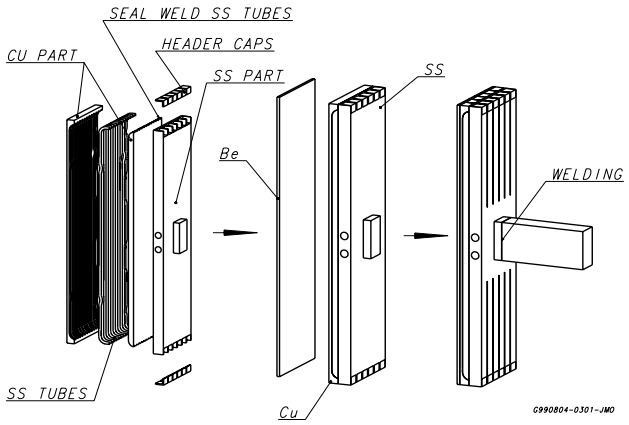

G 16 GR 46 00-12-08 W0.1

Figure 2.3.8-1 FW Panel Fabrication Method for the Option with Central Mechanical Attachment

Shield Block

The procedure of the shield block fabrication is schematically shown in Figure 2.3.8-2. The shield blocks are mainly fabricated by simple drilling and milling, and welding. The feasibility of obtaining drilled forged shield blocks within the required tolerances, and with welding closure plates, has been demonstrated in a module prototype. The manufacturing steps will be:

- producing four separate forged blocks;
- drilling radial coolant holes and the initial machining for headers;
- drilling and machining of slits and FW holes;
- plugging of coolant holes after drilling;
- machining and the fabrication of coolant guides with screws;
- attachment of coolant guides by welding after fixing by screws temporarily;
- milling for the keys and drilling for flexible holes at the rear side as preliminary machining;
- attaching lids to the headers by TIG welds;
- EB welds to assemble separate forged blocks;
- final machining of grooves at the rear side including all slits between the four shield blocks;
- assembling shield blocks and FWs into unit;
- attaching FWs to the shield block;
- welding the hydraulic connections to the respective inlet/outlet headers and attaching electrical straps by bolts**.**

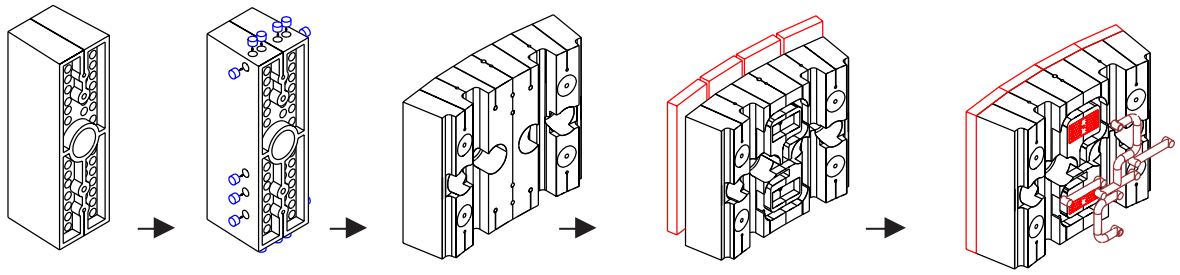

G 16 GR 48 00-12-08 W0.1

1) Drilling & machining
2)Drilling, plugging & machining
3) Welding, milling & machining
4) Final machining & assembly of first walls
5) Welding & setting all attachments

Figure 2.3.8-3 Fabrication Procedures Based on Using Solid Forged Blocks

Powder HIP is also a possible fabrication method for the shield block whose feasibility has been demonstrated by manufacturing a prototype as part of ITER R&D. The fabrication error was still not quite as small as required, but it is expected to be reduced sufficiently in future manufacturing R&D.

2.3.8.2 Limiter Module

Listed below are the main manufacturing steps for the limiter module:

- machine to shape the Cu-alloy heat sink half-plates and machine half-channels;
- attach transition tubes to FW Cu-alloy tubes and join them by brazing or HIP;
- prepare the coolant SS serpentine tube and install swirl tapes;
- machine to shape the shield SS half-plates and the serpentine half-channel;
- bend the heat sink to shape;
- assemble the shield half-plates with the serpentine tube inside, together with the FW Cu-alloy half-plates and the FW cooling tubes; seal weld the tubes to the shield plates and provide canning; HIP the assembled parts at 1,050^{o}C,150 MPa, 2 h;
- machine the component to shape and provide electrical insulation coating;
- attach FW Be castellated plates to the heat sink with fast amorphous brazing (join the castellated side) after jigging;
- machine the continuous part of the Be plates to form tiles;
- make the FW collectors and provide connections to the shield part;
- EB weld the plates using a suitable jig, or bolt plates in sequence to form the module;
- weld coolant manifolds and supply pipes (TIG) and attach supporting fixtures.

If the FW were separately manufactured and attached by laser welding to the shield part of the plates, the HIP parameters of the SS plates can be changed to 1,100^{o}C, 150 MPa, 2 h.

2.3.9 Blanket Assembly

The basic blanket assembly process is as follows (see also 2.10).

1. Pre-assembly stage
   (i) 27 inboard and 27 outboard cooling manifolds (out of a total of 36) are mounted on the plasma-facing wall of VV sectors. The manifolds are checked for leakage.
   (ii) The majority of diagnostics and helium purge lines are mounted on the plasma-facing wall of VV sectors. All the interior cabling and pipelines are routed to the vessel exterior and checked for continuity and leakage.
2. The vacuum vessel torus is aligned to the machine magnetic centreline, all global adjustments made and the vessel supports fixed. The measurement data will be utilised to provide a best-fit determination of the mounting profile information necessary to customise the module attachments.
3. Customisation of the module attachments.
4. Toroidal loops of diagnostics on the plasma-facing wall of the VV are installed and connected to the interior cabling.
5. The remaining 9 inboard and 9 outboard manifolds that cross the VV field joints are mounted on the plasma-facing wall of the VV. The manifolds are checked for leakage.
6. Mounting of module attachments.
7. Pre-mounting of blanket modules by temporary supporting bolts.
8. Fixing of blanket shielding modules. The module flexible support bolts are pretensioned using heat.
9. Welding of branch pipes, and fixing of electrical connectors.
10. Blanket commissioning test: global leak and pressure tests, global flow and pressure drop tests, global/local thermal transient response tests, and electrical resistance test.

2.3.10 Loads and Analysis

2.3.10.1 EM Loads

The plasma disruption database shows that high plasma current density leads to a fast current quench, resulting in a short quench time of 27 ms. By the use of deep slits, electromagnetic (EM) loads on the modules have been reduced to the values shown in Table 2.3.10-1. The FW-normal halo current density is assumed to be 0.18 MA/m^2 under the worst-case halo current event, as specified by I_{halo}/I_{plasma} multiplied by the toroidal peaking factor, TPF = 0.58. The design loads on modules are shown in Table 2.3.10-1.

Table 2.3.10-1 Maximum EM Loads on the Inboard Module (Option B)

		Shield block	FW
1) Centred disruption			
Torque M_r due to I_{rad}	MNm	-1.06	-0.008
Torque M_p due to I_{pol}	MNm	1.12	0.006
2) Fast VDE			
Torque M_r due to I_{rad}	MNm	-0.97	-0.008
Torque M_p due to I_{pol}	MNm	1.47*	0.006
3) Slow VDE**			
I_{halo} / module (FW)	MA	0.28	0.07
EM force F_r on module (FW)	MN	0.32	0.08
EM force F_p on module (FW)	MN	1.1	0.15
EM force F_{tor} on module (FW)	MN	0.21	0.03
Torque M_{tor} on module (FW)	MNm	0.36	0.027

* Maximum torque is produced on module 1 under the downward fast VDE. This torque can be reduced to ~1 MNm by increasing the deep slits as a special module.
** The eddy currents during a slow VDE are very small, thus no radial and poloidal torque are considered

2.3.10.2 Primary Module Structural Analysis

2.3.10.2.1 FW and Shield Block

FW

The FW panel and its attachment system have been sized to withstand the above electromagnetic loads caused by plasma disruption. The slotting of the FW results in a reduction of about 10 times in eddy currents and consequently in the stresses caused by the induced electromagnetic loads. The results of thermo-mechanical analyses performed to verify the FW during normal operation are summarised in Table 2.3.10-2, showing that thermal stresses in the FW panel are well below allowable values. These thermal stresses are somewhat lower in the FW part without penetrations.

Table 2.3.10-2 Main Thermo-mechanical Analysis Results for FW

Location	**T range [°C]**	**Max. σ_{VM} [MPa]**	**Allowable** [MPa]
Be tile	200 - 253	~ 171 (Cu interface)	-
Cu heat sink	165 - 218	~ 152 (Be interface)	294
SS tube	143 - 198	179 (wetted side)	444
SS back-plate	119 - 211	268 (at channels)	465

In the present design of the module, there is only room for a leg of 175 mm. With such a short leg, a scheme with cantilever support (Figure 2.3.10-1) is preferred, being the most reliable. A cantilever supported welded leg should have a big enough diameter to minimise the thickness of the weld. Space allows room for a leg of diameter 168 mm. The required thickness of the weld joint is 14 mm, and the bending stress in the weld joint is within the allowable (207 MPa).

G 16 GR 49 00-12-08 W0.1

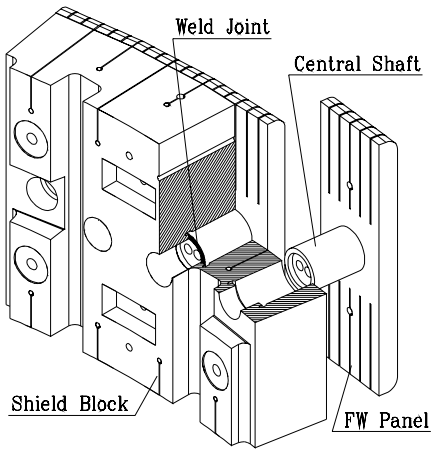

Figure 2.3.10-1
Cantilever-supported Welded Leg

Shield Block

Structural analyses of a 1/8 model of the inboard and outboard blanket modules have been conducted using ANSYS. Figures 2.3.10-2 and -3 show the temperature and stress distributions. Table 2.3.10-3 summarises results of the stress evaluation for the inboard module. The maximum temperatures, 287°C for the inboard module and 338°C for the outboard module, are below the allowable temperature of 427°C for non-active thermal creep. The calculated stress intensity for thermal and pressure loads on both modules are also within the allowable stress ranges of $3S_m$ and thermal fatigue allowable values.

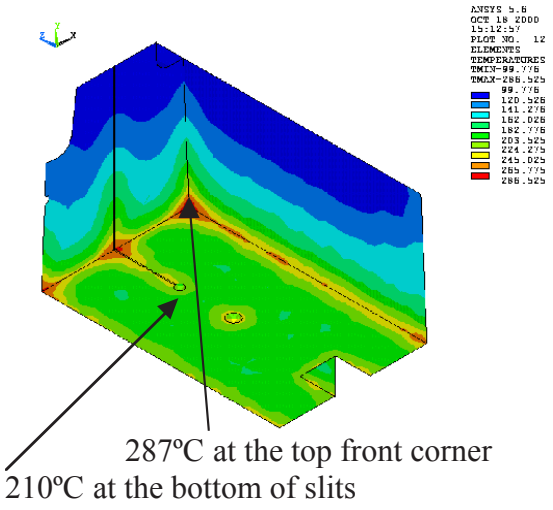

Figure 2.3.10-2
Temperature Distributions in the Inboard Shield Block

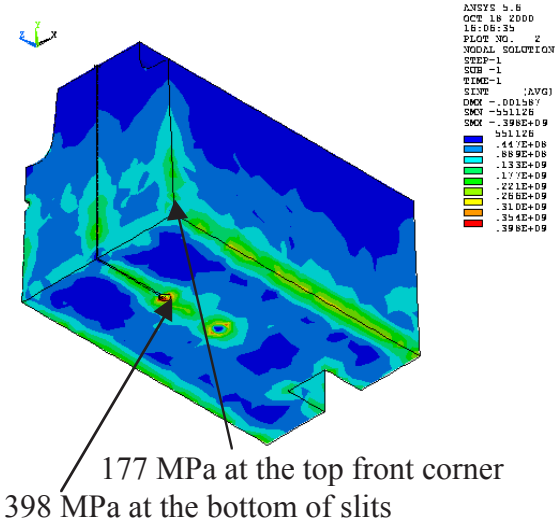

Figure 2.3.10-3
Stress Intensity in the Inboard Shield Block for Thermal and Pressure Loads

Table 2.3.10-3 Results of the Stress Evaluation for the Inboard Shield Block

		Calculated stresses (MPa)		Allowable stresses (MPa)		Accumulated fatigue damage factors	
Evaluation points	Temp (°C)	Press.	Press.+ Thermal	$1.5S_m$	$3S_m$	n/N_d	Allowable value
Bottom of slits	210	32	398 [1)]	202	405	0.06	1.0
Top front corner	287	<10	177 [1)]	184	369	<0.01	1.0

[1)] Values including thermal peak stresses

2.3.10.2.2 Module Attachment

Flexible Support

The loads on the flexible supports are shown in Table 2.3.10-4. The highest stress in the cartridge appears at the ends of the flexible spokes and is kept below the yield of the Ti-6Al-4V alloy at 200°C to avoid any permanent deformation affecting the alignment of the supports; thus the disassembly and the reassembly of the module is reasonable.

Table 2.3.10-4 Stress Components versus Allowables in the Flexible Cartridge

Load	**Load type**	**Stress[MPa]**	**Stress type**
Axial force 500 kN/-600 kN	Primary	+166/-200	membrane
Side displacement 1 mm	Secondary	±153	bending
Flange rotation ± 3 mrad	Secondary	±129	membrane
Combined Stress	**Stress[MPa]**	**Allowable [MPa]**	
Primary membrane	200	S_m	324
Primary (membrane + bending)	200	$1.5\ S_m$	486
Primary + secondary (membrane + bending)	482	$3\ S_m$	972

A high yield stress is important because it triggers buckling. With a combined stress of 500 MPa a margin of 3 on buckling is achieved. This was confirmed on prototypes (see Figure 2.3.10-4), with and without lateral displacements.

Figure 2.3.10-4
Titanium Flexible Cartridge after Compression Buckling at 1.6 MN

The fatigue strength is satisfactory and was validated experimentally up to 10,000 cycles.

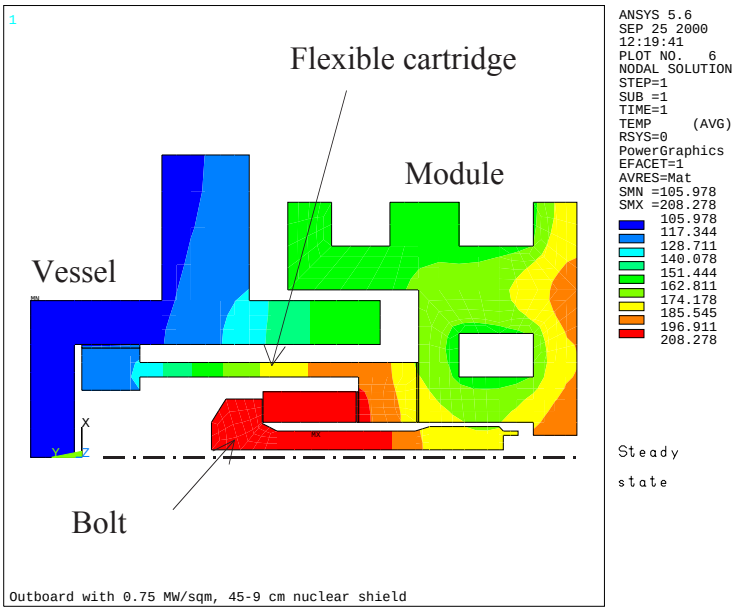

Figure 2.3.10-5 Axisymmetric Temperature Map in the Outboard Support with Stub Key

The temperature of the bolt in the outboard blanket is higher, because the support is partially recessed in the back of the module together with the stub key in the outboard. The analyses show a maximum temperature of 208°C (see Figure 2.3.10-5) in the stem of the bolt which requires a bolt preload of 673 kN for the outboard module instead of 650 kN for the inboard.

Key

The key is cooled through conduction to the vessel. The temperature distribution has been verified with a 3D model to exclude hot spots and large thermal stress in the interface with the VV, and to limit the average shear stress to 35 MPa. In the front of the key at steady state the temperature reaches 256°C, while the inner VV wall reaches 125°C. The thermal stress inside the key is about 50 MPa, but it reaches a peak in the corner of 200 MPa.

Considering the loads from a centred disruption, the fast TF coil discharge and nuclear heating, the Tresca stress (see Figure 2.3.10-6) between the key and the VV reaches 300 MPa over a wide surface of the wall, with a peak of 390 MPa in the corner. These values are within the stress allowable $3S_m$ of the VV, but they require a smooth fillet between the key and the vessel and a defect-free joint. The compressive stress in the contact pad has also been calculated, to verify that local peaks do not reach yielding of the bronze which may break the ceramic electrical insulation. The maximum peak stress of 156 MPa (average 79 MPa) is acceptable, since the yield stress of aluminium bronze at 250°C is above 200 MPa.

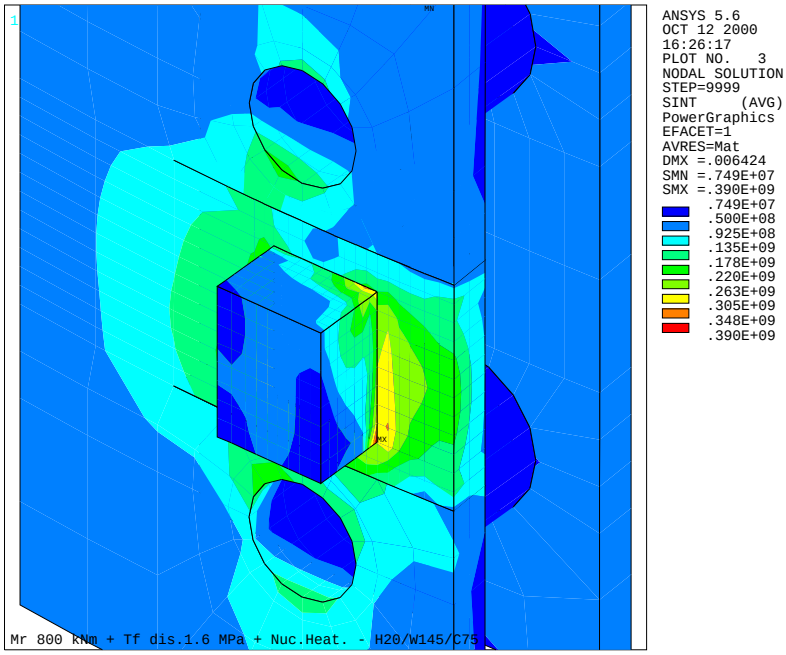

Figure 2.3.10-6 Total Tresca Stress Distribution during a Centred Disruption in the Inboard Key

Electrical Connection

The electrical strap has been analysed under EM forces and thermal displacement (Figure 2.3.10-7). The stress is mainly due to radial displacement and peaks at 315 MPa, below the allowable of 438 MPa for the high strength copper alloy. The experimental validation on a prototype mounted inside a solenoid with 7.5 T magnetic field has been successful completed.

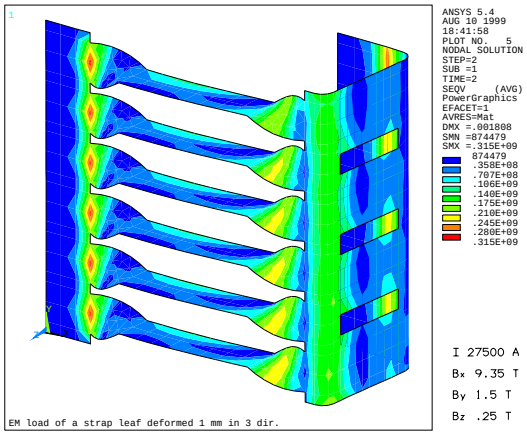

Figure 2.3.10-7 Total von Mises Stress [Pa] in a Typical Leaf of the Electrical Strap

Hydraulic Connection

Structural analysis has been performed for inlet and outlet branch pipes by using a beam model. Four loading conditions have been considered: thermal load, EM load under fast VDE, coolant pressure, and relative displacement between cooling manifolds. The maximum stresses in the inlet pipe are 62 MPa at the elbow portion under the EM load, and 146 MPa at the edge portion of the FW connection pipe under the thermal loads. Both mechanical and thermal stresses are within allowables of $1.5S_m$ (220 MPa) and $3S_m$ (441 MPa), respectively. The maximum stresses in the outlet pipe at 150°C are 71 MPa at the elbow portion due to EM load, and 36 MPa at the other elbow portion due to thermal load. Both stresses are also within allowables. The branch pipe layout and the maximum stress position under the thermal load are shown in Figure 2.3.10-8.

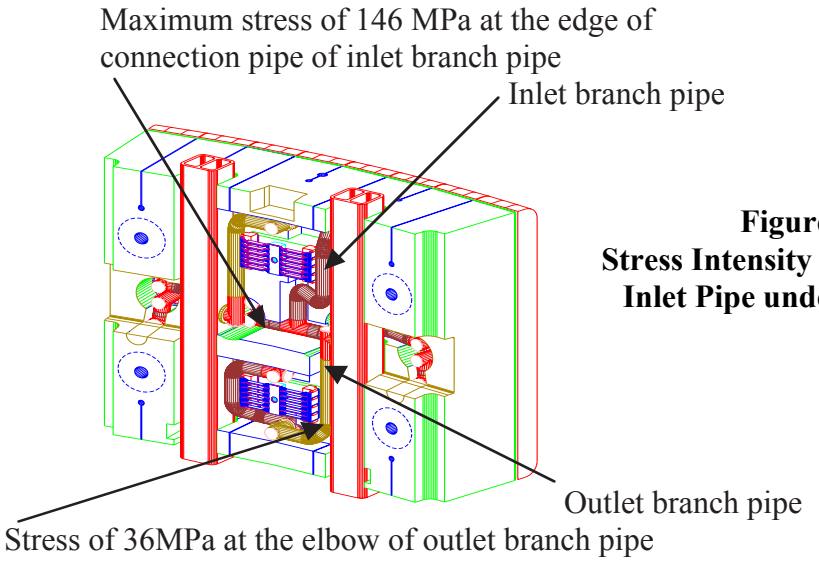

Figure 2.3.10-8
Stress Intensity Distributions of the Inlet Pipe under Thermal Loads

Figure 2.3.10-8 Stress Intensity Distributions of the Inlet Pipe under Thermal Loads

2.3.10.3 Port Limiter Structural Analysis

Port Limiter

In normal operation, only thermal stresses need to be analysed, since primary stresses are low. A transient elasto-plastic thermo-mechanical analysis was carried out for the 1998 ITER design to verify the ability of the limiter to withstand its thermal loads. This analysis is still valid because load conditions and geometry have not been changed significantly. A kinematic hardening model was used with elastic/full plastic material stress strain curves. During start-up the maximum temperature in the Be and Cu-alloy is ~740 and 450°C respectively, for a 4 mm Be armour. The maximum thermal stresses in the limiter structure are below 120 MPa, and the limiter works in low stress condition.

At the Be/Cu-alloy interface, however, plastic conditions are reached during plasma start-up and shutdown. Nevertheless, the maximum plastic strain values present in the DS Cu (Figure 2.3.10-9) are not excessive (max. total strain amplitude in Cu 0.56%), so that ratcheting is not expected. Both in Be and Cu the strain range decreases slightly every cycle. For the full thermal loads (8 MW/m^2), the allowable number of cycles of the FW exceeds 13,000 cycles, which satisfies the limiter design requirements.

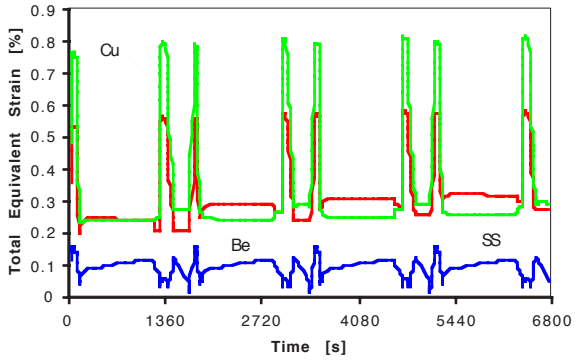

Figure 2.3.10-9 Time Evolution of the Total Equivalent Strain in Be, Cu and SS of Limiter

Port Limiter Supporting and Alignment System

Kinematics performance and the main structural components of the port limiter supporting and alignment system have been analysed. The chosen design of the support provides an accuracy of adjustment higher than required. Regarding EM loads, seismic loads and differential temperatures, maximum stresses of the sub-components in the system are within the allowables.

2.3.10.4 Cooling Manifold Structural Analysis

The highest load for the blanket cooling manifolds is the constrained thermal expansion with respect to the VV, then the coolant pressure, and finally the EM forces. The vacuum vessel and the blanket have the same inlet coolant temperature. Ideally, the inlet manifold has the same temperature as the vessel and no thermal stress, the outlet manifold is 50°C warmer with 157 MPa compressive stress. In reality the control systems of the cooling circuits have some tolerances, therefore the inlet manifolds can be 10°C cooler than the vessel and the outlet manifold can be 55°C warmer. If control fails, the blanket coolant enters at room temperature and quenches the inlet manifold to 70°C below the temperature of the vessel. The outlet manifold is shielded by the heat capacity of the blanket and becomes 30°C colder than the vessel, if the cooling circuit is stopped manually some minutes after the failure, otherwise it reaches also 70°C undercooling. The range of temperature differences is thus 75°C in the inlet and 85°C in the outlet manifolds.

For the assumptions above, the maximum value of the Tresca equivalent stress reaches 312 MPa at the inlet and 343 MPa at the outlet manifolds (Table 2.3.10-5), below the allowable $3S_m$ value of 441 MPa of the SS. If the coolant control is absent indefinitely the range of temperature difference in the outlet manifold becomes 125°C, with an associated Tresca equivalent stress range of 467 MPa (Table 2.3.10-5). The alternate yielding hardens the steel, which can nevertheless still withstand 20,000 cycles before failure.

Table 2.3.10-5 Inboard Manifold Stress [MPa]

Load source, stress component	Allowable stress	Inlet	Outlet
Coolant pressure 3 MPa, membrane (bending)		15 (72)	
EM, membrane shear (bending)		25 (19)	
Thermal range, longitudinal stress		235	267 [392]
All, Primary membrane Tresca	147	52	35
All, Primary membrane +bending Tresca	221	100	93
All, Total stress range Tresca	441	312	343 [467]

The constrained thermal expansion produces mainly longitudinal forces, but in the inboard top curved region the compressive force of the manifolds produces a radial component of 450 kN/m poloidally per 50°C difference. Supports are here spaced 30 cm apart instead of 50 cm as in the straight part.

The moderate effect of the coolant pressure on the manifold cross section is shown by the stress distribution in Figure 2.3.10-10. The finite elements of the mesh, corresponding to the welds between the C, L and T profiles forming the wall, are marked with a different colour.

The resulting stresses in these positions shows no bending and the welds experience only membrane stress as in circular pipes.

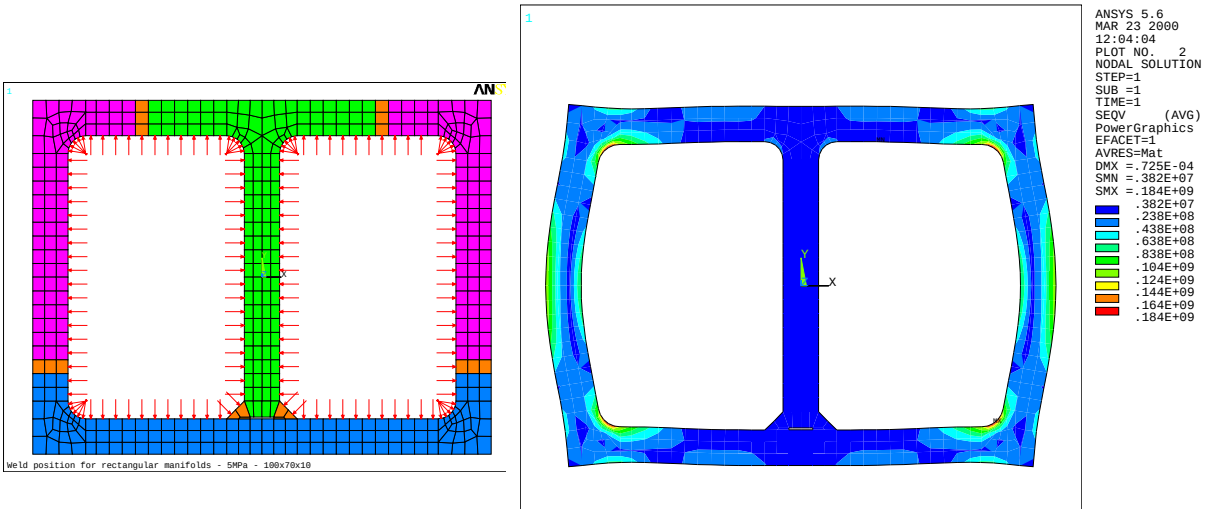

Figure 2.3.10-10 Stress in the Manifold with 5 MPa Pressure during the Baking.
The profiles are welded where there is no bending stress.

In the outboard the manifold is offset to bypass the equatorial port. Above it the channels reduce from 5 to 3 and the manifold has an intermediate restraint to balance the change of the longitudinal force. The support system of the outboard manifold has been assessed by 3D finite element analyses (Figure 2.3.10-11). Poloidal currents are induced in the manifolds by changes in the toroidal flux. They cross the toroidal field and generate radial pushing or pulling forces. At the inboard during a thermal quench of the plasma the pulling force reaches 120 kN/m length of manifold and is reacted by welded sheet clamps (Figure 2.3.6-3). During a TF coil fast discharge the manifolds are pushed against the support sockets on the vessel with a force of 40 kN/m length of manifold. The crossing of the currents with the small radial field generates minor toroidal forces (7.5 kN/m length of manifold in the inboard during the thermal quench) reacted by the indentation of the sockets. All EM loads give stress contributions far smaller than the thermal stress.

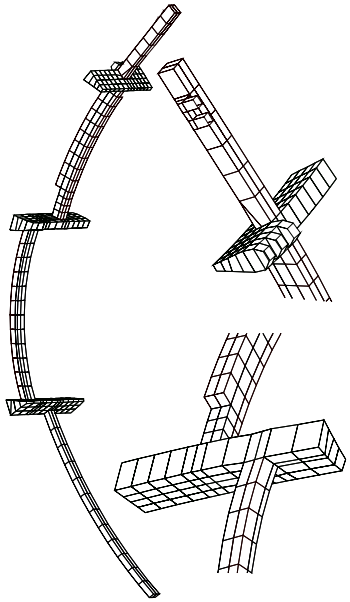

Figure 2.3.10-11 Finite Element Model of the Outboard Manifolds with the Filler Shields

2.3.10.5 Thermal and Hydraulic Analysis

Adequate coolant distribution to each blanket module is important to avoid any overheating in the modules resulting in excessive thermal stress. Coolant hydraulic analysis has been performed to assure that the required coolant can be distributed to each blanket module. The pressure drop has been calculated module 4 under option B. The obtained pressure drop is

0.1 MPa for the first wall and 0.3 MPa for the shield block in the case of a coolant mass flow rate of 7.48 kg/s.

The orifice diameter necessary for correct flow distribution of each blanket module has been calculated. Figure 2.3.10-12 shows the calculation model, with coolant distribution to three blanket modules (4, 5 and 6). The configuration of the blanket modules 5 and 6 are assumed to be the same as that of the blanket module 4. The required diameter for each module is shown in Table 2.3.10-6.

Table 2.3.10-6 Required Orifice Diameter for the Blanket Modules 4, 5 and 6

Module No.	Required Coolant (kg/s)	Orifice Diameter (mm)
4	7.71	42 (no orifice)
5	6.37	24.5
6	5.35	21

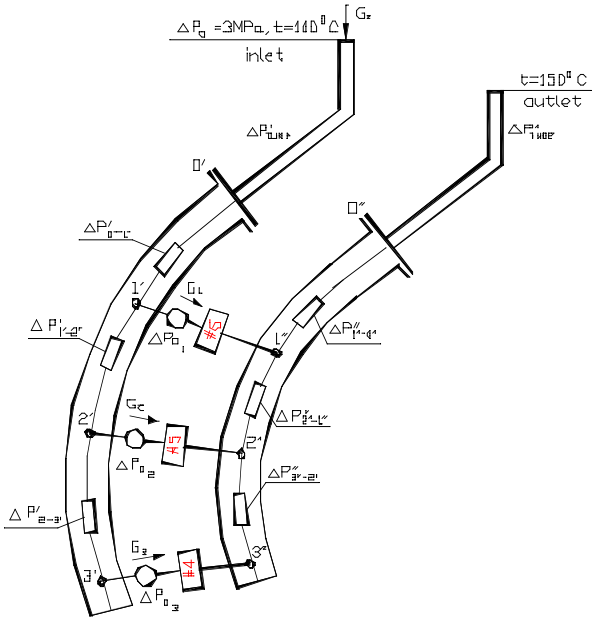

Figure 2.3.10-12 Example of Calculation Model for Coolant Distribution

2.3.11 Blanket Overall Assessment

A modular blanket design with a system of mechanical attachments to the vacuum vessel has been developed. A separate cooling manifold concept has been designed which is located on the vessel inner surface. The installation of a breeding blanket in the outboard area at a later date has not been precluded.

The blanket modules use a separable FW concept with a faceted geometry. Detailed design has been developed for a shield block with radial flow cooling and FW panel attachment structures for two options: (i) central beam and (ii) bolting with shear ribs. These concepts should result in significant cost and activated waste reductions compared to the 1998 ITER design. Fabrication methods for further cost reduction are covered by the on-going blanket R&D program which is investigating (a) the use of CuCrZr heat sink instead of DS Cu, (b) Be joining to Cu-alloy by brazing instead of solid HIPing, (c) powder-HIPed FW panels.

The EM, mechanical, and hydraulic analyses have been done for normal and off-normal events. Stress levels in the shield blanket modules and limiter are below allowable. Fundamental problems completing the further detailed design are not anticipated.

2.4 Divertor

2.4.1 Divertor Function and Main Components

The main function of the divertor system is to exhaust the major part of the alpha particle power as well as He and impurities from the plasma. As the main interface component under normal operation between the plasma and material surfaces, it must tolerate high heat loads while at the same time providing neutron shielding for the vacuum vessel and magnet coils in the vicinity of the divertor. Although good progress has been made in the understanding of divertor plasma physics, there continues to be some uncertainties, and hence the divertor remains an experimental device, which it is anticipated will need to be replaced and upgraded several times during the life of ITER. To facilitate rapid replacement, remote maintainability of the divertor has been given a high priority.

The main components of the divertor system are (see Figure 2.4-1):

- a divertor cassette body, that is reusable to minimise activated waste and provides neutron shielding and a mechanical support for different possible arrangements of plasma interfaces;
- inner and outer vertical targets, which are the plasma-facing components (PFCs) which in their lower part interact directly with the scrape-off layer (SOL) plasma and in their upper part act as baffles for the neutrals;
- the private flux region (i.e. the space below the separatrix which has no flux line connections to the main plasma) PFC which in turn consists of:
  - i) a dome, located below the separatrix X-point, seeing mainly radiation and charge exchange (CX) neutrals - the dome additionally baffles neutral particles and protects the liner and the neutral particle reflector plates from the SOL plasma;
  - ii) inner and outer neutral particle reflector plates that together with the lower ends of the vertical targets form a “V” shape that confines particles in the divertor channels to aid in reduction of peak heat flux by encouraging partial plasma detachment from the plate;
  - iii) a semi-transparent liner that protects the cassette body from direct line-of-sight of the plasma, while allowing He and other impurities to be pumped away;
- support pads integrated into the cassette to provide locking and alignment of the divertor cassettes on the rails;

- divertor to VV gas seals, to prevent back-streaming of gas from the divertor into the main plasma chamber;
- cooling pipe interfaces connecting the divertor cassettes to the radial cooling pipes at each divertor port;
- special diagnostic cassettes providing access for diagnostics;
- rails supporting the cassettes, part of the VV.

Three PFCs (inner and outer vertical targets and a private flux region assembly) are mounted on each cassette body in the hot cell by special semi-automatic tools.

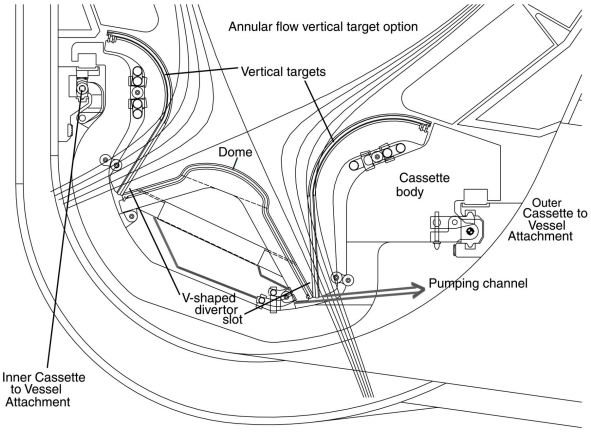

Figure 2.4-1a
Cross-section Through the Divertor
This shows the V-shaped strike zones and the pumping path as well as the attachment to the toroidal rails.

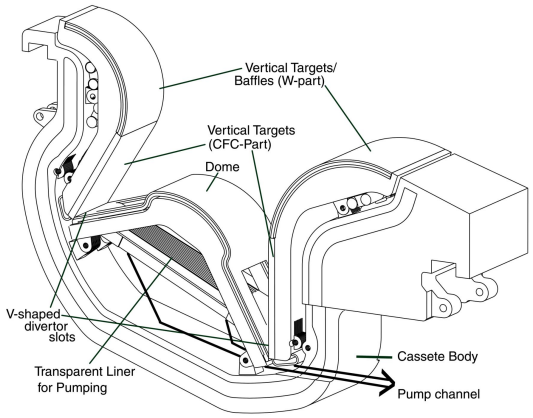

Figure 2.4-1b
Divertor Cassette Showing the Large Openings in the Dome Support
Also shown is the transparent liner allowing pumping access from the private flux region.

2.4.2 General Description

The geometry of the divertor is based on simulations obtained using the B2-EIRENE Monte Carlo code and by extrapolation from results of tokamak experiments[1]. The reference configuration for the ITER divertor is a vertical target/baffle with an open private flux region and a dome below the X-point (Figure. 2.4-1). The vertical target is inclined so as to intercept the magnetic field lines of the separatrix at an acute angle, giving deep inboard and outboard channels in which to establish a partially detached plasma regime. In this regime, while the plasma remains attached in the outer region of the SOL, the plasma is detached from the PFCs in the region near the separatrix, causing the power profile to broaden and power to be radiated to other surfaces. Together with the lower end of each vertical target, a neutral particle reflector plate forms a “V” shape that confines neutral hydrogenic particles in the divertor channels and aids partial plasma detachment.

Compared to a fully attached operating mode, the peak heat flux onto the water-cooled target PFCs is reduced by a factor of two, bringing the target incident heat flux into the range of engineering feasibility (see 2.4.4). For inductive operation, up to 100 MW of thermal power is delivered via the SOL to the inner and outer channels of the divertor, and hence to the PFCs that delimit the divertor channels. According to code simulations, partial plasma detachment will occur and a maximum incident heat flux on the vertical targets of

1ITER Physics Basis, Nuclear Fusion 39 (1999) 2137

< 10 MWm^{-2} is to be expected. For steady-state scenarios up to 136 MW of thermal power is delivered via the SOL to the targets, and preliminary simulations indicate a peak target heat flux in the order of 15 MW m^{-2}. Although the targets can certainly sustain this heat load since they are rated to handle transient (10 s) heat flux perturbations of up to 20 MWm^{-2}, it will be with a reduced lifetime.

In the reference design, inner and outer targets are inclined at 35.5° and 24.5° respectively with respect to the separatrix. Inclining the targets further, to 17.75° and 12.25°, to reduce the target heat flux during Type I ELMs can be achieved by changing the vertical target PFCs, while leaving the rest of the divertor unchanged. In fact, with these "steep" targets the ELM heat flux on the targets is expected to be reduced by 40 to 50% with respect to the reference design (this takes into account toroidal peaking factors). Based on present estimates of Type I ELM energy of 12 MJ, the peak energy deposited on the targets is estimated at 1.7 and 0.8 MJm^{-2} for the reference and steep targets respectively. Some broadening of the SOL is expected to reduce this peak, say a factor 2, to < 0.4 MJm^{-2} for a steep target. This is comparable to the melt limit for tungsten[1]. This value might mean Type I ELMs will have little effect on a steep tungsten target lifetime. However, there are large uncertainties in the estimates of the ELM energy to each target and the extent to which broadening will mitigate the peak flux,. For partially attached plasma operation (normal operation) the heat flux is reduced by ~30% with respect to the reference design. Overall, B2-EIRENE code simulations indicate that operation with steep targets is tenable[2]. However, further study is needed to optimise the geometry and to gain confidence that the minor changes in the re-cycling pattern will not impair good H-mode confinement. The downside with this geometry is that narrower divertor channels are less accommodating to variations in the magnetic configuration than the reference design. Hence the steep target design is at present only considered for installation after initial operational experience has been gained with the more open divertor channel geometry of the reference design.

The baffle region is designed to provide a neutral particle pressure reduction of 10^4 between the divertor and the main chamber and of 10 between the private flux region below the dome and that above the dome. The baffle, positioned immediately below the X-point, is formed by the upper part of the divertor vertical targets and by the divertor dome. The baffle constitutes a toroidally continuous high heat flux surface following the 6 cm flux surface (measured at the outer plasma equator). Using the vertical targets extended upwards to form the baffle means that all the components, with the exception of the limiters, that are required to sustain surface heat loads > 1 MWm^{-2} are integrated into the divertor. This division of PFCs allows a uniform design of blanket modules and is expected to minimise overall in-vessel costs. Furthermore, incorporating the baffles in this way should localise future configuration changes to the divertor cassette alone. In addition, gas seals are employed between the divertor cassettes and the divertor cassette toroidal support rails in order to prevent neutrals from streaming back into the main plasma chamber.

Operating in the partially attached regime also eases the pumping, as the neutral pressure and the helium partial pressure in the private flux region will be increased considerably (0.3 to 10 Pa). This allows sufficiently rapid exhaust of the He ash to keep the He concentration in

[1] G. Federici, J.N. Brooks, D.P. Coster, G. Janeschitz, A. Kukuskhin, A. Loarte, H.D. Pacher, J. Stober, C.H. Wu, "Assessment of erosion and tritium codeposition in ITER FEAT", J. Nucl. Mater. **290-293** (2001) 260-265.

[2] A. Kukushkin et al.,"Operational space of a shaped divertor in ITER", 28th EPS, Madiera, 2001

the main plasma below 6%. This exhaust gas passes through the semi-transparent liners located beneath the dome (see Figure 2.4-1b), from where it flows radially outwards beneath the outboard PFCs, then through a pumping slot (500 mm high by 100 mm wide) formed by matching cut-outs in adjacent cassette bodies, and from there to the cryo-pumps. The slot in the cassette body is behind the outer vertical target where there is low neutron streaming. To maintain a high enough gas pressure to achieve detachment in the outer divertor channel, without recourse to excessive gas puffing, a large unrestricted opening in the private flux region PFC is provided, beneath the dome and above the semi-transparent liner, to connect the inner and outer channels. This allows free re-circulation of neutrals from the inboard to the outboard private flux region and their re-ionisation in the outer divertor plasma (higher pressures in the inner channel are observed in experiments and predicted by modelling).

To maximise the divertor channel lengths, and hence maintain the peak heat flux on the vertical targets to ~ 20 MWm^{-2}, it is necessary to have the lower face of the cassette body closely follow the internal profile of the vessel, especially in the regions immediately beneath the targets. A gap of 70 mm between the bottom of the cassette body and the vessel is maintained to accommodate build tolerances, differential movement of the vessel and divertor under thermal or electro-magnetically induced loads, and to leave space for diagnostic cable runs as well as for pellet injector guide tubes.

The cassette concept employed for the RH class 1 divertor is fundamental for the maintenance strategy as it allows installation to be limited to a few integrated components inside the vessel, thus minimising the maintenance operations in-vessel and allowing short RH intervention times and high reliability. A few complete replacements of the divertor PFCs are anticipated throughout the lifetime of ITER, because of armour erosion and possibly because of changes in the divertor configuration. In these cases, only the PFCs will be substituted, while the cassette body can be re-used, thus minimising the amount of activated waste produced. The divertor is segmented into 54 cassettes, 3 per port. This is based on the maximum size of cassette that can be handled via the maintenance ports and still have an integer number of cassettes per port. Of the 18 lower ports, 3 equally spaced ports are allocated to divertor remote maintenance. These ports are 2 m high, which is large enough to allow the cassettes to pass through them during installation. The ports are inclined so as not to interfere with the inter-coil structure or with the building slab between the equatorial and lower ports. Each cassette is 3.5 m long, ~ 2 m high and 0.4 – 0.9 m wide, and weighs ~ 10.6 t.

The replacement of the PFCs is performed ex-vessel in a hot cell, where the refurbishment of 54 cassettes will take about half a year.

Of the 54 cassettes, 5 are designated diagnostic cassettes and accommodate waveguides and optical diagnostics for studying the plasma. These are located immediately in front of the maintenance ports 3, 9 and 15, and in front of ports 12 and 18. In addition, there are a further 10, “instrumented cassettes”, that carry diagnostics such as thermocouples, which require only minor adaptation of the cassette body and PFCs.

2.4.3 Armour Selection & Armour Issues

Carbon-fibre composite (CFC) is the reference armour for the strike point regions of the targets. Tungsten has been selected for all other plasma-facing surfaces of the divertor, for

the baffle regions of the target and the surface of the dome where there are charge-exchange (CX) neutrals, because of its low sputter yield, and for the private region PFCs because of its low T retention and high melting temperature. Using this armour combination, the erosion lifetime of the PFCs is expected to meet the goal of sustaining 3,000 full-power discharges of 400 s duration, with one in ten discharges ending in a disruption where the SOL becomes fully attached to the target. Although CFC has been selected, an all-tungsten divertor is possible. The merits and demerits of both materials are discussed below.

Carbon is forgiving as an armour material since it will ablate as a result of disruption events or if target misalignments cause leading edges to intercept the SOL (~ 100 MWm^{-2}). There are no concerns over what happens to a melt layer. R&D has developed the technology to manufacture carbon-armoured PFCs with a demonstrated heat flux capability > 20 MWm^{-2}.

Carbon has one major drawback, the potential to chemically trap tritium in co-deposited layers at a rate estimated at 5 g ± 50% T/pulse of 400 s. Besides the presence of He and DT gas in the divertor, there are likely to be significant quantities of carbon and hydrocarbons that have been chemically and physically eroded from the vertical target. It has been shown in laboratory and tokamak experiments[1] that the nature of these hydrocarbons, i.e. the volatile and active species, is such that they can form thick, hydrogenated coatings on cool surfaces. (If they are deposited at high temperature, they form diamond-like hard layers and contain relatively little hydrogen.) Of real concern is the T that will be trapped in soft hydrogenated layers, which have a high proportion of hydrogen, that will build up on cold surfaces of the private flux region and, because of low sticking coefficients of the species that produce these soft layers (e.g. with CH_3 radicals), can migrate downstream of the divertor (and elsewhere in the tokamak).

In order to overcome this, it was suggested that the liner should operate at a high temperature (800 to 1,000°C) and provide sufficient area for surface collisions to recombine the active components, such as H^0 and C_xH_y radicals, into volatile compounds that can be pumped safely away. Although this promises to reduce the amount of co-deposited T, maintaining the divertor exhaust pumping capability is not compatible with providing the required number of wall collisions (~ 1,000) to transform the whole amount to stable compounds that can be pumped.

A second approach considered a hot duct (> 350°C) leading to a cold trap for the hydrocarbons (~ 70K) located in a region sheltered in the cryo-pump ports where the lower neutron flux makes the cryogenic cooling system feasible. The intention is to capture the hydrocarbons that would otherwise contaminate the in-vessel surfaces and in particular, the cryo-pump. The cold traps would need regeneration to reclaim the T, and valves to close off the cold trap from the rest of the in-vessel system during regeneration. Detailed evaluation of this design is underway, but the complexity of including such a system is to be avoided if at all possible.

For both the above options R&D is underway to establish the range and proportions of the C_xH_y species that will be present, and the sticking probabilities versus temperature of these species in the presence of a large flux of atomic hydrogen. It is still possible that results from

[1] G. Federici, et al., Issues arising from plasma wall interactions in reactor-class tokamaks, to appear in Nuclear. Fusion.

this R&D could make one or other of the above options workable, or at least reduce the frequency at which clean-up operations need to be performed. Furthermore, it will be prudent to have available a method than can thoroughly clean C deposits from the in-vessel surfaces of the machine.

Possible methods of using oxygen to release the tritium are under investigation and consider the use of atomic O (molecular oxygen being not efficient enough). The possibilities are baking in ozone, and glow discharge cleaning in O. The results of these studies are as yet inconclusive. Whatever the chosen method, the whole clean-up operation, including re-conditioning, should fit with a tenable machine operation scenario. Introducing O into a tokamak raises concerns over the need to re-condition the first wall of the vessel and also over the damage that might be done to the beryllium surfaces.

On the other hand there are no concerns over T inventory if an all-tungsten armoured divertor is adopted. Encouraged by this possibility, tungsten armour technology has been developed to a level where the feasibility of building reliable targets capable of handling incident heat flux > 20 MWm^{-2} has been demonstrated[1]. Concerns over plasma contamination when operating with tungsten as a plasma-facing material have been partially allayed by the good plasma performance obtained while operating with high-Z, armoured PFCs in Alcator C-MOD[2] and more recently in ASDEX Upgrade[3]. However, there remain concerns over what will happen to the melt layer of the tungsten target (up to 80 μm deep during a disruption) and what effect an uneven re-solidified surface might have on subsequent operations and target life-time. Assuming that 50% of the melt layer is lost in each disruption, then a target lifetime similar to that of carbon is calculated (in fact disruption experiments show a much lower loss fraction). Finally, there are concerns over surface cracking of tungsten due to repeated disruptions and blistering of the tungsten surface due to hydrogen implantation. However, in experiments with tungsten at divertor relevant surface temperatures these effects appear be unimportant. R&D is continuing to study the performance of tungsten armour and the ASDEX Upgrade programme aims to operate with increasing amounts of the first wall covered with tungsten.

During the hydrogen operation of the machine, co-deposition is not an issue, but its importance and possible level can be fully ascertained. Hence, the most prudent scenario is to be able, if appropriate, to remove all carbon deposits at the end of the H phase, and to install an all-tungsten divertor before DT operation begins.

Finally on the issue of plasma-facing materials, the plasma wall interactions in ITER with materials such as Be, W, and CFCs is expected to generate substantial amounts of “dust”, most of which will end up in the divertor region. This dust may be tritiated, radioactive, chemically reactive and/or toxic. Dust on the hot tungsten surfaces of the dome and upper part of the vertical target may promote reactions with steam during a water leak (Be-dust) producing sizeable quantities of hydrogen, or give rise to the possibility of explosion during

[1] M. Merola, et al., "Manufacturing and Testing of a Prototypical Divertor Vertical Target for ITER", 9th Int. Conf. on Fusion Reactor Materials, October 10-15, 1999, Colorado Springs, to appear in J. Nucl. Materials.
A. Makhankov et.al., "Development and Optimization of Tungsten Armour Geometry for ITER Divertor", Proc. 20 Symposium on Fusion Technology, Marseille, September 1998, p.267-270

[2] M. Greenwald, "H Mode confinement in Alcator C-MOD", Nuclear Fusion, 37 (1997) 793

[3] K. Krieger, H. Maier, R. Neu, and the ASDEX Upgrade Team, J. Nucl. Mater. **266-269** (1999) 207

sudden air leaks (carbon dust). The dust on these hot surfaces will be held in the gaps between tiles. The general limit for in-vessel dust, based on allowable release to the atmosphere, is 100 kg for W, Cu, steel and Be, and 200 kg for C because of explosions. The actual rate of dust generation and its distribution in the machine will be studied during the hydrogen operation phase of ITER. In the meantime, R&D has been instigated aimed at finding methods to both measure the quantity of dust inside the ITER machine and to remove it during maintenance periods.

In summary, carbon remains the choice for the lower part of the vertical target where its ablative property makes it a very forgiving material against disruptions and target misalignments that can result in very high heat flux on leading edges. At present all the parties within ITER are investigating the physics of hydrocarbon radicals to decide whether designs incorporating carbon can result in acceptably low T deposition rates or if carbon has to be avoided altogether in a long pulse machine operating with T. In this case, an all-tungsten target is foreseen to be used for the strike point regions of the target.

2.4.4 Vertical Target

Each vertical target is based on a number of thin poloidal elements ~ 23 mm width; 27 elements for the outboard vertical target and 21 for the inboard. The upper part of the element is clad with W tiles and the lower part with CFC monoblocks. All the PFCs are constructed using a similar range of manufacturing techniques, demonstrated to be viable by R&D. This approach is intended to simplify manufacture and minimise costs, as it allows the critical fabrication steps, particularly those involving the armour-to-heat-sink joints, to be performed and qualified on small units. Each poloidal element employs a 10 mm bore, 12 mm outer diameter, copper tube with swirl tape (twist ratio = 2) inserted in the lower part of the vertical target. The swirl tape is required to enhance the critical heat flux (CHF) limit and provides an ~ 1.5 margin on 20 MWm^{-2} slow transients. Uncertainties in the precise location of the SOL strike point require the insertion of the swirl tape over an ~ 500 mm length. High velocity swirl flow (~ 10 ms^{-1}) is employed over the minimum length required in order to minimise the overall pressure drop through the vertical target and maximise the CHF capability (see 2.4.8). For the upper vertical target (heat flux < 5 MWm^{-2}) the swirl tape is not employed and instead the coolant channel is a smooth tube. Figure 2.4-2 shows the geometry of the inner vertical target. The poloidal plasma-facing elements are mounted onto a single steel support structure that incorporates toroidal cooling, resulting in a limited temperature difference (~ 50°C) within the structure, thus providing a stable base for the plasma-facing elements. In fact, finite element calculations show that the maximum deformation caused by the nuclear heating and worst case asymmetric heating of the plasma-facing surface is only 0.25 mm.

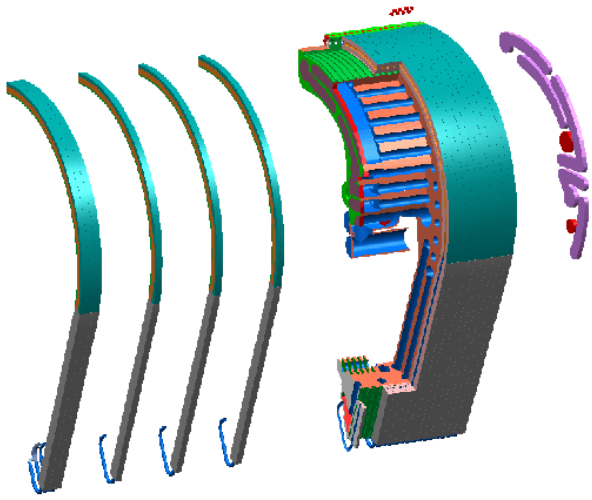

Figure 2.4-2
Exploded View of the Inner Vertical Target

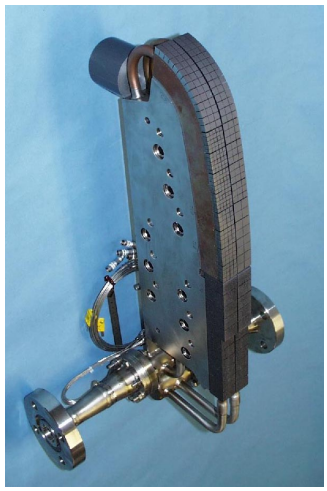

Figure 2.4-3
EU Prototype with CfC & W Armour

The most critical aspect of a PFC is the armour-to-heat-sink joint and the EDA R&D has seen impressive progress made in the development of both CFC to Cu and tungsten to Cu joints.

For the carbon armour joints, the bore of the CFC monoblocks are lined with a pure Cu layer cast onto a laser-textured and Ti-metallised surface, so-called active metal casting (AMC). The Cu in the bore of the monoblocks is machined to size prior to them being low temperature (~ 500°C) hot-isostatically pressed (HIP) to a CuCrZr tube. The precipitation hardened CuCrZr alloy has been selected over other Cu alloys because of its good post-irradiation fracture toughness. In fact, several techniques might be used for making the Cu-CuCrZr joint (furnace braze with fast quench, rapid brazing using ohmic or inductive heating, or HIP-ing), but the HIP process gives optimised mechanical and thermal properties, and minimises the residual strains in the critical Cu-CFC joint. The CFC monoblock has been shown to be a robust design for the CFC armour, and in tests[1] a prototype (Figure 2.4-3) has survived 2,000 cycles at 20 MWm^{-2}. It is preferred over the less expensive flat tile design, because of concerns over the observed tendency for flat tiles to suddenly and totally detach.

For the upper part of the target, 10 x 10 x 10 mm tungsten tiles, with a pure Cu layer cast onto the tungsten to accommodate the differential thermal expansion of tungsten and carbon, are brazed to a CuCrZr alloy rectangular hollow section, a design that has sustained > 20 MWm^{-2} for 2,000 cycles in HHF testing[2]. An added benefit of this design is that, by faceting the surface of the Cu heat sink, the armour can be applied to the curved upper part of the target.

The vertical targets have been analysed for the various operational structural loads. Figures 2.4-4 and -5 show the temperature distribution due to the transient nuclear heating for the ITER duty cycle and the corresponding von Mises equivalent stress. The main loads on

[1] M. Merola, et al, "Manufacture & Testing of a Prototypical Divertor Vertical Target for ITER", 9th Int. Conf. On Fus. Reactor Materials, October 1999, Colorado Springs.

[2] S. Chiocchio et al., "The Divertor for the Reduced Technical Objective/Reduced Cost ITER", SOFE, Albuquerque, Oct. 1999.
R. Tivey et al., "ITER Divertor, Design Issues and R&D", Fus. Eng. & Des. 46(1999) 207-220

the targets are the eddy current loads due to a fast VDE. Finite element analysis shows that the combined loads, secondary plus primary membrane and bending, are within the ITER structural design criteria allowable for category III event.

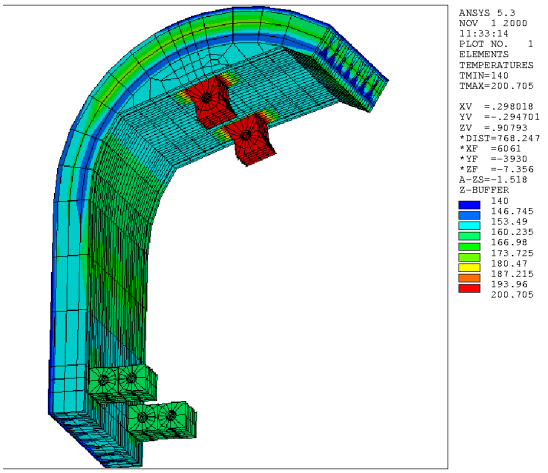

Figure 2.4-4
Temperature Distribution in the Outer Vertical Target for Transient Nuclear Heating

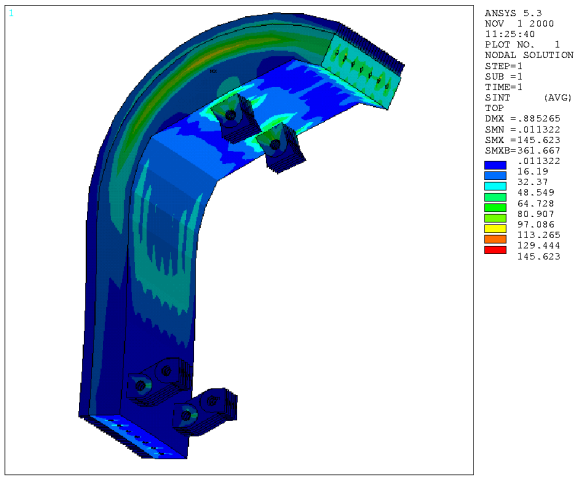

Figure 2.4-5
Stress Intensity (MPa) in the Outer Vertical Target under Thermal Load and Dead Weight

With regard to the low cycle fatigue (LCF) life-time of the heat sink for the reference monoblock design and the coolant parameters described in 2.4.8, analysis indicates a life-time of 2.8×10^5 cycles at 10 MWm^{-2}, and 806 cycles at 20 MWm^{-2}.

An alternative to this reference design that has been investigated is an annular flow heat sink. The advantages of this concept are the removal of expansion pipes at the base of the monoblocks bringing improved reliability and relieving space in an over-congested region and the potential for cost savings due to the lower number of plasma-facing elements (17 instead of 27 elements for the outer vertical target). Unlike the reference design (12 mm OD swirl tube), which needs optimum CuCrZr mechanical properties to satisfy LCF requirements obtained using a low temperature HIP cycle during manufacture, the annular flow monoblock (tube outer diameter 20-22 mm) meets these requirements with the non-optimum CuCrZr properties obtained in a furnace brazed construction. During testing a CFC armoured annular flow mockup, with furnace brazed CFC/CuCrZr joints, survived 3000 cycles at 20 MWm^{-2}, thus demonstrating the viability of the concept.

2.4.5 Private Flux Region PFCs

As mentioned in 2.4.3, there are several options still under consideration for the private flux region PFCs, and the final choice will depend on the armour selected and the success of on-going R&D. However the divertor cassette approach has the flexibility to accommodate any of the likely design solutions. The PFC design described here is the simplest version without cold trap, etc (see Figure 2.4-6).

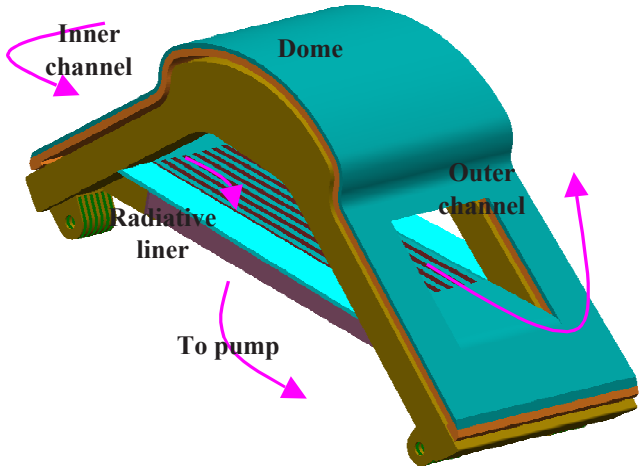

Figure 2.4-6 Open Dome Design with Radiative Liner

The dome and inner and outer short targets of the private flux region PFCs are clad with tungsten tile armour that is attached using a similar technique as used for the upper parts of the vertical targets. The dome is supported on four posts which are protected with a combination of tungsten tile armour (surfaces facing the divertor channels) and radiatively cooled tungsten plates. As part of the PFCs, a semi-transparent liner clad also with radiatively cooled tiles is suspended above the cassette body. In this way, an open duct is formed beneath the dome, connecting the inner and outer channels of the divertor, that is clad completely in radiatively cooled tungsten plates. This allows the surfaces of the duct to be maintained at temperatures > 350°C for the majority of the 400 s discharge.

2.4.6 Divertor Cassette Body

The stainless steel cassette body that supports the PFCs is designed to withstand the electromagnetic forces, provide shielding for the vacuum vessel and coils, and incorporates internal coolant channels, which cool the cassette body and act as manifolds for the PFC coolant. Construction of the cassette body both from steel castings and from forged steel plates have been considered. R&D has shown that either approach has the capability to produce a robust vacuum-compatible component. However, cast 316LN material has ~ 30% lower yield strength than forged material, and hence fabrication from forged steel is preferred, as it allows the cassette thickness capable of sustaining the electromagnetic loads to be ~ 50 mm thinner in the critical region beneath the inner divertor channel, a thickness that can be allocated to the inner channel depth. Two cassette-to-vacuum-vessel support options have been considered, one with the cassette attached to the vessel by a pinned support both inboard and outboard of the cassette, and the second with a pinned connection at the outboard but at the inboard a support that allows radial translation but no vertical displacement (sliding support). The worst case loads are caused by halo currents flowing through the cassette as a result of VDE II and VDE III in combination with internal pressure and thermal loads.

The stress levels are such that only the pinned inboard and outboard option is acceptable, even if preliminary analysis indicates that only ~ 50% of the halo current is carried by the cassette. The resulting maximum primary stress is 64 MPa, assuming all the halo current is carried by the cassette (I_{cass}= 0.29I_pPf / N, where Pf is a peaking factor taken as 2 and N is the number of cassettes).

Figure 2.4-7 shows the von Mises equivalent stress distribution for the combined load case of 100% halo current, internal pressure, and nuclear heating. Table 2.4-1 summarises the different stresses in the cassette body with the corresponding margins on the allowables. For this pessimistic load condition the pinned inner and outer supports provide a margin of > 10%.

Table 2.4-1 Stress Estimations from ANSYS Analysis
For the Case of Inboard and Outboard Supports Pinned

			Dynamic loading factor	Allow. Stress MPa	Halo[1] MPa	Margins	Halo + Nuclear Heating MPa	Margins
CASSETTE BODY	Primary + Secondary Stress	Category I VDE I	1.2	340[2]	32	8.8	291	1.2
		Category II VDE II	1.2	340[2]	48	5.9	297	1.1
		Category III VDE III	1.2	340[2]	64	4.4	304	1.1
	Secondary Stress	Category I VDE I	NA	340[2]	-	-	279	1.2
		Category II VDE II	NA	340[2]	-	-	-	-
		Category III VDE III	NA	-	-	-	-	-
	Primary Stress P_m+P_b	Category I VDE I	1.2	200[3]	32	5.2	12	14
		Category II VDE II	1.2	200[3]	48	3.5	18	9.2
		Category III VDE III	1.2	240[3]	64	3.1	24	8.3

Maximum Displacements			
	Axial Directions	**Positive direction mm**	**Negative direction mm**
U_{MAX}	**Radial**	1 (H+NH)[4]	4.5 (H+NH)
	Toroidal	1.03 (H+NH)	-
	Vertical	1.8 (H+NH)	5.5 (H+NH)

[1] *Internal pressure + Halo (slow VDE).*
[2] *Allowable @Temperature 350°C*
[3] *Allowable @Temperature 200°C*
[4] *Halo + Nuclear Heating (the analysis with the maximum displacement)*

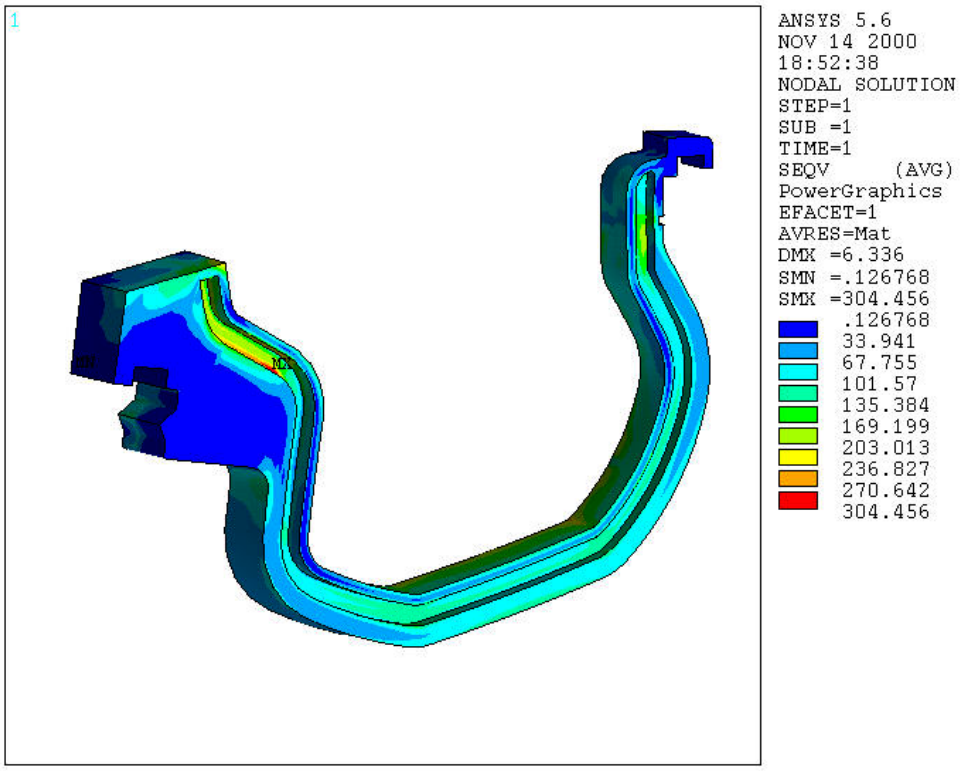

Figure 2.4-7 Von Mises Equivalent Stress in the Central Cassette Body for Primary Plus Secondary Stress with the Inner and Outer Supports Pinned.

The loads caused by eddy currents generated in the PFCs, as a result of disruption types I and II, are less severe for the cassette body than those caused by halo currents during VDEs. However, they determine the cassette body design local to the PFC-to-cassette attachments. A cassette minimum thickness of 240 mm is maintained in order to provide neutron shielding of the VV and coils. The coolant channels within the cassette body that service the PFCs combine to represent an average of 21% of the volume of the cassette body (the acceptable level for both coils and VV being in the range 10-30% water).

2.4.7 Alignment

The scrape-off layer strikes the vertical targets at a glancing angle (< 2°). Targets on adjacent cassettes must be aligned accurately with respect to one another and angled slightly so as to shield the leading edges of the adjacent components from direct incidence of the field lines in the scrape-off layer. A maximum radial step in the toroidal direction between adjacent targets of 4 mm is taken as a requirement. The overall alignment of the divertor is less critical, provided the deviations from the nominal are of a long wavelength (i.e. occurring in an arc spanning several cassettes), and an overall tolerance of ± 10 mm is taken as a requirement. These demanding tolerances are met by a combination of accurate manufacture of the cassettes and in-vessel toroidal rail support points, and if necessary, adjustment of the attachments prior to installation in order to suit the as-built dimensions of the toroidal rails.

2.4.8 Divertor Cooling

The main driver for the cooling layout is the need to maintain an adequate margin (> 1.4 based on experimental results) to the critical heat flux (CHF) limit, and not, as may at first be thought, the total input power to the divertor.

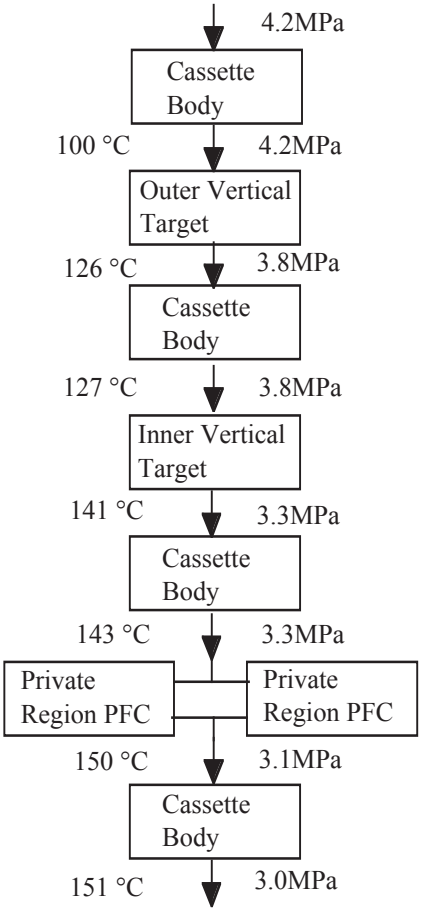

Figure 2.4-8 Schematic of Coolant Circuit in a Divertor Cassette

Table 2.4-2 Divertor Coolant Parameters, and Margins on CHF for each PFC

Inlet pressure (MPa)	4.2
Inlet temperature (°C)	100
Flow rate (kgs^{-1})	734
Total pressure drop (MPa)	1.2
Total temperature increase (°C)	~50
Axial velocity in the swirl section of the outer target (ms^{-1})	9.0
Axial velocity in the swirl section of the inner target (ms^{-1})	11.9
Minimum margin to CHF in the outer vertical target (based on 20 MWm^{-2})	1.65
Minimum margin to CHF in the inner vertical target (based on 20 MWm^{-2})	1.53
Minimum margin to CHF in the dome (based on 3 MWm^{-2})	2.84

Data on the mechanical properties of irradiated CuCrZr indicate that the sub-cooling that a 100°C inlet temperature provides allows the coolant to be fed in series through the PFCs of

the divertor (Figures 2.4-8 & -9). A higher coolant velocity is employed in the downstream inner vertical target in order to compensate for its lower sub-cooling and to achieve a similar margin on CHF as the outer vertical target. The coolant parameters and margins on CHF for each PFC are given in Table 2.4-2 for the reference Inductive Operation Scenario I plasma.

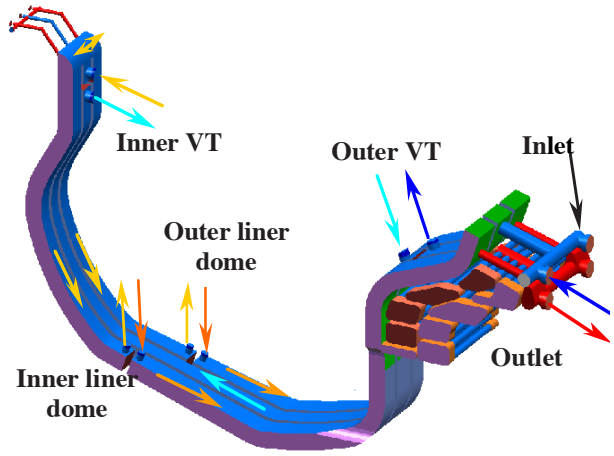

Figure 2.4-9 Coolant Routing within the Cassette Body.

2.4.9 Scheme of PFC Attachment to Divertor Cassette Body

Each of the 3 PFCs are supported from the cassette body using two pairs of remotely maintainable attachments (Figure 2.4-10). One pair of attachments, the lower ones in the case of the vertical targets, accommodates both rotation and translation. A series of links engage at one end in slots in the PFC and at the other in slots in the cassette body. The holes in the links are aligned at one end with holes in the cassette body and at the other with holes in the stainless steel support structure of the PFCs. Thick aluminium-bronze tubes (~ 30 mm outer diameter and ~ 20 mm bore) are then inserted into each of the holes of the inter-linked components (clearance of 0.5 mm) and one at a time the pins are expanded by drawing a mandrel through them. Aluminium-bronze is selected because of good wear characteristic when operating in vacuum against stainless steel. The second attachment uses only one expanded pin and is capable of rotation only. In this case no links are needed, and instead a series of tongues (part of the cassette body) are inserted into slots in the PFC. These links react the loads caused by eddy currents in the PFCs induced during disruptions. For PFC replacement in the hot cell, the attachments are removed by simply drilling out the pins using the central hole as a guide. Coolant pipe connections (60 mm dia) between the PFCs and the cassette body are located adjacent to the pinned supports, where the minimum relative displacement occurs. Helium generation in these tubes is estimated to be ~ 5 appm over the life of ITER, which is beyond the assumed re-weldability limit. However, by ensuring that, at each PFC replacement, part of the tube belonging to the most recently replaced PFC remains with the cassette, the He content in welded material will remain acceptable. Analytical assessments indicate that the attachments can carry the currents flowing between the PFCs and the cassette body during disruptions or VDEs. Preliminary R&D performed in air simulating the electrical and mechanical loads and the applied joint rotation shows no joint degradation and indicates that separate earth straps are unnecessary.

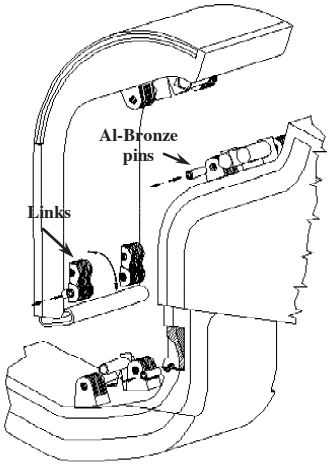

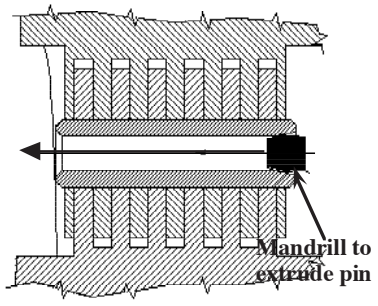

Figure 2.4-10
Attachment Scheme of the PFCs Using Copper Alloy Pin Extruded into Cassette Body and PFC Attachment Lugs.

2.4.10 Cassette to VV Attachments

During operations, the cassettes are accurately held in position on two toroidal rails (Figure 2.4-1), attached to the VV. During shutdowns, these rails are used for remote maintenance of the divertor. The cassette is positively and remotely locked to both the inboard and outboard rails (see above), except in the case of the three cassettes positioned immediately in front of the maintenance ports. These are positively locked at the outboard and held at the inboard by applying a radial pre-load (~ 30 t), which, taking advantage of the radial spring stiffness of the cassette body ($k = 2.5$ t mm^{-1}), radially compresses the cassette by 13.7 mm and results in a peak stress in the body structure of 230 MPa (VDE III + pre-load). The pre-load ensures that the cassette remains in contact with the inner support attached to the VV under all loading conditions, including that caused by the radial differential thermal expansion between cassette and vacuum vessel. Each support allows rotation around a toroidal axis and can sustain all normal and off-normal vertical, horizontal and radial loads. As in the case of the PFC to divertor attachments, R&D is expected to show that separate earth straps are an unnecessary complication.

2.4.11 Divertor Gas Seal

The divertor-to-main-chamber gas "seal" (actually a baffle) is achieved by the cassette-to-toroidal-rail attachments. It is designed to meet a leak tightness of < 5 Pam^{3}s^{-1} for a ratio of 10^4 in pressure between the divertor and main chamber at a pressure of 1 Pa in the divertor area.

2.4.12 Diagnostic Cassettes

The three diagnostic cassettes located in front of the maintenance ports have an appendage that protrudes into the port. This supports wave-guides and optical transmission lines. As a result these cassettes weigh an additional 1.7 t making them 12.3 t.

All the diagnostic cassettes carry diagnostics on the side wall of the cassette body (Figure 2.4-11). These diagnostics include Langmuir probes, thermocouples, pressure gauges etc. The diagnostics are supported on localised stainless steel or copper alloy support structures bolted (or possibly riveted) to the cassette sides and are cooled without water, radiatively and by conduction through the attachments to the cassette body. The side plates, shown in the

figure schematically, are in fact carried on strong-backs/jigs that support and correctly position the diagnostics during handling prior to their attachment to the cassette. The diagnostic support plates then remain with the cassette and use a minimum of material to keep down the nuclear heating. They are locally split so as to allow thermal expansion without distortion and take their strength during operation from the cassette body and PFCs to which they are rigidly attached. As far as possible, the diagnostics, associated cabling, and support plates, are inserted in recesses or grooves in the side plates of the cassette body and the PFCs. In this way the recessed diagnostics are protected during divertor maintenance, and the neutron shielding performance of the divertor as a whole is unaffected.

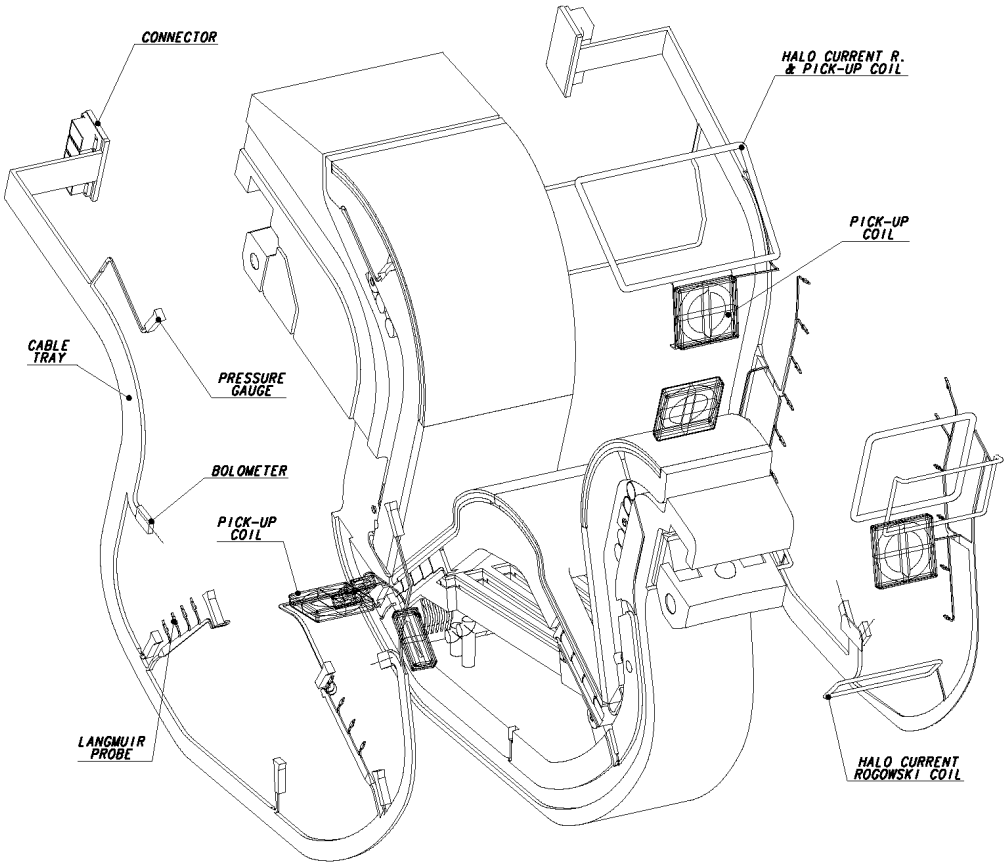

Figure 2.4.11 Exploded View of Instrumented Cassette

Similar side-plates accommodate the wave-guides. However, there are two types of wave-guide (10 mm and 20 mm wide) and the 20 mm wide version will require a deeper cut into the cassette body side wall.

The cassettes that incorporate optical diagnostics have a mirror assembly in the private region beneath a semi-transparent liner with slots are cut in it to allow viewing of the divertor channels. A hole running radially through the outboard region cassette body provides the route for the optical transmission lines.

2.4.13 Further Divertor Integration Issues

Of the 18 lower ports, 10 contain cryo-pumps (see 2.7), 3 are allocated to remote maintenance (see 2.9) and contain diagnostic blocks supporting wave-guides and optical

transmission lines (see 2.6), 2 are allocated primarily to diagnostics, and 3 accommodate part of the pellet and gas injection systems. In addition, the cryo-pump ports host the glow discharge cleaning heads (see 2.7) and the laser-based, in-vessel viewing and metrology system (see 2.9). Detailed integration studies have generated designs that accommodate all the requirements for the maintenance and cryo-pump ports, including remote handling needs and locations for divertor coolant feed pipes (6 per port).

Figure 2.4-12 shows the maintenance ports with diagnostic racks carrying waveguides or optical transmission lines installed. The rack is held on the radial rails that carry and guide the RH transporter during maintenance interventions. Six coolant pipes that feed the divertor cassettes are located either side of the port.

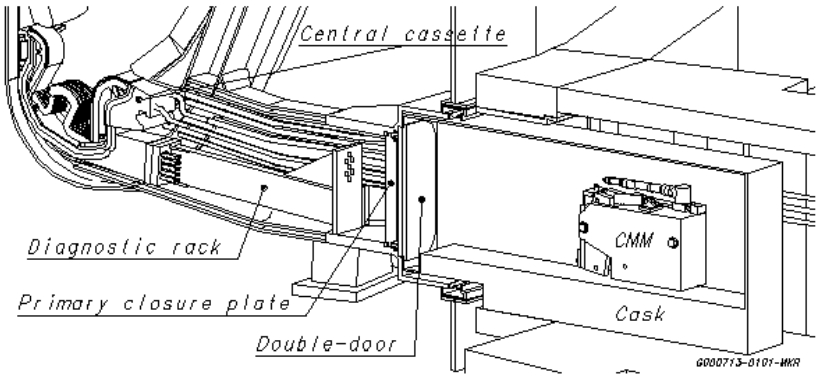

Figure 2.4-12 Maintenance Port with Diagnostic Equipment Installed

For fuelling, the divertor incorporates 3 gas valve lines in ports 1, 7 & 13. The gas is routed via the rail into the cassette, the seal between rail and cassette being achieved by contact pressure alone, which require no in-vessel RH operations. Gas lines are routed, through channels in the toroidal rails and the cassette bodies, to positions beneath the separatrix in the divertor dome. Pellet fuelling gas lines are included in these ports. These closely follow the vessel wall beneath the divertor and pass through the inner toroidal rail to the blanket.

2.4.14 Divertor Overall Assessment

The above divertor design provides an engineering solution compatible with today's plasma physics expectations. Its detailed specification has been thoroughly investigated through R&D, some of which is still underway. Given the uncertainties in the plasma physics extrapolation, and thus the component durability, the design provides a system for rapid replacement and refurbishment. The present design provides an accurate mechanical support, and flexibility to change the plasma-facing geometry as well as the plasma-facing materials on the PFCs. It is expected that R&D already active in present tokamaks (JET, JT60, DIII-D, ASDEX-U) will provide results on which an optimized material choice can be based before manufacturing starts, to be confirmed by initial experimentation in ITER (during the H phase) If needed, the divertor PFCs in the cassettes can readily be replaced to provide a different geometry and/or different plasma-facing material.

2.5 Additional Heating and Current Drive

Multiple roles and a wide range of functions are assigned to the additional heating and current drive (H&CD) systems in ITER.

All key phases of the reference scenario – i) the access to the H-mode regime, ii) the plasma temperature rise, while density is increased to allow the requisite fusion power, iii) the achievement of a steady burn, iv) the control of the excursions about the operating point, v) the suppression of instabilities, and vi) the achievement of a soft termination – are controlled by the input of H&CD power by an appropriate combination of neutral beams (NBs) and three RF H&CD systems operating at the electron cyclotron (EC), ion cyclotron (IC) and lower hybrid (LH) frequency. The last will not be used for initial operation and may be added only in an upgrade of H&CD performance.

The onset of neo-classical tearing modes (NTMs) potentially poses challenges to ITER high-β operation and provisions for active control by ECCD is included.

H&CD systems are required to heat non-fusion plasmas in the early operating phases, for example, to commission the divertor target plates. They are used for plasma initiation and assisted start-up, to control sawteeth and resistive wall modes, to induce a small amount of plasma rotation, and for wall conditioning.

Steady state operation requires an on-axis current seed and active control of the plasma current profile, to access enhanced confinement regimes in which a large fraction of the plasma current is generated via the bootstrap effect.

With the current number and dimensions of the ITER ports competition for access to the plasma is tight. For H&CD systems, this is reflected in the need for high power density operation, close to the practical limit.

Two and possibly three ports are reserved for the NB injectors, two equatorial ports are assigned to RF systems, and three additional upper ports are used for ECCD NTMs stabilisation. For the equatorial ports, the design power density is 20 MW/port for the RF systems and 16.5 MW/port for the NB H&CD system. Seven MW of EC power can be injected in each upper port.

Provision is made in the design for space, auxiliaries and services adequate for the maximum installed power, i.e. for four equatorial ports (and three upper ports) for RF power and 3 NB injectors. With all auxiliary systems operating at the nominal performance in all possible reserved ports, 130 MW of H&CD power would be available, although heating power of only up to 110 MW should be added simultaneously to the plasma.

2.5.1 Neutral Beam Injection System

2.5.1.1 System Parameters

The neutral beam (NB) system design consists at present of two heating and current drive (H&CD) injectors and one diagnostic neutral beam (DNB) injector (2.5.1.5). Each H&CD injector will deliver a deuterium beam of 16.5 MW (total 33 MW), with energy of 1 MeV, and will be able to operate for long pulses (up to 3,600 s for steady state operation). A system based on negative (D^-) ions is necessary, primarily, for better energy efficiency due to its high neutralisation efficiency.

The size of the ion source and the required D^- current density should not require large extrapolations from the largest operational negative-ion-based NB injection systems (JT-60U and LHD N-NB injection systems) in physics (plasma uniformity and negative ion current density) and in engineering (manufacturing, assembly, and maintenance) aspects. The present design assumes 200 A/m^2 as the D^- accelerated current density, at the grounded grid (a reasonable extrapolation from the relevant R&D results), a total accelerated current of 40 A and an ion source roughly twice the size of that on the JT-60U N-NB injection system.

The acceleration voltage remains the only free variable. For the H&CD injectors, higher voltages than the one quoted above could permit to increase the power and the current drive efficiency. On the other hand, higher voltages imply larger insulation distances (both in gas and vacuum) and higher beam shine-through through the plasma. Moreover, the maximum acceleration voltage of the two existing test beds, at Naka and at Cadarache, is 1 MV in both cases. Considering ITER dimensions, 1 MV is considered as a good compromise.

In addition to heating and current drive, a small amount of plasma rotation is also provided by the NB H&CD injectors. For the H operation phase, the H&CD injectors can be operated in hydrogen, with beam energy ≤ 0.8 MeV and beam power ≤ 13 MW.

2.5.1.2 System Layout and Integration

Figure 2.5.1-1 shows the NB layout: the NB injectors are located on the north side, at the equatorial level of the tokamak building. Port 4 is shared between an H&CD injector and the

diagnostic injector, and port 5 is allocated to the second H&CD injector. Space has been reserved for a third injector that could be mounted on port 6. The total NB H&CD power could then reach 50 MW

The horizontal angle of injection is defined by the NB duct size (including beam envelope, vacuum confinement, neutron shielding, tolerances and clearances) and the space available between the toroidal field coils (see Figure 2.5.1-2). The strike area on the far wall of the vacuum vessel is constrained not to include a port so as not to damage items in the port plug. Beam injection is possible when the plasma density is $\geq 0.35 \times 10^{20}\ m^{-3}$, assuming that 1 MW/m^2 is the acceptable power density on the first wall.

Within the NB duct height, the beam can be aimed at two extreme (on-axis and off-axis) positions by tilting the beam source around a horizontal axis on its support flange. In order to cover a range of vertical positions from the machine equatorial plane (at the tangency point) suitable for both on- and off-axis CD, the beam axis is tilted vertically in the range 40 - 60 mrad. This tilted beam geometry enables the NB duct to be compatible with a port of the same height as the regular equatorial port, the other relevant structures of the machine (toroidal field coils, intercoil structures, poloidal field coils and thermal shields) and the building design. The main layout parameters are listed in Table 2.5.1-1.

Table 2.5.1-1 System Layout, Main Parameters

Beam Tangency Radius (mm)	Beam Axis Vertical Position from the Equatorial Plane, at Tangency Radius (mm)		Duct Liner Exit Width (mm)	Duct Liner Exit Height (mm)	Distance from Grounded Grid to Duct Liner Exit (m)
	Highest	Lowest			
5300 ± 60	+ 156	- 417	582	1360	22.8

The injector's vessel is an extension of the primary vacuum boundary and is part of the primary barrier for contamination confinement. The common enclosure for all the injectors, the NB cell, performs the function of a secondary confinement barrier.

2.5.1.3 System Design

Figure 2.5.1-3 shows the NB system design. Since the early stages of the EDA, the injector has been conceived with the aim to reduce its axial length, and hence to limit the cost impact on the tokamak building. The concept[1] is to subdivide the neutralizer, and, consequently, the residual ion dump (RID) to form four vertical channels.

[1] R Hemsworth, et al., "Neutral Beams for ITER", Rev. Sci. Instrum. 67/3 Part II, pp 1120 - 1125, (1996).

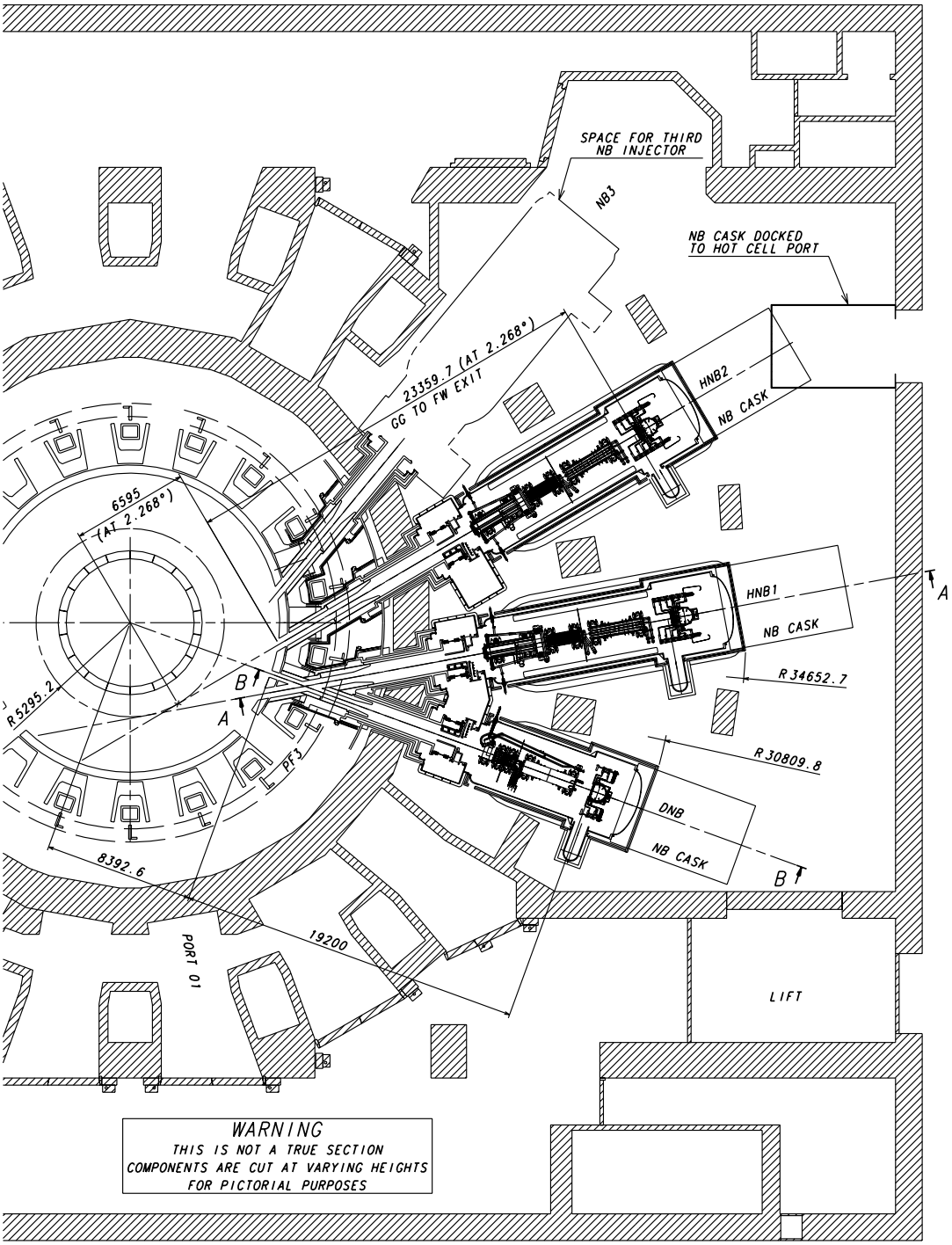

Figure 2.5.1-1 NB System Layout, Plan View

N 53 GR 393 01-06-14 R 0.1

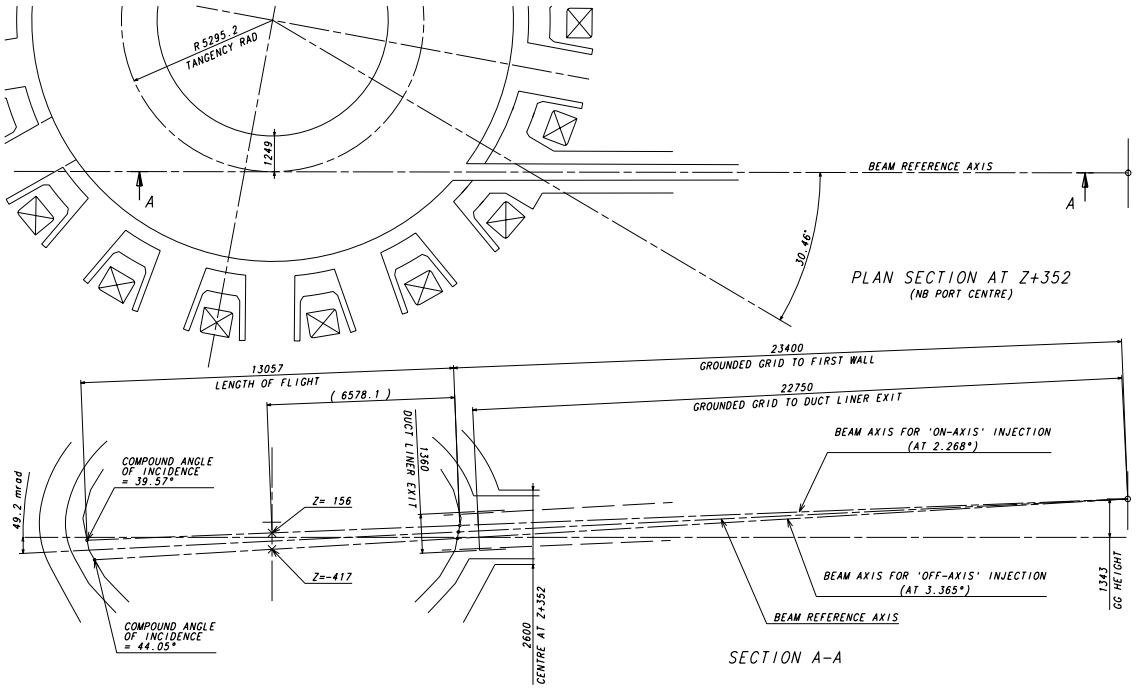

Figure 2.5.1-2 Tokamak and H & CD Neutral Beam Geometry

As the exact characteristics of the beam are unknown, the design has been done assuming a double Gaussian profile for the beamlets forming the beam with a core carrying 85% and with a halo carrying 15% of the beam. The divergence of the core is assumed to be in the range 3 – 7 mrad and the divergence of the halo is assumed to be 15 mrad. Existing R&D results support these assumptions. Moreover, maximum misalignments of 2 and 4 mrad have been added in the horizontal and vertical directions respectively. In considering the beam transmission and the power loading of the beamline components, the "worst case" combination of the assumed beam characteristics has been studied to ensure that the system meets the ITER requirements (see below).

The design of the channels of the neutraliser and of the RID is a compromise between gas flow and beam transmission requirements. In spite of the narrow channels, the NB injection power ~ 16.5 MW and efficiency of ~ 35 % could be achieved even with the 7 and 15 mrad divergence of the core and of the halo respectively, plus 2 mrad horizontal misalignment (worst case).

The magnetic field produced by the tokamak in the spaces where the beam is formed and transmitted is ~ 20 mT in the ion source and ~ 70 mT at the calorimeter exit. A combination of passive shielding (~ 0.15 m thick) and active coils (~ 200 kA turn per coil), reduces the field in the beam volume to an acceptable value which is between 0.1 – 0.2 mT. Moreover the line integrated field from the beam source to the exit of the neutraliser (total length ~ 4 m) should be $\leq 4 \times 10^{-4}$ Tm to improve beam transmission.

2.5.1.4 Component Design

Figure 2.5.1-4 shows the beam source and HV bushing. D^- ions are extracted from an arc discharge produced between tungsten filaments (cathode) and the source body (anode). Small quantities (< 1 g) of caesium are introduced into the discharge as this has been found to enhance the production of negative ions. The overall efficiency of the source is increased by a multi-cusp magnetic field created by permanent magnets on the source body. The plasma grid (PG) operates at high temperature, between 250 – 300°C, as this has been found to further enhance the negative ion production. A current is passed through the plasma grid (2 – 4 kA), which generates a magnetic field (PG filter) that reduces the loss of negative ions by collision with fast electrons, and the number of extracted electrons. The plasma and extraction grids form the extractor (height ~ 1,540 mm, width ~ 580 mm). Each grid is made up of 4 horizontal segments, divided into 4 groups. Each group has 5 x 16 apertures, so that the total number of apertures is 1,280.

N 53 GR 390 01-06-14 R 0.2

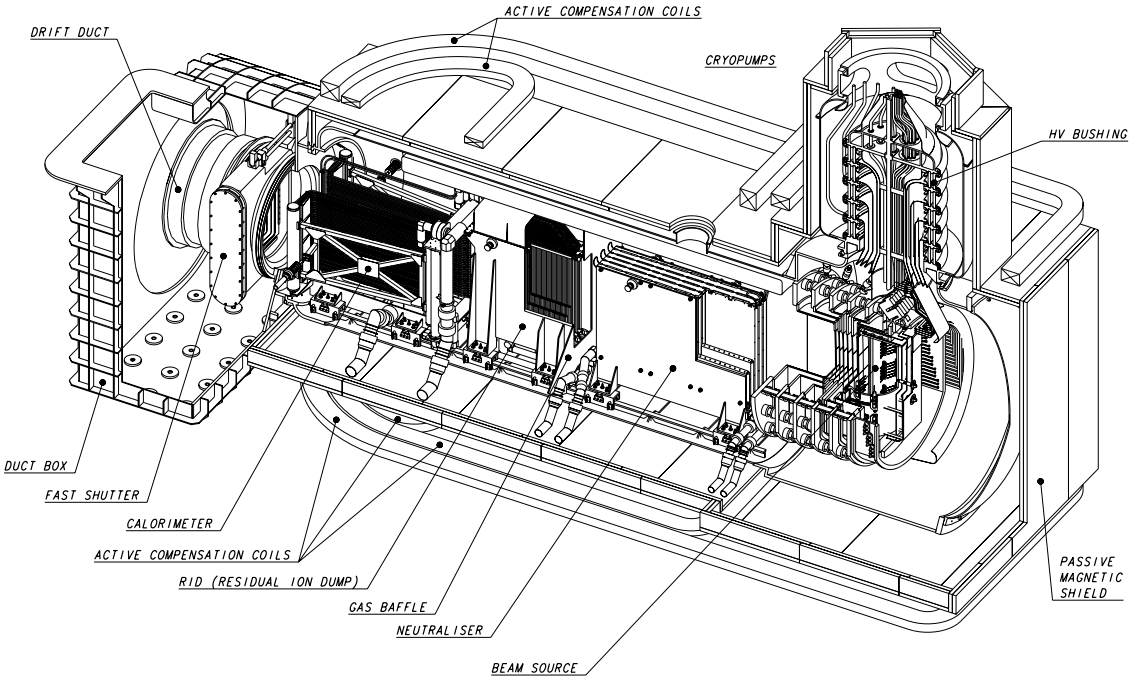

Figure 2.5.1-3 Neutral Beam Injector, Isometric View

R&D is in progress on two accelerators: the multi-aperture multi-grid concept (MAMuG) under development in Naka, and the single gap concept (SINGAP) under development in Cadarache. In the MAMuG concept, the accelerator consists of 5 stages, each stage consisting of 4 grid segments for beam aiming. Post insulators support the intermediate acceleration grids and the ion source. The design current of the negative ion beam, at the exit of the grounded grid, is 40 A. In the SINGAP concept, a pre-acceleration stage (~ 30 keV) follows the extractor, and this is followed by a single acceleration stage. The pre-acceleration grid is similar to those of the MAMuG accelerator with an identical aperture pattern. In the acceleration stage, beamlets from one group of apertures are merged and

accelerated through a single aperture in the final grid. MAMuG is the more conservative extrapolation from experience in positive ion accelerators and electrostatic particle accelerators, and has been considered the basis for the ITER design.

The beam source is in the primary vacuum. The reason for vacuum insulation is to remove the problem caused by the radiation induced conductivity (RIC) in the high pressure gas insulation present in the previous design. Vacuum insulation provides an additional advantage: lateral pumping, through the spaces between the post insulators, reduces the stripping loss of the ions in the accelerator to 25% (instead of 43%). Low stripping losses are the main reason to operate the ion source with low D_2 filling pressure ≤ 0.3 Pa.

The primary vacuum is sealed by a 1 MV, five stage bushing made up of two coaxial insulators: the inner, facing the vacuum, in ceramic (1.56 m outer diameter, OD), and the outer, facing SF_6 gas, in fibre-reinforced plastic (1.76 m outer diameter).

The space between the two insulators is filled with "guard gas" to avoid contamination of the primary vacuum with SF_6. The guard gas could be nitrogen or dry air. Electrostatic analysis of the HV bushing and of the beam source is in progress, and R&D in the JA home team is underway to refine the design criteria. The ceramic insulator with 1.56 m OD is technically challenging, but, in principle, within the present capability of industry.

The gas neutraliser provides ~ 60% neutralisation efficiency for the 1 MeV D^- ions. The beam, at the exit from the neutraliser, consists of neutrals and residual ions (D^- and D^+, each ~ 20%). In the worst case (7 mrad core divergence plus 2 mrad horizontal misalignment) the maximum power deposited on the walls of the neutraliser channels is 4.2 MW and on the neutraliser leading edges is 370 kW; there the maximum power density is 2.1 MW/m^2.

The residual ion dump (RID) uses an electric field to deflect the ions that are dumped on the five RID panels. The field is produced by applying zero potential to the odd panels (the two external and the central panels) and - 20 kV to the two even panels. In the worst case (7 mrad core divergence plus 2 mrad horizontal misalignment) the maximum power deposited on the RID panels is 19.6 MW**.** The maximum power density that could be encountered, 6.0 MW/m^2, occurs if the beam core divergence is 3 mrad.

A movable calorimeter intercepts the neutral beam during the commissioning and conditioning phases. A single V-shaped calorimeter is selected. The maximum power deposited in the panels of the calorimeter, 21.6 MW, and the maximum power density, 22 MW/m^2, arise if the beam core divergence is 3 mrad. The calorimeter panels consist of an array of swirl tube elements, parallel to the beam direction. A limited deflection of the swirl tube array (about 40 mm) can be allowed, and the secondary stresses can be limited to < 200 MPa.

The neutraliser, the RID and the calorimeter are water-cooled. Swirl tube elements made of CuCrZr-alloy are foreseen in the RID, the calorimeter and in the neutraliser leading edge. The overall design guarantees acceptable thermal fatigue of these components throughout the operation life.

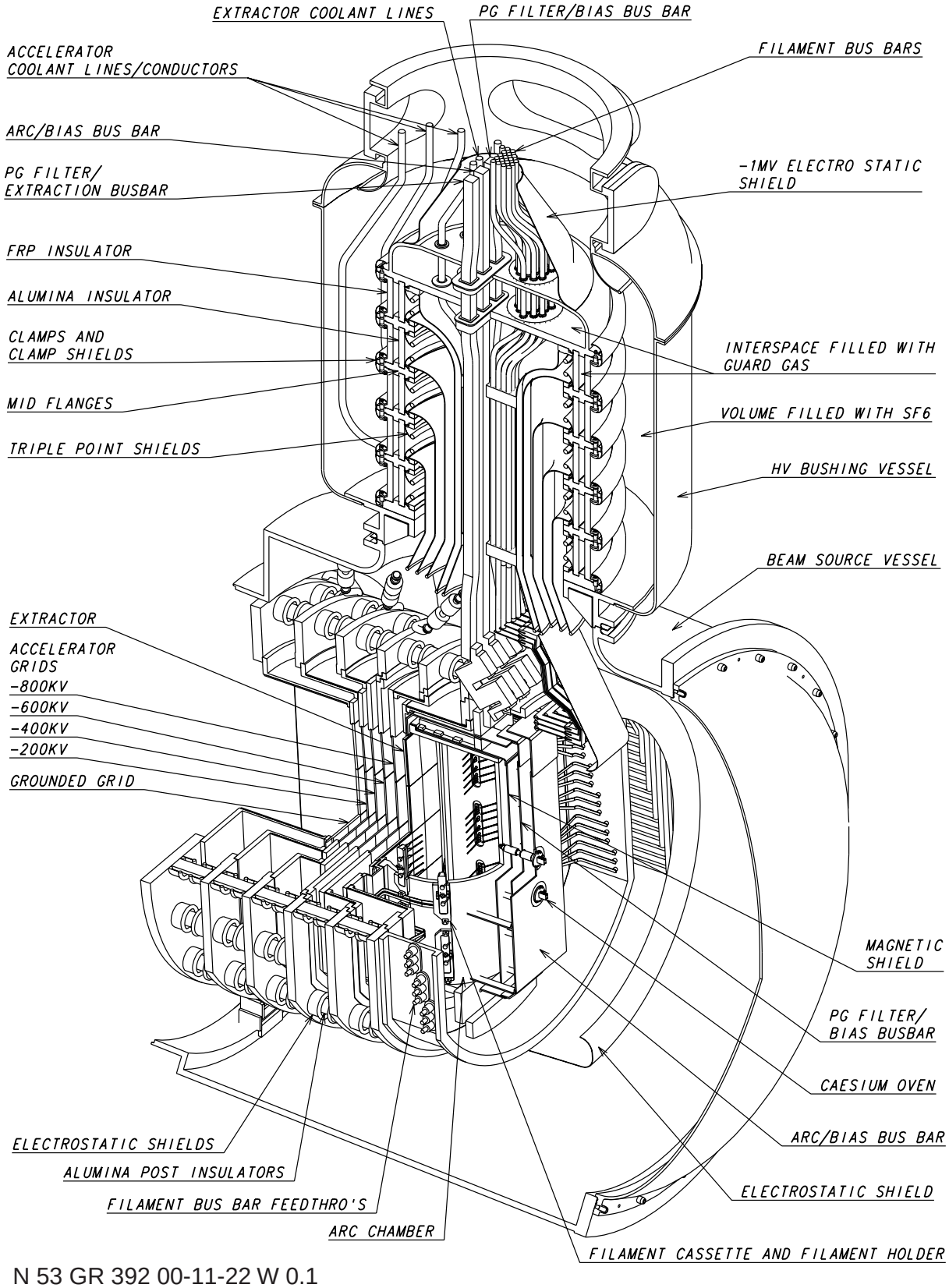

Figure 2.5.1-4 H&CD NB: HV Bushing and Beam Source

Large cryopumps maintain low pressure in the injector outside the ion source and the neutraliser. They are located close to the wall of the beam line vessel from the entrance of the neutraliser to the exit of the calorimeter. They cover all but the lower section of the beam line vessel where the support structure of the beam line components is located together with the coolant and the gas supply lines. The surface allocated to the cryopumps is about 47 m^2 and the assumed absorption probability for the cryopumps is 0.2. A gas baffle is mounted at the RID entrance to subdivide the injector volume and therefore to achieve differential pumping.

The injector is contained inside two large pressure vessels: the beam source vessel and the beam line vessel. Both are designed to guarantee the confinement of radioactive materials in case of an accidental overpressure: they are designed for a maximum internal pressure of 0.24 MPa (absolute pressure).

A "fast" shutter is located at the exit of the injector vacuum vessel to prevent tritium flowing from the torus to the injectors and to allow regeneration of the injector cryopumps without significantly increasing the torus pressure. This is essentially a lightweight "door" which can be moved across the beam path to seal against a frame built into the exit of the beam line vessel. A flexible metal seal on the frame ensures a low conductance between the injector and the torus of $\approx 10^{-4}$ m^3/s for D_2.

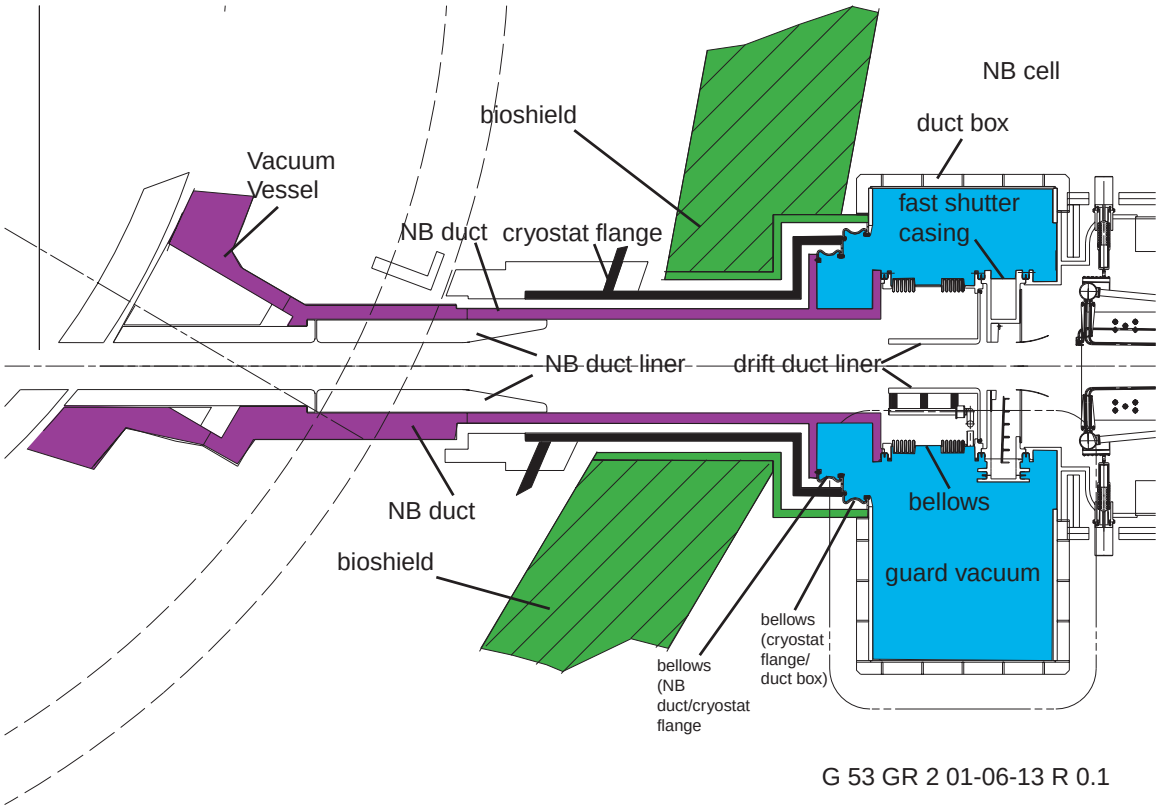

Figure 2.5.1-5 H&CD NB: Connections to the NB Duct and Cryostat Flange

The drift duct is the last component of the NB system and allows the flexible connection between the fast shutter casing (connected rigidly with the beam line vessel) and the NB duct (Figure 2.5.1-5), connected rigidly with the vacuum vessel. Two bellows with equalizing rings connected with an intermediate cylinder are foreseen between the two extremity

flanges. The drift duct liner faces the beam and protects the two bellows. The duct box encloses the fast shutter and the drift duct and provides a double barrier, with guard vacuum, between the NB cell and the primary vacuum. It provides also the nuclear shielding in this region.

The magnetic field reduction system consists of a passive magnetic shield and of active compensation and correction coils. The passive magnetic shield (PMS) encloses the beam line and the beam source vessels, the HV bushing, (and maybe the transmission line and the HV deck). Its purpose is to reduce the magnetic field in the space inside it, and the radiation (neutrons, gamma and X-rays) in the space outside it. The PMS is made of ferromagnetic steel with 150 mm thickness. It is a simple structure made of two construction steel plates each 75 mm thick, bolted together. Six active compensation coils (three above and three below the PMS) limit the flux in the space inside the PMS and reduce the field in the PMS below its saturation value. Finally, an active correction coil, located between the beam line vessel and the fast shutter, could limit, if required, the error field produced by the NB system on the plasma. All coils are made of copper and are water-cooled.

2.5.1.5 Diagnostic Neutral Beam

The main parameters (Table 2.5.1-2) of the diagnostic neutral beam (DNB) have been progressively identified, as a trade-off between diagnostic requirements and engineering feasibility. The beam is injected in a series of modulated "pulse trains" with the repetition time given in the table.

Table 2.5.1-2 Diagnostic Neutral Beam, Main Parameters

Parameter	Unit	Value
Accelerated ion		H^-
Beam energy	keV	100
Injected neutral (H^o) equivalent current	A	≥20
DNB pulse train duration	s	up to 3
DNB pulse train modulation frequency	Hz	5
Modulation wave form		Square (100 ms on/100 ms off)
Repetition time	s	20
Integrated number of pulse trains		1.0×10^6
Integrated number of modulations		1.5×10^7

The overall design concept of the DNB injector is identical to the one used for the H&CD injectors. This allows to utilise most of the R&D and design performed for the H&CD injectors and to standardise the components, maintenance equipment and procedures.

In the beam source, one single stage of acceleration is used. The design assumes 300 A/m^2 as the accelerated current density of H^- corresponding to a total accelerated current of 60 A. For the beam optics and misalignment, the same assumptions are made as for the H&CD injectors.

The requirements for the magnetic field reduction system are about a factor 4 more stringent than in the H&CD injectors, due to the lower beam energy. The line integral of the residual

magnetic field in the space between the accelerator grounded grid and the neutraliser exit (about 4 m) has to stay at the level of $1x10^{-4}$ Tm.

The mechanical design of the neutraliser is similar (4 vertical channels) to the one used for the H&CD injectors, apart for minor differences related to the beam aiming. The same neutralisation efficiency of about 60% can be achieved.

A RID is used for the deflection of the ions (H^- or H^+) exiting the neutraliser. The RID length is 1 m and the required deflecting voltage is limited to 4 kV. During "beam on" time the peak power density on the RID panel is about 0.75 MW/m^2 and total power to the RID is about 2.5 MW. Utilising, for the mechanical design of the RID, the same concept of the H&CD injector RID, the thermal fatigue limits are satisfied.

During "beam on" time the peak power density at the calorimeter position is 12 MW/m^2 (normal incidence) and total power is about 3.5 MW. The power is accommodated by a movable calorimeter with a heat receiving panel inclined 45° with respect to the beam line axis. Peak power density on the panel surface is about 8 MW/m^2 and, utilising the same calorimeter design concept as for the H&CD injectors, the thermal fatigue limits are satisfied.

The blanket segmentation, the DNB duct neutron shielding, and the clearance with the toroidal field coil structures, determine the vertical position of the DNB axis (Z = + 1,070 mm).

2.5.1.6 Maintenance

The NB system will become activated by neutrons streaming directly into each injector and the system will need to be remotely maintained. The whole (remote handling class 3) system does not need maintenance in the lifetime of ITER except for the following.

- The filaments of the ion source (class 1) have a finite life, estimated as > 200 h. They should be replaced twice a year (or less) through the rear formed head of the beam source vessel.
- The caesium oven (class 1) will need to be replaced; this operation is expected to take place every two years.
- Caesium will flow from the ion source to the accelerator and may eventually contaminate the insulator, which might require cleaning. Its frequency is expected to be less than once per year. If this cleaning cannot be carried out in situ, the removal of the source will be required (class 1). This complex procedure has already been studied and considered feasible (see 2.9).
- The fast shutter requires maintenance for seal wear (class 2).

2.5.1.7 Design Assessment

The design is based on the R&D targets which are summarised below and compared with the main results achieved so far.

Ion Source

200 A/m^2 of D^- have been extracted and accelerated (~ 27 keV) for short pulses (5 s) with the arc discharge lasting 150 s in a source with filling pressure of 0.30 Pa. However, the stripping loss in the 1 MeV accelerator will be significantly higher than in the low energy

accelerator used for the R&D. Hence the R&D needs to demonstrate ~ 250 A/m^2, to achieve the required current density at the grounded grid of the ITER accelerator. Moreover continuous pulses of 1,000 s should be produced repetitively and reliably. These are the targets for the R&D in progress. The demonstration of an acceptable source uniformity (± 10%) is also essential in an ITER source.

Accelerator

Experiments in the EU and JA home teams with high energy beams with ITER-relevant current densities have been stopped since December 1998; studies in the beam optics are still at relatively low energies (700 – 860 keV). The main reason has been failures in both test beds of the large cylindrical insulators made of epoxy. These failures were caused either by faulty manufacturing (EU) or outgassing from the fibre-reinforced epoxy to the vacuum (JA). Outgassing of epoxy is irrelevant in the ITER design of the HV bushing (described above), as this has ceramic facing the vacuum and compressed gas on both sides of the epoxy secondary insulator.

The JA HT succeeded in 1 MeV acceleration of H^- ions but at a very low (a few A/m^2) current density (hence with poor optics). The EU HT achieved D^- ion acceleration up to 630 keV at 53 A/m^2 and H^- ion acceleration up 860 keV at 36 A/m^2, with good optics in both cases. The main targets of the 1 MeV accelerator R&D are to demonstrate 1 MeV negative ion beams at the same perveance conditions of ~ 0.5 A, 280 A/m^2 H^-.(MAMuG) and of ~ 0.1 A, 200 A/m^2 D^- (SINGAP). Demonstration of the reliability of such beams (each with pulse length of ≥ 1 s) is one of the targets.

The R&D in progress on these key aspects has to continue with increased effort after the end of the EDA until the targets are achieved. The experimental results obtained in the last two years have been too limited to be appropriate to the challenges ahead.

2.5.2 Radio-Frequency Systems

2.5.2.1 General Design Features of the RF Heating and Current Drive Systems

The design of the radio frequency H&CD systems has been developed with the aim of providing for all systems:

- a credible high-level power performance associated with a high reliability;
- modular construction and identical interfaces wherever possible;
- interchangeable in-vessel assemblies;
- standardised control systems (with an unique man-machine interface) and operation.

2.5.2.2 Layout

The RF H&CD systems use different power generation and transmission components, but have similar general layout. The one of the ion cyclotron system, shown in Figure 2.5.2-1, is used as example, to identify the common components.

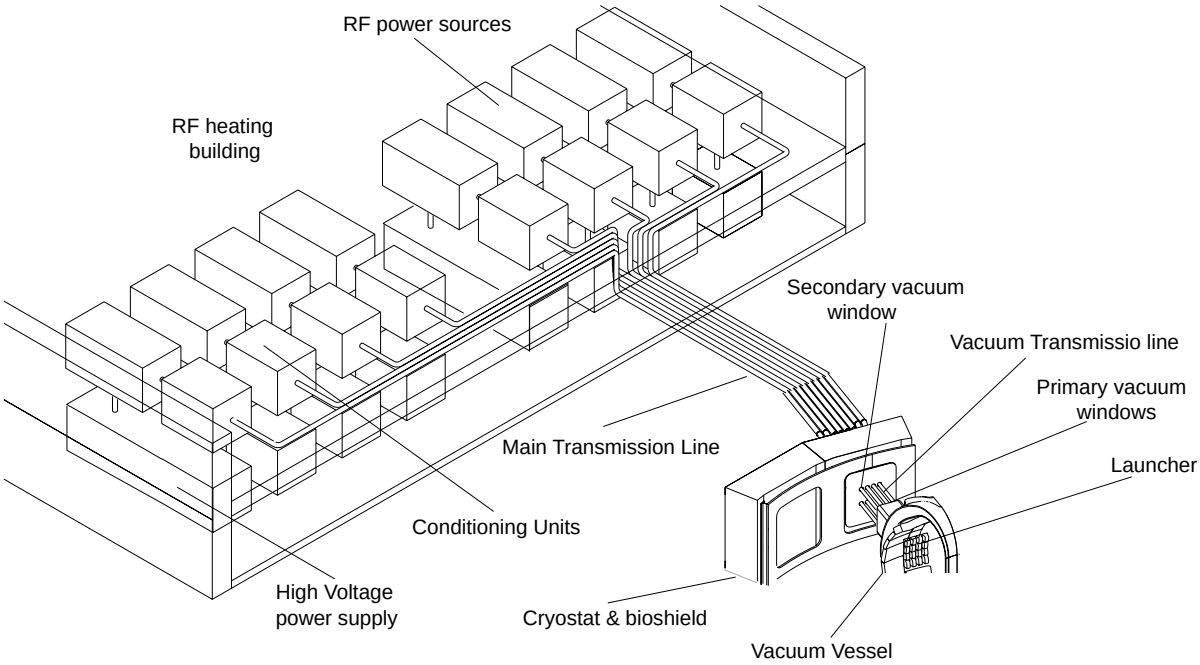

Figure 2.5.2-1 IC System Layout as Example of RF System Layout, Showing the Relative Locations of i) Launcher, ii) Primary and Secondary Vacuum Windows, iii) Vacuum and Main Transmission Lines and iv) Power Sources

The RF launchers are designed as interchangeable plugs inserted in the vessel equatorial ports, featuring:

- the same nominal installed power per port (20 MW/port), corresponding to an average power density of 9.2 MW/m^2 at the plasma boundary;
- the same neutron shielding /activation performance;
- the same confinement boundaries and interfaces with the VV port;
- the same remote maintenance requirements, interface and procedures.

Four equatorial ports can be used to provide a maximum RF power of ~80 MW; two are expected to be used for the initial experiments.

Smaller EC launchers (~ 7 MW/port), specialised for NTMs stabilisation, are integrated in four upper ports. The general layout of the upper launchers is similar to the one described, but with different geometry and dimensions.

The launcher assemblies of all RF systems are supported by the same mechanical structure sketched in Figure 2.5.2-2.

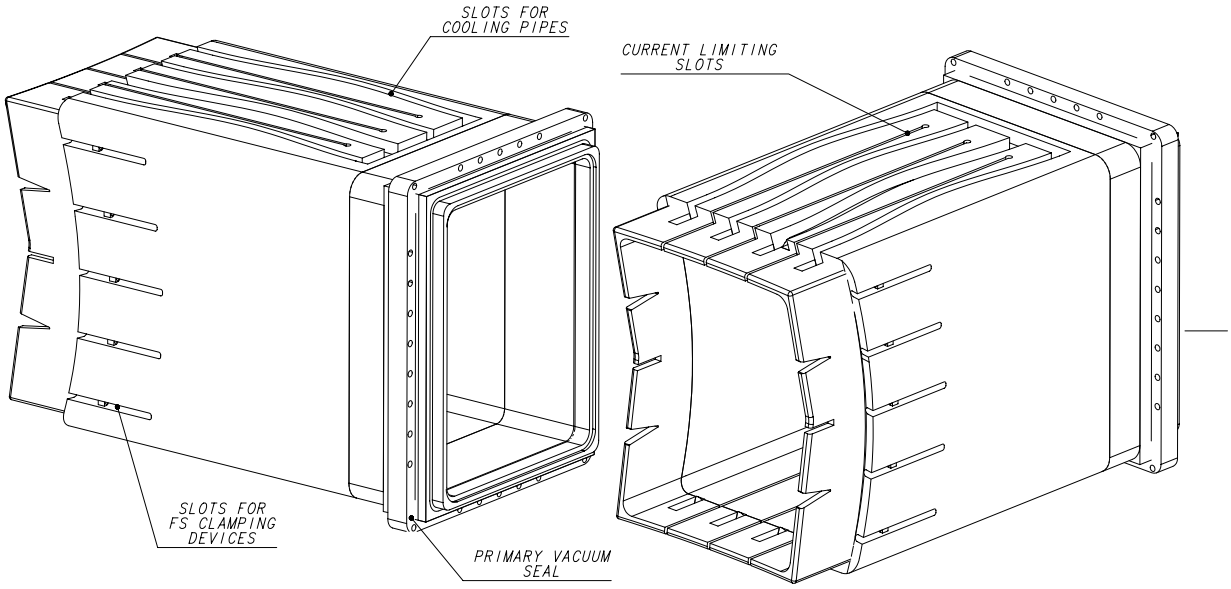

Figure 2.5.2-2 Front and Back of RF Assembly Support Structure, Including Port Flange and Closure Plate

The support structure of the launcher includes the vacuum vessel port closure plate, which transfers to the port the gravity load and the bending moments induced by plasma disruptions. The structure is also used to distribute coolant to the different RF components from blanket and VV cooling loops. The support structure is not in contact with other in-vessel components.

A gap of 20 mm is allowed from the port walls all around the plug perimeter and an overlap of 30 mm is provided by the adjacent blanket modules, to shield direct neutron streaming in the gap. A gap of 120 mm is allowed between plasma separatrix and the first wall in equilibrium conditions at the outboard equator.

The first wall of the RF launcher assemblies is designed to accept the same thermal loads from plasma radiation and neutrons as the adjacent shield blanket modules. However, they are not designed to be exposed to conduction heat loads from the plasma (e.g. during the start-up phase) from which they are protected either by the blanket or by shielding structures built in the blanket.

The RF launchers include a neutron shield, about 1 m thick, which reduces the high energy (E > 1 MeV) neutron flux outside the VV closure plate to 1.18×10^7 n/cm^{2}s, and limits the integrated activation level in the area to produce < 100 μSv/h, 15 days after shut-down. Hands-on maintenance of the components in the port inter-space would be therefore permitted. The neutron shield is penetrated by wave-guides and transmission lines of type specific to the different frequencies. Artificial bends (doglegs) are included in their path, to reduce the radial neutron streaming.

Plasma-facing components and neutron shield are cooled in parallel by pressurised water distributed by the blanket cooling loop. The coolant manifolds are located within the support structure. The closure plate and the components integrated in it (e.g. windows) are instead connected to the VV cooling loop.

The boundary of the primary vacuum confinement is located at the closure plate of the vacuum vessel, and the secondary boundary is at the cryostat closure plate. Water-cooled ceramic windows are used in each wave-guide or coaxial line. The dielectric window materials are different in different systems: BeO is used for IC and LH and polycrystalline diamond for EC.

Sections of evacuated waveguide/transmission line (VTL) join the vacuum vessel closure plate to the cryostat closure plate and penetrate the bioshield (vacuum transmission line). The vacuum transmission lines are manually disassembled, to allow remote-handling cask to dock to the VV port.

Monitoring and safety-related equipment is installed at the end of the VTL, in locations easily accessible for maintenance. Among others, DC breaks (to prevent ground loops being closed outside the pit) and rupture disks, exhausting in the volume served by the detritiation system, are installed.

Outside the bioshield, the VTLs are connected to the main transmission lines (MTLs). These run on the ceilings of the appropriate port cells and gallery, and are then routed to the RF heating area of the laydown, assembly and RF heating building. For continuous operation, VTLs and MTLs are water-cooled by loops of similar specifications, connected to the cooling water system (see 3.3). The MTL of IC and LH use a pressurised gas as waveguide dielectric, whereas the EC lines are evacuated.

The RF power sources (gyrotron oscillators for EC, gridded–tube amplifiers for IC, and klystron amplifiers for LH) are connected to the MTLs by RF conditioning and matching components. In the case of LH, the power of four klystrons is combined, to minimise the number of transmission lines.

The RF power sources are connected to their main DC supply, located at grade in the RH heating area of the laydown, assembly and RF heating building when a voltage fault is detected. Fast protection rapidly (10 μs) removes the DC supplies to prevent arc damage in the tubes. In view of the long pulse operation, the protection is designed for multiple response and power re-application, after a time suitable for the arc to clear.

2.5.2.3 Electro-mechanical Analysis

Owing to the similarity of the mechanical layouts, the electromechanical analyses of the three RF launchers have been performed using the same finite element model, by simply varying the electrical and mechanical properties of the material(s) according to the individual design. A harmonic analysis at 10 Hz frequency has been performed.

The spatial distribution of the disruption-induced currents in the assembly is computed first, from local poloidal and radial magnetic flux variations, inferred from global magnetic field analysis. The intensity of the eddy current is reduced, and their distribution modified, by the introducing radial cuts in both neutron shield and support structure. Different segments are either insulated or electrically connected by low value (typically 0.1-1 mΩ) carbon fibre composite resistors. The results of the analysis are:

- the 3D map of resistive and inductive currents;
- field distribution in assembly metal and voids;

- loads applied to the port closure plate;
- stresses applied to the different assembly components.

In Figure 2.5.2-3a) a stress/strain map computed for the whole IC launcher is shown.
In Figure 2.5.2-3b) a stress analysis output of a section of the EC support structure is shown.

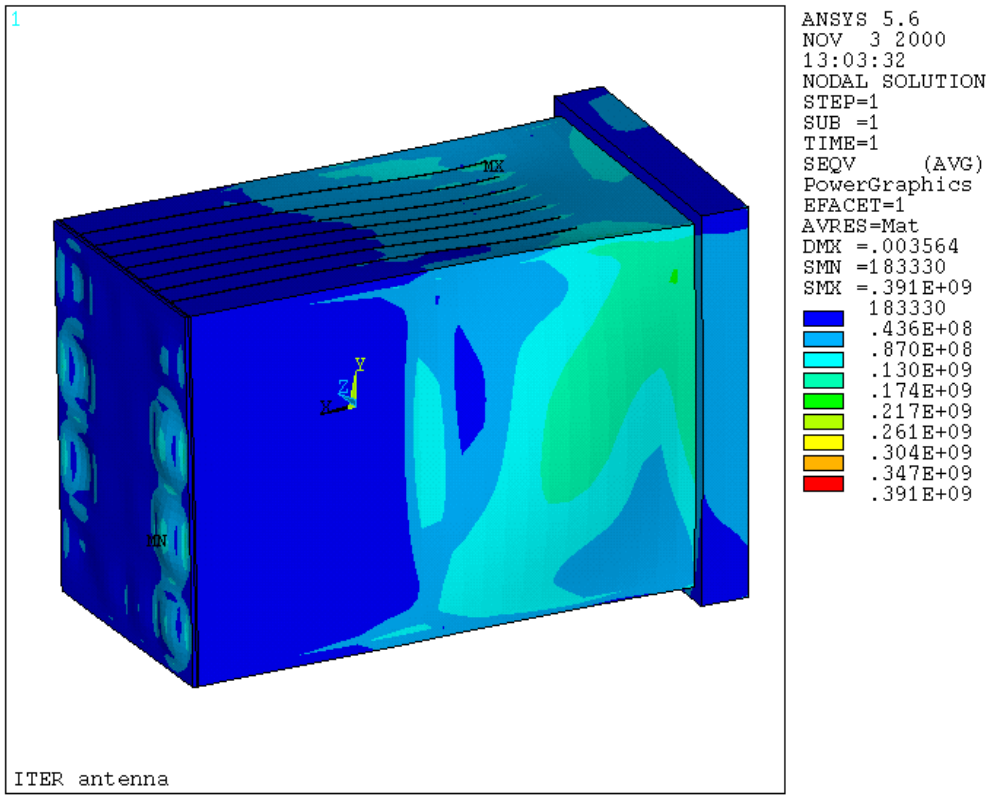

Figure 2.5.2-3(a)
Example of IC Launcher von Mises Stress and Strain Map

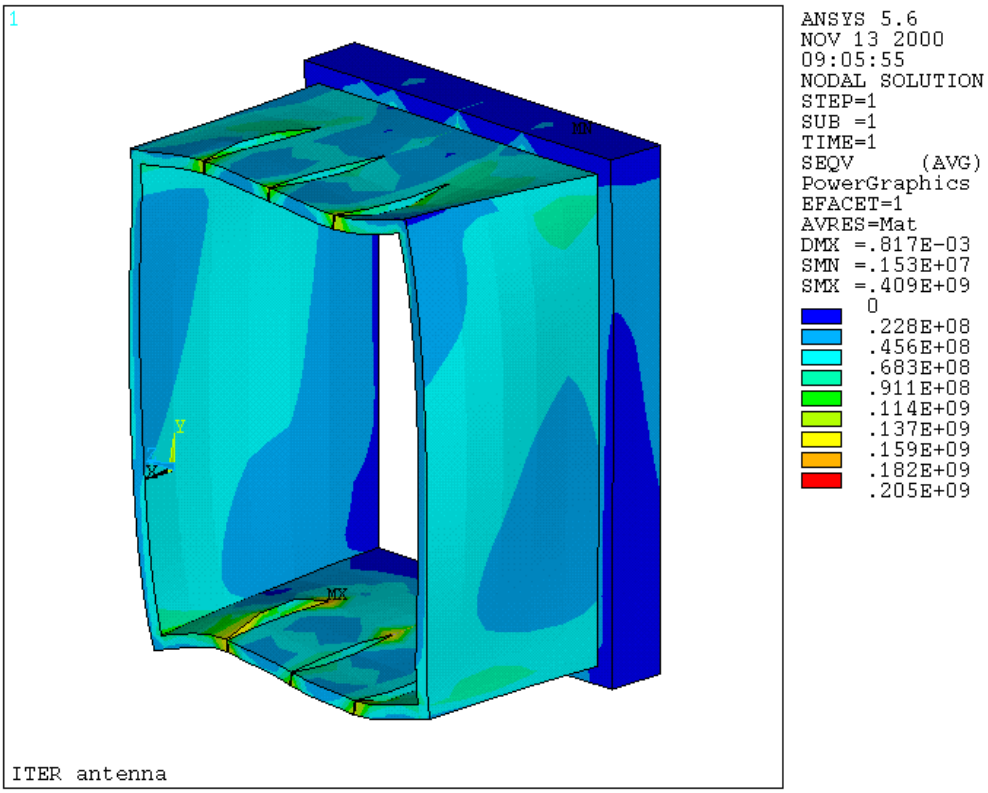

Figure 2.5.2-3(b)
Von Mises Stress and Strain Map in a Section of the EC Support Structure

A summary of the stress analysis is reported in Table 2.5.2-1. These comply with the limits set by the structural requirements for the equatorial ports.

Table 2.5.2-1
Typical Forces and Moments Applied by RF Launcher to the VV Port

Parameter		**EC**	**IC**	**LH**
Radial force	(MN)	-0.93	-0.149	-0.169
Poloidal force	(MN)	-0.165	-0.194	-0.195
Toroidal force	(MN)	0.010	0	0
Radial moment	(MNm)	7.09	5.89	11.99
Poloidal moment	(MNm)	-2.22	-1.53	-2.62
Toroidal moment	(MNm)	0.18	-0.92	-0.14
Max current (kA)		1.070 in Farad. Shield	0.409 in Closure Plate	0. 839 Launcher Front
Max deformation (mm)		0.3	0.4	0.8
Max von Mises stress in SS (MPa)		90	80	120

2.5.2.4 Commissioning and Operation

The in-vessel components of the RF systems are delivered from the manufacturer fully assembled, conditioned for high vacuum and leak-tested at room temperature. Their integration in the port requires installation and vacuum sealing of the closure plate.

For initial commissioning and acceptance tests, and for commissioning tests after refurbishment in the hot cell, the RF systems share the use of a test stand (TS). The TS is a vacuum vessel having dimensions and shape similar to the ITER VV port and can accommodate any of the RF launcher assemblies. It is provided with a flange mating with the port closure plate, and encloses test loads. The test stand is installed in the hot cell, to allow testing on activated equipment.

The RF H&CD systems require a large number of RF and low frequency monitoring channels, control functions and protection circuits. However, monitoring and control functions of the three RF systems are very similar. They can be implemented by a single set of standardised procedures for data handling, control, alarm handling and machine-man interface.

The operation is co-ordinated by a plant control system, responsible for all real time control/monitoring transactions, which reports in real time to the ITER CODAC system.

Three basic states of operation are possible.

- In the normal state of operation, the RF output power is equal to the pre-set power and all other system parameters are within their operational windows.
- The control system switches to power limit operation if one or more system parameters indicate abnormal operating conditions. The RF output power of that system is automatically reduced to the highest level compatible with the current parameter state and is automatically restored when the limiting parameter recovers the normal value. The RF power of the other systems is increased, to compensate the missing power.
- The RF output power of one of the system is temporarily suppressed during a power trip, to allow abnormal load conditions (such as an arc) to clear. The RF power (and in some cases the DC high voltage) is rapidly removed (~ 10 μs), to prevent a large energy being dissipated in the fault, and reapplied through an "intelligent" routine, to avoid re-strikes. The RF power of the other systems is increased, to compensate the missing power.

2.5.2.5 Maintenance

The RF in-vessel assemblies are designed to make maintenance simple in situ and in the hot cell. The use of a single support structure automatically makes all interfaces with the vessel identical, and standardises remote handling equipment and procedures.

The launcher assemblies are designed to allow a RH cask to dock to the VV port, after the manual disconnection of vacuum transmission lines, water cooling pipes and pumping ducts. They are installed in, and removed from the VV port, using standard RH procedures, and transferred by cask to the hot cell.

Hot cell maintenance is meant for:

i refurbishment of damages to plasma-facing sections (such as EC shield, IC Faraday shield, LH outer multi-junction stack. To this purpose, all plasma-facing components are separable from the assembly;

ii preventive maintenance or replacement of defective components. The most critical components (such as mirrors, tuners, actuators and windows) are located either on the front sections or installed on the closure plate using standard flanges. Maintenance is

performed by complete substitution, needing disassembling and re-welding of the substitute.

The RF launcher assemblies are themselves modular in construction, and can be disassembled into mechanical subsets having weight lower than 10 t. The elements composing an IC launcher are shown in Figure 2.5.4-4.

The waveguide/transmission lines located within the secondary vacuum boundary and those running at atmospheric pressure are commercial components of different types (coax transmission (IC), rectangular wave-guide (LH) and circular, corrugated wave-guide (EC). Transmission lines and power sources are commercial items. Maintenance of these is performed according to the manufacturer's user manuals.

2.5.2.6 Design Assessment

The design of the RF systems outlined below underlines engineering solutions that meet ITER physics requirements and are consistent with the current technologies.

The design effort has mainly focussed on assessing the capability of the in-vessel components of surviving and safely operating in the reactor environment. Operational issues, (such as the way of efficiently fulfilling the requirements of an integrated real-time control, protection and data management system, in quasi-continuous operation), have been generically addressed, as they are likely to benefit from future technology advances.

The level of design development is similar for the three systems. The launcher design is still at a conceptual level in some case (e.g. the remote steering design for EC, and the PAM stack for LH still need demonstration). However, for most components, and in particular for those directly facing the plasma, no showstoppers have been identified and there is sufficient information to start manufacturing drawings.

Manufacturing processes were only generically addressed for costing purposes. The technology developed for the first wall and blanket are however generally applicable to the RF plasma-facing components.

Specific R&D programs did not investigate the launcher design specifications. A limited development of mock-ups and high power tests in vacuum was carried out for the IC system launcher (and is still ongoing), and has confirmed the design parameters [1].

The status of development of the power sources is different for the three systems. The 170 GHz, CW, 1 MW, 50% efficiency gyrotron development programme for the EC system is still far from meeting ITER specification. The best results achieved at this frequency are: 8 s pulse length, 0.45 MW and 33% efficiency. For IC, an industrial study has shown that a source fulfilling ITER specification (2 MW-CW-40/60MHz at a VSWR < 2.5) could be constructed using existing tetrodes, although an upgrade of a current tube would lead to a more cost effective source. There are no detailed studies of a 1MW-CW-5 GHz klystrons.

Finally, it should be always kept in mind that the operation of both IC and LH launchers is plasma dependent. Plasma edge parameters and separatrix distance need to be controlled at

[1] ITER/US/98/IV-RF-01(T361 US) Final report

the antenna(s), for an efficient power transfer and to reduce to the very minimum RF losses in the plasma edge, which could otherwise cause wall loading and release of impurities unacceptable for long pulse operation.

It has not proved possible to test RF launcher features on plasma or in otherwise ITER-relevant operating conditions.

The R&D on these key aspects, have to be addressed after the end of EDA until all design parameters are demonstrated. These key aspects are all important and difficult targets, which need an efficient organisation and will to be achieved.

2.5.3 Electron Cyclotron System

2.5.3.1 General Design Features

The EC system uses two types of RF launchers, both operating at a frequency of 170 GHz. One type, located in an equatorial port, has toroidal beam steering capabilities (± 12.5°). The launcher is used for heating and current drive, with a typical on-axis CD efficiency is $\gamma_{20} = 0.2 \times 10^{-20}$ A/Wm^{-3} and to assist start-up at a lower frequency (120 GHz). The other type is located in an upper port, and has poloidal RF beam steering capability (± 5°). This system is mainly used for neo-classical tearing mode (NTM) stabilisation, with the beam, and focussed at resonant flux surfaces (q = 2, 3/2) in a position vertically off-set from the magnetic axis. This allows the use of a single frequency (170 GHz) for H&CD and NTM stabilisation and avoids higher harmonic power absorption during far off-axis CD when the main H&CD is applied. As an example of its use, the density of the driven current is plotted in Figure 2.5.3-1 for an equatorial launcher of 20 MW.

The nominal injection power is 20 MW at 170 GHz and 2 MW at 120 GHz. The RF power at 170 GHz is switched between the upper launcher and the equatorial launcher by changing of waveguide connections as shown in Figure 2.5.3-2. The RF power used for the assisted start-up is transmitted by three waveguides also used for the main H&CD. The power sources at 120 and 170 GHz are switched during a plasma discharge.

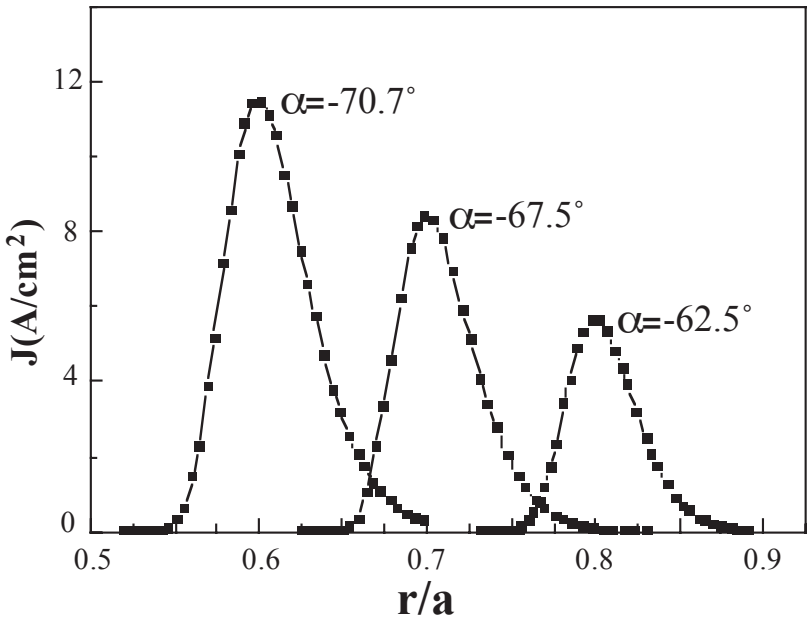

Figure 2.5.3-1 Profiles of Driven Current vs. the Normalised Minor Radius
Injected RF power is 20 MW and α is the angle between the beam and the horizontal plane, at an angle of 24˚ between the beam and the poloidal cross-section)

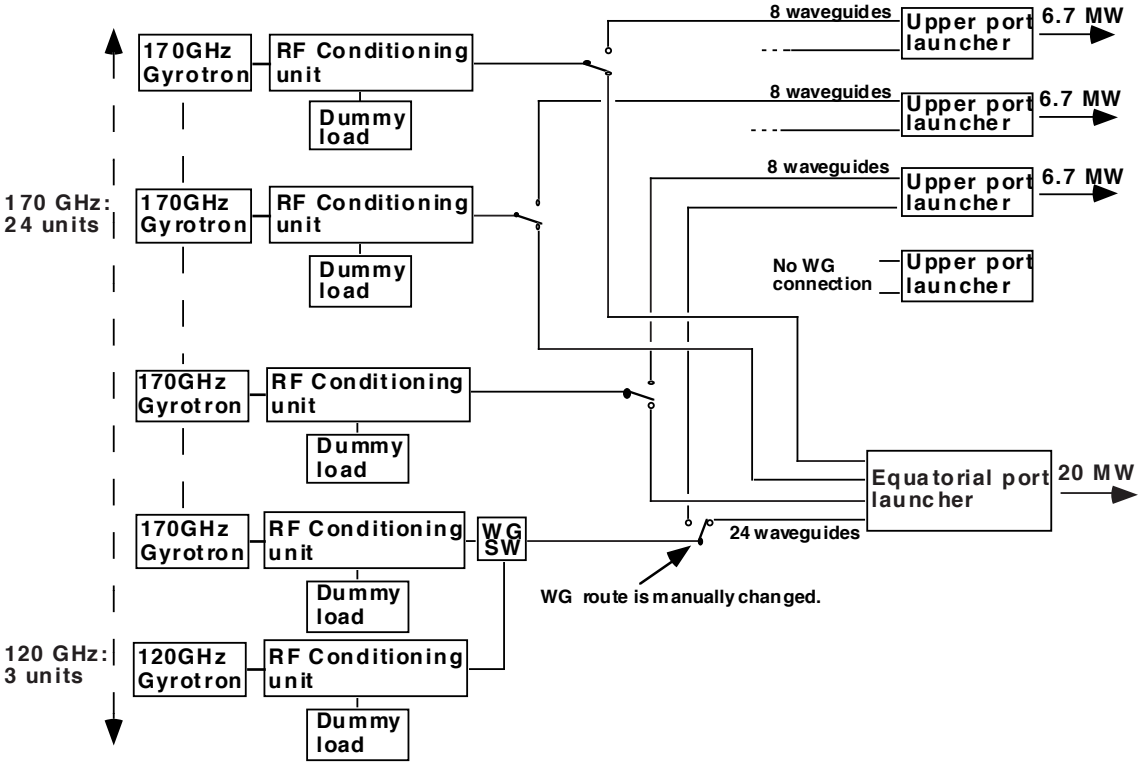

Figure 2.5.3-2 Combination of Launchers and Gyrotrons

2.5.3.2 Launcher(s) Design

There are three upper launchers and one equatorial launcher.

The equatorial launcher (Figure 2.5.3-3a) consists of i) a plasma facing neutron and radiation shield, ii) 3 sets of steerable mirrors, collecting 8 RF beams each, iii) 24 circular corrugated wave-guides, iv) mitre and v) diamond window.

The front shield has 3 horizontal slots and is segmented into modules. The steerable mirrors are made of dispersion strengthened Cu and supported by a pivot mounted on bearings. The mirrors are water-cooled to accommodate RF power losses (about 50 kW/mirror for a Be deposit of several μm thickness on the mirror surface), plasma radiation and nuclear heat.

A stainless steel spiral pipe having a mean diameter of 15 cm, a pipe inner diameter of 8 mm and a pipe thickness of 1 mm is used to supply the coolant to the steerable mirror. A shaft, operated by a pneumatic actuator, drives the pivot, and rotates the mirror without the need of links and cams. Plasma disruption currents induced in the spiral pipes and in the mirror, can be reduced to an acceptable level by electrically insulating the bearings.

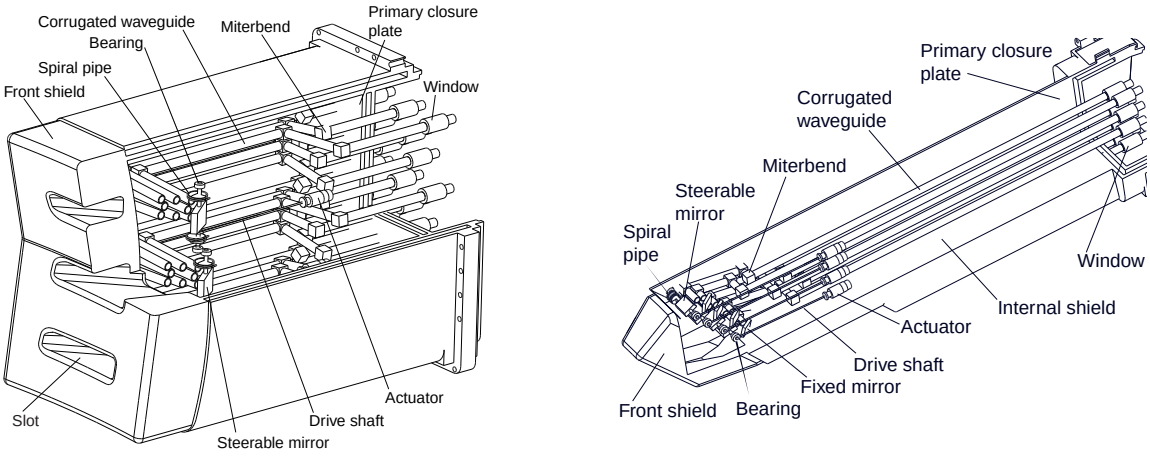

,

Figure 2.5.3-3 a) Equatorial Launcher
b) Upper Launcher (Front-steering Type, see Text Below)

The in-vessel waveguides must include a dog leg in order to avoid excessive radial neutron streaming and satisfy the maintenance dose rate requirement at the primary closure plate. Electrically insulated mitre-bends are used in these sections. These components need water cooling.

A diamond disc obtained by chemical vapour deposition (CVD)[1)] is used in each line as a primary vacuum window. Owing to the crystalline diamond low dielectric losses ($\tan\delta = 2x10^{-5}$) and high thermal conductivity (~ 2,000 W/mK), simple edge water cooling of the window is possible. Disks of different thickness are used: 1.482 mm for the transmission of the 170 GHz wave and 2.592 mm for the transmission of both 170 GHz and 121.4 GHz, as shown in Figure 2.5.3-4.

[1] M Thumm rt al., "Status report on CVD-diamond window development, for high power ECRH" to appear in Fusion Eng. Des.

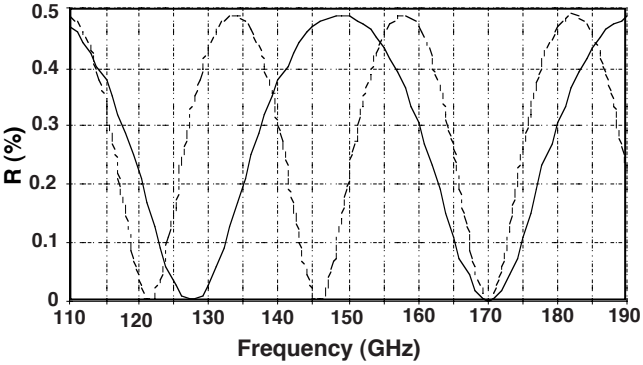

Figure 2.5.3-4
Power Reflectivity of Diamond Disk
(solid line: reflectivity of a 1.482 mm disk;
dotted line: reflectivity of a 2.592 mm disk)

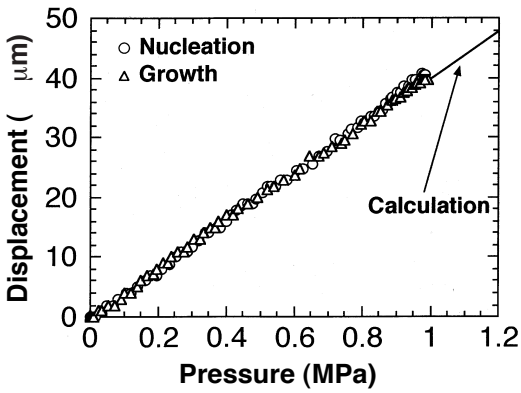

Figure 2.5.3-5
Pressure Test of a CVD Diamond

The disk can withstand pressures up to 1 MPa , as demonstrated by pressure tests on a 70 mm disk, 2.25 mm thick (Figure 2.5.3-5)[1]. This significantly exceeds the required 0.2 Mpa value resulting from a coolant leak in the vacuum vessel.

In the upper launcher[2] (Figure 2.5.3-3b) there are four steerable mirrors. A beam-mirror concept similar to that of the equatorial launcher is used, but now with eight beams, reflected in pairs by four mirrors through a vertical slot at the front shield. An additional fixed mirror is needed to reflect the beam through the slot, with an overall RF power loss of ~ 13 kW. An accurate focussing of the RF power on the m = 2 and m = 3/2 plasma flux rational surfaces is obtained

A complementary concept of remotely steerable launcher (Figure 2.5.3-6), allowing all movable components to be located outside the primary vacuum, has also been developed. Corrugated square cross-section waveguides and a fixed exit mirror are used. The steerable mirror is located outside the primary vacuum, at the input of the waveguide. In a remotely-steered system, the square cross-section dimensions and the total waveguide length, L, must satisfy the relation $L = 4a^2/\lambda$, where λ is a wavelength and a is an internal width of the square waveguide. Here, the length of the waveguides is 6.5 m and a is ~ 50 mm. Fixed mirrors at the waveguide exit are used to reflect the RF beam –60° ~ -70° downward.

For steering angles < 10° the beam optics are not degraded, as shown in Figure 2.5.3-7. It is also found that power transmission efficiency is not too sensitive to corrugation depth and wave guide alignment and steering can be obtained by a single axis rotation, if the steering angle is limited to ~ ± 5°. This allows the use of the same design for front and remote mirror assemblies. Both options are still under investigation.

[1] K.Takahashi et al., "Development and design of an ECRF launching system or ITER" to appear in Fusion Eng. Des.
[2] G. Bosia et al., "Design of ITER-FEAT RF H&CD System", Proc 21th IAEA Fus. Energy Conf., Paper ITERP14 (2000)

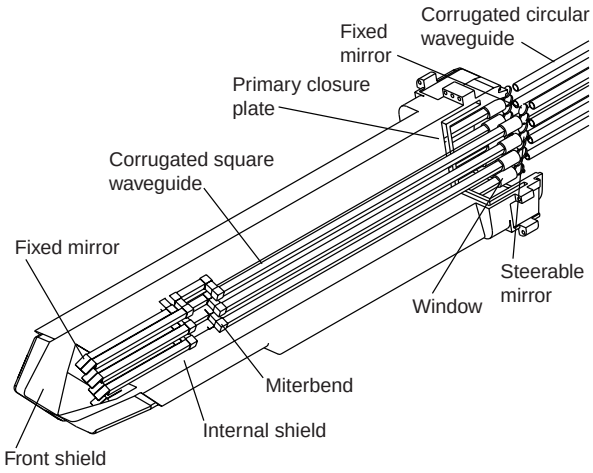

Figure 2.5.3-6
Upper Launcher (Remote Steering Type)

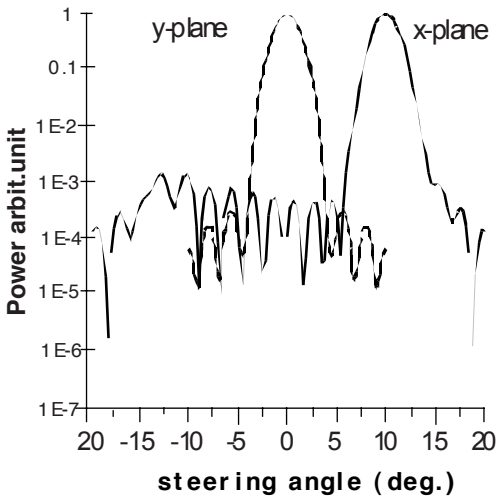

Figure 2.5.3-7
Steered RF Beam Profile

2.5.3.3 Power Transmission Design

Transmission lines used by the EC system are commercial items and consist of:

i) an RF conditioning unit;
ii) straight sections of circular cross section corrugated wave guide;
ii) a number of mitre-bends;
iv) auxiliary equipment such as DC breaks, expansion segments, vacuum pumping sections, damping segments, isolation valves, sections including rupture discs and services (pumping, vacuum monitoring, water cooling, etc).

To reliably transmit the RF power, all sections of the transmission line are evacuated to 10^{-3} Pa and water cooled. Pumping is provided at the RF conditioning unit. This converts the mm-wave power beam at the exit of the gyrotron to the waveguide HE_{11} mode, for long distance transmission. It consists of matching optics and a pair of polarizers.

The routing of the waveguides from the RF power sources to the tokamak is similar to the one shown in Figure 2.5.2-1. Transmission lines are grouped in the central area of the laydown, assembly and RF heating building and then directed to the tokamak. As the same RF sources are used to alternatively power the equatorial launcher and the three upper launchers, switching is provided at the exit of the RF heating area. The waveguides routed to the upper ports run along the tokamak hall south wall and penetrate the wall at different points. The total line length ranges from 70 m to 100 m depending on the gyrotron position. The overall power transmission efficiency, from gyrotron to injection point for both types of launchers, is about 80 %.

One torus window provides the primary vacuum confinement. An isolation valve (closing within 1 s) combined with a rupture disk, and exhausting in a volume connected to the detritiation system (VDS), provides the secondary confinement. When a high pressure accident happens in the vacuum vessel, the isolation valve closes. If the isolation valve shut-off fails, the rupture disc breaks and contaminated steam is conveyed by parallel ducts into the Vent Detritiation System.

2.5.3.4 Power Source

High power mm waves are generated by a gyrotron drift-tube oscillator delivering an RF power of 1 MW in steady state. An efficiency of ~ 50 % is possible using a depressed-collector geometry. As the expected rf transmission losses are ~ 20 %, twenty four tubes and three 120 GHz gyrotrons are needed to inject 20 MW and 2 MW, respectively. An output window similar to the one described above is located at the gyrotron output.

Each power source (gyrotron unit) includes i) a tube and socket, ii) an oil tank, isolating the tube voltage supplies, iii) beam deflecting magnets (both normal and superconducting, and iv) electrical supplies for tube and magnets. The superconducting magnet (SCM) generates the magnetic field of 6.6 T at the cavity centre.

The gyrotron tube and associated power circuitry are protected by fast protection circuits, automatically (< 10 μs) removing the DC body and cathode voltage in case of tube, line or load breakdown. After suitable vacuum conditions are recovered after the arc, the DC high voltages can be automatically re-applied. A regulated and variable DC high voltage power supply is required for the body and for the cathode of gyrotrons.

The gyrotron units located at the mezzanine level of the RF heating area in the laydown, assembly and RF heating building are arrayed in 7 groups (pods). A pod contains 4 tubes for the170 GHz frequency and 3 tubes for 120 GHz. Each pod has common auxiliary supplies such as cooling water. Power supplies, series switches, and other auxiliary support equipment are located immediately below the gyrotrons on the lower level of the RF heating area. Each pod has separate control unit, interfacing to the power supply and capable of an independent operation.

2.5.4 Ion Cyclotron H&CD System

2.5.4.1 General Design Features

The main heating scheme of the IC system (Table 2.5.4-1) is at the tritium second harmonic, in a 50-50% DT mixture at f = 53 MHz and B_T = 5.3 T with typical 50-50% power partition among the bulk ions and electrons. Addition of ^{3}He (< 3%) minority [DT-(^{3}He)] results in a significant increase of the fraction (up to 70%)[1] deposited on bulk ions. The alternative deuterium minority heating scheme is less efficient because it is in strong competition with absorption by Be and α-particles.

The frequency window for on-axis current drive is at the peak of the electron absorption (f = 56 MHz, with a central current drive efficiency of ~ 20 kA/MW). Ion minority current can be driven at the outboard q = 1 for the control of the sawtooth period, at a frequency of 40 MHz.

The operating range Δf = 40 – 55 MHz encompasses all the IC physics scenarios and allows operation at a 70% reduced toroidal field. An extension of the range (35 to 60 MHz), could be desirable for improved flexibility, and would be possible at somewhat reduced performance.

[1] P. Bergeaud et al., Nuclear Fusion 40 (2000) 35

Table 2.5.4-1 Ion Cyclotron Resonances

Resonance	MHz	Comments
$2\Omega_T=\Omega_{^3He}$	53	Second harmonic + minority heating
Ω_D	40	Minority heating. Strong competition of Be and α-particles
FWCD	56	On axis current drive
Ω_{3He}	45	Minority ion current drive at sawtooth inversion radius (outboard)

The IC system is designed to operate, at the nominal power density:

- at a moderate electric field at the plasma interface and in-vacuum ($E_{max} < 2$ kV/mm);
- at a power transfer efficiency essentially constant over the frequency range;
- with a high tolerance to load variations not to require dynamic matching control in ELMy plasmas.

The system performance is computed as a function of plasma loading $R'= (2P/I^2)^{1/2}(\Omega/m)$, where I is the maximum strap current and P is the radiated power per unit length, by modelling the array/tuning system as a network of lossy and coupled transmission lines. The nominal R' value used in the computations (perfect match at 4 Ω/m) is typical for ITER operation at 53 MHz, π phasing, at a gap of 120 mm from the separatrix. The main results are summarised in Table 2.5.4-2.

Table 2.5.4-2 Summary of Array Parameters (at R' = 4 Ω/m and f = 55 MHz)

Parameter	Value	Parameter	Value
Strap length (m)	0.3	MTL Voltage (kV)	12.25
Characteristic impedance (Ω)	~ 35.0	Max voltage in tuner (kV)	32.1 & 40.0
Feeder length(m)	0.3	Max voltage in choke(kV)	5.4
Matched reactances (1&2) (Ω)	-38.3 & -49.7	Max E-field in tuner (V/mm)	1.99 & 2.45
RDL Input impedance (Ω)	6	Max E-field in choke (V/mm)	0.28
Input power (MW)	2.5	Max E-field in strap (V/mm)	1.3
Tuners @ choke char. imp.(Ω)	10	Max E-field in VTL (V/mm)	0.53
Input voltage (kV)	5.5	Power transfer efficiency (%)	~95
Max. strap voltage (kV)	27	Variation of PE with freq. (%)	~5
Max. strap current (kA)	1.30		

All requirements are met. In particular, the voltage standing wave ratio at the input of the resonant double loop (RDL) remains below 1.5 (Figure 2.5.4-1) for any loading $R' > 2.5$ Ω/m. This implies that load variations such as those caused by ELMs can be accepted without the need of real-time re-tuning.

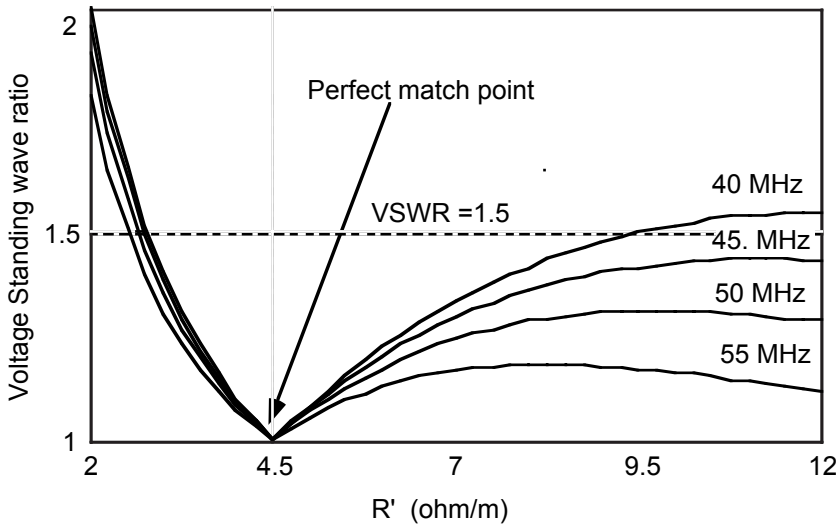

Figure 2.5.4-1 Input VSWR as Function of R' and Frequency

2.5.4.2 Launcher Design

The IC launcher is an array of 4x2 elements fed by eight coaxial transmission lines each carrying a nominal RF power of 2.5 MW (Figure 2.5.4-2).

The electric scheme of the IC antenna is a variation of the resonant double loop (RDL) concept. The RDL consists of a pair of straps with capacitive tuners in series, located at the input (Figure 2.5.4-3a). The straps are short, with one end connected to ground (Figure 2.5.4-3b). This arrangement makes them self supporting and able to operate at low voltage

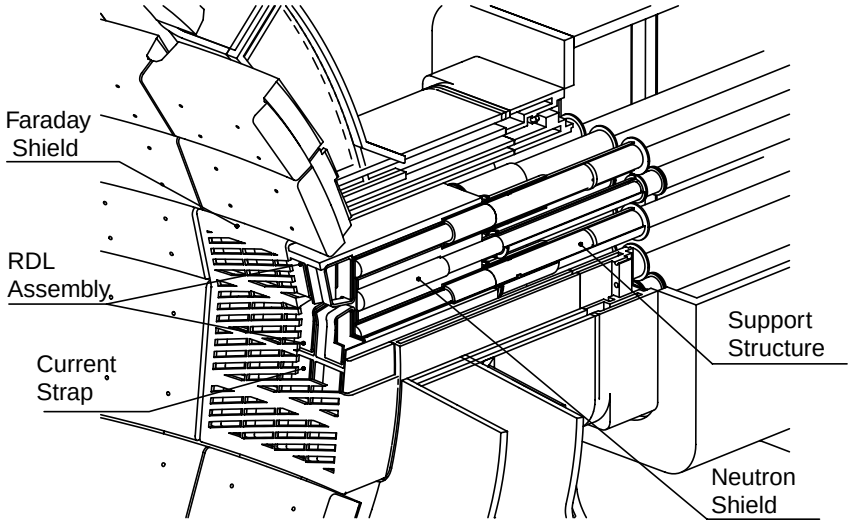

Figure 2.5.4-2 View of the IC Array Seen From the Plasma

The tuners are sections of coaxial transmission lines, the electrical length of which is varied by sliding a short circuit to the opposite end. The adjustable lines and their actuators are located in tubular assemblies (Figure 2.5.4-3b), individually removable for maintenance.

The tuners are inserted in cylindrical cavities of the neutron shield, forming outer coaxial structures (chokes) whose electrical length is set at $\lambda/4$ by sliding short circuits similar to

those of the tuners. The chokes decouple the inputs of the tuners and have all the same length. They are also housed in the removable sections of the tuners.

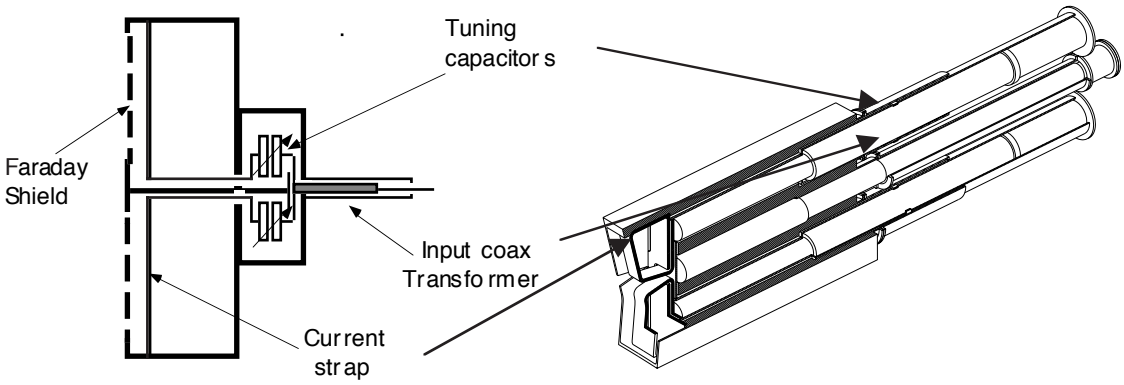

Figure 2.5.4-3 a) Electrical Scheme of RDL Antenna; b) Mechanical Layout

The two-strap/tuner assemblies are connected in parallel to the vacuum transmission line and matched at a low input resistance (6 Ω). It can be shown that this scheme features a large tolerance to load variations. A wide-band impedance transformer, located in the coaxial feeder, transforms the input impedance to the VTL characteristic impedance (30 Ω).

The IC array features a modular construction. A box-like, Be-plated, Faraday shield in Cu-Cr-Zr alloy, is the plasma-facing component, with elements tilted 16º, to be approximately aligned with the local magnetic field. Eight RDL structures, with coaxial tuners inserted in the neutron shield are fed by eight coaxial feeders, (Figure 2.5.4-4).

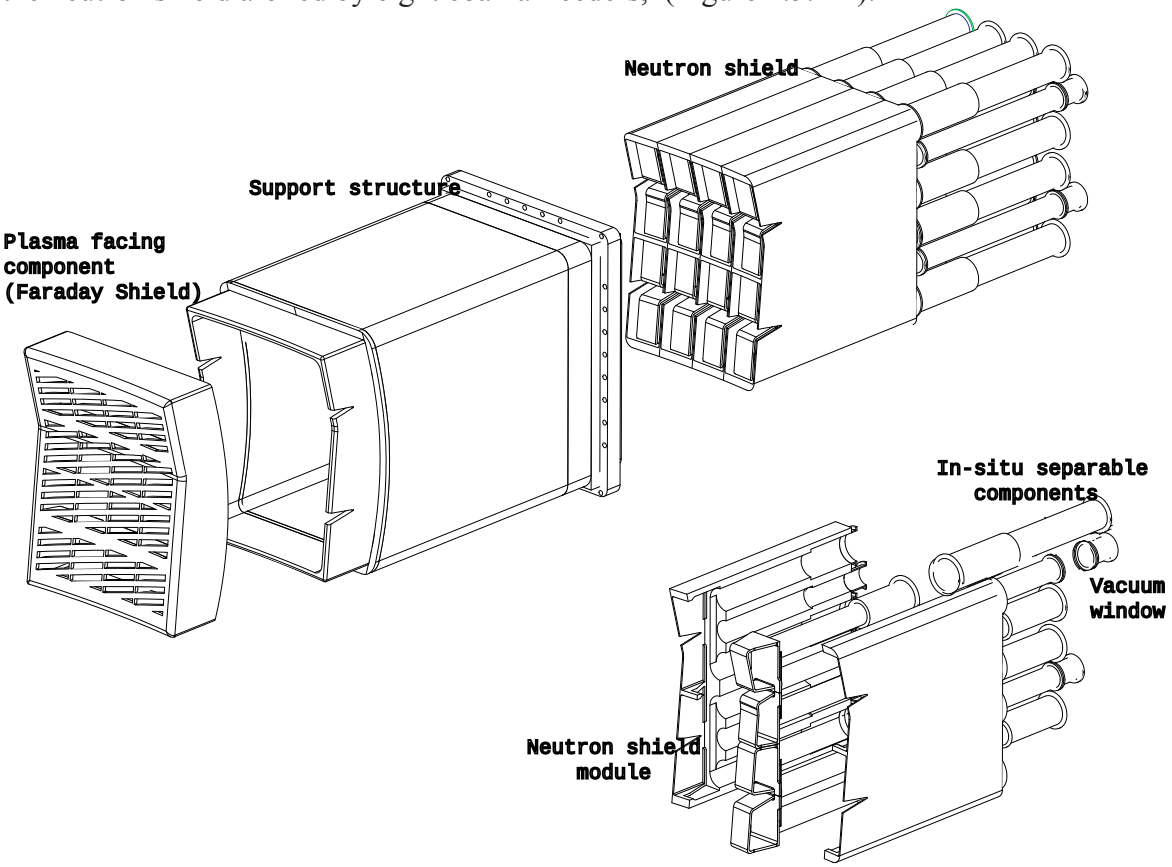

Figure 2.5.4-4 Exploded View of IC Launcher Showing Main Mechanical Components and Ways for Disassembly

These components are mechanically assembled with and supported by the outer mechanical structure (in 316L(N)-IG SS), also enclosing coolant manifolds for the front-end components. The closure plate supports the eight IC vacuum transmission line ceramic (BeO) feed-throughs, contributing to the vacuum and tritium containment. The windows are also accessible from behind and can be easily maintained

2.5.4.3 Power Transmission Design

The coaxial transmission lines used by the IC system are commercial items. The main transmission line is a rigid coaxial of 280 mm OD, having a characteristic impedance of 30 Ω. The inner conductor is radiation-cooled and operates at T_{in}< 110°C. The outer conductor is water-cooled and operates at T_{out} ~ 45°C. The two conductors are coated with high emissivity material to enhance radiative thermal exchanges.

The voltage stand-off of the main transmission line is 80 kV, well in excess of the expected maximum RF voltage (< 15 kV). This large margin should provide low maintenance and a high reliability to this component.

2.5.4.4 RF Power Sources

The IC power sources are commercial multi-stage amplifiers equipped with tetrode tubes. The power source delivers 2.5 MW CW in a mismatched load with VSWR < 1.5. A detailed study has shown that this source can be constructed either using two existing commercial tetrodes combined in the end stages, or by a single-tube end-stage, with an upgraded anode power dissipation.

2.5.5 Lower Hybrid System

2.5.5.1 General Design Features

The lower hybrid H&CD system is specialised for off-axis current drive and current profile control. It is designed to deliver a total power of 20 MW at 5 GHz to the ITER plasma.

Typically, the system can drive a plasma current at a flux surface y such as $n_e(y)T_e(y) \sim 10\text{-}15 \times 10^{20}$ keV m^{-3}, with a typical current drive efficiency between 2 and 3×10^{20} m^{-3} MA/MW, in any scenario and/or discharge phase. In ITER, this is approximately equivalent to a driven current of ~ 1.5 MA in the region $0.5 < r/a < 0.7$.

An efficient coupling of LH to the plasma requires the presence of a sufficient plasma density between the launcher and the separatrix (4×10^{17} $m^{-3} \leq n_e \leq 10 \times 10^{17}$ m^{-3}).

The system is designed to operate at:
- a waveguide maximum electric field of 3.2 kV/mm (or a power density of 33 MW/m^2) at full power;
- a wave number $1.8 < n_{//} < 2.2$ modified by electronically varying the array phasing;
- a maximum load reflection coefficient of 5%, measured at the antenna input.

2.5.5.2 Launcher Design

The LH launcher is shown in Figure 2.5.5-1 The plasma-facing component is a phased array, made of four modules (2x2) of passive-active multi-junction (PAM) stacks. Each PAM module is composed of 24 active and 25 passive, rectangular cross section wave guides, progressively phased in quadrature, so as to synthesize a travelling slow wave propagating in the toroidal direction. The phase shift is obtained by inserting phase shifters of multiples of $\pi/2$ in adjacent groups of waveguides. Details on the mechanical dimensions of the PAM stack are listed in Table 2.5.5-1.

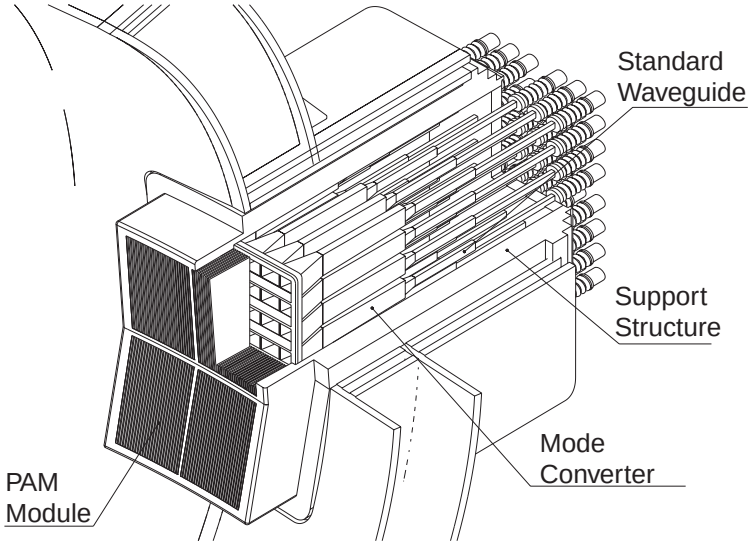

Figure 2.5.5-1 LH Launcher

Table 2.5.5-1 Mechanical Dimensions of Multi-junction Stack

Parameter	Value
Number of active wave-guides	24
Number of passive wave-guides	25
Cross section of active wave-guide (mm^2)	9.25 x 171
Mechanical length (mm)	900
Fundamental transmission mode	TE_{30}
Mechanical length (mm)	925 to 1050
Wall thickness (mm)	13.25
Phasing among active wave-guides	$3\pi / 2$
Phase shifter dimensions (mm)	14 x 750
Typical n// value	1.9-2.1
Max electric field in nominal power (22%) plasma reflection (kV/cm)	3.2

The PAM assembly is constructed in precipitation-hardened copper alloy (CuCrZr) or in dispersion-strengthened copper alloy (Glidcop Al25) and covered by a Be protection plate 18 mm thick. Cooling channels are provided in the thickness of the passive wave guide wall, by twin cooling channels lined with thin 316LN SS tubing, and supplied by a manifold housed in the supporting frame.

Forty-eight $TE_{10}/TE_{30/}$ mode converters form a 2x2 matrix, held in position by a 316LN SS frame, which also provides the attachment of the launcher to the support structure. The mode converters are cooled by means of channels bored in their top and bottom SS walls. The same cooling circuit feeds all cooling channels in the module. The mode converters are fabricated of 316 LN SS, Cu-plated on the inside surfaces.

Forty-eight double-disk ceramic windows (12 per module) are located at the end of each converter, outside the primary closure plate. BeO (99% purity) is used as dielectric material. The windows have an insertion loss of 0.1%, a voltage standing wave ratio VSWR ~ 1.5, and a working frequency of 5 GHz ± 1 MHz. The ceramic disks can withstand 0.2 MPa dry air pressure on one side. The coolant is routed to the components of the four PAM modules from a common manifold located in the support structure, and connected to the primary heat transfer system.

2.5.5.3 Power Transmission Design

The main transmission line (MTL) is in four sections.

i) A vacuum section (Figure 2.5.5-2) which runs between vacuum vessel and cryostat closure plates. The VTLs are commercial rigid rectangular waveguide sections (type WR229), connected in pairs to 24 3-dB hybrid junctions. At the cryostat exit, twenty-four standard vacuum windows or gas barriers are used for secondary vacuum containment.

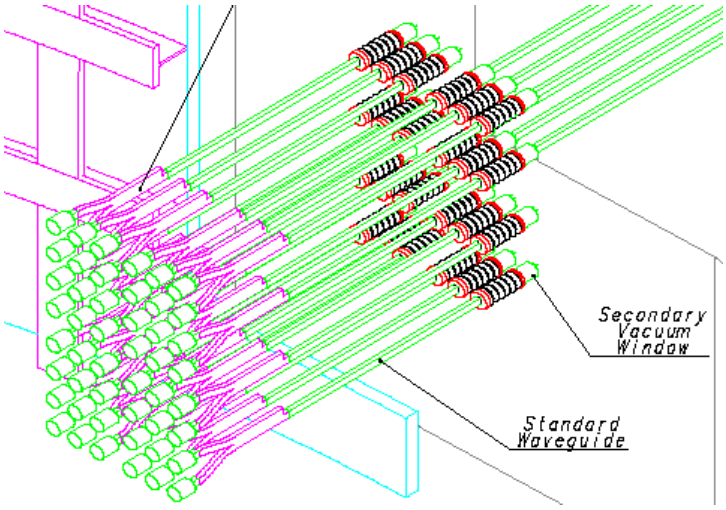

Figure 2.5.5-2 Vacuum Section of MTL

ii) A pressurised splitting network section (SN), running from the cryostat wall and the circular transmission line. Each circular wave-guide feeds 4 standard vacuum transmission lines through its SN.

iii) A pressurised circular transmission line section (CTL), running from the splitting network to the klystron cabinet (Figure 2.5.5-3). The total CTL length is approx. 80 m with six 90° bends. The circular transmission line is made of sections of commercial, rigid circular cross-section waveguide and elbows, filled with pressurised air. The main propagating mode

is TE_{01}. Mode filters are inserted along the line, to avoid propagation of high order modes (see Table 2.5.5-2).

iv) A pressurised recombining network (RN) section (symmetric with the SN), located in the klystron cabinet, running from the CTL to each individual power klystron. Each MTL is fed by 4 klystrons through the RN.

Four klystron generators are connected to the same CTL through the RN, which includes an RF switch and a 1 MW test load.

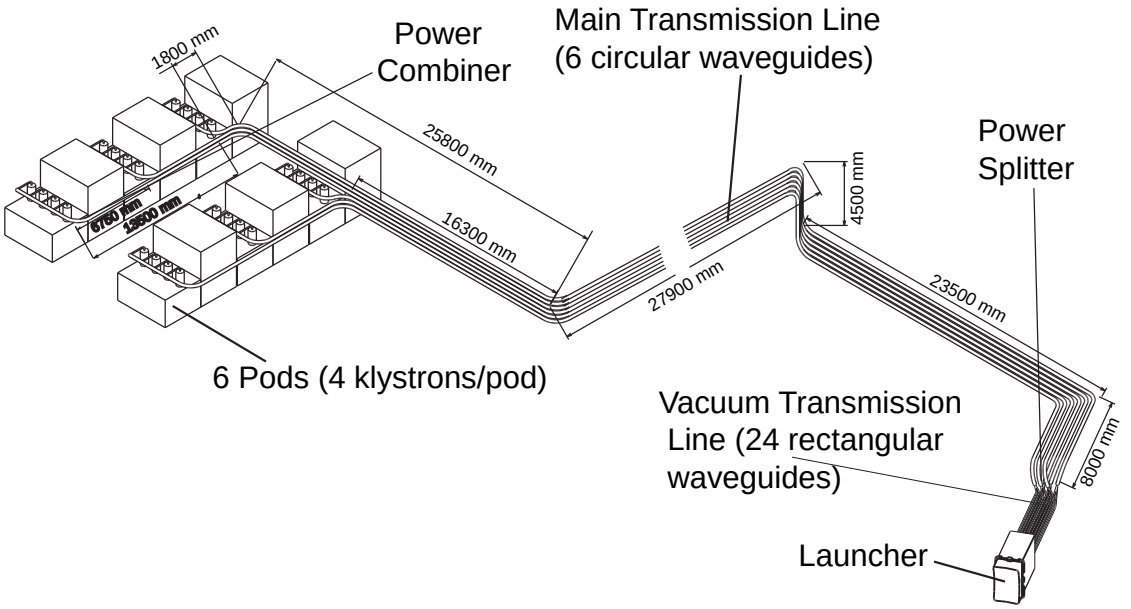

Figure 2.5.5-3 Pressurised Section of MTL and Power Sources Layout

Table 2.5.5-2 Main Transmission Line Parameters

Design	**Feature**	
Wave guide	standard C10: 107.57 mm radius	
Flange	remote handling and standard C 10 types	
Material	OFHC, 3 mm thick	
Attenuation TE_{01} @ 5 GHz (dB/m)		4.2×10^{-4}
RF power rating		4 MW
Electric field for nominal operation at VSWR = 1		822 V/m
VSWR		< 1.4
Admissible operating pressure		4 bar absolute
Sealing material		Silicon rubber
Insertion loss for a 90° bend		< 0.3 %
Insertion loss for mode filter or bellows		< 0.5 %
Bellows span		+/- 10 mm

2.5.5.4 RF Power Sources

The LH RF power system consists of 24 RF power sources, each consisting of one power klystron amplifier (see Table 2.5.5-3) and of auxiliaries (focusing block with superconducting magnet and regulated supply, shielding, filament power supplies, and oil tank). The amplifier is driven by a solid state driver amplifier (10 W).

Phase and amplitude of the output wave of all klystrons are electronically controlled using a single reference. The klystrons are connected in groups of four to the HVDC power supply unit and common protection circuits are installed close by so as to minimize stray capacitance in the connections.

Table 2.5.5-3 Main Features of the Klystron Amplifier

Parameter	**Value**
Nominal power	1 MW (VSWR < 1.4:1 any phase), CW
Duty cycle	CW or 1000s every 20 mn
Frequency	5 GHz
Bandwidth	1 MHz
Efficiency	> 60 %
Gain	53 dB
Amplitude accuracy	1%
Phase accuracy	± 2°

2.6 Plasma Diagnostic System

To meet the requirements for plasma and first wall measurements, an extensive diagnostic set of about 40 individual measurement systems is required. In general, very high levels of reliability are necessary, particularly for systems providing measurements for protecting the in-vessel machine components from abnormal events, and/or used in real-time control. Most systems are based on the experience of similar ones on current machines, but in order to fulfil some measurement requirements it has been necessary to use techniques still under development.

2.6.1 Selected Diagnostic Systems and Startup Set

It is neither necessary nor desirable to build all diagnostics during the machine construction phase: some will not be required until later in the operational programme, e.g. those specific to the DT programme, and a phased installation will permit the most advanced techniques and technologies to be used. However, it will be necessary to assess the interface, space and service requirements of each diagnostic that will eventually be used, and make any necessary provisions during machine construction to avoid expensive modification costs later. The subset of diagnostics for initial machine operation is called the 'startup set'. A provisional selection of the startup set has been made and is included in the list of diagnostic systems and their planned readiness (see Table 2.6-1). For some systems only a limited measurement capability will be available for first plasma. Novel diagnostics still under development are marked with 'N/C' (new concept). Some systems require a dedicated diagnostic neutral beam (DNB), which is also shown in the table.

2.6.2 Diagnostic Integration

Individual diagnostic systems are installed on the tokamak taking into account measurement requirements, shielding, vacuum boundaries and activation requirements, length and complexity of transmission lines, and maintenance requirements as well as requirements for confinement of radioactive and toxic materials. For optical and microwave systems, windows and fibre-optic feedthroughs are used to cross the vessel and cryostat flanges; for electrical signals, vacuum feedthroughs are used.

Diagnostic components are installed in four locations – within the vacuum vessel (VV), in divertor ports, and in equatorial and upper ports. The installation issues are different in these locations and so they are discussed separately.

Table 2.6-1 Status of Diagnostic Systems at the Startup of the H Phase and of the DT Phase

Diagnostic	Status at Startup (H phase)	Status at Start of DT Phase
Magnetic Diagnostics		
Vessel Wall Sensors, Divertor Magnetics, Continuous Rogowski Coils, Diamagnetic Loop	Complete	
Neutron Diagnostics		
Radial Neutron Camera, Vertical Neutron Camera	Interfaces complete	Complete
Micro-fission Chambers (In-Vessel) (N/C)	In-vessel components and interfaces complete	Complete
Neutron Flux Monitors (Ex-Vessel)	Interfaces complete	Complete
Gamma-Ray Spectrometer		Complete
Activation System (In-Vessel), Lost Alpha Detectors	In-vessel components and interfaces complete	Complete
Knock-on Tail Neutron Spectrometer (N/C)		Complete
Optical/IR(Infra-Red) Systems		
Core Thomson Scattering	Complete except for two lasers and one power supply system	Complete
Edge Thomson Scattering, X-Point Thomson Scattering	Complete except for some spares	Complete
Divertor Thomson Scattering	Penetrations, in-vessel optics and interfaces complete	Complete
Toroidal Interferometer/ Polarimeter, Polarimeter (Poloidal Field Measurement)	Complete	
Collective Scattering System (N/C)	Penetrations, in-vessel optics and interfaces complete	Complete
Bolometric Systems		
Arrays for Main Plasma, Arrays for Divertor	Complete	
Spectroscopic and Neutral Particle Analyzer Systems		
H Alpha Spectroscopy, Visible Continuum Array	Complete	
Main Plasma and Divertor Impurity Monitors, X-Ray Crystal Spectrometers	Penetrations, in-vessel optics and interfaces complete. Partial operation	Complete
Charge eXchange Recombination Spectroscopy (CXRS) based on DNB, Motional Stark Effect (MSE) based on heating beam, Soft X-Ray Array, Neutral Particle Analyzers (NPA), Laser Induced Fluorescence (N/C)	Penetrations, in-vessel optics/sensors and interfaces complete	Complete

Table 2.6-1 Status of Diagnostic Systems at the Startup of the H Phase and of the DT Phase (cont'd)

Microwave Diagnostics		
Electron Cyclotron Emission (ECE)	Complete except for one spectrometer	Complete
Main Plasma Reflectometer	One LFS (low field side) X-mode and one LFS O-mode complete	Complete
Plasma Position Reflectometer, Divertor Reflectometer, Divertor EC absorption (ECA), Main Plasma Microwave Scattering, Fast Wave Reflectometry (N/C)	In-vessel components, interfaces	Complete
Plasma-Facing Components and Operational Diagnostics		
IR/Visible Cameras, Thermocouples, Pressure Gauges, Residual Gas Analyzers, IR Thermography (Divertor), Langmuir Probes	Complete	
Diagnostic Neutral Beam		
Diagnostic Neutral Beam (DNB)	Interfaces and main source components complete	Complete

2.6.2.1 In-vessel Installations

The principal diagnostic components mounted in the VV are sensors for the magnetic diagnostics, bolometers, soft X-ray detectors, waveguides for reflectometry, micro-fission chambers, and transmission lines for neutron activation foils. A summary of the diagnostic sensors and their location is shown in Table 2.6-2. The critical design issues for each component are also mentioned. On the inboard side, the sensors are either welded directly on the vessel (e.g. micro-fission chambers, magnetic loops), or are grouped in remote replaceable plugs mounted in bosses on the vacuum vessel. On the outboard side they are mounted on the blanket coolant manifolds. The number and the toroidal and poloidal locations of the diagnostic sensors are defined by the measurement requirements.

Most sensors and cables are shielded by the blanket modules although some sensors, for example bolometers and soft X-ray detectors, would view the plasma through the 20 mm gap between blanket modules.

The principal candidate cable for use in the vessel is mineral insulated (MI) cable, with copper core, alumina insulant and stainless steel sheathing. All wires will be screened or twisted in pairs to cancel inductive pick-up. The sheath of the cable will be grounded. The in-vessel sensor cabling is marshalled in specially constructed cable looms running behind the blanket modules. The cables are brought out along the upper port to feedthroughs.

Table 2.6-2 Summary of Diagnostic Sensors located on the Vacuum Vessel and Blanket

Location	Diagnostic Sensor	Particular Radiation and Environ-mental Effects[1]	Particular Design Problems
Inner wall	High Frequency Response Coils	Heating	Fragile, exposed insulator, RF pickup
	Equilibrium Coils	RIC, RIEMF	Signal drift integration, thermal stability, connector noise
	Joint-less Equilibrium Coils	Heating, RIC, RIEMF	Lifetime
	Diamagnetic Loop	Heating where exposed	Planarity
	Diamagnetic Loop Compensation	Heating, RIC	Size
	Voltage and Saddle Loops	Heating where exposed	Routing conflicts with in-vessel components
	Halo Current Rogowskis		Quantity
	Micro-fission Chambers		
	Neutron Activation Detector		Through vacuum boundaries
Side of blanket	Lost Alpha Detectors		Fragile and exposed to the plasma
Filler module	Interferometer Retroreflectors	Erosion and/or deposition	Degradation in optical performance
Blanket module	Polarimeter Retroreflectors		
Inner wall	Bolometer	He swelling, radiation	Microphony, large cable, many lines of sight (LOS), ECH
	Soft X-ray		Small signal currents, e-m interference
Inner wall and/or blanket	Reflectometer Antennas	Heating where exposed	Wide temperature range

[1] RIC – Radiation Induced Conductivity; RIEMF – Radiation Induced EMF.

2.6.2.2 Equatorial and Upper Ports

Four equatorial ports are dedicated to diagnostics. Two more ports, allocated to remote handling, are foreseen to have diagnostics that can be removed easily before the start of a maintenance procedure. Several factors have to be taken into account in optimising the allocation of diagnostics to the available ports: for example, large aperture systems are placed at port centres and tangential viewing systems at the sides of ports, whereas systems which need to view one of the neutral beams, need to use specific ports. Systems which have complicated transmission lines are located in the ports on the west side of the tokamak near

N 55 GR 25 01-06-11 F1

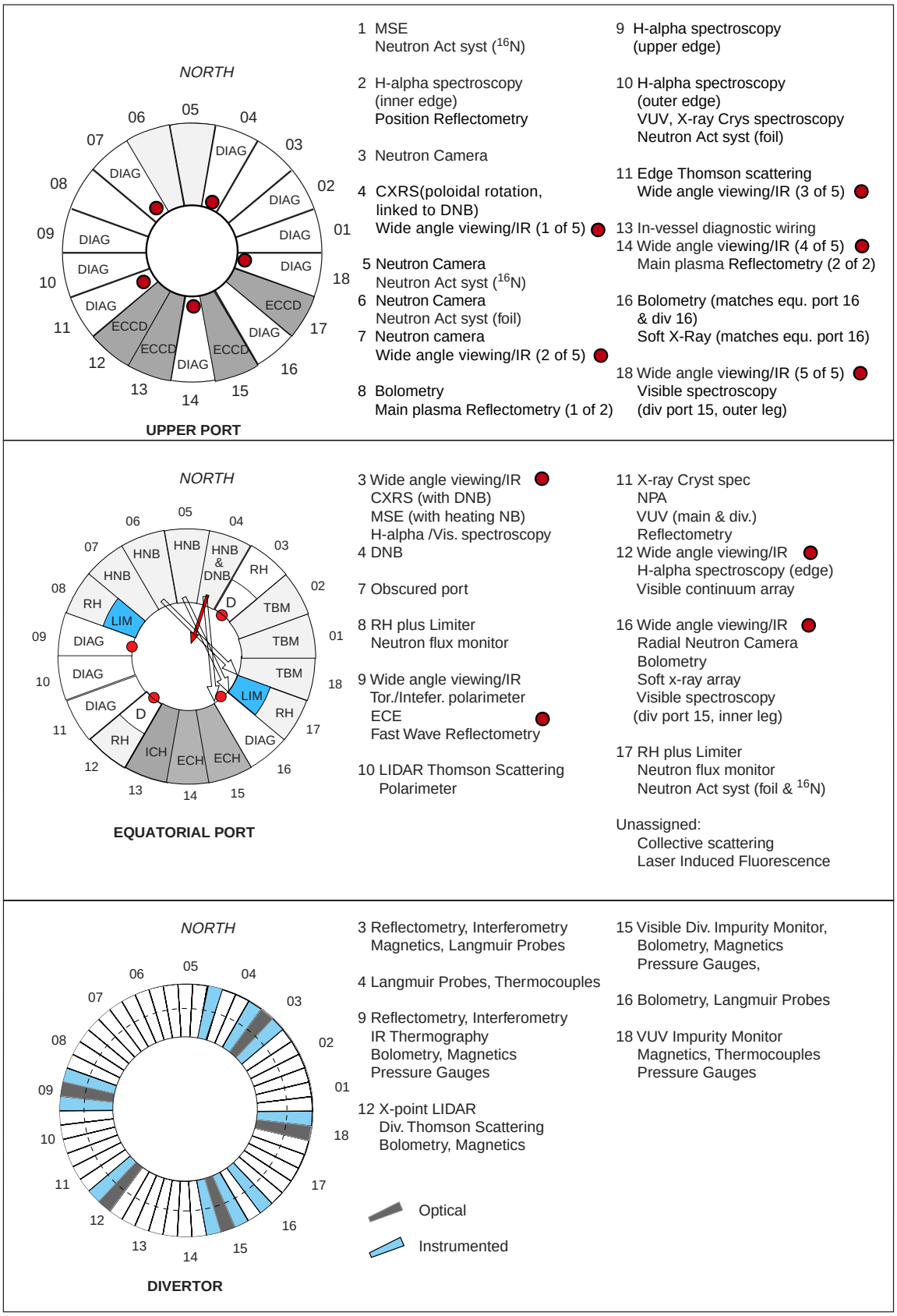

Figure 2.6-1 Provisional Diagnostic Port Allocation at the Upper, Equatorial and Divertor Port Levels

to the diagnostic hall. Some systems, for example the plasma and first wall viewing system, are distributed systems and it is the performance of the combined installation that is important. Figure 2.6-1 shows the provisional port allocation for diagnostics which takes into account these factors.

In most cases, diagnostic equipment in equatorial ports is mounted in a single port plug within the primary vacuum. The principal components of the plug are a special blanket shield module, and a port plug structure incorporating a VV closure plate. The shield module comprises a first wall made from armoured beryllium tiles bonded to seamless stainless steel water cooling pipes and a shielding manifold box, an arrangement similar in design and technology to other equatorial ports, in particular the limiter one. The port plug structure (see Figure 2.6-2) has the dual functions of supporting the diagnostic components and providing the necessary shielding. A single structure similar for all ports is used, containing shielding/diagnostic modules. The common arrangement allows a simple concept for remote maintenance of all the port plugs and the modularity of internal components allows a standardised approach for hot cell maintenance.

Outside the primary vacuum, a structure is located in the connecting duct between the vessel flange and the port interspace closing flange. The connection between vessel and cryostat is relatively simple for the diagnostics which require optical connections, whilst substantial connections are required for waveguides and vacuum extensions.

N 55 GR 10 00-12-08 F1

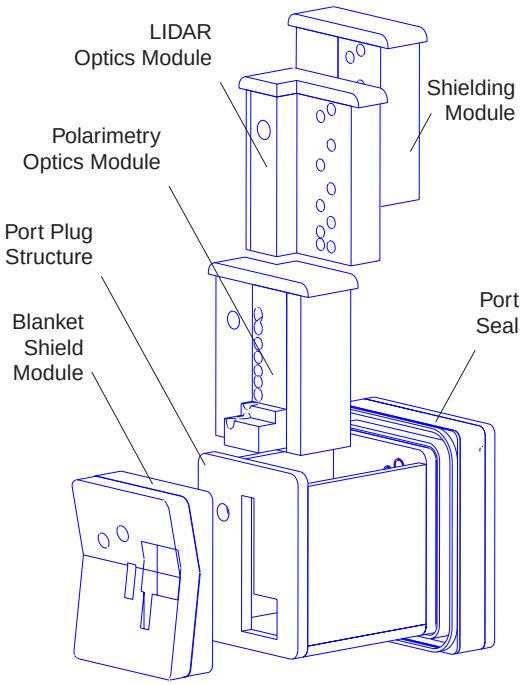

Figure 2.6-2 Assembly of a Typical Diagnostic Equatorial Port Plug Structure with the Diagnostic Systems: LIDAR and Poloidal Field Polarimeter (Port 10)
The apertures in the blanket shield module are also shown.

The VUV, X-ray crystal spectrometry, and the NPA, have to be directly coupled and require an extension of the primary vacuum outside the bioshield, as shown schematically in Figure 2.6-3. The primary vacuum extension is enclosed in a secondary vacuum chamber, which is able to resist a pressure larger than 0.2 MPa, and which is separated from the cryostat vacuum to avoid cross-contamination.

N 55 GR 18 00-12-08 F1

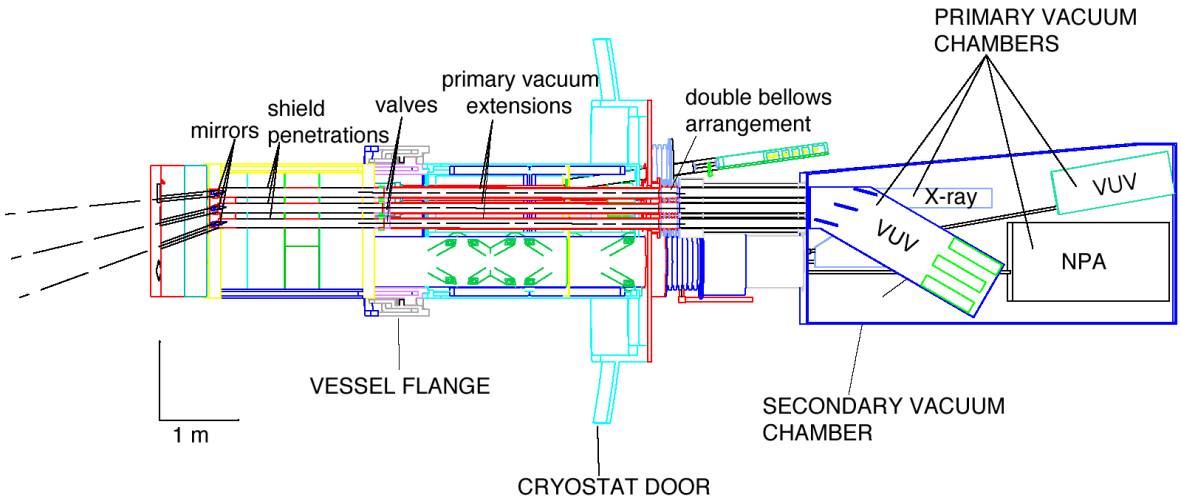

Figure 2.6-3 VUV Vacuum Extension at the Equatorial Port 11

For maintenance operations, the diagnostic port plug will be brought to a dummy port installed in the hot-cell area. While in the dummy port, in-vessel components can be accessed remotely, while the windows and other feedthroughs on the vacuum vessel flange can be replaced hands-on. Tests can be carried out on the port plug and the interspace structure while they are mounted in the dummy port.

The concepts and approach developed for the equatorial ports are also used for diagnostics installed in the upper ports. However, some diagnostic equipment in these ports will have permanent features such as wiring and waveguides with as few connections as practical. The neutron camera will have a special arrangement outside these ports (2.6.3.2).

2.6.2.3 Divertor Ports

In the divertor, diagnostic components are installed in the three remote handling ports and on the divertor cassettes at these positions. At each location there are two instrumented cassettes (with Langmuir probes, bolometers, pressure gauges, etc.) on either side of a central, 'optical', cassette. The latter is modified to incorporate optical and microwave diagnostics and includes a mirror on a central mount (Figure 2.6-9). Side plates, up to 20 mm thick, complete with pre-wired sensors and wiring loom, are bolted to the body of the cassette. These permit relatively simple installation and replacement of diagnostic components (Figure 2.6-4).

Signals are marshalled at the electrical connector on the outboard end of the cassette. In the space between the VV closure plate and the divertor cassette, a diagnostic block is installed

which carries waveguides and optical equipment. Remote maintenance inside the machine is performed for the diagnostic cassettes in the same way as for standard cassettes.

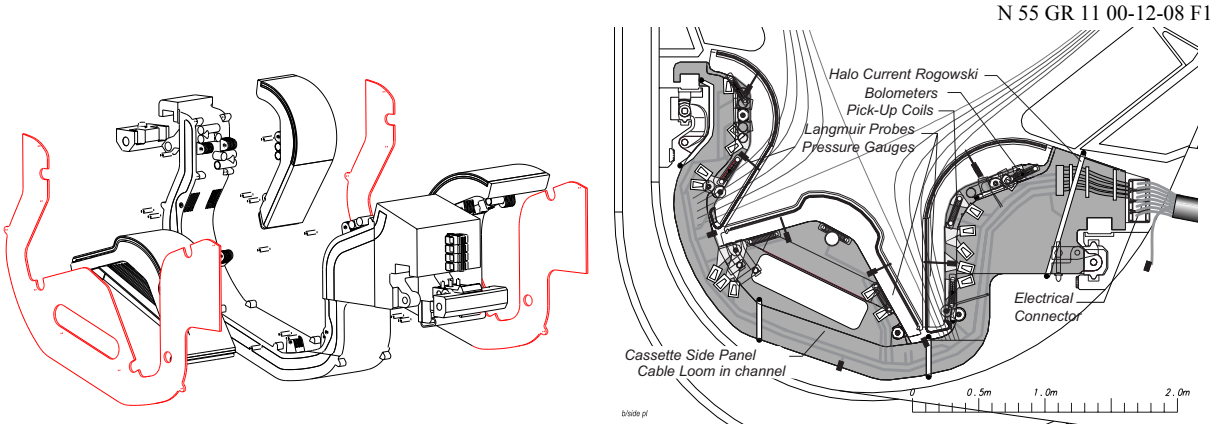

Figure 2.6-4 Side Plate of a Divertor Cassette with Typical Sensor Locations

2.6.3 Diagnostic Systems

The individual diagnostic systems can be grouped into seven generic groups (Table 2.6-1). The different groups of diagnostics have different implementation details and so it is convenient to discuss them separately.

2.6.3.1 Magnetics

The magnetic diagnostics comprise several subsystems:

- sets of pick-up coils, saddle loops and voltage loops mounted on the inner wall of the vacuum vessel for equilibrium and high frequency measurements (in-vessel system);
- sets of pick-up coils and steady state sensors for back-up measurements, currently proposed to be mounted between the VV shells;
- continuous poloidal (Rogowski) loops mounted on the outside of the vacuum vessel;
- sets of coils mounted in the divertor diagnostic cassettes;
- diamagnetic system comprising poloidal loops on the inner wall of the VV and compensation circuits inside and outside the vessel;
- Rogowski coils mounted around earth straps of the blanket/shield modules for measuring the 'halo' currents.

The in-vessel system comprises:

- tangential, normal and toroidal equilibrium coils mounted on the inner surface of the VV;
- tangential high frequency coils mounted on the inner surface of the VV;
- complete and partial flux loops mounted on the inner surface of the VV;
- dedicated saddle loops mounted on the inner surface of the VV;
- a (temporary) PF and TF error field measurement assembly.

The distribution of the main elements of the system is shown in Figure 2.6-5.

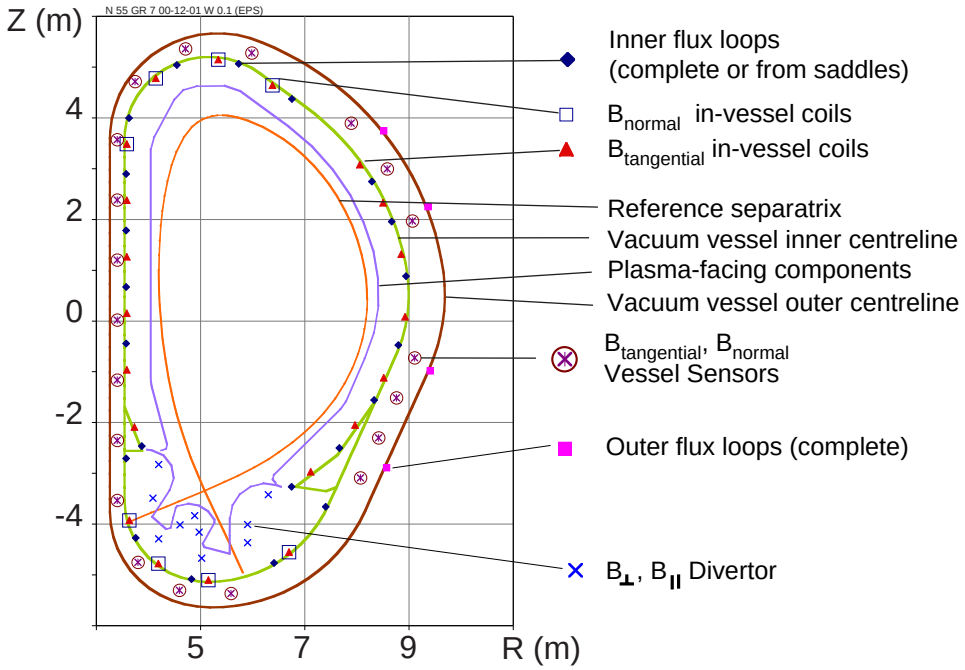

Figure 2.6-5 Poloidal Distribution of Magnetic Sensors
(The diamagnetic loops and external Rogowski coils are not shown)

The pick-up coils mounted on the inner surface of the VV are wound on a stainless steel former with a protective cover. The important irradiation effects, radiation-induced conductivity and radiation induced EMF, are minimised by a careful choice of materials and sensor location. The voltage loops have a bridge at every sector joint. Special connectors are used to permit reconnection of the voltage loop if replacement of a vessel sector were needed. The coils, the cable and other ceramics (e.g. those used in the HF coils) are sufficiently shielded by the presence of the blanket modules that their lifetime is comparable to or longer than the lifetime of ITER.

The coil set proposed to be mounted between the VV inner and outer shells, and on the VV, would form a back-up system for the in-vessel magnetics for long pulses. By placing coils of large effective area in this relatively low radiation environment, it is expected that the signal to noise ratio at the input of the integrator will be significantly enhanced. In addition, this environment allows the use of steady state sensors of the strain gauge type, which do not suffer from drift. Finally, this set is mechanically and electrically very well protected. There is a drawback: the slow frequency response (of order 1.2 s for 2 % error following a step).

The external, continuous, Rogowski coils are located on poloidal contours outside the vacuum vessel and supported by the TF coils, and measure all current passing through their cross-sections, that is, the sum of plasma current, and vessel current. An independent measurement of the vacuum vessel current is needed to derive the plasma current. This is provided by the vessel and in-vessel sensors.

The diamagnetic loop system measures the magnetic flux expelled by the plasma. From this measurement, the perpendicular energy content can be derived. This in turn gives the confinement time. The method is based on a pair of poloidal loops on the inner wall of the vessel, and compensation circuits. The poloidal loop measures the flux change inside its

contour. The compensation circuits measure the vacuum flux inside and outside the vessel, and the local vertical field. The exit wires are twisted and routed out of the vessel through the nearest divertor port, with already existing wiring, feed-throughs and connectors. Multi-turn compensation coils of the same surface area as the diamagnetic loop are placed inside the vacuum vessel below the triangular support frames (see section 2.2), and outside the vacuum vessel, for the same sectors as the diamagnetic loop. In addition, the TF current (including casing) change during the pulse is measured by Rogowski coils around the TF coil cases on the low field side.

Distinct sensors are used to measure halo currents. Since current enters the wall through the blanket/shield modules and these are electrically connected to the VV by means of earth straps, one way of measuring halo currents is to measure the current in the earth straps using Rogowski coils. In addition, the blanket/shield modules provide an opportunity of obtaining higher spatial resolution, required since halo current density varies poloidally and toroidally. However because of the large number of modules, it is impractical to obtain full coverage using this method. The present design attempts to obtain reasonable coverage of the important areas. The inner top and bottom of the vessel have dense coverage. The halo-sensing Rogowski coil is wound on a ceramic body with grooves with a bare wire or within a thin metal case using sheathed cable. Approximately 300 turns are required to give signals of order 1 V during disruptions. Separate sensors are used to deduce the current flowing through selected divertor cassettes.

2.6.3.2 Neutron Systems

The principal neutron systems are a radial neutron camera, a vertical neutron camera, neutron spectrometers, neutron flux monitors, and a neutron activation system.

The radial neutron camera consists of a fan-shaped array of flight tubes, viewing the plasma through a vertical slot in the blanket shield module of an equatorial port plug. The sight lines intersect at a common aperture defined by the port plug and penetrate the vacuum vessel, cryostat, and biological shield through stainless steel windows (Figure 2.6-6). Each flight tube culminates in a set of detectors chosen to provide the required range of sensitivity, and temporal and spectral resolution. Some of the viewing chords will be equipped with high resolution neutron spectrometers, enabling the system to provide emissivity-weighted, chord-averaged measurements of ion temperature. Appropriate spectrometers have not yet been selected but there are several that could meet the measurement requirements with development.

The proposed vertical neutron camera measures the line-integral neutron emissivity along chords viewing downward through the upper ports. Each sight-line views the plasma through long narrow tubes in the upper port plug and vacuum vessel, cryostat and the second collimator in the shield. The first collimators are integrated into the plug of the upper port. For each sight line, a 45 mm inner diameter flight-tube passes through the vacuum vessel and contains a thin stainless steel ‘window’. The detectors and the second collimators are in the space between the cryostat lid and the top bioshield. Shielding on the cryostat lid, around the detectors, provides a beam dump and will allow hands-on maintenance.

Summation of the chordal signals, together with knowledge of the plasma vertical position, gives the global neutron source strength, hence the total fusion power. Combined with data from the radial neutron camera, these measurements allow reconstruction of the spatial

distribution of neutron emissivity, which determines the alpha particle source profile and fusion power density, and serves as a constraint on inferred values of fuel concentrations and effective ion temperature.

N 55 GR 27 01-06-12 F1

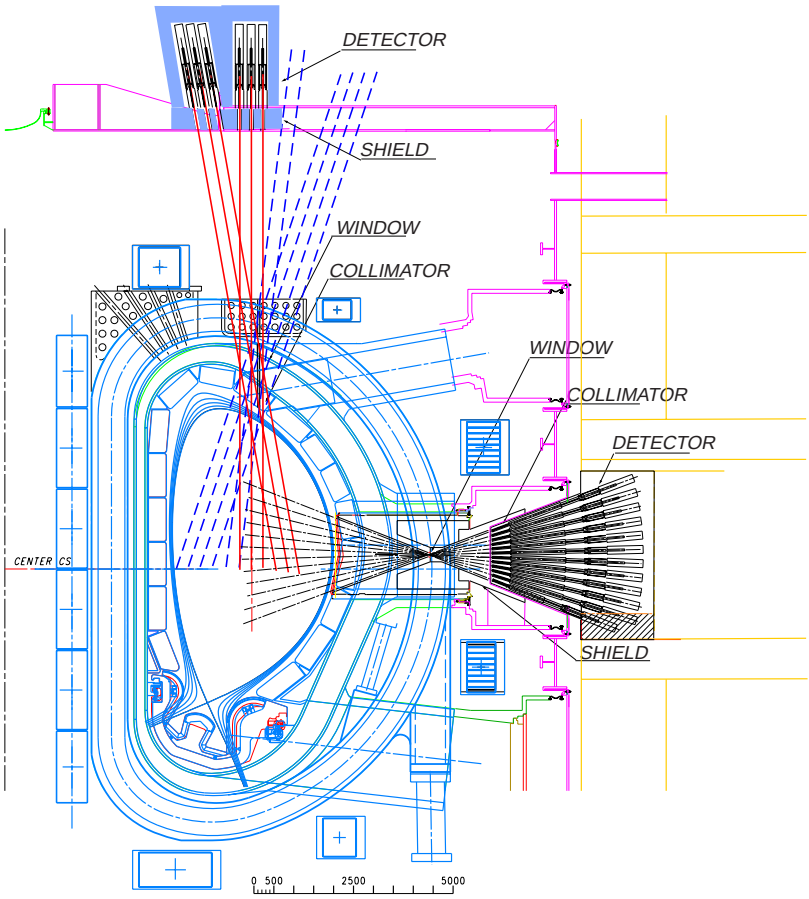

Figure 2.6-6 Schematic of Proposed Radial and Vertical Neutron Cameras
(The sight lines for the vertical camera would be distributed at four different toroidal locations)

The neutron flux is measured by fission chambers containing ^{235}U or other isotopes, situated at different locations in the diagnostic ports and outside the VV. In addition, micro-fission chambers are deployed behind the blanket modules in poloidal arrays at two toroidal locations. These are miniature fission detectors of the type commonly used for in-core neutron flux measurements in fission reactors. The use of multiple locations allows compensation of effects due to changes in plasma position or shape, and provides redundancy in case of detector failure. Together these systems give the global neutron source strength from which the total fusion power is obtained, and the measurement should be insensitive to plasma position.

Two activation systems are planned. One uses pneumatic transfer to place a sample of material close to the plasma for irradiation. This will give an accurate but relatively slow measurement. The second system measures the gamma rays from the decay of ^{16}N produced

in a flowing fluid. This system will be faster (typically several seconds) but less accurate. Taken together these systems will provide a robust, independently calibrated, measure of fusion power.

2.6.3.3 Optical/Infrared Systems

The principal optical systems are two multi-pulse Thomson scattering (TS) systems (core and edge), an equatorial plane interferometer, and a poloidal interferometer/polarimeter.

The core TS system operates on the time-of-flight (LIDAR) principle. Light from a high power laser is transmitted to the plasma using a folded mirror arrangement inside a shielded labyrinth at an equatorial port. The plasma-facing mirror is metallic and actively cooled. Scattered radiation returns along the same labyrinth to remote spectrometers. An active alignment system is employed to compensate for movements of different parts of the system.

The key element in the system is the plasma-facing mirror. The mirror will be located at the bottom of a duct about 2 m in length and view the plasma through a 0.2 m diameter aperture in the blanket shield module. It will be actively cooled. In this location, it can potentially be damaged by two processes. The mirror surface can be eroded due to bombardment from energetic neutrals arising from charge exchange processes occurring in the plasma edge region, and/or it can be covered by a thin layer of first wall or duct material due to erosion of these components. Extensive R&D[1] has shown that mirrors made from low sputtering coefficient materials deposited on a high thermal conductivity substrate are robust against erosion. The chosen mirror for the LIDAR system is Rh on a V substrate. Baffles, cleaning techniques, and/or shutters are possible mitigating methods against deposition.

In order to meet the requirements for high-resolution measurements in the edge region, a conventional Thomson scattering system is employed. The large upper ports permit the installation of separate input and collection lines in the same port (Figure 2.6-7). Moreover, implementation at this level allows advantage to be taken of the flux expansion in this region. The collection line is transmitted beyond the secondary confinement barrier using heated optical fibres (although space is allowed for a conventional optical relay with discrete elements if required).

A vibration-compensated interferometer employing Faraday rotation techniques will be used to measure line-integrated density for use in feedback control. The plasma is probed along lines of sight in the equatorial plane. Each beam path has collinear 10.6 μm (CO_2) and 5.3 μm (CO) laser probe beams. The laser beams paths are generated from one 10.6 μm (CO_2) laser and one 5.3 μm (CO) laser and are spatially separated by a mirror system. They enter and exit the plasma chamber from a single port and are reflected back down the same beam path (with an offset) by retroreflectors. There are several possible locations for the installation of the retroreflectors, including the filler modules between the blanket shield modules and in the special shield modules on other ports.

[1] V Voitsenya et al,, "Diagnostic First Mirrors for Burning Plasma Experiments", Rev. Sci. Instrum, 72, 1 (2001) 475.

N 55 GR 14 00-12-08 F1

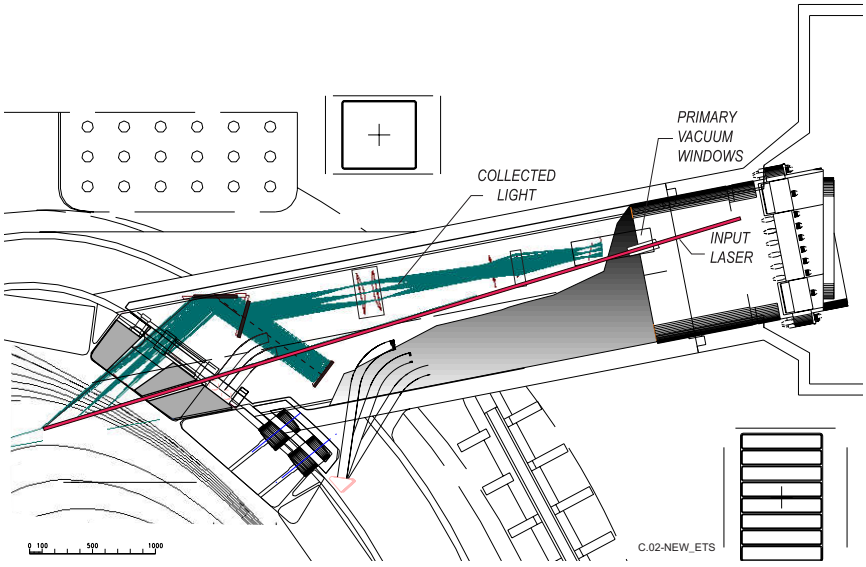

Figure 2.6-7 Schematic of the Thomson Scattering System installed in an Upper Port

The phase change due to the plasma is measured at both 10.6 µm and 5.3 µm. Also, the Faraday rotation is measured at 10.6 µm. Analysis of the data gives the line-integral of the electron density along each line of sight which, when inverted and combined with other measurements, gives the profile of the electron density. Vibration compensation is obtained by taking the difference between the results at 10.6 µm and 5.3 µm. High reliability and high sensitivity are obtained from the Faraday rotation and phase measurements respectively.

A plan view of the beam paths through the port shield plug is shown in Figure 2.6-8.

N 55 GR 15 00-12-08 F1

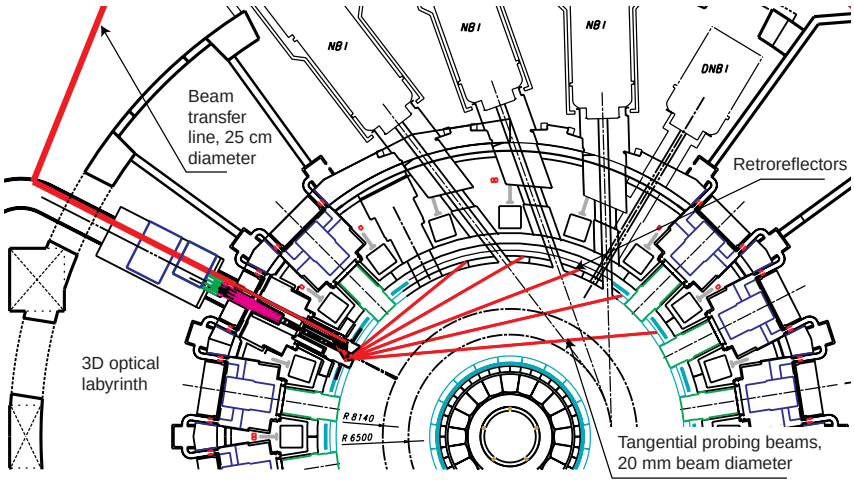

Figure 2.6-8 Schematic of the Layout of the Interferometer/Polarimeter showing the Five Lines of Sight through an Equatorial Port

Multi-chord polarimetry in the poloidal plane will be used to provide measurements of the q profile and/or to anchor reconstructions of the magnetic equilibrium. As for the interferometer, in-vessel retroreflectors have to be used, but in this case it is proposed to mount them in the remote handling vertical slots in the blanket modules.

Additional planned optical systems under investigation are Thomson scattering systems for the X-point and divertor regions, and a collective scattering system to provide measurements of the confined alpha particle population.

2.6.3.4 Bolometry

The bolometric systems aim to provide the spatial distribution of the radiated power in the main plasma and in the divertor region with spatial resolutions of 20 cm and 5 cm, respectively. The proposed method, used on many tokamaks, is sparse-data tomography. This would require a large number of lines of sight (approximately 340).

The bolometer arrays will be installed in the equatorial and upper ports, in the specially instrumented diagnostic divertor cassettes (and possibly at selected locations on the VV). From each of these locations several arrays of lines of sight observe the plasma in a fan-shaped geometry. From the equatorial port, the inner divertor leg and the main plasma are viewed. From the upper port, the main plasma, the area of the X-point, and the largest part of the divertor legs, can be seen. This last view provides the total radiated power. Bolometers mounted on the VV would view the plasma through the poloidal gaps between adjacent blanket/shield modules. This provides some shielding from the nuclear radiation.

In the equatorial and upper ports, the bolometer arrays are integrated rigid units with all wiring attached, mounted in a diagnostic shield plug. In the divertor, there are multiple small heads assembled in a rigid conduit with the wiring attached to the side wall of the instrumented divertor cassette. The wiring runs to an automatic remote handling connector near the exit port. The plasma is viewed through the gap between cassettes, nominally 1 cm. The bolometers, if present on the vacuum vessel, are proposed to be housed in removable carriers that are plugged into permanent bosses. There are remote handling connectors between the bolometers and the wiring runs which are in conduits behind the blanket/shield module.

2.6.3.5 Spectroscopic and Neutral Particle Analyzer (NPA) Systems

An extensive array of spectroscopic instrumentation will be installed covering the visible to X-ray wavelength range. Both passive and active measurement techniques will be employed. The four main regions of the plasma - the core, the edge, the scrape-off layer (SOL), and the divertor - will be probed. The principal diagnostic systems employed are listed in Table 2.6-3. In addition there will be an NPA system which shares access with the X-ray and VUV systems and so is included in this group. A wide range of plasma parameters are determined including impurity species, impurity density and input flux, ion temperature, He density, fueling ratio, n_T/n_D and n_H/n_D, plasma rotation, Z_{eff}, current density, and q profile.

The H-alpha spectroscopy system measures the emission in the Balmer hydrogen lines. Several wide-angular optical systems located in the upper and equatorial ports view the upper, inner, and outer regions of the main plasma and the part of the divertor inner region visible from above. Collected light is transmitted by mirror optics through the labyrinths in

port plugs and then focused onto the fibre light guides leading to the spectrometer installed behind the biological shield. The divertor region is also probed with the divertor impurity monitoring system which views the plasma through the divertor ports and can measure the emission in the Balmer hydrogen lines.

The visible continuum array measures the emission at $\lambda = 523$ nm along multiple lines of sight in the equatorial plane. By using many sight lines (~ 35), an accurate unfolding of the Z_{eff} profile can be obtained. The emission is multiplexed into one transmission line and an optical labyrinth provides the required shielding.

The VUV main plasma impurity monitor has two subsystems: one consists of two spectrometers located at an upper port viewing from the flux expansion region up to 1 m into the plasma, and the other consists of a single spectrometer located at an equatorial port with a radial view through the plasma centre. Both systems measure the emission in the wavelength range 10 – 100 nm. Grazing collecting optics (5º - 7º) and spectrometers are employed, and thereby some shielding of the detectors is achieved. In this wavelength range, it is not possible to use windows, and so direct coupling of the instruments is required.

Table 2.6-3 Summary of Spectroscopy and NPA Diagnostics

Instrument	Wavelength Range	Regions Probed/ Viewing Directions	Function
H_α system	Visible region	Main plasma: inner, outer and upper regions Divertor: inboard and outboard regions	ELMs, L/H mode indicator, n_T/n_D and n_H/n_D at edge and in divertor
Visible continuum array	$\lambda = 523$ nm	Core plasma. Multiple LOS in the equatorial plane	Z_{eff}, line averaged electron density
VUV (main plasma)	10 – 100 nm	Upper and equatorial regions	Impurity species identification
X-ray (survey and high resolution)	0.1 – 10 nm	Core region: five LOS in the poloidal plane	Impurity species identification, plasma rotation, T
Divertor impurity monitor	200 – 1000 nm	Divertor and X – point regions	Impurity and influx, divertor He density, ionisation front position
CXRS	$\lambda = 468.5$ nm	Core and edge	T_i (r), He ash density, impurity density profile, plasma rotation
MSE	Visible region	Core	q (r), E_r (r).
NPA	N/A	Core and edge	n_T/n_D and n_H/n_D at edge and core. Fast alphas

Abbreviations see Table 2.6-1. LOS = Line(s) of sight

For the X-ray region, there will also be two subsystems: a medium resolution spectral survey instrument providing full coverage in the wavelength range 0.1 – 10 nm, combined with a high resolution, multi-channel instrument, with narrow spectral coverage in the range between about 0.1 - 1 nm and multiple radial sight-lines. These will be mounted in an equatorial port along with the VUV system and the NPA in an integrated instrument package.

In addition, there will be a survey instrument mounted in an upper port. This will share access with the upper port VUV system.

The divertor impurity monitoring system measures the emission in a wide spectral range along multiple lines of sight in the divertor region. The plasma is viewed at the divertor level and also from the equatorial and upper ports.

At the divertor level, the light emitted from different chords is collected by mirror optics mounted beneath the dome and on the side, of the special (central) optical divertor cassettes (Figure 2.6-9). It is transmitted through an optical penetration in the divertor remote handling port, the VV shielding plug and the cryostat. A labyrinth in the biological shield provides the necessary shielding. The beams are guided to the collecting and focusing optics where they are focused on to an optical fibre array. The light entering the optical fibre bundles is separated into two wavelength regions: 200 - 500 nm, and over 500 nm. The former enters the spectrometers positioned on a transport cask in the pit. Optical fibre bundles guide light in the wavelength region over 500 nm to spectrometers installed in the remote diagnostic hall, where accessibility for maintenance is better.

The plasma in the upper part of the divertor region to the X-point is observed through the gap between the divertor cassettes. An optical transmission line transmits the emission to the spectrometers and detectors located in the pit, or in the diagnostic hall, depending on the wavelength region.

Additional views of the divertor region are needed in order to meet the measurement requirements for two-dimensional information. These are achieved by viewing the plasma with two separated viewing lines with multi-chords, one from the upper port and the other from the equatorial port.

N 55 GR 16 00-12-08 F1

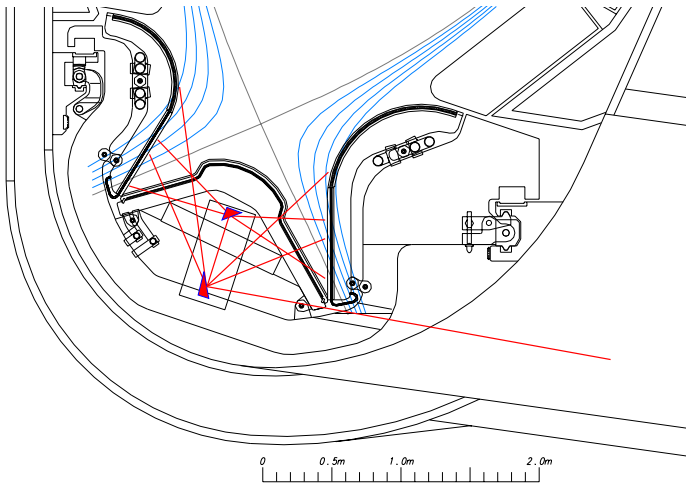

Figure 2.6-9 Viewing Fans in the Divertor Region

Passive spectral measurements in the visible wavelength range are of limited value for probing the core, because of the high temperatures. However, active measurements, employing charge exchange recombination spectroscopy (CXRS) with beams of energetic neutrals, are a rich source of information. For several of the important measurements, the optimum beam energy is ~ 100 keV/amu, well below the energy of the heating beams

(1 MeV). This generates a requirement for a dedicated diagnostic neutral beam (DNB). The beam is viewed through optical labyrinths embedded in shielding blocks in the upper port above the DNB and in an equatorial port. The most important measurement is that of the He ash density. Calculations for standard conditions show that a good signal-to-noise ratio can be achieved in the core region (Figure 2.6-10).

In order to achieve sufficient beam penetration for motional Stark effect (MSE) measurements, a beam energy > 500 keV/amu is necessary. One of the heating beams is therefore utilised for this measurement. The radial electrical field (E_r) can affect the interpretation of the MSE measurements. By using two viewing directions both the E_r and the q profiles can be obtained.

N 55 GR 26 01-06-12 F1

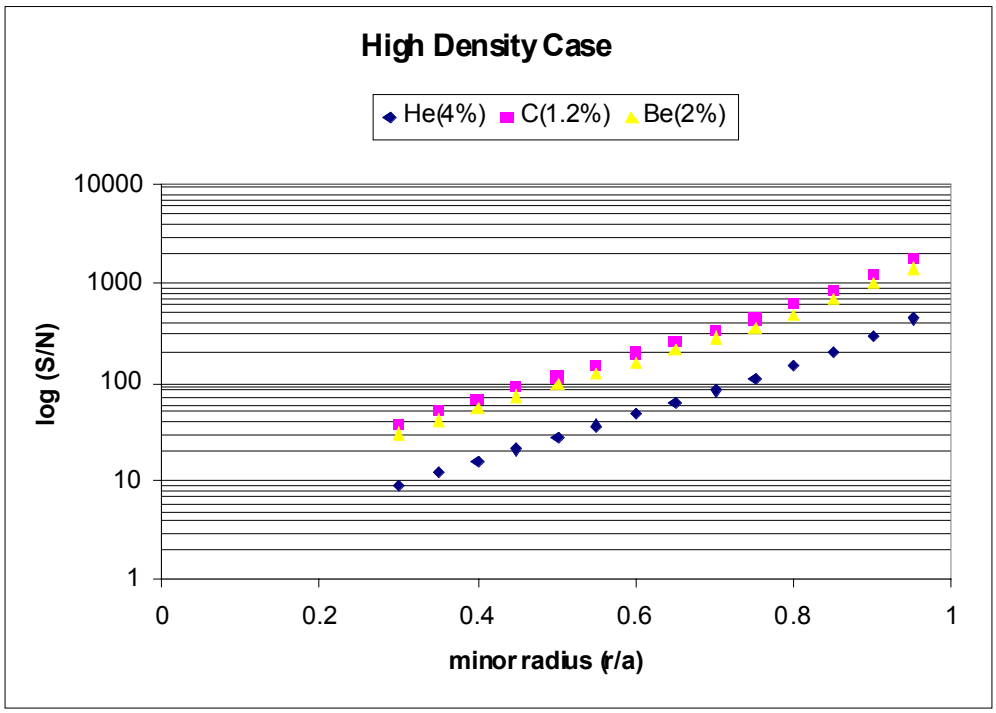

Figure 2.6-10 Signal-to-Noise Ratio at Spectral Half Maximum for the Measurement of 4% Helium, 1.2% C and 2% Be respectively versus Minor Radius for Standard ELMy H-mode Plasma Conditions

The line-averaged electron density is 1.4×10^{20} m^{-2}. The viewing geometry is a poloidal periscope with a typical path length through the plasma of about 6 m.
The integration time is 0.1 s.

The NPA is designed to measure the tritium-to-deuterium ion density ratio n_T/n_D in the plasma and to provide information on the distribution function of alpha particles in the MeV energy range. The system is directly coupled with a 200 mm tapering to 70 mm conical tube, approximately 6 m long, enveloped in a stainless steel shield in an equatorial port. The incoming neutral particles are ionized in a stripping target foil and then pass the magnetic and electric fields of the analyzing magnet and electrostatic condenser before detection. The NPA primary vacuum chamber (located outside the equatorial port 11, is enveloped in a secondary vacuum chamber together with the X-ray and VUV diagnostics.

An enhanced version of the NPA is under development. This will measure the neutral particles emitted at high energy (> 100 keV) and with this detector it is expected that under typical conditions (peaked T_i) measurements of n_T/n_D will be possible in the plasma core (Figure 2.6.11).

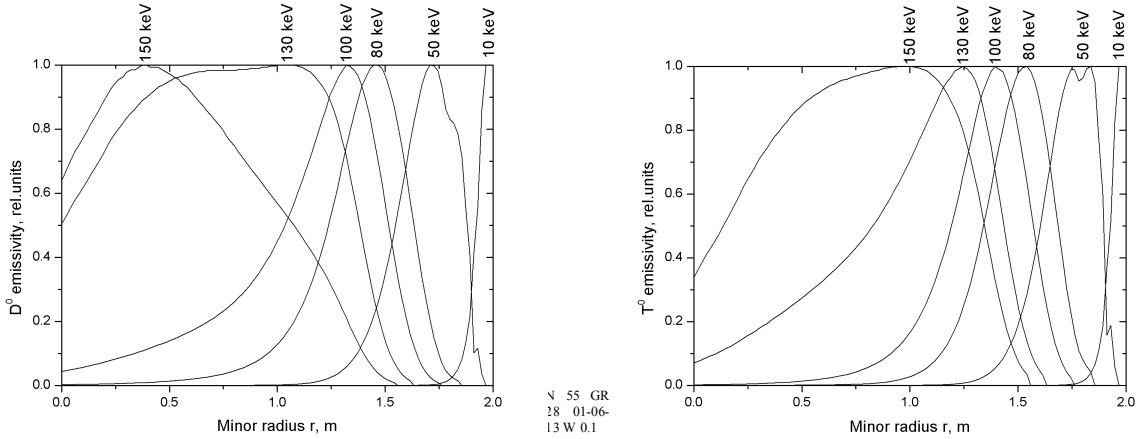

Figure 2.6-11 Calculated Emissivity Functions for D and T under Typical ITER Conditions (Peaked T_i) showing that with the Upgraded NPA Detector Measurements of n_T/n_D should be Possible in the Plasma Core Region

2.6.3.6 Microwave Systems

The principal microwave diagnostics will be a system to measure the electron cyclotron emission (ECE) from the main plasma, and three reflectometry systems for probing the main plasma, the divertor plasma, and for measuring the plasma position. Additional systems under study are an electron cyclotron absorption (ECA) system for use in the divertor region, a fast wave reflectometry system, and a microwave scattering system.

The ECE system consists of two collection antennas in an equatorial port plug, a transmission line set, and spectrometers for analyzing the emission. The antennas are staggered vertically to give access to the core for a variety of plasma heights near the nominal plasma centre height. The antennas are Gaussian beam telescopes. They are subject to surface heat loads of ~ 50 kW/m^2 during plasma operation and therefore are cooled. For each antenna, there are built-in calibration hot sources at the front end. The sources can be intermittently viewed through a shutter.

The radiation from each antenna is transmitted to the pit using wide-band corrugated waveguide with suitable mechanisms to take up machine movements. There, the signal is split into X and O mode components using a polarising beam splitter contained in a box which is an extension of the secondary vacuum. The signals are transmitted to the diagnostic hall through a secondary vacuum window and via a dedicated corrugated waveguide which is open to the pit pressure (see scheme in Figure 2.6-12). In the diagnostic hall, the signal is divided between two survey spectrometers (Michelson interferometers) and two fixed multichannel spectrometers (heterodyne radiometers).

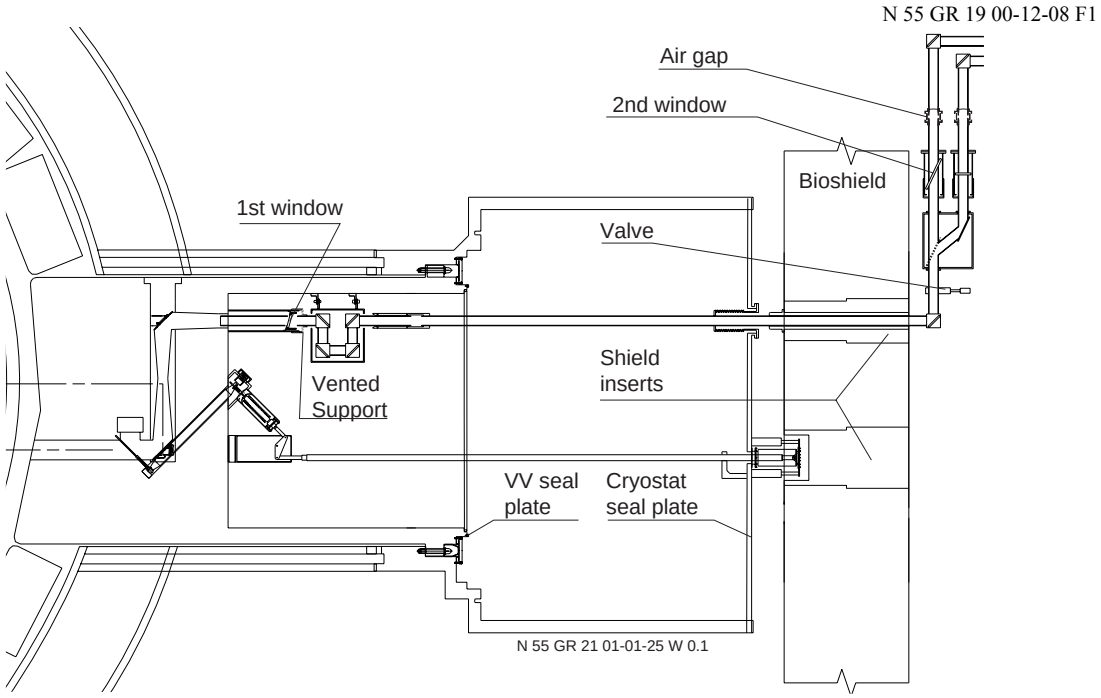

Figure 2.6-12 Schematic View of the Vacuum Boundary and Window Locations in the ECE System

The reflectometer for the main plasma provides essential information on the density profile and density perturbations due to plasma modes, to be used for machine protection, optimisation of plasma operation and for establishing performance characteristics. In addition, it supplies valuable information on plasma turbulence in all regions of the plasma. In order to provide coverage of the full profile, three sub-systems are necessary: (i) an extraordinary mode (X-mode) launch system, reflecting off the upper cutoff on the low-field side which provides measurements of the SOL profile, (ii) an ordinary (O-mode) system to provide the inboard and outboard density profile in the gradient region, and (iii) an X-mode system reflecting off the lower cutoff and launched from the high field side to provide the core profile.

The plasma position reflectometer is designed to act as a stand-by gap measurement, in order to correct or supplement the magnetics for plasma position control, during very long (>1,000 s) pulse operation, where the position deduced from the magnetic diagnostics could be subject to substantial error due to drifts. To meet the requirements for accuracy of the location of the gaps, it is necessary to measure the density profile to a density comparable to, or exceeding, the separatrix density. As for the high field side of the main reflectometer with which it shares one antenna pair, the antenna pairs (about 1.4 cm tall) are mounted in the 2 cm gap between blanket modules on the vacuum vessel and view the plasma between blanket modules. Radiation is routed to them using small bore waveguides. The waveguides are brought out through two of the upper ports to the sources and detectors installed in the pit.

The divertor reflectometer measures the profile of the electron density in the divertor region. It is the only divertor system potentially able to provide good (sub-cm) resolution across the divertor legs for selected sightlines. The waveguide set for this system will also be used for electron cyclotron absorption (ECA) and interferometric measurements.

The wide density operating space forces the use of two distinct types of measurement. In the mm-wave domain, it is reasonable, based on present technology, to plan for continuously swept reflection measurements of the density profile. In the sub-mm domain, spot measurements at a number of frequencies are planned. By combining transmission and reflection measurements, it is expected that the first few moments of the density profile (peak density, width) can be estimated.

Labyrinths in all the transmission lines reduce neutron streaming outside the vacuum vessel and bioshield. Vacuum windows of fused quartz directly bonded to metal structures, and inclined at the Brewster angle for the appropriate polarisation, provide robust, low mm-wave loss, pressure boundaries.

2.6.3.7 Plasma-Facing and Operational Diagnostics

A range of diagnostics will be installed to aid the protection and operation of the tokamak. Several diagnostics will be dedicated to monitoring the condition of the high heat flux components in the main chamber and the divertor. Other systems include Langmuir probes, pressure gauges, residual gas analyzers, and runaway monitors (hard X-ray detectors and tangential view IR systems).

The principal high heat flux protection diagnostic will be a wide-angle camera system which will give views of the in-vessel components (including parts of the divertor) in the IR and visible wavelength ranges. Combining several cameras can achieve high coverage (~ 80%) of the area of the first wall. The first element of the system is a metal mirror and the image is transmitted through a rigid labyrinth to a flattening array immediately before the vacuum window. From here the image is transmitted by lenses to ccd cameras mounted on the shielded side of the biological shield.

Dedicated divertor diagnostics include an IR thermography system for measuring the profile of the power deposition on the target plates, Langmuir probes for local measurements of plasma parameters and as attachment/detachment indicators, and fast pressure gauges, all to be installed in diagnostic divertor cassettes. These have special provisions for diagnostic sensors and provide access for optical and microwave transmission lines. IR thermography provides surface temperature measurements of both divertor target plates in a poloidal plane with good spatial and temporal resolution. Two different methods of implementation are being considered – a conventional optical periscope or a novel multiplexing scheme. In the latter case, the thermal radiation collected at different wavelengths from different points on the target plates is merged into a single beam using a shielded low-frequency grating close to the front mirror. Using this “inverse spectrometer” set-up, the number of optical elements inside the vacuum vessel is drastically reduced and only a small diameter optical window is needed.

2.6.3.8 Diagnostic Neutral Beam and CXRS

The optimum beam energy for the diagnostic neutral beam is ~ 100 keV/amu. This is considerably below the energy of the heating beams (1 MeV), so a dedicated beam is required (see section 2.5.1). To minimise the cost with high reliability, a conservative approach is proposed, i.e. to use the same negative ion source and the same maintenance tools as in the main ITER injectors. The beam would have a beam current of 15 A

(H^o atoms), a footprint of 30 x 30 cm and pulse duration 1 – 3 s every 10 – 20 s. The beam can be modulated at 5 Hz.

2.6.4 Conclusions – System Performance Assessment and Key Issues

Feasible concepts have been developed for the installation and maintenance of diagnostic sensors and components in the upper and equatorial ports, and in the divertor region. In the VV ports, diagnostic components installation faces integration issues: suitable cabling and hardware for the necessary penetrations through the VV and the cryostat have been identified. Detailed analyses are in progress to confirm the compatibility of the in-vessel diagnostics with the vessel fabrication, in-vessel cooling manifolds, blanket support system, and neutron streaming but this work is not yet complete.

At the equatorial and upper levels, promising design concepts for the special blanket shield modules are well developed and it is expected that the required viewing apertures can be provided. The effectiveness of the shielding, the stresses in the structure, and the cooling of the modules, are all being analysed. Margins have been left for design iteration when this is completed.

Guidelines have been developed for optimizing the distribution of diagnostics in the available ports. Application of the guidelines has led to a distribution of diagnostics which, it is believed, enables most of the selected systems to be accommodated. However, detailed neutron calculations have been done on only a few representative ports. It is possible that, when these have been done on all ports, further optimisation of the selection and distribution of the diagnostics will be necessary.

At the divertor level, the concept of installing diagnostic components on, and in, the divertor cassettes allows for relatively easy installation and maintenance. No insurmountable engineering problems are foreseen, but the details have yet to be developed. The major issue at this level is the survivability of the diagnostic components.

The ability of the diagnostic systems to meet their individual measurement requirements depends on factors which are in general different for each generic group of diagnostics, and so these are assessed separately.

For the magnetic diagnostics, it is expected that it will be possible to install a configuration of sensors which will meet the measurement requirements. A key issue is the lifetime of the in-vessel coils and loops. Although it is believed that necessary lifetimes can be achieved using materials examined in the supporting radiation effects R&D programme, at least one backup system should be included for key control measurements. The most vulnerable sensors are in the divertor cassette and have been designed for quick replacement. A particularly difficult area is the repair and maintenance of the in-vessel diagnostic components.

Tests with prototype coils and integrator have shown an unexplained high asymmetric voltage apparently due to the phenomenon of radiation induced electromotive force. However, a recent re-examination of the results suggests that there were problems with the long pulse integrator used in the tests, and/or other sources of voltage, for example thermoelectric effects. Latest tests with a gamma source suggest that the phenomenon will be negligible, as was expected from simple models. Further tests are planned.

No insurmountable difficulties are expected for the implementation of the neutron flux monitors and activation systems. However, the ability of the neutron cameras to provide the measurements for which they are intended, for example the total fusion power and the alpha particle source profile, is directly linked to the available access. A wide angle of view is necessary in both the radial and vertical directions. This is difficult to achieve in the vertical direction due to the limited height of the equatorial port. The view through the upper ports for the vertical camera is a new concept and some key interfaces are not yet developed.

All optical/IR, spectroscopic and microwave systems view the plasma with a mirror and a critical issue is the lifetime of this component. It is believed that solutions for the first mirrors exist for those systems that operate in situations where the dominant potentially damaging mechanism is erosion due to the bombardment of high energy neutral particles. This is likely to be the case for most systems installed in the equatorial and upper ports. However, it is possible that deposition of eroded first wall material or viewing duct material will also occur leading to a degradation of optical performance. Mitigating methods in this case would be baffles in the duct, cleaning techniques, and/or shutters in front of the mirror.

For diagnostic components in the divertor, it is probable that deposition of eroded material will be the dominant potentially damaging mechanism. At this stage, only limited information is available on this process. More investigations and developments are required before the extent of the problem is really known and the most effective countermeasures can be selected. Alternative views from the equatorial and upper ports are also under consideration.

A bolometer which is believed to be sufficiently radiation-hard for use during the initial DT operation exists, but a device with enhanced radiation hardness may be required for the anticipated end-of-life fluence level of the machine. Potentially suitable devices are being investigated in a supporting R&D programme. Dedicated development is likely to be necessary.

A design for the implementation of the spectroscopic systems which require direct coupling to the vessel vacuum (X-ray crystal, VUV spectrometers and NPA systems) has been developed for the measurements on the main plasma and it is believed that good performance will be achieved. In the divertor the VUV measurements are more difficult, and the visible and near UV capability needs to be exploited.

For the microwave measurements (ECE and reflectometry) which are made from the low-field side, no insurmountable problems are foreseen. A conceptual design exists for the installation of the antennas and waveguides for the reflectometry measurements on the high-field side and at various locations in the poloidal cross-section for the plasma position reflectometer. The details of these designs need to be developed.

The integration of waveguides through the divertor ports and in the divertor cassettes has been studied and appears feasible. However, the R&D on the associated diagnostics - electron cyclotron absorption (ECA) and divertor reflectometry - is still in an early stage, and so the information that can be obtained from these measurements is not certain.

A promising design has been developed for the wide angle visible/IR viewing diagnostic and it is expected that it will meet its measurements specifications. A key issue is the extent of surface coverage that is necessary. Presently, sufficient cameras are envisaged to give a coverage of about 80%. Measurement of the surface temperature of the divertor plates is important for operation and conventional imaging systems are difficult to implement in the restricted divertor space. The novel IR multiplexing technique has the potential to provide the required measurements but there is no experience with using such a technique on existing machines. No insurmountable difficulties are foreseen with the basic operational diagnostics such as pressure gauges and gas analyzers.

Substantial progress has been made with design of the diagnostic neutral beam and its integration onto the tokamak (see 2.5.1). However the performance of the active CXRS remains marginal in the core for reference plasma conditions, although it is much better in the edge region and at reduced densities.

In terms of the overall measurement capability, it is expected that all the measurements necessary for machine protection and basic plasma control can be made although the detailed performance has yet to be determined in many cases. There are difficulties with some of the measurements necessary for advanced control, for example the q profile measurement, but it is too early in the design process to determine what limits, if any, there will ultimately be to the operation of the tokamak. Some of the measurements which are intended solely for physics purposes also have implementation difficulties. Current design and R&D work is focussed in these areas.

Considerable further design work is required to permit the implementation of specific diagnostics on ITER. This work requires special skills and knowledge. These are, in particular, available in the fusion laboratories of the home teams, and it is expected that they will take the lead in developing individual diagnostics for ITER.

2.7 Vacuum Pumping and Fuelling

2.7.1 Fuelling

2.7.1.1 Introduction

The fuelling system comprises a main gas supply system and a number of distribution systems i.e. the gas injection system (GIS), the pellet injection system (PIS), the local gas supply system for the neutral beam (NB) injectors and diagnostic neutral beam (DNB) injector, and the fusion power shutdown system (FPSS). The GIS is used for both plasma fuelling and the delivery of gases for wall conditioning. All gases are supplied to the various delivery systems from the tritium plant. Their system diagram is shown in Figure 2.7-1.

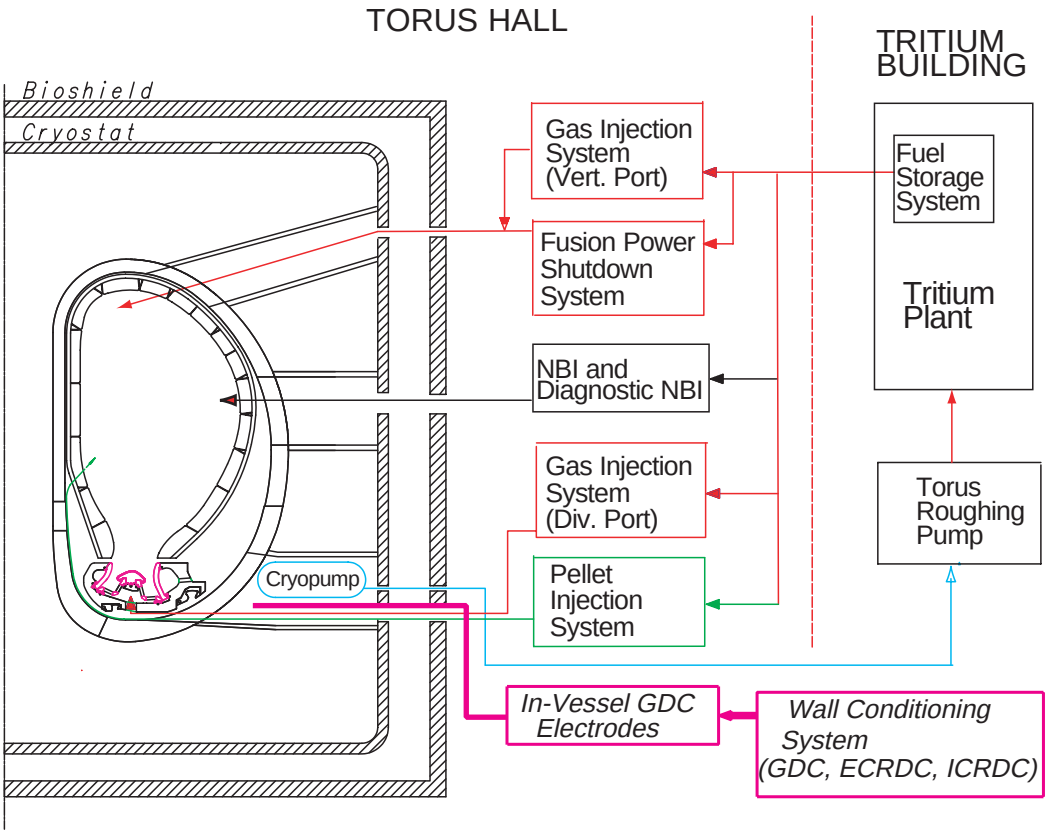

Figure 2.7-1 Fuelling System Diagram

2.7.1.2 Main Gas Supply System

This system delivers all the required gases from the tritium plant. Six lines are used for the supply of plasma fuelling gases for the GIS and PIS, two of these lines also supply gas to the FPSS, and a further two lines supply the gases for the neutralisers and beam sources of the NB and DNB injectors. A common 50 mm evacuation line is provided to allow the recovery of gases from the various local gas supply systems by the tritium plant when not required, to pump and purge lines prior to the changeover to a different gas, and to allow the checkout of delivery systems during non-operational periods. The tritium plant provides this evacuation and purge function. The gases supplied to the various systems are from a common manifold that is routed from the tritium plant to the various distribution points around the bio-shield.

The plasma fuelling supply manifold comprises a single T_2 line and three impurity gas lines (typically Ar, Ne, and He) of 7 mm diameter and two lines of 16.5 mm (typically H_2, DT, and D_2). The lines are sized to provide a peak plasma fuelling rate of 400 Pam^3/s for D_2 and DT gas and 100 Pam^3/s for all other gases at a delivery pressure of 0.12 MPa. The total tritium inventory of the supply lines at this pressure with a 50/50 DT mixture in the 16.5 mm line and T_2 in the 7 mm line is ~ 10 g.

In addition to the above, two 7 mm diameter lines are used to deliver H_2 and D_2 gas to the NB and DNB injectors at a pressure of 0.6 MPa and to provide a minimum flow rate of 120 Pam^3/s.

All the above delivery lines are routed in a common secondary confinement line, nominally 150 mm diameter, rated at 0.6 MPa. The secondary confinement line is actively monitored for both internal and external leaks.

2.7.1.3 Gas Injection System

Plasma Fuelling

During plasma operations (H, D, DT and He) the GIS will be required to provide initial gas filling prior to plasma initiation, supply gas during plasma density ramp-up, control plasma density during steady-state burn, control the scrape-off layer (SOL), and to provide divertor heat flux control by radiative cooling (seed impurities). The system will allow the injection of up to six gases simultaneously, and will typically be used for three hydrogenic species and three impurity gases (e.g., D, T, DT, Ar, Ne, and He).

To provide flexibility for physics operations (e.g., between minimum neutral density in the main chamber and a strong plasma flow in the SOL), gas injection will be provided at two poloidal elevations, the top of the plasma chamber (upper port GIS) and in the divertor private region (divertor GIS). To minimise first wall erosion by charge exchange (CX) sputtering, the gas injected will be uniformly distributed toroidally at six discrete positions at the upper port elevation. The gas injection pipes at the top of the machine will end behind the blanket modules and gas will flow through poloidal slots (~ 1 to 2 m in length) to promote uniform flow and reduce local erosion due to CX sputtering.

The upper port GIS consists of six valve boxes evenly distributed around the outside of the biological shield. The valve box, nominally 0.51 m diameter x 0.66 m high, will be shielded against the magnetic field of ~ 0.1 T present in this location. The valve arrangement inside each valve box allows independent injection of up to six fuelling gases which flow into a common manifold before discharging into the plasma chamber through a single 10 mm discharge line. A 0.12 MPa rated isolation valve is used to isolate this manifold from the line connected to the torus, and a further isolation valve connects the manifold to the pumping and flushing line which allows each gas injection line to be pumped and flushed prior to changeover to a different gas. It also permits gas puffing tests for each gas species to be conducted during commissioning without using the plasma chamber (isolation valve to torus closed, isolation valve to evacuation line open). Incorporated into the upper port GIS valve boxes is the FPSS (2.7.1.4). The gas discharge manifold is routed from the valve box through the guard pipe to the upper port where it runs along the inside of the port and terminates behind the blanket module adjacent to the port. The length of the discharge line from the valve box to an area behind the blanket module is ~ 15 m allowing a fuelling response time of ~ 500 ms to be achieved.

At the divertor level, gas is injected into the divertor private flux region under the dome and into the divertor channels. Since the recycling fluxes are much lower in this region, local erosion due to CX sputtering is not an issue, allowing the selection of only three injection (toroidal) points at this location.

With the exception of the FPSS and the routing of the injection lines, the divertor GIS is identical to that of the main chamber GIS.

Wall Conditioning Gas Delivery

The GIS is also used for the injection of all gases required for wall conditioning. During discharge cleaning the GIS is operated in conjunction with the vacuum pumping system and provides a throughput of < 50 Pam^3/s for impurity removal. If wall conditioning with reactive gases is needed (for example, for the removal of co-deposited layers) then one of the impurity lines will be used for the delivery of this gas.

2.7.1.4 Fusion Power Shutdown System (FPSS)

The capability to inject impurity gases (e.g. Ne, Ar, etc.) into the torus is needed to provide an orderly shutdown of fusion power within ~ 3s so as to limit temperature excursions of the first wall and/or blanket following an ex-vessel coolant leak. Termination of fusion power within this time can be satisfied by the release of ~ 200 Pam^3 of impurity gas into the torus. This quantity of gas is provided by six gas cylinders, each charged with 1,000 cm^3 of the selected impurity gas at 0.12 MPa. The contents of each cylinder is isolated from the torus during normal operation by a 0.2 MPa positive shut-off valve which is opened on receiving a signal from the fusion power shut-down safety control system.

The gas cylinder, shut-off valve, a charging valve and a purge valve make up an individual FPSS mechanical assembly. Each one of these six assemblies is installed in one of the upper port GIS valve boxes. The isolation valve connects the gas cylinder to the common 10 mm discharge manifold of the GIS. Each gas cylinder is charged using the charging valve that is connected to the common supply manifold that also supplies the GIS. The purge valve connects the gas cylinder to the pumping and flushing line, also common to the GIS, allowing the cylinder to be pumped and flushed prior to filling.

2.7.1.5 Pellet Injection Fuelling

The pellet injection system will provide a fuelling rate of 50 Pam^3/s with 90%T/10%D pellets and 100 Pam^3/s for other hydrogenic species in the form of pellets of 3-6 mm diameter, sized to limit density and fusion power excursions to < 10%. The maximum repetition rate varies between 7 Hz for 6 mm pellets to 50 Hz for 3 mm pellets, and is available for pulse lengths up to 3,000s. Pellet speeds of up to 0.5 km/s, from the high field side, are considered necessary to achieve a penetration beyond the ELM-affected zone (~ 15% of minor radius).

Two injectors will be installed, providing not only operational redundancy but also the flexibility to use one of the injectors to deliver impurity pellets for physics studies. Each pellet injector will be capable of steady state operation and will consist of the following major hardware:

- a centrifuge pellet injector driver, for pellet delivery;
- a screw extruder, for pellet production;
- a gas feed manifold connected to the pellet injection gas supply system;
- a pellet injector cask housing the injector assembly (~ 6 m L x 4 m H x 3 m W);
- a single flight tube connected through a divertor port to the plasma chamber;
- a diagnostic, control and data acquisition system.

The pellet injector cask is similar to the remote handling casks, and will be moved by air cushions to allow transportation to and from the hot cell for maintenance. The cask will provide secondary containment for all the equipment located inside and be rated at 0.12 MPa.

Divertor level ports 1, 7 or 13 are allocated for the pellet injectors, two for immediate use and the third fully equipped (excluding injector) for possible future use. The fuelling gas, cryogenic supplies, service vacuum, and electrical connections, are mounted on the rear of the cask allowing hands-on installation.

Each injector has a dedicated pumping system to keep the extruder, centrifuge and the flight tube under high vacuum. The guard vacuum of the injector is pumped by the guard vacuum system of the vacuum pumping system. The 5 cm diameter flight tube exits into the plasma chamber in the gap between two blanket modules on the high field side, after following the contour of the vacuum vessel below the divertor cassette. Outside the cryostat the flight tube is doubly contained, ending in a 0.12 MPa rated valve box which houses one 0.12 MPa rated isolation valve.

2.7.2 Wall Conditioning

2.7.2.1 Introduction

Wall conditioning will be used prior to plasma operation to remove water, oxygen and other impurities from the plasma-facing walls, to clean secondary surfaces not directly interacting with the plasma but potential sources of plasma impurities, to reduce hydrogenic gas recycling from the walls (desorption) during plasma start-up, and to minimise the in-vessel tritium inventory by the removal of co-deposited layers. The reference process for wall conditioning involves baking of all the in-vessel components to 240°C, glow discharge cleaning (GDC) without toroidal field using D_2 and He, and EC-DC or IC-DC (see below) with toroidal field using D_2 and He.

2.7.2.2 Baking

Baking will be undertaken following a vent of the machine to atmospheric pressure. The vacuum vessel will be heated to 200°C and the shield blanket, divertor, and other in-vessel components heated to 240°C by the primary heat transfer systems (PHTSs) of these components. Bakeout will be undertaken for a period of ~ 100 h until the total impurity pressure drops to $< 10^{-3}$ Pa. At the completion of the bakeout cycle, the in-vessel components will be cooled to an operating temperature of ~ 100°C, at which time the total pressure for impurities will be $< 10^{-7}$ Pa and $< 10^{-5}$ Pa for hydrogen isotopes.

2.7.2.3 Glow Discharge Cleaning System

Based on the experience from present day tokamaks, a current density of > 0.1 A/m^2 will be needed for the effective removal of surface contamination. Adequate spatial distribution must be provided to achieve the toroidal uniformity of the GDC current needed and, in addition, sputtering of surfaces especially near to the electrode and of the electrode itself must be avoided. For ITER, with an accessible surface area of ~ 845 m^2, six electrodes extending ~ 1.25 m beyond the plasma-facing surface have been selected, with each electrode operating at up to 30 A.

The electrodes will be supplied from a constant current ~ 1 kV DC power supply located in the vacuum pump room. The working pressure during GDC is ~ 0.1-0.5 Pa and the discharge gases will be H_2 and D_2 for impurity removal, and He for degassing of hydrogenic gases absorbed in plasma-facing components.

2.7.2.4 Electron Cyclotron Resonance Discharge Cleaning System (EC-DC)

The required EC power for wall conditioning is estimated to be about 1 MW. Varying the toroidal field between 4 and 5.7 T between successive discharges allows the EC resonance to be swept across the plasma chamber. The working pressure during the EC-DC is in the range 0.01 Pa to 0.1 Pa and the working gases that will be used are D_2, He or O_2 similar to GDC. In ITER operation, EC-DC could be used between discharges as an option.

2.7.2.5 Ion Cyclotron Resonance Discharge Cleaning System (IC-DC)

The IC H&CD system can be used for discharge cleaning and will require a power of about 1 MW. The working pressure for IC-DC is about ~ 0.01 Pa to 0.1 Pa and the working gases are He or D_2. The use of IC-DC with helium gas is a potential candidate for wall conditioning between shots to remove weakly bonded hydrogen species on plasma-facing components.

IC-DC has also been proposed as a conditioning technique in high magnetic fields where high energy neutral helium atoms with 300 eV to 400 eV energies will be created. In this energy range, the desorption yield of implanted hydrogen species in plasma-facing components is large, and higher than that provided by GDC. However, this mechanism is probably insufficient for removing the co-deposited tritium.

2.7.3 Vacuum Pumping Systems

2.7.3.1 Introduction

The vacuum pumping system comprises the major systems listed below and the system configuration is shown in Figure 2.7.3-1:

- roughing system;
- torus pumping system;
- cryostat vacuum pumping system;
- heating and current drive vacuum pumping systems;
- guard and service vacuum pumping system;
- diagnostic vacuum pumping system;
- leak detection systems.

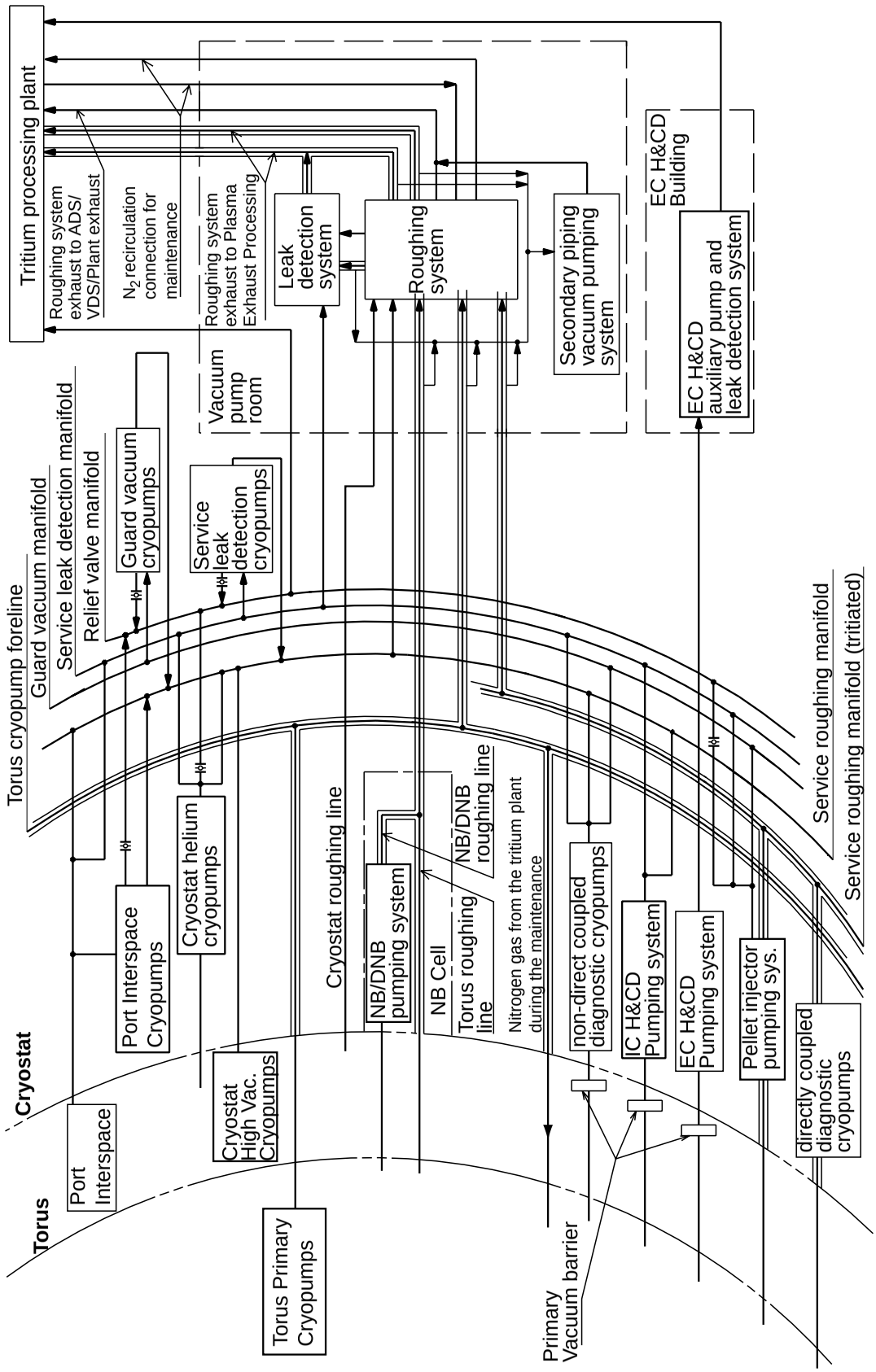

Figure 2.7.3-1 System Diagram of Vacuum Pumping System

2.7.3.2 Roughing System

The roughing system consists of a single integrated system which provides all major roughing functions. The roughing system comprises the following elements:

- four identical roughing pump sets;
- the roughing pump change-over valve box;
- the piping to the tritium plant.

The roughing system is used to evacuate equipment before crossing-over to a high vacuum pumping system, and for regeneration of cryopumps. The roughing system evacuates equipment from an initial pressure of 10^5 Pa to a base pressure of ~ 10 Pa. The primary functions of the roughing system are as follows:

- rough the torus prior to cross-over to the torus primary pumping system and evacuate each of the 10 (initially only 6 pumps may be fitted for short pulse operation) torus cryopumps during regeneration;
- rough the cryostat prior to cross-over to the cryostat high vacuum pumping system;
- evacuate the NB/DNB injectors during regeneration of their cryopanels;
- evacuate port interspaces and other miscellaneous volumes;
- regenerate guard vacuum and service leak detection cryopumps, and regenerate cryopumps for the cryostat high vacuum and cryostat helium pumping systems.

2.7.3.3 Torus Vacuum Pumping System

The torus vacuum pumping system comprises:

- the torus roughing line;
- the torus high vacuum pumping system;
- the torus venting system;
- gas re-circulation connections to the torus standby atmosphere detritiation system.

The torus high vacuum pumping system is used during plasma operations to pump the torus plasma exhaust consisting primarily of hydrogen isotopes together with helium and impurity gases. It also provides high vacuum pumping during all other phases of machine operation, including evacuation during dwell periods between plasma discharges, wall conditioning, bakeout and leak testing.

The design for the torus high vacuum pumping system is based on the use of up to ten batch-regenerating cryogenic pumps installed in the divertor level ports. These pumps are independently controlled to allow individual pumps to be regenerated, and to be shut down in the event of failure. A ring header, located at the lower magnet interface level, is used to connect the regeneration line of each cryopump to the roughing pumps. Mounted on the inlet of each pump is a valve that allows the regulation of pumping speed and also the regeneration of the pump when the inlet valve is closed. The inlet valve and its associated valve drive mechanism are an integral part of the vacuum vessel closure plug to facilitate remote maintenance.

The pumps are operated using supercritical helium at three nominal temperature levels: 4.5K for the cryopanel surfaces, 80K for the radiation shields and inlet baffle, and 300K to maintain the cryopump inlet valve below the vacuum vessel port temperature. The 80K radiation shield and inlet baffle provide an optically tight thermal radiation shield to limit heat transfer to the 4.5K panel. The 80K inlet baffle also serves to cool the incoming gas

before it reaches the 4.5K cryopanel surfaces thereby reducing the heat load to the 4.5K surfaces.

The initial phase of tokamak operations will be limited to short pulses where six pumps are needed to meet pumping speed and throughput requirements. As operations progress, and the length of the pulse is extended, four additional pumps will be added to allow on-line regeneration during the pulse, and bring the total complement of pumps to ten. In either configuration the pumps will provide a throughput of 200 Pam^3/s, and a helium pumping speed of 60 m^3/s is needed to remove the fusion products produced under the various operating scenarios envisioned.

An operational limit is imposed by the hydrogen inventory that can be accumulated in a pump before regeneration is undertaken. This is to ensure that the pressure arising following a deflagration under any plausible combination of upset conditions is limited and can be contained within the pump. A deflagration could arise following the ingress of oxygen (water, steam or air etc) into the pump in the presence of an ignition source. The pump is designed to confine an internal deflagration pressure of up to 0.5 MPa without loss of confinement.

The six cryopumps initially installed will provide an accumulated pulse time of 400 s (short pulse) before regeneration is required, which will be undertaken during the dwell. To overcome the inventory constraint for longer pulses (steady state) the complement of pumps is increased to ten, which allows on-line regeneration to be performed, while limiting inventories to acceptable levels. In this mode of operation six pumps continuously pump the plasma exhaust while four are in various stages of regeneration.

For short pulse operation each pump is regenerated during the dwell time. With a duty cycle of 0.25 this limits the complete regeneration sequence for all six pumps to 1,200 s for a 400 s pulse. Regeneration is undertaken sequentially on each pump with ~160 s being available for the process in this case. The maximum tritium inventory of all six pumps during short pulse operation when fuelled with a 50/50 DT mixture at 200 Pam^3/s is 88 g.

During longer pulses (> 400 s) a new regeneration sequence is started every 75 s (the incremental cycle time, T_{ic}) throughout the burn. The value of T_{ic} is dependent on a number of parameters which include the time needed to heat up and desorb the plasma exhaust gases (hydrogen and helium), the time needed for evacuation of the desorbed gases (sizing of the roughing system), the time needed for cool down (places demands on the cryoplant), and the accumulation of hydrogen and tritium inventories. Based on the results of earlier studies, a T_{ic} of 75 s has been selected as being a reasonable compromise for these parameters while satisfying deflagration limits. The total maximum tritium inventory stored in the cryopumps when fuelled with a 50/50 DT mixture at a fuelling rate of 200 Pam^3/s is 109 g.

The torus venting system is available to vent the torus at a variable rate and to any pressure up to atmospheric pressure. The venting gas used will typically be nitrogen delivered to the torus through the torus roughing line.

During maintenance activities, nitrogen gas will be recirculated through the standby atmosphere detritiation system in order to remove mobile tritium desorbed from the walls of the torus. Three equally spaced lines connected from the cryopump regeneration ring header

to the divertor ports are used to carry the recirculating gas from the tritium plant to the torus. The torus roughing line provides the gas return path.

2.7.3.4 Cryostat Pumping System

The cryostat is pumped from crossover pressure to high vacuum using the cryostat high vacuum pumping system. This system consists of two cryopumps located inside the cryostat suspended underneath the cryostat lid. The pumps are cooled with single phase helium supplied from the cryoplant. They incorporate plain cryopanels (no sorbent coating) to suppress helium pumping, while pumping other gases species. This allows adequate cryostat pressure to be maintained during leak testing and prior to cooldown of the magnets. The net pumping speed provided by both pumps is 500 m^3/s for water vapour and 100 m^3/s for nitrogen. Regeneration of the high vacuum cryopumps is accomplished using the service roughing manifolds. These cryopumps are required only prior to and during cool down of the magnets. The fully cooled magnets provide subsequent pumping of condensables.

For helium pumping during all phases of operation, a pumping system that provides a helium pumping speed of 5.5 m^3/s is installed external to the bioshield on a duct located at the lower magnet interface level. Prior to cooldown of the magnets, the pumps are available for pumping helium but can be valved out while helium leak testing is being conducted. However, after the magnets are cooled the helium pumping system is available to pump small helium leaks from the cryogen lines inside the cryostat. This is necessary to ensure that the total pressure within the cryostat is maintained $< 10^{-3}$ Pa to limit convective heating of the magnets and thermal shields.

2.7.3.5 Heating and Current Drive Vacuum Pumping Systems

NB Injector and Diagnostic Neutral Beam (DNB) Pumping System

Each NB injector and DNB injector module is connected to the torus via a fast shutter valve which does not provide an absolute leak tight isolation from the torus. For initial evacuation, the shutter valves are opened and the injectors are roughed down, together with the torus, using the torus roughing system. Upon reaching crossover pressure of the torus high vacuum system, the shutter valves are closed and the NB cryopanels are cooled down. During their regeneration, the shutter valve is closed and the beamline cryopanel warmed up while being pumped by the roughing system. With the shutter valve closed during regeneration, the leakage into the torus is $\sim 10^{-2}$ Pam^3/s.

IC H&CD Pumping System

The IC H&CD system includes coaxial vacuum transmission lines (VTLs) which are open at one end to the torus vacuum and closed ~ 5 m away by double sets of 0.1 MPa vacuum windows. The annular space in the VTL on the vacuum side of the windows and the annular space between the windows must be maintained below 10^{-2} Pa to avoid arcing.

A pair of vacuum pumps will pump each VTL annular vacuum space. The pumps are non-evaporable getters, which will reside in the secondary volume between the vacuum vessel closure flange and the cryostat secondary closure plate. Each VTL has two pumps, but only one pump is active at any one time, if failure of this pump occurs the second pump is energised to continue the pumping duty.

EC H&CD Pumping System

The EC H&CD system consists of corrugated waveguides that are routed from the gyrotrons up to the torus equatorial and up to the upper ports. The waveguides are open to the torus vacuum at one end. A vacuum window is located at a position corresponding to the VV closure plate and an isolation valve is located at the cryostat secondary closure plate. On the torus side of the vacuum window the waveguides are pumped by the torus. The space between the window and the isolation valve is pumped together with the waveguide run.

LH H&CD Pumping System

A dedicated pumping system is not foreseen for the LH H&CD system. The neutral gas pressure in the waveguides of the LH launcher has to be $< 10^{-4}$ Pa in order to maintain a good high RF power handling capability. The plasma provides adequate pumping at the mouth of the launcher to satisfy this requirement

2.7.3.6 Guard and Service Vacuum Pumping

Overall Configuration

The guard and service vacuum pumping systems are designed to provide common vacuum facilities for numerous users. These common services are provided by a series of vacuum manifolds that completely encircle the bioshield at the various levels of the machine with local connections provided for each individual user.

Service Roughing System

The service roughing system is used for roughdown of various volumes prior to cross-over to their respective high vacuum pumping systems and for cryopump regeneration. The vacuum system pressure varies as various pumps are regenerated and volumes evacuated.

Of the four toroidal ring manifolds installed, one of these, which is located at the equatorial level, will be dedicated to tritium service and used primarily for regenerating the cryopumps of direct coupled diagnostics (i.e. tritiated). The three remaining manifolds will be used for non-tritium service. All the ring headers are pumped by the main roughing system located in the vacuum pump room.

Guard Vacuum System

The guard vacuum system is used to provide pumping at locations where a semi-permanent vacuum is required and is designed to provide a pressure of $< 10^{-2}$ Pa. Examples of guard vacuum applications include pumping cryostat double seal interspaces and pumping of diagnostics that require vacuum but are not connected directly to the torus. The guard vacuum is also used to allow continued tokamak or cryostat operations by differential pumping of the double seal interspaces of otherwise detrimental leaks. The guard vacuum pumping systems consists of three manifolds from which piping and valves branch off to the volumes requiring guard vacuum pumping.

Port Interspace Vacuum System

The port interspaces (i.e., the port volume between the vacuum vessel flange and the cryostat flange) are maintained at ≤ 10^{-2} Pa by a dedicated cryopump for each port. The use of a dedicated cryopump on each port is dictated by the prevention of cross-contamination. Cross-contamination could occur if a leak developed in the primary vacuum boundary or a divertor cooling line. With the selected configuration, each port interspace is completely separated from the others during operations since the cryopump foreline valves remain closed.

A manifold assembly located outside the bioshield and behind each vacuum vessel port is used to connect the port interspaces to the service roughing and service leak detection ring headers. A closed-cycle cryopump is mounted on the manifold to provide medium vacuum after the port interspaces have been roughed out

Service Leak Detection System

The service leak detection system is used to provide a permanent leak detection at locations requiring routine leak checking. Examples are the cryostat double seals, port interspace volumes, the guard and service vacuum manifolds, and the cryogenic valve boxes. Almost every volume requiring hook-up to the guard and service vacuum systems will also include a connection to the service leak detection system.

The piping and pumping configuration is similar to the guard vacuum system and consists of three independent toroidal ring manifolds. The ring manifolds are initially roughed down by the service roughing system prior to entering high vacuum operation.

The pumping system is identical to that of the guard vacuum services system except that the cryopumps do not contain charcoal-coated cryo-pumping arrays so that helium will not be pumped during leak detection.

2.7.3.7 Diagnostic Pumping Systems

The diagnostic pumping systems will be designed on a case-by-case basis as the diagnostic designs are further developed. However, a common design strategy has been developed.

The diagnostics can generally be divided into two types from a vacuum system design standpoint. A window separates the non-direct coupled (non-throughput) diagnostics (type 1) from the torus, whereas the direct coupled (throughput type) diagnostics (type 2) are connected directly to the torus vacuum. The type 1 diagnostics that require vacuum will be pumped, in general, by the guard vacuum system. Closed cycle cryopumps regenerating into the tritiated service roughing system manifold will be used to pump the type 2 diagnostics.

2.7.4 Leak Detection Strategy and Methods

2.7.4.1 Introduction

Plasma performance depends to a large extent on the impurity concentration within the plasma. Water molecules entering the SOL are decomposed and ionised causing a rise in the impurity level within the plasma with oxygen being of particular concern. The formation of

< 0.1 monolayers of oxygen in a 24 hour period is one method that has been successively employed to establish an acceptable leak rate in a fusion experiment. In the case of ITER, formation of 0.1 monolayers in 24 hours equates to a leak rate of ~ 10^{-4} Pam^3/s, which compares with 10^{-6} to 10^{-5} Pam^3/s for current machines due to the size difference[1].

Data from present tokamak operation shows that normal plasma performance can be maintained with leak rates in the 10^{-7} to 10^{-5} Pam^3/s range. Within this range, some machines have also reported a gradual deterioration in leak tightness with time (age) with no noticeable deterioration in plasma performance. From the above, and the relative volume, it can be concluded that a leak rate in the 10^{-6} to 10^{-4} Pam^3/s range would not result in a deterioration of plasma performance in ITER.

Another important quantity influencing plasma operation is the impurity base pressure after baking and conditioning resulting from outgassing and possibly leaks. Given the installed pumping speed (160 m^3/s) the total impurity gas load (outgassing plus leaks) must not exceed 10^{-5} Pam^3/s. This would require both the outgassing rate and the leak rate to be in the 10^{-6} Pam^3/s range. Adding some safety margin leads to an integrated global leak rate of 10^{-7} Pam^3/s, which is therefore the one specified for ITER.

The goal of the leak detection strategy is therefore to guarantee that the leak rate inside the primary vacuum boundary, in operating conditions, shall not exceed 10^{-7} Pa m^3/s.

2.7.4.2 General Strategy

Due to the fact that ~1,000 individual components reside within the primary vacuum boundary, the sensitivity of leak checking on the component level prior to installation in the machine (e.g. in the factory or, if subassembly takes place at the ITER site, at the sub assembly level) should be ~ 3 orders of magnitude better than the global leak rate requirement, i.e. < 10^{-10} Pam^3/s. This leak rate should, however, not be interpreted as the acceptable leak rate for each component. The policy for acceptance must be "if there is a detectable leak fix it". The acceptance of "unfixable" leaks in components must be controlled on a global basis to ensure the global vacuum integrity is not jeopardised. At installation (e.g. installation welds on water cooling pipes inside the machine), a similar detection sensitivity of < 10^{-10} Pam^3/s should be achieved if possible and the same controls applied as with the acceptance of individual components. A special case in this respect is the VV, where leak checking will be performed after subassembly of 2 sectors (in the assembly hall) but the above sensitivity may not be achievable at that time. A global leak check with the fully assembled vessel prior to, as well as after, baking with all in vessel components installed will have to be done, most likely with reduced sensitivity.

To check the above strategy and the required sensitivities one can also use the experience on present day machines. The most complete source of information available on component leaks during operations has been prepared by JET, and of particular interest are the leaks that developed in welds during operations. In this category, leaks were recorded in 0.7% of 1772 installed items over a six year operational period with leaks in the 10^{-9} to 1 Pam^3/s range. This compares with 1.2% that occurred during the assembly phase. Unfortunately the concurrence of individual leaks is not reported.

[1] All leak rates reported in this section are to be intended as equivalent He at 25°C

Using the 1.2 % and the 0.7% failure rate exhibited by JET during assembly and operations, respectively, as a guidance this would indicated that a decrease in the commissioning test sensitivity from 10^{-10} to 10^{-8} Pam^3/s, after assembly is complete, would be reasonable. This relaxation would allow a more flexible selection of leak detection tools, the potential for wet leak testing, and provides shorter times for localising leaks. A similar sensitivity should be the goal for leak checking during operations or during re-commissioning after large maintenance shut downs.

In contrast to existing machines, the ITER VV is embedded in a cryostat vacuum vessel which also needs to be leak checked. In principle the same strategy and also the same tools (see below) will be applied but some special features exist. There are three phases of leak checking in the cryostat: the pump down phase, the coil cool down phase, and the operation phase with cold coils. While, during the pump down phase, air leak checking problems are similar to those inside the VV and limited hands on access may exist under certain circumstances at least for initial commissioning, the other two operation phases are somewhat different. Due to the cool down of the coils, the air leak checking system is increasingly competing with a large pump, and helium leaks may just occur due to the cool down. Therefore the leak checking system will have to use accumulation methods (charcoal coated cryo-pumps) as well as He leak checking. This is in particular true for the operation phase where the coils are at 4.5K.

Port interspaces (i.e. the space between VV flange and the cryostat flange in each port) have their own pumping systems and are also connected to the central leak checking station. Again He spray facilities (most likely to a large extend hands on) will be used to find leaks there.

Following the above general strategy, it is clear that leak testing must be a part of the initial commissioning procedure for all vacuum components, and have the following objectives:

- locate and fix all detectable leaks to the greatest extent practical, with all leak testing conducted dry, and at the highest achievable sensitivity;
- test and catalogue the global leak rates of all components at their lowest testable (sub system) level i.e. water-cooled components at the sub-circuit level (this will use a similar He leak checking strategy to that described below);
- commission, check out, and calibrate specially installed leak test equipment to confirm performance by using simulated leaks (all equipment will have to be tested and from time to time re-calibrated by using calibrated leaks - dependent on the equipment this will have to be done for the global leak checking system as well as e.g. RGAs, etc.);
- commission and check out of leak test scenarios applicable to all phases of operation by using simulated leaks (although this may not be practical in all cases it should be done for some components by introducing a calibrated leak (possibly a reservoir filled with air) and then seeing if the methods work in the machine environment);

During initial commissioning, hands-on access will be available (at least on the subcomponent level prior to installation) allowing the highest possible levels of sensitivity to be achieved. However, also a full shake-down of equipment and procedures that will be needed for all remote leak testing has to be performed at this stage. In particular, after assembly is complete, leak checking inside the VV and for the cryostat will need to be done partly by remote tools anyway due to the size and complexity of the machine.

During this initial commissioning phase, the detection sensitivity and the allowable leak limit for individual components at < 10^{-8} Pam^3/s to < 10^{-10} Pam^3/s, depending on the component, is considered both reasonable and achievable.

Further commissioning and possible improvement of the remote leak checking tools will be possible during the hydrogen operation phase. In this phase, while hands-on access will still be available, remote leak detection techniques and leak test scenarios should be applied to the maximum extent possible in preparation for later DD and DT operations.

During DD and DT operations only remote leak detection techniques and leak test scenarios can be used inside the VV and to a certain degree also inside the biological shield. It is almost certain that during commissioning the levels of sensitivity achieved hands-on (assisted), and with dry components will be higher than can be achieved using "remote" techniques and in particular with wetted components. Nevertheless, the sensitivity for leak detection for each individual component during operation should be < 10^{-8} Pam^3/s, which is most likely achievable for the majority of the components

2.7.4.3 Testing Methods and Installed Equipment

Available leak detection methods for the VV and the in-vessel components are divided into two groups: vacuum methods and methods that require venting of the machine. As already mentioned, the same or similar methods will be applied to the other vacuum systems. The main advantages of vacuum methods is that there is no need of the torus to be vented but application of these methods is restricted to identification of leaks up to ~ 10^{-1} to 1.0 Pam^3s^{-1}. The second group of methods are used at atmospheric pressure and can be applied both for small and large leaks. While, during commissioning, in some cases conventional hands-on He leak checking can be performed also for the in-vessel components, the issue for ITER operation is to find remote methods capable of detecting and localising leaking water cooling circuits inside the VV within an acceptable time frame. In the following paragraphs the main methods and the required tooling are briefly outlined.

A leak in a cooling circuit (the most likely type of leak) or generally inside the VV, will be detected by the global leak detection system. It consists of a leak checking station located in the vacuum pump room which is connected via the torus roughing line to the machine and which monitors the torus vacuum virtually constantly (checking the exhaust gas from the cryo pumps). Similarly the other vacuum systems are connected to a global leak checking station which checks the exhaust gas of all high vacuum pumps with the exception of the cryostat, which is connected via special accumulation cryopumps (long accumulation times) to its leak checking station.

Leak Localisation by Visible Spectroscopy

If a leak detected in the VV is sufficiently small to continue plasma operation or to engage a glow discharge then a spectroscopic method for leak localisation using the plasma wide angle viewing system may be used if the sensitivity of the system will be sufficient (R&D in progress).

In ITER a spectroscopic in-vessel viewing system which covers ~ 90% of the surface is foreseen, aimed at giving first hand visible observation for the machine operators during plasma operation as well as to monitor certain impurity lines by utilising band pass filters and

surface temperatures by infrared spectroscopy. Employing further remotely changeable narrow band pass filters will allow the selection of a spectroscopic emission line of neutral oxygen on this system. This will possibly enable detection of a cloud of increased oxygen light around the leaking component. Pending further R&D, it is expected that a leak of $< 10^{-6}$ Pam^3s^{-1} can be localised within a few m^2, which would thus provide a relatively fast way of pinpointing e.g. a few suspect blanket modules or divertor cassettes or port plugs, i.e the components most likely to develop leaks. This method could be used to localise leaks in a pressure range between 10^{-7} Pa and 1 Pa.

Spiking

Spiking describes a method where a chemical additive which can be easily identified by an RGA (residual gas analyser) is supplied to a sub-loop of the cooling water circuit (typically at the ppm level) in order to identify which system (e.g. divertor, blanket, VV, port plugs….) or which sub-loop of a system is leaking. This will be the reference method employed to pinpoint leaks at the system and subsystem and in some cases even at the component level. The advantage of this approach is that it does not need draining and drying of the water circuit and, depending on the number of components connected to a given sub-loop, is able to provide a rough localisation of the leak.

The major requirements for the spiking element to be added is:
- not to poison the cryopumps;
- not to cause corrosion in the water circuit;
- not to be one of the major outgassing species;
- sufficient vapour pressure at 100 C;
- sufficient solubility in water;
- sufficiently stable in a fusion environment (e.g. high level of γ radiation);
- readily removable from the vessel;
- easily removed from the cooling loop after completion of the test.

Both inert gases and water-soluble compounds are potential candidates for these additives. Inert gases meet nearly all requirements for a spiking element, but their major drawback is their very low solubility in water which will significantly reduce the level of sensitivity that can be achieved. In the case of e.g. krypton, which has one of the highest solubility levels, this is 10^{-5} mole fractions at 50˚C. Whereas the soluble mole fraction for alcohol, one of the water soluble compounds that are being considered, varies from 10^{-4} to infinitely soluble. Outstanding R&D results will determine which of the many possible spiking additives can be used and also which will provide the required sensitivity. For the successful use of spiking, either a few (< 4) different substances are needed, or a fast cleaning (reduction by > 1 order of magnitude) of the tested circuit from the spiking substance has to be possible.

Accumulation method

In the case when the concentration of the tracer element is low, accumulations of leakage gases over time will be required in order to obtain the threshold level of the leak detector and thus detectable readings. The cryopumps are used for this procedure and the regenerated gases are analyzed by the RGA, evaluating the gas content accumulated over the pumping time. The average leak rate can be calculated by dividing the gas content by the pumping time.

The accumulation method could also be used to roughly localise leak sources by using the geometrical features of the pumping system. This modified method compares the integral amount of water or spiking additive in each of the toroidally placed cryopumps during their regeneration, thus allowing the identification of the most likely toroidal quadrant where the leak is located. The sensitivity of this method is determined by the time of integration (pumping time). A model using a Monte Carlo approach was employed to evaluate the different particle fluxes into each cryopump (Figure 2.7.4-1). The difference in particle flux ranges from 3 to 4 which allows at least the quadrant to be identified and thus reduces considerably the area required to be checked.

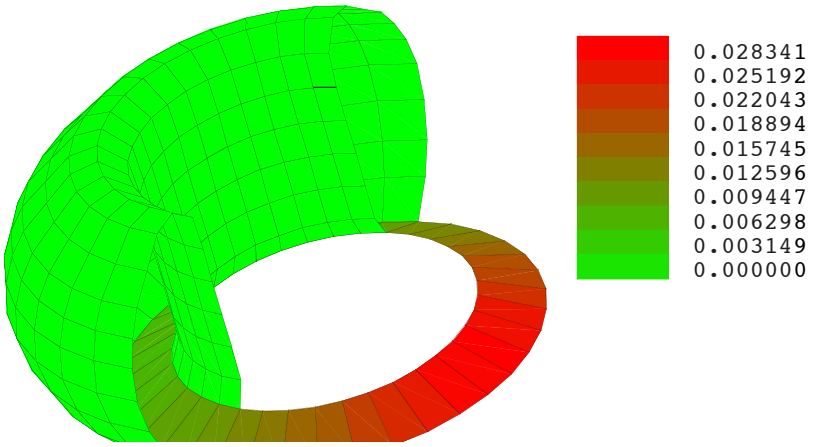

Figure 2.7.4-1 Difference in Particle Flux Ranges

Laser Methods

The existence of a substance (e.g. water or tracers) can be detected through absorption of lines in the UV to IR spectral range since these lines are specific for each material. Both water and also some tracers can be detected by measuring the degree of absorption of the substance. A laser source is particularly convenient for this purpose due to the good controllability and its narrow oscillation lines.

Laser spectroscopic methods that can be applied for gas density measurements are differential absorption lidar (DIAL) and tuneable laser absorption (TLDAS). The DIAL method is based on the comparison of the absorption of two wavelengths: one has a high absorption coefficient and the other one a low absorption coefficient. The TLDAS method is based on the detection of the varying light intensity when the light is passing through the suspected area by sweeping the laser wavelength around the absorption line of the suspected substance.

For the DIAL method, CO_2 and H_2O are considered as probe materials, in the case without and with water, respectively. For CO_2, a leak > 20 μm diameter (~10^{-5} Pam^3/s) is theoretically detectable, while a leak > 5 μm diameter can be theoretically detected for H_2O. For TLDAS, a leak >8 μm diameter (~10^{-6} Pam^3/s) can be theoretically detected with water as the target substance. Both of these methods require a view through the cloud of e.g. water escaping a leak or being reflected back and then detected by the spectrometer. Therefore it may be difficult to use these absorption methods on ITER.

Another possible laser method is laser-induced fluorescence (LIF), which is based on the detection of light emitted by the target substance after exposure to laser light. A theoretical estimate shows that leaks of > 4-6 μm diameter (~10^{-7} Pam^3/s) are detectable by the LIF method when using NO gas without cooling water in the circuits. In the case of using Rhodamine 6G (Rh6G), leaks of >1 μm diameter (~10^{-9} Pam^3/s) are theoretically detectable.

Laser methods seems to be sensitive enough for a precise localization of leaks and can be theoretically applied at the last stage of the leak checking process. However, extensive R&D is needed before this technique can be applied to ITER.

Leak Localisation by Movable Water Sensors Under Vacuum

In cases where the number of possible sub-loops is small and so the identification of a sub-loop by spiking is not sufficient to pinpoint the leak, additional tools can be employed, such as a movable RGA. This method requires the surface of the component to be scanned using a vacuum sensor such as a vacuum gauge or RGA head. Preliminary tests, using a uni-directional vacuum gauge, indicated that 10^{-6} Pam^3/s levels of leaks could be detected with about 1 m between the gauge head and the leak source. The sensitivity of the method depends strongly on the accessibility of the target components by the mounted sensor head. Reducing the distance between the head and the target is a key to improved sensitivity. Presently a "snake arm" which could carry such a sensor is under investigation. This snake arm will be deployed under vacuum from a cask which can be connected to the VV at the divertor level. Since the casks can be connected to the machine at 6 equidistant locations, such a snake arm can reach all in vessel surfaces with a lightweight tool such as an RGA or vacuum gauge.

The above methods conclude the available tools for leak checking under vacuum and without complete draining and drying of the water cooling circuits.

Leak Testing with He in Vacuum and at Atmospheric Pressure in the Vessel

This type of tool will be used to find leaks which are too large to be compatible with vacuum conditions needed for the above methods or will be used to further pinpoint the location of leaks after the above methods have been applied. In cases of large leaks, pressurising the different sub-lops and monitoring the pressure drop and the water leakage rate will allow the identification of the cooling loop responsible. Thus this approach is the equivalent to spiking for large leaks. In order to localise the leak more accurately than with any of the above methods, conventional He leak checking methods have to be applied albeit under rather severe boundary conditions (remote tools needed). To this end, the water containing loop, which has been identified by the above tools, needs to be completely drained and dried before He leak checking can commence.

There are two possible approaches for He leak checking. The first one is after draining and drying to evacuate the water pipes and to rout the exhaust gas to the leak checking station as well as to use a movable tool, e.g. the snake arm, to spray He at the suspected components inside the VV as one would do with hands-on leak checking. The second is to pressurise the water pipes with He gas and to use sniffers or hoods on each of the suspected components, again using the snake arm, and routing the exhaust gas to the leak checking station. The surplus He will be removed by the cryo-pumps (half of the pumps operate at 4.5K and mostly with closed inlet valves, and half of the pumps at > 20K, i.e. without He pumping) in the case of testing in vacuum. In the case of larger leaks, where testing has to be done in atmospheric

pressure, the MDS system will remove the surplus He. As the sensitivity of the sniffer method is in most cases 1 to 2 orders of magnitude lower than one using the leak checking station for pumping the pipes and spraying He from the plasma side, special mechanical enclosures enriching the leaking He around the most sensitive areas, such as e.g. branch pipe welds or divertor cooling pipe welds, may have to be installed. The use of specially built hoods, e.g. for the blanket modules, is not practical due to the complex and different shapes of the in vessel components.

Because of the higher sensitivity and flexibility the most attractive approach from a leak checking point of view would be to evacuate the water pipes and to use a RH tool to move a He spraying gun along the suspected components. However, even if the components are dried, there might be sufficient dirt and water vapour left in the system and also the large gate valves used to close off the cooling manifold may not be sufficiently leak tight to use this method. Therefore sniffer-based methods may have to be employed and are foreseen.

In general, the equipment selected is commercially available although some adaptation and re-configuration will be needed to use it in ITER. The equipment identified above for the various leak detection tasks will, in combination, cover the wide pressure ranges that will be needed. These tools will thus permit gross leak testing, performed in the roughing regime at high pressures, and fine leak testing performed under high vacuum conditions. In the fine leak testing range the sensitivities specified will be achievable, i.e. for the torus, individual leaks of $> 1x10^{-8}$ Pa m^3/s.

2.7.5 Procedure of Leak Localisation in ITER

In order to understand how the above described leak checking methods are applied practically in ITER, the available general leak checking methods have to be translated into a leak checking procedure for each component taking additional boundary conditions such as repair methods into account. Therefore, besides the choice of leak checking tools to find the leak, how long it will take to localise and repair is also important. The permissible localisation time must be seen in relation to the repair time, which in most cases will be several weeks or even month. Therefore the choice of leak checking tools and the adaptation of the component design to leak checking should be such that a leak can be localised within a small part of the repair time, i.e. in most cases within several days to a few weeks.

2.7.5.1 Design Features Required for Leak Checking

The design of components must take full account of the leak detection techniques that are to be implemented to ensure that a plausible overall leak test strategy is developed. For example in order to be able to perform spiking on sub-loops with only a few blanket modules connected to it, the appropriate valves and spike additive supply lines have to be implemented in the design. To this end the following provisions are foreseen in the design of the cooling manifolds. The blanket is anyway divided into 3 large cooling loops each serving ~1/3 of the blanket. In each of these loops at each machine sector 8 pairs of feed and return pipes are supplying 2 to 4 modules each. The divertor has only one cooling loop but can be divided into 3 large subsections (3 large feeder pipes). Each of these feeder pipes serves 18 cassettes from where sub-loops serving 3 cassettes each branch off. The port plugs are cooled by two separate loops, one connected to the same secondary heat exchanger as the VV (cooling the VV flange and the plug) and one connected to the blanket cooling system

(cooling the blanket section of the port plug). Each port plug / flange and blanket section of the plug is a sub-loop and means to separate them are foreseen (see below).

To be able to perform spiking, as well as draining and drying, the following additional connections and closure valves are provided. The spiking additive is added by a small pipe and valve to each of the main cooling manifolds of each of the three blanket, one divertor, the two VV and the two port plug cooling systems. The draining and drying is also performed by a system connected by 2 pipes and valves to the main cooling manifold of each heat transfer system. As the draining plant can only blow out 4 blanket modules and 3 divertor cassettes and one port plug (blanket part or flange / plug part, see 3.3) and as the drying plant can only dry 1/3 of the divertor as well as the blanket modules of one machine sector or one port plug, additional means of separating each sub-loop are implemented.

Two principle possibilities for sub-loop isolation exist, namely to use ice plugs or valves. The ice plugs would be the preferred method because they are simple, relatively cheap and have no mechanical components. However, they are unsuitable for high pressure and thus unsuitable for separating the sub-loops during the blow-out required for draining. Due to this incompatibility, valves are foreseen on each sub-loop inlet pipe. Most likely the spiking additive will not diffuse down the return pipe when the feeder is valved off, therefore no valves need to be installed on the return pipes. However, ice plugging at the returns will be needed during blow-out and may be used during other times as long as the after-heat from the components can be removed.

2.7.5.2 Leak Checking Procedures

Due to the complexity of the in-vessel components, in situ repair for e.g. blanket modules, divertor cassettes, port plugs, port limiters etc is impractical, and repair must be achieved by component replacement. As a result, there is no need to pinpoint the leak on a particular component except for the cooling connections (e.g. branch pipes) and it is thus sufficient to identify the source of the leak to the component level. In some cases it might be even quicker to replace say in the order of 2 to 4 blanket modules instead of introducing more elaborate methods to localise the leak further. More studies are needed to understand the optimal approach. For other components, e.g. the vacuum vessel, the port extensions, etc., are permanently installed, and removal for repair is not an option. There, in-situ repairs must be made and thus the leak localisation has to be more accurate, i.e. the leak has to be localised down to the cm^2 level. With these two distinct types of components, therefore, somewhat different leak checking strategies are dictated. In situ repair will be only possible with draining and drying, and subsequent He leak checking.

To better understand how leaks can be found and repaired in ITER a small leak in a blanket module is taken as an example. A leak will be detected by the global leak checking system which monitors the in-vessel vacuum. It will not be clear which component is responsible for this leak. Therefore the first step is to distinguish in which major system the leak is, i.e. in the divertor, in the blanket, in the port plugs or in the VV. This can be done by supplying the same spiking additive successively to each of the major cooling loops (3 for the blanket, 1 for divertor and limiter, 2 for the VV and 2 for the port plugs) and to monitor the response of the RGA. In case of large leaks, pressure variations will be used instead which should also identify the main cooling loop.

Leak Checking Procedure for the Blanket

Supposing that a small leak is discovered in one of the three major blanket cooling loops, the next stage will be to concentrate the testing onto this loop. There are two possibilities: either to use the spectroscopic approach or to go further with spiking on the sub-loop level. Assuming that the spectroscopic approach is not sufficiently sensitive in this case, the next spiking step is to add a different additive (from the one used to identify the main system) to subsequent sub-loops of the leaking main cooling system and to check with the global leak checking system whether this particular additive can be detected, using direct as well as accumulation techniques (if higher sensitivity is needed). Initially all sub-loops will be valved off and opened one after the other, circulating the water containing the new spiking additive at low speed. The water circulation time will be in the order of 500 s and up to the same time may be needed for checking if the additive shows up in the global leak checking system in particular if the accumulation method needs to be used. So each sub-loop will require in the order of 1000 s to be checked, i.e. ~ 30000 s or ~ one working day to check 1/3 of the blanket.

This method should finally be able to identify the leaking sub-loop and its 2 to 4 blanket modules. Again several methods could then be applied to localise the leak further, namely to use a vacuum water sensor head (RGA), which is remotely operated (by the snake arm) or to drain and dry the sub-loop and commence with He leak checking. The sensor head method will be tried first and if the leak is localised at a particular blanket module or at its branch pipe weld, leak checking is finished and repair can start. Assuming that the sensitivity of the sensor head (10^{-6} Pa·m^3/s) is not sufficient and thus He leak checking will have to be applied, after draining and drying the sub-loop it will be pressurized with He and e.g. the snake arm will be used to move the sniffer over the suspect modules. Possibly only the weld connection should be checked by this method. It is not clear if the design and the sensitivity (in terms of time delays) will be sufficient to distinguish between a leak in the water connection and in the module in all cases. But if the leak is on the FW there should be a distinguishable time delay between sniffing the front of the module and inside the hole for pipe welding and cutting access. If the leak is identified at the pipe connection, re-welding could be tried without the need to remove the module. Otherwise the module will be removed and leak testing on it will commence in the hot cell to clearly identify the leak. The repair approach will depend on the outcome of this test.

Leak Checking Procedure for the Divertor and the Limiter Port Plugs

In cases where the leak is detected in the divertor or in the limiter port plugs (which are in the same cooling loop) again spiking will be used to identify which 3 divertor cassettes or which limiter port plug is responsible. After this, the leaking sector or the limiter plug (see below), which is the one accessed by a particular RH port, is drained and dried. Then the water pipes of the three leaking modules are successively opened outside the bio-shield, a tool is inserted which can isolate the weld connecting the pipe to the cassette by a balloon from the cassette body, and He is sprayed into this area. In the second step the balloon is deflated and the He can also reach the cassette body. This approach can distinguished between a leak in the divertor itself and in the water pipe connection. If the leak is found in the water pipe connection re-welding could be tried, and if the leak is in one of the three cassettes, all cassettes from the RH port up to the leaking ones are removed and further leak checking will be performed in the hot cell.

Leak Checking Procedure for the Port Plugs and VV Flanges

The leak checking for the port plugs (including the VV flange) in the equatorial and top level, as well as for VV flanges at the divertor level, is performed as follows. Presently all port plugs have two independent cooling loops, one serving the front blanket module which is mounted on the plug, and the other one serving the plug body and the VV flange. The latter one is routed through the same secondary heat exchanger as the VV cooling loop, while the blanket part is connected to the blanket cooling system except for the two limiters where it is connected to the divertor loop. Each port plug can be separated by valves from the rest of the cooling system and, in similar fashion to blanket or divertor, successive introduction of the spiking substance by opening the valves isolating each port plug successively will allow the leaking one to be identified (blanket part or plug-flange part). Once the leaking port plug is identified it will be removed and further leak checking will be performed in the hot cell.

Leak Checking Procedure for the Port Interspaces

Leaks into the interspace vacuum will again be identified by the global leak checking system and due to the possibility to valve each interspace connection to the leak checking station off it will be possible to find the leaking port interspace without He spraying or other methods. If the leak is a water leak piping routed through the interspace is to be suspected and a spiking procedure will follow to check which cooling pipe it is. If it is an air leak then the cryostat flange is to be suspected and He spray will be used to localise the leak. This can be performed hands on assisted.

Leak Checking Procedure for the Cryostat

Leaks in the cryostat can have two major origins, one is the He cooling circuit of the coils or thermal shields, and the other one is a possible air leak. An air leak will be very difficult to detect during operation because the cold coils will act as a large cryo-pump, and even with the accumulation method the sensitivity will be low. In case an air leak is detected by the leak checking system or by an increase in the cooling requirement (icing of thermal shields), He leak checking using automated tools (for He spraying) operating between bio-shield and cryostat will be employed. In particular the areas around flanges for the ports and other personnel access holes will be checked first using the accumulation method. If no leak is found but an air leak is suspected (to much heat loss from the coils) the coils have to be warmed up to increase sensitivity and the procedure repeated. If again no leak is found the cryostat body has to be suspected and spraying has to be extended to this large region (an unlikely event).

In case of a He leak from the cooling circuit, operation will be possible for some time but a warm up of the coils and leak checking will eventually be required in particular if leaks are large or increasing. The first step is to identify the leaking circuit by using the He distribution circuit and its numerous valves. Localisation will be done by a sniffer inside the cryostat after warm up of the coils to find the leak while the cooling circuits will be pressurized with room temperature He. In situ repair will be carried out as necessary.

General Remarks

The above descriptions are related to small leaks. In case of large leaks in a water circuit, where the leak checking station cannot be used any more, one has to use pressurization and

possibly the in vessel viewing system to localize leaks. Pressurization will work similarly to the spiking approach, where all sub-loops will be closed, and the pressure will be increased in successive loops in order to find the one leaking by a pressure loss over time.

In conclusion, pending some R&D results which will confirm or define the various leak checking methods better, a leak in ITER will be detectable in a reasonable time and with the required sensitivity. Small design modifications on the in-vessel components, however, may be needed to support leak checking and/or to allow easier pinpointing of leaks. These will have to go hand-in-hand with the improved understanding of leak checking procedures and tools available in the environment envisaged for ITER.

2.8 Cryostat, Vacuum Vessel Pressure Suppression System and Thermal Shields

2.8.1 Introduction

The cryostat provides the vacuum environment to stop convective heat transfer to the superconducting magnets and cold structures, and forms the secondary confinement barrier for the radioactive inventory inside the vacuum vessel (VV).

The thermal shield system minimises heat loads transferred by thermal radiation and conduction from warm components to the components and structures that operate at 4.5K. Reduction of these heat loads by over two orders of magnitude is compulsory to ensure that the residual heat load at 4.5K can be removed by the ITER cryoplant with reasonable capacity.

The vacuum vessel pressure suppression system (VVPSS), which is here described in conjunction with the cryostat due to its considerable similarity to the cryostat vessel in its construction and assembly, and likelihood of procurement as part of the same package, limits the VV internal pressure, in the case of loss of coolant from the in-vessel components, to 0.2 MPa. This is a safety function as a large internal pressure could lead to a breach of the primary confinement barrier.

2.8.2 Engineering Description

2.8.2.1 Cryostat

The design principles of the cryostat are chiefly based on cost minimisation and functionality. The cryostat is a single wall cylindrical shell with flat top and bottom. An elevation view is shown in Figure 2.8-1. Its diameter, 28 m internal, is determined by the dimension of the largest component located inside, the poloidal field coils PF4 and PF5, with an additional small radial clearance of approximately 1 m to facilitate installation of components and for access space for in-situ repair. Its height, 24 m internal, is determined by the size of components inside as well as to provide adequate vertical space for penetrations through the cryostat cylindrical shell needed to make the interconnections with external systems.

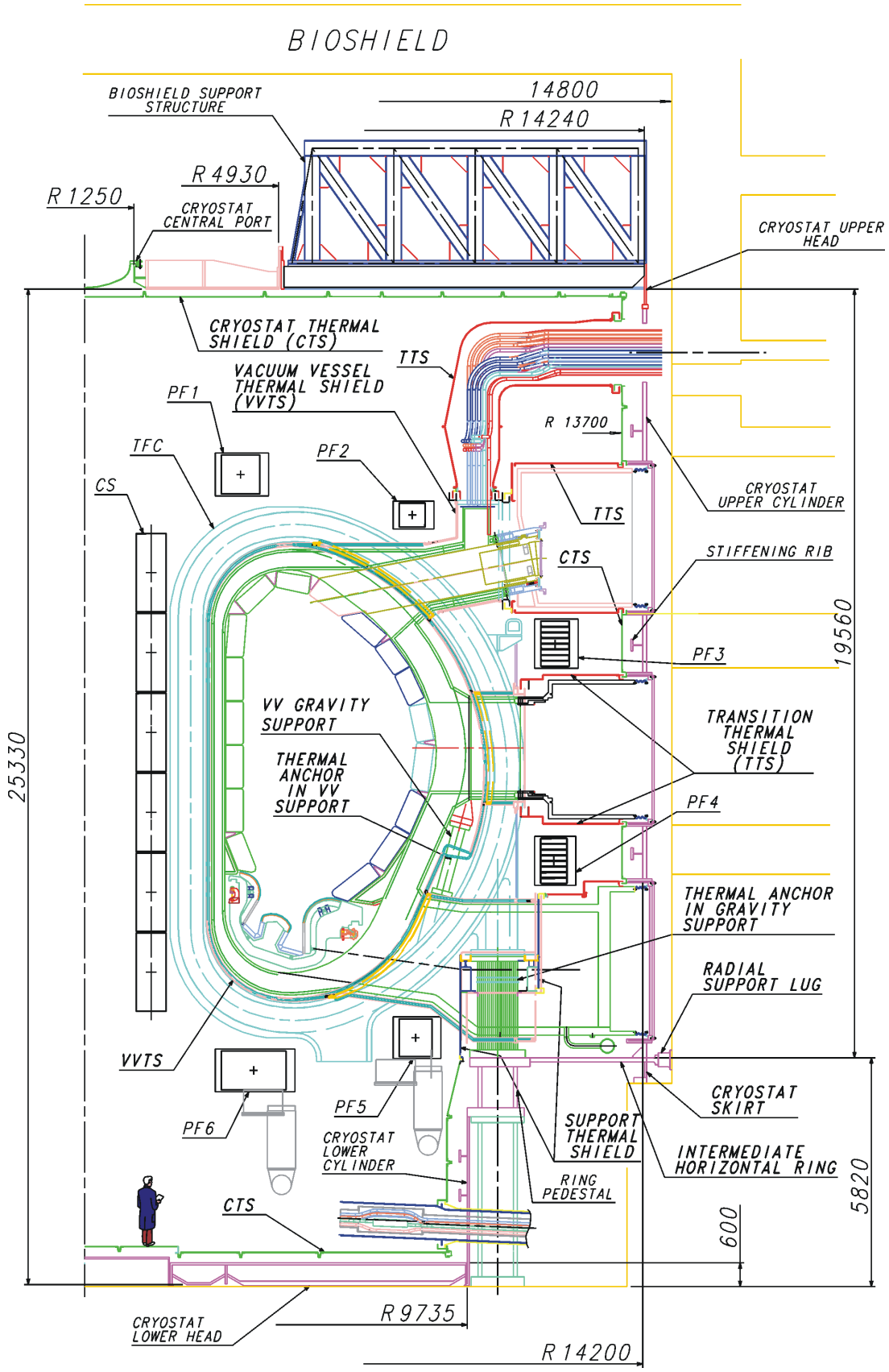

Figure 2.8-1 Elevation View of the Cryostat and the Thermal Shield System

The cryostat is supported by the building and surrounded by a concrete bioshield keeping a radial clearance of approximately 0.5 m. The bioshield extends above the cryostat and includes a 2 m thick slab above the cryostat that is supported by a truss structure connected to the upper head of the cryostat. The diameter of the cryostat cylinder below the VV is reduced in one step to 18 m. The reason is to facilitate a strong lateral connection between the machine supports and the building to minimise lateral movements during design basis loads including seismic events. The connection with the bioshield is at a position where an external floor slab provides additional lateral stiffness. A further feature of this design is that it improves the accessibility, through penetrations in the lower cylindrical part, into the cryostat for eventual repair or inspection access.

The cryostat is a fully-welded, stainless steel vessel with a large number of horizontal penetrations for access to VV ports at three levels and further horizontal penetrations for coolant pipework at upper and lower levels, and cryo and current feedlines to magnets at the upper and lower levels. Furthermore, access penetrations for manned or remote access for repair or inspection are included in the lower cryostat cylinder for horizontal entry and in the upper cryostat head for vertical entry. In the very unlikely case that large components located inside the cryostat need to be replaced, the upper bioshield slab can be removed, and the cryostat head with the support structure can be cut from the cryostat cylinder and also removed.

The total weight of the upper bioshield slab is approximately 3,500 t, which exceeds the capacity of the main cranes (~ 1,500 t). The bioshield slab is therefore designed to be installed and removed in several parts. The weight of the cryostat head, including the truss structure, is below 1,000 t and can therefore be removed by the main cranes without segmentation.

The upper head is a circular flat plate with radial stiffening ribs spaced every 10 degrees and integrated with the bioshield support which consists of a ferritic steel truss structure. The head, through which a neutron diagnostic penetrates, is connected via welding to the vertical cylindrical shell. The lower head is reinforced similarly to the upper head and also connected to the cylindrical shell by welding.

The main design loads considered are external pressure of 0.1 MPa, for normal operation under vacuum, and 0.2 MPa absolute internal pressure, for accidental events involving the simultaneous loss of helium and water from coolant lines routed through the cryostat. Considering the flat upper and lower ends, and particularly the large penetrations for port access, etc., through the cylindrical shell, the stability against buckling is the main driver for the mechanical design. The upper end is stabilised by the stiffening truss structure, whereas the bottom end is stabilised by ribs. The wall thickness of the cylindrical shell is generally 100 mm. Its upper, middle and lower regions are reinforced at the large divertor, equatorial and upper penetration openings. All of these shell portions are stiffened for external pressure by equally-spaced, circumferential and vertical stiffening rings and ribs. The minimum required thickness and distance between stiffening rings have been defined for external pressure in accordance with ASME code section VIII, division 2, article D-3. Because of its minimum intrusion into the inner space of the cryostat, T-section reinforcement profiles with adequate strength margin have been selected.

Large size ducts (~ 3 m H x ~ 2 m W) interconnect the VV ports with corresponding aligned penetrations in the cryostat vessel. Bellows are integrated in the duct to compensate for

differential movements. These bellows have a rectangular shape and are made of reinforced elastomer materials. Development of suitable bellows is the subject of R&D nearing completion. The results show that elastomer bellows designs with adequate pressure bearing capacity, leak tightness and radiation hardness are feasible. It is recognised, however, that outgassing rates of elastomer bellows could be higher than desirable for the operation of thermal shields etc. Hence, suitable metallic coatings or metallic bellows may have to be developed.

2.8.2.2 VVPSS

The VVPSS consists of a large linear tank of 46 m length and a circular cross section of 6 m diameter, containing enough room temperature water to condense the steam resulting from the most adverse in-vessel coolant leak. The tank is connected to the vacuum vessel through two of the H&CD neutral beam boxes and the diagnostic neutral beam box. From these locations, three main relief pipes are routed to the VVPSS tank, each pipe incorporating double rupture disc assemblies which constitute the vacuum boundary between the vacuum vessel and the room temperature suppression water during normal operation. As described in 2.8.3.2, numerical studies predict a total relief pipe area requirement of at least 1.0 m^2, in order to maintain the VV pressure below 0.2 MPa during a category IV coolant leak. In the design, this flow area is provided by two of the relief pipes, the third being redundant. The VVPSS includes a bypass system for the rupture discs, consisting of bypass pipes containing isolation valves, which are designed to open during a small coolant leak, when the vacuum vessel pressure is greater than atmospheric, but less than the opening pressure of the rupture discs. The VVPSS suppression tank is located at level + 19.7 m above the cryodistribution cold boxes in the tokamak building.

During an in-vessel coolant leak the VVPSS acts in concert with the VV drainage system, the former discharging evolved steam to the suppression tank where it is condensed, while the latter facilitates timely drainage of water from the VV to limit the amount of steam that the suppression tank has to condense. The VV drainage system is brought into play automatically by the opening of rupture discs in the VV drainage lines, for a large coolant leak, and by the opening of drainage valves for a small one. These drainage rupture discs and valves are part of the VVPSS. Additionally, the VVPSS is connected to the radioactive gaseous processing system, the low level waste processing system, the liquid and gas distribution system and the leak detection system. The VVPSS has provision to handle gaseous exhaust that could arise during a coolant leak in the VV (concurrent ingress of water, and cryogenic helium or inleakage air), by extracting such gaseous exhaust from the VVPSS tank ullage and transferring it to the standby vent detriation system (S-VDS)

Figure 2.8-2 shows a cross-section of the VVPSS tank at the location of a relief pipe connection. The VVPSS is designed for 0.2 MPa and constructed in ferritic steel. Among the load cases considered in the design is the sloshing effect of the fluid contained within the tank under seismic motion. The anchoring into the building structures is therefore an important feature of the design.

2.8.2.3 Thermal Shields

The thermal shields comprise the vacuum vessel thermal shield (VVTS), between the VV and the cold structures, the cryostat thermal shield (CTS), covering the walls of the cryostat

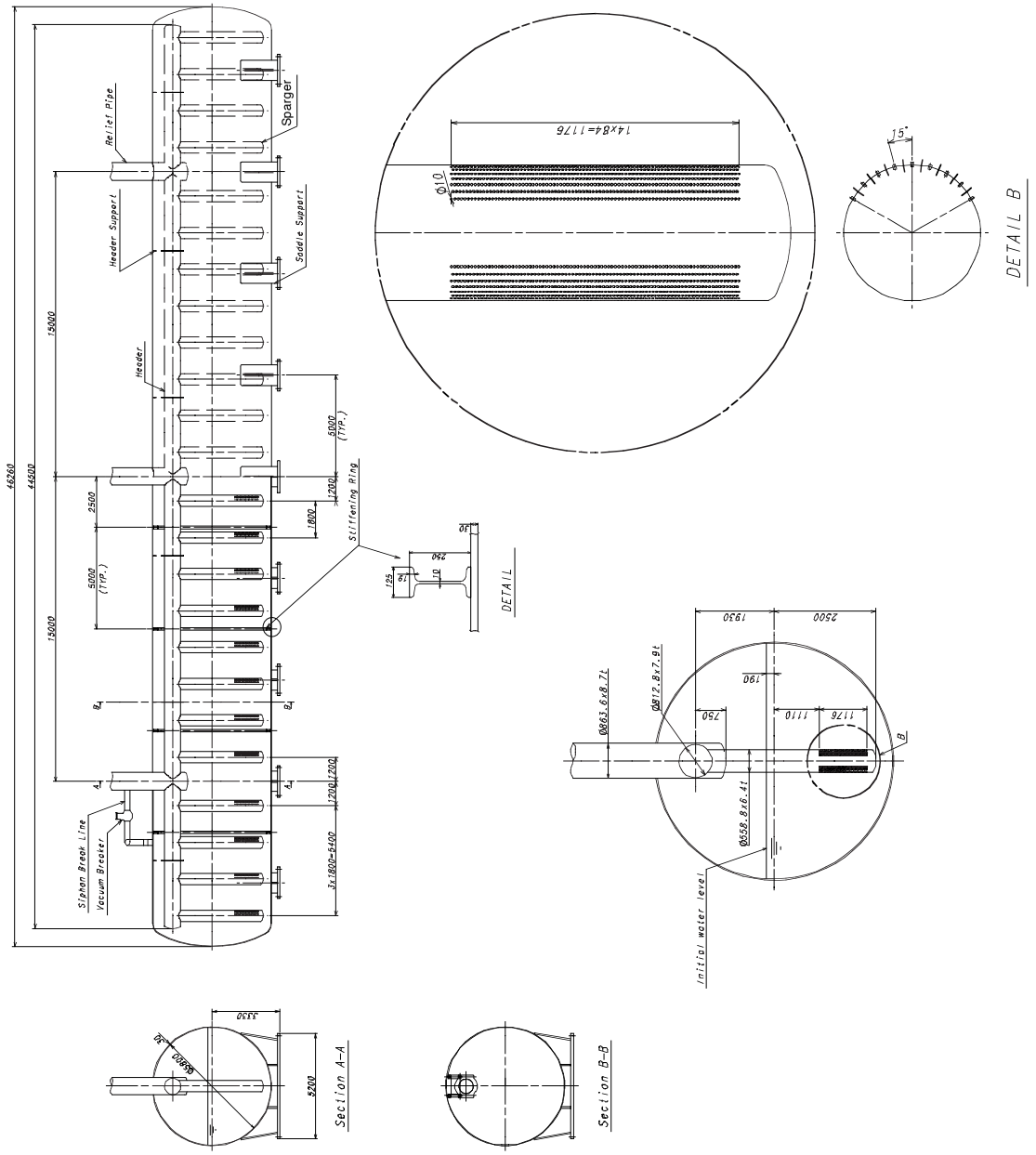

Figure 2.8-2 Vacuum Vessel Pressure Suppression Tank

(bottom, cylinder and upper head), thereby preventing direct line of sight of the room temperature walls to the cold structures, the transition thermal shields (TTS) that enclose the port connecting ducts and service lines that are routed between the cryostat walls and the VV, and the support thermal shields (STS) that enwrap the machine gravity supports. The TS system also provide the thermal anchors in the VV and machine supports to reduce the conducted heat load to the cold (4.5K) structures.

A schematic elevation view of the thermal shields is shown in Figure 2.8-1. The VVTS is self-supporting under its own gravitational and thermal loads and is attached to the toroidal field (TF) coils by inboard and outboard supports. Inboard supports are slender Inconel rods allowing radial and toroidal movements whereas, on the outboard side, plate-type supports are used to fix the radial and toroidal position of the VVTS. All other thermal shields are modular, and fixed on the warm components via low-conductivity titanium alloy supports. Direct line of sight through the gaps between individual thermal shield plates is blocked by labyrinth-type junctions connected to the plates. The same type of labyrinth interface is used at the junctions of the different thermal shields.

In all cases the thermal shields consist of stainless steel panels that are cooled by helium gas with 80K inlet temperature. The cooling lines remove the heat load intercepted from the warm surfaces. The cold magnet structures, operating around 4K, face the TS surfaces only. The conductive heat loads from all thermal shields are merely limited to small losses through their supports. To minimise the heat load received from the warm surfaces and to reduce the heat load radiated to the 4K surfaces, the thermal shield panels are covered on both sides with a thin, low emissivity layer of silver.

While the thermal shields perform no safety function, their repair or replacement, particularly of the VVTS, would involve dismantling major parts of the VV and other in-cryostat components. Therefore, the VVTS is conservatively designed to withstand without damage all design conditions envisaged for the VV, including severe plasma disruption and seismic events, while other thermal shields have the same reliability as the in-cryostat components that surround them. Two cold valve boxes controlling the supply of helium coolant, including control valves and instrumentation, are located external to the cryostat outside the bioshield and are therefore accessible for repair or maintenance.

Furthermore, loss of cooling of the thermal shields, especially the VVTS, would lead to heating up of the cold structures. Recovery times may be very long. Therefore, the cooling system for the thermal shields is designed to be fully redundant. This not only applies to the in-cryostat cryolines, but also to the cryolines between the valve boxes and the cryoplant, as well as to the relevant cryoplant components.

To enhance the mechanical robustness, it has been decided not to employ multilayer insulation or multi-foil stacks on the thermal shields as these can be easily damaged. Moreover, the very large surface areas are difficult to outgas once contaminated by moisture and other condensables. Further enhancements against failure are obtained by having electrical breaks incorporated in VVTS panel joints, reducing the electromechanical loads on the structure and the probability of arcing between components, and by having bumpers mounted on both the inside and external side of the VVTS, thereby mitigating impulse contact loads and avoiding surface and coolant pipe damage during major seismic or off-normal load events.

The space envelope is particularly critical for the VVTS. The gap between the VV and the TF coils, in which the VVTS resides, needs to be kept as small as practical. A considerable effort has therefore been expended on keeping the design of the VVTS as slim as possible. Additional clearance has to be available for component mutual thermal movements, deflections under gravitational loads, and for the VV assembly and disassembly operations. The base design of the inboard VVTS consists of a single stainless steel panel onto which are mounted two independent helium cooling lines. The outboard part of the VVTS is made of double-wall panels for strength reasons and additionally for reducing the radiant heat loads on the magnet structures without overly complicating the cooling tube layout, by interception of heat loads from panels facing the VV and keeping the panels facing the TF coils relatively cold (see Figure 2.8-3).

There are, in principle, two possibilities for the position of the CTS: close to the cold structures to minimise the 80K radiating area, or to connect the CTS to the cryostat wall, i.e., as far as possible away from the cold surfaces. The latter option has been selected for two reasons: (i) it allows good access to the outer perimeter of the PF and TF coils as well as to breaker boxes, clamps etc, and (ii) the overall contour of the CTS follows the cylindrical cryostat shell and is therefore much simpler for the attachment of individual panels than following the complex shape of the cold structures.

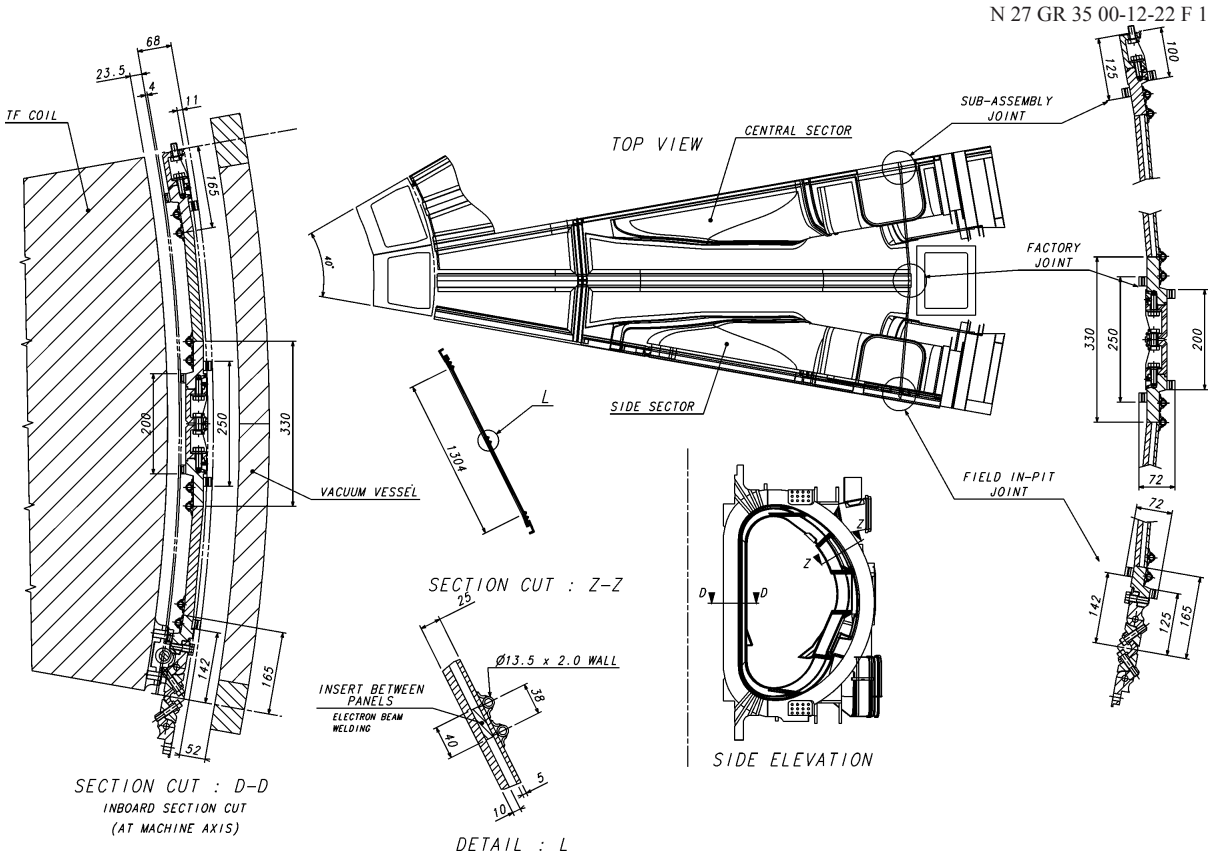

Figure 2.8-3 VVTS Top View and Cross-section Details

Major cost factors are the complexity of design, the high accuracy required, and the total surface area. Simplicity in design is conferred by keeping the basic panels of the CTS, TTS and STS flat and of rectangular shape for most areas. However, the VVTS has to closely follow the shape of the VV, for space reasons, and is therefore of a segmented, toroidal design. Its complexity, apart from the overall shape, lies in the fact that electrically insulated sector joints have to be made suitable for remote operations and even the initial hands-on installation is made more difficult as it is partly made through the narrow VV splice plate gaps. Figure 2.8-4 shows a 20° sector of the VVTS.

N 27 GR 34 00-12-22 F 1

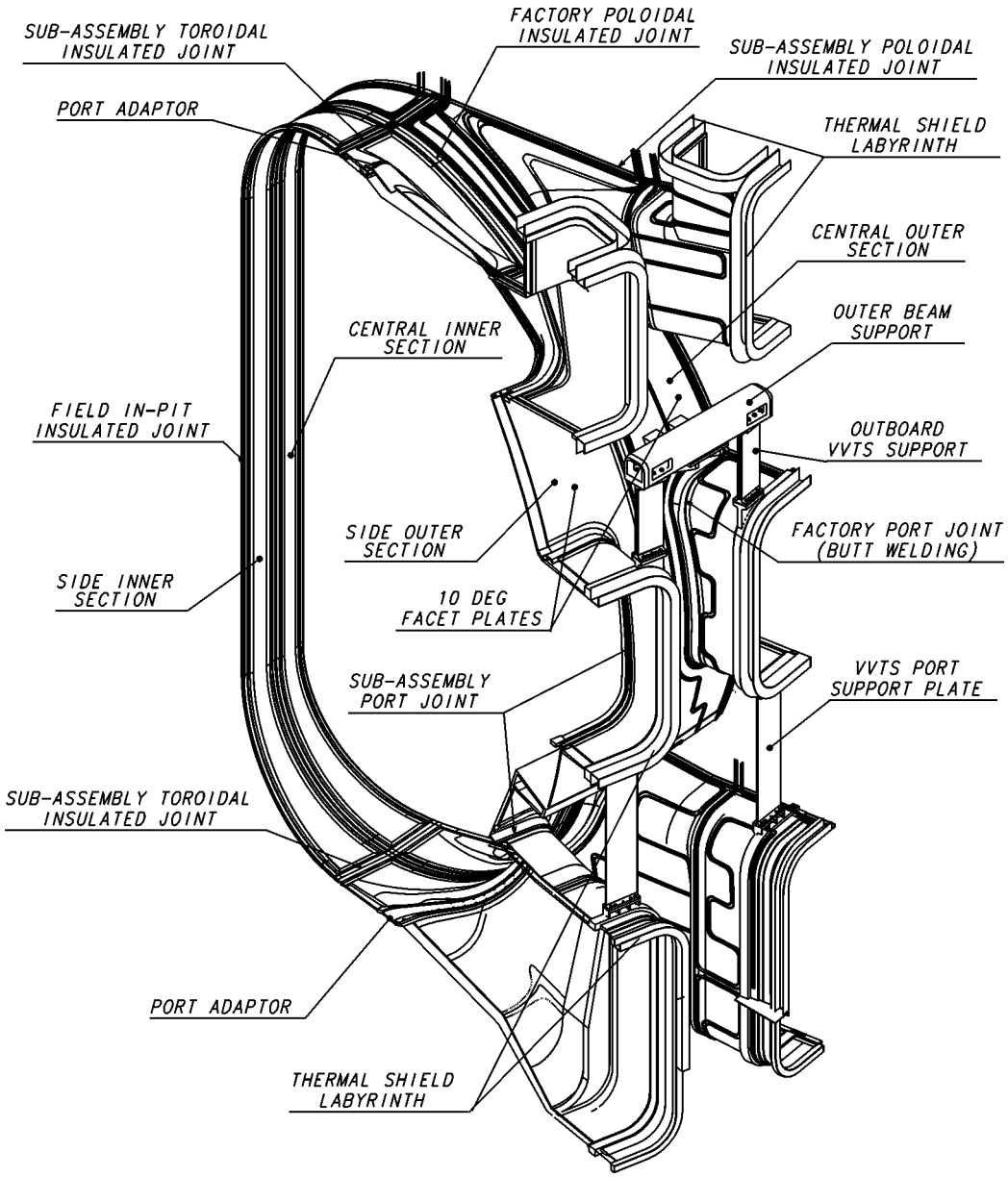

Figure 2.8-4 Vacuum Vessel Thermal Shield 20° Sector

2.8.3 Performance Analysis

2.8.3.1 Cryostat

The cryostat shell is subjected to loading conditions originating from various kinds of events each with its own probability. These are:

(i) category test: dead weight + test pressure
(ii) category I: dead weight + external pressure
(iii) category II: dead weight + external pressure + earthquake SL-1
(iv) category III: dead weight + external pressure + earthquake SL-2
(v) category IV: dead weight + helium and water ingress (internal pressure) + external pressure

Notes:

- Test pressure: The cryostat vessel is pressurised with to 0.23 MPa absolute.
- Dead weight: This loading condition arises as a consequence of gravity and the large mass of the cryostat. It is particularly significant for the top lid where a substantial amount of nuclear shielding is located.
- External pressure: This loading condition arises as a consequence of the vacuum normally present inside the cryostat. It consists of an external applied atmospheric pressure of 0.1 MPa.
- EM loads in category I: Magnet fast discharge, plasma disruption of type I, VDE of type I.
- SL-1: A seismic event of type SL-1 is classified as a likely loading condition.
- SL-2: A seismic event of type SL-2 is classified as an extremely unlikely loading condition.
- Water and helium ingress: Pressurization of the cryostat may occur as a consequence of helium expelled from the magnet into the cryostat simultaneously with hot water.

A finite element model is employed for the analysis of the cryostat vessel. Given the different layout of the smaller openings in different machine sectors, the worst location has been used for modelling, and symmetry boundary conditions have been employed. The analysis model consists of shell elements and beam elements. The analysis for category-test and category I has been performed for the upper cylinder with a model of 10°, which is a half of one cylinder sector. The cylinder and port flanges are modelled with shell elements and stiffening ribs are modelled with beam elements. All stress levels at notable locations are within the allowable stresses. A detailed analysis using a 180° model including other parts of the cryostat is in progress.

2.8.3.2 VVPSS

The bases of the required total flow area of the relief pipes and the quantity of suppression water are results obtained from numerical studies using the MELCOR code.

On the basis of the MELCOR code study, the total relief pipe flow area has to be at least 1.0 m^2. Additionally the code results predict that a drain line flow area of at least 0.1 m^2 is required to drain residual water rapidly enough to keep the final suppression water temperature to the design limit.

The pressure in the VV peaks at 0.17 MPa 10 s after the start of the coolant leak.

The suppression tank is required to have an interior volume of at least 1,200 m^3. A low pressure is maintained inside (0.23 kPa). The tank contains 650 m^3 of suppression water, which is needed to condense the steam arising from an in-vessel coolant leak while subcooled until the end of the event. The tank is subject to loading conditions originating from various kinds of events. A set of loading combinations has been established for evaluation of the VVPSS structure:

(i) category test: dead weight + test pressure
(ii) category I: dead weight + external pressure
(iii) category II: dead weight + external pressure + water head + internal pressure (small coolant leak)
(iv) category III: dead weight + external pressure + water head + earthquake SL-1
(v) category IV: dead weight + external pressure + water head + earthquake SL-2
(vi) category IV: dead weight + external pressure + water head + internal pressure (large coolant leak)

Notes:

- Test pressure: The tank is pressurized to 0.23 MPa absolute to verify its structural integrity after construction.
- Dead weight: This loading conditions arises as a consequence of gravity and the structural mass of the tank.
- Water head: The lower half of the tank volume contains water during normal operating conditions.
- External Pressure: This loading condition arises as a consequence of the near vacuum conditions normally present inside the tank. It consists of an external applied atmospheric pressure of 0.1 MPa.
- Small coolant leak: The steam pressure in the VV will trigger the active opening of bleed lines which will connect the VV to the tank. The peak pressure is less than 0.1 MPa.
- Large coolant leak: The steam pressure in the VV will trigger the passive opening of rupture disks which will connect the VV to the tank. The peak pressure is less than 0.2 MPa.

For protection against buckling due to external pressure, stiffening ribs are welded to the inside surface of the tank at longitudinally equal pitches, in accordance with the requirement of ASME code section VIII, division 2, article D-3.

2.8.3.3 Thermal Shields

The thermal shield system is subjected to a large spectrum of loading conditions and combinations thereof. The main loads are gravity, seismic, electromagnetic and thermal gradients.

Thermal Loads

Detailed analysis of the thermal loads is very important for ensuring that the thermal shields can handle the loads both locally, without excessive stress and thermal traction, and globally to interface with the cryoplant within the specified boundary conditions, and in particular, to ensure that the cryoplant can handle the heat loads in a cost-effective manner. The main results of thermal load analysis for both the plasma operation state (POS) and VV baking state (BOS), together with the associated thermal shield thermohydraulic data, are

summarised in Table 2.8-1. Pressured helium gas from the main cryogenic plant, with an inlet temperature and pressure of 80K and 1.8 MPa respectively, is used to cool the thermal shield system. The total helium mass flow rate for all thermal shields is about 6.0 kg/s.

The total pressure drops are 88 and 98 kPa for POS and BOS respectively. The total heat loads on the magnet system are about 10 kW for POS and the total pressure drop is less than the cryoplant interface limit of 100 kPa. There is potential for a significant reduction in heat load from the labyrinths by further optimising the geometry and surface emissivity. To implement this optimisation, additional refined thermal analysis is required.

Table 2.8-1 Thermal Shield Thermohydraulic Data and Results of Thermal Analysis

	VVTS	**CTS and STS**	**TTS**	**VV Thermal Anchors (TAs)**	**TAs in Machine Gravity Supports**
Surface area, m^2	2,430	2,400	2,330	-	-
Total mass, t	476	280	260	-	25.1
Inner tube diameter, mm	9.5	22.9	22.9	10	7.7
Maximum tube length, m	21	160	110	13.1	4
Inner manifold diameter, mm	70	82.5, 107	54.3	54.3	54.3
Maximum manifold length, m	206	188	216	206	216
Max. outlet He temperature, K:					
POS	100	95	95	100	85
BOS	121	95	119	110	85
Mass flow rate, kg/s	1.87	0.90	2.36	0.2	0.73
Heat loads to shield coolant*, kW:					
POS	194	70	184	19	19
BOS	392	94	386	23	19
Heat loads to cold mass (POS), kW:					
radiation from surface	0.70	0.55	0.95	-	-
radiation from labyrinths	1.55(1)	1.8(2)	0.5(3)	-	-
conductance through supports	0.4	-	-	1.7	2.3
Maximum panel temperature rise, K:					
POS	19/53(4)	-	36	-	-
BOS	32/87(4)	10	60	-	10

*Radiation on surface and captured in labyrinth, nuclear heating and conductance
(1) VVTS/TTS, VVTS/STS labyrinths
(2) CTS/TTS, CTS panels, CTS/STS labyrinths
(3) STS/TTS, TTS panels labyrinth
(4)Values for single and double plate parts of the VVTS respectively

The heat loads to cold mass (radiation from surface and labyrinths, and conductance though supports) are somewhat higher than those quoted in Table 2.1.1-4 based on earlier estimates. Design modifications are being studied to reduce these loads.

Structural Analysis

Hoop stresses induced by the coolant pressure load are very modest. The 1.8 MPa helium in the largest tubes, 23 mm ID with 2 mm walls, gives a hoop stress of only 11 MPa, and in the largest manifold is 27 MPa. Stresses in tube bends and connections are well within allowable values.

Gravity loading is not critical for the thermal shields. The maximum deflection of the VVTS and TTS/CTS panel under gravity loading is less than 2.5 mm and the stress level is within the allowable.

Eddy currents induced in the thermal shields during disruption and fast discharge cross magnetic fields and produce electromagnetic (EM) loads. Electrical breaks in the poloidal and toroidal direction for the VVTS, and judicious selection of the CTS and TTS panel dimensions, is required to mitigate these loads. Detailed finite element static EM analyses and stress analysis for the most adverse design regimes have been performed for the VVTS sector. The main results are presented in Table 2.8-2, and indicate that 36 toroidal and two poloidal breaks are sufficient from the standpoint of limiting stresses and deflections to acceptable values.

Table 2.8-2 Main Results of VVTS Stress Analysis under Dead Weight, EM Loads and TF Coil Out-Of-Plane Deformation

Regime	**Max, Displace-ment,mm**	**VVTS Shell/Flange P_L+P_b*,MPa**	**Inboard Support P_m*,MPa**	**Outboard Support P_L+P_b*,MPa**	**Port Support Plate P_L+P_b*,MPa**
Dead weight (DW)	2.5	21/78	181	38	4.2
Plasma Disruption Types I&II + DW	2.4	23/25	186	151	16
Types III Fast VDE + DW	2.8	40	192	145	26
Types III Slow VDE + DW	3.9	35/135	192	145	36
TF Coil Fast Discharge + DW	1.5	17	178	30	14
		P_L+P_b+Q*, MPa	P_L+P_b+Q*, MPa	P_L+P_b+Q*, MPa	
TF Coil Out-plane Deformation +DW	19	84	138	69	

*P_m – general membrane stress
P_L+P_b – local membrane plus bending stress
P_L+P_b+Q – primary plus secondary stress

The design of the TTS panel has been driven by the large EM loads caused by a central plasma disruption with and without simultaneous PF fast discharge. The maximum deflection is 2.6 mm and the P_{m+L} value does not exceed 190 MPa, confirming that the design of the panel is adequate. The analysis of the TTS and STS panels under EM loads during other design regimes is in progress.

The out-of-plane deflection of the TF coils (17.3 mm during each pulse) results in a bending and shear deformation of outer supports and rotation of the whole VVTS. The stresses in the VVTS for such condition (summarised in Table 2.8-3) are within the acceptable limits for static and cyclic loads.

Both detailed and global FE thermal and mechanical analysis shows that temperature gradients between the coolant tube and panels, caused by the high radiant heat flux (Figure 2.8-5), lead to considerable local stress. However, the stress is less than the $3S_m$ limit for the VVTS and for the CTS/TTS panels for both POS and BOS regimes. Thermal stress for the two-layer outboard VVTS remains to be checked. The stress level in the titanium alloy support for the CTS panels, due to temperature differences between warm components and the TS panel, reaches 500 MPa, but is still within the allowable range, while titanium alloy supports for the TTS panels require further optimisation.

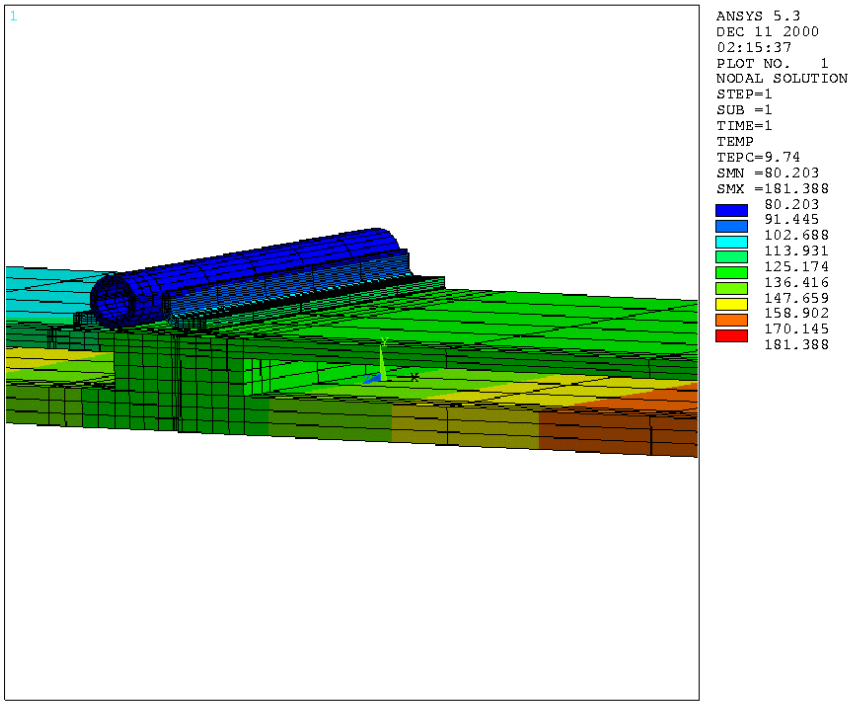

Figure 2.8-5 Temperature in VVTS Outboard Panel (K) at VV Baking, T_{He} = 80K - Detailed View

Seismic Analysis

The results of a seismic analysis of the whole tokamak, which included a model of the VVTS, are presented in Table 2.8-3. After modification of the VVTS support design, the relative displacements between the VV and the VVTS as well as the TF coils and the VVTS are quite small and the existing available gaps can accommodate them.

Table 2.8-3 Mutual Seismic Displacements between VVTS and Adjacent Components (SL-2: Ground Acceleration of 0.2 g)

Name	Radial, mm		Toroidal, mm		Vertical, mm	
	TS/TF coils	TS/VV	TS/TF coils	TS/VV	TS/TF coils	TS/VV
Equatorial inboard	6.6	1.8	6.6	1.8	1.1	2.8
Top	4.4	3.6	4.2	3.4	2.5	2.9
Bottom	8.6	3.2	8.9	3.3	2.0	3.0
Upper port upper outer corner		3.3		4.0		2.9
Lower port lower outer corner		3.2		3.3		2.7
Lower port lower inner corner		3.0		3.6		3.5

As the theoretical contact between TF coil and VVTS is restricted to the bumpers at the inboard and bottom part, it is foreseen that no damage of the VVTS panels will occur during a seismic event. Equivalent static analyses of the CTS and TTS panels have been performed, under an acceleration of 0.8 g and 1.2 g respectively. These seismic loads are considerably less than the EM loads, and does not give problems with stress and deflection in the panels and their supports.

One remaining issue is the upward force in the inboard support, which can lead to increased tensile force during the subsequent downward motion. Further optimisation of the VVTS support structure is in progress.

Seismic analysis of the whole tokamak including cryostat, VV port connecting ducts and a refined VVTS model is important for confirmation of the results presented herein, determination of mutual displacements in other critical regions, and the acceleration of the CTS and TTS support structures.

Fatigue Analysis

A detailed analysis of the fatigue lifetime of the TS under thermal and EM loads has been performed. Even when applying very conservative assumptions, there appears to be no fatigue problems with TS components. However, more detailed fatigue analysis is still required, and planned for the near future, for bolts and dowel pins.

Buckling Analysis

A selective buckling analysis has been performed for the VVTS under dead-weight and most critical EM loads. The safety factor for buckling is higher than 10, which is adequate. Additional analysis has revealed adequate buckling margin for the CTS/TTS panel supports.

Dynamic Analysis

Modal analysis of the VVTS and TS panel has shown that EM loads can lead to significant dynamic effects, and therefore a dynamic analysis of the TS is planned. Meanwhile, a

dynamic coefficient of 2 has been applied to the results of static stress analysis and a peaking factor of 1.3 for VDE regimes. The obtained stress levels and deflections are still very moderate.

Gap Analysis

At the inboard, where the space is at premium, the gap between TF coil, VVTS and VV has to be minimised. The gap analysis had to account for fabrication and installation tolerances, required assembly clearances, mutual seismic and thermal movements, which reach 85 mm in some regions, as well as deflection under all design loads. The allocated clearance between TF coil and VV is 144 mm, which allows a 30 mm gap for the insertion of a backside protection during the cutting of a VV sector. In order to meet these requirements, the VVTS inboard part has been redesigned and the assembly procedures have been checked with 3D CATIA CAD analysis of the clearances.

Thermal Shield Baking

Thermal shield baking is very important for conditioning the TS surface and attaining good cryostat vacuum quality. Thermal shield baking is presently being studied, together with related vacuum quality aspects, with a view to specifying a limit for cryodeposition of condensable gases on the thermal shields during cool-down, which could cause the degradation of the reflective surfaces. Active warm-up of the CTS and STS with acceptable pressure drop requires operation of both active and redundant loops, and additional heaters and coolers of significant size. A temperature of above 110°C can be achieved by passive radiant heating of the VVTS and TTS from the baked VV at 200°C and by simultaneous active warm-up of CTS and STS by pressured He from the cryoplant.

2.9 Remote Handling

2.9.1 Introduction

Due to neutron activation, the repair, inspection or maintenance of ITER in-vessel components has to be carried out remotely. In-vessel first wall components are subject to plasma-wall interaction leading to erosion. This requires regular or infrequent refurbishment, depending on the erosion rate. Furthermore, components may need to be replaced due to unexpected failure. This requires the introduction of common and dedicated remote handling (RH) equipment into the vacuum vessel. Components have been classified according to the frequency with which they are expected to require remote repair or replacement. RH class 1

pertains to components requiring regular planned replacement (e.g., divertor cassettes, test blanket modules). RH class 2 applies to those that are likely to require repair or replacement (e.g., blanket modules, some diagnostics). RH class 3 is for components that are not expected to require maintenance or replacement during the lifetime of ITER but would need to be replaced remotely should they fail (e.g., vacuum vessel). RH class 4 is for components that do not require remote handling. All in-cryostat components are RH class 3, although it is expected that up to the end of ITER operations short-term personnel access will be feasible within the cryostat for simple repair operations.

RH class 1 and 2 procedures and operations (i.e. those involving components in these RH classes) must be verified by tests prior to ITER construction, whereas the feasibility of RH class 3 operations should be verified by studies. Some specific aspects of RH class 3 operations may require testing for verification.

The repair of in-vessel components can, in principle, either be accomplished by in-situ operations, or by removing the component and replacing it by a new one or re-installing the component after repair or refurbishment in a hot cell. However, studies have shown that, mainly due to access problems, in-situ repair operations are generally not feasible. The ITER strategy is therefore based on the removal of components from the vacuum vessel, and remote transfer to the hot cell where the components will be either repaired by common and dedicated RH equipment, or replaced with new components. In the latter case the removed component will be prepared for waste disposal in the hot cell.

The assembly and maintenance of the ITER machine will be affected from the very beginning by the presence of in-vessel components made of, or coated with, beryllium. Because of the health hazards associated with beryllium dust, such components must be handled in a controlled way, starting from the machine assembly stage, to ensure that plant workers are not exposed to unacceptable levels of beryllium. During plasma operation, the machine components will be activated and the in-vessel components will be both activated, and contaminated with tritium. Because of the beta and gamma activation of the component bulk and surface dust (beryllium, carbon, tungsten), and because of the presence of tritium, special handling techniques during machine maintenance periods will also be required. Tritium and dust contamination must therefore be confined during the transfer of components between the machine and the hot cell. A system of sealed, remotely operated transfer casks will be used to assist the above handling operations (port handling). Docking to the machine will be directly at the vacuum vessel (VV) port flanges through openings in the cryostat and bioshield. A similar docking procedure is carried out in the hot cell where adapters are used to cater for different cask sizes. In some cases (neutral beam maintenance, others), due to the large size of the component to be handled, a special cask is provided.

When port handling is required, a cask is positioned inside the designated port cell and docked to the relevant VV port after the port cell has been cleared of all equipment. Such equipment consists mainly of pipes and cables. After this, the bioshield plug in the bioshield wall and the cryostat closure plate in the cryostat wall must also be removed (together with sections of pipes and other feedthroughs) to allow the cask docking to the VV port flange. The radiation level inside the port cell is expected to be negligible a few days after shutdown, thus allowing the above clearing operations to be done manually. However, cutting of the pipes may require the use of tools which, although in principle deployed manually, will most likely be operated remotely. During such operations, the atmosphere inside the port cell is controlled and an intermediate depression is maintained relative to the (higher) pressure in

the building (gallery) and to the (lower) pressure inside the vacuum vessel. For this purpose, sealing (and where required, shielded) doors are fitted at the port cell entrance. The subsequent operations required to remove components from within the VV port (shielding plug, diagnostic/heating systems, etc.) call for the use of a cask and of remote tools operated from within the cask. Typically, these tools perform the bolting/un-bolting of the component as well as the cutting, re-welding and inspection of a vacuum seal. Following these operations, an empty cask is remotely driven to the VV port and docked. The port component is disconnected, extracted from the port into the cask and transferred to the hot cell. Sealing of the VV port opening after removal of the component is performed by the same cask using a dedicated sealing door.

The HC is located adjacent to the reactor building and is connected by a corridor. Component transfers between different floor levels are performed by elevator.

For in-vessel RH operations, components are removed from the vacuum vessel (VV) by accessing the main ports of the VV at three levels, i.e., the upper port level, the equatorial port level and the divertor port level.

At the equatorial level there are four RH ports used for blanket maintenance. During operation, these RH shield plugs are used for diagnostics and the port limiters. Similarly to the other ports housing radio frequency heating system antennae, diagnostics, and test blanket modules, these ports are closed with water-cooled shield plugs that are vacuum seal welded to the outboard end of the port, and have the shielding equivalence of the blanket and the VV. The VV ports are connected to the cryostat wall via rectangular ducts. The corresponding openings in the cryostat shell are closed by a flange at the cryostat wall (secondary closure plate). To gain access to the VV port the cryostat closure plate as well as a bioshield plug have to be removed.

At the divertor port level, three equally spaced RH ports are used for to divertor maintenance (and again for diagnostics during operation). The remaining 15 ports at the divertor level house the in-vessel viewing system, the cryopumps, diagnostics, etc.

At the upper port level, RH class 1 and 2 operations are limited to the replacement of diagnostics and EC systems. Maintenance of these components in the upper ports is performed by the same general methods used in the horizontal ports at the equatorial level.

If a RH class 3 operation is required for components such as the VV and the TF coil (i.e. they need to be replaced) then, after removing intervening systems, a complete vessel sector with TF coils is lifted from the cryostat and moved through the building to the laydown area of the laydown, assembly and RF heating building. Here, if necessary, it is disassembled for repair.

In-cryostat repairs such as inspection and PF coil redundant turn bypassing are performed hands-on. Personnel access is through hatches located at the upper and lower parts of cryostat, and through the hatches located at the equatorial RH port ducts.

Remote handling equipment testing and maintenance, as well as cask storage, will be at the remote handling equipment test stand located at the upper area of the hot cell.

2.9.2 Divertor Maintenance

Due to the erosion of the plasma-facing components and the possible need for improving the design of critical items, the replacement of the divertor and its refurbishment in the hot cell are foreseen a few times during the ITER lifetime. To meet this requirement, a cassette-type divertor has been selected. The cassette is made in two parts: the high heat flux components, which require replacement, and the cassette body (supporting structure, shielding and manifold) which can be re-used.

2.9.2.1 System/Interface Description

The divertor handling concept has the following features.

- Divertor segmentation into 54 cassettes: the cassette width allows installation via the divertor handling ports. A segmentation of three cassettes per port gives the largest cassette size whilst providing an integral number of cassettes per port.
- Three RH ports (Figure 2.9.2-1): these are located 120° apart from each other and allow the radial transport of the cassettes in and out of the vacuum vessel, using radial rails.
- The cassette multi-functional mover (CMM, Figures 2.9.2-1, 2 and 3): the radial transport of the equipment through the RH ports is carried out by the CMM. It includes a radial tractor, together with a set of specific end-effectors, to grip, push, pull, position in a cantilevered manner, and lock/assemble the following equipment using a manipulator arm (MAM):
  - the primary closure plates (closing the RH ports);
  - the diagnostics racks (inside the RH ports);
  - the central cassettes (in front of the RH ports);
  - the second cassettes (located to the left hand-side of the central cassettes);
  - the cassette toroidal movers;
  - the standard cassettes (all other cassettes).

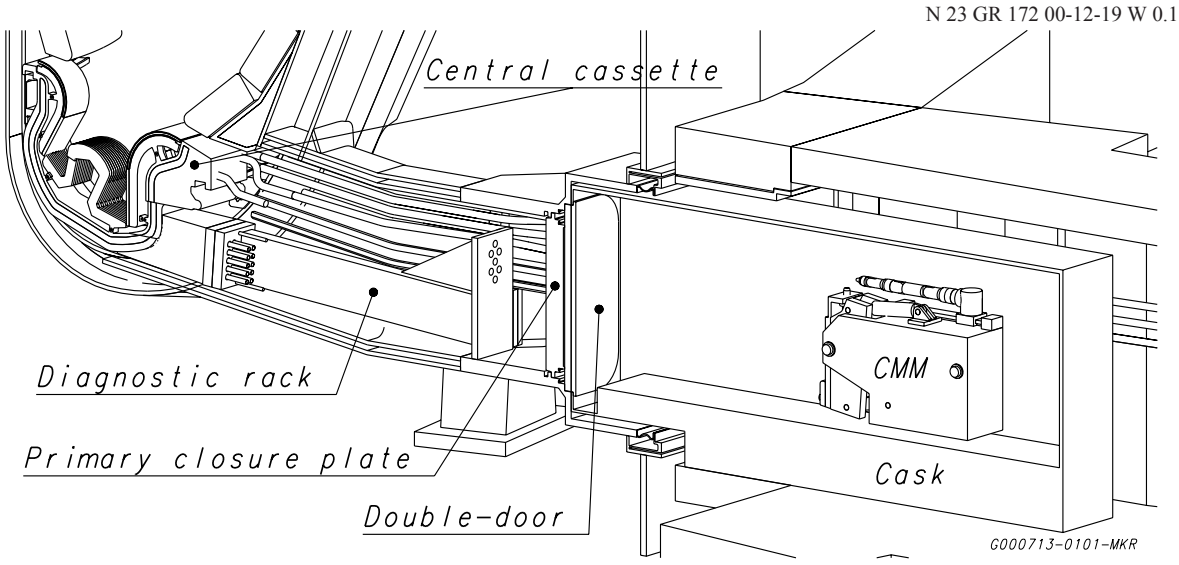

Figure 2.9.2-1 Divertor RH Port

N 23 GR 173 00-12-19 W 0.1

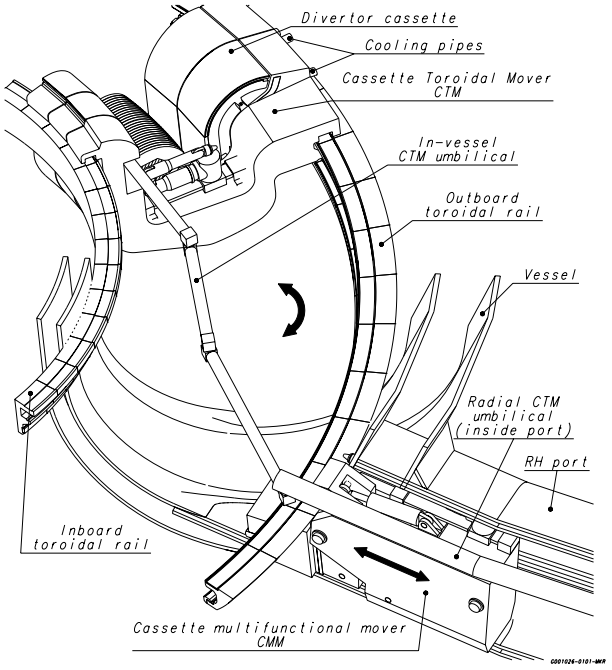

Figure 2.9.2-2 In-Vessel Cassette Handling

N 23 GR 174 00-12-19 W 0.1

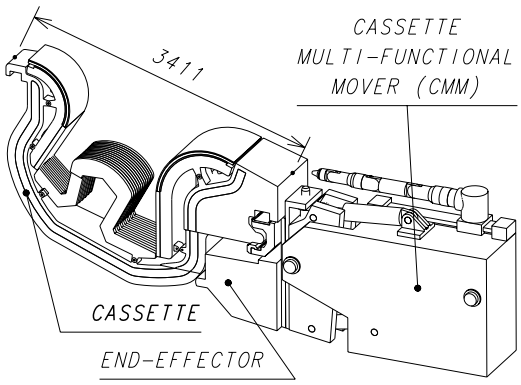

Figure 2.9.2-3 Cassette Cantilevering from the Cassette Multi-Functional Mover

- Two concentric in-vessel toroidal rails (Figure 2.9.2-2): in combination with the inboard and outboard cassette supports, these align the cassettes (maximum step between 2 adjacent cassettes: 4 mm) and sustain the current-induced loads during operation. These two rails are also used to guide the cassette toroidal mover (CTM, see below). While the inboard rail is continuous, the outboard one is interrupted in front of the RH port to allow access. The CMM end-effector includes a rail segment providing the outboard rail with a continuous path for toroidal handling.
- The CTM (Figure 2.9.2-2): this performs the in-vessel toroidal cassette handling operations, the final radial and toroidal positioning, the locking and unlocking of the supports using a manipulator arm (MAM), and the inspection of the assembled cassettes.
- Pipe tools: each cassette is fed by water via curved pipes routed inside the 18 divertor ports. Pipe tools are used for cutting these pipes close to the cassette body prior to cassette removal, and later for welding and inspecting them after installation of the refurbished cassettes.
- Transport casks and double door (Figure 2.9.2-1): divertor cassettes, movers, and diagnostics equipment are transported between hot cell and vessel inside confined and non-shielded casks guided by an air-cushion platform inside the building. Each cask is equipped with a double door to dock at the RH and hot cell ports.
- Control system: this allows the operations of RH equipment from either workstations in the RH control room, or hands-on, using local programmable handheld control panels. Moreover, it allows parallel operation, in RH conditions, of 3 RH ports and 2 hot cell ports, the related RH equipment and two transport casks, using manual, semi-automatic, automatic and computer-assisted tele-operation (CAT) modes.

2.9.2.2 Maintenance Scenario

The divertor removal is in 3 stages (its installation is the reverse) as shown in Table 2.9.2-1.

Table 2.9.2-1 Divertor Removal

Stage 1: Transfer to maintenance configuration. This involves mainly hands-on assisted operations to prepare the RH port pit and inter-space		
Step	**Operations to perform**	**Equipment involved. Hands-on versus full RH operation(s)**
1	The maintenance operations start 2 weeks after shutdown	• Process and circuits
2	Measurement of the dose rates inside the pit prior to access	• Dose measurement package • Hands-on operation
3	Removal and storage of the diagnostics casks from the front of the RH port	• Handling equipment • Hands-on assisted
4	Cassette drainage and drying	• Involvement of DIV/LIM PHTS
5	Cutting of the 2 primary closure plate cooling pipes at each RH port	• Glove-box and pipe tools • Hands-on assisted
6	Installation of the 2 radial umbilicals of the cassette toroidal mover (CTM)	• Glove-box and RH pipe tools • Hands-on assisted
7	Cutting of the divertor cooling pipes at the 3 RH ports (6 pipes /RH port)	• Glove-box and RH pipe tools • Hands-on assisted
8	Removal and storage of the bio-shield plug	• Bio-shield plug handling tool • Hands-on assisted
9	Removal and storage of the secondary closure plate	• Secondary closure plate handling tools • Hands-on assisted
10	Removal of the primary closure plate sealed cover	• Tool box • Hands-on assisted
Stage 2: RH port preparation. This involves mainly RH operations inside the RH port (primary closure plate, diagnostics rack, central and second cassette handling)		
Step	**Operations to perform**	**Equipment involved. Hands-on versus full RH operation(s)**
11	Removal and storage of the primary closure plate in the hot cell	• Cask, CMM & MAM • RH operation
12	Removal and storage of the diagnostics rack in the hot cell	• Cask, CMM & MAM • RH operation
13	Removal and storage of the central cassette in the hot cell	• Cask, CMM & MAM • RH operation
14	Disconnection of the second cassette	• Cask, CMM & MAM • RH operation
15	Removal and storage of the second cassette in the hot cell	• Cask, CMM & MAM • RH operation

Table 2.9.2-1 Divertor Removal (cont'd)

Stage 3: In-vessel handling. This involves mainly RH operations inside the vessel (standard cassettes). Only the cooling pipes are handled in a hands-on assisted manner using RH pipe bore tools confined inside a glove-box		
Step	**Operations to perform**	**Equipment involved. Hands-on versus full RH operation(s)**
16	Cutting of the 2 pipes of the 15 standard cassettes	• Glove-box and RH pipe tools • Hands-on assisted
17	Installation of the right hand side (RHS) CTM inside the vessel	• Cask, CMM, RHS CTM, MAM • RH operation
18	Removal of the 9 next cassettes using RHS CTM	• Cask, CMM, RHS CTM, MAM • RH operation
19	Removal of the RHS CTM from the vessel	• Cask, CMM, RHS CTM, MAM • RH operation
20	Installation of the LHS CTM inside the vessel	• Cask, CMM, LHS CTM, MAM • RH operation
21	Removal of the 7 next cassettes using the LHS CTM	• Cask, CMM, LHS CTM, MAM • RH operation
22	Possibly cleaning (dust removal) of the vessel bottom	• RH cleaning equipment • RH operation

2.9.2.3 Rescue Scenario

A detailed failure mode effect analysis of the movers was performed by the EU-HT. The analysis proposes solutions for the rescue of faulty RH divertor equipment from the vessel. Besides the failure of the RH equipment, faulty in-vessel components might also have to be replaced as shown in Table 2.9.2-2.

Table 2.9.2-2 Divertor-related In-vessel Components for Possible Replacement

RH class 1 components	RH class 3 components
Divertor cassettes and supports	Rail hard-cover plates and bodies
Diagnostics equipment racks	Cooling and gas injection circuits
Primary closure plates	Cable conduits and RH connectors
Radial rail segments	Primary closure plate flange

2.9.2.4 Maintenance Time Estimation

A preliminary time assessment of in-vessel handling shows that it will take approximately 2 months (7 working days a week, 2 (8-hour) working shifts a day and a cask transport (8 hour) shift a day) to replace the 18 cassettes related to a given RH port. As a consequence of this, and managing the 3 RH ports in series, the full divertor replacement would take about 6 months, thus meeting the nominal time requirement. However, in order to account for final inspections (leak testing etc.), and provision for off-normal events (contingencies of the order of 25% needed), it is recommended to adopt some, although limited, parallel work at the 3 RH ports. This can be easily achieved using 2 transport casks and 2 hot cell ports. A logistics study was performed by the EU HT. It assessed the impact of parameters such as cask number, divertor ports number, hot cell ports number, refurbishment workstations number, etc on the overall divertor replacement time. The study indicates that divertor

cassette refurbishment inside the hot cell can be done both on-line (i.e. during the shutdown period) or off-line (i.e. after complete replacement of the old set of cassettes with a new one). In both cases the 6 months maximum shutdown time can be met, although the cassette storage requirement inside the hot cell vary depending on the refurbishment approach which is selected.

The replacement of a single faulty cassette should not take more than 2 months (as required), even in the worst case where it is located in the most inaccessible position.

2.9.2.5 Assessment/Future Work

The principle feasibility of the overall RH procedure that involves the replacement of divertor cassettes by toroidal and radial transporters has already been demonstrated for the 1998 ITER design in a test stand using full-scale prototype equipment within the L7 R&D Project. However, the modified divertor cassette design for the current ITER design requires the adoption of somewhat different handling techniques for the cassettes.

Design tasks are currently being performed on the movers, cassette supports and curved pipe tools which are the most critical items of the divertor maintenance. Nevertheless, significant development/design is still to be done to validate the new scheme, aiming at construction preparation, as listed below.

- Further design activities, including:
  - design task result implementation: movers, supports/rails, other interfaces;
  - cooling circuits: pipe diameter standardisation (2.5 inch), feed-throughs, supports, DIV/LIM PHTS interfaces, full RH process and tools, glove boxes, etc.;
  - divertor port integration: pipes, rails, umbilicals, diagnostics, shielding;
  - sizing rails, pipes, etc.;
  - first installation: procedure, tools, etc.;
  - rescue scenarios: RH equipment and in-vessel equipment.

- Testing activities, including:
  - cassette handling: CMM, CTM, umbilicals, supports/rails, other interfaces;
  - cooling pipe handing;
  - manipulator arm and tools;
  - diagnostics handling: components, interfaces, connectors;
  - radiation hard integrated equipment;
  - basic technology;
  - rescue scenarios: RH equipment and in-vessel equipment.

2.9.3 Blanket Maintenance

The shield blanket is composed of 421 modules (see 2.3). Replacement of some shield blanket modules is likely to be required a few times during the lifetime of ITER due to local erosion or defects, including leaks, and to change the shielding blanket to a breeding blanket (if decided upon).

Each blanket module is equipped with ten remote handling access holes through its plasma-facing first wall (for blanket option A - see 2.3). Four allow access for the tool that bolts and

unbolts the flexible supports, four give access for welding, cutting and inspection of the cooling pipes and for bolting and unbolting of the electrical straps, and two are used to grasp the module and hold it securely during handing into and out of the VV.

As the cost of blanket modules is, to a considerable extent, dependent on the number of modules that are required, the design of the blanket RH system has been optimised with respect to size and weight of modules that can be handled. The result is a system that can handle large modules in terms of weight and size, just leaving sufficient space for manipulations inside the VV and for transfer through the ports.

2.9.3.1 System/Interface Description

The blanket handling concept has the following features.

- One or more in-vessel transporters (IVTs), with manipulator arm and various attachments, is mounted on a monorail deployed inside the vessel from a dedicated port-mounted cask.
- Module transporters, mounted at intermediate ports, are used to load modules into casks, thereby enabling the modules to be shuttled to and from the hot cell. The overall arrangement is shown in Figure 2.9.3-1.
- Each IVT consists of a vehicle manipulator, a segmented rail, rail-deploying equipment, a rail support device, and cable-handling equipment (see Figure 2.9.3-2). The IVT is used for general in-vessel maintenance tasks, and with a variety of end–effectors, depending on the task to be performed.
- The full circumferential rail is made up of two semi-circular rails. For robustness, neither sensors nor actuators are installed on the rails. An important feature of the rail system is that it can function in a reduced configuration. The rail system can be installed and used in the following configurations: 80/100°, 180° and 360° (see below). The rails are held in position by support devices, which are used to install the links that make up the rails.
- Since the vehicle/manipulator moves up to 180° on the rail as it travels around the VV, a trailing, long complex cable with many conductors has to be fed without jamming. To do this, the cable handling equipment is installed in an intermediate cask between the VV port and the RH cask, after the vehicle manipulator and rail are installed in the VV.
- The module receiver portion of the module transporter is moved radially into the VV and the component is transferred to it from the IVT manipulator. Subsequently, the module transporter is moved radially outward and the in-vessel component is transferred into a RH cask docked to the port. The RH cask then transports the component to the hot cell. Figure 2.9.3-3 shows the blanket module transfer to the receiver at the VV port. The module receiver pallet can be retracted from the transporter and exchanged inside the RH cask by an in-cask storage rack system.

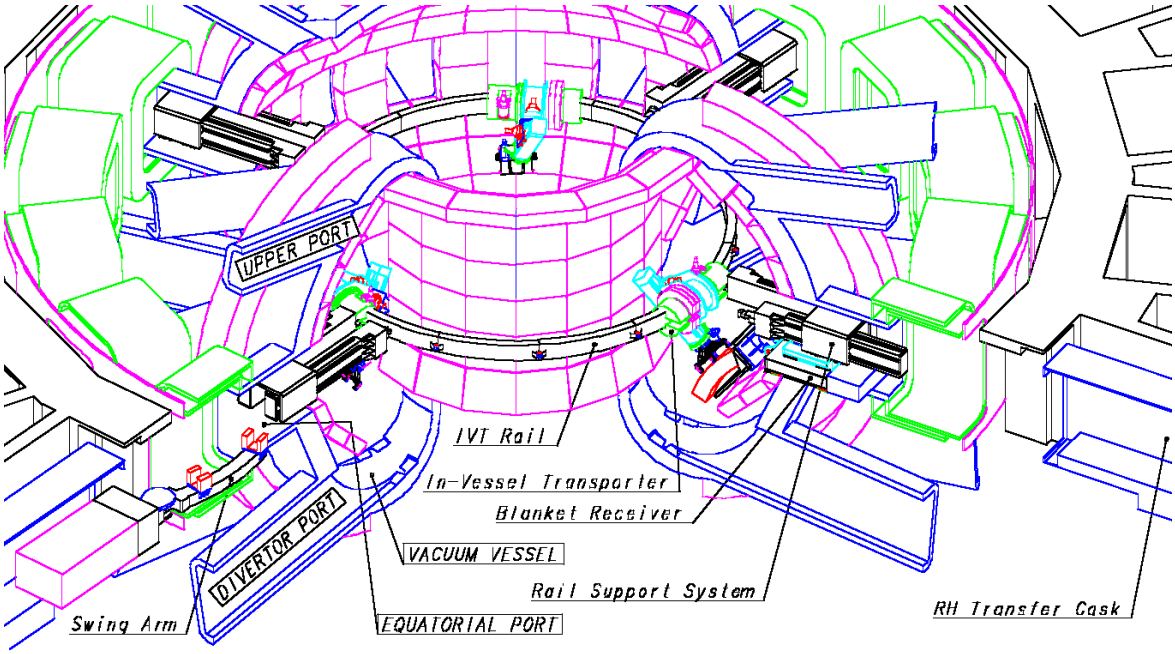

Figure 2.9.3-1 Blanket Maintenance Concept

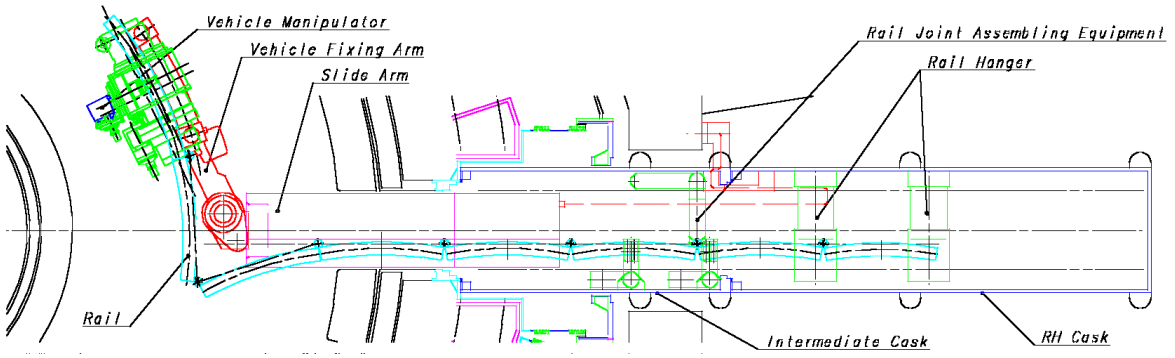

Figure 2.9.3-2 In-Vessel Transporter System

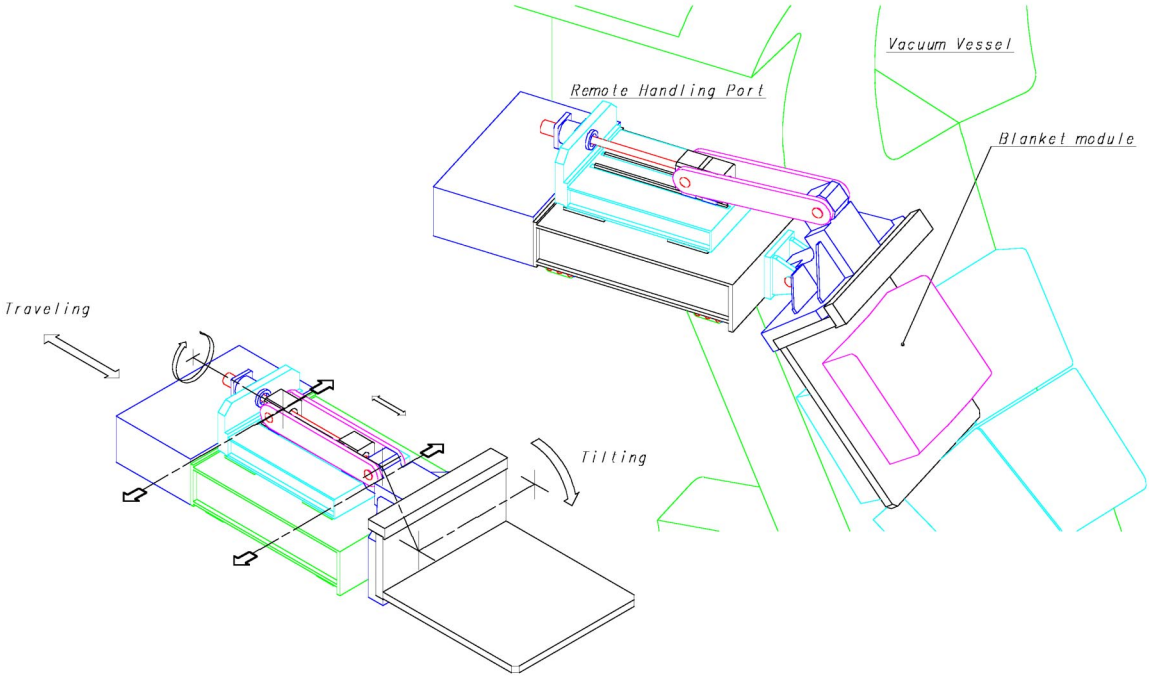

Drawing 23.223.1

Figure 2.9.3-3 Module Transporter

2.9.3.2 Maintenance Scenario

The blanket maintenance procedure is outlined in Table 2.9.3-2.

Table 2.9.3-2 Blanket Module Maintenance Procedure

Sequence No.	Procedure	Operations
1	Port opening	• Removal of service line of port plug • Removal of port plug • Installation of port adapter
2	Intermediate casks docking to RH ports	• Intermediate cask travelling/docking to a RH port • Connection of umbilical for RH equipment and device movement
3	Installation of IVT inside the VV	• IVT system transport by RH cask • Installation of IVT (IVT system transport/rail joint assembly/rail deployment/rail support installation/cable handling equipment installation and cable connection/rail deploying equipment removal)
4	Preparation of tools at RH port	• RH cask-loaded blanket maintenance tools (pipe welding/cutting, bolting, pipe inspection) with blanket transporter docking to RH port

Table 2.9.3-2 Blanket Module Maintenance Procedure (cont'd)

Sequence No.	Procedure	Operations
5	Blanket module removal	• Electrical strap bolts exchanged to temporary fixing bolts (using bolting tool) • Flexible support bolts unbolting (using bolting tool) • Cooling pipe cutting (using pipe welding/cutting tool) • Blanket module removal
6	Blanket module transportation	• Blanket module transportation to the hot cell
7	Blanket module refurbishment	• FW replacement • Electrical straps replacement if necessary - Branch pipes replacement if necessary
8	Blanket module transportation	• Blanket module transportation to the VV
9	Blanket module installation	• Blanket module introduced into the VV by a blanket transporter • Blanket module attached to the VV wall by the IVT • Cooling pipe welding (using pipe welding/cutting tool) • Cooling pipe inspection (using pipe inspection tool) • Temporary fixing bolts attach to electrical strap bolts holes (using bolting tool) • Flexible support bolt fastening (using bolting tool)
10	Removal of tools from RH port	• RH cask loaded with blanket maintenance tools with blanket transporter removing them from the RH port
11	Removal of IVT from the VV	• IVT system transportation by RH cask • Removal of IVT (installation of rail deploying equipment/IVT returning to the vehicle fixing arm/cable disconnection and cable handling equipment retraction/rail support retraction/rail retraction and rail joint disassembly/IVT system removal)
12	Intermediate cask removal	• Disconnection of umbilical for RH equipment and transfer of all RH devices into cask • Intermediate cask undocking and removal from the RH port
13	Port closing	• Installation of port plug • Installation of port plug service lines

To implement the cask-based IVT system, up to four of the equatorial RH ports can be assigned for installation of the IVT system and transportation of the blanket modules. Therefore, both an 80/100° rail and 180° rail deployment system can be used for blanket maintenance, in addition to the full 360° configuration. The configuration of each system variant is shown in Table 2.9.3-3. It is likely that for initial machine operations one 80/100° system will be adequate. Therefore, depending on the location of damaged modules, the 80/100° degree system and 180° degree system can be used.

Table 2.9.3-3 Configuration of System Variant

Equipment and device	80/100° system	180° system	360° system (full system)
Rail	100°	180°	360°
Vehicle manipulators	1	2	4
Rail-deploying equipment	1	1	2
Rail support devices	2	3	4
Cable-handling equipment	1	2	4
Intermediate casks	2	3	4
RH casks	2	3	4
Module/tool transporters	1/1	2/1	2/2
In-cask storage racks for modules/tools	1/1	2/1	2/2
Welding/cutting tools	1	1	2
Bolting tools	1	1	2
Inspection tools	1	1	2
Rescue tools	1	1	1

2.9.3.3 Rescue Scenario

One failure mode that has serious consequences is a malfunction of the actuator in the vehicle manipulator during blanket module handling. To cater for this eventuality, all the mechanisms of the vehicle manipulator have redundant mechanisms, which incorporate an external drive connection that can be accessed by a rescue tool handled by a second vehicle manipulator. The rescue tool then connects to the redundant, healthy actuator and drives it, thereby bypassing the damaged mechanism of the vehicle manipulator.

2.9.3.4 Maintenance Time Estimation

A staged procurement is assumed for the IVT systems. During the first ten years of operation, an 80/100°, or if proven necessary, a 180° system will be used for in-vessel component maintenance. To speed the replacement of blanket modules by a breeding blanket, an additional 180° system may be procured. Estimated maintenance time estimates are shown in Table 2.9.3-4. Single module replacement is expected to be possible within one month, whereas for replacement of a toroidal row of modules approximately 2.5 months, or 1 month are required respectively, depending on whether a 180° or 360° IVT system is deployed.

Table 2.9.3-4 Time Estimates for Blanket Maintenance

Maintenance	80/100° system	180° system	360° system (full system)
One blanket module replacement	25 days	(same as 80/100° system)	(same as 80/100° system)
One toroidal row replacement	No use (151 days)	74 days	32 days
All blanket modules replacement	No use (916 days)	487 days	276 days

2.9.3.5 Assessment/Future Work

An overall RH procedure for replacement of blanket modules has been established. A large in-vessel transporter with telescopic manipulator has been designed. The design has been fully optimised with respect to payload and size. Design concepts of additional equipment and tools are progressing. The main requirements of welding and cutting tools have been confirmed through R&D. The basic scenario and procedure of blanket maintenance using an approximately full scale prototype IVT system have been demonstrated in the large R&D project L6.

The emphasis of present R&D is on developing position and force feedback control for the accurate positioning of blanket modules onto the VV wall, which requires the insertion of keys into keyways with very small gap clearances (fraction of a mm). This has been demonstrated in 2001. Important characteristic data of blanket RH system operation, using a teach-and-playback technique, has been obtained. Furthermore, the remote connection/disconnection of adjacent rail links is being developed in bench tests.

Typical rescue situation were simulated to verify the feasibility of the postulated rescue operations and demonstrate the fail safe behaviour of the remote handling equipment under off-normal conditions. As a result, the respective rescue operations have been successfully performed under the simulated conditions. The respective maximum torque in the rescue tests are 19 Nm for screwing the redundant mechanism to drive the faulty axis, and negligible for disconnecting the jamming mechanism.

After mid-2001 continued development of detailed designs has to be carried out and detailed maintenance procedures, as well as rescue scenarios, have to be demonstrated. This should include:

- demonstration of all module attachment and replacement procedures, including module handling, bolting, welding/cutting, testing;
- demonstration of module transfer procedures (manipulator to receiver, module transporter through port, receiver to rack, rack to receiver, receiver to hot cell receiver);
- optimisation of man-machine interfaces, development of automatic sequences.

To achieve the above demonstrations, relevant full-scale prototype equipment has to be procured.

The above demonstrations must include rescue from upset and failure conditions.

2.9.4 Cask Transfer System

2.9.4.1 System Description

The ITER cask transfer system (Figure 2.9.4-1) consists of a container for the transport of in-vessel components, capable of remotely docking to the vacuum vessel and to the hot cell ports, and travelling by means of a remotely controlled transfer system. Each cask has three main sub-systems: a cask enclosure, a cask transfer system, and remotely operated equipment inside the cask. The cask enclosure shape and dimensions vary, depending on the size of the component to be transported and on the design of the vacuum vessel flange. The cask transfer

system, which allows the cask to travel independently through the building, is designed to be a separate and exchangeable unit. Its design is universal in the sense that it can be used in conjunction with any of the cask envelopes without modification. This approach helps reduce the total inventory of cask system components by allowing total system interchangeability.

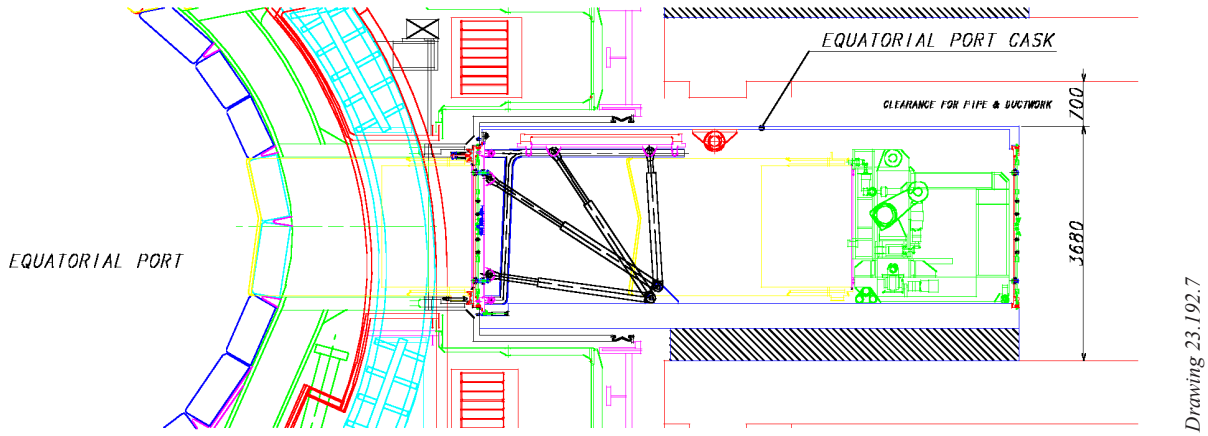

Figure 2.9.4-1 Cask Transfer System

The cask equipment consists of a handling tractor (for the lifting and positioning/removal of the payload), and a manipulator (for the execution of tasks such as bolting and unbolting, seal cutting, welding inspection, etc.). The largest cask size (with the exception of the single, neutral beam injector cask) is 2.6 m wide, 3.7 m high and 8.5 m long, and the maximum weight (unladen/laden) is 40/80 t. In more detail, the transfer cask system includes the components itemised below.

1) Cask platform and enclosure, i.e. the cask load-bearing and envelope structure required for supporting and containing the payload. The load-bearing structure acts also as gamma shielding to prevent radiation damage to the cask transfer system underneath. The envelope is of light construction but strong enough to withstand a maximum internal pressure of 1.05 bar (following air temperature increase caused by the nuclear heating caused by the radioactive payload) and a minimum internal pressure of 0.90 bar. Six different cask envelopes are required to satisfy the need to transfer different sized components while docking simultaneously to four different machine ports.

2) Cask double-seal door system (see Figure 2.9.4-2), fitted to the front end of the cask, allows the component transfer in and out of the cask under contamination-controlled conditions. The function of the double door is to allow connection and disconnection of the cask without the risk of a spread of contamination. The double-seal door is operated by a combination of hydraulic cylinders and by a set of bayonet type mechanisms (for the selective connection and disconnection of the cask door to/from the maintenance door). Where possible, the door actuators are fitted to the fixed part of the cask, thus simplifying cable routing and increasing the overall system safety. The double-seal door opens by tilting upwards and backwards inside the cask, where it is stored near the cask ceiling. A single-seal door is fitted at the rear end of the cask, becoming a full double-seal door system when a rescue cask is docked to the rear end of the cask.

N 23 GR 181 00-12-19 W 0.1

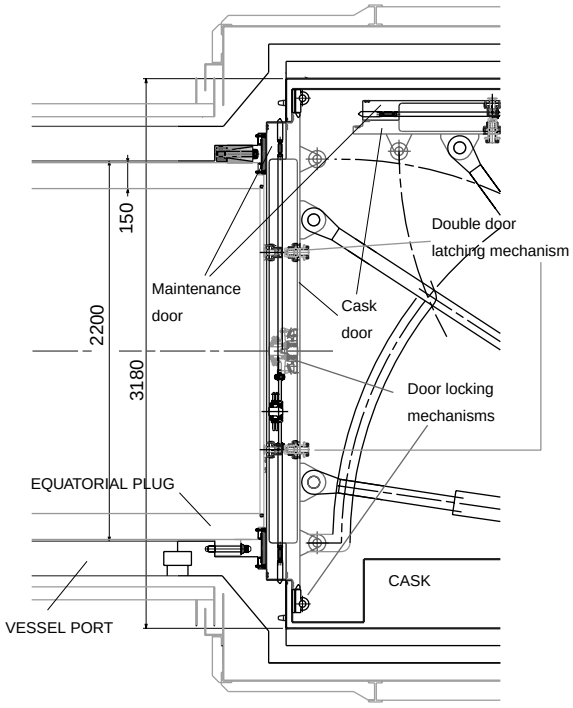

Figure 2.9.4-2 Double-Seal Door System

3) Cask transfer system, allows the cask to be suspended on a virtually frictionless thin air film which acts as a compact, high load capacity, flexible interface between the cask and the floor. Air to the bearings is supplied by a set of on-board compressors. Cask motion (multi-directional) is achieved by a double set of drive wheels powered by electric motors, fed (like other cask onboard electrical components) by a set of onboard batteries. The transfer system design is such that one single transfer unit type can be shared among five different-sized casks.

4) Cask docking and alignment system. The docking system allows all the necessary movements and forces required to adjust the cask position in front of the vessel or hot cell port and keep it there throughout the component transfer operation. This is achieved by means of a jacking system (vertical, tilt and yaw adjustment) and pushing devices reacting on the building floor (providing horizontal adjustment and compression of the docking flange seals).

5) In-cask handling equipment (mainly a combined tractor/manipulator system, remotely controlled) for the disconnection, reconnection, loading, and unloading of the components. For specific operations, the in-cask equipment can be rather complex, as in the case of blanket module replacement.

6) Control system, for the remote control of the cask and of the handling equipment.

2.9.4.2 Rescue Scenario

The issue of rescue in the case of cask failure (such as cask double-seal door failure, or in-cask handling equipment failure) has been addressed. In these cases a rescue cask is delivered and docked to the rear of the failed cask. The front door of the rescue cask is connected to the

main cask rear door. The two doors are then opened inside the rescue cask. At this point two rescue actions are possible:

- if the main cask handling equipment (manipulator, gripper, etc.) is faulty, this is retrieved inside the rescue cask and later replaced with new equipment (i.e. requiring the rescue cask to travel to a free hot cell port and then return to the main cask);
- if the main cask front double seal door is faulty, the rescue cask equipment removes (if present) any component and equipment inside the main cask (plug, manipulator, etc.) returning them to the hot cell; in a second phase, the rescue cask equipment enters the main cask again and, by-passing the double seal door actuator mechanism, closes the double seal door, leaving a maintenance door fitted onto the machine (or hot cell) port and closing the failed cask; the two casks are then removed and a new cask is sent to continue the operation.

The cask transfer system is designed such that in case of failure it can be removed from under the cask (while using temporary jacks) and replaced with a new unit. Redundancy for the main cask transfer components (air bearing units, air compressors and batteries) is included in the design.

2.9.4 3 Maintenance Time Estimation

Maintenance time varies depending on the operation to be performed. In general, the duration of the intrinsic cask operations has to be compatible with the specified overall maintenance time for the components to be replaced. This varies greatly depending on the extent of the replacement operation.

However, there is a minimum time, which must be accounted for to allow the execution of the intrinsic cask functions. These are given in Table 2.9.4-1.

Table 2.9.4-1 Estimated Times for Certain Cask Operations

Operation	Estimated Time
Docking at the vacuum vessel port interface	*h*
Cask alignment	0.75
Cask docking and external power connections	1
Docking surfaces double seal leak check	0.5
Cask door /maintenance door reconnection (1)	0.25
Double-seal door opening	0.25
Double-seal door closing	0.25
Cask/maintenance door disconnection	0.25
Maintenance door leak checking	0.5
Cask undocking and external power disconnection	0.5
TOTAL EST. TIME at VV port	**4.00 ~ 4.25**

Table 2.9.4-1 Estimated Times for Certain Cask Operations (contd.)

Operation	Estimated Time
Docking at the hot cell interface (*)	*h*
Cask alignment	0.75
Cask docking and external power connections	1
Docking surfaces double seal leak check	0.5
Cask/hot cell maintenance door connection	0.25
Double-seal door opening	0.25
Double-seal door closing	0.25
Double door interspace leak checking	0.5
Cask/hot cell maintenance door disconnection	0.25
Cask undocking and external power disconnection	0.5
TOTAL EST. TIME at hot cell interface	**4.25**
Hot cell docking port adapter exchange	*h*
Adapter n.1 double seal leak checking	0.5
Adapter n.1 disconnection	1
Adapter n.2 reconnection	1
Adapter n.2 double seal leak checking	0.5
TOTAL EST. TIME for adapter exchange	**3**

(1) If returning from the hot cell
(*) Assumes that the correct hot cell docking port adapter is already installed, otherwise, in case of adapter exchange, add the time below

2.9.4 4 Assessment and Future Work

Cask docking and double-seal door operation were demonstrated for the 1998 ITER design[1]. However, docking at the vacuum vessel ports for the current design requires that the cask is extended from its support into the cryostat port, and is connected to the vessel port. Moreover, the upper ports are inclined and require more complex handling operations. While good design progress has been made for the current configuration during the period 2000-2001, future R&D needs to address the development and qualification of individual operations.

The transfer cask design and the general port handling using a cask system is now established, but certain areas need further R&D, in particular cask alignment and positioning/docking, double-seal door operation, and the handling tractor development.

2.9.5 Viewing and Metrology

The need for regular viewing inside the vacuum vessel is anticipated for inspection of the inner walls, especially after plasma operations have indicated possible damage to components. Insertion of viewing probes with adequate resolution should allow surveying of the inner walls within a reasonable time, e.g., several hours. A sufficient number of probes should be deployed at toroidal positions to achieve an adequate viewing coverage.

[1] "Technical Basis for the ITER Final Design Report, Cost Review and Safety Analysis (FDR)", ITER EDA documentation series n.16

Metrology may be required to assess the degree of damage after off-normal events and will also be needed to confirm accurate positioning of in-vessel components after replacement. Moreover, metrology may be needed for plasma erosion measurement.

As a result of optimisation considerations, divertor ports were selected for in-vessel viewing (IVV) probe insertion into the vacuum chamber. Deployment of a probe, between the lower outboard module and the divertor cassette, from six, equi-spaced ports, allows nearly 100% viewing of the blanket and divertor first walls. Viewing activity was assumed to be under full vacuum, with the in-vessel components at dwell temperature.

The plug-type system (Figure 2.9.5-1) is permanently parked on the rails inside the port. Due to the configuration of the port and the components permanently mounted inside the port, a curved deployment trajectory is necessary. A cask is required for maintenance.

Such an arrangement requires the use of motors, actuators, sensors, support systems, etc., all operating in vacuum. The technical basis for their radiation hardness also needs to be demonstrated by further R&D, as does the development of viewing and metrology probes. The results so far indicate that the ITER requirements regarding accuracy, resolution and radiation hardness are likely to be met.

The requirements specified for the system are also being scrutinised, e.g., the need for deployment under vacuum and at dwell temperature.

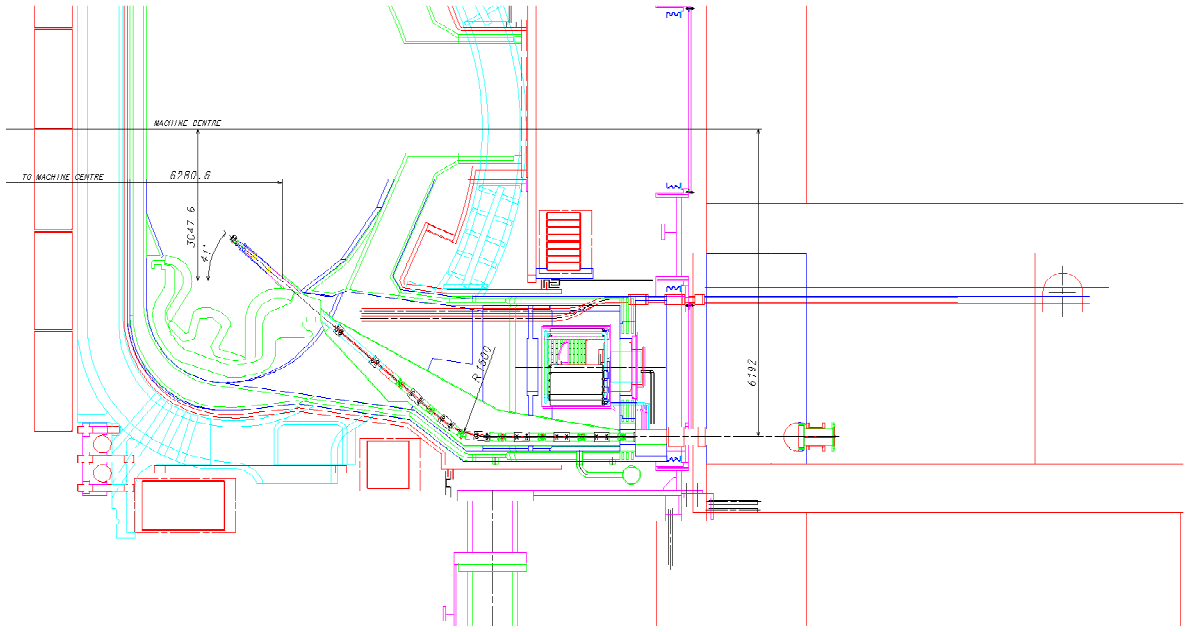

Figure 2.9.5-1 Concept of Plug-type IVV System

2.9.6 Neutral Beam (NB) Injector Maintenance

2.9.6.1 Introduction

Routine remote maintenance of the NB injectors is needed only for the replacement of the ion source filaments, replenishment of the cesium oven and the removal of cesium from the accelerator grids and insulators. Replacement of the source filaments, and replacement of the cesium oven, can be achieved "in-situ", and R&D on removing cesium from the insulators

shows the feasibility of in-situ cesium cleaning, i.e., without removing the ion source. Should in-situ cesium cleaning not ultimately prove feasible, as a back-up solution the beam source from the beam-line can be taken to the hot cell for detailed maintenance. The maintenance sequence of cask travel, docking and ion source removal is shown in Figure 2.9.6-1. The remote handling disconnection and reconnection of the ion sources, while being a complex and time-consuming operation, is nevertheless feasible.

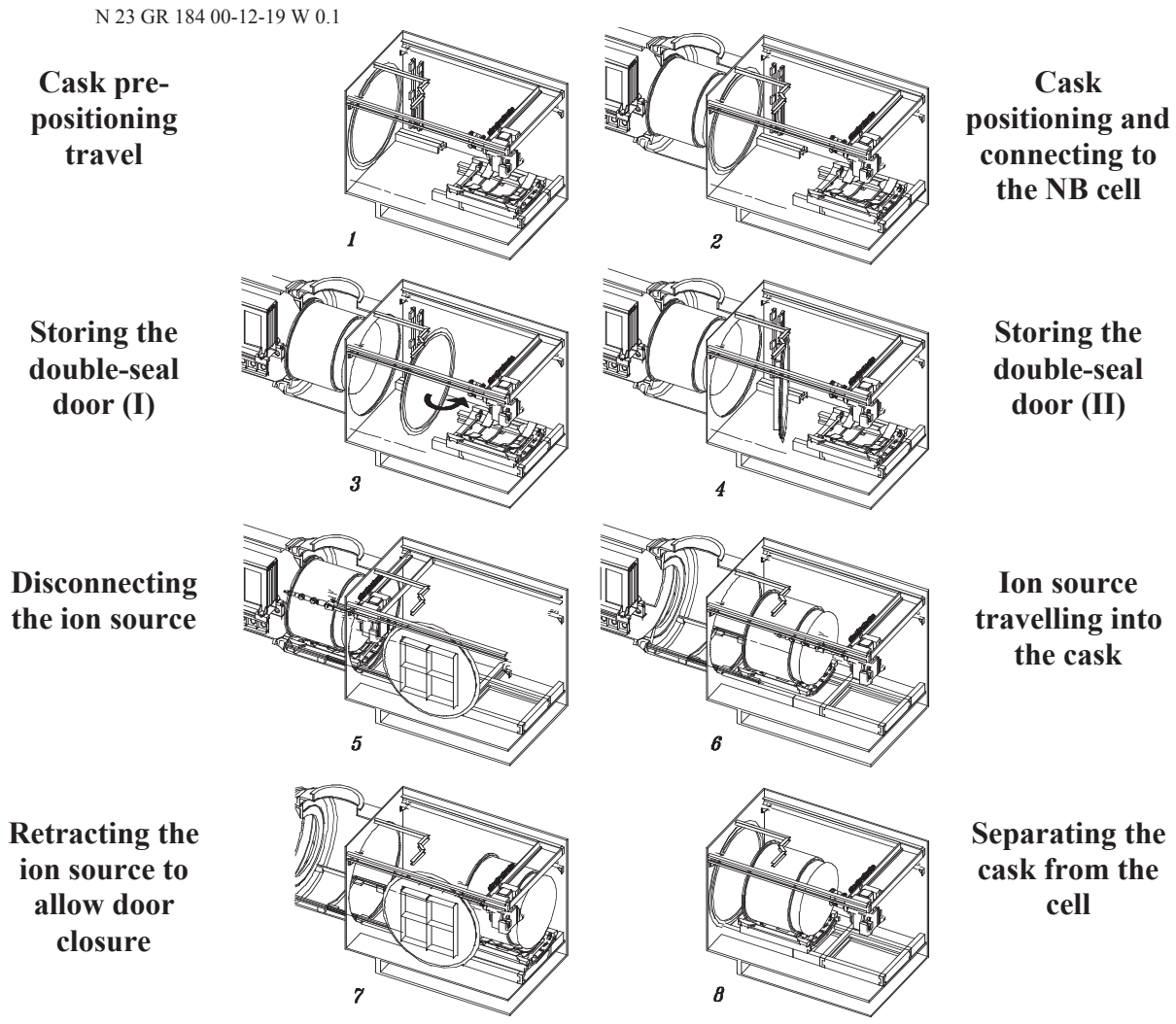

Figure 2.9.6-1 Maintenance Cask Travel, Docking and Ion Source Removal

2.9.6.2 Maintenance Processes

1) Installation of the maintenance cask

The NB injector transfer cask is a dedicated cask used only for maintaining the NB injectors. The ion source pressure vessel has a "race track" shaped dome to which the maintenance cask can be docked. The cask is similar to the other transfer casks operating at the equatorial port level and contains all the remote handling equipment required to carry out a maintenance operation. The installation therefore proceeds as follows.

a) Remove the biological and magnetic shield doors from the required NB cell and re-configure them as temporary gallery shielding.
b) Position the transfer cask at the NB cell using the air bearing support system and the cask driving wheels.
c) Align the transfer cask with the back of the ion source dome, and dock to it.
d) Attach the NB injector ion source dome to the transfer cask door and remove the whole assembly to the back of the cask.

2) Maintenance of ion source filaments

The ion source has 72 filaments arranged radially and longitudinally along the plasma generator, which is in the form of a partial cylinder. The ion source and filament are grouped into sets of six. To ease assembly, the filament housing is provided with a tapered profile. The plasma source chamber is provided with hinge pivots to guide and correctly position a tool installed specifically for assembling the filaments. This tool (Figure 2.9.6-2), engages the hinges on the ion source plasma chamber and automatically aligns the filaments when they are swung into position.

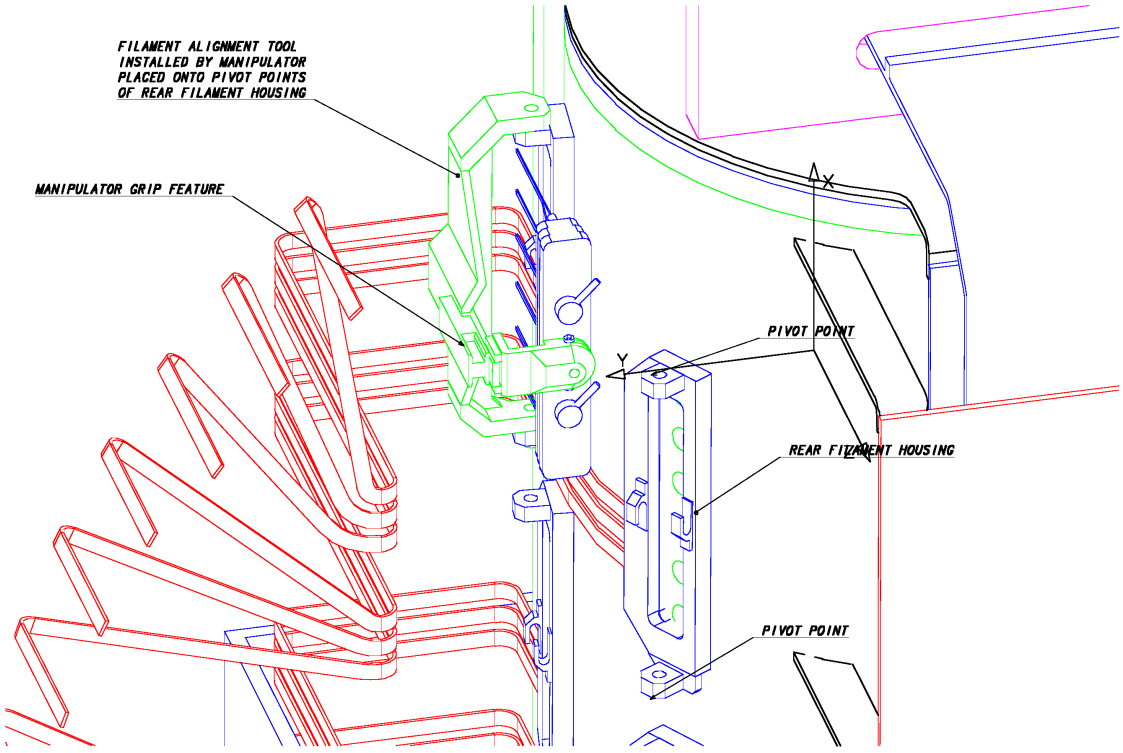

Figure 2.9.6-2 Filament Alignment Tool

3) Replacement of the cesium oven (Figure 2.9.6-3)

There are two cesium ovens per NB injector and they are located at the rear of the ion source. To replenish the cesium source it is necessary to replace the cesium oven. The cesium ovens will be replaced each time the ion source filaments are replaced.

The oven is a self-contained unit and is attached to the ion source plasma generator by a single captive fastener. The ovens are aligned horizontally during assembly by means of a tapered collar and positioned axially by three datum pins attached to the plasma generator housing. An insulated guide pin ensures alignment of the fasteners during assembly.

N 23 GR 186 00-12-19 W 0.1

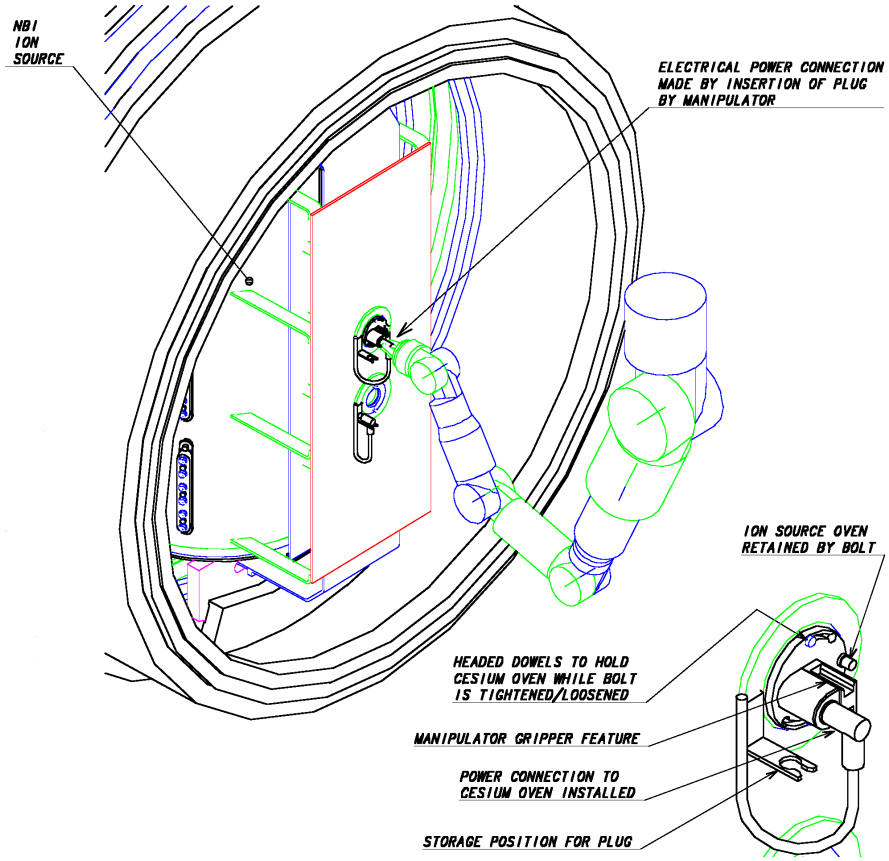

Figure 2.9.6-3 Replacement of a Cesium Oven

4) In-situ cesium cleaning of ion sources (if applicable)

The manipulator delivers cesium cleaning tools to the grids and insulator, where the tools perform laser cesium cleaning.

5) Maintenance of NB injector beam-line components

The beam-line components are generally RH class 3. However, in the event that a beam line component may need replacement, they can be replaced in a manner similar to that described above for the ion source. In this case, the ion source transporter is replaced by a second transporter, which has an upper and a lower set of rails. The lower set aligns with the beam source transporter rails at the bottom of the pressure vessel. The upper set aligns with the beam-line component support rails. Using these rails, beam-line components can be pulled into the transfer cask and subsequently transported to the hot cell.

a) *Neutraliser, Residual Ion Dump (RID), Calorimeter, and Cryopump*
To facilitate remote cutting and welding of coolant pipes, all welded connections are located on the "service flange" at the entrance of the beam-line vessel. The rear flange of the beam line features a reduction ring that can be removed (unbolting followed by cutting of the lip weld. This increases the free passage dimensions so that the largest component (the cryopump panels) can slide out. Prior to cryopump removal, dismantling of all other beam-line components is required.

b) *Fast Shutter*
Two components of the fast shutter are considered for infrequent maintenance. They are the "soft" seal and the pneumatic actuator. The actuator is mounted externally and may be accessed from within the NB cell. The seal is removed after first removing the bellows. The fast shutters on the NB injector systems incorporate the inboard rupture discs of the vacuum vessel pressure suppression system. Maintenance access to the rupture discs is established by removing the bellows.

c) *NB Bellows*
To remove the bellows, whilst at the same time maintaining confinement, the secondary containment surrounding the bellows is provided with a double door system to which may be attached a maintenance cask. All the equipment required to perform maintenance is inside the cask. After cutting the bellows welded lip seal, the bellows are compressed and raised into the maintenance cask. The cask is transported by an overhead monorail to a hatch in the floor, and hence to the hot cell.

d) *NB Duct Components*
The NB injector duct liner replacement will be carried out from within the vacuum vessel using the remote handling in-vessel transporter.

2.9.6.3 Assessment and Future Work

Maintenance concepts have been developed, partly in detail, for the ITER NB injector system. The handling principles are based to a large extent on similar procedures used for the maintenance of other components. Specific procedures are required for cesium cleaning and these are now being addressed in R&D. To qualify the procedures for NB injector maintenance, prototype tools and equipment will need to be tested in mock-ups.

2.9.7 In-Cryostat Repair

2.9.7.1 Design and Interfaces Description

Because of the congested nature within the cryostat and the difficulty of achieving direct access to components located between the outside of the machine and the inside of the cryostat, in-cryostat maintenance is, as far as possible, eliminated by design. Components inside the cryostat are conservatively designed with factors of reliability high enough to render failure very unlikely. All components are designed to last the life of the machine and no components require planned routine maintenance. In the unlikely event that a repair is

required, the strategy for repair within the cryostat is based on human access with hands-on repair. Machine shielding thicknesses are such that any radiation received by operators during maintenance (see 2.14) is below 100 μSv/h two weeks after shutdown, and is as low as reasonably achievable (ALARA).

The specific objectives for in-cryostat repair are as follows.

- To inspect and repair components within the cryostat and located between the cryostat wall and outer surface of the machine, which include the following items:
  - magnet termination joints (current and helium);
  - intercoil structure bolted connections;
  - thermal shields;
  - vacuum or cryogenic leaks;
  - electrical or thermal shorts.
- A less likely objective of in-cryostat operations involves extensive work, mainly related to the replacement of large components, i.e. a PF coil, a TF coil and associated vacuum vessel sector, etc.

Access to the interior of the cryostat for repair is provided at three levels:

- the top of the cryostat which has:
  - a central access hatch;
  - four perimeter hatches.
- the four equatorial remote handling ports;
- four radial access hatches at the basemat level.

Typical access conditions for the upper CS and PF coils are shown in Figure 2.9.7-1.

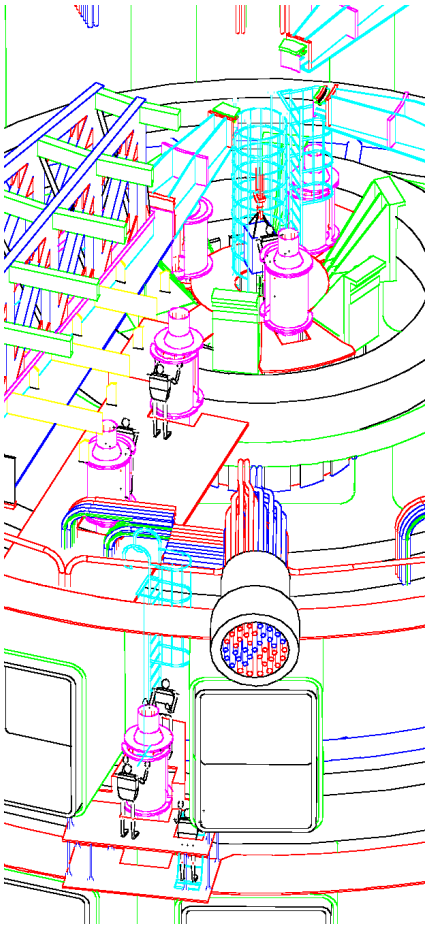

Excerpt from N 23 GR 188 00-12-19 W 0.1

Figure 2.9.7-1
Overview of Upper CS and PF Coil Access

Below each of the hatches at the top of the cryostat is a series of landings, walkways and stairs that allow maintenance personnel to travel to the various sites where repair or inspection may need to be carried out. The equatorial level remote handling ports are provided with hatches in the roof and floor. Ladders, from the remote handling ports, will permit access to the interspaces between the upper and equatorial ports and the divertor and equatorial ports. From the basemat level, stairs and ladders provide access to the overhead repair and inspection sites.

Installed lifting points and rigid set down areas (to protect the delicate thermal shield, etc.) will be provided to assist in the transfer of heavy components and maintenance equipment.

2.9.7.2 Maintenance Scenarios

During maintenance within the cryostat, the magnets will be turned off, warmed to room temperature and the cryostat opened. Only a small residual magnetic field is assumed to remain. Pressure inside the cryostat will be ambient and the atmosphere, normal air. The interior of the cryostat is assumed to be free of radioactive contamination, and maintenance workers will not normally be required to wear plastic suits or be provided with a supply of breathing air.

A typical repair procedure involves the following items.

- Planning to ensure that the estimated radiation dose uptake by personnel entering the cryostat is ALARA. A minimum of two people is assumed, including a maintenance worker and health physics monitor.
- Gaining access to the interior of the cryostat by removing the access hatch by releasing fasteners and cutting the welded lip seal joint, and likewise removing the demountable access panel in the underlying thermal shield.
- Installing walkways and platforms as required (if appropriate) and travelling to the work site along walkways and platforms.
- Assembling equipment.
- Carrying out repairs, reassembly and testing.
- Dismantling equipment, cleaning up and monitoring.
- Retiring from the cryostat.
- Closing the cryostat and checking for leaks.

To access the PF1 coil terminations, a ladder is used to get to the in-cryostat platform via the central access dome in the cryostat lid. Stairs allow access from the pumping platform to the PF2 and PF3 coil terminations. The lower PF coils (PF4, PF5, and PF6) are accessible through a cryostat access port at basemat level. The PF4 coil has the option of being accessed from above. The PF5 coil terminations are mounted on the TF coil clamps and are accessible by ladder and landing from the basemat level. Access to bypass joints or to the PF3 or PF4 coils may also be made via access hatch from the equatorial remote handling ports. A maintenance worker then has access to the area between the equatorial ports and is able to climb up to the PF3 coil or down to the PF4 coil.

The TF coil feed joint can be reached by a maintenance worker on a mobile platform erected on the inside of the cryostat.

Access to the three CS termination joints at the top of the machine is through the upper central dome and onto the vacuum pumping platform. Access to the three at the bottom is via an access port at the basemat level and a walkway through the TF coil support structure. At the top of the machine there is a platform supported off the PF1 coil and the feed joint can be reached from this platform. At the bottom of the machine there is a ladder to an elevated platform from where the lower feed joint can be reached.

2.9.7.3 Rescue Scenario

Two means of access will be provided during personnel entry to the cryostat. The primary access will allow for the transport of personnel and materials, and the second access will provide an escape route in the event of an accident.

2.9.7.4 Assessment and Future Work

Means to access the cryostat for hands-on repair have been established. Critical repair procedures have been developed and the needs for specific access, working space, tools and fixtures have been identified.

Following the detailed layout of components inside the cryostat and a detailed analysis of the radiation levels expected during the operating schedule, there is additional work required to develop the following for in-cryostat repair.

- Devices for deployment of repair equipment.
- Tools for disassembly and assembly of termination and cryogenic isolation joints.
- Repair times and compliance with ALARA and ITER radiation protection program.
- Remote back-up procedures should current estimates of radiation levels prove too optimistic.

2.9.8 Hot Cell Repair and Maintenance

2.9.8.1 Introduction

The hot cell provides space and handling facilities for the reception, dispatch, decontamination, storage, repair, refurbishment and testing of highly radioactive and, or contaminated in-vessel components and materials (divertor cassettes, blanket modules, and other in-vessel component such as diagnostics and port plugs). Facilities are also provided for the maintenance of remote handling tools and for radioactive waste processing and storage prior to disposal by the ITER host.

2.9.8.2 Engineering Description

An overview of hot cell building is shown in Figure 2.9.8-1. The functions performed by the hot cell repair/maintenance equipment are summarised in Table 2.9.8-1 and the system description is as follows.

N23 GR 190

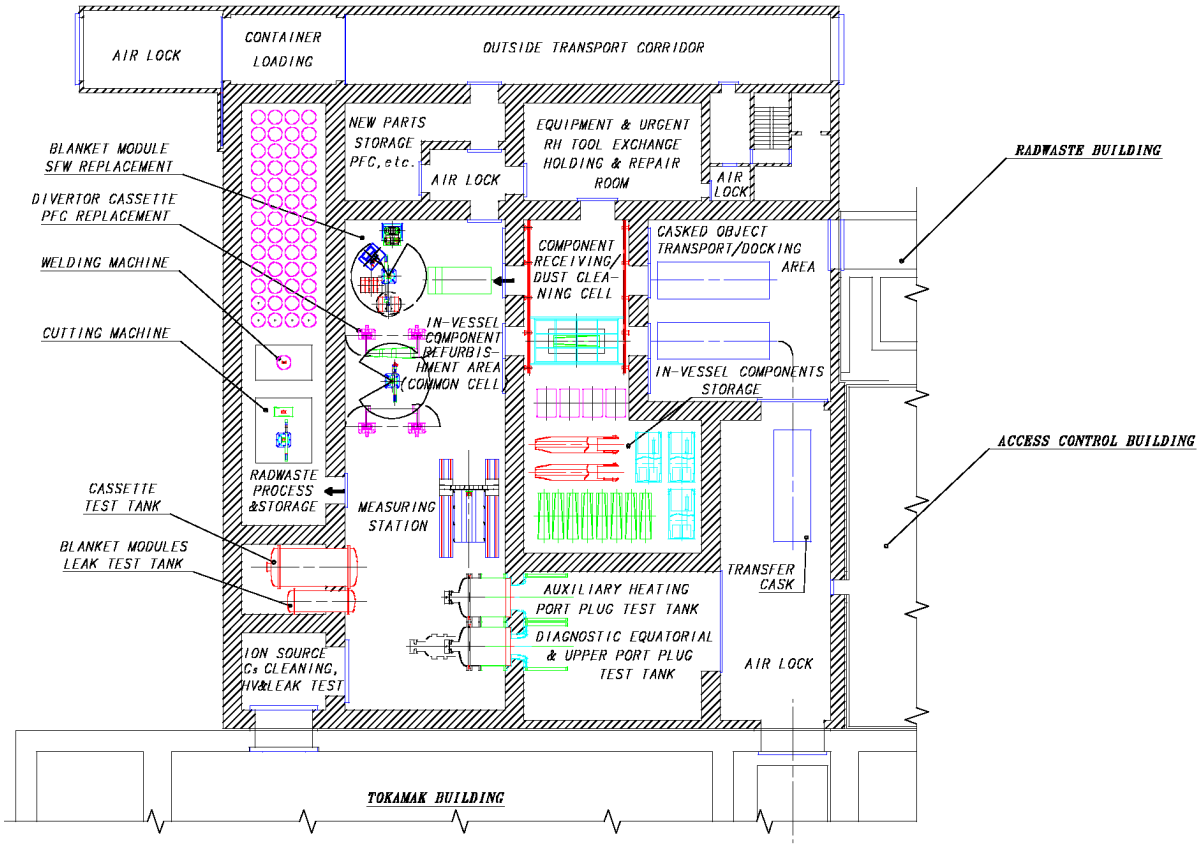

Figure 2.9.8-1 Overview of the Hot Cell (Ground Floor Layout)

Table 2.9.8-1 Hot Cell Repair/Maintenance Equipment

No	Items	Description
1	Dust cleaning system	This facility has two lines to avoid congestion, and consists of the following equipment. • Port number for cask docking system: 2 • Cleaning method: vacuum brush or CO_2 pellet blast • Handling robots: one overhead type arm robot for each line (two robots) • End-effectors/tools: dust cleaning arm, inspecting arm • Overhead crane: 50 t capacity crane with gripper, one rescue crane
2	Blanket module first wall (FW) replacement workstation	This facility has one workstation in the common refurbishment cell, and consists of the following equipment. • Blanket module supporting stand for refurbishment: 1 line • Handling robot: column-type arm robot • End-effectors/tools: - Bolting tool: torque wrench - Cutting tool: with laser cutting head - Welding tool: with TIG welding head - Weld inspection tool: ultrasonic transducer or electro-magnetic acoustic transducer • End-effector and tool storage: all end-effectors and tools are parked in a tool storage rack

Table 2.9.8-1 Hot Cell Repair/Maintenance Equipment (cont'd)

No	Items	Description
3	Divertor cassette plasma-facing component (PFC) replacement workstation	This facility has two identical workstations in the common refurbishment cell and consists of the following equipment. • Cassette supporting stand for refurbishment: 2 lines • Handling robot: column-type robot arm • End-effectors/tools: - Bolting tool: torque wrench - Cutting tool: with laser cutting head - Drilling tool: with drill tool - Expansion tool: with special mandrel to expand fastener connecting PFC to cassette body - Welding tool: with TIG welding head - Weld inspection tool: ultrasonic transducer or electro-magnetic acoustic transducer • End-effector tool storage: all end-effectors and tools are parked in a tool storage stand
4	Pressure and leak test tank for blanket module and divertor cassette	Divertor cassettes and blanket modules must be pressure and leak tested in this facility after exchanging a PFC. • Number of vacuum test tanks: 1 each for blanket module and divertor cassette • Pressure testing line (water) for cooling pipes • Leak testing line (helium gas) for cooling pipes
5	Transporter	For the transport of components in the common refurbishment cell, the following equipment is used. • Floor mobile transporter • Overhead crane: 50 t capacity crane with gripper, 1 rescue crane
6	In-vessel components storage system	Components are stored on the floor. The storage capacity of the storage cell is as follows: • 16 divertor cassettes (12 t each) • 20 blanket modules (4 t each) • 4 port plugs (3 equatorial RH/limiter/diagnostics plugs + 1 dummy plug, or 3 divertor diagnostics racks) • 2-4 upper port plugs (13 t each)
7	Equipment measuring station	Repaired components are brought on their carrying trolleys under the measuring station gantry and examined by the following equipment: • 3D measuring: non-touch method • 3D-examination device: touch sensor • Visual inspection device: CCD camera • Welding inspection : ultra-sonic inspection
8	Radwaste processing and storage facility	The equipment in the radwaste processing and storage cell comprises the following, together with storage drums. • Laser cutter for cutting thin structures. • Diamond blade saw for cutting elements of small pieces. • Canning machine to weld the lids of drums by TIG welding • Overhead crane: 50 t capacity crane with gripper, 1 rescue crane

Table 2.9.8-1 Hot Cell Repair/Maintenance Equipment (cont'd)

No	Items	Description
9	Port plug equipment testing facility	The equipment in the port plug equipment testing facility comprises the following. • Diagnostic, equatorial and upper port plug test tank. • Auxiliary heating port plug test tank
10	Remote handling equipment test stand	The configuration of the maintenance cell is 10.4 m inner length and 100° sector angle with isolation wall of 200 mm concrete. The equipment in the RH equipment test stand is as follows. • Dummy docking port structure (1 dummy upper port, 3 dummy equatorial ports, and 1 dummy divertor port) • Part mock-up vacuum vessel (20° sector) and the support structure • Dummy in-vessel component (1 dummy divertor cassette, and 1 dummy blanket module)

2.9.8.2.1 Description of Hot Cell Areas

The main areas are shown in Figure 2.9.8-1.

a) Dust cleaning area, where components withdrawn from the vacuum vessel (VV) are received and offloaded into a component receiving cell to remove activated dust. After refurbishment and any testing, the components are brought back into the receiving cell and loaded into transfer casks for return to the VV.
b) Common refurbishment area. This area houses dedicated and general workstations, where the layout of the processing area provides flexibility to modify the internal locations of the workstations.
c) Common storage area to store components before repair, after repair, or to await processing for disposal as waste.
d) Radwaste processing and storage area, where the waste is treated for tritium recovery, if required, and segmented and packaged for final disposal.
e) Port plug equipment testing area, where the ex-vessel side of port plugs is accessible for hands-on maintenance and testing, whereas the plasma-facing side is accessible with remote handling equipment from within the hot cell.

Above the hot cell, there is a remote handling (RH) equipment test stand, as shown in Figure 2.9.8-2, designated for the maintenance and repair of RH equipment. Additionally, the test stand is used for operator training, and commissioning of equipment prior to maintenance or rescue interventions in the vessel.

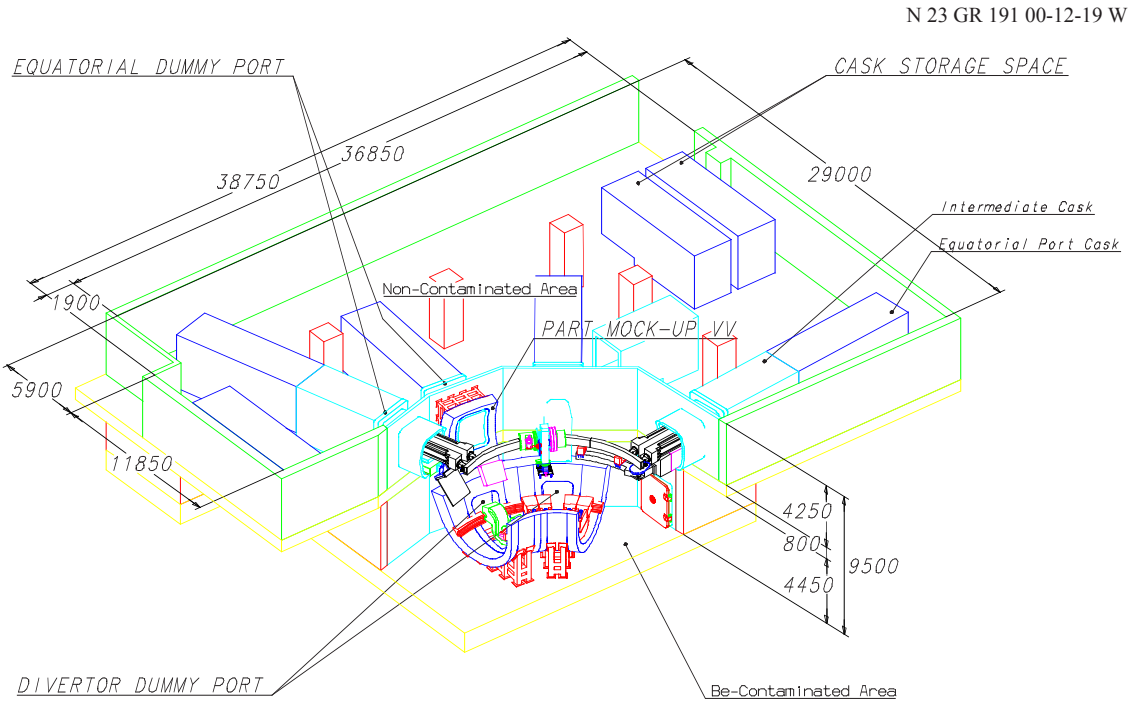

Figure 2.9.8-2 Overview of the Remote Handling Equipment Test Stand

2.9.8.2.2 Layout of the Hot Cell Building

The hot cell building (HCB) is a rectangular reinforced concrete building with a 53.7 x 44.5 m footprint. The HCB is organized on two main levels. Ground level functions include in-vessel component docking, dust cleaning, storage, repair and testing, RH tool exchange and maintenance, waste processing, waste storage and shipping, and the reception and storage of new parts and components. The upper level (+10.56 m) includes space allocation for RH equipment testing, transfer casks storage, and houses equipment for atmosphere confinement control and atmosphere detritiation.

Additionally, the HCB is available, during the initial installation phase of the tokamak in-vessel components, to provide a pre-assembly, beryllium-controlled area, and a facility for loading components into transfer casks.

2.9.8.3 Maintenance Scenario

The basic block diagram for hot cell repair operations is shown in Figure 2.9.8-3. The equipment in these facilities is operated mainly by remote control because the hot cell systems provide space and facilities for highly radioactive and contaminated in-vessel components. The repaired components are stored in the combined storage facility after dust cleaning. For layout flexibility and transfer simplicity, the common refurbishment cell is an open and rectangular space in which are installed the internal work-stations for various repair and refurbishment operations. As in the case of activated and contaminated components of systems such as diagnostics and EC H&CD, some hands-on maintenance will be performed at the port plug test tank area.

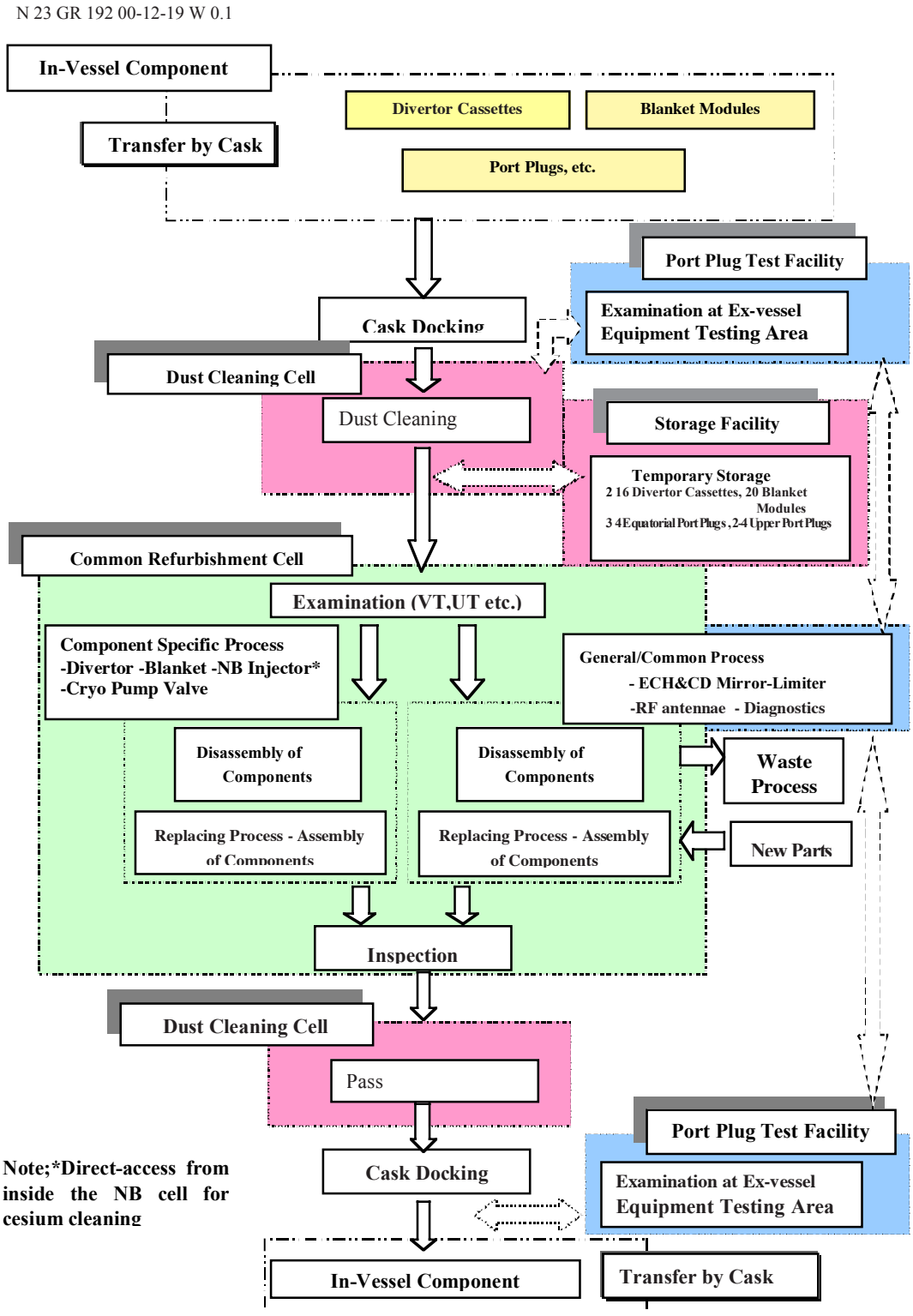

Figure 2.9.8-3 Block Diagram for Hot Cell Repair Operations

2.9.8.4 Assessment

The design of the hot cell is now established and studies done to date confirm that it will meet the design requirements. The work remaining to be done consists chiefly of the detailed design of specialised tools and equipment (including specification and selection of proprietary items) for use in the hot cell, and for further studies to verify the hot cell capacity, both in terms of component throughput and also adequacy of space provision.

2.9.9 Machine Disassembly and Re-assembly

2.9.9.1 Interface Description

The feasibility of disassembly and re-assembly of the magnets or vessel is a basic requirement that affects the machine layout and building design. In particular, during disassembly of a machine 40° sector, (a VV 40° sector with its thermal shield together with its two associated TF coils, the weight to be handled exceeds 1,200 t. Moreover, lifting such a large element out of the cryostat requires that the cryostat lid and bioshield be fully or partly removed, which they are designed to be. Provision also has to be made for the requisite space and facilities.

2.9.9.2 Maintenance Scenarios

2.9.9.2.1 Central Solenoid (CS) Disassembly and Re-assembly

The CS can be repaired in-situ in the event of local failures such as electrical insulator faults or helium leaks. Other, more extensive faults may require that the coil be removed from the machine. For this operation, a lifting device is inserted from the top, after removing the central flange from the cryostat head, and the CS is lifted by the overhead crane without any additional shielding, because the dose rates around the CS are low. A set-down space is reserved to receive the CS in the laydown area of the laydown, assembly and RF heating building.

2.9.9.2.2 Poloidal Field Coils Disassembly and Re-assembly

The PF coils can be repaired in-situ in the event of localised faults such as a helium leak, an electric short circuit, or a ground insulation fault. In the event of failures too extensive to repair in-situ, the faulted PF coil has to be removed. In the case of the upper, untrapped PF coils (PF1 and PF2), these can be removed directly, following the establishment of an appropriately sized aperture in the cryostat upper head and bioshield, and the removal of coolant pipe and vacuum pumping upper headers, as well as coil feeders, etc. However, coils PF3 and PF4 are trapped between the VV equatorial and the upper and lower ports respectively. Their replacement would require a very large amount of preparatory work, including cutting off parts of the VV ports. To minimise the failure probability, these coils incorporate in-built redundancy. The lower coils PF5 and 6 are trapped beneath the VV. Replacement of either of these lower PF coils requires that a new coil is fabricated in-situ. The layout inside the cryostat has been configured such that this can be done.

2.9.9.2.3 Toroidal Field Coils and Vacuum Vessel Disassembly and Re-assembly

In the event of TF coil failure, replacement of a machine 40° sector will be required. This operation follows the assembly procedure in reverse. This complex operation entails the prior dismantling and removal of a large number of the components inside the cryostat using manned interventions, and remote removal of the relevant in-vessel components, followed by cutting out of the affected VV sector. The machine 40° sector is then lifted out of the cryostat by the overhead cranes. The damaged TF coil is replaced by the spare one, and the assembly procedure is started again, using the same vessel sector (there is no spare vessel sector).

While schemes can be devised for this repair operation to be carried out at any time, once the vessel has become heavily activated, their level of difficulty is considerably multiplied. The vessel and coils would have to be accommodated in a shielded cask. Therefore the crane capacity limits the amount of shielding that can be provided. Also the level of neutron and gamma radiation in the hall at the time of replacement due to the open torus provides another limit. This calls into question the feasibility of such a repair for the machine operating programme. Such a procedure will anyway last many months (depending on activation levels). The more likely situation is that failure will occur in the early years of operation, when the vessel is not heavily activated. Should the failure occur after significant activation, the decision whether to repair the device can be taken at the time based on the information to be gained by a repaired machine, versus what has been achieved thus far and the time for repair. The procedures to be used can also be finalised and implemented then.

2.9.9.3 Maintenance Time Estimation

2.9.9.3.1 CS or PF Coils Disassembly and Re-assembly

In comparison to the repair time, the disassembly/re-assembly time for the CS or PF coils is not significant, the repair time of the coils being dominant.

2.9.9.3.2 Machine 40° Sector Disassembly and Re-assembly

When the radiation level is low, the procedure for TFC/VV removal without a shielding cask is as follows.

i) The bioshield lid is removed, transferred to the parking location outside the laydown area.
ii) The cryostat lid is removed to outside the laydown area.
iii) PF1, PF2 coils are removed to the north side floor of the tokamak building.
iv) The machine 40° sector is removed to the laydown area through the west side of the tokamak building. By lifting in this way, it is possible to perform repair and maintenance operations on the laydown area.

The total intervention time for this case is estimated at several months.

2.9.9.4 Assessment and Future Work

The feasibility of TFC/VV disassembly and re-assembly using remote procedures has been studied conceptually and solutions for handling and shielding are proposed.

Further studies and developments are required to verify the feasibility of the disassembly and re-assembly of large components, to a level appropriate to such highly unlikely operations.

2.10 Assembly Equipment and Procedures

2.10.1 Introduction

The assembly plan defines the sequences of operations developed to complete the assembly of the tokamak, which includes the cryostat and the sub-systems contained therein. The scope of the plan includes the on-site transport of the components, preparation (pre-assembly) of the components, sub-assembly of the integrated assembly units, and final assembly inside the tokamak pit.

The assembly plan will be the basis for establishing the scope of the detailed assembly procedures which will be used to assemble the tokamak in accordance with local regulations.

To complete the assembly operations will require both specially designed, purpose-built tools, and standard, commercially available equipment. To support the assembly process, a number of services; metrology, metallurgy, beryllium control, health physics and occupational safety, will be established, and provided at the site.

2.10.2 Basic Concept

The tokamak is assembled from 9 sectors, each with a toroidal angle of 40°, and comprising a sector of VV, two TF coils, the associated VV thermal shield (VVTS), and two VV gravity supports (VVGS), which provide both the vertical support and lateral stabilisation to the VV in the completed tokamak. The components are delivered to the site individually, and sub-assembled into sectors using purpose built jigs and fixtures in the assembly hall.

Prior to installing the sectors in the tokamak pit, the tokamak gravity supports (GS), lower cryostat sections, and the components which cannot be installed following final assembly of the sectors, principally the lower PF coils, lower correction coils (CCs), the lower CC feeders, and the lower pre-tensioning rings, are installed, or placed in the pit.

The sectors are transferred to the pit sequentially. The TF coils and VVTS sectors are connected in the same sequence, whereas the VV sectors are joined (welded) according to a plan which aims to minimise deformations, and the associated technical risk.

Following installation of the final sector, the TF coil pre-tensioning rings are installed, and the pre-load applied to each of the coils. A detailed dimensional survey at this stage provides the

geometrical estimate of the magnetic datums for the as-built TF magnet, and these are used as reference for all subsequent installation operations.

The VV is closed toroidally, with the welding of near-diametrically opposite joints. Clean conditions are then established inside the vessel, and the installation of the in-vessel systems is completed. The completion of the installation of the ex-vessel components proceeds in parallel.

2.10.3 Assembly Strategy

The assembly plan is aimed at achieving the technical requirements for the assembled sub-systems, within the desired assembly schedule. There are three main issues:

- the tight installation tolerances required for the major components of the tokamak, considering the large size and weight of the components - to achieve these, the assembly plan must follow sequences and processes which minimise both deviations and the residual stresses in the components, and which allow for the correction of any deviations as they occur, so that alignment errors do not accumulate;
- routing of components through the building complex to avoid potential conflicts between activities that are carried out in parallel - this must be carefully planned, and also includes the routing of systems which must be transferred via the assembly facilities, and be installed elsewhere in the building, such as in the galleries;
- use of appropriate clean conditions - to meet the vacuum requirements, the assembly of all of the tokamak components must be carried out under clean conditions, and the assembly of the components containing beryllium will require additional precautions.

2.10.3.1 Tolerance Requirements

With the alignment tolerances close to the limit of what is achievable, the accumulation of deviations must be strictly controlled. The assembly plan is therefore designed to correct alignment deviations at each step of the assembly sequence. This strategy relies on linking a sophisticated optical metrology system (OMS) to a CAD system, which can generate and analyse complex 3-D models in near-real time, and provide a complete, evolutionary database of the as-built (i.e. assembled) components and of the overall tokamak geometry.

With respect to the major components, it is essential that most geometrical interfaces have the provision for adjustment (generally shimming) included in their design.

The strategy for controlling the dimensions of the tokamak build is illustrated in Figure 2.10.3-1. Component installation will be preceded by a comprehensive survey of the tokamak pit, and a best-fitting process will then be used to define the "pit assembly datum" with respect to the as-built pit geometry. Prior to completion of the TF magnet, the large components will each be independently aligned with respect to these datums. In principle, the datums will be fixed for the duration of this part of the assembly, although, in practice, it may be advantageous to progressively modify the datums, and the assembly of the TF magnet would then proceed via a process of best-fitting (adjusting) of the datums to the as-built geometry of the TF magnet.

On completion of the assembly (and pre-tensioning) of the TF magnet, a comprehensive survey of the TF coils will be combined with manufacturing dimensional control data to provide a geometrical estimate of the magnetic axis of the machine; this is referred to by the

term "tokamak assembly datum" in Figure 2.10.3-1. Subsequent alignment operations, primarily on the components which are tightly toleranced, will be carried out relative to the tokamak assembly datum.

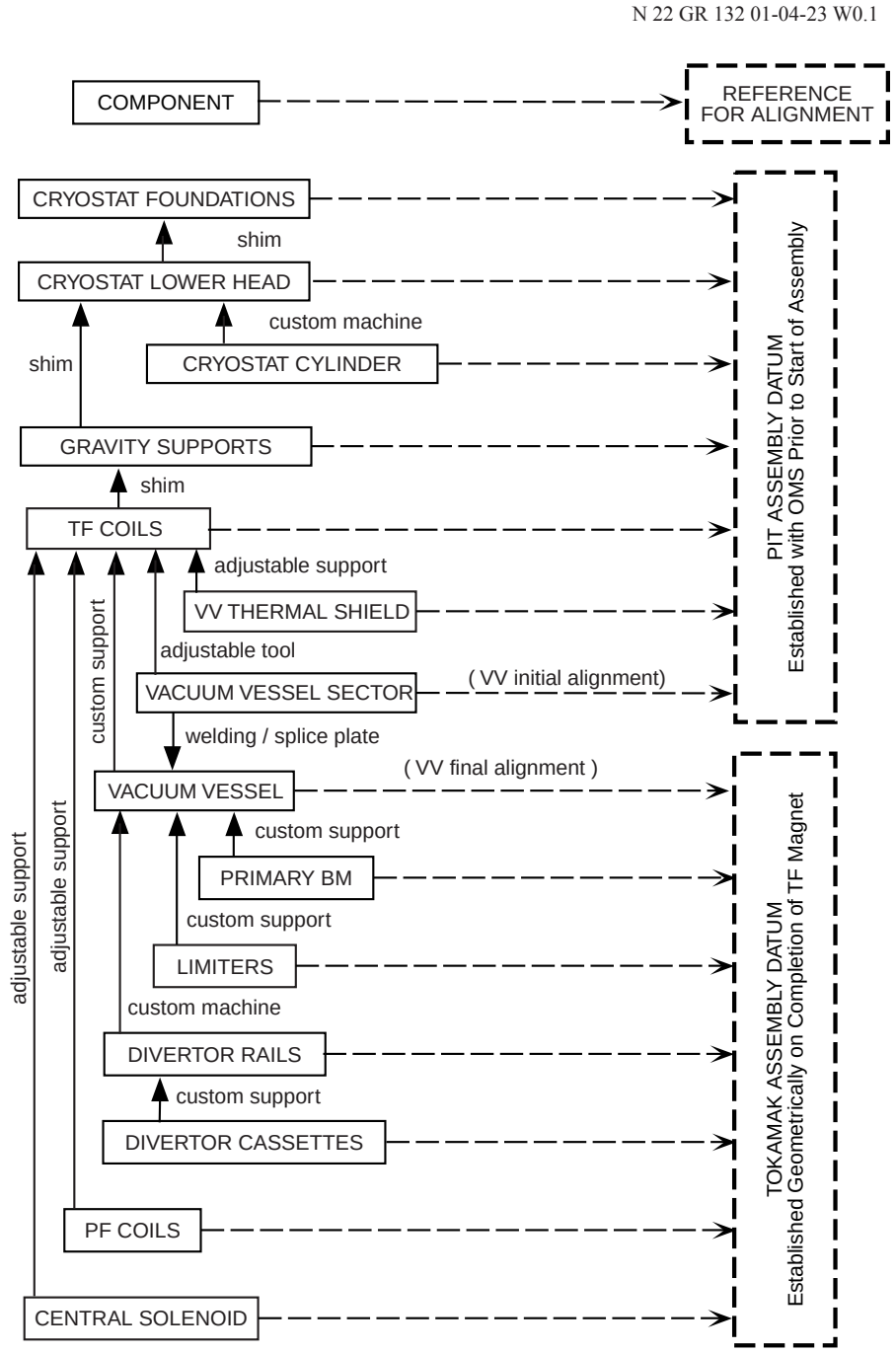

Figure 2.10.3-1 Tokamak Alignment Strategy

Figure 2.10.3-1 also identifies the proposed method of adjusting the component interfaces at each assembly step.

2.10.3.2 Building Utilisation

The assembly processes in the assembly hall of the laydown, assembly and RF heating building are aimed at obtaining the maximum utility from the available layout, which is constrained by crane coverage limitations for the heavy lifts.

A temporary area will be established outside the south end of the building complex (see Figure 2.10.3-2) in which to unpack and/or clean the large components before entry into the assembly hall. A similar, but smaller, area will be established in the hot cell building, to the north. The routing of the components into and through the building will conform to the following basic plan.

Initial assembly phase:

- the sub-assembly tooling and workstations for the VVTS, TF coils and VV will be cleaned, installed and tested in the assembly hall;
- the cryostat foundations, base sections and cylinder, and the lower, trapped PF coils, PF5 and PF6, will be cleaned, and then prepared in the laydown area prior to installation in the pit (this will require lifting these components over the sub-assembly tooling and work stations, with consequent limitations on the height of these lifts).

This strategy will allow the sub-assembly of the 40° assembly sectors, which affects the critical path of the assembly schedule, to begin in parallel with, or prior to, the installation of the lower cryostat components. In this way, the start of installation of the 40° assembly sectors in the pit may be advanced, and the assembly schedule minimised.

TF coil, VV, VV ports and in-vessel components:

- the VV sectors, VVTS sectors and TF coils will be cleaned in the south facility, and then prepared, sub-assembled and controlled in the assembly hall;
- the VV port sections, and the blanket modules, divertor cassettes and other in-vessel components will be unpacked and cleaned, prepared and controlled in the hot cell, located to the north of the tokamak hall; these components will then be routed to the VV via the tokamak hall lift and galleries.

The routing of the components through the building complex is also indicated in Figure 2.10.3-2.

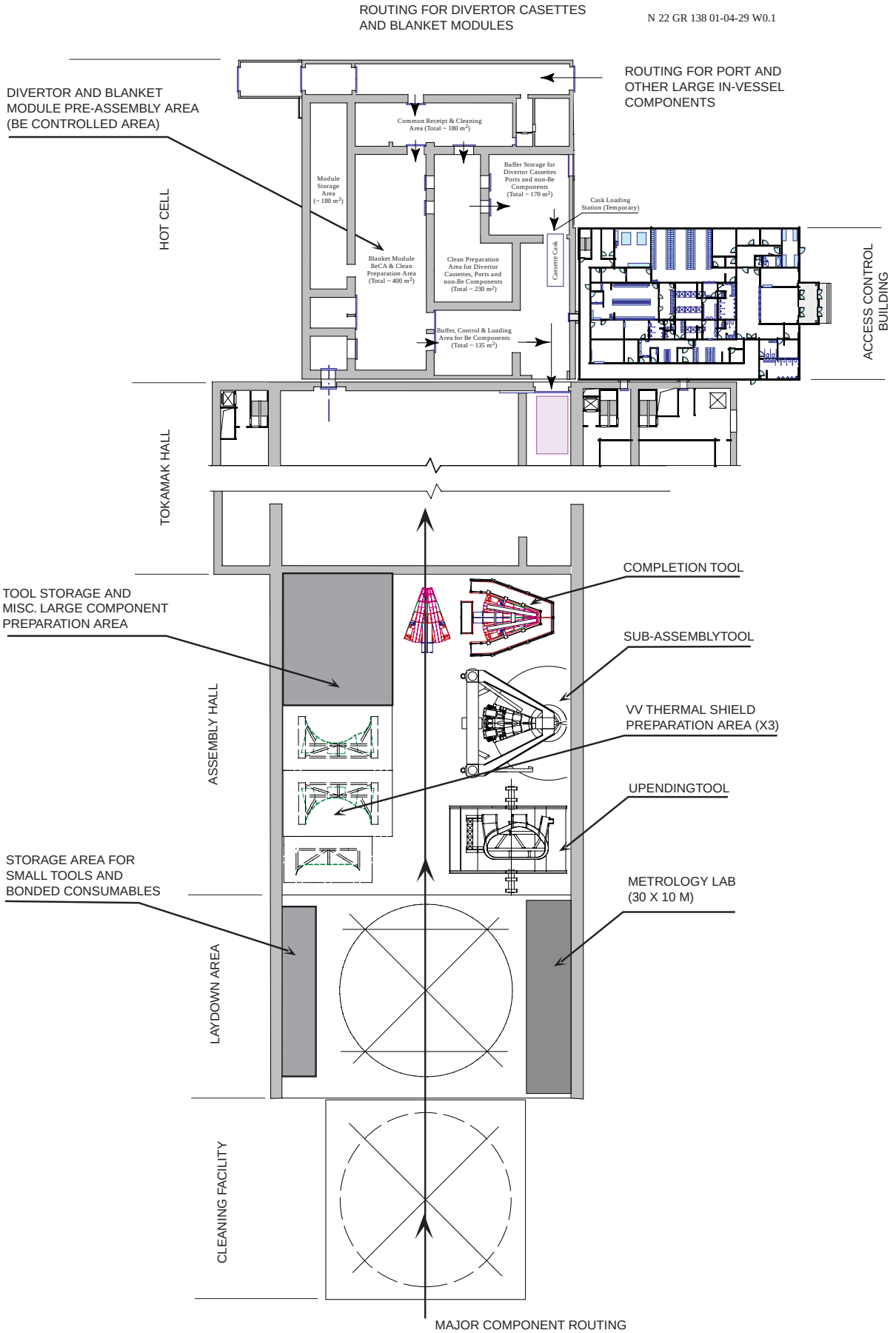

Figure 2.10.3-2 Utilisation of Tokamak Building during Initial Assembly

2.10.3.3 Clean Conditions and Be Control

The correct functioning of the in-vessel and in-cryostat components necessitates the achievement of a high level of cleanliness prior to operation. To ensure cleanliness of the in-cryostat components, for which a systematic, post-assembly cleaning is unfeasible, the building complex will be operated under conditions equivalent, or near to class 100,000 clean room conditions (target conditions); components will be cleaned prior to entry, personnel will be appropriately dressed, and "dirty" processes and tooling specifically excluded from the area.

To ensure compatibility with the achievement of ultra-high vacuum operating conditions, a higher standard of cleanliness will be required for the interior of the VV, and for the in-vessel components. The following strategy will permit the establishment and maintenance of clean conditions for the in-vessel assembly operations, whilst minimising the detrimental effect on the productivity of the workforce:

- the assembly of the VV will be carried out under the same conditions as for the cryostat and other in-cryostat components;
- following toroidal closure of the VV, and installation of the VVGS, an independent ventilation and access system will be installed in the galleries surrounding the bioshield, and connected to the VV via a number of its ports: the remaining ports will be sealed using temporary blanking plates;
- the interior of the VV will be cleaned to the required standards using techniques applicable for ultra-high vacuum components, e.g. scrubbing and pressure washing with approved detergents and solvents, rinsing with demineralised water and "warm" air drying, and clean conditions established;
- in-port and in-vessel assembly shall then be carried out under clean conditions.

Beryllium is a material which in dust form is classified as hazardous to health, and special precautions will be necessary when components containing Be and its compounds are being handled, prepared and assembled. The principle source of Be in ITER is the blanket modules, which are clad with a solid layer of metallic Be. For preparatory operations, a dedicated Be control area will be established in the hot cell building, see Figure 2.10.3-2, and, prior to installation of the first blanket module, similar controls will be applied to the VV. The two areas will be maintained under negative pressure via separate, local ventilation systems, which will exhaust via HEPA filters.

Access to the Be-controlled areas will be restricted to a specific group of registered workers, strictly regulated, and extensive routine monitoring for surface and airborne Be dust will be required. The Be components will be exposed only in these areas; for transit to, and between, the areas the components will be packaged in sealed containers (such as the gallery transport casks).

2.10.4 Tokamak Assembly Plan

2.10.4.1 Tokamak Boundaries

The tokamak assembly plan will require approximately 10^6 man hours to complete. The estimated duration for the activities is approximately 4 years.

The assembly plan covers the cryostat and the sub-systems contained therein. A limited number of components external to the cryostat are also included in the scope of the assembly plan; typically these are attached to the cryostat, and form the interface with the surrounding building/systems, e.g., gravity support pedestals and the penetrations for the magnet feeders. The following sub-systems are included in the scope of the assembly plan:

•	Cryostat and penetrations;	
•	Bioshield lid;	
•	Magnet system, comprising;	Toroidal field coils and structures
		Gravity supports
		Poloidal field coils and supports
		Central solenoid and supports
		Correction coils and supports
		In-cryostat feeders
•	Vacuum vessel;	Vacuum vessel
		Ports
		VV gravity supports
•	Thermal shields, comprising;	Vacuum vessel thermal shields
		Cryostat thermal shields
		Transition thermal shields
•	In-vessel components, comprising;	Divertor
		Blanket modules
•	In-port components, comprising;	Cryopumps
		Diagnostics
		Test blanket modules
		Additional heating systems.

and all associated in-cryostat pipework, instrumentation and cabling.

The overall dimensions and approximate mass of each of the major components in its assembly configuration is given in Table 2.10.4-1.

Table 2.10.4-1 List of Major Tokamak Components

Component	Qty	Overall Dims (m)	Mass (tonne)
Cryostat Base Section	1	Ø 28.6 x 6.0	1187
Cryostat Lower Cylinder	1	Ø 28.6 x 10.2	730
Cryostat Upper Cylinder	1	Ø 28.6 x 8.8	680
Cryostat Lid	1	Ø 28.6 x 4.2	700
Bioshield Lid	1	Ø 12.0 x 2	500
Bioshield Lid	4	21.2 x 10.8 x 2	750
Gravity Support Pedestal	18	Ø 1.35 x 4.32	13.5
VV Sector (with some separate manifolds and fixtures)	9	14.0 x 8.0 x 8.0	700
VV Gravity Supports	18	1.9 x 1.4 x 0.5	5.3
TF Coil	18	16.6 x 9.0 x 2.7	325
Gravity Support	18	2.6 x 2.3 x 1.4	25.6
PF1 incl. Clamps	1	Ø 9.4 x 1.1	218
PF2 incl. Clamps	1	Ø 17.8 x 0.7	271
PF3 incl. Clamps	1	Ø 25.1 x 1.3	627
PF4 incl. Clamps	1	Ø 25.0 x 1.3	600
PF5 incl. Clamps	1	Ø 18.1 x 1.1	404
PF6 incl. Clamps	1	Ø 10.7 x 1.1	453
Central Solenoid	1	Ø 4.2 x17.8	1117
Upper Correction Coil	6	7.0 x 4.2 x 0.2	14.7
Side Correction Coil	6	7.9 x 7.2 x 0.8	27.3
Lower Correction Coil	6	7.0 x 4.2 x 0.8	20.2
Divertor Cassette	54	3.4 x 2.1 x 0.8	12
Blanket Module (max)	421	(1.3-2.0) x (0.9-1.2) x 0.45	4.5
Inboard Cooling Manifold	9	6.9 x 3.2 x 1.0	2
Outboard Cooling Manifold	9	8.0 x 2.4 x 1.8	3

2.10.4.2 Scope of the Operations

The tokamak assembly plan includes all the operations required to progress the components from their point of reception, storage or manufacture on the ITER site, to their final installed position in the tokamak device. The following, generic sequence describes the scope of the operations for a typical component:

Initial Status of the Components

With the exception of the large components to be fabricated on site, i.e. the cryostat sections, and the PF2, PF3, PF4 and PF5 coils, each component to be assembled will be located in one of the paved, on-site storage areas.

The component will be contained in a "transport package" designed to support the component during shipping and handling, and to provide environmental protection and maintain cleanliness during transport and on-site storage.

Generic Operations

In general, each component will then go through the following process:

i. the package containing the component will be rigged and positioned on a suitable transporter, and transferred to the appropriate cleaning facility, see Figure 2.10.3-2;
ii. the component will be rigged and removed from its packaging: the packaging, and the external transporter will be removed from the cleaning facility, and the component placed on an internal, standardised air pallet; the temporary cranes and rigging will be removed from the cleaning facility;
iii. the component will be unpacked, visually inspected, and cleaned as necessary;
iv. the component will be transferred into the laydown area, pre-assembly inspections performed, and the component prepared for subsequent assembly;
v. the component may be transferred to the designated sub-assembly area, and the sub-assembly operations completed;
vi. the component will be transferred to the pit, either as an individual component or as a part of a sub-assembled unit, and assembled into the tokamak.

2.10.4.3 Outline Assembly Procedure

An outline procedure has been developed for the assembly of the tokamak as the basis for the elaboration of the detailed assembly sequences, conceptual design of the associated assembly tools, the evaluation of the assembly schedule, manpower and tooling requirements, and of the associated cost.

A high level summary is provided by the logic diagrams shown in Figures 2.10.4-2 to 2.10.4-6. The overall procedure is divided into the following six main sub-sections, see Figure 2.10.4-1:

2.2.A.1 Lower Cryostat Activities: (Figure 2.10.4-2) the sub-section includes the assembly procedures for the bottom of the cryostat, the gravity supports, and the lower PF coils; this section covers activities from the initial assembly in this area up to the placement of the first 40° assembly sector;

2.2.A.2 40° Sector Sub-Assembly: (Figure 2.10.4-3) includes installation of the VVTS workstations, the upending tool, the sector sub-assembly jig, and the sector completion tool, in addition to the procedures necessary to sub-assemble each of the nine sectors; each sector includes a pair of TF coils, a 40° segment of the VV and three VVTS parts, an inboard 40° sector and two outboard, opposite hand 20° sectors;

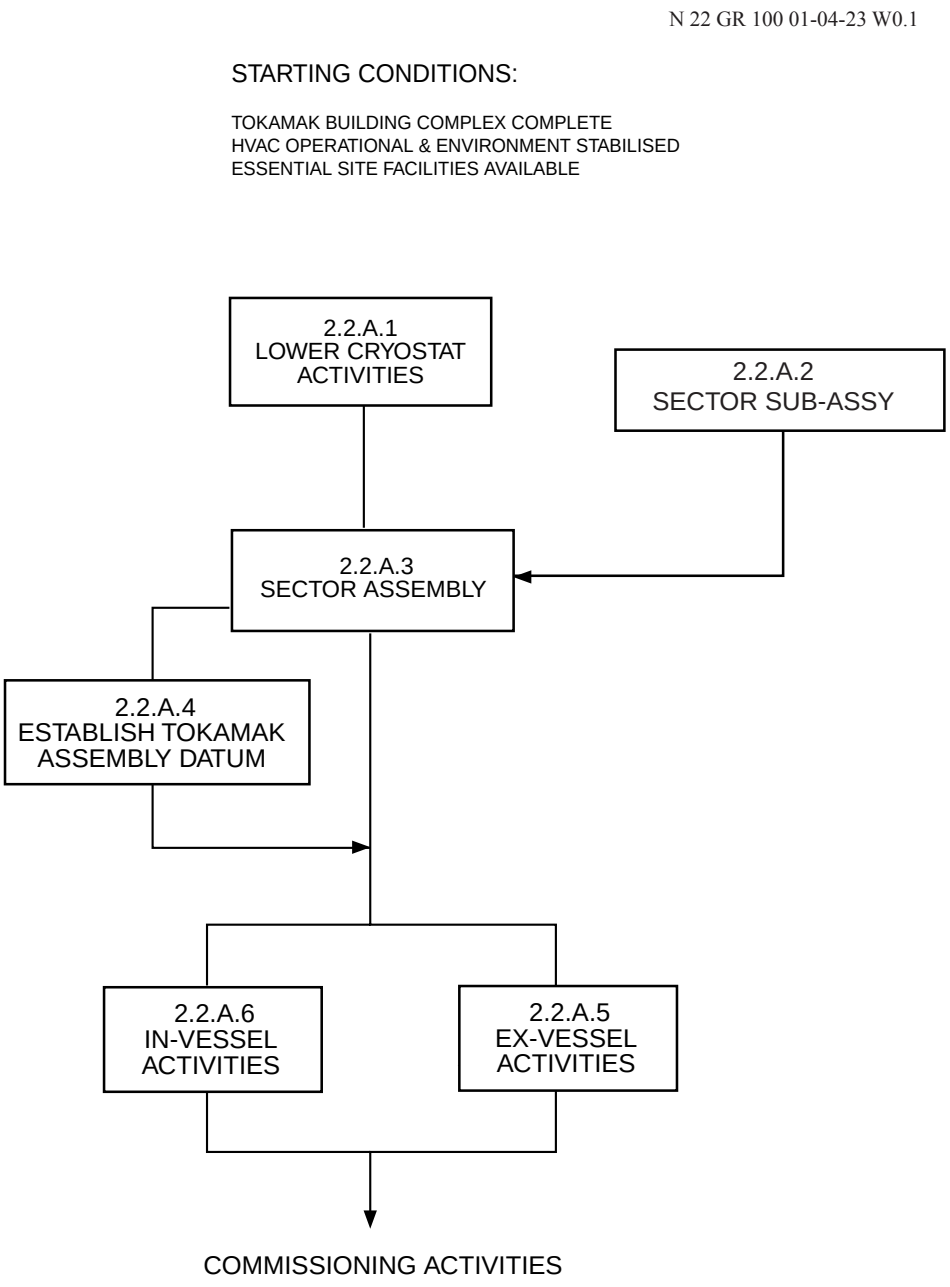

Figure 2.10.4-1 Overall Assembly Sequence – Top Level

N 22 GR 101 01-04-23 W0.1

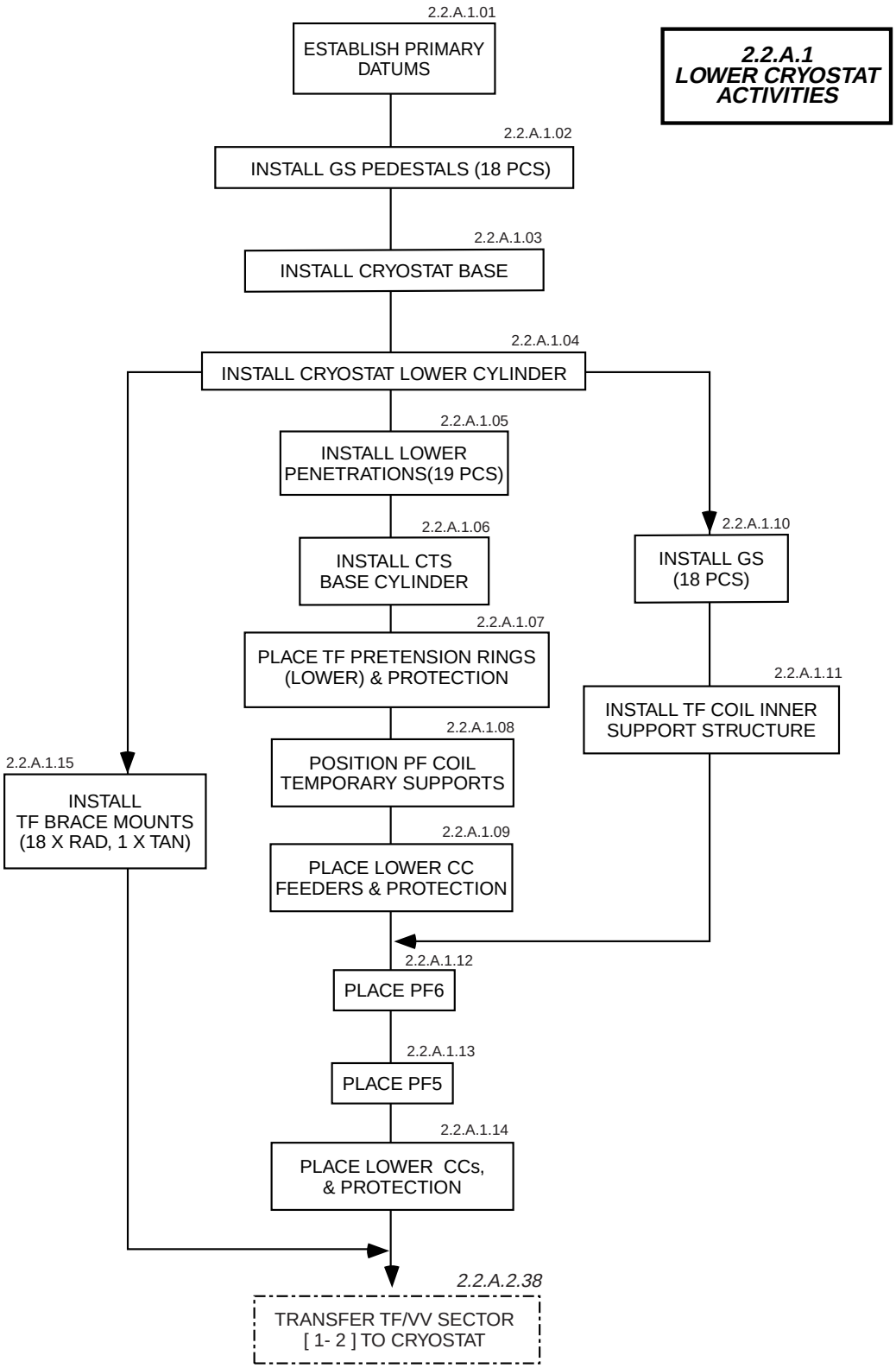

Figure 2.10.4-2 Assembly Sequence – Lower Cryostat Activities

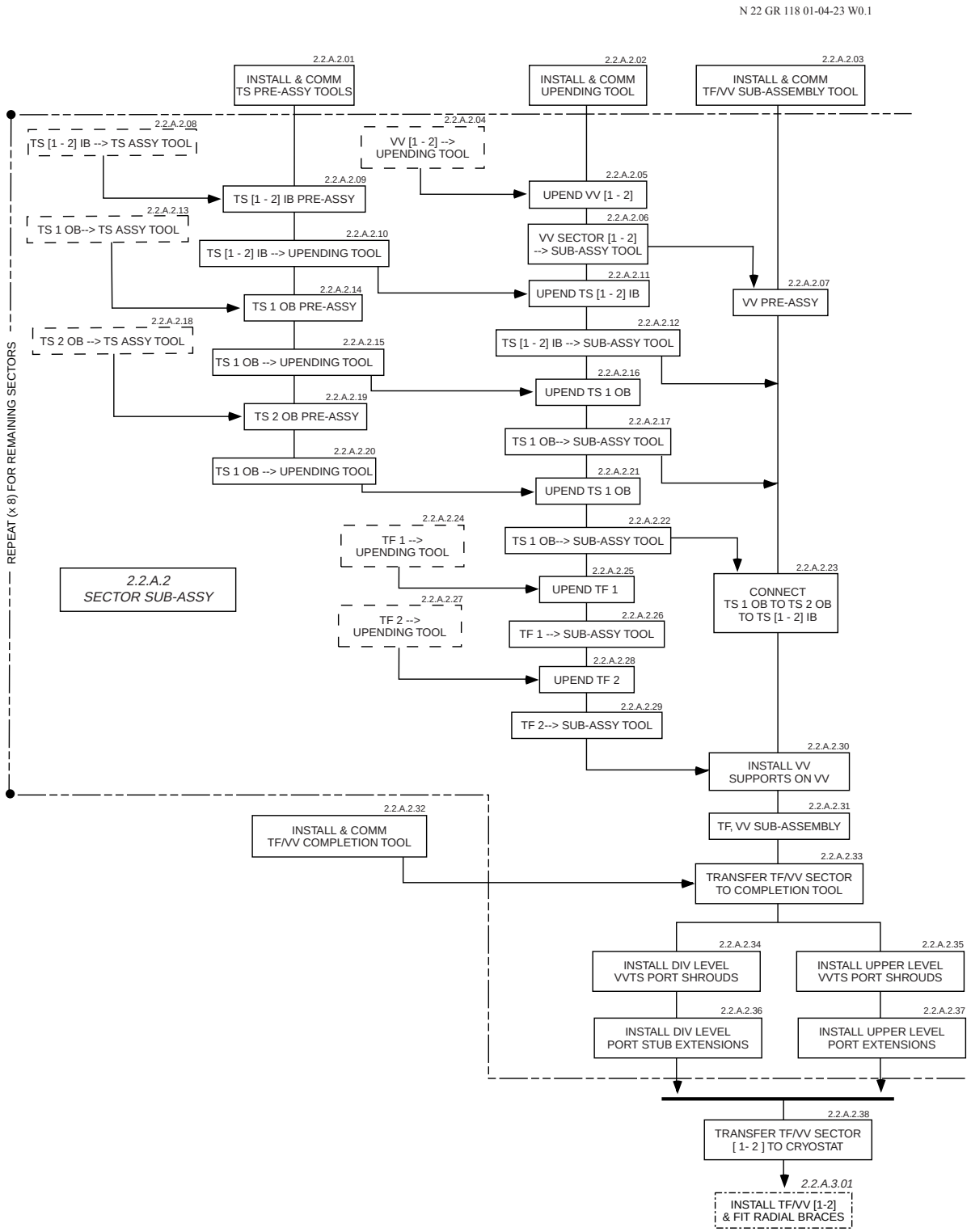

Figure 2.10.4-3 Assembly Sequence – Sector Sub-Assembly

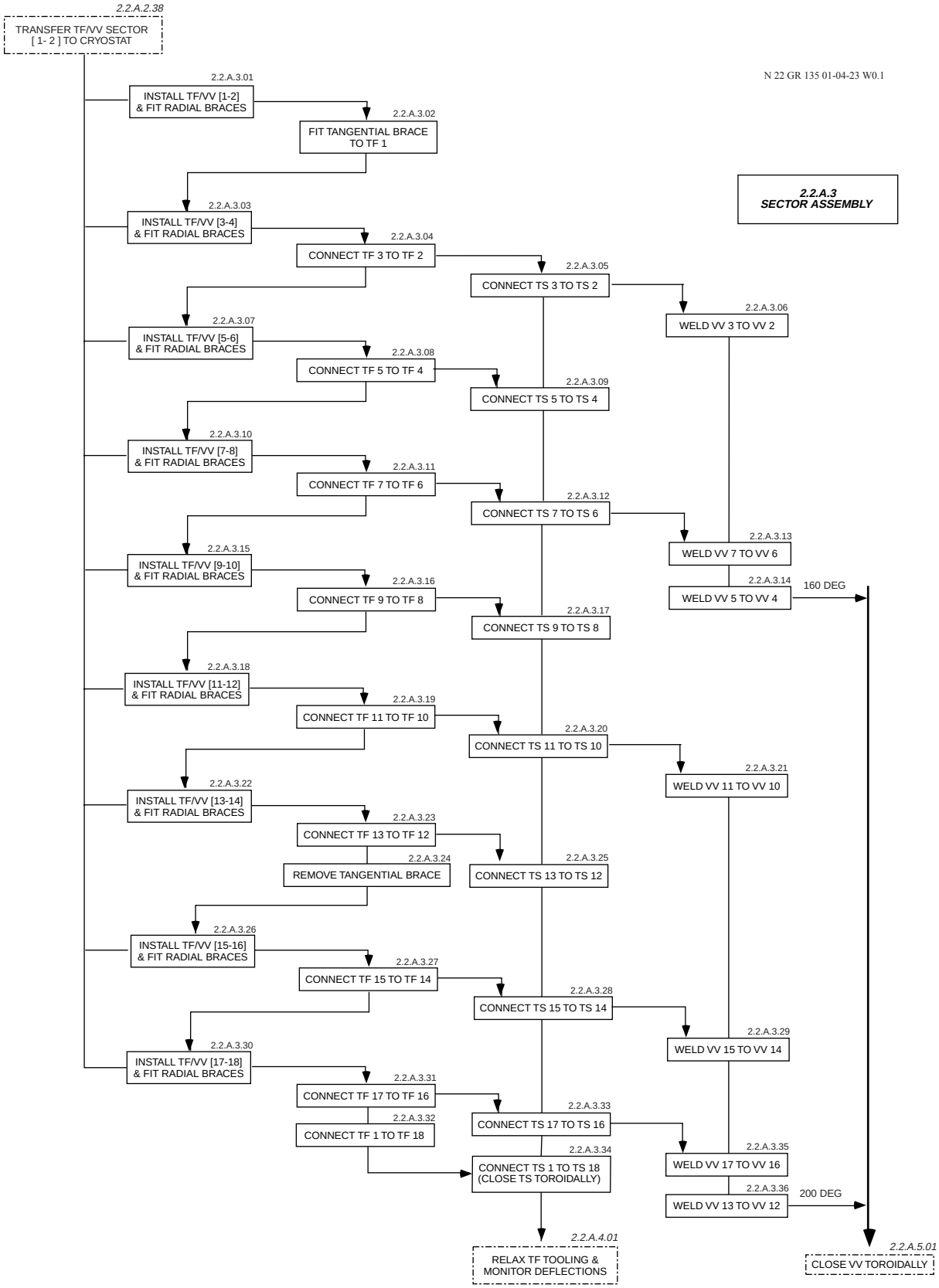

Figure 2.10.4-4 Assembly Sequence – Sector Assembly

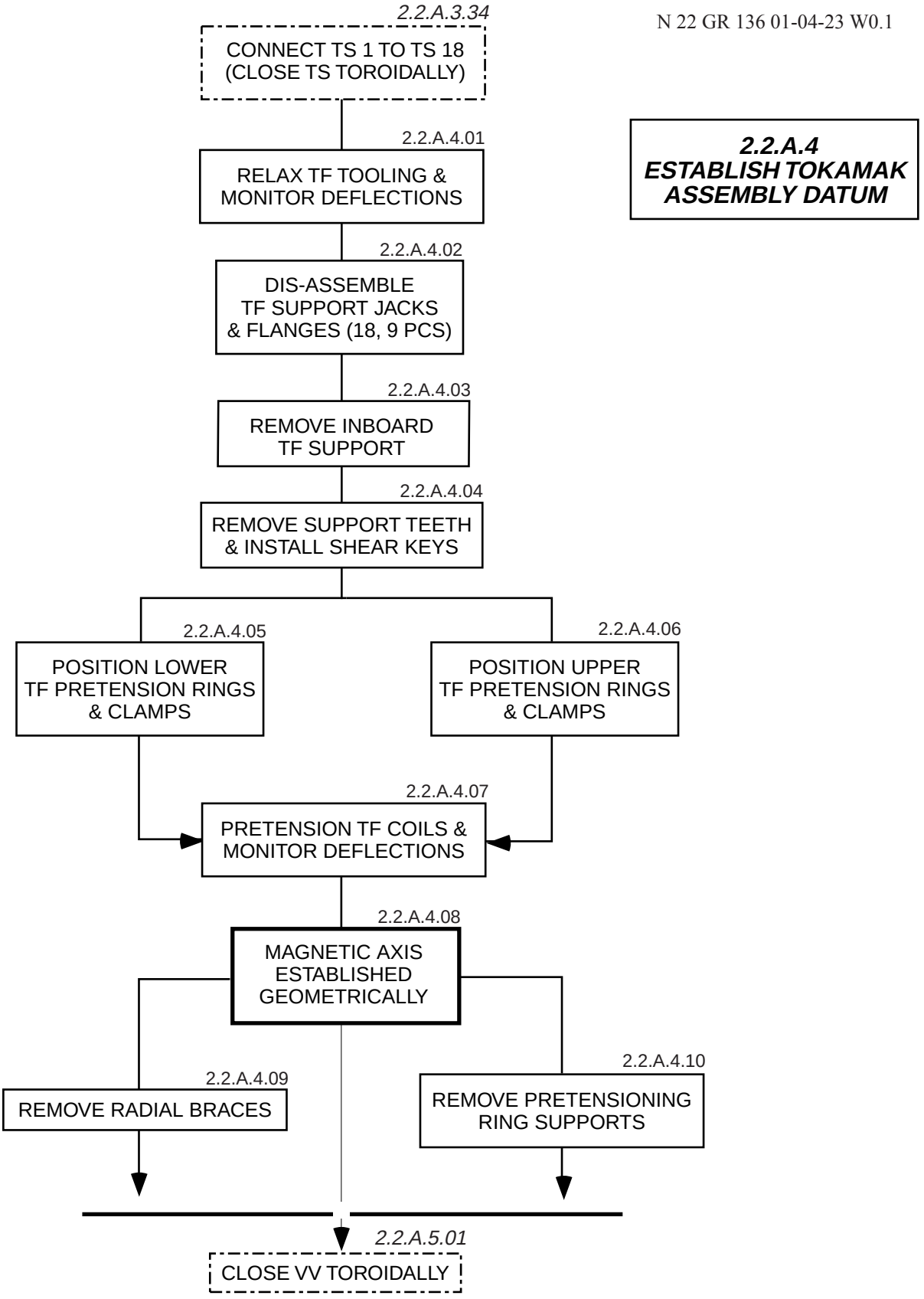

Figure 2.10.4-5 Assembly Sequence – Establish Assembly Datums

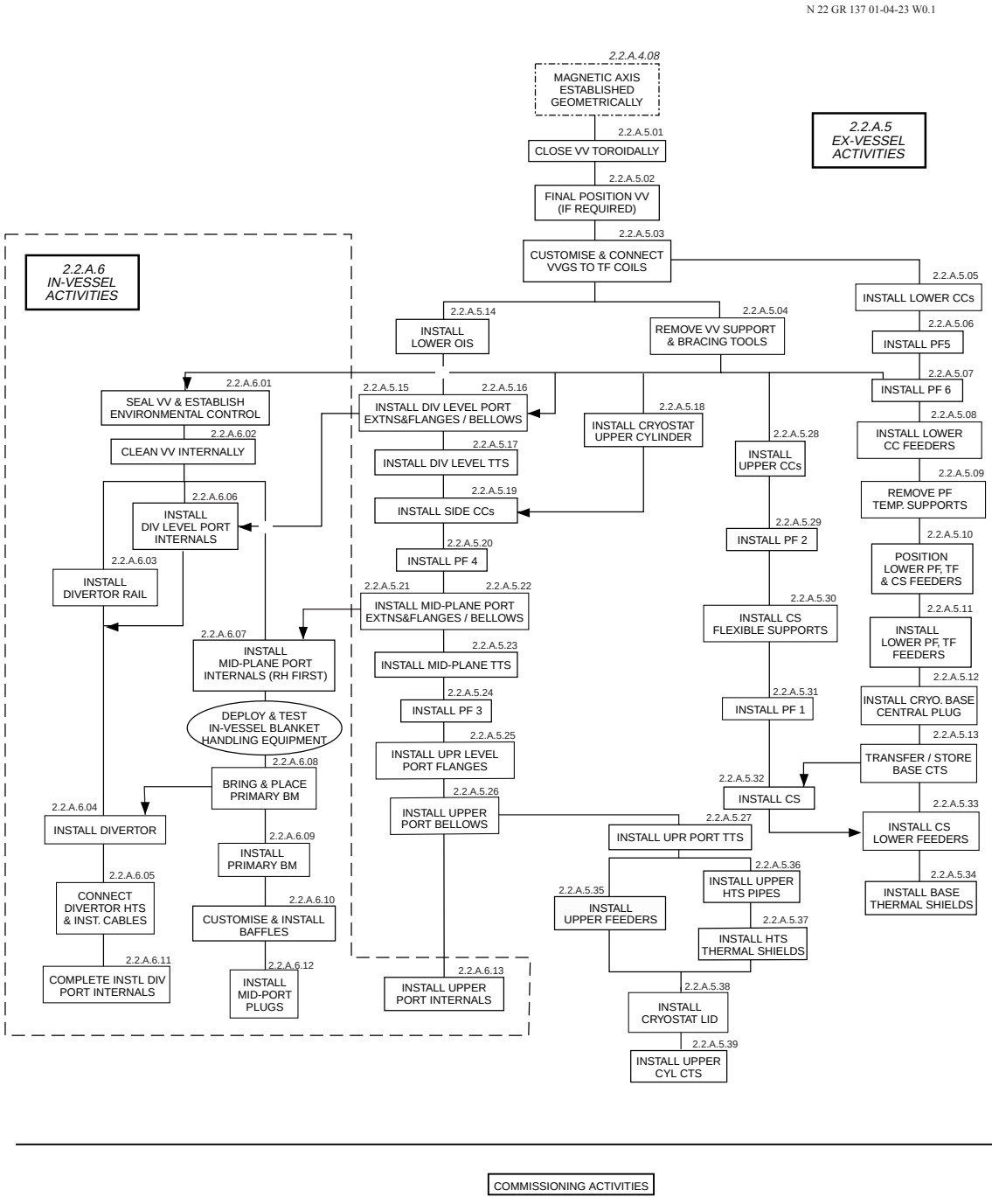

Figure 2.10.4-6 Assembly Sequence – Ex-Vessel & In-Vessel Assembly

2.2.A.3 40° Sector Assembly: (Figure 2.10.4-4) covers the sequencing of the sector assembly in the cryostat;

2.2.A.4 Establish Tokamak Axis: (Figure 2.10.4-5) this section includes the pre-tensioning of the TF magnet, and the survey procedures by which the tokamak assembly datum is geometrically established, see also Figure 2.10.3-1;

2.2.A.5 Ex-Vessel Activities: (Figure 2.10.4-6) includes the welding of the final VV field joints (toroidal closure), and all of the assembly procedures for the components and systems external to the VV and ports, from the establishment of the magnetic datum to the preparation for commissioning; these activities, occur largely in parallel with the in-vessel assembly procedure;

2.2.A.6 In-Vessel Activities: (Figure 2.10.4-6) includes all of the assembly procedures specific to the VV and port internals, up to the preparation for commissioning.

2.10.5 Assembly Tools

To complete the assembly operations described in the assembly plan will require a comprehensive package of tools; this will include both purpose-built jigs, fixtures and handling tools, and standard, commercially available equipment. A list of the major tools is provided in Table 2.10.5-1.

2.10.5.1 General Design Principles

Although the assembly tools comprise a diverse range of equipment, with highly different functions, requirements and capacities, a number of common design principles/philosophies have been universally applied to their design.

Accuracy

The positioning tolerances for the major components are typically in the low mm range. The accuracy of the positioning features of the tools have to be compatible with this requirement.

Capacity

Prior to the availability of final design data, the design of the major tools is presently based on 110% of the current component weights, to accommodate possible future design changes and to provide an allowance for any small ancillary tooling, work platforms, etc., which may be attached to the components.

Currently an absolute limit of 1,500 t is imposed on the weight of any single lift, plus rigging, by the capacity of the dual crane lifting system. The limit for single crane lifts is 750 t. To increase operational flexibility, where possible, the combined weight of tooling plus component should not exceed the capacity of the single crane.

Handling

All component parts of the tools, e.g. component support members, access platforms etc., shall be provided with handling features to interface with standard lifting eyes or shackles, to facilitate their lifting with standard equipment.

Materials

Special consideration has to be given to the selection of the materials to be used in the construction of the tools. The most severe requirements are applied to the tools which will be used inside the vacuum vessel, where conditions of cleanliness suitable for ultra high vacuum operation must be established and maintained.

Multi-functionality

The design of single tools with the capability of performing multiple operations, or the use of common elements in different tools, is a potential reducer of the overall cost of the assembly, and this shall be considered in the design of each tool.

Table 2.10.5-1 List of Major Tokamak Assembly Tools

WBS Identifier	Tool	Comments
2.2.B.01	**Assembly Control Tools**	
2.2.B.01.01	Metrology laboratory	
2.2.B.01.02	Metallurgy laboratory	
2.2.B.01.03	Beryllium analysis laboratory	
2.2.B.01.04	Health physics laboratory	
2.2.B.01.05	Machine shop	
2.2.B.02	**Assembly Support Tools**	
2.2.B.02.01	Cleaning facilities	
2.2.B.02.02	Cryostat access equipment	
2.2.B.02.03	VV access & control system	
2.2.B.02.04	Be enclosure and environmental control	Blanket Module preparation area
2.2.B.02.05	Clean preparation area	Divertor Cassette preparation area
2.2.B.03	**Sector Sub-Assembly Tools**	
2.2.B.03.01	Upending Tool	Multiple purpose
2.2.B.03.02	TF Coil, VV and VVTS Handling Tools	1 each: TF coil horizontal lifting tool; VV sector horizontal lifting tool; TF coil vertical lifting tool; VV sector vertical lifting tool
2.2.B.03.03	Sector sub-assembly tool	
2.2.B.03.04	Sector lifting tool	
2.2.B.03.05	Sector completion tool	Alternatively, 2nd sub-assembly tool (2.2.B.03.03)

WBS Identifier	Tool	Comments
2.2.B.04	**TF Coil, VV and VVTS assy. tools**	
2.2.B.04.01	TF gravity support assy. tools	
2.2.B.04.02	TF coil inner support	
2.2.B.04.03	TF coil bracing tools	
2.2.B.04.04	Guides and positioning jacks for TF coil placement	
2.2.B.04.05	TF coil assembly tools	
2.2.B.04.06	VVTS assembly tools	
2.2.B.04.07	VV welding tools	
2.2.B.04.08	VV gravity support survey tool	
2.2.B.04.09	TF coil pre-tensioning ring installation tools	
2.2.B.05	**Cryostat assembly tools**	
2.2.B.05.01	Cryostat survey tools	
2.2.B.05.02	Cryostat installation tools	
2.2.B.05.03	Cryostat welding tools	
2.2.B.06	**Cryostat thermal shield assembly tools**	TBD
2.2.B.07	**PF coil assembly tools**	
2.2.B.07.01	PF coil handling tools	
2.2.B.07.02	PF coil survey tools	
2.2.B.07.03	PF coil installation tools	
2.2.B.08	**Port & piping assembly tools**	
2.2.B.08.01	Port handling tools	sets. 1 x upper, 2 x mid-plane & 2 divertor
2.2.B.08.02	Port welding tools	
2.2.B.08.03	Port bellows installation tools	sets, 1 x upper, 1 x mid-plane, 1 x divertor
2.2.B.08.04	Port pipework installation tools	sets, handling tools (orbital / bore welding tools incl. in standard tools
2.2.B.09	**CS assembly tools**	
2.2.B.09.01	CS assembly tool	support & access facility installed in assembly hall
2.2.B.09.02	CS lifting tool	incl. interface for independent support from upper TF coil
2.2.B.09.03	CS installation tools	
2.2.B.10	**Correction coil & feeder assembly tools**	
2.2.B.10.01	Correction coil assembly tools	
2.2.B.10.02	Feeder positioning tools	

WBS Identifier	Tool	Comments
2.2.B.11	**In-vessel assembly tools**	
2.2.B.11.01	Vessel washing equipment	sets
2.2.B.11.02	In-vessel staging	modular on per VV sector basis
2.2.B.11.03	In-vessel component installation tools	
2.2.B.12	**Common handling tools**	
2.2.B.12.01	Integrated heavy transporter system	Heavy roller system Air bearing system Self-propelled modular transporter system Boom gantry system Gallery transporter system Standardised air pallet system
2.2.B.12.02	Common heavy lifting tools	Dual hoist lifting beam Universal lifting beam
2.2.B.12.03	Standard handling tools	Temporary crane Flat bed truck Fork lift truck
2.2.B.13	**Standard tools**	Welding tools (manual, orbital & bore welders), pipe cutting tools, jacks, assembly hall machining facilities (bed plate & tools), fastening tools (torque wrenches, stud pre-tensioners, etc.), standard handling tools, hydraulic pressure testing equipment, temporary clean room

Safety/Personnel Access

The design and operation of the machine assembly tools shall conform to good industrial safety practices. In particular, the following specific issues shall be addressed by the design:

- the installation of the components will require personnel to work at significant heights (25 – 30 m) above the effective floor level, i.e. the cryostat base; personnel access to the sectors shall, preferably, be provided via specifically designed platforms, or temporary staging; the use of scaffolding, which could be erected in such a way as to interfere with the safe operation of the tools, is discouraged;
- with a combined mass of ~ 1,400 t, the 40° assembly sectors and their associated lifting equipment, are substantial loads, which require accurate alignment; the design of the tools must allow personnel access to check alignment and/or level during lifting and placement, whilst ensuring that the operations do not necessitate personnel moving or working below the suspended load.

2.10.5.2 Tool Description

Assembly Control and Support (2.2.B.01, 2.2.B.02)

These groups of "tools" include the facilities necessary to control the quality of the work (metrology and metallurgy), and to ensure that the project's statutory obligations in terms of worker safety (beryllium control, health physics, and occupational safety). It may be cost-effective to sub-contract some of the required services to outside suppliers. This will be investigated following site selection, when the local engineering infrastructure is known.

Also included is an on-site workshop (it may also be possible to contract-out this service), and the specialised access and control equipment required for the VV, cryostat and for the preparation of the beryllium containing components.

Sector Sub-Assembly (2.2.B.03)

The sub-assembly of the 40˚ assembly sectors is carried out in the assembly hall, with the components in their final, vertical orientation, see Figure 2.10.5-1. This option is preferred over "horizontal" sub-assembly because: for vertical sub-assembly the footprint of the tooling is smaller, and the reduction in the required floor space yields a corresponding reduction in building cost; vertical sub-assembly is less sensitive to component delivery scheduling; the capacity and cost of the upending tool is lower for vertical sub-assembly, without a corresponding increase in the other tooling.

The tooling comprises: an upending tool, which rotates the components to the vertical orientation; a sub-assembly tool, see Figure 2.10.5-2, which supports the VV, and, via a rotary motion about the "machine axis", incorporates first the VVTS, and then the TF coils; a completion tool, to which the sector is transferred for the installation of the VVTS port shrouds and VV port stub extensions. To maintain the desired schedule, and minimise overall cost, the completion tool, envisioned originally as a cost effective solution for the sub-assembly operations not requiring the specific functionality of the sub-assembly tool, may be replaced by a second sub-assembly tool.

The sub-assembly tools also include a number of handling tools for lifting the major components in both horizontal and vertical orientations.

Sector Assembly (2.2.B.04)

The principal sector assembly tools comprise an integrated system of supports and braces. These are used to position and align the components, and to stabilise them against lateral loads, such as seismic loads. The layout of the tools is shown in Figure 2.10.5-3.

The most substantial of the assembly tools is the inboard support for the TF coils. This tool, located inboard of the centre of gravity of the sectors, supports approximately 30% of their weight (~ 3,300 t) prior to toroidal completion of the TF magnet. For each TF coil, a radial slot in the support provides the means of registering the coil toroidally, and a system of lateral wedges provides the capability to adjust the toroidal position of the coils. A hydraulic jack installed in the base of each of the slots provides the capability to adjust the height at which each sector is supported independently, and, following completion of the assembly of the TF magnet, to unload the tool for disassembly and removal. A mechanical lock on each jack avoids the need to maintain hydraulic pressure throughout the assembly process, and the jacks are only pressurised to effect adjustment and/or unloading of the system.

During the initial stages of assembly, the coils are also restrained radially via a rigid connection to the support. As more sectors are installed, and connected, the GS of the TF coils become more effective at immobilising the sectors radially and, progressively, this function is shared between the tool and the GS.

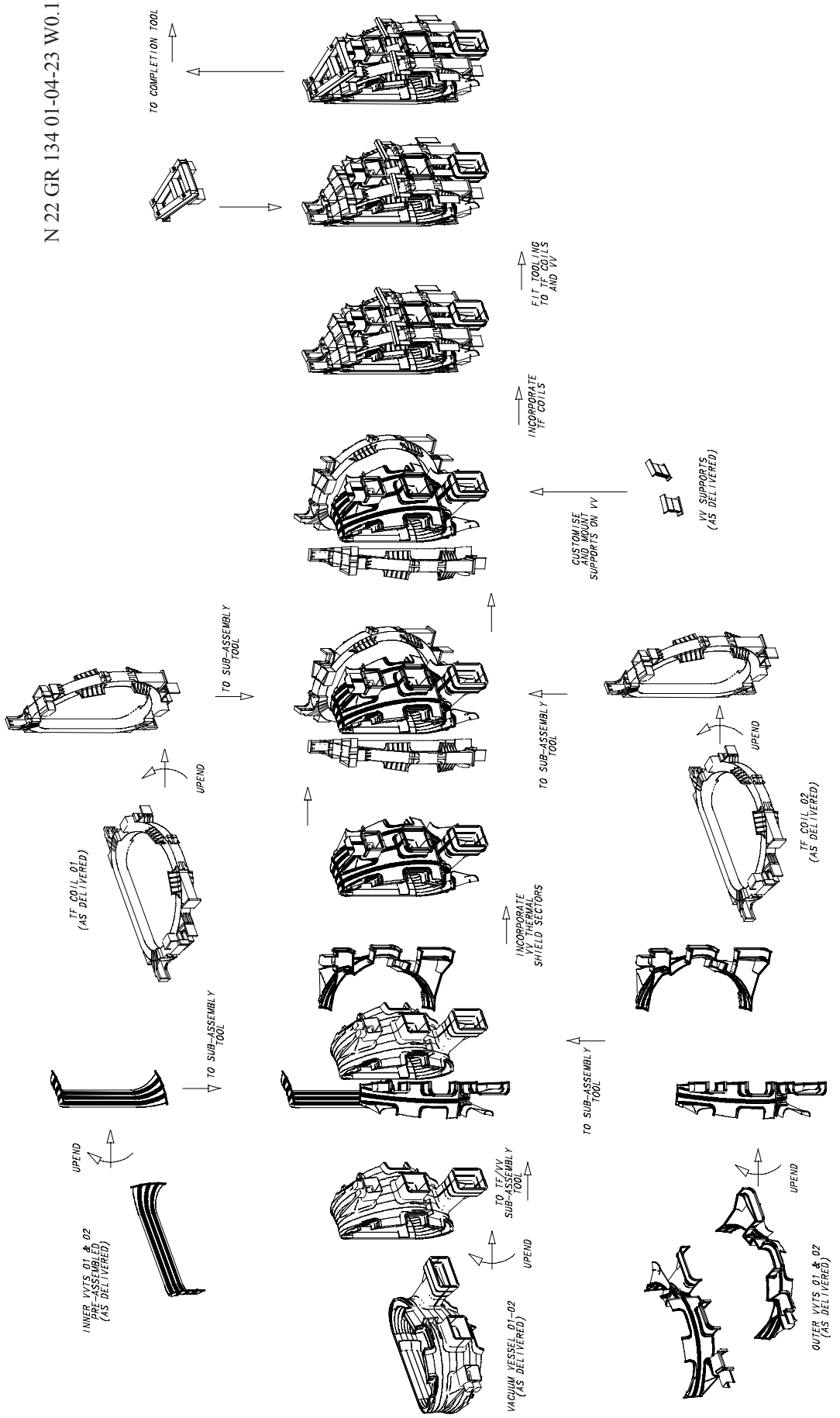

Figure 2.10.5-1 Sector Sub-Assembly Procedure

N 22 GR 188 01-05-30 W0.1

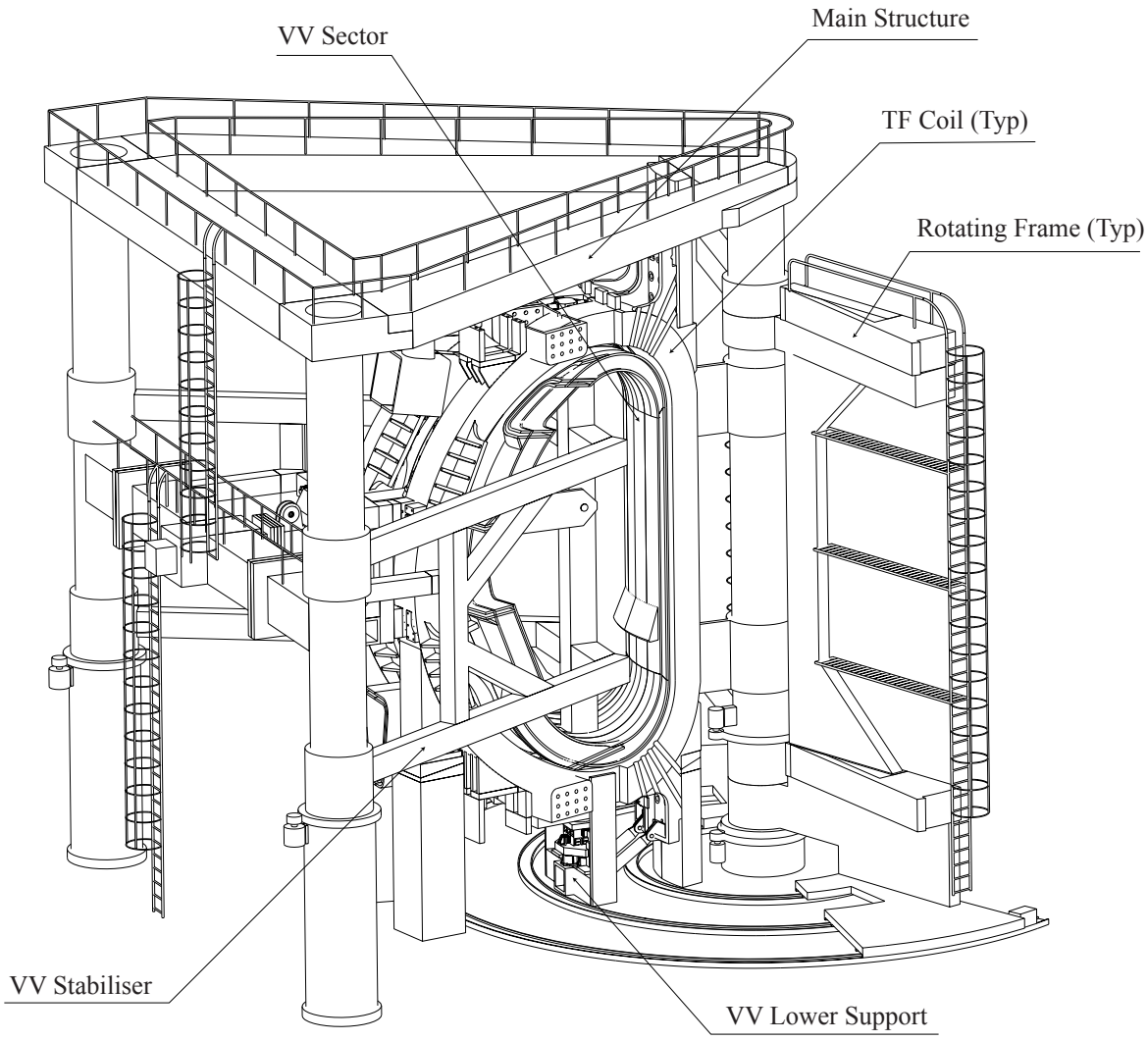

Figure 2.10.5-2 Sector Sub-Assembly Tool (2.2.B.03.03)

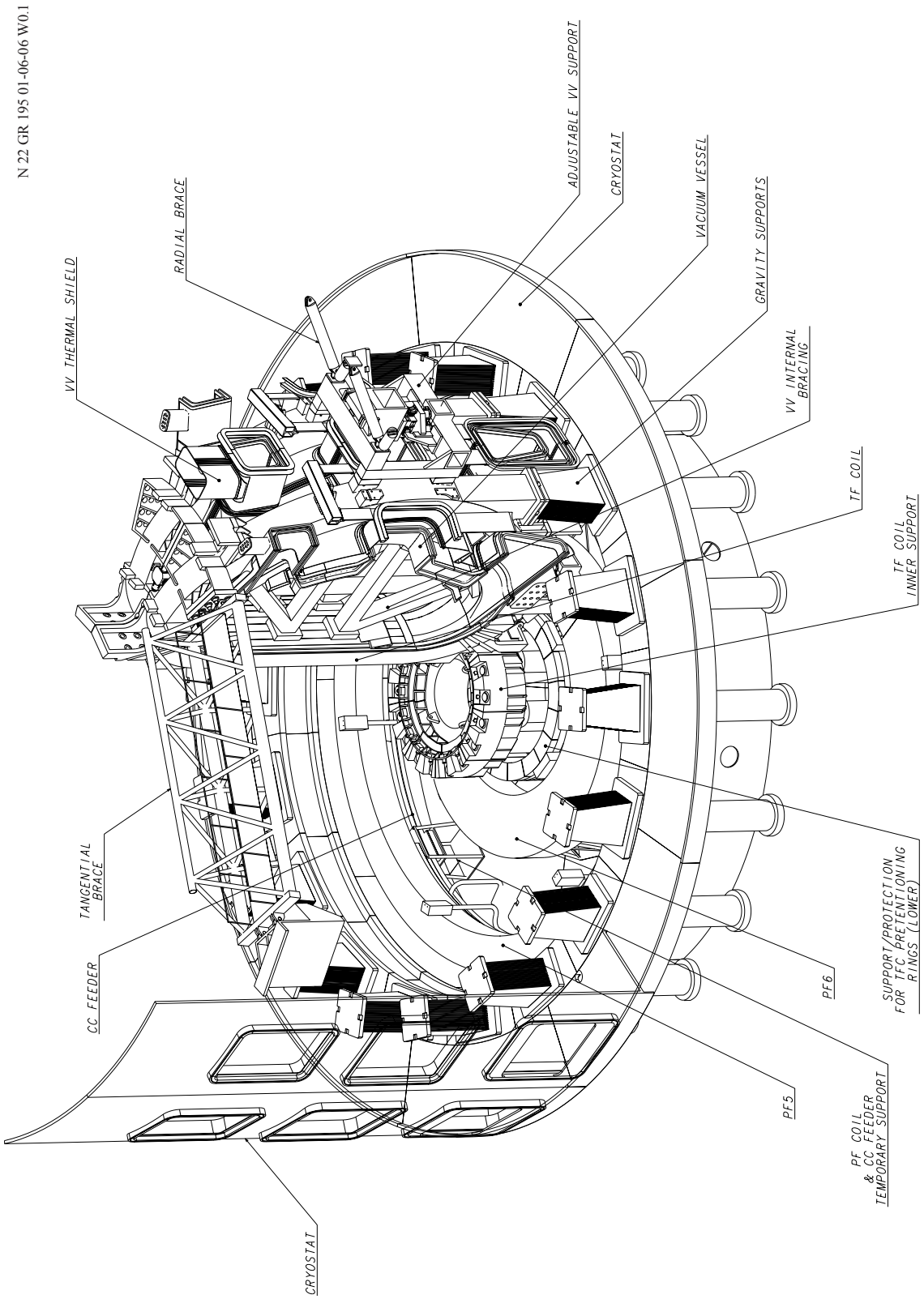

Figure 2.10.5-3 Layout of Assembly Support and Bracing Tools (2.2.B.04)

The assembly tooling also includes the VV support tools, contained in 2.2.B.03, and a series of upper braces which connect: the outboard regions of the TF coils to the bioshield (radial braces); the top of the first coil to the bioshield (tangential brace); and provide temporary connection between the top of the TF coils of neighbouring sectors prior to connection of the respective intercoil structures (TF-TF braces).

Cryostat and Cryostat Thermal Shield Assembly (2.2.B.05, 2.2.B.06)

The cryostat assembly tools include the installation tools: purpose built fabrication/transport frames, for transporting the large sections from their sub-assembly area to the assembly hall; adapters that interface with the 4 universal lifting beams (2.2.B.12), for lifting the sections into the pit with the overhead cranes; and the support and guides which align the field joints as the sections are installed.

Specialised survey tools will be required to control the interfaces between the cryostat base and support pedestals, and also the interfaces between the cryostat base and the bioshield. The welding tools comprise the clamps which hold the field joints in alignment during the welding operations, the NG-TIG welding machines on which the welding process is based, and a purpose built track to support and guide the welding machines.

PF Coil Assembly (2.2.B.07)

This group of tools includes, for each coil: a transportation frame, to support and protect the coil during on-site transit; purpose-built survey tools; lifting adapters to interface with the universal lifting beams (2.2.B.12); and installation tools, mainly temporary, as well as adjustable supports.

In addition, for the two lower trapped coils (PF5 and PF6), an array of support frames are provided to support the coils from the cryostat base, at the minimum height consistent with providing the required “ground” clearance for the coil feeders, for the duration of the sector assembly stage; and a distributed jacking system, to raise the lower coils to their final, installed elevation.

Port and Piping Assembly (2.2.B.08)

The port assembly tools comprise: the handling and positioning equipment necessary to introduce the port through the bioshield and align it with the port stub/stub extension, a machine tool to correct the perimeter of the port stub to provide the correct welding fit-up for port installation (the port handling and positioning equipment will be used to introduce, support and align the machine tool), survey tools for the field joint splice plates, welding clamps; welding rail and NG TIG welding tools, and installation tools for handling and positioning the splice plates.

The piping assembly tools consist of handling fixtures, and standard orbital welding tools.

Central Solenoid Assembly (2.2.B.09)

The principal assembly tool for the CS is a lifting tool with the capability of adjusting the vertical alignment of the coil with high precision. The tools must also interface with the upper

region of the TF coils, to provide the required support to the CS during installation, without unnecessarily occupying the overhead cranes, which are heavily utilised for assembly. Survey tools will be required to determine the custom dimensions for the CS flexible supports.

In addition, a support and positioning fixture will be required to facilitate installation of the lower centring device.

Correction Coil and Feeder Assembly (2.2.B.10)

This group of tools comprise, for each design of CC, a handling strongback, to stiffen and protect the coil during handling, survey tools for the CC supports, and welding fixtures to position and support the coil clamps during installation.

In-Vessel Assembly (2.2.B.11)

For the two major in-vessel systems, the blanket and divertor, the approach will be to use the remote handling tools to transport and manipulate the components inside the vessel, possibly operated in a hands-on mode. Also, variants of the remote welding tools, adapted for hands-on operation, may be used if commercially proven alternatives cannot be found for the specialised weld geometries which exist, for example, between the blanket modules and their co-axial feed pipes. Elsewhere, commercially available equipment will be used for the installation of the in-vessel components.

Common Handling (2.2.B.12)

The common handling tools include the lifting tools required to interface the overhead cranes with various, purpose-built component lifting tools. Presently these comprise: the dual hoist beam - a device with a single, centrally located, slewing attachment with 750 t capacity. This lifting beam, which will be attached to the two hoists of a single crane beam, will be used for lifts in the 375 t to 750 t range, thereby freeing the second overhead crane for increased operational flexibility; a set of 4 universal lifting beams, spreader beams that will be connected to each of the four 375 t crane hooks via a central attachment, and to the component via an attachment at each of their extremities, to provide a low mass, toroidally distributed 8 point lift for the large diameter components, such as the cryostat sections and the PF coils.

The other major handling tool is an integrated system of heavy, surface-based transporters based on a diverse range of technologies. Generally, the large components will be moved between the on-site fabrication/storage areas and the cleaning facility via a customised arrangement of self-propelled modular transporters. These are self-levelling, multi-wheeled, flat bed devices, with the capability of operating in the confined spaces of the compact ITER site, and, if required, on unpaved surfaces. It is anticipated that the self-propelled modular transporters will also be required for delivery operations, leading to heavy utilisation of the units.

Specifically for the cryostat sections, which will be fabricated in an area aligned with the centreline of the building, rail-mounted, heavy roller units will provide an inexpensive and robust solution for transport to the cleaning facility, without imposing unnecessary burdens on the heavily utilised self-propelled modular transporters.

The systems for moving the components inside the clean areas will utilise air pad technology. The purpose-built transport frames for the larger, heavy components, such as the PF coils and cryostat sections will integrate provision for handling with air pads once the cleaning operations have been completed. For the other movements inside the assembly hall and galleries, a standardised range of air pallets will be used.

For loading and unloading components between the various transport systems, where overhead crane capacity is not available, a boom-gantry system is proposed.

In addition, a number of conservatively sized portable cranes, flat bed trucks and fork lift trucks will be required.

Standard Tools (2.2.B.13)

This group includes the standard, commercially available tools required to complete the assembly operations, which are not covered elsewhere in the tooling list. One major item is the assembly hall bed-plate and machining centre, which, given the prohibitive cost and logistical difficulties associated with the return of even one of the large components to the supplier for modification or rework, will provide a cost effective, on-site machining capability for the largest of the components.

2.10.6 Assessment and Future Work

The strategies required to assemble the tokamak have been developed, and an overall assembly plan established. The reference assembly plan has been assessed, and the major, critical tools conceptualised, within the scope of design tasks to the Home Teams, and no lack-of-feasibility issues have been identified. The principal aims of the activities foreseen for the period prior to construction are the widening of the scope of the design and planning base to cover all of the tokamak systems and tools, and their elaboration to a greater level of detail than was previously warranted. More specifically:

- for the assembly plan, there remains an uncertainty concerning the dimensional control of the major components in the pit; the assembly plan depends on the assumption that survey techniques and procedures can be developed that will allow the metrology system to function at the limit of its capability under the non-ideal geometrical constraints which exist in the VV and pit, and this remains to be confirmed via a testing program;

- the effort in terms of man hours and schedule for the assembly have been evaluated, but there is room for further optimisation, by means of the development of a resource-loaded schedule - such work would also confirm and optimise the building utilisation;

- although the details of many of the critical assembly procedures have been developed, the scope of this work needs to cover all the major procedures envisaged; the fully detailed procedures for all assembly sequences can be finalised only after the design of the components is fully frozen, and the applicable regulations are known, following site selection;

- the conceptual design of the major tools is well advanced; the scope of the design activities now needs to be extended to include the minor tools; the design of all the

tools must be reviewed following site selection, when the applicable codes and standards will be defined, and may be incorporated into the design of the tools.

2.11 ITER Decommissioning Procedures

The present document gives a brief description of the ITER decommissioning plan, its phased pattern, and some indications of the activities expected to be required.

2.11.1 Decommissioning Phase 1 – De-Activation

The aim of phase 1 is to bring the machine into a safe state soon after the end of operation, in preparation for the subsequent phase 2 tasks, utilizing the facilities and manpower still available on site from the previous operation phase. The responsibility for phase 1 belongs to the ITER organization and will terminate with the handing over of the facility to a new organization inside the ITER host country in a ready-for-decommissioning status. Phase 1 will consist mainly of the removal of mobilizable tritium from the in-vessel components and of any recoverable activated dust (beryllium, tungsten, carbon). Also, the in-vessel components are removed.

During phase 1, hot cell operations are expected to be intensive due to the large number of components that needs to be processed prior to disposal.

Tritium will first be removed from the surfaces of the in-vessel components by established techniques and stored prior to its removal from site. Beryllium dust and any recoverable activated dust will also be removed to the greatest possible extent from the vacuum vessel using the existing remote handling equipment.

During phase 1, the de-activation of the coolant in the loops of the tokamak cooling water system (TCWS) will start with the removal of activated corrosion products and the de-tritiation of the (water) coolant. Throughout this period, the WDS plant is required to assist continuously the hot cell operations (with the ADS and VDS, atmosphere and ventilation de-tritiation systems), the tritium plant normal ventilation de-tritiation system (N-VDS) and the stand-by atmosphere de-tritiation systems (S-ADS/S-VDS - this is used only in case of a tritium release accident). As for the tokamak vault dryers/coolers, the WDS plant is needed only until after complete TCWS dismantling. As a result, it is estimated that approximately 50% (i.e. 10 kg/h) of total WDS capacity can be used to remove tritium from the TCWS coolant water (max 600 t). Under this condition, the TCWS coolant tritium removal process time can be estimated at about 8 years. This figure may possibly be reduced to about 5 years, depending on the WDS requirements in other parts of plant.

2.11.1.1 Removal of In-Vessel Components

The aim of this phase is to remove all in-vessel components, i.e. blanket, divertor, and all upper, equatorial and divertor port-mounted systems. All in-vessel components are dismantled according to established procedures that are part of the facility remote maintenance plan. This means that only a minimum amount of additional equipment and procedures need to be provided for phase 1.

During phase 1, the following operations could also be carried out, mainly to take advantage of the available remote handling equipment already deployed inside the vessel. After removal of the in-vessel components, the vacuum vessel may be cut from the inside along the field joints and the corresponding interspace shielding blocks removed. The outer vessel skin would not be cut to preserve structural integrity and guarantee confinement during the radioactivity decay period and during the early part of phase 2, provided that the structural integrity against SL-2 earthquake can be retained with outer skin only. The poloidal rail required to drive the cutting tools is left in place for future use in phase 2.

The vacuum vessel is eventually cleaned to remove any remaining dust prior to the start of the radioactivity decay period. Shielding plugs are installed inside the equatorial and divertor ports, and the vessel is sealed.

2.11.1.2 Removal of Ex-Vessel Components

Two options are available:

Option 1 – Anticipate the dismantling of some ex-vessel components during phase 1

According to option 1, some activities could be performed inside the cryostat and pit in parallel with the in-vessel operations. In order to be performed under hands-on conditions, although still time limited, such activities must wait at least ~ 4 years after end of machine operations before the following operations are safely initiated:

- opening of the cryostat top central bioshield/lid assembly and of other cryostat access points as required;
- dismantling of cryostat thermal shield (part), all coils feeders, central solenoid, PF1 coil;
- possibly disconnect and remove CS;
- possibly cut and remove correction coils;
- possibly lowering onto cryostat floor of PF5 and PF6 coils;
- close cryostat openings.

The above operations can be performed using the existing equipment plus, possibly, some additional new equipment and tools, as required. However, new staff would have to be recruited because it has been assumed that for the initial ~ 4 years waiting period no such staff would be required on site (at least not for the above operations). The above operations will not increase the duration of phase 1 because they are entirely in parallel with the in-vessel operations and they are not on the critical path. Removed ex-vessel components, which are not activated, are transferred outside the tokamak building for temporary storage or size reduction, prior to disposal, re-use or material re-cycling.

Option 2 - Ex-vessel components are dismantled during phase 2

This option is desirable if:
- overall decommissioning time is not an issue;
- early re-cycling or re-use of some machine components is not required;
- there is an advantage or a specific requirement by the host country organization;
- there is a decision to delay the decommissioning work and related expenditure until later, i.e. in phase 2.

2.11.1.3 Other Plant Systems Decommissioning

Other activities performed during phase 1 are:
- removal of the remaining activated/contaminated systems, such as parts of the neutral beam (NB) injectors/diagnostics;
- at the end of hot cell operation, the tritium plant is not further required - all tritium in the plant is removed and the plant is dismantled;
- all tritium and beryllium can be removed from the ITER site;
- the hot cell radwaste processing operations are completed and the hot cell is decontaminated and dismantled.

2.11.1.4 Disposal

Disposal of radwaste will take place during and/or after the dismantling operations, depending on the policy adopted by the host country organization at the time. Depending on the local requirements, disposal may be preceded by temporary storage.

2.11.1.5 Hot Cell Building Operation

During phase 1, hot cell operation is expected to be continuous due to the large number of components that needs to be processed prior to disposal. It has been identified that, during phase 1, the hot cell may be the bottleneck in the components waste processing and disposal path, creating hold-ups in the flow of components from the machine to the hot cell building. To ensure that the hot cell activities do not take longer than other phase 1 work, additional hot cell building equipment must be provided. The hot cell needs to be provided, for increased radwaste processing efficiency, with the following equipment:
- 2 or more vacuum furnaces for tritium removal from components;
- 2 or more cutting stations for components size reduction;
- equipment and tools for the removal of beryllium pellets and breeder material from the breeding blanket modules;
- facility for materials re-cycling;
- additional radwaste temporary storage.

2.11.1.6 Phase 1 Duration

The estimated duration of phase 1 is approximately 5 years. The drivers of phase 1 duration are:
- hot cell building waste processing activity duration;
- tritium removal from the coolant.

2.11.1.7 Radioactivity Decay Period

During this period, radioactivity inside the vacuum vessel will continue to decay. The estimated duration of the time at which the contact dose rate for hands-on operations falls, on average, below 10 μSv/h is estimated as approximately 23 years. During this phase, site activities are reduced to a bare minimum and consist mainly in the following:

- vacuum vessel radioactivity monitored to establish when final dismantling (in phase 2) can be initiated;
- cranes periodically maintained in preparation for phase 2 activities;
- plant systems (such as ventilation, etc.) required for phase 2 maintained as necessary (possibly not running continuously, but inspected periodically);
- monitoring of the environment from a safety point of view.

2.11.2 Phase 2 – Final Dismantling and Disposal

2.11.2.1 Final Dismantling – General Description

The main activity during phase 2 is the removal of the machine 40° sectors (each consisting of a vacuum vessel 40° sector and its thermal shield, and two TF coils) and the dismantling of the vacuum vessel. Further, if option 2 of phase 1 is adopted, all ex-vessel dismantling operations are also performed in phase 2. Phase 2 operations are carried out using, in part, components and plant, which have been maintained or kept in an operational state during the radioactivity decay period. Dismantling of the vacuum vessel is done using remote techniques. Dismantling of any ex-vessel components is mostly done hands on. In principle, remote handling equipment used previously for the removal of the in-vessel components could be used. However, it is expected that because of its age and the intensive usage in previous years, this equipment will require upgrading or, most likely, will need to be entirely replaced. Other, general, handling equipment (for example cranes) would have been maintained during the radioactivity decay period and will be used for both the vessel and ex-vessel dismantling. Other activities during this phase include the completion of the dismantling of the NB lines and the removal of the vacuum vessel pressure suppression system (VVPSS) and drain tanks. Separation of the TF coils from the associated VV sectors is performed hands-on or remotely inside a cutting bay which has to be provided and equipped with all the associated systems before the start of the cutting operations. The two major sources, which may contribute to the dose during phase 2, are:

- the torus: after the removal of one or more machine 40° sectors a large opening is exposed;
- the machine 40° sectors : during their transfer from the machine to the shielded area of the assembly hall (cutting bay) where the TF coils are separated from the vessel sector and the vessel sector reduced in size for disposal.

The requirement that radiation doses of a member of the public and workers due to the two sources should be maintained ALARA is satisfied after approximately 23 years decay period from the end of machine operation. After this period, the machine 40° sectors can be extracted and transferred to the cutting bay without time limiting restrictions. Further, the additional sky-shine and direct radiation from the machine after removal of one or more TF/VV sectors is insignificant.

2.11.2.2 Removal of Ex-Vessel Components

During this phase, all ex-vessel dismantling operations are, with a few exceptions (as indicated below), carried out hands on. In case of the option 2 of phase 1, all operations described in 2.11.1.2 must be carried out. In addition, the following operations must be performed:

- PHTS pipes cutting (semi-remote operations);
- coils PF3 and PF4 are removed;
- remaining sections of the cryostat thermal shield are removed;
- all VV ports are cut and removed (semi-remote);
- coils PF5 and PF6 and any remaining correction coils are cut and removed;
- top part (above the equatorial ports) of the cryostat cylinder is cut and removed;
- install TF coils lower support structure;
- TF intercoil structures are disconnected.

2.11.2.3 Machine Sectors Removal and Vacuum Vessel Cutting

Vessel sector separation is achieved by cutting, from within the vacuum vessel, the inner vessel skin (if not done in phase 1) and the outer vessel skin. The vessel thermal shield at the outer field joint region will also need to be cut through using new remote handling equipment. The divertor, equatorial and upper ports extensions are progressively cut and removed. During port extension removal and after the start of the external vacuum vessel splice plate cutting, human access inside the cryostat will be time limited or semi-remote. Tables 2.11.2-1 and 2.11.2-2 give the basis for the time estimates for these operations.

Table 2.11.2-1 Vacuum Vessel Inner Wall Cutting

Operation	Time	Total
Assumptions: 16 h/day, 6 days/week, 380 mm/min cutting speed using plasma cutting, 4.3 weeks/month		
9 vacuum vessel inner skin poloidal cuts, processing time	~ 26 m outer wall perimeter x 9 40-degree sectors x 2 cuts (inner splice plate) /380 mm/min plasma cutting = ~ 0.9 days	~ 1 d
Tools set up & remove, cleaning area, using transfer casks for vacuum vessel inner skin poloidal cuts	(8 h insertion + 8 h disengage/tool exchange/removal + 8 h cleaning) x 18 sectors	~ 18 d
Tools set up & remove, cleaning area, using transfer casks for ports cutting	(8 h insertion + 8 h disengage/tool exchange/removal + 8 h cleaning) x 18 sectors x 3 port levels	~ 54 d
TOTAL		73 d
Contingency 30 %		22 d
TOTAL		~ 95 d

After cutting, the machine 40° sector is lifted out of the cryostat and transferred to a cutting bay in the adjacent assembly hall. The bay consists of a work area surrounded by steel walls. The bay top can be removed to allow use of a crane. The top is needed to prevent the escape of dust during cutting. Near the cutting bay a temporary facility is set up to allow for the transfer of the cut VV sections into containers prior to shipment. The facility also provides space for the storage and maintenance of the equipment required throughout the VV cutting period. Within the cutting bay, the sector is positioned on a special purpose stand (possibly similar to or the same which was used for initial machine 40° sector assembly). The stand should be such as to prevent collision between a sector and the wall due to earthquakes during storage. The vacuum vessel is first cut into two halves, which are separated from the

TF coils. The vessel halves are then cut into pieces, which are placed into containers for disposal. Table 2.11.2-3 gives the basis for the time estimates for the cutting bay operation.

Table 2.11.2-2 Vacuum Vessel Outer Wall and Thermal Shield Cutting

Operation	Time	Total
Assumptions: 16 h/day, 6 days/week, 380 mm/min cutting speed using plasma cutting, 4.3 weeks/month		
Cut and remove all cryostat ports and ports extensions	Assume 5 days/port x 54 ports	~ 270 d *
9 vacuum vessel outer skin poloidal cuts, processing time	˜ 30 m outer wall perimeter x 9 sectors x 2 cuts (outer splice plate) /380 mm/min plasma cutting = ˜ 0.98 days	~ 1 d
9 vacuum thermal shield poloidal cuts, processing time	˜ 38 m outer wall perimeter x 18 sectors /380 mm/min plasma cutting = ˜ 1.22 days	~ 3 d
Cutting of vessel divertor, equatorial and upper ports, processing time	˜ 6 m cut length through the port double wall x 18 sectors x 3 port levels x 2 cuts (inner+outer port wall) / 380 mm/min plasma cutting = ˜ 1.2 days	~ 2 d
Tools set up & remove, cleaning area, using transfer casks for vacuum vessel outer skin poloidal cuts	(8 h insertion + 8 h disengage/tool exchange/removal + 8 h cleaning) x 18 sectors	~ 18 d
Tools set up & remove, cleaning area	(8 h insertion + 8 h disengage/tool exchange/removal + 8 h cleaning) x 18 sectors x 3 port levels	~ 54 d
Vessel port sections handling and removal	Assume 30 % of the above time	~ 16 d
TOTAL (operations from 2 to 7)		94 d
Contingency 30 % (operations from 2 to 7)		28 d
TOTAL (operations from 2 to 7)		~ 122 d
TOTAL (operations from 1 to 7)		~ 392 d

* This can be done in parallel with the in-vessel cutting activities. Some series operations expected where ports are used for in-vessel access therefore the overall period can be somewhat shorter, about 1 year

Table 2.11.2-3 Vacuum Vessel Cutting - Cutting Bay Operations

Operation	Time	Total
Assumptions: 16 h/day, 6 days/week, 380 mm/min plasma cutting speed, 4.3 weeks/month		
Rig up, lift, transfer and drop TF/VVsectors in cutting bay	4 days/sector x 18 sectors	72 d
Poloidal cut to free TF coil	~ 30 m av.VV perimeter x 2 walls x 3 cuts (inner splice + 1 outer cut) x 12 sectors / 380 mm/min = 3.9 days	4 d
Removal of shield blocks (after inner splice plate cut and removal above)	Assume 36 blocks x 2 h/block x 18 sectors = 54 days	54 d
Rig up 1/18 VV sector, remove TF coil	7 day x 18 = 36 days	126 d
Cut 1/18 VV sector in pieces	Assume 45 cut pieces x 6,000 mm perimeter x 18 sectors x 3 cuts (2 inner wall cuts + 1 outer wall cut) /380 mm/min	27 d
Transfer 1/18 VV sector from tokamak pit into cutting bay	3 day x 18 sectors = 8.5	54 d
Cut pieces removal time, clean up area after each cut sector, put pieces into container, transfer to hot cell/storage	(650 shield blocks+810 vv cut pieces) x 3 h	183 d
TOTAL		520 d
Contingency 30 %		156 d
TOTAL		676 d 1.8 yr

Once the vacuum vessel is completely removed from the pit, the remaining components left inside the cryostat (gravity supports, tools and fixtures, etc.) are removed and final cryostat dismantling can take place.

2.11.2.4 Disposal

Disposal of radwaste will take place during and/or after the dismantling operations, depending on the policy adopted by the host country organization at the time. Depending on the local requirements, disposal may be preceded by temporary storage. Further information and details of the ITER general decommissioning waste management policy can be found in 5.

2.11.2.5 Re-Cycling or Re-Use

Materials re-cycling after dismantling or components re-use is desirable. This depends on:

a) for re-cycling:
- ability to rescue base material without extensive intermediate processing (i.e. reduced smelting requirements) while still retaining sufficient commercial value;

b) for re-use:
- ability of the original components (designed some forty years earlier) to satisfy the functional requirements of the new plant.

Preliminary indications suggest that ex-vessel components like the magnets (except for the central solenoid) and the cryostat will have a contact dose rate of ~ 10 μSv/h after a machine decay period varying between 5 and 50 years. Therefore, depending on the component irradiation history and decay time, it may be possible to re-cycle materials either under supervised conditions (and the re-cycled portion of such material will have to be treated as radioactive for some time) or, in the best case, without any specific precaution. Similar considerations apply to entire components (toroidal field coils, poloidal field coils). Materials and components originally installed beyond the biological shielding and which have never been in contact with active gas, fluid, dust or affected by neutron flux, can be re-cycled or re-used without specific precautions.

2.11.2.6 Phase 2 Duration

The estimated duration of phase 2 is approximately 6 years. This duration is essentially driven by the vacuum vessel removal and size reduction/waste processing operations.

2.11.3 Overall Schedule

The estimated decommissioning schedule is summarised in Figure 2.11-1.

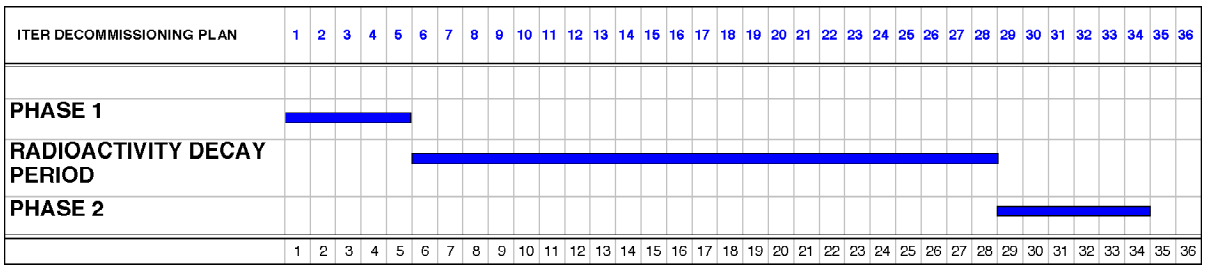

Figure 2.11-1 Estimated Overall Decommissioning Schedule

2.12 Mechanical Loads and Machine Supports Configuration

2.12.1 Overview of Mechanical Loads

Part of the technical difficulties associated with the design of the ITER tokamak are due to the substantial mechanical loads which can develop in multiple components. This section will briefly describe the main static and transient loading conditions that concern the ITER system design.

The mechanical loads acting on ITER can be divided into four independent categories.

1. *Inertial loads*: these are due to accelerations due to gravity and seismic events.
2. *Kinetic pressure loads*: significant on the ITER vessels, include coolant pressure (e.g., vacuum vessel cooling water), and externally applied atmospheric pressure to vacuum (e.g., cryostat vessel).
3. *Electromagnetic loads*: these are normally a strong design driver and not only affect, in their static form, the magnet system (e.g., TF magnet) but also act upon nearly all conductive structures during fast transients (e.g., plasma disruptions and resulting induced currents on the in-vessel components).
4. *Thermal loads*: these often induce mechanical loads, and are typically circumscribed within a single component and thus do not give rise to significant global effects.

To better explain the mechanical loads from a system point of view it is worth briefly describing the general layout of the main component supports (as shown in Figure 2.12.1-1).

The support schemes for the tokamak magnet and vacuum vessel systems have a number of constraints. The supports must allow for radial shrinkage of the magnets, and radial growth of the vacuum vessel, due to thermal differentials, while providing adequate resistance to seismic and disruption forces. Moreover, the general arrangement of supports has been developed to minimise the reaction of each support to loads internal to the component, with the following consequences.

- The tokamak gravity support from the basemat acts exclusively through the TF magnet assembly and consists of support pedestals made up of flexible compression plates resting on a support ring. The gravity support pedestals are rigid in the toroidal and vertical directions to resist inertial loads, but they are flexible in the radial direction to allow TF coil case thermal movements. These pedestals are supported on a steel support ring beam that is a part of the cryostat vessel. This ring is in turn supported, vertically, by a set of columns, and horizontally by a radial shell also part of the cryostat floor which, mainly by shear, carries the load onto the lower part of the bioshield.
- The vacuum vessel is supported by the TF magnet assembly also by means of a set of flexible plates located between the two components in the outer region of the machine. These supports have been located in this region to be efficient in the reaction of

seismic loads as well as to minimise the cyclic toroidal motion which the VV undergoes as a consequence of the out-of-plane loads and deflections of the magnet system.

- Each PF coil is connected directly to the TF magnet assembly by means of radially unconstrained supports.
- The in-vessel systems (blanket modules, divertor) are directly supported by the vessel.
- Cryostat and building are supported from the basemat.

The support hierarchy can therefore be schematically drawn as in Figure 2.12.1-2.

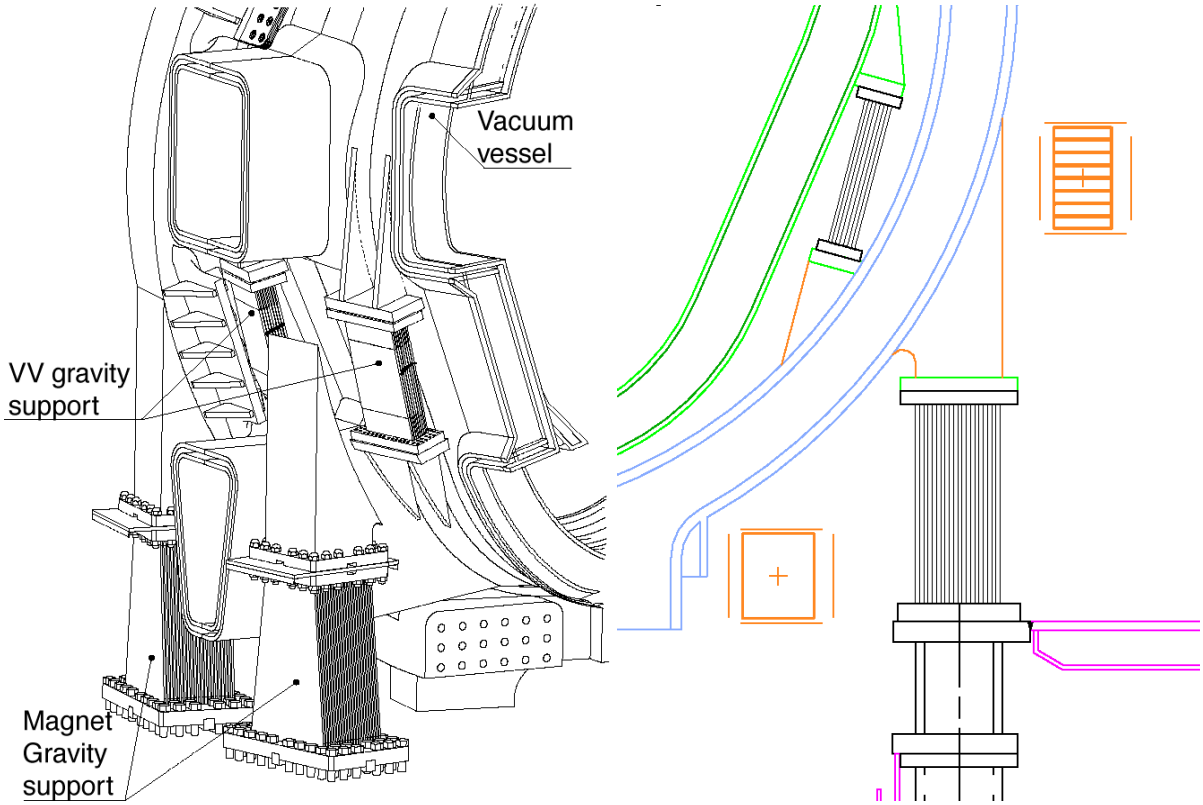

Figure 2.12.1-1 Vacuum Vessel to Magnet Supports and Magnet Gravity Supports

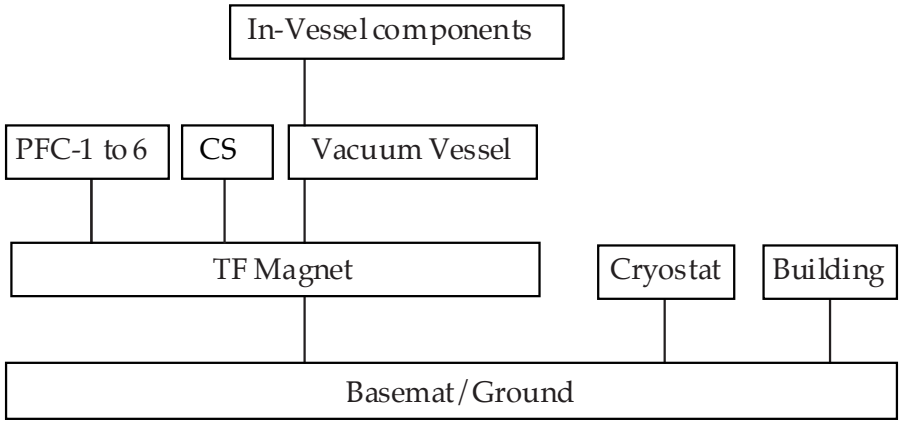

Figure 2.12.1-2 Schematic of Supports Hierarchy

The general philosophy utilised in the design of the support scheme has been to interconnect components and choose the load paths so to increase as much as possible the stiffness associated with the load path itself. This is quite evident with the choice of the supporting scheme of the vacuum vessel which has been directly connected to the magnet. In so doing, the relative deflection between the two components, and therefore the allocated radial build space, has been minimised while also avoiding any load through the main machine gravity supports during a plasma electromagnetic fast transient such as a vertical displacement event (VDE) or a disruption.

The ITER design uses a classification of plant conditions which divides them into categories in accordance with the anticipated likelihood of occurrence. This categorization is chosen to accommodate design criteria for safety importance components as well as in order to obtain a well balanced design also for non-safety importance components. The categories are:

Category I:	Operational events	(Normal)
Category II:	Likely event sequences	(Incidents)
Category III:	Unlikely event sequences	(Accidents)
Category IV:	Extremely unlikely event sequences	(Accidents)

Some type of loads, for example seismic or plasma events, have different events with different intensity defined in different categories.

2.12.2 Seismic Loads

Earthquakes produce random ground motions which are characterised by simultaneous but statistically independent horizontal and vertical components. Their severity is typically associated with the peak ground acceleration. The ground acceleration can be both in the horizontal and in the vertical direction and typically has a spectral content which leads to some level of support reaction load amplification.

The effect of seismic events on ITER are described in the specially devoted section 2.15.

2.12.3 Electromagnetic Loads, Slow Transients

Energies in excess of 40 GJ are normally stored in the ITER superconducting magnet system in the electromagnetic fields that provide stability to, equilibrium in, and drive current in the plasma. Associated with the provision of such strong fields, considerable magnetic loads have to be reacted by the magnet assembly.

2.12.3.1 TF Magnet Loads

During normal operating conditions, the TF magnet system has to withstand the EM loads arising from the interaction of its conductor current with both the toroidal and poloidal fields.

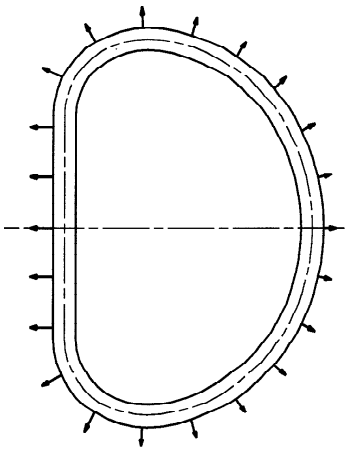

Figure 2.12.3-1 In-Plane Loads on a TF Coil

The interaction with the toroidal field gives rise to a force distribution (see Figure 2.12.3-1) acting in the plane of the each coil, and which can be pictured as a pressure acting from the vacuum vessel side outward with an intensity which reduces as the distance from the machine centreline increases. These loads are referred to as “in-plane“ loads in section 2.1.

As a consequence of this load distribution, each coil experiences a strong internal tension along its length as well as a radially directed force towards the machine centreline which is reacted in hoop compression by the straight legs of the TF magnet which behave as a vault. Even if this load is basically internal to the TF magnet assembly in that no *net* loads are transmitted onto other components, it is certainly one of the most important loading conditions for the whole machine with significant structural consequences. The sheer tension in each TF coil is about 100MN thus requiring a significant amount of structural steel over the TF cross section. The radial force in each coil is about 400MN giving rise, as a consequence of the "wedged" type of structural support, to a toroidal wedging load of about 1150MN, requiring a thick enough vault in the innermost region of the TF cross section.

The interaction of the TF magnet current with the poloidal field, present only during plasma operation or when the CS or the PF coils are energized, gives rise to a load which is normal to the plane of each TF coil. This load is referred to as “out-of-plane” load in section 2.1. This load does not produce a net moment around the vertical axis of the machine but tries to twist the whole TF magnet with opposing sign toroidally directed forces. While being a load of somewhat smaller intensity, when compared with the in-plane load, it is of a pulsed nature

and hence is rather challenging to react as a consequence of the cyclic nature of the arising stresses. The reaction of this load is accomplished by the TF coils casings and the intercoil structures, which increase both stiffness and strength of the magnet assembly. Also in this case no net load is reacted by the gravity supports and, by careful choice of the support location, cyclic loadings on them are minimised.

An extensive amount of finite element analyses have been performed to investigate the mechanical behaviour for several design options of the TF-coil system. For these investigations, several non-linear, two and three dimensional finite element models have been used, most often representing a 20 degree symmetry section of the TF coil. The present ITER design takes into account the results of these studies.

A discussion of the main analysis of the TF magnet loads is given in 2.1.

2.12.3.2 PF Magnet and Plasma Loads

The PF magnet system includes the CS and the PF coils and produces the poloidal magnetic field necessary for plasma equilibrium and shaping, as well as the toroidal electric field needed to build and sustain the plasma current. The forces acting on the PF coils are radially and vertically directed and are essentially axisymmetric in their distribution (except for the small ripple effect due to the discrete TF coils).

During the development of slow transients (e.g., plasma initiation, shutdown, etc...), the net force on the whole PF magnet system is nearly zero due to the essential absence of induced currents in the passive structures (VV, Blanket, etc.).

Net vertical loads acting on each PF coil and the central solenoid (CS) are reacted through the TF magnet structure but without affecting its supports to ground (Figure 2.12.3-2). In this scheme the TF magnet is acting as the main load path. Radial loads, acting on the CS and the PF coils, are instead reacted within each coil by the development of toroidal hoop stress in the conductor jacket. Radial expansion due to this hoop stress is accommodated by supports which are radially flexible.

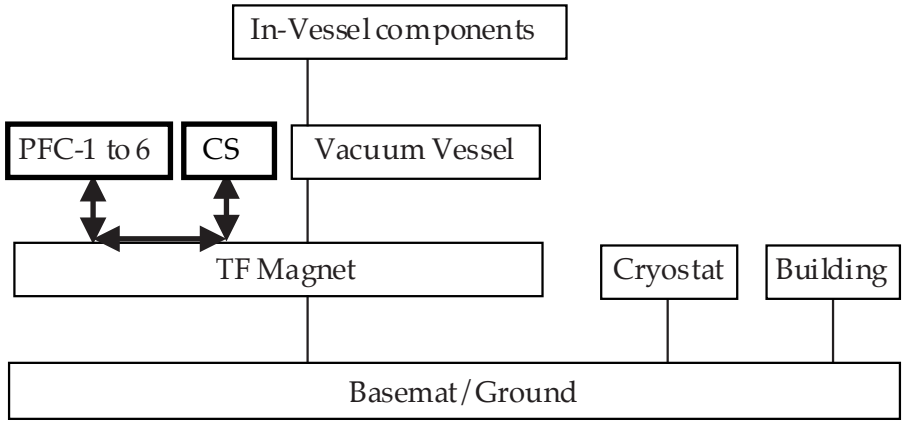

Figure 2.12.3-2 Load Paths between PF Coils

The load on each PF coil (and within the CS coil) varies greatly as a function of other PF coil currents, plasma current, plasma profiles, etc. Therefore, in order to size these coils and their

supporting structures, the envelope of all conditions must be considered. In particular it has been necessary to verify the capability to withstand each design reference plasma with its different ranges of plasma internal inductance and beta poloidal as well as induced currents and loads arising during plasma electromagnetic fast transients such as VDE's and disruptions.

2.12.4 Electromagnetic Loads, Fast Transients

Electromagnetic fast transients typically will occur as a consequence of problems encountered in sustaining currents (e.g., fast magnet discharge, and plasma disruption) or loss of vertical position control of the plasma (VDE).

Due to the experimental nature of ITER where different plasma operation modes will be explored, these loads, such as plasma disruptions and VDE's, are considered part of the (normal) operational (Category I) loading events[1]. For this reason, the systems in ITER are designed to withstand a large number of them.

Typically, fast electromagnetic transients produce significant forces and stresses in all in-vessel components and are a determining factor in their structural design.

2.12.4.1 Disruptions

The tokamak disruption is a severe instability in which the plasma confinement is suddenly destroyed, both thermal and magnetic plasma energies are rapidly dissipated, and the discharge is terminated.

If the plasma current quench takes place in a time short compared with the vertical resistive plasma motion (e.g., < 100 ms) no significant total net vertical forces are generated in the whole passive structure. Nonetheless, given the up-down asymmetric coupling of the ITER plasma with the passive conducting structure, significant plasma fast vertical displacements may take place. A significant poloidal current may also be induced in the passive structure as a consequence of the variation of toroidal flux (during thermal and current quench). This current leads to loads internal to the vessel without significant transfer of forces to the magnet.

The most important structural consequence of a plasma disruption is the induction of local loads on the blanket modules, vacuum vessel, and plasma facing components. The severity of this event depends on the assumed total current quench duration.

A more severe condition takes place during the current quench phase where toroidal currents are induced in the vacuum vessel, applying a pressure toward the plasma in the order of 1 MPa. This is nevertheless a rather unchallenging loading condition for the vacuum vessel itself, which is sized to withstand larger magnetic pressures during a TF coil fast discharge and/or VDEs.

The current quench phase is a significantly demanding condition for the design of the blanket modules where significant saddle current loops are induced.

The interaction of these current loops with the toroidal field, generates significant radial and poloidal moments which determine in large part the type and sizing of the blanket module

[1] Other loading categories are II (likely), III (unlikely), and IV (extremely unlikely).

support scheme (Figure 2.12.4-1). For this type of loads the current quench duration is the single most important design parameter. In the worst case this could be ~ 25 ms, and the disruption analysis has shown that the arising maximum moment in a single module is about 0.6 MNm in the poloidal direction and 0.7 MNm in the radial direction (see 2.3).

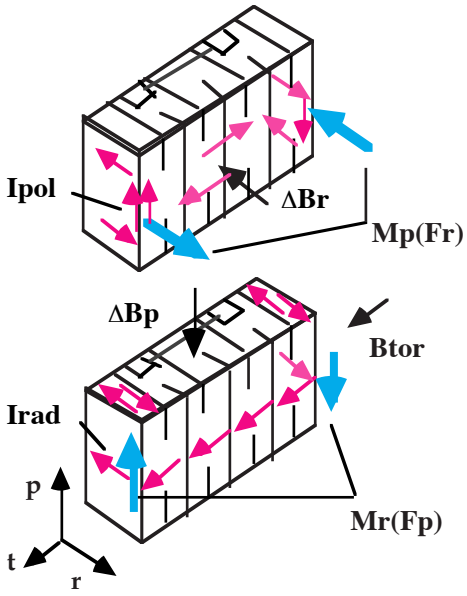

Figure 2.12.4-1 Current Loops in the Blanket Module During a Plasma Current Quench

The electromagnetic (EM) and structural modelling of an EM transient, such as a disruption, is usually performed in three steps.

- Several cases of axisymmetric MHD plasma equilibria transients are analysed to obtain a proper modelling of the plasma motion during the thermal and current quench phases. This is essential to make sure that the plasma is in equilibrium and hence no artificial loads are introduced in the analysis, where also the PF coils response is self-consistently taken into account.
- The results of the initial analysis are then used to introduce current changes (plasma and/or magnet) into three-dimensional EM models which include all significant parts of the passive structure. Several different finite element meshes may be used to model with a sufficient level of detail, all the regions of interest.
- The mechanical loads are passed into a suitably meshed structural model used for the evaluation of mechanical stresses. Also in this case, several meshes are used to describe, for example, the global overall behaviour of the vacuum vessel, the local structural response of the blanket module supports on the vacuum vessel, the blanket modules themselves, the divertor cassette, etc.

Figures 2.12.4-2, 2.12.4-3 and 2.12.4-4 below show some of the models employed in the process outlined. Detailed analytical results are reported in 2.2 to 2.4.

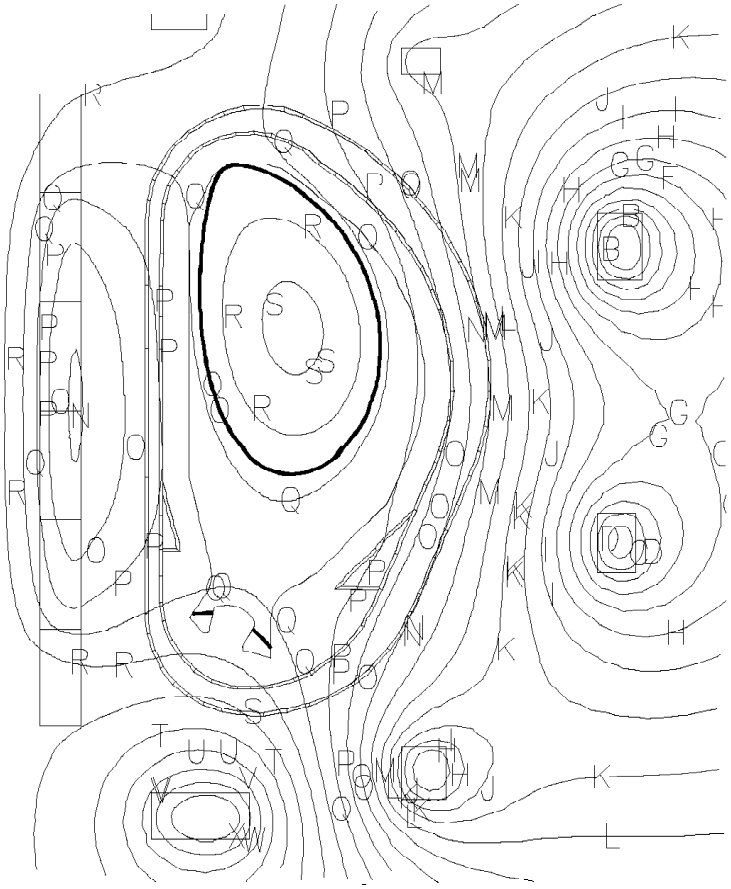

Figure 2.12.4-2 First Step in a Disruption Analysis, Plasma Modelling.

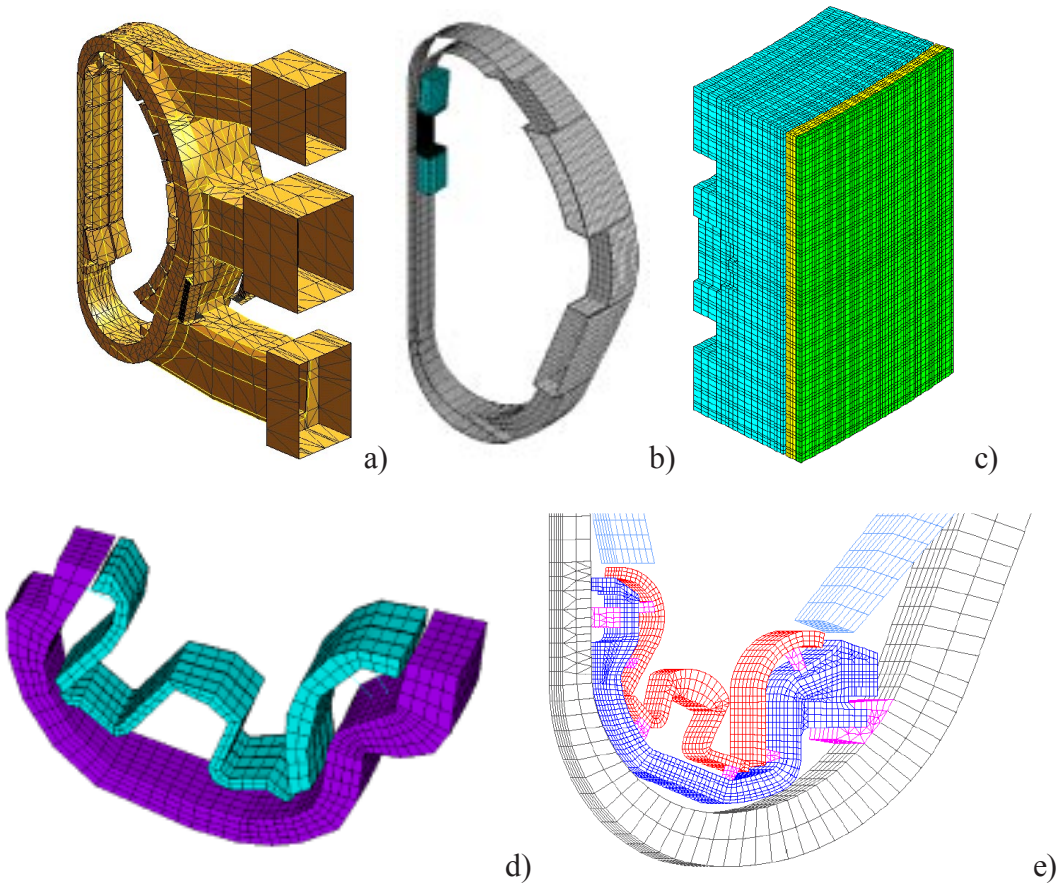

Figure 2.12.4-3 The Second Step - Several Types of EM Analysis 3D Models Using the Results of Step 1 as Input.
The vessel (a,b), a detail showing the module (c), and the divertor (d,e)

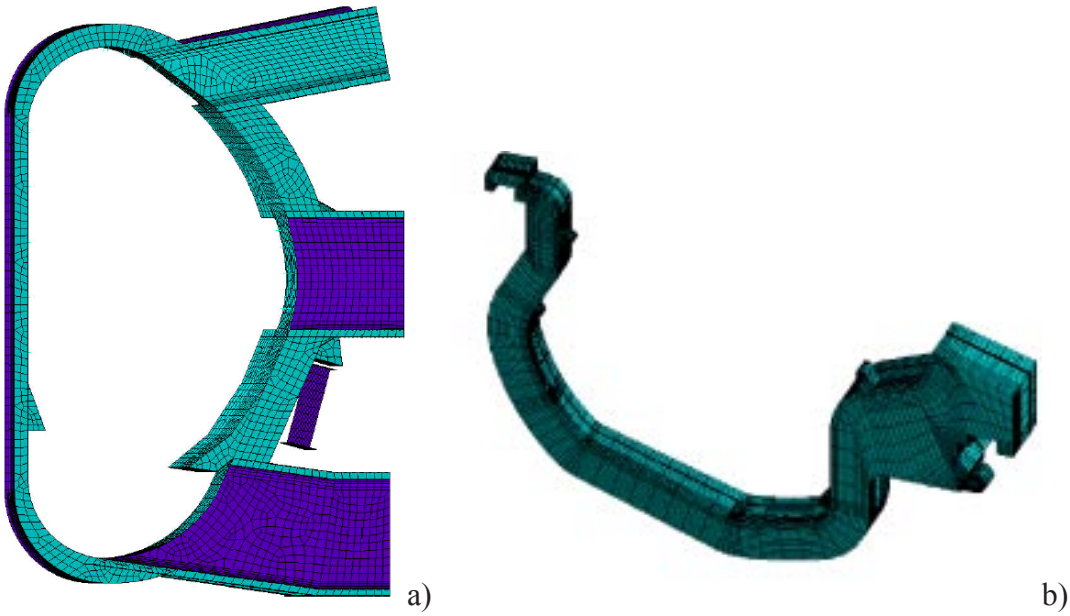

Figure 2.12.4-4 The Third Step - The Use of Structural Codes Applied to a Suitably Meshed Model Taking Loads from the Outputs Obtained in Step2.
The example models shown are the vessel (a) and the divertor cassette (b).

2.12.4.2 VDE's

In a VDE the vertical position control of the plasma is lost as a consequence of a failure of the feedback control system. The plasma motion, in this case, may take place initially without significant plasma current reduction (current quench) and would progress relatively slowly (on the time scale determined by the resistance of the passive structure). This type of instability takes place in elongated plasmas that require for their stability an external feedback system. The loss of vertical position can be caused by external malfunctioning of the control system or by too fast and large variations in the plasma profiles (e.g. major disruptions) to be stabilised by a system with finite voltage limitation.

The VDE is composed of an initial slow vertical drift phase, when the plasma vertical position follows an exponential growth, an onset of plasma-wall contact followed by the onset of a disruption and/or rapid loss of remaining plasma thermal energy. Halo currents may appear as soon as the plasma comes in contact with the first wall. The thermal quench is assumed to start in either of the two cases: one is at the same time as the plasma contact with the first wall; the other is when the plasma edge safety factor q_{edge} reaches a critical value which has been conservatively assumed to be 1.5.

During a VDE, the forces acting on the plasma during its motion are mainly (but not only):

- destabilising force due to the external applied quadrupolar poloidal field;
- stabilising force deriving from the plasma motion in a conducting shell;
- destabilising force due to up-down asymmetric toroidal current induced in the passive structure by the decay of the plasma current.

Since VDE's terminate with a plasma current quench, their severity depends on the delay between the onset of the VDE and the onset of the current quench as well as the duration of the latter. If the onset of the current quench is delayed, the plasma moves further into the destabilising quadrupolar field giving rise to higher net loads on the passive structure.

In other words, the plasma current quench causes a transfer of current from the plasma to the passive structure which, while still continuing to interact with the destabilising poloidal field, forces it to stop drifting vertically. For this reason the worst (higher vertical force) VDEs are typically the ones where the plasma current does not decay before the plasma has undergone a large displacement from its initial position. This is because the destabilising force is roughly proportional to the plasma displacement multiplied by the plasma current itself. The exchange of forces between plasma and passive structure is sustained by the presence of eddy currents as well as poloidal currents which flow through both plasma and passive structure. These are known as halo currents.

The VDE typically gives rise to significant net forces between the PF magnet and the passive structure. The typical load path of these forces can be visualised in Figure 2.12.4-5.

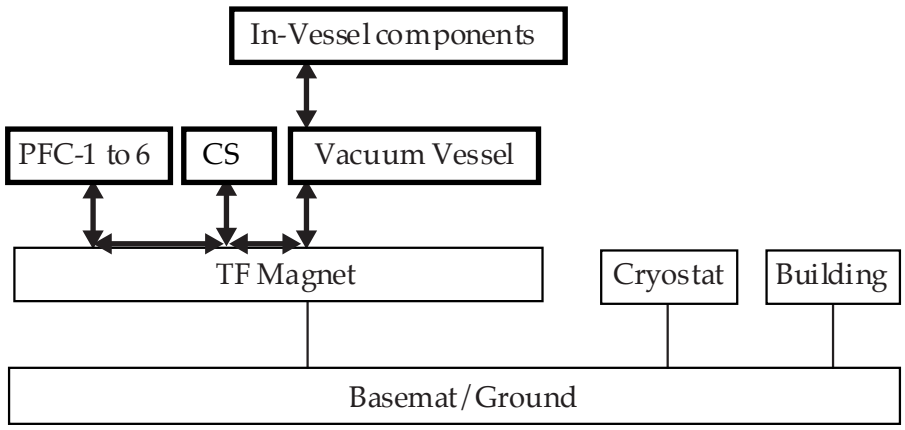

Figure 2.12.4-5 Mechanical Load Paths During a VDE

VDE's can be divided into two classes with slightly different EM load consequences: one is a VDE followed by a fast current quench, that results in more demanding eddy currents on modules, divertor, and vacuum vessel; the other is a VDE followed by a slow current quench that results in higher halo currents and vertical loads on the structure. The estimated current quench time depends mainly on the assumption on halo and plasma temperatures. A lower halo temperature leads to higher resistance in the plasma region and results in the fast VDE and lower halo current, and the higher one results in the slow VDE and higher halo current. For the modelling of both fast and slow current quench types of VDE's the initial scenario is the same. The vertical control system is deactivated and the plasma is given, from its initial unstable equilibrium point, a small initial upward or downward kick. The plasma then drifts in the direction of the displacement and rapidly becomes limited by the first wall. The plasma remains limited and shrinks in cross-section while maintaining its current as it continues to drift. During the drift phase, which typically lasts a few hundreds of milliseconds, no power is supplied to the plasma and the plasma energy slowly decays at a rate determined by the thermal transport in the equilibrium state.

It has also been observed, in present experiments, that VDE's sometimes give rise to net horizontal loads between magnet and passive structure as a consequence of plasma instabilities of a non-axisymmetric nature. The understanding of these phenomena is not clear and their modelling is still somewhat primitive. Nonetheless, some design guidelines have been established for ITER.

The effects of VDE's on in-vessel components can be very severe. It is therefore essential to be able to predict, with some degree of confidence, what will be the loading conditions caused by these events.

Some initial numbers can be estimated by simple force balance considerations.

- The destabilising force on the plasma will have to be transferred to the passive structure by electromagnetic force exchange (between the plasma and the passive structure).
- The external quadrupolar (destabilising) field is well-known and therefore the destabilising force can be easily found once a maximum plasma displacement for the VDE is established.

- The latter is strongly linked with the value of the safety factor at the plasma edge. In fact, during the VDE, the plasma soon becomes limited, and the more the plasma displaces the smaller it becomes and hence (since plasma current ~ constant) the more q_{edge} decreases.
- Once the destabilising force is known, the total value of halo currents can be simply estimated by ascribing the totality of the stabilising force (on the plasma) to the latter.
- It is therefore essential to establish a reference value of q_{edge} at which the plasma will start its current quench. Various considerations lead to setting the lower bound to 1.5. This should be a sufficiently conservative value especially because in ITER the plasma motion during the VDE is very slow (growth time >0.5s).

Given the above, and with simple additional geometrical considerations, the upper bound of the vertical destabilising force can be calculated to occur for a downward VDE and to be about ~70 MN, and that the needed halo current will have to be in the order of 6 MA.

In ITER, several numerical studies have been carried out to verify the upper bound of vertical forces. Generally, numerical modelling of VDE's is carried out with free-boundary plasma axisymmetric equilibrium codes solving the Grad-Shafranov equation with the inclusion of eddy currents and halo current terms. The main conclusions which can be drawn from these analyses are the following.

1. The ITER control system is capable of maintaining plasma vertical position control for all nominal plasma disturbances, including minor disruptions. A VDE, in ITER, is therefore expected to occur only as a consequence of a major disruption or a failure of the control system.
2. Should the VDE be caused by a major disruption followed by the plasma current quench, the plasma is expected to undergo an upward VDE. This is a consequence of the asymmetric vertical inductive coupling between plasma and passive structure. Furthermore, upward VDE's give rise to vertical forces on the passive structure substantially smaller than downward VDE's as a consequence of the smaller quadrupolar field present in the upper section of the vacuum chamber.
3. Smaller vertical forces are generated when the plasma current quench takes place early in the vertical drift. This aspect has generated the idea of using a plasma terminating impurity gas puff, to trigger a plasma disruption, should the vertical position of a ‘healthy’ plasma be lost.
4. When the vertical position of a ‘healthy’ plasma is lost for no reason other than a functional failure of the controller, there are equal chances for the VDE to be downward or upward. Should, in this event, a plasma terminating impurity gas puff be used to trigger a plasma current decay early enough, (the displacement would be less than ~30cm), and the plasma would go upward.
5. The worst case peak vertical load has been observed for downward VDEs. The main results of this loading condition are shown in Table 2.12.4-1. Figure 2.12.4-6 shows the magnetic flux in a particular point during this simulation.

Several additional scenarios of VDE's, as well as fast central disruptions analyses, have been performed. These analyses have then been utilised in a self-consistent way to perform more detailed stress analyses of all affected components.

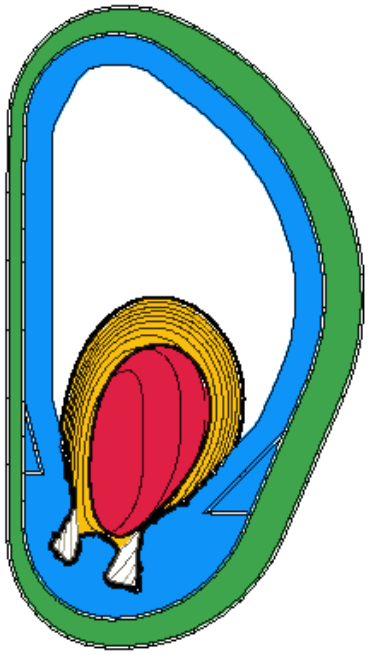

Figure 2.12.4-6
Worst Case Downward VDE

Table 2.12.4-1 Main Results of a Worst Case Slow Downward Category III VDE

Input Data	
Initial plasma state	EOB
Current quench initiator	q=1.5
Additional Assumptions	
Peak (I_{halo}*P_f/I_{plasma})	0.58
Peak total net horizontal load	-25 MN
Main Results of Simulation: Downward VDEIII	
Peak Z force on passive structure (eddy+halo)	-72 MN
Peak total halo current	~7 MA
Peak Z force due to halo currents	-68 MN
Peak Z force due to toroidal eddy currents	-66 MN

2.12.4.3 Magnet System Fast Discharge

A magnet fast discharge is an event where the current flowing in the magnet (TF, PF, or both) is rapidly brought to zero by means of discharge resistors which dissipate the large stored magnetic energy. Such an event is usually triggered by the magnet quench detection system which intentionally does so to protect the conductor from overheating or, in other words, to limit the hot spot temperature of the magnet superconductor.

In particular in the case of the TF magnet, where a significant energy is involved during the fast discharge of the coil circuit, the passive structures surrounding the TF coil conductors, i.e. the radial plates, the coil cases and the vacuum vessel, will absorb part of the stored magnetic energy of the TF coils. This implies that significant currents (Figure 2.12.4-7), in the order of 4MA, will be induced in the VV, producing electromagnetic forces to be also

combined with loads which may arise simultaneously such as halo currents arising during a VDE.

The forces acting on the VV act like an internal pressure but with a local value proportional to the local toroidal field. The force distribution is similar to the in-plane load on the TF coils and results (similarly to the TF coils) in a toroidal compressive load at the inboard region of the VV. This inboard compressive load is a structural design driver for the VV.

The mechanical loads arising as a consequence of a TF coil fast discharge are a rather strong function of the discharge time constant that hence is an important machine design parameter (11 s in ITER) subject to trade and system studies. A longer discharge time constant allows a reduction of the EM pressure acting on the VV, but this choice implies that a larger energy is deposited in the quenched conductor, thus requiring a smaller cable space current density and hence a larger TF winding pack dimensions. This type of trade study has been performed so as to find a near optimal configuration which depends on many other design inputs and choices such as magnet conductor design criteria, material choice for the VV, assumptions on VDE's and halo currents, etc.

As far as the load path through the supporting structure is concerned, due to symmetry, all loads can be considered internal and no significant net loads are exchanged between components other than between the VV and the divertor cassette.

Also with regard to the PF magnet system fast discharge, as a consequence of the decay of the poloidal field a toroidal electric field is generated and subsequent eddy currents are induced in the passive structure. These are, in this case, typically smaller than the ones generated by the quench of the plasma current (disruption) which involves similar field variations but in much shorter times. However, from the support structure standpoint, during the transient, some net loads may be exchanged between the passive structure and the PF magnet.

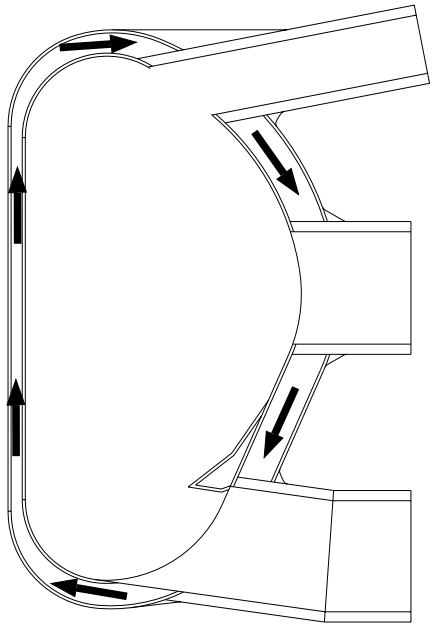

Figure 2.12.4-7
Circulation of Induced Poloidal Currents in VV During TF Magnet Fast Discharge

2.13 Materials Assessment

2.13.1 Introduction

The material choice for ITER has been orientated toward industrially available materials and well-established manufacturing technologies, while taking account of physical and mechanical properties, maintainability, reliability and safety requirements. The materials chosen not only need to have good basic material properties, but also to maintain these properties sufficiently through component manufacture. Materials proposed for ITER can be divided into two groups:

- standard materials with well-established manufacturing technologies, which do not require any modifications (e.g. AISI 304L, 316L, 316LN, Inconel 718, etc.);
- standard materials, which require some modifications, such as more stringent limits on the alloying elements, some changes of the processing technology, etc.

To support the materials selection, ITER R&D has been carried out with the following objectives:

- characterisation of selected materials, study of the critical issues, and provision of the required database for the design;
- justification of the materials selection.

The following sections briefly describe the selection and assessment of materials for vessel and in-vessel components, diagnostic components, and magnets, indicating the reasons for the choice and the advantages of these particular materials over the alternatives.

2.13.2 Materials for Vessel and In-Vessel Components

2.13.2.1 Plasma-Facing Materials

2.13.2.1.1 Rationale for the Selection of Armour Materials

The choice of plasma-facing materials for different components is determined mainly by plasma compatibility and erosion lifetime (ion erosion and thermal erosion during disruption and transient events).

Beryllium (Be) has been chosen as the armour material for ~ 80% of the total surface exposed to the plasma (primary first wall and port limiter). The main reasons for the selection of Be are the low effect on plasma contamination, low radiative power losses, good oxygen gettering ability, absence of chemical sputtering (in comparison with carbon), low bulk tritium inventory, and the possibility of in-situ (or in hot cell) repair of damaged surfaces using plasma spray.

Tungsten (W) has been selected as the material for the divertor baffle areas where there exists a high concentration of neutral particles. In this area the key issue is erosion lifetime, and W has a lower erosion rate, due to its low sputtering yield and its higher sputtering threshold energy, as compared to those of beryllium and carbon. Another advantage of W is its low tritium retention. The plasma compatibility of W is an issue, because a small amount of W in the confined plasma region could lead to a very large radiation power loss from the plasma.

In areas exposed to high thermal fluxes during normal operation, and large energy excursions during plasma disruptions (lower part of the divertor vertical target), carbon fibre composite is selected. Use of carbon fibre composite (CFC) in this area can provide the needed erosion lifetime, whereas the use of W and Be in this area is limited due to the creation and loss of a melt layer during disruption events. However, the use of CFC as armour has to be restricted, because of chemical erosion and tritium retention, especially in co-deposited layers.

All plasma-facing components will create dust which can interfere with plasma operation, and which will generally end up in the divertor region (see 2.4).

2.13.2.1.2 Beryllium

Commercially available beryllium grades from the USA and from the RF have been evaluated as candidate materials. The selection of the optimum grade is driven by those properties which are very sensitive to the impurity levels - grain size, method of production, thermomechanical treatment - which usually differ for the different Be grades.

Among various industrial beryllium grades, S-65C VHP (vacuum hot pressed) grade (manufacturer Brush Wellman Inc., USA) has been selected as a reference grade. The main reasons were:

- lowest BeO and metallic impurity content among the other structural grades;
- high elevated temperature ductility;
- excellent low cycling thermal fatigue performance and thermal shock resistance;

The similar DShG-200 (manufactured by the RF) was selected as a back-up.

The base properties of these grades are well documented. The key issue for application of Be as armour is its behaviour after neutron irradiation and thermal transient events. Neutron irradiation typically leads to degradation of the Be properties. For first wall irradiation conditions (temperature range 240-480°C, maximum damage level ~ 1.7 dpa, He concentration 1,700 appm) the main concern is the embrittlement of Be at low irradiation temperatures (less than 300°C). It is expected that the ductility of Be at this temperature and conditions will be at the level ≤ ~ 1%. The embrittlement of Be at low temperature could lead to brittle destruction of the tiles and affect the thermal erosion of Be during transient events. The study of thermal erosion and damage of the neutron irradiated Be S-65C VHP confirms that this grade has better thermal shock resistance. The use of Be tiles, without critical defects that may result in crack initiation, could partly solve this problem.

Another possible material is plasma-sprayed beryllium. Be plasma spray (PS) has the potential to be used for the manufacturing of the first wall modules and for in-situ or hot cell repair of the damaged armour, which would save maintenance time and reduce radioactive waste. By comparison with S-65C, plasma-sprayed Be has lower thermal shock resistance, lower mechanical properties, and higher porosity.

2.13.2.1.3 Tungsten

A preliminary selection of W grades has been made taking into account the near term availability, cost, technological features, and behaviour under thermal fatigue and disruption conditions. Several W grades from different suppliers (pure sintered W, cast W alloys, W-1%La_2O_3, chemical vapour deposited (CVD) W etc.) were selected for investigation. The recent results from the different tests have demonstrated that among the studied materials, pure W has lowest thermal erosion (in comparison with W-1%La_2O_3) and adequate thermal fatigue resistance (also at heat fluxes much higher than required). The key issue is the proper design of the W armour (size of tiles, grain orientation): the recommended grain orientation is parallel to the direction of the heat flow, in which case possible delamination is not so critical.

Pure sintered W is recommended as the reference material for divertor components. This material is available in a wide range from different suppliers. The W properties database is also well established.

Typically for bcc metals, irradiation leads to an increase in the ductile-to-brittle transition temperature (DBTT). Based on the available data, all W grades have the problem of brittleness at the expected fluence of 0.1-0.5 dpa in the region near the heat sink, for an irradiation temperature less than ~ 500°C. To avoid damage and possible delamination of this brittle material it is recommended to avoid the use of W in geometries with crack initiators. One way to solve this problem is to orient the W armoured design toward concepts

that reduce thermal stresses in the armour and in the joints i.e. brush, rod or lamella structures.

2.13.2.1.4 Carbon Fibre Composites

Carbon fibre composites have been selected as the reference material in certain parts of the divertor due to the absence of melting, their high thermal shock and thermal fatigue resistance (low crack propagation) and their high thermal conductivity in comparison with conventional graphites. The preferable materials are CFCs with:

- high thermal conductivity: the higher the thermal conductivity, the larger the sacrificial thickness and hence the higher the erosion lifetime;
- 3D fibre structure is preferable because it results in more isotropic properties and higher thermal shock resistance in comparison with 1D and 2D materials;
- high density and porosity: higher density and lower porosity are preferable to minimise gas absorption and outgassing.

Among the available CFC grades, the 3D CFCs Sepcarb®NB 31 (produced by Société Européene de Propulsion (SEP), France) and NIC-01 (produced by Nisseki-Corporation, Japan) have been selected as the references. The back-up option is CFC CX 2002U (2D felt-type material, produced by Toyo Tanso Co., Japan). CFC with 10%Si doping (Sepcarb-inox NS31) has also been developed by SEP. The goal of the Si doping is to reduce the chemical erosion. This material is therefore still under study as a possible candidate material.

The properties of CFCs strongly depend on the fibre type, the architecture (size of cells, volume of fibres), the method of production, and the thermal treatment. Being newly developed materials, the existing database on their properties is usually more scattered than that of metals. For the reference materials, data are available only up to ~ 800-1,500°C.

For a damage fluence ~ 0.1-0.3 dpa and irradiation temperature 150-1,200°C the changes in properties are not expected to be crucial except for the thermal conductivity. CFCs with high initial thermal conductivity retain high conductivity after irradiation, but at low irradiation temperatures (less than 300°C) the thermal conductivity could be ~ 3-5 times lower than the unirradiated CFC. The performances of mock-ups using the Sepcarb®NB 31 and NIC-01 armour tiles have been studied including irradiation effects. Generally, the performance was as expected (higher temperature due to the loss of thermal conductivity). The decrease in the thermal conductivity due to neutron irradiation leads to an increase in thermal erosion under disruption conditions and this may have to be taken into account during the erosion lifetime assessment.

2.13.2.2 Structural Materials

2.13.2.2.1 Stainless Steels

SS 316L(N)-IG Type

Austenitic stainless steel (SS) of 316 type is the main structural materials for the ITER vacuum vessel and for in-vessel components (shielding blanket, divertor cassette body) because this steel is qualified in many national design codes, has adequate mechanical properties, good resistance to corrosion, weldability, forging, and casting potential, is industrially available in different forms, and can be manufactured by well-established

techniques. Among the 316 steel family, 316L(N) type SS (based on 316L(N)-SPH SS developed for the European Fast Breeder Reactor program) has been selected for ITER application.

The main reasons for the selection of this grade are the following.

- The proposed grade has an optimal combination of the main alloying elements (C, N, Ni, Cr, Mn and Mo) with a tight specification of their allowable composition range. The narrow specification provides an optimal microstructure (austenitic phase with a δ-ferrite content ≤ 1%) and good control of the heat-to-heat variation of mechanical properties.
- The tight control of the carbon and nitrogen provides a satisfactory resistance to stress corrosion cracking of base metal and welds, and an adequate level of material strength.
- The mechanical properties of the proposed grade are better than those of 316L and 316LN steels. The higher strength is combined with a good ductility. The design allowable stress is higher than in the other SS grades.
- The proposed grade is less prone to delayed reheat cracking than Ti or Nb stabilised steels.
- 316L(N) is less sensitive to irradiation embrittlement than 304 steel.
- There is a comprehensive database for this grade, including heat-to-heat variations and product size.

For ITER, only minor modifications in chemical composition are required, in order to cope with the radiological safety limits and with the re-welding requirement. The safety implications of the Co and Nb content show the following.

- For a fusion reactor, activated cobalt in corrosion products plays an important role in determining the occupational dose level during maintenance after a coolant leak.
- Reducing the Co content from 0.25% to 0.05% decreases the total decay heat in the vacuum vessel by ~20% and helps to reduce the activation of components.
- Further decrease of Co to 0.01% does not further reduce the decay heat because the Ni^{60} (n,p)->Co^{60} reaction becomes dominant.
- Cobalt is one of the main components of activated corrosion products in the water cooling system.
- Nb produces long-lived radioisotopes that could become important for the decommissioning and waste disposal of in-vessel components. In 316 type SS, niobium is present as a trace element picked up during the melting process from the ferroalloy addition: existing data indicate that it is possible to reduce Nb to ≤ 0.01%.

To provide a common designation and to avoid any confusion with similar steel grades, the designation 316L(N)-IGX is used, where 316 indicates the type of steel, L low carbon content, (N) controlled nitrogen content, and IG - ITER Grade. X is a progressive number indicating the procurement specification, which defines the additional requirements in terms of product form, impurity content, QA procedure, and delivery conditions needed for the different components as follows:

- 316L(N)-IG1 for the modules of the primary wall should have a cobalt content < 0.05%;
- 316L(N)-IG2 for the vacuum vessel should have a cobalt and niobium content as low as possible; cobalt and niobium < 0.05% and < 0.01%, respectively, have been assumed as industrially feasible limits; taking into account the requirement of re-welding the irradiated material, the boron content should be limited to 10 wppm;

- 316L(N)-IG3 cast plus HIPed steel for one of the options for the divertor cassette body; cobalt is limited to 0.05%;
- 316L(N)-IG4 thin walled tubes for the primary first wall; the cobalt content is limited to < 0.05%;
- 316L(N)-IG5 in in-vessel cooling pipes: Co < 0.05% and B < 0.0010%;
- 316L(N)-IG6 produced by the powder HIP process; the composition is the same as IG3 with the exception of higher oxygen and silicon concentrations.

The physical and mechanical properties of the 316L(N)-IG steel which is available in the different forms (rolled stocks, bars, plates, tubes, etc.) are well known and sufficient for design evaluation. For some components (e.g. shield blanket modules) high temperature hot isostatic pressing (HIP) at ~ 1,000-1,100°C will be used for the manufacturing. In some cases a few HIP cycles may be applied. Also, a manufacturing option is to use stainless steel powder and HIP as a consolidation technique. As a result, the properties of the HIPed steel may differ from those of wrought material. A study of the effects of HIP cycles on the mechanical properties of solid and powder HIPed steels has been performed in the frame of ITER R&D. It was shown that the tensile properties of HIPed steel are within the design allowables. In some cases the yield strength of solid-HIPed base metal is close to the minimum specified values. Powder-HIP gives tensile properties above the average of the wrought material, but fracture toughness of powder-HIPed steel degrades faster under irradiation than wrought material.

Neutron irradiation is another factor which affects the properties of stainless steel. At the maximum expected neutron fluence ~ 0.3 MWa/m^2, the peak damage in the steel for the in-vessel components will be ~ 2 dpa with a peak He generation of about 55 appm. The irradiation temperature for these components is in the range 100-300°C. Hardening of the steel will occur, but predicted uniform and total elongation of the wrought steel will remain higher than 10% and 20%, respectively, at the end of the operation phase. For the solid-HIP steel, the estimated uniform and total elongation will be above 18% and 31%, respectively. Therefore, materials will be relatively ductile and retain work hardening capability. Initial neutron data on 316L(N)-IG, prepared by powder HIP and irradiated at ~ 75°C to 2 dpa, indicates that the tensile properties are similar to those of wrought material. However, for powder HIPed material, the fracture toughness decreases with increasing dose from ~ 1,000 kJ/m^2 in the unirradiated steel to ~ 250 kJ/m^2 after 2-2.5 dpa at 75-290°C.

For the blanket manifolds and vacuum vessel the irradiation dose will be low, less than 0.06 dpa for an average first wall 14 MeV neutron fluence of 0.3 MWa/m^2. This dose will not result in significant property changes, and design allowables for the unirradiated steel have been used for these component designs.

Vacuum vessel, manifold and branch pipe connections must remain weldable throughout the machine lifetime in spite of the He generated by neutron irradiation. The helium content generated by gaseous transmutation should be kept below a threshold value, which depends on the welding method. Based on existing data, re-welding of 316L type SS can be successfully carried out on thick welds when the He content is 1 appm. For thin single-pass welds, low energy welding can raise this limit to 3-10 appm. Helium generation in the vacuum vessel will be below the re-weldability limit of 1 appm. For the blanket manifolds, the helium generation exceeds this value.

He generation can be minimised by reducing the boron content of the steel. Neutronics calculations show that decreasing the boron to 10 wppm lowers the helium generation by ~ 44% in the vacuum vessel to a level less than 1 appm (for 1 MWa/m^2). Reducing the boron even further results in more than a factor of two suppression in the helium production. Therefore, the boron concentration in the steel used for the manifold should be as low as feasible industrially. The effect of boron on He generation is most significant for the steel close to the water cooling channels due the thermalisation of neutrons by water.

Borated Steel

A standard borated stainless steel is proposed for the shielding inserts of the VV to increase the shielding efficiency. 304B7 (UNS designation S30467) steel is used in the form of plates fixed between two VV walls. The ASTM standard A 887-89 is referred to for the base properties and the procurement specifications. Cobalt concentration should be limited to 0.2% max, unless a lower concentration can be agreed upon between the purchaser and the supplier.

Precipitation-Hardened Steel

High strength precipitation-hardened stainless steel type 660 (also known as A-286) is proposed for the port stiffening extensions and bolting the port plugs. The UNS designation of SS 660 (A-286) grade is K66286.

The heat treatment indicated by ASME SA 638 can be used for SS 660. It should be performed in two stages: solution annealing (from 900 ± 15°C, 2 h, oil or water quench) and ageing for 16 h at 705-760°C, air or furnace cooling. This is a well-known standard material, and a large database is available.

For the port plugs, doses of irradiation are relatively low (< 0.1 dpa). These doses will not result in significant property changes. Thus, properties of unirradiated material can be taken for the design analysis.

Ferritic Steel

Inserts of ferromagnetic material are used in the outboard area inside the vacuum vessel in the shadow of the TF coils to reduce the toroidal field ripple. The working temperature is ~ 20-200°C, the irradiation damage less than 0.03 dpa, and the environment is water, in galvanic contact with the VV material. SS 430 is recommended for the ferromagnetic plates, because it has relatively good corrosion resistance in spite of its slightly lower magnetisation than the best materials. The procurement specification ASTM A 240-86b and/or ASTM 883 (alloy 2) can be used for the required product form. The UNS designation is S43000.

No specific data on the corrosion of SS 430 is available for the water chemistry specified in ITER. However, SS 430, which has a chromium content of ~ 17%, should have a uniform corrosion rate similar or better than that of 304 type SS.

2.13.2.2.2 Copper Alloys

Heat-sink Copper Alloys

Cu alloys are considered as heat sink materials for the ITER first wall, divertor and limiter. Two materials have been retained as candidate heat sink materials for the high heat flux components: CuCrZr and GlidCop® Al25. The main differences between these materials are:

- the properties of CuCrZr alloy strongly depend on thermomechanical treatment which could be part of the manufacturing cycle, whereas properties of GlidCop® Al25 alloy are relatively independent of the heat treatment;
- fracture toughness of CuCrZr alloy is significantly higher at high temperatures (>~ 200°C) than that of GlidCop® Al25;
- CuCrZr is a weldable material, whereas fusion welding is not recommended for GlidCop® Al25;
- CuCrZr alloy is available from different suppliers, whereas GlidCop® Al25 is produced by one firm, OMG Americas, USA.

Starting from the original specification, a tighter limitation for composition and a specific heat treatment were proposed for the CuCrZr alloy, with the definition of an ITER grade specification, CuCrZr-IG. The proposed composition of CuCrZr alloy differs from the standard one, mainly by its narrower range of the Cr (0.6-0.9%) and Zr (0.07-0.15%) content. In different national standards the chromium content varies from 0.4% to 1.5% and the zirconium content varies from 0.03% to 0.25%. The reason for limiting the Cr content to the narrower range in the alloy is that otherwise it may result in the formation of coarse Cr precipitates which affect the radiation resistance. Zr promotes hardening of the alloy by providing a good homogeneity of precipitates. Limitation of oxygen (< 0.002%) and of the total amount of impurities (< 0.03%) is required for the same reason and for a better resistance against embrittlement. Based on industrial experience, the reference ITER heat treatment for CuCrZr-IG is the following: solution anneal at 980-1000°C for 1 h, water quench then age at 450-480°C for 2-4 hours. Ageing can be performed at any time during component manufacturing.

For ITER application, the fabrication process of GlidCopAl25 was optimised, with an improvement of ductility and reduction of anisotropy. The material is provided by the manufacturer under the trademark Glidcop® Al25-LOX-CR (low oxygen, cross-rolled). A high temperature annealing (at 950°C) is performed after cross rolling. The optimised grade is indicated as CuAl25-IG.

During component manufacturing, the base material is generally subjected to additional thermal cycles e.g. welding, brazing, HIPing, etc. Brazing, even at relatively low temperatures, results in a significant decrease of strength in the case of long term exposure and/or slow cooling rates. Brazing or HIPing at high temperature can be combined with solution annealing. In this case the brazing/HIPing temperature should be about 950-980°C, followed by fast cooling and ageing at 475-480°C. The most critical step is the cooling rate from the brazing/HIPing temperature. If a fast cooling rate can be realised after high temperature brazing/HIPing, the loss of strength is minimised.

CuAl25-IG shows much less sensitivity to heat treatment than CuCrZr-IG. Thermal stability is one of the main advantages of CuAl25-IG. This allows a wider flexibility in the use of different joining technologies for high heat flux components.

Irradiation results in an increase of strength of Cu alloys at low temperatures, below 300°C. Properties of unirradiated materials should be used in this temperature range to be conservative for analysis. At temperatures > 300°C, the strength of irradiated materials is lower, and irradiated material strength properties should be used.

Ductility of CuCrZr alloy increases with increase of irradiation temperature. At irradiation temperatures < 200-250°C, criteria for immediate plastic strain localisation and fracture due to the exhaustion of ductility are paramount in structural assessments. Above these temperatures the material will be ductile, and creep and creep fatigue properties are more critical. For CuAl25-IG in all temperature ranges, ductility decreases significantly with irradiation, and plastic strain localisation and local fracture criteria should be used for structural analysis.

Nickel-Aluminium Bronze

Nickel-aluminium bronze C63200 (82Cu-9Al-5Ni-4Fe) is proposed for nuts, bearings and rods connecting plasma-facing components to the divertor cassette. Several standard specifications can be used for the material procurement (ASTM B150, ISO 428 CuAl10Fe5Ni5, DIN CuAl10Ni and BS CA 104). High strength, low friction and spark resistance are the key properties for these applications.

The typical tensile strength of C 63200 bronze is 540-725 MPa, and yield strength is ~ 330-380 MPa, depending on the heat treatment. The ultimate compressive strength is ~ 760 MPa. There is experience of using this material in JET for similar applications, and testing for ITER is now under way. The properties of irradiated C 63200 bronze are unknown.

DS Copper Alloy, Glidcop Al60

DS Cu alloy, Glidcop® Al60, is proposed for the compression collar of the bolt fastening of flexible supports. The material is manufactured by OMG Americas Company under the trade mark Glidcop® Al60-LOX. The UNS alloy number is C15760. High material strength is provided by aluminium oxide (~ 1.1 %) particles uniformly distributed in the copper matrix. The material is used to compensate for a pre-load decrease due to thermal expansion of bolt and flexible cartridge materials, and to equalise temperatures in the module support unit due to high thermal expansion and thermal conductivity. Strength and thermal resistance of Glidcop Al60 are superior compared with other Cu alloys (ultimate strength ~ 500-530 MPa and yield strength ~ 400-440 MPa).

Irradiation results in a decrease of ductility and increase of strength for compression collar working conditions. However, the material of the collar is under compression stresses, and fracture due to immediate plastic flow localisation and fast fracture is avoided in this configuration. Irradiation may accelerate creep that should be taken into account in the design analysis.

2.13.2.2.3 Ti Alloys

For the blanket flexible supports, a flexible cartridge in the form of a cylinder with axial slots is screwed into the vessel from one side and bolted through access holes in the blanket. The design requirement for the material of the flexible cartridge is complex and somewhat

contradictory. The material should have a high strength, because of high axial loading force, and at the same time allow for a wide range of elastic deformation during bending. The estimated temperature range of the flexible cartridge is between 100 and 260°C, and damage is ~ 0.1 dpa.

A comparative analysis of the properties of several candidate materials was performed. The ability of materials to withstand impact loading is proportional to $U = 0.5 (YS)^2/E$, where YS is yield strength, and E is Young's modulus. Comparison of the candidate materials shows that titanium alloy has a yield strength slightly less than that of Inconel 718, the highest flexibility and the best U parameter, because of the relatively high strength, and low Young's modulus (approximately a factor of two less than Inconel 718 and 316 steel). Also, Ti alloys have lower resistance to buckling compared with high strength nickel alloys, since the buckling stress limit is proportional to Young's modulus.

Titanium alloys are widely used in the chemical and aerospace industries. Among the commercial Ti alloys, Ti-6Al-4V ($\alpha+\beta$ alloy) was proposed as reference grade. Since it is widely used in different countries, there is an industrial experience in many fields and the database of unirradiated material is relatively complete. Ti-6Al-4V can also be used according to ASME specification SB-381, "Titanium and titanium alloy forgings".

Ti alloy property change due to irradiation was studied for doses in the range 0.01-0.4 dpa and temperatures 40-350°C. The following general conclusions can be drawn from the available R&D results.

- Strength of all materials is increased due to irradiation.
- Ductility is decreased. However, in all experiments (even at ~ 0.4 dpa) the uniform elongation was above 2%. Irradiation dose expected for flexible cartridges in the ITER design is below 0.1 dpa. Structural criteria of unirradiated materials therefore should be used for the design analysis.
- There was no significant alteration of fatigue lifetime due to irradiation.
- Fracture toughness decreases (2-5 times) due to irradiation. Nevertheless, J_c (or K_c) values remain at a relatively high level (~ 20-60 kJ/m^2) at room temperature.

α-based Ti alloy (Ti-5Al-2.4Sn) exhibited less embrittlement due to irradiation. However, the strength of the alpha-based alloy is lower than that of the $\alpha+\beta$ alloy. Ti-5Al-2.4Sn alloy is thus considered as a back-up.

The cartridge operates in the environment of the vacuum chamber, but it is shielded from the direct bombardment of energetic particles by the module itself. The possibility of hydrogen or helium implantation by energetic particles is, therefore, eliminated. Available data indicates that a relatively high hydrogen content of 3-5 wt. % is necessary to produce significant embrittlement, in terms of impact fracture energy, in Ti alloys. ITER R&D shows that hydrogen saturation of Ti-6Al-4V alloy up to 200 wppm of hydrogen did not result in changes of tensile properties.

2.13.2.2.4 Ni Alloys

Inconel 718

High strength, fatigue and fracture toughness are required for the bolt attaching the shielding blanket modules through the flexible support, to minimise the size of attached units and to

provide reliability of the attachment. The operational conditions for bolts are the following: temperature ~ 150 – 300°C, damage dose ~ 0.5 dpa, and a design fatigue lifetime that is ~ 30,000 full power cycles.

Inconel 718 is selected as the reference material due to its high strength and good ductility. As a back up the high strength grade 660, also known as A-286, precipitation-hardened stainless steel could be considered. Inconel 718 has satisfactory fracture toughness and fatigue lifetime. The limited data available suggest that SS 660 has lower stress relaxation than Inconel 718 under low dose irradiation.

Inconel 718 is used in the nuclear industry. The material is produced commercially in forms of bars, rods, plates, strips, etc. The specifications, chemical compositions, required heat treatments and properties of these materials are well established. Selecting the correct heat treatment provides materials with a high level of strength and ductility. Inconel 718 has higher strength allowing for a higher pre-loading and a reduction of the bolt diameter. Careful control of the grain size of the mill product of Inconel 718 is needed to provide good fatigue lifetime. The material has relatively good fracture toughness after appropriate heat treatment.

Data on the irradiation behaviour of Inconel 718 is sparse. Preliminary results shows that irradiation up to 0.5 dpa will result in an increase of strength and in a slight decrease of ductility that will not affect the component structural integrity and lifetime.

Significant stress relaxation is expected under irradiation. Results show that for the bolts of flexible cartridge fastenings where the irradiation dose is ~ 0.02-0.1 dpa, the stresses reduce by 10-20% from initial pre-load to the end of life, so, the required pre-stress should be ~ 800 MPa.

Nimonic 80A

Superalloy Nimonic 80A is proposed for the divertor keys (elements for fixing PFCs in the cassette body) where high strength is required. This material is produced by Inco Alloy International under the specifications ASTM B637, DIN 17742, DIN 17754 and BS 3076. The UNS designation of alloy is N07080. High strength can be achieved in the aged state. The ultimate tensile strength is about 1,250 MPa, and yield strength is about 780 MPa at RT. The material is used for components where relatively low doses of irradiation will be achieved at the end of life, i.e. < 0.1 dpa. These low doses will not result in significant properties changes, and properties of unirradiated material should be used for the design analysis.

2.13.2.3 Joining Technologies

The design of the ITER PFCs involves various combinations of joints between armour materials and Cu alloy heat sinks, and between Cu alloys and austenitic steels. The joints must withstand the thermal, mechanical and neutron loads, the cyclic mode of operation, and operate under vacuum, while providing an acceptable design lifetime and high reliability. This section summarises the results of the R&D program on the development of joining technologies. Further developments are still needed with the goal of improving reliability and improving manufacturing efficiency, and the final selection must take into account the estimation of the cost of these technologies.

2.13.2.3.1 Be/Cu Joints

The main problem of bonding Be to Cu alloys is that Be reacts with almost all metals at moderate and high temperatures and forms brittle intermetallic phases that are detrimental for the joint reliability and the fatigue lifetime. To solve this problem and to provide good quality Be/Cu joints, different approaches have been studied.

- Use of materials as fillers or interlayers between Be and Cu alloy which do not form intermetallic phases with Be (e.g. Al, Ge, Si, AlSi or AlBeMet). The joining temperature for these materials is typically equal to or less than the melting temperature of these filler materials.
- Use of diffusion barrier materials with less affinity for the formation of beryllide intermetallics. Different types of these barriers have been studied: Ti, Cr, Ti/Ni, Al/Ni Ti/Cu, Al/Ti/Cu, Cr/Cu. Typically for this type of joints, HIP is used as a joining procedure with the temperature range 500 - 850°C.
- Brazing with Cu-based brazing alloys. At a brazing temperature more than 650°C (typical temperature for these types of brazing alloys) intermetallic formation occurs, but using a "fast" brazing technique, this formation can be limited.
- Direct bonding of Be to Cu alloy (with or without a soft intermediate layer of Cu) at moderate temperature (~ 500-700°C). Direct Be plasma spray can also be carried out under this condition.

Based on the result of tests on small scale mock-ups, the following joining technologies have been determined as references.

- For ITER first wall, HIP at 850°C with a Ti interlayer. Be plasma spray could also be used. Both technologies have demonstrated satisfactory performance at a heat flux ~ 1- 2.5 MW/m^2.
- For high heat flux components (port limiter): "fast" brazing with CuInSiNi alloy and HIP at 625°C with AlBeMet interlayer. These technologies demonstrated the best thermal durability, e.g. fast brazing resisted 4500 cycles at 12 MW/m^2.

Based on preliminary data, both methods (HIP and brazing) seem to be resistant to neutron irradiation.

2.13.2.3.2 W/Cu Joints

The main problem in the development of W/Cu joints is the large difference in the coefficient of thermal expansion and of elastic modulus. With a conventional flat tile geometry, this difference creates very large stresses at the W/Cu interface. From an engineering point of view the solution is to use brush-like (rectangular or rod) or lamella type W armour design. The advantages of the brush structure are that the stresses at the W/Cu interface may be reduced as the single elements are free to expand under the heat flux, reducing the thermal stress in the tile.

Several joining methods have been developed.

- Casting of pure Cu onto W. This process consists of casting a soft compliant layer of pure copper onto the activated/or not activated surface of W. The good joint during casting is based on the high wettability and high creep relaxation ability of pure Cu. The W/cast Cu elements are then joined by different methods such as e-beam welding, brazing or HIP to the copper alloy heat sink.
- High temperature brazing technology using CuMn base braze alloy has provided reliable and good quality joints of W tiles and copper heat sink.

- Several methods for joining W rods (1.6-3.2 mm dia) to CuCrZr heat sinks have been developed. One of them is the diffusion bonding of W rod tips directly into the OFHC/CuCrZr substrate at 450°C.
- The use of CVD (chemical vapour deposition) of W onto Cu also produces good joints, but has limitations in thickness. The use of W plasma spray also gives good joints with a Cu alloy heat sink. Both these methods have been successfully applied for manufacturing of components with curved surfaces. However, as was demonstrated by testing of representative mock-ups, these technologies can be applied only for components with low and moderate heat flux.

Several technologies (casting, brazing, direct diffusion bonding of W into Cu) provide excellent high heat flux durability performance of W/Cu joints and can be recommended for the manufacturing of the divertor components. Further development has to be focused on the cost optimisation of these technologies.

2.13.2.3.3 CFC/Cu Joints

The problem in the development of CFC/Cu joints is worse than for the W/Cu joints, due to the even larger difference in the coefficient of thermal expansion of the materials. To provide a high quality CFC/Cu joint, the surface of the CFC has to be activated to increase the wetting and a compliant layers between the CFC and Cu alloy heat sink is needed to relieve the residual stresses. Several joining technologies have been developed and studied.

- Active metal casting (AMC®) technology, which was originally developed for the Tore Supra limiters. This technology includes special laser treatment of the CFC surface, followed by casting of pure Cu onto CFC, machining and final joining with the Cu alloy heat sink. In the monoblock configuration, CFC tiles with AMC® Cu can be joined to Cu alloys by brazing or HIP. For flat tiles, the same joint could be obtained by e-beam welding. AMC® technology was applied to different CFC grades (SEP N11, SEP N31, etc.).
- Brazing with silver-free alloys (CuMn, CuSiAlTi) and HIP-assisted brazing with CuMn and CuTi alloys. The best high heat flux results have been observed for CuMn brazes.

Few technologies (AMC® and brazing with CuMn) provide the required high heat flux durability performances of the CFC/Cu joints. Based on preliminary data, both methods are resistant to neutron irradiation.

2.13.2.3.4 SS/Cu Joints

Plasma-facing components involve the use of three different types of SS/Cu joints: tube-to-tube, plate-to-tube, and plate-to-plate. For the first wall, solid HIP is considered as the most promising method of achieving the required quality of joints. Two ranges of HIP temperatures have been studied: high, ~ 1,050°C, which permits the combination in one treatment of the joining of Cu to steel and steel to steel, and moderate temperatures ~ 920°C, in which case steel-to-steel joining has to be performed by a separate procedure. For HIP joining the use of CuAl25-IG alloy is preferable due to its excellent resistance to high temperature heating. With fast cooling (~ 2°C/s) and applying further ageing, the properties of CuCrZr-IG after HIP are acceptable. Both methods give high quality bonding and tensile properties of joints very close to the strength of Cu alloys. Optimised SS/CuAl25-IG joints have good radiation resistance. Strength of the HIP-bonded joints after 0.4 dpa irradiation

dose at 150 and 300°C is higher than or equal to that of the base metal, with the failure location within the Cu part close to the interface.

Another joining method, i.e. explosion bonding, seems promising and provides a good quality of joint, but it is applicable only for simple geometric component shapes. For Cu tube to stainless steel tube joining, friction welding, diffusion bonding (for DS Cu) and TIG welding with Ni interlayer (for CuCrZr-IG) can be used. The casting of CuCrZr onto stainless steel also gives a good quality of joint, that is also resistant to neutron irradiation.

2.13.2.3.5 SS/SS Joints

All austenitic stainless steels are readily weldable with a wide range of well-established methods, such as narrow gap TIG welding, electron beam welding, and laser welding. The weld joints should be performed in accordance with internationally accepted procedures such as described in ASME section IX. 316L(N)-IG can be considered to be a member of the P-8 Group 1 weld joints. Narrow gap TIG welding is selected as reference for the vacuum vessel manufacture. The properties of the weld are well-defined and compatible with the load requirement of these components. For TIG joints, the unirradiated welded material shows, in general, a higher yield stress, lower ultimate tensile strength and lower ductility than plate material. The effect of neutron irradiation on the tensile properties is similar to that for plate material, i.e. significant hardening and loss of ductility occurs. It is expected that the worst ductility reduction occurs in the irradiation temperature range of 275-375°C, well above that appropriate for ITER.

For some components, the welding of irradiated steel is needed. From the material point of view, helium content generated by gaseous transmutation should be kept below a threshold value. The threshold He content is rather low and although it will not cause any change of the mechanical property of the base material, it can still promote the formation of cracks in the heat-affected zone during welding. Certain precautions have to be taken, such as low weld heat input, surface preparation, avoiding high tensile stresses, etc. The welding method must therefore be carefully chosen.

The joining of stainless steel to steel by HIP is considered as the main method for the manufacture of the shield blanket modules. The quality of joint strongly depends on the quality of the base metal and on the surface preparation during the HIPing process. The base metal should be vacuum re-melted for a low content of impurities and of non-metallic inclusions. The surfaces should be polished, etched and HIPed right after surface preparation. Any delay in HIPing may result in the formation of an oxide layer with unsatisfactory properties of the joint. The manufacturing process should be carried out under strict quality control.

Most of the tensile data for SS/SS HIP joints are within the design allowable but close to the lower bound of the specified strength. Neutron irradiation has a slight effect on the mechanical properties of the joints, demonstrating a similar behaviour as for the base metal.

2.13.2.4 Ceramics for Electrical Insulation

Aluminium oxide and aluminium magnesium oxide (spinel) are proposed for the insulation of the modules and for the limiter plates. The same materials are used as for electrical insulator for the diagnostic components. The main difference between the diagnostic application and

that in the blanket module and in the limiter and baffle plates is the additional requirement to sustain significant static and dynamic loads. The ceramic provides not only passive electrical insulation but also fulfils a structural function.

Plasma spray is one of the most promising options for components manufacture where insulation is required. Coatings have good mechanical properties in the unirradiated state. Results of R&D shows that the coating is not damaged if the compression stress does not exceed the yield point of the substrate material. In ITER, the maximum design load during operation, 200 MPa, is below the yield point of 316L(N)-IG.

Impact tests of unirradiated and irradiated ceramic coatings have been performed. ITER R&D has demonstrated that a 12 kg weight falling from 20 mm did not cause the coating to disintegrate (> 10,000 cycles).

The radiation-induced conductivity is estimated at about 10^{-6} - 10^{-4} S/m for the ITER working conditions (first wall and limiter). Therefore the estimated electrical resistivity of coatings will be no worse than ~ $3x10^{2}$-10^{5} Ω. Dielectric breakdown strength either does not change or decreases under irradiation depending on the material. But in the worst case the estimated dielectric breakdown strength of alumina and spinel is almost one order of magnitude better than required for the insulators of the first wall module. It is not expected that significant strength degradation of the ceramic materials, alumina and spinel will occur for the dose of irradiation anticipated within the flexible attachment, ~ 0.3 dpa.

2.13.2.5 Material Selection for Vessel/In-Vessel Components

A summary of the materials grades selected as reference for ITER vessel/in-vessel components is given in Table 2.13-1. Behind the use of each material is a substantial body of R&D to substantiate the properties and the materials use, in the main carried out in the frame of ITER EDA R&D. For the current ITER design a proven material solution exists for each component. However, work is continuing so as to confirm that material properties can be preserved under the most cost-effective component manufacturing processes.

Table 2.13-1 Materials for Vacuum Vessel (VV) and In-vessel Components

Material	Material Grade	Components
Beryllium	S-65C VHP (backup DShG-200)	• Armour tiles for first wall and limiter
Tungsten	Pure sintered W	• Armour tiles for divertor components
Carbon fibre composite (CFC)	SEP NB 31, NIC 01 (back-up CX 2002U, SEP NS31)	• Armour tiles for divertor vertical target
Cu and Cu alloys	CuCrZr-IG	• Heat sink for plasma-facing components (PFCs) and for heating systems
	CuAl25-IG	• Heat sink for PFCs
	Nickel-aluminium bronze	• Nuts, bearings and other friction parts
	Glidcop Al60	• Compression collar of the flexible support bolts
Austenitic and precipitation hardened steels	316L(N)-IG1 plates and forgings	• Shield modules
	316L(N)-IG2 plates and forgings	• Vacuum vessel, blanket cooling manifolds
	316L(N)-IG3 cast	• Some vacuum vessel components and back-up material for divertor body
	316L(N)-IG4 tubes	• Thin walled tubes for first wall
	316L(N)-IG5 tubes	• In-vessel cooling pipes
	316L(N)-IG6 powder HIP	• Back-up material for shield modules
	AISI 660 (A-286)	• Fastening components for the port plugs (e.g. fixing wedges and bolts)
	SS 30467	• Boronised steel for in-wall shielding structures (plates)
Ni alloys	Inconel 718	• Bolts for the flexible supports and electrical straps, blanket cooling manifold support
	Nimonic 80A	• Keys in divertor PFCs
Ti alloy	Ti-6Al-4V	• Flexible cartridges for the module support
Ferritic steel	SS 430	• Ferromagnetic insert
Ceramic	Al_2O_3 or $MgAl_2O_4$	• Electrical insulators of module attachment and limiter plates

Note: Materials used for commercial components are not included in the table

2.13.3 Materials for Diagnostic Components

Diagnostic components use a variety of different materials. These materials are distributed at different locations within ITER and, as a result, the operational conditions for them are very different. However, the key issue for these materials is radiation resistance under ITER conditions.

2.13.3.1 Electrical Insulators/Ceramics

Insulating ceramics will be used in feedthroughs, connectors, mechanical supports and general stand-offs, mineral insulated (MI) cables and their seals, substrates of bolometers, and other sensor devices such as pressure gauges. Ceramic windows are also used in diagnostic systems and heating/current drive systems. Almost all the candidate ceramics retain the geometrical stability demanded by the design, namely within ± 5% (± 1% for magnetic coils) for the full temperature and neutron fluence. In nearly all cases they must be high-vacuum compatible, and the electrical conductivity of ceramics should remain below a specified value depending on the diagnostic systems. This in general is ~10^{-6}S/m.

For ceramics, radiation induced conductivity (RIC), radiation induced electrical degradation (RIED), dielectric, thermal and mechanical properties, and tritium diffusion, are the key properties.

Present data indicates that, with careful choice of material and operating temperature range, the long-term volume degradation of the electrical insulation (bulk RIED) should not impose serious technological problems for ITER conditions (up to 2 dpa). RIC plays a major role in determining the electrical insulating ability at the onset of operation, and is quantitatively well evaluated. In general, RIC will not impose a serious technological problem except possibly for applications such as the bolometer substrate, where cross-leakage may be important.

Additional problems which have been identified during RIED investigation, such as surface conductivity, insulator cracking and electric charging effects, require further investigation to determine the physical mechanisms responsible for associated RIED-like electrical degradation, and to assess their possible influence on the insulator performance and lifetime. The possibilities of surface contamination and degradation must be taken into account and countermeasures to mitigate such effects should be considered.

2.13.3.2 Wires/Cables

Different cable types (mineral-insulated, steel and glass-braided) with different configurations (twisted pairs, coaxial, multi-axial etc.) are under consideration. For cables/wires, RIC, RIED, radiation induced electromotive force (RIEMF) between sheath and centre conductor of mineral insulating (MI) cables, conductor resistance, and dielectric breakdown strength, are important properties. Reliable cable termination techniques with low leakage currents for MI cables are also an important issue.

RIC and RIEMF are quantitatively well documented. RIC is evaluated to be ~10^{-10} S/Gys. RIEMF current will be ~10^{-10} A/Gysm for typical MI-cable below 600˚C.

Magnetic coils made from MI-cable require an insulating conductivity of less than 10^{-6} S/m. This requirement for magnetic coils set behind shield blankets will be satisfied.

In ITER geometry, the voltage generated between two ends of a centre lead by the RIEMF is evaluated to be of the order of 1 μV. However, the full resolution of the RIEMF topic is still to be completed due to uncertainties in the interpretation of the results. Indications are encouraging but further tests and analytical work are required to clarify the matter.

2.13.3.3 Windows

Windows, acting as vacuum and tritium confinement barriers, transmit optical and microwave signals. Window assemblies must be vacuum tight to UHV standards and also be able to withstand the potential 0.2 MPa pressure rise during an in-vessel coolant leak.

Some issues for windows are common with ceramic issues. For potential window materials, the optical properties including radioluminescence and optical transmission have been extensively studied. In addition to enhanced tritium diffusion, there is a possibility of enhanced tritium leaks due to microcracking in the ceramics-to-metal joints due to effects such as radiation-enhanced segregation and sub-critical crack growth (SCCG). For LIDAR applications, synergistic effects of high power laser-beams and irradiation and/or surface degradation are very important from the mechanical damage point of view.

Based on ITER R&D, fused silica glass or quartz windows are recommended for spectroscopic systems for the visible region, and sapphire windows should be used for the IR region. From the viewpoint of radioluminescence, fused silica has an advantage over sapphire as a window material. On the other hand, optical absorption in silicas (covalent-bonding) is sensitive to gammas (ionising radiation), namely radiolysis, as well as to atomic displacements. Optical absorption in sapphire is relatively insensitive to gamma radiation and only displacement damage associated with neutron irradiation induces notable absorption. Thus, under high-flux ionising-radiation, sapphire will have some advantages over fused silica. Crystalline quartz is more resistant to radiolysis than fused silica.

The availability in quantity and in sizes of window materials made of fused silica (synthesised silica especially for large windows and optical fibres) should be considered. Two possible fused silicas which have been found to have radiation-resistant optical properties are KU-1 (high OH) and KS-4V (low OH). In the case of diamond, excellent material grades have been developed in the EC H&CD programme (at 145 GHz), which may possibly be used for diagnostic windows from the GHz region to the IR /visible range.

2.13.3.4 Optical Fibres

For a large variety of optical diagnostics it is extremely desirable to be able to use fibre optic transmission close to the plasma region to take advantage of the limited spatial access and easy alignment of optical components.

Important issues for ITER diagnostics are radiation resistance of optical fibres especially for the visible region, and their application in the vicinity of the first wall. (Optical fibres will be employed in such a way that only a few metres will be exposed to the high radiation flux region.) Irradiation effects on radioluminescence and degradation of optical transmission due to permanent and transient absorption are important. Key parameters of optical fibres, which

affect radiation resistance, are fibre composition (dopants, OH-content, impurities, cladding type), fibre fabrication (manufactured drawing speed and temperature) and preform fabrication.

The behaviour of optical fibres is excellent in the IR region (low absorption and low radioluminescence). Serious technical problems are not anticipated and suitable fibres already exist. The main problem will be in the associated electronics in an optical communication system. R&D indicates that the radiation-induced loss could be less than 10 dB/m in the wavelength region of 800-1,200 nm for some optical fibres, with a fast neutron fluence of 10^{25} n/m^2 and ionising radiation dose of 10^{10} Gy.

Recently developed fluorine-doped optical fibres revealed better radiation resistance, 20 dB/m or less in the visible region for a fast neutron fluence of 10^{23} n/m^2 and 10^8 Gy. Taking into account these results, there is a possibility to use the optical fibres for the visible region inside the cryostat during operation. More detailed, specific and extensive studies, including manufacturing processes, are needed before final conclusions can be made for the application of optical fibres in ITER. Further radiation-resistant optical fibre development, and round robin irradiation tests, are underway.

2.13.3.5 Mirrors/Reflectors

The first mirrors will experience the most severe environmental conditions in the ITER device. In addition to irradiation effects on mirrors, other adverse effects of sputtering, evaporation or coating on the mirror surfaces can change the reflectivity of the mirrors.

R&D has been focused on the irradiation on metal bulk mirrors, single coated mirrors, dielectric coatings on ceramics for high power laser beams, layered synthetic microstructures for UV reflectors, crystalline materials for X-ray spectroscopy, and graphite elements for submillimetre plasma diagnostics.

It is believed that solutions now exist for situations where the dominant potentially damaging mechanism is erosion due to the CX flux of energetic neutrals. This is likely to be the case for the plasma facing mirrors mounted in the equatorial and the upper ports.

For mirrors mounted in ducts in the shielding labyrinths however, deposition could be the dominant potentially damaging mechanism. This will most likely be the situation in the divertor where there may be substantial erosion. There are only limited experimental results on deposition and models of the process are still at an early stage. There is therefore a need for controlled experiments on present-day devices and the development of models and possible mitigating methods.

Dielectric mirrors and layered synthetic microstructures should be used in well-shielded locations and under temperature control, to avoid differential nuclear and thermal swelling.

Some inorganic X-ray crystals, though they are vulnerable to radiation damage, do not have a change in their reflectivity, interplane distance, and width and form of diffraction lines, up to 10^{23} n/m^2 for Ge, Si, SiO_2 and Graphite, and to 10^{22} n/m^2 for Mica monocrystals.

Table 2.13-2 Materials for Diagnostic Components and Results of Irradiation Tests

Diagnostic components/ sensors	Candidate materials	Main R&D results: Accumulated effects (Dose)	R&D results: Dynamic effects (Dose rate)
Ceramics (electrical insulators)	Single crystal and polycrystal alumina (Al_2O_3)	2 dpa in helium atmosphere (RIED: < 10^{-6} S/m)*1	10^4 Gy/s (RIC: < 10^{-6} S/m)
Wires /Cables	MI-cables: SUS, Inconel (sheath)/MgO, Al_2O_3 (insulator)/ Cu, Ni (centre conductor)	1.8 dpa (RIED: No catastrophic degradation)*2	10^4 Gy/s (RIC: < 10^{-6} S/m) 10^3 Gy/s (RIEMF: < 10V)
Windows	Fused Silica/Quartz KU-1 (400-1500 nm; high OH)	10^{-3} dpa (Transmission: 5% degradation; 8 mm thickness) $6x10^{19}$ n/cm^2 , $2.5x10^9$ Gy (High trans. for λ > 350 nm)	Radioluminescence: 10^7 photons/Gy.Å.sr.cm^3 at 410 nm
	Sapphire (800-5000 nm)	0.4 dpa (Transmission: No degradation; 1mm thickness)	Radioluminescence: 10^{10} photons/Gy.Å.sr.cm at 410 nm
	Diamond (GHz-IR)	10^{-2} dpa	
Optical fibres (Visible region)	Pure silica (core)/F doped (clad)/Al jacket (RF:KS-4V)	10^7 Gy (pure gamma) (Transmission loss: 2-2.5 dB/m)	Radioluminescence: (Cerenkov + 450-650 nm)
(Visible region)	F doped silica (core)/F doped (clad)/Al jacket (JA F-doped)	10^{-2} dpa (10^8 Gy) (Transmission loss: 20 dB/m)	Radioluminescence: (Cerenkov + 450-650 nm)
(IR region)	Pure silica, F doped (core)/F doped (clad)/Al jacket	0.5 dpa (10^{10} Gy) (Transmission loss: 5 dB/m)	Radioluminescence: (Cerenkov + 1270 nm)
Mirrors /Reflectors	First mirrors: Metal (Cu, W, Mo, SS, Al)	40 dpa (Cu)*3 (Reflectivity: No degradation)*4 0.1 dpa (Mo, Al) (Reflectivity: No degradation)	
	First mirrors for LIDAR: Single coated (Rh/V)*5		
	Dielectric mirrors: (HfO_2/SiO_2, TiO_2/SiO_2)	< 10^{-2} dpa *6 (Flaking, blistering)	
	LSMs *7: (Mo/Si, W/B_4C and W/C)	< 10^{-2} dpa (the shift of the peak reflectivity to shorter wavelength)	
	X- ray crystals: (Ge, Si, SiO_2, Graphite)	10^{-2} dpa	
Magnetic coils	MI cables	10 dpa (Dimensional stability)	Asymmetry in output voltage
Bolometers	Mica substrate*8	10^{-2} dpa (Expansion: 0.15% at 150˚C)	
	Au meander	10^{-2} dpa (Resistivity: 20% increase)	
Pressure gauges	Alumina feedthrough, W filament, SS frames		

*1 Substantial surface degradation in Wesgo 995 and Ruby is observed.
*2 Some long-term degradation even without voltage application is observed.
*3 Simulation experiment using Cu+ ions of 1 or 3 MeV.
*4 Sputtering by energetic particles near plasma will affect reflectivity seriously.
*5 Sputtering and redepostion will be important.
*6 Partially damaged. Dielectric mirrors are used as second mirrors.
*7 LSM (Layered Synthetic Microstructures): in well-shielded location and temperature control.
*8 Al_2O_3, AlN being considered for thin substrate.
Note: Abbreviations are defined in the text.

2.13.3.6 Materials Selection for Diagnostic Components

Reference materials for application in the diagnostic components in ITER have been selected (Table 2.13-2). This choice depends on a comprehensive irradiation database of diagnostic components which has been accumulated during ITER EDA R&D. While not all material choices are yet proven, promising candidates exist for nearly all applications. The most serious potential problem identified so far concerns noise, for example from radiation-induced emfs, and its effect on plasma control sensing magnet coils, which could cause the baseline to drift to the point at which control becomes difficult for very long pulses (> 1000 s), and alternative solutions would then be needed.

2.13.4 Materials for Magnets

2.13.4.1 Introduction

The magnets have two classes of structural materials: metallic and non-metallic, and one class of electrically conducting materials. Within the metallic materials, there are two subclasses: conductor jackets and structural elements. The conductor jackets require special consideration because of their close association with the superconductor fabrication and (for Nb_3Sn) their potential influence on its superconducting properties. Within the non-metallic components, there are four subclasses: high voltage insulation, low voltage insulation, non-metallic structural components and low friction surfaces. The only fully non-metallic component (apart from small local fillers that form part of the electrical insulation although they have no role in forming the electrical barrier) is the pre-compression ring. The electrically conducting materials have four subclasses: Nb_3Sn cables, NbTi cables, joints and current leads.

2.13.4.2 Metallic Materials

2.13.4.2.1 Requirements

The operating temperature of the magnet structures is predominantly in the range 4.5-20K. Under fault conditions loads can occur up to 300K but these do not influence the material choice. The gravity supports and the vacuum vessel supports have a temperature gradient, from 4.5K at one end to 300K or above at the other. Some keys and bolts (especially those associated with pre-compression structures) require pre-loading at room temperature.

The nuclear radiation levels on the magnets are low (in terms of the potential impact on material properties) since the most sensitive components are the organic fillers used in the electrical insulation. There is a requirement to reduce impurities that result in long life residual radioactivity (cobalt and niobium).

There is a generic need for good material properties for the magnets. The critical properties are those relating to plastic yield, fast fracture and fatigue crack growth rate. For keys and bolts, typically a high yield strength at room temperature is required.

2.13.4.2.2 Material Characteristics for Structural Elements

The most obvious material to meet most of the structural requirements is austenitic steel. There are two well known classes frequently used in cryogenic applications, AISI 304L(N)

and 316L(N). Unstabilised austenitic steels such as 304 can, under some conditions, undergo a martensitic transition in association with fatigue crack growth, which at 4K can lead to fast fracture. This is not generally acceptable for stressed components, and the fully stabilised 316 class is required. The cost penalty of this choice is small.

The 316L and LN class has a fairly wide range of chemical compositions and the properties at 4K have a substantial range. To achieve properties towards the upper end of the range for yield stress and fracture toughness K_{ic} (typically over 1000 MPa and 200 $MPam^{1/2}$ respectively), a narrower composition range is required, typically with nitrogen, nickel and chromium levels at the maximum allowable for 316LN. This has led to the definition of a class of 'strengthened austenitic steels' for the magnet structural elements. These are steels with a specific individual composition that are close to the 316LN range. In some recent developments, the composition is extended outside the 316LN range, usually by the addition of extra manganese to increase nitrogen solubility. These new steels have been qualified after trial component fabrication to confirm that the manufacturing route does not lead to martensite formation. For less critical components, 316LN and 316L remain suitable candidates (yield stress and fracture toughness K_{ic} in the range 700-900 MPa and over 200 $MPam^{1/2}$ respectively).

The fatigue properties of these steels are generally associated with impurity content, grain size, and the formation of brittle phases as the result of heat treatments (including welding). For high performance components, removal of impurities using vacuum oxygen degassing and electroslag refining are required for the material preparation. Welding procedures and weld fillers have to be qualified on an individual basis and avoidance of brittle delta ferrite formation is a strict requirement.

The main welding techniques qualified are:

- electron beam (EB) of strengthened austenitics (forgings and castings) for thicknesses up to 50 mm;
- submerged arc welding of strengthened austenitics (forgings and castings) for thickness up to 250 mm (also used combined with EB);
- gas tungsten arc welding of strengthened austenitics (forgings and castings) for thicknesses up to about 30 mm (to be used combined with submerged arc welding where low heating is required for the initial weld passes, as in the TF coil case closure).

In addition to the austenitic steels, exceptionally high strength materials may be required for local components such as keys and bolts. Two standard varieties of Inconel are selected for this purpose.

2.13.4.2.3 Material Characteristics for Conductor Jackets

The material for the conductor jacket has an important structural role in the CS and PF coils.

For the PF coils, the cable material is NbTi. The jacket is fabricated as extruded or drawn sections which are assembled onto the cable by butt and/or longitudinal welding. The stress issues are entirely tensile fatigue (the jacket does not operate at high Tresca stress levels) and a refined 316LN or L austenitic steel is suitable.

For the CS, the cable material is Nb_3Sn and the material choice is much more complicated. The jacket material may have to be co-reacted through the Nb_3Sn heat treatment (approximately 200 h at 600-650°C) and both high yield strength and good fatigue resistance are required. Assembly onto the cable after heat treatment is possible but requires extreme care as the Nb_3Sn cable is brittle (a thin protecting jacket is used). It is preferable (but not an absolute requirement) for a co-reacted jacket to have a thermal contraction coefficient close to that of the Nb_3Sn strands, since the strand superconducting properties are decreased by strain.

Three materials are available for the conductor jacket which can be co-reacted with the cable. In addition, any of the strengthened austenitic steels or standard 316LN can be used as a jacket material if assembled onto the cable after the heat treatment.
The following materials are all specially developed for co-reaction:

- Incoloy 908;
- pure titanium (with controlled oxygen content);
- modified 316LN.

The first two of these have thermal contraction coefficients that match the Nb_3Sn. Incoloy 908 is a nickel-based superalloy that undergoes precipitation hardening in the reaction heat treatment, leading to a good fatigue performance. It is however extremely sensitive to stress accelerated grain boundary oxidation and results in stringent requirements on oxygen in the heat treatment atmosphere. Pure titanium is not sensitive to oxygen but has a low modulus. The final option, a modified 316LN steel, has a significantly higher thermal contraction. It has a low carbon level to avoid embrittlement by carbide precipitation during the heat treatment, and enhanced nitrogen to improve the yield strength.

2.13.4.2.4 Material Selection

Table 2.13-3 gives a summary of materials allocated to the various components. EK1, EC1, JJ1 and JK2 refer to specific varieties of strengthened austenitic steels that have been qualified by particular suppliers.

Table 2.13-3 List of Materials for Magnet Structures

Class	Specification	Components
Strengthened austenitic steel	EK1 or JJ1 for cryogenic applications as forged sections	• TF coil case (inner leg basic elements) including stub elements • Pre-compression ring flanges
	EK1 or JJ1 for cryogenic applications as forged plates	• Gravity support stacked plates, flanges and joint keys • Friction joints • Webs of intermediate outer intercoil structure stub elements (fabrication option)
	JK2 as extruded/rolled sections	• Reinforcing for Ti CS conductor jacket
	JK2 as forged plates	• Buffer elements of CS pre-load structure (due to low thermal contraction of JK2)
	EC1 for cryogenic applications as cast sections	• TF coil case (outer leg basic elements) including (fabrication option) outer intercoil structure stub elements
316 austenitic steels	316LN as forged plates	• PF coils supports (frames, clamp plates, tie rods, flexible plates and bolts) • Parts of radial plates and covers • CS supports • Tie plates, flanges, adjustable wedges of CS pre-load structure
	316L as extruded square tubes, circular tubes and circular sections	• PF coil jackets • Parts of radial plates and covers • VV support stacked plates and flanges • CCs supports • Cooling pipes
Nb_3Sn conductor jacket materials	Incoloy 908 extruded square tubes	• CS conductor jacket
	Modified 316LN	• TF conductor jacket
	Titanium	• CS conductor jacket
Inconel	718 as fasteners	• Pre-compression ring bolts, inner intercoil structure poloidal keys and outer intercoil structure bolts • Joints bolts for gravity support and VV support

2.13.4.3 Non-Metallic Materials

2.13.4.3.1 Requirements

Electrical Considerations

The high voltage insulation in the coils is designed for a maximum level of 20 kV which allows for anticipated levels of faulted operation as well as effects such as switching jitter that increase the nominal maximum operating level. All high voltage insulation must incorporate a true electrical barrier which is capable of withstanding the electrical fields without a filler material (because filler materials may contain gas-filled voids which can break down). Low voltage insulation must withstand < 10 V and the insulation has only to maintain separation of the conducting surfaces. The insulating breaks are electrical breaks that have to be placed in each helium cooling pipe that is connected to the coil and which have to withstand a maximum voltage level of 20 kV.

Mechanical Considerations

The insulation material contributes to the support of the magnets by acting both as a bonding agent within a coil (only for high voltage insulation) and a filler material that transmits pressure loads.

The non-metallic insulation material used in the coil has an important secondary role as a filler that is used to absorb conductor manufacturing and winding tolerances.

The pre-compression ring is required to have high tensile strength in the circumferential direction both at room temperature and 4K.

Some structural supports (for the PF coils) must provide a reaction against vertical load, while allowing relatively free component movement parallel to the surface. This requires generally a non-metallic interface that can provide low sliding friction and is wear resistant under high compression loads.

The insulating breaks may be loaded by extension loads due to relative movement of the coil and the cryostat.

Manufacturing Considerations

The filler material used in vacuum impregnation processes (usually a form of epoxy resin) has several constraints because of the small gaps that have to be filled. The resin must have a low viscosity and a pot life significantly longer than the filling time at the filling temperature (a minimum of several hours, depending on the precise resin composition) to allow proper filling of the insulation. Flexibiliser is generally used to increase the resin fracture toughness and therefore to reduce the susceptibility to cracking at low temperature.

The reinforcement material and electrical barrier used together with the filler for high voltage insulation is required to be sufficiently robust (i.e. resistance to tearing if in the form of tapes) during manufacturing to allow easy wrapping of the conductor and a high filler density to be obtained by compression.

Nuclear Radiation

Extensive investigations of candidate insulation materials have been performed, based around mechanical and electrical tests of insulation systems after irradiation in a fission reactor.

Tetraglycidyl diaminodiphenyl methane epoxy (TGDM) and polyimide resin systems, suitable for pre-impregnation and high-pressure laminates, lose little strength and stiffness and do not change dimensionally after irradiation at 4K as high as 1.8×10^{22} fast (>0.1 MeV) neutrons/m^2.

Diglycidyl ether of bisphenol A (DGEBA) epoxy resins are more sensitive to radiation than TGDM systems. The principal deleterious characteristics of this resin system following irradiation are significant loss of shear strength and the expansion caused by increased porosity from gas evolution during warm-up to room temperature. Despite this, it is the first choice for impregnated systems because of its low viscosity and long pot life.

Mica barriers do not offer improved radiation resistance compared to other electrical barrier systems and have a low shear capacity. The use of polyimide film or inorganic coatings for electrical barriers will provide higher shear strengths and better radiation resistance.

2.13.4.3.2 Material Selection

Table 2.13-4 Potential Non-metallic Materials

Material		Process
Resins		
DGEBA	diglycidyl ether of bisphenol A epoxy, anhydride curing agent	VPI*
flex. DGEBA	flexibilized diglycidyl ether of bisphenol A epoxy, anhydride curing agent	VPI*
TGDM	tetraglycidyl diaminodiphenyl methane epoxy, amine curing agent	PP*
Reinforcements		
S-2 glass (also known as R-glass or T-glass)	S-2 glass (boron free) with silane finish	wrapped as tapes or injected with resin as chopped fibres
Electrical Barriers		
PI (HA) film	polyimide film, 0.025 mm thick, relatively amorphous structure	
PI (H) film	polyimide film, 0.025 mm thick	
PI (HPL)	polyimide	HPL*
Low Friction Surface		
Fibreslip	woven mat of PTFE and glass fibre with epoxy binder	bonded to support surface

*VPI: Vacuum pressure impregnation; PP: Pre-impregnation; HPL: High pressure laminate

The list of potential non-metallic materials is given in Table 2.13-4 and the materials applicable to the various magnet components in the current design are given in Table 2.13-5. The high voltage insulation system is chosen on the basis of its manufacturing convenience which outweighs its sensitivity to radiation damage. High pressure laminate is chosen for the low voltage insulation because of its high compressive strength and tolerance to small local gaps and sliding of the contact surfaces.

The pre-compression ring is formed by winding glass filaments coated with epoxy binder around the circumference. The winding-case filler is applied by mixing the resin and filler before filling the case with a VPI process. The insulating breaks are preformed (i.e. before welding into the helium cooling tubes) by winding glass filaments coated with epoxy binder around a central former which includes the steel end connections and the central electrical break. Steel reinforcement and voltage screens may be included within the winding.

Table 2.13-5 Non-Metallic Materials for Magnets

Components	Material and Form
TF, CS, PF Turn Insulation	Pre-impregnated glass epoxy TGDM type with polyimide film barrier and S-2 glass reinforcement or VPI DGEBA flexibilised epoxy with polyimide film barrier and S-2 glass reinforcement
Filler for Radial Plate Grooves, CS, PF Winding Pack Filler	VPI DGEBA flexibilised epoxy with S-2 glass reinforcement (only if pre-impregnation used for turn insulation)
Radial Plate Insulation	VPI DGEBA flexibilised epoxy with S-2 glass-kapton barrier (with bonded or unbonded sheets)
TF, CS, PF Ground Insulation	VPI DGEBA flexibilised epoxy with S-2 glass-kapton barrier (with bonded or unbonded sheets)
TF winding - Case Filler	VPI DGEBA flexibilised epoxy glass with S-2 chopped glass filler
Low Voltage Insulation	High pressure laminate
TF Coil Pre-compression Ring Insulating breaks	High density unidirectional glass fibre reinforced epoxy
PF1, 6 sliding surfaces at the supports	Fibreslip bonded to coil ground insulation

2.13.4.4 Conductor Materials

2.13.4.4.1 Requirements

The main coils are superconducting and the type of superconductor used depends on the field, temperature and current levels associated with the different coils. Two types of superconductor are commercially available and can be considered: Nb_3Sn and NbTi. The choice is related to the overall machine design (see 2.1). Nb_3Sn is of the A15 type and has the the highest critical temperature at high field. However it is a brittle compound and all of the mechanical forming operations associated with the coil have to be completed before the compound is formed by a reaction heat treatment at about 600°C for about 200 h. This reaction forms the Nb_3Sn from niobium filaments distributed in a tin-bearing matrix (either bronze or copper with a central tin core). NbTi is a metal alloy and is ductile.

Nuclear Radiation

Nb_3Sn and NbTi filaments show negligible effects of radiation at levels up to those corresponding to the coil insulation limits. At higher levels, there is evidence of changes in critical properties of the strands (initially an improvement, followed by degradation). The copper stabiliser in the conductor undergoes a resistance increase with neutron irradiation at 4K that can be largely recovered by annealing on warm-up of the coils. For the expected dosage over the lifetime of the machine, about 5 warm-ups of the TF coils will be required to keep within the electrical conductivity specification of the stabiliser.

Joints

Each coil is made up of a stack of pancakes (or multiple pancakes) of wound superconductor, with a joint at each end. The joints of adjacent pancakes are connected together and those at the ends are connected to the coil busbars. The joints generally represent a structurally weak point in the conductor, as the current must be transferred from the superconducting strands to a copper interface before entering the next conductor. In some joint techniques it is possible to join the cables directly and extend the jacket containment around the whole electrical contact part. However, in some locations (the coil terminals to the busbars), this is not practical and the copper must form part of the jacket containment. In this case, methods of joining the copper contact interface to the conductor jacket are required.

2.13.4.4.2 Material Selection

Nb_3Sn strands are formed in a multistage drawing process with intermediate re-stacking of the billets. The strand layout consists of a core of a bundle of filaments in a matrix, surrounded by a diffusion barrier (that prevents the tin contaminating the outer copper during the heat treatment). Outside the diffusion barrier there is a layer of copper stabiliser and then a coating which controls the contact resistance to adjacent strands (Table 2.13-6). NbTi strands consist of NbTi filaments in a copper matrix with again a surface coating to control the contact resistance (Table 2.13-6).

Table 2.13-6 Materials Selected for Nb_3Sn and NbTi Strands.

Type	Matrix	Diffusion Barrier	Filaments	Stabiliser	Coating
Nb_3Sn	Bronze or tin in copper	Tantalum or tantalum/niobium, thickness about 10μm	Ti doped with Ta, diameter about 2-5μm	High conductivity copper, RRR*>120	Electroplated Cr
NbTi	Copper	none	NbTi, diameter about 5μm	High conductivity copper, RRR>120	Electroplated Ni

*residual resistivity ratio

Jointing techniques that are available are defined in the Table 2.13-7, and those selected are given in Table 2.13-8.

Table 2.13-7 Jointing Techniques

Type	Jacket Seal	Electrical Seal
Lap	Explosion bonded steel-copper, steel-jacket weld	Solder
Butt	Jacket-jacket weld	High pressure sintering

Table 2.13-8 Superconductor and Joint Types Used in the Various Coils

Coil	Superconductor Type	Internal Joint Type	Terminal Joint Type
Toroidal Field	Nb_3Sn	Lap/Butt	Lap
Central Solenoid	Nb_3Sn	Butt	Lap
Poloidal Field	NbTi	Lap	Lap
Correction	NbTi	Lap	Lap

2.14 Nuclear Assessment

Radiation transport calculations are very important in the assessment of the ITER design, particularly with regard to operational constraints, access for reactor maintenance and unscheduled repairs, and activated waste (see 5). These calculations are carried out in a progression which begins with 1D studies for scoping, that take into account the reactor operating conditions, followed by 2 and 3D calculations that take into account streaming through penetrations, as well as the complexity of the geometry and the different material thicknesses and compositions.

An accurate map of the radiation fields is necessary all around the system. Component design and disposition of shielding must be decided to meet the objective of getting dose levels within imposed limits on surrounding systems, e.g. magnets, or to ensure personnel safety during operation and after shutdown if access is required for maintenance activities.

The shielding efficiency of the blanket plus the vacuum vessel should satisfy limits which include, for example, the total nuclear heating in the magnet (~14 kW), the helium production in the vacuum vessel at points where rewelding may be necessary (~1 appm), and the dose rate after shutdown in areas requiring access (< 100 μSv/h), etc.

For radiation transport calculations, mainly two types of models have been used: 1) 1 and 2D models for deterministic transport codes (ANISN, DANTSYS) and 2) 3D models using a Monte Carlo transport code (MCNP[1]). The 1D method is used to identify ranges of nuclear responses and provide initial design guidance. 3D models have been used to give specific nuclear responses in complex geometries that are more representative of the actual ITER systems.

[1] "MCNP 4B, Monte Carlo N-Particle Transport System", Los Alamos National Laboratory, Los Alamos, New Mexico. Ed. by J. Briesmeister, LA-12625-M, Nov. 1993.

The 1D model shown in Figure 2.14-1 is a "toroidal" cylindrical representation of the radial build-up of ITER at the equatorial plane. Such configurations simultaneously include the inboard and the outboard parts of the reactor with the main machine vertical axis as the axis of symmetry.

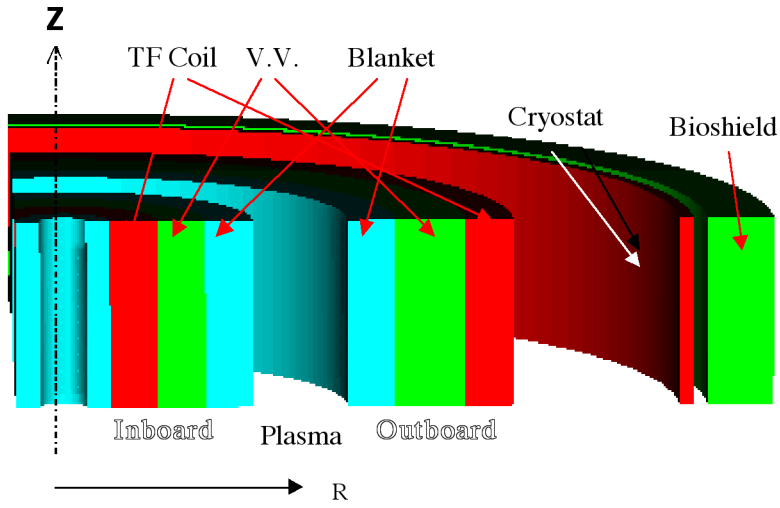

Figure 2.14-1 One-Dimensional "Toroidal" Model

For more accurate prediction of the nuclear responses, a fully detailed 3D MCNP model, with 20˚ symmetry, has been constructed. This includes (Figure 2.14-2) a careful representation of the poloidal and toroidal segmentation of the blanket modules, divertor cassettes, vacuum vessel, TF coil, intercoil structure, and cryostat envelope. A few details (which may have some effect on the results) have been neglected, for example, the cooling channel in the blanket modules and heterogeneity of the vacuum vessel (including the flexible joints). A source routine has been written so that the neutron distribution probability emission is very close to the real one, using a matrix whose elements are proportional to the fusion power.

The 3D model with 20˚ symmetry is the basis of all analyses for ITER. For detailed analyses around the ports, modifications have been introduced in the basic model to insert details relevant to the specific study. For the NB injection port analysis, for instance, the standard model has been expanded to 80˚ to take into account the relevant toroidal asymmetry, and the two tangential neutral beam lines have been modelled in full detail (see 2.14.4).

The following sections range across the whole machine, presenting a summary of the means by which the analyses have been performed, and the main results.

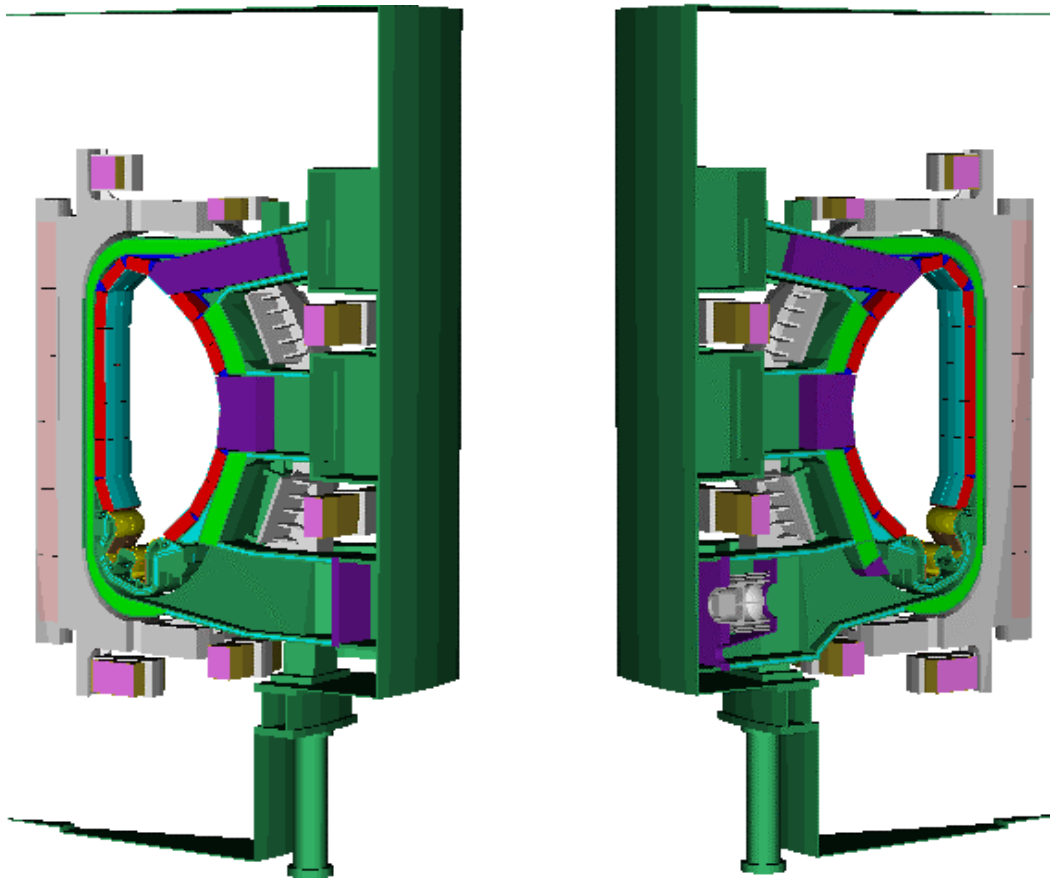

Figure 2.14-2 Outboard View of the ITER Standard Model for the Monte Carlo Calculations showing Different Lower Port Geometry (a) At the Mid-plane of a Divertor RH Port and (b) At the Mid-plane of a Pumping Port

2.14.1 Neutron Wall Loading Distribution on the First Wall

The neutron wall loading (the 14.1 MeV neutron current through the first wall) is usually used by designers as a normalisation factor for a quick estimate of nuclear responses in different parts of the blanket, vacuum vessel and others structural elements of the reactor. The poloidal distribution of the neutron wall loading is shown in Figure 2.14-3 for design scenario I (P_{fus} = 500 MW).

The neutron wall loading, averaged over the inboard part of the first wall (~ 200 m^2), the outboard part (~ 470 m^2) and the divertor surfaces facing the plasma (~ 60 m^2) is ~ 0.55 MW/m^2 at this level of fusion power. The inboard maximum is about 0.59 MW/m^2, and the outboard one ~ 0.78 MW/m^2.

In the case of the hybrid non-inductive operation (design scenario 3, P_{fus} = 400 MW) with a smaller minor radius and outward shifted plasma, the relative peak value at the outboard equatorial plane is slightly (by ~3%) higher than during the reference inductive operation. However, as the fusion power is lower, the average neutron wall loading is 0.44 MW/m^2, and the maximum inboard and outboard neutron wall loads are ~0.46 and ~0.64 MW/m^2 respectively.

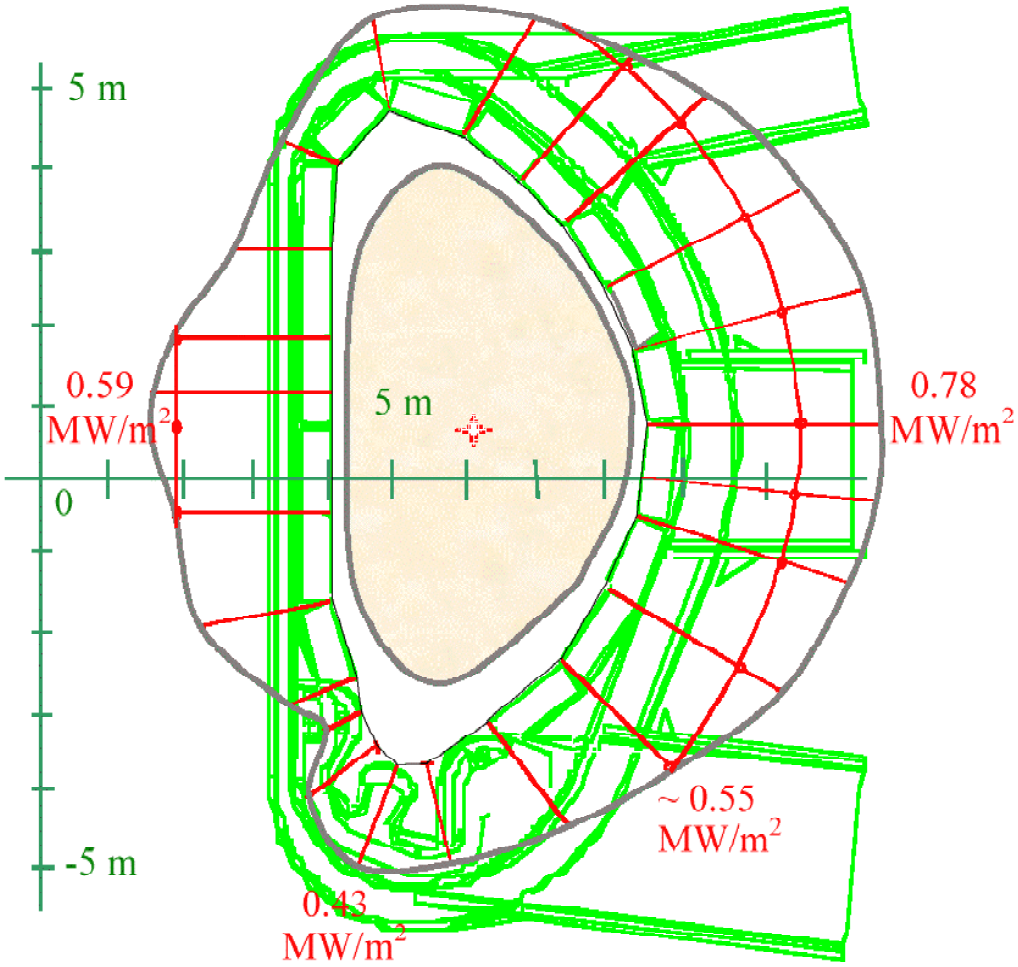

Figure 2.14-3 Poloidal Distribution of the Neutron First Wall Loading (fusion power 500 MW)

2.14.2 Nuclear Power Deposition in the Main Systems

2.14.2.1 Nuclear Energy Multiplication and Total Power

The total power balance in the reactor includes three main components: the fusion power, auxiliary heating, and additional nuclear energy release in the structural components of the reactor.

Under nominal operation, plasma heat radiation (~100 MW) which is ~20% of the fusion power (500 MW), and the auxiliary heating power (P_{heat} = 73 MW), will be deposited in the plasma-facing components of the first wall and the divertor.

As a result of the various reactions of neutrons with materials in the blanket, divertor and vacuum vessel structural elements, the total nuclear energy release from both neutrons and secondary photons is about 20 MeV per incident 14.1 MeV source neutron. Table 2.14-1 shows the neutron energy multiplication factors based on 1D and 3D neutron and gamma transport calculations at a nominal fusion power of 500 MW (i.e. 400 MW of 14 MeV neutrons).

Table 2.14-1 Neutron Energy Multiplication by 1D and 3D Transport Calculation

	1D (MW)	3D (MW)
First Wall and Blanket	584	502
Vacuum Vessel	3.6	7.1
Divertor Cassettes	-	49.4
Total	588	559
Neutron energy multiplication factor	1.47	1.40

The 4% difference between two estimates comes mainly from geometric effects (torus versus cylinder) and nuclear data uncertainty. A factor of 1.44 was used as a reference value to avoid underestimating neutron energy multiplication in the blanket.

A more detailed distribution of nuclear energy deposited in each major system of the machine is indicated in the following paragraphs.

2.14.2.2 Heat Deposition in the Blanket Modules

In the standard 3D model, a careful description of the segmentation of the inner vacuum vessel components has been made. Streaming through the poloidal and toroidal gaps between the blanket modules can have a strong impact on nuclear responses in the components behind. There are 17 modules poloidally. The toroidal segmentation is different in the inboard and outboard part: per 20˚ sector there are 2 outboard modules and 1 inboard.

The overall radial thickness of each blanket module is 45 cm. The radial layout of the module has been modelled with the front beryllium armour (1 cm thick) followed by a 2 cm thick heat sink. The remaining 42 cm is the bulk shield. It has been represented as a homogenised mixture of 84% steel and 16% water.

Other components relevant to the shielding performance have been described in addition. Where used, filler shield elements are inserted in between the blanket modules. Bearing in mind that the blanket coolant manifold is combined with the filler shields, an assumed homogenised material composition of 50% steel and 50% water has been used. The poloidal layout of blanket coolant manifolds has also been included.

The nuclear heating in the blanket system components is summarised in Table 2.14-2

Table 2.14-2 Nuclear Heating in the Blanket Modules (MW)

Inboard first wall	30
Inboard shield module	104
Outboard first wall	59
Outboard shield module	230
Filler wedge elements	7
Manifolds	4
Equatorial port plug	58
Upper port plug	9
Total	502

2.14.2.3 Nuclear Heating in the Divertor Cassette

The divertor cassette has a complex geometry and is made of two kind of components that have different purposes: plasma-facing components for very high heat load removal, and an underlying robust cassette body.

A very detailed model has been made for the divertor. Account has been taken of the heterogeneity and the complicated curvature of the components, the pumping slots and the gap in between the cassette, which affect the streaming through the lower ports. A fine cell subdivision has been made in order to have a detailed poloidal and radial distribution of the nuclear heating. In the 20˚ model one whole cassette and two half cassettes are described to keep the exact symmetry of the system with respect to the port. Table 2.14-3 summarises the heat deposition results.

The analysis refers to an earlier version of the design, whereas the divertor design has since been updated. The update affects mainly the void region under the dome. The cassette itself is not substantially different in thickness and composition. Thus the bulk shielding properties are expected to be the same, as is the average heat production. Some differences are expected in the poloidal distribution of the nuclear responses in the front layers of the plasma-facing components.

Table 2.14-3 Integrated Nuclear Heat Deposition within the Complete Divertor System

Divertor Component	Heating[MW]
Outer Target	19.5
Inner Target	7.2
Dome	14.5
Cassette	13.4
Total	54.6

2.14.2.4 Nuclear Heating in the Vacuum Vessel

The vacuum vessel has been modelled according to its layout by three layers. There are two robust shells 6 cm thick, both made of pure SS 316 L(N) IG. The thickness of the filler region between the two shells varies poloidally and has been described as an homogenised material

mixture which was assumed to be borated steel 60% ($2^{w}/_{o}$ of natural boron) and 40% water. The overall thickness of the vacuum vessel at the equator is 33.7 cm at the inboard and 75 cm at the outboard.

Results of analysis are summarised in Table 2.14-4. The maximum power density on the surface of the inner layer of the vacuum vessel is 0.3 W/cm^3. This value takes into account the enhancement due to both poloidal and toroidal gaps in between the modules.

Table 2.14-4 Nuclear Heat Deposition in the Vacuum Vessel (kW)

Inboard Vacuum Vessel	997
Top Vacuum Vessel	819
Outboard Vacuum Vessel	3260
Bottom Vacuum Vessel	324
Triangular Support Structures for Modules	1296
Port Walls	396
Total	7092

2.14.2.5 Nuclear Heating in the Superconducting Magnets System

Minimal nuclear heat deposition in the superconducting coils is one of the strong design requirements. The analysis shows that nuclear heating of the toroidal and poloidal field coils and intercoil structures is mainly due to the neutron and gamma rays leaking through the bulk shield and the vacuum vessel port extensions, with some contribution from ^{16}N-decay gamma rays emitted by the outlet blanket water coolant, activated by DT neutrons in the first wall region.

The estimated total nuclear heating in the TF coils and intercoil structures from neutrons and prompt gamma rays is ~13 kW, depending on the in-port plug shielding efficiency. The main part (~ 10 kW) is deposited in the inner straight TF coil legs (Figure 2.14-4) in front of which the thickness of the shielding blanket and vacuum vessel is smallest (~79 cm).

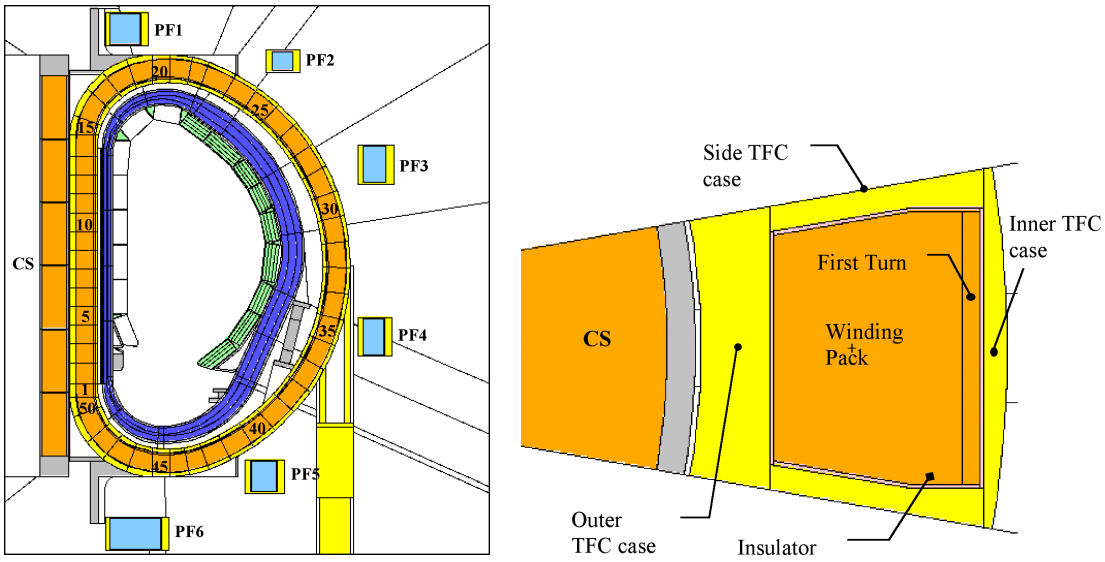

Figure 2.14-4 Superconducting Magnet Model and the Inner TF Coil Leg Cross-section

The specific nuclear heating must also be limited within the local capacity of the He cooling. In the vertical mid-plane of the TF coil legs the local maxima do not exceed ~1 mW/cm^3 and ~0.3 mW/cm^3 in the front steel cases and in the first superconductor layer, respectively. Other magnet nuclear responses, such as the damage to the copper stabiliser, the total insulator dose, and the fast neutron fluence in the first superconductor at the end of the DT operational campaign (at first wall neutron fluence of 0.3 MWa/m^2), are below possible limiting values for these components.

The thickness of the outboard bulk shield is 45 cm (blanket) + ~ 75 cm (vacuum vessel) due to the desire to be able to allow hands-on maintenance within the cryostat two weeks after shutdown. Reducing the shutdown dose rates at the maintenance locations requires a factor of one hundred more attenuation than required to reduce the magnet nuclear heating. Thus the nuclear heating of the outer TF coil parts is much lower than the inner TF coil legs.

The total nuclear energy deposition in six poloidal coils varies between 2 W in the upper PF1 and ~ 250 W in PF5 below the divertor port walls (Figure 2.14-4). The total heating rate in all PF coils is < 0.5 kW. The maximum specific nuclear heating in the poloidal field coils is ~ 0.01 mW/cm^3.

The specific ^{16}N-activity in the water coolant in the upper port is ~1.5 x 10^9 Bq/cm^3 or ~ 0.04 Ci/cm^3. The total ^{16}N-decay gamma ray source in the outlet cooling pipes passing through the upper port walls at the cryostat releases ~ 9 kW. The largest fraction of this is released in water itself, in the pipe walls and in the room temperature components inside the cryostat. About 300 W is distributed between different cryogenic components.

The estimated specific nuclear heating in the poloidal field coils and the coil clamps from ^{16}N-decay photons is low, < 0.03 mW/cm^3.

2.14.2.6 Nuclear Heating in the Cryo-pump

A 3D calculation has been carried out to obtain the heating in the cryo-pump system (Figure 2.14-2b). In the 3D standard model, the cryo-pump port has been partially closed by an extension of the vacuum vessel into the port from above. In such a configuration, the overall heat on the pump assembly is 160 W (for one single pump system). Only a small amount (1.8 W) goes to the 4K array, with an average 0.15 mW/cm^3 volumetric power density. A fine subdivision of the 4K array into 12 cells (3 in the radial direction, and 4 in the axial direction) has shown that the peak value is 30% above the average value. If the partial closure at the port entrance were removed, the heating would be 3 times higher.

2.14.2.7 Thermal Shield Nuclear Heating

The vacuum vessel thermal shield (VVTS) is located between the vacuum vessel and the superconducting magnets and covers both inboard (~ 970 m^2) and outboard surfaces (~ 580 m^2) of the vacuum vessel and the port extensions (~ 1030 m^2). A compressed 80K helium gas flow provided by the cryogenic system will be used for an active cooling of the VVTS inside the cryostat.

The heat loads to the VVTS are nearly all by thermal radiation from the room-temperature components. Additional nuclear heat loads are small and are determined mainly by the secondary gamma ray absorption in the steel VVTS structure. The nuclear energy deposition in gaseous helium in the pipes attached to the thermal shield is insignificant.

The specific nuclear heating ~ 2 x 10^{-4} Wcm^{-3} is expected in the innermost part of the thermal shield (~2.2 cm steel) in front of the straight TF coil legs, where the thickness of the bulk radiation shield including the ~ 45 cm blanket and the 34 cm vacuum vessel is minimal.

The specific nuclear energy deposition in the outer ~ 1.8 cm thermal shield behind the 45 cm blanket and thick 75 cm vacuum vessel is ~ 1.0x 10^{-6} Wcm^{-3}. This is much lower than in the inboard part for reasons stated earlier. The main contributors potentially increasing this value locally are the diagnostic and other in-port structures, such as the NB injector.

Additional nuclear heating from the ^{16}N decay gamma source in the outlet water pipes in the locations of the stiff ring that supports the thermal shield and the VVTS-holders is about ~ 2 x 10^{-6} W/cm^3.

The overall nuclear heat load on the VVTS at the nominal fusion power of 500 MW is ~1.7 kW. The largest fraction (~ 69%) is deposited in the inner part of the thermal shield. A further ~ 27% is deposited in the bottom part just below the inner divertor targets. The remaining 3% is deposited in the vacuum vessel and port coverage (~ 60-90 W), the stiff ring (~ 35-50 W), and the thermal shield holders (~ 3-5 W). The overall nuclear heating of the VVTS appears to be much smaller than other heat loads and does not cause a significant problem for the cryogenic system.

2.14.3 Other Nuclear Responses

2.14.3.1 Damage in the Blanket and Vacuum Vessel Materials

The damage accumulated in materials, and pre-loading relaxation induced by radiation, is an important design constraint for the development of the separate first wall fasteners and blanket attachments.

Principally, the damage cross sections depend on the material and the neutron spectrum. About 90% of the damage production in metals is determined by fast (E > 0.1 MeV) neutrons. For this reason, the damage production rates are not too sensitive to local non-uniformity in the blanket structure. Their spatial distribution through the blanket depth follows the fast neutron flux distribution.

Figure 2.14-5 shows the radial 1D dpa distributions in the bulk shielding blanket from the first wall to the vacuum vessel ignoring possible local peaking due to the neutron streaming through access holes.

The peaking factor for damage at the bolt end surface does not exceed ~1.3 in comparison with the value in the bulk shield at the same distance (~33 cm) from the first wall. The peaking factor, estimated for the 13 mm hole to access the bimetallic stud at the distance ~70 mm from the first wall inner surface, is about ~1.1.

Figure 2.14-5 compares also the damage accumulated in different materials. The damage in titanium alloys resulting from fusion neutron irradiation is ~10-30 % higher than that in steel. The damage in other materials are nearly the same for the same locations in the blanket depth as that in steel: in Inconel by ~5-15 % higher, in Cu-alloy by ~ 0-10 % higher.

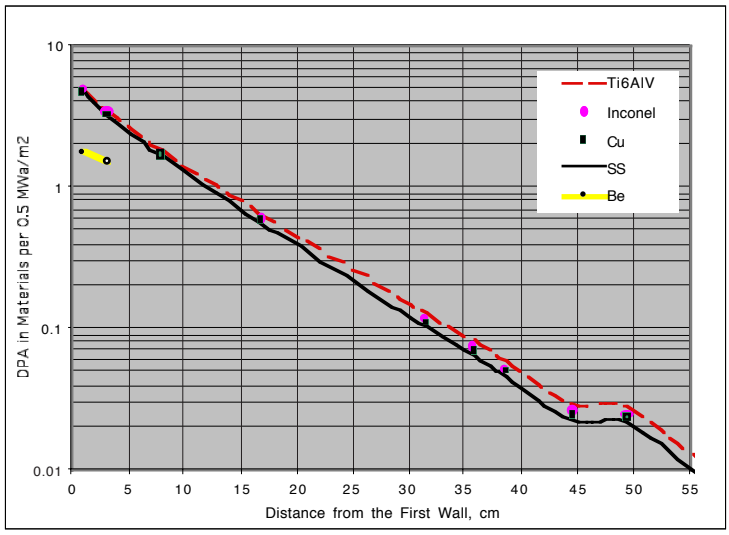

Figure 2.14-5 1D Radial Distributions of Damage in the Blanket and Attachment Materials (Neutron Fluence 0.5 MWa/m^2)

The first wall fastener assemblies (in blanket option A) are located at a distance of ~ 6-15 cm from the inner surface of the plasma chamber and attach the separate first wall panels to the shielding blanket blocks. The damage accumulated in different elements of the first wall

fasteners (such as the threaded bush and bimetallic stud made of Inconel with a copper rod) and calculated in a 2D geometry are shown in Figure 2.14-6.

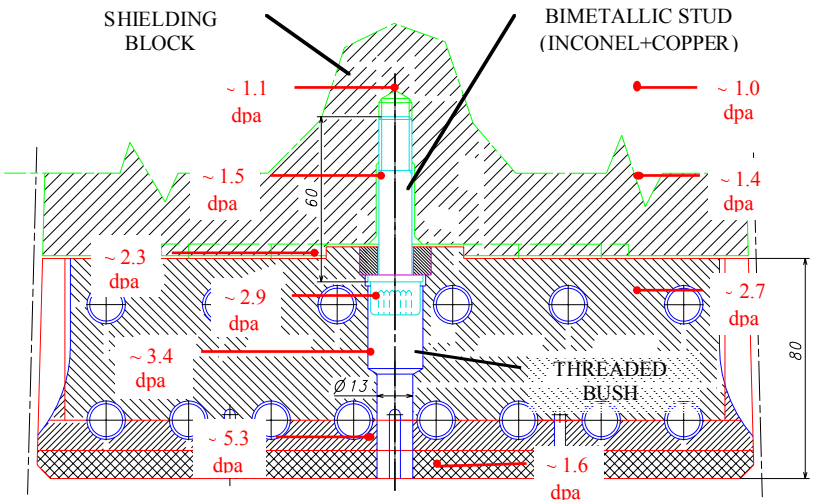

Figure 2.14-6 Damage Expected in Some Elements of the First Wall Fastener (Neutron Fluence 0.5 MWa/m^2)

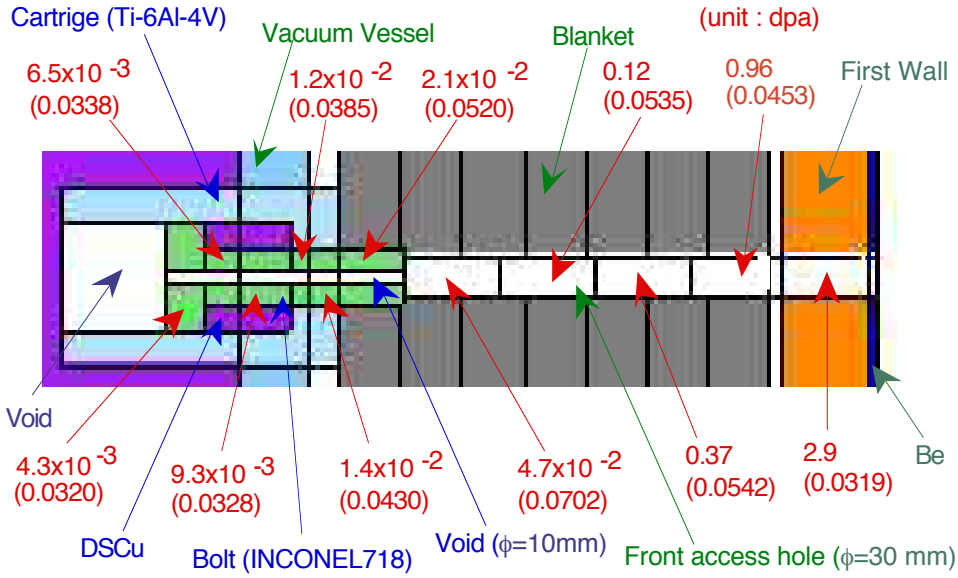

Figure 2.14-7 Damage in Flexible Support Assembly and Surrounding Region (Neutron Fluence 0.5 MWa/m^2)

The maximum damage in the Inconel threaded bush is ~3.4 - 2.9 dpa on its axis. A factor of two lower values are expected in the lower part of the bolt shank.

The maximum damage in the Inconel bolt end of the blanket attachment system (Figure 2.14-7) is ~ 0.02 dpa.

In the vacuum vessel the damage production attenuates exponentially beginning from ~0.02 dpa in the front steel layer. This “dose” is low and will not result in significant property changes of the structural materials.

All the above values are normalised to the maximum local neutron fluence of 0.5 MWa/m^2, which is the local maximum expected in the outboard first wall at the end of the DT-operation campaign with a nominal average neutron fluence of 0.3 MWa/m^2. The dpa-values and the spatial distributions presented may be used for scaling to other local fluence and bolt positions.

2.14.3.2 He Production

He production in stainless steel is an important parameter for those parts of the vacuum vessel and blanket that need to be rewelded during maintenance or replacement. He-production rates have been estimated for two critical locations where the capability of re-welding is required: the front layer of the outboard vacuum vessel, and the cooling branch pipes in the blanket modules. An average first wall neutron fluence of 0.3 MWa/m^2 is assumed in this analysis.

By 1D calculation, the He-production is estimated to be ~ 0.13 appm at the front part of the vessel, which is made of the SS316L(N)-IG with low boron content (~ 10 wppm). About six times higher values are expected behind gaps (2 cm) between blanket modules, giving ~ 0.8 appm as a local peak value, which is below the limit of 1 appm.

Figure 2.14-8 shows the helium production in the front access hole and branch pipe of the blanket module obtained with the 3D model for the reference structural material, SS316L(N)-IG, which has low boron content (~ 10 wppm). Boron in the steel makes a large contribution to helium production through its large $B^{10}(n,\alpha)$ reaction cross section in the region where thermal neutron flux dominates. The helium production at the welded part of the branch pipe is estimated to be 1.2 dpa.

The design limit of helium production for a re-welded part is 1 dpa for thicker welds. For thinner welds, like that of the branch pipe, the limiting value is now under investigation, but there are indications that higher values can be tolerated. If it is the same as that for thicker welding, branch pipe re-welding could be a serious problem. If higher dpa values are acceptable (for example 3 dpa), re-welding of the branch pipe would be possible.

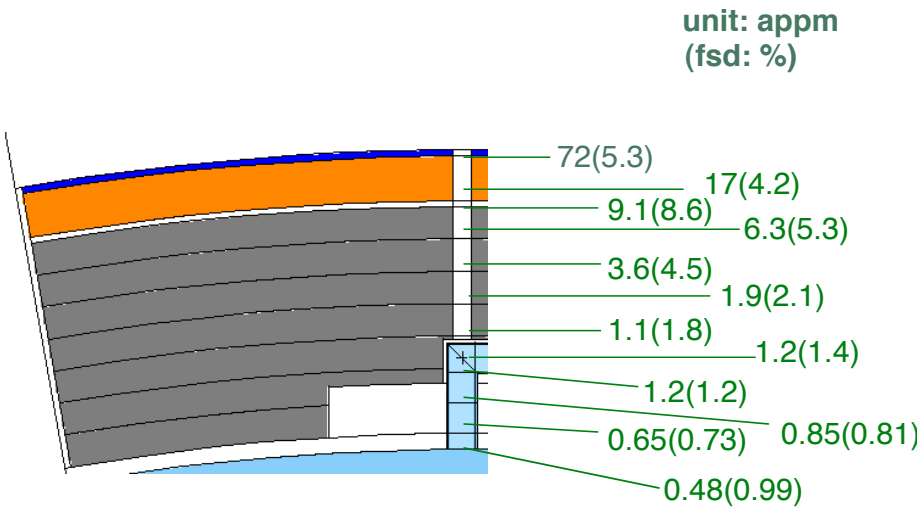

Fig.2.14-8 Helium Production Distribution in SS with 10 wppm B Along the Front Access Hole and the Cooling Water Branch Pipe (Neutron Fluence: 0.3 MWa/m^2)

2.14.4 Dose Rate

In the space inside the cryostat, limited personnel access is envisaged for repair of unexpected defects. At the port locations where personnel should have access for maintenance, the dose rate should be less than 100 μSv/h about 2 weeks (~ 10^6 s) after shutdown. Dose rate behind the bioshield, where more frequent and longer access is necessary, is required to be less than 10 μSv/h.

In order to satisfy these limits, the design relies on the performance of the bulk shielding provided by the outboard blanket and vacuum vessel as well as the bioshield. These alone would bring the dose rate well below the above limits. However the dose rate is dominated, both inside and outside the bioshield, by the presence of numerous penetrations (including NB ports) which are necessary to provide various access routes to the plasma and which affect the shielding capability of both vacuum vessel and bioshield.

The required shielding of these penetrations has been subject to exhaustive dose rate analyses which have been and will be carried out in increasing detail. The main results so far are reported here.

During machine operation, the dose rate around the torus is too high for personnel access. Figure 2.14-9 shows the operation dose rate distribution obtained by a 1D calculation. Although the dose rate behind the bio-shield is shown to be low enough (~1 μSv/h) for personnel access, in practice it is impossible to access there because of radiation streaming through the many penetrations in the bio-shield. (Such access during operation will of course anyway be ruled out by the presence of strongly varying magnetic fields.)

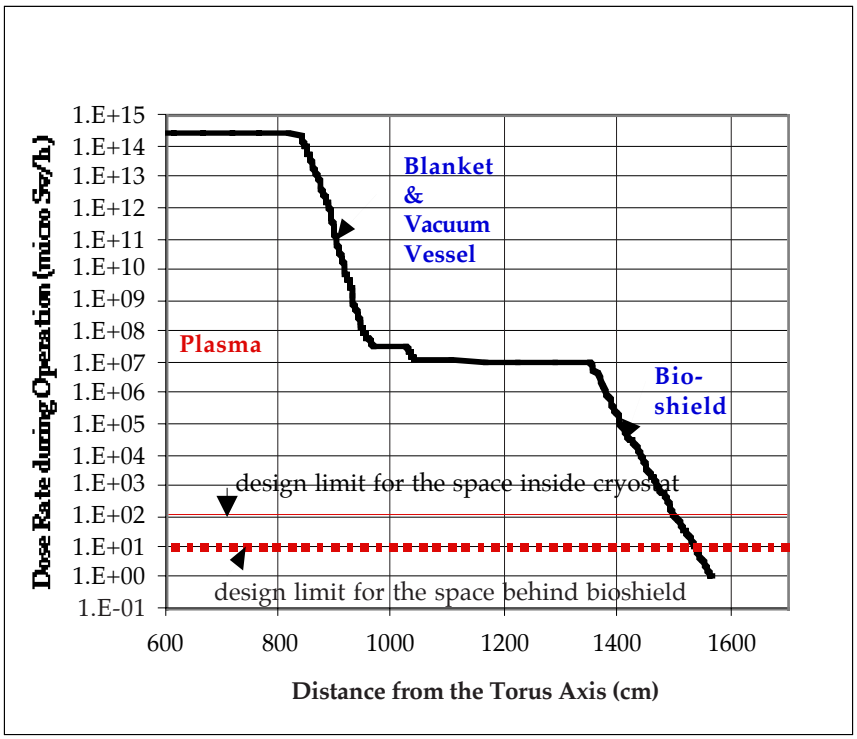

Figure 2.14-9 Dose Rate Distribution During Operation

2.14.4.1 Shutdown Dose Rate Outside Maintenance Port

There are four ports for blanket module maintenance purposes (3, 12, 8 and 17). During operation, plugs are inserted in all of those ports. Two of them have limiters with alignment adjusting mechanisms in their plug. The other two contain diagnostics.

Figures 2.14-10 and -11 show a 3D model of the maintenance port with the limiter. Calculated dose rates due to decay gamma rays around the port 10^6 s after shutdown are shown in Figures 2.14-12(a) and (b). The dose rate levels are generally low in comparison with the design target of 100 μSv/h. This means that there will be no significant problem caused by these ports for personnel access for the preparatory work involved in the removal or re-installation of those plugs.

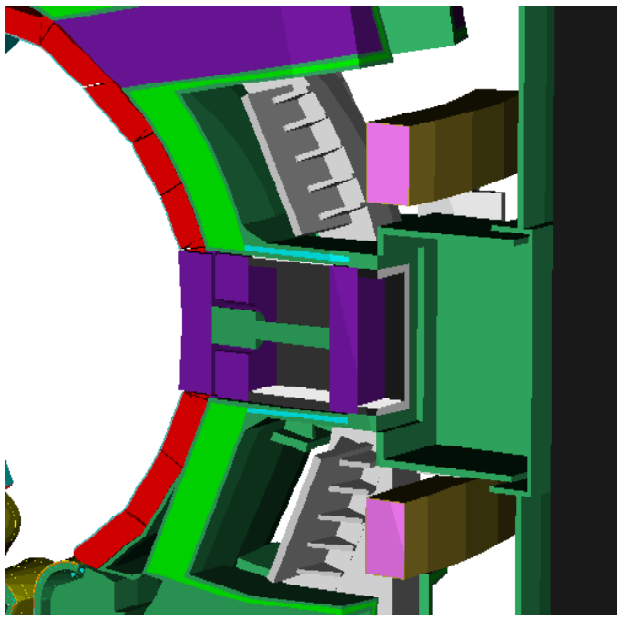

Figure 2.14-10
Limiter Port 3D MCNP Model

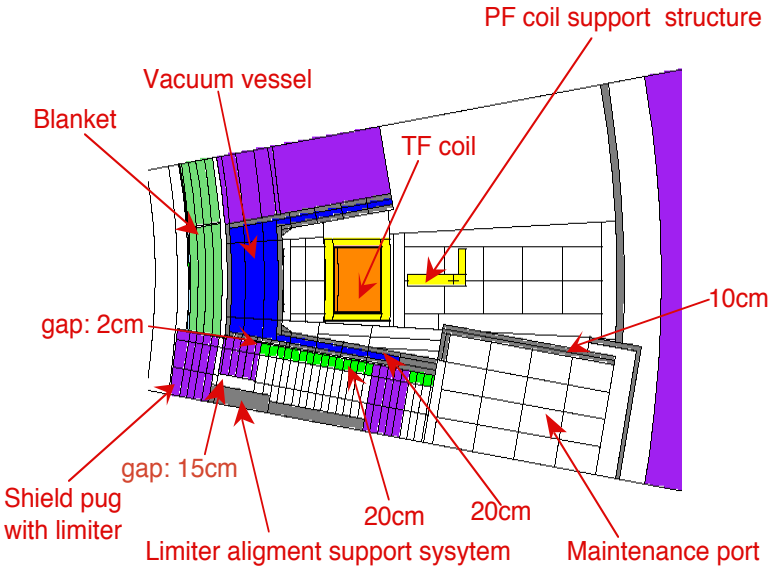

Figure 2.14-11
Horizontal Cross- section of the Limiter Port 3D Model

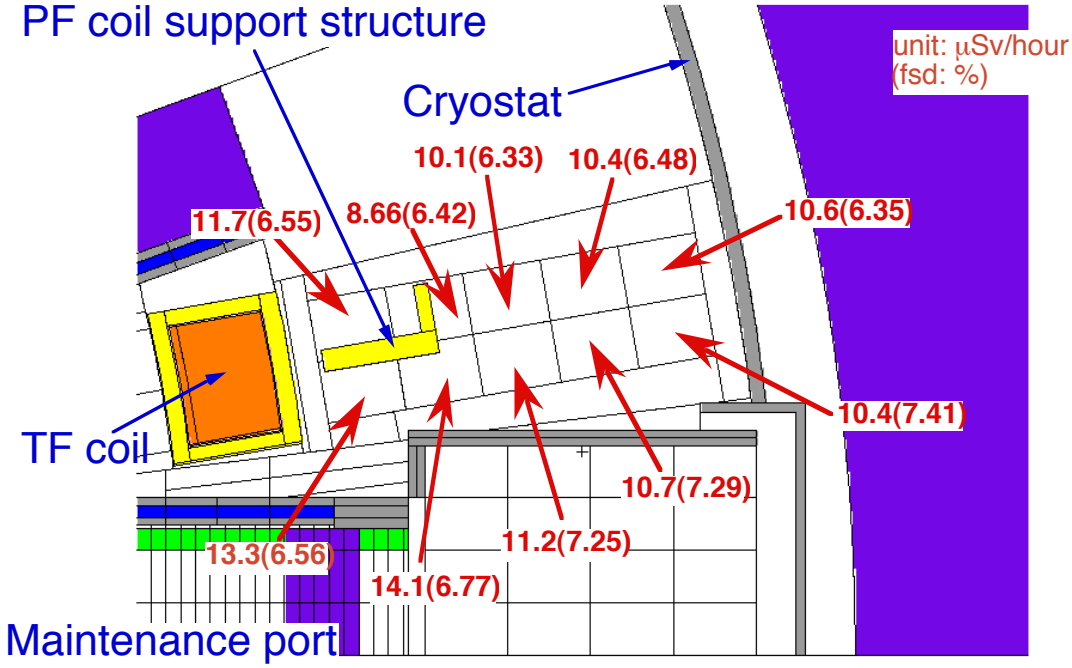

Figure 2.14-12(a) Shutdown Dose Rate Distribution (after 10^6 s)
Outside the Limiter Port
(for average neutron fluence of 0.3 Mwam^{-2})

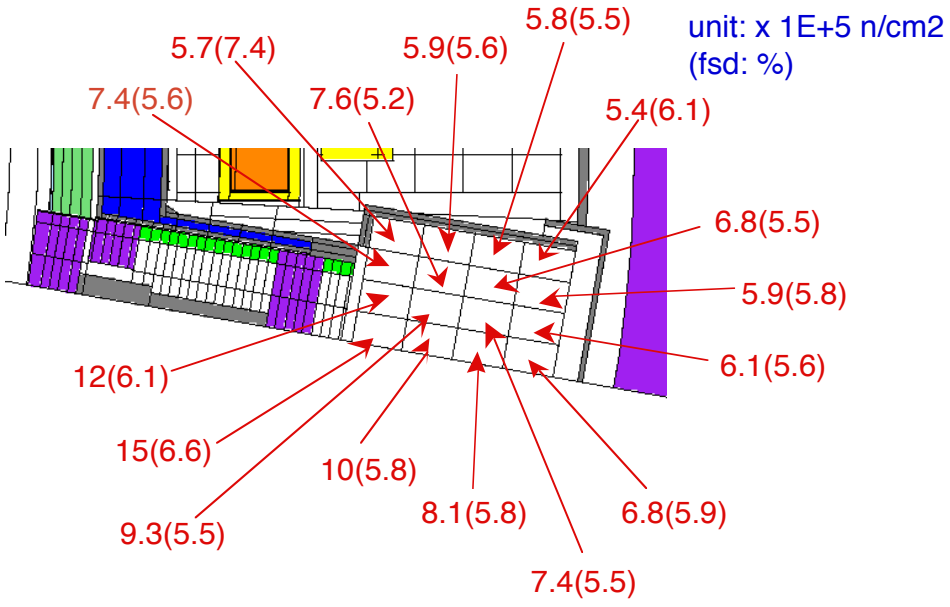

Figure 2.14-12(b) Shutdown Dose Rate Distribution (after 10^6 s)
Inside the Limiter Port
(for average neutron fluence of 0.3 Mwam^{-2})

2.14.4.2 Shutdown Dose Rate Outside NB Injection Port

Equatorial ports 4 and 5 are used for NB injection for plasma heating. A diagnostic NB injector is also installed on port 4. Since the NB lines in these ports are completely open, NB injection ports are a major concern for neutron streaming from the plasma, and a careful shielding design is required.

Previous calculation has shown that a total wall shielding thickness of about 60 cm is enough to provide the required attenuation. However the present design, in order to provide a suitable NB current drive capacity as well as additional strength for the inter-coil structure, provides a local minimum shielding thickness around the NB duct of only about 45 cm. This causes some unacceptable dose rates in the neighbourhood of the duct itself. However this problem is under additional detailed investigation, and it is expected to be solved by providing additional local shielding around the weak point of the port wall.

Figures 2.14-13 and -14 show the 3D Monte Carlo calculation model for the NB injection ports. Calculated dose rates due to decay gamma rays around the port 10^6 s after shutdown are shown in Figure 2.14-15. They are higher than the design limit of 100 μSv/h in some positions and suggest the necessity to avoid access of personnel at these positions (if shielding improvements turn out to be too difficult to achieve).

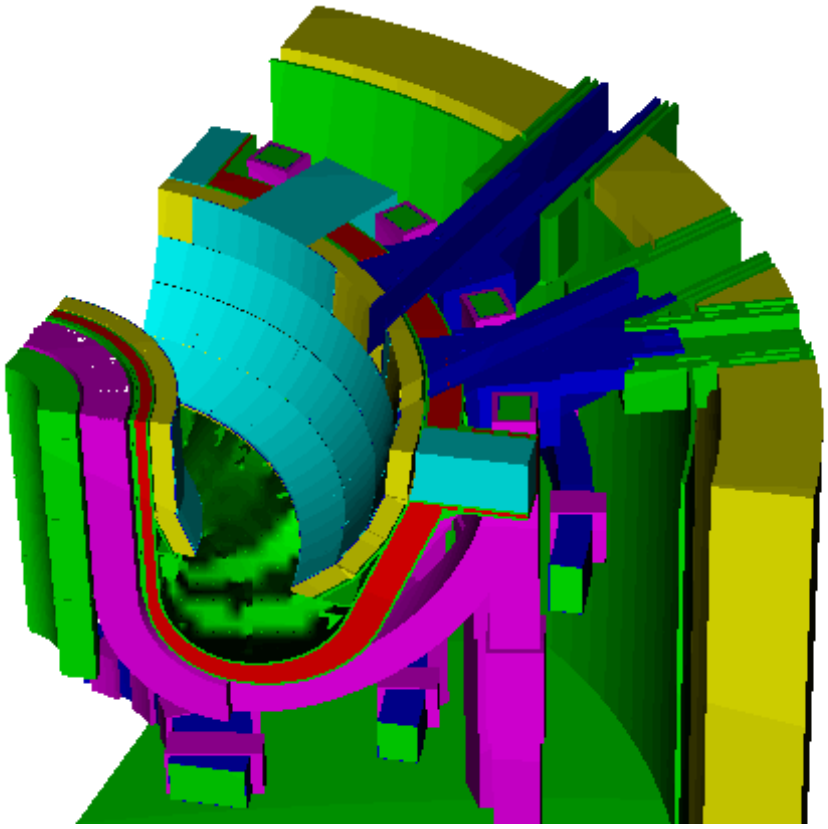

Figure 2.14-13 NB Injection 3D MCNP Model

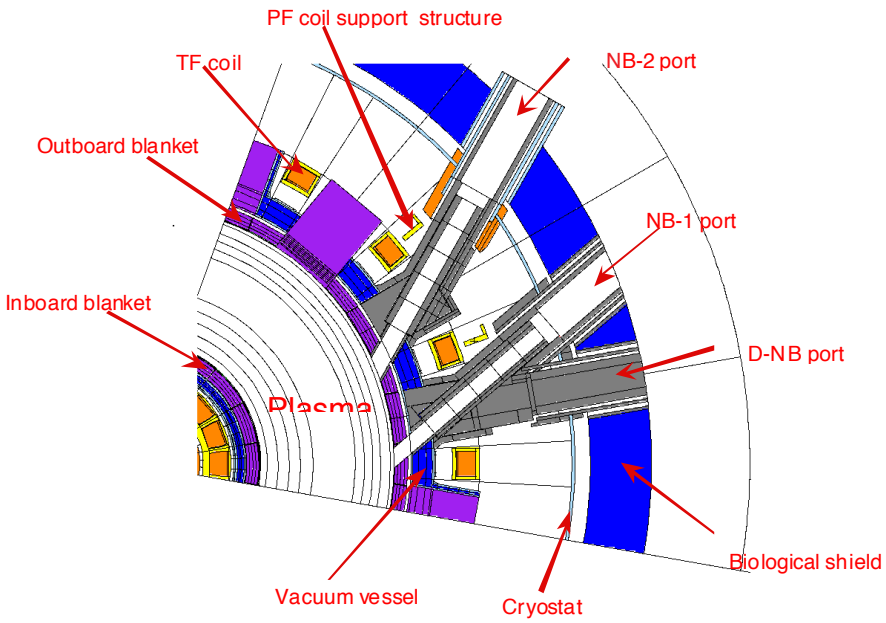

Figure 2.14-14 Horizontal Cross-section of the NBI 3D Model

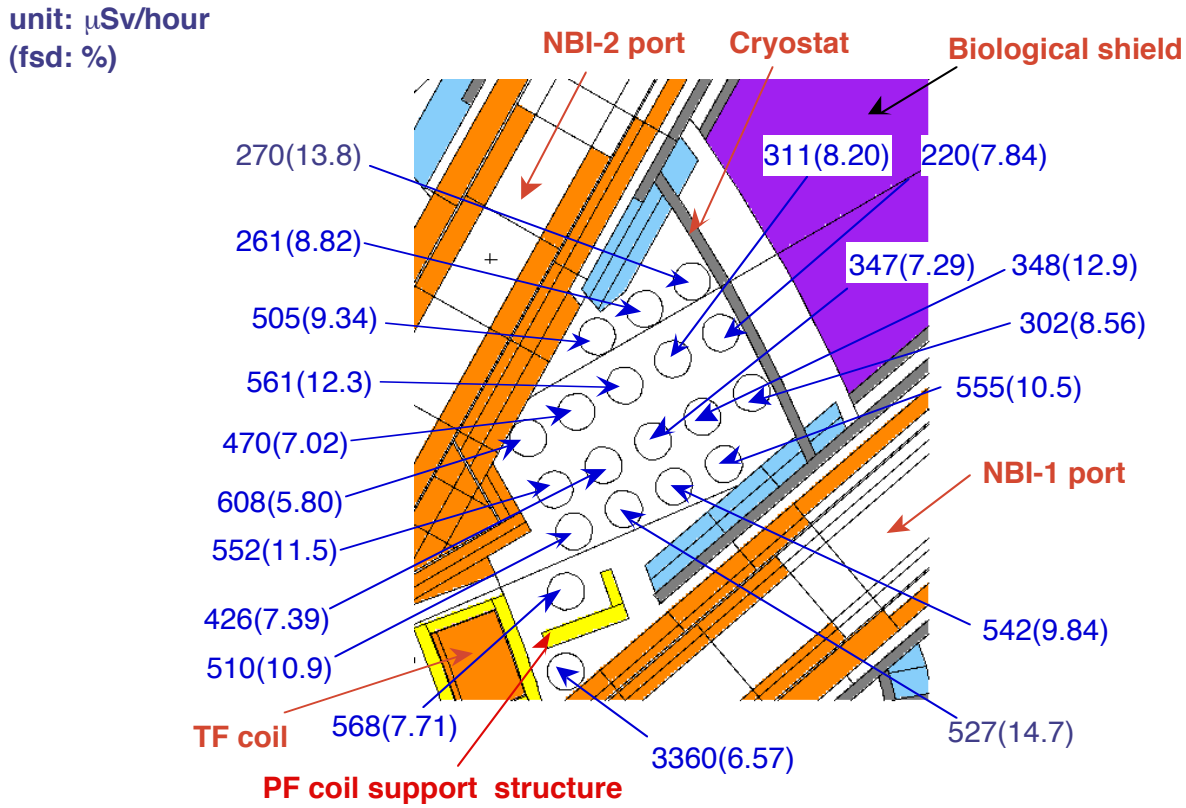

Figure 2.14-15 Shutdown Dose Rate Distribution (10^6 s After Shutdown) Around the NBI Port (for average neutron fluence of 0.3 Mwam^{-2})

2.14.4.3 Divertor Port

The dose rate level around the divertor ports is a problematic issue, mainly as a consequence of the need to have high gas conductance between the divertor plasma region and the cryopump. Dose rates have been calculated using a new methodology, the so-called "one-step" method.

Different shielding configurations have been considered to see the impact on the response functions. The reference port configuration (for all ports except the remote handling ports) foresees (Figure 2.14-16) an extension of the vacuum vessel into the port down to the rail supporting the divertor cassette ("port closed"). This additional shield reduces the poloidal mouth entrance of the port itself, without great impedance increase to the pumps. The in-vessel viewing system (IVV) channel has been considered void in some cases (IVVC open) or closed by a plug (IVVC closed). Values are in Table 2.14-5. In the table not all the figures are completed for tallying region number 5, but nevertheless it can be seen that a viable solution close to cryostat can be achieved when all the penetrations are reduced. Borated steel added to wall ports can help, removing low energy neutrons from the system.

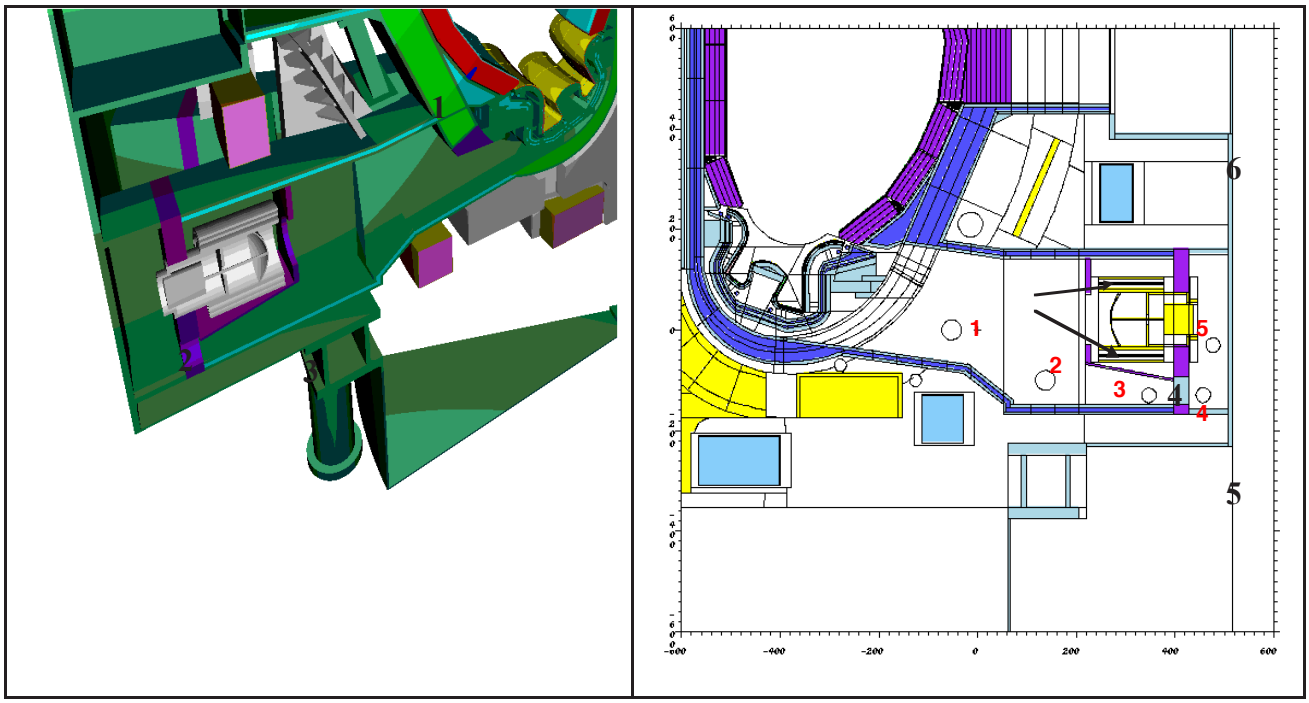

Figure 2.14-16 Section of the Model Cryopump (section AA, left), and Toroidal Section at the Level of the Divertor Region (section BB, right)

Table 2.14-5 Dose Rate Values [μSv/h] Calculated in 5 Positions Inside the CP Port for Different Shielding Configurations.
The last column refers to a configuration with all the penetrations open but with borated steel in the walls covering the walls of the port.

Location in Figure 2.14-16	Open port IVVC open	Open port IVVC closed	Closed port IVVC open	Closed port IVVC closed	Open port IVVC open, borated steel in the walls
1	$7.74\ 10^4$	$8.11\ 10^4$	$6.12\ 10^4$	$5.82\ 10^4$	$7.73\ 10^4$
2	$2.05\ 10^4$	$3.37\ 10^4$	$9.43\ 10^3$	$1.14\ 10^4$	$1.65\ 10^4$
3	$1.33\ 10^4$	$1.50\ 10^4$	$7.11\ 10^3$	$8.73\ 10^3$	$8.60\ 10^3$
4	$3.21\ 10^3$	$6.78\ 10^2$	$2.77\ 10^3$	$2.27\ 10^2$	$1.07\ 10^3$
5	$9.01\ 10^2$	$7.13\ 10^2$			

2.14.4.4 Shutdown Dose Rate Outside RF H & CD Port

The IC H & CD launcher plug is installed in equatorial ports 13 and 15. While this plug provides rather good bulk shielding, it has been necessary to verify the adequacy of the dogleg in the gap between plug and port wall to avoid excessive neutron streaming. 3D pictures of the model are shown in Figures 2.14-17 and -18.

The calculated dose rates due to decay gamma rays around the port, 10^6 s after shutdown are shown in Figure 2.14-19. It can be concluded that the shutdown dose rates outside the port are generally below the target of 100 μSv/h.

The EC H&CD launcher plug is installed on the equatorial port 14. Calculated dose rates due to decay gamma rays around the port are similar to those for the IC H&CD port. The EC H&CD system also uses upper ports. Calculations are underway to assess the dose rates.

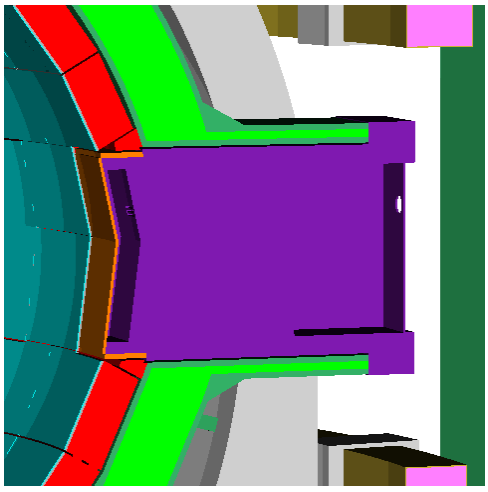

Figure 2.14-17
IC H&CD Port 3D MCNP Model

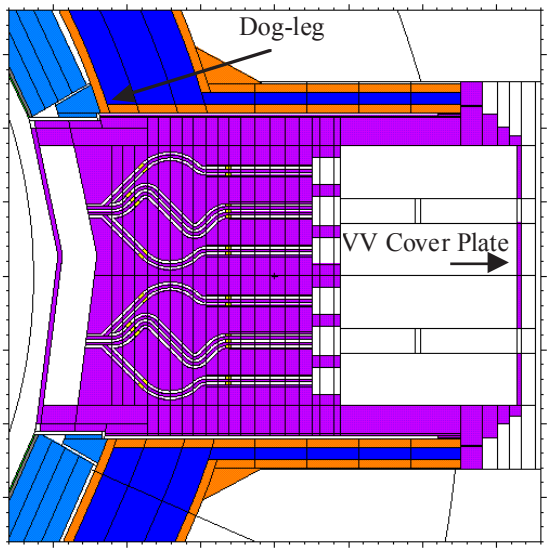

Figure 2.14-18
IC H&CD Port Vertical Cross-section

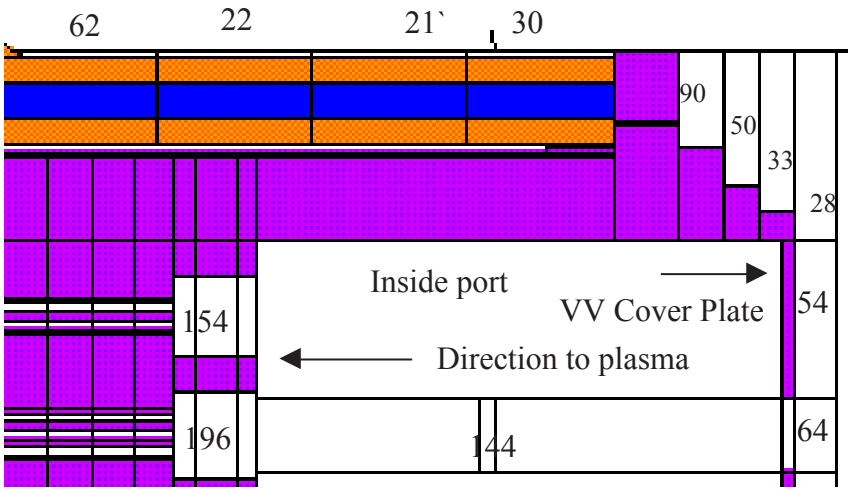

Figure 2.14-19 Dose Rates Around IC H&CD Port in µSv/h 10^6 s After Shutdown

2.14.4.5 Diagnostic Ports

A number of diagnostic plug layouts have been and will be analysed to cover the requirements of all diagnostic systems[1]. Some of them do not alter the bulk shielding efficiency. In other cases, when diagnostic access apertures affect the effective blanket/vacuum vessel shielding capability, this is recovered by labyrinthine access penetrations in special steel/water shielding plugs.

Representative configurations are shown in this section. For example, the 3D model of the edge Thomson scattering system in the upper port is shown in Figure 2.14-20.

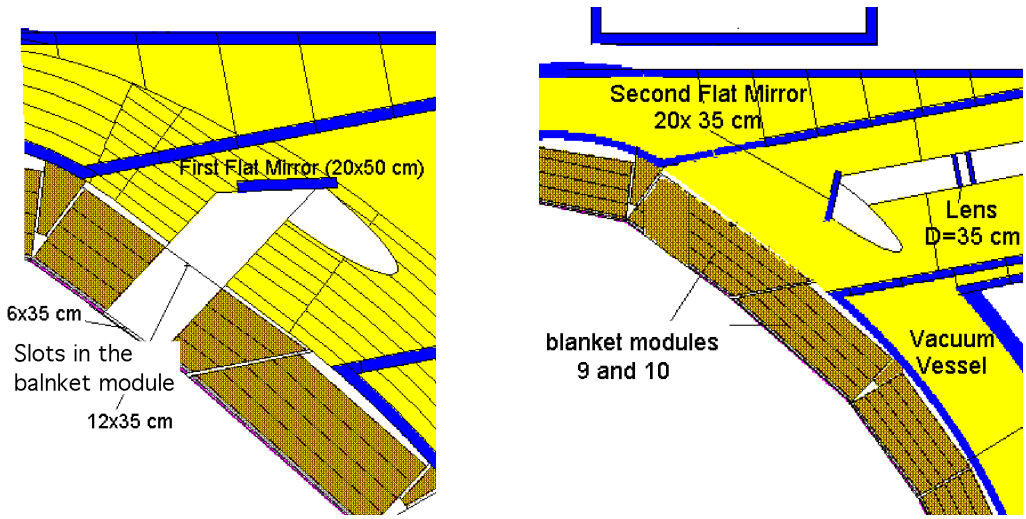

Figure 2.14-20 3D Model of the Edge Thomson Scattering System in the Upper Port

[1] C. I. Walker, S. Yamamoto, A. Costley, L. de Kock, K. Ebisawa, P. Edmonds, G. Janeschitz, V. Khripunov, E. Martin, G. Vayakis, "Nuclear Aspects of Diagnostics for RTO/RC-ITER", Proceedings of the 5th International Symposium on Fusion Nuclear Technology (ISFNT-5), 19-24 September 1999, Rome, Italy.

The first mirror of the system is located ~1 m behind the first wall in order to reduce the radiation loads and neutron streaming to the cover plate. The calculated specific nuclear heating here does not exceed ~ 20 mW/cm^3, the fast neutron flux ~ 5.6 x 10^{11} cm^{-2}s^{-1} and total neutron flux ~ 1.2 x 10^{12} cm^{-2}s^{-1}. This is by 2-3 orders of magnitude lower than at the first wall. Thus simple water-cooled, stainless steel mirrors can be used here.

Due to the "dog-leg" configuration, the neutron and photon fluxes attenuate along the channel by 5 orders of magnitude at the outlet lens. This does not change the average flux level inside the cryostat from that expected with a solid plug. Nuclear heat loads on the nearest cryogenic systems will not be disturbed by this diagnostic plug.

Another representative example is the combined LIDAR and polarimetry diagnostic system in the equatorial port (Figure 2.14-21) where the resulting streaming through the large channel (diameter 18-22 cm) might be a matter of concern.

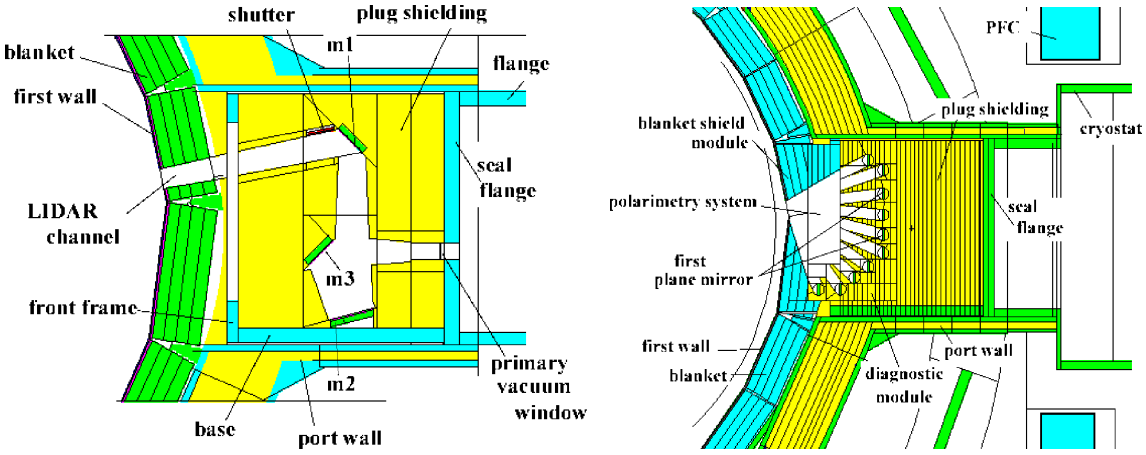

Figure 2.14-21 LIDAR and Polarimetry Diagnostic System Models for Nuclear Analysis

This streaming has in fact been evaluated to be acceptable adding only ~30% to the nearest PF3 and PF4 nuclear heating and to the neighbouring TF coil heating. Other limits for the magnet structure are also not exceeded.

The specific nuclear heating in the optical elements of the polarimetry system, which essentially consists of two fan-shaped vertical rows of 14 cm diameter angled tubes passing through a 23 x 14 cm aperture at the first wall, decreases from 50-150 mW/cm^3 in the mirrors to 1-7 μW/cm^3 in the quartz windows. The total neutron flux at the VV cover plate ("seal flange") surface is ~ 0.15-1 x 10^8 cm^{-2}s^{-1}. The residual dose rate between the seal flange and the cryostat due to neutron streaming throughout the diagnostic structure is below 80 μSv/h two weeks after shutdown. The total nuclear heat deposition in the diagnostic plug is ~ 2.9 MW which is a typical value for the blanket modules.

2.14.4.6 Dose Rate Outside Bioshield

2.14.4.6.1 Dose Rates from Irradiated Water Coolant Behind the Biological Shield

The outlet water coolant activated in the ITER plasma-facing regions is a source of high energy (~6 or 7 MeV) ^{16}N-decay photons and 0.9 MeV ^{17}N-decay neutrons ~ 1 minute after irradiation.

Operational dose rates at the outlet "hot" pipes outside the biological shield will be caused mainly by ^{16}N-decay photons. The estimated ^{16}N-specific activity in water here is ~1.3 x 10^9 Bq/cm^3. The corresponding absorbed dose rate is ~300 Gy/h at the pipe surface and ~5 Gy/h on the distance ~1 m from the pipe. Personnel access during operation in the outlet water pipe room, even behind the biological shield, is not allowed.

The ^{17}N-activity in water coolant is by 3 orders of magnitude lower than the ^{16}N-activity. The maximum expected residual dose rate initiated by the ^{17}N-decay neutrons at a steel pipe surface (0.10 wt% Co) is ~ 1.5 - 4 μSv/h two weeks after shut down, at the end of the first and the second decade of the DT operation campaign, respectively. This is several times lower than the expected corrosion product effects. The residual dose rates decrease rapidly, by 1 - 2 orders of magnitude at a distance ~ 0.5 - 1 m from the pipes.

2.14.4.6.2 Effect of Penetrations in Bio-shield

As mentioned previously, the bioshield has a thickness of 2 m and provides ~ 8 orders of magnitude attenuation during operation without considering penetrations. However, outside operation phases, assuming that the required 100 μSv/h is achieved in the cryostat, the bioshield only needs to produce one order of magnitude to reduce the dose rate to 10 μSv/h 10^6 s (~ 11 days) after shutdown. For places where more quick access (less than one day after shutdown) is required, two orders of magnitude reduction may be necessary, since dose rate at the shutdown is higher by ~ an order of magnitude than that 10^6 s after shutdown. There therefore seems to be plenty of margin in the bioshield to accommodate access after shutdown in the region outside it, providing penetration effects do not dominate.

Many penetrations are necessary to route hydraulic, electrical guides, etc. in the bioshield. Preliminary estimation shows that a hole with 50 cm radius provides an order of magnitude attenuation and that with 15 cm two orders of magnitudes. Most of the holes in the bio-shield have a radius less than 15 cm, for example the IC H&CD transmission line (R < 10 cm) and the EC H&CD waveguides (R < 10 cm).

In some cases, the size of penetration exceeds the above 15 cm or even 50 cm radius. As a typical case, penetrations for blanket cooling pipes have a 64 cm radius, including 36 cooling pipes. Proper shielding material should therefore be provided in the hole in order to give the required attenuation.

The above discussion assumes that the effect of concrete activation will be eliminated where it is necessary. This effect is important only when quick personnel access is required. Adding small amount of boron in the concrete, for example, will eliminate this effect.

2.14.5 The DD Phase Nuclear Performance

During the D phase preceding the DT phase, the DD (2.45 MeV) neutron yield ~ 3.5 x 10^{18} n/s will be accompanied by considerable tritium production. Assuming conservatively that all the generated tritium will react with the available deuterium, then a DT (14.1 MeV) neutron yield of ~ 3.5 x 10^{18} n/s is expected, leading to conditions which cannot be ignored from the radiation safety and maintenance standpoints.

The main nuclear characteristics of ITER, evaluated[1] for the two-component (2.45 MeV and 14.1 MeV) neutron source experienced in the proposed D operation phase, may be as high as: a high energy (> 0.1 MeV) neutron flux of ~ 2 - 4 x 10^{12} n/cm^{2}s, a neutron wall loading ~ 0.003 - 0.01 MW/m^2, and a first wall neutron fluence ~ 0.0006 - 0.002 MWa/m^2. These and other nuclear responses, are ~30 - 300 times lower than the values for the nominal DT-operation, depending on the tritium burn-up and gas removal (pumping) capability.

Taking into account the DD and DT neutron energy multiplication in the blanket (~ 4.2 and ~ 1.4 for the DD and DT neutrons), the secondary photon energy release and also the charged particle energy deposited in the plasma facing structures, a total nuclear power ~ 12 - 23 MW is estimated. (Auxiliary heating power of ~ 50 - 100 MW was not included in this value.)

Under this operation, the plasma chamber activation is three orders of magnitude lower than expected after the DT phase. Nevertheless, personnel access to the plasma facing structures, such as the first wall and the divertor targets, will be restricted already after only a few tens of seconds of “full scale” DD operations. At the same time the radiation conditions outside the machine behind the bulk radiation shield will allow for hands-on-maintenance almost immediately after reactor shutdown.

Thus, the foreseen DD operation phase can be treated as an initial nuclear phase, and for this reason tritium production and removal, active cooling during the DD plasma burn and after shut down, as well as remote handling of the in-vessel components, neutron diagnostics, and many ancillary systems, will need to be available from the very beginning of the DD phase.

2.14.6 Conclusions

A fairly sophisticated nuclear analysis has been performed on ITER by means of the most detailed models and the best assessed nuclear data and codes. This has mainly been focused on:

- global and local nuclear heating for the component design;
- global and local shielding optimization;
- radiation conditions in different plasma heating and diagnostic systems;
- radiation conditions in and around the divertor port;
- activation of materials including the cooling water (see 5).

In the area of nuclear heating in the superconducting magnet system, the principal source is caused from neutrons and promptly emitted gamma rays. The total amount of TF coil heating

[1] V. Khripunov, "Nuclear Performance of the D-D Phase of ITER", Proceeding of the 5th International Symposium on Fusion Nuclear Technology (ISNFT-5), 19-24 September 1999, Rome, Italy

has been computed to be less than 13 kW including the effect of shielding penetrations such as VV ports. The main contribution to this heating is localized in the inner leg of the magnet where the shielding has been optimized so as to reduce the overall radial build of the reactor. The volumetric local nuclear heating as well as the radiation damage to the copper and insulation materials of the magnet has been computed to be far below the respective limits.

In the light of the sufficiently thick blanket, helium production in the regions of required re-weldability in the vacuum vessel has also been evaluated to be within limits at the end of life.

Another important area of consideration, in view of its consequences for hands-on maintenance and unscheduled repairs, has been the dose rate for maintenance inside and outside the cryostat shell. In fact, neutrons do activate the reactor components during operation but, as a consequence of the presence of sufficient shielding, in most of the places the residual dose rate two weeks after shutdown is the level of the target for personnel access (100 μSv/h). Some local improvements have been identified to be required, in particular in the area around the NB system, and the shielding of the torus cryopumps, but no fundamental problems are foreseen.

In summary, the ITER nuclear response has been evaluated to be sound in all respects including magnet nuclear heating, radiation damage, activation, vessel helium production, etc. Further work in this area is needed to verify the local response of components still to be developed in full detail, such as port plugs and diagnostics systems.

2.15 Tokamak Seismic Analysis

2.15.1 Introduction

Even if the ground peak acceleration is a small fraction of gravity (e.g. 0.2 g for SL-2) the effects of earthquakes on ITER are significant and have to be carefully taken into account in its design. A seismic event is in fact, in many cases, the most demanding loading condition, in particular for the interface structures (e.g. supports) which must be sized for high strength, and often also for high stiffness.

The two main reasons why these events are of so much importance are as follows.

1. Seismic motion has a relatively broadband spectral content which encompasses the typical natural frequencies of structures (e.g. 1 to 10 Hz) with therefore spectral amplifications likely to take place. Spectral amplification factors are a function of both damping and natural frequency of the structures and are established by enveloping charts, called design response spectra (see paragraph 2.15.2.1). The typical value of acceleration amplification factors (for structures with natural frequency between 1.5 and 10 Hz) is about 3.
2. Structures are usually weaker when loaded by horizontal inertial loads, even when these are a small fraction of gravity.

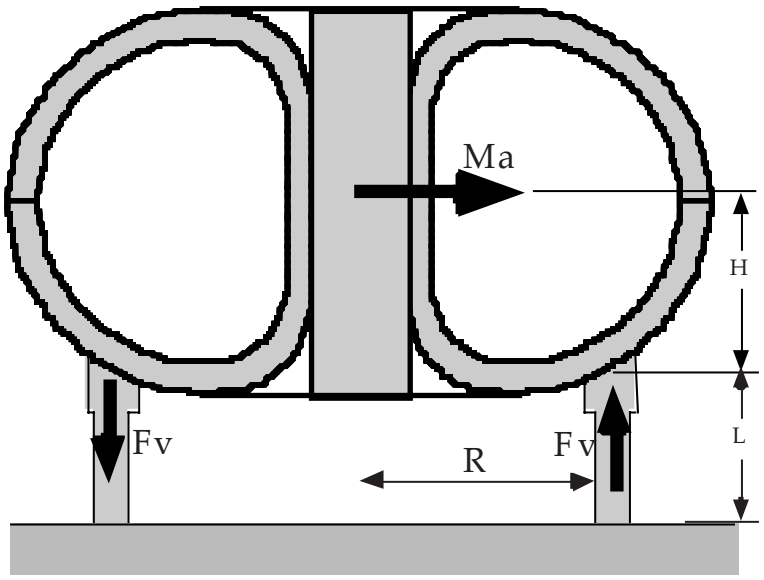

Figure 2.15.1-1

Example of Vertical Reaction Loads at the Main Gravity Supports when the Tokamak is Subject to a Horizontal Seismic Acceleration

The response of the tokamak system when loaded by a vertical seismic excitation is fairly easy to consider as a repetitive increase/reduction of the normal gravity load.

However, under horizontal excitations, the ITER global tokamak structure exhibits oscillatory modes which involve horizontal shearing as well as rocking motions around a horizontal axis perpendicular to the direction of the initial excitation.

The rocking motion is determined by the vertical distance from the basement to the centre of gravity of the system. For example, Figure 2.15.1-1 shows a schematic of the magnet system and the main machine gravity supports. The moment originated by rocking mode is reacted by the axial tension/compression of the gravity supports. Since the gravity supports must be radially flexible to accommodate thermal contractions of the magnet, they are able to react a horizontal force only on a line orthogonal to their azimuthal position.

In fact, the rationale for the use of reacting members between VV and magnet, roughly positioned vertically in the plane of the centre of gravity of the VV, is to minimise the relative displacements between VV and Magnet system during both seismic events and VDE's.

The ITER reference design considers seismic ground motion up to 0.2 g. The design, however, is such that if ITER is sited in a region with higher seismicity, the pit can be seismically isolated. The use of horizontal seismic isolators would effectively lower the peak acceleration, lower the frequency of seismic oscillations, and increase the motion and deflection of the tokamak and other isolated components relative to the non-isolated structures and the earth. The isolation schemes that would be considered utilise horizontal isolation pads made of alternating layers of steel plate and rubber. The tokamak and tritium buildings would be isolated to minimise the services that must cross the gap between isolated and non-isolated buildings. All services and plant systems which cross this gap would be designed to accept the consequences of relative motion of this gap, either by flexing or by failure and repair for non-safety-related items.

During the course of the EDA, several seismic analyses have been performed on the various design evolutions in order to always maintain and often improve the support scheme and to guarantee the required structural performance both from the displacements and stresses points of view.

The analysis summarised in this section has been performed by using the response spectrum method which has been chosen owing to its simplicity in comparison with a full dynamic analysis (time history method). According to this method a response spectrum at the tokamak anchor points, called the floor response spectrum (FRS), is utilised. It has been a priori assumed that the FRS is the same at all the anchor points of the machine, namely the basement, the cryostat skirt base, and the pit at the cryostat cover lid elevation.

The specific effect of soil-structure-interaction (SSI) is therefore neglected in this analysis. An SSI analysis is site specific as it strongly depends on geological data with its effects being of particular importance, together with the effect of excavation and embedment, for foundations on soft soils. The main effect of taking SSI into consideration is that the seismic input motion acting on the structure-soil system will change. On the other hand, SSI results in the radiation of energy of the waves propagating away from the structure which will result in an increase of the damping of the final dynamic system.

The design response spectra employed in this analysis, described below, has been specified by the U.S. Nuclear Regulatory Commission (NRC) in a Regulatory Guide[1] with the objective to be applicable to a wide range of sites, with the exclusion of those with unusually soft soils.

2.15.2 Input Conditions

2.15.2.1 Design Response Spectra

The ground motion DRS to be used for seismic analyses is specified in accordance with the guidelines of ASME[2] and NRC[3]. The primary scaling parameter used in the construction of this spectrum is the design maximum ground acceleration. The horizontal component ground DRS for both SL (seismic level)-2 and SL-1 can be linearly scaled from the DRS shown in Figure 2.15.2-1, which corresponds to a maximum ground acceleration of 1 g and accompanying peak ground displacement of 91.4 cm. A slightly different DRS spectrum is utilised for the vertically directed component of the seismic excitation.

The DRS curve shows the peak response of a single-degree-of-freedom oscillator of a given resonant frequency and damping coefficient excited by the ground motion as a function of the oscillator's resonant frequency. Different curves are given for different damping coefficients.

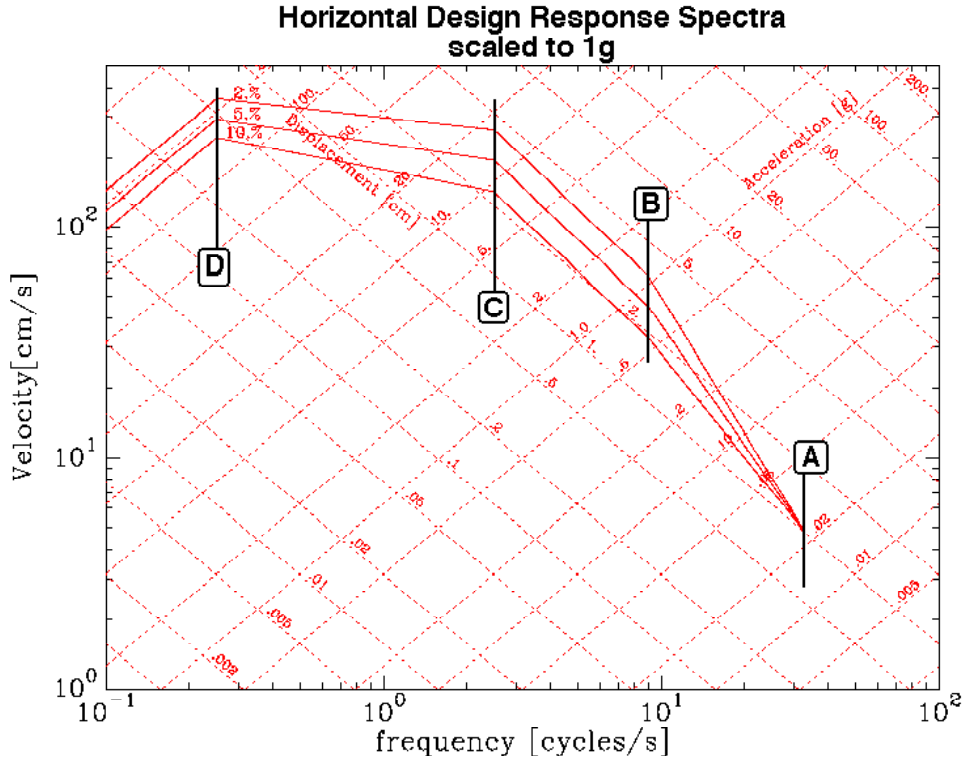

Figure 2.15.2-1 Horizontal Ground Acceleration DRS Scaled to 1 g at point A
The points A, B, C, D are reference frequencies defined in the NRC guides.

[1] NRC Guide 1.60
[2] ASME III Appendix N- Dynamic Analysis Methods
[3] NRC Guide 1.92, NRC Guide 1.60, NRC Guide 1.61

2.15.2.2 Damping Coefficients

The energy of a vibrating system is dissipated by various mechanisms. In materials, these include plasticity, thermal effects of repeated elastic strain, and internal friction. In structures, other effects can contribute to energy absorption such as friction at mechanical connections. For analysis convenience, damping is generally assumed to be viscous in nature.

The damping values in Table 2.15.2-1, expressed as a percentage of the critical damping coefficient, are the ones recommended by the NRC. The lower levels of the values given for each item are generally considered to be nearly lower bounds and highly conservative.

Considering that an SL-2 earthquake is to be analysed and that the ITER tokamak structure is built by a composition of both welded and bolted components, a single realistic damping ratio of 5% is used for the main calculations. However, different damping coefficients for each component of the tokamak were also used for comparative calculations to check the sensitivity of the results[1].

Table 2.15.2-1 Damping Factors for Seismic Analysis

	SL-0/SL-1	**SL-2**
Welded steel	2%	4%
Bolted steel	4%	7%
Reinforced concrete	4%	7%
Large diameter piping D>12in	2%	3%
Small diameter pipes D≤12in	1%	2%

2.15.3 Model Overview

The reported analysis has been performed using ANSYS and a global 3D finite-element beam-shell model which, while being sufficiently simplified to allow the execution of the model, is sufficiently detailed to properly model stiffness, deflections, and forces.

Due to cyclic symmetry of the system, one 20° sector of the tokamak with symmetric boundary conditions has been used for the modal and spectrum analyses for vertical (Z-directed) seismic excitation.

Under horizontally directed seismic excitation, in light of the double-symmetry of the system, a model of 1/4 of the tokamak may be used with the boundary conditions of symmetry in the ZX - plane and anti-symmetry in the ZY - plane. However, if the cyclic symmetry of the structure and sinusoidal distribution of the horizontal response in the toroidal (azimuthal) direction are taken into account, the model dimension may also be reduced to 1/18 of the tokamak. This model would require the use of so-called harmonic boundary conditions which allow only the modes with one nodal diameter to develop.

To obtain the mutual (relative) displacements between the major tokamak parts with the same degree of accuracy and reliability as for usual displacements several "key" pairs of nodes have been chosen where mutual displacements are to be determined. Then special additional

[1] V Sorin et al., "Seismic Response of the tokamak ITER updated model under combined loads", Plasma Devices and Operations,1999, Vol. 7, pp267-291

indicative nodes are introduced in the model where, by means of constraint equations, the displacements of these indicative nodes are set to be the difference between corresponding displacements of initial "key" nodes.

The one sector model is shown in Figure 2.15.3-1. For clarity, the vacuum vessel thermal shield model is shown separately. A 180° model is shown in Figure 2.15.3-2, whose mesh has also been used to verify the validity of the one sector model with harmonic boundary conditions.

The model includes a) the TF magnet with intercoil structures, b) the central solenoid together with its supports and preloading structure, c) the complete set of poloidal field coils with their radially flexible supports, d) the vacuum vessel also supported to the magnet by means of radially flexible supports, e) the VV thermal shield, f) the divertor cassette, g) the gravity supports, h) the blanket modules modelled as distributed masses and the port plugs, i) the lower set of supports consisting of vertical columns and radially directed "washer" shaped lower part of the cryostat, J) the VV port extensions and port plugs, and k) the cryostat.

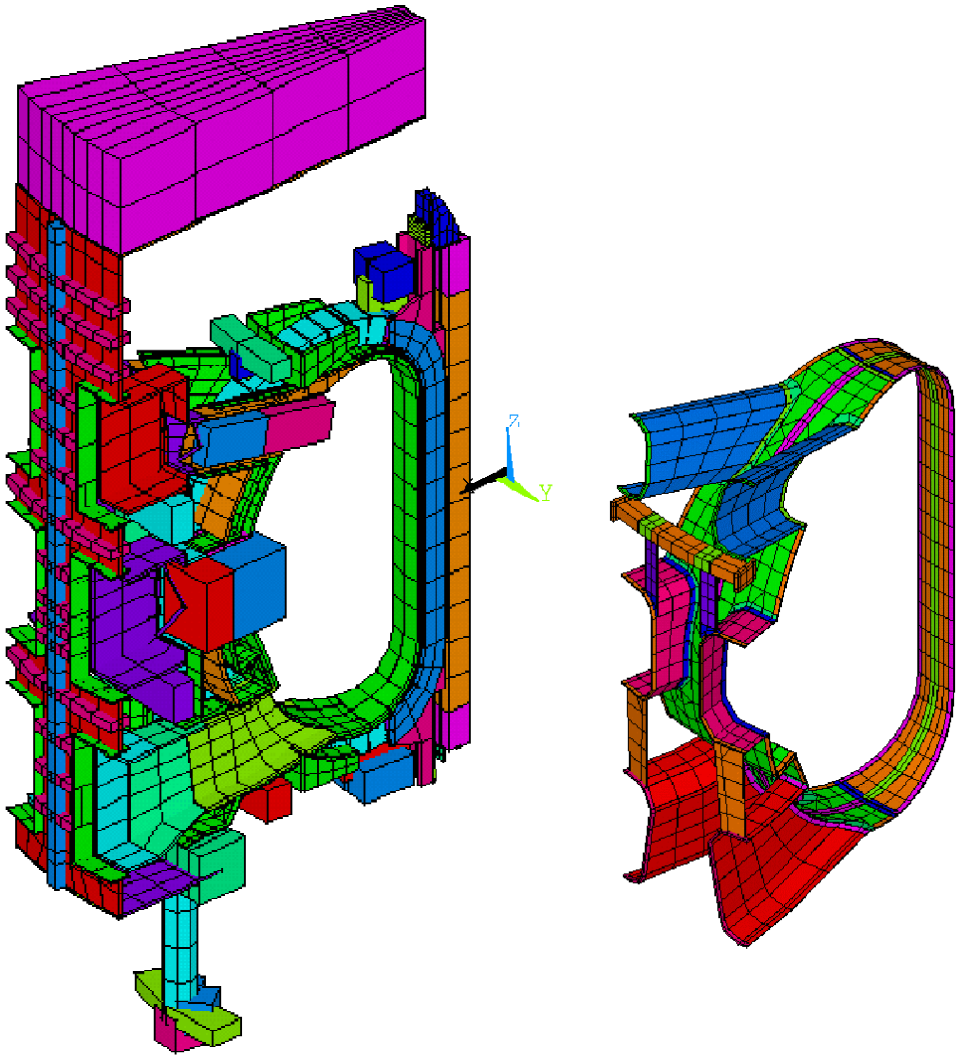

Figure 2.15.3-1 Finite Element Model Used for the DRS Seismic Analysis of ITER
The thermal shield model is shown on the right.

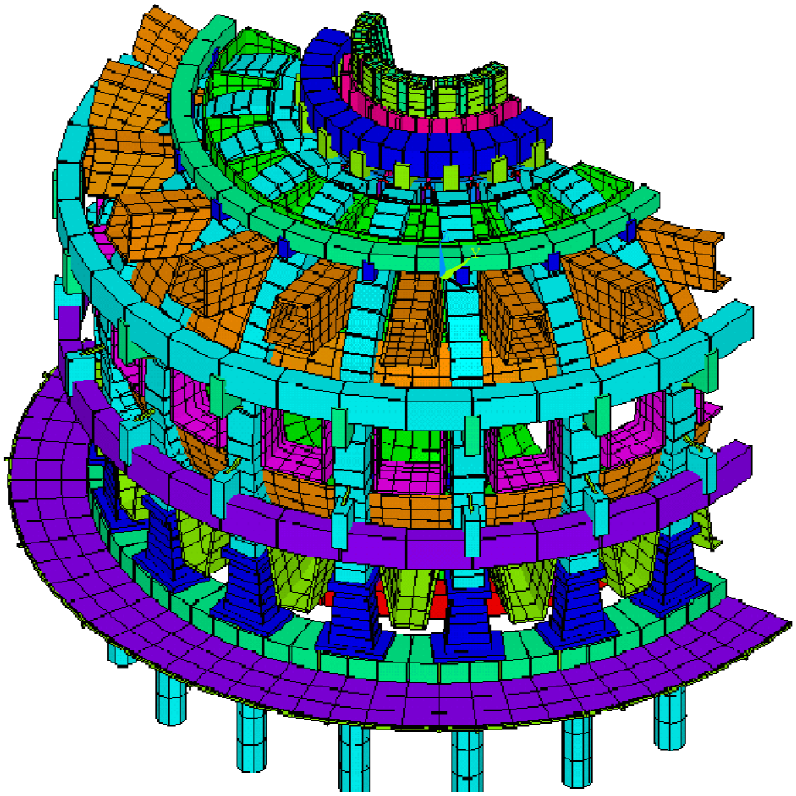

Figure 2.15.3-2 Seismic Model of the Tokamak Extended to 9 Sectors

2.15.4 Main Results Under SL-2 Seismic Excitation

In the modal analysis ten natural frequencies have been extracted both for a horizontal and a vertical seismic excitation. In both cases these frequencies model the movement of more than 95% of the total mass.

The first most significant four natural frequencies obtained for both horizontal and vertical seismic excitation are shown in Table 2.15.4-1.

Table 2.15.4-1 First Four Eigenvalues for Both Vertical and Horizontal Excitation of the Tokamak

	Horizontal excitation	Vertical excitation
1 Frequency	2.82 Hz	8.10 Hz
2 Frequency	3.40 Hz	8.54 Hz
3 Frequency	5.37 Hz	9.90 Hz
4 Frequency	6.56 Hz	11.2 Hz

The first horizontal eigenvalue of about 2.8 Hz corresponds to a mode where the entire tokamak rocks on top of the gravity support and is responsible for a large fraction of the overall effective modal mass. In this mode the supports aligned with the direction of the earthquake are loaded axially whereas the supports whose radial flexibility is normal to the earthquake direction react the horizontal inertial load by means of shear and bending.

The second horizontal eigenvalue of 3.4 Hz corresponds to the cryostat horizontal translation/rocking. The cryostat has its own independent horizontal support; and hence its seismic motion is mainly independent from the tokamak.

The third and fourth horizontal modes correspond to the horizontal oscillation of the thermal shield and the vacuum vessel with respect to the magnet system.

Table 2.15.4-2 shows the most important relative displacements between major components for a triaxial earthquake:

Table 2.15.4-2 Relative Displacements Obtained in the SL-2 Seismic Analysis.

Name	Radial mutual displac. mm	Vertical mutual displac. mm
VV – TFC, equatorial inboard	6.7	2.5
VV – TFC, top	7.4	2.0
VV – TFC, equatorial outboard	6.9	2.2
CS – TFC, equatorial inboard	1.4	0.7
TS – TFC, equatorial inboard	6.6	1.1
TS – VV, equatorial inboard	1.8	2.8

The relative deflections between TF magnet and vacuum vessel are within the allowable space allocation also in the case of an SL-2. In the inboard region this motion is in fact limited to less than 7 mm with an allowable (radial build allocated) value of 10mm. The TFC-VV and the TFC-TS relative displacements are in large part determined by the first overall tokamak mode and for this reason the relative displacements VV-TS is relatively small.

Table 2.15.4-3 gives the computed reacted loads at the gravity and VV supports under dead weight and SL-2 seismic loads.

Table 2.15.4-3 Absolute Values of the Reaction Loads in the Main Machine Supports

	Triaxial Earthquake	Dead Weight	Triaxial and Dead Weight
Gravity Supports Response:			
Axial load, MN	7.8	-10.9	18.6
Toroidal load, MN	12.4	0	12.4
Radial moment (top), MNm	7.64	0	7.6
Radial moment (bottom), MNm	35.4	0	35
Toroidal moment, MNm	0.44	-0.7	1.1
Axial (torsion) moment, MNm	3.0	0	3.
VV Supports Response:			
Axial load, MN	4.6	-6.4	11.1
Toroidal load, MN	9.1	0	9.1
Radial moment, MNm	9.1	0	9.1
Toroidal moment, MNm	0.2	0.11	0.3

2.15.5 Seismically Isolated Tokamak

The above analysis, which shows sound overall tokamak behaviour and has been the basis for the detailed design of the supports, is based on a generic site seismicity where the peak acceleration is assumed to be 0.2g. If ITER is to be sited in regions with higher seismicity, the use of seismic isolation has been foreseen. Its spatial extension would be limited to the tokamak and tritium building, thus encompassing also the primary heat transfer system. An optimisation procedure has been performed to establish the best compromise between isolation pad effectiveness and mutual displacements between the isolated island and ground. The challenge is to design power, signal, and cooling lines to cross the isolation boundary with sufficient compliance.

With the support concept discussed in the previous sections, the ITER tokamak is able to withstand earthquakes up to 0.2g. This makes the required isolation scheme rather straightforward since, for example, a reduction factor of only 2 would be required by the isolation if an SL-2 event if it were raised to a 0.4g specification. A natural frequency of about 1 Hz would provide the required reduction in the event of a doubling of site seismicity specification.

If ITER is to be sited in a location with a significantly higher level of seismicity, it will be possible to incorporate seismic isolation at the bottom of the reactor pit. With this concept, the seismic isolation will not change the machine design and general equipment layout, requiring only some structural modifications of the pit and building.

2.15.6 Conclusions

For the employed concept of both magnet and vacuum vessel support design it has been found that the entire tokamak is strong and rigid enough so that the use of seismic isolation can be avoided for the presently specified seismic conditions. The use of a stiff and strong horizontal linkage between magnet structure and vacuum vessel has been shown to be essential and effective to react both horizontal VDE loads and seismic ground motions.

3 Plant Description: Plant Systems Design and Assessment

3.1 Tritium Plant and Detritiation

3.1.1 System Description

The functions of the tritium plant can be summarised as:

- processing all tritiated gas streams from sources within the plant to produce the gas streams for fuelling (at specified flow rates and isotopic compositions);
- confinement of tritium with multiple barriers (such as a primary component, secondary enclosures and rooms);
- detritiation of a number of tritium-containing waste streams and contaminated room air, and detritiation of tritiated waste water to reject the detritiated remnants to the environment.

The main design guidelines for the tritium plant are:

- minimisation of tritium inventories;
- reduction of occupational exposure;
- low generation of effluents and wastes;
- reduction of costs by standardisation of components.

The design is based upon well-proven technology to ensure the safe handling and credible accountancy of tritium, and high reliability.

3.1.1.1 Tokamak Fuel Processing Subsystems

The outline flow diagram, shown in Figure 3.1-1, depicts the tokamak fuel processing subsystems, which consist of the storage and delivery, tokamak exhaust processing, hydrogen isotope separation, and the tritium plant analytical systems. The diagram identifies and defines all interfaces within this group of subsystems, enabling the process conditions at the interfaces to be defined systematically and consistently. In addition, there are further subsystems which participate in the fuel processing: glow discharge gas processing, gamma decay and auxiliaries.

The diagram also indicates the connections between these systems and the fuelling system, torus, torus exhaust pumps, and the water detritiation system.

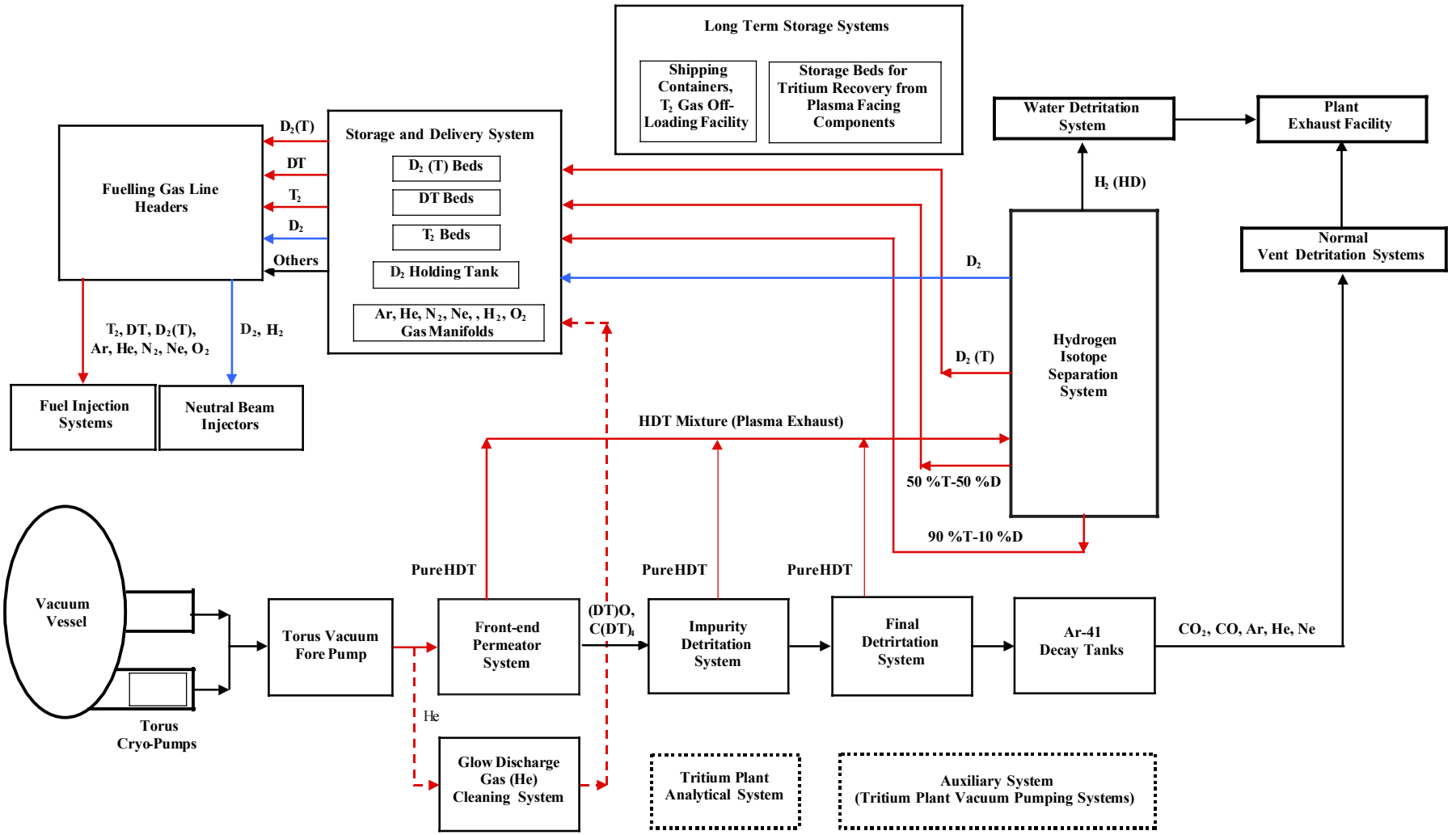

Figure 3.1-1 Outline Flow Diagram of ITER Fuel Cycle Systems and Interfaces

Storage and Delivery Systems

These systems include the long-term storage, and the short-term fuel storage and delivery systems. Transport beds containing tritium delivered from off-site are unloaded in the long-term storage. Prior to unloading, calorimetric determinations of the amount of tritium contained in the transport beds are made. Tritium is transferred as required for machine operation to the short-term storage and delivery system. In addition, between operational campaigns, when tritium is recovered from plasma-facing components, it will be necessary to transfer much of the tritium to the long term storage, which requires a capacity of 1,000 g. At the maximum tritium concentration available from the isotope separation system (purity of T ≥ 90%) this will correspond to ~ 200 moles.

The short-term storage and delivery system receives tritium containing hydrogen gases from the isotope separation system, tokamak exhaust processing system, and long term storage, at specified isotopic compositions (10/90 DT, 50/50 DT, and two D_2(T) streams for the NB injectors and gas puffing) during plasma operation, and stores them on getter beds and in holding tanks. The gases are delivered on demand to the fuelling system at specified isotopic compositions and flow rates. The design delivery rate from each bed is 20 Pam^3s^{-1}. The delivery of DT mixtures with compositions other than those listed above involves mixing the gases evolved from the storage beds, the proportions of each component being metered by mass flow controllers. For D plasma operation, D_2(T) may be delivered to the fuelling system from storage beds, the holding tank or from both these sources.

The storage beds in the storage and delivery system are each equipped with an integral calorimetric capability, achieved by temperature differential measurement in an external loop in which helium is circulated at a precisely controlled flow rate.

A further requirement is the recovery of the ^{3}He tritium decay product, which is achieved by periodically releasing the gas inventory from each of the beds in turn and transferring it to a dedicated getter bed which pumps the hydrogen isotopes, allowing the helium to pass through and be directed to a collection tank. The hydrogen absorbed by the getter bed is then returned to the main battery of storage beds.

Tokamak Exhaust Processing System

The main function of the tokamak exhaust processing system is to recover unspent DT fuel yielding a product stream suitable for transfer to the isotope separation system, or for transfer to the storage and delivery system during all modes of tokamak operation, including plasma operation, pump-down, wall-conditioning, leak detection, and tritium recovery from the plasma-facing components. In addition, tritiated gaseous process wastes from other sources (NB injector cryopump impurities, fuelling system purge, tritium plant analytical system, regeneration of helium glow discharge cleaning molecular sieve beds, and ultimately from the test blanket module purge gas loop) are also accepted and decontaminated by the tokamak exhaust processing system. The tokamak exhaust during plasma operation also includes inert gas activated by neutrons. The expected overall detritiation factor verified by R&D[1] is ≥ 10^8. The waste gas stream from the tokamak exhaust processing system, although it contains an extremely low level of tritium (less than 1 mCi/d), is sent to the normal vent detritiation system.

[1] H. Yoshida et al. “ITER R&D Auxiliary Systems”, Fus. Eng. Design 55 (2001), pp 313-323

The tokamak exhaust processing system (see Figure 3.1-1) is composed of the following three processing subsystems:

- front end permeator;
- impurity processing;
- final clean-up.

The first subsystem (once-through process) comprises front-end membrane permeators (palladium/silver alloy) for separation of elemental hydrogen isotopes from tokamak exhaust gas during plasma operation and wall conditioning with D_2 gas, and a nickel catalyst reactor for direct conversion of tritiated impurities into elemental tritium during plasma operation and co-deposited tritium recovery campaigns. A separate permeator receives the NB injector cryopump regeneration gases and separates this stream into a pure molecular hydrogen stream, which is mixed with the tritiated protium stream from the water detritiation system and sent to the protium column of the isotope separation system. The impurities are sent to the impurity processing subsystem of the tokamak exhaust processing system.

During the special operation mode for tritium recovery from the plasma-facing components, the tritium recovery gas may include high concentrations of tritiated hydrocarbons, water vapour (DTO), CO, CO_2, O_2 and carrier gas (N_2 or Ar). The tritiated impurities are directly converted into elemental hydrogen (DT) in the nickel catalyst reactor, and the product gas sent to one of the front-end permeators for separation of DT from impurities and carrier gas. The DT stream is transferred to the isotope separation system. The major portion of the carrier gas is sent to the normal vent detritiation system via the impurity processing system.

The second subsystem (re-circulation loop process with continuous feed and bleed) comprises a small nickel catalyst reactor and a small membrane permeator for continuous recovery of elemental tritium from tritiated impurities by heterogeneously catalysed cracking or conversion (chemical) reactions. This subsystem also treats impurity streams from other sources including during glow discharge cleaning, cryogenic molecular sieve bed regeneration, and the analytical system.

The third subsystem (once-through final cleanup process) comprises a small counter-current membrane reactor for final detritiation of waste gas by means of isotopic exchange with protium. The detritiated impurity gas is then routed to the gamma-decay system. These three subsystems and gamma-decay system are placed in a shielded room.

Gamma Decay System

A system of tanks equipped with γ activity monitors and transfer pumps has the function of temporary retention of activated (short half-life) inert gas species to allow for their decay to an acceptable level, at which point they are discharged through the normal vent detritiation system to the environment.

Glow Discharge Gas Processing

During glow discharge cleaning, deuterium and helium will be purged over prolonged periods (up to 100 h) through the plasma vacuum vessel, at a flow rate of ~ 50% of the nominal fuelling rate for plasma operations. The gas stream from the torus roughing pumps during the helium glow will be processed through one of a pair of 77K liquid nitrogen-cooled

molecular sieve beds to trap the impurities, and the helium is recycled directly back to the tokamak. The molecular sieve beds will be regenerated every 24 h, by warming to room temperature for elemental hydrogen desorption, and (at a lower frequency) to higher temperatures for tritiated moisture desorption. The desorbed gas is directed to the impurity processing loop of the tokamak exhaust processing system. This processing system will also be used for helium plasma operation.

Hydrogen Isotope Separation System

The isotope separation system utilizes cryogenic distillation to separate hydrogen isotope mixtures. The feeds originate from the sources shown in Table 3.1-1 with the indicated schedules.

Table 3.1-1 Isotope Separation System Operation Schedules for Different Feeds

Feed	Schedule
Plasma exhaust	Intermittent
Neutral beam injection	Intermittent
Water detritiation	Continuous
First wall conditioning	Occasional (not simultaneously with intermittent feeds)

These feed streams are introduced at two feed locations in the column cascade to produce up to five different products. These are a detritiated protium effluent for discharge to the environment, two distinct deuterium streams for gas fuelling and NB injector source gas, and two tritium fuelling streams, one with 50/50 DT and one with 10/90 DT isotopic composition. The column cascade consists of four distillation columns (CD1, CD2, CD3 and CD4). The purpose of the first column (CD1) is to remove tritium from predominantly protium-rich streams and to produce a virtually tritium-free protium stream as the overhead product. The function of the second column CD2 is to separate H and D from the CD4 overhead stream, and produce a partially-purified D_2 stream which is used for gas fuelling and as the feed to the third column CD3. CD3 removes tritium and protium from the deuterium for NB injector source gas. The bottom product of CD2, a D_2-DT mixture stream, is fed into the high-tritium-column CD4, which also receives elemental hydrogen separated in the tokamak exhaust processing system from the plasma exhaust stream.

Dominant design inputs for the isotope separation system are (1) the dynamic characteristic of some of the feed stream flow rates and compositions, and (2) tritium (and total hydrogen) inventory minimisation. These necessitate optimisation of the cascade configuration and column design to reduce column diameters and lengths to the maximum extent consistent with maintaining product quality. In addition, the cascade is equipped with several equilibrators, which are small catalytic reactors operating at ambient temperature to promote isotope exchange reactions. These reduce the required number of theoretical stages and therefore the total inventory of the cascade. The circulation pumps for equilibrator loops and transfer pumps are located in ambient temperature locations. As a result, the entire isotope separation system has no moving parts operating at cryogenic temperatures. This, with the use of redundant electric reboiler heaters, minimises the maintenance needed for components inside the cold box.

In order to facilitate the transition from standby to intermittent plasma operations, a set of recycle lines is provided to permit temporary operation at closed recycle without external feed and product flows.

Tritium Plant Analytical System

In addition to local instrumentation, a central analytical system is an integral part of the tritium plant with the main functions:

i) verification or additional control of the correct functioning of various processes by determination of the composition of various gas mixtures;
ii) determination of tritium concentrations in various gas mixtures for inventory accounting;
iii) monitoring and calibration of local instrumentation, e.g. ionisation chambers.

Samples from the storage and delivery system, tokamak exhaust processing system, and isotope separation system, are sent to the analytical system via interconnecting lines. Four manifolds are installed in the analytical system to receive samples, and are organised to minimise cross contamination between samples of different compositions. The samples to be analysed are injected into analytical gas chromatographs for determination of their gas composition.

Five gas chromatographs (three micro-gas chromatographs and two cryogenic micro-gas chromatographs) are chosen to perform the analytical tasks required, i.e. determination of the tritium concentration, as well as of the six hydrogen molecular species and of the other impurities expected.

The exhaust gases of the five gas chromatographs containing carrier gas and injected samples are either sent for final detritiation to the normal vent detritiation system or to the tokamak exhaust processing system, depending on their tritium concentrations.

The gas chromatographs, manifolds and pipework connected to the tokamak exhaust processing system are placed in a shielded barrier.

Auxiliary System

The auxiliary system (see Figure 3.1-1) is composed of a high vacuum manifold and a vacuum manifold. The former receives high vacuum pump exhaust from the tritium process component vacuum jacket. The latter receives vacuum pump exhaust from various other sources. Gases collected by this system are delivered to an appropriate point in the tokamak exhaust processing system, depending on their composition.

3.1.1.2 Tritium Confinement and Detritiation Subsystems

The heating, ventilation and air conditioning systems (HVAC) and detritiation systems form an essential part of the ITER tritium confinement. HVAC and detritiation subsystems for the tokamak building, tritium building, hot cell and radwaste buildings are operated in various modes depending on the plant operation states, such as normal operation, maintenance and off-normal events.

Tokamak Building HVAC and Detritiation Systems

The HVAC and detritiation systems for the tokamak building are composed of two dedicated heating, ventilation and air conditioning systems for the gallery areas (HVAC-I) and for the containment volume (the tokamak cooling water system vault and annex, CVCSs area, NB cell, upper and lower pipe chases, and vertical pipe shafts) (HVAC-II), and various atmosphere detritiation systems such as the normal vent detritiation system, the standby room air vent detritiation system, the standby room air detritiation system, and the tokamak vent system for these areas. As an additional function of the HVACs for the gallery and the containment volume, local air coolers are incorporated for continuous removal of the heat load from various equipment and lighting.

Figures 3.1-2 and -3 show the integrated confinement and detritiation system configurations for the tokamak building. During plasma operation and baking, a negative relative pressure of -1 mbar in the gallery areas is maintained by HVAC-I. Through a small duct the gallery area is connected with the tokamak pit free volume (~ 5,000 m^3, leakage rate 10 vol%/d) in between the cryostat outer surface and the bioshield inner surface. This ensures that air leakage between the crane hall and the pit free volume (~ 20 m^3/h) is always in the direction of the pit.

Ducts are installed between the bioshield inner wall and the cryostat outer wall enclosing the port openings. This effectively seals off the port area from the pit free-air volume and prevents the cross-contamination from one port to another.

To avoid condensation of the moisture, which is included in the external air, onto the cryostat surface, a forced air circulation system with a small rotary air dryer unit (throughput 150 m^3/h) composed of a compressor and an internal gas/water heat exchanger is utilized.

As schematically shown in Figure 3.1-2, the port cell pressure is kept at -2 mbar differential pressure by continuously extracting air by the normal vent detritiation system to form a pressure gradient from the gallery areas (-1 mbar) to the ports. With this confinement configuration, it is possible to localise tritium contamination, and to eliminate the risk of tritium release to the environment during port maintenance.

It is intended to route all tritium-bearing pipes, e.g. vacuum and fuelling lines, that interconnect the vacuum vessel with the tritium plant, and hence cross the gallery areas, inside the floor slabs of the galleries, such that their secondary containment volume is either pumped or purged to the tritium plant. This design configuration makes release from these lines into the gallery areas a beyond-design-basis event, and avoids the need to have emergency isolation valves in the gallery areas HVAC system.

HVAC-II (Figure 3.1-3) for the containment volume (volume 51,000 m^3, air leakage rate 10 vol%/d at a room internal pressure of 2 bar(abs)) is not operated during plasma operation and baking, and a differential room pressure of -3 mbar is maintained by the normal vent detritiation system by extracting room air with a flow rate equivalent to the volume air leakage rate.

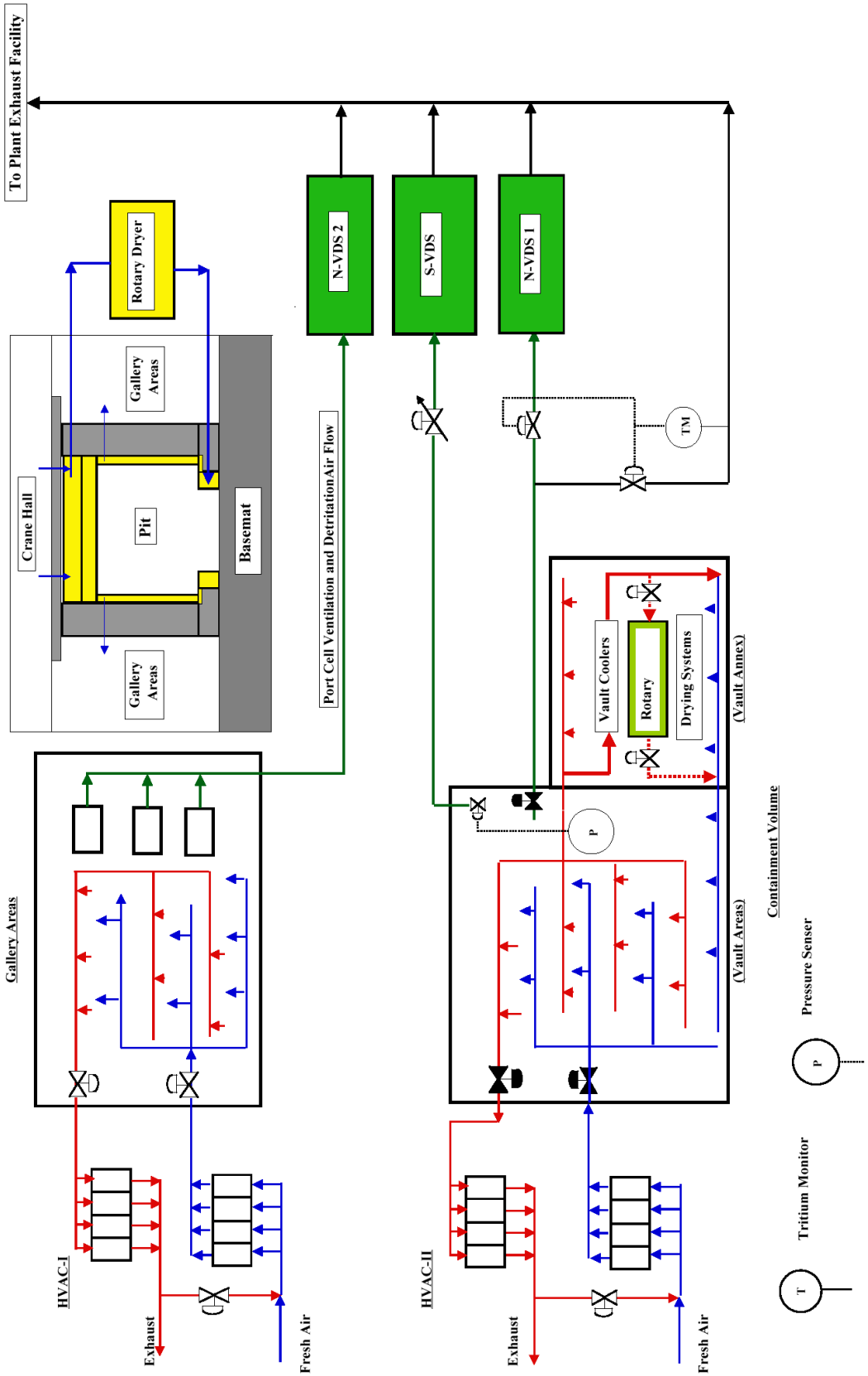

Figure 3.1-2 Configuration of HVAC Systems

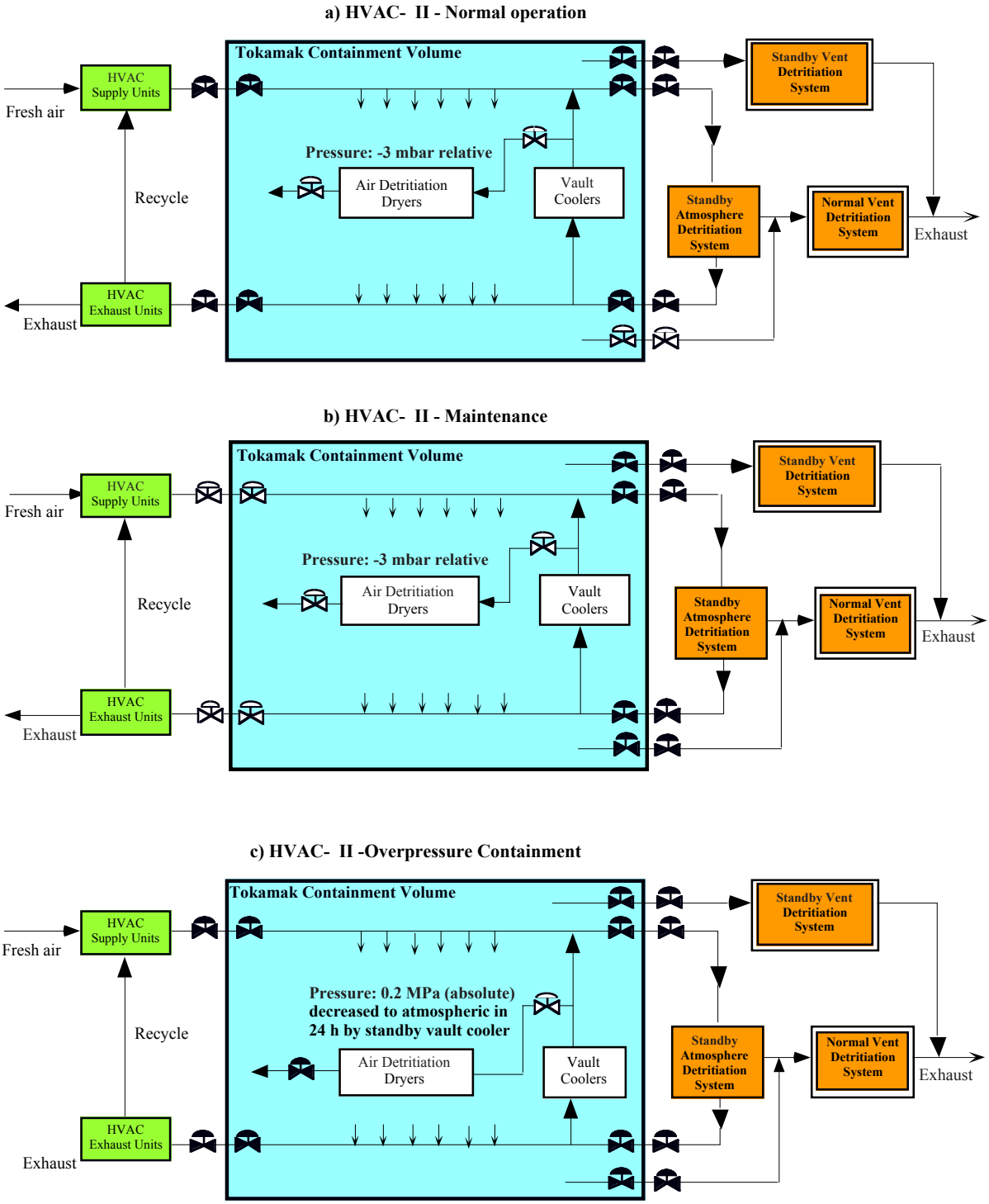

Figure 3.1-3 Tokamak Building Confinement and Detritiation System Configuration of HVAC II (TWCS Vault and Vault Annex Upper and Lower Pipe Chases, Vertical Pipe Shafts, NB Cell)

N 32 GR 105 01-02-26 W 0.1

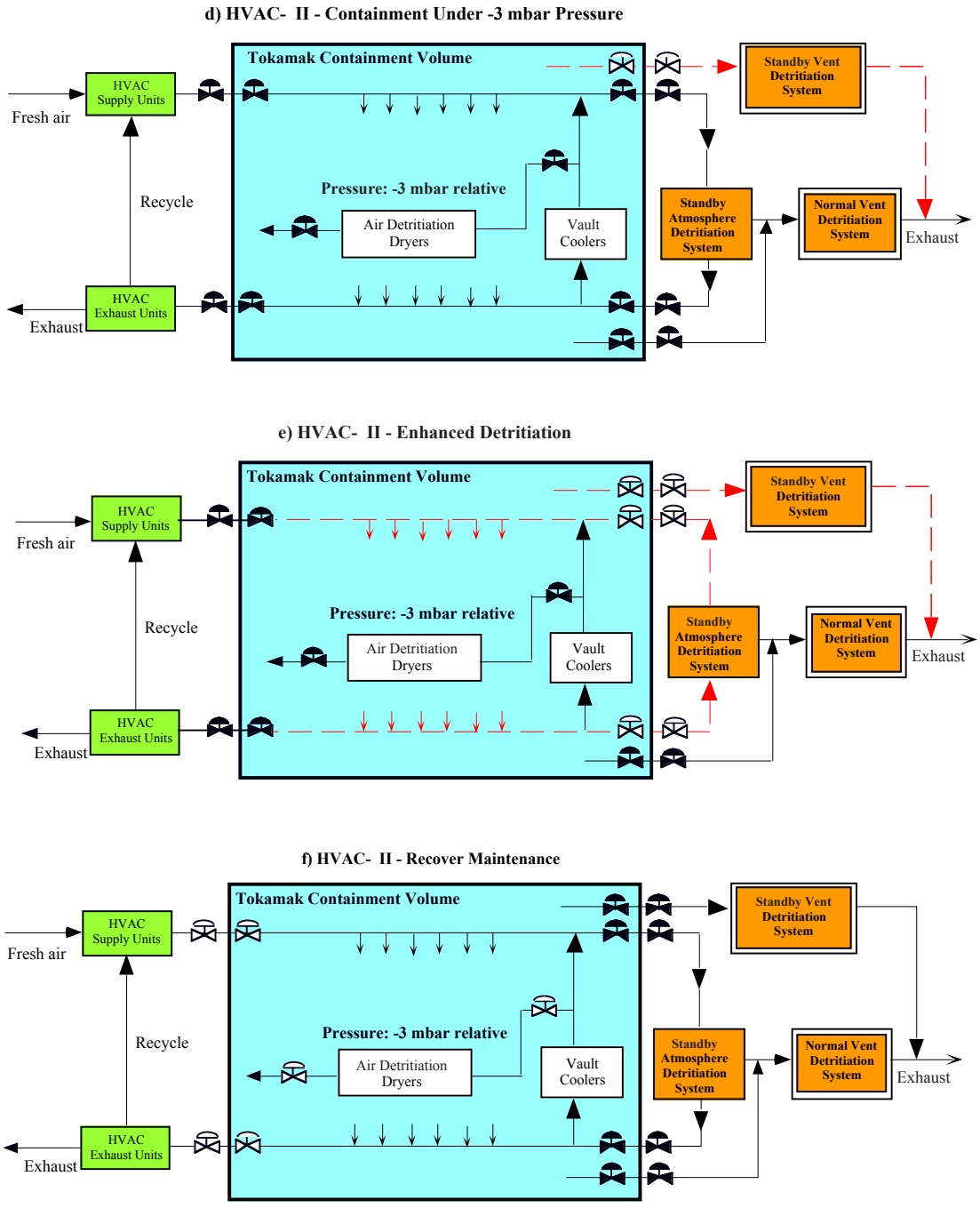

Figure 3.1-3 Tokamak Building Confinement and Detritiation System Configuration HVAC II (continued) (TWCS Vault, Vault Annex, Upper and Lower Pipe Chases, Vertical Pipe Shafts, and NB Cell)

The heat load (plasma operation: 0.8 MW, baking: ~ 1 MW) in the containment volume generated by pump motors and losses through the thermal insulation around pipes and components of the tokamak cooling water system, is continuously removed by the

containment volume air coolers (cooling capacity 1.2 MW). Moreover, in the case of a large ex-vessel coolant leak (~ 100 m^3 water), the resulting steam pressure (below 0.2 MPa) is reduced to ambient within 24 h by steam condensation at the containment volume coolers.

Tritiated moisture leaking from the tokamak cooling water system is also continuously removed by air detritiation dryers. The condensate of the coolers and the air detritiation dryers may include tritium, thus it is sent to the water detritiation system before its rejection to the environment. Tritium permeation into the tokamak cooling water system coolant is estimated to be relatively small, therefore the air detritiation dryers will be installed later when required in the operation programme.

In case an ex-vessel leak occurs and/or a wet bypass event (bypass between the tokamak cooling water system vault to the vacuum vessel interior via a failed tokamak cooling water system loop) is caused as a consequence of an ex-vessel coolant leak, the normal vent detritiation system is isolated and the standby vault cooler (0.2 MW capacity) is started up. When the normal temperature and pressure in the containment volume are regained in 24 h, the standby vent detritiation system (throughput 3,000 m^3/h) and the standby atmosphere detritiation system (throughput 4,500 m^3/h) will be operated to enhance detritiation, which may allow early entrance to the vault areas to repair and/or replace failed piping and components.

An emergency water holding sump tank system of 400 m^3 capacity is installed in the basement room of the tritium building, to collect tritiated water generated (~ 100 m^3/month) by the operation of these detritiation systems.

Another type of wet bypass scenario (opening size < 0.02 m^2) due to the failure of a vessel penetration and/or a failure of diagnostic windows (both primary and secondary confinement), which may occur as a consequence of in-vessel coolant leakage, has been considered. In this case, the tokamak vent system (throughput 150 m^3/h) connected to the normal vent detritiation system, is started up within 3 minutes to prevent the internal pressure of the vacuum vessel from exceeding the area room pressure. During this scenario the tokamak vent system receives a stream from the tokamak vessel of high temperature (up to 300°C) and high humidity (up to 0.1 MPa vapour pressure).

In the case of a small-scale dry bypass event (opening size ~ 0.02 m^2), which may be caused by a failure of both primary and secondary confinement boundary windows attached to a diagnostic or heating system, allowing penetration of both the vacuum vessel and the cryostat boundaries, the air is immediately heated by the first wall and the volumetric expansion of the air results in a back flow of tritium containing air to the port cells. A relatively high level of leak tight design (in-leakage rate ~ 100 vol %/day) is applied to all port cells, and the atmosphere of the port cells is detritiated by a permanent connection to a dedicated normal vent detritiation system.

For tokamak maintenance through the vessel ports, the standby atmosphere detritiation system is switched to tokamak maintenance mode by connecting it to the tokamak vessel via the torus vacuum pumping ducts. The closed loop through the standby atmosphere detritiation system and tokamak vessel circulates dry air and continuously removes tritium outgassing from the first wall. The flow rate is adjusted to ~ 2,000 m^3/h to avoid wide dispersion of fine particles of tokamak dust due to turbulent flow in the vessel. This

maintenance loop is also connected to the normal vent detritiation system, and a small flow is extracted from the loop to maintain negative pressure in the tokamak vessel.

The atmosphere detritiation systems, HVACs and containment volume air cooler equipment are located in the tritium building. The condensate of the equipment is sent to the tritiated water holding tank systems in the tritium building.

Tritium Building Confinement and Detritiation Systems

The confinement and detritiation systems for the tritium building are composed of tritium process equipment (primary barrier), enclosures such as glove boxes (secondary barrier), and tritium process rooms (final barrier). The secondary confinement is implemented by the glove box atmosphere detritiation system and/or the dry N_2 gas purge to the normal vent detritiation system. The tritium process rooms are backed up by the tritium building HVACs, the normal vent detritiation system (500 m^3/h) and the standby atmosphere detritiation system.

Figure 3.1-4 shows the concept of the confinement and detritiation system configuration for the tritium building. It also shows the interface with the ADS and VDS units for the tokamak building. The dotted lines indicate the possibility to connect the vault volume to the S-ADS and S-VDS. The HVAC is composed of a white zone HVAC and two green zone HVACs, i.e. one for the water detritiation system room and tritiated water holding tank rooms, another one for other tritium processing subsystems rooms. During normal conditions, the room atmosphere pressure in the green zone is maintained at - 1 mbar differential by the HVAC. When the room air tritium concentration exceeds a set point, the relevant room isolation valves in the HVAC are closed, and triggers cause the isolation valves connected to the normal vent detritiation system to open.

In the case that large room areas are contaminated simultaneously, the standby vent detritiation system (3,000 m^3/h) will be operated with a required flow rate. The standby vent detritiation system can be switched to three main areas, i.e. the tokamak building gallery area, the containment volume, and the tritium building green zone areas. The standby atmosphere detritiation system (4,500 m^3/h) is operated to enhance decontamination of the contaminated rooms to ensure early entry to reestablish normal conditions.

In addition, the normal vent detritiation system (throughput 500 m^3/h) receives various exhaust gases from different sources depending on their operation modes, maintenance schedule and their off-normal conditions. The normal vent detritiation system has a standby capacity (~ 200 – 300 m^3/h) to meet such intermittent gas sources.

Figure 3.1-5 shows the concept of an integrated atmosphere detritiation for both the tokamak and tritium buildings. The equipment of all atmosphere detritiation systems is located in the tritium building. Figure 3.1-6 shows an integral configuration of the glove box atmosphere detritiation system (throughput 150 m^3/h) and glove boxes. All glove boxes are purified by re-circulating the atmospheric gas (N_2) through the glove box atmosphere detritiation system during normal conditions. In case the tritium concentration in one of the glove boxes exceeds a set point (1 mCi/m^3) due to a failure of equipment or process piping, other glove boxes are isolated from the glove box atmosphere detritiation system gas circulation loop, and the full glove box atmosphere detritiation system capacity, is dedicated to the contaminated glove box for enhanced detritiation. Even if the maximum tritium inventory of 100 g in the tritium

storage bed is instantaneously spilled in a representative glove box (volume 30 m^3), 99.9 % recovery is achieved in a few hours. The resulting tritium permeation into the room through the gloves will be less than a few Ci, and retained by the normal vent detritiation system.

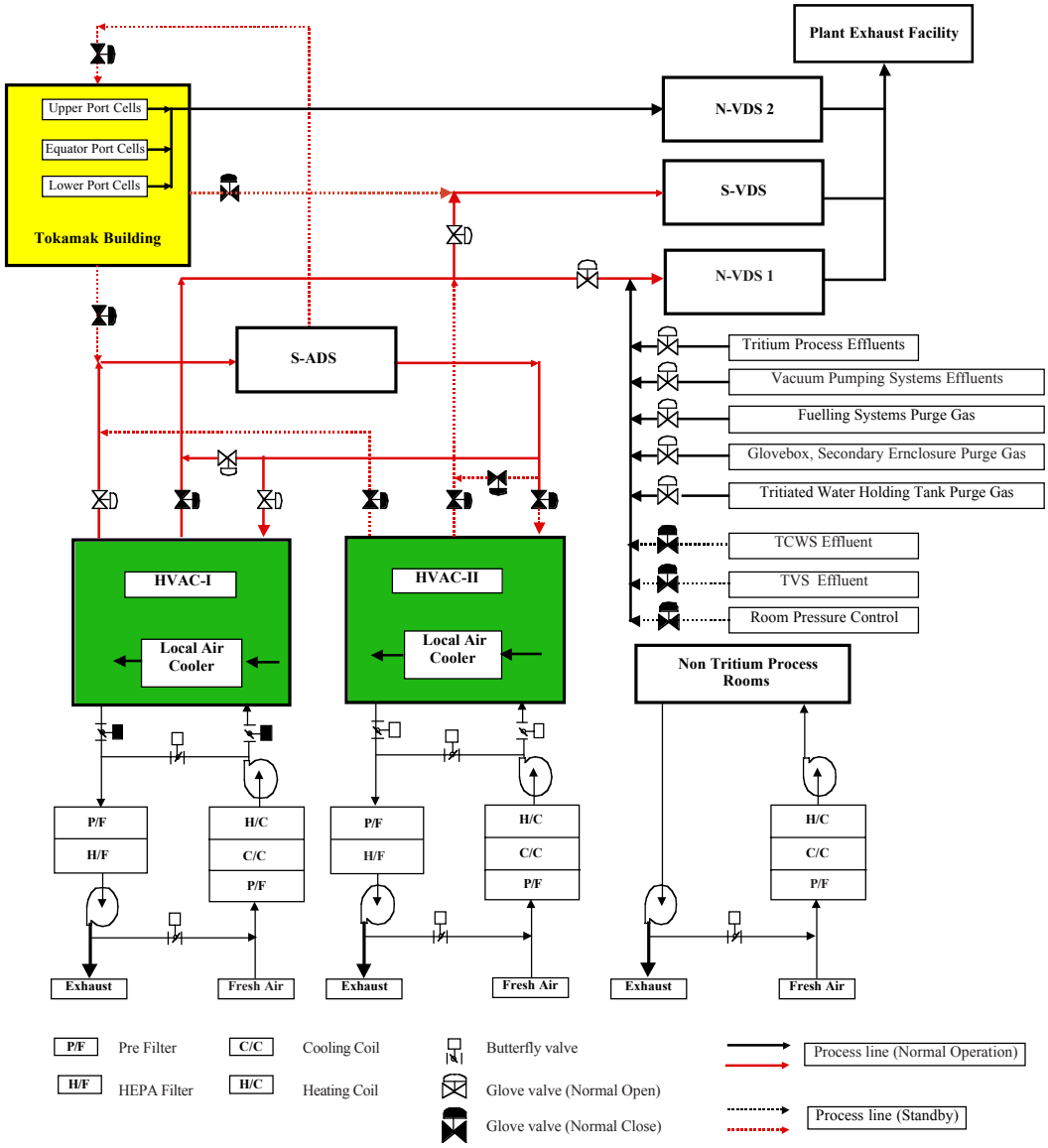

Figure 3.1-4 Concept of Confinement and Detritiation System Configuration for the Tritium Building

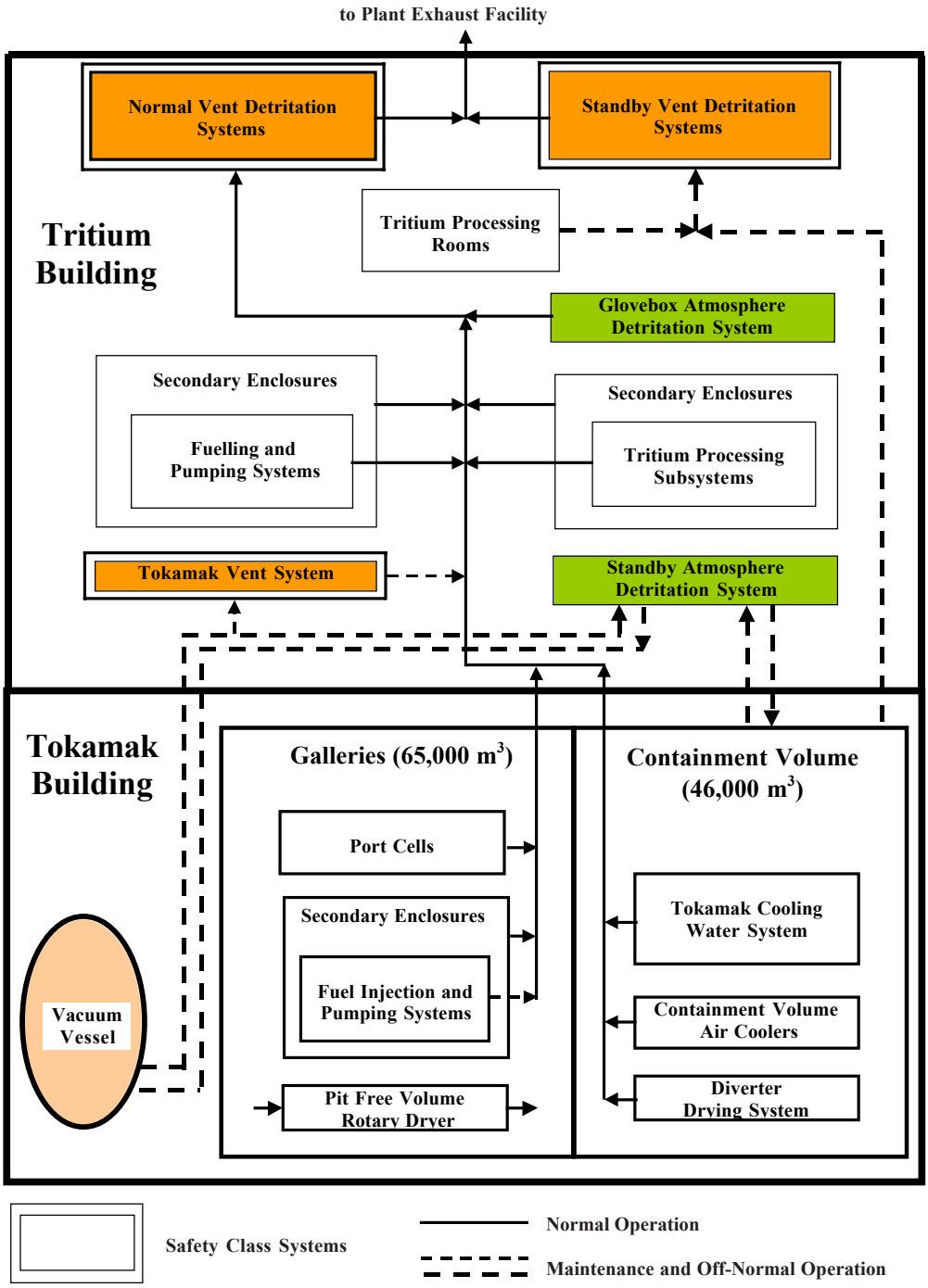

Figure 3.1-5 Integrated Atmosphere Detritiation System Configuration for the Tokamak and the Tritium Buildings

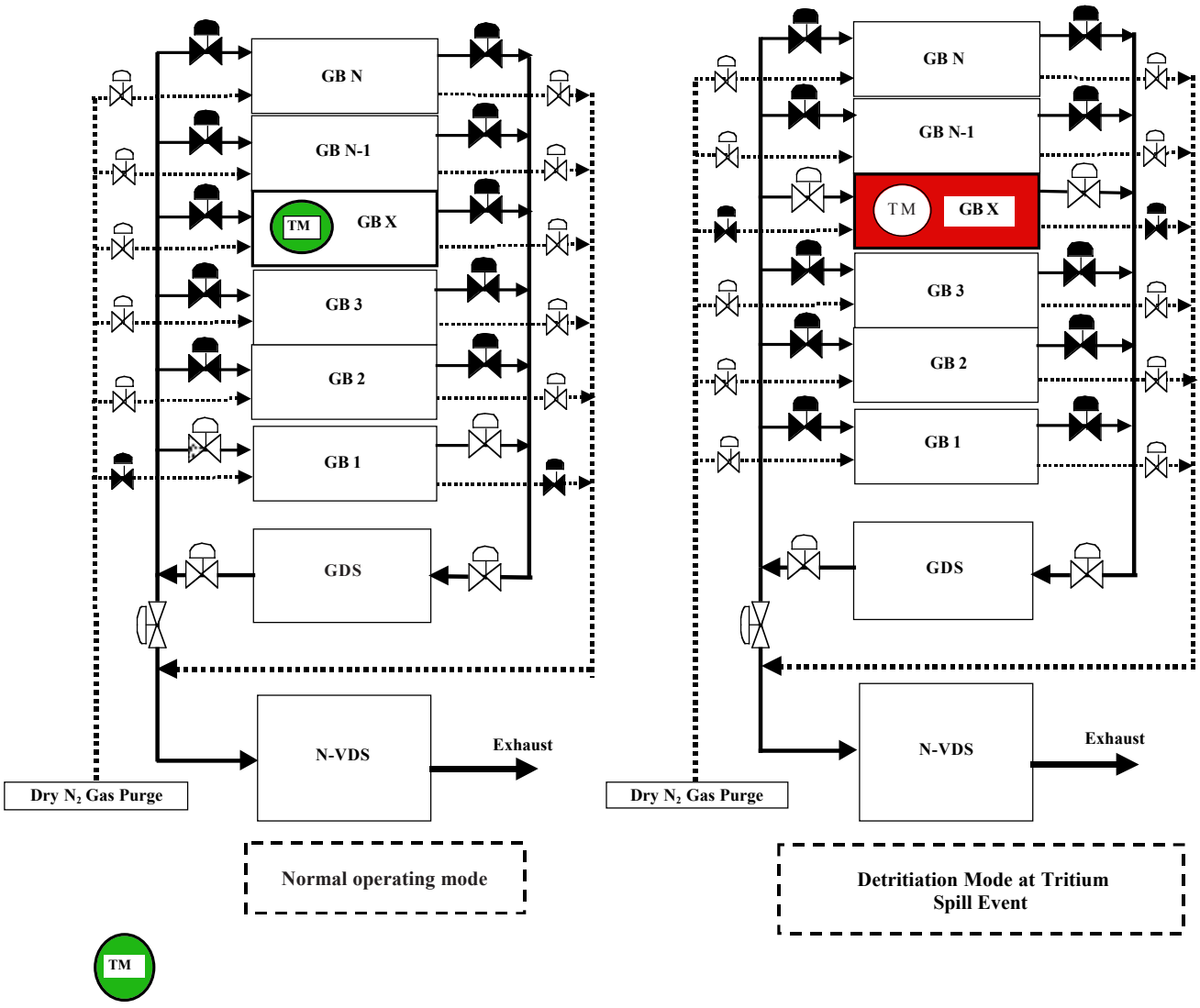

Figure 3.1-6 Integral System Configuration of the Glove Box Atmosphere Detritiation System, Glove Boxes and the Normal Vent Detritiation System

Tritiated water produced by the operation of these detritiation systems is collected by an intermediate measuring tank and then sent to the tritiated water holding tank systems after measurement of the tritium concentration levels. Condensate of the HVAC and local air coolers is sent to the tritiated water holding tanks in a similar manner.

Hot Cell and Radwaste Building Confinement and Detritiation Systems

The confinement and detritiation systems for the hot cell and the radwaste buildings are composed of their HVACs, a hot cell red zone detritiation system, and the vent detritiation system. Activated dust and decay heat from in-vessel components introduced in the red zone are separately removed by local filters and local air coolers installed in a green zone in the hot cell. Figure 3.1-7 shows the configuration of an integrated confinement and detritiation system for these buildings. The atmospheric pressure of the hot cell green zone is maintained at a differential of - 1 mbar by the HVAC during normal conditions, and the pressures in the amber and the red zone are maintained at differentials of - 2 mbar and - 3 mbar, respectively by the hot cell vent detritiation system. The hot cell vent detritiation system capacity (700 m^3/h) includes standby capacity for an emergency tritium confinement for any green

zone rooms in the hot cell and the radwaste buildings, where the relevant HVAC isolation valves are closed.

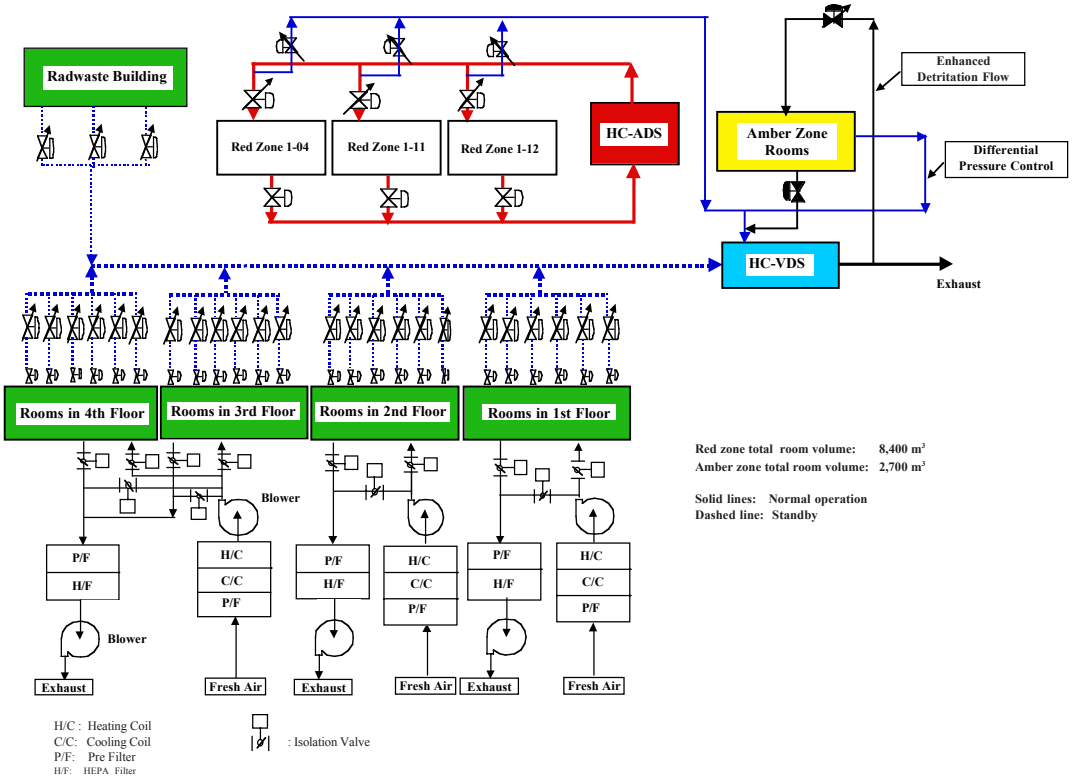

Figure 3.1-7 Hot Cell and Radwaste Buildings - Confinement and Detritiation System Configuration

The hot cell atmosphere detritiation system (capacity 4,500 m^3/h) is manifolded to all red zone rooms to control the air flow rate required in each room depending on their operation states. The achievable room air HTO concentration during occupancy by the maximum number of divertor cassettes (estimated tritium outgassing rate ~ 18 Ci/h) is 500 DAC (Derived Air Concentration: unprotected exposure to 1 DAC = 10 µSv/h), or 1.6 $x10^8$ Bq/m^3. The reduction rate of the HTO concentration after removal of divertor cassettes or other tritium source terms from the room depends on the decontamination characteristics of the wall surface, and based on recent R&D results, the tritium concentration can be lowered to 1 DAC within approximately 5 days using the atmosphere detritiation system at full capacity.

Saturated molecular sieve beds in these detritiation systems are regenerated by a hot cell dedicated regeneration system. The recovered condensate from the regeneration system and the HVAC is sent to the tritiated water holding tanks system located in the tritium building in a manner similar to that for the tritium plant systems.

In order to reduce the generation rate of tritiated water from hot cell operation, minimization of the leakage rate in the building walls, doors and other penetrations is being investigated. The tentative estimate of water generation based on the present design parameters (room volume, leak tightness, humidity and temperatures) is ~ 0.3 m^3/d.

Water Detritiation System

During operation of ITER, tritiated water will be produced in various systems. The expected sources are:

(a) condensate generated from the normal operation of various atmosphere detritiation systems and HVACs,
(b) tritium process component maintenance,
(c) condensate from the air coolers in the containment volume (designed to limit overpressures from an ex-vessel coolant leak),
(d) air detritiation dryers in the containment volume,
(e) the tokamak cooling water system maintenance drain and the tokamak cooling water system vent gas condensate,
(f) in-vessel component maintenance drain collected in the hot cell, and
(g) condensate from the standby vent detritiation system and the standby atmosphere detritiation system operated during tritium contamination accidents.

The source water (a) - (d) will be processed by the water detritiation system to minimize tritium-bearing waste water to be rejected to the environment, whereas the water (e) and (f) is recycled to the tokamak cooling water system. The water (g) will be stored in the emergency holding sump tanks.

The source water will be stored in the holding tank system with the following level classification:

- H Level > 100 Ci/kg;
- M Level 10^{-3} Ci/kg – 100 Ci/kg;
- L Level 1.6×10^{-6} Ci/kg - 10^{-3} Ci/kg;
- LL Level < 1.6×10^{-6} Ci/kg for direct release after assaying;
- emergency holding sump tanks: total capacity 400 m^3

The high (H) level and the medium (M) level tanks receive condensate from the atmosphere detritiation systems and the local air coolers in the hot cell building and the tritium plant building, and the process blow-down water of the water detritiation system at maintenance. In case of an event leading to a large amount of tritium contamination, condensate produced by the standby atmosphere detritiation system and the standby vent detritiation system will be stored in either the H level or the emergency holding sump tanks. The low (L) level tanks receive drainage from tritium process equipment during its maintenance. The low low (LL) level tank receives water generated in the HVACs, and the water can be directly rejected to the environment after assaying the tritium concentration.

Figure 3.1-8 shows the outline flow diagram for the water detritiation system, but does not show the LL level or emergency holding sump tanks. Tritiated water sent from the holding tank system is purified by the front-end processing system composed of demineralizer and charcoal beds to remove hazardous ions and organic species to the catalytic exchange process and electrolysis. The purified water (tritium concentration < 10 Ci/kg) is then fed (~ 20 kg/h) either to the catalytic exchange towers (tritium feed concentration < ~ 10 Ci/kg) or to the electrolysers (tritium feed concentration ~ 100 – 500 Ci/kg). Pure water is fed (~ 20 kg/h) to the top of the catalytic exchange tower.

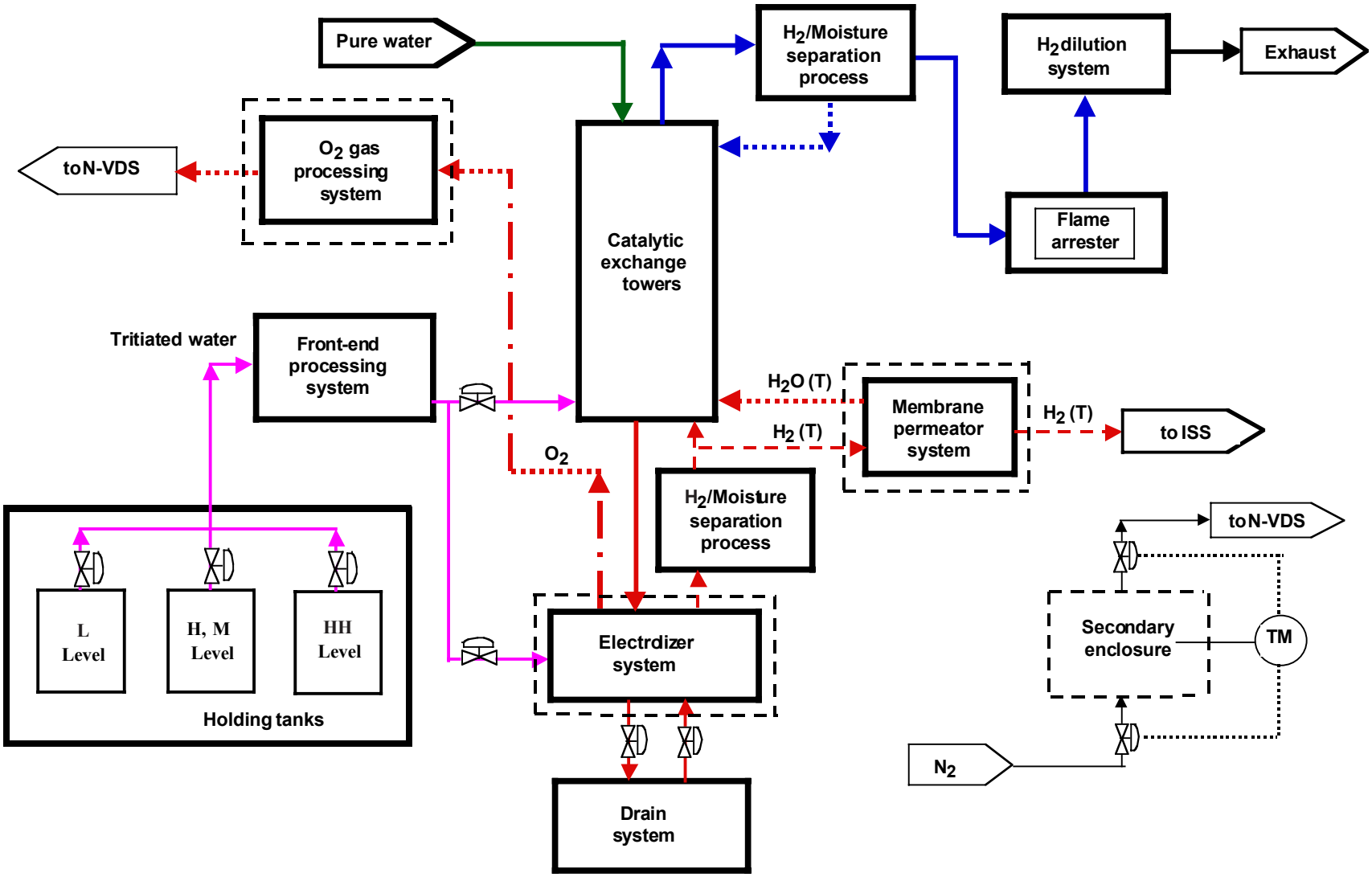

Figure 3.1-8 Block Flow Diagram for the Water Detritiation System

The catalytic exchange towers are composed of hydrophobic catalyst-packed sections and a hydrophilic-packing section (sieve tray). The isotopic exchange reactions taking place in each section are:

$HT\ (G) + H_2O\ (V) = H_2\ (G) + HTO\ (V)$: Hydrophobic catalyst section

$HTO\ (V) + H_2O\ (L) = H_2O\ (V) + HTO\ (L)$: Hydrophilic packing section

where, G, V and L in these equilibrium reactions mean gas, vapour and liquid phases, respectively.

Through these counter-current catalytic exchange reactions, tritium (T) is enriched in the water which is flowing to the bottom of the towers, and hydrogen gas which contains virtually no tritium is flowing to the top of the tower. The enriched water is then dissociated into hydrogen gas H_2 (T) and O_2 gas by the electrolysers. The H_2 (T) is returned to the bottom of the tower, and a part of the hydrogen gas stream (280 mol/h) is sent to the hydrogen isotope separation system to recover tritium via a membrane permeator system. The hydrogen stream from the top of the tower is rejected to the environment through the flame arrester. The O_2 stream from the electrolysers is sent to the normal vent detritiation system via the O_2 gas processing system composed of molecular sieve dryers.

The membrane permeator and molecular sieve dryer, which are operated at elevated temperature, and electrolysers, are placed in a secondary enclosure to avoid tritium leakage/permeation to the room. The atmosphere (dry N_2 gas) of the secondary enclosure is sent to the normal vent detritiation system with a small flow rate.

The water detritiation system can be operated with high availability (more than 300 days/year). Demineralizers and charcoal beds require frequent replacement (every two years), and the electrolyser, based on solid polymer electrodes, may need electrode replacement once per year due to expected deterioration caused by β-ray exposure from tritium-enriched water. A detailed maintenance procedure, which can handle components contaminated by highly concentrated tritiated water, has been developed and reflected in the water detritiation system design.

3.1.1.3 Design Integration

General

Components have been standardised across the whole tritium plant to the maximum extent consistent with the functional requirements of each application, in order to minimise the costs of spare parts and maintenance.

Process interconnections between systems located in different glove boxes consist of stainless steel piping/tubing within a secondary enclosure. The atmosphere of the secondary interspace will communicate with the secondary confinement volume of either the upstream or downstream system, and a bulkhead at the other end of the secondary jacket will ensure segmentation of these volumes as necessary.

Plant Layout

A detailed layout of the tritium plant in the building (which also houses other equipment, such as the roughing pump system and the HVAC systems for both the tritium plant and tokamak buildings) has been developed. The arrangement of the constituent process systems, together with their secondary confinements, and the infrastructure systems, has been optimised in terms of minimising the length of interconnections, and has taken into account provision of adequate space for operation and maintenance, incorporation of shielding (for some specific systems), separation of areas of the building into zones, assurance of satisfactory working conditions in all locations by the HVAC systems, and definition of access and escape routes. Analysis of the layout is essential to ensure that the functionality of the tritium confinement by the HVACs and the atmosphere detritiation system/vent detritiation system is maximised, and that the potential for and consequences of hydrogen deflagration/explosion are reduced to acceptable levels. The building design and locations of equipment within it enable the seismic response at the locations of critical components to be calculated, to serve as a basis for seismic analysis of components as necessary.

3.1.1.4 Performance Analysis/Design Integrity

The principal design features, which have been implemented to preclude or mitigate hazards common to multiple systems in the tritium plant, are reviewed briefly in the following.

Overpressure Protection

Pressurization from external systems is avoided by backflow prevention units in the supply lines which close at a pressure well below that needed. In addition, the feed gas pressures are limited by pressure relief valves in the respective systems.

Primary system vacuum pumps and compressors are equipped either with a relief valve which opens a bypass from the discharge side to the suction side of the pump, or with two redundant pressure transducers on the pump discharge which trip the pump at a preset pressure.

In systems operating at cryogenic temperatures, such as the isotope separation system and the glow discharge cleaning gas processing system, the dominant potential cause of over-pressurisation is a malfunction of the refrigerant supply, leading to regeneration of the

inventory, and/or failure of pipes or valves leading to plugging of gas exhaust lines. The protection against this is an expansion vessel downstream of a rupture disc. The rupture disc is designed to burst at a pressure below the system design pressure, and the expansion vessel is sized to accept the gas expanded from the process system under the most severe combination of inventory and warm-up postulated.

Over-temperature Protection

Each heater is thyristor-controlled and the temperature of adjacent components monitored by thermocouples, which causes the programmable logic controller (PLC) to give a warning at high/low deviations from the set point. If the temperature reaches a second set point closer to the design temperature, the heater is tripped and an alarm given by the PLC.

In parallel, other thermocouples give a warning if the temperature is above a certain level. Heater trip and alarm functions are redundant for the above-mentioned thermocouples.

The readings of the two thermocouples are continuously compared by a virtual instrument in order to detect any off-normal condition in either of them.

Tritium Permeation Mitigation

Heated components in the fuel cycle subsystems such as permeators and catalytic reactors, in which the working tritium inventory exceeds 1 g, are equipped with internal thermal shields and a vacuum jacket which is held at close to ambient temperature at which no measurable hydrogen permeation occurs. The evacuated interspace allows confinement and recovery of tritium which has permeated through the primary vessel wall. The presence of permeated gas can be detected either by pressure monitors in the interspace, or by a deterioration in the thermal insulation performance of the vacuum interspace, which can then be pumped out and the gas returned to the primary circuit.

Redundancy/Diversity

The system design embodies no redundant components for the purpose of enhancing availability. Due to the fact that, wherever possible, commercially available components are employed, a certain margin of over-capacity exists in some systems, which will mitigate short-term failures or unavailability of components. The control system incorporates redundant and, where possible, diverse components and cable routes in order to provide a fully independent hard-wired alarm and emergency shut-down function.

3.1.2 Assessment

3.1.2.1 Fuel Cycle Subsystems Design

The design of the fuel cycle subsystems is based on either well-proven processes and components, or on comprehensive R&D carried out at near ITER scale over the full range of anticipated parameters.

The storage and delivery system utilizes ZrCo as the metal hydriding material. This has been tested under the full range of operating conditions to ensure that the potential drawbacks of this material will not compromise performance. Combinations of pressure and temperature

under which disproportionation can occur can be avoided, and even if under upset conditions this took place, the getter material can be reproportionated at moderate temperatures (450°C). The tendency for deviations in isotopic composition as the beds deliver gas has been demonstrated to be acceptable (within ~ 2%). Determination of in-bed tritium inventories can be made by calorimetry with an accuracy of 3% within a working shift and to within 1% over longer periods. The capability of the reference-bed design to maintain required delivery rates (20 Pam^3s^{-1} per bed) consistent with ITER fuelling scenarios over extended ranges of bed-loading fractions should be demonstrated with a full-scale prototype, in order to confirm the results of laboratory tests with a 1/5 scale unit.

The mechanical integrity of Pd/Ag membrane permeators used in the tokamak exhaust processing system (and other systems) has been demonstrated at representative tritium and impurity concentrations over operating periods of several years. The poisoning effects (in presence of CO) have been shown to be fully reversible. System optimization studies, supported by R&D on the overall detritiation achievable by the tokamak exhaust processing system[1], have enabled permeator pumping requirements to be considerably reduced compared with earlier designs. The design of the impurity processing module has been simplified by combining the reactors for cracking (for hydrocarbons) and shift reactions (for water), and by the adoption of a single catalyst (nickel on kieselguhr, a naturally occurring material used as a catalyst carrier) for all duties (chemical and isotope exchange reactions) throughout the tokamak exhaust processing system. The evolution of the design into an essentially once-through process has contributed to a reduction in tritium inventory and improvement in detritiation performance (by maintaining nearly constant isotopic compositions at specific locations within the system, thereby minimizing memory effects). The ability of the process to achieve the required detritiation factor of 10^8 with a reasonable margin in steady state has been proven. Further tests are required to confirm the performance over the full range of operating conditions.

The process used for separation of the impurities from the circulating He during glow discharge cleaning (trapping on cryogenic molecular sieve beds) is well-established technology.

Hydrogen isotope separation by cryogenic distillation has been demonstrated under steady-state conditions in fission applications and by R&D over many years. For ITER, recent R&D has focussed on tritium inventory minimization by the selection of optimized column packing materials and operating conditions. A consensus has been reached on the database to be used for design and safety analysis, and the tritium inventory of the whole system has been reduced by refinement of the column sizes and detailed design improvements of other components. R&D to demonstrate that the design is capable of handling the expected rapid fluctuations in feed compositions and flow rates has been successfully completed. The development of steady state and dynamic simulation computer codes has enabled design calculations and R&D results to be benchmarked against each other.

Advances in the development of analytical techniques have been incorporated in the design for the tritium plant analytical system. Substantial progress in micro-gas-chromatography performance enables quantitative measurements in ~ 60 s for hydrogen isotope mixtures and ~ 160 s for impurity mixtures to be achieved with very small samples, in the nanolitre range.

[1] H. Yoshida et al., “ITER R&D Auxiliary Systems”, Fus. Eng. Design 55 (2001), pp 313-323

Developments in laser Raman spectroscopy include the application of an external resonator which enables quantitative analysis of hydrogen isotope mixtures to be carried out. This technique is proposed for periodic calibration of the on-line pressure and temperature measurement techniques used for the product quality control of the isotope separation system.

The layout of tritium plant systems within the building has been reviewed to ensure that all requirements for space, access, and environmental conditions are met. The effect of the equipment on the building design such as mechanical loads and heat dissipation requirements, have been taken into account. Access routes for the introduction of deferred equipment and for the replacement and removal of components during maintenance and routine operations, such as the import of tritium transport containers, have been checked. The design of the building is conventional, and consistent with the practice followed at existing tritium laboratories, upgraded where necessary to provide additional features such as shielding capability.

The distributed control system with PLCs and a hardwired system for alarm and emergency shut-down developed for the ITER tritium plant (Figure 3.1-9) is consistent with systems currently in operation in tritium laboratories. It is to be expected that advances in system and hardware design will occur prior to the implementation of the ITER tritium plant and these will be reviewed and adopted where appropriate.

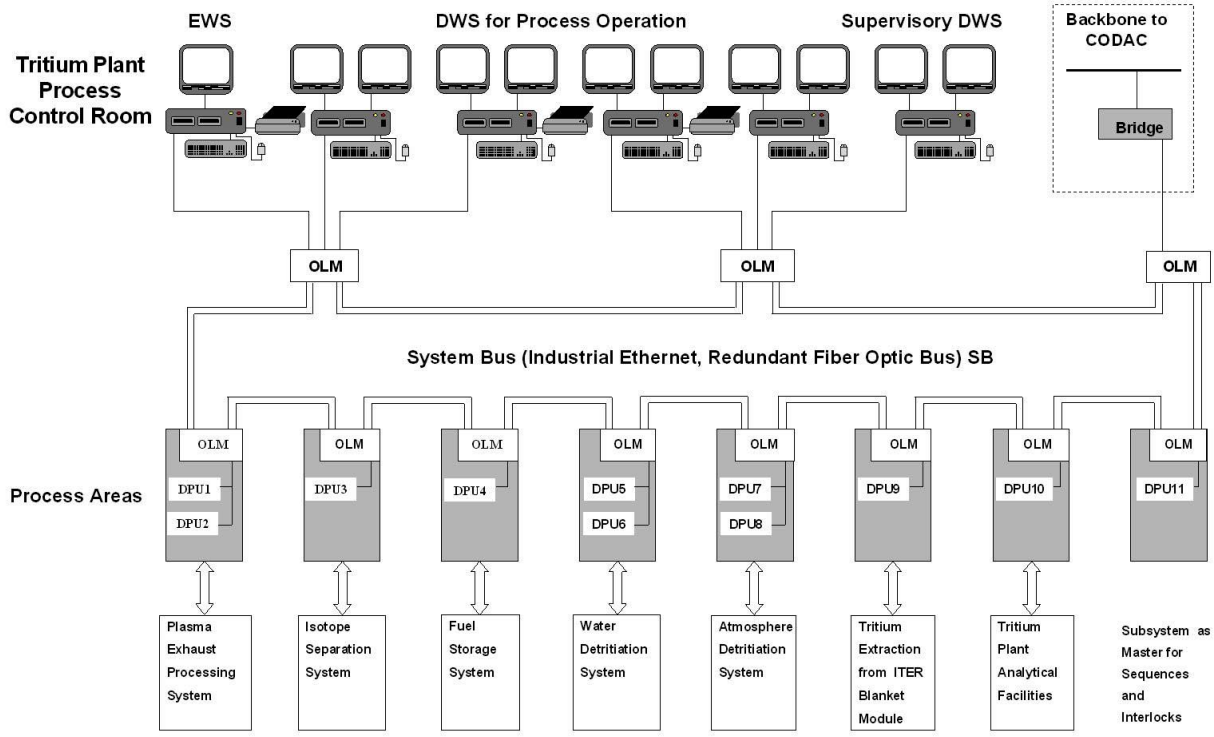

Figure 3.1-9 Tritium Plant Automated Control System Configuration
DWS: Display Work Station, EWS: Engineers' Work Station
OLM: Optical Link Module, DPU: Distributed Process Unit

3.1.2.2 Development of Tokamak Fuel Cycle System Dynamic Simulation Code

The fuel cycle dynamic simulation code CFTSIM[1] was developed during the ITER EDA through a design task. This code provides an integrated dynamic simulation of the ITER fuel cycle. It presents the user with a graphical representation of the ITER tritium plant. The code models the ITER fuel cycle pathways for deuterium and tritium, including the following system models, in varying degrees of detail.

(i) Fuelling System Model (Storage and Delivery System Model);
(ii) Co-deposited Layer Dust Model;
(iii) First Wall Model;
(iv) Tokamak Model;
(v) Tokamak Chamber Model;
(vi) Tokamak Exhaust Processing System Model;
(vii) Hydrogen Isotope Separation System Models;
(viii) Neutral Beam Injectors Model.

3.1.2.3 Analysis of the Tritium Inventory Dynamics for DT Pulsed Plasma Operations

For the purpose of design improvement in the interfaces between the SDS, TEP and ISS, a series of preliminary studies of the tritium inventory dynamics were implemented by using the CFTSIM code. The following cases of DT plasma operation were selected as being representative of the plasma operation:

(i) short DT pulse operation (450 s burn, 1,350 s dwell) with 200 Pam^3/s total fuelling flow rate (deep fuelling 50 $Pam^3s^{-1}T_2$, shallow fuelling 100 Pam^3/s DT + 44.5 Pam^3/s D_2 + 5.5 Pam^3/s T_2);
(ii) long DT pulse operation (3,000 s burn, 9,000 s dwell) with 200 Pam^3/s total fuelling flow rate (deep fuelling 50 Pam^3/s T_2, shallow fuelling 100 Pam^3/s DT + 44.5 Pam^3/s D_2 + 5.5 Pam^3/s T_2). Table 1-7 summarizes the input parameters selected for these representative cases.

Figures 3.1-10 (a) and (b) show the results of the tritium inventory dynamics over five repetitive pulses. In the present preliminary analysis, the entire column cascade of the ISS was started up with pure D_2 gas immediately after receiving the feed stream (tokamak exhaust stream) via the front-end permeator. The time to establish steady-state concentration profiles of the 6 possible hydrogen isotope mixtures (permutations of H, D and T) in cascade, will require a distillation time of 1,000 s or more.

The total tritium inventory shown in these figures does not include the following inventory elements:

(i) tritiated impurities trapped in the torus cryo-pump during the five pulses;
(ii) tritium trapped by the plasma-facing components, and co-deposited material in the vacuum vessel;
(iii) tritiated impurities processing in the tokamak exhaust processing unit.

[1] A. Busigin and P. Gierszewski, "CFTSIM-ITER dynamic fuel cycle model", Fus. Eng. Design 39-40 (1999), p 909

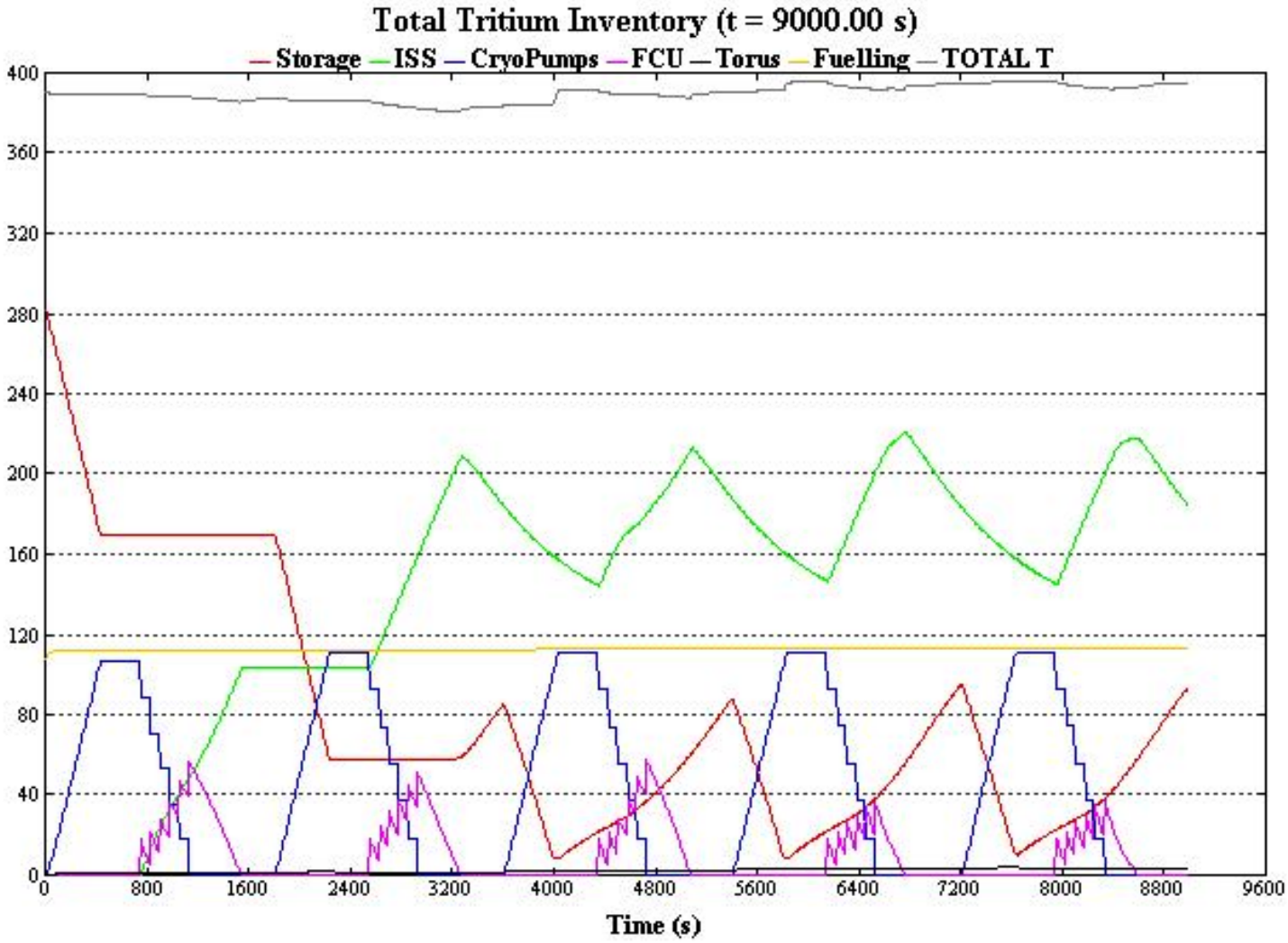

Figure 3.1-10 (a) Tritium Inventory Dynamics in the Fuel Cycle Systems (for Short DT Pulses)

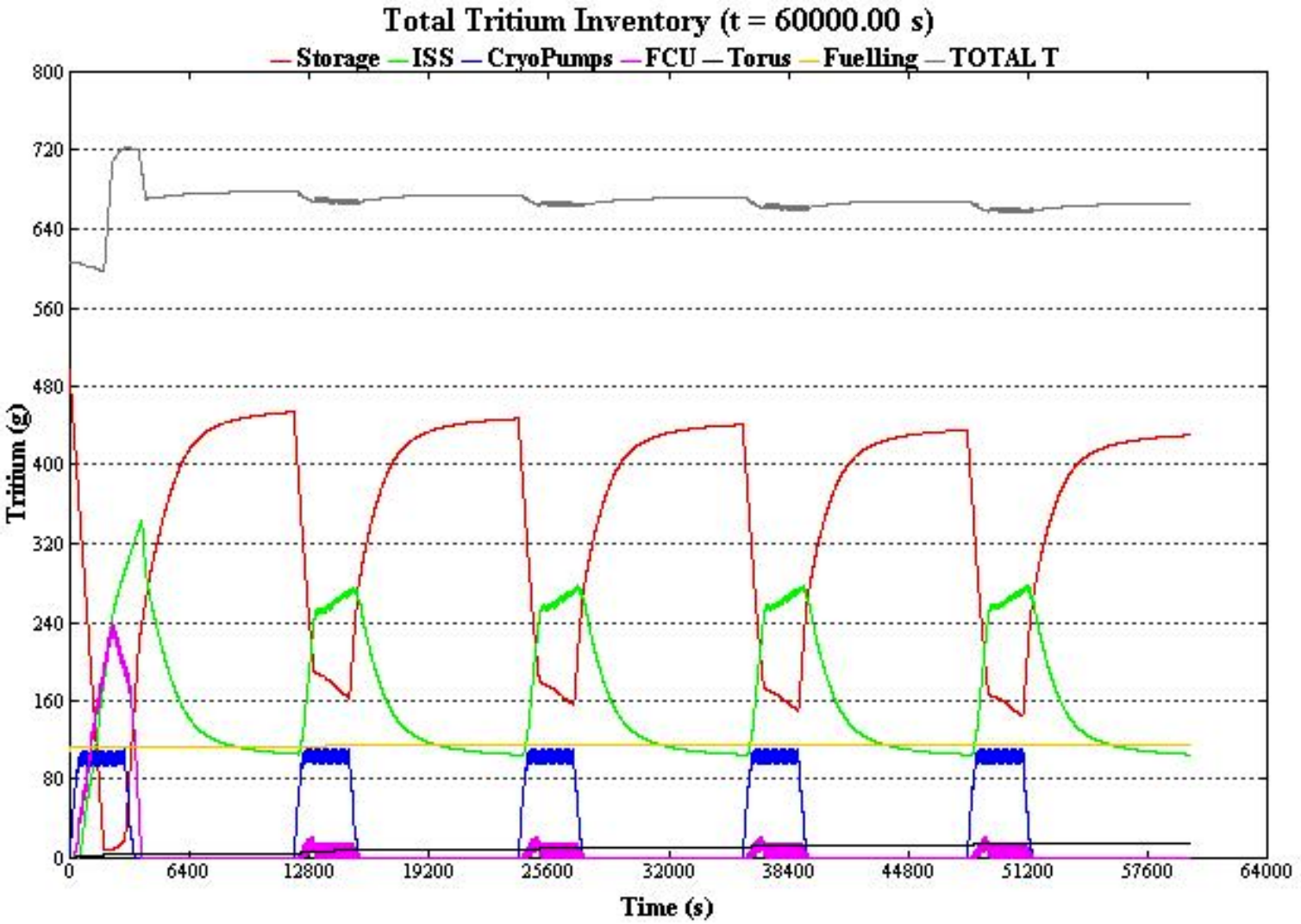

Figure 3.1-10 (b) Tritium Inventory Dynamics in the Fuel Cycle Systems (for Long DT Pulses)

3.1.2.4 Tritium Confinement and Detritiation Subsystems

HVAC

Because of their functional requirements during off-normal events in the tokamak, tritium, hot cell and radwaste buildings, the HVAC systems are safety classified systems – therefore there are two emergency room isolation dampers (high leak tightness butterfly valves) in series backed up by emergency power and/or emergency compressed gas (N_2). However, all HVAC equipment such as blowers, heating and cooling coils, pre-filters and HEPA (high efficiency particulate) filters, emergency isolation dampers, and fire isolation dampers are industrial items, and no specific R&D has been required for their use in ITER.

Atmosphere Detritiation Systems

As described in 3.1.1.2, different atmosphere detritiation systems are employed to meet the confinement and detritiation requirements at different operation states of the tokamak, tritium, hot cell and radwaste buildings. The process configurations of these atmosphere detritiation systems are different, based on the confinement strategy and safety requirements (off-normal event scenarios).

Figure 3.1-11 shows a conceptual process flow diagram of the standby atmosphere detritiation system, which is a typical safety classified atmosphere detritiation system similar to the normal vent detritiation system, standby vent detritiation system, hot cell atmosphere detritiation system and the hot cell vent detritiation system. The standby atmosphere detritiation system is designed to process various tritiated source gases containing high levels of elemental tritium, tritiated hydrocarbons, and saturated moisture. The process configuration is characterised by the three loops described below.

a) Recombiner loop composed of inlet filter (F-1), inlet blower battery (BL1-A/B/C: 50% capacity/each blower; one blower is redundant), two stage recombiners (Rec-L, Rec-H), two stage recuperative heat exchangers (HX-1, HX-2), one stage electric heater (EH-1), one stage condenser (CX-1), and one stage molecular sieve dryer bed battery (DX-A/B/C). Elemental tritium included in the source gas/air is catalytically converted (conversion factor > 10^4) into tritiated water molecules by the first stage recombiner (operating temperature 150°C), and tritiated organic species are oxidised (conversion factor > 10^3) to tritiated water molecules and CO_2 by the second stage recombiner (operating temperature 500°C). The converted tritiated water molecules are adsorbed by the molecular sieve dryer bed. Thus, overall tritium permeation through vessel walls and pipe lines in the recombiner loop can be minimised by the two stage recombiner configuration. This configuration was selected as an essential design feature to process tritiated source gases containing elemental tritium and organic tritium. The glove box atmosphere detritiation system process uses only a one stage recombiner (operating temperature 150°C) because the expected tritiated species in the glove box atmosphere are elemental tritium and tritiated moisture (HTO).

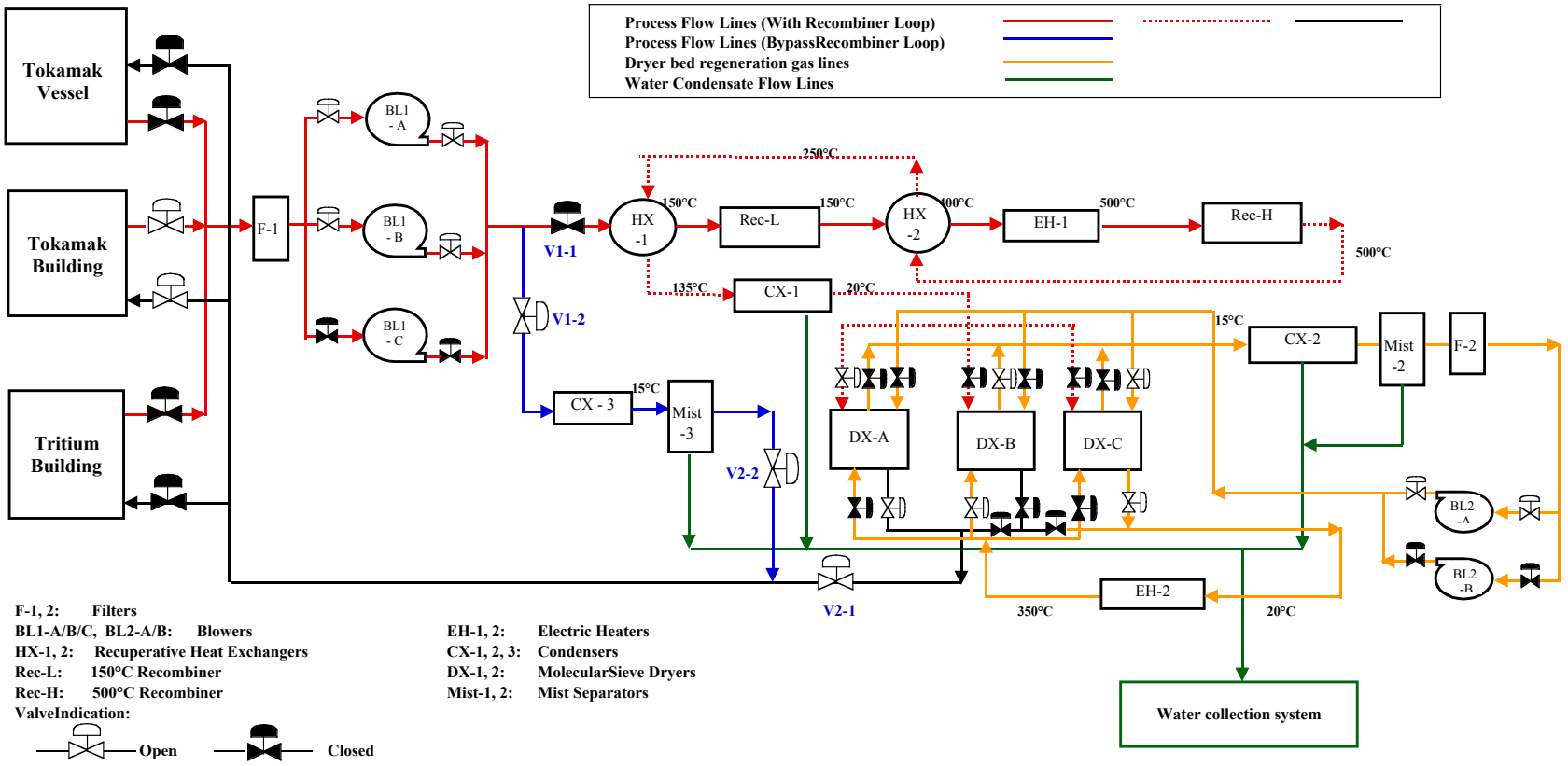

Figure 3.1-11 Conceptual Process Flow Diagram of the Standby Atmosphere Detritiation System

(b) Molecular sieve dryer regeneration loop composed of regeneration gas heater (EH-2), dryer bed cross-over valve headers, one stage condenser (CX-2), mist separator (Mis-2), filter (F-2) and blower battery (BL2-A/B). Tritiated water produced in the recombiner loops and/or included in the source gas/air is adsorbed by the dryer bed. When the decontamination factor (DF) defined by the tritium concentration ratio between inlet and outlet streams around the dryer is > 100 (design value $10^2 – 10^4$), the saturated dryer bed is then switched to the regeneration mode.

(c) Direct condensing loop composed of a one-stage condenser (CX-3) and mist separator (Mist-3). In case humidity in the source gas/air is very high or saturated, this bypass loop is started for direct condensing of the moisture, and the recombiner loop is isolated until the room moisture level is reduced to an acceptable level for the standby atmosphere detritiation system dryer bed battery capacity.

The use of the direct condensing loop is an important design feature which results in a large reduction of water load on the molecular sieve dryer regeneration loop.

All atmosphere detritiation systems utilise proven technology and components such as canned type blowers, recuperative gas/gas heat exchangers, gas/water heat exchangers, electrical gas heaters, catalytic recombiners and molecular sieve dryer beds.

The design value of the detritiation factor of these atmosphere detritiation systems (glove box atmosphere detritiation system > 10^2; standby atmosphere detritiation system > 10^3; normal vent detritiation system, standby vent detritiation system > 10^4) has been well proven in the existing tritium facilities, and no further R&D is required.

Common Dryer Regeneration System

It is expected that the usage of dryer regeneration systems, which is required for all atmosphere detritiation systems, will be very low for the standby detritiation systems (S-VDS, S-ADS). To maximize the effective usage of the dryer regeneration system, a common dryer regeneration system was employed for ITER instead of a distributed regeneration system in each detritiation system. A similar design (use of common regeneration system) was applied to the atmosphere detritiation systems located in the hot cell building.

Water Detritiation System

The water detritiation system selected for ITER is based on the existing plant technology using catalytic exchange towers and electrolysers, which has been operated over 13 years in a Japanese fission reactor. The advantages of the plant technology are compact size due to its very high separation efficiency, no production of tritium-bearing waste water due to a complete decomposition of the water into molecular hydrogen and oxygen, and operation flexibility over a wide range of tritium concentration (1 mCi/kg – 500 Ci/kg) by the combination of a tritium-scavenging catalytic exchange process with tritiated water electrolysis. The long-term operation of the existing plant has indicated that tritium levels in the exhaust hydrogen stream can be directly rejected to the environment with suitable air dilution to meet the deflagration limit (1 vol% in air).

3.2 Cryoplant and Cryodistribution

3.2.1 System Description

One of the key requirements for the cryogenic system is to operate in a steady state cooling mode as is usual for conventional large cryogenic plants. However, the heat load of the magnet system is largely deposited in pulses due to magnetic field variation, DT neutron production, etc. Each of plasma scenarios results in different nuclear and other heat loads and consequently the liquid He (LHe) plant must be able to cope with varying ratios of refrigeration to liquefaction capacity as well as with different total plant loads. The smoothing of the pulsed heat load, the maintenance of stable operation over the wide range of plasma scenarios, as well as cost minimisation by using standardised components, are the main guidelines for the design of the ITER cryogenic system.

The ITER cryogenic system is subdivided into three parts: the cryoplant, the cryodistribution system and the system of cryogenic lines and manifolds.

3.2.1.1 Cryoplant

The principal process and flow diagram of the cryoplant is shown in Figure 3.2.1.1-1. The cryoplant equipment includes the following components:

- four identical cold process boxes of the LHe plant;
- helium gas compression station of the LHe plant;
- external He gas purification unit;
- 1.8 MPa warm (300K) and 80K tanks for storing the gaseous He;
- two identical 80K He cold boxes linked to two identical liquid nitrogen (LN_2) auxiliary cold boxes for final cooling of the He flow to 80K;
- helium gas compression station of the 80K He loop;
- LN2 subsystem with two identical cold process boxes and LN_2 storage;
- nitrogen gas compression station.

The cryoplant equipment is located in two buildings: the cryoplant compressor building and the cryoplant cold box building (see Figure 3.2.1.1-2). The compressor building houses all the warm compressors for the LHe plant, the liquid nitrogen (LN_2) subsystem and the 80K He loop as well as the He and N_2 gas dryers. All cold boxes of the LHe plant, the LN_2

N 34 GR 20 00-12-22 F 1

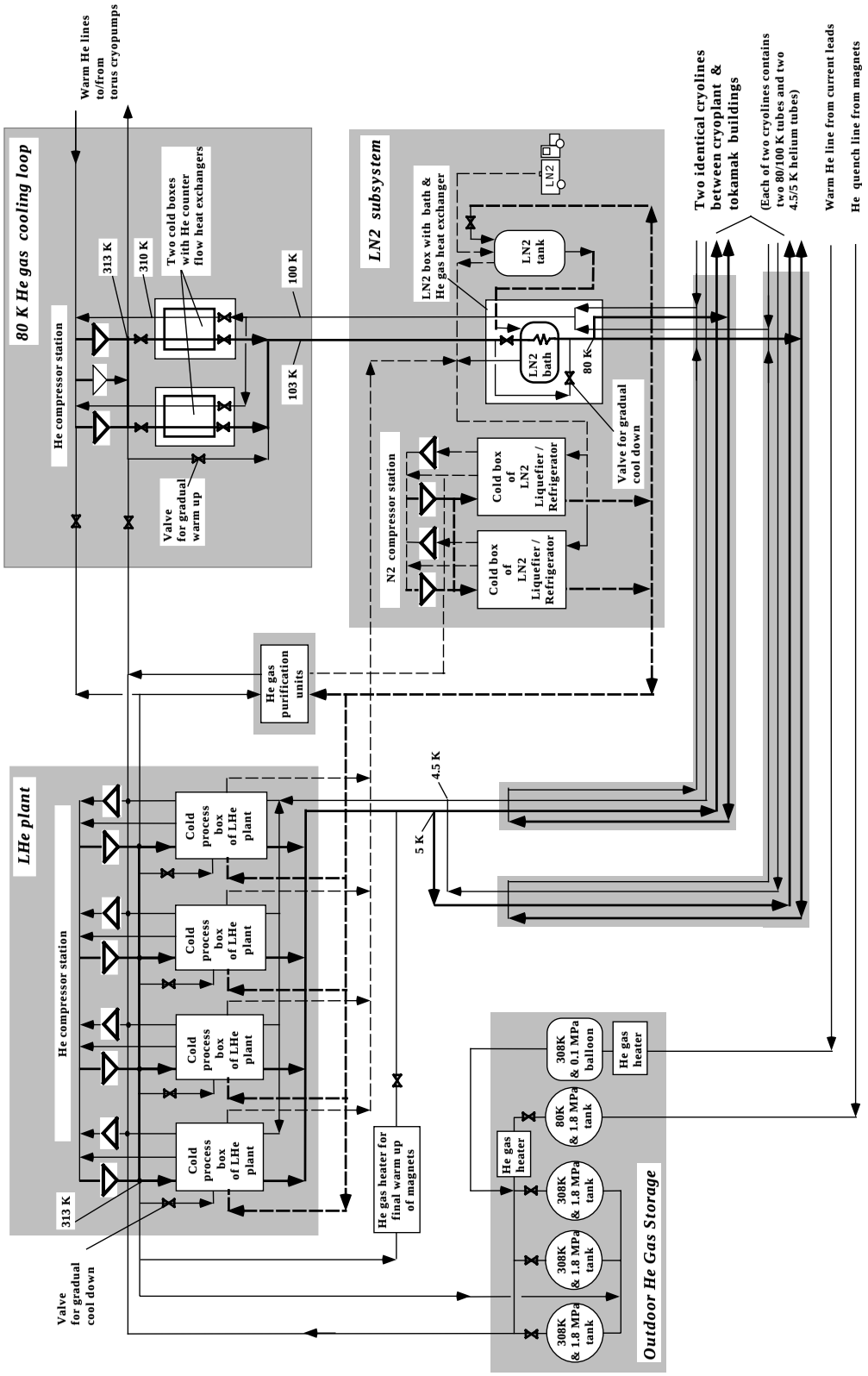

Figure 3.2.1.1-1 Process Principles and Flow Diagram of ITER Cryoplant

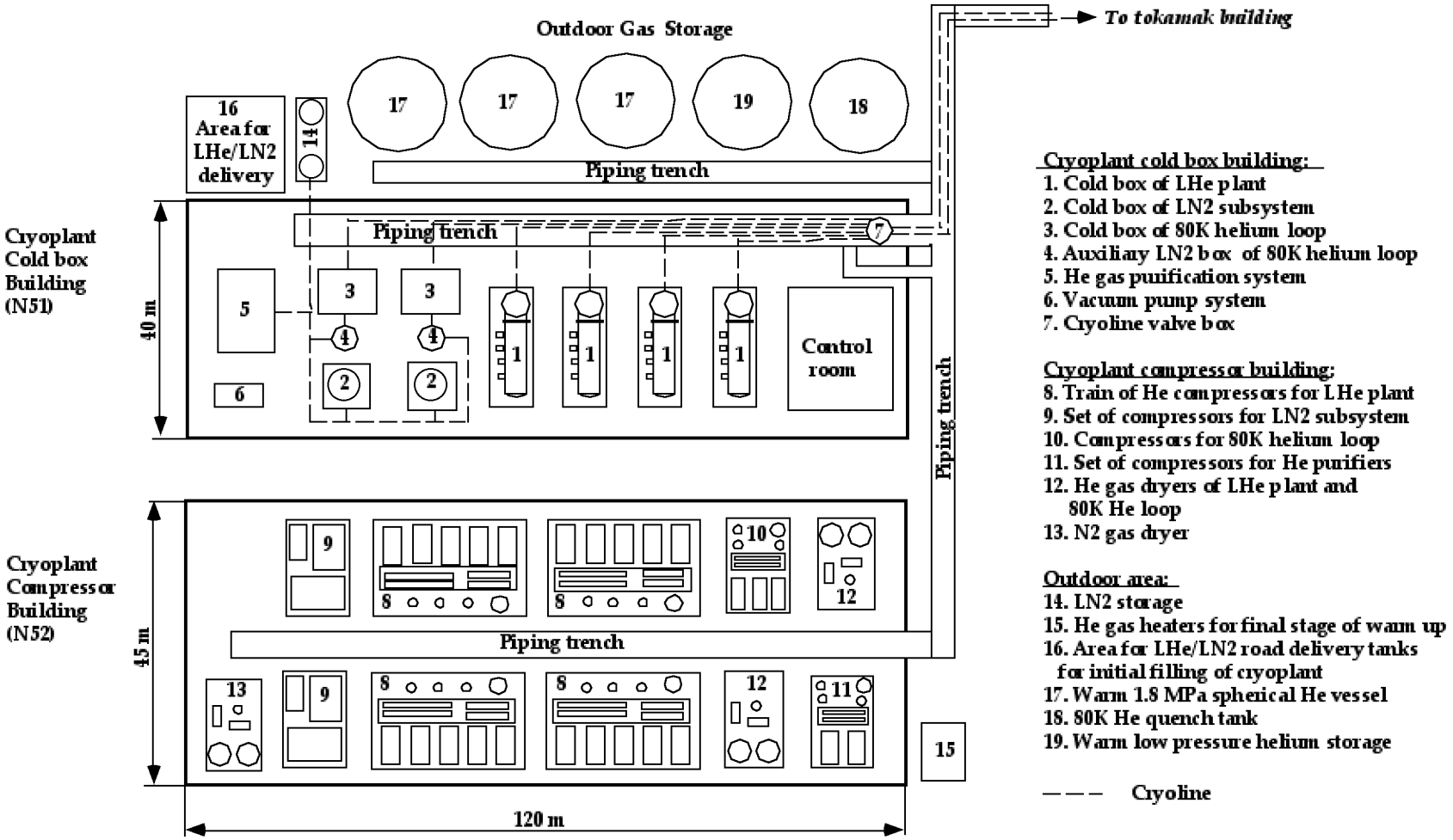

Cryoplant cold box building:
1. Cold box of LHe plant
2. Cold box of LN2 subsystem
3. Cold box of 80K helium loop
4. Auxiliary LN2 box of 80K helium loop
5. He gas puification system
6. Vacuum pump system
7. Cryoline valve box

Cryoplant compressor building:
8. Train of He compressors for LHe plant
9. Set of compressors for LN2 subsystem
10. Compressors for 80K helium loop
11. Set of compressors for He purifiers
12. He gas dryers of LHe plant and 80K He loop
13. N2 gas dryer

Outdoor area:
14. LN2 storage
15. He gas heaters for final stage of warm up
16. Area for LHe/LN2 road delivery tanks for initial filling of cryoplant
17. Warm 1.8 MPa spherical He vessel
18. 80K He quench tank
19. Warm low pressure helium storage

– – – Cryoline

N 34 GR 21 00-12-22 F 1

Figure 3.2.1.1-2 ITER Cryoplant Layout

subsystem, the 80K He cooling loop, and He gas purification unit, are installed in the cryoplant cold box building. The external dual-operated purification unit is incorporated in the LHe plant to allow continuous processing during normal operation of about 5% of the total mass flow rate produced by the He gas compressor station. The capacity of the He purification system is also available for cleaning the gaseous He from all the ITER cryogenic components within 7 days before starting the cool-down of the tokamak.

Three 1.8 MPa warm He tanks, one 80K He quench tank, a low pressure He balloon, and liquid nitrogen tanks, are placed in an outside area, adjacent to the cryoplant cold box building. The 1.8 MPa warm He tanks are used to store the He inventory of the cryogenic components of ITER after machine warm-up. The cold 1.8 MPa tank is needed for expelling cold He from the TF coils during fast energy discharge (see 3.2.3.3).

Two 25 m^3 LHe tanks are used for storing LHe when the plasma pulsing allows an accumulation of LHe. These tanks are installed in the main tokamak building.

All cryoplant components are of a high industrial quality standard and are chosen from industrially proven technology.

3.2.1.2 LHe Plant

The heat loads for the different components of the ITER machine are summarised in Table 3.2.1.2-1. The design point of the LHe plant is 43.2 kW of refrigeration plus 0.17 kg/s of liquefaction to satisfy the nominal plasma pulsing with 1,800 s plasma repetition time and 400 s burn at 100 % availability for plasma pulsing.

The total refrigeration capacity of the LHe plant includes both the heat load deposited in the different ITER components and an additional heat load associated with the work of He circulating pumps and cold compressors.

Table 3.2.1.2-1 Total Heat Load Requirements of the LHe Plant

Liquefaction to cool the current leads	kg/s	0.1
Static heat load to the magnet system	kW	11.8
Averaged pulsed heat load to the magnet system	kW	10.9
Heat load of the He circulating pumps[1]	kW	11.4
Heat load of the cold compressors[2]	kW	4.3
Torus and other cryopumps, including liquefaction for cool-down during their regeneration	kW/kgs^{-1}	4/0.07
Small cryogen users[3]	kW	0.8
Total	43.2 kW + 0.17 kgs-1	

[1] The requirements on each He pump are shown in Table 3.2.1.4-1.
[2] The cold He compressors operate at 4.3K for cooling the magnet system.
[3] NB injector system, the pellet fueling system and the EC H&CD gyrotrons.

The largest cryogenic user is the magnet system that includes the 18 TF coils, the CS, 6 PF coils together with the correction coils (CCs) and the magnet mechanical structures (MS). Liquefaction capacity of 0.1 kg/s is required for cooling the coil current leads. The heat load deposited in the magnet system includes both the static loads due to thermal radiation from 80K shields, and the thermal conduction through gravity supports, as well as the averaged value of the large pulsed heat loads of electromagnetic losses and nuclear heating. The

electromagnetic losses and nuclear heating are intrinsically pulsed heat loads and the ITER cryogenic system is designed to smooth this pulsed heat load to enable steady state operation of the LHe plant (see 3.2.3.1).

Another large cryogenic user is the tokamak vacuum pumping system that includes the 10 cryopumps of the torus primary vacuum system, the 4 cryopumps of the neutral beam injector system and the 2 cryopumps of the cryostat. The mean value of the liquefaction capacity for the fast cool-down of the torus cryopumps together with the total refrigeration load and work of the circulating He pump of other cryopumps is shown in Table 3.2.1.2-1.

The LHe plant consists of four identical LHe process modules each of the equivalent refrigeration capacity of 18 kW. The unit size of 18 kW is used in CERN and therefore is within the current manufacturing technology base.

3.2.1.3 80K He Loop and LN_2 Subsystem

An 80K flow of compressed He is used for the active cooling of the 80K thermal shields of the ITER machine. For nominal operation, the He temperature at the inlet and outlet of the shields is 80K and 100K respectively. Liquid nitrogen is used for pre-cooling He to 80K for the thermal shields.

The LN_2 production subsystem together with the 80K He loop provides for cooling the following ITER components:

- VV and other 80K thermal shields inside the cryostat;
- gravity supports of the magnet system and the VV;
- 80K chevron baffles and thermal shields of the cryopumps;
- 80K thermal shields of all cryogenic transfer lines and cryo-manifolds;
- pre-cooling the He to 80K as required for the cryogenic cycle of the LHe plant;
- external He purification unit.

The cooling scheme of the 80K He loop together with the LN_2 subsystem and the LHe plant is shown in Figure 3.2.1.1-1. The 80K He cooling loop includes two identical cold He boxes and two LN_2 auxiliary cold boxes. If one 80K He box or LN_2 auxiliary box is removed from service, another box will cool the thermal shields with a higher outlet temperature of 120K. This design provides a very high level of reliability for keeping the magnet system at low temperature despite some malfunction in the cryoplant.

Each 80K He box contains a counter flow He heat exchanger (HX) for cooling the supply He flow from 310K to about 103K by a return He flow heated from 100K to 307K. The temperature difference between the supply and return He flows of this HX is 3K. Final cooling of the He flow from 103K to 80K occurs in the LN_2 auxiliary cold box.

The heat loads of the 80K He loop for the nominal operation and baking of the VV together with requirements for the LN_2 supply are summarised in Table 3.2.1.3-1.

Table 3.2.1.3-1 Heat Loads on the LN_2 Subsystem (kW)

Components	Normal operation	VV baking
Thermal shields and gravity supports of the tokamak	385	740
Thermal shields of all cryogenic lines	50	50
Thermal shielding of cryopumps	180	60
LN_2 for supplying the LHe plant	280	70
Total heat load of different components	895	930
Total cooling capacity of the LN_2 refrigerators	987	1,000

The LN_2 subsystem operates close to the refrigeration mode. Two LN_2 refrigeration units each of 450 kW are incorporated in the cryoplant. These units are of conventional design, such as used in air separation plants. The LN_2 subsystem includes also two LN_2 tanks (see Figure 3.2.1.1-2), each of 50 m^3, to improve operation flexibility of the cryoplant.

3.2.1.4 Cryodistribution System

The principal process and flow diagram of the cryodistribution system is shown in Figure 3.2.1.4-1. The cryodistribution system provides forced flow cooling of the magnet system and cryopumps by using cold circulating pumps. These pumps are able to deliver circulation of large He flows in the ITER cryogenic components that are much higher than the He flow produced by the LHe plant itself. The cold circulating pumps of the ITER machine are located in five separate auxiliary cold boxes (ACBs). A typical ACB for the magnet system is shown in Figure 3.2.2.3-1.

The cryodistribution system contains also two identical cryoplant termination cold boxes (CTCBs) that are required for final cooling of the supercritical He (SHe) flow of the coil current leads to 4.6K.

Cold compressors are incorporated in the cryodistribution system for maintaining a temperature of 4.3K in the boiling He baths of all the ACBs of the magnet system. These compressors are located in a cold compressor box (CCB).

All cold boxes of the cryodistribution system are installed inside the main tokamak building, as shown in Figure 3.2.1.4-2. Each ACB is connected through long cryolines and ring cryogenic manifolds with several cold termination boxes (CTB) or cold valve boxes (CVBs) of each individual cryogenic ITER user. These CTBs and CVBs are not part of the cryodistribution system and belong to the individual cryogenic user system.

The principle arrangement of a typical ACB of the magnet system is described in 3.2.2.3. Each ACB contains two circulating pumps. Using two pumps for each ACB provides redundancy against pump failure. Since each pump will be equipped with variable speed motor and be operated at 50% of its full capacity, the nominal He flow rate can be maintained when one of the two pumps is suddenly stopped, or can be minimised when the plasma experiments allow reduced pump parameters.

The He mass flow rate and pressure drop requirements for the He circulating pumps and cold compressors as well as the heat loads on the heat exchanger of each ACB are summarised in Table 3.2.1.4-1.

N 34 GR 22 00-12-22 F 1

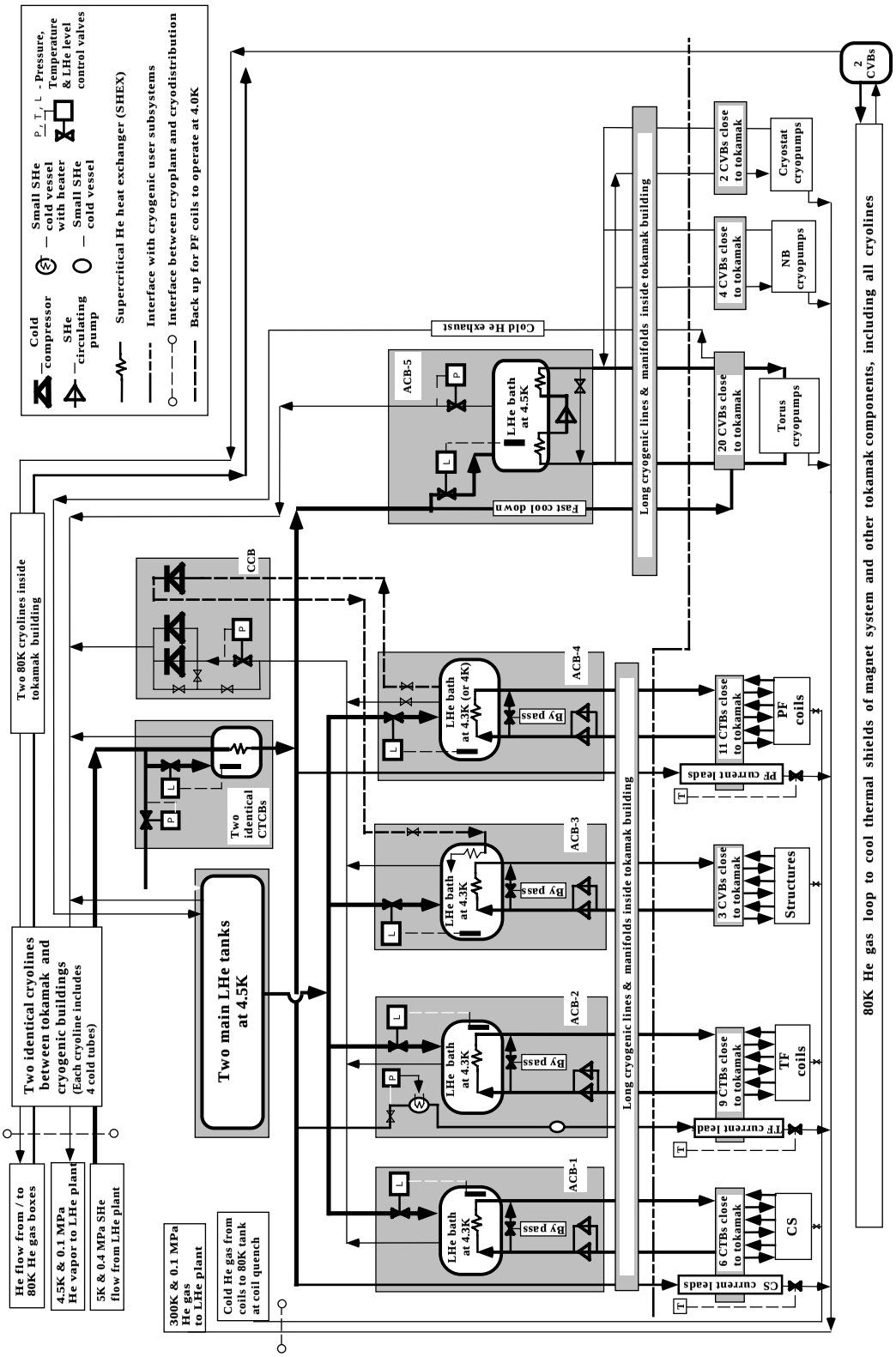

Figure 3.2.1.4-1 Process Principles and Flow Diagram of ITER Cryodistribution System

N 34 GR 23 00-12-22 F 1

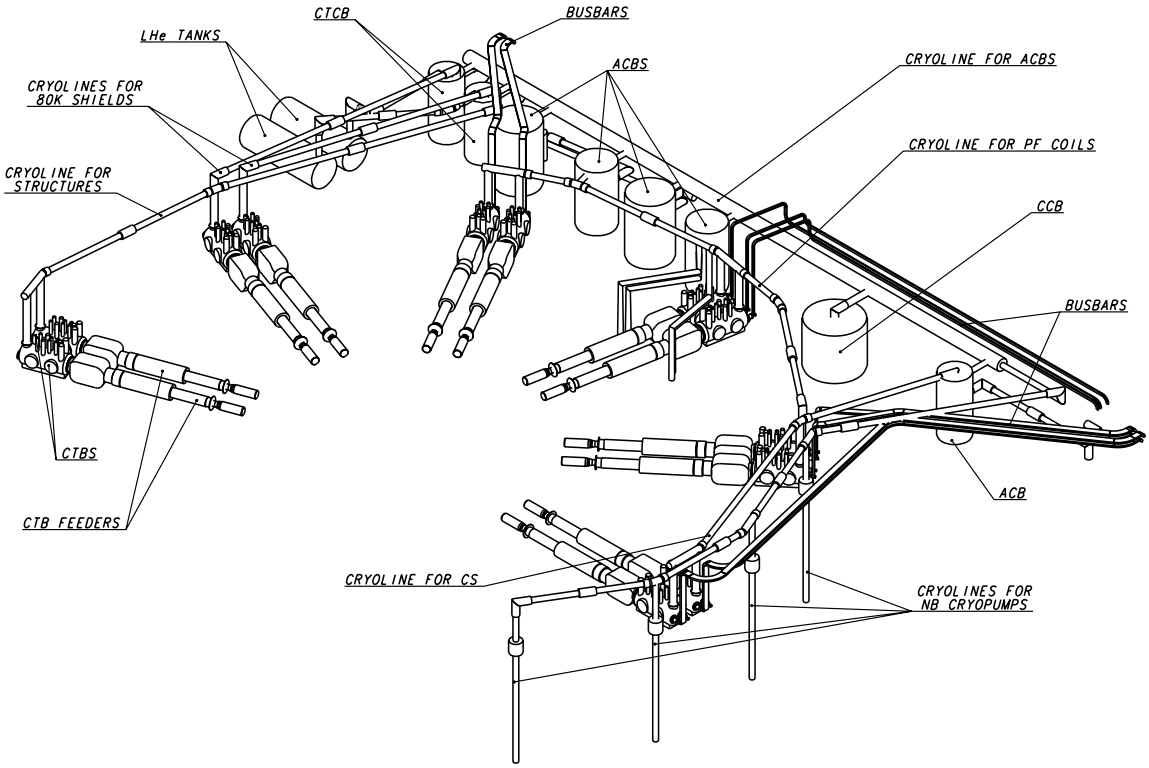

Figure 3.2.1.4-2 Isometrical View of Cryodistribution Boxes and Cryolines at the Upper CTB Level of the Tokamak Building

Table 3.2.1.4-1 Requirements for Cold Pumps and Compressors

	He flow (kg/s)	Pressure drop (MPa)	Work of pump (kW)	Heat load on heat exchanger of ACB (kW)
Pumps of TF Cases and Structures	4.5	0.04	2.0	12.6
Pumps of TF Coil Winding Packs	3	0.12	5.0	12.4
Pumps of PF and Correction Coils	2	0.1	2.2	4.5
Pumps of Central Solenoid	2	0.1	2.2	5.4
Pump of Torus Cryopumps	2.1	0.07	1.7	4.0
Cold Compressors	2.0	0.03	4.3	--------

One type of large capacity pump with variable motor speed has been designed. The design point is 1.5 kg/s and 0.12 MPa. The design efficiency of the pump is 0.8.

Cold compressors with variable motor speed have been designed to operate with the magnet system. The cold compressors compress the 4.3K He vapour from the saturated pressure of 0.1055 MPa to 0.1355 MPa that is equivalent to the saturated He temperature of 4.5K.

3.2.1.5 System of Cryogenic Lines and Manifolds

The system of the cryogenic transfer lines and manifolds that is located inside the tokamak building includes the following components:

- manifold for connecting the ACBs, the CCB and the two CTCBs;
- two cryolines and two half ring manifolds for supplying the 9 CTBs of the TF coils;
- cryoline and two manifolds for supplying 11 CTBs of the PF coils and correction coils;
- cryoline and two manifolds for supplying the 6 CTBs of the CS;
- two cryolines for supplying the 3 CVBs of the magnet structures;
- two cryolines from the CTCBs for supplying the 2 CVBs of the 80 K thermal shields;
- cryoline and manifold for supplying the 4 CVBs of the NB cryopumps;
- cryoline for supplying the one CVB of the cryostat cryopumps;
- four cryolines and four manifolds for supplying the 20 CVBs of the torus cryopumps;
- four short cryolines to connect the ACB of the magnet structure with the two CTCBs and two LHe tanks.

The cryolines and ring-shaped manifolds that connect the ACBs with the CTBs and CVBs of each individual ITER cryogenic component are located around the tokamak cryostat on three different levels of the tokamak building, in particular the TCWS vault level (upper CTB level), the basemat level (lower CTB level) and the lower pipe chase level. The routing of the cryolines and manifolds of the upper and lower CTB levels is shown in Figures 3.2.1.4-2 and 3.2.1.5–1.

To minimise cost and allow space allocation for all the cryolines and manifolds in very restricted areas of the tokamak pit, the following design principles have been used:

- design of the cryolines and manifolds is simplified, no cold valves or temperature/pressure sensors are installed in the cryolines or manifolds (all cold valves and cryogenic sensors are housed in the ACBs, CTBs and CVBs);
- manifolds are designed with a minimum (50 mm) separation between cold tubes for using a welding (or cutting) tool for installation or repair;
- only welded joints are used for connecting the sections of the cryolines or manifolds during their assembly;
- minimum numbers of vacuum barriers are installed in any manifold. These vacuum barriers are located only between the manifold and each CTB, and between the cryoline and ACB.

The typical design of the manifold for the magnet system has been developed on the basis of designing the two half ring manifolds of the TF coils. These two manifolds are terminated with two cryolines that lead to the ACB. The TF manifold or manifolds of other coils consists of several straight pipe sections of 10 to 15 m in length and several bend sections of short length (1.5 to 2.2 m) which are connected in a such a way as to build the ring-shaped manifold.

A cross sectional view of the TF manifold is shown in Figure 3.2.1.5-2. The manifold includes five internal cold tubes. One of the two 80K He tubes is attached to the aluminium shield for its active cooling.

Each straight pipe section of the manifold includes cold bellows, to allow free longitudinal thermal contraction of cold tubes, one fixed support, and several sliding supports for guiding the bellows.

N 34 GR 30 01-01-22 F 1

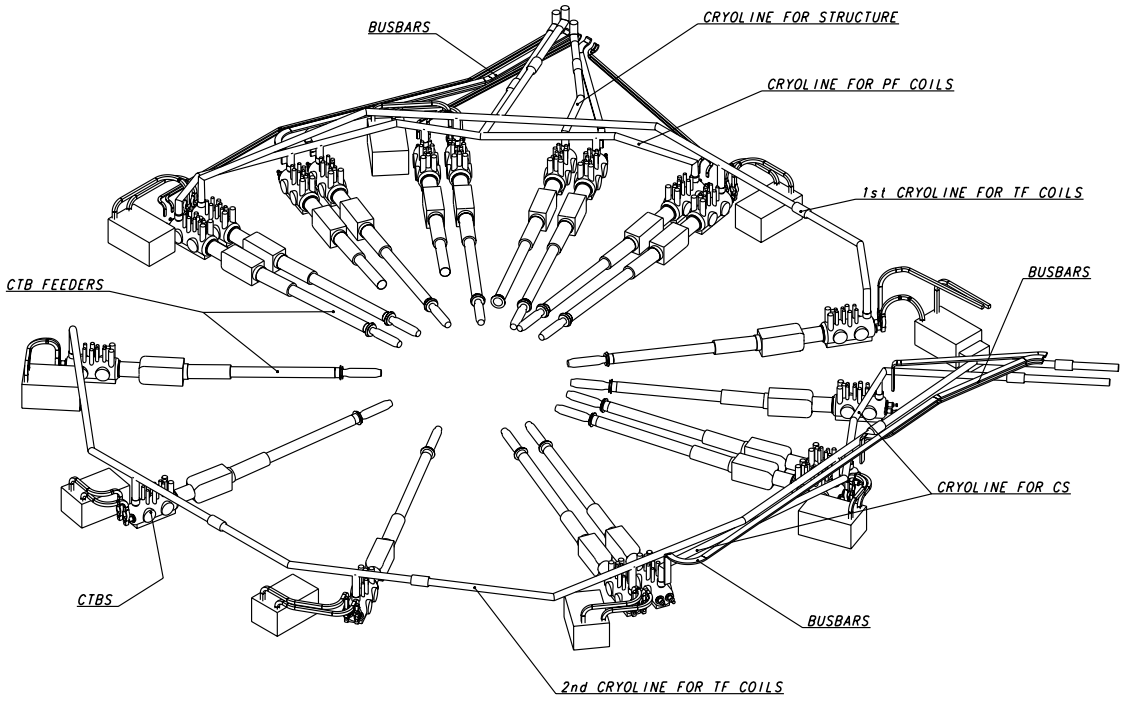

Figure 3.2.1.5-1 Isometrical View of Cryolines at the Lower CTB Level of the Tokamak building

N 34 GR 26 00-12-22 F 1

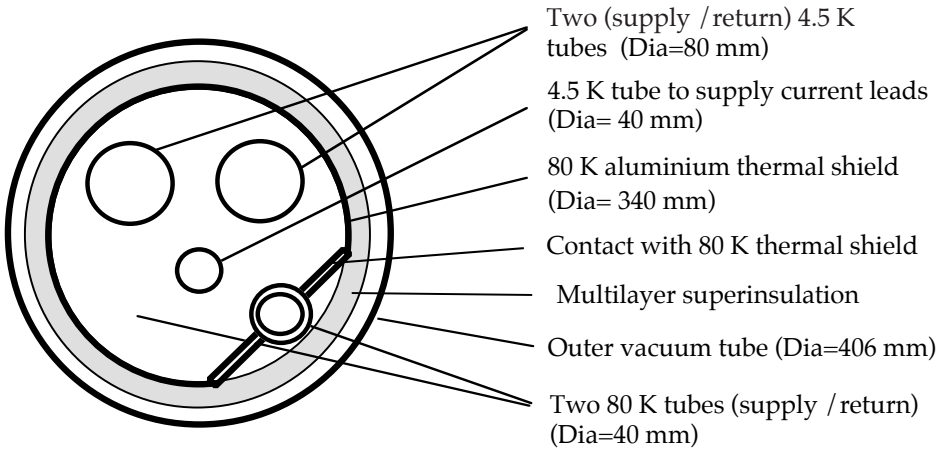

Figure 3.2.1.5-2 Cross Sectional View of TF Ring Manifold

The bend section has an internal design identical with that of the straight section. The outer vacuum tube has a mitre-type design and the inner cold tubes are bent to the required angle. Each bend section contains one fixed support. The cold tubes include a bellows section to facilitate thermal contraction.

Nine tee-sections are used for connecting the TF manifold with the 9 CTBs. Each tee section contains a vacuum connector with the branched cold tubes for attaching to the CTB. Each branched tube is formed to allow free thermal contraction, or has a flexible braided hose (bellows section). Each tee section has a vacuum barrier with the CTB.

The same internal design as for the TF manifolds has been used for the cryolines and manifolds of other components of the magnet system as well as for the torus and other cryopumps. The difference is that the supply (and return) manifolds of the torus crypumps includes three internal cold tubes, and six cold tubes for the NB and cryostat cryopumps.

The system of the cryolines includes also two, identical cryolines of 100 m in length to connect the cold process boxes of the cryoplant with the main tokamak building in which the CTCBs are installed.

There is also a system of long quench manifolds and lines that allow the exhaust of cold He from the TF coils during fast energy discharge or coil quench. (see 3.2.3.3).

3.2.2 Component Design Descriptions

3.2.2.1 Warm Gaseous Compressors

Oil injection screw type compressors are the reference design for the LHe plant. Four He compressor trains are installed in the cryoplant compressor building as shown in Figure 3.2.1.1-2. One compressor train consists of 3 units for the first compression stage (from 0.1 to 0.36 MPa), 2 units for the second stage (from 0.36 to 1.9 MPa), and two oil separators and water coolers for He and oil. The small amount of oil remaining in He after the oil separator of the second pressure stage is separated with three coalescing filters connected in series and finally with an activated charcoal adsorber. Two oil injection screw-type compressors are also used for the 80K He loop. One screw-type compressor set is installed in the cryoplant compressor building for operation with the He purification unit. Two sets of centrifugal compressors are used for the LN_2 subsystem. The two dual-operated He gas dryers are installed in the cryoplant compressor building for operating with both the LHe plant and 80K He loop. One dual-operated N_2 gas dryer is used for the LN_2 process boxes.

3.2.2.2 Cold Process Boxes of the Cryoplant

The cold box reference design is based on a modified 18 kW CERN 4.5K process module using a LN_2 pre-cooled, three-pressure He cycle as shown in Figure 3.2.2.2-1. The LHe module contains the first stage with LN_2 pre-cooling, several counter flow He HXs, and four cold He turbines (expanders).

The cold box of the LHe module consists of two vacuum cylinders, a vertical one and a horizontal one, connected together forming an L-shape as shown in Figure 3.2.2.2-2. The vertical cylinder of 4 m in diameter and 9 m in height contains all the He HXs. The horizontal cylinder of 3.5 m in diameter and 12 m long includes all the cold turbines, cryogenic valves and a LN_2 bath.

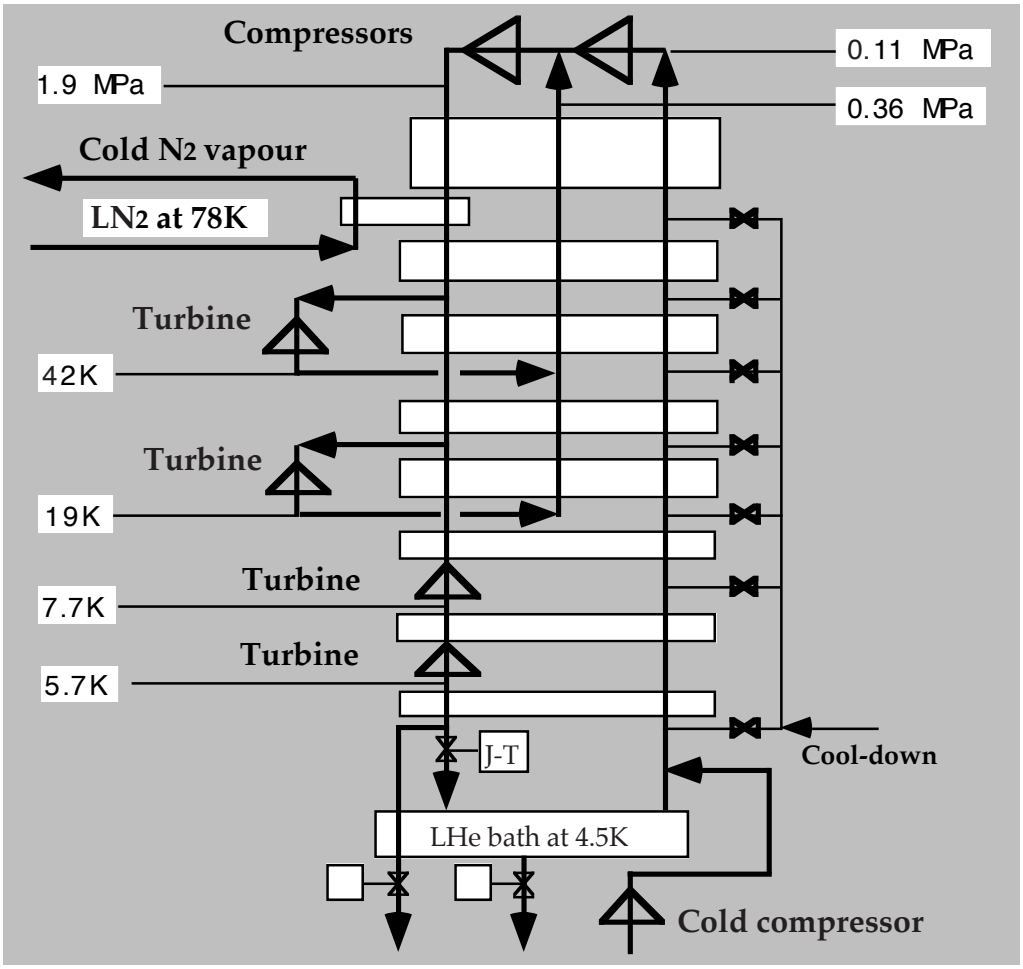

N 34 GR 31 01-01-22 F1

Figure 3.2.2.2-1 Cooling Cycle of the ITER Lhe Plant

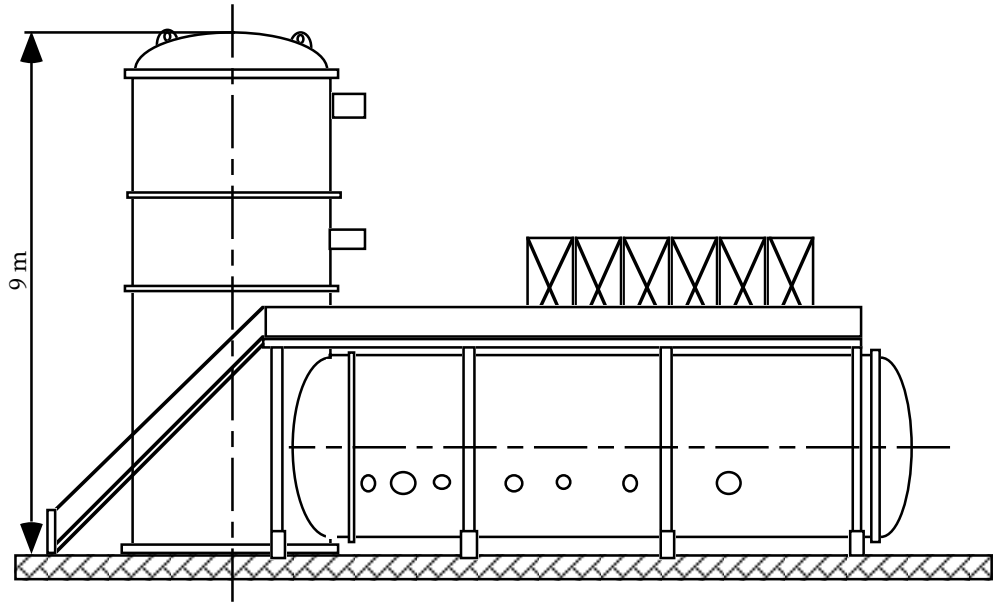

N 34 GR 32 01-01-22 F1

Figure 3.2.2.2-2 Sketch of the 18 kW CERN Module of the LHe Plant

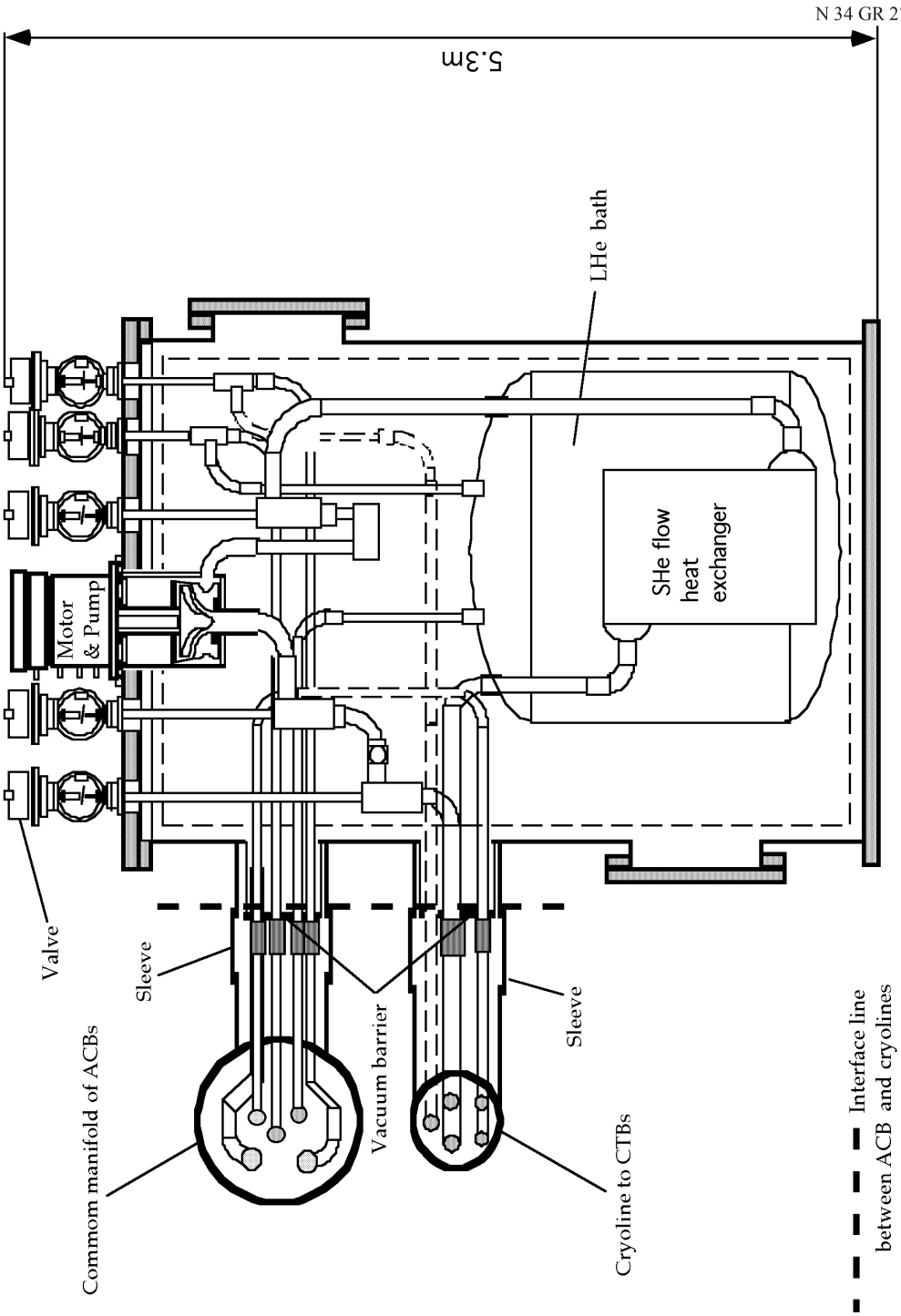

Figure 3.2.2.3-1 Vertical Cross Sectional View of Typical ACB of Magnet System

The 80K He loop includes the two vertical He cold boxes of 8 m in height, and two auxiliary LN_2 boxes of 5 m in height. All these boxes are of conventional design. The 80K box contains the He counter flow HX and the auxiliary LN_2 box includes the LN_2 bath and He HX immersed in this bath.

The LN_2 subsystem includes two, vertical, 10 m high cold boxes plus two appendages for locating expander machines. These boxes are of conventional design as used in industrial air separation plant.

3.2.2.3 Typical ACB of the Magnet System

All the ACBs of the magnet system are of identical design. The vertical cross sectional view of the ACB of the TF coils is shown in Figure 3.2.2.3-1. This ACB contain the following components:

- vertically-oriented cylindrical vacuum enclosure with connectors for attaching the common manifold of the ACBs and two cryolines of the TF coils;
- two He-circulating pumps (only one pump is shown in Figure 3.2.2.3-1);
- a bath with boiling He;
- a supercritical flow heat exchanger of fin-plate type immersed in the He bath;
- cold control, isolating and bypass valves;
- set of cryogenic sensors and a heater as a dummy load.

Note that the arrangement of the cold compressor box (CCB) is similar to the ACB design. The CCB contains a warm vacuum enclosure, cold valves and cold compressors. The possibility to install an additional cold compressor for allowing back-up operation of the PF coils at a reduced inlet temperature of 4.1 - 4.2K is also considered for this CCB.

3.2.3 Performance Analysis

Detailed evaluation of plant performance has been largely limited to plasma scenarios with up to 400 s burn. Initial comparison with the conditions for the hybrid scenario with 1,000 s burn indicates that the present plant design should meet the requirements. As for the non-inductive, 3,000 s burn, scenario operation details have still to be developed, and detailed analyses performed.

3.2.3.1 Controlling a Constant Heat Load on the LHe Plant

ITER plasma experiments start with hydrogen (then deuterium) plasmas (minimum cooling demands for plasma pulsing). Then tritium plasma experiments will be conducted at reduced requirements on the duration of plasma burn and plasma current, or with increased dwell time between pulses (reduced cooling demands for plasma pulsing compared with the reference plasma scenario).

The LHe plant is designed to be adjustable for plasma operation during the initial years at any reduced cooling demand as well as for the nominal pulsed plasma operation. The LHe plant can be also adjusted for stand-by, cool-down and ready-for-plasma-pulsing operating modes. The liquefaction vs. refrigeration working characteristics of the LHe plant cope with varying operation patterns for plasma pulsing, including the situation where one period of several hours is devoted to plasma pulsing at the maximum possible heat loads to the LHe plant, and the subsequent period of several hours is performed at reduced plasma pulsing parameters.

During the reduced plasma pulsing, net liquid He production takes place and this LHe is stored in the LHe tanks for use during a further period of plasma pulsing at maximum heat loads. This operating pattern can be repeated indefinitely.

The following, simplified sequence of active operating actions is required during preparation for each set of plasma pulses.

- The level in the main LHe storage of 50 m^3 is examined. If the volume of LHe is greater than 20 m^3, the maximum cooling capacity is available for plasma pulsing. If the volume is less than 20 m^3, plasma pulsing at reduced cooling capacity can be performed to increase the level in the LHe tanks to 20 m^3 in 4 - 10 hours.
- According to the intended plasma operation scenario, the heat load for the next set of pulses is specified and the speed of the cold circulating pumps and cold compressor is adjusted and held constant during those pulses.
- Reduction of the cooling capacity of the LHe plant for stand-by can be achieved by reducing the operating pressure in the compressors of the LHe plant from 1.8 MPa to 1.3 MPa.

One of the most challenging requirements for the LHe plant is the removal of large, pulsed heat loads deposited in the magnet system, because conventional LHe plant operation can become unstable above a certain (small) level of heat load fluctuation.

For smoothing the pulsed heat load, a special cooling procedure has been developed. Each ACB contains a bypass valve (see Figure 3.2.1.4-1) that allows part of the He flow heated in the magnet system to be returned to the coils or structures without passing through the heat exchanger of the LHe bath. This control procedure is based on periodic opening and closing of the bypass valve so as to maintain a constant total heat load on the supercritical He flow heat exchanger of the ACB.

The following additional automatically controlled valves and regulators (see Figure 3.2.1.4-1) are incorporated in the ACBs and CCB for active cooling control:

- control valves to maintain a constant level of boiling He in the LHe baths of each ACB at any instantaneous heat load;
- regulators to adjust the revolution rate and hence capacity of the cold compressors and the He circulating pumps in accordance with the heat load expected for the next plasma operating period;
- control valves of the current leads to maintain the minimum mass flow rate in the current leads under conditions with maximum electrical current or without current in the leads;
- a regulator interconnected with an electric heater, to maintain the heat load on the LHe bath constant when the heat load on the LHe baths coming from the magnet system is suddenly less than specified for this plasma pulsing period;
- a cold valve of the CCB to maintain He vapour pressure constant at the inlet of the cold compressor - due to operation of this valve a constant He flow returns through the cold compressor to the LHe plant, even though the heat load on the LHe baths rises above the value for which the revolution rate of cold compressor is fixed.

An active cooling control procedure using the bypass valves has been analysed for the PF coils, the CS and TF winding packs together with TF cases. The comprehensive

VINCENTA[1] code v.4.2 has been developed and used for these cooling simulations. The VINCENTA code allows combined 1D, 2D and quasi-3D transient thermal and hydraulic analysis of the coils and magnet structures to be made. The code allows investigation of the detailed temperature profiles along the conductor length when there is a thermal contact between the different turns and layers of each coil as well as between the coil and magnet structure. This code models (in space and time) non-uniform distributions of the heat loads due to AC/eddy losses and nuclear heating along and across the coils and magnet structures. The models of the cryogenic lines, He feeders, the heat exchanger of the ACB, the bypass valves for active smoothing the pulsed heat loads, as well as the circulating He pumps, are also included in this code.

The active cooling control associated with repeated opening and closing of the bypass valves results in repeated increases of the He temperature at the inlet of the conductor or increase of the heat load from the TF case to the conductor. The VINCENTA code allows careful checking of the possible temperature rise of the conductor, and hence guarantees that its temperature is within the limit for its design despite the active cooling control of the LHe plant.

The results of the numerical hydraulic and thermal simulations of the cooling control demonstrate that the temperatures of the TF, CS and PF conductors do not exceed maximum allowed values despite the inlet temperature variation. However, the cold He compressors must maintain an operating temperature of 4.3K.

As an example, Figures 3.2.3.1-1 and 3.2.3.1-2 show the results of the thermal simulations for the largest component of the magnet system i.e. the TF coil winding packs and their cases. Two different cooling procedures has been studied: one without smoothing the pulsed heat loads, and the other with active cooling control. As shown in Figure 3.2.3.1-1, the heat load on the LHe plant varies during each plasma pulse from 20 kW to 30 kW, if there is no active cooling control. Figure 3.2.3.1-2 illustrates that practically a constant heat load of 25 kW is maintained on the LHe plant for the active cooling control after the third plasma pulse.

[1]"Design of the ITER-FEAT cryoplant to achieve stable operation over a wide range of experimental parameters and operation scenarios", G. Claudet, N. Chatil, V Kalinine, N. Mitchell, P. Roussel,. 21st SOFT, Madrid, Spain, 11-15 September 2000 (to be published).

N 34 GR 28 00-12-22 F 1

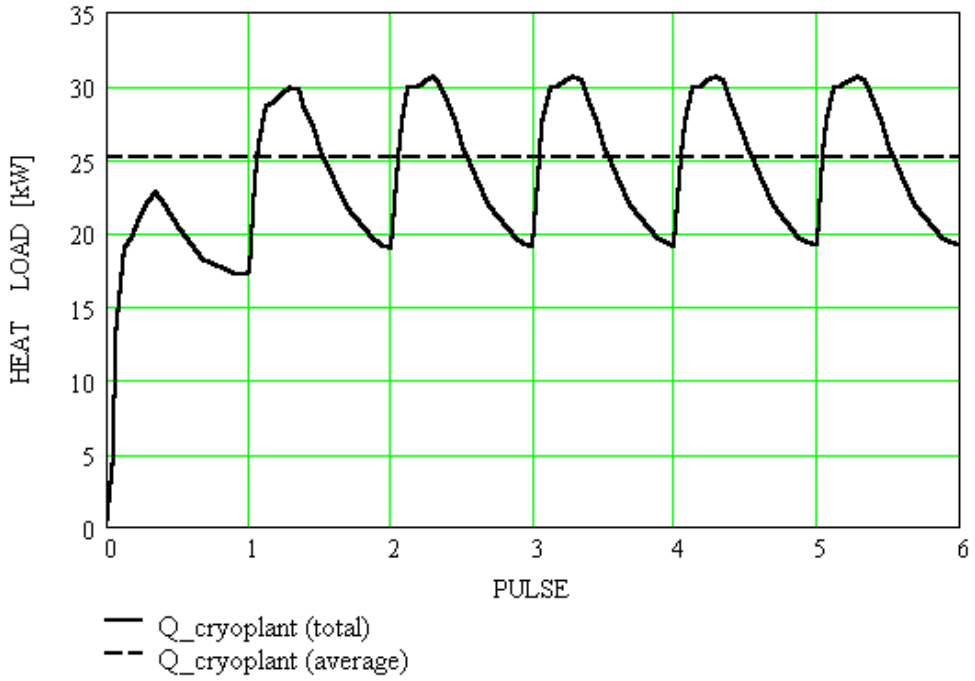

Figure 3.2.3.1-1 Evolution of the Total Heat Load from the TF Winding Packs, their Cases and Circulating Pumps for No Active Cooling Control

N 34 GR 29 00-12-22 F 1

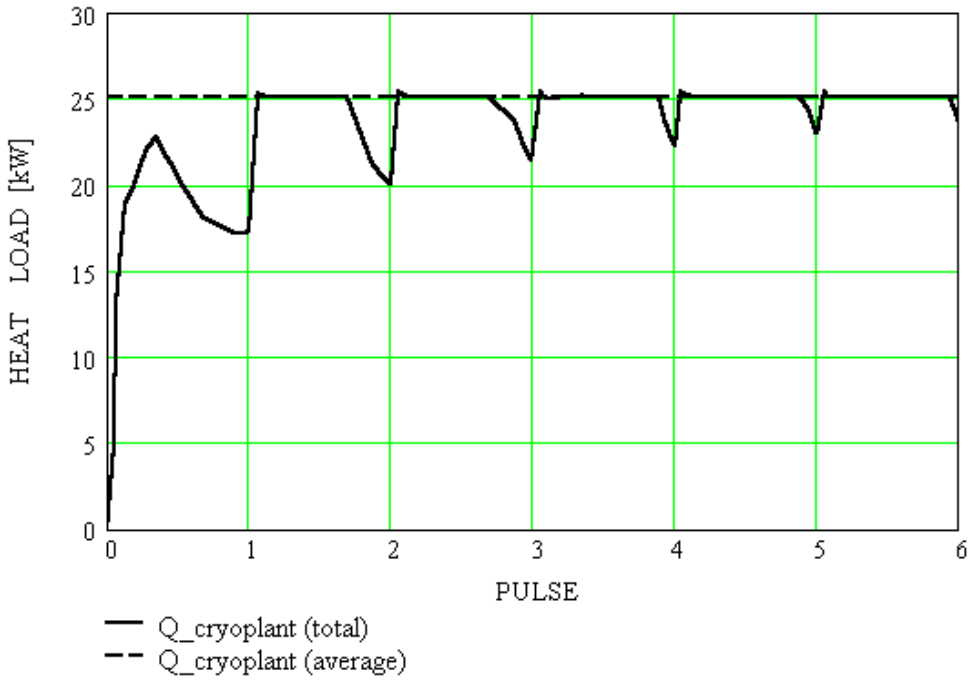

Figure 3.2.3.1-2 Evolution of the Total Heat Load from the TF Winding Packs, their Cases and Circulating Pumps for Active Cooling Control

3.2.3.2 Cool-Down of the ITER Machine from 300K to 4.5K

The cool-down scenario of the ITER machine is mainly determined by cool-down of the magnet system. The cool-down is subdivided in two stages, namely from 300K to 80K and from 80K to 4.5K. During the first cool-down stage, the inlet He temperature is gradually decreased at a rate of 0.4 - 0.5K per hour. This gradual cool-down is required to limit mechanical stresses in the magnet system to acceptable values. The gradual cool-down is provided by compressed He flow from the LHe plant.

A transient cool-down analysis of the magnet system has shown that the most restrictive hydraulic parameters are those of the TF coils. A temperature gradient of 40K arises along the TF conductor during cool-down at the temperature decrease rate of 0.5K per hour. The PF coils, the CS, the magnet structures and the 80K thermal shields will follow the same cool-down scenario as that of the TF coils, because all portions of the magnet system must be simultaneously cooled to keep them as closely as possible in thermal equilibrium.

A special cooling scheme for the gradual decrease of the He flow temperature at the inlet of the magnet system has been developed. This cooling scheme is based on mixing in a controlled way the warm and 80K He flows. This cooling cycle, in which the He flowing out of the coils returns to the heat exchanger of the LHe plant, and cold N_2 vapour returns to the LN_2 subsystem, allows operation of the LN_2 subsystem in the most effective refrigeration mode. The cooling capacity of the installed LN_2 subsystem can thereby be maximised. The total refrigerating capacity of the LN_2 subsystem for the cool-down of the magnet system, together with the thermal shields and gravity supports is 900 kW, as shown in Table 3.2.1.3-1. It is expected that the duration of the first cool-down stage of the ITER machine will not exceed 20 days.

Supercritical He is used during the second stage of cool-down from 80K to 4.5K. The return cold He gas at gradually decreasing temperature can be recycled to the LHe plant cold boxes to reduce LN_2 consumption during this cool-down stage. Cold valves are incorporated in the LHe cold boxes to return He flow to the heat exchangers at the requisite temperature level. With this cool-down technique, the LN_2 consumption will be the same as that for the nominal operation of the LHe modules at 4.5K. It is expected that the duration of the second cool-down stage will not exceed 7 days.

A procedure that is the reverse of cool-down is expected for the warm-up of the ITER machine. The gradual temperature increase of 0.5K per hour is maintained for warm-up from 80K to 310K. The heaters (see Figure 3.2.1.1-1) are incorporated in the cryoplant for final warm-up of the magnet system to 310K before opening the cryostat.

3.2.3.3 Helium Exhaust to the Cold Quench Tank during Fast Energy Discharge

A large energy of approximately 5 GJ will be deposited inside the radial plates of the 18 TF winding packs and the 18 TF coil cases during a fast TF coil discharge. This energy deposition has a transient nature and results in a temperature increase of the radial plates and TF coil cases from 4.5K to approximately 50K in 15 s. Due to the high temperature rise the He inventory of 40 m^3 and 12 m^3 will be expelled from the 18 TF coil winding packs and their cases respectively.

To avoid loss of a large quantity of He to the atmosphere, a cold quench tank of 700 m^3 is incorporated in the ITER cryoplant. This tank has active cooling at 80K. The cold tank is installed at a distance of 60 m from the tokamak building and connected with the magnet system through a system of half-ring shaped manifolds and long He quench lines.

The VINCENTA code v.4.2 (see 3.2.3.1) has been used for the transient analysis of the He exhaust to the cold quench tank. In this analysis it was assumed that the fast energy discharge appears at the end of the plasma burn phase of the fourth nominal plasma pulse. The He relief valves of the CTBs and CVBs are opened when the pressure is increased to 1.6 MPa at the inlet of the relief valves.

The main purpose of this transient analysis is to quantify the required diameters of the long quench He lines. The diameters of the quench lines should be chosen to limit He exhaust pressure to approximately 2.5 MPa in the cryogenic manifolds and He circulating pumps.

The main results of the analysis as the follows:
- the quench lines should be designed for expelling the maximum He flow of 140 kg/s that occurs 15 s after beginning the fast energy discharge - then He flow rate exponentially decays to zero during the next 130 s;
- the common quench line is 60 m in length and 300 mm in diameter;
- the diameter of each of the two parallel ring-shaped 100-m manifolds that connect the CTBs of the TF winding packs with the common quench line is 100 mm;
- the TF case manifold that connects the CVBs of the TF coil cases with the common quench line is 150 mm in diameter and is 40 m in length;
- the maximum He pressure inside the 18 TF winding packs is 12.0 MPa, but the maximum pressure at the inlet of the relief valves is 2.5 MPa and 2.0 MPa respectively for the TF coil cases and TF coil winding packs;
- quench of the TF coil winding pack occurs after 12 s of the energy discharge due to active thermal contact between the ‘hot’ radial plates and the ‘cold’ TF conductor. However, this additional energy deposition does not exceed 10 % of the total energy of 5 MJ and does not practically affect the pressure rise in the quench lines.

3.2.3.4 Cool-Down of the TF Coils after Fast Energy Discharge

The TF coil fast energy discharge results in temperature increase of the TF coil winding packs and TF coil cases to 50K, and cool-down is required for restoring the operating temperature of these two components of the magnet system.

A special cooling procedure has been developed for the cool-down of the TF coil winding packs and TF coil cases and maintaining in parallel a 4.5K stand-by for the PF coils and CS. This cool-down procedure allows maximum reduction of cool-down time and is subdivided in the following two stages:
- cool down of the TF coil winding packs and cases from 50K to 10K - during this stage the LHe plant operates at the maximum refrigeration capacity of 72 kW;
- filling the TF winding packs and cases with supercritical He - during this stage the LHe plant operates at the maximum liquefaction capacity of 0.2 kg/s.

During the first stage, a part of the cooling capacity of about 20 kW is required for maintaining the PF coils and CS at 4.5 K, and 52 kW can be used for cool-down of the TF coil winding packs and TF coil cases. The cold mass of the 18 TF coil winding packs and

their cases is 1,710 t and 1,840 t respectively and 25 kW of the refrigeration capacity is available for cooling the TF coil winding packs and 27 kW for cooling the TF coil cases.

The second cool-down stage starts, when the heat load on the LHe plant is getting lower than 72 kW, despite increasing the He flow through the TF coil winding packs and their cases. At this cool-down stage the He stored in the cold quench tank is re-liquefied for filling the cooling channels of the TF coil winding packs of 40 m^3 and TF coil cases of 12 m^3 with supercritical He at 4.5K and 0.5 MPa. The refrigeration capacity of 20 kW is also required for maintaining the stand-by capability of the PF coils and CS.

Transient thermal hydraulic analysis (using VINCENTA v3.9) has been carried out to quantify the time required for cool-down of the TF coil winding packs. The constant refrigeration heat load of 25 kW is maintained on the LHe plant and the He mass flow rate through the TF coil winding packs varies from the minimum to the maximum in such a way as to keep the constant heat load of 25 kW.

The main results of this analysis are the following:

- time for cool-down of the TF coil winding packs from 50K to about 10K is 28 hours;
- 12 hours will be required to fill the TF coil winding packs of 40 m^3 with 4.5K He if the liquefaction capacity of the LHe plant is 0.1 kg/s.

It is expected that the time for the cool-down of the TF coil cases will be the same as for the cool-down of the TF coil winding packs, because the cold masses of these two components are very similar. Taking into account that there is a transition period for changing the operation of the LHe plant from the total refrigeration to the liquefaction mode, the cool-down of the TF winding packs plus the TF coil cases is expected to be 2 to 2.5 days.

3.3 Cooling Water

3.3.1 Overview of the Cooling Water System

The cooling water system (CWS) consists of the tokamak cooling water system (TCWS), the component cooling water system (CCWS), the chilled water system (CHWS), and the heat rejection system (HRS).

The main drivers of the CWS design are cost reduction, segmentation and standardisation of the in-vessel components, facilitation of installation and maintenance, staged procurement, and acceptable impact on the building of pressure loading following an ex-vessel coolant leak.

The TCWS consists of the primary heat transfer systems (PHTSs) and their supporting systems, i.e. the chemical and volume control systems (CVCSs), the draining and refilling systems, and the drying system. The schematic flow diagram of the CWS is shown in Figure 3.3.1-1. The PHTSs are the:

a) vacuum vessel (VV) PHTS;
b) primary first wall/blanket (PFW/BLK) PHTS;
c) divertor/limiter (DIV/LIM) PHTS;
d) NB injector PHTS.

The systems a) – c) cool components inside the VV, and the vessel itself. The system d) (low and high voltage) serves the NB injectors installed at VV ports. The systems b) to d) are sometimes referred to as “in-vessel” PHTSs.

The schematic pipe routing of PHTSs is shown in Figure 3.3.1-2. The upper and lower pipe-chases are located above the upper port level and below the divertor port level respectively, and are interconnected by vertical shafts. Three pairs of inlet/outlet C-shaped manifolds of the PFW/BLK PHTS, two outlet C-shaped manifolds of the VV PHTS and inlet/outlet pipes for the NB cell are located in the upper pipe chase, and one pair of the inlet and outlet C-shaped manifolds of the DIV/LIM PHTS and two inlet C-shaped manifolds of the VV PHTS are located in the lower pipe chase. The east side of the upper pipe chase is integrated with the TCWS vault of the tokamak building, and it is vertically separated by a mezzanine floor.

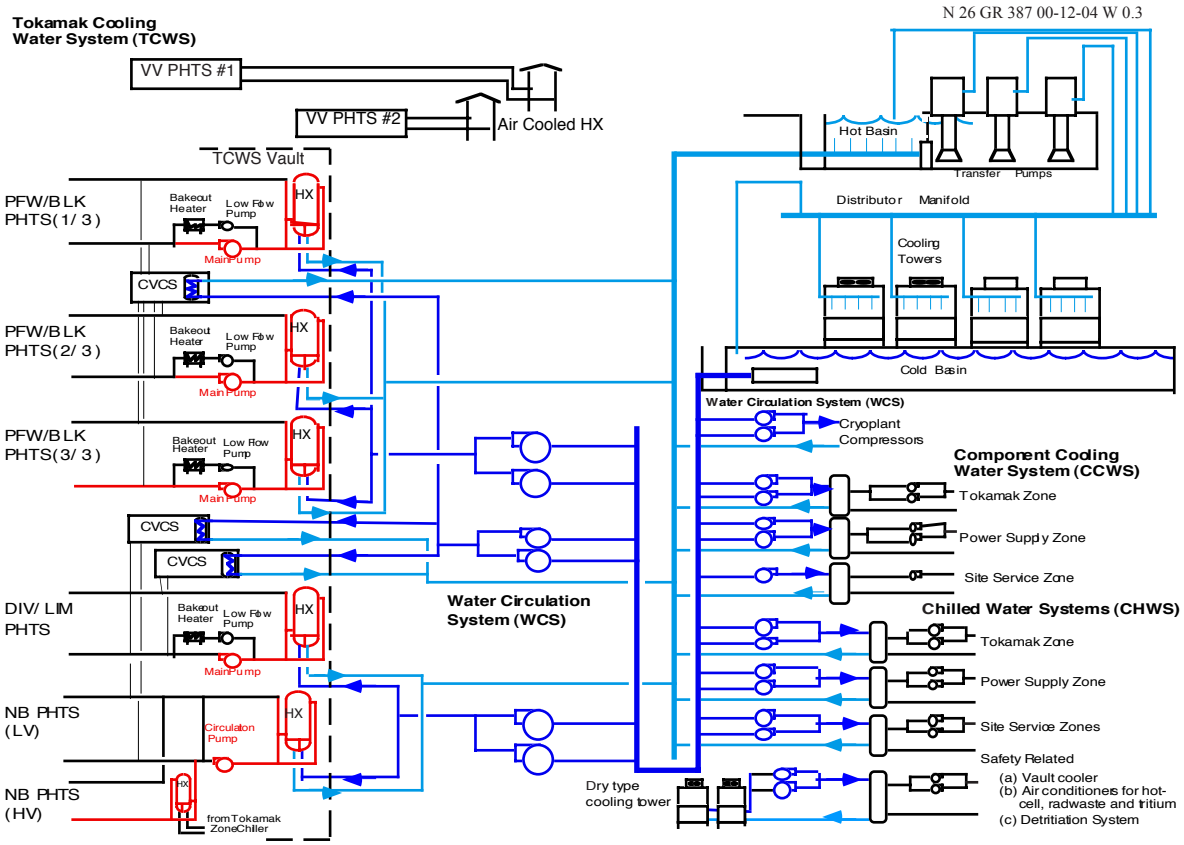

Figure 3.3.1-1 Schematic Flow Diagram of the Cooling Water System

The main loop components of the PHTSs, except for the VV PHTS, are sited in the upper area of the rectangular TCWS vault above the magnet and CVCS levels, and the components of the CVCSs are sited in the lower TCWS vault area at the magnet and CVCS level. The HRS pipes that serve PHTSs are routed below the mezzanine floor.

The closed volume formed by the pipe chases, vertical shafts, the NB cell, the TCWS vault, the TCWS vault extension, and the area for the CVCSs, constitutes a secondary confinement boundary for an ex-vessel coolant leak as shown in Figure 3.3.1-2.

The main components for the VV PHTS are located on the tokamak building roofs on the east and west sides, and at the divertor level in the drain tank area.

The components of the TCWS are based on fission power plant experience, and no difficulties are expected in their commercial availability. The same holds for the CCWS, the CHWS and the HRS. The layout of the TCWS components and the pipework is a standardised configuration for modularised installation and minimisation of impact by the magnetic field on the components. The layout agrees with the footprint allowed in the building design and with the safety strategy regarding the ability of the TCWS vault to withstand 0.2 MPa mixed steam/air peak overpressure following a large pipe break during operation.

N 26 GR 422 01-06-27 W 0.1

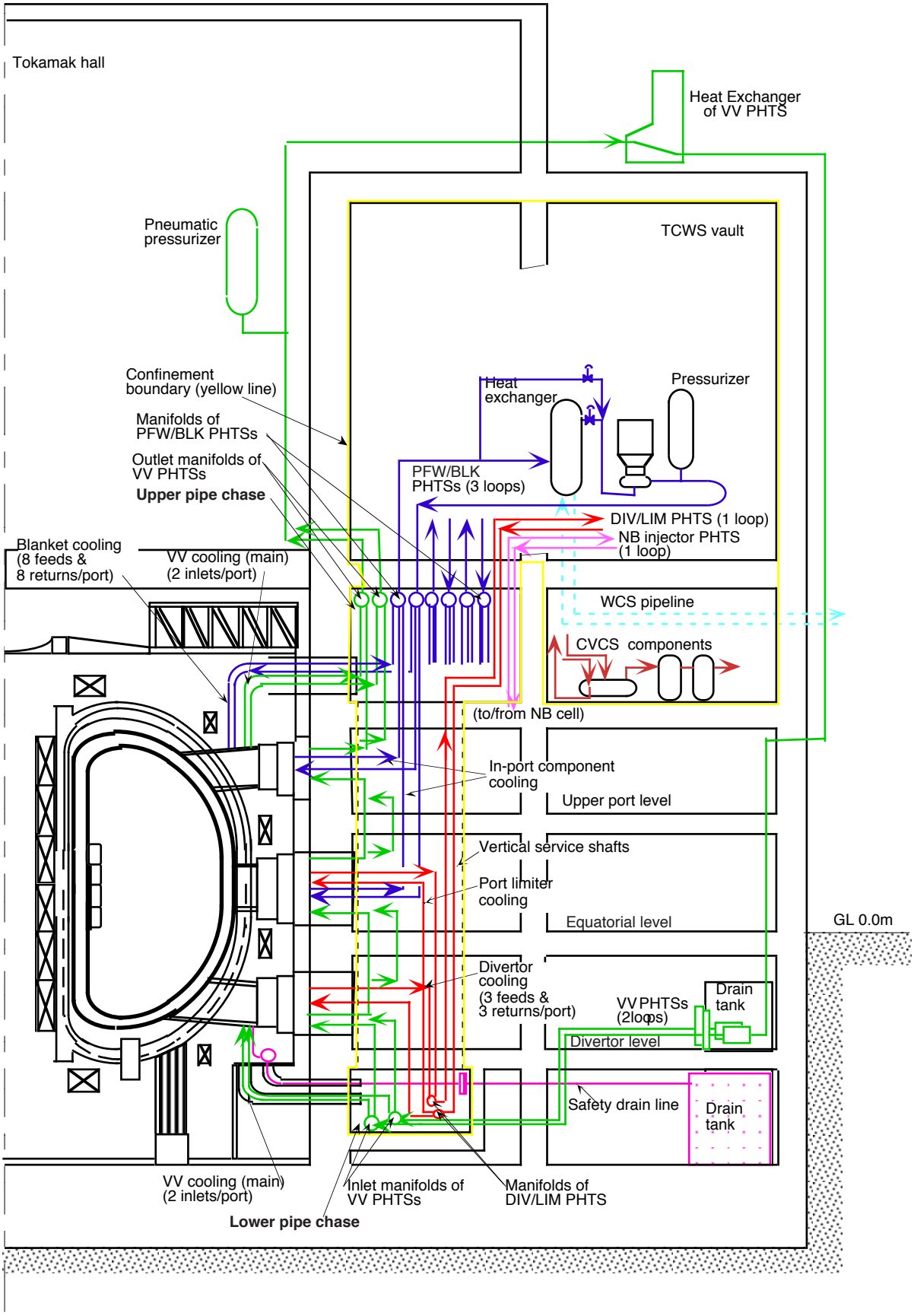

Figure 3.3.1-2 Concept of PHTS Pipe Routing

From a cost and maintenance point of view, the number of PHTS loops should be reduced as much as possible. This also aids in minimising radiation exposure of maintenance workers, which is an ALARA requirement. However, a reduction in the number of loops increases the coolant inventory per loop and consequently also the peak pressure experienced in the containment vault during a postulated ex-vessel coolant leak. As a result, the pressure retention and leak tightness requirements, and hence the building costs, increase. The optimisation is therefore a trade off between these variables. The segmentation adopted is based on the premise that a containment volume with a pressure-bearing capacity of not exceeding 0.2 MPa would be feasible and cost effective. The full containment of the pressure has been adopted for postulated ex-vessel coolant leaks during plasma operation. This leads to three loops for the PFW/BLK PHTS and one for the DIV/LIM PHTS.

The peak pressures in the building vault have been estimated tentatively by simplified calculation and ~ the results showed that a large ex-vessel leak during plasma operation generates a peak pressure of ~ 0.17 MPa. Using more refined analysis with the MELCOR code, a peak pressure of 0.141 MPa was obtained. During baking, a peak pressure of 0.17 MPa would be obtained in the case of a small ex-vessel coolant leak (LBB case). However, the limit of 0.2 MPa would be exceeded in the case of a large leak. Therefore, for this event, the ITER strategy is based on the adoption of the LBB philosophy. Added to this, an engineered pressure relief system is provided that will open if the peak vault pressure exceeds 0.2 MPa and it will reseal at ~ 0.2 MPa under a hypothetical double-ended guillotine break during baking.

Tritium permeation into coolant loops is calculated to be very low. Latest test data and numerical calculations have given enhanced confidence that, in combination with an efficient coolant chemistry control and purification system, the concentration of activated corrosion products (ACPs) will be continuously kept at very low levels. The levels of tritium and ACPs in the coolant are monitored to ensure they are within safety limits, and the possibility of an additional communication with the detritiation system is allowed for in the design in case it is needed.

The CCWS removes heat from large process components which do not become activated. The CCWS transports heat from the components to the HRS, which is the ultimate heat sink. The system provides high quality cooling water where necessary for components with sensitive water chemistry needs. The maximum temperature of the CCWS feed water is basically 40°C. Loops in the CCWS for some of the power supply components, which require temperatures lower than 35°C, are served by the CHWS.

The CHWS services components and loops in the CCWS which require coolant temperatures lower than can be provided by the normal CCWS and HRS. The CHWS utilizes industrial chiller units to provide cooling water at 6°C with a return temperature of 12°C. The CHWS has separate loops for “safety-related” circuits (to the vault, hot cell and tritium plant) which may need to confine radioactivity.

The HRS is the final heat sink and uses cooling towers to reject heat to the environment. The HRS includes water circulation systems (WCSs) for the TCWS, the cryoplant warm compressors, the CCWS, and the CHWS. The safety-related CHWS circuits reject heat to separate dry cooling towers which form a separate part of the HRS.

The CCWS, the CHWS and WCSs in the HRS are zoned as shown in Figure 3.3.3-1, and the components for each zone are sited in the buildings in each zone and connected to pump stations outside the buildings. The pipework interconnecting the cooling tower, pump stations of WCSs and the buildings are routed inside service tunnels and trenches.

3.3.2 Functions of the Cooling Water System

The CWS has the following functions:
(1) TCWS
- remove the heat deposited in the in-vessel components and VV during a plasma pulse to the HRS by way of the WCSs, or directly to air;
- control the coolant temperature, flow rate and pressure for the in-vessel components and VV during normal operation as required;
- remove decay heat from the in-vessel components and the VV after plasma shutdown;
- provide the ability to bake the in-vessel components and the VV;
- provide safe confinement of the radioactive inventory of the coolant;
- confine radioactive materials from the tokamak following any failure of in-vessel component boundaries;
- measure the heat removed from the in-vessel components and VV to contribute to the determination of the overall fusion power balance;
- control the water chemistry in the in-vessel components and VV;
- allow in-vessel components to be isolated to facilitate leak localisation.

(2) CCWS
- remove the heat from components to the CHWS or to the HRS;
- control the coolant temperature, flow rate and pressure for the components as required;
- control the water chemistry in the components.

(3) CHWS
- provide low temperature coolant for the components;
- remove the heat from components to the HRS.

(4) HRS
- provide HRS coolant for the TCWS, CCWS and CHWS;
- remove the heat from the TCWS, CCWS and CHWS, and release it to the environment.

3.3.3 System Description

3.3.3.1 Tokamak Cooling Water System (TCWS)

3.3.3.1.1 PFW/BLK PHTS

The PFW/BLK PHTS is divided into 3 loops. Each of these loops supplies coolant to the blanket modules in three 40° sectors, three sectors apart. This cooling system also supplies coolant to the in-port components inside the equatorial and the upper ports.

All of the 32 cooling water pipes from each adjacent pair of upper ports, 8 feeds and 8 returns for each upper port, that pass through the cryostat vacuum are integrated into one pipe bundle, and connected to the C shaped manifolds in the upper pipe chase. The pipe

bundles at the cryostat penetration are contained within a guard pipe of approximately 1.4 m diameter that connects the cryostat and the biological shield wall.

The main data for the PFW/BLK PHTS are listed in Table 3.3.3-1 and a flow diagram for the PFW/BLK PHTS is shown in Figure 3.3.3-1. The loop is pressurised by a steam pressuriser connected to the cold leg. The heater is used to maintain coolant inlet temperature during baking.

Table 3.3.3-1 Main Data for the PFW/BLK PHTS

	Normal Operation	**Baking**
Thermal Power/Loop	230 MW	-
Coolant Inlet Temp.	100°C	240°C
Coolant Outlet Temp.	148°C	~240°C
Coolant Pressure at Inlet	3 MPa	4.4 MPa
In-Vessel Pressure Drop	1.0 MPa	~0.01 MPa
In-Vessel Water Holdup/Loop	~ 28 m^3	
Loop Number	3	
Flow Rate/Loop	1,130 kg /s	120 kg/s
Loop Pipe Inside Diameter[1]	0.514 m	
Pressure Drop[2]	2.0 MPa	0.1 MPa
Total Water Holdup/Loop	~ 130 m^3	
Pump - Pumping Power/Loop	Main pump 3,660 kW	Low flow pump 25 kW
Heat Exchanger - Exchange Heat - Heat Transfer Surface Area	234 MW 2,710 m^2 /unit	
Pressurizer Size	16.5 m^3	
Heater	~ 1,400 kW	

[1]Coolant velocity = approx. 6 m/s
[2]Total pressure drop including in-vessel components, heat exchanger and piping

The low flow pumps are also used for maintaining coolant circulation during long shutdown periods, for good chemistry control of the coolant throughout the loop. During loss of off-site power or loss of flow in category II events, the small pump units are automatically switched to class III power to remove decay heat for investment protection.

3.3.3.1.2 DIV/LIM PHTS

There is one DIV/LIM PHTS loop and it provides the primary coolant to 54 divertor cassettes as well as 2 port limiters. The main PHTS parameters are given in Table 3.3.3-2, and a flow diagram is shown in Figure 3.3.3-2. The loop layout, temperature control, and other characteristics are almost identical to that of the PFW/BLK PHTS loops.

The feed and return pipes to the divertor cassettes penetrate the cryostat inside the divertor ports, where they are routed, six per port, through the upper part of the ports. Outside the ports, the cooling pipes are individually routed from/to the C shaped manifolds in the lower pipe chase and finally to the TCWS vault via a vertical shaft.

Table 3.3.3-2 Main Data for the DIV/LIM PHTS

	Normal Operation	Baking
Thermal Power/Loop	202 MW (at flat-top)	-
Coolant Inlet Temp.	100°C	240°C
Coolant Outlet Temp.	150°C (for DIV) 128°C (for LIM)	~ 240°C (for DIV) ~ 240°C (for LIM)
Coolant Pressure	4.2 MPa	4.4 MPa
In-Vessel Pressure Drop	1.6 MPa	~ 0.02 MPa
In-Vessel Water Holdup/Loop	~ 23 m^3	
Loop Number	1	
Flow Rate/Loop	1,000 kg/s	100 kg/s
Loop Pipe Inside Diameter[1]	0.514 m	
Pressure Drop[2]	2.3 MPa	~ 0.1 MPa
Total Water Holdup/Loop	~ 145 m^3	
Pump - Pumping Power/Loop	Main pump 3,670 kW	Low flow pump 19 kW
Heat Exchanger - Exchange Heat - Heat Transfer Surface Area	206 MW 2,410 m^2 / loop	
Pressurizer Size	23.0 m^3	
Heater	1,600 kW	

[1]Coolant velocity = approx. 6 m/s
[2]Total pressure drop including in-vessel components, heat exchanger and piping

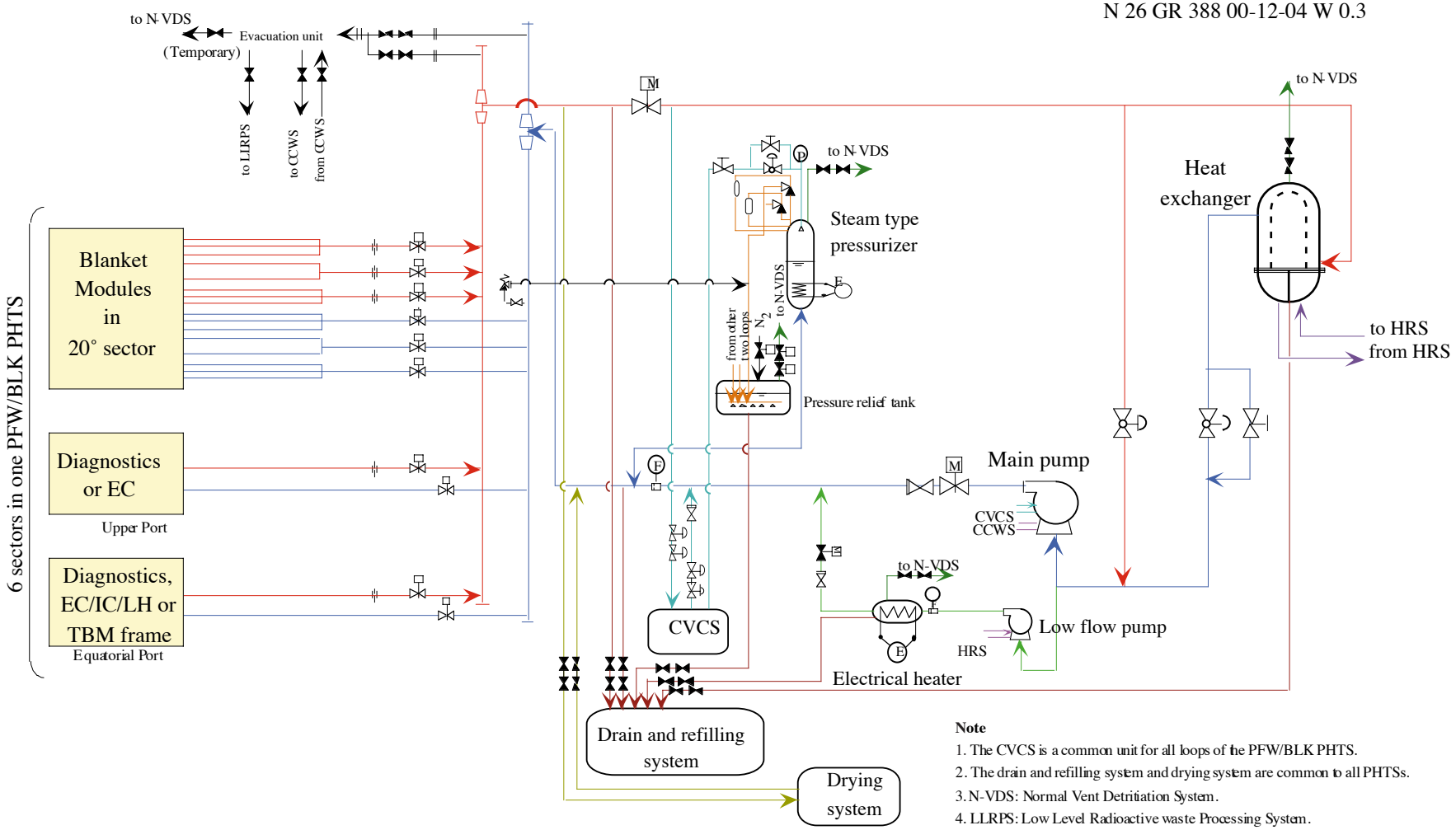

Figure 3.3.3-1 Flow Diagram of the PFW/BLK PHTS

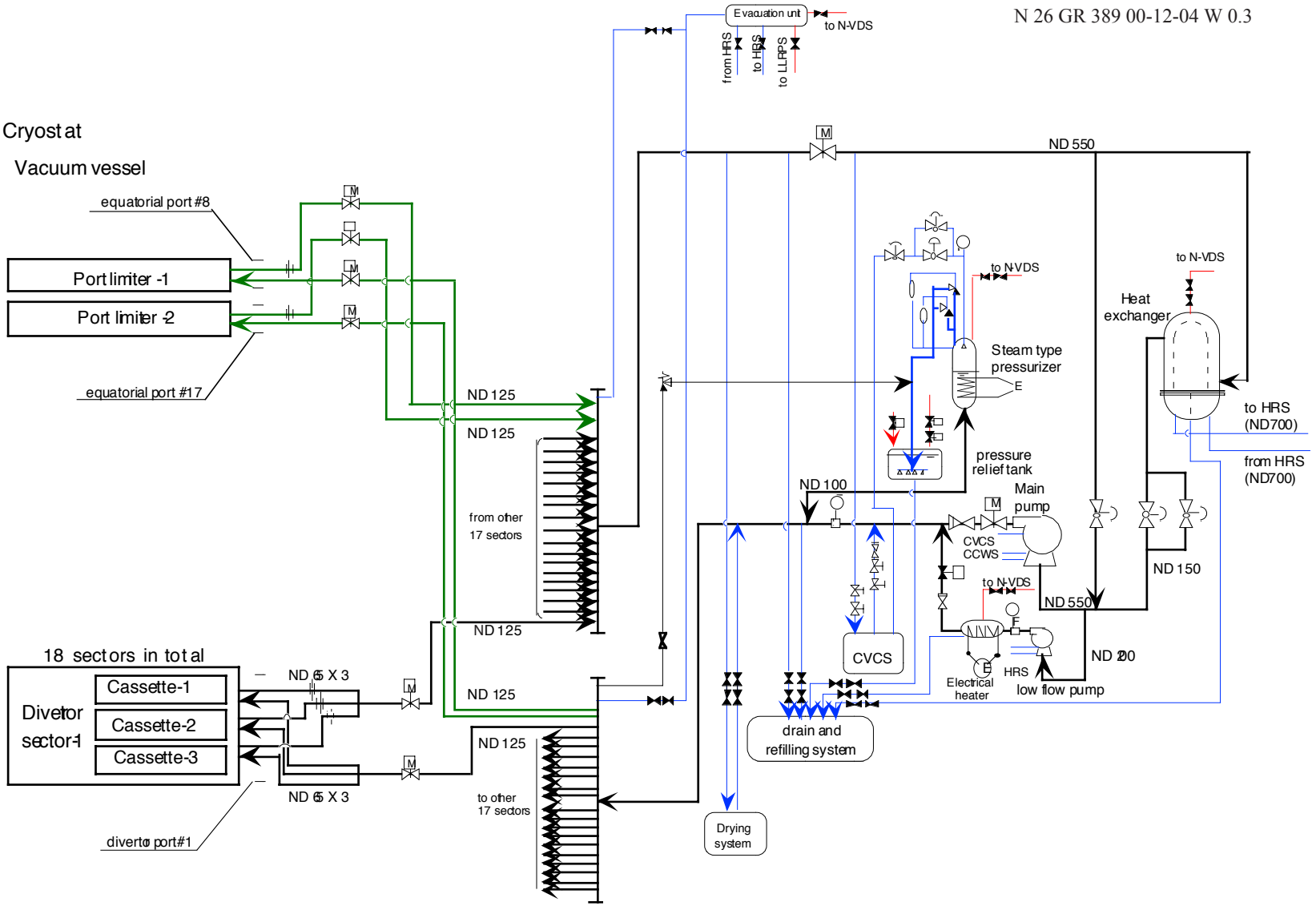

Figure 3.3.3-2 Flow Diagram of the DIV/LIM PHTS

3.3.3.1.3 VV PHTS

The VV PHTS has a safety role in that it provides the ultimate decay heat removal for all in-vessel components should the other PHTSs be unavailable. For this reason, the VV PHTS is required to have a passive heat removal capability, i.e. by means of natural convection.

The VV PHTS is divided into two loops, and each loop is connected to alternate halves of the 9 VV 40° sectors. This configuration confers redundancy in that decay heat can be adequately removed by one operational cooling loop in the event that the other becomes unavailable. Two inlet pipes (from different loops) penetrate the lower faces of each divertor port on either side of the port centreline, and the corresponding outlet pipes penetrate the top faces of the upper port in the same cooling path in 20° of the machine (10° of the machine either side of the ports). Two feeds per 20° sector from adjacent ports ensure that there are no stagnation zones in the flow fields of the inclined (upper and lower) ports. The cooling paths of pairs of feed and return pipes per 20° sector are connected alternately to the feed and return manifolds of the two VV PHTSs which are located in the lower and upper pipe chases, respectively. The main pipes are then routed through the upper pipe chase and tokamak hall to the top of the tokamak building where they connect with the air-cooled heat exchangers. In parallel with the main VV cooling lines, branch lines are connected in series to the VV closure plates at each divertor, equatorial, and upper ports of the sector. The main VV PHTS data are given in Table 3.3.3-3, and a flow diagram is shown in Figure 3.3.3-3. Each of the two loops is also designed to be able to remove the total heat load on the VV during off-normal conditions.

Table 3.3.3-3 Main Data for the VV PHTS

	Normal Operation	**Baking**
Thermal Power/Loop	5 MW	--
Coolant Inlet Temp.	100°C	200°C
Coolant Outlet Temp.	~ 103°C	~ 200°C
Inlet pressure	1.1 MPa	2.4 MPa
In-Vessel Pressure Drop	< 0.05 MPa	
In-Vessel Water Holdup/Loop	~ 110 m^3	
Loop Number	2	
Flow Rate/Loop	475 kg/s	
Loop Pipe Inside Diameter	0.33 m	
Pressure Drop	~ 0.6 MPa	
Total Water Holdup in a Loop	~ 160 m^3	~ 175 m^3
Main Pump - Pumping Power	1 / loop 450 kW	
Heat Exchanger - Heat Transfer Surface	3 / loop 1,591 m^2 /unit	
Heater - Size	1 / loop 1.7 MW	
Pressurizer (pneumatic type) - Size	1 / loop 30 m^3	

The VV PHTS does not have to have further confinement due to the low ACP and tritium level in the loops, thereby allowing the HXs and other loop components to be positioned outside the TCWS vault.

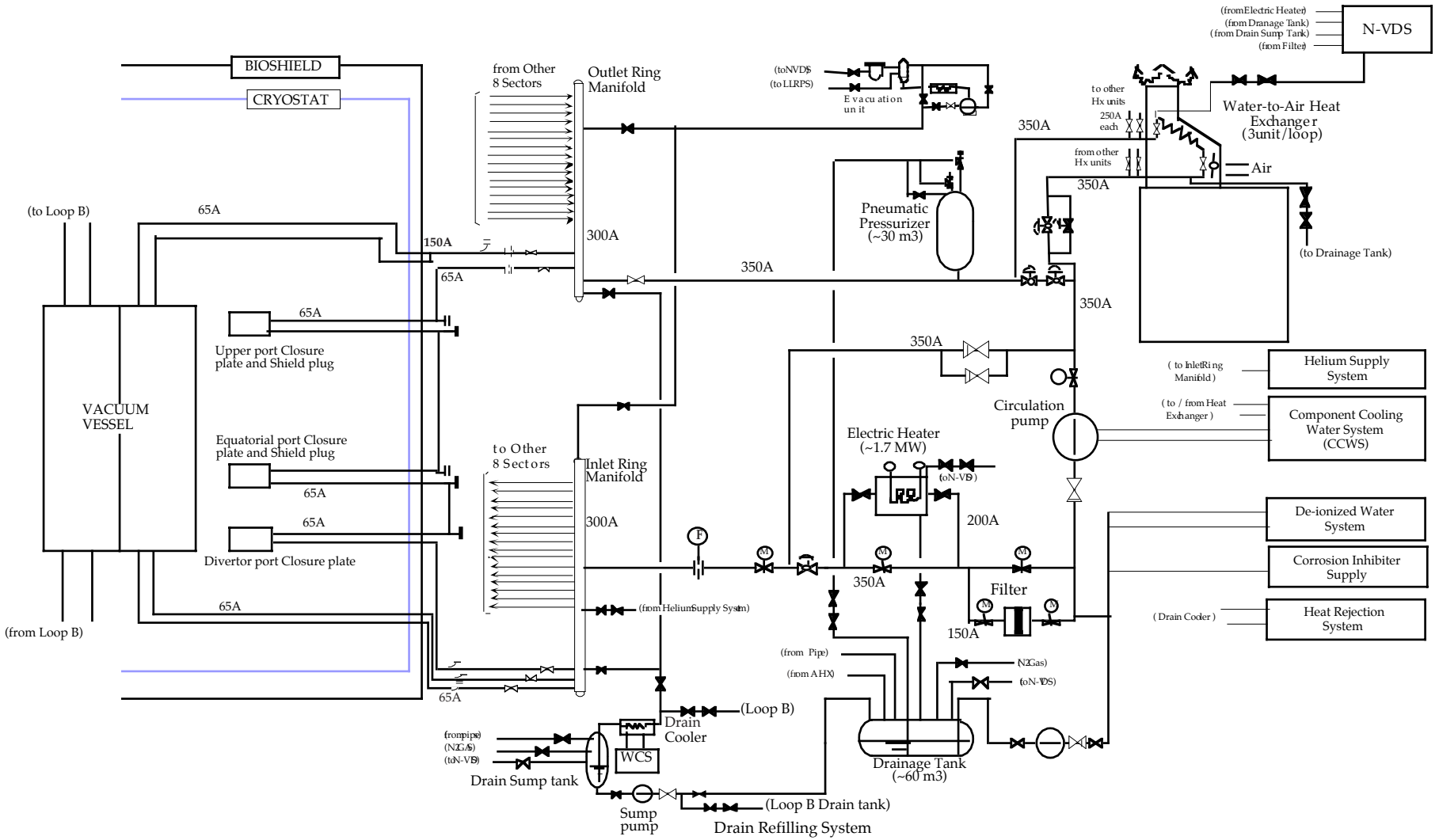

Figure 3.3.3-3 Flow Diagram of the VV PHTS

The main loop components except for the pneumatic pressurizer, i.e. pumps, filters and electrical heaters, are located in the gallery at the divertor level. Water-to-air HXs are located on the roof of the TCWS vault on the east (elevation + 34 m) and west (elevation + 31m) side of the tokamak hall and are enclosed with a chimney to enhance the natural convection of air.

The pneumatic pressurizer is located inside the tokamak hall and its volume is sufficient to accumulate the expansion volume from room temperature to baking temperature, and therefore no volume control system is needed.

Due to the relatively large thermal mass of the VV PHTS, the heat load during a plasma pulse is accumulated in the coolant and VV materials and released slowly, thereby smoothing the pulsed heat load. Numerical studies demonstrate that the same basic smoothing action occurs during 3,000 s non-inductive pulses, and confirm the feasibility of temperature control under these conditions. During normal plasma operation, forced circulation is used and the total flow is fed through the HX. The HX bypass is used only during the baking operation to control the VV inlet temperature at 200°C.

The valves in the main loop of the water-to-air HX line are the fail-open type. A non-return valve is provided in the bypass line for the main circulating pump, so that natural convection is ensured in case of pump trip.

3.3.3.1.4 NB injector PHTS

A single loop supplies coolant to both the low and high voltage components of the NB H&CD system, which are located in the NB cell at the equatorial port level. The main loop data are summarised in Table 3.3.3-4, and a flow diagram is shown in Figure 3.3.3-4.

Up to three NB injectors and one diagnostic NB system can be cooled by this PHTS.

Table 3.3.3-4 Main Data for the NB Injectors PHTS

	Low voltage components	**High voltage components** (ion source)	(other)
Thermal Power	86.9 MW	4.8 MW	10.5 MW
Coolant Inlet Temp.	75°C	20°C	55°C
Coolant Outlet Temp.	~110°C	40°C[3]	95°C
Coolant Pressure	2.0 MPa	2.0 MPa	
In-Vessel Pressure Drop	1.0 MPa	0.9 MPa	
Loop Number	1		
Flow Rate	591.7 kg/s	48.8 kg/s	65.6 kg/s
Loop Pipe Inside Diameter[1]	428.6 mm		
Pressure Drop[2]	1.4 MPa		
Total Water Holdup	87 m^3		
Pumping Power	1.6 MW		
Pump Size (Vertical type)	5 m-D x 5.4 m-L		
Heat Exchanger - Exchange Heat - Heat Transfer Surface Area	Main heat exchanger 87.7 MW ~2,310 m^2	Chilled cooler 6.7 MW ~ 430 m^2	Pre-cooler 9.2 MW ~ 560 m^2
Pressuriser Size (Pneumatic type)	4.7 m^3		

[1]Coolant velocity < 6 m/s
[2]Total pressure drop including LV/HV components, heat exchanger and piping
[3]For the main components with 4.0 MW heat load

During operational periods, the inlet coolant temperature to the NB injector components must be maintained less than 80°C for the low voltage system and less than 20°C for the ion source and 60°C for the other components in the high voltage system despite the pulsed nature of plasma operation. However, there is no particular requirement for lower temperature limits and decay heat removal, such as for the other in-vessel PHTSs. Therefore, a HX bypass for temperature control and a low flow pump are not necessary, which simplifies the loop configuration.

A bypass line around the main pump and a stop valve with intermediate opening in this bypass line provide a trickle flow to the NB injectors during standby to reduce erosion of the Cu material in the NB injectors and to prevent freezing.

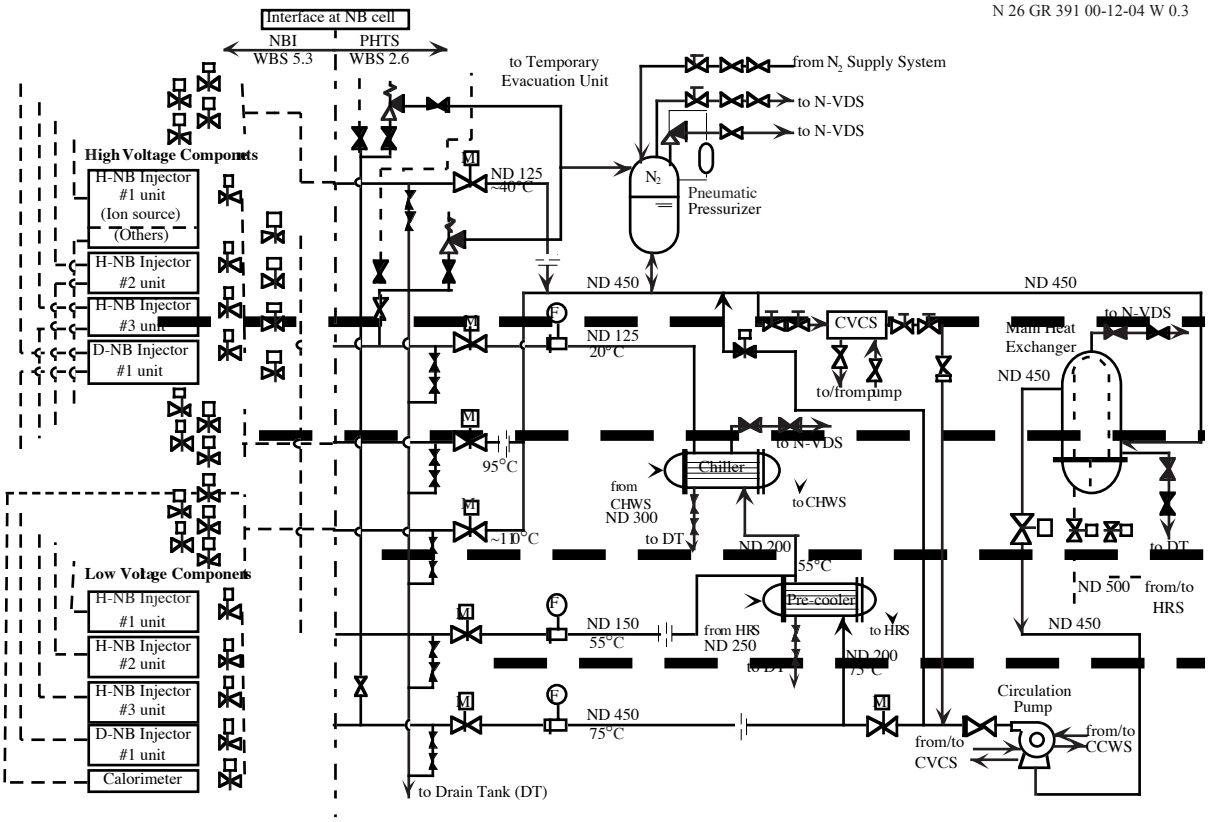

Figure 3.3.3-4 Flow Diagram of NB Injectors PHTS

3.3.3.1.5 Chemical and Volume Control Systems (CVCSs)

The CVCSs consist of three units for in-vessel PHTSs. These systems are installed in the TCWS vault below the mezzanine floor. A flow diagram of the CVCS for the PFW/BLK PHTS is shown in Figure 3.3.3-5, and the main data are summarised in Table 3.3.3-5.

The filtered stream is cooled in a recuperative HX to below ~100°C. Then it passes through a pressure reducer, where the coolant pressure is reduced from PHTS loop pressure to 0.5 - 1 MPa, being kept at this value in the remainder of the unit up to the re-injection pump. In a second HX called the letdown cooler, the temperature of the stream is reduced to ~50°C. At this temperature, the water is further purified in mixed ion-exchange resin beds.

After the resin bed, the stream is led to a volume control tank in which the hydrogen concentration is controlled. Via a high pressure re-injection pump, the coolant is re-pressurised and re-injected back into the loop, via the recuperative HX, or is pumped to a pressuriser or drain tank. A small bleed stream is also provided for the main pump shaft seal.

Table 3.3.3-5 Main data for the CVCS for PFW/BLK PHTS

Operational state or mode	Plasma Operation State	Baking	Decontamination Mode
Volumetric Flow Rate (at inlet)	45 m^3/h	45 m^3/h	90 m^3/h
Feed Coolant Temp.	148°C	240°C	100°C
Return Coolant Temp.	120°C	190°C	83°C
Feed Coolant Pressure	1.7 MPa	4.3 MPa	1.7 MPa
Return Coolant Pressure	3.4 MPa	4.6 MPa	3.4 MPa
Number of Inlet Filters in Service	1	1	2
Number of Resin Beds in Service	1	1	2
Number of Re-injection Pumps in Service	2	2	4
Loop Pipe Inside Diameter[1]	78 mm		
Recuperative Heat Exchanger - Exchange Heat (Max) - Heat Transfer Surface Area	3 modules 6.5 MW 213 m^2		
Letdown Cooler - Exchange Heat (Max) - Heat Transfer Surface Area	1 unit 2.6 MW 178 m^2		
Volume Control Tank	1 unit		
Inlet Filter	2 units		
Resin Bed	2 units		
Re-injection Pump - Pumping Power	4 units 70 kW		

[1]Coolant velocity < 6 m/s

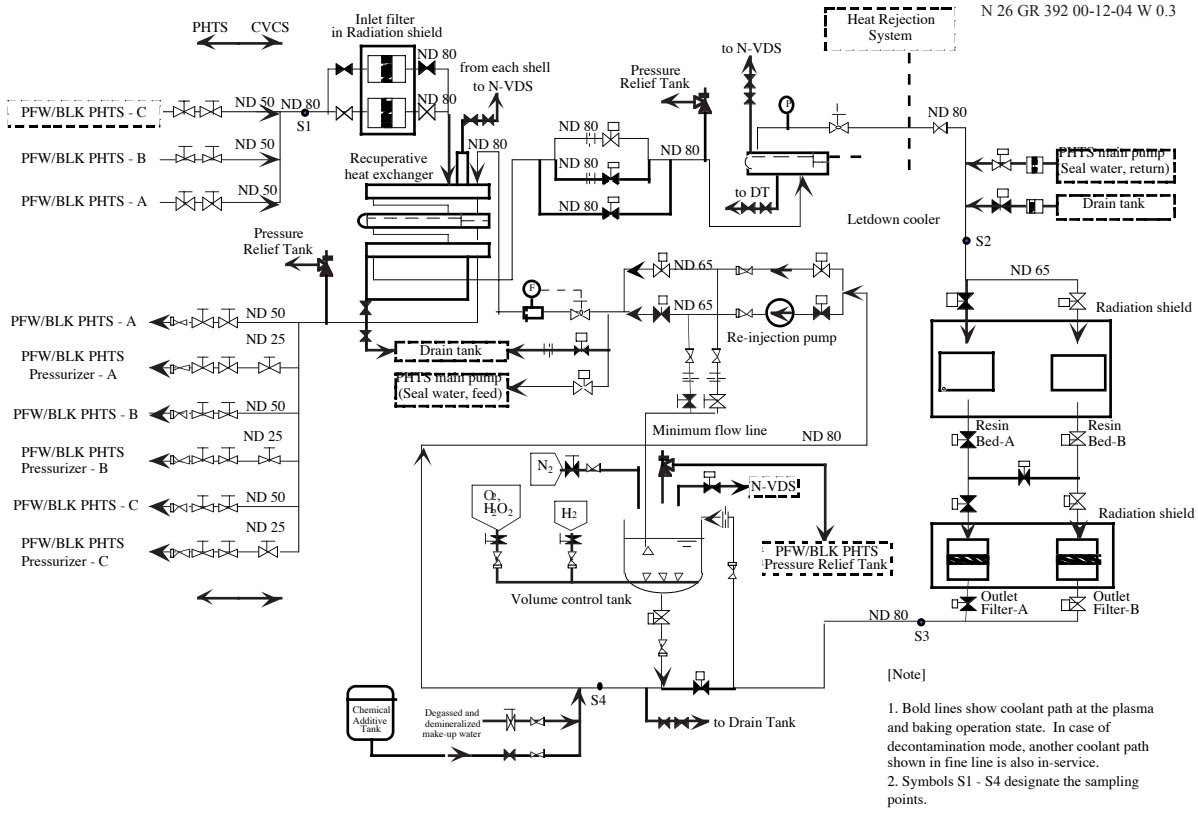

Figure 3.3.3-5 Flow Diagram of the CVCS for the PFW/BLK PHTS

Controlled oxidation is implemented to form a protective passivating oxide layer on the wetted surfaces after installation or maintenance, prior to plasma operation, in order to reduce the subsequent oxidation rate. Oxygen is added to the coolant to promote the formation of stable spinel-rich (mixed chromium/iron/nickel oxide) films.

During normal operation, the coolant chemistry will be controlled such that the further deposition of oxide layers on top of the stable spinel film is kept low. This is achieved by lowering the oxidation potential by adding and dissolving hydrogen in the coolant. Continuous circulation will be maintained through the filters and resin beds to remove suspended and dissolved compounds respectively in order to reduce the concentration of ACPs (activated corrosion products) in the coolant and keep the plate-out rates along the loop surfaces at an acceptably low level.

To lower the dose burden to maintenance workers, the ability to undertake an intensive campaign of ACP removal is foreseen. The flow rate through the CVCSs is in this case increased to approximately twice the normal processing rate and the chemistry is changed to remove deposited ACPs by dissolving oxygen and/or hydrogen peroxide in the coolant.

For the VV PHTS, a filter located on the divertor level of the tokamak building removes ACPs in the coolant, instead of the CVCS unit.

3.3.3.1.6 Draining and Refilling Systems

For maintenance and inspection operations, loops have to be drained partly or fully. Storage segmentation is based on avoiding the mixing of coolant at different contamination levels or chemistry requirements.

Some of the drain tanks are also used to receive the drain water from the VV via the emergency drainage lines during an in-vessel coolant leak. The assigned drain tanks, which have a total volume ~ 400 m^3, are maintained in a partially-evacuated condition, ~ 10 kPa, during operation, and they have a safety function.

To accommodate expelled coolant from the CVCSs, caused by expansion of the coolant during heating up from pulse operating temperature to baking temperature, separate drain tanks for volume control are required for the PFW/BLK and DIV/LIM PHTSs. The NB injector PHTS does not need a drain tank for volume control because there is no baking operation.

Refilling of the PHTSs loops is performed by the injection pumps through the CVCSs.

The draining and refilling systems, except that for the VV, are located in the drain tank area at the basemat level of the tokamak building. Valves, instrumentation and refilling pumps are also located in a room connected to the detritiation system. The draining and refilling system for the VV PHTS is located on the same floor but outside the room.

Table 3.3.3-6 shows the drain tank volumes of the draining and refilling system.

Table 3.3.3-6 Draining and Refilling System Tank Volumes

System	Number of drain tanks*	Total internal volume (m^3)
PFW/BLK PHTS	2 (1)	~ 500
DIV/LIM PHTS	2 (1)	~ 200
VV PHTS	2	~ 120
NB injectors PHTS	2 (2)	~ 120

* number of tanks in parentheses indicates those used for drainage following an in-vessel coolant leak

3.3.3.1.7 Drying System

After drainage, the residual water in the in-vessel components, the VV inter-wall space and the port closure plates must be dried to facilitate leak testing of the in-vessel components. The procedure is to blow out most of the residual water with nitrogen gas, from all modules that are open to the gas flow. Subsequently, hot nitrogen gas is introduced to evaporate and thereby remove the remaining liquid. It is intended that the system be used for both the blow-out and drying stages, in order to minimise the capital cost, and the capacity of the compressor and heat exchanger. Although two independent compressors for the blow-out and drying are designated because of the different working conditions (the compressor shaft powers required are ~500 kW for the blow-out and ~300 kW for the drying), the other components are used for both stages.

The design accounts for counter current flow limiting behaviour in the cooling paths and the flow area of the paths that have to be blown out concurrently. The limiting condition for the blow-out is 8 blanket modules to be blown concurrently: the residual water after the blow-out

is evaluated as ~5% in this case. This evaluation has large uncertainty, depending on the configuration, and a confirmatory blow-out test will be needed, using the actual configuration.

The drying system data are given in Table 3.3.3-7. A simplified flow diagram of this system is shown in Figure 3.3.3-6.

The drying procedure can be roughly divided into two stages: a heat-up stage with the nitrogen at 150 - 200°C, 2.1 MPa, and a dry-out stage with the nitrogen at 150 - 200°C, 0.6 MPa. During the heat-up stage, the component and the residual water are heated to above 150°C. Then the gas pressure is reduced to ~0.5 MPa (i.e. saturation pressure at 150°C). The residual water is vaporised and extracted by the drying system.

This system has the capability to dry the blanket modules in two 20° sectors or the divertor cassettes in six 20° sectors in a single operation to a residual steam partial pressure of ~0.002 MPa (saturation pressure at 20°C). The estimated drying time, following the blow-out, is ~3 days for the blanket modules connected to one PFW/BLK loop and for all the divertor cassettes. The major components of the drying system are located in the TCWS vault cooler and dryer room in the tritium building.

At the price of reducing the number of components that can be blown out concurrently, the simplification of the common use of a single 300 kW compressor for all operations may be possible. Further development of the leak checking procedure detail is necessary before the requirements can be finalised.

Table 3.3.3-7 Main Data for the Drying System

	Blow-out mode	**Heat-up mode**	**Dry-out mode**
Fluid	Nitrogen	Nitrogen	Nitrogen + H_2O (steam)
Fluid Inlet Temp.	40°C	210°C	210°C
Fluid Outlet Temp.	40°C	160°C	160°C
Fluid Inlet Pressure	4.0 MPa	2.1 MPa	0.6 MPa
Number of loops	1		
Main piping size	ND 250		
Compressor - Compressor Power	Magnetically floating bearing type ~500 kW, 1 unit	~300 kW, 1 unit	
Electrical Heater - Heater Power	Shell and baffle type, 1 unit 690 kW		
Cooler Condenser #1 - Exchange Heat	Cooled by HRS cooling water, 1 unit 370 kW		
Cooler Condenser #2 - Exchange Heat	Cooled by chilled water, 1 unit 190 kW		
Drain Separator	Cyclone separator type, 1 unit		
Mist Separator	Vane separator type, 1 unit		
Filter	2 units, 3 μm (Mesh fineness)		

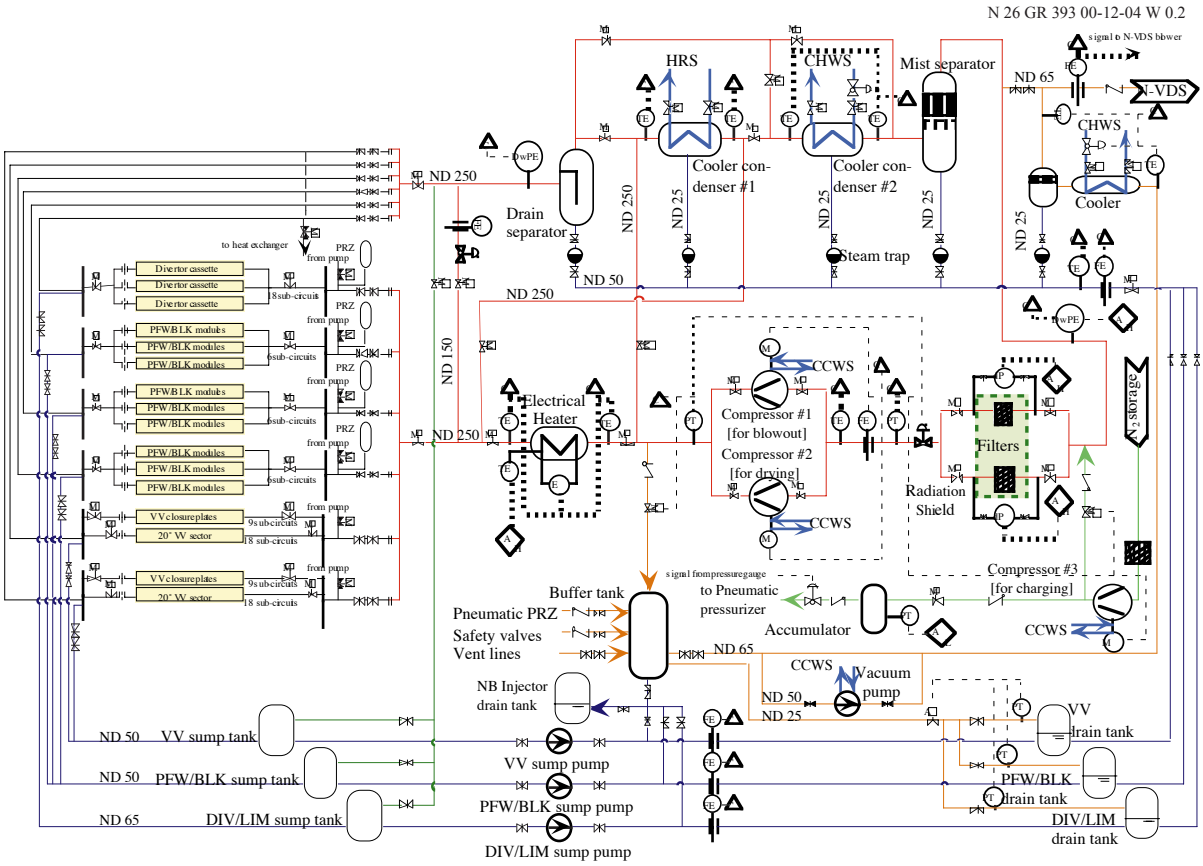

Figure 3.3.3-6 Flow Diagram of the Drying System

3.3.3.2 Component Cooling Water System (CCWS)

The CCWS provides demineralised cooling water flow at a specified quality to components and systems, and transfers heat to the circulating water via intermediate HXs. The total heat rejected through the CCWS is ~ 120 MW when operating at full capacity.

The heat loads of clients, and the flow rate and temperature condition in each CCWS, are summarised in Table 3.3.3-8. The schematic flow diagram is shown in Figure 3.3.3-7. The intermediate HXs are of the plate type.

The CCWS is partitioned into three zones.

(i) Tokamak zone

This serves pumps inside the tokamak building, NB active compensation/correction coils, and the RF heating components inside the assembly building. As the power supply components for the RF H&CD require an inlet temperature less than 35°C, the corresponding CCWS sub-loop (CCW-1C) is interfaced with a CHWS.

The inlet and outlet temperatures in Table 3.3.3-8 are those under the most adverse conditions. As a lower inlet temperature is acceptable, no temperature control is foreseen. The loop (CCW-1C) for the power supply components has a bypass line on the intermediate HX to avoid the component temperature becoming lower than the dew point.

(ii) Power Supply zone

This serves power supply components, and the loops are located in the magnet power supply switching network building. The CCWS for some power supply components requires an inlet temperature of less than 35°C, and the corresponding CCWS sub-loop (CCW-2B) is interfaced with the CHWS. Two sub-loops have demineralisers to maintain the required electric conductivity of the coolant.

(iii) Site services zone

This serves components in the site services building, the control building, the laboratories and offices.

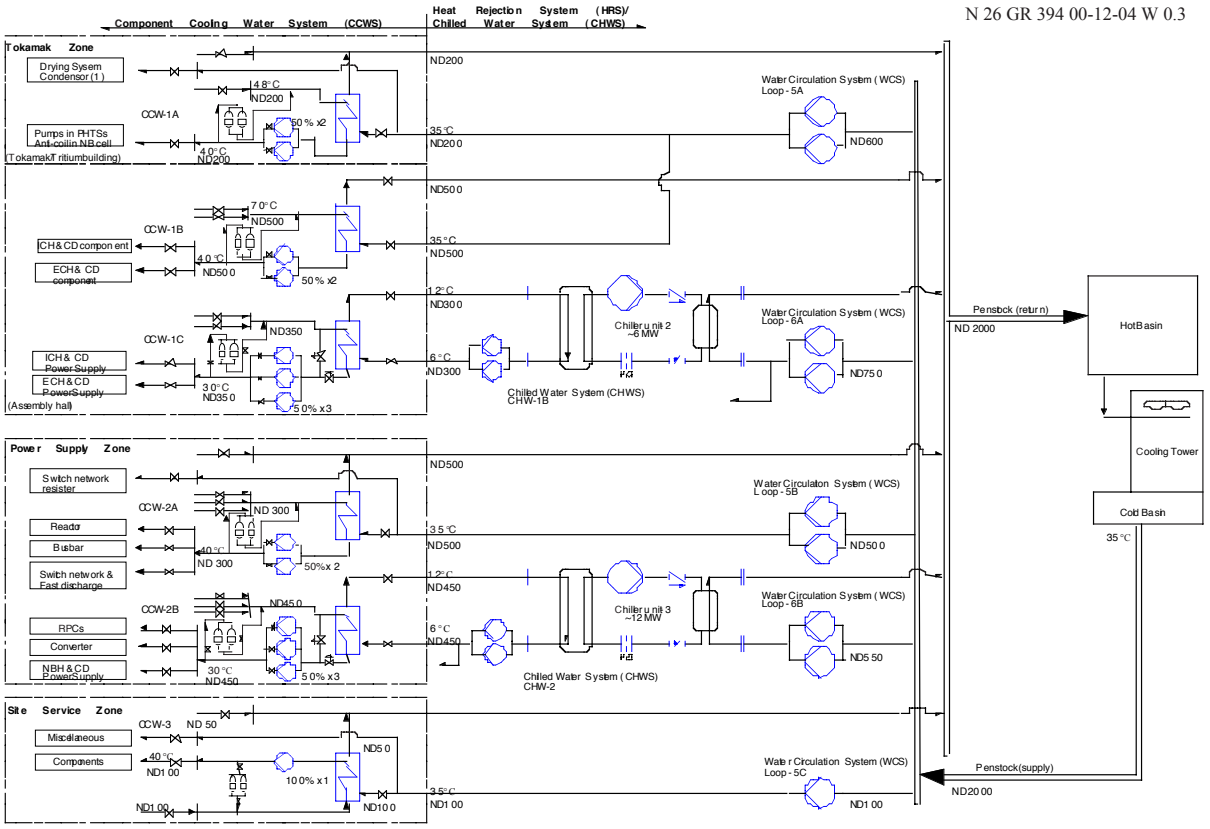

Figure 3.3.3-7 Schematic Flow Diagram of the CCWS

Table 3.3.3-8 Heat Loads and Flow Rates for the CCWS

System (Loop)	Clients		Heat Load of Clients		Flow Rate		Inlet/Outlet Temp. (°C)	
	Name	Location	MW	Sum.	(kg/s)	Sum.	In	Out
CCWS in tokamak zone [Loop CCW-1A]	PHTSs pumps	Tokamak building	1.8	3.3	85.3	94.3	40	45
	NB ACCC*	NB cell	1.5		9.0		40	80
CCWS in tokamak zone [Loop CCW-1B]	IC H&CD components	Assembly hall	21.6	81.6	172.1	650.1	40	70
	EC H&CD gyrotron	Assembly hall	60.0		478.0			
CCWS in tokamak zone [Loop CCW-1C]	IC H&CD power supply	Assembly hall	1.92	5.9	222.2	322.2	30	34.4
	EC H&CD power supply	Assembly hall	4		100.0			
CCWS in power supply zone [Loop CCW-2A]	Reactors	Power supply zone	5.84	18.8	94.4	228.1	40	59.7
	Busbars	Power supply zone	10.11		111.4			
	Switching network and fast discharge	Power supply zone	2.83		22.2			
CCWS in power supply zone [Loop CCW-2B]	RPCs** + coil converters	Power supply zone	5.73	9.2	291.7	475.0	30	34.6
	NB injector power supply	Power supply zone	3.45		183.3			
CCWS in site services zone [Loop CCW-3]	Component in building	Site service zone	0.6	0.6	28.7	28.7	40	45

* Active Compensation/ Correction Coils ** Reactive Power Compensating Units

3.3.3.3 Chilled Water System (CHWS)

The CHWS provides a flow of chilled water (~ 6°C) to those plant systems which require low temperature, such as HVAC, and CCWS for the power supply components. The total heat rejected through the CHWS is ~ 41 MW when operated at full capacity. There are two CHWS loops for the tokamak zone, one for the power supply zone and one for the site services zone. In addition, two independent "safety-related" loops of the CHWS are installed in the tokamak zone. The heat load for the safety-related CHWS is ~ 4 MW, and full redundancy appropriate to its safety importance classification (SIC) is provided.

The heat loads required by the clients, and the flow rates and temperature conditions in each CHWS are summarised in Table 3.3.3-9. The system configuration is shown in Figure 3.3.3-8.

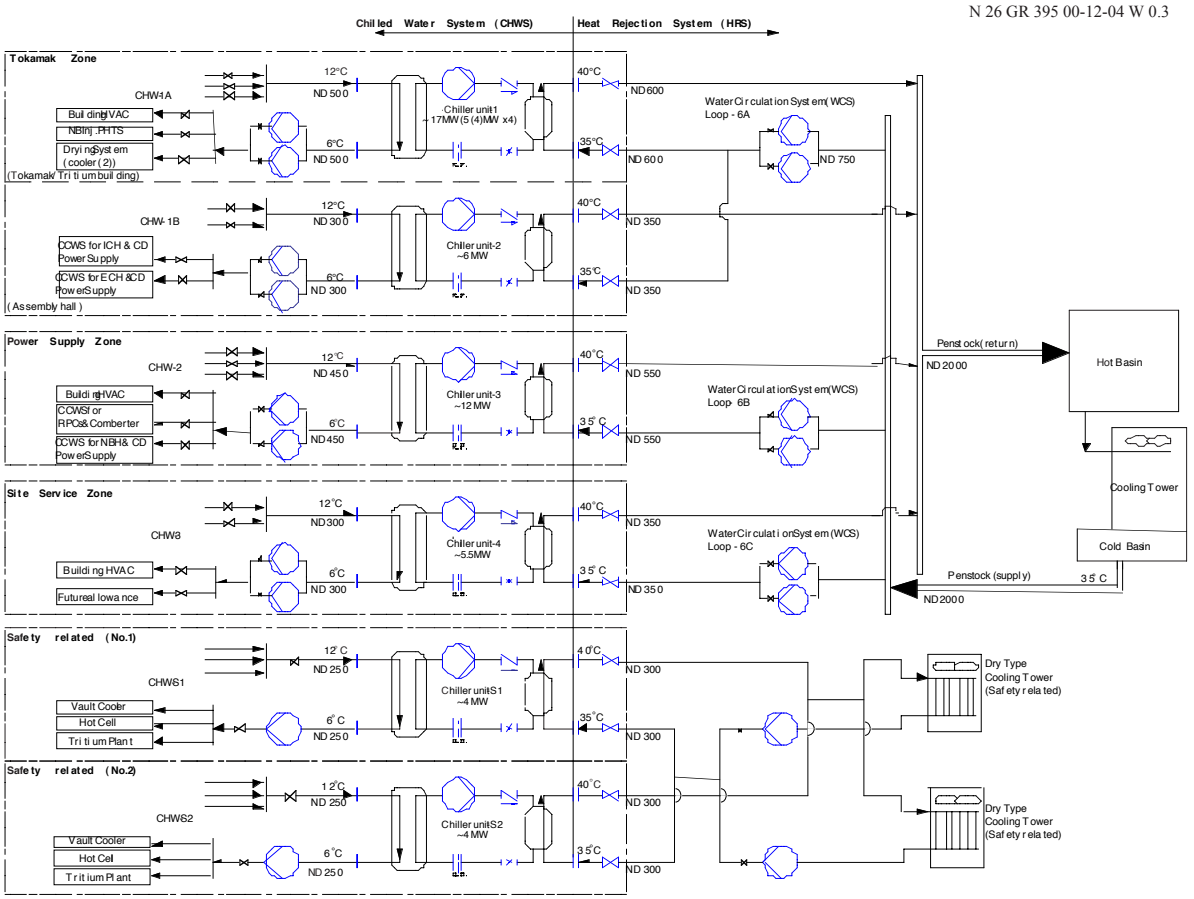

Figure 3.3.3-8 Schematic Flow Diagram of the Chilled Water System (CHWS)

Table 3.3.3-9 Heat Loads, Temperatures and Flow Rates for the CHWS

System (Loop)	Clients		Heat Load of Clients		Flow Rate		Inlet/Outlet Temp. (°C)	
	Name	Location	MW	Sum.	(kg/s)	Sum.	In	Out
CHWS in tokamak zone [Loop CHW-1A]	Tokamak building HVAC	Tritium building	9.3	17.0	370.4	675.2	6	12
	Radwaste/ personnel building HVAC	Radwaste building	0.75		29.9			
	NB injector chilled HX (for HV)	Tritium building	6.7		266.9			
	Drying system: condenser #2	Tritium building	0.2		8.0			
CHWS in tokamak zone [Loop CHW-1B]	CCWS for ICH&CD power supply	Assembly hall	1.9	5.9	76.5	235.8	6	12
	CCWS for ECH&CD power supply	Assembly hall	4		159.3			
CHWS in power supply zone [Loop CHW-2]	Buildings HVAC	Power supply zone	2.9	12.1	115.5	481.2	6	12
	CCWS for RPCs* + coil converters	Power supply zone	5.73		228.3			
	CCWS for NB injectors power supply	Power supply zone	3.45		137.4			
CHWS in site services zone [Loop CHW-3]	Buildings HVAC	Site services zone	5	5.5	199.2	219.1	6	12
	Future allowance load	Site services zone	0.5		19.9			
Safety-related CHWS [Loop CHW-S1]	TCWS vault cooler	Tritium building	1.1	4.0	43.8	159.3	6	12
	Hot cell HVAC	Hot cell building	0.9		35.9			
	Tritium plant	Tritium plant building	2		79.7			
Safety-related CHWS [Loop CHW-S2]	TCWS vault cooler	Tritium building	1.1	4.0	43.8	159.3	6	12
	Air conditioning in hot cell	Hot cell building	0.9		35.9			
	Tritium plant	Tritium plant building	2		79.7			

* Reactive Power Compensating Unit

3.3.3.4 Heat Rejection System (HRS)

The HRS provides the final heat sink and rejects all heat loads in the ITER plant. It consists of water circulation systems (WCSs) and the cooling tower system (CTS). Water is provided at a maximum temperature of 35°C and returned at a maximum temperature of 75°C.

The WCSs provide pipeline connections for cooling water feed and return streams from the HXs of all heat transfer systems to the heat sink, i.e. the CTS. The WCSs interface with the CTS at the collecting hot basin and the distribution cold basin. The HRS has 3 loops for the TCWS, one for the cryoplant warm compressors, 3 loops for the CCWS and 3 loops for the CHWS. Water is circulated from a cold penstock, through pumps situated in pump stations

which are located just outside the clients' buildings. The heat loads, temperatures and flow rates in the WCSs are summarised in Table 3.3.3-10.

The design of the circulating pump motors allows polarity changeover to enable the main pumps to change to low pump speeds during low flow operation (including the case of loss of site power) for the WCSs serving the PHTSs. This enables the elimination of separate low flow pumps and associated piping and valves. In the event of a single main pump trip, the remaining pump will supply sufficient flow to maintain the return temperature to less than 90°C, and thus prevent boiling.

The design of the CTS, including the basins, is based on a cost optimisation between cooling tower heat rejection capacity and temperature levelling capacity in the hot basin. The capacity of the cooling tower units is based on the most thermally adverse burn (3,000 s of burn with 350 MW of fusion power, see 3.3.4.4). Based on ITER site reference conditions, the system is envisioned to consist of 8 cooling cells and 4 fans. The volume of the hot basin is 12,000 m^3 and the cold basin 20,000 m^3.

Additionally, a dedicated dry type CTS with a capacity of ~ 5 MW is adopted for the safety-related CHWS. The heat loads and flow rates in the safety-related HRS are shown in Table 3.3.3-11. This system is connected to class III power during off-normal conditions.

Table 3.3.3-10 WCS Heat Loads and Flows (non-safety related)

System name	Clients		Design heat Load in HRS		Flow Rate		Inlet/Outlet Temp. (°C)	
	Name	Location	MW	Sum.	kg/s	Sum.	In	Out
Primary first wall and blanket WCS [Loop 1]	PFW/BLK heat exchanger #1	TCWS vault	234	702	1,400	4,195	35	75
	PFW/BLK heat exchanger #2	TCWS vault	234		1,400		35	75
	PFW/BLK heat exchanger #3	TCWS vault	234		1,400		35	75
Divertor and limiter & neutral beam injectors WCS [Loop 2]	DIV/LIM heat exchanger	TCWS vault	206	303	1,230	1,980	35	75
	NB injector heat exchanger	TCWS vault	88.0		600		35	70
	Pre-cooler for NB injector (HV)	TCWS vault	9.2		147		35	70
CVCS WCS [Loop-3]	PFW/BLK CVCS-1	TCWS vault	3.5	11.2	55.8	118	35	50
	DIV/LIM CVCS-1	TCWS vault	1.4		22.3		35	50
	NB injectors CVCS-1	TCWS vault	0.3		4.0		35	50
	Test blanket modules PHTSs	TCWS vault	6.0		35.8		35	75
Cryoplant compressor WCS [Loop 4]	Cryoplant compressor	Cryoplant building	25	25	854	854	35	42

Table 3.3.3-10 WCS Heat Loads and Flows (non-safety related) (cont'd)

System name	Clients		Design heat Load in HRS		Flow Rate		Inlet/Outlet Temp. (°C)	
	Name	Location	MW	Sum.	kg/s	Sum.	In	Out
Component cooling water system(1) [Loop 5A]	PHTS pumps	Tokamak zone	1.8	85.7	85	755	35	40
	NB ACCC**	Tokamak zone	1.5		9		35	75
	IC H&CD (components outside VV)	Tokamak zone	21.7		173		35	65
	EC H&CD gyrotron	Tokamak zone	60.2		480		35	65
	Drying system: Condenser #1	Tokamak zone	0.5		8		35	50
Component cooling water system(2) [Loop 5B]	Reactors	Power supply zone	5.89	24.6	201	684	35	42
	Busbars	Power supply zone	10.3		352		35	42
	Switching network and fast discharge	Power supply zone	2.88		98		35	42
	Switching network resisters	Power supply zone	5.50		33		35	75
Component cooling water system(3) [Loop 5C]	Components in building	Site services zone	0.6	1.2	21	26.2	35	42
	Miscellaneous in building	Site services zone	0.6		6		35	60
Chilled water system(1) [Loop 6A]	Tokamak buildings HVAC	Tritium building	11.6	28.6	556	1,368	35	40
	Radwaste/ personnel building HVAC	Tritium building or Radwaste building	0.94		45		35	40
	NB injectors chiller (for HV)	Tritium building	8.4		400		35	40
	IC H&CD power supply	Assembly hall	2.40		115		35	40
	EC H&CD power supply	Assembly hall	5.00		239		35	40
	Drying system: Condenser #2	Tritium building	0.25		12		35	40
Chilled water system(2) [Loop 6B]	Buildings HVAC	Power supply zone	3.63	15.1	174	722	35	40
	RPCs*** + coil converters	Power supply zone	7.16		342		35	40
	NB injectors power supply	Power supply zone	4.31		206		35	40
Chilled water system(3) [Loop 6C]	Buildings HVAC	Site services zone	6.25	6.9	299	329	35	40
	Future allowance load	Site services zone	0.63		30		35	40
HRS TOTAL	-	-	-	1,205*	-	11,030	-	-

* Total capacity in clients. Maximum heat load for CTS is ~ 1,120 MW
** Active Compensation/Correction Coils
*** Reactive Power Compensating Units

Table 3.3.3-11 WCS Heat Loads and Flows (safety-related)

System name	Clients		Design Heat Load in HRS		Flow Rate		Inlet/Outlet Temp. (°C)	
	Name	Location	MW	Sum.	kg/s	Sum.	In	Out
Safety-related [Loop 7]	TCWS vault cooler	Tritium building	1.4	5.0	67	239	35	40
	Hot cell HVAC	Hot cell building	1.1		53		35	40
	Tritium plant	Tritium building	2.5		120		3	40

3.3.4 System Performance Analysis Summary

3.3.4.1 Stress in PHTS Piping

A complex pipe network is laid out inside the TCWS vault and the upper and lower pipe chases. Thermal and seismic stress analyses have been performed confirming the design feasibility.

(1) The piping stress in the in-vessel PHTSs are below the allowable values for both of ASME III class 2 and ANSI-ASME B.31.3 codes.
(2) The piping stresses in the VV PHTS are below the allowable values for MITI Bulletin 501 and JEAG-4601 code (similar to the ASME III code).

As a result, the PHTS layout has been confirmed to be satisfactory for the stress.

3.3.4.2 Temperature, Pressure and Flow Rate Control in PHTSs

Due to the pulsed nature of machine operation the coolant temperatures, pressures and flow rates have to be controlled within certain ranges. These ranges are determined by a number of limiting parameters including nominal coolant inlet temperature, pressure and flow conditions that guarantee a safe margin from critical heat flux at any location inside the components, as well as avoiding excessive thermal stresses in the in-vessel and ex-vessel loop components.

(i) In-vessel Component PHTSs

Temperature control in the PFW/BLK and DIV/LIM PHTSs is achieved by controlled bypassing of the HX. During a plasma pulse, the coolant exit temperature follows the power deposition profiles of the in-vessel components, delayed by the thermal capacity of the components subject to transient temperature conditions. During fusion burn, therefore, up to the full primary coolant flow may be routed through the HX, thereby raising its temperature while the component inlet temperature is controlled at 100°C within a control band. During dwell, the inlet temperature to the in-vessel components has to be maintained at nominally 100°C. This requires full bypassing of the HX, except for any small heat load due to decay heat and pumping power. Temperature changes in the coolant lead to concomitant volume changes which are accommodated by the pressuriser. Pressure changes in the steam pressurisers corresponding to water insurge or outsurge resulting from thermal expansion or contraction of the loop water, are controlled by the use of cool water spray or heaters in the pressuriser.

A thermohydraulic analysis has been performed using the ATHENA code, and the results show that the fluctuations in temperature and pressure during the burn are within +8/-0°C and ± 0.2 MPa, respectively The analytical results for the PFW/BLK PHTS are shown in Figure 3.3.4-1. The fluctuation is within the acceptable band, and this indicates acceptable controllability of the systems.

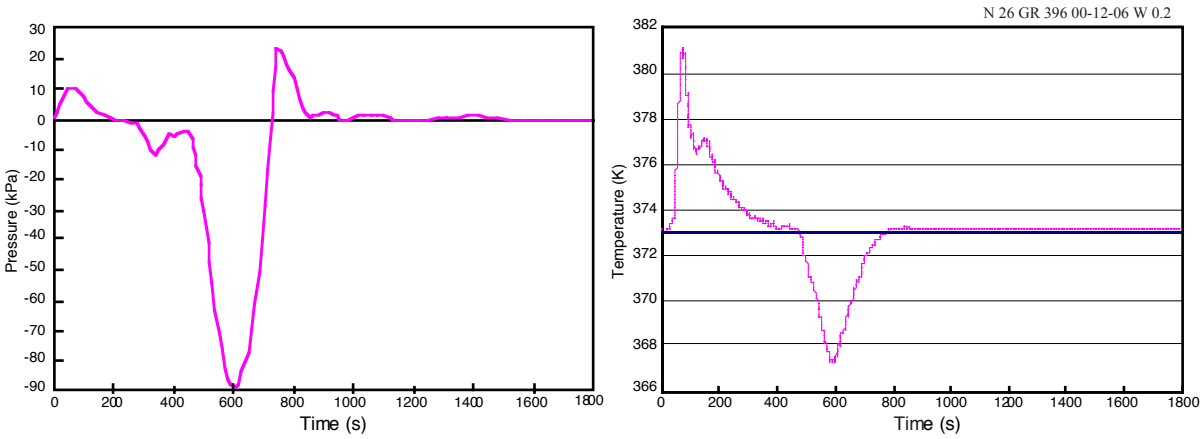

Figure 3.3.4-1 Trends of Pressure and Temperature in the PFW/BLK PHTS (100% power pulse)

The heat load of ITER is expected to cover a very wide range (i.e. zero to full power) and to change between zero power and full power in a short time (i.e. about 50 s at fusion start-up). This operating condition is quite different from that for conventional large heat transfer systems. Parametric thermohydraulic analyses are ongoing using the ATHENA code, and the preliminary results show that fluctuations in temperature and pressure during the burn cycle are within acceptable limits.

The total flow rate must be maintained within an acceptable range during normal operation. Deviation of flow rate caused by a change of flow resistance around the HX and its bypass line, as a result of the operation of control valves, is maintained within the allowable range by adoption of an appropriate control logic for the independent, cage-type, control valves.

(ii) VV PHTS

Temperature control in the VV PHTS is achieved by air-flow control in the air chimney which surrounds the air-cooled HXs. The control variable is the inlet air damper opening, with a feedback signal derived from the HX outlet temperature excursion from the setpoint. The HX bypass is used only during the baking operation to preclude heat rejection through the HXs.

Numerical studies predict a ~ 500 s delay for temperature perturbations, corresponding to a long coolant transit time through the VV cooling path, and a high degree of levelling of the pulsed heat load, on account of the large thermal mass of the VV thermally coupled materials. To reach a quasi-steady temperature condition in the VV structure requires 3 reference plasma pulses due to the large thermal mass of the VV. The VV inlet temperature during the second pulse increases because the heat transferred from the VV is larger than the HX capacity. The temperature in the VV, however, reaches the maximum in the third pulse, and it fluctuates corresponding to the heat balance in the loop. As shown in Figure 3.3.4-2, the temperature fluctuation at the VV inlet is within +2.7/-0.2°C.

For a 3,600 s pulse with 500 MW of fusion power, a more conservative condition than the current design reference, the inlet temperature increases continuously because of a lack in the heat release capability of the HX. The maximum temperature increase during the burn duration is ~ 7°C, and this is within the control band.

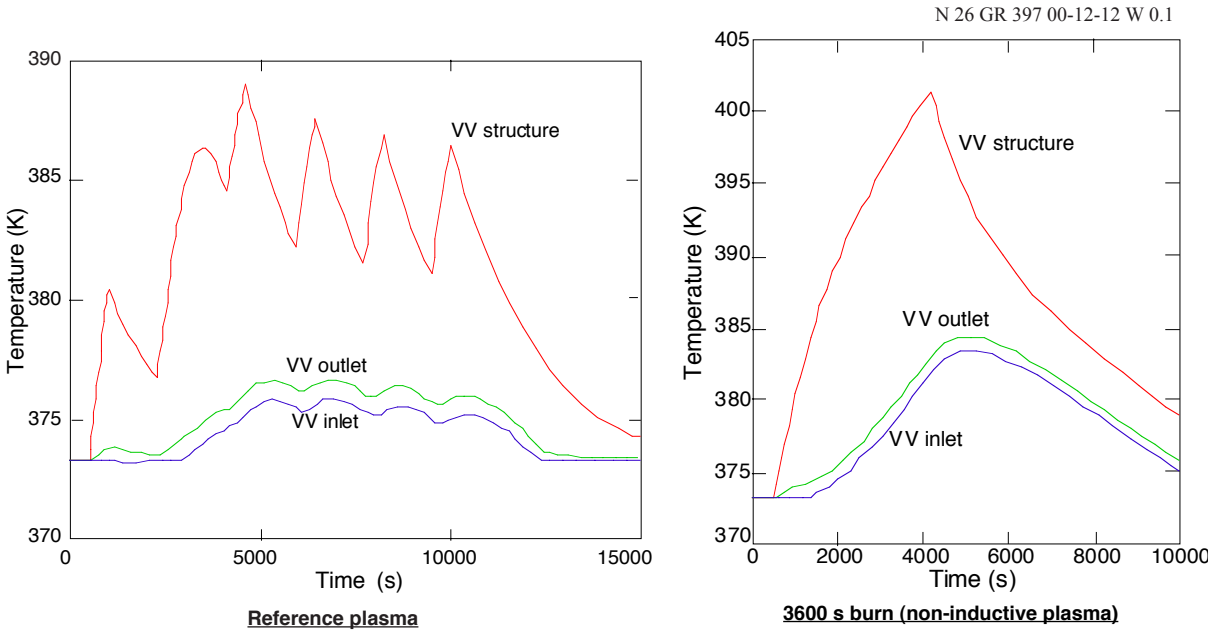

Figure 3.3.4-2 Trends of Temperature in the VV PHTS under Reference Plasma and Long Burn Conditions

Pressure regulation is achieved by either supplying nitrogen gas to, or abstracting it from, the pneumatic pressuriser. Pressure regulation is needed during normal operation, particularly during the operation mode change between pulsed and baking. However, pressure regulation is not needed during off-normal conditions.

3.3.4.3 Decay Heat Removal

Decay heat removal is performed by the heat transfer loops, i.e. the complete "train" formed by the PHTSs and the HRS, or directly to the environment (for the VV PHTS). Since the amount of decay heat to be removed is only a small fraction of the nuclear heat load during a plasma pulse, most PHTSs loops employ a low flow pump of approximately 10% of full flow throughput, to remove decay heat from the in-vessel components. These pumps are connected to class III power to protect investment in case of a loss of site power or a loss of flow during a category II event. Since loss of coolant flow in the HRS leads to the loss of the heat sink, one pump in the WCSs for the PFW/BLK and DIV/LIM PHTSs is also connected to class III power (non-safety), utilising polarity changeover type pumps to minimise the class III power requirement.

The role of the VV PHTS as the safety system for decay heat removal, in the event that all other systems fail, is to be able to remove decay heat in a passive mode, i.e. by natural convection. To fulfil this role, two fully independent loops are employed, each loop being capable of safely removing the entire decay heat, acting alone. This capability has been confirmed by numerical studies. It has also been confirmed by numerical studies that the

coolant temperature during the winter season (-15°C outside air temperature) is above 0°C for at least 6 days after event initiation. Therefore, the anti-freeze system is not safety importance classified.

3.3.4.4 Operation under 3,000 s Pulse Conditions

The PHTSs are designed for the maximum heat load, and they impose no limitation on longer pulse duration. On the other hand, the HRS has been designed for 3,000 s pulse length operation with 350 MW fusion power.

The hot basin size and the cooling tower capacity in the HRS depend on the temperature levelling (mixing) efficiency in the hot basin. Mixing within the basin is promoted by injecting the inlet hot water into the basin through a spatially distributed injection system, and by turbulent convection. The mixing behaviour has been analysed using the FLUENT code, and an almost simultaneous, complete mixing is predicted.

The numerical studies indicate that the maximum basin temperature increases as the basin volume decreases, and that higher basin temperatures require a higher cooling tower (CT) capacity (number of CT cells). The limiting condition for the cold basin (CT outlet) temperature is 35°C, which is the maximum temperature condition for the client systems such as the PHTSs. The most thermally adverse design condition is that for the 3,000 s pulse length operation with 350 MW of fusion power. Under this condition, the numerical study predicts that a cold basin volume of 12,000 m^3 is required, and this is adopted as the reference volume.

The maximum temperature for a CT is ~ 48°C under the reference plasma conditions, and the corresponding required number of CT cells is ~ 6. The maximum value of the CT inlet temperature during a 3,000 s burn is predicted to be ~ 54°C, so two additional CT cells are required to maintain the maximum CT outlet temperature below 35°C. Therefore, 8 CT cells are specified as the reference design. However, installation of the additional two CT cells can be deferred until the 3,000 s burn operation is initiated. The ability of the supply water subcooling to compensate for evaporation from the free surface of the CT is not significant, because the evaporation is less than 4 % of the circulation flow rate.

One way to attain a longer burn duration is to prescribe less adverse atmospheric conditions. The CT performance under lower atmospheric (air) temperature conditions has been investigated numerically. The required atmospheric temperature to cool the water to 35°C decreases as the CT inlet temperature increases. The maximum CT inlet temperature is 55°C, and under this condition, an atmospheric temperature of 27.8°C is required to cool the cold basin water to 35°C. For atmospheric temperatures below 27.8°C, the numerical studies indicate that the cold basin temperature does not exceed 35°C, and under these conditions, there is no limitation on the operation duration without two additional CT cells.

3.3.4.5 Operating Duration under Higher Power Plasma

The allowable operating duration of the TCWS under a higher fusion power (~ 700 MW) has been investigated numerically. The blanket PHTS is taken as the study case. The integrity of the in-vessel components under higher power conditions is outside the scope of this study.

The coolant temperature in the blanket modules responds to an increased heat load with a time delay, and this coolant temperature propagates through the cooling loop at the flow velocity. The overall heat transfer rate in the HX increases in correspondence with the primary coolant temperature rise, and the temperature in the cold leg depends on the overall heat transfer rate in the HX.

The temperature trends at each location, the hot leg, the HX inlet, the main pump inlet, and the cold leg have been investigated using a simplified numerical model.

The allowable burn duration with a fusion power 40% greater than the reference value is ~ 60 s, due to the limitation of the blanket inlet temperature needed to keep sufficient thermal margin inside the blanket modules. This is the only factor from the heat transfer system side limiting the duration of high-beta plasma operation. Other aspects related to the higher temperature conditions do not generate additional constraints.

A countermeasure to prolong the allowable duration is to set a lower inlet temperature for the blanket modules in advance of the expected ~ 40% higher fusion power, and to set a lower HRS temperature for the HX to keep the requisite heat transfer capacity in the HX. In this case, the cold leg temperature during the first pass will be lower than the upper limit of the blanket module inlet temperature, and longer operation will be possible.

The thermal hydraulic behaviour under various temperature conditions has been investigated. These temperature conditions are compatible with the heat transfer capacity of the HRS, with the logarithmic mean temperature difference between the shell and tube sides in the HX remaining virtually the same across the range of temperature conditions. Therefore, the same temperature conditions can be maintained as during normal conditions.

Although the HX heat transfer capacity is increased corresponding to increases in the HX inlet temperature and the logarithmic mean temperature difference, the heat transfer capacity cannot match the thermal load with a ~ 40% higher fusion power. This means that the allowable duration cannot be extended without a bound under the conditions that have been investigated. The attainable duration, however, is extended under lower temperature conditions. The allowable duration under various conditions is summarized in Table 3.3.4-1.

Table 3.3.4-1 Allowable Operation Durations under Various Conditions

Condition	Case-1*	Case-2**
100°C (Blanket inlet) 35°C (HX inlet of HRS)	~ 60 s	~ 60 s
90°C (Blanket inlet) 25°C (HX inlet of HRS)	~ 160 s	~ 180 s
85°C (Blanket inlet) 20°C (HX inlet of HRS)	~ 260 s	~ 360 s

* with fouling and 5 % HX plugging
** with fouling and no plugging

Fatigue of the tube sheet in the HX would be larger under lower temperature conditions because of the relatively high temperature difference between the shell and tube sides.

Therefore, fatigue analysis is required in the detailed design phase if lower temperature operation is selected as one of the operation conditions.

3.3.5 Assessment of the Design

The cooling water system and its functions required to accomplish the ITER mission have been defined and the basic system design has been completed. The design operating conditions of critical components has been established. The cost reduction, segmentation of the in-vessel components, standardisation of components, feasibility of the installation and maintenance, staged installation, and acceptable impact for the building design due to peak pressures under ex-vessel coolant leaks, are the main drivers in these designs. These drivers lead to the number of loops and the layout adopted.

It has also been confirmed that the systems as designed satisfy the requirements on temperature and pressure control in the PHTSs, passive decay heat removal capability in the VV PHTS, and operational capability for 400 s pulses under reference plasma conditions and 3,000 s burn in non-inductive operation. The operable duration under 40% higher fusion power will be between 60 s and 360 s depending on the season (ambient atmospheric conditions) and inlet temperature pre-cooling.

In addition to site-specific design, further activity is desirable in the following areas to improve plant performance, to support an operating license application, and to optimise the system design:

1. demonstration and measurement of data validating the natural convection characteristics of VV PHTS;
2. plant operation/control system design (including plant shutdown sequence after off-normal events);
3. optimisation of layout considering facilitation of installation and maintenance, particularly for the upper pipe chase (including the pipe freeze method for leak localisation);
4. clarification of requirements for drying such as the maximum number of in-vessel components to be dried concurrently, and drying duration;
5. clarification of counter current flow limiting correlation for the blanket module and divertor cassette configuration, and optimisation of the system to blow-out the residual water after gravity drainage.

3.4 Pulsed and Steady-State Power Supplies

The pulsed and steady state power supplies consist of the following four major systems:

- pulsed power distribution system;
- coil power supplies;
- heating and current drive (H&CD) power supplies (PS);
- steady state electric power network (SSEPN).

The pulsed power distribution system will supply ac power to the coil PS and H&CD PS, while the SSEPN will provide ac power to different loads (mainly motors) within the plant systems, such as the cooling water system, cryoplant etc. The coil PS and H&CD PS will supply their corresponding loads, the magnet coils and H&CD systems, in general with dc power.

The main general functions of the pulsed power distribution system PS systems are:

- to supply the ITER machine and ITER plant systems with electric power;
- to protect them in case of electric faults;
- to provide proper grounding of the machine and power supply components.

3.4.1 Pulsed Power Distribution System

The ITER pulsed power distribution system will be connected to a powerful high-voltage (HV) grid capable of providing the large pulsed power needed to supply the superconducting coils and the H&CD systems.

Ac power is assumed to be received from the HV grid at 400 kV voltage and is transformed to an intermediate level (69 kV) via 3 step-down transformers, each rated at 300 MVA continuous power (see the simplified one-line diagram in Figure 3.4.1-1). All loads (ac/dc converters for the TF coils, CS, PF coils and CCs, and H&CD systems) are shared among the three 69 kV busbars as equally as possible. Most of these loads are directly supplied from the 69 kV busbars. The loads with relatively lower power per unit (normally less than 20 MVA) are connected to the medium, 22 kV, busbars, which are powered from the 69 kV busbars through 3 step-down transformers, 50 MVA power each.

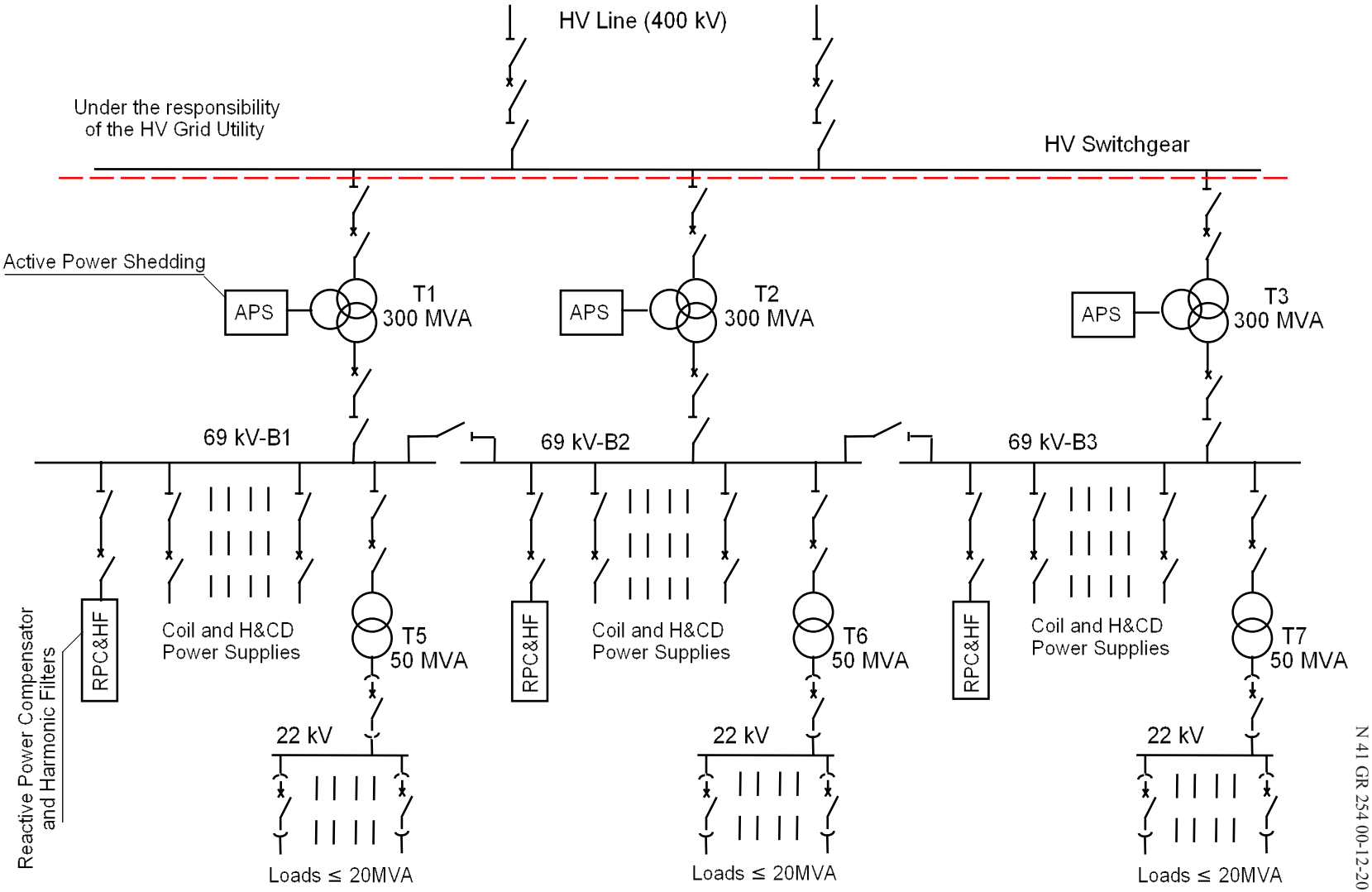

N 41 GR 254 00-12-20 F 1

Figure 3.4.1-1 Pulsed Power HV Substation and Distribution System– Simplified Diagram

The total peak pulsed power demand will be limited to 500 MW active power and 400 Mvar reactive power. This includes power required for the pre-programmed PF scenarios, power needed for the plasma current, position and shape control, including the vertical stabilisation, and power to supply the H&CD systems. The active power demand will be limited in derivative to 200 MW/s, with maximum step changes of 60 MW in normal operation. (The power steps are defined as the variation of the total power during the time when the absolute value of the power derivative is higher than 250 MW/s.)

A 180 Mvar reactive power compensation unit, including harmonic reactive power and high frequency filters, is connected to each 69 kV busbar to compensate for the ac/dc converters. Each unit consists of one thyristor-controlled reactor and 6 LC filters.

In addition, a system for active power shedding is foreseen. It consists of 3 identical units supplied by the tertiary (33 kV) winding of the 400/69 kV step-down transformers. Each unit consists of 3 three-phase resistor banks connected to the transformer via 3 vacuum circuit breakers. Altogether the three units, if switched on, may absorb up to 350 MW, thus preventing large negative power steps in the HV grid. Such steps are expected in case of plasma disruption, when all H&CD systems have to be simultaneously switched off. Later the resistors are progressively switched off in about 3 s, providing the smooth variation of the active power (about 40 MW per step). This system, however, cannot be used for the correction of steps caused by fast plasma control, which in some cases are very high (up to 90 MW). If measures to improve plasma control are unsuccessful in reducing the power step to less than that presently specified (60 MW), an increase in the power step should be considered as part of the work on the power supplies for site adaptation.

An alternative design has been developed of a power supply system fed from a HV grid with a more limited capability (e.g. 400 MW, 300 Mvar). In this design, a local energy storage will supply power required for fast control to stabilise plasma disturbances. Several options were considered, but the preference is for ac-excited flywheel motor-generators with controlled output voltage frequency, that allows them to be synchronised with the HV grid. Therefore, the common 69 kV busbars for ac power distribution can be used, and no changes are needed for the ac/dc conversion system.

3.4.2 Coil Power Supplies

The coil power supplies include the following 9 systems supplying controlled dc current to the TF and PF coils and the CS modules:

- one common power supply system for the 18 TF coils;
- 5 PS systems for the CS modules: 4 individual PS systems for CS2 and CS3 upper and lower modules, and one common PS system for the CS1 upper and lower modules connected in series;
- 2 PS systems for individual supply of the PF1 and PF6 coils;
- one common system for the 4 outer PF coils, PF2 - PF5, used for plasma vertical stabilisation.

In addition, 9 relatively small PS systems with identical configuration will supply the 9 correction coils (CCs).

3.4.2.1 TF Coil Power Supply System

The TF coils are combined in nine groups, each containing two coils which are connected in series inside the cryostat. These groups are connected in series and supplied with power by one 12-pulse, 2-quadrant thyristor-converter rated for 68 kA current, 900 V no-load voltage (see Figure 3.4.2-1). When the TF system has been charged and the current has reached the requested constant value, the primary winding of the rectifier transformer is switched from the 69 kV ac supply to the 22 kV supply. This results in a corresponding reduction of the output converter voltage and, therefore, of reactive power, for the long (a few weeks/months) period of operation with constant current. To discharge the coils, the ac power supply from the 69 kV busbar has to be restored. The minimum charge/discharge time is about half an hour. The energy stored in the TF coils at the maximum (68 kA) current is about 40 GJ.

In case of quench or a failure in the power supply system requiring immediate extraction of the coil energy, 9 fast discharge units interleaved in series with each coil pair are activated to rapidly discharge the stored energy. These units consist of circuit breakers and discharge resistors, which are rated to absorb 35 GJ and provide the discharge with an equivalent time constant of 11 s. About 5 GJ will be dissipated in the vacuum vessel, TF coil radial plates and cases, and other passive components. The maximum voltage on the discharge resistors will not exceed 8 kV.

Two circuit breakers are included and connected in series in each of the fast discharge units. The first, called the current commutation unit, is designed for multiple operation and will open when a quench is detected. In case of failure in one current commutation unit, the second circuit breaker (pyrobreaker), not suitable for repetitive operation but very reliable, will interrupt the current.

The circuit breakers for fast discharge are located in the tokamak building gallery, near the coil terminal boxes. A fast make switch also located in the gallery is switched on simultaneously with the initiation of the fast discharge. Therefore, the whole discharge circuit will be closed within the gallery and detached from the ac/dc converters and the busbars between the converters and the fast discharge units. The discharge resistors, and the counterpulse capacitor banks used to create the current zero in the current commutation unit, are located in the diagnostic building adjacent to the tokamak building, and are connected with the switches by coaxial cables.

Other provisions aimed at increasing the coil protection reliability include, in particular, the use of capacitors and reservoirs for compressed gas to provide autonomous operation of electromagnetic and pneumatic drives, redundancy, and uninterruptible supply for instrumentation and control devices and others. Moreover, two or more “lines of defence” are foreseen for the detection of, and protection against, over-current in the coils, as well as excessive or deficient values of parameters within the power supplies, e.g. over-temperature of busbars, low flow rate of cooling water etc.

3.4.2.2 Power Supplies for the CS Modules and for the Coils PF1 & PF6

These power supplies drive one CS module or PF coil, as shown in Figure 3.4.2-2 for the PF1 system (as an example), or drive two modules in series, as shown in Figure 3.4.2-3 for the CS1.

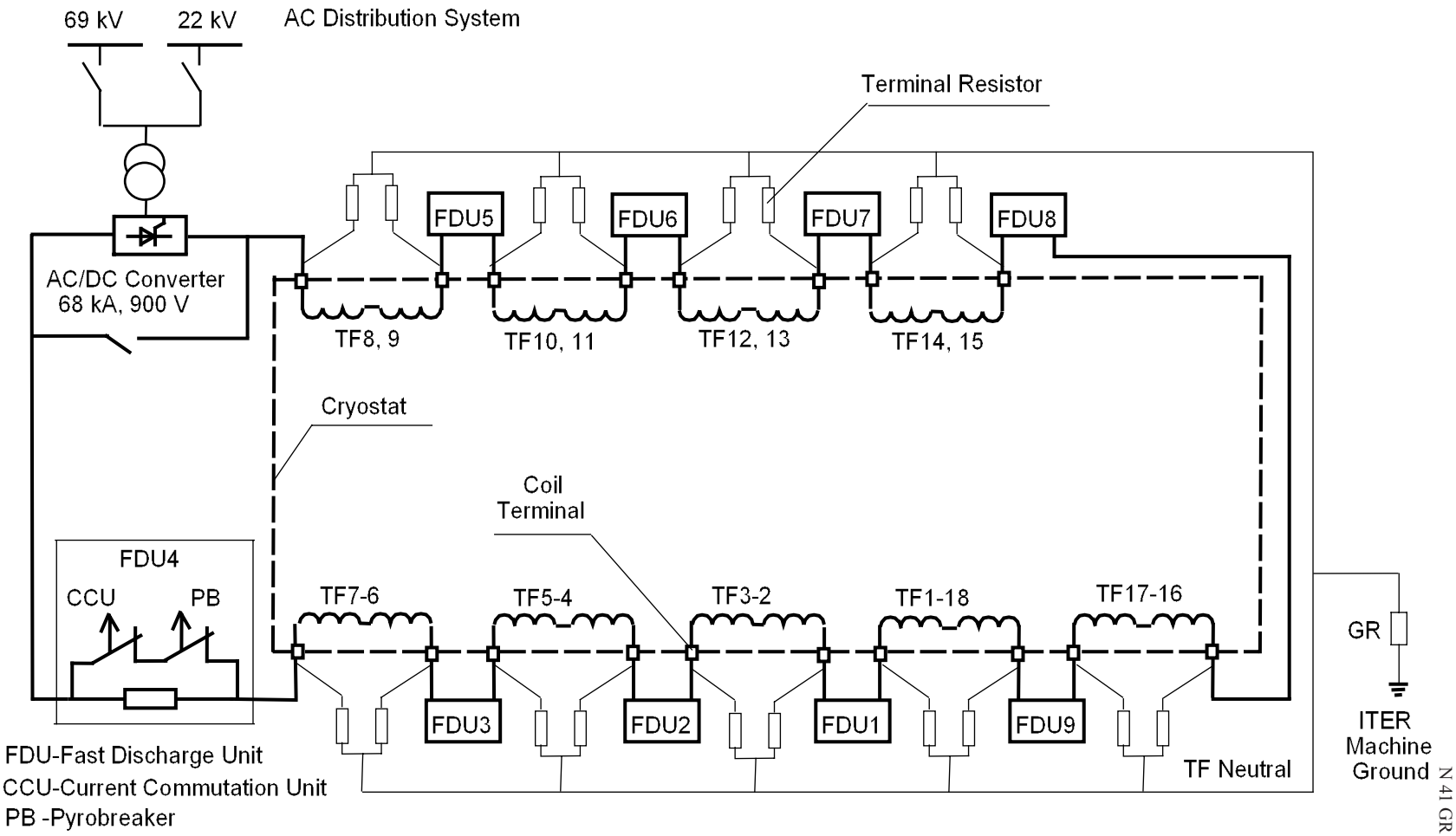

N 41 GR 255 00-12-20 F 1

Figure 3.4.2-1 TF Coil Power Supply – Simplified Diagram

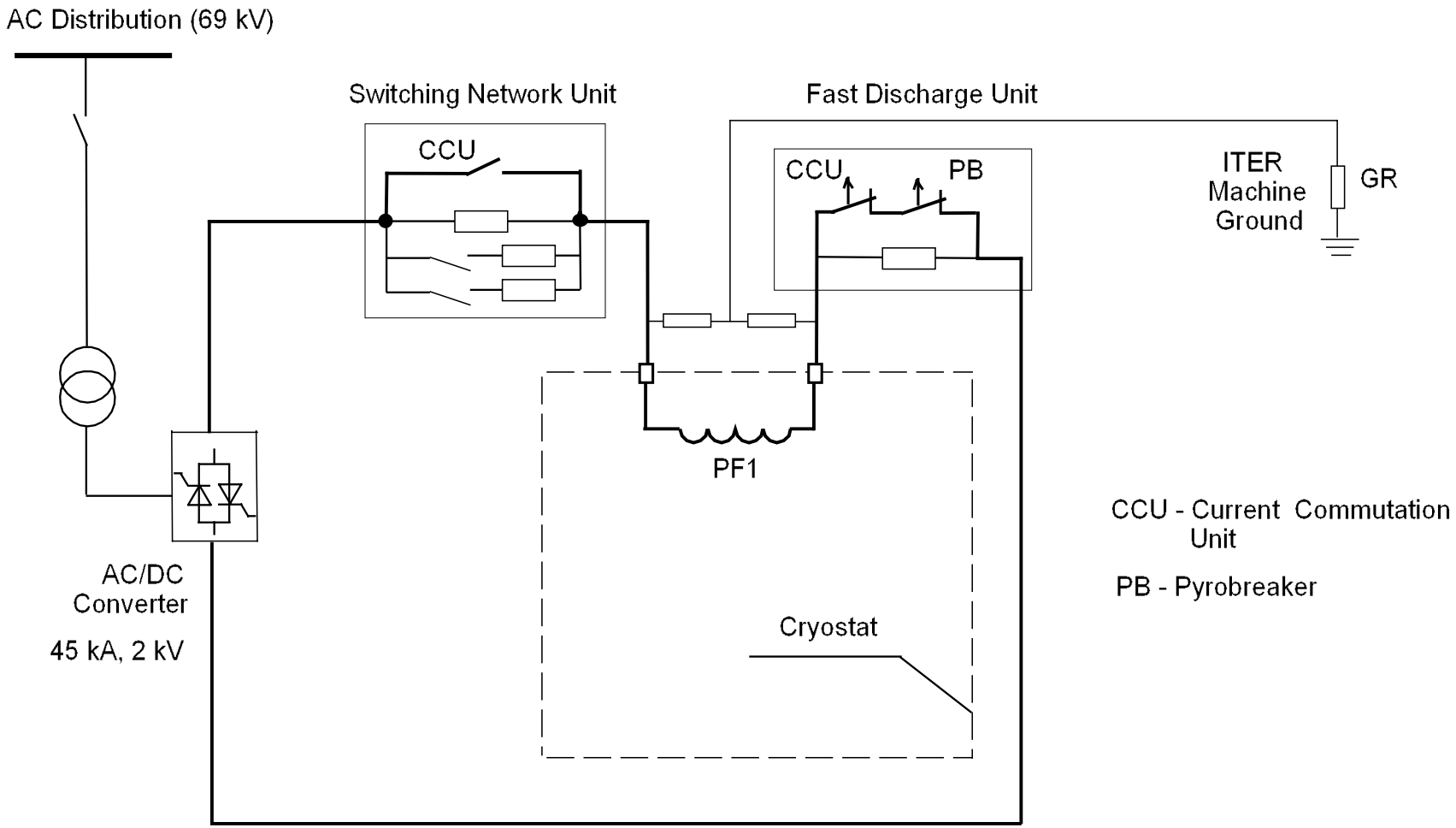

Figure 3.4.2-2 **Coil PF1 Power Supply – Simplified Diagram**

N 41 GR 257 00-12-20 F 1

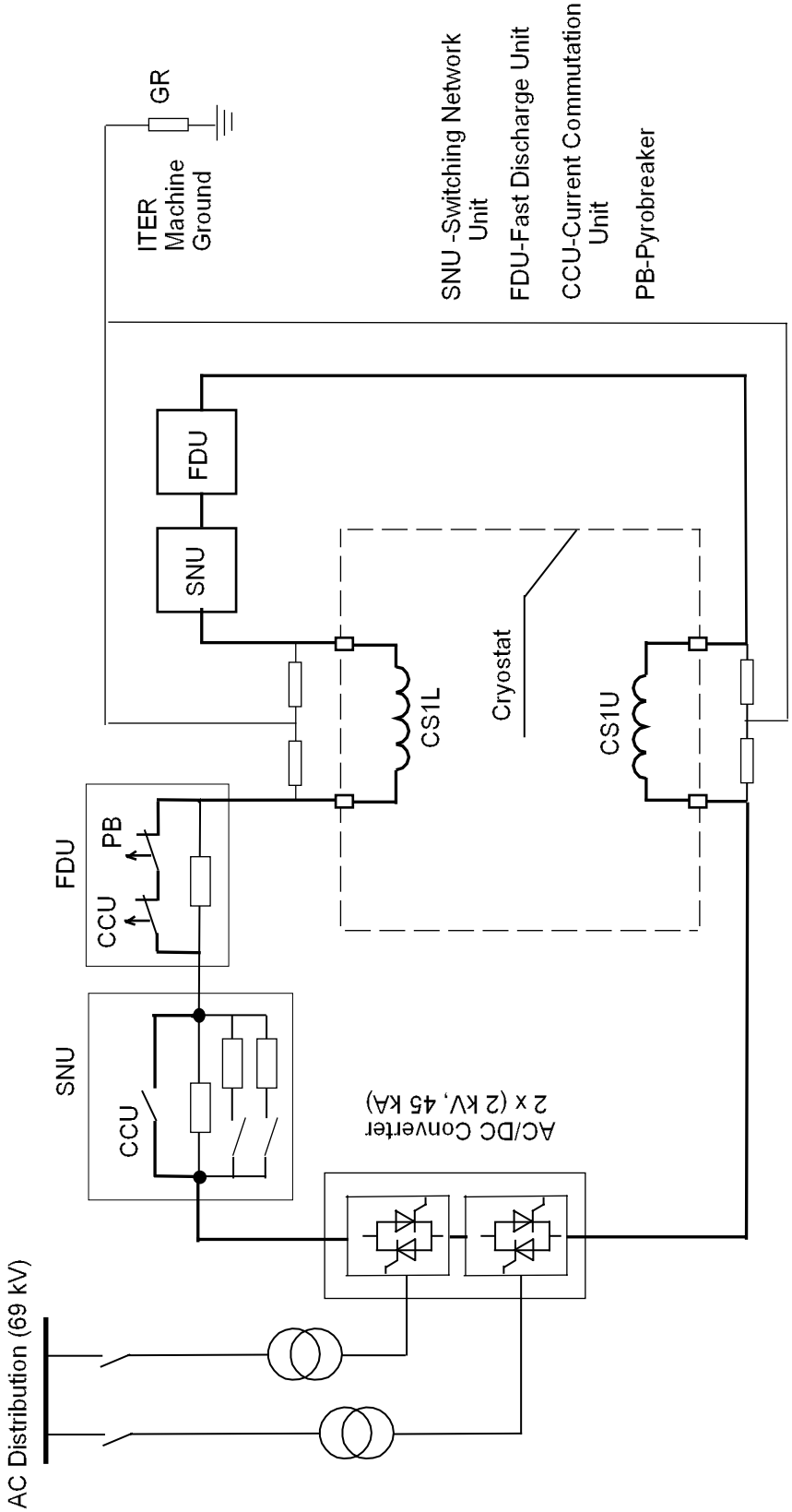

Figure 3.4.2-3 CS1 Power Supply – Simplified Diagram

The loop voltage required for breakdown and plasma initiation is obtained by connecting resistors in series with the CS modules, PF1 and PF6 coils, causing a very large amount of power (about 2 GW) to be extracted. These circuits, called switching networks, are made up of circuit breakers, make switches and resistors. A switching network unit contains three resistors banks connected in parallel to the current commutation unit: one resistor bank directly and the other two through make switches. When the current commutation unit is open, the first resistor is inserted simultaneously in series with the coils. Then, at predetermined time steps, the other two resistors are progressively included in parallel with their own make switches.

After plasma initiation, the power required for plasma current, shape, and position control is provided by one 12-pulse, 4-quadrant thyristor converter, rated for 45 kA continuous current, 2 kV no-load voltage.

The fast discharge units for coil energy discharge are identical with those used for TF coil protection. A fast discharge with the equivalent time constant of 7.5 s for the CS and 14 s for the PF coils is provided with a voltage not exceeding 7 kV. The maximum energy dissipated in the discharge resistors is in the range of 1-2 GJ per system.

3.4.2.3 Power Supply System for the Coils PF2-PF5

The quasi-symmetrical distribution of currents in these coils make it possible to use one fast-response thyristor converter, dedicated to plasma vertical stabilisation, in an integrated power supply system, as shown schematically in Figure 3.4.2-4. The two pairs of quasi-symmetrical coils (PF2-PF5 and PF3-PF4) are connected in parallel to the vertical stabilisation converter. Within each pair, the two coils are connected in anti-parallel.

Three types of thyristor-converters are utilised in this scheme. The main converter, rated for 45 kA, 1.5 kV (on-load), provides relatively slow variation of coil current needed for the plasma current and shape control. The design is the same as that of the CS/PF converter. The “booster” converter generates a relatively high voltage (up to 4.2 kV at the maximum current 10 kA) that, together with the voltage of the main converter, creates the conditions required for breakdown at plasma initiation. When this phase is over, the booster converter is switched into freewheeling mode and then bypassed by the make switch. Finally, the 22 kA fast response vertical stabilisation converter generates a voltage up to 6 kV (on-load) when requested by the plasma feedback control system.

The fast discharge units are identical with those described previously. When a fast discharge is initiated, the vertical stabilisation converter is bypassed by the protective make switch. The fast discharge is characterised by an equivalent time constant of 14 s, a maximum voltage up to 7 kV and a maximum energy per coil of 1.8 GJ.

3.4.2.4 Power Supply System for the Correction Coils

Three groups of correction coils (CCs), top, side and bottom, are included in the design of the magnet system. Each group consists of 6 identical modules shifted toroidally with respect to each other by 60°. The opposite modules are connected in anti-series, forming together three

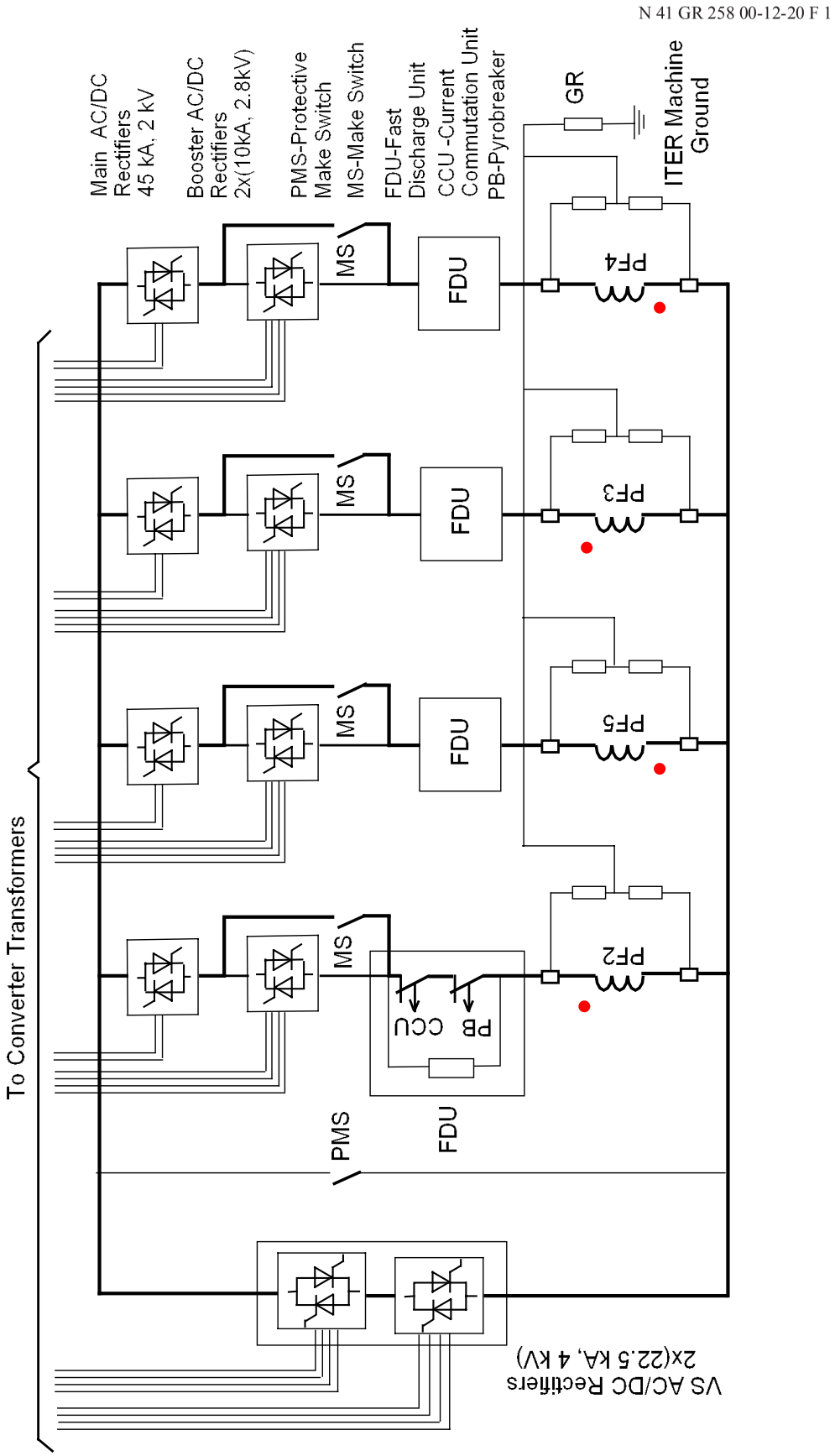

Figure 3.4.2-4 Coils PF2 - PF5 Power Supply – Simplified Diagram

N 41 GR 259 00-12-20 F 1

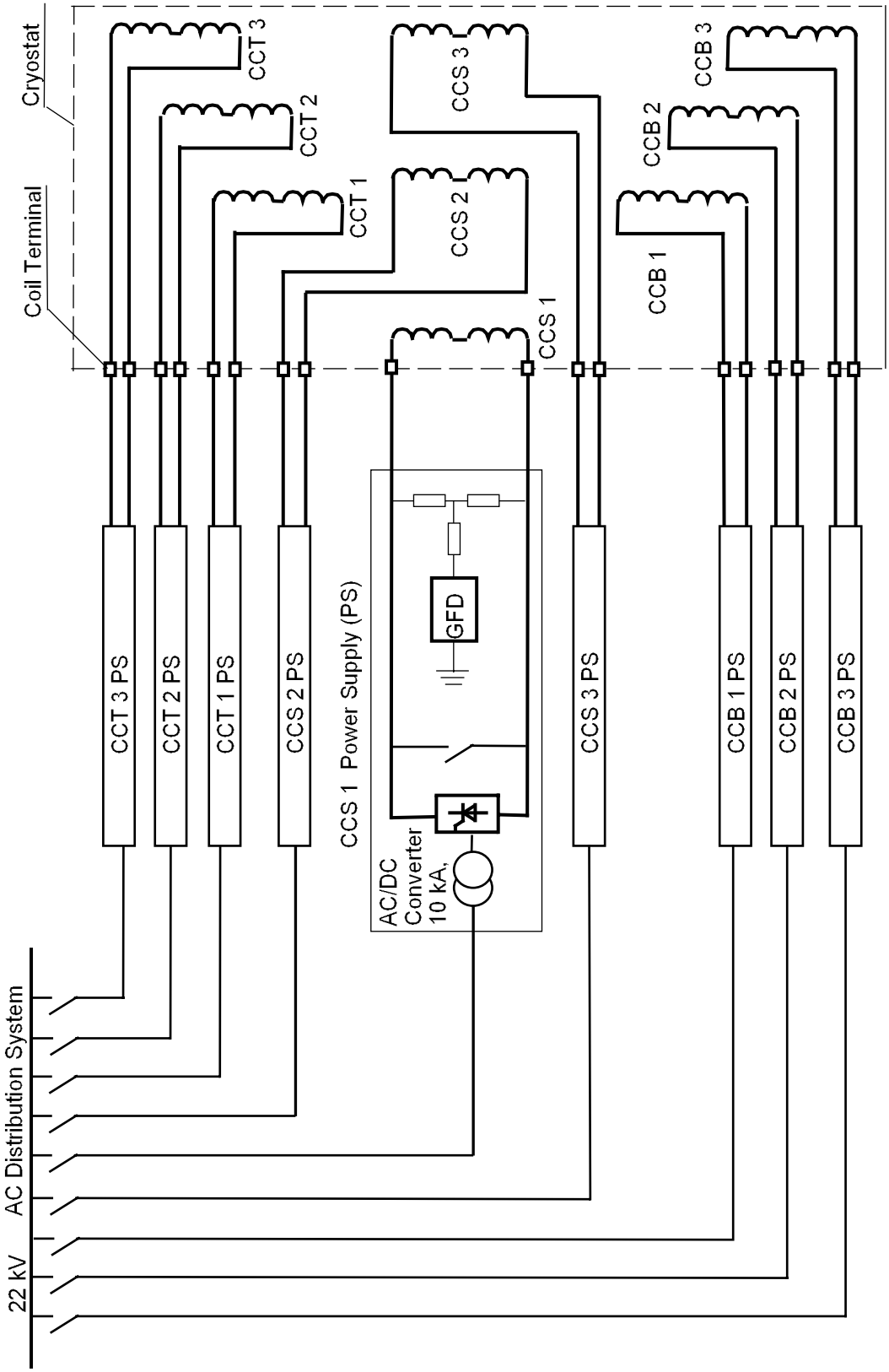

Figure 3.4.2-5 Correction Coils Power Supply – Simplified Diagram

top CCs (CCT1, 2 and 3), three side CCs (CCS1, 2 and 3) and three bottom CCs (CCB1, 2 and 3). Each CC set has its own power supply system, as shown schematically in Figure 3.4.2-5.

All 9 power supplies have the same, simple, configuration: an ac/dc converter supplies dc power to the coil. Acting in inversion mode it also provides fast discharge of the coil energy in case of quench. If the converter fails to perform this action, it will be bridged by a parallel-connected make switch, and the coil energy will be dissipated in the busbars with a time constant less than 20 s (backup protection). All converters are rated for 10 kA current, but have different output voltages in the range 100 - 800 V, depending on the coil contribution to the stabilisation of resistive wall modes.

3.4.2.5 Coil Grounding

A soft grounding via high impedance (1-2 kΩ) resistors is provided for all the coils. This approach is illustrated by the grounding scheme of the TF coils shown in Figure 3.4.2-1. The TF system is grounded through a set of identical resistors connected in parallel to each coil pair. Their midpoint is connected to the TF neutral, which is a common busbar connected to the ITER machine ground, through one resistor (GR). Its resistance is about 1 kΩ to limit the fault current to ground and the related arc energy in the case of a single failure in the ground insulation of the TF system. The leakage current to ground will be measured and used for ground fault detection. A similar concept is used for the CS, PF coils and CCs (see Figures 3.4.2-2 to -5).

3.4.3 H&CD Power Supplies

The H&CD power supply (PS) systems will supply dc or ac controlled voltages and/or currents to the H&CD equipment, which are radio frequency (RF) generators or neutral beam (NB) injectors. In particular the PS systems will be connected to:

- the anodes and driver stages of the IC H&CD tetrodes;
- the cathodes, anodes and bodies of the EC H&CD gyrotrons;
- the collectors of the LH H&CD klystrons;
- the acceleration grids and auxiliaries of the NB H&CD and DNB injectors.

The different components are ac/dc converters, dc/ac inverters, etc., based mainly on solid-state devices (diode, thyristor, gate-turn-off thyristor, insulated gate bipolar transistor, etc.). The ac power will be supplied from the pulsed power distribution system at the 69 kV or 22 kV busbars, according to the level of power required for their operation.

The basic combination of heating systems (for initial operation) will deliver 73 MW to the plasma (20 MW IC, 20 MW EC and 33 MW NB). The power delivered to the plasma can be upgraded to 110 MW, by increasing the number of IC, EC or NB units and/or by adding the LH system. The total peak power demand on the pulsed power system will be around 210 MW (330 MW with upgrade). Differing requirements have led to the use of different power supply technologies for each of the H&CD systems. These PS systems are briefly described below.

3.4.3.1 IC H&CD Power Supplies

One IC H&CD PS unit feeds one tetrode with controlled dc voltages between anode and cathode and between driver stage and cathode. A simplified scheme of this unit is shown in Figure 3.4.3-1. The parameters of the PS units are given in Table 3.4.3-1.

N 42 GR 29 00-12-20 F 2

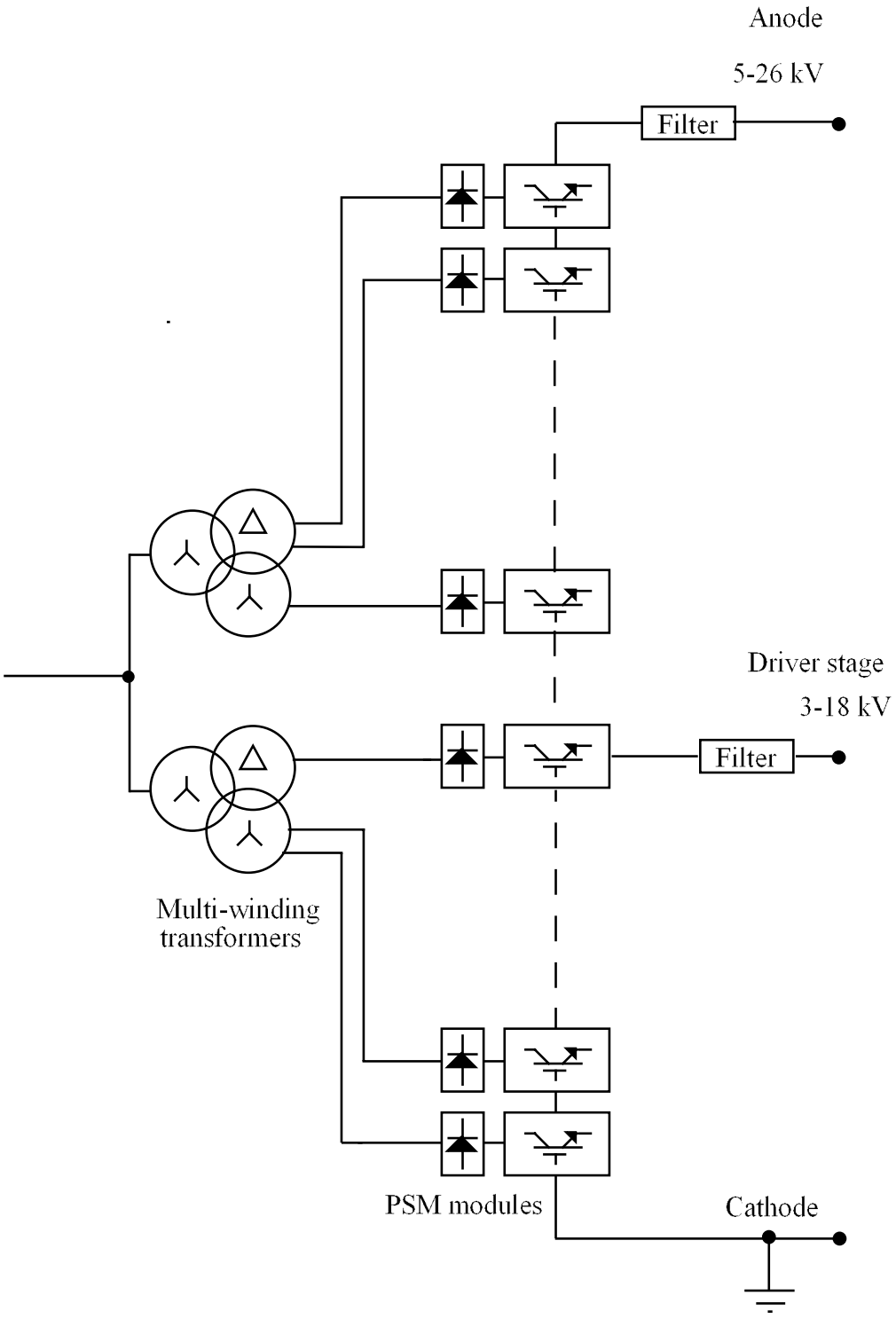

Figure 3.4.3-1 IC H&CD PS Unit – Block Diagram

Table 3.4.3-1 Parameters of the IC H&CD PS Units

Parameters	Unit	Value
Number of IC H&CD PS units		8
Anode maximum power per unit (150 A)	MW	3.9
Driver stage maximum power per unit (25 A)	kW	450
Maximum current per unit	A	175
Anode voltage range	kV	5 - 26
Anode voltage modulation frequency	Hz	200
Driver stage voltage range	kV	3 - 18

The use of individual PS units for the tetrodes of the IC H&CD, based on "pulse step modulator" (PSM) technology, has been adopted to control with high accuracy the voltage applied to the tetrodes. This technology uses 36 separate voltage steps, which can be electronically switched in and out of the circuit. In this way, the output voltage can be rapidly varied to meet the voltage requirements of the tetrode. Moreover, pulse width modulation, with an overall effective frequency per PS unit of 90 kHz, is employed to regulate the voltage with more accuracy, to smooth the 12-pulse rectification ripple, and to provide required 200 Hz modulation of the anode voltage.

Load protection is accomplished by the insulated gate bipolar transistor, which is part of the switched PS module; all modules are switched off in less than 10 μs, limiting the energy dissipated in a fault to 10 J.

3.4.3.2 EC H&CD Power Supplies

The gyrotrons require two types of HV dc power sources to supply its cathode, anode and body as shown in Figure 3.4.3-2. The main, cathode, PS consists of 2 units each feeding six pairs of gyrotrons with a controlled dc voltage between cathode and collector. A simplified scheme of this unit is shown in Figure 3.4.3-3. Another PS (one for each gyrotron) supplies a controlled and modulated (1 kHz) voltage between body and cathode (see Figure 3.4.3-2). Part of this voltage is derived between anode and cathode, through a resistive voltage divider. The parameters of the PS units are given in Table 3.4.3-2.

The use of one main PS unit for twelve gyrotrons, based on a conventional ac/dc thyristor converter, has been adopted for its limited cost, and its capability to control the cathode voltage with the requested accuracy. Connection, protection and commutation, between the H&CD gyrotrons and those used to assist the plasma start-up, are performed by insulated gate bipolar transistor switches for every pair of gyrotrons. Voltage overshoots and undershoots, which can appear in the case of an intervention of the protective switch of a pair of gyrotrons on the cathode voltage of other gyrotrons connected to the same power supply, remain within ± 1% of the maximum voltage. The high dynamic accuracy in the control of body-to-cathode voltage (± 0.5%) is obtained with an individual generator for every gyrotron.

Load protection is accomplished by the insulated gate bipolar transistor switch, which is in series with the faulty gyrotron. This acts in less than 10 μs, limiting the energy dissipated in a fault to 10 J.

N 42 GR 30 00-12-20 F 2

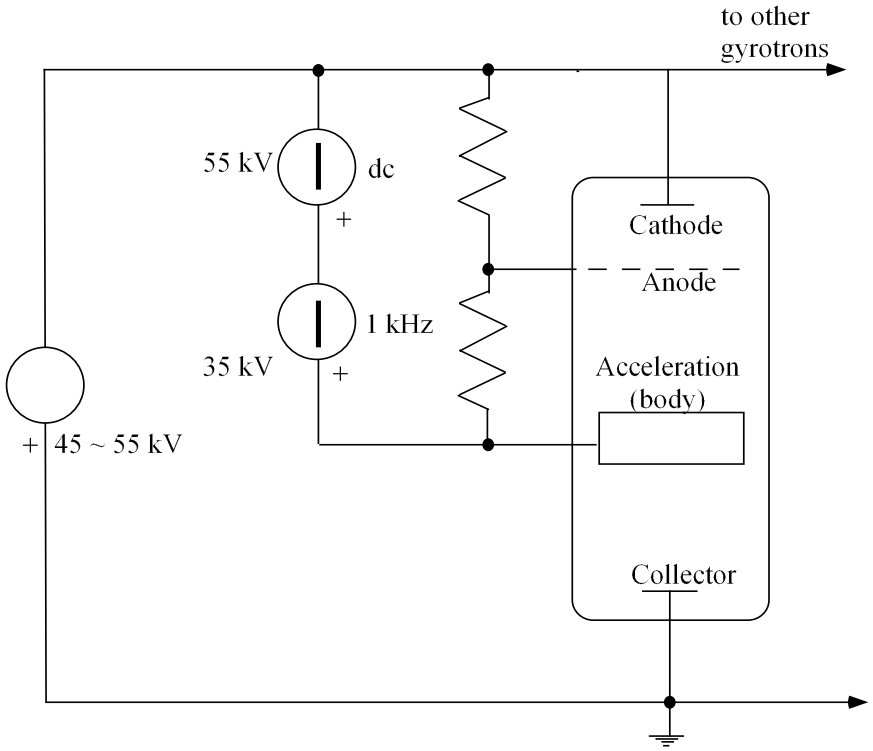

Figure 3.4.3-2 Connection of the EC H&CD PS to Gyrotron Electrodes

N 42 GR 31 00-12-20 F 1

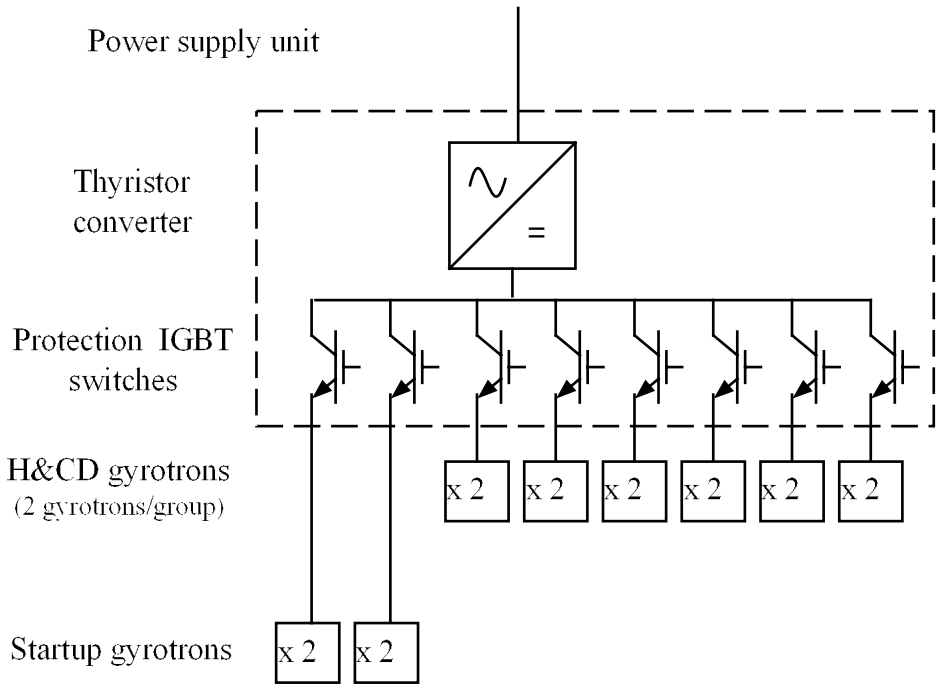

Figure 3.4.3-3 EC H&CD PS Unit - Block Diagram

Table 3.4.3-2 Parameters of the EC H&CD PS Units

Parameters	Unit	Value
Number of main (cathode) PS units		2
Cathode-to-collector voltage range	kV	- 45 to - 55
Nominal cathode current per unit	A	540
Maximum power per unit	MW	30
Number of body/anode PS units		24
Body-to-cathode voltage range	kV	+ 45 to + 90
Maximum body current	A	0.1
Anode-to-cathode voltage range	kV	0 to + 50
Anode and body voltage modulation range	kV	35
Anode and body voltage modulation frequency	kHz	1
Maximum anode current	A	0.1

3.4.3.3 LH H&CD Power Supplies

One PS unit feeds six pairs of klystrons with a controlled dc voltage between collector and anode, with a scheme similar to that for EC H&CD, shown in Figure 3.4.3-3. The parameters of the PS units are given in Table 3.4.3-3.

Table 3.4.3-3 Parameters of the LH H&CD PS units

Parameters	Unit	Value
Number of LH H&CD PS units		2
Collector voltage	kV	80
Nominal collector current per unit	A	300
Maximum power per unit	MW	24

The use of one PS unit for twelve klystrons, based on the "star point controller" technique[1], has been adopted due to its limited cost even with high values of dc voltage (80 kV load voltage), capability to control the collector voltage with the requested accuracy, and the limited amount of energy released in case of a fault. (This solution was not adopted for the EC H&CD PS because it is more expensive than the thyristor converter solution at the 55 kV voltage level). Connection and protection are performed by insulated gate bipolar transistor switches for every pair of klystrons.

Load protection is accomplished by an insulated gate bipolar transistor switch, which is in series to the faulty klystron. This acts in less than 10 μs, limiting the energy dissipated in the fault to 10 J.

[1] R. Claesen and PL Mondino, "Neutral Beam Injection and Radio-Frequency Power Supplies", in Fusion Technology, Vol.11, January 1987, pp 141-162.

3.4.3.4 NB H&CD Power Supplies

The NB H&CD PS provides:

- frequency and voltage conversion for voltage control and fast power interruption at low voltage level;
- voltage transformation rectification and filtering, to provide high voltage power to the beam sources, with different levels for the different source grids;
- dc power transmission to the beam sources;
- auxiliary power (both ac and dc) to produce and extract the negative ion beam; the power supplies are floating at a high voltage level (-1 MV) and are contained in a HV deck, located in the machine gallery;
- power to the active correction/compensation coils and the residual ion dump at ground reference level.

One PS system feeds one NB injector. The PS system is split into three parts. An acceleration PS provides a negative voltage (up to 1 MV to ground) to the beam source, together with intermediate voltages to the acceleration grids. An ion source PS provides different voltages and current to several items of equipment in the HV deck (SF_6-insulated). A third group of power supplies provides individual dc voltages to seven active correction/compensation coils and to the residual ion dump. A simplified scheme of the acceleration PS is shown in Figure 3.4.3-4, where frequency and voltage conversion is provided by gate-turn-off thyristor inverters and voltage transformation is provided by five transformers, connected in series, with 1 MV insulation between primary and secondary windings. The parameters of the PS system are given in Table 3.4.3-4.

The connection between power supply and beam source is done by a multi-axial, SF_6-insulated, HV transmission line (see 3.4.5.3). The line is split in two parts by the HV deck, where the ion source power supply is located.

The load protection is obtained by fast switch-off of the gate-turn-off thyristor inverters. These act in less than 200 μs, limiting the energy dissipated in a fault to 50 J.

Table 3.4.3-4 Parameters of the NB H&CD PS System Unit

Parameters	Unit	Value
Number of units		2
Acceleration supply voltage/current	kV/A	- 1000 / 59
Grid 1 voltage/current	kV/A	- 800 / 7
Grid 2 voltage/current	kV/A	- 600 / 6
Grid 3 voltage/current	kV/A	- 400 / 3
Grid 4 voltage/current	kV/A	- 200 / 3
Current at ground level	A	40
Rated power per acceleration unit	MW	48
Rated power of ion source PS per unit	MW	6
Rated power of active correction/compensation coils and residual ion dump PS per unit	MW	6

N 42 GR 32 00-12-20 F 1

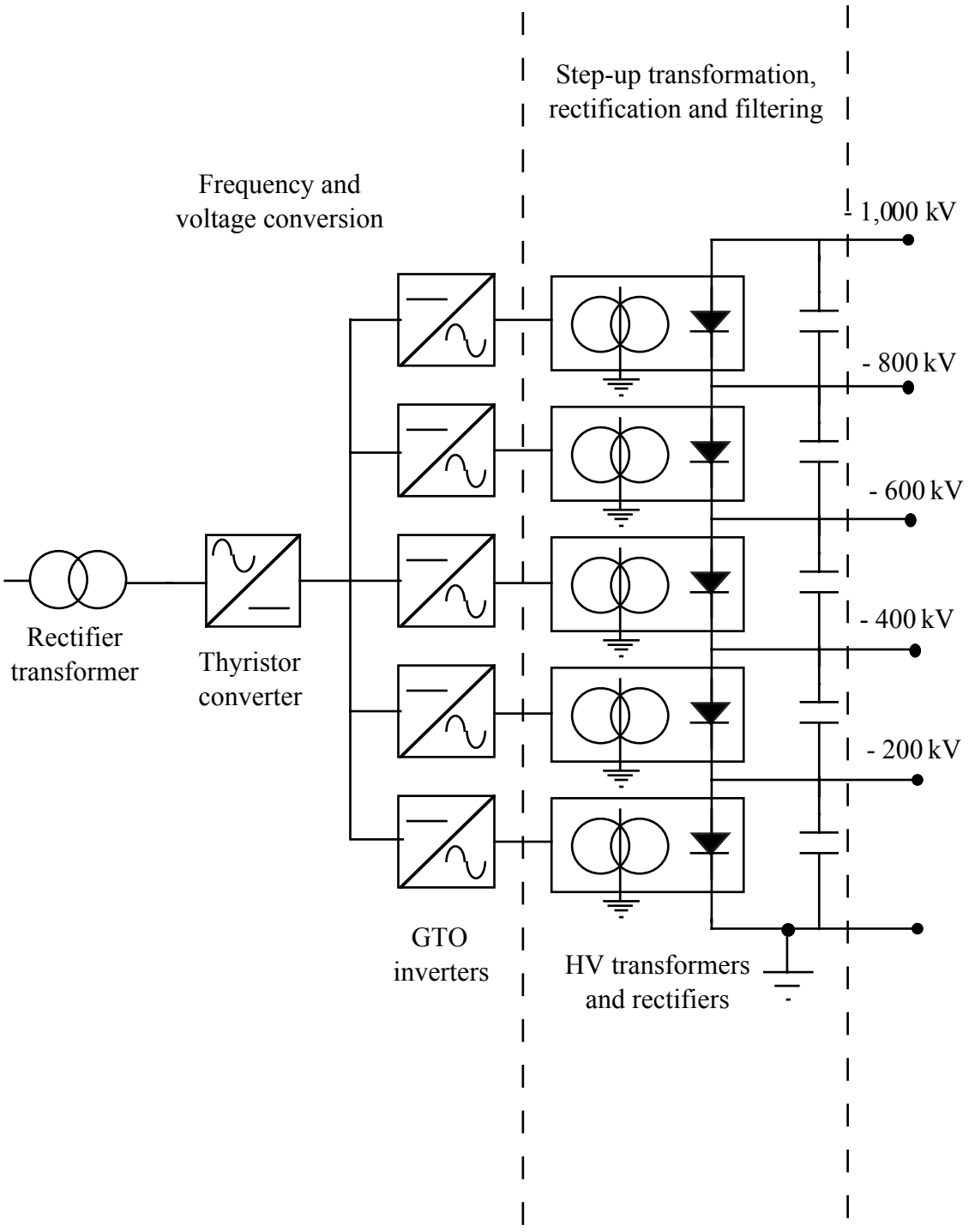

Figure 3.4.3-4 NB H&CD PS - Simplified Diagram

3.4.3.5 DNB Power Supplies

The DNB injector will provide a hydrogen beam for pulsed operation (1 to 3 s) with trains of pulses at 5 Hz (100 ms beam on/100 ms beam off) and 20 s between pulse trains. The PS system is split into three parts, with a structure very similar to the NB H&CD one. The main differences are that only one voltage (- 100 kV) is provided to the beam source and only five active correction/compensation coils are used. The parameters of the DNB power supply units are given in Table 3.4.3 5.

Table 3.4.3-5 Parameters of the DNB PS unit

Parameters	Unit	Value
Acceleration supply voltage/current	kV/A	- 100 / 71
Rated acceleration power	MW	7.1
Rated power of ion source PS	MW	1.5
Rated power of active correction/compensation coils and residual ion dump PS	MW	1.8

3.4.4 Steady State Electric Power Network

The SSEPN will provide ac power to all plant electric loads, except those supplied by the pulsed power distribution system. These are listed in Table 3.4.4-1. The major consumers are the cooling water and cryogenic systems requiring together about 80% of the total demand of 112 MW. About 6 MW (or 5.5% of the total amount) must be provided even in case of a loss of off-site power. Backup, autonomous power generators will be used in such a case. Loads that would not tolerate the 30 s interruption needed to start up the backup generators, will get power from ac or dc uninterruptible power supplies. This service will not be centralised: the uninterruptible supplies will be part of those individual systems requiring them.

The SSEPN will receive up to 120 MW continuous power from a HV grid through two independent transmission lines, each capable of supplying the entire plant maximum load. The nominal voltage of the grid power source is assumed to be 220 kV. The grid power is then transformed to the 11 kV level by four, 3-winding, step-down transformers, each rated at 40 MVA, and is distributed among 8 Class IV (i.e. infinitely interruptible AC) power busbars, as shown in Figure 3.4.4-1. Three 1.8 Mvar capacitor banks for the reactive power compensation are connected to each busbar. Having a 43.2 Mvar total capacity, they will improve the power factor in nominal operating conditions to 0.95.

Emergency backup power will be generated by two diesel generators, each rated for 6.3 MW. These generators are connected to two separate 11 kV busbars for supplying Class III (i.e. temporarily interruptible AC) power to the loads, most of which are safety classified. The two redundant channels for the supply of the safety-related loads, starting from the diesel generators and including switchgear components, transformers and cables, are entirely segregated from each other.

The most powerful loads (larger than 400 kW) are directly supplied from the 11 kV busbars. The loads with power in the range of 100-400 kW are supplied at the 3.3 kV level, through additional, 11 kV/3.3 kV, step-down transformers and 3.3 kV, class IV and class III, busbars.

The remaining, less powerful, loads will be connected to the 400/230 V network created with the help of 12 transformer load-centre substations, or load centres (LC).

Table 3.4.4-1 Steady-state Power Supply and Emergency Loads

System	Connected loads (MW)	Class IV Power in POS (MW)	Class IV Power in LTM (MW)	Class III Power (MW)
Cooling Water	60.4	46.1	21.1	2.1
Cryoplant & Cryodistribution	33.9	26.7	8.5	[3]
Buildings and Layout	12.3	5.5	6.8	0.9
Heating &Current Drive (total)	2.9	2.6	0.3	[3]
-IC H&CD (for 20 MW)	2.3	2.2	0.3	[3]
-EC H&CD(for 20 MW)	0.6	0.4	[3]	[3]
-NB H&CD(for 33 MW)	[3]	[3]	[3]	[3]
Remote Handling Equipment	3.0	0.0	1.0	0.0
Liquid and Gas Distribution	2.8	1.8	1.8	0.5
Tritium Plant & Detritiation	1.6	0.5	0.5	0.6
Diagnostic	2.0	2.0	0.2	0.1
Power Supplies	1.9	1.4	0.3	0.3
Vacuum Pumping & Fuelling	1.1	0.5	0.7	0.2
Hot Cell and Waste Processing	1.1	0.4	0.5	0.0
Radiological and Environmental Monitoring	0.4	0.2	0.2	0.1
Supervisory Control, Interlock and General Alarm System	0.2	0.2	0.2	0.2
Magnet	0.1	0.1	0.1	0.1
Others	0.3	0.2	0.1	0.1
Total	124.0	88.2	42.3	5.2
Total, including uncertainty factor[1]		101.5		5.7
Total, including future growth factor[2]		112.0		6.2

[1] 15% for class IV, 10% for class III

[2] 25% for class IV, 15% for class III, with exception of the Cooling Water system, the requirements of which correspond to the extended capability

[3] Less than 100 kW - accounted in Others

N 43 GR 16 00-12-20 F 1

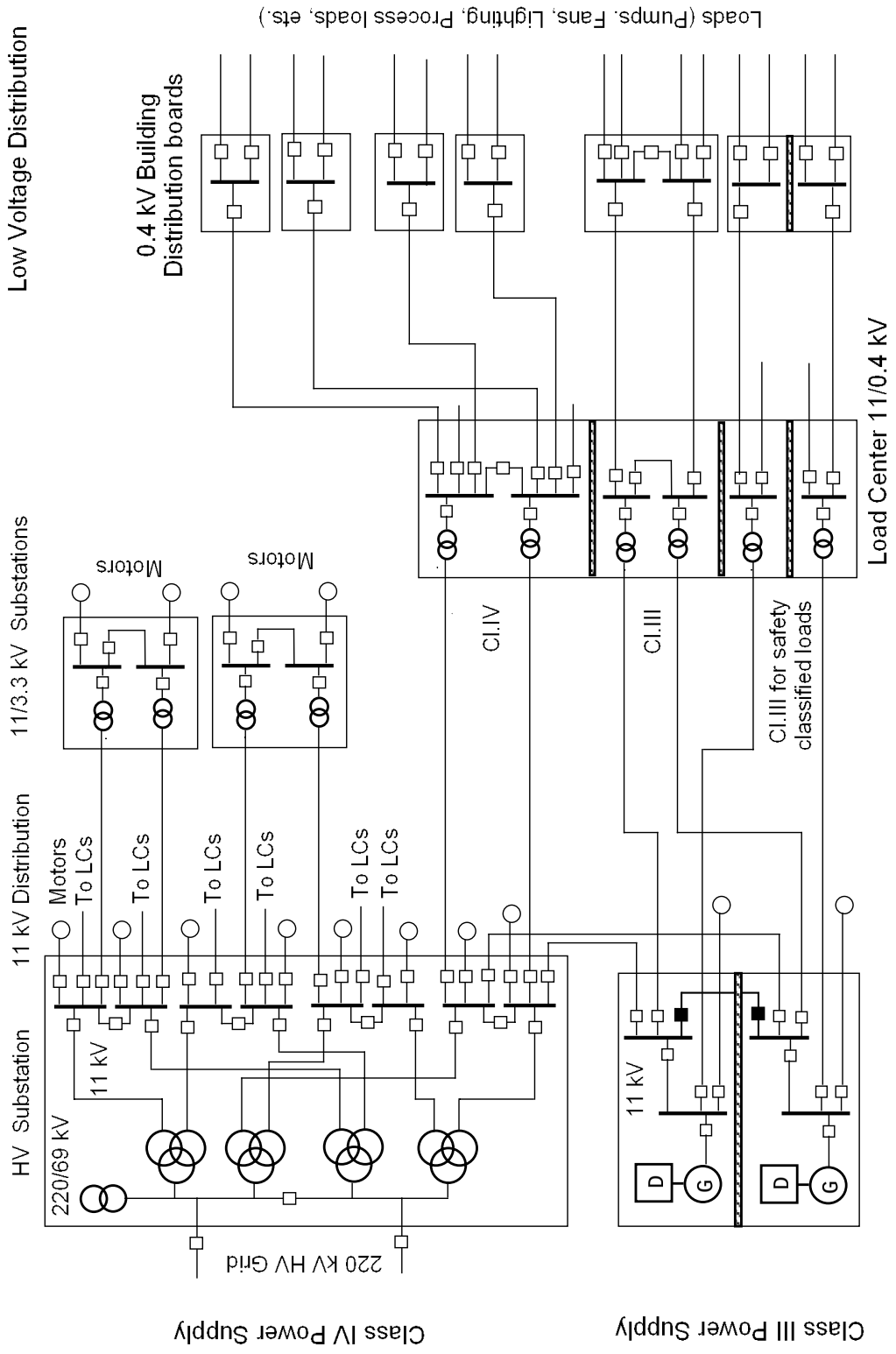

Figure 3.4.4-1 Simplified Diagram of the SSEPN

3.4.5 Components

The reference designs described above are mainly based on existing technology and products available in the world market, or on progress that is expected to be achieved in the near future. However, design issues existed, mainly relating to the dc current switches for the extraction of energy stored in the coils, and to the super-high voltage (1 MV) equipment for the NB H&CD power supplies. Therefore, R&D was undertaken during the EDA with the overall aim of demonstrating the feasibility of those components. In addition, limited R&D was necessary to verify the design of the 90 MVA basic module for the thyristor converters of about 1500 MVA total power, which will supply controlled dc power to the magnet coils.

3.4.5.1 AC/DC Converters

Different types of converter units have to be used in the TF and PF circuits due to the various operating requirements: the current and voltage ratings vary from 10 kA to 68 kA and from 0.9 kV up to 5.6 kV correspondingly. Nevertheless, some common criteria have been used in the design.

In particular, the converters are designed both for fault suppression and for operation in internal bypass (internal no-cycled freewheeling) mode. The former implies the capability to clear the over-current due to the most frequent internal faults by gate pulse suppression without melting the internal fuses, thus improving the availability. It is normally used in converters without fuses with one thyristor per arm, but its extension to cases with many thyristors in parallel had to be proved by R&D.

A 4-quadrant 6-pulse bridge was designed, built and tested[1]:

- to verify the feasibility of design solutions able to reduce the maximum current imbalance among 10 thyristors in parallel below 1.4, both in normal operations and fault conditions;
- to demonstrate that fault suppression can be achieved in ac/dc converters with several thyristors in parallel;
- to demonstrate the converter capability to repeatedly withstand the severe electromechanical stresses due to the high value of the current to be cleared by fault suppression.

The framework built could integrate a 12-pulse 4-quadrant 2 kV, 45 kA continuous operation converter with a power density of more than 3 MVA/m^3. The results of the tests were completely successful and confirm the viability of the design.

3.4.5.2 DC Switches for Current Commutation

The key components in the coil energy discharge systems are the current commutation units used in both the switching networks and discharge circuits. DC circuit breakers rated at 45-68 kA steady state and 10-15 kV are required to transfer current from the coil to discharge resistors. A scheme consisting of two parallel-connected devices, a mechanical bypass switch and a pulsed circuit breaker, equipped with a counterpulse system to create an artificial current zero, is foreseen.

[1] E. Gaio et al., "Main technological aspects of the ITER ac/dc converter system". Proceedings 20th SOFT, Marseille, 1998, pp 861-864.

The program established to develop and test these switches has been implemented by the EU and RF Home Teams. The EU HT concentrated on the development of a conventional current commutation units with a vacuum circuit breaker[1] for the fast discharge units, starting from industrial components with lower current and/or voltage ratings. The RF HT has developed a novel scheme[2] in which a mechanical bypass switch with arcless commutation is to be used in a current commutation unit together with a thyristor circuit breaker. This design is more challenging but may assure the very long lifetime (10^4 cycles or more) necessary for the switching network units. In addition, the RF HT developed a fast make switch intended for long term repetitive operation within the switching network units, and two explosively actuated switches for backup protection: a circuit breaker and a make switch. All these switches have been successfully tested at continuous current up to 60 kA and at switching currents up to 66 kA. Additional R&D activities are now in progress with the aim of assessing the margins and of demonstrating the capability of operating at a current of up to 70-75 kA for the TF coil system.

3.4.5.3 Transmission Line and HV Bushing for NB H&CD PS

One of the crucial elements in the neutral beam power supply system is a dc HV transmission line, which connects the NB injector to the remotely located power supply. The transmission line has multiple conductors at intermediate potentials. A high voltage (1 MV dc) bushing, called the "transmission line bushing", which can support and insulate these conductors, is essential for a practical power supply system.

An R&D program was established to design this bushing, to develop the required manufacturing techniques, and to test the prototype. The program has been implemented by the JA Home Team and the bushing has been realised with alumina-ceramic powder mixed with epoxy resin, hardened twice under vacuum in an electric oven and then finished up. First electrostatic field analyses have been performed, in order to outline the electrical design of the bushing. Then a computer simulation using a 3D code was performed to investigate the mechanical strength of the bushing. Finally, the fabrication technology developed for making UHV bushings for ac lines was adopted for fabricating the transmission line bushing.

Due to limitations of the manufacturing facilities, the prototype was built with a reduction to 90% of the final dimensions and the test voltages were chosen accordingly. The prototype withstood all the tests performed.

3.4.6 Performance Analysis

Computer simulation studies of the entire ac/dc conversion plant, including pulsed ac power supply, have been performed. The results show that, with the selected parameters of the reactive power compensation and harmonic filter system, the level of reactive power, and the content of harmonics in the reference HV grid, do not exceed specified limits.

---

[1] T. Bonicelli et al., "The Development and Testing of a 66 kA Bypass Switch with Arc Commutation Capability for the ITER Coil Power Supply System", Proceedings 17th SOFE, San Diego, 1997, pp 1129-1132
F. Bellina et al., "Design, Construction and Operation of the 66 kA Life Tests Facility for the ITER Magnet Protection Vacuum Circuit Breakers", Proceedings 17th SOFE, San Diego, 1997, pp 1137-1140

[2] S.D. Avanesov et al., "The High DC Current Commutating Devices for the ITER Power Supply System developed in Russia", presented at the EPTR-6 conference, May 1997, St. Petersburg, RF.

The typical active (P) and reactive (Q) power pulse, corresponding to the 15 MA plasma inductive scenario with 73 MW heating power starting in the current ramp-up phase, is shown in Figure 3.4.6-1. The dashed line shows that the compensation systems in the design are effective in reducing the reactive power taken from the grid (Q_{grid}) to the 400 Mvar generic site assumptions indicated in the PDS, section 4.II.C.2. The variations of reactive power "Q" and "Q_{grid}" during the fast (≤ 10 s duration) plasma control actions, which are not shown in Figure 3.4.6-1, are insignificant.

N 41 GR 260 01-01-11 F2

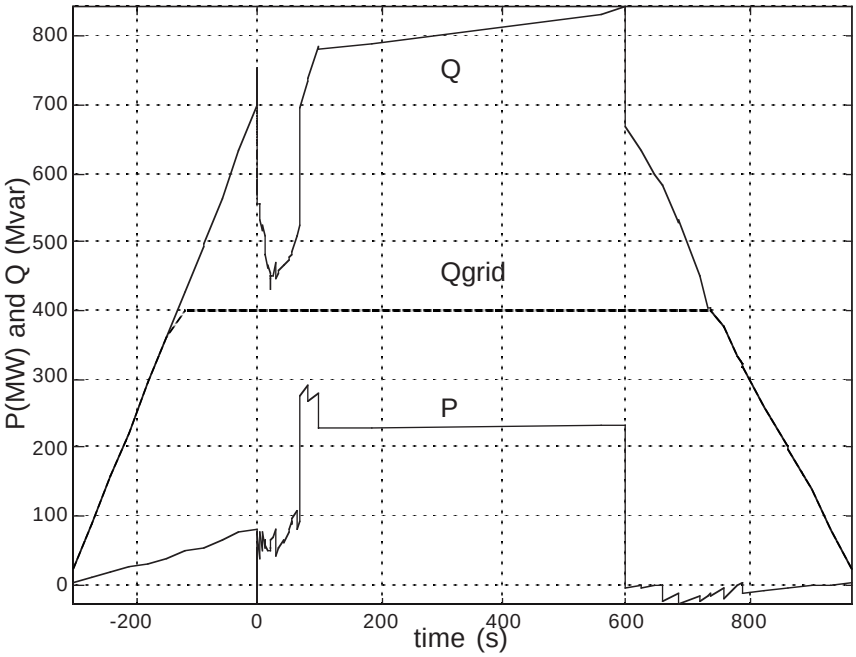

Figure 3.4.6-1 Active (P) and Reactive (Q) Power Plot for 15MA/73MW Additional Heating

Intensive studies have been carried out to define extreme conditions in case of faults. For the magnet coils, one of the most important parameters is overvoltage on the coil terminals that can cause an insulation breakdown and trigger a chain of other fault events. The results of fault analysis have shown that the highest voltage to ground in case of a single fault or malfunction within the coil PS system, aggravated by a coil terminal short circuit to ground, may reach 12.4 kV in the TF system and 15.6 kV in the CS/PF systems. With regard to the H&CD systems, it has, in particular, been verified that the reference PS designs meet the most critical restriction related to the energy dissipated in the load (50 J for the NB source and 10 J for the RF generators) in case of its breakdown.

Among several trade-off studies aimed at the optimisation of the PS schemes and parameters of components, the most important was the comparison of two technical solutions for the EC H&CD power supply. The first is based on the pulsed step modulator technology and is similar to that used for the individual supply of the IC H&CD generators; the second includes a powerful thyristor converter supplying 12 gyrotrons in parallel. The latter solution has been selected as the reference, because of its lower price.

3.5 Miscellaneous Plant Systems

The ITER plant has a number of miscellaneous systems that are required to support the operations of the plant, as categorised in Table 3.5-1.

Table 3.5-1 Miscellaneous Plant Systems

Category	System Name
Personnel and Environmental	
	Radiological and Environmental Monitoring
Liquid Distribution	
	Potable and Fire Protection Water
	Sewage (Sanitary & Industrial)
	Steam, Condensate, and Demineralized Water
Gas Distribution	
	Compressed Air
	Breathing Air
	Nitrogen, Helium and Other Special Gases
Other	
	Plant Sampling

3.5.1 Radiological and Environmental Monitoring Systems

3.5.1.1 Functions

The radiological monitoring system is designed to monitor personnel, and plant areas, to protect people against exposure to ionising radiation.

The environmental monitoring system provides information suitable for monitoring compliance with environmental regulations applicable to the site.

3.5.1.2 Specific Functions

3.5.1.2.1 Radiological Monitoring System

The radiological monitoring system for a generic site, according to present assumptions, provides the following specific functions:

- personnel dosimetry, for all radiation and contamination hazards appropriate for the radiation zones;
- dedicated radiation and contamination monitors, separate from others, which are located at strategic points in the ITER plant, and specified to remain functional during and after postulated accidents.

The latter are to provide an assessment of the conditions as part of an emergency preparedness program. In particular, air radiation monitoring is provided in all areas where tritium is handled, processed or stored. The tritium monitoring system in the plant gaseous exhaust is redundant and is designed to remain operable under accidents and loss of normal electrical power. It provides real-time indication of tritium releases. The sensitivity of the monitors enables the detection levels of tritium in air as low as 10^{-6} Ci/m^3.

3.5.1.2.2 Environmental Monitoring System

The environmental monitoring system inside the generic ITER site provides a number of fixed environmental monitors, to monitor designated gaseous and aqueous pathways to the environment. These measure the following:

- airborne tritium (oxide and elemental);
- aqueous tritium oxide (tritiated water);
- airborne and aqueous neutron activation products;
- airborne beryllium;
- CO_x, NO_x emissions;
- hydrocarbon emissions;
- suspended solids;
- other hazardous/radioactive materials in the ITER plant.

The environmental monitoring system is designed to demonstrate that radiation and/or contamination releases to the environment are within the requirements established.

3.5.1.2.3 Testing Requirements

All monitors have the capability of being tested in-situ. If the monitor has a circuit which actuates equipment or alarms, these functions have a bypass and “return-to-armed” capability such that unwanted alarms and actions during testing are avoided.

3.5.1.2.4 Operations/Maintenance Requirement

Monitored data is transmitted to the CODAC system via a dedicated network.

3.5.2 Liquid Distribution Systems

The liquid distribution systems include:

- potable and fire protection water;
- sewage (sanitary & industrial);
- steam, condensate, and demineralized water.

3.5.2.1 Potable and Fire Protection Water

The potable water system distributes water suitable for human consumption, provided by the host to the site in quantities suitable for up to 1,000 persons. A reserve tank holds capacity for up to three days of normal use. About 10 per cent of the capacity is reserved for fire protection water. One day's usage is based on the widely used "rule of thumb" 380 ℓ/d/person. This translates to 380 m^3/d, and a storage tank volume of 1,250 m^3.

A distribution system for pressurised, plant-wide fire protection water distributes water supplied by the host to the site. The fire protection system provides the following specific functions:

- it provides a flow rate of 0.4 m^3/s at a pressure of 1 MPa;
- it is configured as two independent feeds, so that water can be delivered at any point by at least two independent means - routing is such that leaks will not imperil systems important to safety;
- it is designed to withstand earthquake level SL-0.

The fire protection system is designed with sufficient redundancy to allow the maintenance of all active components without removal of the entire system from service, and without incapacitating the ability of the system to perform its function.

3.5.2.2 Sanitary and Industrial Sewage

The sanitary and industrial sewage system is designed to collect the sanitary and industrial drainage from the ITER plant and feed it to the sanitary and industrial sewage treatment system to be provided by the host. The industrial sewage system is designed to include coarse separators to provide a discharge quality satisfactory for the treatment system. However, should the host require additional treatment of filters, precipitators and/or ion exchange equipment in order to provide the necessary quality, those would have to be added outside the scope of the ITER plant design.

3.5.2.3 Steam, Condensate, and Demineralized Water

The steam and condensate system supplies and distributes saturated steam at 0.5 MPa, to components, systems and areas within the plant which require auxiliary or area heating, and collects and returns condensate to the steam-making equipment in the site services building. The steam condensate system uses carbon steel piping. Preliminary estimates of steam requirements are given in Table 3.5-2.

The demineralized water system supplies and distributes deionised water to be used directly for process purposes or as makeup to all other ITER closed cooling water loops. The de-ionised water system provides a maximum flow rate of 300 m^3/d at pressures ranging from 0.2 to 1 MPa. The system is designed with stainless 304 steel.

Table 3.5-2 Steam Load List (Preliminary)

Interfacing Systems	Required Heat kW(t)	Steam Flow kg/h	Remarks
Tokamak Complex Buildings	4,576	7,075	HVAC use
Hot Cell Building	1,307	2,020	HVAC use
Radwaste Building	279	431	HVAC use
Personnel Building	43	67	HVAC use
Cryoplant Compressor Building Cryoplant Cold Box Building During PF Coil Fab. in Cryoplant Buildings	268 299 2,509	415 462 3,880	HVAC use HVAC use HVAC use
Magnet Power Supply Building	144	223	HVAC use
Magnet Power Conversion Building	331	511	HVAC use
Laydown, Assembly & RF Heating Building (and Tokamak Crane Hall)	534	826	HVAC use
NB Power Supply Building	8	12	HVAC use
Emergency Power Supply Building	102	158	HVAC use
Laboratory Office Building	298	460	HVAC use
Control Building	174	270	HVAC use
Site Services Building	335	517	HVAC use
Water Detritiation		3,150	Process use
Freeze Protection etc.		5,400	Equipment Protection
Distribution Loss ~ 10%		3,015	
Total	**12,133**	**30,424**	

3.5.3 Gas Distribution Systems

The gas distribution systems include:
- compressed air;
- breathing air;
- nitrogen, helium and other special gases.

3.5.3.1 Compressed Air

The compressed air system is designed as a distributed system comprising compressors, receivers, dryers and other equipment needed to meet the air specifications for the specific equipment or personnel needs that it serves. An independent compressed air subsystem will be designed, if appropriate, for each of the following combinations of buildings:
- tokamak and tritium;
- hot cell, radwaste and personnel;
- cryoplant, emergency power supply;
- site services and control;
- magnet power supply.

The compressed air system satisfies the following specifications:
- the capacity of each independent subsystem is greater than 10 m^3/min (STP) and less than 50 m^3/min (STP);

- all subsystems which provide instrument air are designed to provide air with less than 10 ppm oil content;
- all subsystems are designed to provide high pressure (590 kPa to 865 kPa) and low pressure (270 kPa to 450 kPa) air.

The gas distribution system is designed such that all gas taps on the distribution system have check valves to isolate the tap from the distribution system if the gas pressure applied to the tap is greater than the distribution system pressure. This is to protect users' systems against overpressure.

3.5.3.2 Breathing Air

The primary function performed by the breathing air system is to supply and distribute "breathing quality" compressed air to enable personnel wearing plastic suits or respirators to enter and work in contaminated or potentially contaminated areas of the ITER plant. With plastic suits, about 80 percent of the air is used for suit cooling with the balance used for respiration. Breathing air is also used by workers wearing respirators when entering enclosed work locations without adequate ventilation. The function is accomplished by compressors, air receivers, air dryers, air distribution, filters and other equipment needed to meet the requirements. The breathing air system is required to perform this function during normal plant operating and shut-down conditions.

An important feature for the function of the breathing air system is that it must not be connected in any way to the plant compressed air systems.

Breathing air is supplied on an entire ITER plant basis at a nominal pressure of 520 kPa(g). The single, centralized system of compressors with a distribution system is justified on an economic basis. The duplication of breathing air system components and controls is minimized. The breathing air system equipment is located in the site services building (Figure 3.6.1-1, building 61). The main distribution headers distribute breathing air to the complex of buildings which are the tokamak, hot cell, radwaste and tritium buildings. Each of these buildings is supplied by a separate distribution system from the main distribution header.

For access to areas that are too far away to connect into the distributed breathing air system, or for when the air compressors are not running, bottled breathing air is provided in addition to the plastic suits.

3.5.3.3 Nitrogen, Helium and Other Special Gases

The primary function performed by this system is to provide nitrogen, helium and other gases for equipment and other plant needs.

Currently, all needs for special gases are small, such that a single central distribution system is not economical. Rather, the special gas system will consist of primarily "multi-bottle" stations located near the point of use. The stations have regulators and pressure monitors to assure safe and reliable delivery to the user. There is a large multi-bottle station adjacent to the tritium building, along the east wall.

For the very large volumes of helium in the cryoplant, dedicated storage tanks and distribution lines are provided by the cryoplant and the cryodistribution system.

3.5.4 Plant Sampling Systems

3.5.4.1 Functions

The function of the plant sampling systems is to collect and evaluate the chemical and radiological attributes of key plant systems samples. The plant sampling system is designed to obtain samples for chemical and radiological analysis, so as to provide supporting operational information for the process systems of the ITER plant.

3.5.4.2 Configuration

3.5.4.2.1 General

Two separate laboratory analysis subsystems, within the plant sampling system, are located in separate facilities to avoid cross contamination. The first subsystem, "hot" laboratory analysis, will be capable of handling radioactive samples in solid, liquid or gaseous form. The second subsystem, "cold" laboratory analysis will handle non-radioactive samples including potentially hazardous chemicals in solid, liquid or gaseous form.

Both subsystems are designed to be available on demand such that no maintenance or operations activity will be delayed beyond the minimum practical sample processing time. Routine samples that may be safely contracted to outside laboratories will be routed to the off-site laboratories only if such action is cost effective.

3.5.4.2.2 Beryllium

Special attention is required for the handling and the control of materials containing beryllium. Components with Be surfaces, such as blanket modules, will first be handled in the hot cell area during machine assembly. These Be-containing components will be received in the hot cell area and a temporary Be analysis laboratory will be set up close to the hot cell building, or in a separate area of the hot cell building, so as to avoid cross-contamination, to analyze samples from smears and from sample air filters to determine the presence of airborne Be. The permanent Be analysis function will be combined with the hot laboratory functions in the radwaste building once that portion of the radwaste facility is available.

3.6 Site Layout and Buildings

3.6.1 Site Layout

The site layout (Figure 3.6.1-1) and the buildings have been designed for a generic site[1]. Before construction, certain design modifications shall be implemented to meet actual conditions on the selected site such as seismicity, topology, geology, hydrology, and access routes.

The layout has been designed for the minimum floor area, to reduce the complexity of system interfaces, and to minimise the connection distances, by following these key design strategies:

- a general layout policy to avoid the crossing of different service types such as electrical power, cooling water, and waste handling - clearly, the extent to which services can be segregated decreases as they get closer to the tokamak;
- separation of services: with the tokamak building located in the centre, the site is arranged so that electrical services enter from the west, cooling systems are located on the east, personnel-related functions are concentrated on the south, and waste management functions are located on the north (these directions are for identification purposes only);
- staged construction and expandability: to the maximum extent possible, the design of systems, buildings, and the site will be such that future additions in system capacity are not precluded.

The ITER site is enclosed by two fence systems. The outer fence encompasses the compulsory area, which means all the land area under control of the ITER operating entity. The inner fence surrounds a high security area and prevents unauthorised entry by persons or vehicles. All ITER buildings and structures except the cooling basins and structures, the laboratory office building, and the pulsed and steady state switchyards, are inside the high security area. In addition to the space required for buildings, structures and areas, the site layout allows for access, roadways and future expansion.

Space is allowed for the passage of services such as electrical power, cooling water, and movement of personnel and materials. Access is available for all phases of the project, including construction, operation, maintenance, and decommissioning.

During the construction of the tokamak itself, the primary access is from the south, but alternative construction accesses for the site are available from other points as well.

3.6.2 Buildings

ITER buildings house, support, protect, control access to, provide suitable environmental conditions for, and provide services to the components, systems, and operations which are selected to be located within them. The ITER buildings have been optimised to provide the lowest cost design solution which adequately meets the mission requirements and the appropriate standards for the public and workers, as well as investment protection.

The ITER buildings can be grouped in two main classes:

- the radiologically controlled buildings;
- the conventional buildings.

[1] Plant Design Specification (PDS)

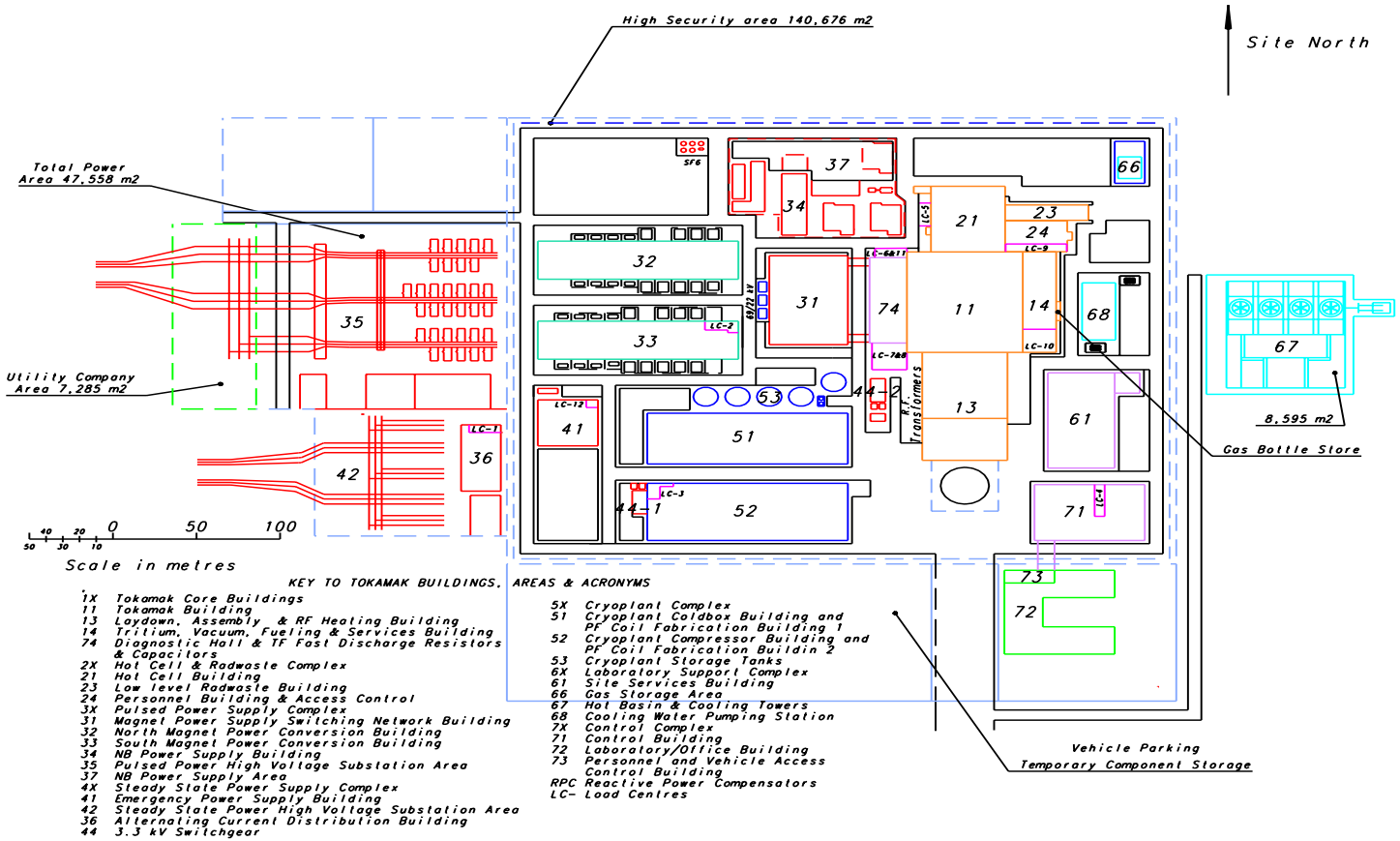

Figure 3.6.1-1 ITER Site Layout

The following description concentrates mainly on the radiologically controlled buildings.

3.6.3 Specific Design of the Radiologically Controlled Buildings

The radiologically controlled buildings include the tokamak building (11), tritium building (14), hot cell building (21), low level radwaste building (23), and personnel access control building (24).

These are the core of the ITER plant and, beyond their specific functional requirements, have been designed:

- to complement the protection of the personnel from exposure to radiation and contamination;
- to complement the confinement barriers that limit the spread of contamination to the external environment in accidental conditions.

As a consequence, the radiologically controlled buildings have been designed to provide appropriate radiation shielding, ventilation, drainage, and access control. They are designed to resist an SL-2 earthquake[1].

3.6.3.1 Radiation Shielding

The general philosophy in the design of the ITER buildings that enclose radiation sources or potentially radioactive components or may become contaminated by radioactive products, is to provide shielding using the building structure itself to keep radiation exposure to the workers as low as reasonably achievable (ALARA).

The radiation sources are of three main types:

- radiation deriving directly from tokamak operation (mainly during the DT phase);
- radiation deriving from activated components removed from the vacuum vessel during maintenance;
- radiation deriving from the inventory of radioactive materials directly (e.g. tritium) or indirectly (activated corrosion products and dust) connected with tokamak operation, but present also when the tokamak is not in operation.

The radiation deriving directly from tokamak operation is primarily a factor in the tokamak building. During tokamak operation, the radiation sources include X-rays, gamma and neutron radiation from neutral beam injectors, gamma and neutron radiation from inside the vacuum vessel (VV), and gamma and beta (tritium) radiation from activated coolant. The radiation fields which will exist during and after the start of the DT phase have been estimated throughout the tokamak building (see 2.14). The shielding in the latter case is required to limit gamma ray fields from activated materials in the volumes where human access is required. These fields are constituted by the emissions from a few isotopes. The field strength decreases rapidly as short-lived isotopes decay, then remains fairly constant as longer-lived isotopes dominate. Shielding thickness is, in general, sufficient to reduce the dose rate in the tokamak galleries and in the tokamak crane hall below 10 μSv/h, within 24 hours of a DT pulse, allowing personnel access without special supervision or requirements.

[1]Plant Design Specification (PDS)

The shielding for this tokamak radiation is initially provided by the bioshield, a hollow cylindrical concrete structure located around the cryostat, forming the "pit". Bioshield plugs installed in front of each of the ports, designed for removal in pieces, provide access for remote maintenance activities inside the vacuum vessel. The tokamak crane hall is shielded from radiation effects by a 2 m thick bioshield lid on the top of the cryostat. The lid is made up of removable concrete blocks to allow controlled access into the pit should any repairs be required.

During maintenance, gamma and beta radiation comes from the plasma-facing components which have been extracted through the ports from inside the VV. These components are handled in casks which move on floor-supported air-bearing vehicles (see 2.9). To reduce the weight of the casks, no shielding materials are used in the casks themselves. The shielding function is performed instead by the buildings, structures, and passageways through which the casks move. Most radioactive components and materials are moved to either the hot cell building or the low level radwaste building. Objects will exit the tokamak building via a lift shaft located in the gallery space and be delivered to the hot cell complex. Shielding is provided, along this path, by the building structural elements. A concrete thickness of 1 m is provided in the floor slabs; in certain locations, a wall thickness of 500 mm is used where it provides both adequate strength and sufficient shielding.

All other radioactive materials are located in the tokamak complex, the hot cell, or the radwaste buildings, except for packaged radioactive waste which has been prepared for off-site shipment and disposal. Also for this source of radiation the shielding is provided by the thickness of the building structures supplemented, where necessary, by local shielding.

3.6.3.2 Radioactive Contamination Confinement

The ITER plant is designed to limit releases of radioactive material to the environment, and radioactive exposure to workers and the public. Buildings where tritium or tritium-bearing components/materials or activated components/materials are handled have been designed accordingly.

Confinement is achieved by establishing barriers around the various radionuclide sources. In certain areas, the buildings provide a confinement barrier. In addition, building atmosphere pressures are arranged to ensure that the pressure gradient is always in the direction towards higher potential contamination, and discharge flow is always directed to the plant exhaust.

The vault that houses the TCWS equipment is connected to adjacent rooms and volumes and the overall volume is designed to limit overpressures resulting from postulated accidents within the capacity of the structure, especially an ex-vessel coolant leak. This building volume is called the "containment volume" (Figure 5.2.4-1), and includes:

- the TCWS vault;
- the CVCSs area;
- the TCWS vault annex;
- the NB cell;
- the vertical pipe shafts;
- the upper and lower pipe chases;
- the lower pipe chase sump.

The structures of the “containment volume” are designed to withstand an internal absolute pressure of 0.2 MPa (absolute) and to keep the leakage under 10% per day at this pressure. In case of an ex-vessel coolant leak, this overpressure is reduced to sub-atmospheric as the resulting gas and vapour is processed by the vault coolers and the vent detritiation system.

The heating, ventilation, and air conditioning (HVAC) systems are designed to provide suitable air change rates to remove heat released to air in the building as well as to maintain acceptable levels of airborne radioactive contamination within the ITER plant and to limit or eliminate contamination spread in the external environment, both for normal operation and for a number of postulated off-normal events.

The radiologically controlled buildings are divided into areas (see Table 5.4.2-1), based on their potential contamination ranging from "white" (uncontaminated) through "green" and "amber" to "red" (with different degrees of airborne and surface contamination). The design of HVAC systems ensures appropriate pressure and flow gradients within the buildings so that air flows from areas of lowest probability of contamination towards areas of higher probability. The HVAC air flow is passed through appropriate filters, and, if necessary, through the detritiation systems, before being released through the plant exhaust. The HVAC system is specifically designed to respond to potential off-normal events. In locations that may be involved with such events due to loss of vacuum or coolant leakage, the HVAC systems are equipped with high-efficiency particulate filters. Areas where the release of elemental tritium or tritiated water is possible are equipped so that the exhaust flow can be passed through a vent detritiation system (VDS).

Floor drainage from radiologically controlled areas is collected in tanks where it can be monitored and, if necessary, treated before it is released to the environment. Details of the detritiation capabilities of the HVAC system are given in 3.1.

3.6.3.3 Personnel Access Control and Evacuation Routes

During operation, all access (personnel and vehicular) to the ITER high-security area of the site is through the single access control gate and gatehouse (73), located on the south side of the site, outside the security fence.

For workers operating in the radiologically controlled buildings, access is through the personnel access control building (24). This is contiguous with the tokamak complex and provides a controlled pathway and change facilities for personnel access to the potentially contaminated zones in the radiologically controlled buildings.

Access control to the tokamak complex is through the common stairway between the tokamak and the tritium buildings, in the north end of the complex on a floor-by-floor basis, with an air-lock that incorporates card readers as well as “step-off-pads” and hand and foot radiation monitors at each point of access. This airlock provides for radioactive contamination control to avoid spreading contamination into the stairways and into other floors of the building.

Access to the other radiologically controlled buildings is controlled in a similar manner. For the hot cell building and the low level radwaste building, truck access is required periodically.

The areas of the plant where access is normally forbidden under certain operational conditions include:

- the tokamak galleries (the areas below the crane hall of the tokamak building) during tokamak operation (including baking);
- the tokamak crane hall during tokamak operation, due to the intensity of the magnetic field ;
- the parts of the hot cell building where radioactive components have been accepted;
- the tokamak galleries and hot cell, and the passageway between these buildings, during the non-operational shift when casks transfer radioactive components.

Protection of workers from beryllium inhalation and contamination is according to common industrial practice by personal protection and ventilation. Access control is implemented according to the beryllium zones defined in Table 5.4.2-5.

The radio-frequency power guidelines defined in the Table 5.4.2-7 are used to ensure that the limits recommended by the international non-ionising radiation committee (INIRC) for high frequency radio-waves are not exceeded for personnel working in areas adjacent to sources of hazard.

Access is also controlled to limit exposure of personnel to potentially harmful electromagnetic fields, according to Table 5.4.2-6.

There are at least two independent emergency evacuation routes from each location or room on each floor of each of the buildings, including the tokamak building, leading to the evacuation stairways and to an outside exit. The routes of exits as a rule do not exceed a length of 60 m. The width of the emergency escape doors are not less 800 mm and the height of doors and escape routes are not less than 2 m. Evacuation exits lead directly to, or through a lobby to, a street or to an outdoor area.

3.6.3.4 Decommissioning

At the end of ITER operations, the radiologically controlled buildings and their internal walls (including the bioshield) will not have become significantly more activated than when they are built. The hot cell and radwaste buildings may have some local contamination, but the walls and floors will be pre-treated with epoxy paint which can be removed to clean them. It will therefore be possible to re-use all the buildings on the site, if necessary to return the site to a “green field”, once the final packages of radwaste are removed from the site following the plant decommissioning process (2.11).

3.6.3.5 Quality Assurance

The buildings and structures which are safety importance classified (SIC) are designed and constructed in accordance with American Concrete Institute (ACI)-349 (or equivalent), and ACI-318 (or equivalent) for specified seismic conditions, and all the quality assurance and inspections contained therein, plus any additional requirements specified by the ITER QA program.

3.6.4 Tokamak Complex

The tokamak complex includes the tokamak building (11), the laydown, assembly, and RF heating building (13) and the tritium, vacuum, fuelling and services building (14). The tokamak building and the tritium, vacuum, fuelling and services building are integrated into a large reinforced concrete structure on a common rectangular basemat with dimensions of approximately 79 m in the north-south direction, and 90 m in the east-west direction. The main reason for placing the tokamak and tritium building on a single foundation is to minimize possibilities of relative displacement due to seismic events in any of the large number of pipes and ducts that run between them.

The tokamak complex design is capable of accommodating seismic isolators if the actual ITER site requires an SL-2 earthquake tolerance significantly greater than the generic site design basis of 0.2 g peak horizontal and vertical ground acceleration.

3.6.4.1 Tokamak Building

The building arrangement is designed to permit assembly and operation of a tokamak with 18 sectors with radial ports at three vertical levels. The general architecture is arranged around the cryostat. The development of floor levels and radial wall or pillar positions is directly related to port access and the remote handling cask docking and transport system. On the north side, the layout accommodates the space requirements for the secondary confinement of the NB H&CD system (the NB cell). A plan and an elevation (east-west section) of the tokamak building are shown in Figures 3.6.4-1 and -2, respectively.

The tokamak building is arranged in three major volumes:
- the pit;
- the galleries;
- the crane hall.

The tokamak pit is that volume surrounded by the cylindrical bioshield wall, that houses the cryostat, the vacuum vessel, the magnets, and all the other in-cryostat and in-vessel components. The tokamak pit is configured to permit the replacement of the central solenoid, the replacement or in-situ repair of any PF coil, and any 40° machine sector (which consists of a 40° VV sector, associated thermal shields, and two TF coils), without dismounting the other TF coils, cutting cables or pipes belonging to other TF coils or machine sectors. The cryostat in turn is supported on the tokamak building basemat. There is sufficient access through the bioshield at the basemat level, via temporary removable blocks, so that the in-situ rewinding of a faulted lower PF coil (PF5 or PF6) is possible if required.

The rooms and access areas under the crane hall floor and outside the bioshield, plus the TCWS vault and the VV pressure suppression tank vault, are organised in several levels (see Figure 3.6.4-2):
- basement level;
- divertor level;
- equatorial level;
- upper port level;
- upper magnet or CVCS level;
- crane hall and TCWS vault level.

At the divertor, equatorial, and upper port levels, the areas are divided into port cells and galleries. A port cell is defined as the volume from the bioshield wall out to the end of the vertical pipe shaft alongside each port. Typical locations of pipe shafts are shown in Figures 3.6.4-1,-2, and -4. The gallery is the space outside the port cells and connects all the port cells circumferentially around the tokamak. If the port cell is used for class 1 remote handling, it will be closed by a sliding full shielding leak-tight door across two adjacent vertical pipe shaft end walls (see Figure 3.6.4-1). This allows personnel access and parallel maintenance activities in the galleries and nearby port cells after a cask has been placed inside the port cell. For ports requiring class 2 or 3 RH operations, shielding for parallel maintenance is to be decided on a case-by-case evaluation.

The tokamak crane hall is connected to the laydown, assembly and RF heating building to form a contiguous crane hall, about 175 m in length, with the crane rails being approximately 47 m apart. This south end of the crane hall, the laydown, assembly and RF heating building, will initially have no internal structure, as it will be used to assemble the tokamak and other components.

The architecture and dimensions of the tokamak building, shown in Figures 3.6.4-1 and -2, are determined through a complex trade-off between various functional and structural constraints:

- equipment sizes;
- service routing;
- internal transport;
- shielding and structural elements;
- initial assembly and maintenance requirements.

The room heights at the port levels are dictated by the height available or necessary for the ports. The room heights at the other floor levels are determined by the equipment that is located on those floors.

The building size is influenced in the vertical and horizontal planes as described below.

Tokamak building vertical layout

The tokamak building height (Figure 3.6.4-2) is determined by two factors:

- the height of the pit below the bioshield top, which is dependent upon the machine port arrangement and the equipment on the tokamak gallery floors that, in turn, set the floor slab heights;
- the height of the hall above the bioshield, which is dependent upon the maximum crane lift for the largest machine component during the assembly process.

In the tokamak galleries, the size and position of the port extensions limits the available locations for slab elements. However, the building design must accommodate clear spans on the order of 10 m and maintenance loads on the order of 100 t and it is not practicable to size slab elements generally less than about 1 m thick. As a consequence the residual clearance between the bottom of the slabs and the top of the remote handling casks is on the order of 0.5 m. This height must be sufficient for installing, at the roof of each level, all the services connecting to the ports or the port area and, in particular, the coolant pipes for in-vessel component cooling. In order to connect the coolant pipes to the ports without crossing the

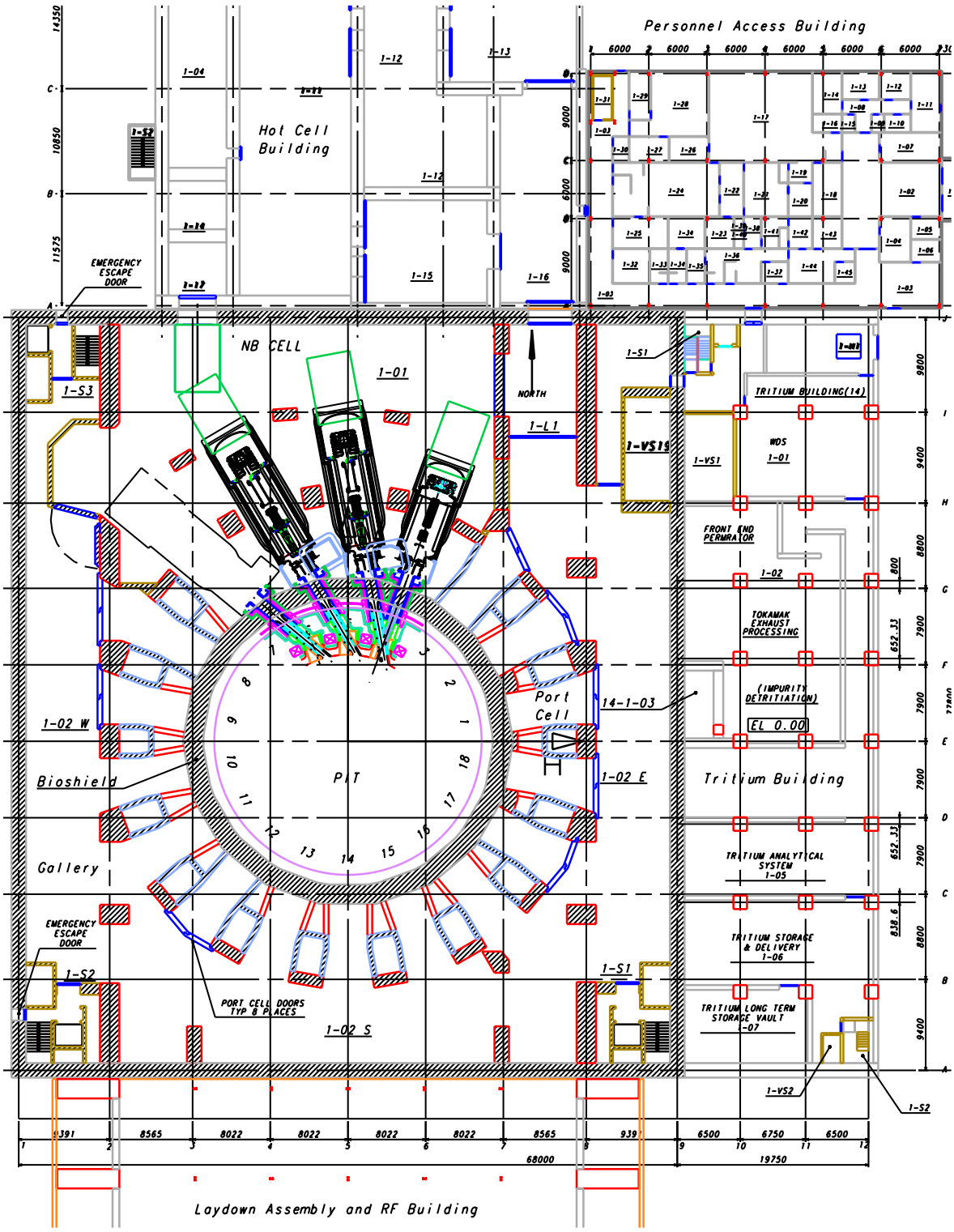

Figure 3.6.4-1 Tokamak Building – Plan View of the Equatorial Level

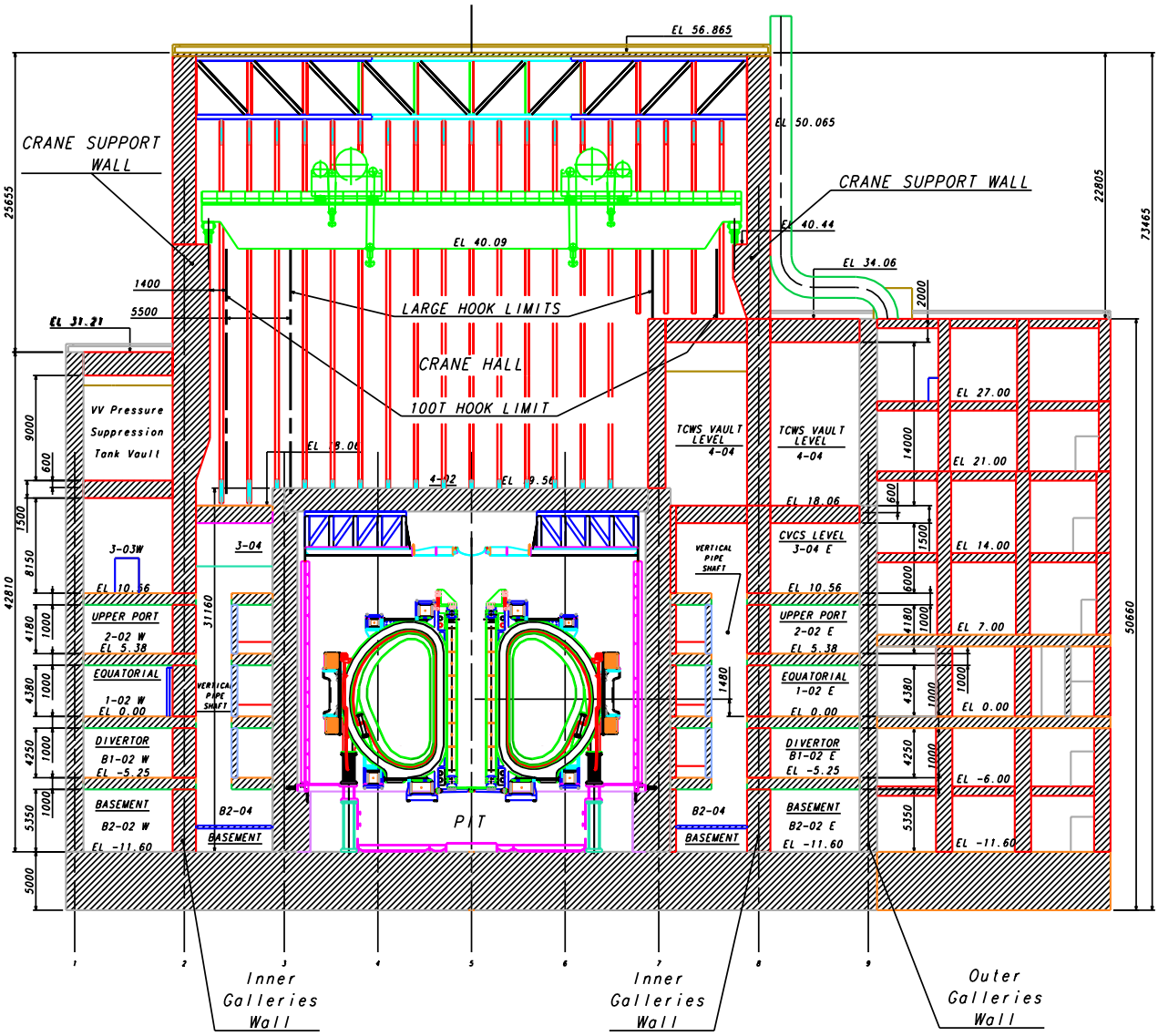

Figure 3.6.4-2 Tokamak Building Elevation (E-W Section)

gallery and thereby blocking the movement of remote handling vehicles, they go in vertical pipe shafts between the ports. The toroidal connections and routing of the coolant pipes is made in two annular pipe chases located at the CVCS level and at the basement level.

The NB injectors require a clear space about 6.4 m high, more than the space between the equatorial level floor and ceiling slabs. Consequently, the upper port level floor slab in the area of the NB cell is replaced by a metallic mezzanine floor.

This mezzanine floor can be more easily integrated with the injector structures and provides limited access to the upper horizontal ports above the NB injector locations.

The toroidal field coil terminal boxes (CTBs), and those for the lower poloidal field coils and lower half of the central solenoid, are located in the basement level below the divertor port level. The upper poloidal field coils, the upper half of central solenoid coil modules, and upper correction coils, are served by CTBs located at the CVCS level, either above the NB cell or on the west side of the tokamak building.

The bioshield roof design is a 2 m thick concrete shield with steel lattice girder supports, with the dual purpose of providing reinforcement to the cryostat head, and access to the upper cryostat area for maintenance.

The tokamak crane hall height is set by the tallest component lift. The height of a 40º sector is approximately 18.5 m, the specific lifting tool is 1 m deep, plus a manoeuvring height of 0.5 m ground clearance. Hence, the overall height is approximately 20 m. The lifting beam arrangement for the crane requires an additional vertical space, estimated at 3 m, but this has been partly accommodated by incorporating a removable section in the bioshield wall. This feature will save 2 m from the crane clearance height.

There will be two, independent, identical 750 t capacity bridge cranes. Each crane will be equipped with two trolleys. Each trolley has a 375 t capacity main hoist and a 100 t auxiliary hoist. The rail-to-rail spacing of the crane rails is 44.82 m. By synchronising the operation of the four main hoists, loads up to 1,500 t can be raised (including jigs). The rail height has been set at EL + 40.595 m. In addition, it is anticipated that the crane lifting beam could be designed to allow the lift to rise between the two cranes, saving a further 3 m in building height. This latter option, however, would be a trade-off between cost reductions from lowering the building height by 3 m, against the cost of procuring the special crane lifting tools.

Tokamak Building Plan Layout

The plan layout (Figure 3.6.4-1) is primarily defined by the space requirements for the cryostat which define the inner diameter of the biological shield wall. The thickness of the biological shield (2 m) wall is then defined, providing both the necessary structural strength and the radiation shielding for the port cells.

The level of embedment of the tokamak building into the ground is defined by choosing as reference grade the equatorial level. This choice is favourable for two reasons. Primarily the access from other buildings into the tokamak building is easier than a deeper embedment and a rectangular layout has been designed, with a better location of plant components, and other

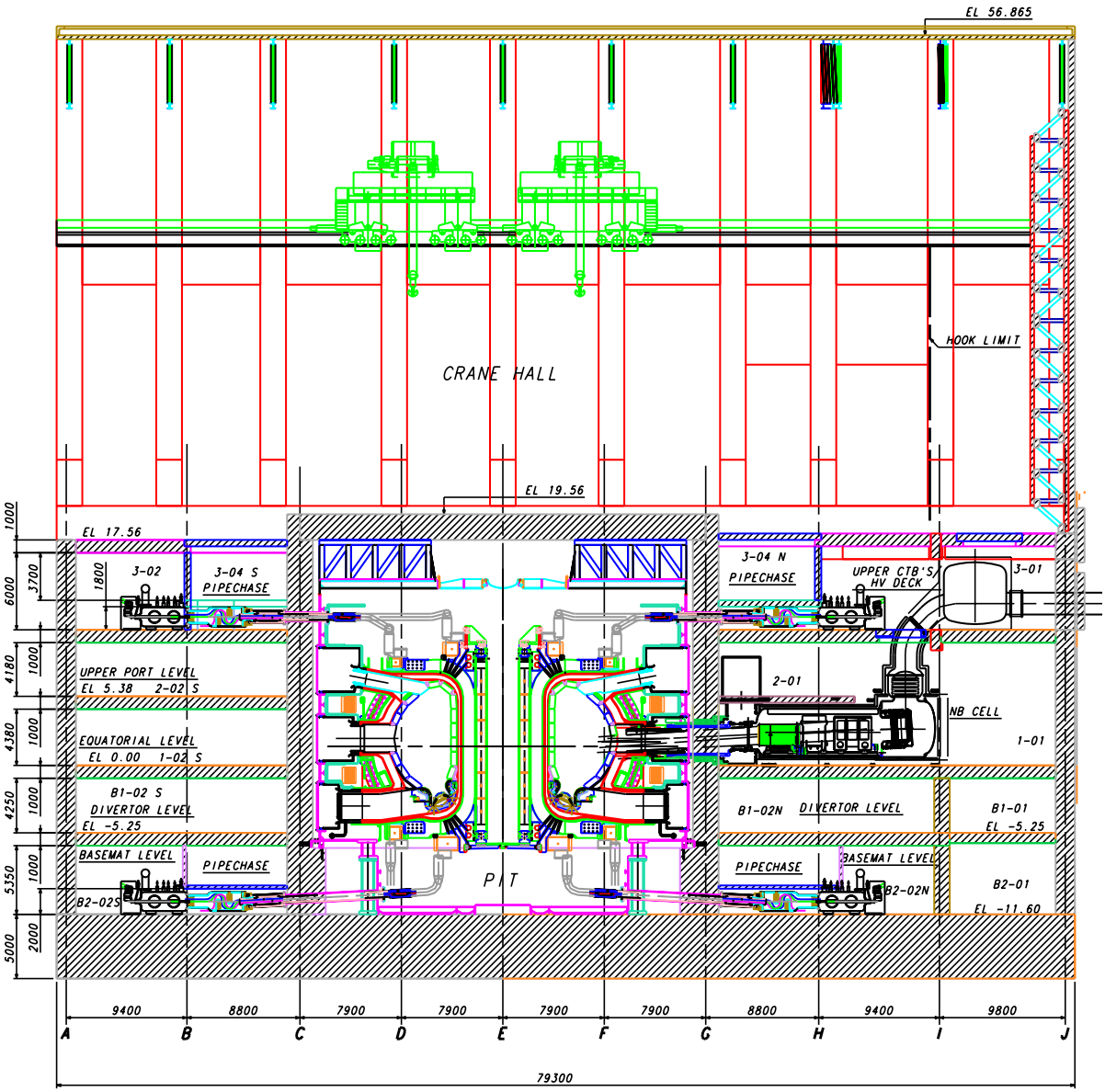

Level	Room no.	Room Designation
Basemat	B2-01	TCWS Drain Tanks
	B2-02	Basemat Galleries
	B2-L1	Elevator (Lift) Area
	B2-VS19	HVAC Shaft
	B2-SU1	Sump
	B2-04	Lower Pipe Chase
Divertor	B1-01	TCWS Drain Tanks Upper Level
	B1-02	Divertor Galleries
	B1-L1	Elevator (Lift) Area
	B1-VS19	HVAC Shaft
Equatorial	1-01	NB Cell
	1-02	Equatorial Galleries
	1-L1	Elevator (Lift) Area
	1-VS19	HVAC Shaft
Upper Port	2-01	NB Cell Mazzanine
	2-02	Equatorial Galleries
	2-L1	Elevator (Lift) Area
	2-VS19	HVAC Shaft

Level	Room no.	Room Designation
Magnet & CVCS	3-01	HV Deck & CTB Area North
	3-02	CTB Area South
	3-03	Cryodistribution Area
	3-04	CVCS Area East
	3-L1	Elevator (Lift) Area
	3-04	Upper Pipe Chase
Crane Hall & TCWS Vault	4-01	Crane Hall
	4-02	Top of Bioshield
	4-03	VV Suppression Tank
	4-04	TCWS Equipment
	4-L1	Elevator (Lift) Area
West Roof		VV PHTS Air Heat Exchanger
Main Roof		Plant Exhaust Duct (el 60.000)
East Roof		VV PHTS Air Heat Exchanger

Figure 3.6.4-3 Tokamak Building Elevation (N-S Section)

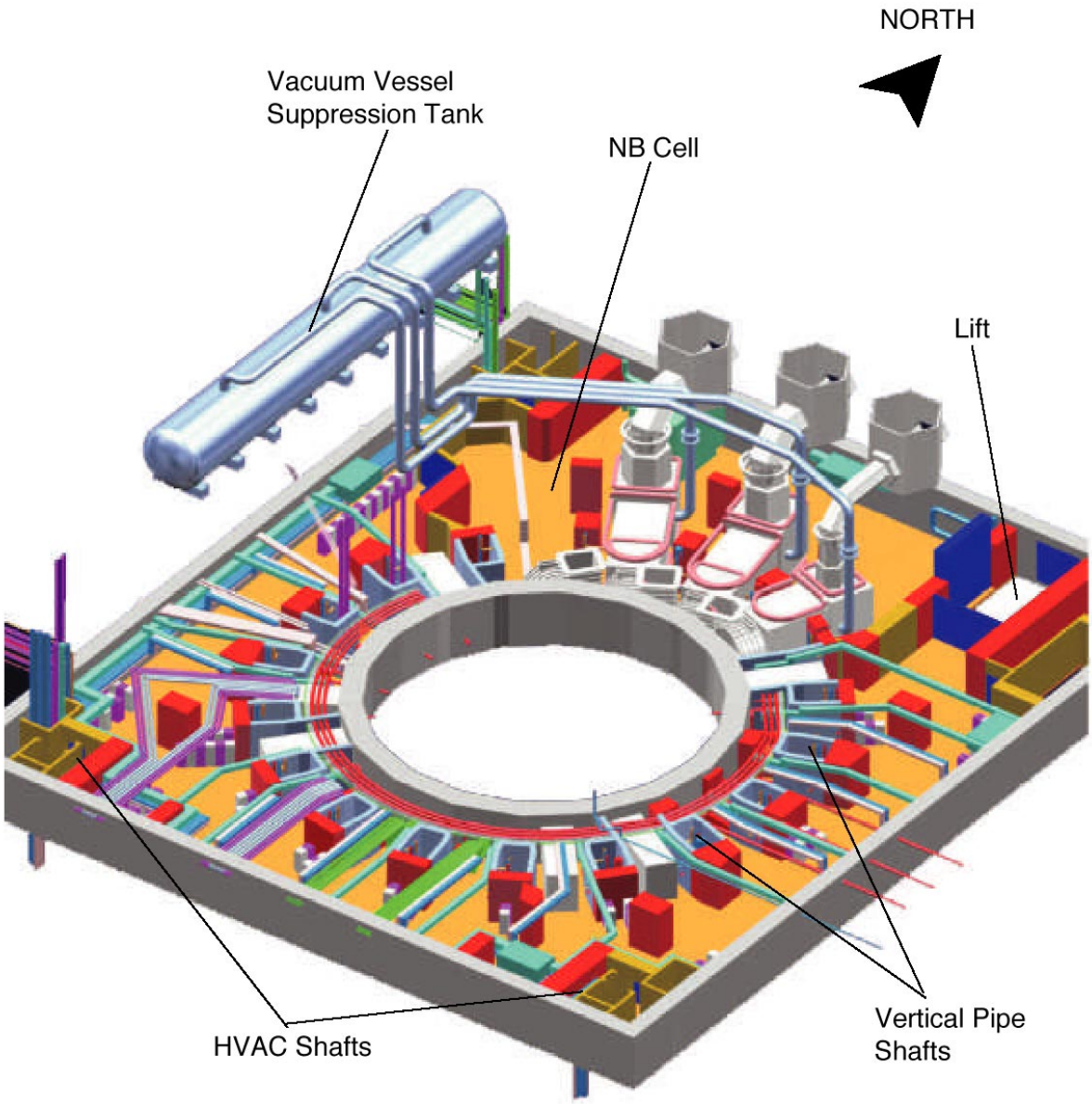

Figure 3.6.4-4 Tokamak Building – Isometric View of the Equatorial Level

services not directly connected to bioshield penetrations. Ground water is assumed at 10 m below nominal grade. This assumption may require engineered ground water control during the construction of the tokamak building.

The floor space required by the additional heating system is then allocated. In particular the volume for the NB cell, the secondary confinement for that H&CD system, occupies part of the north side of the equatorial level and of the upper port level. The floor space is defined by the need to integrate in the NB cell up to three NB injectors plus one smaller diagnostic neutral beam. The location on the north side is defined by the proximity of the NB power supply switch-yard.

The heat transfer equipment is located above grade on the east side of the tokamak building in a single TCWS vault. From the TCWS vault, cooling water is distributed to the blanket modules, divertor cassettes, and vacuum vessel at every sector.

This level of embedment, making the building rectangular, and locating the heat transfer equipment into a single vault, produces some options for placement of the crane support structures. Several options were considered for the structural support wall for the crane rail. On the west side of the building, the crane support wall is located over the inner gallery wall, based on input from the assembly process, to maximise the utility of the assembly hall and to offer full crane cover over the tokamak pit. On the east side of the building, the crane support wall interacts with the TCWS vault by means of pillars through the vault and suitable penetrations to accommodate the TCWS equipment and piping layout. The crane beam overhangs the bioshield, resulting in a distance between the crane rails of approximately 47 m. The operating scope of the crane is maximized, including all of the area inside the bioshield.

Remote handling cask access to each of the ports is required, with the exception of the equatorial ports 4, 5 and 6, allocated to the NB injectors. Cask envelope dimensions are specified by the port size and design of on-board tooling. Casks of 8.5 m long have been assumed as the standard length for analyzing cask access routes. Kinematic analyses of remote handling vehicle motion have been performed to set wall and column positions so that all available ports are accessible. Current analysis shows that casks of this size can be accommodated on the three port levels. All ports allocated for remote handling can be accessed by casks which are able to manoeuvre via the galleries to the building-high 100 t capacity lift in the north east corner of the building. The only exception is for the ports to be accessed from the mezzanine above the NB injectors. At this level, the mezzanine is restricted by the diagnostic neutral beam injector. This issue is under study.

The location for the remote handling lift is on the east crane wall. The lift opens into the passageways to the hot cell building at the equatorial level, for the hot cell processing, and to the RH test stand areas in the hot cell building at elevations + 10.56 m and at + 15.81 m.

Provision has also been made for cask rescue, in the event of breakdown, by an alternative route to the lift on both the equatorial and divertor levels of the building. At the equatorial level the NB cell includes a corridor on the north side that provides a route for the NB maintenance casks to exit to the main equipment lift on the east side. This corridor also provides an alternative access route for the remote handling casks if the gallery is obstructed by a temporarily disabled transport vehicle. The corridor is connected to the gallery by an airtight door. The alternative path for cask rescue is not available on the upper port level due to the additional height requirement of the NB cell. This issue is under study.

Additional Space Requirement

A preliminary layout and evaluation of space availability has been conducted for:
- HVAC ducts;
- cable trays;
- cubicles.

The arrangement of the HVAC system at the basement, three port levels and magnet levels has been developed using ring ducts (750 mm x 650 mm cross section) fixed to the outer gallery walls. At each floor level, these ring ducts have four air handling chiller units symmetrically distributed around the gallery perimeter. The intake air from the cooler end is redistributed by the ring duct through outlets around the perimeter of the outer gallery wall. A

similar arrangement is used to allocate HVAC duct space at the basement and magnet levels. Each port cell is closed by either a shielding door or a closing membrane that seals against the wall, thus separating the port area from the gallery area. During normal operation, air is extracted from each port cell area and processed through a vent detritiation system prior to external release through the plant exhaust system. This creates a differential pressure of -1 mbar between the port cell inside and the gallery atmosphere.

When the shielding doors or membranes need to be opened for cask or personnel access, the depression in temporarily lost. During this period, no operations are permitted within the port cell that could release any tritium or activated products.

A preliminary conceptual design has been decided for the routing of cable trays. Space has been allocated for a minimum of two separate cable trays; one for interlock/signals and one for power cables, for each port cell area, excluding the RH cells. These two trays feed into two rings of cable trays situated just inside the outer gallery wall. These two rings feed into the two vertical shafts on the south-west and south-east corners of the building behind the lift shafts. From there, they feed between floors or out of the building, to their respective sources and destinations.

Specific cubicle requirements have not yet been defined. Early estimates indicate a need for about 355 cubicles in the gallery area and another 400 in the diagnostic hall. Over 660 standard-sized cubicles (800 mm x 800 mm x 2,000 mm high) have been placed in the 3D model of the tokamak building, throughout the galleries, as follows:

- upper port level ~ 200
- equatorial port level ~ 260
- divertor port level ~ 200

Cubicles for the magnet current and cryogenic feeders in the basement and the magnet levels have also been located.

The estimated heat load from these cubicles in the tokamak building is about 500 kW, and may need to be cooled by a chilled water system rather than by the building HVAC system, thus minimizing the number of local gallery air conditioning units

3.6.4.2 Laydown, Assembly, and RF Heating Building (13)

This is a large, rectangular, reinforced concrete building that is the southward extension of the tokamak crane hall, and houses several vital functions.

During the machine assembly phase, the building will be used for the assembly of the ITER machine. At this time, the building will consist only of the shell: the walls, the roof, the interface with the adjacent tokamak building, and the south wall with a 30 m wide door. The floor at grade-level allows easy access of material and components into the area, enabling the pre-assembly of the two TF coils with a 40º vacuum vessel sector and its thermal shields, using the large pre-assembly tools necessary for handling these heavy and large components. The 1,500 t main cranes will be used extensively during this period, and the crane rails are designed to allow smooth transition from the tokamak building to the laydown, assembly, and RF heating building. Preliminary design studies of the main crane and its support structure under design-basis earthquake conditions indicate that adequate safe performance would be sustained.

Assembly will take about 39 months (to month 84). However, as the workload in the assembly hall diminishes towards month 66, the conversion of the assembly area to incorporate the RF heating can begin in time for completion and commissioning by month 96. In order to make this viable, a temporary screen would have to be installed between the RF heating construction and installation area and the still busy assembly area. Commissioning of the RF heating equipment could be delayed to a later stage of the commissioning of the tokamak without seriously affecting the schedule of tokamak activities.

3.6.4.3 Tritium, Vacuum, Fuelling, and Services Building (14)

This building, more simply called the tritium building, is located immediately adjacent to the tokamak building to minimise the length of vacuum and tritium process lines. It is built on the same basemat as the tokamak building, and is 21 m in the east-west direction, and about 79 m in the north-south direction. The bottom floor of the tritium building is at elevation - 11.6 m, and has six additional floors at elevations up to 27 m. The roof is contiguous with the east side of the tokamak building roof, at elevation + 34 m.

The tritium building is structured to house the major systems and components on the various floor elevations as shown in Figure 3.6.4-5 and -6.

The room heights at the 7 floor levels are determined by equipment located on those floors:

- 11.6 m level:	4.600 m
- 6 m level:	5.000 m
+ 0 m level:	6.000 m
+ 7 m level:	6.000 m
+ 14 m level:	6.000 m
+ 21 m level:	6.000 m
+ 27 m level:	6.060 m

The building drawings have been prepared to show these minimal dimensions, which results in column spans and room heights in non-standard distances. A final site-specific design would incorporate some standardisation in these areas, where possible.

TRITIUM BUILDING PLAN VIEW AT ELEV. : -11.600 (Basement 2)

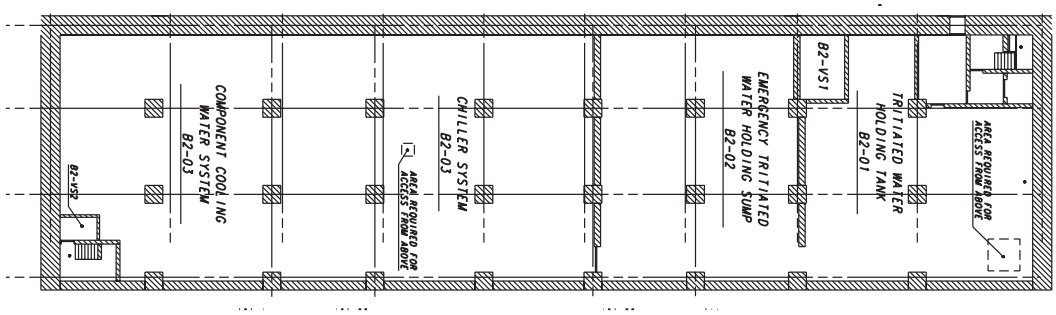

TRITIUM BUILDING PLAN VIEW AT ELEV. : -7.000 (Basement 1)

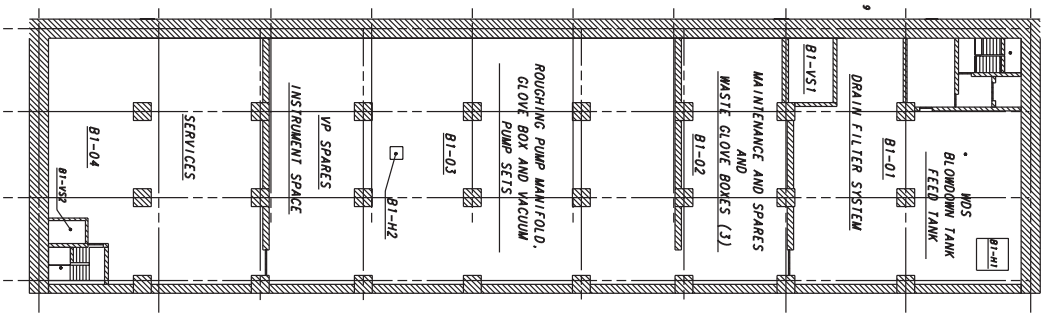

TRITIUM BUILDING PLAN VIEW AT ELEV. : 0.0 (Grade)

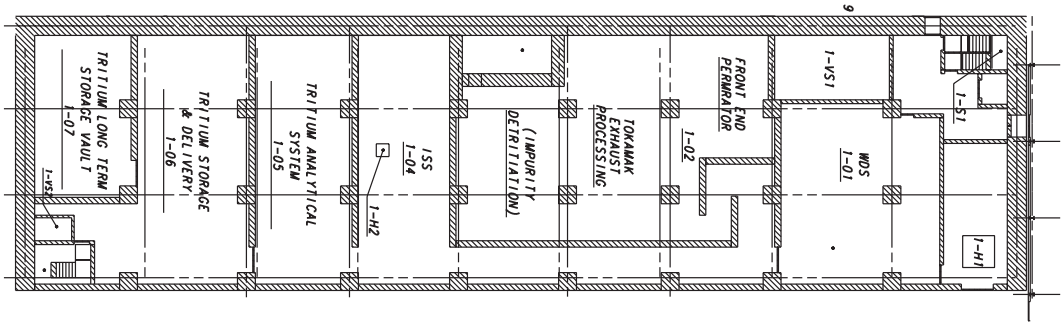

TRITIUM BUILDING PLAN VIEW AT ELEV. : +7.000

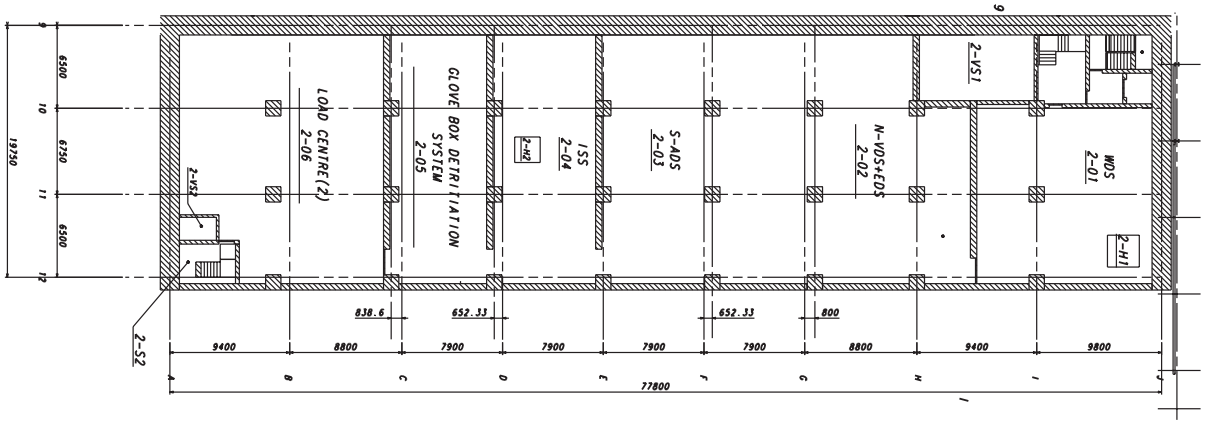

Figure 3.6.4-5 Tritium, Vacuum, Fuelling, and Services Building Plan View at Elevations: - 11.6 m , - 7.0 m, 0.0 m and + 7.0 m

TRITIUM BUILDING PLAN VIEW AT ELEV. : +14.000

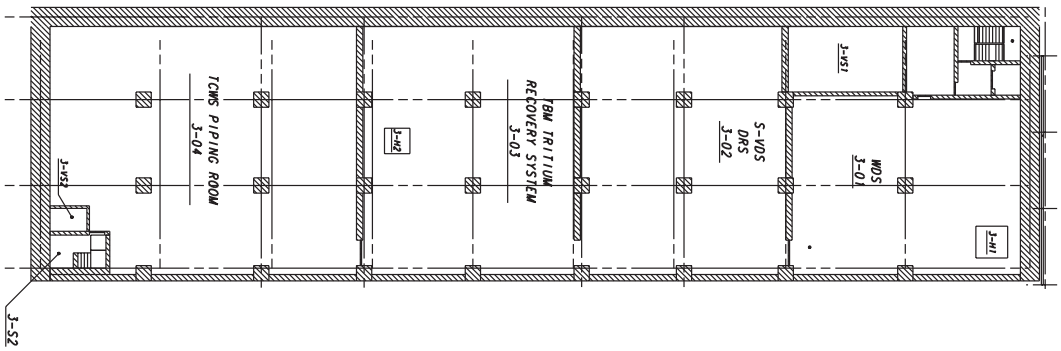

TRITIUM BUILDING PLAN VIEW AT ELEV. : -+21.000

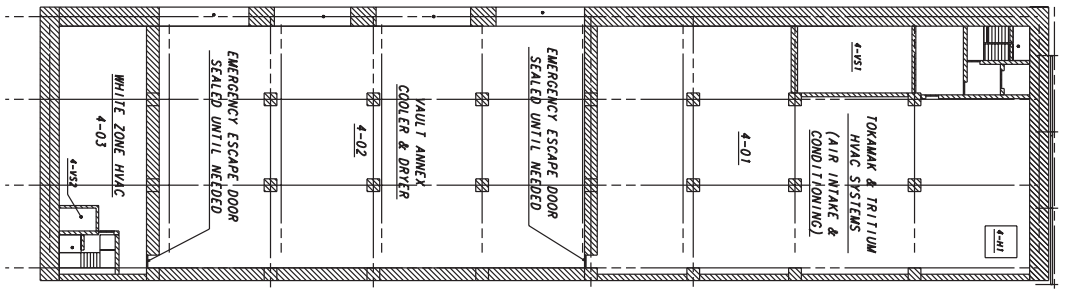

TRITIUM BUILDING PLAN VIEW AT ELEV. : +27.000

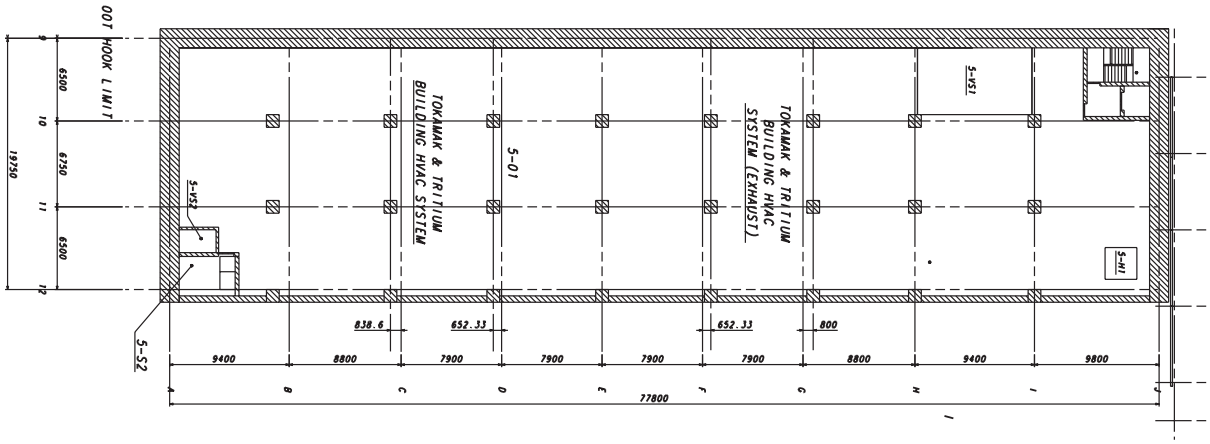

Figure 3.6.4-6 Tritium, Vacuum, Fuelling, and Services Building Plan View at Elevations: + 14.0 m , + 21.0 m, + 27 m

3.6.4.4 Diagnostic and TF Coil Fast Discharge Resistors and Capacitors Building (74)

This building is a reinforced concrete building with four stories above grade and one below, containing the following diagnostic systems and equipment:

- shielded neutron test area;
- cubicles;
- spectrometers;
- reflectrometry;
- toroidal interferometer and polarimeter;
- LIDAR.

In addition, the building houses the TF coil fast discharge resistors and capacitors, and the busbars supplying DC power to the magnet coils. The number of floors, their heights, and equipment layout are determined by the space requirements for the diagnostic cables or waveguides. The TF coil fast discharge resistors are located on the third floor. Also on the third floor, at the north and south ends of the building, is space for routing the busbars between the tokamak complex and the magnet power supply switching network (31).

3.6.5 Hot Cell and Radwaste Complex

3.6.5.1 Hot Cell Building (21)

The hot cell building is located close to the tokamak building to facilitate the transportation of objects removed from the tokamak.

The hot cell building is a rectangular reinforced concrete building with a 53.7 x 44.5 m footprint. It is organised on two main levels (see 2.9). Ground level functions include in-vessel component docking, dust cleaning, storage, repair/testing, remote handling (RH) tools exchange and maintenance, waste processing and waste storage and shipping, and new parts and components receiving and storage. Upper level (+ 10.56 m and +15.81 m) functions include RH equipment test, transfer casks and RH equipment storage, atmosphere confinement control and atmosphere detritiation equipment.

The rationale for the hot cell building layout and size is determined in the first instance by the maintenance requirements, and secondly by a few main design features which have evolved from a number of studies and reviews which particularly aimed at simplification of the remote handling processes. The main features and requirements for space are given below:

a) hot cell arrangement on one (ground) level;
b) in-line repair and refurbishment concept (assumption for the present layout);
c) common in-vessel component refurbishment area is used instead of dedicated hot cells;
d) common in-vessel component receiving/dust cleaning and storage cell with two docking ports that, together with current dimensions of transfer casks, determine the size of the hot cell transportation/docking area;
e) common radioactive waste processing and storage area is used instead of dedicated cells;
f) common repair/test area for all diagnostic, test blanket modules (TBMs) and RF heating port plugs including interspace blocks;
g) equipment and RH tool exchange holding and repair/storage area;
h) new parts and components receiving and storage area;
i) cranes/manipulators and transportation devices retraction/maintenance space;

j) RH equipment test stand and transfer cask and RH equipment storage area on top of the hot cell building;
k) space for atmosphere detritiation system (ADS), the vent detritiation system (VDS), and HVAC;
l) biological shielding, air locks, access and escape routes for personnel.

Figure 3.6.5-1 shows the hot cell building layout on grade level and its proximity to the adjoining personnel, radwaste, tokamak, and tritium buildings.

The sizing of the hot cell receiving room, processing room and storage space is based on meeting the requirements for the maximum allowable maintenance durations, together with the above design features and assumptions.

The sizing of the hot cell receiving/dust cleaning and in-vessel component storage cell is based on unloading and loading of two casks during the same shift and required storage space for the simultaneous storage of 4 blanket modules, 16 divertor cassettes, 4 equatorial port plugs and up to 4 upper port plugs or, instead of the upper port plugs, 3 diagnostic racks (structures for diagnostics at equatorial and upper port plugs).

The process cell size is based on simultaneous refurbishment of two divertor cassettes and one blanket module. In parallel, port plugs can be refurbished and tested by insertion in special port interfaces (test tanks).

The current hot cell building size is defined to satisfy the minimum requirements of all hot cell facility users. However, the detailed refurbishment procedures and the necessary RH equipment are still under detailed study. It may therefore be expected that further design optimisation will be possible at a future date.

Most of the other room sizes are a logical consequence of their functional requirements, i.e. space needed for casks to manoeuvre, space for equipment, e.g. HVAC, etc.

The hot cell building is available during the initial installation phase of the tokamak in-vessel components to provide a pre-assembly, Be-controlled area and a facility for loading components into transfer casks.

The hot cell building is designed such that it can be expanded to meet future, increased processing capacity needs, e.g. for the decommissioning phase of ITER.

To minimise the amount of tritiated water generated because of air inleakage, the leak-tightness of the building must be verified by detailed design, and the same attention to penetrations must be made as is required for the containment volume.

There is still the issue of mixed wastes arising because of the possibility of generating waste materials that contain both toxic Be and radioactive materials. This is an issue that will have to be dealt with in the host country licensing discussions.

Finally, the hot cell building will be built early in the schedule, and will be available for the temporary storage of RH equipment used for in-vessel assembly, as well as the storage and assembly of some of the in-vessel assembly components. This will obviate the need for a temporary facility to serve these functions.

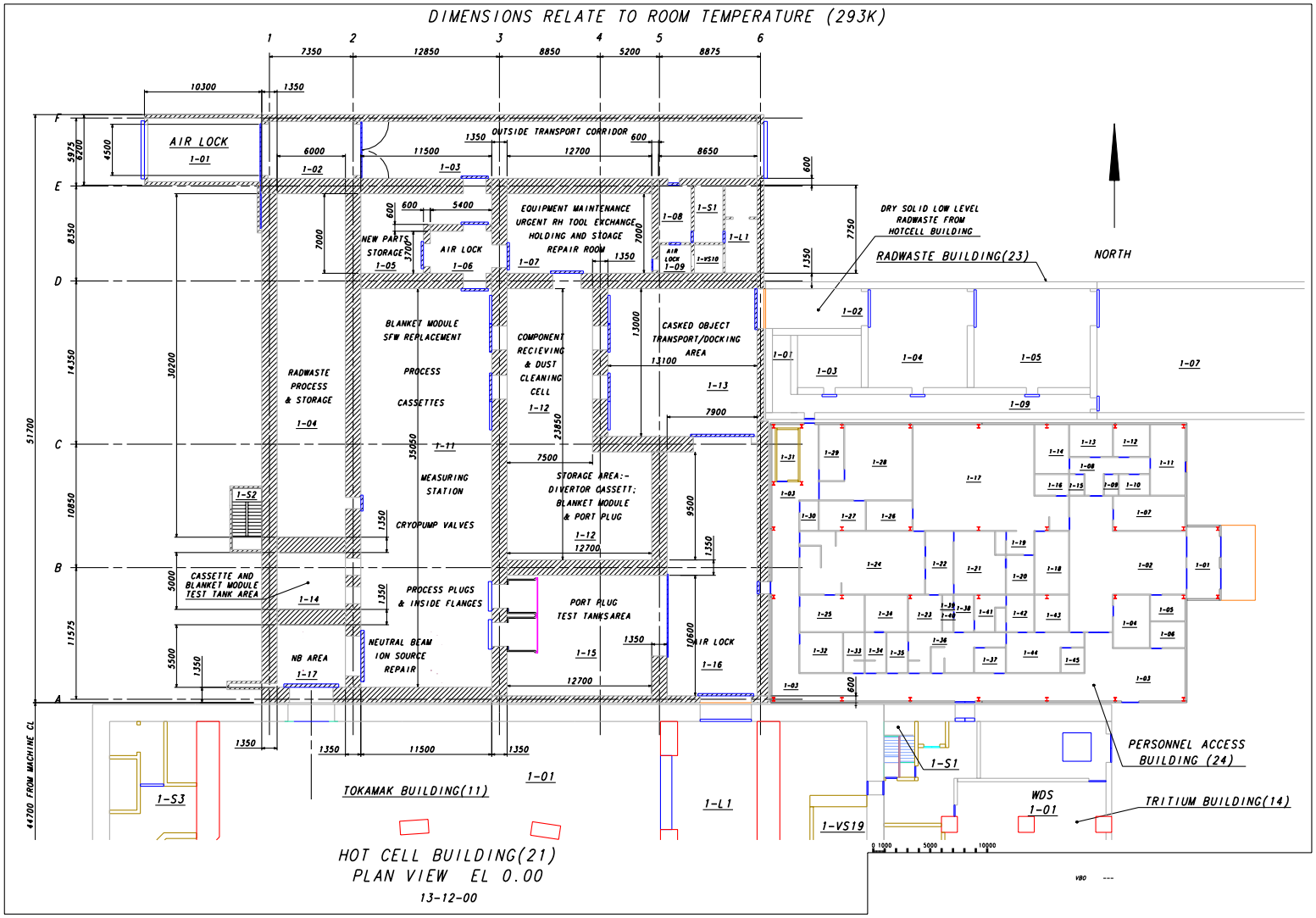

Figure 3.6.5-1 Hot Cell, Low Level Radwaste, and Personnel Access Control Buildings (plan view at grade level)

3.6.5.2 Low Level Radwaste Building (23) and Personnel Access Control Building (24)

As seen in Figure 3.6.5-1, these buildings are located close to the tokamak, the tritium, and the hot cell buildings to facilitate the management of personnel exposure and health physics, and to minimise the length of radioactive waste treatment connections.

The low-level radwaste building provides space for systems which process mildly contaminated water. Floor drainage from radiologically controlled buildings, active laboratories, tokamak cooling water system equipment drains, and shower and laundry drains, are treated here. Paper, plastic, and other dry solid material are collected and stored for appropriate packaging. The low-level radwaste building is configured to facilitate the handling of loaded filter and demineralizer beds. Filters and demineralizers are designed so that the beds can be sealed in a disposable liner and handled as wet solid waste. A de-watering step may be necessary before these materials can be transferred for disposal, and a connection to the hot cells provides for a common exit for this transfer. Materials are sealed in containers for off-site disposal by the host country. It is intended that the radwaste facility will be able to package materials so that they do not require any further processing prior to disposal by the host. The low-level radwaste building will be constructed using cast-in-place reinforced concrete.

Primary coolant will be continuously cleaned by the CVCSs to remove particulate and ionic material, some of which may have become activated. When the CVCSs filters and demineralizer beds reach their end-of-service life, the filter medium or demineralizer resin bed will be replaced. The spent filters and demineralizer beds may be treated as wet solid radioactive waste and packaged for disposal. Alternatively, ITER may have features which would allow backwashing of filters or regeneration of CVCS demineralizer beds thereby reducing the waste volume.

When primary coolant is intentionally removed from the system, it will be collected in drain tanks. Normally, primary coolant systems will be refilled from these tanks to resume operation.

Occasionally, it will be necessary to remove primary coolant to the waste systems. Primary coolant, water which is spilled onto the floor and collected in drains within the radiologically controlled areas, fluid from active laboratory drains, and decontamination fluid, will be collected in tanks in the radwaste building and treated in a dedicated waste process stream. Fluid will be sampled before and after processing. This process stream will include oil separators, filters, and demineralizers. If the product water meets the specifications for primary coolant, but exceeds the allowable tritium content for release to the environment, it will be sent to a water detritiation system where tritium will be extracted and detritiated water can be discharged. If the water does not meet primary coolant specifications, it must be recycled until additional particulate and ionic activity have been removed. The filter beds and demineralizer resins from this stream will also be treated as waste and handled in a manner similar to the primary coolant CVCS filters and demineralizers.

As with the hot cell, the low level radwaste building has been reduced to the minimum, because rather than designing and installing a comprehensive radwaste processing facility, the use of contractors for further waste processing is foreseen.

There is still the issue of mixed wastes arising because of the possibility of generating waste materials that contain both toxic Be and radioactive materials, an issue that will have to be dealt with the host country licensing regulations.

The personnel access control building is a rectangular steel frame building on a slab at ground level in plan 36.0 m x 24.0 m, with a height of 7.4 m. This building is on two floors and located so that it is contiguous with the tokamak building, the tritium building, the hot cell building and the low level radwaste building. The above-grade structures use structural steel framing. The building has floor levels at grade (0.00 m) and at + 3.60 m, and a roof at + 7.40 m, and is divided into white and green zones, based on their potential contamination. There are separate HVAC ducts to separate the rooms with different degrees of airborne and surface contamination. This building provides the single, controlled pathway for personnel access to the potentially contaminated zones in the connected buildings.

3.6.6 Pulsed Power Supply Complex

3.6.6.1 Magnet Power Supply Switching Network Building (31)

The main function of the MPSSN building is to house the busbar connections for incoming DC electric power from the magnet power conversion buildings (32 and 33), plus the magnet power switching network, poloidal field (PF) circuit protective equipment, and dump resistors. Included is an instrumentation room, personnel support facilities, as well as general services such as HVAC, lighting, power, drainage, fluids, and lifting capability. A compressed air system and water cooling supply system are located at grade.

The MPSSN building is a rectangular steel frame structure, with dimensions 46 m wide by 70 m long by 14 m high, running north and south. The structure is set on a cast-in-place reinforced concrete slab, with two floor levels at grade 0.00 m, + 7.00 m and a roof level at + 14.00 m. The foundation of the building is set below grade by 0.2 m so that the finished floor level matches grade level. It is located inside the ITER high security fence on the west side of the tokamak building, in order to minimize the length of magnet power busbars.

3.6.6.2 North and South Magnet Power Conversion Buildings (32 and 33)

The two magnet power conversion buildings are two-level structures arranged as relatively long and thin structures to provide adequate indoor space for rectifier sets and related equipment, while also providing large exterior walls for connections to transformers. The steel frame buildings are each set on a reinforced concrete foundation. Rectifiers and power conditioning equipment are floor-supported, along the edge of each building. Power supply circuit transformers are located outdoors on foundation structures, including blast/fire walls to protect equipment inside. Busbars are routed vertically from the rectifier sets to an upper level. Large doors, at grade level and at +10 m on an intermediate floor, allow the installation and removal of equipment using portable equipment. The roof level (+16 m), is structurally flat, with only HVAC equipment located there.

High current power supply output is collected in air-cooled busbars, located on a second level above the converter sets in each building. The building provides general services such as HVAC, lighting, power, drainage, fluids, and lifting capability, as well as personnel support areas, including an office.

3.6.6.3 NB Power Supply Building (34)

The NBPS building provides space for neutral beam injection converters, inverters and control cubicles for delivering 33 MW to the plasma. The building includes a control room, facilities for personnel support, and general services such as HVAC, lighting, power, drainage, fluids, and lifting capability. It is located inside of the ITER high security fence on the north side of the tokamak building, adjacent to the NB power supply area, that contains the power supply units for the NB and DNB injectors.

The NBPS building is structural steel, column and beam frame, 15 m wide by 45 m long and 11 m high, with two floor levels at grade 0.00 m, + 6.00 m and a roof level at + 11.00 m. The structure is set on a cast-in-place reinforced concrete slab foundation, 0.2 m below grade so that the finished floor level matches grade level. The second level contains power conditioning equipment and the control room, while the HVAC is located on the flat roof.

3.6.6.4 Pulsed Power HV Substation Area (35)

This pulsed power area is an outdoor switchyard and serves the magnet and plasma heating systems. The site infrastructure includes cast-in-place equipment foundations for transformers, circuit breakers, pylons, switchgear and other switchyard equipment. No building structure is required to protect this equipment.

3.6.6.5 NB Power Supply Area (37)

The power supply units for the NB injectors and DNB will be placed in the NB power supply area at the north side of the MPSSNB and near the hot cell building. This NB power supply area has the size of about 100 m x 80 m and it includes one building (the NB power supply building), which houses the static converters and inverters of the power supplies for both the NB and DNB injectors. All step-down and isolating transformers, as well as the HV rectifiers for the acceleration power supplies, are placed outdoors, around the building. Moreover, space is reserved for a NB power supply test facility, and for future extension (power supplies for a possible 3rd NB injector).

Power for the NB acceleration is taken from the pulsed power HV substation to the west. The output power is delivered to the NB sources located in the NB cells (tokamak building) via HV transmission lines which cross the hot cell building to the HV deck in the gallery of the tokamak building.

The site infrastructure includes concrete firewalls for the large transformers, and cast-in-place equipment foundations for transformers and rectifiers, etc.

3.6.7 Steady State Power Supply Complex

3.6.7.1 Emergency Power Supply Building (41)

The EPS building is a rectangular reinforced concrete three-level structure, 36 m by 42.7 m by 14.4 m high, located at the west end of the high security area, next to the steady state power supply switchyard. It houses two diesel electric generator sets, each rated at 6.3 MW_e, plus control and switchgear equipment, to supply plant power in case of emergency.

The generators are set on separate foundations, to isolate their vibration. Diesel engine exhaust muffler, stack and heat rejection systems are located on the roof. Diesel fuel is stored in nearby underground tanks.

3.6.7.2 Steady State Power HV Substation Area

This steady state power area is an outdoor switchyard and serves "house" loads, including the cryoplant, cooling systems, hot cell systems, HVAC, etc. The site infrastructure includes cast-in-place equipment foundations for transformers, circuit breakers, pylons, switchgear, and other switchyard equipment. No building structure is required to protect this equipment.

3.6.7.3 Alternating Current Distribution Building (36)

The AC distribution building is a reinforced concrete, two-level structure. Reinforced concrete is used because the DC battery room requires the strength of massive and strong walls to resist a potential hydrogen explosion. Heavy equipment is located at grade.

3.6.7.4 3.3 kV Power Supply Structures (44)

Two independent 3.3 kV power supply (PS) structures (44-1 and 44-2) are dedicated to motor loads up to 400 kW. PS 44-1 is just west of the cryoplant compressor building (52), and PS 44-2 is located south of the diagnostic building (74) between the cryoplant coldbox (51) and the tokamak assembly hall (13).

Each of the 3.3 kV power supply structures is a single-level, rectangular structural steel, column and beam configuration unit, set on a concrete slab at grade, with a roof level at + 4.70 m.

Siding is architectural metal with integral insulation, supported on horizontal stringers. Non-structural concrete walls separate the transformers and switchgear along building walls. Two power transformers for each structure, are located outdoors on concrete foundations, which incorporate oil catch basins and fire/blast separation walls. Roofing is structurally flat with built-up insulation to provide slopes to drainage points. Each structure provides general services such as ventilation, lighting, power, fire protection, fluids and drainage.

There are no operator support facilities.

3.6.7.5 Electrical Load Centres

LCs are located throughout the site to efficiently consolidate the electric power requirements for a particular area, building, or a group of buildings. Currently, ten load centres are served by tunnels from the main power supply areas, feeding the end users in the vicinity.

3.6.8 Cryoplant Complex

3.6.8.1 Cryoplant Coldbox Building (and PF Coil Fabrication Building 1) (51)

As with the cryoplant coldbox building, the cryoplant compressor building is built in the early stages of construction, and used initially for PF coil fabrication. It is configured in the same manner as the PF coil fabrication building 2, below, and will be used to simultaneously

fabricate coils PF3 and 4. After the coil fabrication campaign, the building will be converted to the cryoplant coldbox building.

The cryoplant coldbox building is a single-level structure with clear span. The building provides space for process equipment and is serviced by an overhead main 50 t bridge crane and by a 5 t bridge sub-crane, suitable for servicing and assembly and disassembly of the helium coldboxes. The general configuration of the building is the same as for the cryoplant compressor building. The cold process boxes contain series of counter-flow regenerative heat exchangers, cold turbines and valves. The streams of compressed helium and nitrogen are supplied to these cold boxes from the cryoplant compressor building. The space for mechanical and electrical services, parts storage, and personnel areas such as local control room, offices, lavatories, and other worker support functions will be provided at the east end of building. Additional cryoplant equipment, including gaseous helium storage tanks, and LHe and LN_2 tanks, are located outdoors.

3.6.8.2 Cryoplant Compressor Building (and PF Coil Fabrication Building 2) (52)

The cryoplant compressor building is built in the early stages of construction, and used initially for PF coil fabrication. It is a single-level steel frame structure with a space for mechanical and electrical services. The building footprint is sufficient to provide for simultaneous fabrication of coils PF1, 2, 5, and 6. Each coil type, i.e. l and 6 or 2 and 5, will occupy 5 equivalent coil diameters, plus space for conductor laydown and spooling for a two-in-hand winding operation. The height of the building is controlled by the height of the winding operation plus room for pancake and module handling tools, crane, and roof truss depth.

The tools, jigs, and winding fixtures needed for the largest coil determine the space requirements for the building. The heaviest module determines the crane capacity. The manufacturing process involves the application of epoxy insulating and bonding materials, vacuum impregnation steps, and preparation of conductor joints. The process requires cleanliness, lighting, and environmental control, which are similar to modern aircraft manufacture.

The building includes space for an electrical load distribution centre, which is part of the plant steady-state electrical power distribution system. Personnel areas such as offices, lavatories, change facilities, and other worker support functions, will be provided using temporary buildings.

After the coil fabrication campaign, the PF coil fabrication building 2 will be converted to the cryoplant compressor building.

The cryoplant compressor building is a single-level structure with clear span. The building provides space for process equipment and is serviced by an overhead main 40 t bridge crane as well as by a 5 t bridge sub-crane, suitable for servicing and assembly and disassembly of the compressors. To maintain stability, the crane columns are built up with an effective width of 2.5 m, resulting in 40 m between crane rails. The maximum hook height for the crane is 18 m. The north aisle is used for interior truck access and routing of services, both overhead and in a below-grade utility trench. Large doors are provided at the east end of the building. The spaces for mechanical and electrical services, parts storage, and other worker support

functions are provided at the west end of the building. Additional cryoplant equipment, and helium gas heaters for the final stage of warm-up, are located outdoors.

3.6.8.3 Cryoplant Storage Tanks

Three warm and one 80K helium tanks, all rated at 1.8 MPa, a low pressure He balloon, and liquid nitrogen tanks, are located in an outside area, adjacent to the cryoplant coldbox building. The site infrastructure includes cast-in-place tank foundations.

3.6.9 Laboratory Support Complex

3.6.9.1 Site Services Building (61)

The site services building provides space for industrial support systems including compressed and breathing air, miscellaneous gas distribution, chilled water, demineralized water, potable and hot water treatment, auxiliary steam for space heating, and electrical power distribution. It contains space dedicated to non-radioactive waste handling, the non-active chemical laboratory, spare parts warehousing, machine shops, and offices.

The building has two parts: the main building and a small auxiliary boiler annex.

The main building is a single-level structure, 75 m long x 40 m wide and 12.5 m high, internally divided into three bays. Two 17 m wide bays, at each side of the building, provide space for process equipment and are serviced by overhead bridge cranes 20 t and 5 t. The centre bay , 6 m wide, is used for interior truck access and routing of services, both overhead and in a below-grade utility trench. Large doors at several locations provide access to interior equipment during operation. The roof is structurally flat.

The separate auxiliary steam boiler annex is 16 m x 15 m x 7.3 m high, set on a concrete slab at ground level.

3.6.9.2 Gas Storage Area

This area is allocated for the storage of hydrogen, deuterium and possibly nitrogen.

3.6.9.3 Hot Basin and Cooling Towers (67)

The ITER cooling system is based on generic site conditions, which include the use of mechanical draft cooling towers. Since the power production is not steady state, the cooling system is optimized by providing separate hot and cold water basins. The cooling towers are set on a foundation built as part of the cold water basin.

The cooling water for the tokamak systems is drawn from the cooling tower cold basin, extracts heat throughout the tokamak systems, and is returned to the hot basin. The flow rates between the basins and through the cooling towers are used to control the water temperature in the two basins. A spillway allows excess hot basin water to overflow into the cold basin.

The volume of the hot basin is 12,000 m^3 while that of the cold basin is 20,000 m^3. Make-up water pumps beside the cooling towers have a foundation which is 10 m x 8 m . The main pumps feeding the cooling towers are on the hot basin.

3.6.9.4 Cooling Water Pumping Station (68)

The main cooling water pumping station is located east of the tritium building to minimise the distance that the cooling water needs to be pumped. It is connected to the cold basin via a utility tunnel. The structure for the pumping station is 18 m (EW) x 50 m (NS) x 14 m (height) with walls, a simple roof, and natural ventilation, housing ten (10) pumps and two safety-related chiller cooling towers, one at each end. Power for lighting and small power users, and a welding outlet, are provided. There is no crane, as pump maintenance will use temporary lifting devices.

3.6.10 Control Complex

3.6.10.1 Control Building (71)

The control building is located south and east of the tokamak complex, within the high security fence boundary. It houses:

- basement level: machinery room, load centre, cable room, transformer room, library, meeting room, storage, offices;
- ground level: control room, computer room, change area, visitors' rooms, offices, incident response area (with vehicle).

The control building is designed so that essential systems can be operated after a seismic event, and has the following size and characteristics.

- building dimension : 40.4 m (E-W) x 70.4 m (N-S) x 7.2 m (from grade);
- depth of basemat bottom: 8.8 m;
- footprint: 2,844 m^2;
- total floor area: 5,688 m^2 (2,844 m^2 above ground, 2,844 m^2 below ground).

3.6.10.2 Laboratory/Office Building (72)

The ITER office building, located outside the ITER high security fence, is a five-level rectangular structure with an appendage to house an auditorium. HVAC and elevator equipment are located on the roof. The building provides some general services such as lighting, power, HVAC, fluids and is linked to other parts of the ITER site through communications networks.

It is a structural steel framed building which has floor levels at grade 0.0 m, + 3.60 m, + 7.20 m, + 10.80 m, + 14.40 m, and a roof level at + 18.00 m. Ground floor building amenities include a lobby and display area at the building entrance, cafeteria and kitchen facilities, locker and exercise area, computer room, library, conference rooms, auditorium, and various areas to house building support personnel and equipment. Floors 2 through 4 provide staff offices, workstations (cubicles), and meeting or conference rooms.

Two roof structures are provided to house HVAC and elevator equipment.

3.6.10.3 Personnel and Vehicle Access Control Gatehouse

The gatehouse is located just west of, and connected at grade level to, the laboratory/office building on the south, and to the control building on the north. The gatehouse provides access control to the high security area, such that all personnel and vehicle access is granted through this building. All personnel proceeding through on foot to the control building or other areas within the high security fence pass through this gatehouse.

3.6.11 Utility Tunnels and Service Structures, and Site Improvements

3.6.11.1 Utility Tunnels

Underground tunnels between buildings provide a protected route for cooling water piping, cryoline piping, electric power, communication services, instrumentation and control wiring, fibre-optic cables, and general services such as lighting, power, and fluids. The tunnels form a network around the site, with combination tunnels being internally segregated for protection of the services from each other.

The major use of the tunnels is for the ITER cooling system piping, going from the cooling tower basin to the tokamak building via a pumping distribution station, located just north of the site services building, and east of the tokamak complex. These pipe tunnels are equipped with sumps and sump pumps to collect rainwater and leakage, and to pump the water collected to the site storm drain system. For areas of the tunnels containing potentially contaminated water, any collected leakage is first sent to the radwaste building for confirmation of the acceptability of discharging the water.

The next major use is for electrical power. These tunnels link both the steady state electrical power switchyard and the pulsed power switchyard on the west side of the site with the various buildings and electrical load distribution centres throughout the plant.

3.6.11.2 Service Structures

Electrical load centres are located inside or adjacent to buildings. Those adjacent to buildings require only a minimum structure to protect the equipment from the elements, and to provide an area for inspection and maintenance. Similar protection is required for the 3.3 kV power supply structures, and for the AC distribution building. In some cases, electrical power is transferred on bridge structures where the required access to a building is above grade.

Other systems require foundations for equipment or tanks, and, in some cases, include the concrete storage tanks themselves. Such service structures include:

- foundation pads for large helium storage tanks used by the cryoplant, for fuel tanks used by the auxiliary boiler, for fuel tanks associated with the emergency power supply, and for water tanks associated with the demineralised and potable water systems;
- a reinforced concrete potable water basin sized to provide for three days of makeup for demineralised water and potable water storage systems including fire-water reserve;
- a large holdup basin available for temporary storage of industrial sewage so that, if the sewage streams become contaminated, the industrial sewage can be held while corrective action and procedures for processing are established.

3.6.12 Specific Areas and Site Improvements

Each of the ITER buildings includes appropriate outdoor lighting. In addition, the site infrastructure includes outdoor overhead lights. Lighting covers the switchyards, cooling towers, security fence, perimeter road, personnel and vehicle gate areas, and parking areas.

The assembly of the ITER tokamak involves the receipt and on-site handling of numerous large heavy objects. Site-fabricated PF coils, off-site shop-fabricated TF coils, vacuum vessel segments, and other tokamak parts, must be delivered to the tokamak buildings. For such purposes, there are wide paved areas to the south of the tokamak building. There is also a wide, heavy duty transport path able to move the site-fabricated coils from the east end of the coil fabrication buildings to the south entrance of the tokamak hall. The pathway is smooth enough for heavy haul vehicles, and has sufficient surface drainage. Also, there is a temporary building to the south, designed for the fabrication of the cryostat sections.

3.6.13 Internal Communications

A site-wide internal communication system is provided in most buildings, including telephone connections, public address system, and appropriate warning systems for plant emergency, crane movement, fire, radiation monitoring, access control, etc. In addition there will be dedicated intercommunication systems between the control room and important plant locations and access control points.

3.6.14 Fire Protection

The fire protection strategy at ITER is that the building materials and installed components make extensive use of non-flammable or low-flammable materials, such as concrete, steel, and fire retardant cable insulation, etc. Nonetheless, the buildings and structures provide fire detection, alarm, and mitigation systems commensurate with the occupancy and fire risk loading. There will be an on-site incident response team which will be able to carry out fire-fighting duties. This team will be supplemented by off-site emergency services as required.

3.6.15 Assessment of Design

The design of the ITER site and buildings has progressed in a varied manner across the site. Those buildings that are involved with the tokamak machine, that house the systems and the components that interact directly with the machine, that are required for close support of the tokamak machine, have received the greatest degree of attention. These buildings, in order of highest degree of design completion to lowest, are the:

- tokamak building;
- tritium, vacuum, fuelling and services building;
- hot cell building;
- low level radwaste building;
- personnel access control building.

Other buildings which are also associated with the above, have received preliminary and detailed design attention, but will need to be studied further, include:

- laydown, assembly, and RF heating building;
- diagnostic building.

The rest of the buildings have received only preliminary design attention.

The site and building structures, except for the nuclear-related buildings, are relatively conventional in design and construction technology for industrial buildings. There are no site or building problems with these buildings that require extraordinary efforts.

3.6.15.1 Tokamak Building

General Layout

The tokamak building provides a minimum size layout for the contained systems and equipment. This results in column spans and room heights in non-standard dimensions. A final site-specific design might well incorporate some standardisation in these areas, where possible.

In addition, some size constraints may be relieved by adopting special forms of concrete: in areas where shielding thicknesses govern the building size. Floor thicknesses could be reduced by the use of high density concrete (with a density of 3.5 t/m^3), rather than normal density concrete (2.5 t/m^3), thus allowing an increase in room height of approximately 285 mm. This extra space could be taken up, if necessary, for fitting extra services, especially the HVAC ducting and any required cable trays, in the space above the cask travel paths. However, the present layout, which does not use heavy concrete, is found to provide sufficient space for all services and utilities within the building.

Structural – Seismic Verifications

In areas where special strength properties are required, high performance concrete or the use of a larger fraction of steel might still allow for some relaxation of column, beam, floor or wall thickness. With the present thickness and design, walls and floors are generally close to the allowable stresses, especially for the design basis earthquake.

The tokamak complex has been analysed by the JA HT, and the study concludes that the combined tokamak and tritium building will behave satisfactorily during the design basis seismic event. The evaluation showed:

- the maximum response shear stress at the shear wall is within the allowable value;
- the maximum response axial stress at the wall is 4.0 kg/cm^2 (EL- 5.25m), and the building has enough strength to resist this;
- even when vertical seismic motion is considered, the contact pressure is 100% at the NS-direction and the EW-direction;
- the maximum contact pressure at the bottom of the foundation is 90.4 t/m^2 (NS-direction) and 80.5 t/m^2 (EW-direction), and is well within the short-term allowable bearing capacity, 130 t/m^2 (which comes from twice the maximum soil bearing capacity for the generic site).

If it proves necessary to protect the tokamak complex from large seismic forces, the building will be placed on seismic isolation bearings.

Structural – Containment Volume Overpressure Verifications

Current calculations, using self weight and component weight, combined with the load imposed by an internal overpressure of 0.1 MPa as loading conditions, predict that surface cracks will appear at certain sections of the concrete structure. The main cracking occurs at corners and in the middle of side walls (predominantly TCWS vault, vertical pipe shafts and slabs of NB cell). These cracks are caused by tensile stresses due to bending, and hence occur mainly at the external surfaces of the walls and slabs loaded by the internal pressure. Additionally, cracking is likely at the internal surfaces at or near corners where walls meet floors, ceilings or intermediate floors and where pillars interface with slabs. The crack depth

remains small relative to the slab thickness, and therefore the predicted surface cracking has no consequences for the structural integrity and acceptance of the building design. It may only matter for licensing the vault as a containment volume, which must therefore have a high degree of leak tightness.

For CANDU reactors, pre-stressed concrete vacuum buildings are designed and constructed to contain steam pressures arising from a postulated LOCA event. Their design is based on limiting surface cracking during the LOCA to such values that the internal liner can "bridge" the cracks and maintain a seal against leaks. The combination of a glass fibre and epoxy liner was developed for this purpose restricting the crack width to 0.2 mm. In the ITER case, the calculation predicts cracks up to 0.5 mm in width for concrete with rebar.

There are a number of possible measures under consideration to decrease or eliminate the possibility of concrete cracks or effects of cracks due to low-probability accidental events, as indicated below. A decision on their possible use can be expected as part of site licensing considerations, when more detailed analysis will be available on crack occurrence and characteristics.

Reinforced Corners

External or internal reinforcement or a combination of both may be applicable to reduce the stress concentration at corners. External reinforcement is easily achieved by increasing the corner radii, or increasing (locally) the slab and wall thickness. Reinforcement internal to the concrete is possible using special structures connected firmly by welding or other means to the rebar structures in slabs and side walls. Such measures are neither expected to cause feasibility problems nor add substantial cost.

Prestressed Concrete

This method uses special cables and ducts embedded in the concrete, with large tensioning bolts/nuts at one or both ends to apply additional compressive stresses to the concrete structure, thereby reducing or eliminating the tension stress and as a result eliminating the predicted concrete cracking.

Due to the complexity of the current structures, it may be difficult to incorporate this method of construction. However, by concentrating on certain connections between the TCWS Wall and the various floors, and allocating sufficient space for the tensioning cables and end-point mechanisms, the strength of the concrete structures in these areas is expected to be able to be increased sufficiently to eliminate the cracking.

Special Concrete Mixes with Rebar, Fibre and Cement

Certain matrix combinations of short fibres (e.g. graphite, aramid, vinylon, or steel), concrete and rebars are possible in tokamak building structures to provide strength to weight ratios greater than current concrete mixes. In addition, the fibres make the cracks small but numerous. An R& D program would be needed to further investigate suitable mixtures and resulting behaviour under postulated stress conditions.

Multiple Surface Layers of Epoxy Liner + Flexible Coatings

This approach would use the current concrete mixtures but apply a viscous, semi-plastic, deformable layer of appropriate organic substances, on top of concrete, then cover it with fiberglass-epoxy liner. Even if cracks were to occur in the surface, they would be covered over, or "healed" with the deformable layer. An R& D program would be required, to investigate feasibility, costs, and schedules.

Steel liner

Applying and attaching a flexible thin steel liner to the inside of the confinement volume concrete would prevent leakage into and through any postulated cracks in the concrete. Considerable design changes would be required, both for attaching the liner, as well as construction sequencing, and subsequent testing. This method would be expensive.

3.6.15.2 Tritium, Vacuum, Fuelling, and Services Building

The tritium plant building and its equipment is being designed by Home Team effort, using a conventional 2D approach, and has not yet been incorporated into the ITER standard building 3D models Likewise, the other equipment, such as the vacuum pumping systems, the fuelling systems, and HVAC, have not been modelled in 3D, which is planned for the next phase of work.

The building drawings have been prepared to show these minimal dimensions, which results in column spans and room heights in non-standard distances. A final site-specific design might well incorporate some standardisation in these areas, where possible.

3.6.15.3 Laydown, Assembly and RF Heating Building

The detailed analysis for this building is yet to been done, but initial indications are that the building supports appear to be suitable for these loads.

The tokamak assembly has imposed stringent requirements on maintenance of temperature within ± 2°C in the areas where the large components are to be assembled, and in the tokamak pit as well. A conceptual HVAC design meeting this requirement has been completed.

Once the tokamak assembly has been completed, the RF power supplies will be installed on the basemat, and a non-magnetic mezzanine will be installed to support the RF H&CD generators. A preliminary layout of the RF H&CD equipment has been prepared, with detailed design of the internal structure to be done in the next phase.

3.6.15.4 Hot Cell Building

The hot cell building has been reduced to the minimum possible size, dictated by the necessary RH operations that are required to be performed in the building, according to the maintenance requirements. Further, to minimise the amount of tritiated water generated because of air inleakage, the leak-tightness of the building must be verified by detailed design, with the same attention to penetrations as is required for the containment volume.

3.6.15.5 Personnel Access Control Building

The personnel access control building has been reduced to the minimum, with minimum-sized laundry facilities, relying instead on external laundry contractors. Such a plan may be problematic because of the potential for Be contamination, so further investigations are required.

3.7 Plant Control

3.7.1 Introduction

A highly integrated plant control scheme is necessary for the efficient operation of the ITER device. This section describes the Plant Control System (3.7.2), which is composed of a number of subsystems: Supervisory Control System (3.7.2.2), Subsystem Control System (3.7.2.3), Interlock System and Fusion Power Shutdown System (3.7.2.4). Also described is Plant Operation Sequence (3.7.3), where various states of plant operation are defined and discussed. Finally, in 3.7.4, magnetic, kinetic and disruption control are discussed.

3.7.2 Plant Control System

The ITER command control and data acquisition and communication (CODAC) system is structured in a hierarchy composed of the supervisory control system (SCS) and individual dedicated control subsystems to ensure the integrated control of the whole ITER plant. The CODAC system, through its supervisory system provides high level command to subsystems dedicated to the control and operation of each subsystem.

In the hierarchical structure of CODAC:

- subsystem controllers are supervised from the SCS;

- individual plant subsystems and diagnostic subsystems are directly controlled and monitored by their dedicated control systems;
- the limits in the autonomous behaviour of a subsystem are always determined by the SCS, allowing the possibility of going from complete autonomy during tests for example, to a total subordination when all parameters of the subsystem process are fixed from the supervisory control system.

To achieve integrated hierarchical control of the ITER plant, CODAC will provide general software functions for the benefit of the individual subsystems, a synchronization system, large bandwidth backbone communication networks with gateways and communication protocols which allow real time participation from remote ITER work sites. In addition, CODAC coordinates data acquisition & processing of data from the plant subsystems and manages the experimental database.

Software applications, common to many subsystems, will be provided by the SCS in order to make the control system as uniform as possible and to minimize the cost for design and maintenance. A formalism can be used to describe the logic of all operation sequences in a sequential function chart (SFC). For effective implementation, the same SFC methodology will be used for control and command design at all levels (supervisory or subordinate), for machine process operation and diagnostic data acquisition.

The individual subsystem SFC describes the logic of the subsystem control, operation, alarm and interlock functions. The subsystem also provides the instrumentation and control to implement the SFC logic. Data acquisition for plant subsystems will use conventional methods such as data scanning, data conversion, alarm limit checks and trend data processing.

With regard to the process of diagnostic data acquisition, the ITER tokamak operation will involve very long time scales, but events of interest will occur on short time scales. The length of the cycle for a given parameter would be controlled at a higher level so as to correlate with other timing signals. The memory would act as a buffer in line with the sensors.

3.7.2.1 Overall Plant Control System Function and Architecture

The ITER plant operation is controlled and monitored by the command control and data acquisition and communication (CODAC) system during normal operation modes. The CODAC system consists of a centrally positioned supervisory control system (SCS) and sub-control systems dedicated to each plant subsystem under the supervision of the SCS. A concept of ITER control system is schematically shown in Figure 3.7.2-1.

The SCS controls transition of the entire ITER plant operation state, and provides high level commands to plant subsystems, in order to achieve integrated control of the entire plant. The SCS also monitors the operation state of each plant subsystems to ensure it is operating within the proper operational envelope of the ITER plant operation state.

The interlock system, in parallel with the CODAC system, ensures plant-wide machine protection, as well as personnel protection, in case of off-normal events. In addition, the interlock system monitors operational events of the plant, and performs preventative and protective actions to maintain the system components in a safe operating condition. The

interlock system is also hierarchically structured and has individual interlock subsystems which are dedicated to each plant subsystem.

The fusion power shutdown system (FPSS) is the safety class plasma shutdown system used in case of an off-normal events. The FPSS is triggered by detection of off-normal events occurring in the tokamak cooling water system (TCWS).

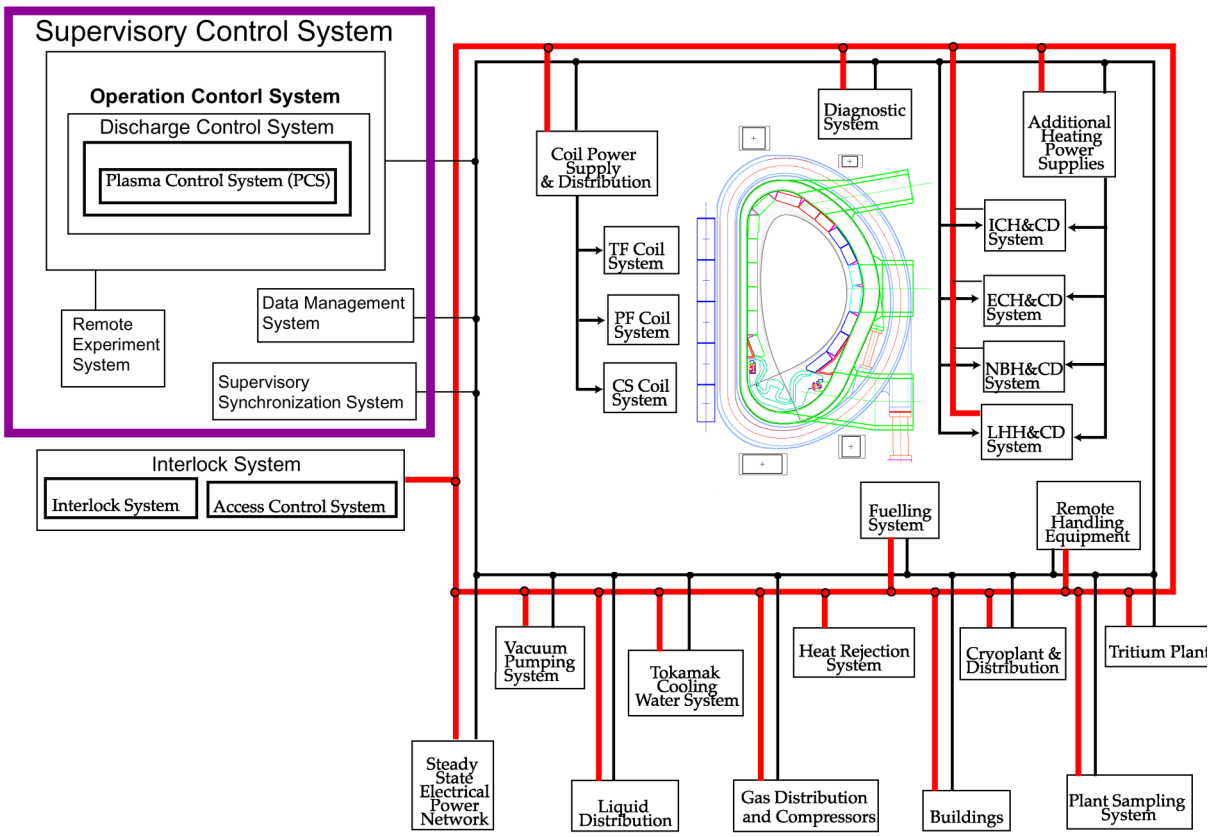

Figure 3.7.2-1 ITER Control System

3.7.2.2 Supervisory Control System

3.7.2.2.1 Functions

The SCS supervises the ITER plant operation, controls the plasma discharge, imposes selected plasma parameters, acquires plant and scientific diagnostic data, displays alarms, creates the ITER database, and communicates with both on-site and remote site control rooms. The functions of the SCS are summarized as follows:

- overall ITER plant operation, management and data monitoring;
- plasma discharge sequence management;
- plasma operation support;
- diagnostic data processing support;
- data management of experimental results;
- the synchronisation system for plasma discharge and data acquisition;
- communication functions and communication networks;
- remote-site experiment capability;
- plasma control system (PCS).

3.7.2.2.2 System Architecture

Operation control system

This provides the supervisory function of the ITER operation state management, and configuration control at the highest level of the control architecture. When the ITER plant is in a plasma operation state, operation of the plant and the discharge sequence are managed and controlled by the discharge control subsystem (DCS). When the ITER plant is ready to initiate plasma operation, the PCS will assume responsibility for controlling the ITER device components and systems which directly affect plasma operation. After completion of the plasma discharge operation and resetting of the system, the control is returned back to the DCS. The PCS has four major functions: plasma operation scenario sequencing, plasma magnetics control, plasma kinetics and divertor control, and fast plasma shutdown. It also displays monitoring signals for the plant operation. Relations between the phases controlled by DCS and PCS are shown in Figure 3.7.2-2. Throughout these operation sequences and phases, the operation control system always maintains the ultimate responsibility for operation, control and protection of the ITER facility and device.

Machine data acquisition system

This also globally monitors all plant subsystems and interlocks.

Diagnostic control and data acquisition system

This provides the supervisory function of the ITER diagnostic subsystem control and operation, configuration control and plasma parameter computation.

Data management system

This provides the supervisory function of the creation and management of the ITER experimental database as well as data storage and archiving. In addition, it also provides a computational capability for detailed data analysis.

Supervisory synchronisation system

This provides the supervisory function of the synchronisation system which consists of the master clocks, clock distributions, timing signal input/output portions and their logic control.

Supervisory network and communication system

This provides the supervisory backbone networks and message communication software, which handle all data and command communications among the entire ITER plant control system. This communication software will be used for all ITER subsystems as a standard software package.

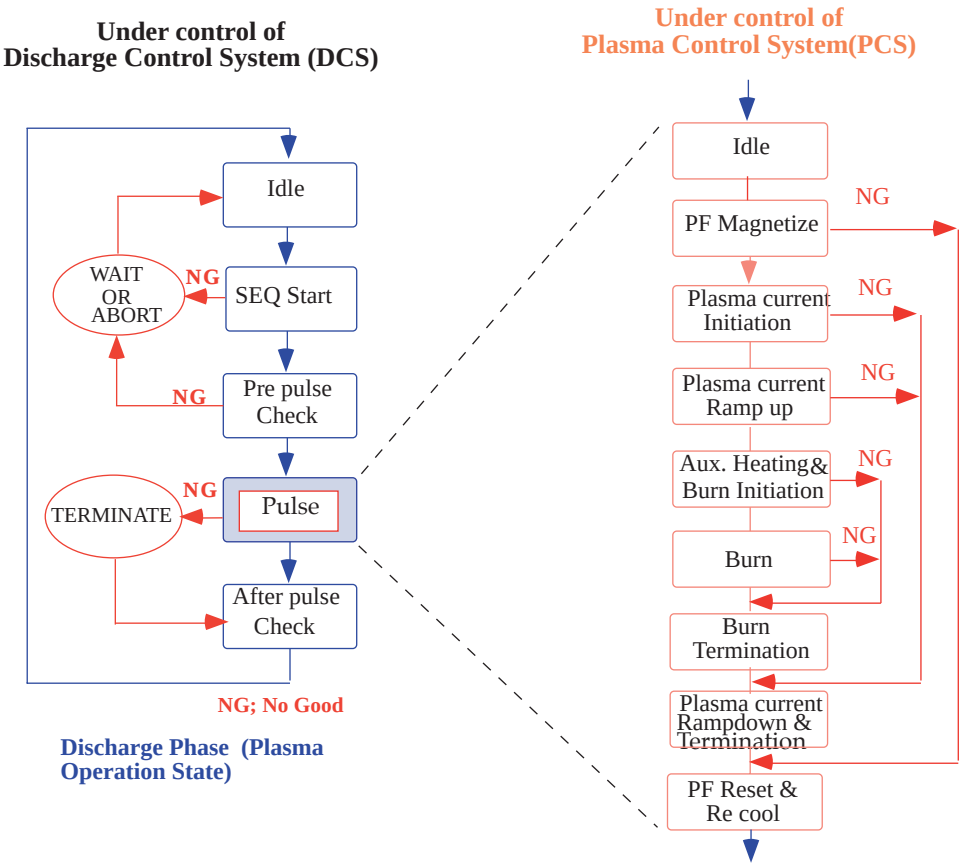

Figure 3.7.2-2 Plasma Discharge Control Phase

Remote experiment system

This provides the wide area network (WAN) node processor to communicate with each remote work site. The necessary information from the ITER plant and experimental database are extracted through each subsystem of SCS, which also communicates with individual subsystems if required through the ITER CODAC network and WAN node processor.

Plasma Control System (PCS)

The scope of plasma control and the corresponding requirements for the PCS comprises four major categories:

- Plasma operation scenario sequencing (see 3.7.3.2);
- Magnetics control (see 3.7.4.1);
- Kinetic control (see 3.7.4.2);
- Disruption Control (see 3.7.4.3).

3.7.2.3 Subsystem Controllers

The CODAC system is structured in a hierarchy composed of the SCS and individual dedicated control subsystems to ensure integrated control of the entire ITER plant. The Control subsystems need to satisfy the following requirements:

- subsystem controllers are supervised by the SCS;
- individual plant subsystems and diagnostic subsystems are directly controlled and monitored by their dedicated control subsystems;

- limits in the autonomous behaviour of a subsystem are always determined by the SCS, allowing for the possibility of going from complete autonomy during tests to a total subordination when all parameters of the subsystem process are fixed by the SCS.

The ITER plant control system is composed of the following subsystem controllers (with the exclusion of diagnostics):

1) TF, CS, PF coils, correction coils and structure instrumentation and control system (includes power supply control for coil system);
2) vacuum vessel (VV), blanket, divertor instrumentation system;
3) pellet fuelling instrumentation and control system;
4) gas fuelling instrumentation and control system;
5) wall conditioning instrumentation and control system;
6) tokamak cooling water and CVCS control system;
7) vacuum pumping control system (includes cryostat instrumentation);
8) tritium plant control system;
9) cryoplant control system (includes cryostat instrumentation);
10) RF power supply and control system (IC, EC and possibly LH);
11) NB power supply and NB control system;
12) steady state power supply control system;
13) radiation monitoring system;
14) liquid and gas distribution control system;

The individual control subsystems have similar functions to the SCS, but perform their dedicated duties for operation, control and data acquisition. These are:

- control of operations;
- alarm handling;
- monitoring and display;
- data acquisition and storage;
- synchronisation;
- data communication.

3.7.2.4 Interlock System and FPSS

The interlock system, through its supervisory system, ensures plant-wide machine protection as well as personnel protection with graded approach, and must act rapidly and directly in case of off-normal events or conditions. For that reason, the interlock system is fully independent of the CODAC system except for the data monitoring communication bus, which is shared with CODAC.

The FPSS secures the safe shutdown of the fusion power in case of an ex-vessel coolant leakage. Off-normal events will be displayed and recorded. A dedicated network will be used for off-normal event detection and dispatch of the command signal to the fuelling system for power shutdown. Because of its dedicated safety function, the FPSS is independent from other interlock systems.

3.7.2.5 Functional Interface between CODAC, Interlock System and FPSS

Reliable operation of the ITER plant will be achieved through an integrated plant control. The CODAC has the primary function of maintaining the plant operating condition in normal

states. The interlock system tries to avoid or minimise machine damage from operational events with or without availability of the CODAC. This is why the interlock system is separated from the CODAC and FPSS.

Even though the interlock system is in principle designed to be independent of the CODAC, some level of coordination between the interlock and CODAC systems will be essential. Some interlock actions can be executed by the CODAC as long as it is operational. Also, the interlock system is a back-up machine protection system in case of CODAC failure.

In general, the interlock protective actions are graded at three levels.

Level 1: (fast shutdown)

Whether the CODAC is functional or not, plasma discharge is terminated by the direct command of the interlock system. Possible scenarios are as follows:
- immediate shutdown by D_2 gas injection;
- immediate shutdown by the killer pellet injection;
- immediate shutdown of auxiliary systems like additional heating systems.

Level 2: (fast or accelerated shutdown)

Detected deviation of the process value from the normal operation range is not as gross as the case of Level 1. Compared with the Level 1 interlock actions, slower actions are expected. Interlock actions will be executed through the coordinated operation of the CODAC. The following scenarios are presently foreseen:
- a time delay (~ 150 s) will be set after the interlock trigger expecting a recovery by the normal control function of the CODAC during this delay period; after a certain delay time (~ 150 s), if the recovery is not yet achieved, a fast shutdown will be triggered;
- the interlock system requests the SCS to shift the discharge phase to fast or accelerated plasma shutdown phase (~ 150 s).

Level 3: (shot sequence inhibition)

Compared to the previous two levels of interlock events, this is a case of minor deviation of the interlock process values, which does not require immediate termination of the discharge.
- the discharge sequence will be stopped if it is prior to the plasma initiation;
- if the plasma is already initiated, the plasma discharge will be completed but the following discharge sequence will be suspended;
- in case of discharge cleaning such as EC discharge cleaning, this interlock event stops the sequence immediately.

Set point on certain process value for interlock event trigger will be shown in Figure 3.7.2-3 for illustrative purposes.

When a process value deviates beyond its interlock Level 1 set point value and reaches the safety system trigger level, the safety system is then activated for reliable and robust shutdown of the system. FPSS is one of the safety systems which shuts down the fusion power production in case of an off-normal event such as ex-vessel coolant leakage. In this

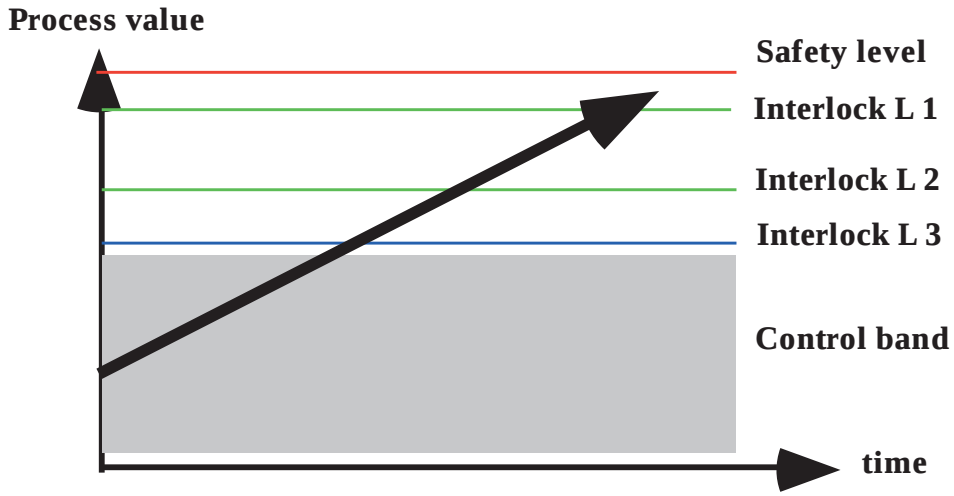

Figure 3.7.2-3 Interlock Level Set Point

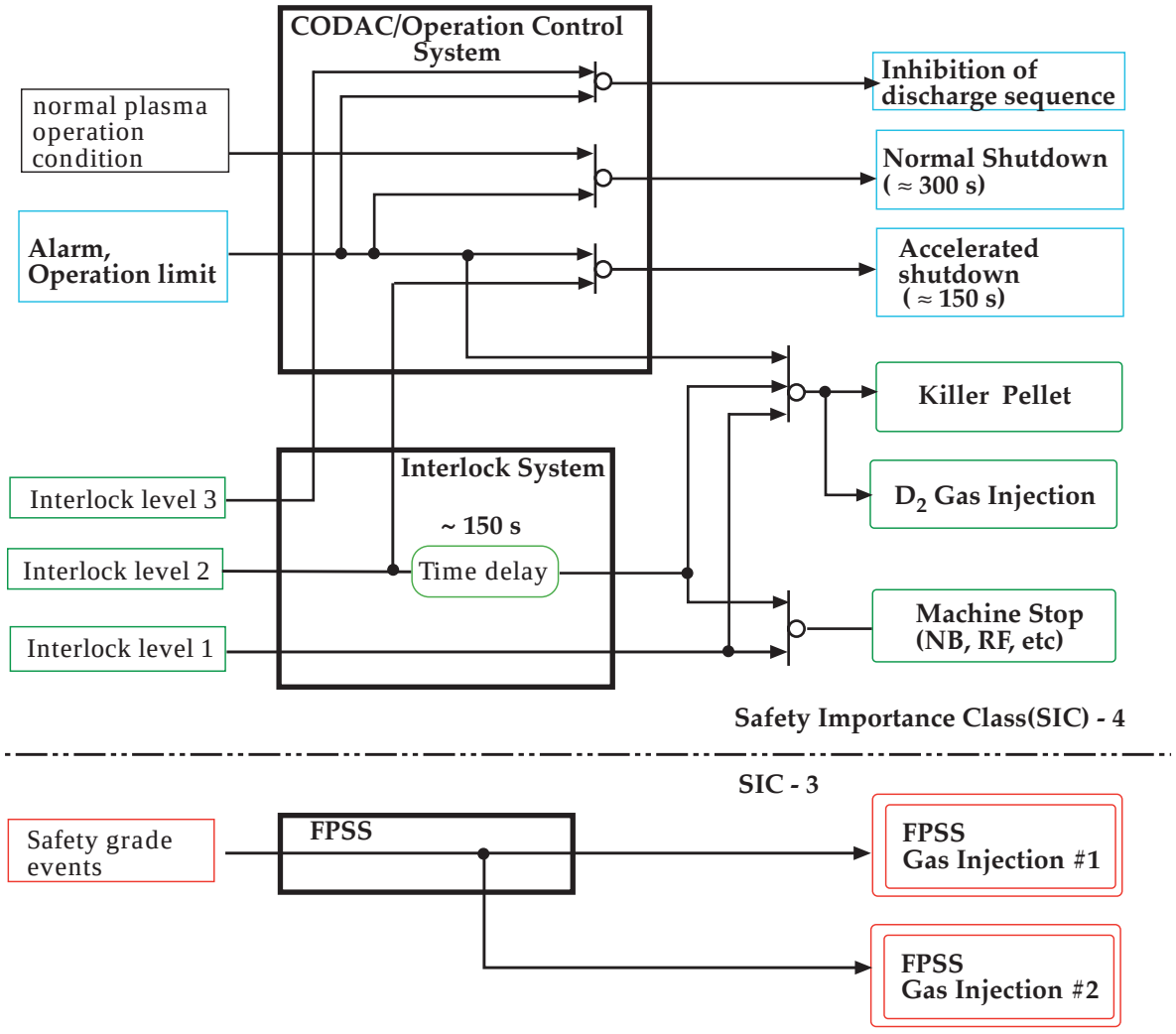

Figure 3.7.2-4 Functional Relations between CODAC, Interlock, and FPSS

case the FPSS monitors the primary heat transfer system coolant parameters for the safety event trigger.

Functional relations between CODAC, interlock and FPSS are summarised in Figure 3.7.2-4.

3.7.3 Plant Operation

This section schematically describes the operational sequences of the ITER plant by using a sequence function chart (SFC). A SFC describes the control process for the plant using an implementation-independent graphical representation.

The process described by the SFC can be divided into a number of well-defined, successive "steps", separated by "transitions". The purpose of each step, when it becomes "active", is to launch new actions. The subsequent transition of the system describes a condition or conditions that must occur before the next step can become active. The "state" of part of the plant may indicate the last step it passed (e.g. "operating"), or in which transition it is engaged (e.g. "waiting for temperature to reach 200˚C").

Macroscopically, the operation of the ITER plant is characterised by major plant states, in which most of the plants are waiting for some command before relatively rapidly changing to another state, and some plant items are undergoing maintenance or testing, or are in operation.

Construction and Long-Term Maintenance State (LTM)

This state is applied to periods of major machine modification. Long term maintenance is defined as that taking >30 days. In this state, most of the tokamak subsystems which require maintenance may be shut down. Decay heat is passively removed. For example, the cryoplant may be shut down, the VV and cryostat may not be actively pumped, and large in-vessel and ex-vessel component replacement and maintenance may be conducted. Coil excitation and any power injection by an additional heating system to the tokamak is prohibited.

Short-Term Maintenance State (STM)

This state allows maintenance activities which typically last for 1 to 30 days. Relatively long time periods of plasma operation stoppage such as night times and weekends may require that the plant be placed in this state with reduced or without toroidal field coil current. Decay heat removal may be taking place, if appropriate. In this state, component maintenance and replacement needs to be carried out under high vacuum conditions in the VV and, if in the cryostat, also under cryogenic temperature conditions. The vacuum and cryogenic temperature conditions must also reach or regain their operational levels during this state. PF coil excitation is prohibited in this state.

Test and Conditioning State (TCS)

Wall conditioning operations such as baking, glow discharge cleaning and EC discharge cleaning, with or without baking, are major actions. TF and PF coil excitation tests may be carried out. Additional heating system tests such as NBI ion source conditioning, RF dummy load tests, and fuelling system tests are allowed without any tokamak plasma. During the

TCS no in-vessel or major ex-vessel maintenance may be initiated. However, minor ex-vessel component maintenance and trouble-shooting is allowed outside the pit area.

Short-Term Standby State (STS)

Final preparation of each subsystem is completed and all systems are ready for plasma operation. Limited troubleshooting is allowed within 8 hours of the last pulse. Maintenance and conditioning operations are not allowed.

Plasma Operation State (POS)

All of the plant subsystems are supervised or directly receive commands from the SCS during plasma operation. No maintenance activities are allowed in this operation state.

3.7.3.1 Overall Plant Operational Sequences

The relationship between states can be presented by the sequential function chart, shown in Figure 3.7.3-1. The basic direction of evolution in the chart is from top to bottom unless indicated by arrows. Operation sequences covering the transfers between states are macroscopically represented by boxes labelled SEQn (n=1–10).

3.7.3.2 Plasma Operation Sequences

When ITER is permitted to operate and produce plasma pulses, operation of the plant is managed and controlled by the discharge control subsystem (DCS). When the ITER plant is ready to initiate the plasma pulse, the plasma control system (PCS) will assume responsibility for controlling ITER device components and systems which directly affect plasma operation. DCS and PCS mainly play the role of supervisory control and each subsystem under DCS and PCS has its own dedicated local control system.

After completion of the plasma pulse and resetting of the system, control is passed back to the DCS. This operational sequence of the control system is shown in Figures 3.7.3-2 and 3.7.3-3.

First, the discharge parameters are selected and transferred to the DCS. After checks for consistency of these discharge parameters, the discharge sequence will be started. First, pre-pulse checks will be carried out for the availability and operational readiness of all the necessary plant systems. After these tests are completed and satisfied, the PCS will take over the control of tokamak-related operation.

Figure 3.7.3-4 illustrates the key features of plasma operation scenarios. The parameters of the scenario – current, fusion power, auxiliary heating and/or current drive input and burn duration – can vary, but the sequencing requirements and general waveforms remain invariant.

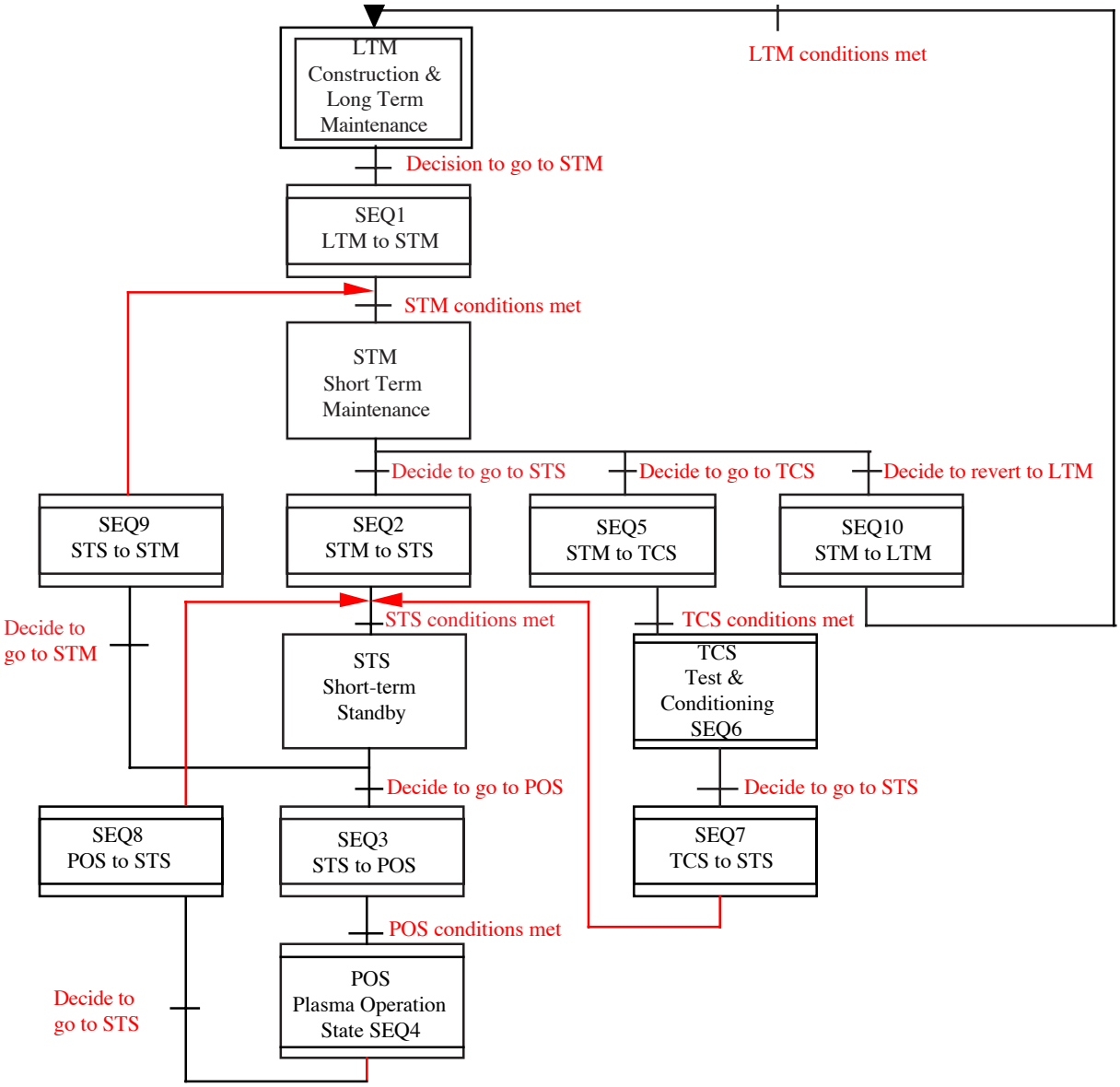

Figure 3.7.3-1 ITER Plant State Transitions

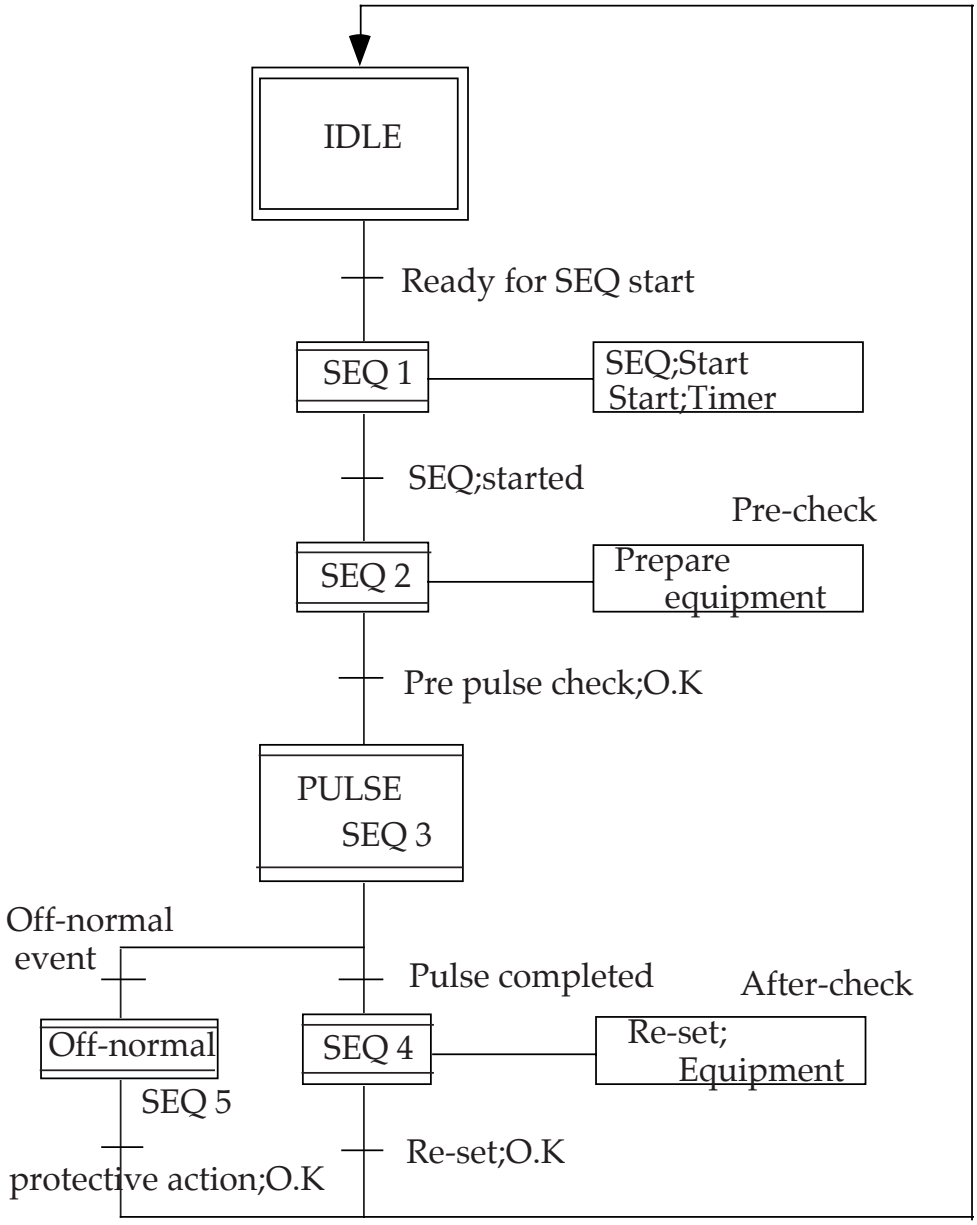

Figure 3.7.3-2 Overall Plasma Pulse Sequence

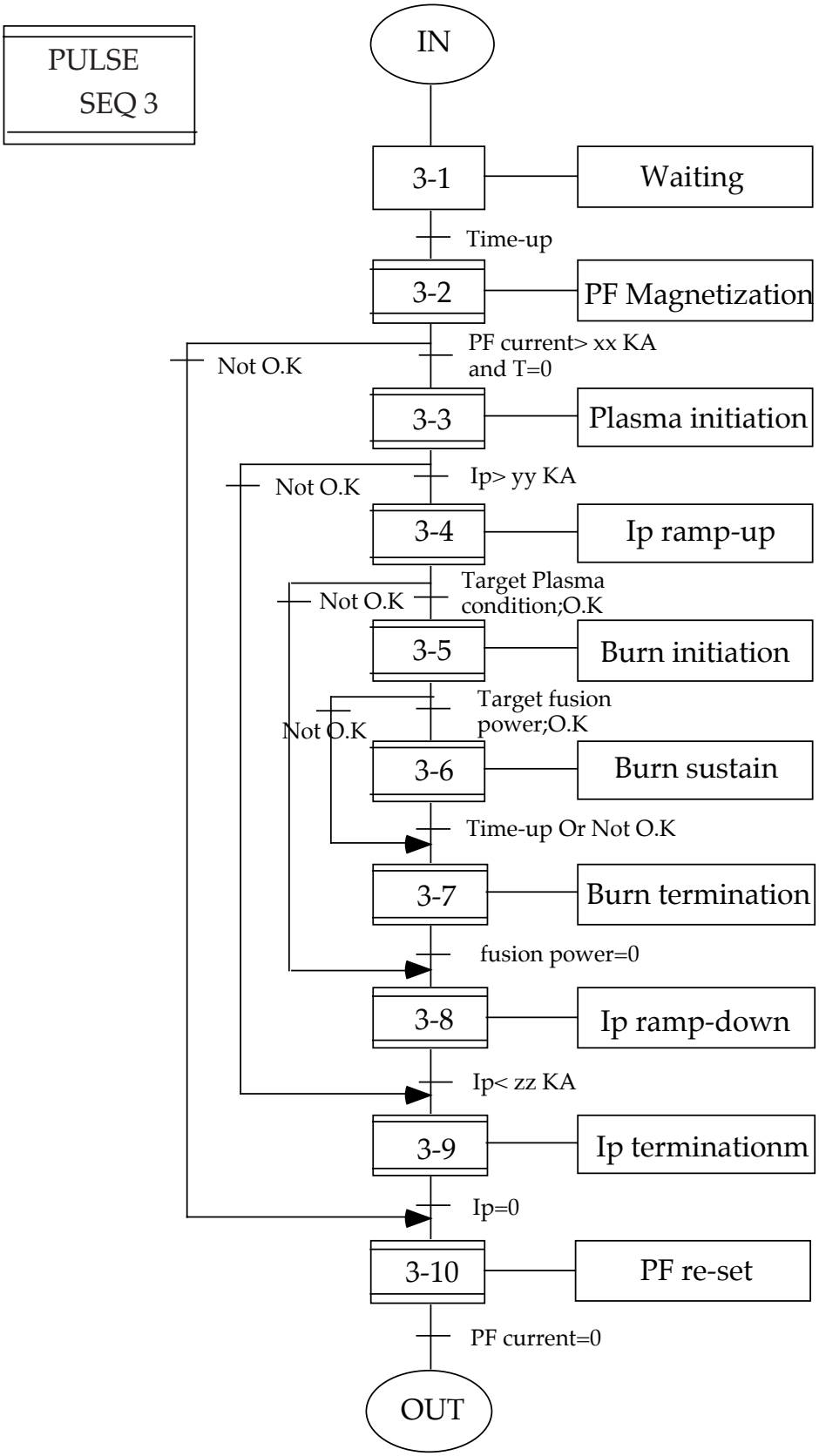

Figure 3.7.3-3 Detailed Sequence of "Pulse" State (SEQ.3)

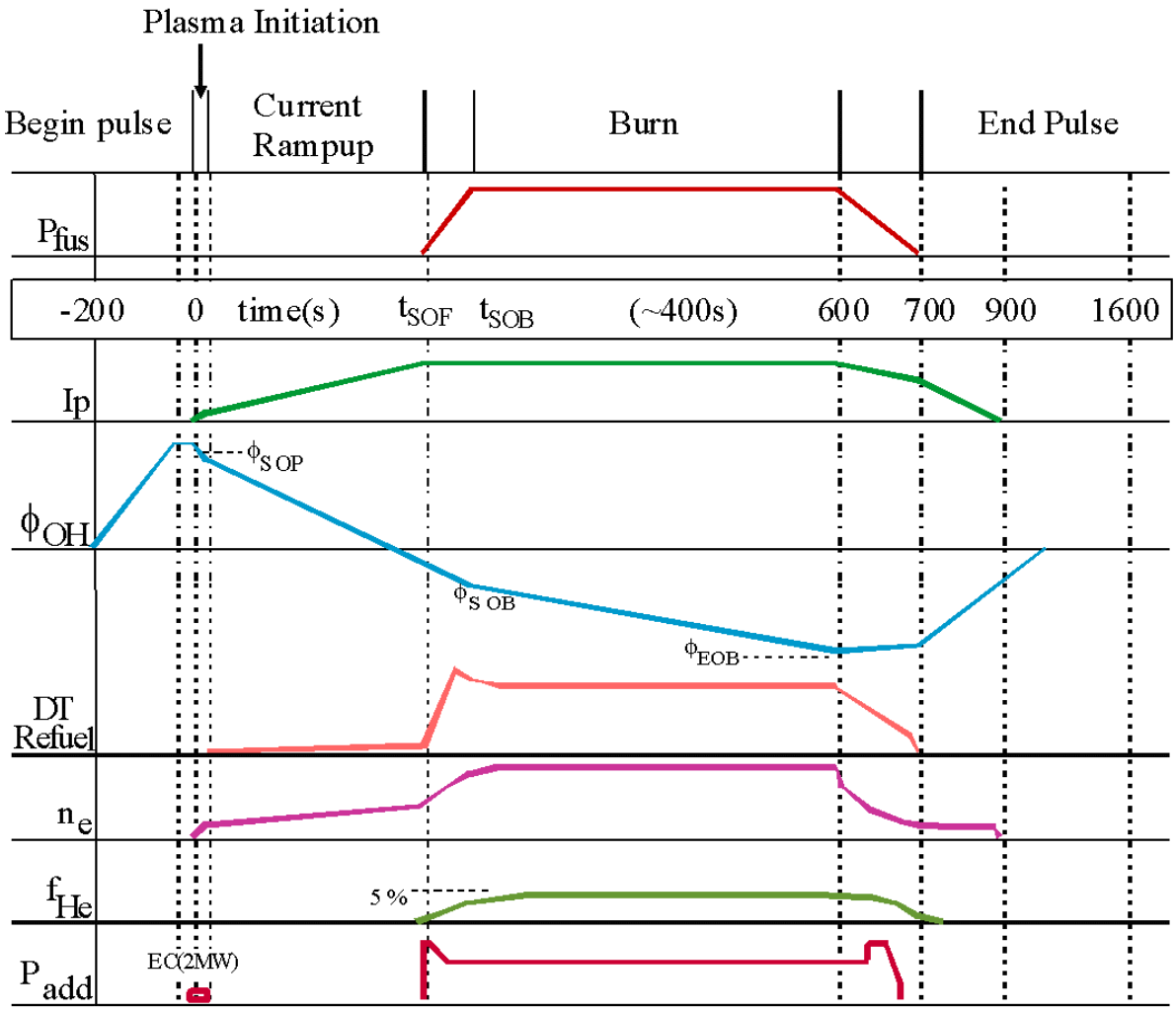

Figure 3.7.3-4 Waveforms for Standard Driven-burn Operation Scenario

3.7.3.2.1 Plasma Discharge Sequence

Plasma Initiation

A pulse proceeds from pulse initiation with attainment at t = 0 of PF coil system pre-magnetisation with a plasma-axis flux linkage of ϕ_{SOP}(start of pulse), as shown in Figure 3.7.3-4. This is followed by a 2 s plasma initiation phase that begins with the application of pre-determined voltages to the PF coils. These voltages and the initial PF currents are chosen to produce a dynamic multipole field null with a low poloidal field (< 2 mT within an 0.8 m radius) that is positioned near the port-mounted start-up limiters at t ≈ 1 s. The in-vessel loop voltage is ~ 12 V (E ≈ 0.3 Vm^{-1}) at this time. With a gas fill pressure of about 1.3 mPa, Townsend avalanche breakdown occurs within 50 ms.

During start-up, 2 MW of EC power at 120 GHz will be provided for 2 s to facilitate initial breakdown over a range of pre-fill pressures and error-field conditions, and will also provide supplemental heating after breakdown to ensure rapid ionisation (burn-through) of impurities in the initial low-current startup plasma.

Current Ramp-up

The current ramp-up with average dI/dt ≈ 0.15 MAs^{-1} is coordinated with a minor radius expansion and elongation increase to maintain a nearly constant edge safety factor $5 \leq q \leq 6$. The plasma remains limited until I_{SOD} (start of divertor) (≈ 0.5 I_{P0}) is reached, when a single null (SN) divertor configuration is formed ($q_{95} \approx 4$). Continuation of the current ramp-up results in an I_{P0} current flat-top ($q_{95} \approx 3$) at t ≈ 100 s.

Shape and Configuration Control

Dynamic control of the plasma shape and position is required throughout the scenario. The clearance gap between the first wall and the separatrix are controlled, in particular near the outboard equatorial plane to permit and efficient coupling to the plasma from IC and LH launchers.

Heating to Driven Burn

Following SOF (start-of-flat top), auxiliary heating is applied. This, coordinated with plasma fuelling, results in the attainment of H-mode confinement and sustained fusion burn with ~ 500 MW of fusion power within ~ 50 s. Attainment of the rated fusion power is denoted as the start-of-burn (SOB). The most demanding requirement in this phase is the transition from L to H mode confinement, which requires that a certain threshold heating power, linked with plasma density, be provided. It is assumed that the required plasma shape and current are achieved at SOF and that plasma heating and β increases are carried out at constant shape and current. Scenarios, which modify plasma shape and current during the plasma heating before SOB, can also be considered.

In extended-pulse-duration/steady state operation, the scenario is more complicated. Following SOF, auxiliary power heats the plasma and generates a toroidal current which, together with the bootstrap current, replace the Ohmic current. Generally, the current profile before the addition of auxiliary power is somewhat different from the final profile. The current diffusion time across the whole plasma volume is large, e.g. ~ 200 s for $T_e \approx 5$ keV and ~ 800 s for $T_e \approx 10$ keV. So during the sustained burn, the current profile will evolve to the final state over several 100 s.

Sustained Burn

Once SOB is attained, accumulation of thermal helium results in the need to further increase the plasma density to maintain a fixed fusion power: the approach to sustained burn with stationary helium level requires a few tens of seconds. The burn proceeds until the end-of-burn (EOB) inductive flux limit of the PF coil system is reached. For nominal conditions, the duration from SOB to EOB is about 400 s for the driven-burn.

Burn Termination

The burn is terminated by reducing the fuelling to ramp-down the fusion power, followed by current, auxiliary heating and density ramp-down and plasma termination, with measures to avoid plasma disruptions.

3.7.3.3 Off-normal Plant Operation Sequences

ITER plant off-normal conditions are classified following three different levels of protection from relation to the ITER plasma discharge:

Level 1: fast plasma termination
Level 2: controlled plasma termination
Level 3: pulse inhibition

All of the off-normal events are classified into above three levels of protection and initiate corresponding actions when off-normal events are enabled at any operation state. Individual subsystem component protective actions such as coil fast discharge, slow discharge, additional heating power off, isolation from leakage are also included within above protections. Figure 3.7.3-5 represents the scheme of actions for off-normal event.

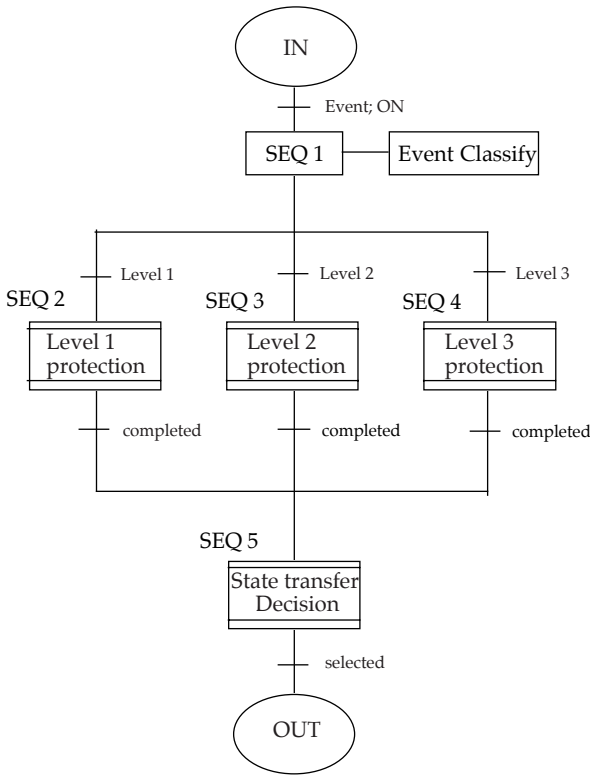

Figure 3.7.3-5 Overall Off-Normal Sequence

3.7.4 Magnetic and Plasma Control

Plasma control is an essential element to achieve the goals of the ITER experimental programme. Its objectives include machine protection and plasma operation. Successful plasma operation requires a control system monitoring the plasma status by diagnostic sensor signals and able to counteract the deviations from the reference values by controlling the relevant actuators. A list of sensors and actuators needed for plasma control is shown in Table 3.7.4-1.

Table 3.7.4-1 Sensors and Actuators for Plasma Control

Category	Sensor or Indication	Actuator or Action
Key machine protection	Gaps between the separatrix and first wall/divertor, first wall temperature	PF coils
	Fusion power	P_{add}, fuelling/pumping
	Div. Plate temperature	Impurity gas-puff in divertor
Additional machine protection (disruption)	Disruption precursors (particularly detection of locked modes)	I_p, P_{add}, fuelling/pumping, killer pellet
	Halo currents	
	Runaway electrons	PF coils ($q<2$)
ELM heat load	Type of ELM, divertor plate. temp.	I_p, shaping, fuelling/pumping, selection of PFC
Shine-through	Shine-through power, n_e	NB
Plasma-wall contact	Impurity emission lines	PF coils
Conventional control	B_p, flux loop	PF coils
	I_p	PF coils
	n_e	fuelling/pumping
Burning plasma control	Fusion power	P_{add}, fuelling/pumping
	Divertor heat load	Impurity seeding, fuelling/pumping
	Helium ash, impurity	Fuelling/pumping
Beta	Stored energy	P_{add}, fuelling/pumping
Threshold power	Fusion power, P_{rad}, n_e	P_{add}, fuelling/pumping
Advanced control	q profile	CD, P_{add}, fuelling/pumping
	Pressure profile	
	Rotation profile	
Neoclassical tearing mode control	NTM mode amplitude and location	ECCD, saddle coils
Resistive wall mode control	RWM mode amplitude, phase	Saddle coils

The first set of control loops, shown with bold letters are categorised as machine protective control. Machine protective control involves prediction, avoidance and mitigation of disruptions and avoidance of abnormal heat loads to protect the components inside the vacuum vessel. The control in this category has the highest priority and the control commands generated thereby override the other control commands.

Some control loops aim at protecting key machine components, these include the monitoring of the gaps between the separatrix and first wall/divertor, wall/divertor temperature and fusion power, the detection of contact of the plasma to the wall, of excessive heat to the divertor, and of unwanted excursions of fusion power. Wall contact of the plasma can be detected by impurity line emission or by magnetic signals. Such an event would invoke correction of plasma position and shape, increase of radiation power, and reduction of auxiliary heating and fuelling.

Other control loops are for additional machine protection against disruption. Protection of components inside the vacuum vessel requires failure-free detection of disruption precursors, avoidance, and mitigation of disruptions. The precursors of disruptions can be detected by monitoring the fluctuation of the magnetic signals and ECE and soft X-ray emission. Of particular importance is the recognition of locked modes. Recently, disruption detection systems have been developed using neural networks. Once a disruption is recognised in advance, it may be avoided by reducing the plasma current, β, or density. A decision has not yet been made on whether to include a killer pellet injection system to distribute the plasma energy over a large area to mitigate the consequences of disruption, on the understanding that adequate plasma termination can be achieved using an edge impurity gas puff. The runaway electrons can be eliminated by shifting the plasma and reducing the edge safety factor to 2.

Finally, some additional control loops are for ELM heat load control. This system recognises the type of ELM and measures the divertor heat load associated with it. If the heat load due to ELMs is excessive, the operation has to be shifted to a regime with more benign ELMs. Possible methods include increasing the fuelling rate, increasing the safety factor, and changing the plasma geometry.

The set of controlled plasma parameters will include those currently considered in the present generation of tokamak plasmas, in particular the plasma shape and position, the plasma current, and the electron density. Operation with a burning DT plasma results in additional plasma control requirements, in particular a simultaneous control of the fusion power, divertor heat load and helium-ash is needed. The ITER divertor is designed for a high steady state peak power load but, at full power, a substantial fraction (~ 75%) of the total power must be radiated to keep the power deposited on the divertor plates to acceptable levels. This operation may require injection of a controlled amount of a specific impurity or a combination of impurities (e.g. Ne, Ar) to the divertor and scrape-off layer (SOL) plasma but, at the same time, the bremsstrahlung power loss and plasma dilution in the core must be maintained at acceptable levels for the plasma burn. The kinetic control must also keep the plasma away from the β and density limits and provide sufficient power flow through the separatrix to ensure H-mode plasma operation. It is clear that a sophisticated multi-input, multi-actuator feedback control scheme is required for the successful operation of ITER even in the basic driven burn regime. Therefore a wide range of additional plasma measurements is required for control, including radiative power loss from the plasma core, SOL, X-point region and from the divertor, plasma density profile, β, n_T/n_D ratio, rotating MHD modes, and the degree of divertor detachment, i.e. "ionisation front" position and/or T_e and n_e at the divertor plate.

Further, sustained operation in high confinement modes, for example reverse shear, is a fundamental part of the ITER experimental programme. This operation is likely to require control, and hence measurement of the spatial profile, of key parameters such as q, pressure and rotation. For sustained operation near the β-limit, it is expected that detection and suppression of neoclassical tearing modes (NTMs) will be required, and for resistive wall modes (RWMs) in steady state operation at high β levels. Measurement of the location and amplitude of these modes, and active stabilisation by ECCD and saddle coils, will therefore be required.

3.7.4.1 Plasma Control by the Poloidal Field System

3.7.4.1.1 Requirements of the Poloidal Field System

The ITER poloidal field (PF) system has been designed to support all the design scenarios (the first four scenarios from Table 3.7.4-2). Its overall operational flexibility was also assessed by studying the feasibility of a high current scenario. This is named scenario 5 in the table below and reaches 17 MA of plasma current (fusion power 700 MW, Q = 20).

For each scenario seven key states were identified: the start of the magnetised central solenoid (CS) discharge (SOD), the X-point formation (XPF), the start of plasma additional heating (SOH), the start of plasma current flat-top (SOF), the start of driven burn (SOB), the end of burn (EOB) and the end of plasma cooling (EOC). Table 3.7.4-2 shows the values of plasma current at these key states. Up to XPF the plasma touches the central part of the

limiter. The PF system drives the plasma cross-section expansion during the current rise, keeping the edge safety factor roughly constant at a value of about 4.8. At XPF, transition from a limited to a fully developed diverted configuration takes place. Further ramp-up of the plasma current continues in the diverted configuration.

Table 3.7.4-2 Plasma Current (MA) at the Key States of the Scenarios

State	SOD	XPF	SOH	SOF/SOB	EOB	EOC
Scenario 1	0	7.5	13	15	15	12.3
Scenario 2	0	7.5	15	15	15	12.3
Scenario 3	0	7.5	9.5	13.5	13.5	11
Scenario 4	0	5.4	7	9	9	8
Scenario 5	0	7.5	15	17	17	13.2

As an example, Figure 3.7.4-1a shows the evolution of the plasma aperture during the current ramp-up in scenarios 1 and 2. In scenario 2, additional heating is initiated at the start of the current flat-top. In all other scenarios, the SOH is before SOF. At EOB, a controlled termination of the fusion burn is initiated. The plasma must be cooled prior to the current ramp-down, in order to avoid the large negative currents at the plasma edge arising when a negative surface voltage is applied. Finally, at EOC, the transition from a diverted to a limited configuration takes place.

The plasma in scenarios 1, 2, 3 and 5 is characterised, during the current flat-top, by the following parameters: R = 6.2 m, a = 2 m, $\kappa_{95} \approx 1.70$, $\delta_{95} \approx 0.33$. The plasma of scenario 4 (at burn) is shifted outwards: R = 6.35 m, a = 1.85 m. This plasma has higher elongation, $\kappa_{95} \approx 1.85$, and higher triangularity, $\delta_{95} \approx 0.42$, than the standard plasma of scenarios 1, 2, 3 and 5. Table 3.7.4-3 presents the values of the plasma main parameters during the driven burn. Figure 3.7.4-1b shows the overlay of the separatrices of the inductive scenarios and of scenario 4 during the burn.

Table 3.7.4-3 Plasma Parameters, Magnetic Flux Available for Burn, and Expected Duration of Burn

Scenario	**1**	**2**	**3**	**4**	**5**
I_p, MA	**15**	**15**	**13.5**	**9**	**17**
R/a, m	6.2/2.0	6.2/2.0	6.2/2.0	6.35/1.85	6.2/2.0
$\kappa_{sep}/\delta_{sep}$	1.85/0.48	1.85/0.48	1.85/0.48	1.97/0.58	1.85/0.48
κ_{95}/δ_{95}	1.70/0.33	1.70/0.33	1.70/0.33	1.85/0.42	1.70/0.33
R_{axis}/Z_{axis}, m [1)]	6.42/0.54	6.41/0.54	6.45/0.54	6.69/0.51	6.42/0.54
R_X/Z_X, m [2)]	5.09/-3.36	5.09/-3.36	5.09/-3.36	5.09/-3.35	5.09/-3.36
q_{95}	3.0	3.0	3.3	5.0	2.7
q_{axis}/q_{min}	1/1	1/1	1/1	2.8/2.4	1/1
reference l_i	0.85	0.85	0.90	0.61	0.77
min l_i/max l_i	0.7/1.0	0.7/1.0	0.7/1.0	-	0.7/0.9
β_p/β_N	0.70/1.88	0.65/1.75	0.80/1.94	1.9/3.0	0.7/2.1
$\Delta\Psi_{burn}$, Wb	37	30	53	≈10	20
Δt_{burn}, s	500	400	1000	∞	200

[1)] "axis" = magnetic axis [2)] "X" = X- point

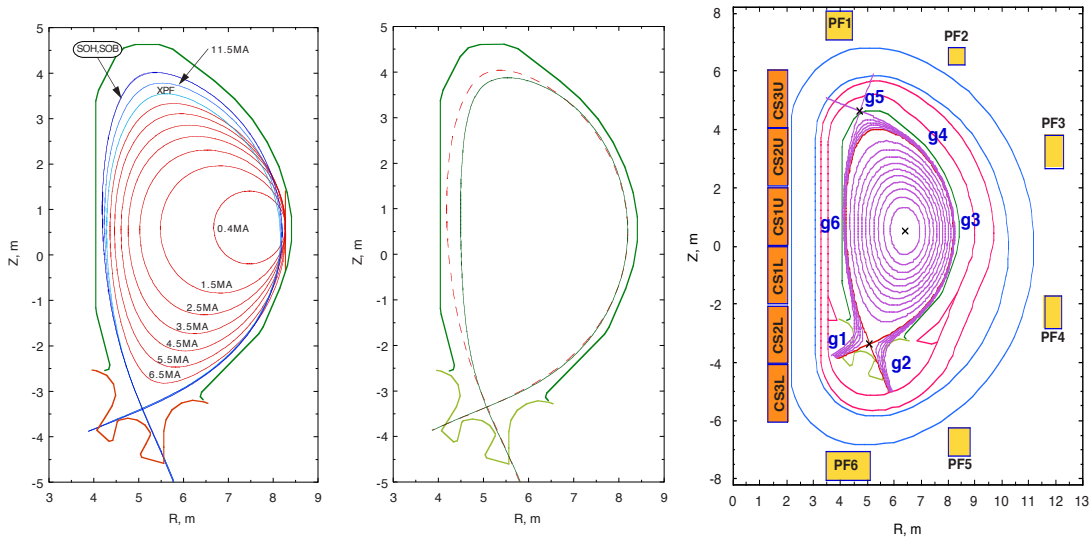

a **b** **c**

Figure 3.7.4-1a - Plasma Boundary during the Current Ramp-Up, Heating and Burn Phases of Scenarios 1 and 2; b - Separatrices during the Burn in the Scenarios 1, 2, 3, 5 (dashed line) and in the Steady State Scenario 4 (solid line); c - ITER Magnetic Configuration at Burn in Inductive Scenarios, Vacuum Vessel, CS, PF, TF Coils and the Locations of the 6 Controlled Gaps

The PF system has been designed to provide a sufficient degree of shaping flexibility. The CS consists of six modules. All PF coils and all CS modules, except for the two central modules, have independent power supplies, used for plasma current, position and shape control. The two central modules of the CS are, instead, connected in series to a common power supply unit.

3.7.4.1.2 Analysis of Poloidal Field Scenarios

All the scenarios mentioned above were at first studied using plasma equilibrium codes (EQUCIR[1] or TOSCA[2]) with partly prescribed plasma position and shape. The codes use prescribed values of l_i and β_p. The deviation of the separatrix from the target separatrix, shown by the dashed line in Figure 3.7.4-1b, was minimised. The assumptions on the resistive losses of the poloidal magnetic flux are given in Table 3.7.4-4.

Table 3.7.4-4 Assumptions on the Resistive Consumption of the Poloidal Magnetic Flux

Resistive flux loss at breakdown	10 Wb
Resistive flux loss during the plasma current ramp-up until SOH	$0.45\mu_0\Delta(R_pI_p)$*
Resistive flux loss from SOH to SOB for inductive scenarios	10 Wb
Resistive flux loss from SOH to SOB for hybrid and non-inductive scenarios	17 Wb
Resistive flux loss during the plasma cooling (till EOC)	10 Wb

* $\Delta(R_pI_p)$ represents variation of the parameter (R_pI_p)

Two types of studies have been performed with the above codes.

[1] H.Ninomiya, K.Shinya, A.Kameari, "Optimization of Currents in Field-Shaping Coils of a Non-Circular Tokamak", Proceedings of the 8th Symposium on Engineering Problems of Fusion Research, (1979), p.75

[2] H. Ninomiya, A. Kameari and K. Shinya; report: JAERI-M 9127 (1980). K. Shinya and H. Ninomiya; report: JAERI-M 9278 (1981). K. Shinya and S. Nishio; report: JAERI-M 87-133

- A complete study of the operational range of l_i in order to obtain the magnetic flux available for burn, the maximum values of the (scenario) currents in the CS and PF coils, and the CATIA plasma models. Three different values of l_i (minimum, reference and maximum), shown in Table 3.7.4-3, were considered for scenarios 1, 2, 3 and 5 at SOH, SOF, SOB and EOB. For scenario 4 only, plasma with reference values of l_i was analysed. The magnetic flux available for burn in these scenarios (reference l_i) is given in Table 3.7.4-3. The table also shows the expected duration of the burn, assuming the appropriate plasma loop voltages in each case. The maximum value of the total flux swing of the PF system is about 280 Wb (17 MA scenario 5). The maximum values of the coil currents and of the magnetic fields at SOD and in the l_i survey at SOH, SOF, SOB, EOB states, are within the coil capabilities with some margins left for plasma control actions.
- A design of all PF scenarios in terms of plasma equilibrium snapshots. The goal was to provide the time evolution of all plasma parameters (e.g. major and minor radii, elongation, triangularity) and of the coil currents, voltages and power for the design of other systems (i.e. the power supplies).

PF scenario 2 was verified and simulated with a free-boundary time evolution plasma equilibrium code MAXFEA. This code takes into account eddy currents in the vacuum vessel and the models of power supplies. Moreover, the code simulates the feedforward and feedback control of the plasma current, position and shape, according to the control scheme described in 3.7.4.1.3. However, the evolution of l_i, β_p and the resistive flux loss needs to be prescribed as inputs in this analysis. The waveforms of the plasma parameters and of the coil currents obtained with EQUCIR were used as reference in MAXFEA simulations.

The PF system operation and the plasma evolution in scenario 2 and in scenario 4 were self-consistently simulated with the DINA[1] code, using feedback and feedforward control of the plasma current, position and shape. In addition to the MAXFEA capabilities, DINA calculates the evolution of the plasma temperature and current profiles (i.e. l_i, β_p and the resistive flux loss). The evolutions of the plasma density, Z_{eff}, and the power of the additional heating and non-inductive current drive are prescribed as inputs in this analysis. Control of the plasma current, position and shape was performed with the "JCT/February 2001" controller described in 3.7.4.1.3. DINA simulations based on the studies of these scenarios performed with the transport code ASTRA (see 4) and with the plasma equilibrium codes (EQUCIR or TOSCA).

The inductive scenario 2 was simulated in two variants: the nominal scenario and a scenario with accelerated transient phases (before and after driven burn). To check the capability of the PF system to operate in the presence of large-scale recoverable disturbances, simulations of scenario 2 with nominal transient phases were also repeated with minor disruptions (see 3.7.4.1.3). As an example, Figure 3.7.4-2 shows results of the simulation of scenario 2 with the nominal ramp-up of the plasma current (100 s) and two minor disruptions incurred at 60 s (current ramp-up) and 140 s (driven burn).

The waveforms of plasma current, minor radius, κ_{sep}, β_p, l_i, and total power required for the PF system are shown in Figure 3.7.4-2a. The positive peak of the total power is less than

[1] Khayrutdinov, R., Lukash, V., "Studies of plasma equilibrium and transport in a tokamak fusion device with the inverse-variable technique", J. Comput. Phys. 109 (1993) 193

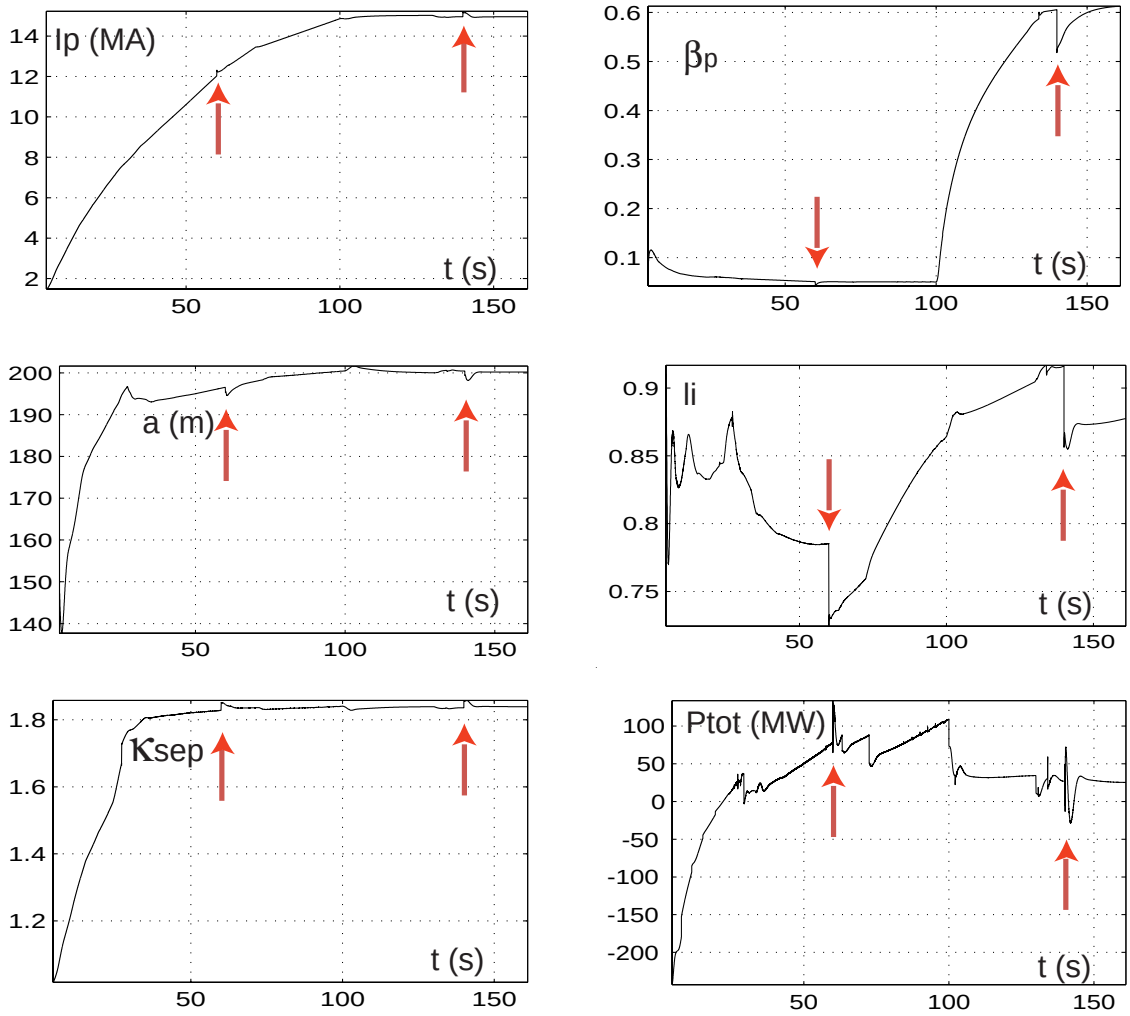

Figure 3.7.4-2a DINA Simulation of Scenario 2 with Minor Disruptions (see below) at 60 s and 140 s (arrows)

Waveforms of plasma parameters and total coil power

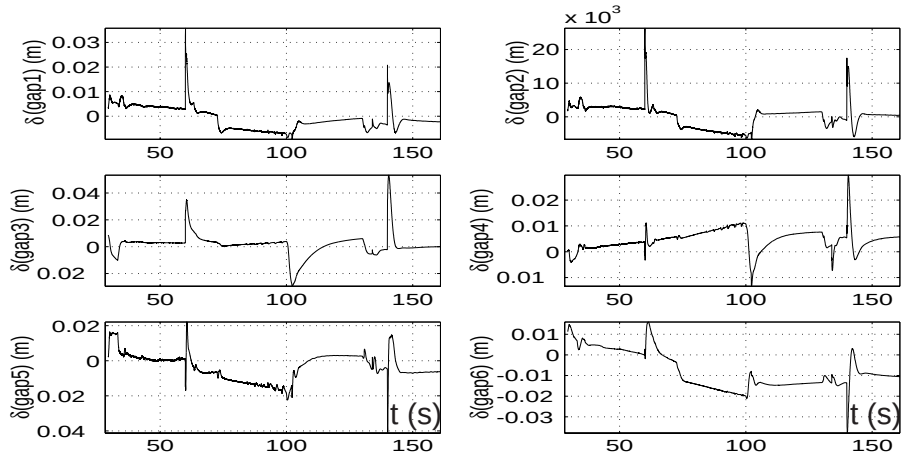

Figure 3.7.4-2b DINA Simulation of Scenario 2 with Minor Disruptions at 80 s and 140 s

Deviation of the controlled gaps relative to their reference values
(see comments on the signs of the gap deviations in Figure 3.7.4-5)

100 MW. Deviations of the controlled gaps relative to their reference values are shown in Figure 3.7-2b. The deviations of all gaps during the plasma current ramp and early part of flat top are well within acceptable limits. The value of deviations is less than 40 mm.

The plasma current ramp-up and the driven burn in the steady state scenario 4 were also simulated with the DINA code in two variants. In the first variant inductive control of the plasma current is continued till the end of the simulation (300 s). Only 9 Wb of magnetic flux is required to sustain a driven burn with 9 MA plasma current for3000 s. In the second variant the control of the plasma current by the PF system is switched off at 60 s. This leads to a plasma current reduction, over about 150 s, from 9 MA to the steady state value of 8 MA. At steady state the value of Q is 5.5 and the loop voltage is zero. The plasma current ramp-up rate in scenario 4 is higher than that in scenario 2. The positive peak of the total power is about 120 MW, higher than in scenario 2.

Studies of plasma initiation and verification of the assumptions used in the studies presented above (i.e. the magnetic flux at breakdown) were performed by simulations which take into account eddy currents in the conducting structures, plasma displacements, models of the power supplies, plasma ionisation and transport. The analysis was done with the set of the switching network resistors considered in the power supply design (see 3.4). Several codes were used in this study: the 2D electromagnetic code TRANSMAK with the 0D transport code SCENPLINT and the 2D electromagnetic code BDOS[1]. 3D electromagnetic analysis was also provided (effect of the vacuum vessel ports and ferromagnetic inserts on plasma initiation). The studies have shown the capability of the PF system to provide outboard plasma initiation, starting from 45% to 100% of the maximum magnetic flux at SOD and assuming 2 MW of EC power is transferred to the electrons.

To summarise, all the scenario studies mentioned above have demonstrated the capability of the PF system to support the scenarios 1-5 with the limits imposed on the coil currents, voltages and total power.

3.7.4.1.3 Plasma Current, Position and Shape Control

The ITER elongated plasma would be vertically unstable without the use of an active feedback control system. The double shell (each 60 mm thick) stainless steel vacuum vessel, shown in Figure 3.7.4-1c, provides the main contribution to the stabilisation of plasma vertical displacements. Important elements of the plasma passive stabilisation are also the toroidally continuous rings (stainless steel, 60 mm thick) attached to the blanket module triangular supports (shown in Figure 3.7.4-1c above the outboard divertor region). The total toroidal resistance of the vacuum vessel with the stabilising rings is 7.4 μΩ. These stabilising rings improve the up/down symmetry of the conducting structures as they couple well with any plasma vertical motion and in particular render the passive structure more symmetric with respect to the plasma. They in fact decrease the initial values of the plasma vertical displacement after a plasma disturbance by about a factor of 2. As far as the instability growth rate is concerned, the contributions to the plasma stabilisation force (participation factors) from the different conducting elements are shown in Table 3.7.4-5.

[1] I. Senda, et al., “Optimizing voltage wafe forms of poloidal field coils at the plasma breakdown”, JAERI-Tech 96-016, Japan Atomic Energy Research Inst., Itaraki (1996)

Table 3.7.4-5 Participation Factors (%) of the Vacuum Vessel (Inner and Outer Shells), Stabilising Rings and Coils in Passive Stabilisation of the Plasma Vertical Displacements (Scenario 2 with l_i = 0.85)

State	VV inner shell	VV outer shell	Stabilising rings	CS and PF coils (each coil is short circuited)
SOF	54.8	27.1	11.7	6.4
SOB	52.6	27.4	11.2	8.8

One interesting feature of the design is that the quasi-symmetrical configuration of the PF coils (see Figure 3.7.4-1c) allows the use of one AC/DC converter, dedicated to plasma vertical stabilisation (VS), which is connected to the coils PF2 - PF5, as shown in the simplified schematic of Figure 3.7.4-3. Compared to the main AC/DC converters connected in series with each coil, the VS converter has a higher output voltage and shorter response time. The on-load voltage limit of the VS converter is 6 kV. The on-load voltage limit of the CS and PF coil converters (main converters) is set at 1.5 kV, except for the one driving the CS1U and CS1L coils (the coil modules nearest the machine mid-plane) connected in series, which is set at 3 kV. The VS converter carries only the imbalance current, which is the algebraic sum of the currents in the coils PF2 through PF5. The scenario value of the imbalance current is typically limited to 12 kA, while the total admissible value is 22 kA.

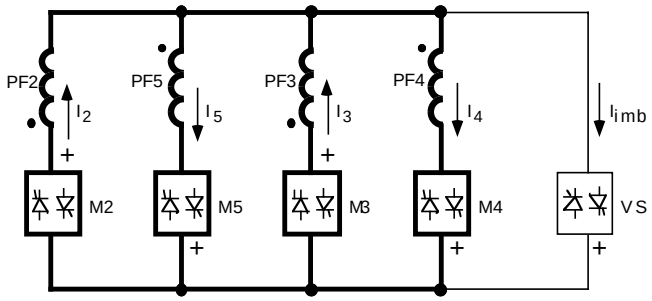

Figure 3.7.4-3 Vertical Stabilisation Circuit

For an optimal use of these features, a control scheme with two feedback loops acting on different time scales has been designed and is schematically shown in Figure 3.7.4-4. In the fast VS loop, the feedback algorithm determines the voltage of the VS converter using as input the vertical velocity of the plasma current centre. Its identification, performed by magnetic diagnostics, is simulated with a first order transfer function with 3 ms time constant. The slow feedback loop provides control of plasma current and shape by acting on the CS and PF coil main converters. Plasma shape control in divertor configurations is realised with the control of the six gaps between the separatrix and the plasma-facing components (the first wall and the divertor) shown in Figure 3.7.4-1 (c). Figure 3.7.4-4 shows the transfer functions of the various components present both in the fast loop and in the slow loop. Current and shape identification, performed again by magnetic diagnostics, is simulated with a longer time constant, 150 ms.

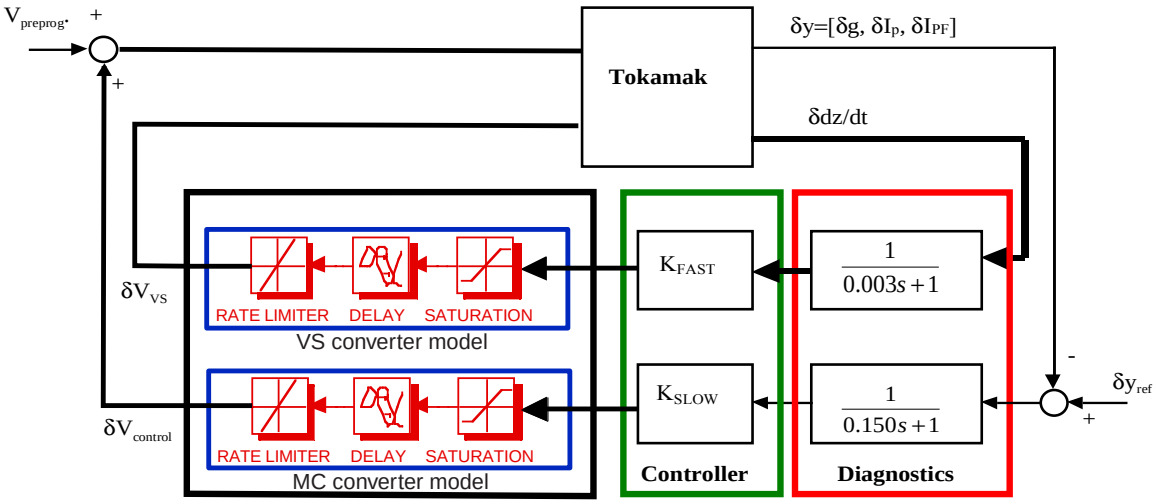

Figure 3.7.4-4 Plasma Current, Position and Shape Control
A two loop control scheme is adopted
(fast loop for vertical stabilisation shown in bold arrows)

The resulting closed loop bandwidth of the fast loop is about 20 rad/s, whereas the slow loop bandwidth is about 1 rad/s; the two loops are therefore well decoupled in the frequency domain.

Two types of large-scale recoverable plasma disturbances, minor disruptions (MD), are used for the design of the controllers and for their studies in the inductive scenarios.

- MD1: an instantaneous l_i drop of 0.2 (l_{i0} – 0.5) without recovery, simultaneous with a β_p drop of 0.2 β_{p0} followed by 3 s exponential recovery.
- MD2: an instantaneous β_p drop of 0.2 β_{p0} followed by 3 s exponential recovery.

The corresponding instantaneous variation of the plasma current is calculated assuming conservation of magnetic helicity.

Several controllers have been designed on the basis of the linear, non-rigid plasma displacement model derived from the PET code. Several controllers for the divertor phases were analysed. The "RF/April 2001" controller design uses the linear quadratic Gaussian (LQG) approach for both the fast and the slow feedback loops. The "JCT/February 2001" controller design combines the LQG VS controller with the LQG controller for the plasma current and shape. The "EU/April 2001" controller design combines a lead network VS controller with two separate decoupling controllers for plasma current and shape, including integral actions to eliminate the static errors. The controllers were used to simulate minor disruptions in the key states of the scenarios described in 3.7.4.1.1. Different possible strategies for controlling the plasma during the limiter phase were also investigated. Various types of these controllers were designed, differing in the set of controlled variables and in the design technique.

Linear plasma models were used for design of the controllers and for preliminary analysis of the controller performance in the case of minor disruptions. Figure 3.7.4-5 shows, as an example, waveforms of gaps, coil currents, voltages and power in the simulation of plasma current, position and shape control during an MD1 (scenario 2, SOF, l_i = 0.85).

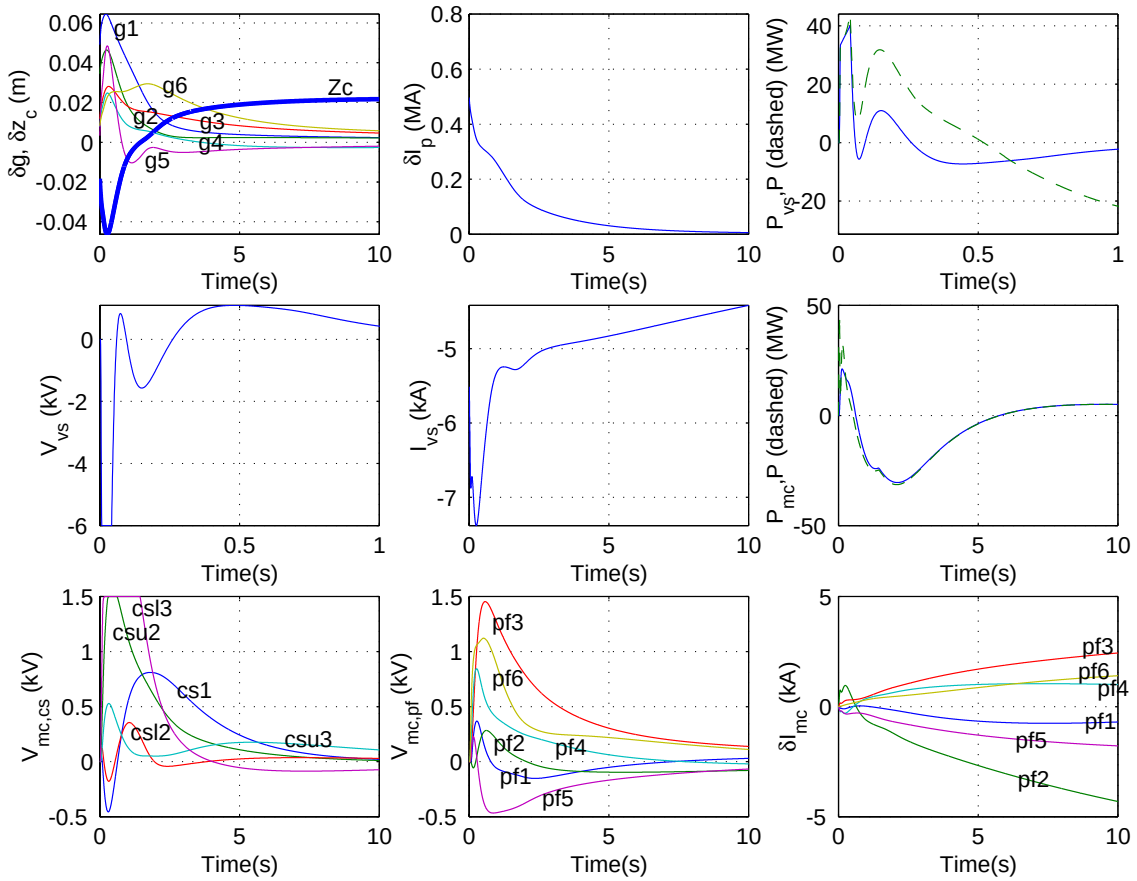

Figure 3.7.4-5 Plasma Current, Position and Shape Control during MD1 in Scenario 2 (SOF, l_i = 0.85).

Linear model derived from PET code, "JCT/February 2001" controller.
δg – deviation of the gaps from the reference values, δz_c – displacement of the current centroid from the reference value, δI_p – variation of plasma current, P – total active power, V_{VS}, I_{VS} and P_{VS} – voltage, current and power of the VS converter, V_{mc} – voltage of the main converter, δI_{mc} – variation of current in the main converter

Positive g1 and g2 deviations correspond to displacement of the separatrix legs towards the divertor dome. Negative g3 – g6 deviations corresponds to decrease of the gap between the separatrix and the first wall.

Similar simulations were provided for the key states of scenarios 1, 2, and 5 with the various plasma equilibria having different l_i. Both minor disruptions (MD1 and MD2) were considered during the burn. The studies were done with the controllers described above. The main results of the linear model simulations can be summarised as follows. The settling time of the gap control, defined as the time needed for the deviation of all the gaps to become less than 10 mm, is about 5-20 s. The maximum displacement of gap 1 (inner separatrix leg) towards the divertor dome is within 100 mm. In a few cases, the separatrix inner leg slightly interacts, during a minor disruption, with the divertor dome (by less that 20 mm for less than 5 s), but these plasmas have low β_p. The maximum displacement of gap 2 (outer separatrix leg) is within 70 mm, which does not lead to interaction of the outer separatrix with the dome. For controllers having a settling time for plasma shape control of 5-10 s, the maximum displacement of the separatrix towards the first wall is about 30 mm for gaps 3 and 4, whereas for gaps 5 and 6 it is about 90 mm. These values are within the acceptable limits.

The "EU/April 2001" controller has been also validated in simulation on the linear model including the plasma shape reconstruction algorithm in the feedback loop and taking into account the effects of noise on the magnetic flux and field measurements.

The overall performance of the shape control has been found to be satisfactory. However, the relatively high plasma elongation with its short growth time implies peak power requirements, of about 100 MW (positive active power). Moreover, the largest power steps found in the simulations with the linear models are of about 90 MW. A preliminary study of the power management system was provided with the goal to reduce the power steps. The system is based on the possibility of transferring electrical power from one coil to other coils. In addition to the linear plasma models, the MAXFEA, PET and DINA free plasma boundary time varying codes have been used in order to analyse the performance of the controllers (see, for example, the results presented in Figure 3.7.4-2).

Possible abnormal operational regimes, due to failure of one PF converter or current saturation in one PF coil, were also studied at a preliminary level. The analysis concludes that in all key states of scenario 2 the "EU/October 2000" controller is able to counteract a minor disruption and restores the plasma shape in 20 s, even if one of the PF converters fails (produces zero voltage). The shape control accuracy is affected by the failure but the controller limits the plasma wall interaction to reasonable values. A strategy to counteract the possibility of current saturation in the PF coils was also developed. An anti-saturation controller, changing the reference signals for the gaps, was proposed. The simulations performed with such a device, both on linear and non-linear models, show the effectiveness of such a system in keeping the coil currents far from their saturation limits with a moderate deterioration on the shape control accuracy.

Several studies were done to estimate the effect of the vacuum vessel ports and other conducting structures on the plasma current, position and shape control. The results can be summarised as follows. The vacuum vessel ports decrease the growth time of plasma vertical instability by 10-20%. The blanket modules have deep cuts in the poloidal direction which, for a model with five plasma facing slits, decreases the eddy current decay time to about 2 ms. This leads to an insignificant effect of the blanket modules on the plasma vertical stabilisation. The TF intercoil structures, the cryostat and the outer-cryostat structures affect insignificantly the plasma current, position and shape control.

3.7.4.1.4 Error Fields, Correction Coils and RWM Stabilisation

Error Fields

Error fields (any perturbation of the axial symmetry of the magnetic field) can drive the formation and growth of locked modes in otherwise MHD-stable plasmas. The most critical period for the locked modes is the last phase of the current ramp-up when the plasma density is low. Recent experiments in DIII-D[1] have also shown that correction of the error field allows the plasma rotation to be maintained above the threshold for rotational stabilisation of the resistive wall mode (RWM).

The following "3-mode" error field criterion has been adopted for the ITER design:

[1] DIII-D Weekly Reports, 2001

$$B_{3-\mathrm{mode}}/B_0 = \sqrt{(B_{2,1}/B_0)^2 + 0.8(B_{3,1}/B_0)^2 + 0.2(B_{1,1}/B_0)^2} \le 5\times10^{-5},$$

where $B_{1,1}$, $B_{2,1}$ and $B_{3,1}$ are the amplitudes of the (1,1), (2,1) and (3,1) modes of the normal component of the non-axisymmetrical magnetic field to the q = 2 surface, and B_0 is the value of toroidal magnetic field (5.3 T), at R = 6.2 m.

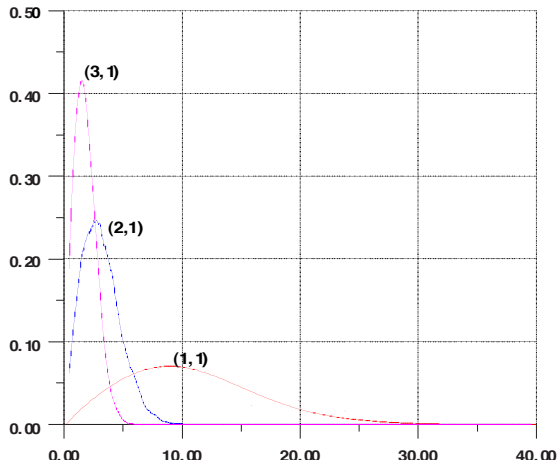

$B_{m,1}$ / B_0 (in 10^{-5})

a) Probability Density of (m,n) = (1,1), (2,1) and (3,1) Error Field Mode Amplitudes.

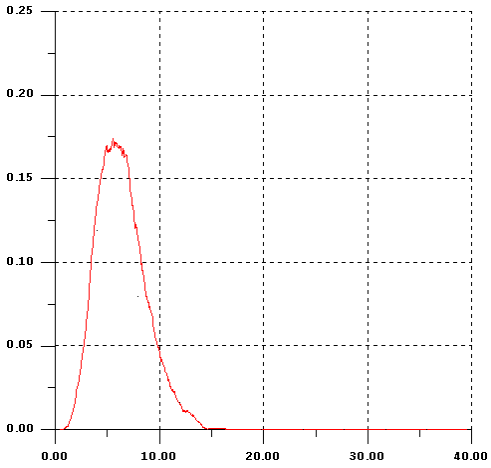

$B_{3\text{-mode},1}/B_0$ (in 10^{-5})

b) Probability Density of 3-mode Error Field Amplitude.

Figure 3.7.4-6 Error Fields from CS, PF and TF Coils Misalignment at SOF in Scenario 2

The misalignments of the TF, CS and PF coil current centrelines, arising during the coil manufacture, installation and assembly, are the main contributors to the error field. A tolerance analysis has been used to estimate the deviation of the coil centrelines from their nominal position and shape. The expected error fields have been calculated with Monte-Carlo simulations using the various degrees of freedom in the coils deviation. A uniform distribution of these deviations, within the limits resulting from the tolerance analysis, was assumed. The probability density of the error field modes expected at SOF in scenario 2 is shown in Figure 3.7.4-6. From Figure 3.7.4-6b the expected "3-mode" error field is less than $9.5\text{x}10^{-5}$ with probability 90% and less than $15\text{x}10^{-5}$ with probability 99.9%.

Additional error fields are produced by the neutral beam magnetic field reduction system (NB MFRS) and by ferromagnetic materials used in the Test Blanket Modules (TBM). The "3-mode" error field due to the NB MFRS (two NB injectors and the diagnostic injector) is about $1.1\text{x}10^{-5}$, whereas five TBMs, having the ferromagnetic material, produce $3.1\text{x}10^{-5}$.

Correction Coils

A correction coil (CC) system has been designed for ITER to bring the above-mentioned error field down to an acceptable level. The CCs (shown in Figure 1.4.1-3) consist of three sets of superconducting coils (top, side and bottom) distributed poloidally to provide control of poloidal fields with several m mode numbers. Each coil is connected to the opposite coil in

anti-series, to produce an n = 1 asymmetric mode and to avoid coupling with axisymmetrical magnetic fields. Three power supplies are used for each CC set to provide toroidal directionality for the error field components. The CC current limits based on the requirements and on the design consideration are: 140 kAt for the top coils, 200 kAt for the side coils and 180 kAt for the bottom coils.

Currents in the CC required to correct the total error fields from the three NB MFRSs and from the five TBMs are as follows: 8 kAt in the top CC, 20 kAt in the side CC and 16 kAt in the bottom CC. A Monte-Carlo simulation has shown that, with a probability of 99%, the rest of the CC currents, available for the correction of other error fields, are sufficient to reduce the error field anticipated from the CS, PF and TF coils to the design criterion of $5x10^{-5}$. The top and side CCs have margins in the currents for this error field correction: about 20 kAt in the top CC and about 55 kAt in the side CC. The margin in the current of the side coils is important also for active stabilisation of the resistive wall modes (RWM).

RWM Stabilisation

The main approach to steady state operation in ITER is via a weak or negative central magnetic shear, high-bootstrap-current discharge. In the absence of a nearby conducting wall, such discharges are unstable to the n = 1 external kink mode at $\beta_N \approx 3$ (due to the low value of l_i), while equal or larger values of β_N are needed to achieve Q = 5. When a resistive (i.e. not perfectly conducting) wall is present, these modes are no longer ideally unstable but can develop RWMs, which grow on the time scale of the magnetic field penetration through the wall, τ_w.

Detailed studies of RWM stabilisation in ITER have not been performed. However, an estimate of the requirements for the currents and voltages in the side CCs was made. A 3D electromagnetic model (without plasma) was used in the analysis. The penetration time of the CC magnetic field through the vacuum vessel was estimated to be about 0.3 s. This time defines the frequency of the CCs currents required for the stabilisation, i.e. about 2 Hz. A 20 kAt current is required for the side CCs to produce, at this frequency, a radial magnetic field of about 1 mT inside the vacuum vessel (several times above the level of detection of the RWM). 13 V/t is required for the side CCs to provide this current amplitude at the 2 Hz frequency, assuming that the single turn inductance of a pair of coils is 50 $\mu H/t^2$.

Parameters of the ITER power supply, chosen for the side CC, can be compared with the AC capability of the new power supply of CCs used in the DIII-D for RWM stabilisation[1]. The DIII-D power supply has frequency f = 100 Hz with maximum current I = 5 kAt. Taking into account the position and size of the DIII-D C-coils normalised by the plasma minor radius, which are then very similar to the ITER side CCs, parameters for the ITER power supply can be scaled from the corresponding DIII-D parameters as follows:

$$f(ITER) = f(DIII-D) \times \frac{\tau_w(DIII-D)}{\tau_w(ITER)}, \quad I(ITER) = I(DIII-D) \times \frac{I_p(ITER)}{I_p(DIII-D)}.$$

Substituting τ_w(DIII-D) = 5.8 ms, τ_w(ITER) = 300 ms, I_p(DIII-D) = 1.5 MA, I_p(ITER) = 9 MA (scenario 4), one obtains for the ITER power supply the frequency 1.9 Hz

[1] A.M. Garofalo et al., Nucl. Fusion 40 (2000) 1491

and the current 30 kAt. These values are consistent with the power supply parameters chosen for the ITER side CC.

3.7.4.2 Kinetic Control

3.7.4.2.1 Kinetic Control Requirements in ITER

Tokamak plasma control encompasses both magnetic configuration control, covered above, as well as kinetic control. There is a clear distinction between magnetic control and kinetic control in terms of the actuators used (the PF coil system is used for magnetic control whereas heating, fuelling and pumping systems are used for kinetic control). In this section, kinetic control in the inductive operation is mainly described although many of the issues are also relevant to steady state operation. Current profile control in the start-up phase is also investigated in its relation to MHD stability.

At the simplest level, the key kinetic attributes of the core plasma control are density, temperature, impurity content, current density, and fusion power. The key attributes of the divertor plasma control are density, temperature, impurity content, radiation power in the core and the divertor region, and the power to the divertor target. Among these attributes, the most important attributes to be controlled are fusion power P_{FUS} and the power to the divertor target plates $P_{Divertor}$. In addition also the power P_{LOSS} across the edge pedestal region should be controlled for the transition from L- to H-mode (in the start up phase) and H- to L-mode (in the shutdown phase).

To control the above three variables (P_{FUS}, $P_{Divertor}$ and P_{LOSS}), there are four main actuators: 1) additional heating power P_{ADD}, 2) DT gas or pellet injection rate, 3) high-Z impurity (for example, argon) injection rate, and 4) pumping rate.

The control system is non-diagonal as every input variable has an effect on every desired output. However, the strongest effect on fusion power is given by changing the particle density. Additional heating has a major impact on both fusion power and L-H transition control, whereas heavy impurity injection has its main impact on the local radiated fraction in the divertor region.

3.7.4.2.2 Kinetic Control in the Reference Inductive Scenario

Fusion Power and Divertor Power Control after Sudden Increase of Confinement Time

The dynamic response of the fusion power to internal (plasma-induced) perturbation is an important issue. Modelling of the plasma burn dynamics with a time-dependent simulation model provides insight into both the inherent response of the plasma and the effectiveness of various burn control systems.

Figure 3.7.4-7 shows a simulation of the response of the power control system to a hypothetical plasma disturbance in which a sudden change of energy confinement occurs. Confinement enhancement factor $H_{H98(y,2)}$ is increased by 20% during the current flat top (t = 300 s) in the reference scenario. The electron density $\langle n_e \rangle$ is controlled to keep the fusion power constant. By controlling argon impurity fraction, the power to the divertor region is also maintained at 30 MW, which approximately corresponds to 5 MWm^{-2} heat load on the target. This analysis also shows that the direct use of fuelling control, for example by

cutting back the fuel injection rate, is an effective method in limiting fusion power excursions.

Control of Fusion Power in High-Q Operation by Impurity Seeding

The control of fusion power excursion is one of the most important issues in the fusion reactor. In the case of high-Q or ignited operation, fusion power can not be controlled only by the additional heating power. In this case, high-Z impurity seeding or density control has been considered as one of the means for burn control.

Figure 3.7.4-8 shows a simulation where the suppression of the fusion power excursion is achieved by impurity injection. Here, $I_P = 17$ MA, $\langle n_e \rangle = 1.18\times10^{20}m^{-3}$ ($\langle n_e \rangle / n_G = 0.87$), $\tau_{He}^*/\tau_E = 3$, $H_{H98(y,2)} = 1.0$ and, as an artificial disturbance, a heating power P_{ADD} is added from 10 s to 13.7 s. The dotted line denotes the case without impurity seeding. In this case, a large overshoot of fusion power is observed. In the case of the solid line, argon impurity (Ar) is injected and the overshoot of fusion power is suppressed.

3.7.4.2.3 Control of Current Profile in Start-up Phase

In the start-up phase, the current profile can be modified by changing the current ramp-up rate and/or the timing of the heating. In this case, magnetic control and kinetic control are linked to each other.

Figure 3.7.4-9 shows various start-up scenarios of ITER. Cases (a) and (b) are with heating after current flat-top, and case (c) is with heating during current ramp-up. In cases (b) and (c), the current ramp-up rate is reduced by a factor of 2 at the final stage of current rise. It is seen that the plasma internal inductance $l_i(3)$ increases by decreasing the current ramp-up rate. Higher $l_i(3)$ indicates a more peaked current density profile.

The figures on the bottom row show the trajectory in q_{95}-$l_i(3)$ space. X-point formation (XPF), start of heating (SOH), start of flat-top (SOF), start of burn (SOB), end of burn (EOB) and end of cooling (EOC) are shown. Dotted lines show the empirical stability boundary. The trajectory in q_{95}-li(3) space can be controlled by the start time of the additional heating.

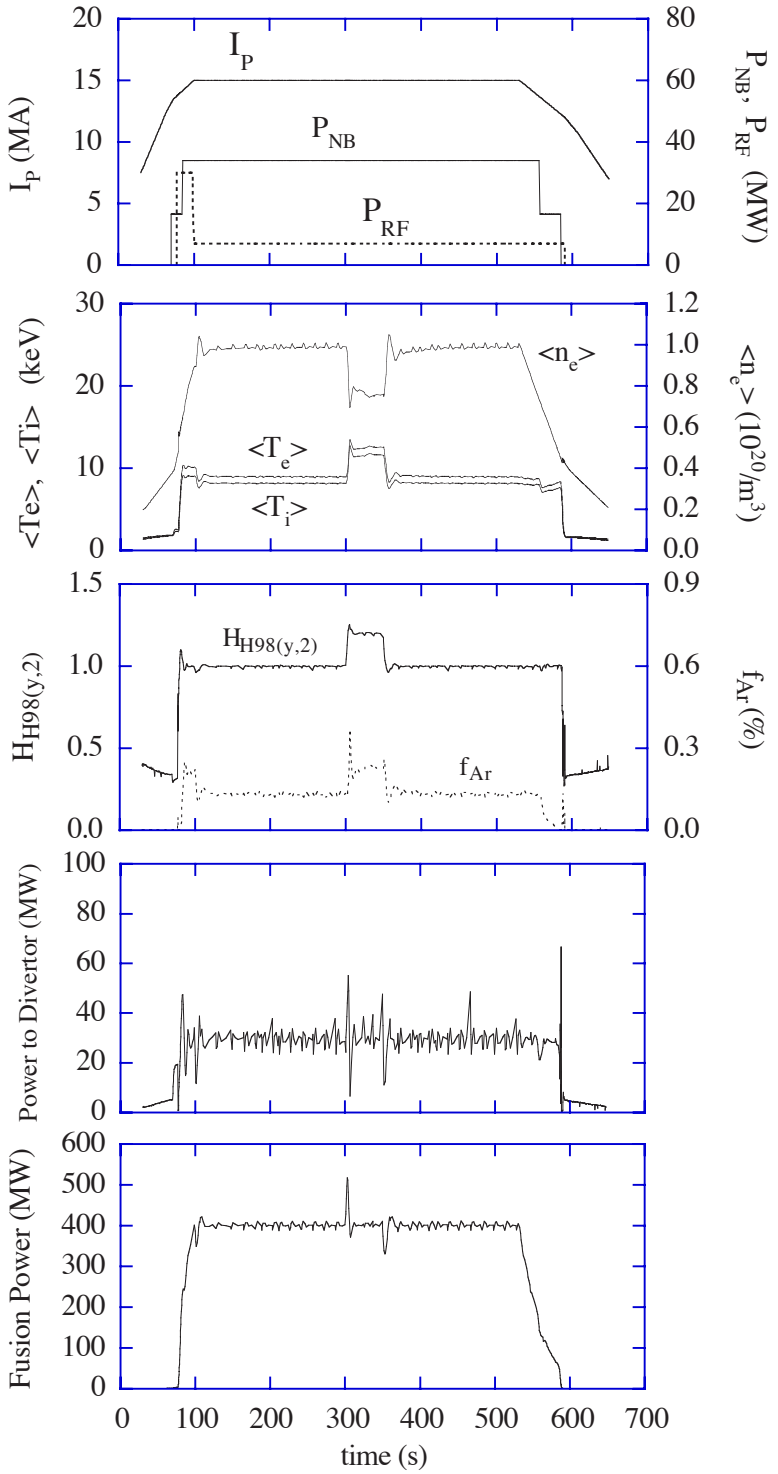

Figure 3.7.4-7 Fusion Power Control by Density Control after Sudden Increase of Energy Confinement Time

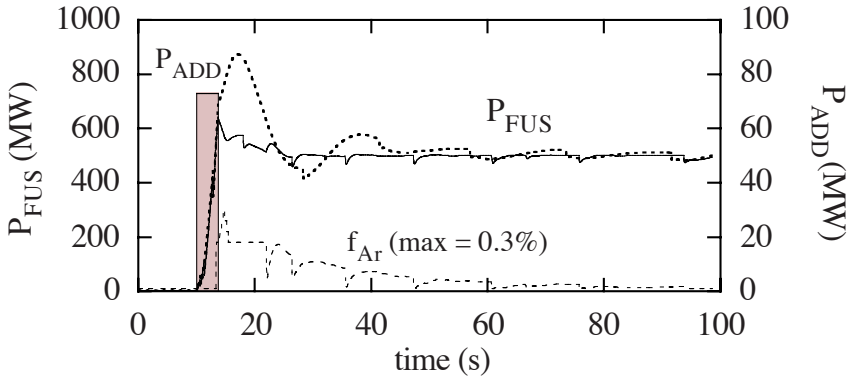

Figure 3.7.4-8 Suppression of Fusion Power Excursion by Impurity Seeding in Ignited Operation

Here, I_P = 17 MA, τ_{He}^*/τ_E = 3, $H_{H98(y,2)}$ = 1.0 and 73 MW of additional heating power (P_{ADD}) is added from 10 s to 13.7 s.

solid line: with argon (Ar) impurity seeding, dotted line: without impurity seeding

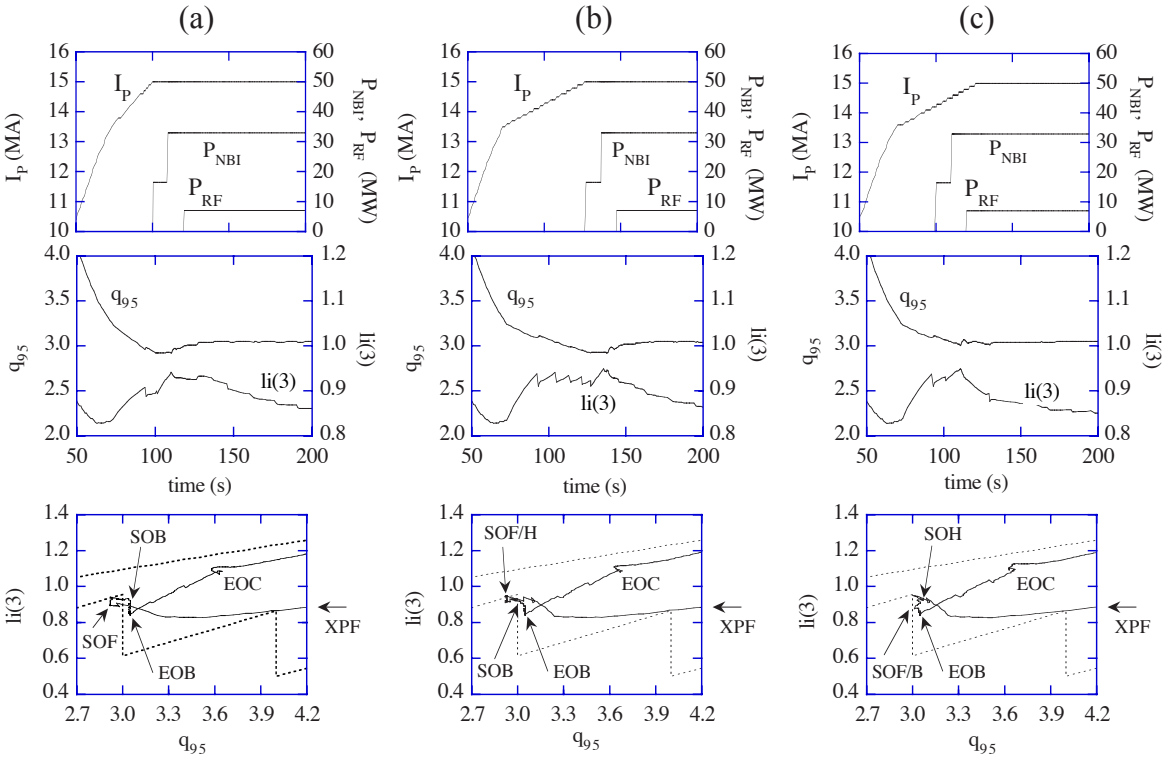

Figure 3.7.4-9 Various Start-up Scenarios

(a) and (b) with heating after current flat-top, (c) with heating during current ramp-up

3.7.4.2.4 Control of Magnetic Shear and ITB Formation from Conventional q-profile

In non-inductive operation, current profile control is an important issue. Figure 3.7.4-10a shows a demonstration of ITB (internal transport barrier) formation from a conventional q-profile by using a simple model in which an ITB is formed when magnetic shear rq'/q is < 0. Here, I_P = 9 MA and $<n_e> = 0.67 \times 10^{20} m^{-3}$. Starting from a normal shear plasma ($P_{FUS}/P_{NB}/P_{RF1}$ = 140 MW/20 MW/20 MW), peripheral current drive (P_{RF2} = 40 MW) is added at t = 300 s. An ITB is formed at 640 s and steady state conditions with Q = 3.5 (P_{FUS} = 280 MW) are obtained at about 2000 s. Here, current drive efficiencies assumed are $\gamma_{20}(NB) = 0.18 - 0.28$ and $\gamma_{20}(RF2) = 0.3$. Figure 3.7.4-10b shows plasma profiles corresponding to a). Here, the RLWB transport model[1] is assumed. Thermal diffusivity χ (and also particle diffusivity) is reduced to the neo-classical level at r/a < 0.7 where magnetic shear rq'/q < 0. A large current drive power (~ 40 MW) in the peripheral region is required in addition to 40 MW of on-axis (RF) and off-axis (NB) current drive.

For the non-inductive operation mode, time response of plasma parameters to various perturbations (confinement, impurity fraction, current drive power, pumping speed and fuelling rate) has been investigated. Current penetration determines the rate of profile changes and the time constant of any plasma parameter is usually longer than 100 s.

a)

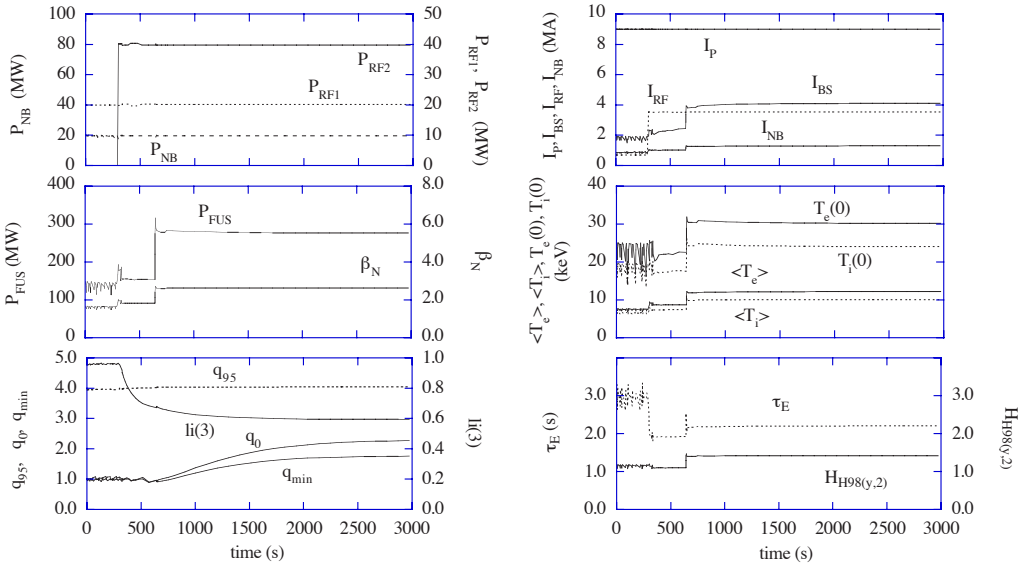

b)

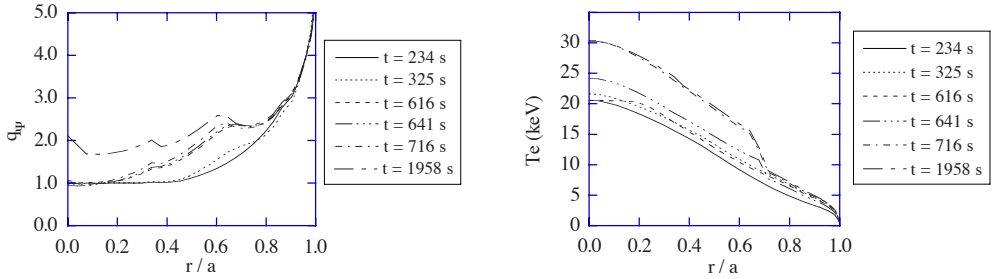

Figure 3.7.4-10 ITB Formation from a Conventional q-profile

a) Time histories of current drive powers (P_{NB}, P_{RF1}, P_{RF2}) and plasma parameters
b) Profiles of mhd safety factor (q_ψ) and electron temperature T_e corresponding to a)

[1] D. Boucher, et al., in Proc. 16th IAEA Fusion Energy Conference, Montreal, 1996 (IAEA,Vienna, 1997) p945

3.7.4.2.5 Start-up Scenario in Non-inductive Operation

In this section, more realistic start-up scenario including growing plasma size is described. Here, the 1.5D transport code ASTRA[1] is used. Figure 3.7.4-11 shows the simulation result for the start-up of non-inductive operation with weak negative shear (WNS). Simulation starts from a limiter plasma with small plasma minor radius (R/a = 7.4 m/0.8 m). After plasma initialisation phase, the plasma current profile is almost flat with high central $q_o \sim 2$. Such profile is close to the desirable one at the current flat-top phase. To prevent current peaking, a fast current ramp-up rate and an additional heating power are required. For example, the average current ramp-up speed is increased to 0.25 MAs^{-1}, 6 MW of the ECRH power is applied at t = 0.1 s and then increases to 8 MW at t = 6 s. 3 MW of LH power is also applied at t = 3.5 s. At this limiter phase, the input power is kept smaller than the maximum limiter heat load $P_{loss} < 15$ MW. After the X-point formation (t = 15.7 s, I_p = 5 MA), the LH power is increased to 15 MW at t = 24 s, to 25 MW at t = 25 s and to 29 MW at t = 26 s to provide the L-H transition at low density and replace the ECRH power, which is switched off. One NB injector is switched on at t = 27 s, and the other at t = 28.5 s, when plasma density reaches $4\times10^{19}m^{-3}$ and shine-through losses drop to an acceptable level. Each of two NB injectors (on-axis and off–axis) delivers 15 MW. The gradual replacement of carbon by argon (27 s < t < 40 s) enables reduction of the loss power from the core to the level compatible with the divertor constraints $P_{loss} < 100$ MW. In this scenario, the resistive voltage drops to zero in ~ 100 s. The total required flux consumptionis about 5 Wb. Although a complete steady state current profile relaxation takes about 2000 s from a conventional centrally-peaked current profile(see the previous section), an almost steady state condition is achieved within 300 s by optimisation of the current ramp-up rate.

3.7.4.2.6 NTM Stabilisation

ITER can achieve its goal of Q ≥ 10 with β_N as low as 1.5 and even at fusion power levels of 500 MW, β_N is ~ 2. Nevertheless, in present experiments with long-pulse, low collisionality plasmas, neoclassical tearing modes (NTMs) can limit β and degrade energy confinement within the range of β_N foreseen for ITER operation[2] (and well below the ideal mhd stability limit). The predominant modes are (m,n) = (3,2) and (2,1), with the former typically producing a 10 - 30% degradation in confinement, while the latter results in major disruptions.

Although a scatter in available data does not allow a precise scaling of critical quantities, such as the minimum seed island width, it has been found in several tokamaks that the minimum β for the onset of NTMs falls approximately linearly[3] with the normalised Larmor radius ρ_i *.

[1] G. V. Pereverzev, et al., IPP 5/42 (1991)
[2] O. Sauter, et al., Phys. Plasmas **4** (1997) 1654 M.N. Rosenbluth, Plasma Phys. Control. Fus. **41** (1999)
[3] R.J. La Haye, et al., Phys. Plasmas **7** (2000) 3349

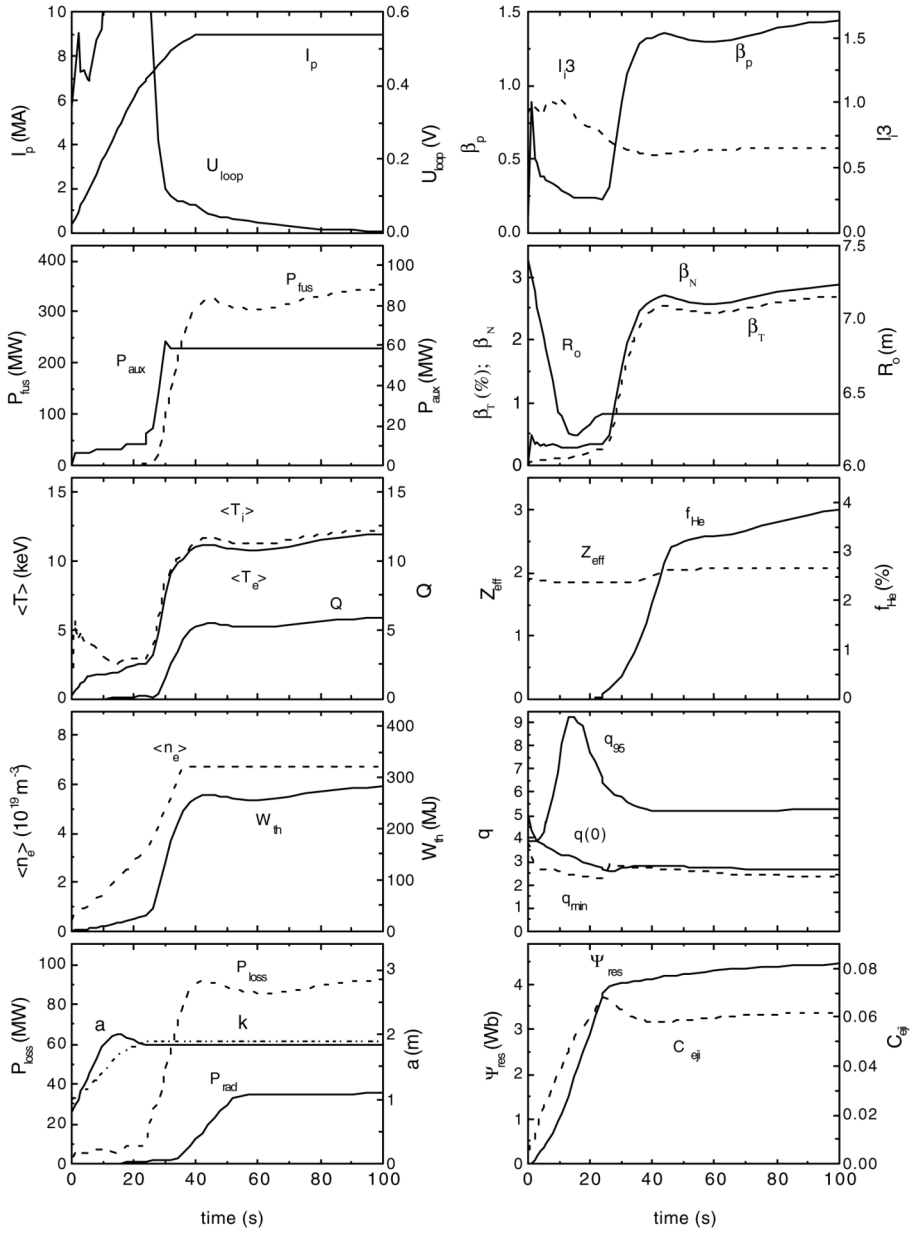

Figure 3.7.4-11 Start-up Scenario for Non-inductive Operation

X-point formation corresponds to t = 15.7 s, start of flat-top corresponds to t = 40 s and start-of-burn corresponds to t = 40 s.

If this scaling is valid in the range of small ρ_i *, the critical β_N in ITER would be about 0.5, which is below the operational value. Since this prediction is based on limited data in the range far from ITER, and since at very low ρ_i * the seed island is expected to be too small to overcome the stabilising factors (polarisation current and incomplete pressure flattening in the island), usually higher estimates for critical β_N for ITER are given[3]. However, given a large uncertainty in prediction, it is necessary to develop NTM stabilising techniques.

The growth time of NTMs is determined by the timescale for resistive reconnection in the vicinity of the relevant rational q surface, which is long enough to permit stabilisation by ECCD in present experiments[1], and should lie in the range 10 -30 s in ITER. Therefore, an ECCD-based stabilisation system for NTMs will be installed to suppress (3,2) and (2,1) modes. Two possibilities have been explored computationally: (i) mode stabilisation by ECCD modulated in phase with the island O-point, and (ii) reduction in width of the saturated island by continuous ECCD. Theoretical calculations show that a modulated ECCD current density exceeding 1.5 times the bootstrap current density in the neighbourhood of the rational surface (driven in the forward direction in the island O-point) will stabilise an arbitrarily small island.

Initial analyses of power requirements have shown that (3,2) and (2,1) NTMs could be stabilised (individually) in a time of order 10 s by 10 - 30 MW of modulated ECCD power[2] in devices of the ITER class (see Figure 3.7.4-12). There is a satisfactory agreement between different approaches. The scatter in the predictions is partly related to the island detection size. For example, an estimate of modulated ECCD power[3] for ITER varies from 28 MW for saturated islands to 18 MW for a smaller detectable size of island $w/a \approx 0.04$ (see Figure 3.7.4-13), indicating that detection of small islands of $w/a \approx 0.04$ would reduce the required ECCD power to <20 MW.

Feedback stabilisation by ECCD seems at present to be the most promising route to ensure control of NTMs in ITER. Direct control of the q profile, shown experimentally to affect the NTM threshold[4], might also be feasible, but requires further investigation. Also, further theoretical work and experimental proof are needed, before it could be recommended to ITER, for the recent proposal[5] to stabilise NTMs by an externally applied static helical field with a helicity different from that of NTMs.

3.7.4.3 Disruption Control

Disruptions and VDEs have a significant effect on the overall design of ITER[6]. The neutral point position in ITER, halo currents, runaway electrons and methods of avoidance and mitigation of the disruptions and VDEs are discussed in this section.

[1] H. Zohm, et al., Proc. 26th EPS Conf. on Controlled Fusion and Plasma Physics (Maastricht, 1999) 1373
[2] G. Giruzzi, et al., Proc. 13th Topical Conf. on Applications of RF Power to Plasmas (Annapolis, USA, April, 1999); A.V. Zvonkov, "Electron Cyclotron Current Drive Optimisation for Control of Neoclassical Tearing Modes in RTO/RC-ITER", unpublished (1999)
[3] V.D. Pustovitov, et al., 18th IAEA Fusion Energy Conference, Sorrento, (2000) IAEA-CN-77/ITERP/07
[4] R.J. La Haye, et al., Nucl. Fusion **40** (2000) 53; T.C. Hender, et al., 18th IAEA Fusion Energy Conference, Sorrento, (2000) IAEA-CN-77/EXP3/02
[5] Q. Yu, et al., Phys. Rev. Lett. **85** (2000) 2949
[6] ITER Physics Basis, Chapter 3 Section 4, Nucl. Fusion **39** (1999) 2321

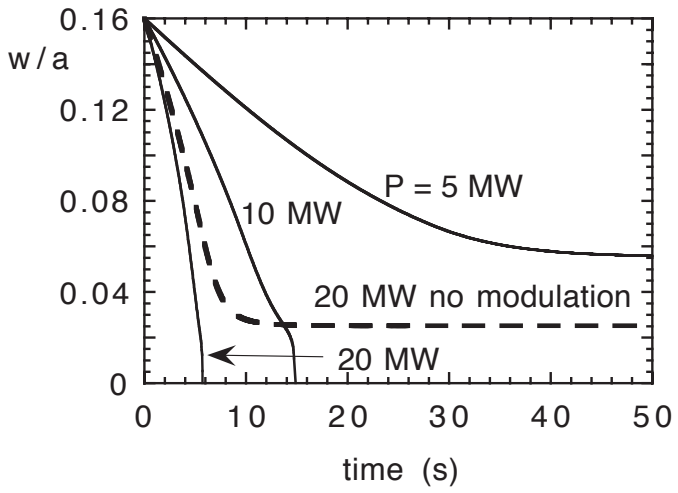

Figure 3.7.4-12 Predictions of Power Requirements and Timescales for (2,1) Neoclassical Tearing Mode Stabilisation by ECCD for Nominal Conditions in a Device with Parameters similar to ITER

Results are shown in terms of the initial island width, w, normalised to the plasma minor radius, a, at ECCD switch-on. It is assumed that the ECCD power is modulated in phase with the island rotation, except for the dashed curve.

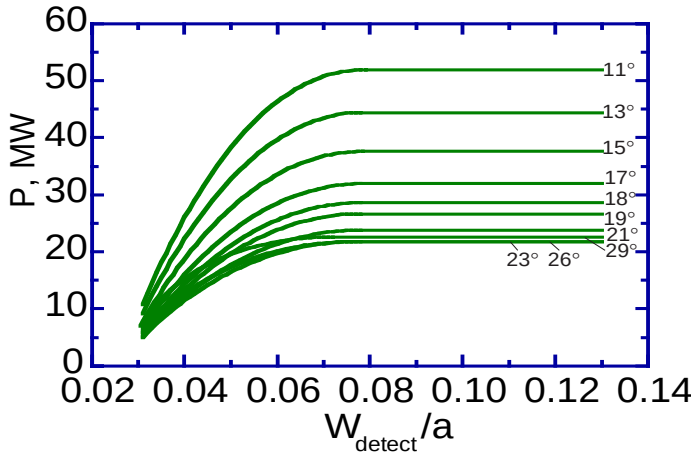

Figure 3.7.4-13 Necessary EC Power (Modulated ECCD) versus Detectable Si e of Island for Upper Launching with Angles between the Wavebeam and the Poloidal Plane in the Range 11 - 29 for ITER

The minimum power for the $q = 2$ case is obtained for angles between 23° and 26°.

3.7.4.3.1 Plasma Neutral Point Position

Investigation of the vertical instability demonstrates the presence of the so-called passive-stability 'neutral point', where the initial vertical displacement of the plasma magnetic axis or current centroid that occurs after disruption, or fast shutdown β_p loss, is small or zero. The onset of vertical instability following fast shutdown in a vertically-elongated plasma can be avoided if the initial plasma position is chosen to be close to the neutral point. The resulting plasma motion is predominantly radially inward, and a major vertical excursion and the associated halo currents in the upper or lower in-vessel and vessel structures are absent. This type of passive neutral-point instability avoidance was investigated for fast current quenches in JT-60U[1]. The neutral point VDE and halo-current avoidance technique was extended in JT-60U to slow current quenches with active control of the plasma position. Such control is made possible by a plasma-axis vertical position magnetic diagnostic signal that includes compensation for the effect of the toroidal vacuum-vessel eddy currents that develop during the current quench[2]. The resulting actively stabilised single-null divertor plasmas can be controlled vertically down to low plasma current ($\leq$ 10% I_p) and halo currents in the divertor region are avoided. Detailed study of the poloidal field system feasibility of maintaining vertical control after disruption in ITER remains to be performed.

Post-disruption plasma motion was investigated for ITER by means of the DINA code[3]. It has been found[4] that the plasma will generally drift downward for a drop of l_i, upward for a drop of β, and even more significantly upward for any reduction of plasma current. The triangular frames mounted on the vacuum vessel structure to support the lowest blanket modules are an important factor for these motions. The position of the neutral point in ITER is approximately only 10 cm below the plasma centre, thus causing a relatively slow initial plasma speed in response to plasma perturbations.

3.7.4.3.2 Halo Currents

During a vertical disruption (VDE), both the plasma current and cross-sectional area (which encloses toroidal flux) decay to zero. Both decays generate an electric field, which can drive current flow along the helical field lines in the wall-connected scrape-off-layer (SOL) region of the plasma. This so-called 'halo' current[5] flowing helically on wall-intersecting plasma flux surfaces makes a complete circuit by flowing from the strike points at one end of the open SOL field lines, through the conducting first wall structures, and out onto the other end of the SOL field lines. Interaction of the halo current flowing through the wall in the poloidal direction and the toroidal magnetic field produces both vertical and lateral forces. A toroidal asymmetry of the halo current leads not only to local enhancement of the vertical force but also to a net lateral force. The halo current toroidal asymmetry is usually characterised by the toroidal peaking factor TPF, the ratio of maximum halo current density to toroidally averaged halo current density.

[1] R. Yoshino, Y. Nakamura, Y. Neyatani, Nucl. Fusion **36** (1996) 295
[2] R. Yoshino, J. Koga, T. Takeda, Fusion Technology **30** (1996) 237
[3] R. Khayrutdinov, V. Lukash, J. of Comput. Physics **109** (1993) 193
[4] V. Lukash, Report from ITER Physics Design Group at RRC Kurchatov Institute, "Analysis of RC-ITER Plasma Dynamics during VDE" (2000)
[5] P. Noll, et al., in Fusion Engineering (Proc. 11th Symposium on Fusion Engineering, Austin 1985), IEEE, New York (1986), **Vol. 1** 33; E.J. Strait, L.L. Lao, J.L. Luxon, E.E. Reis, Nucl. Fusion **31** (1991) 527

The question of the possible tokamak size scaling of the maximum halo current fraction I_h/I_p and TPF is one of the principal remaining uncertainties. Information on the fraction I_h/I_p and TPF in a number of tokamaks assembled as part of the ITER Disruption Database (DDB) indicates that the higher peaking factors tend to be seen only at lower normalized halo currents[1]. The ranges of data from medium-sized and small tokamaks, described in the ITER Physics Basis, are $I_h/I_p \leq 0.4$ (≤ 0.25 typical), $1.2 \leq TPF \leq 4$ and $(I_h/I_p)\times TPF \leq 0.75$ (≤ 0.50 typical)[2]. The database extended with JET and JT-60U data indicates a favourable machine size scaling of $I_{h,max}/I_{p0}$[3], and hence that the bound on maximum halo current fraction in ITER may eventually lie well below ~ 0.3. Furthermore the highest values of TPF x $I_h/I_{p0} \sim 0.5$ are from low current discharges ($I_p/I_{pmax} = 0.35$ - 0.5, where I_{pmax} is the maximum plasma current achieved in the machine), and the other data satisfy $(I_h/I_p) \times TPF \leq 0.4$. This indicates that the present guideline is conservative.

3.7.4.3.3 Runaway Electrons

The generation of multi-MeV runaway electrons, following onset of plasma disruption at low densities, is a well-known effect in tokamaks. High-current tokamaks such as ITER are theoretically expected to be susceptible to runaway current conversion following disruption even at high density by an avalanche process[4]. The conversion of plasma current magnetic energy to runaway currents leads to localization of the magnetic energy deposition in poloidal direction. Beside this, the first-wall misalignment in the toroidal direction is estimated[5] to increase local deposition by a factor of ~5. Self-consistent studies of ITER runaway conversion and wall-interaction using the DINA code[6] illustrate the potential magnitude of the runaway deposition problem for different post thermal quench values of temperature (T_e = 5 eV, 20 eV, and 35 eV), internal inductance (l_i = 0.7, 0.85 and 1.0) and plasma density ($n_e = 0.6\times10^{20}$ m^{-3}, 0.9×10^{20} m^{-3}, 1.2×10^{20} m^{-3}). Direction of the plasma movement before touching the wall is upwards and to the inner part of the wall. After touching the wall, the plasma moves in the clockwise direction. It is assumed in these calculations that runaway electrons are not confined and that they are expelled from the plasma when the safety factor at the boundary reaches $q_b = 2$, as observed in JT-60U experiments[7]. Because of this effect, the estimated heat load by runaway electron is reduced by an order of magnitude from the estimate made for ITER-1998 design[8]. The simulations demonstrate that both runaway current I_{ra} and runaway electron energy deposited to the first wall Q_{ra} are diminished with growth of the electron density and/or electron temperature. The runaway current can replace up to the full pre-disruption plasma current, I_{ra} = 14.6 MA at T_e = 5 eV and l_i = 1.0. The maximum Q_{ra} = 25.7 MJ is estimated at T_e = 5 eV and l_i = 0.7.

[1] ITER Physics Basis, Chapter 3 Section 4.3.5, Nucl. Fusion **39** (1999) 2343
[2] ITER Physics Basis, Chapter 3 Section 4.3.6, Nucl. Fusion **39** (1999) 2343
[3] R. Yoshino, et al., 17th IAEA FEC (Yokohama,1998) IAEA-CN-69/ITERP1/14
[4] M.N. Rosenbluth, S.V. Putvinski, Nuclear Fusion, **37** (1997) 1355
[5] ITER Physics Basis, Chapter 3 Section 4.4.4, Nucl. Fusion **39** (1999) 2351
[6] V. Lukash, ITER Physics Design Group at RRC "Kurchatov Institute", "Runaway Electrons and Halo Currents in FEAT Plasma", Moscow, (January 2000)
[7] H. Tamai, et al., "Runaway Current Termination in JT60-U", in Proc. of 18th IAEA Fusion Energy Conference, 2000, Sorrento, Italy, IAEA-CN-77-EX9/2
[8] "Technical Basis for the ITER Final Design Report, Cost Review and Safety Analysis (FDR)", IAEA, Vienna (1998) Chap. III. 62

3.7.4.3.4 Disruption Avoidance and Mitigation of Consequences

ITER components are designed to withstand the electromagnetic and thermal loading stress and erosion consequences of disruptions. The disruption erosion may consume approximately 50% of the overall component lifetime, and sometimes long term reconditioning of plasma-facing surfaces after disruptions will be required before normal plasma operation can be resumed. It is desirable to avoid the occurrence of disruptions whenever possible and to reduce the direct and consequential effects of such disruptions in ITER. The subjects of disruption effect amelioration can be divided into three aspects: (1) *a priori* avoidance of the operation conditions that lead to disruption, (2) active intervention in a discharge scenario after early prediction of disruption onset, and (3) mitigation of unavoidable disruption effects by after-onset actions. All of these methods have been tested and/or demonstrated with some degree of success and reactor relevancy in present tokamaks.

Avoidance of Operation Conditions that Lead to Disruption

The disruptions can, in principle, be avoided during tokamak operation by the use of a discharge scenario which circumvents the various operational limits and conditions that cause disruptions, and by the provision of adequately reliable plasma operation and control systems such that all critical parameters of the prescribed scenario can be reliably obtained and repeated. Operational scenarios to avoid six different types of disruptions were developed in JT-60U[1]. Disruptions caused by the density limit, the error field, β collapse, a high l_i during the plasma current ramp-down at low density, a low l_i during the plasma current ramp-up, and vertical instability, have been studied and successfully avoided in these experiments.

Selection of a scenario that maintains a relatively wide margin against known disruption-initiating conditions is an obvious benefit in the development of such 'disruption-free' scenarios. Under such "reference pulse" conditions, discharges with high plasma performance and low per pulse disruption rates can be obtained. The standard TFTR 'supershot' regimes[2] used for DT experiments were characterised with disruption frequency of ≤ 1%.

Disruption-Onset Predictions

The "reference pulse" scenarios are often based upon conservative plasma operation parameters that do not press close to known disruption-initiating limits or plasma configuration control limits. The *a priori* disruption avoidance procedures can in principle be extended to operation scenarios that come closer to several operational limits. In these cases, observation of the limits involved, and provision of real-time disruption prediction (onset warning) capability, become important. Here, monitoring of various plasma performance indicators, including safety factor, internal inductance, plasma density relative to the Greenwald density, radiated power fraction, and status of MHD activity, become essential operation scenario development tools. Monitoring of such indicators can provide warning of the potentially impending onset of disruption. Using a warning indicator to effect feedback-controlled intervention (e.g., feedback[3] from β_N to control P_{add}) can lead to reliable operation near a limit that can initiate disruption.

[1] R. Yoshino, et al., Journal of Japan Society of Plasma Phys. and Contr. Fusion (1994) 1081
[2] E.D. Frederickson, et al., Phys. Plasmas **2** (1995) 4216
[3] D. Mueller, et al., Fusion Technology **30** (1996) 251

Basing disruption prediction on single parameter proximity or the confluence of several single parameter limits may not necessarily provide complete certainty for disruption avoidance, or conversely, may unduly restrict the accessible operation domain. A possible improvement can be made by implementation of a neural network disruption predictor, wherein multiple disruption-related indicators or diagnostic signals are combined via a neural network to provide a composite impending disruption warning indicator that is more robust and reliable than simple single- or multiple-parameter indicators. For example, after training, a neural net successfully predicts disruptions in DIII-D[1]. Enhanced predicting capabilities (85%) were achieved in ASDEX Upgrade using a neural network disruption predictor[2]. More complex systems[3] are capable of disruption prediction with a probability of 95%. About 100 disruptions are sufficient to train a neural network. However, how to directly apply training obtained in a present experiment to ITER, or how to shorten the period required for network training in ITER (which will require producing disruptions), remains to be assessed.

The result of any of these prediction methods or of the more traditional approach of detection of disruption MHD precursor growth is an indication of the possible or likely occurrence of a disruption. Such indication can form the basis for initiating avoidance and/or mitigation procedures. The time needed for the implementation of such a procedure determines the 'look-ahead' time-horizon capability needed for the predictor. Reliability of the predictor is a second key consideration: simultaneous achievement of highly reliable prediction of disruption and low (ideally zero) occurrence of 'false alarms' is important.

Softening of the Disruption Consequences

The risk of onset of vertical instability following a disruption in vertically elongated plasma can be reduced if the initial plasma position is chosen to be close to the passive-stability neutral point.

If a full blown VDE can not be avoided, a fast discharge shutdown can be implemented by the injection of impurity or hydrogen species. This injection serves to distribute energy more uniformly by radiation and to limit the severity of VDEs and the resulting vessel vertical and radial forces.

Three methods of injection are being discussed: intense gas puffing, liquid jet injection and solid pellet injection. The pellet injection seems to be most attractive for ITER, although injected impurity may produce runaway electrons. Numerical simulations of the injection of a sequence of 30 - 50 deuterium pellets doped with a small concentration of krypton with a simultaneous controlled rampdown of the poloidal fieldcoil currents, show that benign fast shutdown without generation of a large number of runaway electrons can be achieved[4]. A cryogenic system for gas pellet preparation is not ideal for stand-by operation. Beryllium pellets or pellets based on polyethylene doped with titanium or silicon are proposed instead of the cryogenic pellets. No long-lived runaway electrons were observed with doped

[1] D. Wróblewski, G.L. Jahns, J.A. Leuer, Nucl. Fusion, **37** (1997) 725
[2] G. Pautasso, et al., Journal of Nucl. Materials, 290-293 (2001) 1045
[3] F.C. Morabito, et al., "Fuzzi-Neural Approaches to the prediction of disruptions in ASDEX-Upgrade", Nucl. Fusion, to be published; F.C. Morabito, et al., "Progress in the prediction of disruption in ASDEX-Upgrade via neural and fuzzi-neural techniques", in Proc. of 18th IAEA Fusion Energy Conference, 2000, Sorrento, Italy, IAEA-CN-77-EXP3/17
[4] Jardin, et al., Nucl. Fusion **40** (2000) 923

polyethylene pellet injection in ASDEX-Upgrade[1]. Avoidance of runaway electron formation under disruptions was achieved at low values of safety factor, $q_{95} \leq 2$ and in the presence of large-scale magnetic disturbances, $\tilde{B}_r / B_T \approx (2 \div 8) \times 10^{-4}$ in JT-60U[2].

For safety, reduction of fusion power must be achieved in a simple, reliable way. For this purpose, intense impurity gas-puffing will be adequate.

3.7.5 Summary

The ITER plant control is achieved by a CODAC system, which is structured in a hierarchy composed of the SCS and individual dedicated control subsystems to ensure integrated control of the entire ITER plant.

The SCS supervises the ITER plant operation, controls the plasma discharge, imposes selected plasma parameters, acquires plant and scientific diagnostic data, displays alarms, creates the ITER database, and communicates with both on-site and remote site control rooms.

Control subsystems, dedicated to each plant and diagnostic subsystems, are supervised from a central control system, control directly and monitor the individual plant and diagnostic subsystems, and perform limited actions of autonomous operation of a subsystem even though they are always determined by the supervisory control system.

The above philosophies are adopted to all ITER control systems, and more detailed functional definition and distribution between the SCS and individual subsystems will be determined as for the future work.

The plasma control system takes on discharge sequencing, and magnetic, kinetic and disruption control. The poloidal field (PF) system is capable of supporting all the design scenarios and the assessed scenario with high plasma current of 17 MA. Simulations show that the PF system can control and recover the plasma position and shape in the case of minor disruptions.

The key elements of kinetic control have been studied for inductive and non-inductive operations. In the inductive operation mode, particle control or helium accumulation determines the time constant of kinetic control, which is typically less than 50 s. Therefore, an inductive burn pulse length of 100 - 400 s is adequate to investigate transient plasma behaviours. The fusion power can be controlled by fuel density and heating power. The divertor heat load can be controlled by impurity seeding. Stable quasi-steady state plasma will be achieved with various values of Q. High Q operations might be associated with fusion power excursions, which can be suppressed by impurity injection.

For the non-inductive operation mode, time response of plasma parameters to various perturbations (confinement, impurity fraction, current drive power, pumping speed and fuelling rate) has been investigated. Current penetration determines the rate of profile changes and the time constant of any plasma parameter is usually longer than 100 s. A complete current profile relaxation takes about 2000 s, e.g. from a conventional mode to a

[1] Pautasso, et al., Journal of Nucl. Materials 290-293 (2001) 1045
[2] R. Yoshino, S. Tokuda, Nucl. Fusion **40** (2000) 1293

weak reverse shear mode. However, an almost steady state is achieved within 300 s by optimising the current ramp up phase. Therefore**,** a pulse length longer than 1000 s is not always necessary to study a non-inductive operation mode.

Feedback stabilisation by ECCD system seems to be the most promising route to control neo-classical tearing modes (NTMs). Analyses have shown that detection of small islands (w/a ~ 0.04) would enable stabilisation of NTMs by <20 MW of ECCD power.

Reduction of error-field is very important to prevent locked modes. By a Monte-Carlo calculation, the probability is calculated for a range of the error-field amplitude. In non-inductive regimes with Q > 5, resistive wall modes (RWMs) pose a major concern since the normalised beta exceeds the ideal limit without the wall. Recent experiments show that reduction of error field is essential to maintain the rotation speed and thus stability at normalised beta above the no-wall limit. A correction coil (CC) system is adequate to reduce the error field and to stabilise these modes. Active stabilisation with this coil system would be necessary in ITER because of difficulty of large momentum input to the plasma to provide sufficient rotation, an alternative stabilising mechanism.

The ITER device is designed to withstand the consequences of disruption (i.e. electromagnetic and heat loads). This assessment is carried out with conservative assumptions based on the experimental database of current quench time and halo current. Experiments show that runaway electrons are eliminated as soon as the boundary safety factor reaches 2, which reduced the estimated heat load by runaway electron by an order of magnitude. A number of disruption prevention and amelioration measures has been tested in recent experiments, e.g. on disruption avoidance by careful selection of discharge scenarios away from the operation limit, prediction of disruption by neural network, and reduction of halo current by strong gas-puff. To summarise, disruption is acceptable for ITER, and the frequency and consequence of disruption can be further reduced in future.

4 Plasma Performance Assessment

4.1 Introduction

ITER will be the first fusion device with significant Q (the ratio of fusion power to additional heating power) and extended burn. ITER is designed as an experimental device with extensive diagnostics and a considerable flexibility in fusion power, plasma density, beta, shaping, heating and current drive, fuelling methods, and replaceable in-vessel components. This flexibility has been deemed essential for accommodating uncertainty in projection, and

for investigating and optimising the burning plasmas well as to facilitate the exploration of new operation regimes attractive for a reactor. The principal physics goals of ITER are:

(i) to achieve extended burn in inductively-driven plasmas with Q of at least 10 for a range of operating scenarios and with a duration sufficient to achieve stationary conditions on the time scales characteristic of plasma processes;

(ii) to aim at demonstrating steady state operation using non-inductive current drive with a ratio of fusion power to input power for current drive of at least 5.

In addition, the possibility of higher Q operation will be explored if favourable confinement conditions can be achieved.

The reference plasma operating scenario for ITER inductive operation is the ELMy H mode, which has been observed reliably and reproducibly in many tokamaks. Furthermore, the properties of H-mode have been investigated over the last 18 years, establishing the scaling laws for projection. The rules and methodologies for projection of plasma performance to the ITER scale are basically those established in the ITER Physics Basis (IPB)[1]. After completion of the IPB document, continued physics R&D has yielded new results, which are reflected in the present analyses.

The key physics issues relating to plasma performance in the ELMy H-mode regime are the following:

- H-mode confinement at sufficiently high density and beta to produce the requisite fusion power, and hence Q value;
- power and particle exhaust to ensure acceptable levels of helium, plasma impurities and heat load on the divertor target;
- small losses of α-particles via TF ripple or collective instabilities, to enable efficient transfer of α-particle energy to the thermal plasma and to prevent damage to the plasma-facing components;
- global magnetohydrodynamic (mhd) stability and plasma control capability to reduce heat and/or electromagnetic loads due to disruptions and ELMs to ensure adequate life time of the in-vessel components.

The development of plasma operation scenarios that exploit active profile control to access enhanced confinement regimes with an internal transport barrier (ITB), which has occurred in the course of the EDA, has allowed greater emphasis to be placed on the use of such scenarios in ITER. In particular, these regimes offer the prospect of establishing reactor-relevant, steady state operation in which a significant fraction of the plasma current is generated via the bootstrap effect. Although the precise conditions for the development of ITBs are uncertain, the aim has been to provide ITER with the necessary plasma control tools to facilitate access to such modes of operation. Flexibility in the ITER design through plasma shaping, a mixture of heating and current drive systems, and availability of techniques for suppression of neoclassical tearing modes (NTMs) and resistive wall modes (RWMs), favours the exploitation of plasma scenarios with either shallow monotonic or negative central shear. Sophisticated diagnostics of key profiles such as q, pressure, and rotation will be required to operate with a high level of reliability from the first phase of plasma experiments, and this has been acknowledged in assigning measurement priorities. The

[1] ITER Physics Expert Groups et al., ITER Physics Basis, Nucl. Fusion 39 (1999) 2137

question of α-particle losses, via TF ripple, is anticipated to be particularly pronounced in these regimes, and the design of the ferromagnetic inserts reflects this consideration. It is also possible that collective instabilities, e.g. TAE modes, are excited in these regimes, but these instabilities are expected to be tolerable in scenarios with flat or weakly inverted q profiles. High-field-side pellet injection would create a significant density gradient in the far off-axis zone, which is shown to be essential for reducing or eliminating the need for far off-axis current drive. Predictions of steady state operation in ITER, therefore, build upon these recent developments and reflect the expectation that considerable further progress can be achieved in the fusion programme in the future to resolve remaining uncertainties.

This section presents the analysis results on plasma performance, control and operation. In subsection 4.2, the bases of performance analysis are summarised. In subsection 4.3, plasma operation scenarios are described for inductive, hybrid and steady state operation. Subsection 4.4 presents the analysis results of plasma performance. Operation boundaries, sensitivity to assumptions, high-Q, and ignition operation, are assessed. Also discussed are the projections of hybrid and steady state operation, and the requirements for current drive for steady state. The performance projection of the divertor pedestal and ELMs is presented and assessed in subsection 4.5. Subsection 4.6 deals with energetic particle confinement issues, i.e. TAE modes and ripple losses. Subsection 4.7 elaborates the conclusions.

4.2 Performance Analysis Basis

In this subsection, the basis of performance analysis is summarised.

4.2.1 Global Scaling Expression for the Thermal Energy Confinement Time

The thermal energy confinement time of ELMy H-mode, the reference confinement regime for inductive Q = 10 operation, is described by the ITERH-98P(y,2) empirical scaling as

$$\tau_{E,th}^{IPB98(y,2)} = 0.0562 H_{H98(y,2)} I_p^{0.93} B_T^{0.15} \bar{n}_e^{0.41} P^{-0.69} R^{1.97} M^{0.19} \kappa_a^{0.78} \varepsilon^{0.58} \qquad (4.2.1\text{-}1)$$

where the units are s, MA, T, 10^{19}m^{-3}, MW, m, and amu, respectively, $\varepsilon = a/R$, and the elongation κ_a is defined as $\kappa_a = V/(2\pi^2 R a^2)$ with V being the plasma volume. $H_{H98(y,2)}$ denotes a constant normally taken to be unity but varying here between 0.85 and 1.15 in order to assess the sensitivity of the machine performance to energy confinement changes.

4.2.2 Radiation Correction for the Energy Confinement Time

The power P used for scaling derivation is the total heating power with the deduction of power lost through the charge exchange and unconfined ion orbits only[1]. No correction for radiation losses was applied. In ITER, the fraction of the input power lost by radiation is estimated to be more than 30%. The numerical simulations for ITER have led to the following radiation loss account in the expression for the net heating power:

$$P = P_\alpha + P_{oh} + P_{add} - (P_{brem} + P_{cycl} + P_{line}/3) \qquad (4.2.2\text{-}1)$$

[1] K. Thomsen, D.J. Campbell, J.G. Cordey, et al., Nucl. Fusion **34** (1994) 131

where P_α is the α-particle power, P_{oh} the ohmic power, P_{add} the additional heating power, P_{brem} the bremssrtahlung power, P_{cycl} the cyclotron radiation power, and P_{line} the line radiation power.

4.2.3 Temperature and Density Profiles

The temperature and density profiles are estimated using 1.5D transport codes, PRETOR and ASTRA. There are two approaches to calculate the radial dependencies of transport coefficients. It is possible to use the radial dependencies from any specific model[1] or to use formal dependencies such as D and $\chi \sim \gamma_1(1 + \gamma_2 (\rho/\rho_{edge})^2)$ with $\gamma_2 \sim 3$ similar to many experiments[4], and a normalisation factor γ_1 chosen to fit the scaling law for τ_E. The formal approach assumes also some relations, based on the experimental background[3] $\chi_i/\chi_e = 2$, $\chi_i/\chi_\phi = 1$, $D_e/\chi_e = 1$, where χ_ϕ is momentum diffusivity. For helium diffusion, both $D_{He} = \chi_i$, or $D_{He} = \chi_e$ are assumed.

4.2.4 Additional Heating and Current Drive

For nominal operation, the additional heating power of 40 MW is made up of 33 MW of NB and 7 MW of RF heating.

In 1.5D transport simulations using the PRETOR code[2], the RF power is assumed to be deposited in the core region (normalised minor radius r/a < 0.3), with 50% of the power heating the ions and 50% the electrons. For more detailed analysis, the RF power deposition profile and ion heating fraction can be obtained numerically, for example by coupling with the PION ICH&CD simulation code[3]. For sensitivity analyses, the ion heating fraction is varied as a parameter. The normalised current drive efficiency ($\gamma_{CD} = I_{CD}\langle n_e\rangle R/P_{CD}$) for RF is also an input parameter. A typical case for ECCD has $\gamma_{CD} = 0.3\times10^{20}AW^{-1}m^{-2}$ for on-axis current drive and $\gamma_{CD} = 0.1\times10^{20}AW^{-1}m^{-2}$ for current drive in the periphery.

In the ASTRA code[4], the ECCD efficiency and absorption width are calculated by approximate formulae obtained using the OGRAY[5] code, in which ray tracing and Fokker-Planck equations are solved for the fast electrons. For the case of LHH&CD, the driven current profile is prescribed and γ_{CD} is assumed to be $0.3\times10^{20}AW^{-1}m^{-2}$ in the peripheral region.

NB injection in the ASTRA code is calculated using a Fokker-Planck solver taking account of shape of power distribution within the beam footprint, multi-step ionisation cross sections, orbital losses and neo-classical effects[6]. In the PRETOR code, the NB power deposition profile is calculated with a pencil beam assumption and the current-drive efficiency is given with the Mikkelsen-Singer approximation[7]. The ACCOME code is used for detailed analysis and verification of the PRETOR calculation. The injection energy is 1 MeV, and the injection radius and height are varied within the available design range.

[1] ITER Physics Basis, Nucl. Fus. **39** (1999) 2225-2228
[2] D. Boucher, et. al., in Proc. 16th IAEA Fusion Energy Conference, Montreal, 1996 (IAEA,Vienna, 1997) 945
[3] V. Bergeaud, L.-G. Eriksson, D.F.H. Start, Nucl. Fusion 40 (2000) 35
[4] G.V. Pereverzev, et. al., IPP 5/42 (1991)
[5] A.V. Zvonkov, A. Yu. Kuyanov, A.A. Skovoroda, and A.V. Timofeev, Plasma Phys. Rep., 24 (1998) 389
[6] A.R. Polevoi, H. Shirai and T. Takizuka, JAERI Data/Code 97-014
[7] D.R. Mikkelsen and C.E. Singer, Nucl. Technol. /Fusion **4**, 237 (1983)

4.2.5 Helium Contamination and Impurities

The simplest models used for the ITER predictive simulations consider a reduced set of one-dimensional fluid-like equations, which represent the evolution of plasma density, momentum and energy for each of the plasma species[1]. In the reduced version, the charged particle density transport is simulated only for the electron and helium components n_e and n_{He}. For the other impurity species, the fractions of the electron density $n_{zk} = f_k n_e$, are assumed and the fuel densities n_D, n_T are calculated from the quasi-neutrality condition: $n_e = n_D + n_T + 2\, n_{He} + \Sigma_k Z_k n_{zk}$. The electron source S_e is defined from pellet injection and/or from edge neutral fuelling modelling. The helium source S_{He} is defined from fusion reaction calculations. An alternative version of this approach is an n_D, n_T transport simulation with n_e calculated from quasineutrality. The impurity charge Z_k is determined from a coronal equilibrium model[2]. The momentum transport is considered only for the toroidal component. The heat transport description is reduced to the electron heat transport equation with T_e, n_e, and a summarised ion heat transport equation with T_i, $n_I = n_D + n_T + n_{He} + \Sigma_k n_{zk}$, since all ion species have the same temperature on the transport time scale.

4.2.6 Divertor

Divertor modelling is carried out with the B2-Eirene code[3]. This package consists of a two-dimensional, multi-fluid model for the DT and impurity ions and electrons coupled to a Monte-Carlo model for the neutral particles. The main physical assumptions used in the B2-Eirene code package are described in the ITER Physics Basis[4].

4.2.7 Beta Limit

Ideal MHD alone constitutes the basis for the experimental observation that kink and/or ballooning instability onset develops in most cases for $3 \leq \beta_N \leq 4$ (i.e. at ideal MHD limit) or for $\beta_N > 4l_i$ (the wall-at-infinity limit).

Neo-classical tearing modes (NTMs) pose a potential challenge to ITER operation. If NTMs are triggered and uncontrolled in ITER, they will likely limit the attainable normalised β to values of $\beta_N < 2$.

In some steady state scenarios, the minimum safety factor can be made above 2, thus eliminating the possibility of tearing modes of (m,n) = (2,1) and (3,2).

4.2.8 Plasma Density

For ITER, two distinct density-limiting processes observed in present tokamaks are relevant, namely a disruptive limit, and a performance limit causing a confinement degradation in H-mode and ultimately a return to L-mode confinement. The disruptive empirical limit is usually (but not inevitably) characterised by $n_{max} \sim n_G$, (Greenwald density

[1] ITER Physics Basis, Nucl. Fus. **39** (1999) 2178-2184
[2] D.E. Post, et al., Atomic Data and Nuclear Data Tables, **20** (1977) 397
[3] D. Reiter, et al., Plasma Phys. Contr. Fusion **33** (1991) 1579; R. Schneider, et al., J. Nucl. Mater, **196-198** (1992) 810
[4] ITER Physics Basis, Chapter 4: Power and Particle Control, Nucl. Fus. **39** (1999) 2391

n_G [10^{20} m^{-3}] = I[MA]/πa^2[m]). The fraction of Greenwald density where the performance limit sets in is also dependent on the triangularity and on the onset condition for type II ELMs. In the performance calculations here it was characterised by the H-L back-transition based on the H-mode power threshold scaling and is described in the next section.

4.2.9 L to H-Mode Power Threshold

The recommended form for the H-mode power threshold empirical scaling[1] is

$$P_{L\text{-}H} = 2.84 M^{-1} B_T^{0.82} \bar{n}_e^{0.58} R^{1.00} a^{0.81} \quad \text{(rms err. 0.268)} \qquad (4.2.9\text{-}1)$$

in MW, amu, T, 10^{20} m^{-3} and m, respectively, with M being the effective isotopic mass of the plasma fuel. This scaling expression is based on the latest version of the threshold database (DB3) including results from recent dedicated H-mode threshold experiments in Alcator C-Mod and JT–60U, the latter using the new 'W' shaped divertor. For ITER-like devices, this scaling yields an H-mode power threshold prediction which is approximately a factor of 2 lower than that predicted by an earlier version[2]. $P_{L\text{-}H}$ is defined as the total input power in the threshold database. In ITER analyses $P_{L\text{-}H}$ is calculated by Eq. (4.2.2-1), which gives an about 30% more conservative value.

4.3 Plasma Operation Scenarios

4.3.1 Inductive Operation Scenarios

The time evolution of plasma parameters is investigated by the 1.5D transport codes PRETOR[3] and ASTRA[4]. Here, the plasma shape is fixed during the simulation and the 2D equilibrium is re-computed if the pressure change exceeds a given value. The PF coil system is consistent with the scenarios throughout the whole phase of the plasma operation. Time histories of plasma parameters such as plasma current (I_P), electron density (n_e), electron and ion temperature (T_e, T_i), heating power by NB (P_{NB}), heating power by RF (P_{RF}), safety factor at 95% flux surface (q_{95}), safety factor at the magnetic axis (q_0) and fusion power (P_{FUS}) are calculated.

Figure 4.3.1-1 shows the time evolution of plasma parameters in a typical operation scenario with the flat-top current of 15 MA. The simulation is performed from the X-point formation (XPF) to the end of burn (EOB). Plasma heating starts just after the current flat top. At this time, the electron density should be small enough to keep the threshold power (P_{LH}) for L-H transition low and large enough to avoid shine-through of neutral beams. In this case, NB heating (16.5 MW, 1 MeV) starts at 100 s when $\langle n_e \rangle = 4\times10^{19} m^{-3}$. In the simulation, the H-mode transition occurs at 110 s when the second NB is started and the total NB power increases to 33 MW. During the flat top phase, 33 MW of NB and 7 MW of RF heating are used and about 400 MW of fusion power is produced (Q = 10). 2% impurity of beryllium is assumed and the helium accumulation is calculated for the pumping speed which provides $\tau_{He}^*/\tau_E = 5$.

[1] J.A. Snipes et al., Plasma Phys. Control. Fusion **42** (2000) A299-A308
[2] ITER Physics Basis, Chapter 2 Section 4.3 (Eq. (5) in Table 2), Nucl. Fus. **39** (1999) 2196
[3] D. Boucher, et al., in Proc. 16th IAEA Fusion Energy Conference, Montreal, 1996 (IAEA,Vienna, 1997) 945
[4] G.V. Pereverzev, et al., IPP 5/42 (1991)

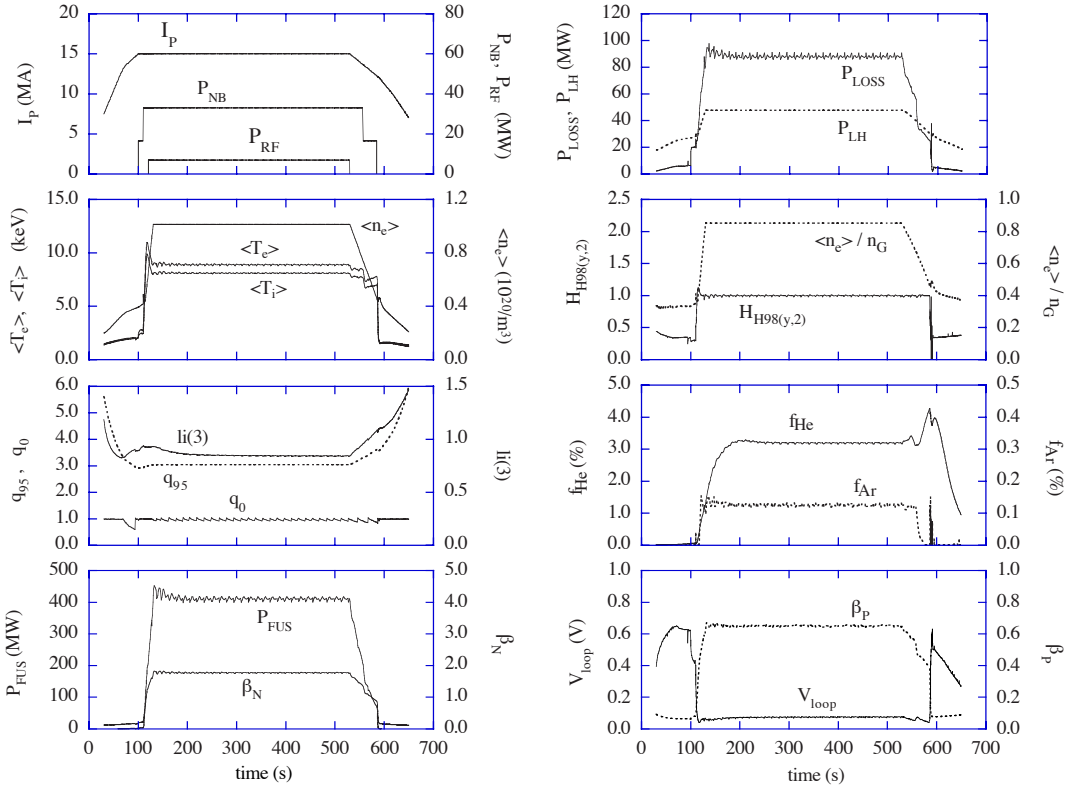

Figure 4.3.1-1 Time Evolution of Plasma Parameters

Here, plasma current (I_P), neutral beam heating power (P_{NB}), RF heating power (P_{RF}), volume-averaged electron density ($<n_e>$), electron and ion temperatures ($<T_{e,i}>$), safety factor at 95% flux surface (q_{95}), safety factor at the magnetic axis (q_0), internal inductance ($l_i(3)$), fusion power (P_{FUS}), normalised beta (β_N), loss power (P_{LOSS}), L-H transition threshold power ($P_{L\text{-}H}$), Greenwald parameter ($<n_e>/n_G$), HH-factor ($H_{H98(y,2)}$), average helium fraction (f_{He}), argon fraction (f_{Ar}), loop voltage (V_{loop}), and poloidal beta (β_P) are shown.

Argon impurity up to 0.12% is seeded. The necessary seeding fraction is calculated on the basis of a simplified divertor model[1] to keep the power to the divertor region at a conservatively low value, i.e., about 30 MW, which gives less than 5 MW/m^2 on the divertor target. In this example, additional 37 % is radiated outside the separatrix and the total heat load to the divertor target is 30 MW. However, the allowable heat load is 60 MW on the divertor target, therefore, the minimum requirement for the radiation cooling outside the separatrix is 13%.

The corresponding effective charge (Z_{eff}) of 1.66 and a helium contribution of about 0.16 with f_{He}(axis) = 4.3% are obtained. The power P_{LOSS} across the pedestal top is 87 MW (the power P_{SOL} across the separatrix flux surface is about 75 MW). This power and a separatrix density of 3×10^{19}m^{-3} are taken as input for a 2D divertor simulation code and are shown to be consistent with acceptable divertor conditions[2], where the separatrix density of 3×10^{19}m^{-3} is assumed as a conservative estimate. The loop voltage at the flat top is about 75 mV and the burn time is estimated to be 400 s with an available flux of 30 Vs. To come to the final plasma shutdown, the transition to L mode occurs at 580 s, when all the heating power is

[1] M. Sugihara, et al., 12th PSI Conference in Controlled Fusion Devices, St. Raphael (1996)
[2] A. Kukushkin, et al., 14th PSI Conference, Rosenheim (2000)

switched off. The main physics parameters during flat top for both 400 MW and 500 MW operation scenarios are summarised in Table 4.3.1-1.

Table 4.3.1-1 Parameters of ITER Inductive Operation Scenarios

Parameter	400 MW	500 MW
R/a (m/m)	6.2/2.0	6.2/2.0
Volume (m^3)	831	831
Surface (m^2)	683	683
Sep.length (m)	18.2	18.2
$S_{cross\text{-}sect.}$ (m^2)	21.9	21.9
B_T (T)	5.3	5.3
I_P (MA)	15.0	15.0
κ_X/δ_X	1.85/0.48	1.85/0.48
κ_{95}/δ_{95}	1.70/0.33	1.70/0.33
l_i (3)	0.84	0.84
V_{loop} (mV)	75	75
q_{95}	3	3
β_N	1.8	2.0
$<n_e>$ (10^{19} m^{-3})	10.1	11.3
$<n_e>/n_G$	0.85	0.94
$<T_e>$ (keV)	8.8	8.9
$<T_i>$ (keV)	8.0	8.1
$<\beta_T>$ (%)	2.5	2.8
β_p	0.65	0.72

Parameter	400 MW	500 MW
$P_{RF} + P_{NB}$ (MW)	7 + 33	17 + 33
P_{OH} (MW)	1	1
P_{TOT} (MW)	121	151
P_{BRM} (MW)	21	26
P_{SYN} (MW)	8	8
P_{LINE} (MW)	18	27
P_{RAD} (MW)	47	61
P_{FUS} (MW)	400	500
$P_{LOSS}/P_{L\text{-}H}$	87/48	104/51
Q	10	10
τ_E (s)	3.7	3.4
W_{th} (MJ)	320	353
W_{fast} (MJ)	32	34
$H_{H98\,(y,2)}$	1.0	1.0
τ_{He}^*/τ_E	5	5
$Z_{eff,\,ave}$	1.66	1.72
$f_{He,axis\,/\,ave}$ (%)	4.3/3.2	4.4/3.2
$f_{Be,axis}$ (%)	2.0	2.0
$f_{Ar,axis}$ (%)	0.12	0.14

4.3.2 Hybrid Operation Scenario

A hybrid mode of operation, in which a substantial fraction of the plasma current is driven by non-inductive current drive power and the bootstrap current, is a promising route towards the establishment of true steady state modes of operation. Operation longer than 1,000 s with Q = 5 is investigated with current drive power up to 100 MW and a modest requirement on confinement ($H_{H98(y,2)}$ = 1.0). In this section, the burn time of hybrid mode operation is estimated. In order to optimise the plasma parameters such as plasma current, a simple formula[1] is used for the estimation of flux available for the burning. Current-drive efficiency of NB injection is given by the Mikkelsen-Singer approximation[2] and the normalised current drive efficiency for RF is fixed to $0.3\times10^{20}AW^{-1}m^{-2}$. A Gaussian-type RF power deposition profile in the core (normalised minor radius r/a < 0.3), with 50% to ions and 50% to electrons, is assumed. The NB current drive efficiency was verified by the ACCOME code.

Figure 4.3.2-1 shows the achievable burn duration as a function of fusion gain Q. Here, 0D modelling is used and the plasma current is optimised under the condition that the maximum normalised beta β_N and the ratio $<n_e>/n_G$ of electron density to Greenwald density are given. It is seen from Figure 4.3.2-1 that the maximum burn time for operation with Q = 10 is about 500 s when full size plasma (R/a = 6.2 m/2.0 m) is adopted. In this case, I_P = 14.2 MA and P_{FUS} = 320 MW for the flat density profile. Operation with Q > 10 is possible with a limited

[1] Y. Murakami and M. Sugihara, Fusion Technology, **24**, (1993) 375
[2] D.R. Mikkelsen and C.E. Singer, Nucl. Technol., Fusion **4**, (1983) 237

burn time. The burn time increases with decreasing Q and I_p. It is seen that operation with burn time of 1000 s is possible when Q = 5. In the low-Q region (Q < 10), the burn time can be prolonged by adopting a plasma with a smaller minor radius (R/a = 6.35 m/1.85 m). The achievable burn time is about 1300 s when Q = 5, β_N = 2.0 and $<n_e>/n_G$ = 0.85. In this case, the fusion power is 350 MW, and the current drive power is 70 MW. (The fusion power depends on the plasma profiles). If β_N can be increased to 2.5, the expected burn time becomes longer than 2000 s. In the high-Q region, the burn time is not sensitive to β_N but can be prolonged by increasing the operating density. The burn time can be prolonged further if the flux Ψ_{HEAT} used for heating (10 Vs) at the plasma current flat top is reduced by heating the plasma before the flat top.

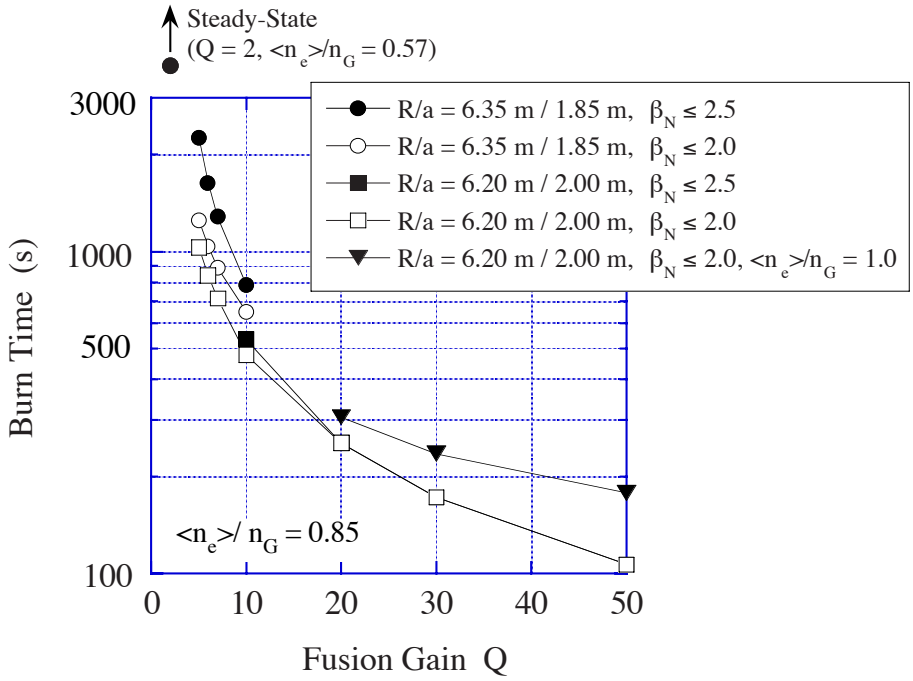

Figure 4.3.2-1 Fusion Gain and Burn Time for Hybrid Mode of Operation

1.5D transport simulation is also done for the hybrid operation. The results are shown in Table 4.3.2-1 (#1 ~ #4). All of these scenarios satisfy Q ≥ 5 and a burn time ≥ 1000 s at $H_{H98(y,2)}$ = 1.0. The scenarios #1 and #3 are compatible with the additional heating power available in the initial phase of operations (73 MW), while #2 and #4, with a fusion power of 500 MW, require a total additional heating power of 100 MW. The scenarios #1, #2 and #3 use full-size plasmas (R/a = 6.2 m/2.0 m) and #4 uses the plasma with a smaller minor radius (R/a = 6.35 m/1.85 m). This plasma can be produced in the vacuum vessel of ITER by shifting the magnetic axis outward. In this case, the plasma elongation can be increased to 1.8. These scenarios are also consistent with the magnet system.

The advantage of scenarios using a plasma with smaller minor radius is a longer burn time, consequent to the smaller plasma current, larger required β_N and available bootstrap current fraction. These scenarios show that very long pulse operation regimes are accessible in ITER with a modest improvement.

Table 4.3.2-1 PRETOR Simulation Results for Hybrid Operations

	Scenario 3			
	Hybrid #1	Hybrid #2	Hybrid #3	Hybrid #4
R (m)/a (m)	6.2/2.0	←	←	6.35/1.85
κ_{95}/δ_{95}	1.7/0.33	←	←	1.8/0.35
V_P (m^3)	831	←	←	770
B_T (T)	5.3	←	←	5.17
I_P (MA)	13.8	14.4	13.3	12.6
q_{95}	3.3	3.2	3.5	3.1
$<n_e>$ ($10^{19}m^{-3}$)	9.3	10.0	9.0	11.0
$<n_e>/n_G$	0.85	←	←	0.94
$<T_i>$ (keV)	8.4	9.4	8.2	8.5
$<T_e>$ (keV)	9.6	10.9	9.1	9.7
β_N	1.9	2.2	1.9	2.3
P_{FUS} (MW)	400	500	350	500
P_{NB} (MW)	33	60	33	60
P_{RF} (MW)	40	40	40	40
$Q = P_{FUS}/(P_{NB}+P_{RF})$	5.4	5.0	4.8	5.0
P_{LOSS}/P_{L-H}	114/45	151/47	113/45	154/47
τ_E (s)	2.73	2.40	2.62	2.26
$f_{He,\,axis/ave}$ (%)	3.5/2.5	3.9/2.7	2.9/2.2	3.3/2.5
$f_{Ar,\,axis}$ (%)	0.19	0.25	0.15	0.20
$Z_{eff,\,ave}$	1.85	2.03	1.73	1.88
P_{RAD} (MW)	55	72	44	67
P_{Sep} (MW)	99	128	100	133
β_p	0.76	0.83	0.77	1.01
l_i (3)	0.91	0.87	0.88	0.81
I_{CD}/I_P (%)	25	32	28	29
I_{BS}/I_P (%)	17	20	18	21
γ_{20}^{NB} ($10^{20}A/Wm^2$)	0.24	0.26	0.26	0.23
γ_{20}^{RF} ($10^{20}A/Wm^2$)	0.30	←	←	←
γ_{20}^{TOT} ($10^{20}A/Wm^2$)	0.27	0.27	0.28	0.26
τ_{He}^*/τ_E	5	←	←	←
$H_{H98(y,2)}$	1.0	←	←	←
V_{loop} (mV)	56	46	53	46
Burn flux (Vs)	60	56	68	74
Burn time (s)*	1070	1220	1280	1610

* Burn time for the case that the flux used during the heating phase is saved

If the erosion due to type I ELMs gives a short life time of the divertor target, a hybrid operation with a larger q_{95}, typically ≥ 3.5, and small ELMs would be suitable for high fluence tests. One possible example is Hybrid #3 shown in Table 4.3.2-1.

The results for plasmas with smaller minor radius (R/a/κ = 6.35 m/1.85 m/1.8) are also shown. (This plasma can be produced in the ITER vacuum vessel by shifting the magnetic axis outward.)

4.3.3 Steady State Operation Scenario

In the steady state (SS) operation scenario the total plasma current at the current flat-top phase is generated non-inductively by additional current drive (NB and RF) and bootstrap current. A conventional ELMy H-mode with $H_{H98(y,2)}$ gives a low Q, i.e., Q ~2 in a steady state operation. To provide SS operation in ITER with Q > 5 with the available additional power (P_{NB} < 50 MW,P_{IC} + P_{EC} + P_{LH} < 80 MW) it would be necessary to decrease the plasma current to I_p ~ 9 MA. In this case the bootstrap current fraction will increase due to an increase of the poloidal beta ($I_{bs}/I_p \propto \beta_p \propto I_p^{-1}$). To obtain the required CD efficiency for full steady state operation with Q > 5, an improved confinement with $H_{H98(y,2)}$ ~ 1.5-1.6 is necessary. In present-day experiments such confinement is achieved and sustained up to ~2.6 s in regimes with specially shaped safety factor profiles, associated with internal transport barriers (ITB)[1,2]. The ITB appears in the discharges with strong negative shear (SNS) with q(0) ~q_{95} ≥ q_{min} ≥2, weak negative shear (WNS) with q_{95}> q(0) > q_{min} > 1, or weak positive shear $rq'/q < 1$ (WPS) with q(0) > 1.

An example set of steady state plasma parameters and profiles for WNS snenario is shown in Table 4.3.3-1 and Figure 4.3.3-1. Here, the 1st NB is injected at the position closest to the magnetic axis (distance from the magnetic axis ΔZ ~ 0.38 m at R = 6.2 m) and the 2nd NB is injected at the outer most position (ΔZ ~ 0.95 m). LH power is also injected at R_{LH}-R=1.25m and the normalized current drive efficiency is assumed to $\gamma_{20} = 0.3 Aw^{-1}m^{-2}$. In this scenario, the zone of the improved confinement propagates to 70% of the minor radius but the central electron and ion temperatures are moderate because of high neoclassical heat conductivity χ_{iNeo}. The shape of the profiles is similar to what is obtained in some present day ITB experiments[1].

[1] F.X. Soldner et al., Nucl. Fus. **39** (1999) 407
[2] Y. Kamada and the JT-60 Team, "Extended JT-60U Plasma Regimes toward High Integrated Performance", Proc. 18th IAEA Fusion Energy Conference, Sorrento, Italy, (2000), IAEA-CN-77/OV1/1

Table 4.3.3-1 ITER Parameters for the Non-Inductive Scenario

Parameter	WNS	Parameter	WNS	Parameter	WNS
R/a (m/m)	6.35/1.85	β_N	2.95	f_{He} (%)	4.1
B_T (T)	5.18	β_p	1.49	f_{Be} (%)	2
I_p (MA)	9.0	P_{fus} (MW)	356	f_{Ar} (%)	0.26
κ_{95}/δ_{95}	1.85/0.4	$P_{L-H} + P_{NB}$ (MW)	29 + 30	Z_{eff}	2.07
$<n_e> (10^{19}m^{-3})$	6.7	Q	6.0	P_{rad} (MW)	37.6
n/n_G	0.82	W_{th} (MJ)	287	P_{loss} (MW)	92.5
$<T_i>$ (keV)	12.5	$P_{loss}/P_{thr. L-H}$	2.59	τ_E (s)	3.1
$<T_e>$ (KeV)	12.3	β_T %	2.77	τ_α^*/τ_E	5.0
I_{CD}/I_p (%)	51.9	l_i (3)	0.72	$H_{H98\,(y2)}$	1.57
I_{bs}/I_p (%)	48.1	$q_{95}/q_o/q_{min}$	5.3/3.5/2.2		
I_{OH}/I_p (%)	0				

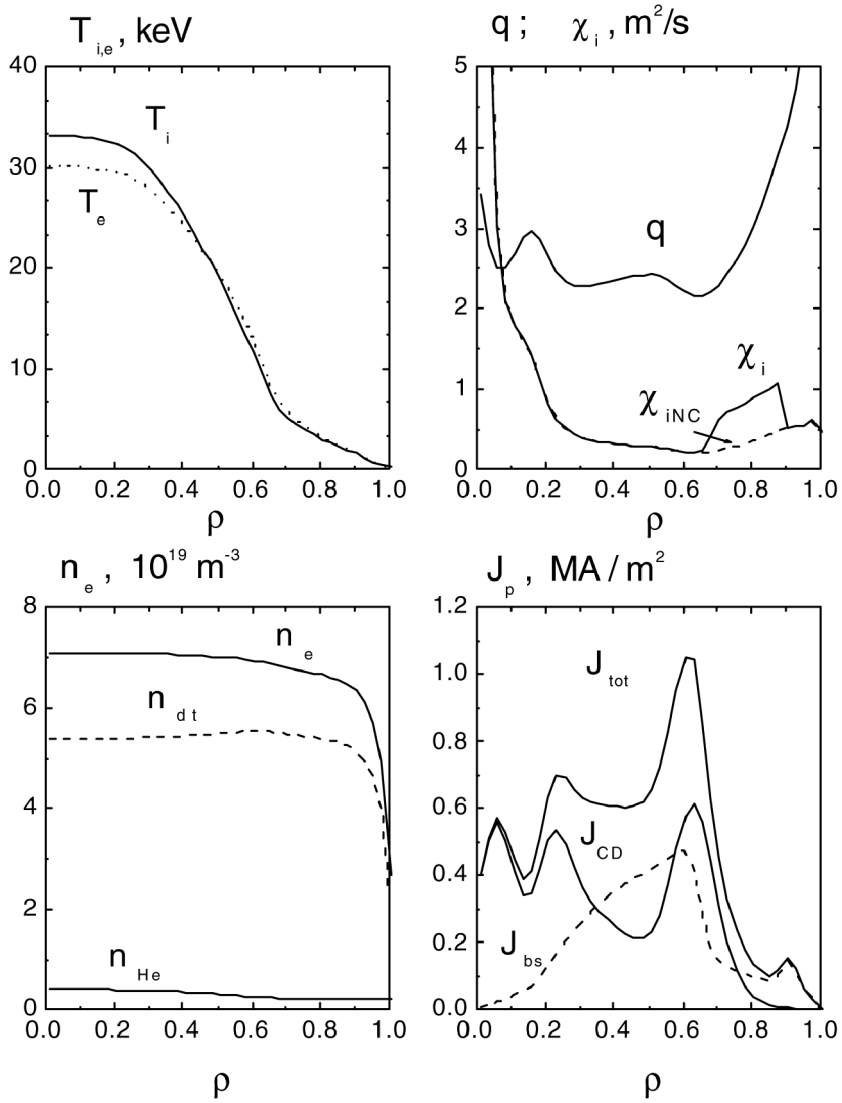

Figure 4.3.3-1 Plasma Parameter Profiles at the Current Flat-top Phase (t > 1000 s) for the Steady State WNS Operational Scenario

4.4 Plasma Performance Assessment

4.4.1 Flexibility and Plasma Performance Optimisation

4.4.1.1 Operation Boundary

The operation domain plot in H_H factor and fusion power space is a useful tool to analyse the performance of ITER. Figure 4.4.1-1 shows such a plot resulting from 1.5D simulations using PRETOR[1]. Here, the fusion power as a function of $H_{H98(y,2)}$ for various operation conditions is presented when I_P = 15 MA. Each point of the domain corresponds to a fusion gain Q = 10. Here, β_N is the normalised beta, n_G is the Greenwald density P_{LOSS} is the power across the H-mode edge pedestal and P_{L-H} is the power required for the H-mode transition[2]. The power assumed to be required for a good confinement is $1.3\times P_{L-H}$. When $H_{H98(y,2)}$ = 1.0 and $<n_e>/n_G$ = 0.85, 400 MW of fusion power is produced.

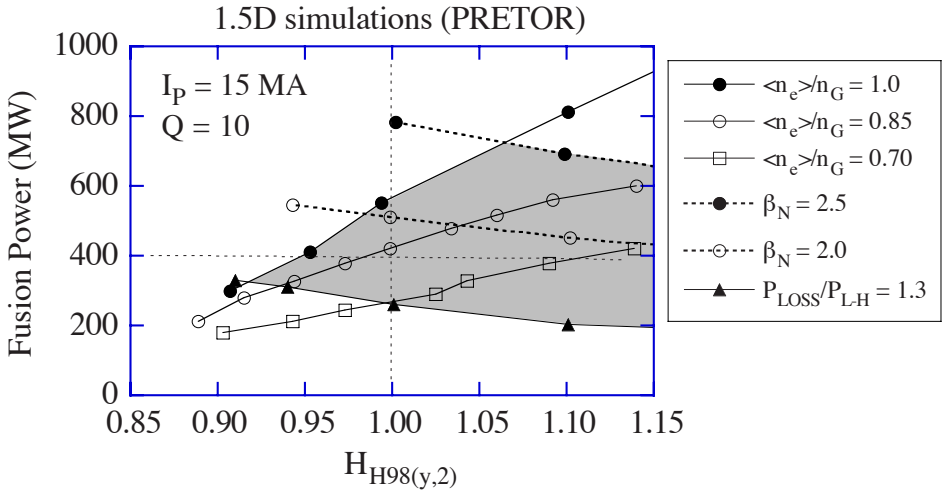

Figure 4.4.1-1 Operation Domain in H_H-factor and Fusion Power Space when I_P = 15 MA and Q = 10

If the operation boundaries are given by $<n_e>/n_G$ = 1.0, β_N = 2.5 and P_{LOSS}/P_{L-H} = 1.3 (shaded area in the figure), the maximum and minimum fusion powers are 560 MW (point B) and 260 MW, respectively, when $H_{H98(y,2)}$ = 1.0. It is also seen that about 8 % of confinement margin (margin in H_H factor to achieve operation with Q = 10) exists.

A possible range of Q is given in Figure 4.4.1-2, showing results of PRETOR calculations of fusion power, Q values, $<T_e>$, $<T_i>$, β_N, f_{Ar}, Z_{eff}, P_{BRM}, P_{LIN}, and P_{SYN} as a function of P_{ADD} for a plasma with I_P = 15 MA, τ_{He}^*/τ_E ~ 5 and $<n_e> = 1.19\times10^{20}m^{-3}$ ($<n_e>/n_G$ = 1.0). Ar is seeded to limit $P_{Divertor}$ ~ 30 MW(~5 MWm^{-2}). As the additional heating power is reduced, Q increases, to exceed 20 at Padd ≤ 20 MW. The upper limit of Q is determined by the H-L transition. The boundary given by the condition of P_{LOSS} greater than than 1.3 x P_{L-H} is indicated in the Figure.

[1] D. Boucher, et al., Proc. 16th IAEA Fusion Energy Conference, Montreal, 1996 (IAEA,Vienna, 1997) 945
[2] ITER Physics Basis, Nucl. Fus. **39**(1999) 2137

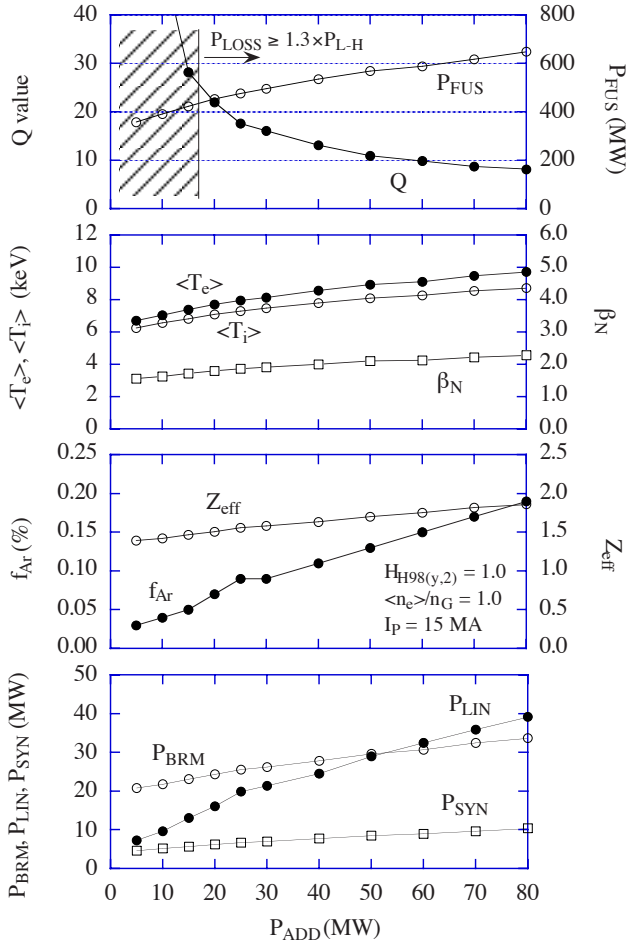

Figure 4.4.1-2 1.5D Simulation Results of Plasma Performance
Here, I_P = 15 MA, τ_{He}^*/τ_E = 5 and $<n_e> = 1.19\times10^{20}m^{-3}$ ($<n_e>/n_G = 1.0$).
Ar is seeded to limit $P_{Divertor} \sim$ 30 MW(~ 5 MW/m^2)

4.4.1.2 Sensitivity Analyses

(1) Density and temperature profile effects
In general, peaked density profiles tend to produce larger fusion power for the same average density and even more for the same pedestal density. Here, the density profile effect is examined by including the inward pinch effect, as an example. This kind of profile could be achieved also with deep fuelling by high field side (HFS) pellet injection. Figure 4.4.1-3a shows the density profiles when a pinch term proportional to the thermal diffusivity χ and to the magnetic shear is included with a different pinch coefficient V_P. In this modelling, the pinch effect is not significant in the core region (r/a < 0.5) where the shear is small. Figure 4.4.1-3b shows the fusion power for various pinch coefficients. Here, the volume-averaged density is fixed to $1.0\times10^{20}m^{-3}$, which corresponds to n_e/n_G = 0.85 for the flat profile. It is seen that significantly higher fusion power is available in the nominal to high H_H factor region, while the margin below 1.0 in H_H factor is not increased in the lower fusion power region. Helium accumulation due to the pinch effect also degrades performance. If a peaked density profile is achieved by using HFS pellet injection, a more significant improvement is expected.

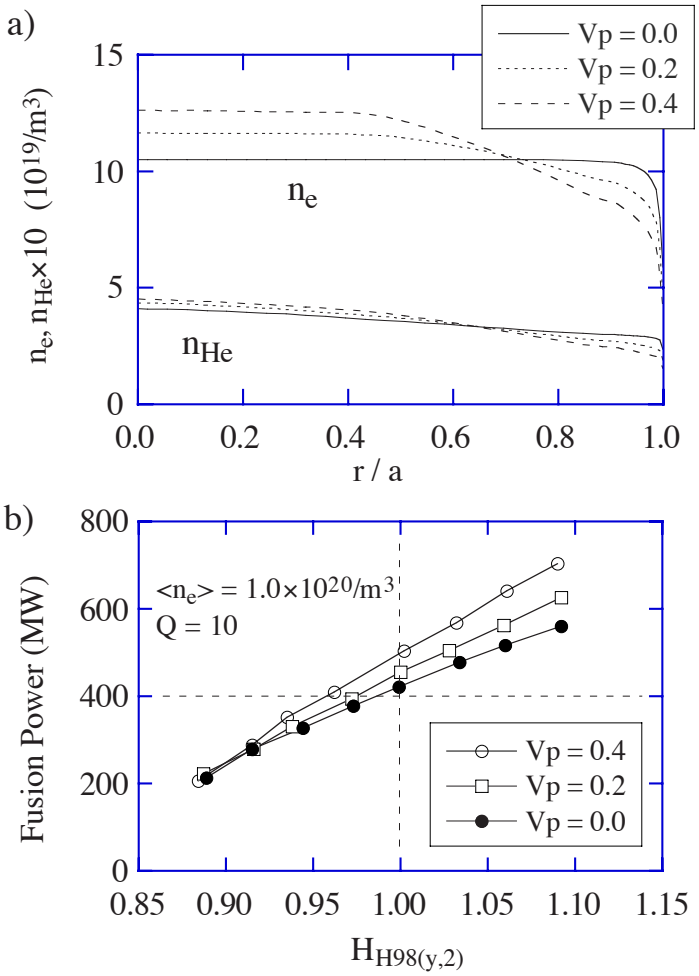

Figure 4.4.1-3 a) Density Profiles for Various Pinch Coefficients V_p, b) Dependence of Fusion Power on the H_H Factor for the Pinch Coefficients shown in (a)

(2) Dependence on χ_i/χ_e ratio

The ratio of ion thermal diffusivity to electron thermal diffusivity χ_i/χ_e is assumed to be 2 for the reference case with additional dependencies such as $(T_e/T_i)^{0.5}$. This χ_i/χ_e value was chosen as a conservative assumption although $\chi_i/\chi_e < 1$ is obtained in many experiments. Figure 4.4.1-4 shows the relation between χ_i/χ_e and fusion power for two types of transport coefficients profiles, the RLWB model[1] and parabolic model ($\chi_e = c_0(1+4(r/a)^2)$) both with normalisation factor c_0. It is seen that the fusion power increases with decreasing χ_i/χ_e for both models and the present assumption ($\chi_i/\chi_e = 2$) is conservative.

[1] D. Boucher and P-H. Rebut, in Proc. IAEA TCM on Advances in Simulations of Modeling of Thermonuclear Plasmas, 1992, IAEA, Vienna, (1993) 142

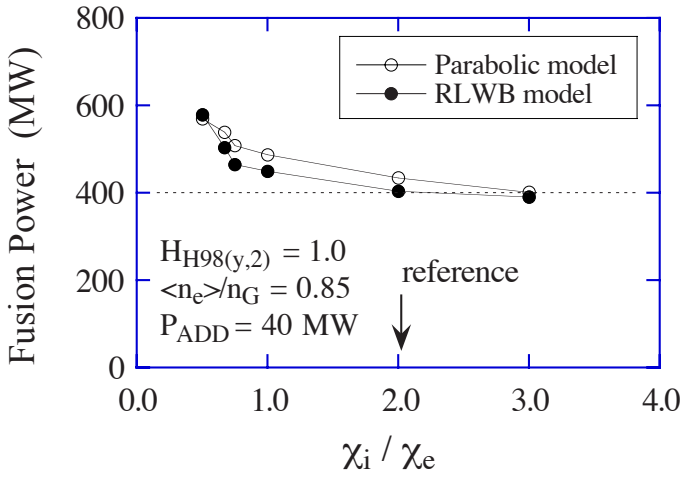

Figure 4.4.1-4 Dependence of Fusion Power on χ_i/χ_e when $H_{H98(y,2)} = 1.0$, P_{ADD} = 40 MW and $<n_e>/n_G = 0.85$

(3) Effect of ion heating fraction

The increase of the ion heating fraction is also favourable for the improvement of operation performance. Figure 4.4.1-5 shows the relation between the H_H factor and fusion power for different ion heating fractions P_i/P_{RF}. Here, all heating power is RF and the total heating power $P_{RF} = P_i+P_e$ is adjusted to Q = 10 with $<n_e>/n_G = 0.85$. In the figure, the NB-heating-only case is also shown. It is seen that the fusion power increases with P_i/P_{RF} through the H_H range, and the lower H_H margin is also improved.

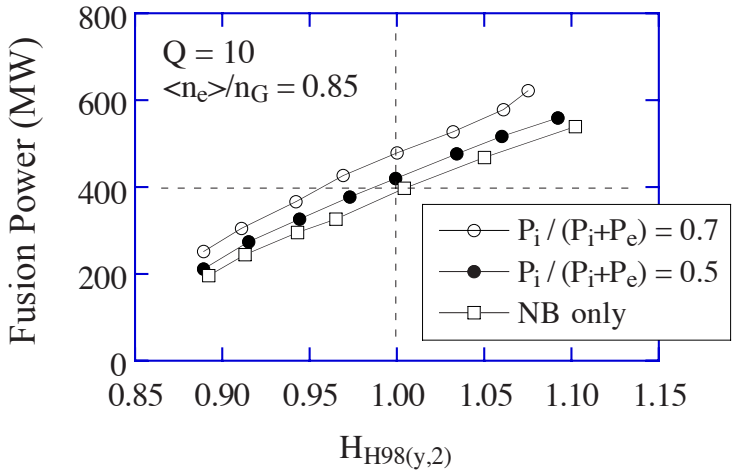

Figure 4.4.1-5 Dependence of Fusion Power on H_H-factor for Various Ion Heating Fractions

4.4.1.3 Operation with Higher Plasma Current, High Q and Ignited

One of the possible scenarios in ITER foresees a total plasma current up to 17MA albeit with some additional engineering margins which may or may not actually apply given inevitable conservatism in the design. Under the condition of an increased plasma current to 17 MA, clearly the operation boundary is significantly expanded, leaving ignition as a possibility even when $H_{H98(y,2)} = 1.0$ and $<n_e>/n_G = 0.85$.

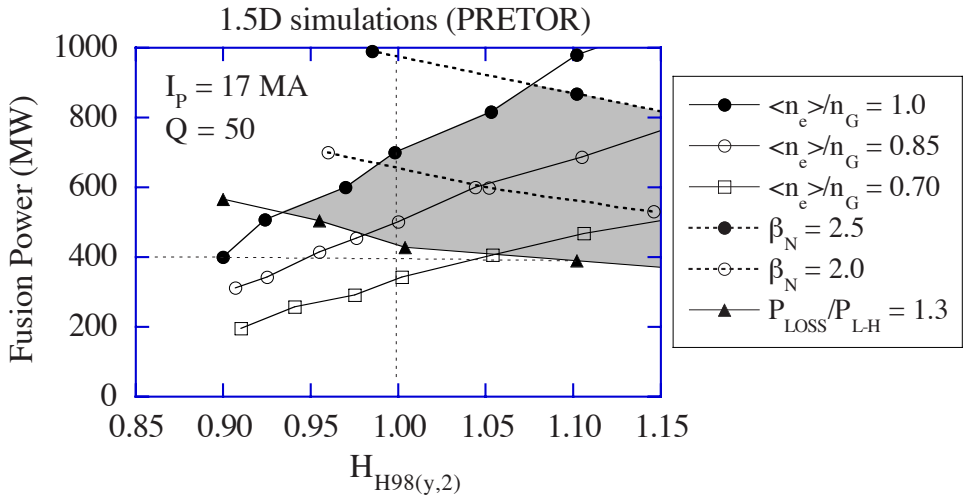

Figure 4.4.1-6 Operation Domain in H_H factor and Fusion Power Space when I_P = 17 MA and Q = 50

Figure 4.4.1-6 shows the operation domain in $H_{H98(y,2)}$ and fusion power space when Q = 50 and I_P = 17 MA. If the operation boundaries are given by $<n_e>/n_G = 1.0$ and $P_{LOSS}/P_{L-H} = 1.3$ (shaded area in the plot), the minimum and maximum fusion powers are 450 MW and 650 MW respectively, when $H_{H98(y,2)} = 1.0$. It is also seen that operation with Q = 50 is possible with certain margin even if the density boundary is set to $<n_e>/n_G = 0.85$.

Figure 4.4.1-7a shows PRETOR simulation results for high-Q operation when the plasma current is 17 MA and the electron density is 1.1×10^{20}m^{-3} ($\sim 0.81\times n_G$). The helium accumulation is again calculated by assuming $\tau_{He}^*/\tau_E = 5$. During the plasma flat top, the additional heating power (P_{ADD}) is 10 MW and about 450 MW (Q = 45) of fusion power (P_{FUS}) is produced. In this scenario, 73 MW of additional heating power is required from 10 s to 13.5 s to achieve the H-mode transition. Here, P_{L-H} is the threshold power for the L-H transition and P_{LOSS} is the power across the H-mode pedestal. In the early phase of the discharge, fusion power excursion is observed. This result implies that ignition is possible by turning off the additional heating power for a short period.

Figure 4.4.1-7b shows a simulation for a fully ignited operation. The heating power P_{ADD} is turned off at t = 13.5 s and other assumptions are the same as for Figure 4.4.1-7a. When the heating power is turned off, the helium level is very small and the self-heating power is large enough for H-mode operation. Therefore, the ignition state is maintained for about 40 s and the L-mode transition occurs at t = 55 s. In this study, a hysteresis for HL-transition is conservatively not assumed.

Since the pumping rate can be increased up to 400 Pa m^{3}s^{-1} for a short period, operation with $\tau_{He}^*/\tau_E < 5$ could be even more likely. Figure 4.4.1-8 shows the results for various helium accumulation levels. The ignition operation continues in steady state when $\tau_{He}^*/\tau_E = 4$. It is seen that the transient ignition experiment can be performed even for lower pumping efficiency ($\tau_{He}^*/\tau_E = 7$).

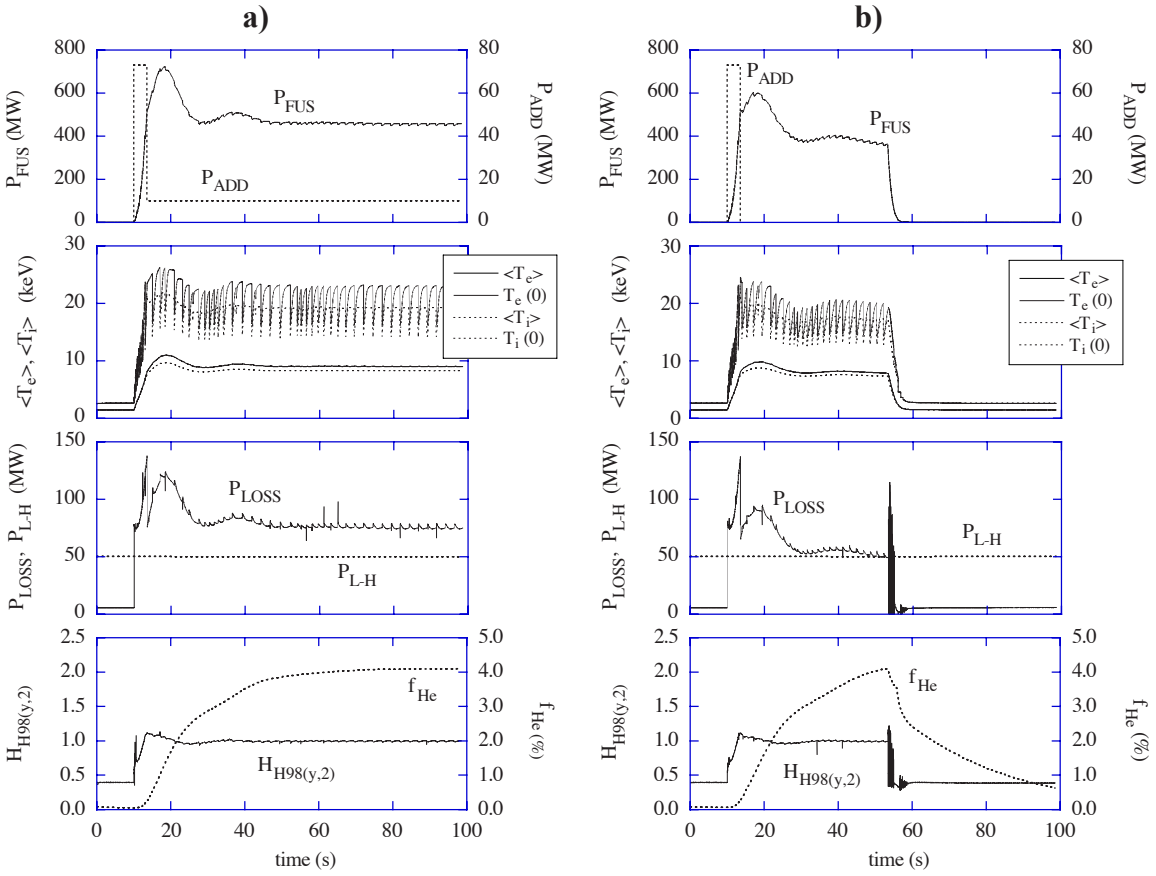

Figure 4.4.1-7 Evolution of Plasma Parameters for High-Q Operation
I_P = 17 MA, $\langle n_e \rangle = 1.1\times10^{20}/m^3$ ($\langle n_e \rangle / n_G = 0.81$) and $\tau_{He}^*/\tau_E = 5$. a) Q = 45, b) Q = ∞

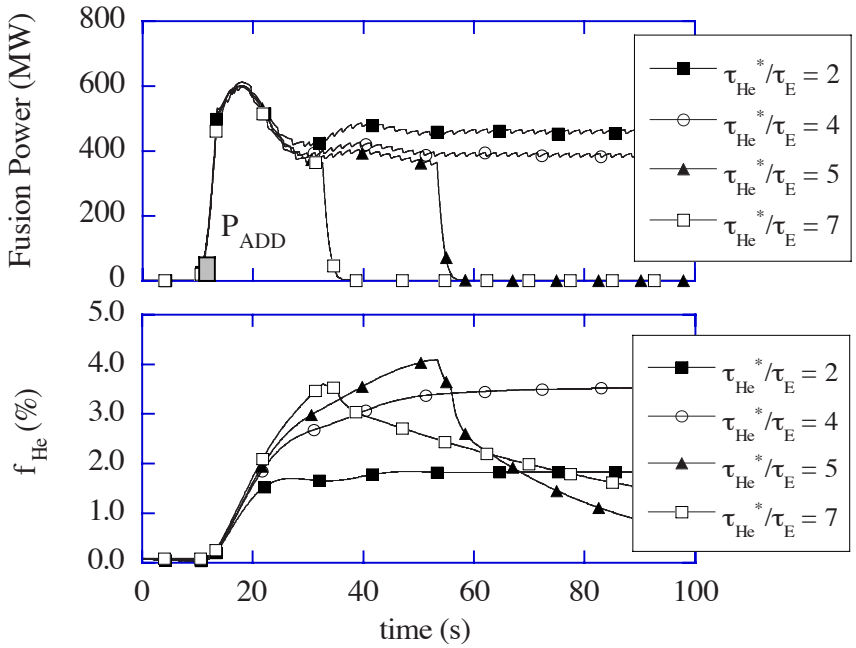

Figure 4.4.1-8 Evolution of Fusion Power and He Fraction for Various τ_{He}^* Assumptions

Here, I_P = 17 MA, $\langle n_e \rangle = 1.1\times10^{20} m^{-3}$ ($\langle n_e \rangle / n_G = 0.81$) and P_{ADD} = 73 MW from t = 10 s to t = 13.5 s. L-mode transition occurs when $P_{LOSS} < P_{L-H}$

4.4.2 Projection of Steady State Operation and Assessment

Here, the SS operation scenario is described on a basis similar to present day experiments. The results of 1.5D transport simulations with ASTRA code[1] are presented. In these analyses, realistic NBH&CD modelling[2] in ITER geometry has been used. ECCD parameterisation for absorption width and CD efficiency has been computed based on the OGRAY simulations[3], and for LHCD a semi-empirical approach was utilized, prescribing absorption width and position (in the outer region r/a > 0.5) with a CD efficiency $\gamma_{20} = 0.3$ $AW^{-1}m^{-2}$. The plasma parameters for WNS, WPS, SNS and Low-Q scenarios are presented in Table 4.4.2-1. Absence of q = 2, 1.5 and 1 surface inside the plasma eliminates the growth of tearing modes.

4.4.2.1 Weak Negative Shear Scenario

After the plasma initialisation phase, the plasma current profile is almost flat with high central q(0) ~ 2. Such a profile is close to the desirable one during the current flat-top phase. To prevent current peaking, a fast current ramp-up rate and an additional heating power are required.

After the X-point formation, the RF heating power is increased gradually to 29 MW to provide the L-H transition at low density. Each of two NB injectors (on-axis and off-axis) delivers 15 MW. The gradual replacement of carbon by argon keeps the loss power from the core to the separatrix at a level compatible with the divertor constraints, i.e. $P_{loss} < 100$ MW.

In the considered scenario the resistive voltage drops to zero in ~ 100 s. A complete steady state current profile relaxation takes about 2000 s. The steady state plasma profiles of scenario 4 are presented in Figure 4.3.3-1. The scenario 4 requires $\beta_N = 2.95$, which is slightly above the no-wall limit (~ 4 $l_i = 2.88$). The second scenario of WNS requires a lower value of $\beta_N = 2.69$, but li is low (4 $l_i = 1.72$).

4.4.2.2 Strong Negative Shear Scenario

Early application of 9 MW of ECRH power and 2 MW of RFheating power increases the skin time and prevents the current redistribution. After the X-point formation the RFpower is increased to 40 MW to provide the L-H transition. After the density reaches sufficiently high value, neutral beam injection is started and P_{NB} increases to 20 MW.

The high central q values would increase alpha particles losses and reduce plasma performance. For these reasons the SNS configuration looks less promising for ITER SS operation. In all of these regimes, Q > 5, but the normalised beta exceeds the ideal mhd limit without wall, thus requiring stabilization of resistive wall modes (RWMs).

[1] G.V. Pereverzev, et al., IPP 5/42 (1991)
[2] A.R. Polevoi, T. Takizuka, H. Shirai, “Benchmarking of the NBI Block in ASTRA Code Versur the OFMC Calculations", JAERI Data/Code 97-014, (1997)
[3] A.V. Zvonkov, A.Yu. Kuyanov, A.A. Skovoroda, and A.V. Timofeev, Plasma Phys. Rep., **24** (1998) 389

Table 4.4.2-1 Parameters for Non-Inductive Scenarios at the Flat Top

		Scenario 4		Scenario 6	Scenario 7
		WNS	WNS	SNS	WPS
R/a	(m)	6.35/1.85	6.35/1.85	6.35/1.85	6.35/1.85
B_T	(T)	5.18	5.18	5.18	5.18
I_P	(MA)	9.0	9.5	9.0	9.0
κ_{95}/δ_{95}		1.85/0.40	1.87/0.44	1.86/0.41	1.86/0.41
$<n_e>$	($10^{19}m^{-3}$)	6.7	7.05	6.5	6.7
n/n_G		0.82	0.81	0.78	0.82
$<T_i>$	(keV)	12.5	11.6	12.1	12.5
$<T_e>$	(keV)	12.3	12.6	13.3	12.1
β_T	(%)	2.77	2.67	2.76	2.75
β_N		2.95	2.69	2.93	2.92
β_p		1.49	1.25	1.48	1.47
P_{fus}	(MW)	356	338	340	352
$P_{LH} + P_{NB}$	(MW)	29 + 30 *1	28 + 35	40 + 20 *2	29 + 28 *3
$Q = P_{fus}/P_{add}$		6.0	5.36	5.7	6.2
W_{th}	(MJ)	287	272	287	285
P_{loss}/P_{LH}		2.59	2.74	2.63	2.6
τ_E	(s)	3.1	2.92	3.13	3.07
f_{He}	(%)	4.1	4.0	4.0	4.0
f_{Be}	(%)	2	2	2	2
f_{Ar}	(%)	0.26	0.16	0.2	0.23
Z_{eff}		2.07	1.87	1.89	1.99
P_{rad}	(MW)	37.6	30.6	36.2	34.6
P_{loss}	(MW)	92.5	93.2	91.6	92.7
l_i (3)		0.72	0.43	0.6	0.69
I_{CD}/I_p	(%)	51.9	49.7	53.7	50.2
I_{bs}/I_p	(%)	48.1	50.3	46.3	49.8
I_{OH}/I_p	(%)	0	0	0	0
$q_{95}/q_o/q_{min}$		5.3/3.5/2.2	5.01/3.8/2.7	5.4/5.9/2.3	5.3/2.7/2.1
$H_{H98(y2)}$		1.57	1.46	1.61	1.56
τ_{He}^*/τ_E		5.0	5.0	5.0	5.0

∗1 ΔZ1(NB) ~0.38 m (P = 0.5 P_{NB}), ΔZ2(NB) ~0.95 m (P = 0.5 P_{NB}), R_{LH} - R = 1.28 m (γ = 0.3A/Wm^2)
∗2 ΔZ1(NB) ~0.38 m (P = 0.35 P_{NB}), ΔZ2(NB) ~0.95 m (P = 0.65 P_{NB}), R_{LH} - R = 1.2 m (γ = 0.3A/Wm^2)
∗3 ΔZ1(NB) ~0.38 m (P = 0.67 P_{NB}), ΔZ2(NB) ~0.95 m (P = 0.33 P_{NB}), R_{LH} - R = 1.37 m (γ = 0.3A/Wm^2)

4.4.2.3 Weak Positive Shear Scenario

The waveforms of plasma parameters in the WPS scenario are similar to those in the WNS scenario. The main difference is in the redistribution of the NB power 2/3 of which should be injected near the plasma centre. In the WPS scenario the target central q value is smaller, so 5 MW of the ECRH power is applied later.

4.5 Divertor and Edge Pedestal

4.5.1 Divertor Performance

Divertor modelling with the B2-Eirene code package[1,2] has become an important tool in the ITER divertor design. This code, which is constantly validated against data from various experiments, predicts the divertor plasma performance in ITER and its dependence on geometry[3] as well as on various other parameters[4] (e.g. gas throughput, upstream density n_s, etc.). The fact that similar behaviour can be found in experiments on JET and other divertor tokamaks gives credibility to these modelling results and allows their use as design guidance.

Most of the modelling studies performed to date assume CFC-clad vertical targets in the strike zone areas and W cladding on all other surfaces. While self-consistent sputtering and impurity transport of W is not treated in the code calculations, the self-consistent behaviour of C is taken into account by assuming physical sputtering as well as chemical sputtering, the latter with a constant yield of 1%. Thus the main radiation losses in the SOL and in the divertor originate from carbon radiation. A few calculation runs were performed assuming a pure W divertor and N, Ne or Ar seeding in order to replace the C radiation losses. In all cases a Z_{eff} at the core-edge interface (CEI, a surface assumed ~ 5 cm inside the separatrix at the outer equator) and at the separatrix is calculated taking He and other impurities such as C, N, Ne and Ar into account. Note that no realistic transport model for the region inside the separatrix, which would correctly describe the "transport barrier" and "pedestal" physics is implemented in the code. At the same time, the relation between the divertor performance and the upstream plasma parameters at the separatrix is insensitive to the detail of the transport inside the separatrix, therefore the interface parameters such as Z_{eff} or helium concentration are in most cases determined at the separatrix.

4.5.1.1 Target Geometry

It was found[3] that the peak power loads on the divertor targets depend strongly on the arrangement of the divertor target, and the bottom part of the divertor chamber. If the bottom part of the divertor chamber makes a distinct corner (V shape) with the target, and if the separatrix strike-point is located near this corner (Figure 4.5.1-1), then the neutrals become locked in the vicinity of the strike-point, thus favouring partial detachment at the separatrix. The results are consistent with experiments at JET for which the strike point was swept across the target[5]. The effect is strong: introduction of a V, about 10 cm deep near the separatrix strike-point, reduces the peak power load by 30% compared with a straight vertical target for ITER conditions. This can outweigh the effect of the variation of the divertor length or the divertor closure. Optimisation of the divertor geometry and pumping speed reduces the power loading further. A reduction of the pumping speed causes a similar effect, i.e. increased neutral pressure in the divertor and reduced power load, but leads to a deterioration of helium removal - which is not the case for the modification of the target shape.

[1] D. Reiter, H. Kever, G.H. Wolf, et al., Plasma Phys. and Contr. Fusion, **33** (1991) 1579
[2] R. Schneider, D. Reiter, H-P. Zehrfeld, et al., J. Nucl. Mater., **196-198** (1992) 810
[3] A.S. Kukushkin, G. Janeschitz, A. Loarte, et al., "Critical Issues in Divertor Optimisation for ITER-FEAT", Proc. 14th PSI Conference, Rosenheim, 2000 (to be published in J. Nucl. Mater.)
[4] A.S. Kukushkin, et al., "Basic Divertor Operation in ITER-FEAT", 18th IAEA Fusion Conference, Sorrento, Italy, Oct. 2000
[5] A. Loarte, Nucl. Fus. **38** (1998) 587; R. Monk, et al., Proc. 24th EPS Conf. Contr. Fusion Plasma Phys., Berchtesgaden, 1997, Vol. 21A (1997) 117

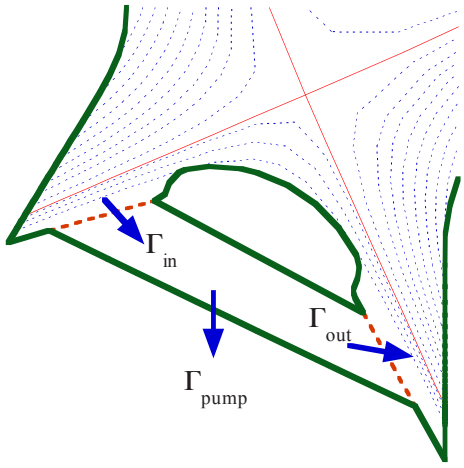

Figure 4.5.1-1 Divertor Geometry Used in the Calculations
Arrows indicate the direction of neutral flows in the private flux region.
The dome-supporting structures are represented by two surfaces (dotted lines) with transparency of 0.56 for the neutrals

4.5.1.2 Gas Flow Between the Divertors

Gas conductance in the private flux region (PFR) between the inner and outer divertors also plays an important role. Indeed, because the neutral pressure in the inner divertor is normally higher than in the outer, the resultant gas flow between the divertors increases the neutral-induced energy loss in the outer divertor and thus reduces the power loading there. In a real divertor, there are supporting structures beneath the dome which hinder the gas flow. This effect was modelled[1] by introducing two semi-transparent surfaces connecting the dome edges with the divertor bottom, as in Figure 4.5.1-1. The effect is clear: reduction of the gas conductance between the divertors results on the whole in a considerable, up to a factor 2, increase of the peak power loading. This observation is consistent with JET experiments[2], where the introduction of a "septum" separating the inner and outer divertors was found to increase the asymmetry of the divertor parameters, i.e., the outer divertor became hotter and the inner one more detached. In that experiment, it was found that symmetry of the divertor parameters can be recovered by gas puffing in the outer divertor and pumping from the inner. However, this approach is not feasible in ITER because the gas throughput between the divertors at fully transparent structures in PFR is calculated to be 300 to 400 Pam^3/s which is far beyond the pumping capability of ITER (200 Pam^3/s). Sufficient gas conductance between the divertors in the PFR is therefore necessary in ITER.

4.5.1.3 Operational Window

The window for divertor operation in ITER is delimited by several constraints arising from core plasma and technology requirements.

First, the divertor plasma must be compatible with core plasma conditions ensuring the necessary reactor performance, as given by core plasma modelling for ITER. The upstream

[1] A.S. Kukushkin, et al., "Basic Divertor Operation in ITER-FEAT", 18th IAEA Fusion Conference, Sorrento, Italy, Oct. 2000
[2] C.F. Maggi, et al., Proc. 26th EPS Conf. on Contr. Fusion and Plasma Phys., Maastricht, 1999, ECA Vol. 23J (1999) 201

plasma density at the separatrix, n_s, which is the edge density for the core plasma, is expected to be limited from one-third to two thirds of the core density. In a reference inductive operation, an edge density equal to $3.3\times10^{19}m^{-3}$ is therefore taken as a conservative assumption. The helium concentration in the core, c_{He}, is limited by fuel dilution. Z_{eff} at the core is limited by the acceptable impurity radiation and fuel dilution. The values of c_{He} and Z_{eff} at the separatrix are taken as representative for the core plasma. The particle control in the recent calculations is accomplished by specifying the gas puffing rate (puffing from the top of the plasma), the pumping speed (the pumping duct is located in the PFR, beneath the dome), and the plasma flow from the core. The difference between the latter and the calculated neutral flow into the core is supposed to be balanced by some deep core fuelling $\Gamma_{core} \geq 0$ provided by e.g. pellet injection. The value of the neutral flux Γ_0 crossing the separatrix and providing the ion source in the core plasma should be compatible with the core conditions – that is, sufficient to maintain the density pedestal and low enough not to cause deterioration of the core confinement. In fact, in all calculations performed to date, less than 20% of the gas fuelled into the main chamber cross the separatrix as neutrals – i.e., the neutral influx into the core does not exceed about 50 Pam^3/s.

Secondly, the plasma parameters must be compatible with various technological requirements. The peak power on the targets, q_{pk}, must be below a certain value to satisfy constraints on the plasma-facing components (20 MW/m^2 is the maximum limit and 10 MW/m^2 or less is desirable.). The particle throughput, Γ_{DT}, is limited by the capacity of the pumping and tritium processing facility and tritium inventory considerations. Γ_{core} is limited above by the capacity of the core fuelling system (pellet injection, neutral beams). Other constraints could arise from wall and target erosion but these are not considered yet.

The limits of this operational window are given in Table 4.5.1-1. Different means to control the divertor operation can be used to explore the window. In recent calculations, the gas puffing rate was varied in order to achieve the desirable density variation. The core fuelling varied slightly (10 to 15 Pam^3s^{-1}) along with the change in the neutral influx across the separatrix. The pumping speed, S_p, was kept constant in the density scans and varied between scans. Impurity seeding (neon, nitrogen, or argon) was used to explore the margins in Z_{eff}. The input power, P_{in}, depends on the plasma core conditions and it has been varied from 86 MW (P_{fusion} = 410 MW, Q = 10, 30% core radiation) to 100 MW (P_{fusion} = 600 MW, Q = 24, 30% core radiation, or Q = 13, 40% core radiation) and to 130 MW (P_{fusion} = 600 MW, Q = 9, 30% core radiation). He production rate was consistent with the fusion power. The divertor geometry was also varied to optimise the divertor operation window.

A point for a full-tungsten target with argon-seeded plasma is also shown. The drops in peak power load at certain upstream densities are related to partial detachment at the inner and outer strike zone, respectively.

The 6D operating window (q_{pk}, n_s, Z_{eff}, Γ_0, c_{He}, Γ_{DT}) for the reference ITER target geometry, Figure 4.5.1-1, is shown in Figure 4.5.1-2. Operational points inside the 6D window are seen to exist for the input power as high as 100 MW. Even at higher power, 130 MW, all the parameters except the peak power and upstream density are within the acceptable limits. If the restrictions on n_s can be relaxed (2/3 instead of 1/3 of the core density), then operation with higher input power becomes possible. There is a considerable

margin in Z_{eff} for the carbon cases which implies a possibility of impurity seeding, and some margin in c_{He} which may be necessary to cope with the uncertainty of the helium transport in the core.

Table 4.5.1-1 Limits of the Operational Window of the ITER Divertor for the Reference Inductive Operation

Peak power load on the targets	$q_{pk} \le 10$ MW/m^2
D-T particle throughput	$\Gamma_{DT} \le 200$ Pa·m^3/s (1.1 10^{23} s^{-1})
Core fuelling	$0 \le \Gamma_{core} \le 50$ Pa·m^3/s (2.7 10^{22} s^{-1})
Upstream plasma density	$n_s \sim 0.33\times10^{20}$ m^{-3}
Helium concentration in the core plasma	$c_{He} \le 0.06$
Z_{eff} in the core plasma	$Z_{eff} \le 1.6$
Neutral influx to the core	$\Gamma_0 \sim 50$ Pa·m^3/s (2.7 10^{22} s^{-1})

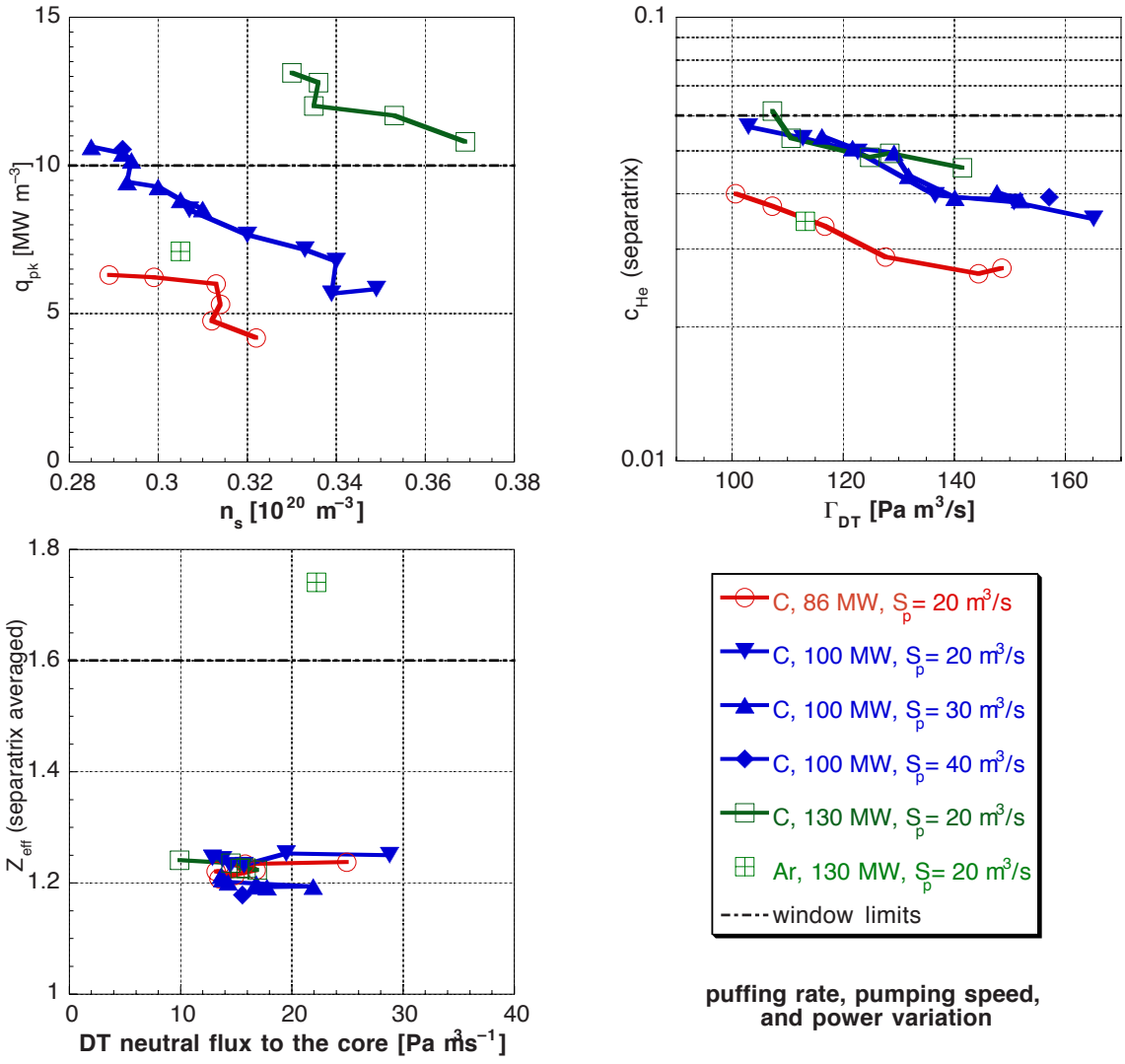

Figure 4.5.1-2 Three Views of the 6D Operational Window for the ITER Divertor, for V-shaped Carbon Targets, Varied Pumping Speed S_p, No Impurity Seeding, Three Levels of Input Power

4.5.1.4 Pumping Speed

To trade off the margin in c_{He} against throughput, one can reduce the pumping speed to reduce the throughput while keeping the same neutral density in the divertor. Reducing the pumping speed leads to higher c_{He} at the same upstream density while the particle throughput goes down. It is therefore a control tool allowing, together with the fuelling rate, the plasma density and helium concentration to be tuned separately.

4.5.1.5 Impurity Seeding

Impurity seeding in addition to the sputtered carbon is not very efficient in enhancing the divertor radiation[1]. Indeed, radiation from seeded impurity reduces the power left for recycling, thus the particle flux to the surfaces drops together with the influx of sputtered carbon, resulting in a reduction of the radiation from carbon.

Another option would be to replace carbon completely with a seeded impurity. This could become necessary if carbon presence in the machine is deemed undesirable due to the tritium co-deposition problem. Limited modelling studies of the effect of this replacement were done for a simpler, straight target geometry. The results shown in Figure 4.5.1-3 suggest that the main trade-off is between the radiation power and Z_{eff} while the kind of seeded impurity is less important.

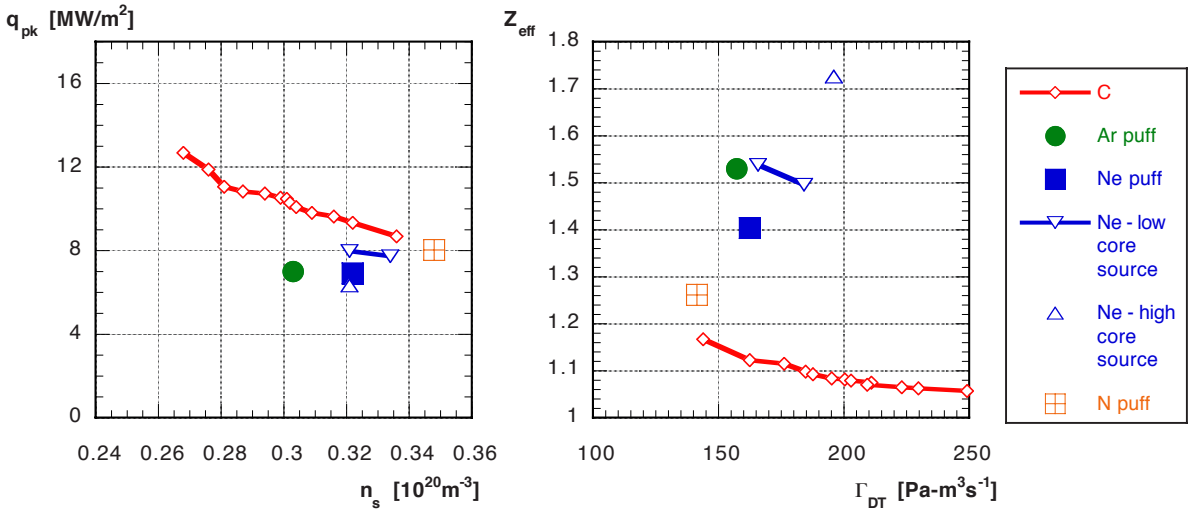

Figure 4.5.1-3 Divertor Performance with Impurity Seeding: Peak Power Loading vs. Upstream Plasma Density (left) and Z_{eff} at the Core-edge Interface vs. DT Particle Throughput (right)

The curve corresponding to the intrinsic carbon impurity as the radiator is also shown for comparison. The input power is 86 MW, pumping speed 75 m^3/s, straight target. The seeded impurity is either puffed as neutrals into the outer divertor (N, Ne, Ar) or supplied from the core as ions (Ne).

[1] A.S. Kukushkin, G. Janeschitz, A. Loarte, et al., "Critical Issues in Divertor Optimisation for ITER-FEAT", Proc. 14th PSI Conference, Rosenheim, 2000 (to be published in J. Nucl. Mater.)

4.5.1.6 Prospects for Steady State Operation

Steady state operation with non-inductive current drive implies higher input power (low Q), lower upstream density, and greater connection length (high q). Initial studies done for the reference ITER geometry with reduced current and 100 MW input power show that the increase of the connection length reduces the q_{pk} at given n_s and improves helium pumping. At present, the results are only available for carbon divertor plates, without impurity seeding, Figure 4.5.1-4.

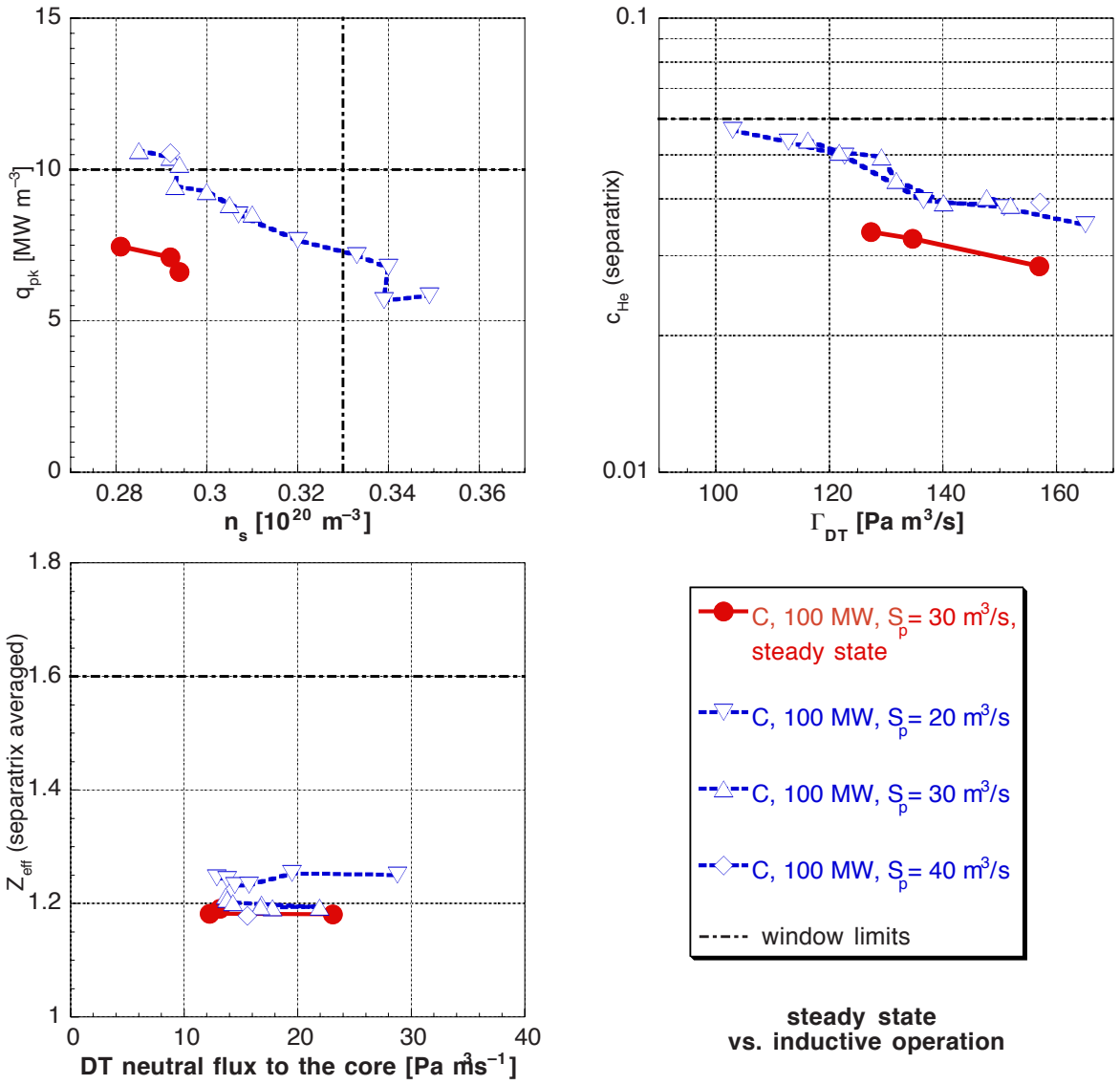

Figure 4.5.1-4 Three Views of the 6D Operational Window for the ITER Divertor for Steady State Operation with Carbon Target

The data for inductive operation are also shown for comparison.

4.5.1.7 Conclusions

An acceptable operational window for the ITER divertor in inductive operation has been identified.

A V-shaped configuration of the target and divertor floor is beneficial for divertor performance, providing a considerable reduction of the peak power load on the target without adversely affecting helium removal. The effect is mostly due to accumulation of neutrals near the strike point when the V is plugged by plasma, as confirmed by the available experimental data from JET. However, such a configuration can negatively affect the operational flexibility of the machine by reducing the freedom of positioning the strike point. On balance, as a result of these studies, a V-shaped target configuration is foreseen for ITER.

Efficient particle exchange between the inner and outer divertors, via neutral gas in the private flux region, is essential to achieve an acceptable operational regime for the ITER divertor. The high gas throughput between the divertors, typically above 300 Pam^3/s, enhances the neutral-induced power dissipation in the outer divertor thus reducing the peak power load there. These results are consistent with JET experiments using the "septum" in the divertor, and the latest ITER divertor design takes them into account.

Impurity seeding can be used as an alternative to natural carbon radiation if the use of carbon were to become undesirable because of tritium co-deposition. Different radiating impurities can be used. In impurity seeding, the main trade-off is between the radiated power and Z_{eff} in the core, and the first results suggest that this trade-off is not strongly affected by the choice of impurity. The difference in fuel dilution, compared to C and among different seeded impurities, is also not large, unless the Z_{eff} is allowed to reach a value well above 2.

Further work is necessary to study the compatibility of acceptable divertor performance with steady state operation using non-inductive current drive in ITER, which requires an increase of the power entering the scrape-off layer and a decrease of the upstream plasma density. The first results suggest that the increase of the connection length caused by the reduction of the plasma current ensures lower peak power loading for the same upstream plasma density.

4.5.2 H-Mode Edge Pedestal and ELMs

4.5.2.1 H-Mode Edge Pedestal

In many tokamaks energy confinement during H mode strongly depends on the temperature at the top of the H-mode pedestal[1]. This pedestal temperature is determined by the pressure gradient and the width of the edge pedestal and the pedestal density. In the case of the type I ELMy regime, which is assumed for inductive operation in ITER, the pressure gradient is widely observed to be close to the ideal ballooning (first) stability limit. In DIII-D, the gradient is observed to be much steeper and it is suggested that the gradient is in the second stable region. However in this case the pedestal width is ~ half of the one in ASDEX Upgrade and thus the pressure on top of the pedestal is comparable between DIII-D and ASDEX Upgrade.

[1] M. Greenwald, R.L Boivin, F. Bombard, et al., Nucl. Fusion **37** (1997) 793; W. Suttrop, F. Ryter, V. Mertens, et al., 17th IAEA Fusion Energy Conference, Yokohama, 1998, IAEA-F1-CN-69/EX2/06; G. Janeschitz, Yu. Igitkhanov, M. Sugihara, et al., 26th EPS Conference on Contr. Fusion Plasma Physics, Maastricht, 1999, p1445

Experimental examinations of the pedestal width in individual machines[1], and also comparisons between two machines (C-MOD and DIII-D[2], JT-60U and DIII-D[3]) show that the pedestal width follows largely a thermal ion poloidal Larmor radius (ρ_{pol}) like dependence[4]. However, the actual pedestal width is several times wider than the poloidal Larmor radius and varies with the operational regime, e.g. is generally narrower in ELM free or in discharges in the second stability regime against ballooning than in ELMy discharges and is wider with a high z impurity injection in ELMy discharges than without the impurity injection[5].

A model for the pedestal width, which could partly explain these characteristics[6] is used to predict the pedestal width for ITER. It is based on turbulence suppression by the combined effects of the magnetic shear and the $\boldsymbol{E} \times \boldsymbol{B}$ shearing rate using the ITER pedestal database[7] for comparison to experimental data. The basic idea of the model is that the transport barrier is formed in the region where the turbulence is suppressed by a stabilizing $\boldsymbol{E_r} \times \boldsymbol{B}$ shearing rate, which is generated by the ion pressure gradient. The magnetic shear plays an essential role through two facts, namely that the critical pressure gradient at the ideal ballooning limit increases with increasing shear and that the turbulence growth rate decreases with increasing shear. The turbulence is completely suppressed when the $\boldsymbol{E_r} \times \boldsymbol{B}$ shearing rate is larger than the turbulence de-correlation rate[8] or its surrogate linear growth rate. The resulting expression of the pedestal width includes the toroidal Larmor radius and the magnetic shear. A plasma current dependence of the width appears indirectly through the magnetic shear, and thus the dependence becomes poloidal-Larmor-radius-like as observed on many machines. An approximately linear machine size dependence of the pedestal width appears through the magnetic shear profile.

Figure 4.5.2-1 shows a systematic density scan for type I ELMy discharges in JET with fixed toroidal field (2.3 T) and plasma current (2.5 MA) shown by closed squares. Also shown are predictions by several pedestal width models, namely a pure poloidal Larmor radius dependence (dashed), a constant pedestal width and thus pedestal pressure (dotted) as well as the above described ITER reference model (open circles). Predictions by the ITER model uses the magnetic shear calculated at the 95% flux surface by the EFIT code. Also the pedestal pressure in C-MOD can be reproduced as well by the ITER model as by the poloidal

[1] A.E. Hubbard, R.L. Boivin, R.S. Granetz, et al., Phys. Plasmas **5** (1998) 1744; T.H. Osborne, K.H. Burrell, R.J. Groebner, et al., J. Nucl. Mat. **266-269** (1999) 131; R.J. Groebner, T.H. Osborne, Phys. Plasmas **5** (1998) 1800; J. Lingertat, V. Bhatnager, G.D. Conway, et al., J. Nucl. Mat. **266-269** (1999) 124; Y. Kamada, A. Isayama, T. Oikawa, et al., 17th IAEA Fusion Energy Conference, Yokohama, 1998, IAEA-F1-CN-69/CD2/EX9/2; W. Suttrop, M. Kaufmann, H.J. de Blank, et al., Plasma Phys. Control. Fus. **39** (1997) 2051

[2] R.S. Granetz, T.H. Osborne, R.L. Boivin, et al., 17th IAEA Fusion Energy Conference, Yokohama, 1998, IAEA-F1-CN-69/EX6/2

[3] T. Hatae, Y. Kamada, S. Ishida, et al., Plasma Phys. Control. Fusion **40** (1998) 1073

[4] M. Greenwald, R.L. Boivin, F. Bombard, et al., Nucl. Fusion **37** (1997) 793; W. Suttrop, F. Ryter, V. Mertens, et al., 17th IAEA Fusion Energy Conference, Yokohama, 1998, IAEA-F1-CN-69/EX2/06; G. Janeschitz, Yu. Igitkhanov, M. Sugihara, et al., 26th EPS Conference on Contr. Fusion Plasma Physics, Maastricht, 1999, p1445; T.H. Osborne, K.H. Burrell, R.J. Groebner, et al., J. Nucl. Mat. **266-269** (1999) 131; R.J. Groebner, T.H. Osborne, Phys. Plasmas **5** (1998) 1800; J. Lingertat, V. Bhatnager, G.D. Conway, et al., J. Nucl. Mat. **266-269** (1999) 124; Y. Kamada, A. Isayama, T. Oikawa, et al., 17th IAEA Fusion Energy Conference, Yokohama, 1998, IAEA-F1-CN-69/CD2/EX9/2

[5] H. Kubo, S. Sakurai, N. Asakura, et al., Nucl. Fusion **41** (2001) 277

[6] M. Sugihara, Yu. Igitkhanov, G. Janeschitz, et al., Nucl. Fusion **40** (2000) 1743

[7] M. Sugihara, Yu. Igitkhanov, G. Janeschitz, et al., 26th EPS Conference on Contr. Fusion Plas. Physics, Maastrich, 1999, p1449

[8] H. Biglari, et al., Phys. Fluids **B2** (1990) 1; T. Hahm and K. Burrell, Phys. Plasmas **2** (1995) 1648

Larmor radius scaling. In addition, the observation that ELM free discharges and second stable discharges tend to show, in general, a smaller width than ELMy and first stable discharges, can be also reproduced by this model (shear changes with bootstrap current).

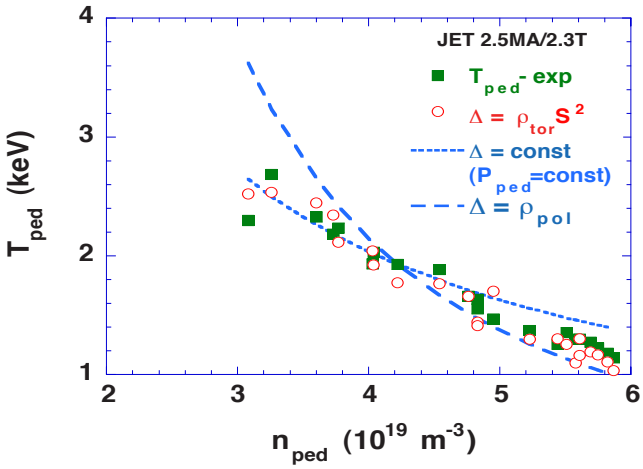

Figure 4.5.2-1 Pedestal Temperature T_{ped} vs. Pedestal Density n_{ped} for Type I ELMy Discharges in JET with Fixed Toroidal Field (2.3 T) and Plasma Current (2.5 MA) (closed squares)

Open circles are obtained from the width scaling with toroidal Larmor radius times shear squared (ITER model). Dashed and dotted lines are obtained from the width scaling based on poloidal Larmor radius and constant pedestal width, respectively.

Application of the above described reference model to ITER suggests that the expected pedestal pressure is (80-100) kPa. The pedestal density can be estimated by the experimental observation that the ratio of line average density and pedestal density is in the range of (0.7-0.9) for high density discharges close to the Greenwald density. Thus, for $\bar{n} \approx 10^{20} m^{-3}$ in ITER, $n_{ped} \approx (7-9) \times 10^{19} m^{-3}$ is expected. With this pedestal pressure and density, the expected pedestal temperature is $(3-4)\ keV$. The estimated pedestal temperature for ITER will be within the range where good confinement of the core plasma is maintained by ion temperature gradients. The expected range of pedestal values for ITER is summarised in Table 4.5.2-1.

Table 4.5.2-1 Reference Pedestal Parameters for ITER

Temperature T_{ped} (keV)	**Density** n_{ped} $(10^{19} m^{-3})$	**Energy** W_{ped} (MJ)	**Width** Δ_{ped} (cm)
3 - 4	7 - 9	100 - 120	10 - 15

This expected pedestal pressure (or pedestal energy) is also consistent with another observation of present day experiments, where the pedestal energy is approximately in the range of 1/3 of the total stored energy in good confinement H-mode discharges. Also, predictions based on non-linear offset type scaling laws used to extrapolate the pedestal energy to ITER provide similar values, albeit at present with a large uncertainty.

4.5.2.2 Energy Loss during Type I ELMs

The energy loss ΔW_{ELM} caused by type I ELM is relatively large and can potentially produce significant erosion of the divertor target plates in a reactor like machine with high plasma energy content.[1]

Impact of the ELM energy deposition on the divertor plate due to sublimation (graphite) or melting (tungsten) can be characterised by $\Delta W_{ELM}/(S_{ELM}\sqrt{\delta_t})$ that is proportional to the surface temperature rise of the plate. Here S_{ELM} is the ELM energy deposition area and δt is the energy deposition time. Experimental database gives $\delta_t \cong$ (0.1-0.2) ms in JET and JT-60U, $\delta_t \cong$ (0.2-0.3) ms in DIII-D, and $\delta_t \cong$ 0.4 ms or more in ASDEX Upgrade. Majority of the machines (JET, ASDEX Upgrade[2], JT-60U) observe that the ELM energy deposition area expands only slightly from the steady state heat deposition area S_{SS}, i.e., $S_{ELM} \equiv \zeta S_{SS} = (1\text{-}2)S_{SS}$ while $\zeta > 4$ in DIII-D[3]. IR measurements show that the energy deposition on the inner divertor plate is larger than the outer plate, although detailed specification is difficult due to the modified surface property by the deposited materials on the surface of the divertor plate. Radiation energy loss during the energy deposition is rather small, especially in the low to medium density discharges.

Critical values of deposited energy density, $E = \Delta W_{ELM}/S_{ELM}$, with which ITER divertor plate can withstand many numbers of ELM events, are calculated for CFC (2cm thick) and W (1cm thick) divertor plates for the expected range of deposition time δt = (0.1 - 1) ms. In the case of tungsten, melt limit is much stringent limitation than the evaporation limit. The critical values of the energy and flux densities for $\approx 10^6$ ELM during about 10^6 s burn with δt = (0.1 - 1) ms are (0.2 - 0.7) MJ/m^2 and (2 - 0.7) GW/m^2 in the case of CFC plate and (0.3 - 1) MJ/m^2 and (3 - 1) GW/m^2 in the case of W plate. In ITER, $S_{ELM} = 8\zeta$ m^2 and the critical energy is (1.6 - 5.6)ζ MJ for CFC and (2.4 - 8)ζ MJ for W with δ_t = (0.1 - 1) ms.

In several tokamaks, the ratio $\Delta W_{ELM}/W_{ped}$ has been investigated where W_{ped} is the pedestal stored energy. The ratio is 0.13 - 0.18 at low-to-moderate plasma density[4]. But the ratio is not constant and is strongly reduced in high density[5]. The ratio is well correlated with the pedestal collisoinality ν^* as shown in Figure 4.5.2-2.[6] Assuming that this collisionality dependence originates from the parallel ion transport process, the value of $\tau_{//} \propto 2L/c_s(1+\sqrt{3}/2\nu^*)$ relating to the parallel ion loss time (collisionless or collisional) would be the fundamental parameter (Figure 4.5.2-3).[7] Note that $\tau_{//}$ should include the transport time not only in the SOL region, but also in the ergodised (by an ELM) region inside the separatrix. Both figures suggest $\Delta W_{ELM}/W_{ped} \geq 12\%$ or $\Delta W_{ELM} \geq 12$ MJ for ITER in the case of $n_{ped} = 8\text{x}10^{19}$ m^{-3} and $T_{ped} = 3.5$ keV. If the expansion factor ζ is less than 2 and the ELM pulse length δ_t is much shorter than 1 ms, the estimated value of

[1] ITER Physics Basis, Nucl. Fus. **39** (1999) 2430-2431
[2] A.W. Leonard, A. Herrmann, K. Itami, et al., J. Nucl. Materials **266-269** (1999) 109
[3] C.J. Lasnier, et al., 14th Int. Conf. on Plasma Surface Interactions in Controlled Fusion Devices, May 22-26, 2000, Rosenheim, Germany, Report GA-A23399 to be published in J. Nucl. Mater
[4] A.W. Leonard, A. Herrmann, K. Itami, et al., J. Nucl. Materials **266-269** (1999) 109
[5] A. Mahdavi, et al., 18th IAEA Fusion Energy Conference, Sorrento, Italy (2000) IAEA-CN-77-EXP1/04
[6] A. Loarte, G. Saibene, R. Satori, et al., 18th IAEA Fusion Energy Conference, Sorrento, Italy (2000) IAEA-CN 77/ITERP/11(R)
[7] A. Loarte, G. Saibene, R. Satori, et al., 18th IAEA Fusion Energy Conference, Sorrento, Italy (2000) IAEA-CN 77/ITERP/11(R)

$\Delta W_{ELM} \geq 12$ MJ will exceed the critical energy. The heat flux density is not clear from this study.

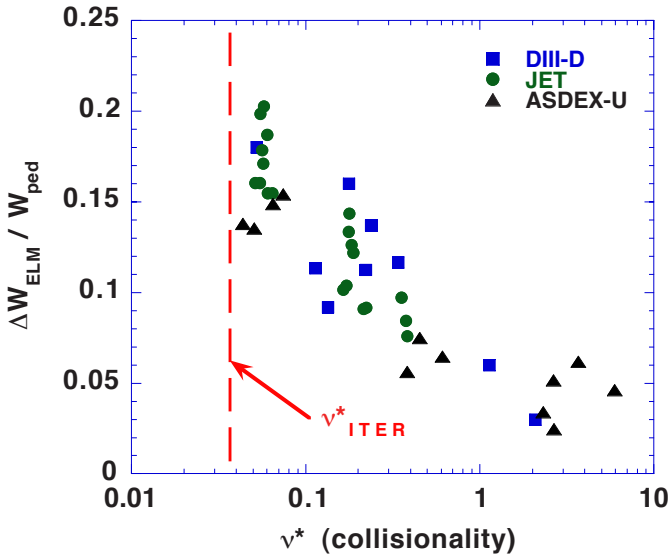

Figure 4.5.2-2 Energy Loss Fraction for ELMs as a Function of Pedestal Collisionality ν*

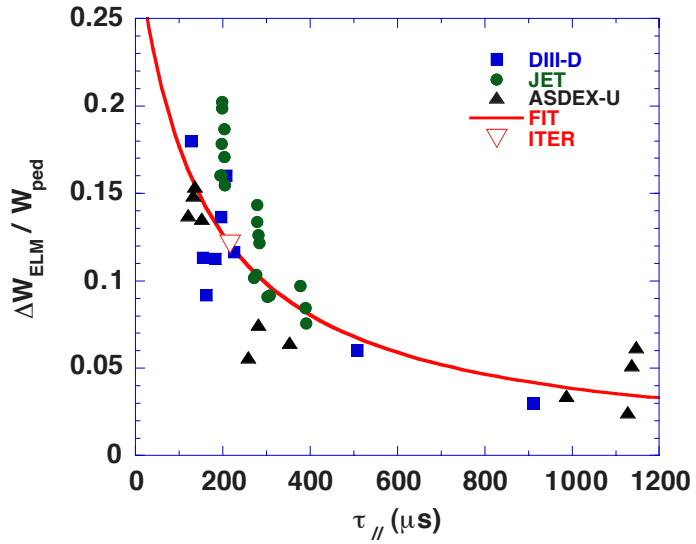

Figure 4.5.2-3 Energy Loss Fraction per ELM as a Function of Parallel Transport Time

The possible maximum heat flux density would be estimated from a sheath model by assuming pre-ELM pedestal density and temperature in the divertor region. The heat flux density on the divertor plate can be expressed as:

$$q_{target} = \gamma k \Gamma_s T_s \sin\alpha, \qquad (4.5.2\text{-}1)$$

where γ is the heat transmission coefficient,[1]

[1] P.C. Stangeby, "The Plasma Boundary of Magnetic Fusion Devices", Plasma Physics Series, Ed. P.Stott and H. Wilhelmsson, Institute of Physics Publishing, Bristol and Phyladelphia, 2000, p. 649

$$\gamma = \frac{2.5T_i}{T_e} + \frac{2}{1-\delta_e} - 0.5\ln\left[2\pi\frac{m_e}{m_i}\left\{1+\frac{T_i}{T_e}\frac{1}{\left(1-\delta_e\right)^2}\right\}\right], \qquad (4.5.2\text{-}2)$$

δ_e is the secondary electron emission coefficient, $\Gamma_s = n_s c_s \approx 0.5 n_{div} c_s$ is the particle flux density along the field line (c_s is the sound velocity), and T_s is the electron temperature at the entrance of the sheath. The value of $\sin\alpha$ is evaluated from the magnetic equilibrium and divertor target geometry. This gives for ITER the upper limit of the heat flux density $q_{target} = 3.39$ GW/m^2 for the typical ITER conditions: $T_{ped} = 3.5$ keV, $n_{ped} = 8\text{x}10^{19}$ m^{-3}, and $\sin\alpha = 0.037$. It is assumed here that the incident ion energy at the sheath is $\approx 5T_{ped}$, the secondary electron emission[1] is ~ 0.2 giving $\gamma \sim 7.8$ for a DT plasma at $T_i = T_e$. This heat flux density would exceed the critical heat flux of (2 - 0.7) GW/m^2 for CFC and (3-1) GW/m^2 for W. It should be noted that the sheath model might overestimate the ELM energy loss.

A design solution exists for this problem: a tungsten target, inclined by a factor of two from the reference design, would withstand the type I ELM heat load of most conservative estimation. The helium exhaust efficiency and heat load during steady state are tolerable. However, this design solution is associated with possible melting at disruptions and high particle recycling at upstream, i.e. some concern on the compatibility of H-mode confinement. Therefore the initial operation will use CFC as the target. The tungsten target may be used in the later stage after an experimental verification is made on ELM heat loads being unacceptable and control schemes are developed to reduce heat load during disruption to a tolerable level for tungsten.

Further studies are definitively needed to improve prediction of the divertor heat load associated with ELMs. In particular, the density scans for the ELM energy loss in various machines are particularly important for this purpose.

4.5.2.3 H-mode Regimes with Small ELMs

It is desirable to reduce the heat energy deposition to the divertor target due to ELM in order to increase the lifetime of the target. The pedestal energy can be reduced by reducing the pedestal density. This can be achieved with high-field-side pellet injection allowing, by density peaking, to reduce the pedestal density while maintaining the same temperature averaged density. The fast energy loss associated with the type I ELMs was reduced by a factor of 2 by pellet injection in experiment. Further studies should be performed in order to understand these possibilities and to study applicability of these methods to ITER.

Alternative high confinement modes with small ELM amplitude have been observed in most of the divertor tokamaks, e.g., grassy ELMs in DIII-D[2], 'minute' ELMs in JT-60U[3], and the enhanced D_α (EDA) mode in Alcator C-Mod[4] and recently in ASDEX Upgrade[5]. Previously

[1] K. Ertl, and R. Behrisch, "Electron emission from Solid Surfaces", Physics of Plasma Wall Interactions in Controlled Fusion, Ed. D.E. Post and R. Behrisch, NATO ASI Series, Plenum Press, New York, 1986, pp. 515-538
[2] T. Ozeki, et al, Nucl. Fusion **30** (1990) 1425
[3] Y. Kamada, et al., Plasma Phys. Control. Fusion **38** (1996) 1387
[4] M. Greenwald, et al., Plasma Phys. Control. Fusion **40** (2000) A263
[5] J. Stober, O. Gruber, A. Kallenbach, V. Mertens, F. Ryter, et al., Plasma Phys. Control. Fusion **42** (2000) A211

JET observed this mode as a so-called low particle confinement H-mode[1]. Although it is not yet verified that all these modes correspond to the same phenomenon, they are all classified as type II ELMs here for convenience.

Stability analyses and observations from DIII-D edge stability experiments[2] support an ideal stability based model of type I ELMs as low to intermediate toroidal mode number, n, kink-ballooning modes. In this model, second stability access plays a supporting role by facilitating the build-up of the edge pressure gradient and associated bootstrap current density, which then drives lower n MHD modes. The ELM amplitudes are assumed to be determined by the radial width of the unstable modes. Predictions from this model are consistent with many observed features of DIII-D edge stability experiments, as well as the observed increase of the edge pressure gradient with triangularity δ in DIII-D, JT-60U and ASDEX Upgrade.

In JT-60U, large amplitude low frequency ELMs (~100 Hz) are found to disappear and small high frequency grassy ELMs (~500-1000 Hz) to appear at sufficiently large δ ($\delta \geq 0.45$), q_{95} ($q_{95} \geq 6$) and β_p ($\beta_p \geq 1.6$).[3] At higher δ (0.54), type I ELMs can disappear at a lower q_{95} (~4). In the grassy ELMy H-mode, the peak heat load on the divertor plates is much smaller than that at type I ELMs. Edge stability analyses have revealed that the edge plasma is accessing to the second stability regime of high n ballooning modes in the grassy ELM discharges. Ideal stability analyses with careful equilibrium reconstruction including edge bootstrap current using EFIT[4] shows a possibility of intermediate n (= 5 - 10) modes as the trigger mechanism for type I ELMs and modes with $n \geq 10$ as the trigger for grassy ELMs. Modes with higher n are expected to be more localised due to shorter wavelength and will perturb a smaller edge region.

In the C-Mod EDA regime, periodic MHD relaxations are normally not observed.[5] The enhanced particle transport is caused by continuous, quasi-coherent density fluctuations which are localised in the density pedestal region. These have f~ 100 kHz in the laboratory frame and $k_\theta \sim 3\text{-}6\ cm^{-1}$. Perhaps because of their high k_θ, no magnetic signature has been observed so far. The 'low particle confinement' H-mode regime reported on JET[5] shares many characteristics of the EDA regime, but has not been as extensively studied or readily reproduced in their recent campaigns.

Most of the type II ELMy H-modes have similar pedestal parameters as type I ELMs and, thus, comparable energy confinement. The EDA mode like other 'small ELM' regimes, have the advantages of being steady state and avoiding impurity accumulation. The thermal energy confinement times agree well with type I ELMy H-mode.

The operating conditions required to attain regimes with small ELMs are now being investigated in many machines. It has been found that the most important parameters for obtaining such regimes are high triangularity and high safety factor. These operation conditions are summarised in Table 4.5.2-2.

[1] M. Bures, D.J. Campbell, N. Gottardi, et al., Nucl. Fusion **32** (1992) 539
[2] J.R. Ferron, M.S. Chu, G.L. Jackson, et al., Phys. Plasmas **7** (2000) 1976
[3] Y. Kamada, et al., Plasma Phys. Control. Fusion **42** (2000) A247
[4] L.L. Lao, et al., Nucl. Fusion **41** (2001) 295
[5] M. Greenwald, et al., Plasma Phys. Control. Fusion **40** (2000) A263

Table 4.5.2-2 Summary of Operation Regime in Terms of q_{95} and δ for Grassy or EDA ELMs in Various Devices

Tokamak	Regime	δ_x	q_{95}
ASDEX-Upgrade[1]	Type II ELMy H-mode	≥ 0.4	≥ 4.2
C-MOD[2]	Enhanced D_α (EDA) H-mode	≥ 0.4	≥ 3.5
DIII-D	Type II or Grassy ELMy H-mode	≥ 0.4	
JET	Low Particle Confinement (LPC) H-mode		
JT-60U[3]	Grassy (minute) ELMy H-mode	≥ 0.4	≥ 4

The operational spaces for the grassy ELMs in JT-60 and EDA in C-Mod are similar. The similarity suggests that, despite the differences in observed edge phenomena, there may be similarities in the physics of the two regimes. Relatively high edge density and/or neutral pressure also appear to play a role in accessing the EDA mode on C-Mod. In ASDEX Upgrade, type I ELMs gradually decrease from the mixture of type I and II ELMs with increasing density and pure type II ELMs appear at relatively high density ($\bar{n}/n_G > 0.8$). For higher density ($\bar{n}/n_G > 0.95$), the discharge suffers of a sharp transition to type III ELMs, which leads to reduced confinement. Small ELMs have been observed in various machines with ohmic, ICRF and NB heating, showing that they are not related to heating method or fast particles. There does not seem to be a clear power threshold, as long as the power outflow through the separatrix is sufficient to avoid type III ELMs.

According to the present database, the type II ELM regime requires higher q_{95}, and thus lower plasma current, than the type I ELM regime thus leading generally to a reduced confinement time. The amount of plasma current reduction required for achieving the type II ELM regime is uncertain and might be somewhat mitigated when a second separatrix is very close to the first one at higher triangularity (higher shear). Type II ELM regime could be also used for hybrid or steady state operations with higher q. Further systematic experimental studies in existing machines should be performed more extensively to extend this ELM regime even into the reference operation mode of ITER.

Another possible way to improve confinement in regimes with reduced ELMs is creating a peaked density profile by pellet injection. Pedestal pressure can be reduced to the extent, where the associated confinement degradation can be compensated by the density profile peaking. This has been demonstrated by the high field side (HFS) pellet injection in ASDEX Upgrade.[4] Essential point of this mode of operation is the pellet penetration depth and the resultant profile peaking. Although the HFS pellet injection is planned in ITER for this purpose, the effectiveness still needs to be confirmed in large machine with high pedestal pressure.

Improved confinement due to the density profile peaking has also been observed in RI mode.[5] In this case, the profile peaking is produced spontaneously with impurity puffing. In

[1] F. Ryter, J. Stober, A. Stäbler, et al., 18th IAEA Fusion Energy Conference, Sorrento, Italy (2000) IAEA-CN 77/EX2/2
[2] M. Greenwald, et al., Phys. Plasmas **6** (1999) 1943
[3] Y. Kamada, et al., Plasma Phys. Control, Fusion **40** (2000) A247-A253
[4] P.T. Lang, J. Gafert, O. Gruber, et al., Nucl. Fusion **40** (2000) 245
[5] A.M. Messian, et al., Nucl. Fusion **34** (1994) 825

TEXTOR, with neon seeding,[2] the H_{H93} factor larger than 1.2 has been achieved and sustained for about $100\tau_E$ in discharges with L-mode edge at 1.2 times the Greenwald density. Confinement improvement in experiments with impurity injection was observed also in DIII-D,[1] JET[2] and JT-60U[3] (see also Section 2.2.2 and Annex A2.2.3). Further systematic studies of RI-mode in large machines are needed for extrapolation of this mode to ITER conditions (e.g. in JT-60U with 16-20 MW of heating power).

4.6 Energetic Particle Confinement

In ITER plasmas, a variety of suprathermal ions will be produced by NB injection, ICH&CD and fusion reactions. Good confinement of energetic alpha particles produced by fusion reactions is essential for attaining and sustaining high Q operation in ITER. It is expected that the energetic ion behaviour will be close to classical in a quiescent plasma, based on the present experimental results with additional heating in large tokamaks.

Different loss channels have been analysed in order to develop the design specification and requirements. The major potential loss channels for energetic particles in ITER are TF ripple and the effect of collective instabilities including those excited by energetic particles such as TAE (toroidal Alfven eigenmode) and fishbone instability.

4.6.1 Ripple Loss of Energetic Ions

Potentially significant loss of fusion alpha particles and high-energy ions produced by NB injection or ICH&CD can occur in ITER due to toroidal field (TF) ripple, i.e. perturbations of the toroidal magnetic field due to discreteness of the TF coils[4]. The TF ripple amplitude is defined as:

$$\delta(R,Z) = \frac{B_{max} - B_{min}}{B_{max} + B_{min}} \qquad (4.6.1\text{-}1)$$

where B_{max} and B_{min} are maximum and minimum magnetic field strengths at a circular line with given (R, Z). Without Ferromagnetic Inserts (FI) the maximum ripple amplitude at the plasma separatrix in ITER is 1.1%. An essential reduction of ripple amplitude can be achieved using ferromagnetic inserts[5]. At the nominal value of toroidal field, the planned configuration of the FI set[6] provides a reduction of the ripple amplitude by a factor of 1.5 at the separatrix and is even more effective in the inner plasma regions.

Alpha particle loss rates have been calculated for the nominal Q = 10 inductive and two reverse shear (RS) steady state operating scenarios using the HYBRID Monte-Carlo numerical code.[7] Results are shown in Table 4.6.1-1 for the cases with and without FI. In the absence of FI, the particle and power losses in the inductive regime as well as in the steady state regime with a weak RS ($q_{min} \approx 2$) are tolerable. In the scenario with a strong RS ($q_{min} \approx$

[1] M. Murakami, et al., Nucl. Fusion **41** (2001) 317
[2] G.P. Maddison, et al., 18th IAEA Fusion Energy Conf., Sorrento, Italy (2000) IAEA-CN-77/EX5/4
[3] H. Kubo, et al., 18th IAEA Fusion Energy Conf., Sorrento, Italy (2000) IAEA-CN-77/EX5/3
[4] ITER Physics Basis, Chapter 5 Section 3, Nucl. Fus. **39** (1999) 2475-2478
[5] H. Kawashima, et al., 18th IAEA Fusion Energy Conference, Sorrento, Italy (2000) IAEA-CN-77/EX9/3
[6] A. Alekseev, E. Lamzin, et al., "Calculation of Ripple in the ITER Facility", Final Report, Efremov ITER Design Office, July 2000
[7] S. Konovalov, T. Takizuka, K. Tani, K. Hamamatsu, and M. Azumi, JAERI-Research 94-033, 1994

3.75), α-particle losses in the absence of FI are rather large. The peak power load on the first wall produced by the escaping α-particles in this scenario exceeds the wanted level of 0.5 MW/m^2. Ripple losses of fast ions produced by NB injection are also rather large in this case (Table 4.6.1-2). In the presence of FI the ripple losses of alpha particle and NB ions become negligible in the ITER inductive scenarios and are reduced to values well below the permissible level in the reverse shear steady state scenarios.

Table 4.6.1-1 Ripple Loss of Fusion Alpha Particles in Various ITER Scenarios With and Without Ferromagnetic Inserts (FI)

	Inductive		Weak RS (#4)		Strong RS	
	No FI	With FI	No FI	With FI	No FI	With FI
Total particle loss fraction (%)	2.15	negligible	6.5	0.08	21	0.75
Total power loss fraction (%)	0.65	negligible	2.5	0.04	9.3	0.13
Peak FW heat load (MWm^{-2})	< 0.1	negligible	0.23	0.005	0.8	0.025
Plasma current (MA)	15		10		10	

Table 4.6.1-2 NB Ion Ripple Loss with and without Ferromagnetic Inserts in Configuration with Strong Reversed Shear for Off-axis NB Injection

	No FI	With FI
Particle loss fraction	15.5%	0.5%
Power loss fraction	3.2%	0.05%
Maximum heat load at P_{NB}=50 MW	230 kWm^{-2}	< 10 kWm^{-2}
Plasma current (MA)	10	10

In ITER plasmas, the reversal of the ion [**B**×∇B] drift direction weakly affects the α-particle and NB ion ripple loss. Counter (to the plasma current) NB injection will be accompanied by an appearance of prompt (first orbit) losses. These losses could be substantial due to a high density at the plasma periphery where a significant fraction of the beam atoms will be ionized**.**

4.6.2 Fast Ion Instabilities

A variety of collective instabilities with a wide range in frequency may be driven by energetic particles including alpha particles. Results from present day experiments have shown that two classes of instabilities are effective in causing anomalous transport of energetic ions: 1) high frequency instabilities such as the shear Alfven eigenmodes and 2) lower frequency instabilities such as the fishbones associated with the toroidal precession of trapped fast particles.

4.6.2.1 Alfven Frequency Modes

Toroidicity causes the continuous frequency spectrum of shear Alfven waves in a tokamak plasma to exhibit a radial "gap". Within this gap the discrete frequency modes called toroidal Alfven eigenmodes (TAE) can exist. The frequency gap is centred at:

$$\Omega_{TAE}(r_0) = v_A k_{//} = v_A/(2qR) \qquad (4.6.2\text{-}1)$$

with v_A the Alfven speed, q the safety factor at the gap location, and R the major radius. The relative gap width of the frequency is of the order of inverse aspect ratio. Since alpha particles in thermonuclear plasma have velocities that are typically super-Alfvenic, they can resonantly interact with weakly damped TAE modes and destabilise them.

Various forms of Alfven eigenmodes exist in a toroidal plasma which can be spontaneously excited by energetic alpha particles. These modes present a potential danger to fusion reactors, because they can eject high energy alpha particles from the plasma before their thermalisation. Since they can carry considerable energy, these losses may damage the first wall of reactors.

During the past years, the close interaction between theory and experiment has led to many discoveries on Alfven eigenmodes in toroidal plasmas. Most of data come from experiments with neutral beams and ICRF heating. A great deal of theoretical work have been carried out on energetic particle pressure gradient drive and competing damping mechanisms for both thermal and fast ions, electron Landau damping and trapped electron collisional damping.

Recently detailed comparisons have been carried out in conventional JET discharges, showing a quantitative agreement between first principle gyrokinetic calculations and measurements of Alfven eigenmode damping rates.[1] They provide the theory required to make extrapolations for a reactor, since the thermonuclear conditions with a significant alpha-particle power cannot be accessed with similarity experiments and dimensional scalings based on the results from tokamaks that are now in operation.

The results of calculations with the global gyrokinetic PENN code predict that conventional burn scenarios, with monotonic safety factor around unity in the plasma core, exist where all the AEs of global character with low to intermediate n (= 1–12) are stable.[2]

Calculations using the MISHKA1 code have shown that high-n ($17 \leq n \leq 26$) AEs are stable at (flattened) post-sawtooth β_α profiles in the ITER-98 ignited scenario but unstable at peaked pre-sawtooth profiles.[3] Analysis of the nonlinear evolution of unstable spectrum of these modes, restricted to the radial domain $0.2 \leq r/a \leq 0.4$, in a simplified circular geometry under otherwise ITER-like conditions, indicates that such group of modes leads to rather insignificant anomalous alpha-particle redistribution even in worse than expected conditions. The possibility of significant redistribution via interaction with more radially extended modes remains to be clarified.

Modelling of the drift kinetic Alfen eigenmodes (DKAEs) using the PENN code has revealed[4] a strongly unstable $n = 3$ mode in ITER like plasma with a deeply reversed magnetic shear ($I = 8$ MA, $q(0)=4.5$, $q_{min} = 3.77$) and $\omega_{*,bulk}/\omega_{TAE} \approx 0.01n$. The theoretical understanding of DKAE instabilities is however still limited. With the present knowledge, it is advisable to avoid scenarios where the ratio $\omega_{*,bulk}/\omega_{TAE}$ exceeds $\approx 0.002n$, in order to remain in a regime where little degradation of fast particle confinement has been observed experimentally in JET.

[1] A. Jaun, et al., Phys. Plasmas **5** (1998) 2952; A. Fasoli, et al., Phys. Lett. **A265** (2000) 288
[2] A. Jaun, et al., Nucl. Fus. **39** 11Y (1999) 2095
[3] J. Candy, et al., Phys. Plasmas **4** (1997) 2597
[4] A. Jaun, et al., Nucl. Fusion **40** (2000) 1343

It is therefore desirable to develop advanced tokamak burn scenarios with a flat or weakly inverted safety factor ranging between $q \approx 1$ - 2 in the core.

4.6.2.2 Fishbone Instability

The fishbone instability is the resonant wave-particle interaction between the toroidal precession of trapped energetic particles and the toroidal wave velocity of m = 1, n = 1 MHD perturbations. Fusion alpha particles typically have energies such that their magnetic precession frequency $\omega = E_\alpha/(ZeBRr)$ is much higher than the thermal ion diamagnetic precession frequency. In this case, the threshold for the excitation of alpha-driven precessional drift fishbones depends on the alpha particle β. An analytic study including the effects of shaping, finite aspect ratio and finite beta, found fishbone instability occurred when the alpha particle β exceeds 1% on axis. As this is only slightly higher than the normal value expected in ITER, alpha-particle-driven fishbone oscillations may actually occur. However, according to calculations of anomalous transport of alpha particles due to fishbones, although redistribution of the alpha particle profile is caused, loss of trapped alpha is not expected.[1]

4.7 Conclusions

The physics analysis outlined in this chapter demonstrates that ITER satisfies its objectives: inductively-driven DT discharge with Q > 10 lasting for 300-500 s with sound margins in confinement, β and L-H transition power. The nominal operation density is 85% of the Greenwald density, which enables operation with high reliability, particularly with high plasma triangularity. Recent results from JET and ASDEX Upgrade have given confidence on maintaining $H_{H98(y,2)} \sim 1$ at $n \sim n_G$. Even with I_p = 15 MA and $H_{H98(y,2)} = 1.0$, operation with reduced additional heating with $n = n_G$ would enable achievement of Q ~ 20. High current (e.g. 17 MA) operation will enable studies on plasmas with high Q ~ 50, i.e. plasmas which are almost fully self-sustained. Improved confinement by a factor of 1.2 or improved confinement up to the Greenwald density would also allow sub-ignition studies at 15 MA.

The operational scenarios that are under consideration for steady state operation involve modest currents (~ 9 MA) with negative shear. However, modest current, steady state operation requires challenging values of confinement improvement ($H_{H98(y,2)} \sim 1.5$) and β ($\beta_N \sim 2.7$). Although these values have been obtained in recent experiments, further investigation will be required to establish the operation scenarios: pressure and current profile control, stability control, and divertor compatibility. Hybrid operation, with combined inductive and non-inductive current drive, will provide long pulses (e.g. > 1,000 s) with a more modest requirement on confinement ($H_{H98(y,2)} \leq 1.0$). This scenario offers a candidate operation mode for material tests.

ITER has the capability to exploit NB, EC, IC and/or LH for heating and current drive, which, taking advantage of their different characteristics, offers flexibility and variation in experimental operation. In addition, the diagnostics system is designed to satisfy the profile control needs of enhanced modes of operation.

The advanced features of ITER include ECCD for stabilising neoclassical tearing modes, saddle coils external to the toroidal field coils for stabilising resistive wall modes, and high-

[1] ITER Physics Basis, Chapter 5 Section 4, Nucl. Fus. **39** (1999) 2478

field-side pellet injection, all of which will expand the operational space and/or improve the stability characteristics of discharges with high β and high density.

The reference operation at $q_{95} \sim 3.0$ is associated with large uncertainty in projecting the ELM heat load onto the divertor targets. All available models lead to values of the energy density on the divertor target larger than what would be permitted to achieve an acceptable target lifetime due to erosion. Even if the most conservative value based on sheath-limited power transfer to the target is not too much larger than the acceptable value (less than 2), it is important to consider a number of alternative scenarios to be used to reduce the ELM amplitude. A design solution exists for this problem: a tungsten target, inclined by a factor of two from the reference design, would withstand the type I ELM heat load of most conservative estimation. The helium exhaust efficiency and heat load during steady state are tolerable. However, this design solution is associated with possible melting at disruptions and high particle recycling at upstream, i.e. some concern on the compatibility of H-mode confinement. Therefore the initial operation will use CFC as the reference target. The tungsten target may be used in the later stage after an experimental verification is made on ELM heat loads being unacceptable and control schemes are developed to reduce heat load during disruption to a tolerable level for tungsten. High density or density peaking by pellet injection and ion heating by IC H&CD would facilitate reaching $Q \geq 10$ at 13 MA ($q_{95} \sim 3.5$), where more benign ELMs are expected (type II ELM regime). Furthermore, weak-negative-shear operation would provide a scenario for reaching $Q \geq 10$ at $q_{95} \sim 4$.

To summarise, the physics design concept of ITER satisfies the stated mission, embodies all the state-of-the-art tokamak physics knowledge available to date, and is compatible with the constraints of engineering and cost. ITER will allow, for the first time, plasma physics studies on confinement, MHD stability, divertor, and energetic particle confinement, under completely integrated, reactor-relevant conditions, and for pulse lengths significantly longer than the characteristic times of plasma processes. Also, its flexibility in fusion power, plasma density, beta, shaping, heating and current drive methods, fuelling, and replaceable in-vessel components, will accommodate uncertainty in projection, and facilitate the investigation and optimisation of burning plasma. Furthermore, significant α heating, high β, large size and long burn, are expected to define and optimise operation regimes attractive for a reactor as well as new aspects of plasma physics. ITER, with its extensive diagnostics and considerable flexibility, is an essential and powerful vehicle for the exploration of these frontiers.

5 Safety

5.1 Introduction

It is a goal of ITER to demonstrate the safety and environmental potential of fusion and thereby provide a good precedent for the safety of future fusion power reactors. To accomplish this goal, ITER needs to address the full range of hazards and minimise exposure to these. However, it is necessary to account for ITER's experimental nature, the related

design and material constraints, and the fact that not all design choices are suited for future fusion power reactors.

With regard to the above goal, the ITER work programme has always included extensive safety and environmental assessments and aimed at a design that can be sited in any of the sponsoring Parties' countries with a minimum of site-specific adaptations. There can be a number of acceptable safety approaches and different choices or emphasis made in implementing a safety approach to meet a particular country's concerns and regulations. This section describes a generic safety approach and its implementation for a generic site. The safety guidelines for the project are based on internationally recognised principles and criteria, most notably the International Commission on Radiological Protection (ICRP) and the International Atomic Energy Agency (IAEA) recommendations. The approach to safety[1] is summarised in the following sections in terms of safety objectives, safety principles, safety and environmental criteria, and the elements of the generic safety approach.

5.2 Safety Approach

5.2.1 Safety Objectives

With regard to the safety of individuals, society and the environment, the potential hazards in ITER from normal operation, off-normal operation and waste are addressed as follows:

(1) ensure in normal operation that exposure to hazards within the premises is controlled, kept below prescribed limits, and minimised;
(2) ensure in normal operation that exposure to hazards due to any hazardous effluents from the premises is controlled, kept below prescribed limits, and minimised;
(3) prevent accidents with high confidence;
(4) ensure that the consequences, if any, of more frequent events are minor and that the likelihood of accidents with higher consequences is low;
(5) demonstrate that the consequences from internal accidents are bounded as a result of the favourable safety characteristics of fusion together with appropriate safety approaches so that there may be, according to IAEA guidelines[2], technical justification for not needing evacuation of the public (external hazards are site dependent, but are considered for the generic site);
(6) reduce radioactive waste hazards and volumes.

It is against these objectives that ITER has been assessed as summarised here.

5.2.2 Safety Principles

The principles[3] associated with the safety approach that have guided the design are listed below.

(1) As a basic principle, exposures to hazards shall be kept as low as reasonably achievable (ALARA), economic and social factors being taken into account.

(2) Defence-in-depth is used so that all activities are subject to overlapping levels of safety provisions in that a failure at one level would be compensated by other provisions. Priority shall be given to preventing accidents. Protection measures shall

[1] Plant Design Specification G A0 SP 2 00-06-01 R2.0, section 3
[2] International Atomic Energy Agency, International Basic Safety Standards for Protection against Ionizing Radiation and for the Safety of Radiation Sources, Safety Series No. 115, IAEA, Vienna (1996)
[3] Plant Design Specification G A0 SP 2 00-06-01 R2.0, section 3.2

be implemented in sub-systems as needed. In addition, measures to mitigate the consequences of postulated accidents shall be provided, including successive or nested barriers for confinement of hazardous materials.

(3) Passive safety shall be given special attention. It is based on natural laws, properties of materials, and internally stored energy. Passive features, in particular minimisation of hazardous inventories, help assure ultimate safety margins.

(4) The safety approach shall be driven by a deployment of ITER's favourable safety characteristics to the maximum extent feasible: the fuel inventory in the plasma is always below 1 g so that the fusion energy content is small; plasma burn is terminated inherently when fuelling is stopped due to the limited confinement by the plasma of energy and particles; the plasma burn is self-limiting with regard to power excursions, excessive fuelling and excessive additional heating; the plasma burn is passively terminated by the ingress of impurities under abnormal conditions; the radioactive decay heat density is low; the energy inventories are relatively low; large heat transfer surfaces and large masses are available as heat sinks; confinement barriers exist and must be leak-tight for operational (non-safety) reasons.

However, the experimental nature of the facility shall also be addressed. A conservative, fault-tolerant safety envelope shall be provided to enable flexible experimental usage. In view of the limited operational experience with DT plasmas and hence some plasma physics uncertainties, experimental components will be conservatively designed considering the expected loads from plasma transients so as to reduce the demands on systems which are required for safety. A safety function shall not be assigned to experimental components, but faults in these will be considered as expected events in the safety assessments. The experimental programs and related machine modifications and operations shall be developed to take advantage of preceding operations.

(5) Safety assessments shall be an integral part of the design process and results will be available to assist in the preparation of safety documentation for regulatory applications. These analyses shall comprise normal operation, all categories of off-normal operation, and waste.

5.2.3 Safety and Environmental Criteria

Since regulatory approval is required before the construction of ITER, preparations to assist in the future application for approval have been included in the design. In the absence of an actual ITER site, the design has followed international recommendations (ICRP and IAEA), in particular technology-independent ones, such as limits on doses to the public and staff.

The project guidelines for doses from occupational exposure[1] are given in Table 5.2.3-1. The work towards the establishment of best practices is consistent with the ICRP and IAEA recommendations. In particular, efforts have been made to design such that exposures during operation, maintenance, modification and decommissioning are ALARA.

[1] Plant Design Specification G A0 SP 2 00-06-01 R2.0, Table 3-2

Table 5.2.3-1 Limits and Project Guidelines for Doses from Occupational Exposure

Dose Limits	
ICRP[1] recommended limit for annual individual worker doses	20 mSv averaged over 5 consecutive years not to exceed 50 mSv in any year
Project Guidelines	
Annual individual worker doses	< 5 mSv/year
Individual worker dose for any given shift	< 0.5 mSv/shift

The project has established guidelines for radioactivity releases to the environment[2] given in Table 5.2.3-2. The design has aimed at ensuring margins between calculated values and project guidelines. The favourable characteristics of ITER can be further demonstrated if, even for hypothetical events (see section 5.5.5) that can be postulated, the calculated doses to the local population are below 50 mSv (early dose). This would be below the generic optimised intervention level for temporary evacuation developed by the IAEA[3] which is 50 mSv avertable dose within a period no more than 1 week. Following site selection, host country regulations will apply.

Table 5.2.3-2 Project Release Guidelines

Events or Conditions	Goal	Project Release Guideline
Normal Operation, comprising events sequences and plant conditions planned and required for ITER normal operation, including some faults, events or conditions which can occur as a result of the ITER experimental nature.	Reduce releases to levels as low as reasonably achievable but ensure they do not exceed project release guideline for Normal Operation.	< 1 g T as HT and 0.1 g T as HTO and 1 g metal as AP and 5 g metal as ACP per year.
Incidents, comprising deviations from normal operation, event sequences or plant conditions not planned but likely to occur due to failures one or more times during the life of the plant but not including Normal Operation.	Reduce likelihood and magnitude of releases with the aim to prevent releases, but ensure they do not exceed project release guideline for Incidents.	< 1 g T as HT or 0.1 g T as HTO or 1 g metal as AP or 1 g metal as ACP or equivalent combination of these per event.
Accidents, comprising postulated event sequences or conditions not likely to occur during the life of the plant.	Reduce likelihood and magnitude of releases but ensure they do not exceed project release guideline for Accidents.	< 50 g T as HT or 5 g T as HTO or 50 g metal as AP or 50 g metal as ACP or equivalent combination of these per event.

HT: elemental tritium (including DT); HTO: tritium oxide (including DTO); AP: divertor or first wall activation products; ACP: activated corrosion products.

In the absence of an actual ITER site, activated materials that do not meet the criteria for unconditional clearance following IAEA recommendations[4] after a decay period of up to 100 years are considered long-term waste.

[1] 1990 Recommendations of the International Commission on Radiological Protection, ICRP Publication 60, Pergamon Press, 1991

[2] Plant Design Specification G A0 SP 2 00-06-01 R2.0, Table 3-1

[3] International Atomic Energy Agency, International Basic Safety Standards for Protection against Ionizing Radiation and for the Safety of Radiation Sources, Safety Series No. 115, IAEA, Vienna (1996)

[4] "Clearance Levels for Radionuclides in Solid Materials", International Atomic Energy Agency, IAEA-TECDOC-855, Vienna, 1996

5.2.4 Implementation of the Safety Approach

5.2.4.1 Overview

This section describes the current implementation of the safety design principles and elements of a generic safety approach[1].

The ITER safety approach has been implemented by:

- enhancement of fusion's intrinsic safety characteristics to the maximum extent feasible, which includes a minimisation of the dependence on dedicated 'safety systems';
- conservative design to accommodate uncertainties due to the limited operational experience and data with DT plasmas;
- integration of mitigation systems to enhance safety assurance against potentially hazardous inventories in the facility by deploying well established safety approaches and methodologies tailored for ITER;
- use of a step-by-step approach through progressive stages of operation to further validate safety data and analyses.

ITER is a research facility, and its experimental nature requires a design that permits flexible operation, facilitates experimentation, and can accommodate changes. Changes, for example, could include testing of alternative divertor designs, different plasma-facing materials, etc. These needs drive the safety design in three ways:

- provision of a conservative safety envelope;
- minimisation of the safety role and influence of experimental components such as the divertor and blanket;
- minimisation of the safety role and influence of experimenters' equipment such as plasma diagnostics.

Protective measures and safety functions have been identified to ensure protection of the personnel, public and the environment. Design requirements have been derived from the safety principles and release guidelines by identifying the systems, structures, components, and procedural or administrative measures that can prevent or mitigate releases, and by allocating performance targets (both in terms of capability and reliability) to these. The design requirements are iterated and refined as a result of systematic safety analysis.

The elements of the implementation of the ITER safety approach are listed below.

Design
- confinement and protection of confinement
- component classification
- structural design
- materials
- quality assurance

Ability to withstand events
- earthquake and other common cause events
- equipment (environmental) qualification
- fire protection

Protection of public and environment in normal operation

[1] Plant Design Specification G A0 SP 2 00-06-01 R2.0, Section 3.4

effluents
decommissioning
waste
Safety of workers
radiation protection
hazardous materials
conventional hazards
Legal and international obligations
security and proliferation
Human Factors
organisational aspects, user interfaces, etc.

From a review of the nature of the hazards in ITER, protective measures or safety functions are identified and assigned to implementing systems and components.

Restricting inventories is an effective method to control hazards.

Confinement of hazardous materials is the most fundamental safety function, where confinement refers to all types of physical and functional barriers which provide protection against the spread and release of hazardous materials. Confinement is implemented by:

- sets of successive physical envelopes (including process enclosures, secondary confinement, port cells, containment volume, etc.) around each of the principal source terms (in-vessel, fuel cycle, heat transfer systems, hot cell, and in-vessel components during maintenance);
- systems (vacuum vessel pressure suppression system, tokamak vent system, tokamak cooling water system (TCWS) vault coolers, and normal and standby vent detritiation systems) which provide the functions of pressure control in and removal of radioactive materials from these envelopes.

Releases would most significantly occur upon breach of barriers. Hence, protection of confinement and the following needs to be evaluated, taking into consideration ITER's safety characteristics.

Control of coolant enthalpy to prevent damage to barriers from overpressure or underpressure.

Control of chemical energy to avoid energy release and pressurisation threats to confinement barriers.

Heat removal to protect against mobilisation of hazardous materials or damage to barriers.

Control of magnetic energy to avoid damage to confinement barriers from mechanical impact, pressurisation or electric arcs in the event of faults.

5.2.4.2 Inventories

The ITER project has set itself challenging guidelines for the maximum amounts of tritium and dust inside the vacuum vessel and the fuel cycle. Further design studies have to show their feasibility. These ambitious guidelines were set to push the design into a direction of minimising inventories. If further studies showed that the guidelines needed to be increased to allow practical operation of ITER, this would not invalidate the ITER safety approach, since wide margins are built into the confinement of inventories such that predicted releases are significantly below project release guidelines. More details of the radioactive inventories and energies in ITER are given in subsection 5.3.

5.2.4.3 Confinement

ITER protects personnel and the public by using confinement barriers. Successive physical and functional barriers protect against spread and release of hazardous materials. The confinement barriers are as independent from each other and passive where possible with minimal dependence on new components that cannot practically be tested in the appropriate service environment before construction. Every radioactive inventory is contained in its vessel, process piping, component, etc. which serves as the first confinement barrier. This confinement barrier is designed to have high reliability to prevent releases. Another barrier is provided, usually close to the first one, to:

- protect personnel and limit the spread of contamination from leaks;
- mitigate consequences in the event of failure of the first barrier to assist in meeting the project release guidelines.

The design maximises structural and spatial separation and independence from the first confinement barrier to prevent a common failure mode of both barriers. Exhaust from rooms that can be contaminated is treated by filters and/or detritiation systems and is monitored.

Inventories of tritium or activated materials reside within the vacuum vessel, in the fuel cycle (vacuum pumping, tritium plant, fuelling), within the hot cell, and in the TCWS. The confinement approach for accidents for each of these is illustrated in Figure 5.2.4-1 and described below.

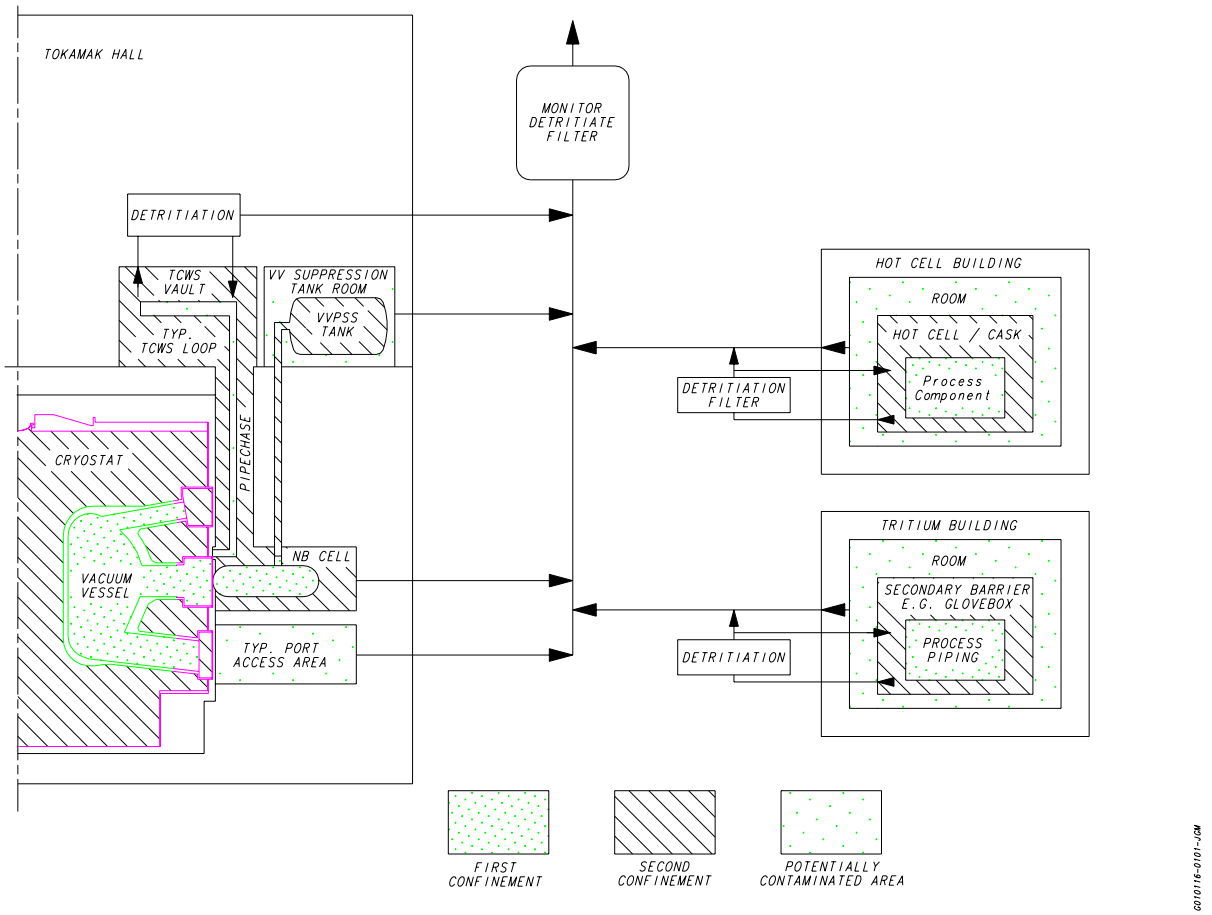

Figure 5.2.4-1 Schematic of Confinement Approach for Accidents Illustrating the Successive Confinement Barriers that are Available

The primary confinement for the source term within the vacuum vessel is the vacuum vessel and its extensions including the neutral beam (NB) injector vessels and confinement barriers in the radio-frequency (RF) heating systems and diagnostics. The TCWS piping forms the primary confinement for tritium and activated corrosion products in the loops of its constituent primary heat transfer systems (PHTSs). Since experimental components inside the vacuum vessel are not assigned a safety function, the TCWS must also confine the in-vessel source term for events such as an in-vessel coolant spill. The vacuum vessel pressure suppression system (VVPSS) reduces peak pressures inside the vacuum vessel if there is an ingress of coolant, and the parts of the VVPSS that are external to the cryostat would then also form part of the confinement barrier.

For the in-vessel and TCWS source terms, another barrier is available. Penetration confinement barriers or windows, typically at the cryostat closure plate, in the RF heating systems and diagnostics form part of this barrier. The TCWS vault, the area where the CVCSs are, the TCWS vault extension, the NB cell, the vertical pipe shafts, the upper and lower pipe chases and the lower pipe sump, collectively referred to as the containment volume, are designed to be leak tight and withstand over-pressures following coolant spills. Exhaust from the containment volume, port access areas and gallery areas, etc. that can be potentially contaminated (e.g. due to accidental leakage past confinement barriers or during maintenance) can be treated by filters and detritiation systems and is directed to the monitored plant exhaust.

The stainless steel piping used in the TCWS piping is ductile and incipient failures should be revealed by leaks before any crack reaches a critical crack size. For such materials and with a reasonable leak detection system, double-ended guillotine failures can be considered 'hypothetical events'. The containment volume, at minimum, is designed to confine the pressures resulting from a leak in the TCWS piping under any foreseen conditions. Due to the higher temperatures, pressures resulting from a leak during machine baking (when the coolant temperature is ~ 240°C) is limiting. A building design pressure of ~ 200 kPa (absolute) is adequate to confine any such leak with a margin to allow for computational uncertainty.

Nonetheless, the containment volume can also confine the pressure caused by any pipe failure during plasma operation up to and including a double-ended guillotine rupture. It is only during pulsed operation of the plasma (coolant temperatures ~ 150°C) that an ex-vessel piping failure could lead to in-vessel failures (due to resulting overheating of in-vessel components or disruption damage), and hence potentially release the in-vessel source term (tritium, dust) into the containment volume. A building design pressure of ~ 200 kPa (absolute) is also adequate to confine any such release with a margin to allow for computational uncertainty. This approach of confining breaks even up to double-ended guillotine failures during operation adds margin to the design and decreases the importance to public safety of being able to correctly predict critical crack sizes and leak rates, and of having a sensitive leak detection system capable of working under transient conditions such as during a pulse.

Leaks through PHTSs heat exchangers can be isolated (e.g., isolation valves on the heat rejection system). The vacuum vessel primary heat transfer system (VV PHTS) is somewhat different from the others in that it is very well shielded from the plasma and neutrons by the in-vessel components. As a result the VV PHTS contains very low inventories of tritium and

activated corrosion products even under accident conditions and hence does not require a secondary confinement barrier.

Heating, ventilation and detritiation systems provide additional confinement functions (isolation, detritiation, filtering) for the port cells surrounding the tokamak. These systems service rooms where a release of tritium or tokamak dust is possible. Releases to the environment would be reduced by providing filters to remove particulates, dryers to remove tritiated water vapour, or detritiation systems to remove elemental tritium. Releases are routed to a monitored release point.

The primary confinement for the fuel cycle tritium inventory is the process equipment and pipes of the vacuum pumping system, tritium plant, and fuelling system. These are surrounded by secondary barriers such as glove boxes, cold boxes, vacuum jackets, and other enclosures. For example in the isotope separation system, tritium is contained by the high quality piping and components of the distillation columns which are themselves within in a cold box under high vacuum for thermal insulation and which also forms another confinement barrier. Rooms are maintained at a negative pressure with respect to the external atmosphere, and the exhaust can be treated by detritiation systems and is directed to the monitored plant exhaust.

The hot cell source term includes tritium and activated materials that arise from the refurbishment and the storage of in-vessel components. Hot cells, casks, and process equipment (e.g. for tritium recovery from plasma-facing materials) form the primary confinement barrier, and the hot cell building exhaust can be treated by filters and detritiation systems, and is directed to the monitored plant exhaust.

Other buildings with radioactive materials include the low level radwaste building and the personnel building. Floor drainage from such radiologically controlled areas is collected to tanks where it can be monitored and, if necessary, treated before it is discharged to the environment. Ventilation from the potentially contaminated, radiologically controlled spaces in these buildings is routed to the monitored plant exhaust.

Using the vacuum vessel and cryostat as confinement barriers takes advantage of the inherent magnetic fusion characteristic that high quality and high reliability vacuums are needed for fusion operation. Failures of these barriers or leakage through them inherently (passively) terminate plasma or super-conducting magnet operation. The other confinement barriers are tailored to the nature of hazards in each compartment. The vacuum vessel and its extensions (including penetration barriers), the fuel cycle process piping, hot cells, etc. that form the primary enclosures for radioactive inventories, together with the building and detritiation/filter systems, may be considered a minimum set of systems to meet project release guidelines. The additional confinement barriers described in this section are available to reduce the spread of contamination in the facility and help protect personnel from exposures, and they also further enhance public safety.

5.2.4.4 Coolant Enthalpy

The use of pressurised water and cryogenic coolant requires consideration of the consequences of failure for the protection of confinement barriers, and design of the confinement barriers for accident pressures.

The vacuum vessel is connected to a pressure suppression system by ducts with rupture disks and bleed valves that permit connection at pressures below the rupture disk setpoint. Steam from an in-vessel coolant leak is routed though the ducts and condensed in the large tank of water of the VVPSS, which limits the pressure in the vacuum vessel to below its design pressure. Operation of the VVPSS is passive, relying only on pressure differences to open the rupture disks and force the steam through the water in the VVPSS tank to condense the steam. The bleed valves are provided to permit connection to the VVPSS at lower pressures which may avoid use of the rupture disks and limit recovery time and operator exposures. A drain line allows water to be drained from the vacuum vessel to the drain tank, limiting the generation of steam in the longer term. The VVPSS also provides vacuum vessel overpressure protection in case of cryogenic leaks into the vacuum vessel (e.g. from cryopumps).

The ex-vessel primary heat transfer system piping is surrounded by guard pipes, pipe chase structures, or is within the TCWS vault and/or NB cell (see section 5.2.4.3). Water and steam released if piping fails are routed to the vault. In the TCWS vault, coolers are provided to return the pressure to sub-atmospheric within 24 hours in the event of a steam discharge.

5.2.4.5 Hydrogen Inventories and Chemical Reactions

The potential for the following chemical reactions exists in ITER:

- hydrogen - air reaction with hydrogen isotope inventories in process systems in case of leaks from or into process piping;
- beryllium/carbon/tungsten - steam/air reactions inside the vacuum vessel at elevated temperatures following in-vessel coolant spills or air ingress;
- ozone formation (and the attendant explosion hazard) in liquid/frozen air caused by air in-leakage in a radiation field.

In the case of systems containing hydrogen, basic hydrogen safety design principles applied in the design include:

- preventing leakage of hydrogen isotopes (also required for radioactive material confinement);
- eliminating the formation of hydrogen/air mixtures by use of inert or vacuum second confinement or isolation;
- preventing the formation of flammable hydrogen/air mixtures in rooms by adequate ventilation;
- eliminating ignition sources.

Reduction of hydrogen generated by potential in-vessel chemical reactions consists of:

- limiting the quantities of chemically reactive dust on hot plasma-facing components of the divertor to less than 6 kg each of beryllium, carbon and tungsten;
- terminating fusion power to prevent heat up to high temperatures of in-vessel components by terminating the heat load in the event of an upset in their heat transfer systems to limit hydrogen production from Be-steam reactions[1];
- ensuring heat removal to reduce temperatures and hence reduce reaction rates - the design ensures that in-vessel temperatures remain below 385°C for the beryllium surfaces except during the few tens of minutes of initial transient after fusion power shutdown (see section 5.2.4.6).

[1] for example, M.J. Gaeta, B.J. Merrill, H.-W. Bartels, L.N. Topilski, and C. Laval, "Short term hydrogen production issues for ITER", Fusion Technology, Vol. 32 (1997), pp 23-34

The design of the cryostat must limit air leakage in the cryostat below an acceptable value to maintain thermal insulation for cryogenic cooling of the superconducting magnets, and this also prevents the potential ozone production (and hence explosion) hazard. Provision is made to detect cryocondensates on the cryostat interior cold surface. All cryogenic needs across the ITER facility (except inside the cryoplant) are met by helium, not by liquid nitrogen to avoid the formation of ozone.

5.2.4.6 Heat Removal

Heat must be removed during normal operation to prevent component failures and following events to limit chemical reactions, to limit source term mobilisation, and/or to help ensure confinement integrity is maintained.

The decay heat time evolution after shutdown is shown in Figure 5.2.4-2. At the end of life (conservatively assuming a fluence of 0.5 MWa/m^2 to maximise predicted decay heat) the ITER global decay heat amounts to ~11 MW at shutdown and decreases to 0.6 MW after one day.

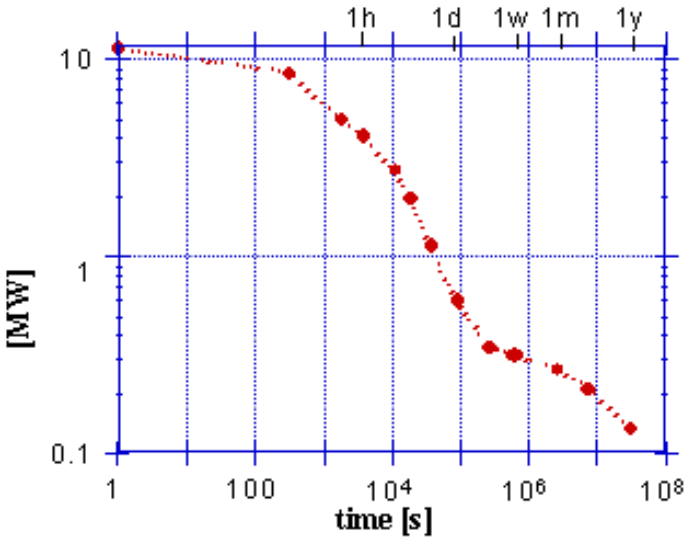

Figure 5.2.4-2 Global Decay Heat In ITER at End of Life (fluence 0.5 MWa/m^2)

Successive lines of defence of systems to provide heat removal are available:

- multiple normal heat removal paths and systems provided for machine operation (which are assumed not to function for safety assessment);
- two independent loops of the vacuum vessel cooling systems;
- a natural circulation capability of the vacuum vessel PHTS should electrical power for its pumps be lost;
- thermal radiation to the magnet structures and cryostat and ultimately to the environment;
- the possibility of assisting ultimate decay heat transfer by introducing gas into the cryostat, degrading the vacuum insulation.

The VV PHTS has a natural circulation capability and is divided into two independent loops. Each loop is capable of removing decay heat and slowly cooling down the structures in the

long-term following an accident (~ 0.8 MW). Initially the in-vessel components cool off as the plasma heat load is removed. No cooling is needed for several hours (> 12 h) as temperatures remain < 330°C. Subsequently, the in-vessel components slowly heat up until the decay heat levels decrease to within the vacuum vessel heat transfer system capability (~ 17 hours). The acceptability of the intermediate heat-up is confirmed in accident analyses. In the safety assessments, only the vacuum vessel cooling system is assumed to provide the decay heat removal function.

For hypothetical sequences (when all in-vessel and vacuum vessel cooling is assumed not to be functioning), investigations conclude that filling the cryostat with helium even weeks after the loss of cooling and ensuring air convection at the outer surface of the cryostat is sufficient to limit in-vessel component temperatures to < 650°C, precluding failure of confinement barriers and limiting any potential for chemical reactions.

Decay heat removal by radiation and natural circulation is an example of passive safety integrated into the ITER safety approach.

5.2.4.7 Magnetic Energy

The function of the magnet system is to provide the toroidal and poloidal magnetic fields necessary to initiate, contain and control the plasma during the various phases of machine operation. Since the magnets occupy valuable space around the machine, and are difficult to repair, the primary design considerations are compactness and reliability. However, the magnets contain large amounts of magnetic energy, are subjected to large electromagnetic loads, and are in proximity to confinement barriers. Safety is therefore also an aspect that requires consideration at the design stage. The magnet system is designed to be built and operated so that its failures cannot cause damage to confinement barriers that would result in a release of radioactivity exceeding the project release guidelines.

Because of the need for high availability levels required for machine operation, the magnets have multiple levels of defence against operational faults, so that the likelihood of any fault developing to the point where permanent magnet damage occurs is very low. For the same reason, margins are provided in the magnet design criteria, and the quality assurance procedures to be applied during manufacturing, pre-testing and commissioning of magnet components must be very thorough. Again, for investment protection, multiple diagnostics and/or inherent design features are included to achieve an inherently low probability of faults and/or a minimisation of their impact. Where active protection is used, the instrumentation and intervention systems are fully separate from the fault location and entirely independent of it. Reliance on the functioning of single critical components or diagnostics to achieve the desired low probability of magnet damage is avoided.

Nonetheless, to assess the design performance for safety, the inherently low fault probability has been neglected, and faults have been postulated and analysed with particular attention to the failure of the manufacturing inspection and active protection systems. Potential damage mechanisms are:

- structural: mechanical impact on other components due to abnormal loads on magnets caused by postulated faults or due to postulated structural failure of magnet components;
- thermal: energy deposition from the magnets into other components due to arcs

arising from postulated faults.

The magnets are massive components, and the magnet structural elements are distributed and contain large redundancy against failure. The design of these structural elements take into account normal and abnormal loading conditions to prevent structural failure or thermal damage to the point where the vacuum vessel or its extensions are damaged. Fault detection to switch off power to the PF coils is included to mitigate damage that may be caused by arcs. Damage from postulated arcs is limited to cryostat feedthroughs and there is no release of radioactivity as a consequence of magnet system failures.

5.3 Radiological Source Terms

ITER will contain radioactive and hazardous materials as well as energy inventories. They have been quantified as part of the safety assessment since they are the basis for virtually all safety and environmental analyses.

The relevant source terms are:
(1) tritium,
(2) tokamak dust,
(3) activated corrosion products (ACPs).

The total site inventory of tritium will be < 3 kg. The ITER project has set an ambitious guideline for initial operation of 450 g tritium for the maximum mobilisable amount of tritium inside the vacuum vessel or the fuel cycle subsystems. The cryogenic pumps have a maximum tritium inventory of 120 g. Thus the maximum amount of tritium in co-deposited layers and implanted in plasma facing material should be limited to less than 330 g by regular removal (see section 2.4). Tritium bred inside the beryllium of the first wall is considered to be immobile because of the limited temperatures in ITER off-normal operation. These ambitious guidelines were set to push the design into a direction of minimising tritium inventories. For safety assessments, larger values were used (1000 g in vessel and 700 g in the fuel cycle) to provide margins for measurement uncertainties. Because of the wide margins adopted in the confinement of these inventories, operating values above the guidelines would not invalidate the safety approach. The tritium inventory is segmented such that only a relatively small fraction is available for mobilisation and release during any specific event. Multiple confinement barriers including tritium cleanup systems are provided to mitigate the consequences of any tritium release.

The vast majority of the activation products are tightly bound in solid metallic structures and are not mobilisable during any credible off-normal scenario. ITER energy sources are controlled such that activation product mobilisation is generally limited to erosion (dust) and corrosion of structural materials.

The plasma-facing components are beryllium, carbon, and tungsten. A guideline to limit the mobilisable tungsten dust to 100 kg inside the vacuum vessel has been established due to its radiological hazard. For safety assessments, larger values were used (350 kg in vessel) to provide margins for measurement uncertainties. Dust particles are prone to chemical reactions with steam, forming hydrogen in off-normal situations when coolant is leaked into the vacuum vessel. To limit this potential source of hydrogen, guidelines are set for the maximum amount of dust on the divertor surface. These surfaces can be hot enough in off-normal situations to cause oxidation of dust and subsequent hydrogen production. The

guideline is 6 kg dust each for carbon, beryllium and tungsten (see section 5.2.4.5). Dust production and removal is further discussed in Section 2.4.

Some ACP will be present in the various in-vessel and vacuum vessel coolant loops as well as in coolant loops for the test modules, auxiliary heating and diagnostic equipment exposed to a neutron flux. The ACP affect occupational exposure, routine effluents to the environment and potential releases due to accidents. The amount of ACP has been assessed to be < 10 kg as deposits, < 60 g as cruds and ions per cooling loop. The hazard potential of the ACP in the vacuum vessel (VV) HTS is < 1% of the hazard potential of the ACP in the primary-first wall/blanket (PFW/BLK) HTS because the neutron flux is reduced by several orders of magnitude inside the vacuum vessel. Specific radionuclide concentrations used in the safety assessments are presented in Table 5.3-1.

Table 5.3-1 Activity of Tungsten and FW/shield Activated Corrosion Products (ACPs)

Tungsten activation (plasma surface layer: 25 micro-m)			**ACP deposits (steel)**			
isotope	half life [y]	activity [Bq/kg]	isotope	half life [y]	deposit activity [Bq/kg-deposit]	ion and cruds in solution activity [Bq/kg-ion/crud]
W 187	2.72E-03	5.24E+14	Fe-55	2.73E+01	2.07E+12	9.61E+11
W 185	2.06E-01	3.71E+13	Mn-54	8.55E-01	9.86E+10	3.49E+11
W 185m	3.17E-06	3.64E+13	Mn-56	2.94E-04	1.35E+12	1.19E+13
W 181	3.31E-01	1.43E+13	Co-58	1.94E-01	1.06E+11	3.92E+11
Re188	1.94E-03	6.01E+12	Co-60	5.27E+01	1.41E+11	2.39E+11
Re186	1.03E-02	2.20E+12	Cr-51	7.59E-02	1.14E+11	4.54E+08
Re188m	3.54E-05	5.79E+11	Ni-57	4.11E-03	4.52E+10	8.85E+10
W 179	7.13E-05	2.56E+11	Co-57	7.44E-01	2.64E+11	4.96E+11
Ta182	3.14E-01	1.54E+11				
W 179m	1.22E-05	1.02E+11				
Ta186	2.00E-05	6.34E+10				
Ta183	1.39E-02	6.18E+10				
Ta184	9.92E-04	4.34E+10				
Ta182m	3.04E-05	2.88E+10				
Ta179	1.61E+00	2.74E+10				
Re184	1.04E-01	1.99E+10				
Ta180	9.22E-04	1.15E+10				
Hf183	1.22E-04	9.64E+09				

5.4 Normal Operation

The assessment of normal operation addresses potential effluents and emissions to the environment, occupational safety of personnel working at the facility and radioactive materials generated during operation and decommissioning of ITER. The design and operation of ITER strives to reduce effluents, occupational exposure and wastes in accordance with the ALARA principle. Efforts to ensure very low levels will continue, but no concerns have been identified by the assessments.

5.4.1 Effluent Sources and Control

The ITER design incorporates many features to ensure that environmental impact during normal operation will be low. The hazards are known and the control technologies are well established. According to the analyses performed, the facility can be operated to satisfy the conservative safety and environmental guidelines that have been established by ITER. Continuing application of the process to implement the ALARA principle may further reduce the estimated normal effluents.

This section discusses effluents that may be expected during normal operation. The primary materials of concern are tritium and activated materials. In addition, the facility will produce electromagnetic fields at the site boundary less than the earth's natural magnetic field and will reject thermal energy. Normal operation includes operation of all systems required to carry out the experimental programme, as well as maintenance, hot cell operation, and radioactive materials management operations.

5.4.1.1 Summary of Effluents Estimates

ITER has set restrictive project release guidelines, as given in Table 5.2.3-2. In addition to meeting prescribed host country limits, the ALARA principle is recommended by international nuclear safety experts and incorporated in national regulations of many countries. The International Basic Safety Standards[1] explain ALARA as the objective to keep all exposures to values such that further expenditures for design, construction, and operation would not be warranted by the corresponding reduction in radiation exposure. For ITER this process involves a systematic review of systems, activities and pathways with a potential of effluents, estimating effluents, and examining ways to reduce the main contributors.

Sources of potential effluents have been identified, discharge pathways determined, and design features and active discharge control systems assessed for expected end of life conditions which are assumed to include extensive maintenance and refurbishment in the hot cell. Conservative assumptions are made so as not to underestimate potential effluents. Effluents pathways are controlled and monitored through the plant exhaust, the liquid discharge pathways, and the heat rejection system. Table 5.4.1-1 provides a summary of estimated annual effluents and compares these to the project guidelines. Annual effluents will increase with time from the start of operation as activation levels increase and tritium permeates, and will vary from year to year depending on activities undertaken, but are unlikely to exceed the values in Table 5.4.1-1 given the conservative assumptions used in making the estimates.

[1] "International Basic Safety Standards for Protection against Ionizing radiation and for the Safety of Radiation Sources", International Atomic Energy Agency, Safety Series No. 115, Vienna, 1996

Table 5.4.1-1 Estimates of Effluents at Expected End of Life Conditions and Comparison with Project Guidelines

Species	Estimate	Project Guideline	% of Guideline
Tritium – as HTO in air	0.05 g tritium /a (18 TBq/a)	0.1 g tritium /a	50
Tritium in water	0.0004 g tritium /a (0.14 TB/a)		
Tritium – as HT in air	0.18 g tritium /a (67 TBq/a)	1 g tritium /a	18
Activated dust	0.25 g metal/a	1 g metal/a	25
Activated corrosion products (ACP)	0.85 g metal/a	5 g metal/a	17
Species with no specified project guideline			
Species	**Estimate**	**Notes**	
Activated gases ^{41}Ar ^{14}C	 <1 TBq/a 10 MBq/a	Release limits not specifically established for these isotopes but not significant at these levels	
Direct radiation at 250 m	4 µSv/a	< 0.5% of background	
Beryllium (not activated)	~ 0.1 g/a	This is well below current limits for public protection as based on reviews of existing regulatory limits, official investigations and other publications	
Magnetic fields at 250 m	< 20 µT	Less than Earth's magnetic field (25– 65 µT)	
Thermal	411 MWt (pulsing at 25% availability) 180 MWt (shutdown)	Not significant	
Cryogen – Helium	~ 1-3 t/a	Not significant	

A detailed effluents assessment was performed for each system to ensure that no significant discharge pathway was missed. This detailed information has been further analysed to provide:

- a breakdown of effluents by discharge points (Figure 5.4.1-1);
- a comparison of effluents from operations and maintenance (Figure 5.4.1-2).

There is some uncertainty in any estimate of effluents, since ITER is a first-of-a-kind experimental facility, that will be resolved only when ITER begins operation. However, any radioactive effluents will increase slowly over the project lifetime, so there would be adequate time to upgrade discharge control systems if needed to maintain effluents at low levels. The pulsed nature of the operation also provides some flexibility in scheduling operations with potential effluents to ensure that effective control measures are in place beforehand. The preliminary estimates of effluents, and flexibility in the design to add additional or upgraded discharge control measures, provide confidence that the design can meet the project guidelines. Furthermore, a process is in place to ensure that effluents will be ALARA.

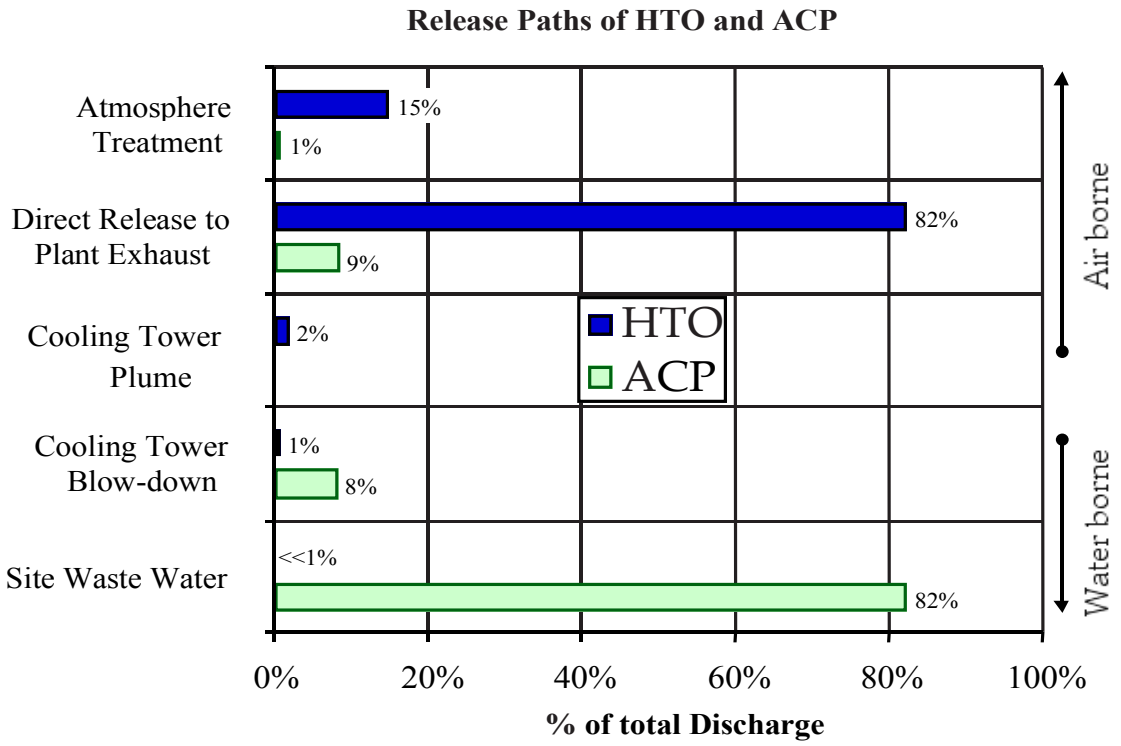

Figure 5.4.1-1 Fraction of the Total Amount of Tritium (HTO) and of Activation Corrosion Products (ACPs) Effluents from Specific Release Points or Paths

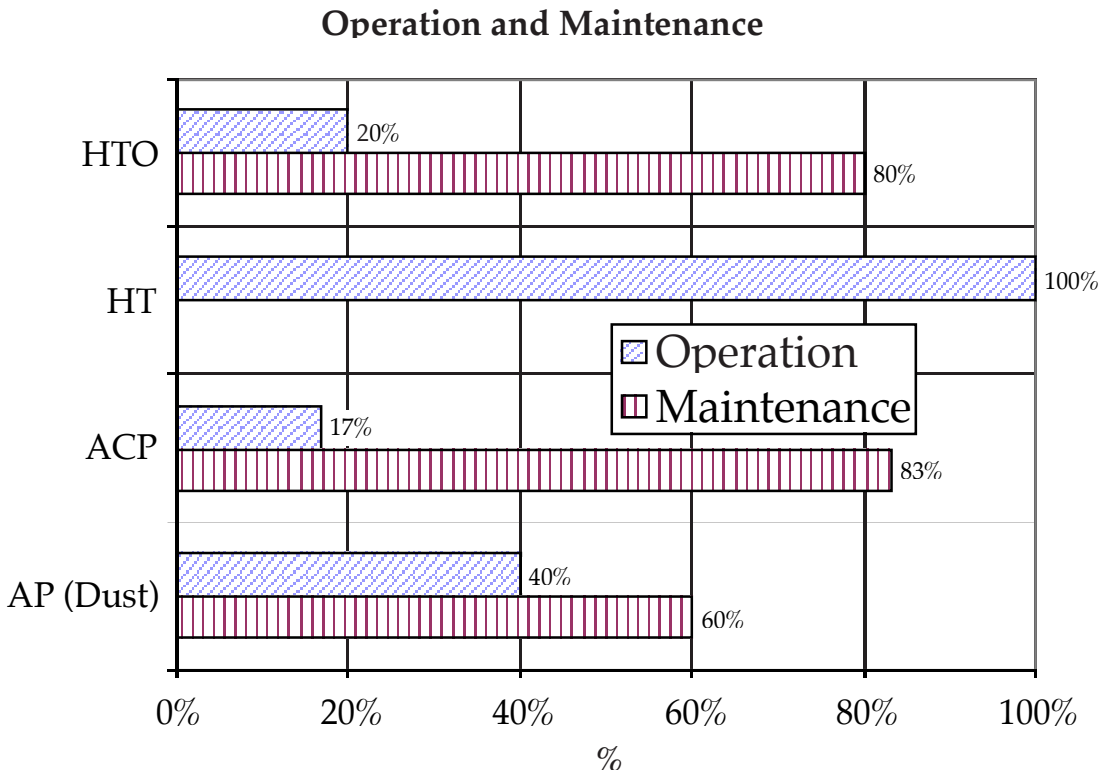

Figure 5.4.1-2 Fraction of the Total Amount of Tritium (HT or HTO), Activated Corrosion Products (ACP) and Activation Products (AP) Effluents during Operations or Maintenance

5.4.1.2 Tritium

There is a potential for tritium effluents from the following monitored release points:
- discharge from atmosphere detritiation systems through the plant exhaust;
- low concentrations discharged through the HVAC directly to the plant exhaust;
- discharge through the cooling tower plume;
- low contaminated water discharged with site waste water.

For each of these, effluents for normal operation and maintenance have been assessed and are summarised above in Figure 5.4.1-1. The tritium loss through HVAC to the plant exhaust results from numerous maintenance operations of large components where each individual discharge is small and further reduction by additional control systems is not warranted. The small amount of discharge from operational atmospheric detritiation systems results from the high removal efficiency, 99.9%, of these systems.

A small amount of tritium in the cooling tower blowdown as liquid effluent is included in the estimate, which is only due to the conservative assumption that the heat exchangers may have chronic leaks.

5.4.1.3 Activation Products

The primary contributors to operational effluents with activation products are the following:
- corrosion products from primary heat transfer systems (PHTSs);
- activated dust from the vacuum vessel;
- activated gases.

ACPs from Coolants

Activated material enters the PHTSs coolant by corrosion of the activated cooling channels in the components (e.g., blanket modules) within in the vacuum vessel. The isotopes entering the coolant depend on the material at the water interface. The three loops for the primary first wall/blanket (PFW/BLK) PHTS have stainless steel at the water interface. The vacuum vessel also has a steel/water interface but the neutron fluence is significantly lower. The divertor/limiter (DIV/LIM) PHTS loop has steel and copper at the interface. This is also the case for the NB PHTSs but the neutron fluence is lower for those systems.

The corrosion rate and solubility are strongly affected by the water chemistry and the extent of the water treatment during operation. The treatment during operation is performed by the chemical and volume control systems (CVCSs) described in section 3.3. This system employs chemical control, filtering, and ion exchange to remove ACPs. Table 5.4.1-2 lists the most significant isotopes for the coolant systems with stainless steel at the interface.

Table 5.4.1-2 Key Isotopes for the Coolant Systems with SS316 at the Water Interface

^{51}Cr	^{54}Mn	^{55}Fe	^{56}Mn	^{57}Ni	^{57}Co	^{58}Co	^{60}Co

The pathways for effluents are by leakage from the TCWS via the heat exchangers to the heat rejection systems, and leakage from components into the TCWS vault. Potential pathways and release points include the following:

- water discharged with the site waste water;
- water leakage into the TCWS vault and released by the HVAC system;
- leakage through the heat exchangers and loss to the cooling tower.

Operational effluents directly from the TCWS components not including heat exchanger leakage are primarily through the TCWS vault atmospheric control systems or from releases not captured by dryers or filters. During operation, the airflow in the vaults is continuously circulated through air filters with only a small stream extracted to maintain negative pressure. The resulting decontamination efficiency is very high, so losses will not be significant. During maintenance operations in the TCWS vault, when worker doses are an important consideration, air flow may be increased by directing flows directly to the plant exhaust filters. ACP effluents from the cooling tower blowdown is only due to the conservative assumption that the heat exchangers may have chronic leaks late in their lives.

The estimated ACP effluents are dominated by discharges from the site waste water originating from the PHTSs. The waste water is filtered, but these effluents have been conservatively estimated without crediting filtering.

Activated Dust

The pathway for dust from the vacuum vessel includes the following steps.

- Dust is carried outside the vacuum vessel, for example during movement of in-vessel components, it is likely that some dust will remain in crevices of the component, even after cleanup. During the cutting and rewelding required for divertor removal, some activated particulates could enter the contamination control areas.
- Dust is lofted into the air. A significant fraction of the dust is of small particle size (< 2 μm) and conservatively assumed be lofted into the air during maintenance and cleanup operations.
- Dust transported through high efficiency filters. During the maintenance operations, contamination control barriers will be in place with air filtration. Any dust by-passing these barriers would be in controlled areas served by the plant exhaust filters. Dust removal by high efficiency filters is a function of particle size, and removal efficiency is expected to exceed 99.9% for particles > 0.3 μm in diameter.

In-vessel components are brought into the hot cell for refurbishing that could produce significant dust. For each divertor replacement, ~ 8 t of plasma-facing material could be processed, and the yearly amount of dust produced could be several tens of kilograms. Since all operations are done in the hot cell that is continually vented to maintain a negative pressure, the primary pathway for effluents is the ventilation system. During cutting operations, the dust produced is captured by high-flow air cleaners and filtered with multiple banks of high efficiency filters.

Activated Gases

Analyses have been performed to estimate the production and release of various activated gases that may be produced during ITER operation. These releases are small and include:

- activated air between the cryostat and bioshield - the main isotope of concern is ^{41}Ar;

- activated divertor gases - nitrogen, argon, and/or neon may be pumped into the divertor to produce line radiation leading to ^{37}S, ^{41}Ar, etc. The half-lives for the most significant isotopes are short, so that hold-up in processing of less than a day before discharge would reduce the estimated effluents by an order of magnitude.

5.4.1.4 Non-nuclear Effluents and Emissions

Beryllium

Non-activated beryllium effluents would come primarily from installation of plasma-facing components and refurbishing the divertor cassettes in the hot cell. After the machine is activated, installation would be done in the circulating gas that is maintained within the vacuum vessel. Particulate filters with an efficiency of better than 99.9%, would maintain effluents to very low levels. It is estimated that a few tens of kg of beryllium dust could be produced from preparation of replacement in-vessel components in the hot cell, which would lead to a discharge below 0.1 g/a.

Cryogens

Cryogenic systems are required by ITER to cool the superconducting magnets and operate cryopumps for hydrogen pumping. A large cryoplant will be on site to provide refrigeration and storage of cryogenic helium. Losses of cryogenic helium and nitrogen will be minimised for economic reasons. The environmental impact of these discharges should be minimal.

Heat

The heat rejected from ITER operations originates from nuclear heating (primarily during plasma pulsing with only a small amount of decay heat between pulses) and non-nuclear systems (during pulsing, the dwell between pulses, and periods between pulsing scenarios). The non-nuclear systems include additional heating systems, component cooling, and chilled water. The thermal discharge will be primarily from the cooling towers; however, there will be some direct losses (see 3.3). The design and selection of an appropriate ITER site should allow dissipation of these heat loads without adverse environmental impact.

5.4.2 Occupational Safety

ITER has established a program for personnel protection against hazards anticipated during construction, operation and maintenance activities. The program addresses radiation protection and conventional hazards protection. The objective of this work is to ensure that occupational safety is adequately considered in the design of systems and components and, thereby, to gain confidence that a high level of worker safety will be achievable during operation and maintenance activities. Such confidence can be built only by developing a sound occupational safety program and performing ongoing assessments.

Programs and guidelines have been established for both radiological and conventional hazard protection. A preliminary occupational safety assessment has been performed, and the requirement for continuing analysis as the design progresses is recognised. The level of detail is commensurate with the information available and the relative safety risks, and further development is anticipated as the design progresses. Since ITER is a first-of-a-kind and an experimental facility, there are no definitive benchmarks for the guidelines and

uncertainty cannot be completely avoided during the assessment. This uncertainty is balanced by conservatism in the analysis, and the time delay for the build-up of radiological hazards. Hazard sources will increase slowly with successful experimental campaigns, allowing the future operating organisation to acquire maintenance and operating experience during lower hazard conditions. This experience will provide a basis for improving the maintenance methods for enhanced worker safety. The current assessment does not credit improvements anticipated with experience nor the initially lower radiological hazards. The hazards considered in these occupational safety assessments include:

- radiological hazards from activated components, tritium, tokamak dust and activated corrosion products;
- industrial hazards, such as exposure to beryllium, electromagnetic fields, cryogenic fluids, inert gases, high voltage, and other hazardous substances.

5.4.2.1 Radiation Protection Program

Objectives

The radiation protection program (RPP) provides a set of systematic processes that identify and control both the radiation hazards and the exposure of personnel to these hazards. The RPP is based on internationally accepted radiation protection principles and well-established precedents. The objectives of the RPP are to:

- prevent occupational doses over legal limits;
- maintain personnel doses As Low As Reasonably Achievable (ALARA);
- prevent unplanned exposures;
- minimise the spread of contamination.

To meet these objectives, the RPP employs the principle of ALARA, the establishment of exposure limits and guidelines, and processes for controlling the movement of personnel and materials.

ALARA

ALARA is a key safety principle for ITER[1] and is applied to occupational safety as follows:
"The radiation protection practices shall be consistent with the IAEA and ICRP recommendations and should make use of best practices. In particular, efforts shall be made to design such that exposures during operation, maintenance, modification and decommissioning are ALARA, economic and social factors being taken into account."

The ALARA principle underlies each element of the RPP and is applied in the analysis of the maintenance scheme of each system. This is done using an ALARA process which is described in Section 5.4.2.2.

Exposure Limits

Limits for occupational exposures are taken from the ICRP recommendations[2]. The annual limit for radiation workers (RW) is 20 mSv measured over 5 years, not exceeding 50 mSv in any single year, and the annual limit for members of the public, non-radiation workers (NRW), is 1 mSv.

[1] Plant Design Specification G A0 SP 2 00-06-01 R2.0, Section 3.3
[2] "1990 Recommendations of the International Commission on Radiological Protection", ICRP Publication 60, Pergamon Press, 1991

These limits are not directly used for design or operation, but they are used as a basis to derive the guidelines given in Table 5.2.3-1 for exposure control. It is anticipated that during operation, ITER will operate within guidelines that will be a fraction of the regulatory limit of the host country.

Table 5.4.2-1 Area Classifications and Radiation Access Zones

Access Zone (Area Classification)	Access Limitations	Airborne / Total Dose Rate / Area Contamination Characteristics
Zone A (Non-Supervised Area)	Unlimited Access	• No airborne contamination. Dose rate < 0.5 μSv/h • WHITE contamination control zones only: No surface or airborne contamination and no reasonable possibility of cross-contamination.
Zone B (Supervised Area)	Limited Access for NRW [(a)] Unlimited Access for RW [(a)]	• Total dose rate (internal + external) < 10 μSv/h • GREEN contamination control zones acceptable: No loose contamination tolerated. May be subject to temporary surface or airborne cross-contamination, airborne should not exceed 1 DAC.
Zone C (Controlled Area)	Limited Access for all workers Access requires planning and an appropriate level of approval for the hazards and the class of personnel requiring access.	• < 100 DAC and < 1 mSv/h • AMBER contamination control zones acceptable: Airborne and loose surface contamination tolerated but must be identified and controlled. Contamination levels shall be maintained ALARA taking into account the risk of exposure, capability of available protective equipment, possibility of contamination spread, and cost. Airborne contamination in AMBER zones should not exceed 100 DAC.
Zone D (Controlled / Restricted Area)	These are restricted access areas, entry occurs only with a high level of approval from both an operational and a radiological safety view. These areas shall have physical barriers to prevent inadvertent personnel entry.	• Airborne >100 DAC or external dose rate > 1 mSv/h • RED contamination control zones are only tolerated in Zone D. These areas have permanent or higher than AMBER levels of contamination.

[(a)] Personnel performing work requiring exposure to radiological hazards will be designated as Radiation Workers (RW). All other personnel, including non-designated visitors, will be treated as Non-Radiation Workers (NRW).

Notes: DAC = Derived Air Concentration: unprotected exposure to 1 DAC = 10 μSv/h
1 DAC HTO = 3.1×10^{5} Bq/m^3 = 8.4×10^{-6} Ci/m^3
For internal dose rate, hazard defined in DAC of airborne contamination
For external dose rate, hazard defined as μSv/h

Access and Zoning

A process to ensure safe personnel access is fundamental to meeting the RPP objectives. This requires a well-designed and properly implemented system of radiation access zones and the operational procedures to ensure proper use. This also forms a framework for contamination control, dose control, and prevention of unplanned, acute over-exposures. Access zones are defined[1] in Table 5.4.2-1. Hazard levels will build with operation. The zoning has been determined to be consistent with expected conditions at end of life to ensure adequate design provisions are in place at the start of operation to avoid the need for design

[1] Plant Design Specification G A0 SP 2 00-06-01 R2.0, Table 3-3.

modifications as operation progresses. Actual zoning during operation will be determined to be consistent with the hazards present and will change with time.

All rooms or areas are classified based on the exposure and contamination conditions estimated for 24 hours after shutdown for maintenance. This allows the accessibility of an area to be determined when access would be normally required. Any activities or operating conditions that can cause an otherwise accessible area to have prohibitive occupational hazards will cause such an area to be Zone D. Because of the changing hazard conditions and the potential for error that this creates, these locations will have a physically interlocked system that has two requirements (1) to prevent the particular activity or operating condition if an affected location is occupied, and (2) to physically prevent human access for the duration of the activity or condition. A formal change control process will be implemented to allow the re-designation of locations from restricted to accessible.

Ultimately, accessibility of an area will depend on the zoning, actual hazard level, worker classification and current worker exposures. The RPP includes requirements, guidance, and good design practices to assure control of exposures and contamination during operation. Basic hazard control and monitoring, and radiation protection administration and management, are also included.

5.4.2.2 Radiation Protection Assessment

A radiation protection (RP) assessment process has been developed to gain confidence that a high level of worker safety will be achievable during operation and maintenance activities. The highest exposure and risk areas are identified as highest priority for potential design improvements aimed at reducing overall exposures and assuring good contamination control. Since ITER is not yet an operating facility, the assessment is of the planned activities for the given design and the proposed maintenance schemes. More refined assessments are performed as the design progresses, and greater design and operational detail is available. In addition, there will be several years of operation prior to introducing tritium for further learning and optimisation.

The radiation safety assessment involves two steps. The first is to review exposure conditions to assure that the access control and contamination control zoning requirements are met for the anticipated activities. The second is to apply the ALARA process which requires an estimate of collective occupational exposure. The assessment methodology for ITER is graphically presented in Figure 5.4.2-1. The iterative process begins with the review of the entire facility to prioritise systems for further detailed assessments. It then proceeds to the development of goals and criteria, the application of these goals to the specific systems, and possible modification of the facility or activities. Each repetition may result in a new set of goals and criteria being developed as the assessment is refined and the design is optimised. Dose reduction methods are first applied to those areas where it is identified that the impact would be the greatest. The process continues throughout design and operation to optimise the activities and reduce risk.

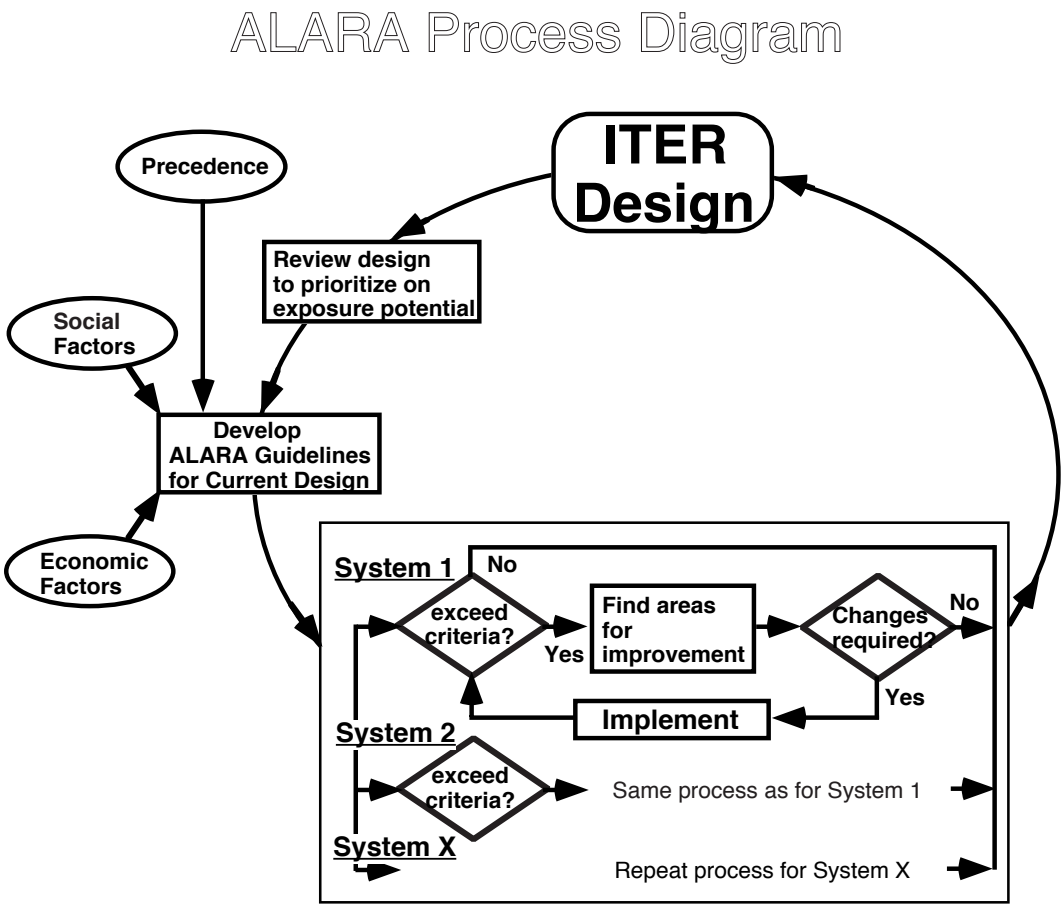

Figure 5.4.2-1 ALARA Process Diagram

Radiation Hazard Information and Zoning

The estimated radiological hazard information is used with the zoning criteria to define the access zone maps for ITER. The radiological conditions are based on neutron activation analysis modelled for the end of 20 years operation. This modelling is based on the reference operating scenario of 0.3 MWa/m^2 modified with 6 days added operation at 25% duty cycle at the end of each 10-year period. This is used for both neutron activation of in-vessel components and structures (see section 2.14) and for calculation of ACPs in the coolant systems. Tritium permeation and production in the coolant is considered along with component location and leakage rates, based on heavy water fission reactor (CANDU) experience, to estimate the potential levels of tritium in air. Finally, sources of contamination are identified along with potential pathways. The above is used to prepare access zone maps that illustrate accessibility of the various locations and ensure the viability of the proposed maintenance and operation schemes.

Access zone maps have been developed for the tokamak building, the tritium building, the hot cell building, the low level radwaste building, and the personnel and access control building.

ALARA Implementation

The ALARA process for ITER has already gone through one iteration, and the estimated occupational exposures reduced. A larger number of systems are being assessed in a more

detailed manner as the design and operational and maintenance schemes become more detailed, and dose estimates become more refined. The process has been executed in three steps.

1. Preliminary qualitative review: Each system was initially reviewed for problems in accessing components for operation and maintenance activities, possible deterioration of contamination control, or significant potential for individual or collective exposure during required operation and maintenance activities.
2. Judgement of occupational radiological safety risk of systems: An initial judgement was made on the relative radiological risk posed by the maintenance of the various systems to prioritise the subsequent more detailed reviews. The systems in Table 5.4.2-2 were selected for more detailed review.

Table 5.4.2-2 Systems Selected for ALARA Review

WBS No	System
1.6	Blanket
1.7	Divertor
1.8	Fuelling and wall conditioning
2.6	Cooling water system
3.1	Vacuum pumping
5.1	Ion cyclotron heating and current drive
5.2	Electron cyclotron heating and current drive
5.3	Neutral beam heating and current drive
5.4	Lower hybrid heating and current drive
5.5	Diagnostics
5.6	Test blanket modules
6.3	Hot cell processing and waste treatment

3. Detailed analysis: The prioritised systems were scrutinised using the criteria as described below. The criteria are not absolute levels below which there is no further concern, but as described previously, the process is an iterative one that will continue into the operations stage, and the screening criteria reviewed and revised (downward) in subsequent iterations.
   (a) The design is reviewed to identify any locations where the exposure conditions exceed 100 μSv/h, and it is determined whether the access and associated exposure warrants efforts to either reduce the dose rates or to change the maintenance procedure to reduce worker exposure to these conditions.
   (b) The design is reviewed and if an activity is identified that would require an individual to exceed 0.5 mSv in one shift, then either the activity or the system is modified.
   (c) The collective dose required for operation and maintenance activities for the system is estimated. Dose reduction methods are considered for systems with annual activities that exceed a total of 30 pers-mSv, or for tasks performed less often than annually if the occupational exposure for the task is estimated to exceed 30 pers-mSv. Steps to reduce the estimated exposure are taken, unless it is judged that "deployment of resources is seriously out of line with the consequent reduction."[1]

[1] 1990 Recommendations of the International Commission on Radiological Protection, ICRP Publication 60, Pergamon Press, 1991 (para 117)

This iterative process is used to optimise shielding and maintenance procedures during design evolution. It has led to stricter project guidelines and significant reductions in the estimated occupational exposure for systems which have undergone additional iterations. The initial analyses were performed for divertor cassette replacement and tokamak cooling water system (TCWS) maintenance, and the improvements are presented below. Analyses for the other systems in Table 5.4.2-2 (such as RF heating and current drive and diagnostic systems) are underway.

Tokamak Cooling Water System (TCWS) Maintenance

TCWS occupational exposure estimates have been ongoing during the EDA, following the design as it evolves and demonstrating a reduction in estimated exposure of two orders of magnitude. The estimated exposure has been systematically reduced from 1,400 pers-mSv estimated in 1996, to 250 pers-mSv for the 1998 ITER design, and to ~65 pers-mSv for the current design. This is the result of changes in the baseline operating scenario, improvements in the TCWS and CVCS designs, improvements in the inspection and maintenance programs, and improved accuracy of the code modelling and exposure assumptions. Table 5.4.2-3 shows the evolution of the TCWS occupational exposure analysis.

Table 5.4.2-3 Evolution of TCWS Occupational Exposure Estimates

Design Version	Major Changes	Collective Dose per Year person-mSv
1996	Initial design and assessment assumptions	1,400
Early 1997	CVCS decontamination factor increased from 2 to 10	500
1998 ITER Design	CVCS decontamination factor increased to 50, modification of CVCS units, improved inspection and maintenance plan	250
ITER	Reduced number of components, increased pipe-wall thickness, adopted realistic operating scenarios and worker positions	~65

The evolution of the analysis, as well as of the design, has resulted in reduced estimates and in increased confidence in the estimates.

Divertor Replacement

The assessment of the divertor replacement has been performed several times during the design evolution to optimise the shielding design and the maintenance procedure. The latest occupational exposure for divertor replacement was estimated based on dose rates in the divertor maintenance ports of about 100 μSv/h outside the VV closure plate but inside the cryostat and 50 μSv/h outside the cryostat but within the bioshield. The dose rates used in the estimates reflect those achieved in other port maintenance areas.

The considerable reduction in estimates of occupational exposure is illustrated in Table 5.4.2-4. Compared with the initial analysis which used conservative gamma field levels for the tokamak design before optimisation, the current estimate shows almost two orders of magnitude improvement. The estimates are lower due to the introduction of shielding into the divertor port to reduce neutron streaming, and improved maintenance procedures.

Table 5.4.2-4 Example of ALARA Application for Divertor Maintenance

Design Version	Major Changes	Collective Dose per Year, person-mSv
Initial	Initial design and assessment assumptions	404
1998 ITER Design	Shielding improvements including increasing port wall thickness and replacing 3 cm gas seal with 15 cm plate between VV and blanket	120
ITER	Improved maintenance procedure for pipe cutting and port seal cutting	~6

RF Heating and Diagnostic Maintenance

The most recent occupational exposure assessments are for the port plugs of the three RF heating systems plus diagnostics. These systems have similar remote maintenance requirements and maintenance procedures. For example, the standard port plugs are taken to the hot cell for refurbishment. The preliminary results indicate that much of the estimated exposure is due to pipe cutting or to activities immediately behind the port plugs. Current efforts are focussed on reducing the hands-on time for these two activities by optimising the use of remote cutters. These enhancements are expected to not only benefit the RF heating and diagnostic component maintenance, but also potentially reduce divertor, test blanket, blanket, and cryopump maintenance occupational exposures.

Overall Assessment

The project's commitment to ALARA ensures the continuing review, analysis, and improvement of design and maintenance procedures to ensure that exposures and radiological risks are not only below the guidelines, but also maintained as low as reasonably achievable. The current assessment of all major systems points to ITER successfully maintaining occupational exposures below the project guidelines. The reduction of estimated occupational exposure for the TCWS and the divertor systems has been successful enough to move the focus from these systems to the RF heating and the diagnostic systems. The iterative ALARA process systematically analyses and improves the systems of greatest concern. The widening application of systematic reviews ensures that potential contributors to occupational exposure are identified and addressed. Assessments of systems already reviewed are continuing with the objective of further decreasing the expected exposure and increasing confidence in the results.

5.4.2.3 Conventional Occupational Safety

Occupational safety protective measures will be implemented to assure worker protection against non-radiation hazards in compliance with the industrial safety standards of the host country.

Beryllium Hazard

Similar to radiation zoning, beryllium zoning and design measures for monitoring and control have been developed using JET experience[1]. The beryllium zoning criteria are defined in Table 5.4.2-5.

[1] Code of Practice for the Safe Use of Beryllium at JET, July 1989

Table 5.4.2-5 Beryllium Zoning

Zone	Hazard Level		Access and Control Conditions
	Airborne	Surface	
Uncontrolled Zone	< 0.01μg/m^3	< 0.1 μg/m^2	No reasonable possibility for beryllium exposure. Time unlimited access areas with no protective or monitoring devices. Control Rooms, ordinary offices, all other areas not directly or indirectly connected to operations with beryllium.
Controlled Zone	0.01 μg/m^3 - 0.2 μg/m^3	0.1 μg/m^2 - 10 μg/m^2	Beryllium measured or anticipated. Only designated beryllium workers are allowed access. Access time and protective equipment will be determined by the activities with beryllium bearing equipment and the potential for airborne beryllium.
Respiratory Protection Zone	> 0.2 μg/m^3	> 10 μg/m^2	Airborne beryllium is either measured or expected to exceed levels requiring respiratory protection. These areas must be physically enclosed and outfitted with appropriate ventilation to ensure the areas outside this zone do not experience elevated beryllium due to the work within the zone. Workers will require respiratory protection commensurate with the work and the hazards measured.

Table 5.4.2-6 Electromagnetic Field Zones and Conditions

Zone Name	Field, B [mT]	Access and Control Condition
Uncontrolled Zone	B < 10	Unlimited access
Controlled Zone	10 < B < 100	Access is limited during tokamak operation such that individual exposures to EM fields are ≤ 60 mT h per day.
Prohibited Zone	B > 100	Entry is prohibited, aside from exceptional circumstances where up to 60 mT h may be allowed with a high level of approval.

Electromagnetic and Radiofrequency Field Exposures

Electromagnetic (EM) and radiofrequency (RF) field exposure limits presented in Table 5.4.2-6 and Table 5.4.2-7 are consistent with a survey of national regulations and international recommendations. With the poloidal field coils energised, working restrictions will be required in the tokamak hall and possibly in portions of the buildings immediately surrounding the tokamak hall. Design and administrative measures have been foreseen to monitor and control workers' electromagnetic exposure.

Table 5.4.2-7 Guidelines Related to Radio-Frequency Powers

Leakage at ECRH joints	< 5 mW/cm^2
Leakage at ICRH joints	< 1.0 mW/cm^2

Industrial Hazards

Other hazards that are likely at the ITER facility during construction and/or operation include high voltage, cryogens, confined spaces, fires, chemical hazards, mechanical hazards, rotating machinery, and lifting equipment (cranes). These hazards will be treated according to the industrial safety regulations and practices of the host country.

5.4.3 Radioactive Materials, Decommissioning and Waste

In the frame of ITER's safety objectives, the issue of radioactive materials, decommissioning and waste is carefully considered. It is important in this context to discriminate between the radioactive materials generated and that materials fraction actually remaining 'waste' after the decay time selected. All activities associated with radioactive materials and waste will comply with the host country regulations and practices. The management will be co-ordinated between the ITER project and the host country.

5.4.3.1 The Concept of Clearance

In the absence of an actual host country for ITER, the ultimate waste amounts are estimated provisionally on the basis of 'clearance'[1]. By this process, radiation sources can be released from regulatory control (i.e. control is removed). The "Interim Report for Comment" in the reference provides "unconditional clearance levels" for radionuclides in solid materials. According to the IAEA concept, materials with lower activation levels can be cleared, irrespective of how and where they may be used in the future.

Natural background radioactivity provides a reference level for the assessment of man-made radioactivity. Relative to this reference, doses around 10 μSv/a are commonly considered as insignificant, called[2] "trivial". The perception that a dose of 10 μSv/a appears to be insignificant has been used by IAEA for quantifying the concept of 'clearance' by evaluating credible scenarios for the potential use and the associated exposure hazard of man-made solid radioactive materials after removal from nuclear facilities. The result of conservatively evaluating these scenarios is dose rates and doses, from which in turn "clearance levels" are derived to categorise radioactive materials. The radionuclide-by-radionuclide clearance levels are supplemented by a linear summation rule to be used for nuclide mixtures which are the most common case in practice. The numerical values of the clearance levels[3] have been supplemented by calculated values[4] consistent with the reference. In the actual evaluation, each isotope is characterised by its "clearance index" (actual specific radioactivity divided by the clearance level). A material for which the sum over the clearance indices of all constituent isotopes is above unity after the decay time considered cannot be cleared.

[1] "Clearance Levels for Radionuclides in Solid Materials", International Atomic Energy Agency, IAEA-TECDOC-855, Vienna, 1996
[2] "Principles for the Exemption of Radiation Sources and Practices from Regulatory Control", Safety Series No. 89, IAEA, Vienna, 1988
[3] "Clearance Levels for Radionuclides in Solid Materials", International Atomic Energy Agency, IAEA-TECDOC-855, Vienna, 1996
[4] R.A. Forrest, J-Ch. Sublet, "EAF-99 biological, clearance and transport libraries", Report UKAEA FUS 410, December 1998

5.4.3.2 Scope and Scale

The radioactive materials arising during operation and remaining after final shutdown include activated materials (due to fusion neutrons) and contaminated materials (due to activated tokamak dust, activated corrosion products and tritium) and mixtures thereof. Almost all radioactive materials present at final shutdown would be considered as waste if immediate disposal in final repositories was necessary. Actually, decay and decontamination will reduce the radioactivity with time after final shutdown. Therefore, not all radioactive materials may need to go into waste repositories; rather a significant fraction has the potential to be 'cleared'. Since this fraction increases with time, a criterion with regard to time has to be set. At present the ITER project provisionally assumes that radioactive material not allowing for clearance after a decay time of up to 100 years is 'waste' needing disposal in a repository. The time period beyond 100 years will be called the 'waste time scale' in the following.

To guide the analysis of radioactive materials, assessments have been performed in parallel to the evolving ITER design. These 1D analyses are generally consistent with the more detailed neutronic analyses in section 2.14. The scale is shown by preliminary numbers in Table 5.4.3-1. About 90 % of the radioactive material is predominantly activated, the rest is predominantly contaminated. The waste masses do not include the bioshield for two reasons: Firstly its radioactivity is not due to activation by fusion neutrons, rather it stems from the natural radioisotope ^{40}K in the impurity element potassium in the concrete; secondly the clearance index of the concrete including reinforcing steel is always below unity, around 0.1. Relative to the indicative numbers, the actual ones will vary to a certain extent due to changes of the developing design, analyses details, dismantling possibilities, etc.

Table 5.4.3-1 Rounded Masses of Radioactive Materials and Waste

Total radioactive material	31,000 [t]
Material remaining as waste after a decay time up to 100 years*	6,100 [t]

* The waste mass results from assuming that component parts with clearance indices[1] above unity can be separated from the parts with indices below unity.

A sensitivity assessment indicates that the material remaining as waste after a decay time of only 30 years is about twice that after 100 years.

The mass of operational waste from component maintenance, repair and replacements has been estimated to be about 750 t. This mass and the associated volumes are such that on-site accommodation in the hot cell storage area up to the final shutdown of ITER can be envisaged.

[1] "Clearance Levels for Radionuclides in Solid Materials", International Atomic Energy Agency, IAEA-TECDOC-855, Vienna, 1996

5.4.3.3 Conclusions from the Analyses

Relevant Isotopes

The vacuum vessel is a major contributor to the radioactive masses. The surface separating the non-clearable inner materials from the more peripheral, clearable ones is located inside the vacuum vessel walls. Therefore, the plasma side and rear side of the vacuum vessel have been selected as representative locations for most of the scoping studies.

Figure 5.4.3-1 shows specific activities vs. decay time after final shutdown (total fluence 0.5 MWa/m^2) of the transmutation products in the ITER reference structural steel (SS 316 L(N)-IG with 0.01 and 0.05 wt.% of Nb and Co, respectively) at the plasma-side surface of the outboard vacuum vessel.

Figure 5.4.3-2 shows clearance indices vs. decay time after final shutdown of the transmutation products at the plasma-side surface of the outboard vacuum vessel.

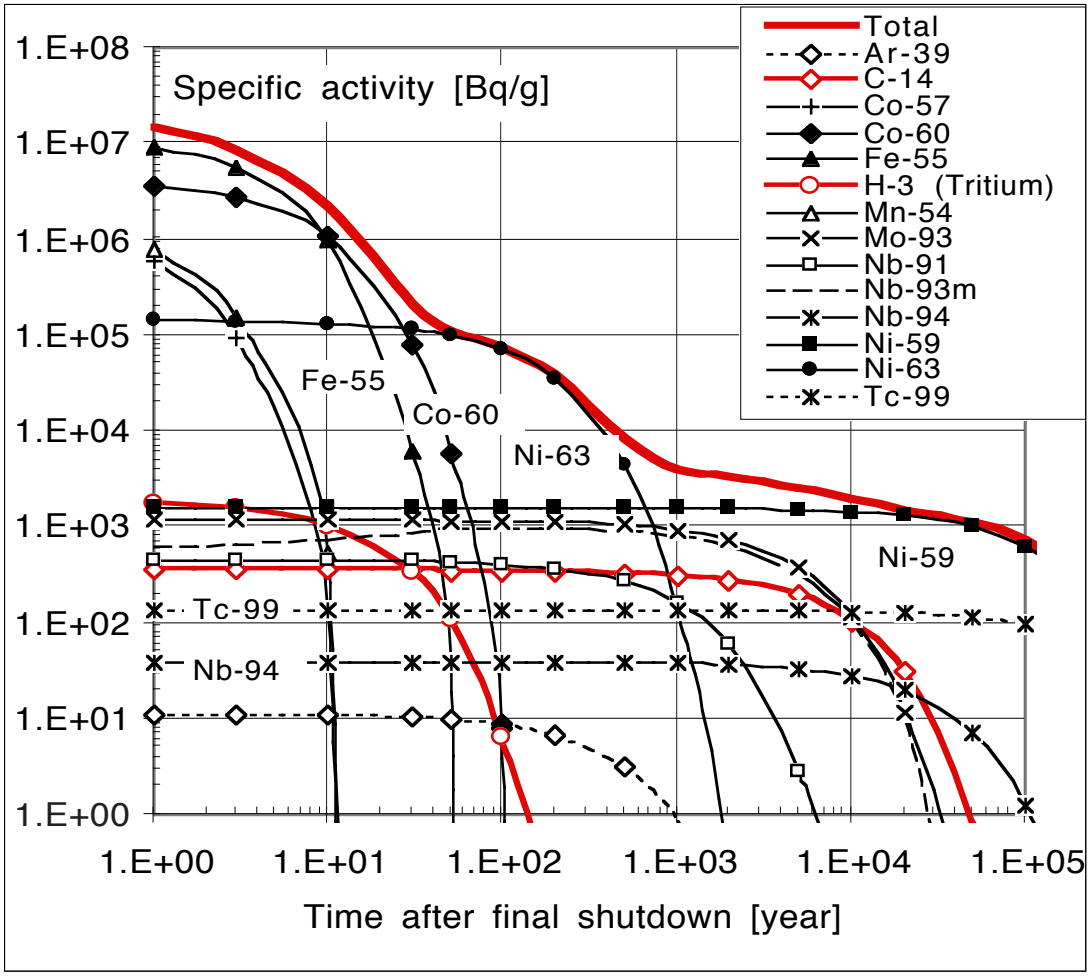

Figure 5.4.3-1 Specific Activities (vs. decay time after final shutdown) of the Transmutation Products in the Structural Steel (SS 316 L(N)-IG with 0.01 and 0.05 wt.% of Nb and Co, respectively) at the Plasma-side Surface of the Outboard Vacuum Vessel

The legend is ordered alphabetically. The four most important isotopes are marked by solid symbols and explicit labels (such as 'Co-60') are attached to the respective curves.

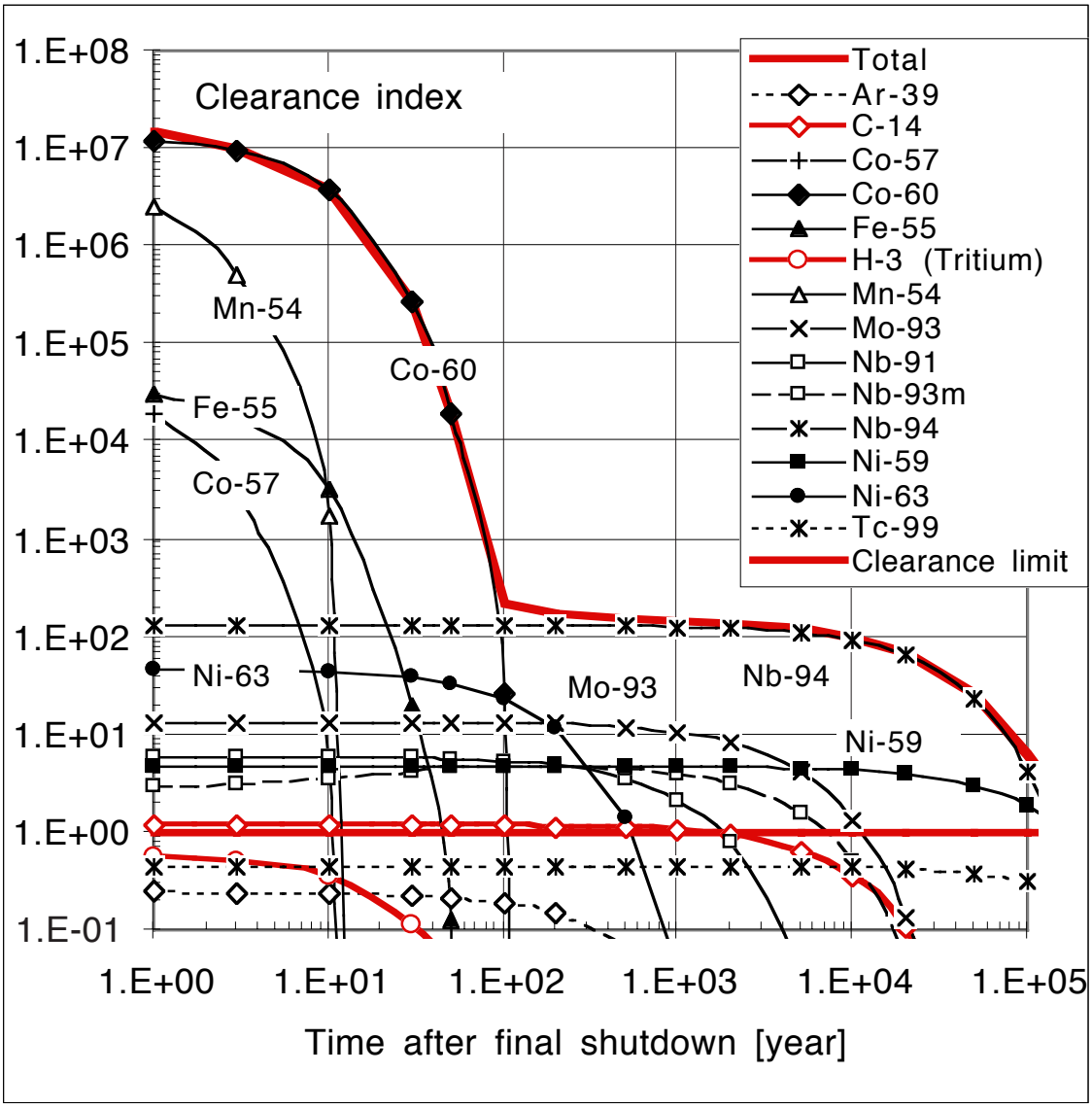

Figure 5.4.3-2 Clearance Indices (vs. decay time after final shutdown) of the Transmutation Products at the Plasma-side Surface of the Outboard Vacuum Vessel (SS 316 L(N)-IG with 0.01 and 0.05 wt.% of Nb and Co, respectively)
The legend is ordered alphabetically. The five most important isotopes are marked by solid symbols and explicit labels (such as 'Co-60') are attached to the respective curves.

The steel alloying elements Ni, Mo and N in the plasma-side part of the outboard vacuum vessel give rise to the transmutation products ^{63}Ni, ^{93}Mo, ^{59}Ni, ^{14}C, ^{93m}Nb, and ^{99}Tc which are relevant since they significantly contribute to the activation level on the waste time scale. Some ^{94}Nb is also produced from the alloying element Mo by threshold reactions. The contribution of alloying elements to the total activation cannot be markedly reduced in the frame of ITER without having an impact on the properties of the reference structural steel.

The impurity elements Co and Nb are the only relevant ones in the reference structural steel since the other impurities and the so-called trace elements do not significantly contribute to the activation. The upper limits of 0.01 wt.% and 0.05 wt.% specified, respectively, for the Nb and Co concentrations in the reference structural steel are reasonable with regard to

clearance and are technically feasible. The impact of these specifications on cost is negligible.

Table 5.4.3-2 shows a list of the most relevant radioisotopes (in alphabetic order), based on analyses of both the vacuum vessel front wall and the blanket first wall at 100 years after final shutdown. The most relevant isotopes with regard to clearance indices (shown in Figure 5.4.3-2) are also most relevant for the specific ingestion dose which is a measure of the radiotoxicity potential.

Table 5.4.3-2 The Most Relevant Radioisotopes for ITER Steels 100 Years after Final Shutdown

^{39}Ar	^{14}C	^{60}Co	^{93}Mo	^{91}Nb	^{93m}Nb	^{94}Nb	^{59}Ni	^{63}Ni	^{99}Tc

The relevance is determined by the concentrations of the parent elements in the reference steel together with the long half lives of the daughter radioisotopes. The only exception is ^{93m}Nb. It makes a noticeable long-term contribution in spite of its relatively short half-life (16.1 years) due to the continuous generation of ^{93m}Nb by capture of an orbital electron by ^{93}Mo nuclei.

Tritium in the Vacuum Vessel Walls from Transmutation and Permeation

Tritium generated by transmutation reactions in the steel of the plasma-side part of the vacuum vessel (see Figure 5.4.3-1) makes a negligible contribution to the total activation on the waste time scale. This implies that the same conclusion is true for the entire vacuum vessel.

Tritium due to permeation into the plasma-side parts of the vacuum vessel is not very relevant if considered only from the radioactivity point of view since the high activity of these parts is dominated by neutron activation. An impact is expected, however, from permeated tritium on decommissioning and disposal (outgassing, leaching, etc.), expressed by associated national requirements. The concentration of permeated tritium in the rear sections from the coolant side is expected to be very low but remains to be assessed.

Figure 5.4.3-3 shows a tritium concentration profile across the plasma-side vacuum vessel wall for an operation scenario that leads to a total neutron fluence of 0.5 MWa/m^2 after 17 years of operation. The peak tritium concentration (at the plasma-side surface) is about 16 mg tritium per m^3 of steel corresponding to a peak specific activity of 0.7 MBq/g. The total tritium inventory is about 0.25 g in the wall, causing an average specific activity of 0.2 MBq/g. Parametric analysis shows only moderate sensitivities on assumptions thus providing confidence in the calculated orders of magnitude.

Similar to the situation in the vacuum vessel walls, transmutation reactions of fusion neutrons with the elements in the in-vessel materials generate tritium. The specific activities of this tritium have been determined by the one-dimensional activation calculations.

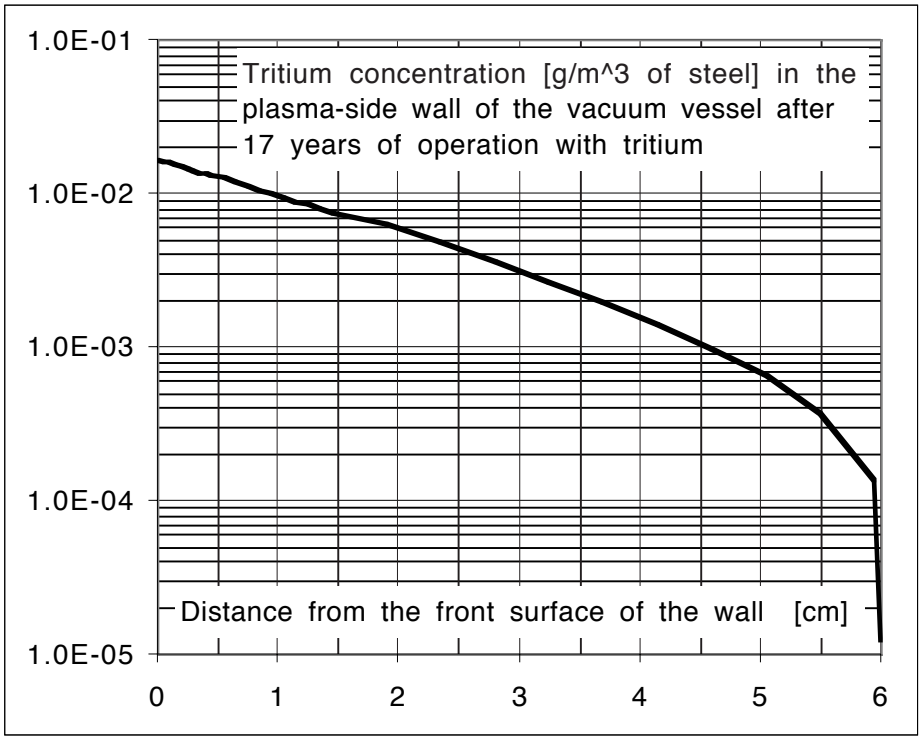

Figure 5.4.3-3 Tritium Concentration Profile Across the Plasma-side Wall of the Vacuum Vessel at Final Shutdown
(for an operation scenario that leads to a total neutron fluence of 0.5 MWa/m^2 after 17 years of operation)

The clearance indices in the blanket steel and copper are significantly above unity for at least the front half of the blanket up to 10 years. This implies that detritiation early after removal of the components from the device in the course of replacements or final decommissioning would be beneficial from the radiation protection point of view, possibly also with regard to tritium economy. The specific activity of tritium in divertor tungsten is about one order of magnitude above the clearance level, whereas the tritium activity in the first wall beryllium is much higher.

For tritium due to permeation into steel of the in-vessel components, the inventories calculated for the vacuum vessel front are used as a zero order approximation. These values are somewhat lower than the blanket front steel tritium activities from transmutation reactions which implies that the tritium from transmutation reactions alone warrants de-tritiation of in-vessel components after removal from the device, so that possibly higher tritium concentrations from permeation may add an additional incentive for detritiation but would not change the basic judgement on its necessity.

Relevance of Carbon-14

^{14}C is considered with increasing scrutiny due to carbon's major role in the biosphere. Dedicated work with regard to doses (both collective and individual ones) in particular from fusion device decommissioning and waste disposal has been launched recently, and provisional results have been obtained[1].

[1] T. Hamacher et al., "Radiological impact of an intense fusion economy", Proceedings 21st Symposium on Fusion Technology (SOFT), Madrid, Spain, September 2000

Figure 5.4.3-1 shows the specific activity of ^{14}C in the vacuum vessel versus time after final shutdown. The value at shutdown is about 600 Bq/g: the clearance level of 300 Bq/g is reached after about 5,000 years. Figure 5.4.3-2 shows that the contribution of ^{14}C to the total clearance index is masked by the much larger long-term contributions from ^{94}Nb, ^{63}Ni, ^{93}Mo and ^{59}Ni, but nevertheless the ^{14}C clearance index remains around unity for a long time. Eventually, dedicated considerations may be required with regard to specific regulations of the ITER host country.

Clearance Potential of the Vacuum Vessel

The profile of the total clearance index across the outboard vacuum vessel wall is displayed in Figure 5.4.3-4. About 30 cm at the plasma side of the outboard vacuum vessel will remain above the clearance limit beyond 100 years. Virtually the same thickness holds for the inboard vacuum vessel. The activity distribution implies that a significant fraction of the outboard vacuum vessel has the potential for clearance. A breakdown into clearable and non-clearable parts would require that the vacuum vessel be disassembled at decommissioning. A disassembly concept which exploits the vessel's shell structure and applies plasma cutting has been addressed in the design. The associated reduction in radioactive mass which would be waste is about 3000 t.

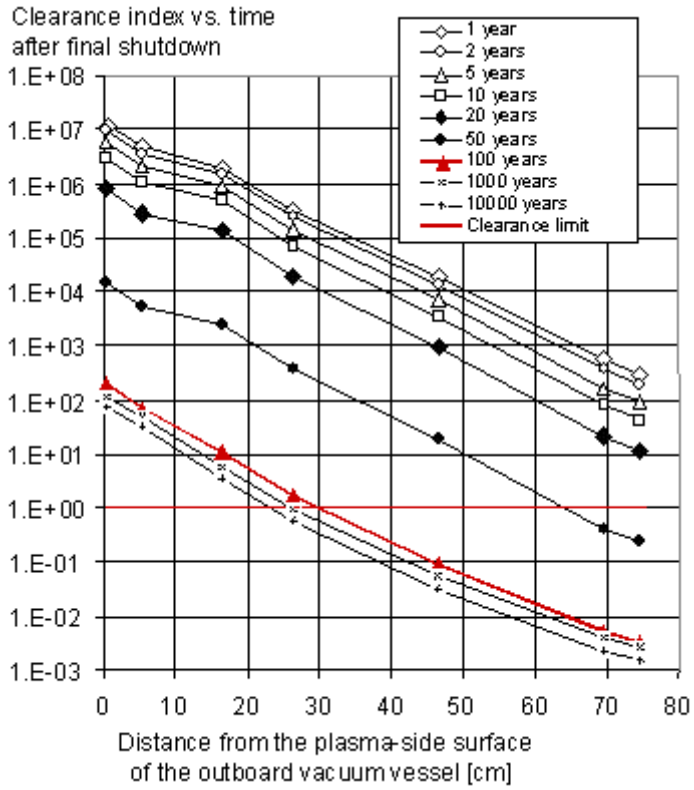

Figure 5.4.3-4 Profile Across the Outboard Vacuum Vessel Wall of the Total Clearance Index in the Structural and Shielding Steels for Various Decay Times After Final Shutdown

Clearance Potential of the Toroidal Field Coils

The toroidal field coils are major contributors to the mass of radioactive materials since they become activated by neutrons in spite of the shielding by the in-vessel components and the vacuum vessel. The long-term activation is dominated by ^{94}Nb. It is generated in particular from the Nb which is inherent to the superconductor in the coil winding packs and also from the Nb impurity in the cryogenic structural steels.

Virtually the entire inboard winding pack has clearance indices (ranging from about 100 down to about one) above the clearance limit beyond 100 years so that no clearance potential exists. The index for the outboard plasma-side of front winding pack is only marginally below the clearance limit at 100 years and beyond. The index in the rear part of the winding is more than two orders of magnitude below the clearance limit so that a potential for clearance exists.

The clearance indices of the coil cases show the usual cross-over of two different decay curves around 100 years: the curve up to 100 years is dominated by ^{60}Co, the curve beyond 100 years is dominated by ^{94}Nb. For the outboard field coil case, the concentration of the Nb impurity in the coil cryogenic steels, specified to be 0.01 wt.%, is sufficiently low from the clearance index point of view, with a margin of more than two orders of magnitude. The situation is less clear for the inboard coil case since its clearance index between 0.1 and 1 at 100 years is only marginally below the clearance limit.

Overall, the activity distribution inside the toroidal field coils is such that part of the coil cases and possibly the outboard winding pack have a clearance potential. A breakdown into clearable and non-clearable parts would require that the toroidal field coils can be disassembled at decommissioning. Therefore, a concept for the removal of the winding packs from the coils has been addressed in the design. The associated reduction of the radioactive mass which would be waste is about 2000 t.

Contact Dose Rates

Figure 5.4.3-5 shows contact dose rates vs. time after final shutdown at various vacuum vessel locations. These are average values since they have been calculated by a 1D model. The dose rates at the outboard rear surface of the vacuum vessel are particularly important since, together with the extent of remote operations and handling times, they determine staff exposure during decommissioning. At present it is assumed that dose rates around 10 μSv/hr may allow for prolonged hands-on operations. On average, the vacuum vessel's outboard rear surface reaches this value after about 10 to 20 years. Of course, more detailed calculations are required for an actual decommissioning program to determine the expected local dose rate peaks.

Decay Heat

Nuclear decay heat has been calculated for the time point 100 years after final shutdown which is the starting time of the ITER waste time scale. A typical value is 30 μW/kg for blanket modules.

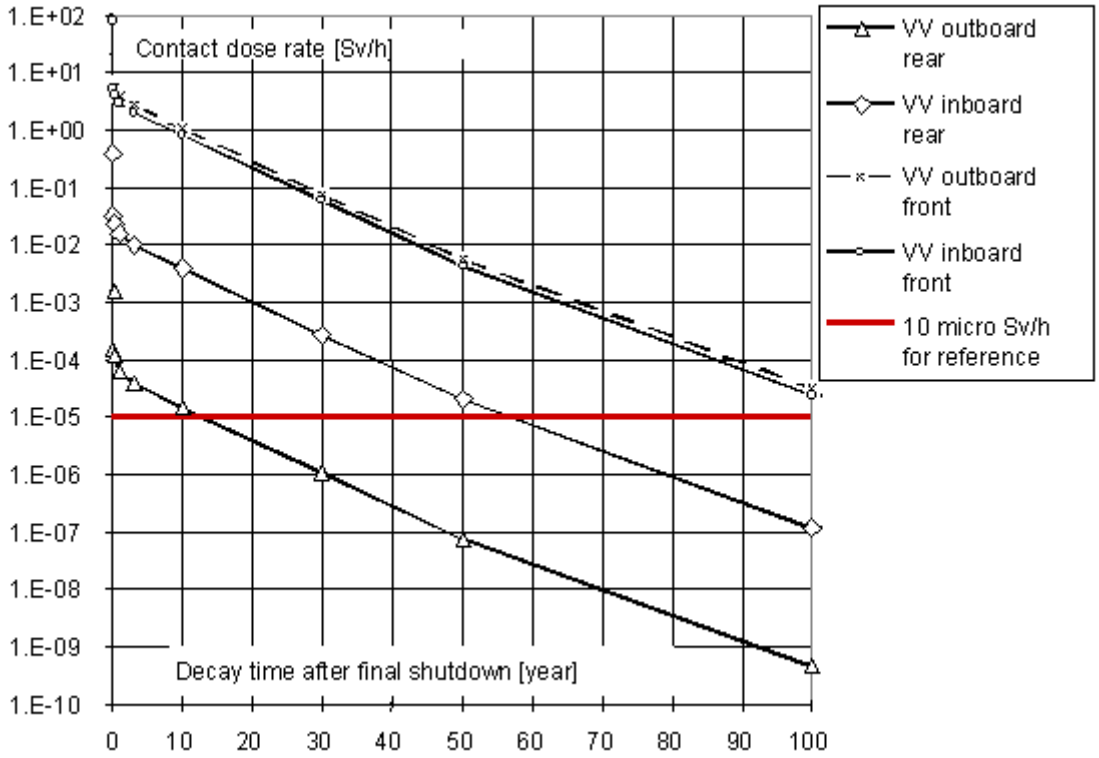

Figure 5.4.3-5 Contact Dose Rates at Various Vacuum Vessel Locations vs. Decay Time after Final Shutdown

Radiotoxicity Potential

'Radioactivity' is supplemented by the important notion of 'radiotoxicity potential'. Total radioactivity (in Bq) from operation, replacements and decommissioning remaining after final shutdown is not an adequate measure for the hazard associated with a nuclear facility. For example, the total radioactivity from component activation in a steel-based model fusion power reactor[1] - after a decay time of 100 years - is about four orders of magnitude higher than the total radioactivity of the ash from an equivalent coal-fired plant, whereas potential doses associated with the two plants differ by only an order of magnitude or so after 50 years. Therefore, it has become common practice[2] to use a 'radiotoxicity potential' (expressed by doses) to characterise the hazard potential of nuclear installations. The radiotoxicity potential is the hypothetical dose due to incorporation in the body of all radioactive material under assessment.

The radiotoxicity of ITER is dominated by the in-vessel components and decreases by several orders of magnitude within 50 to 100 years followed by a much slower decrease afterwards due to longer-lived radioisotopes. After about 100 years, the radiotoxicity of ITER is comparable to the total ash from a large coal-fired power plant. The most relevant isotopes are ^{54}Mn, ^{55}Fe and ^{60}Co in the shorter term and ^{63}Ni and ^{93}Mo in the long term.

[1] J. Raeder, I. Cook, F.H. Morgenstern, E. Salpietro, R. Bünde, E. Ebert, "Safety and Environmental Assessment of Fusion Power (SEAFP)", Report of the SEAFP Project, European Commission, EURFUBRU XII-217/95, Brussels, 1995.

[2] H. Röthemeyer, A.G. Herrmann, H. Salewski, "The influence of radioactive waste disposal on natural activity, heat production, and radiotoxicity", Kerntechnik 61, 5 – 6, 1996, pp245 – 250 (for example)

5.4.3.4 Decommissioning Assumptions

It is assumed that the ITER organisation at the end of operation will be responsible for starting the machine decommissioning through a de-activation period after which the facility will be handed over to the responsible organisation inside the ITER host country.

The envisaged decommissioning scenario (see section 6.8) accounts for the impact of the essential drivers, such as availability of equipment, facilities, staff, activation decay time, etc. Flexibility is provided by the use of two separate phases. The duration and activity of each phase can be modified to a certain extent to accommodate organisational requirements and constraints.

During the first phase, immediately after shutdown, the machine will, in particular, be de-activated and cleaned by removing tritium and any removable dust from the in-vessel components. The necessary activities will be carried out by the ITER organisation by using the remote handling facilities and staff existing at the end of the project. At the end of the first phase, the ITER facility will be handed over to the responsible organisation inside the host country that will be responsible for the subsequent second phase of decommissioning and disposal. The scenarios demonstrate the feasibility of decommissioning considering worker and public safety.

5.5 Event Analysis

To assess the potential for public radiation exposures and the effectiveness of implementation of the safety requirements and functions in the ITER design, a comprehensive analysis of reference events has been performed. Failures and combinations of failures have been postulated to show that the design is tolerant to such failures and to ensure a conservative operating envelope is achieved. The analyses included conservative assumptions of initial facility operating and off-normal conditions and examined possible ways for tritium, activated corrosion products in coolants, and neutron-activated tokamak dust, to be released to the environment. The results showed that radioactive releases for all of these reference events are well below the project release guidelines in Table 5.2.3-2. In addition, ultimate safety margins of the facility were examined by analysis of hypothetical events. Analysis shows that safety margins degrade gradually, and that the ITER design provides a high level of public protection even for these hypothetical events. The assessments provide confidence that the operation of ITER will result in no significant risk to the general public from postulated accidents.

5.5.1 Determination and Categorisation of Event Sequences

In the safety analyses, events and plant conditions are categorised as follows:

- **normal operation** - events and plant conditions planned and required for normal operation, including some faults and events which can occur as a result of the experimental nature of ITER;
- **incidents** - deviations from normal operation, event sequences and plant conditions not planned but likely to occur one or more times during the life of the plant as the result of components failures (excluding normal operation events);
- **accidents** - event sequences and plant conditions not likely to occur during the life of the plant but postulated to assess the safety of the facility.

The basic principle in relating design requirements to each of the conditions is that the most probable occurrences should yield the least radiation exposure to the public, and those conditions having the potential for the greatest exposure to the public should be those least likely to occur.

5.5.1.1 Reference Events

Table 5.5.1-1 shows the 25 different reference events that have been analysed in-depth with their respective categories. These were selected to cover the major systems, the radioactive inventories distributed amongst these systems, and initiator types that have the potential to cause releases, as well as the above event categories. The appropriateness of this set of reference events is confirmed by detailed event sequence studies as described in the following sections.

Table 5.5.1-1 Reference Events Analysed in Detail

Event Family	Events
Plasma events	Loss of plasma control/exceptional plasma behaviour (i,a)
Loss of electrical power	Loss of off-site power for up to 1 h (i)
	Loss of off-site power for up to 32 h (a)
	Loss of off-site power and on-site class III power for up to 1 h (a)
In-vessel events	In-vessel first wall pipe or coolant channel leak (i)
	Multiple first wall pipe or coolant channel damage (a)
	Loss of vacuum through a vacuum vessel penetration line (a)
Ex-vessel HTS events	Loss of heat sink in divertor HTS (i)
	Pump trip/loss of flow in divertor HTS (i)
	Pump seizure in divertor HTS (a)
	Vacuum vessel HTS break (a)
	Large ex-vessel divertor HTS break (a)
	Heat exchanger leakage (i)
	Heat exchanger tube rupture (a)
Tritium plant and fuel cycle events	Tritium process line leakage (i)
	Transport hydride bed mishandling (a)
	Isotope separation system failure (a)
	Fuelling line with impaired confinement (a)
Maintenance events	Stuck divertor cassette in transport cask (a)
	Maintenance accident on vacuum vessel (a)
Magnet events	TF short (a)
	Magnet arc (a)
Cryostat event	Air ingress (a)
	Water/air/helium ingress (a)
Hot cell events	Failure of confinement (a)

(i) Incidents are deviations from normal operation, event sequences or conditions not planned but likely to occur during the life of the plant (see Table 5.2.3-2).

(a) Accidents are event sequences or conditions not likely to occur during the plant life but are postulated to demonstrate the safety of the plant (see Table 5.2.3-2).

The reference events are analysed using detailed quantitative modelling and integrated system simulation codes and conservative or bounding conditions. In addition, all accidents are analysed assuming a coincident loss of off-site power and additional failures in mitigating systems. The plasma behaviour is addressed in a conservative way to show the limited effects of loss of plasma control or exceptional plasma behaviour. Loss of power is investigated to determine if there are requirements for emergency power. Many events are grouped around the cooling water systems which are a key element to demonstrate the safety

approach. Air and water ingress into the vacuum vessel and cryostat under various off-normal plant conditions are investigated. Potential events during maintenance of the vacuum vessel are considered since maintenance will be a typical state of the ITER plant. Safety of the tritium plant with its significant inventory is addressed in four reference events. Magnet system structural integrity and consequences of arcs are examined. Consequences of failures in confinement and decay heat removal in the hot cell are investigated.

5.5.1.2 Enveloping by Reference Events

For the analysis to be complete, it must address the comprehensive list of fault conditions, or initiating events, covering all conceivable hazards arising in the facility. Thus sequence identification studies have been carried out with this objective, and more specifically to confirm that an appropriate selection has been made of the postulated events which are analysed in detail.

To help ensure that all aspects of plant operation have been considered, two fundamentally different approaches have been applied to the identification of potential initiators. These are the component-level (bottom-up) and the top-down approaches. The former is based on the application of systematic methods which seek to catalogue all potential faults in the plant components and subsystems, and to consider the conceivable consequences of these faults. The focus is on the failure of individual components, and it is based on the design in as much detail as is available.

In contrast, the top-down approach starts at the plant level, and takes a global view of the potential hazards and the safety functions which provide protection. By considering the abnormal events which would have to occur to realise these hazards, a list of event initiators is again produced, in terms of system or in some cases component faults.

The concluding part of both the bottom-up and top-down studies is to show that all identified sequences have in some way been addressed by analyses which show that all potential consequences are within acceptable limits. The catalogue of events and the event sequences resulting from these studies identifies the radioactive inventory at risk, the confinement barriers challenged, the mitigating systems that must fail for a hazardous plant state to occur and the release pathway and have been evaluated to ensure that each one is either clearly insignificant or is covered, directly or indirectly, by a detailed analysis. It has been confirmed that the consequences of all identified sequences are enveloped by the assessed consequences in one or more of the analyses of reference events in Table 5.5.1-1.

5.5.1.3 Component-level Studies

The principal technique used in the bottom-up studies was failure modes and effects analysis (FMEA). The level of detail of the application has varied by system, because studies have proceeded in parallel with the evolution of the ITER design, resulting in systems being studied at various stages of their design maturity. FMEA catalogues all conceivable failures in every plant component, and the potential consequences. It allows frequencies to be assigned to each identified fault based, where possible, on failure frequency data gathered from operational experience on existing similar systems.

The outcome of FMEA studies is lists of fault conditions which could initiate an accident sequence. These are sorted into groups of initiators referred to as postulated initiating events

(PIEs) which would lead to similar plant response. Some other, less formal, assessments of initiating events have also produced lists of PIEs. Table 5.5.1-2 summarises those systems that have been studied and the resulting number of PIEs listed for the normal operation phase.

Table 5.5.1-2 Postulated Initiating Events Identified in ITER Systems

System	Identification Method[1]	Number of PIEs
Magnet systems	IE list	1
Vacuum vessel	FMEA	15
First wall//blanket cooling water system	FMEA	13
Divertor cooling water system	FMEA	9
Fuelling system	IE list	8
Divertor remote handling	FMEA	5
Cryostat	FMEA	9
Heat rejection system	FMEA	6
Vacuum pumping	IE list	4
Tritium plant	FMEA	9
Cryoplant	FMEA	2
Coil power supplies	FMEA	6
Electrical power network	IE list	3
Neutral beam	FMEA	11
Hot cell	FMEA	6

[1]. IE list Initiating Event list (by informal method)
FMEA Failure Modes and Effects Analysis

Each PIE was assessed to determine event sequences which may result from it, and the possible consequences. A selection of PIEs was made for development using event trees to depict event sequences in which successive lines of defence of systems and equipment providing the required safety function were considered to fail. These show the potential hazardous consequence of each sequence, for example the release of tritium, tokamak dust or activated corrosion products, but in many cases the sequence frequency is extremely low, in the 'hypothetical' range.

5.5.1.4 Top-down Study

One of the motivations for performing a top-down study, to complement the already voluminous bottom-up studies, was that it can provide a clarity of presentation. Another benefit of this approach is to ensure completeness in identifying hazardous situations that could lead to the event of unacceptable radioactive release to the environment. By expanding this unacceptable event into all possible categories of events that could cause it to occur, the same initiators should be identified as with the bottom-up approach, ensuring the consistency and completeness of the analysis.

In order to start with a plant-level, safety functional approach, and work down to initiating faults, a global fault tree is required. To implement this, a master logic diagram (MLD) has been developed.

The top levels of the MLD are shown in Figure 5.5.1-1, and as an example the expansion of one branch in Figure 5.5.1-2, this representing the release of tritium from plasma-facing components. The top-level event in the MLD is 'excessive off-site release', meaning the release of radiological materials which exceed the project release guidelines. Subsequent levels in the diagram show the confinement barriers and supporting safety functions that protect against the release, and finally the potential initiators of accident sequences. Several failures must occur to give rise to a release based on the logic of the ITER MLD, indicated by the Boolean “AND” gates in the diagram (for clarity, "AND" gates are filled black in the diagram, "OR" gates are not). For example in Figure 5.5.1-2, an ingress of coolant into the vacuum vessel will create the conditions in which mobilisation of tritium could occur, but a large release to the environment would only result if, additionally, other failures occurred resulting in loss of confinement.

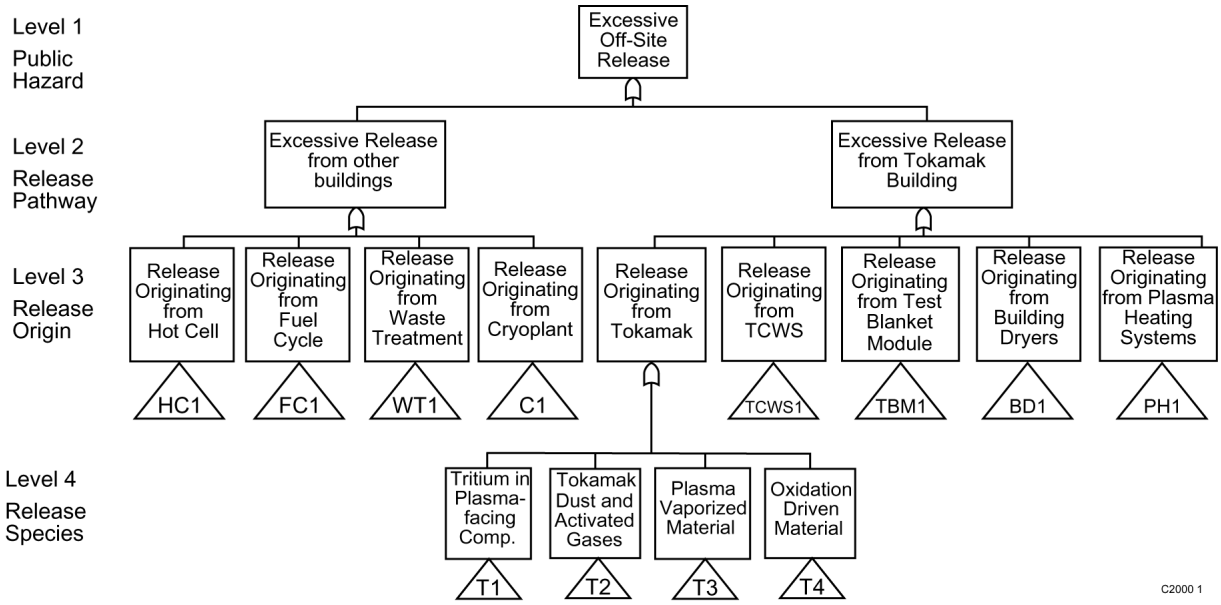

Figure 5.5.1-1 Top Levels of the Master Logic Diagram

As with the bottom-up studies, the initiating events can then be developed into sequences. The event sequence development leading to environmental releases is more straightforward in the top-down approach because all failures leading to environmental releases have been identified during the process of identifying initiating events.

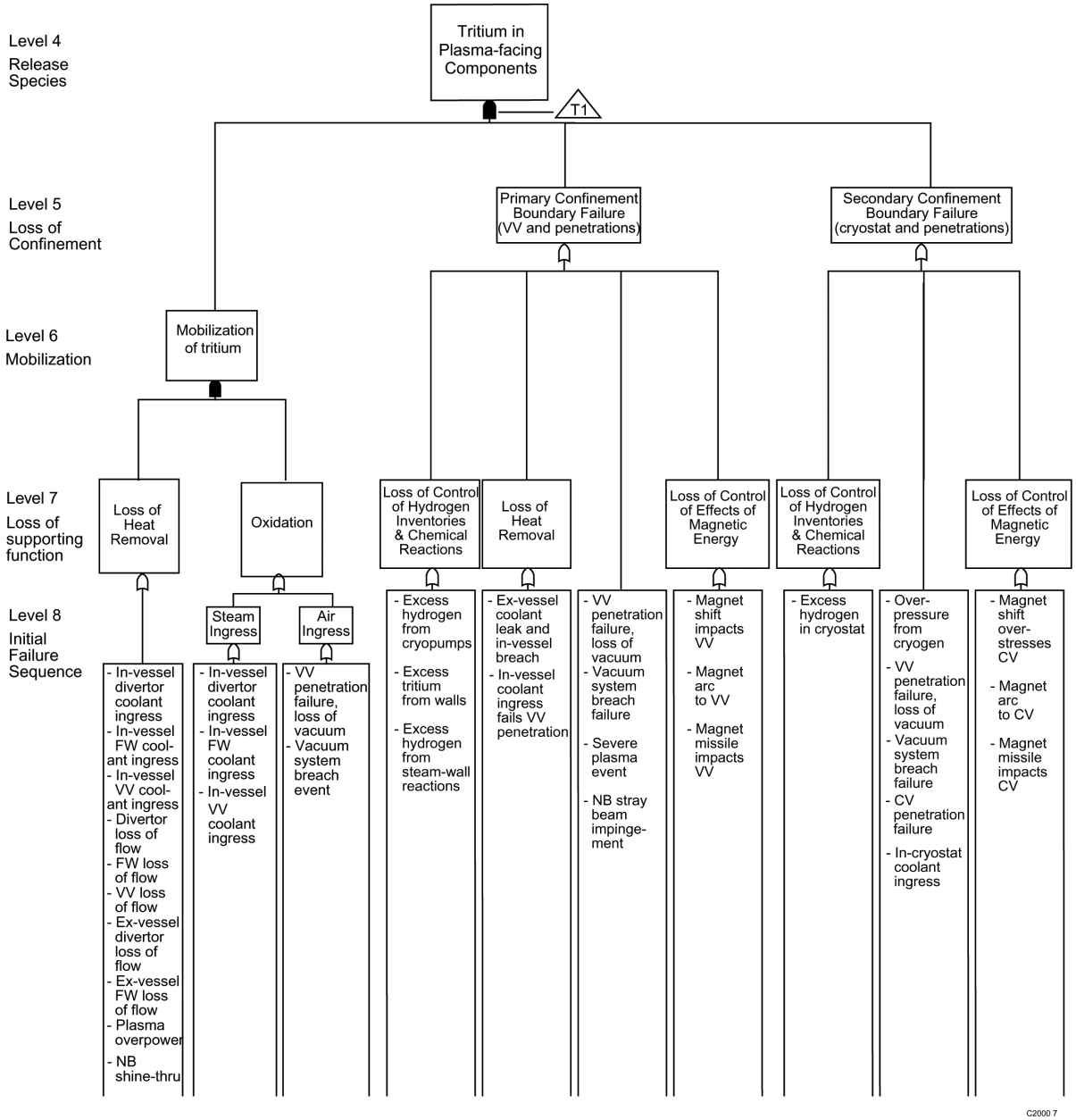

Figure 5.5.1-2 Branch of the Master Logic Diagram Representing the Release of Tritium from Plasma-facing Components

5.5.2 Acceptance Criteria

Project release guidelines for tritium and activation products, which are the top level acceptance criteria used, are given in Table 5.2.3-2. The project imposed restrictive release guidelines so that the design would not have to be significantly modified after site selection. They will be reviewed after a site for ITER is chosen.

Other acceptance criteria adopted for these analyses are:

- maximum pressure inside the vacuum vessel is below 200 kPa (absolute);
- stresses in the cryostat are below allowable (maximum pressure below about 300 kPa (absolute));
- maximum containment volume pressure is below 200 kPa (absolute);

- flammable mixtures of hydrogen and air are avoided; the following acceptance criteria quantify this further:
  - hydrogen production inside the vacuum vessel is below 4 kg;
  - maximum first wall beryllium short-term (< 1h) temperature during plasma burn (excluding disruption) is < 700°C to avoid excessive hydrogen formation in case of beryllium/steam reactions if a water ingress into the vacuum vessel were to occur;
  - maximum long term (beyond one hour after shutdown) first wall beryllium temperature is < 385°C to avoid hydrogen formation in case of beryllium/steam reactions if a water ingress into the vacuum vessel were to occur;
- maximum temperature of components in casks once outside the vacuum vessel is 150°C to limit tritium outgassing;
- ozone formation in the cryostat is below 50 g to limit the explosive hazard.

5.5.3 Reference Events

The estimated releases are below the project release guidelines for all reference events, in most cases by orders of magnitude. The large margins are an indication of the favourable safety characteristics of ITER and the extent to which the safety approach has been successfully implemented in the design to further reduce the consequences of potential accidents to very low levels. Considering the wide breadth and depth of the cases analysed, the conclusion is drawn that there would be no significant risk to the public from accidental releases of radioactivity resulting from the operation of ITER.

Table 5.5.3-1 summarises important parameters and phenomena in the key event analysis. The key events in the table are those events where the fraction of release (a ratio of the predicted release to the release guideline) is larger than ~1% and events where the analysis demonstrates that confinement integrity (H_2 in vacuum vessel, cryostat pressure).

This section summarises the results of the analysis for the most important PIE families shown in Table 5.5.1-1.

5.5.3.1 In-vessel Coolant Leak

A family of potential accidents is grouped around the ITER cooling systems. Sequences starting with coolant pipe failures in various cooling loops and locations have been investigated and show the high degree of robustness in the design.

The thermal loads of a disruption of unexpectedly large magnitude can potentially threaten the integrity of the first wall and divertor cooling channels. Since the in-vessel components are not assigned a safety role, the consequences of a water ingress have been assessed. Different first wall damage sizes are investigated ranging from a single first wall coolant pipe failure (~ 1.6 cm^2) to multiple first wall pipe failure sizes up to 0.2 m^2, which is the maximum effective break size due to limited flow though upstream piping. This is done to show that the ITER design can accommodate the worst possible damage of in-vessel components

.

While it is assumed that such events could cause substantial damage to components in the vacuum vessel, the vacuum vessel pressure remains well below 0.2 MPa and any off-site

releases remain very small. This is because part of the tritium and most of the corrosion products and dust will enter into the coolant leaked into the vacuum vessel and remain in the liquid pool in the pressure suppression system. All releases remain more than two orders of magnitude below the project release guidelines for incidents in Table 5.2.3-2.

Table 5.5.3-1 Important Parameters and Phenomena in the Key Event Analysis

PIE Family	Important parameters	Important phenomena
In-vessel events In-vessel coolant leak	VV pressure and temperature	Effect of discharge of water from loop into the vacuum volume (flashing , impingement)
	Break water flow rate, loop water pressure and temperature	Break coolant flow to vacuum
	Flow rate into VVPSS, volume's pressure and temperature	Condensation in VVPSS
	In-vessel component's surface temperature	Heat transfer by radiation, conduction, convection in air/steam/vacuum
Loss of vacuum	Flow rate through the penetration line	Air exchange flow
	Dust/tritium concentration	Dust/tritium mobilisation and transport
Ex-vessel HTS events Large DV ex-vessel coolant pipe break	HTS vault pressure and temperature	Effect of discharge of water from loop into volume with air
	Break flow rate, loop pressure and temperature	Break flow to volume with air
	Flow rate through the failed DV loop between VV and HTS vault	Air/steam exchange flow
	Dust/tritium concentration	Dust/tritium mobilisation and transport
Heat exchanger leakage	Leak rate through HX tube cracks	Assumption (assumption based on fission industry experience)
Maintenance Stuck DV cassette	Component's temperature due to decay heat	Radiation, convection and conduction in air
	Aerosol/tritium concentrations	Aerosol/tritium mobilisation and transport
Tritium system Isotope separation system failure	Tritium inventory ISS system pressure Leak rate	Tritium transport
	Hydrogen concentration	Release rate, mixing, ventilation
Failure of fuelling line	Fuelling rate, isolation time	Tritium transport
Cryostat event Cryostat water and helium ingress	Cryostat pressure and atmosphere temperature	Heat transfer by radiation, conduction, convection in air/steam/vacuum
	Magnet structures and thermal shield temperatures; condensed (frozen) water masses	Effect of discharge of water and liquid He into the cryostat volume (flashing, condensation)
	Break water and helium flow rate, loop's water pressure and temperature	Steam condensation on cryogenic surface; ice formation in presence of He
Magnet events Arcs near confinement	Arc propagation; location; duration	Magnet quenches; arc formation; metal melting
TF coil short	Structural deformation	Electromagnetic forces

5.5.3.2 Ex-vessel Coolant Leakage

A range of postulated coolant leaks outside of the vacuum vessel was investigated to ensure that the consequences and releases from such events will be acceptably small. The most severe case is discussed below.

During plasma operation, a double-ended pipe rupture of the largest pipe (0.4 m^2 flow area) is postulated to occur in the ex-vessel section of a DIV/LIM PHTS coolant loop. Coolant is

discharged at a high rate into the containment volume. The fusion power is terminated to limit heat up of in-vessel components either passively by tiles that detach above the bond melting temperature or by an active system that injects impurities and uses signals from TCWS parameters. Even if the plasma is terminated, there is a possibility that the in-vessel cooling channels could be damaged because of a disruption that could follow the abnormal plasma termination. Since in-vessel components are not assigned a safety role, an in-vessel water ingress is also postulated to occur to demonstrate that any off-site consequences would be below the project release guidelines.

Only small amounts of hydrogen are generated by steam reacting with the uncooled plasma-facing components (PFCs). The containment volume pressure remains below 0.2 MPa. Failure of cooling channels in PFCs would cause pressurisation within the vacuum vessel. The vacuum vessel pressure peaks at 150 kPa, which is the setpoint for opening the pressure relief lines connecting the vacuum vessel and the pressure suppression system. Some fraction of the in-vessel inventories is transported to the TWCS vault by thermally driven exchange flow through the failed divertor loop, although most remains in the water pool of the suppression system or in condensed steam in the vault. The corrosion products, dust and tritium in the vault may leak to the environment before the vault pressure is restored to sub-atmospheric pressure within 24 hours after the event. Releases are about a factor of three below the project release guidelines for Accidents.

5.5.3.3 Loss of Vacuum

Although vacuum vessel penetrations are designed with care to provide two confinement barriers, the large number of these penetrations suggests that failure of a penetration line should be investigated to demonstrate the tolerance of the design to such failures. A loss of vacuum event results from this. Failure of windows/valves in a vacuum vessel penetration line (0.02 m^2 cross-sectional area) was selected to encompass all kinds of postulated loss of vacuum events. The penetration line is assumed in the analysis to be connected to the gallery with air atmosphere. Air ingress into the plasma chamber terminates the plasma with a disruption. Loss of off-site power is also assumed to coincide with the initiating event and to last one hour.

The vacuum vessel and room pressures equalise about 25 minutes after event initiation. The air in the vacuum vessel heats up but stays below 200^{o}C during the event. Chemical reactions do not occur due to the limited temperatures. In-vessel tritium and dust are mobilised by the air ingress, and some of them are transported to the vacuum vessel pressure suppression system. No mobilised radioactivity is transported out of the vacuum vessel due to the operation of the tokamak venting system, which pumps out the air in vacuum vessel through the normal vent detritiation system to prevent a back flow. Environmental releases are below project release guideline for Accidents by a factor of eight.

5.5.3.4 Tritium Process Pipe Leakage

Failures of the tritium processing equipment have been investigated because of the large tritium inventory in these systems. In such an event, the process gas will be released into the secondary confinement if the primary system pressure is higher than the confinement pressure, or the confinement atmosphere will equalise inside of the primary component if initial pressure is lower. There would be no flammable hydrogen mixtures since the secondary boundary will either contain an inert gas or be evacuated. The tritium release is

the total of tritium losses from the secondary confinement (e.g. glove box) to the process room and the releases through the glove box atmosphere detritiation system in series with the vent detritiation system. The expected tritium atmospheric release is below the expected daily normal effluents.

The extremely unlikely event of failures in both the process and secondary confinement piping was postulated to ensure the fault tolerance of the design. The bounding case is a failure of the fuelling header between the tritium plant and the fuelling system valve boxes in the tokamak building. Tritium will leak into a room in the tritium building. The room will be isolated from normal ventilation and connected to the standby vent detritiation system (S-VDS). A time delay of 30 s between detection and isolation was assumed. The total tritium content of the room is about 13 g at 30 s when the header is isolated from the pump for the bounding case. The tritium inside the room atmosphere is detritiated by the S-VDS. Instrumentation and control systems are provided with un-interruptible power, and the S–VDS can be supplied with emergency class III power that would be available within 30 seconds if a loss of off-site electrical power were also to occur. The total expected tritium release is about 0.17 g, which is one order of magnitude below project release guidelines for Accidents in Table 5.2.3-2. No flammable hydrogen-air mixtures are formed in the room.

Failure of the cryogenic distillation columns and helium coolant lines in the isotope separation system was examined since it has the highest tritium inventory (~220 g). Pessimistic assumptions for initial conditions and confinement equipment performance are used, and additional independent failures are postulated to demonstrate the tolerance to failure of the design. The tritium inventory spilled into its secondary confinement leads to a small tritium release to the environment (~ 54 mg), which is two orders of magnitude below project release guidelines for accidents. Releases from the isotope separation system are contained within secondary confinement and no flammable hydrogen-air mixtures are formed.

5.5.3.5 Magnets

The magnets are designed to ensure that the energy stored in them is controlled and off-normal events in the magnet system do not jeopardise confinement barriers. However, events that could potentially damage confinement barriers are examined in section 2.1 because of the large energy stored in the toroidal field coils (~ 40 GJ) and the geometrical location of the magnets near confinement barriers (vacuum vessel and cryostat). Pessimistic assumptions are made throughout to construct bounding scenarios and to demonstrate that faults in the magnet systems do not create safety concerns.

One event postulated is a full terminal short of a TF coil, which is an extremely unlikely event that requires two ground faults in the coil busbar circuit, one on each side of the TF coil, while undergoing a fast discharge, plus the failure of the monitoring systems to detect these faults. This event is analysed to investigate the potential for structural damage to the confinement barriers. The maximum current induced in a shorted TF coil during a fast discharge is limited by both inductive coupling with the other coils during the fast discharge, and by the quench as the superconductor is driven to critical conditions. Extensive local plastic deformation can be expected to occur in the TF case (in the shorted coil and the adjacent coils) and intercoil structures. There may be some shear key and bolt failure and a loss of cryostat vacuum due to thermal shield damage, but gross structural failure is not predicted. The deflection of magnets is limited, and they do not touch the vacuum vessel or

cryostat wall (or their thermal shields). There may be damage to the CS coil possibly leading to limited short circuits but arcing is confined to the coil. No radiological consequences are expected.

Another event postulated is an arc inside a coil. The arc is postulated to develop as a result of a failure (or more probably an inability) to discharge the coil when a quench occurs. The effects of arcs in the TF coils is contained within the massive coil case. External shorts on the CS and PF busbars (superconducting or normal) can potentially lead to molten material generation in the coils themselves (not significantly in the busbars) due to the coupling of extra energy into the coil, followed by a quench in a coil that cannot be discharged. Only in three of the outer PF coil winding packs will the quench propagate slowly, and local conductor melting, followed by the development of arcs, will be possible. The melted material produced by the coil internal arcs (about 750 kg) may not be contained by the thin coil casing and would be spread over components in the cryostat in the vicinity of the shorted coil. Due to arc movement in the winding pack, the melted material will be distributed around the circumference of the coil, covering several square metres. It is possible that external arc energy associated with the coil short is sufficient to melt the conductor of the superconducting busbars (depending on the location of the initial short and the action of the coil power supplies) and cause local melting around the cryostat feedthroughs No failure of primary confinement barriers is predicted and no radiological consequences are expected.

A combined leak of helium and primary coolant into the cryostat was analysed to bound potential damage from the magnet system. The maximum pressure reached in the cryostat depends on the number of helium and TWCS loops postulated to be damaged. In the bounding case, the cryostat pressure reaches a maximum value of 220 kPa in 82 s. Almost all steam condenses on cold surfaces in about 200 seconds after initiating the event. After 1,000 s, the pressure drops to 150 kPa due to cooling by cold surfaces such as the TF coil cases. Pumping of the cryostat volumes can restore sub-atmospheric conditions within 24 hours. Due to the condensation, the environmental releases are about three orders of magnitude below project release guidelines for Accidents in Table 5.2.3-2.

5.5.4 External Hazards

In addition to the reference events that envelope the safety consequences of internal failures, an assessment has been made to show that ITER is adequately designed against site hazards consistent with the ITER generic site requirements and site design assumptions, specifically earthquakes. An assessment of site-specific natural and man-made external hazards will be carried out following site selection to confirm the ability to perform the required safety functions.

An infrequent, severe earthquake (SL-2) which, although unlikely to occur during the lifetime of the facility, is assessed to demonstrate adequate protection of the public. This earthquake is assumed to have a peak ground acceleration of 0.2 g horizontal and vertical with a return period of ≥ 10,000 years. The design requirement is to ensure that required safety functions are provided and prevent releases from the facility.

Analysis of the tokamak and tokamak building have been carried out using the response spectra based on the assumed design basis ground motions. A 3D finite element shell-beam model has been built to perform seismic analysis as described in section 2.12. There is a high probability that a seismic event that leads to in-vessel motion would trigger a disruption, for

example, due to dust falling into the plasma, loss of magnetic signals, false (motion induced) signals, or loss of plasma control. Control failures under some circumstances may lead to VDEs which in turn lead to higher loads on structures. For these reasons, a disruption or VDE load is assumed in addition to that from the earthquake.

The first horizontal eigenvalue of 2.8 Hz corresponds to the entire tokamak horizontal rocking on top of the gravity support. The vacuum vessel-magnet horizontal mutual rocking eigenvalue is 6.6 Hz. Displacements obtained from the model are relatively small and within the 10 mm radial build value allocated. The computed loads at the gravity support and vacuum vessel support under deadweight loads and SL-2 seismic loads are within acceptable limits.

A thorough seismic safety assessment will be undertaken as part of the site-specific adaptation, based on site-specific seismic hazards, final design and layout of the equipment. The preliminary seismic safety assessment demonstrates that ITER can be adequately designed for earthquakes. A system-by-system review of the consequences of a SL-2 level earthquake found possible releases that would not exceed release guidelines for Incidents in Table 5.2.3-2.

Seismically-qualified systems will survive, and their safety function will not be impaired. In particular, there will be no TCWS pipe ruptures (although some minor leakage may occur). Adequate radioactive confinement barriers will remain intact and sufficient heating, ventilation and air conditioning systems are qualified to ensure control of releases, if any.

It is concluded that ITER can be designed such that postulated earthquakes would not cause releases. Design changes of the tokamak building can be introduced to accommodate seismic loading up to 0.4 g, if judged necessary for a site specific design.

5.5.5 Ultimate Safety Margins

ITER is expected to be 'safe' with little dependence on dedicated 'safety systems' for public protection because of the fail-safe nature of the fusion energy reaction, modest mobilisable radioactive inventories, multiple layers of confinement, and passive means for decay heat removal. However, the inventories are large enough to warrant a detailed assessment of events that are very low in probability, so called hypothetical events, to demonstrate the tolerance to failures in the design and the lack of sharp increases in consequences if further degradation is postulated ('cliff-edge effects').

Hypothetical scenarios are developed by considering reference events (section 5.5.4) and postulating additional independent failures. Some bounding cases are analysed for safety functions, such as decay heat removal without any coolant or failure of all active plasma shutdown. For confinement, scenarios are investigated to show that the internal energy sources do not have the capacity to fail confinement and that enough margin is built into confinement to exclude cliff-edge effects.

Analysis of hypothetical events shows that the ITER design has sufficient safety margins to provide a high level of public protection and to meet the 50 mSv no-evacuation criterion. Releases for the events considered are summarised in Table 5.5.5-1. The most limiting cases are the confinement bypass events. Releases in these events are below or near 15 g of tritium which is roughly 20% of the no-evacuation threshold. Significant environmental releases can

only occur in ITER if several confinement barriers fail independently of each other. So far, no single event has been identified which can simultaneously damage the multiple layers of confinement in ITER.

The absence of cliff edge effects and robustness of the defence-in-depth approach are demonstrated in the postulated confinement bypass events which lead to the most limiting releases. In hypothetical confinement bypass events in the fuel cycle (where failure of two barriers is postulated) the amount of tritium released into the last confinement room is limited to less than 14 g tritium by process isolation. Postulating failure of room isolation would lead to an environmental release of this tritium.

Another extreme situation postulates common cause failure in vacuum vessel penetrations which would lead to significant transport of radioactivity into connecting rooms. Use of detritiation systems would limit environmental releases for these events. The largest environmental releases are expected for vacuum vessel bypass events which are combined with an extended blackout situation lasting one shift (8 hours). Postulating such a situation in combination with an in-vessel coolant leak would lead to environmental releases of about 15 g tritium and about 10 g of activated tungsten dust. Condensation inside the connected room plays an important role in limiting the environmental release of tritiated water. In a dry bypass event less radioactivity is transported from the VV to the connected room because there is no driving pressure pushing mobilized tritium and dust out of the VV.

Another hypothetical event is the postulation of failure of all cooling systems in ITER when removing decay heat. Even for this extreme situation the first wall only heats up to a maximum temperature of about 650ºC.

Postulating damage of both the vacuum vessel and cryostat boundary by some unidentified magnet energy release event would not lead to large environmental releases because the cryogenic surfaces would effectively capture most of the mobilized source term.

Table 5.5.5-1 Summary of Releases for Hypothetical Events

Event (Type of Release)	% of No-evacuation Threshold Average Weather	% of No-evacuation Threshold Conservative Weather
Wet bypass	<~ 1	<20
Dry bypass - loss of vacuum accident	< 1	<10
Tritium plant, fuel cycle	~ 1	15
Decay heat	< 1	< 1
Ex-vessel/in-vessel loss of coolant	< 1	< 1
Magnet energy release	< 1	< 1

Safety margins are maintained in ITER for these hypothetical events because of the following.

- Structural margins in the design of the vacuum vessel maintain integrity for the range of potential in-vessel coolant leaks from one cooling channel to a hypothetical break of all in-vessel pipes.
- The structure is robust such that there will be no catastrophic failure (or gross loss of geometry) due to plasma or magnetic forces.

- Inherent passive shutdown of the plasma occurs when the first wall reaches 700°C - 1100°C due to mechanical failure or beryllium evaporation, and intrinsic fail safe termination of the plasma occurs in case of in-vessel water or air leaks.
- Mobilisable radioactive inventories of tritium and activation products are modest. Therefore, ultimate performance of confinement barriers that must be assured in hypothetical accidents is not very stringent - about one order of magnitude release reduction for tritium and mobilisable metallic dust.
- Releases from the vacuum vessel even in the case of an in-vessel coolant leak with a bypass of the confinement barriers are limited due to limited inventories, isolation of the affected room, filtration and detritiation of leaks, and operation of the vacuum vessel pressure suppression system.
- A passive heat removal system (the VV HTS) exists.
- Long time scales are required for component heat-up following events because of heat removal by radiation from in-vessel components to the vacuum vessel and by natural circulation of the vacuum vessel heat transfer system.
- The decay heat density is low enough not to melt the structure even if all the heat transfer systems including the VV HTS are hypothetically assumed to be lost. Injection of helium (or air) into the cryostat within a few days will bridge the thermal isolation between vacuum vessel and the huge heat sink of the cryogenic structures of the magnet system. The maximum temperatures in such a case are low (< 650°C).
- The design is tolerant of failure of mitigating systems, such as failure of penetration line isolation and failure of the fusion power shutdown system.

6 Plans

This chapter describes the ITER construction, commissioning, operation and decommissioning plan. The corresponding plan for human and financial resources is addressed in the next chapter.

6.1 ITER Construction and Commissioning Plan

6.1.1 Introduction

The planning schedule for supply, construction/assembly and commissioning set out below depends on a number of assumptions detailed in the following. As the design progresses decisions reached by the Parties may confirm or alter the assumptions that have led to the schedule's present status. The actual plan will depend on the licensing procedure, as well as the organization and arrangements that will be put in place for the procurement, construction and commissioning.

6.1.2 Initial and Background Conditions

The construction agreement is expected to be signed at the end of 2002 or the beginning of 2003 following formal negotiations. The ITER legal entity (ILE) will be established after ratification of the agreement within each Party. This organisation will start the formal regulatory procedure and procurement process for the long lead-time items. The regulatory approval process, however, will remain speculative until a site is formally selected. As the site proposals are received before or at a sufficiently early stage of negotiations, it will be possible to assess the time needed for licensing in the various possible host Parties and the effects on the overall schedule. Since the start of the actual construction on the site depends upon when the license to construct is issued by the regulatory authority, dates in the construction and commissioning plan are, therefore, measured in months from a start date ("T = 0") defined as the date at which the actual construction work of excavation for the tokamak buildings is started.

Furthermore, the following assumptions pertain at T = 0.

- Informal dialogue with regulatory authorities should be established and should orientate the technical preparation toward a license application with a view to solving the major technical issues prior to establishment of the ILE. Documents required for the formal regulatory process are assumed to be prepared before the ILE exists, so as to allow the ILE to begin the formal regulatory process immediately after its establishment.
- Procurement specification of equipment/material for the longest lead-time items and critical buildings are assumed to be finalized during the co-ordinated technical activities (CTA).
- Procurement sharing is assumed to be agreed among the Parties during the CTA so as to permit the placing of all contracts at the appropriate time. Particularly the longest lead-time items and the on-site fabrication buildings for magnets which are not related directly licensing issues are procured immediately after the establishment of the ILE and before T = 0.
- The construction site work starts immediately at T = 0. It is assumed that site preparation has been started sufficiently early by the host Party so as not to place constraints on the start of construction.

6.1.3 Overall and Summary Schedule

The overall schedule that leads up to the first hydrogen plasma operation is shown in Figure 6.1.3-1. It represents a reference scenario, which is a success-oriented schedule of

procurement, construction, assembly and commissioning of ITER, based on the assumptions. It is concluded that the construction period is eight years from the start of construction on site (T = 0) to the first hydrogen plasma operation. To meet this schedule, the procurement contracts for the longest lead-time items, particularly the superconducting strands and the TF coils have to be started about 15 months before T = 0. Assuming a reasonable duration for receiving bids, contracting and designing the manufacturing process, the bid cycle must be started 21 ~ 24 months before T = 0 under the ILE. If the license is obtained from the Host Country Regulators within a period of 2 years after the ILE is established (including the case where it will be available immediately after) the overall schedule will be unchanged, saying about ten years from the establishment of the ILE to the first plasma. On the contrary, if it takes longer to obtain the license, the schedule will slip in time by the equivalent amount.

The detailed construction schedule is developed to correspond to each procurement package specified for the cost estimate. The schedule for each package includes procurement specification preparation, bid process, vendor's design (if appropriate), manufacturing (if appropriate), transport to site (if appropriate), installation and commissioning. The summary level of the construction schedule, which includes, in general, one line per procurement package, is shown in Figure 6.1.3-2.

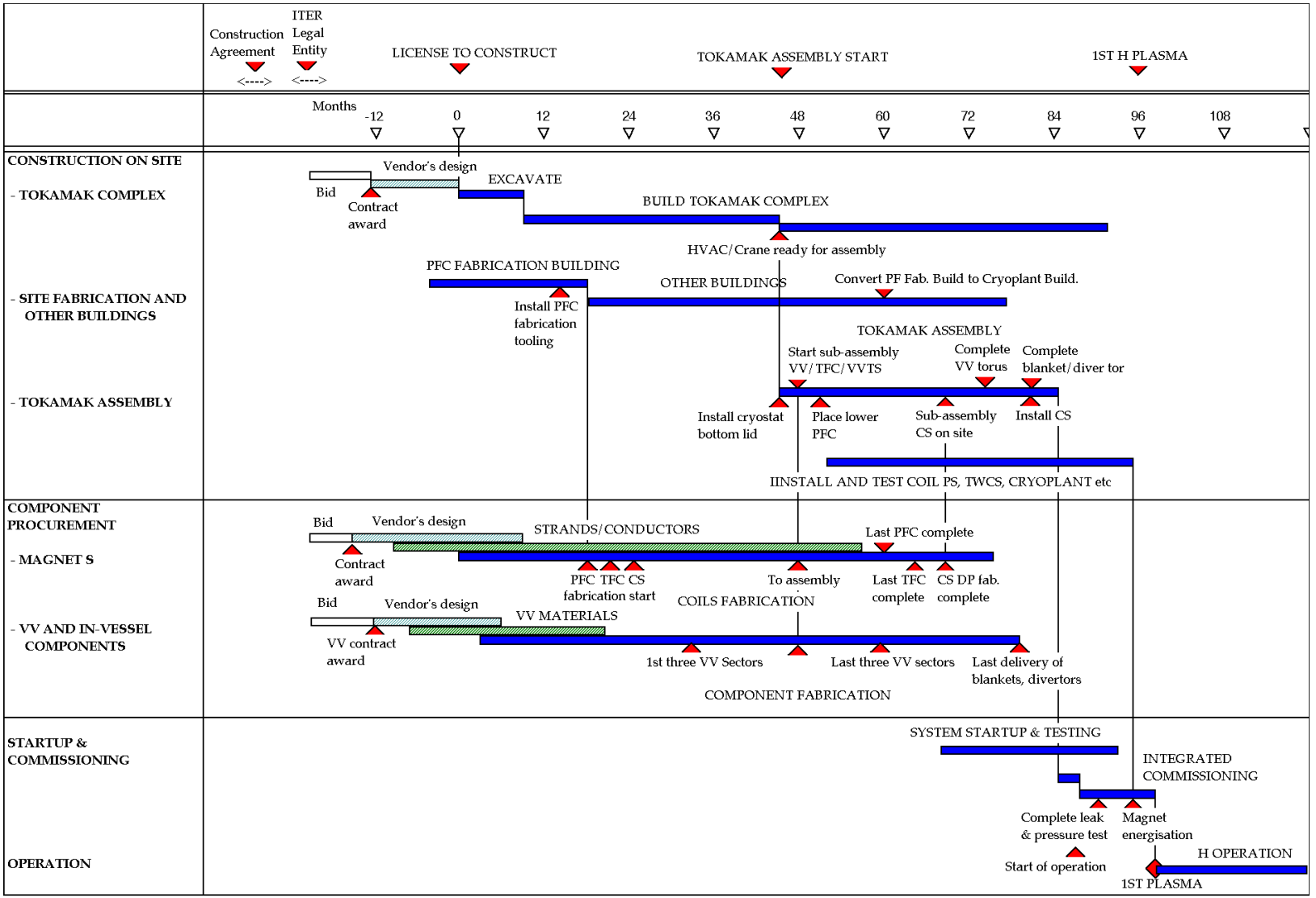

Figure 6.1.3-1 Overall Schedule up to First Plasma

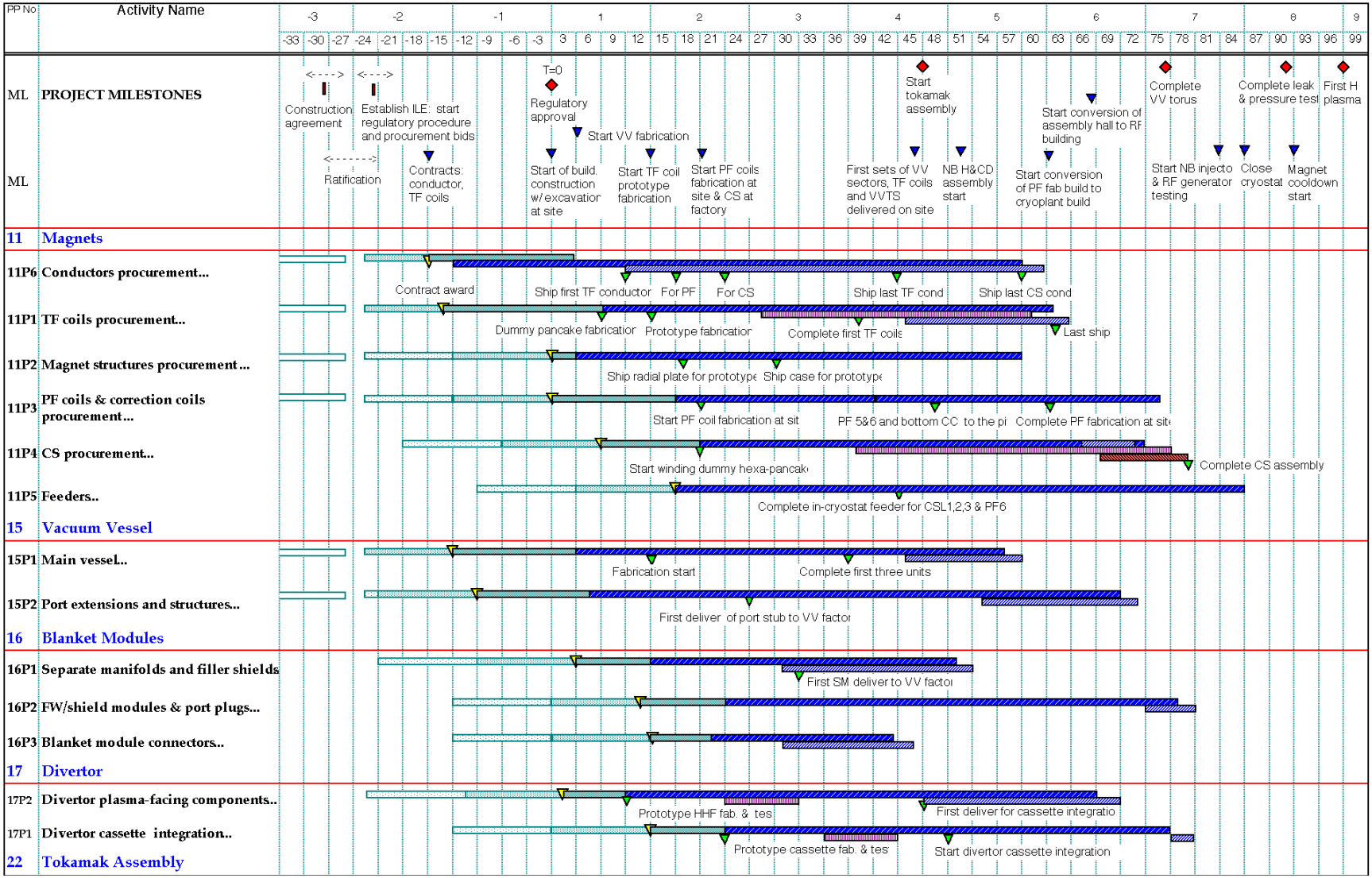

Figure 6.1.3-2 Summary Construction Schedule by Procurement Package (1)

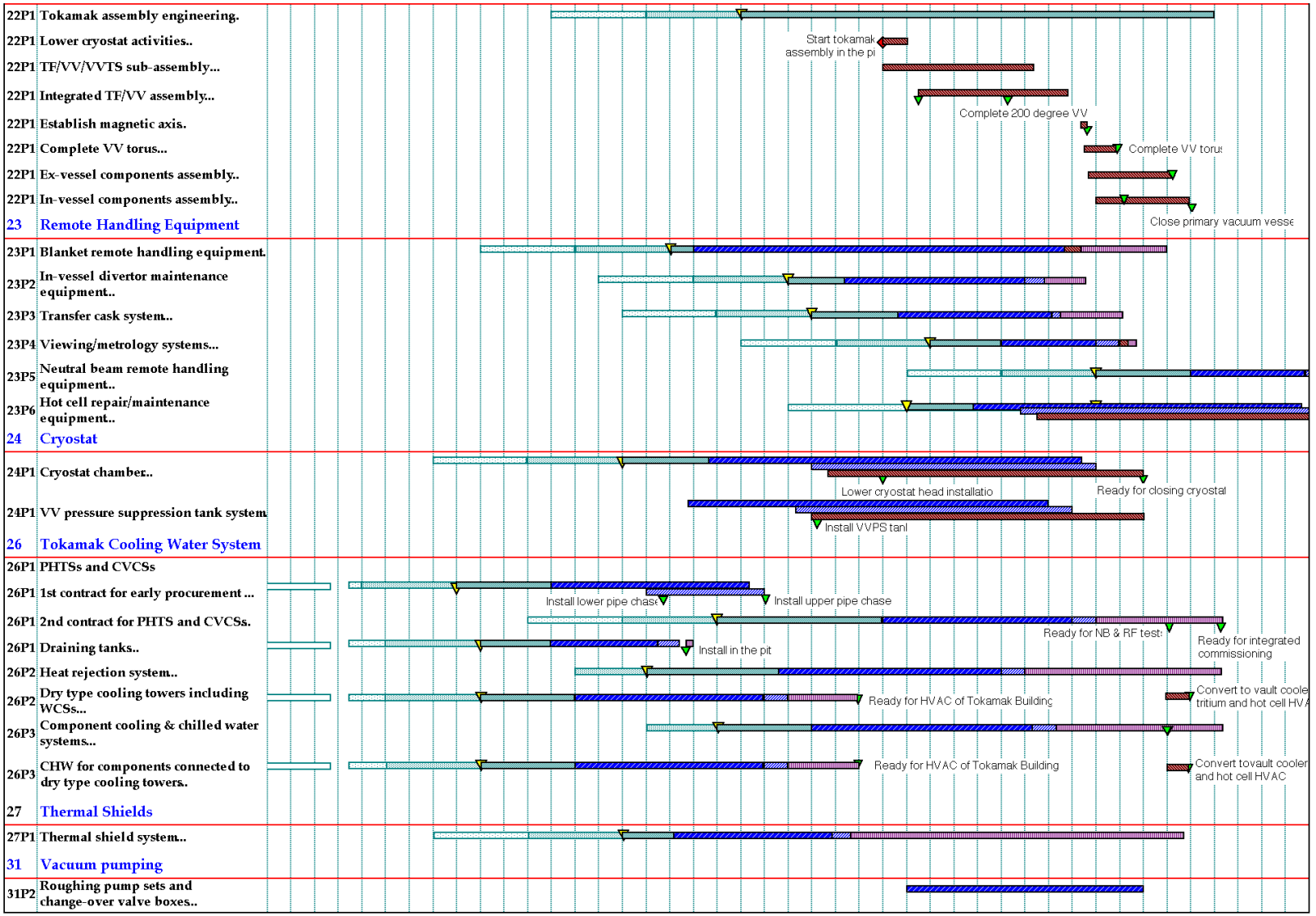

Figure 6.1.3-2 Summary Construction Schedule by Procurement Package (2)

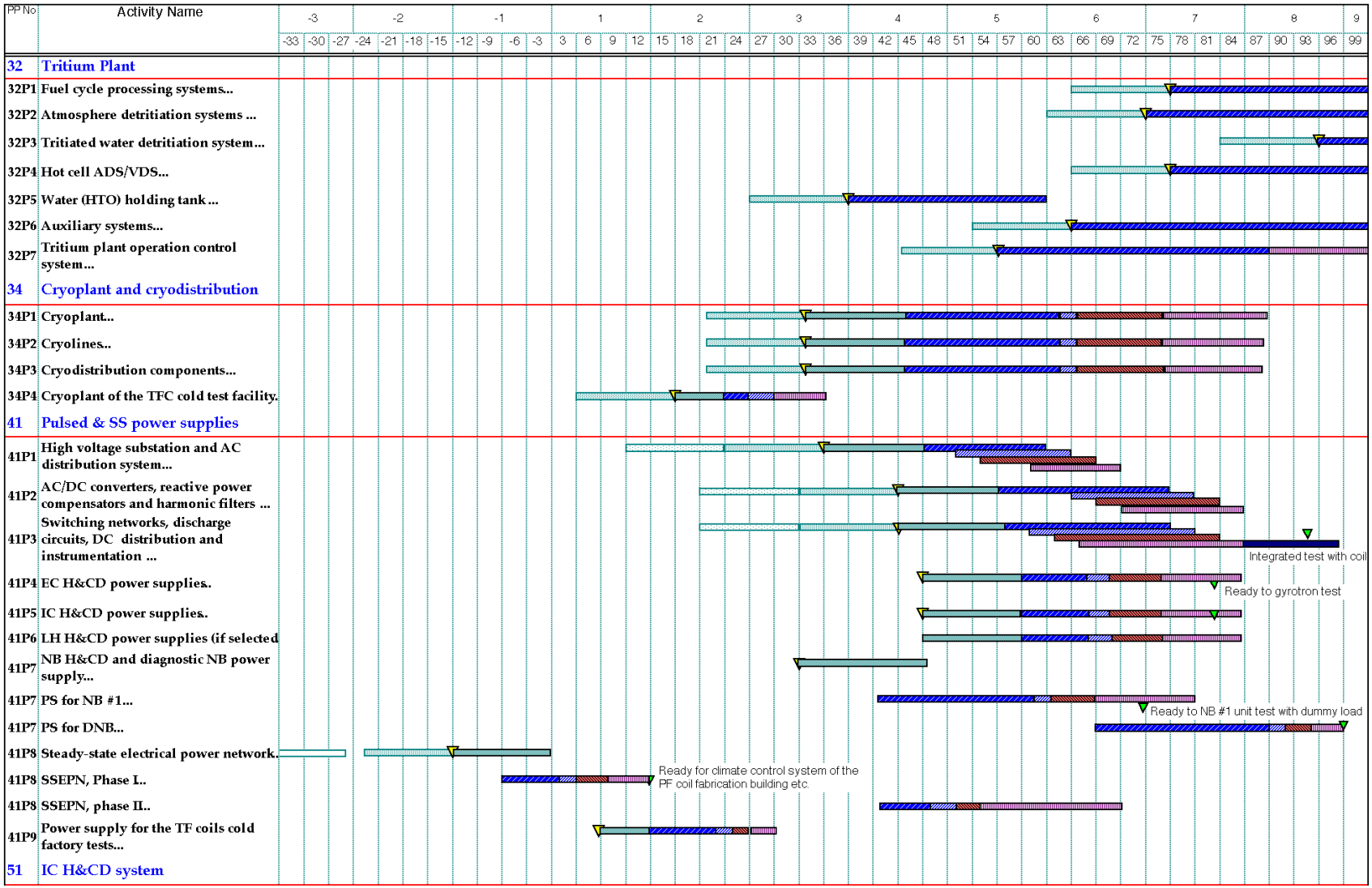

Figure 6.1.3-2 Summary Construction Schedule by Procurement Package (3)

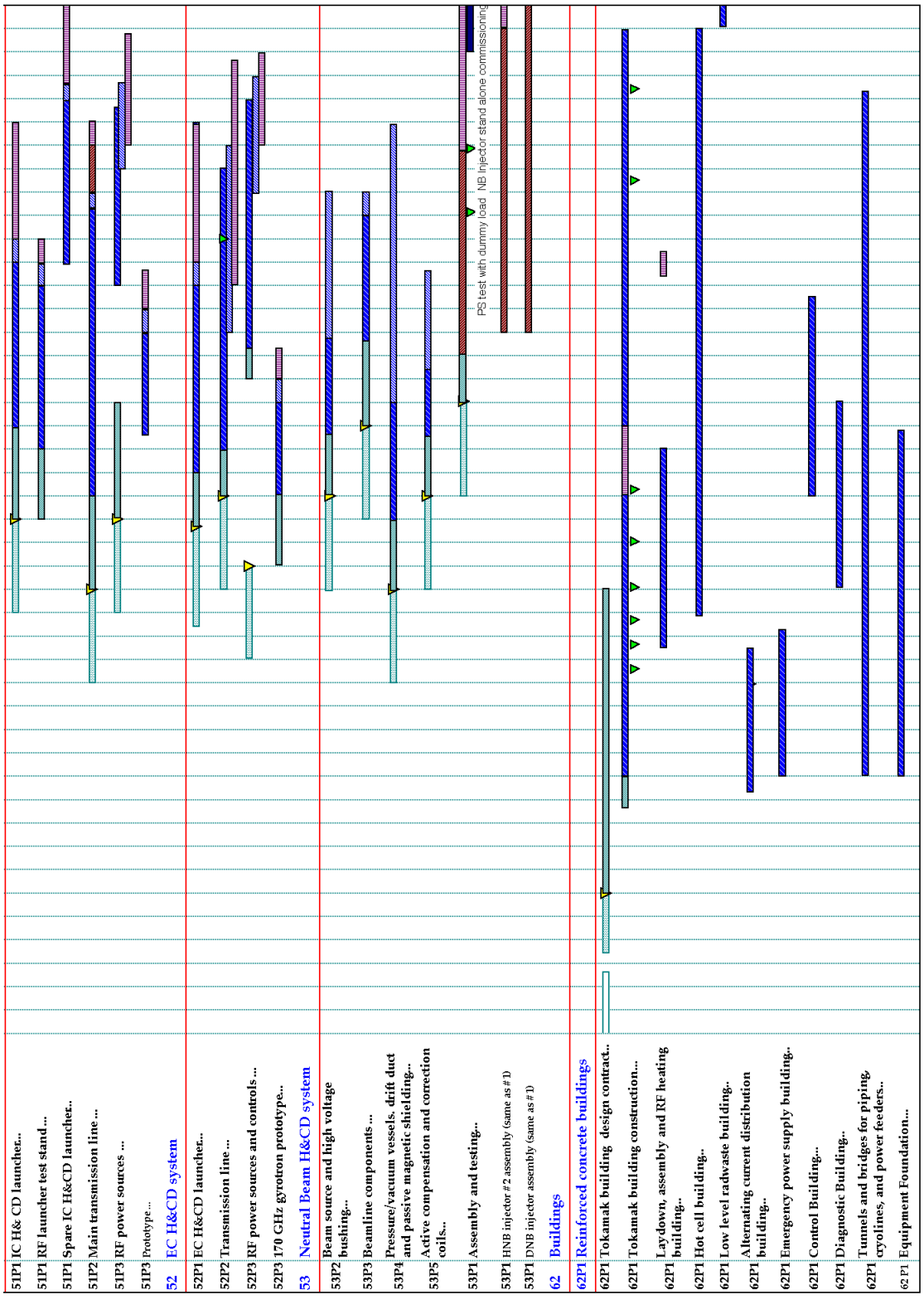

Figure 6.1.3-2 Summary Construction Schedule by Procurement Package (4)

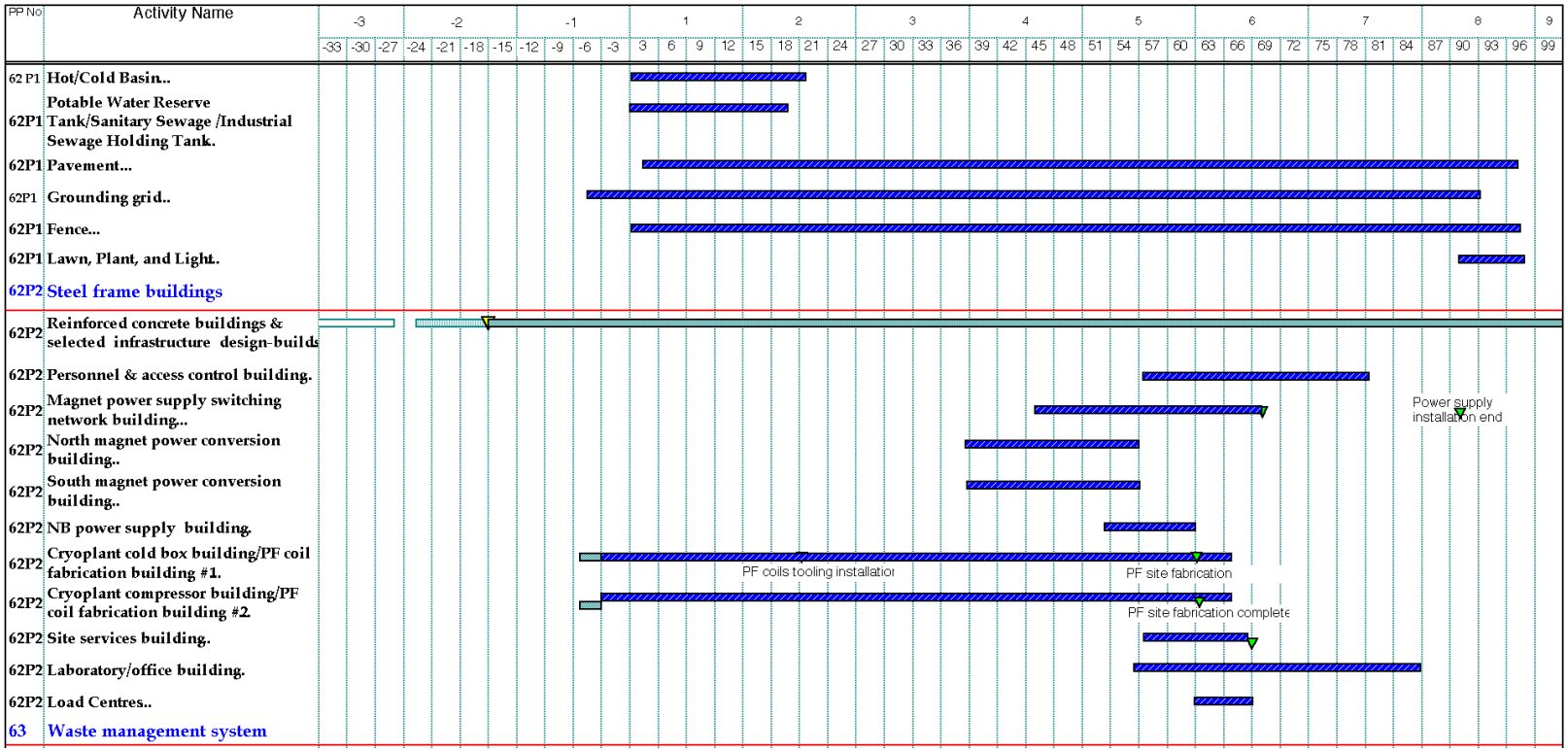

Figure 6.1.3-2 Summary Construction Schedule by Procurement Package (5)

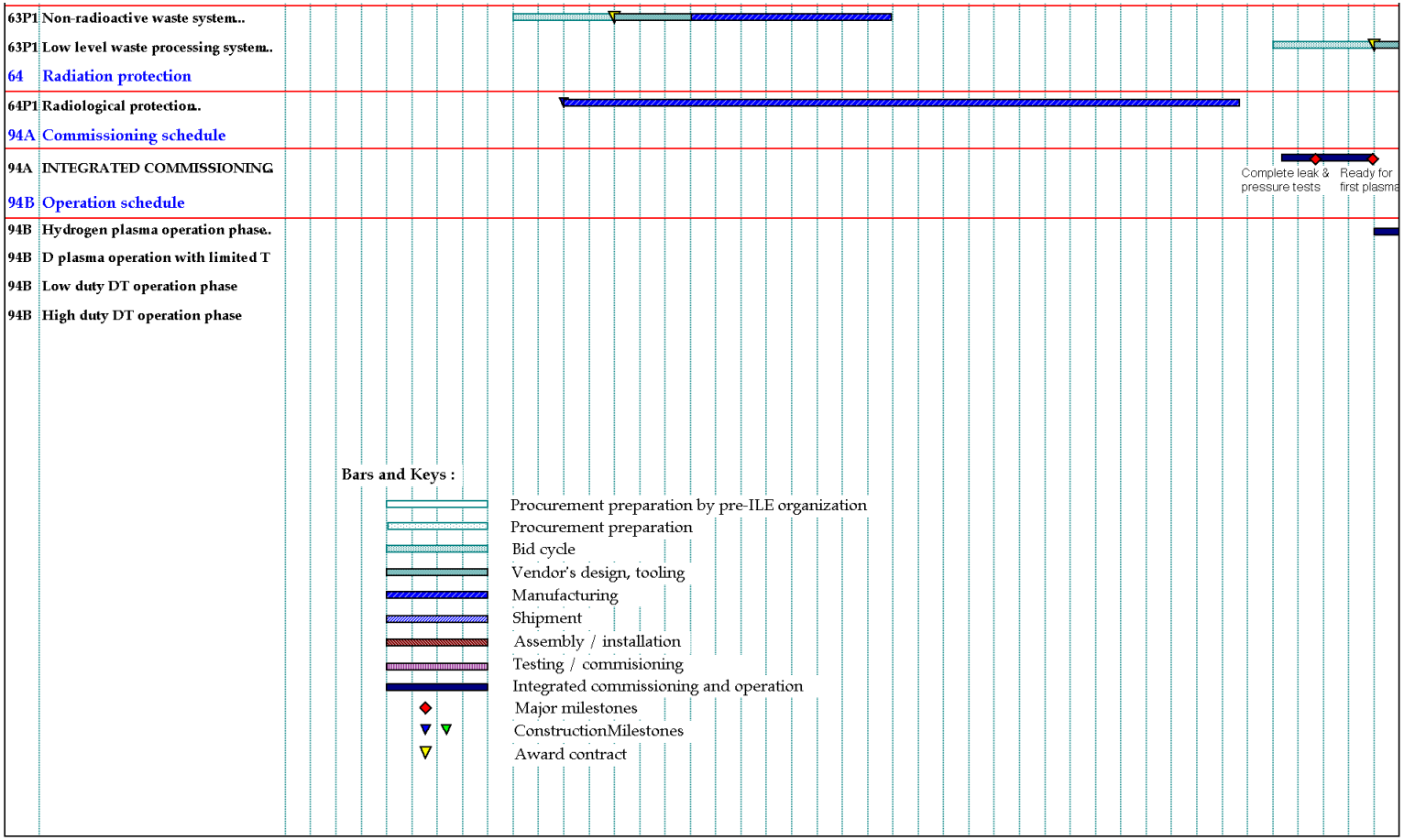

Figure 6.1.3-2 Summary Construction Schedule by Procurement Package (6)

6.1.4 Construction and Early Procurements

6.1.4.1 Procurement Assumptions

The lead-times for the different components of ITER vary widely. Also some items – including the tokamak buildings with parts of water cooling pipes, parts of the cryostat, magnets, and vacuum vessel - are logically on the critical path irrespective of their time schedule, whereas others can be delayed until the date when they would lie on the critical path. In addition, cash flow may pose constraints which conflict with the need to make procurement at a date compatible with the smooth planning of implementation. For the purposes of evolving this schedule, procurement is assumed to occur such that systems/components are delivered just in time, i.e. at the latest time, on the critical path, for assembly and installation/construction, in accordance with the construction logic. In a second evolution of this plan, some items could be moved earlier in the schedule to gain some margins, which would remove those items from the critical path. If cash flow peaks caused by critical items are high, items which is not on the critical path are procured earlier than the just-in-time plan in order to avoid peaky cash flow.

Another important assumption is that the placing of purchase orders is allowed on the establishment of the ILE, in order to allow vendor's design and tooling preparation for the critical lead-time components and buildings. In reality, for non-safety-related items (e.g. magnets), manufacturing can even be started before the granting of a construction licence, provided it is clear one will eventually be granted. For safety-related items, however, construction can start only after the license to construct is issued, if necessary through a second contract. Documentation required for purchasing the various items will be completed in time for the scheduled procurement. The procurement bid process is assumed to take typically six to twelve months from the release of tender documents to industries to the awarding of contracts.

6.1.4.2 Buildings and Licence to Construct

In order to start excavation immediately at T = 0, the design of the complex must be complete by then. The contract for the vendor's preparation of the complex, thus, has to be awarded at least twelve to fifteen months before. Considering a period for procurement bid process, the tender documents have to be released by the ILE 21 to 24 months before T = 0. If the regulatory licensing procedure is required more than 21 to 24 months at the host country, the start of the Tokamak complex construction is delayed and licensing become critical path. If it takes less than two years, the critical path is not the license and construction of the buildings but the procurement of long lead-time items by the ILE.

Excavation is to be completed within 9 months. Installation of the large pipes of the primary heat transfer system that are installed in the tokamak building below grade will follow after basemat construction. Drain tanks are also installed to the bottom of the tokamak building around month 20. The major part of the tokamak building must be functional, including cranes and HVAC system, by the end of 45 months from T = 0 in order to allow the timely start of tokamak assembly. With these assumptions, the large pipe chase, drain tanks and heat rejection system for the HVAC is needed to start procurement before T = 0.

Two cryoplant buildings are to be built and serve dual purposes, as the PF coils fabrication buildings in the early stage, and cryoplant cold box and compressor buildings later. To

maximise the time available for PF coil manufacture and to allow the cryoplant to be used for NB injector stand-alone commissioning and magnet cooldown in time, the construction of these buildings is also started at T = 0, or sooner.

6.1.4.3 Procurement of Long Lead-Time Items

6.1.4.3.1 Magnets

Magnets are definitely on the critical path if license process does not require more than two years. It is essential to purchase an initial quantity of Nb_3Sn conductor to train the firms for the forthcoming series strand production, and to award the contract for the design of the TF coils manufacturing prior to T = 0, as soon as the ILE is established. This should be possible if (1) a sufficient number of contractors in the world have been qualified and trained, (2) the detailed specifications for manufacturing TF coils are fully available by the time of the signing of the construction agreement, and (3) procurement sharing is agreed among the Parties before the signing of the construction agreement. This allows the call for tender to be issued immediately after the establishment of the ILE.

A prototype TF coil is fabricated in order to establish technical basis for the manufacturing process. It will be a spare coil later. In order to meet the pre-assembly of TF coils and vacuum vessel sectors in the assembly hall, the first TF coil at least must be delivered by month 45, and the last one by month 62. Manufacturing time for one TF coil including a cold test of the winding pack is 17 months. Fabricating two TF coils simultaneously after one prototype, the manufacturing time for 19 coils takes 57 months, almost five years in total. Allowing a reasonable duration for establishing the manufacturing process, procuring materials and preparing toolings, the contracts should be awarded at least 12 to 15 months before T = 0.

Figure 6.1.4-1 shows the plan of the TF coils and VV sectors procurements linked to the tokamak assembly. The VV11-12 sector is delivered just in time for sub-assembly with the TF11 and TF12 even if the VV procurement started at T = 0. The delivery of the last two TF coils, TF17 and TF18 also just coincides with the last sub-assembly of the VV and TF coils with the VV thermal shield.

Most of the PF coils are too large to consider their transfer from the factory to the site (unless both factory and ITER site have deep water access). Thus, fabrication on site is planned. To save cost, the cryoplant buildings are used for fabrication. After the fabrication of all six PF coils, the buildings have to be converted to install cryoplant cold boxes and compressors. In order to meet the plan for the magnets cool-down test at month 91, the conversion of the buildings has to be started at month 61. The fabrication of all six PF coils is required 42 months. Thus, the fabrication of the PF coil at site must start at month 18. Another four to six months are needed for installation and commissioning of the PF coil winding tools. It is concluded that the construction of the PF coils fabrication buildings have to start four months before T = 0 at site. The lower PF coils, PF5 and PF6 are easily ready for placement at the bottom of the pit at the beginning of the tokamak assembly starting in month 46 and the other coils are stored until the time of installation.

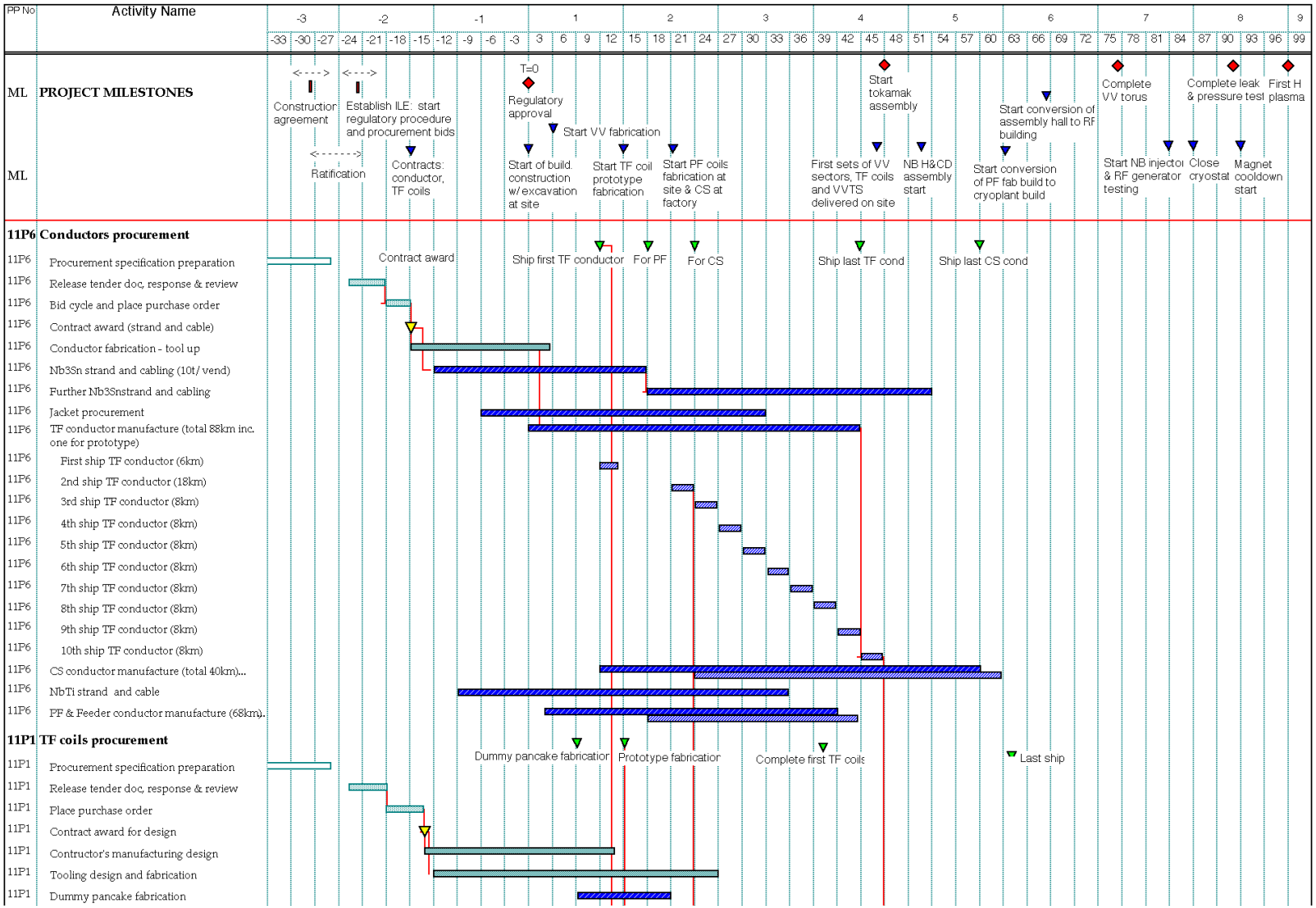

Figure 6.1.4-1 TF Coils and Vacuum Vessel Procurements to meet Assembly (1)

Figure 6.1.4-1 TF Coils and Vacuum Vessel Procurements to meet Assembly (2)

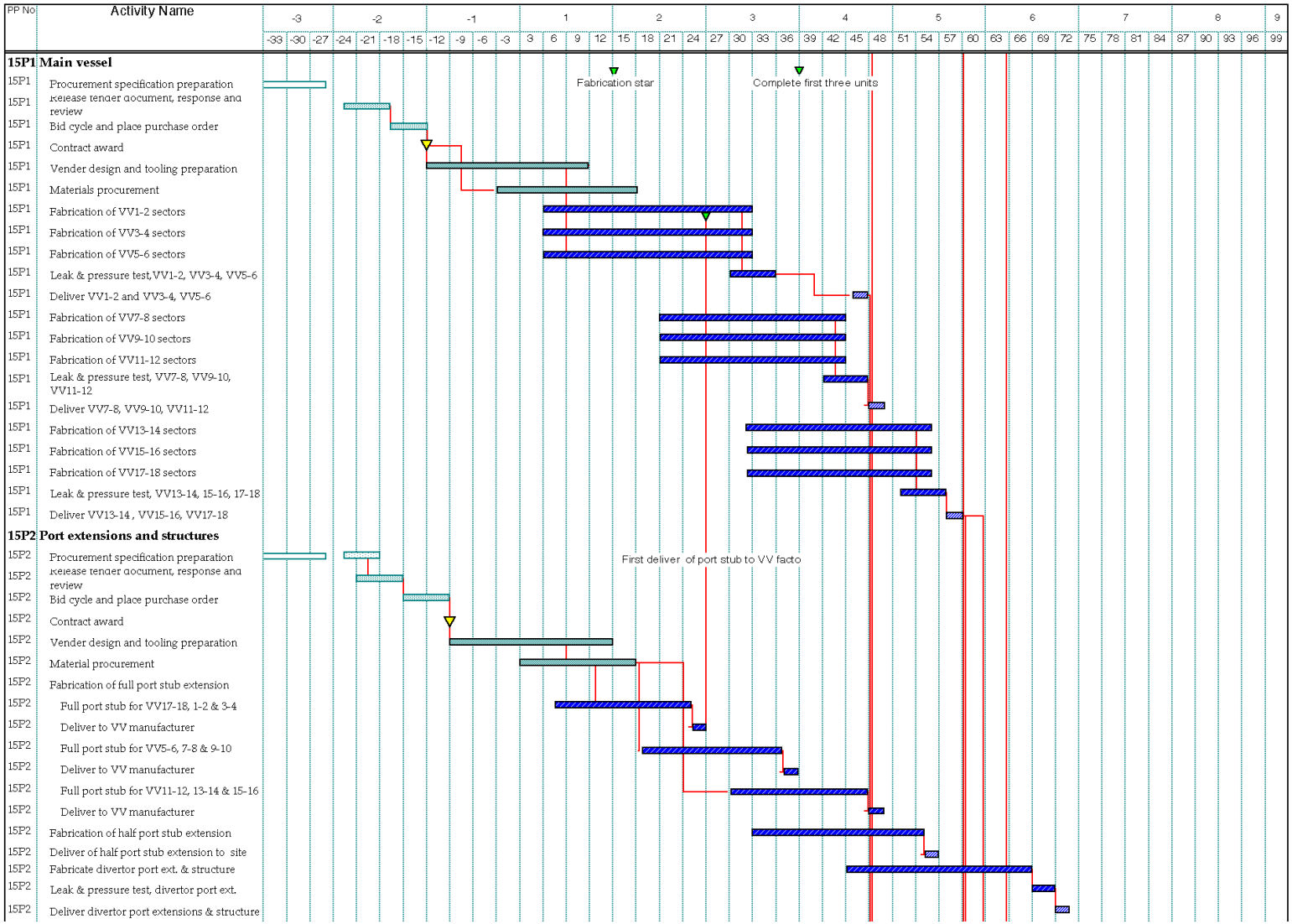

Figure 6.1.4-1 TF Coils and Vacuum Vessel Procurements to meet Assembly (3)

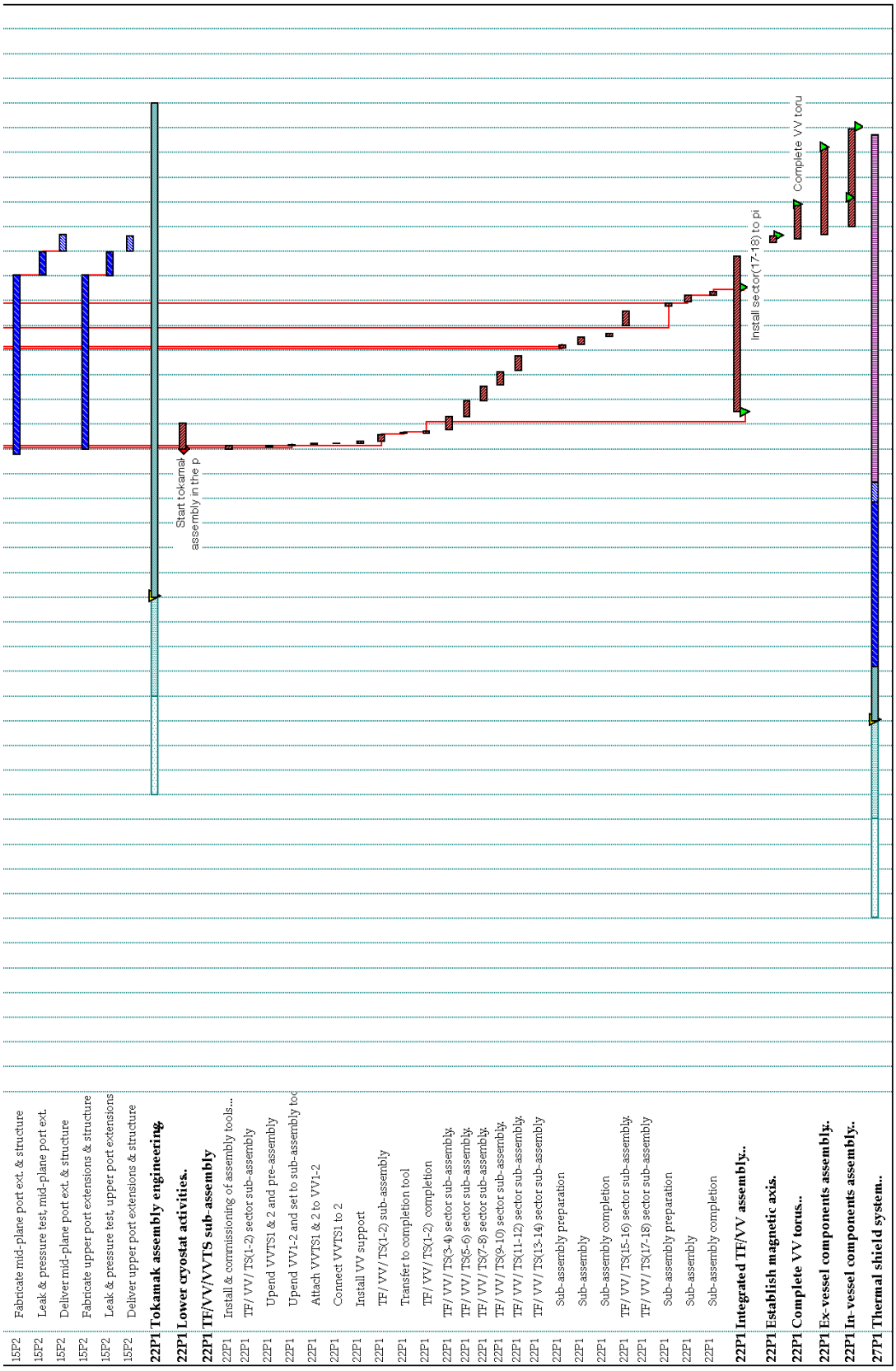

Figure 6.1.4-1 TF Coils and Vacuum Vessel Procurements to meet Assembly (4)

6.1.4.3.2 Vacuum Vessel and Port Stub Extensions

Nine (40º) sectors are shipped to the construction site and pre-assembled with the TF coils and vacuum vessel thermal shield (VVTS) in the assembly hall before being installed in the pit. Three VV sectors are simultaneously at different stages of manufacture. The manufacturing time for one sector including the welding of a port stub extension at the factory is 27 months. Another 3 months are taken into account for shipping and inspection for acceptance at the site. The manufacturing time for the 9 sectors is 54 months in total. The last sector should be accepted on site at month 62. Allowing a reasonable duration for establishing the manufacturing process and materials procurement, the contracts must be awarded 12 months before T = 0 although the fabrication of the VV sector is started after regulatory approval.

6.1.5 Tokamak Assembly and Plant Installation

6.1.5.1 Tokamak Assembly

6.1.5.1.1 Tokamak Assembly Plan

The tokamak assembly logic and procedure are described in detail in 2.10. The assembly procedure is grouped in five activities, lower cryostat assembly, TF/VV/VVTS (machine 40º sector) sub-assembly in the assembly hall, integrated TF/VV/VVTS assembly in the pit, in-vessel component assembly after completion of the torus and establishment of the magnetic axis, and ex-vessel component assembly. It takes two and a half years to complete the assembly of the vacuum vessel torus with TF coils and VV thermal shields. About a year is needed to assemble the in-vessel components and ex-vessel components simultaneously after completion of the torus and establishment of the magnetic axis.

6.1.5.1.2 Cryostat

The tokamak assembly starts with the installation of the ring pedestal support column and the bottom lid of the cryostat, placed on the basemat of the pit at month 45. The lower cryostat cylinder is then installed. For manufacturing of the bottom lid 12 months are needed at the factory and a further 6 months for construction work on the site before installation. Early procurement is required, namely within nine to twelve months after T = 0. The upper cylinder and top lid of the cryostat will be fabricated to match the tokamak assembly process. The completion of the cryostat with the installation of the top lid is at month 84.

6.1.5.1.3 Divertor and Blanket Modules

In-vessel components such as the divertor cassettes and shield blanket modules are installed after the completion of the vacuum vessel torus. The procurement of those components is not critical and it is sufficient to award the contracts between month 3 and month 12.

6.1.5.1.4 Divertor and Blanket Remote Handling Systems

The full operation of the remote handling system will be required just before D and DT plasma operation. However, the handling equipment without full remote capability will be used for the initial assembly of the divertor cassettes and shield blanket modules. This

equipment should be available before the installation of the divertor cassettes and shield blanket modules.

6.1.5.2 Procurement and Installation of Major Subsystems

The installation and assembly of all sub-systems and most of their functional acceptance tests should be completed before the integrated systems commissioning preceding the first plasma. Relevant parts of the CODAC system, to allow individual sub-system testing, must also be ready by then.

6.1.5.2.1 RF H&CD System

A prototype of 170 MHz gyrotron is to be fabricated and tested before manufacturing 24 gyrotron units. A prototype RF power source for the IC H&CD system is also expected to be developed before manufacturing 8 units. Performance testing of those prototype power generators has to be started at month 60 or earlier. It is assumed that those tests are performed at off-site facilities. The RF launchers of both IC and EC systems need to have performance tests before installation in the VV ports. A common RF test stand is provided for these performance tests, on site.

RF power sources and power supplies are installed in the laydown, assembly and RF heating building after the sub-assembly of the VV, TF coils and VV thermal shields are completed at month 66. The RF power supplies are installed and tested first. Performance and acceptance tests of the gyrotron and IC power sources are started at month 81.

6.1.5.2.2 NB H&CD System

The vessel of the NB injector system is a part of the primary vacuum boundary. It is assumed that the final connection to the primary vacuum is made after a stand-alone commissioning test of the NB injector at month 90.

The NB injectors require about six months for stand-alone commissioning before integrated commissioning. Another six months are required for a power supply test with dummy load before the stand-alone commissioning. The construction schedule of the NB power supplies therefore allows them to be ready at month 72.

6.1.5.2.3 Cooling Water System

The tokamak cooling water system is procured and installed in order to meet the first hydraulic test of the VV and in-vessel components at month 91 during integrated commissioning. The construction schedule of the components and chilled water cooling systems is therefore linked to the plan to begin NB injector stand-alone commissioning at month 75. However, It is sufficient to start procurement of the tokamak and component water cooling systems from month 15 to month 24, except for embedded pipework in or between buildings.

The lower pipe chase of the primary heat transfer loops and drain tanks are placed on the basement level of the pit during the construction of the tokamak building and in the surrounding service tunnels. Thus these components have to be procured early as discussed at 6.1.4.2.

The HVAC systems of the tokamak buildings must be ready before the start of tokamak assembly in month 46. It is not necessary to construct the full heat rejection system with wet cooling towers by then just for the ventilation of the building. Instead, the chilled water system can be used for the HVAC system of the building during tokamak assembly etc. The chilled water system must be procured 6 months before T = 0 - the cooling tower it needs initially, before the full heat rejection system is ready, could serve as the safety-related HVAC system.

6.1.5.2.4 Tritium Plant

Most of the tritium plant facilities are not needed before the start of D and DT operation. The procurement activities are introduced later phase of the construction and installation and commissioning tests are performed through hydrogen plasma operation phase.

6.1.6 Commissioning Plan

6.1.6.1 Individual Subsystem Test

Testing of each individual plant subsystem has to start immediately when permitted by their delivery and by the corresponding assembly work. Individual plant subsystem tests will be done by simulating interfaces with other systems or by using dummy loads or bypasses. Links with the CODAC supervisory control system are compulsory at this time. Each individual subsystem must be ready before the next phase of integrated testing with other subsystems. Subsystems, not needed in an early phase will be commissioned in parallel with operation.

The following system tests will be carried out:
- magnet power supply with dummy load (one by one);
- cryoplant and cryodistribution with bypasses (one by one);
- tokamak cooling water system with bypasses;
- vacuum roughing pumps by closing gate valve to the main chamber;
- additional heating, current drive and diagnostics;
- gas fuelling without tritium.

A more complex example is that of the remote handling (RH) equipment. Many RH tools, especially transporters, will be tested on mock-ups during the construction phase. Some complete RH techniques will be used as part of the initial installation either because it is more efficient or for demonstration purposes. Therefore, the major RH equipment will be installed and commissioned before first plasma.

6.1.6.2 Integrated Commissioning up to the First Plasma Discharge

6.1.6.2.1 Preparation for Integrated Commissioning

The integrated commissioning is a start of machine operation performed by the operation staffs. There will be the need for adequate testing of controls and interfaces between subsystems. CODAC is designed to permit testing of the complete system in the absence of one or more of the sub-subsystems. Subsystem controllers are designed to provide simulated data for equipment status, alarm monitoring and responses to command. (In reality, it is too

complicated to provide perfectly simulated data and responses in many systems. However, at a minimum, simplified data and responses will be provided.)

At the conclusion of this phase the whole CODAC system is ready.

6.1.6.2.2 Integrated Commissioning Procedure

All systems are tested to the extent possible without plasma. This includes the following major items.

(1) Vacuum leak and pressure test
The pumpdown of the cryostat and vacuum vessel for leak tests starts at month 86 with the following test sequence:
(i) all components will be individually tested at operating pressure (with helium);
(ii) a global leak test will be conducted with all components pressurized to operating pressure;
(iii) pressure testing of the vacuum vessel and cryostat will be made, if required;
(iv) a final global leak test will be conducted with all components pressurized to operating pressure, and VV and cryostat under vacuum.

(2) Hydraulic test and baking

(3) Magnet cooldown
After completion of a global leak test of the cryostat, the cooldown of the magnets can be started at month 91. It takes 40 days to cool down all TF coils, CS, PF and correction coils. Information for optimization of the cooldown procedure is obtained during this testing period.

(4) TF coil energisation
Main testing activities are (1) the energisation of all superconducting coils, (2) operation of fast discharge units and power supply units with coils and (3) AC loss measurements of each coil. These are scheduled to take about four months for the first coil energisation test. Error field measurement and checks of accuracy of alignment of the first wall to the toroidal magnetic field are also performed during this phase.

(5) Pulsing without plasma
Wall conditioning including baking and glow discharge cleaning starts at month 94 and the commissioning of pulsed operation without plasma, including calibration of magnetics, is continued until the first plasma discharge at the end of month 96.

At the end of this phase the following will be achieved:

- readiness of operation of the tokamak machine (e.g., vacuum, baking, sufficiently high toroidal magnetic field (4 T) to match ECH&CD for start-up and discharge cleaning, and more than 50% of coil currents in all PF coils);
- readiness of all subsystems, including the additional heating and current drive system, start-up diagnostics set, and fuelling (except the tritium system), which are needed for H plasma operation. Initial test blanket modules (or blanking plugs) have been installed and commissioned. Some subsystems may be completed later.

6.1.6.3 Commissioning after First Plasma

After the first plasma there will be further integrated commissioning over about four years leading to full operation in DT. The first 2.5 years of operation without DT is defined as a "pre-nuclear commissioning phase" and "nuclear commissioning" (about one year) will be done by using DD discharges with limited amounts of tritium. These commissioning activities are treated as part of the operation plan set out in the next section.

6.2 ITER Operation Plan

6.2.1 Introduction

Operation is divided into 4 phases: hydrogen phase, deuterium phase with limited tritium use, and two deuterium-tritium plasma phases. As a plasma experimental facility, the operation starts from the first plasma with hydrogen. However, as a nuclear fusion experimental facility, the hydrogen phase is defined as a "pre-nuclear commissioning phase", and the ITER machine will be fully commissioned and operated with the full plasma current and the full heating power with H plasma discharges. Then, after nuclear commissioning by using D plasma discharges with a limited amount of tritium, the full deutrium-tritium operation starts to develop high-Q inductive and fully non-inductive operation and highly reliable operation. Operational modes will be continuously improved and the more reliable operation will be used for the breeding blanket tests. In this section, the operation plan of these phases is summarized.

6.2.2 ITER Plant Operation and Constraints

6.2.2.1 General Considerations of ITER Operation

The following principles and assumptions are adopted for ITER operation.

(1) It is essential that all the individual subsystems be separately tested to the greatest extent possible before being linked to ITER to minimize the time devoted to integrated commissioning and troubleshooting at the full plant level.

The operation schedule should be as time efficient as possible. Commissioning should proceed as rapidly as possible, but with adequate time devoted to identifying and fixing machine problems. Before starting D operation with a limited use of tritium, all pre-nuclear commissioning should be completed with/without hydrogen plasma with the full engineering parameters except those relating only to DT operation.

(2) ITER operation will have to be efficient in order to make optimum use of the machine. Methods foreseen for ensuring this include:
- participation of remote experimental sites;
- continuous operation, i.e. 3 shifts - 24 hours/day;
- long operation phases with a relatively long break, e.g. 10 days continuous operation and 1 week break;
- a few months break per year for maintenance, further installation and commissioning.

Very careful planning is essential for ITER operation. The permissible parameters and conditions will have to be authorized in advance and the operation must be within the envelope of the approved conditions. In order to assess the planned operation, a comprehensive simulation code, including both engineering and physics, is essential. It will have to be developed during the construction phase, tested during the commissioning phase and improved during operation. This code will be essential also during operation for real-time or almost real-time analyses and display to understand plasma and machine behaviour and to optimize operation conditions.

6.2.2.2 ITER Tritium Breeding Blanket and DEMO-Relevant Blanket Testing

One of the objectives of ITER is to demonstrate fusion technologies in an integrated system by performing integrated testing of nuclear components required to utilize fusion energy. In the detailed technical objectives, it is stated that "ITER should test design concepts of tritium breeding blankets relevant to a reactor. The tests foreseen on modules include the demonstration of a breeding capability that would lead to tritium self-sufficiency in a reactor, the extraction of high-grade heat, and electricity generation."

ITER has assigned 3 equatorial ports for testing tritium breeding blankets. At present, six tritium-breeding reactor-relevant blanket concepts are planned in the Parties' programme which is intended to achieve the following main objectives:

1) demonstrate tritium breeding performance and verify the on-line tritium recovery and control systems;
2) demonstrate high-grade heat extraction suitable for electricity generation;
3) validate and calibrate the design tools and the database used in the blanket design process including neutronics, electromagnetics, heat transfer, and hydraulics;
4) demonstrate the integral performance of the blanket systems under different loading conditions;
5) observe early irradiation effects on the performance of the blanket modules.

The test program requires installing the test blanket modules early in ITER operation, before the DT operation. The first 10 years testing schedule is shown in Figure 6.2.3-1 featuring the main test items. This test plan will be integrated with the different phases of the physics programme, with emphasis on test campaigns of a few days of repetitive pulses, dedicated to functional blanket tests mostly during the 8^{th} –10^{th} year of operation and beyond.

6.2.3 Operation Plan

6.2.3.1 Summary of the First Decade of Operation

The operation phase of ITER begins with a year of integrated commissioning of subsystems, followed by the first period of machine exploitation, lasting roughly a decade. The plan is shown in Figure 6.2.3-1. About 2.5 years of initial operation in hydrogen, and a 1 year DD phase with limited use of T will be followed by operation with full DT. Various operational modes are envisaged, including initial ohmic and auxiliary heated pulses in H, 400 s high Q pulses, and longer pulses with non-inductive current drive. Although the main emphasis will initially be on studies of the reference scenarios, blanket module testing will also be carried out whenever significant neutron fluxes become available. The operating plan allows for maintenance, further installation and commissioning.

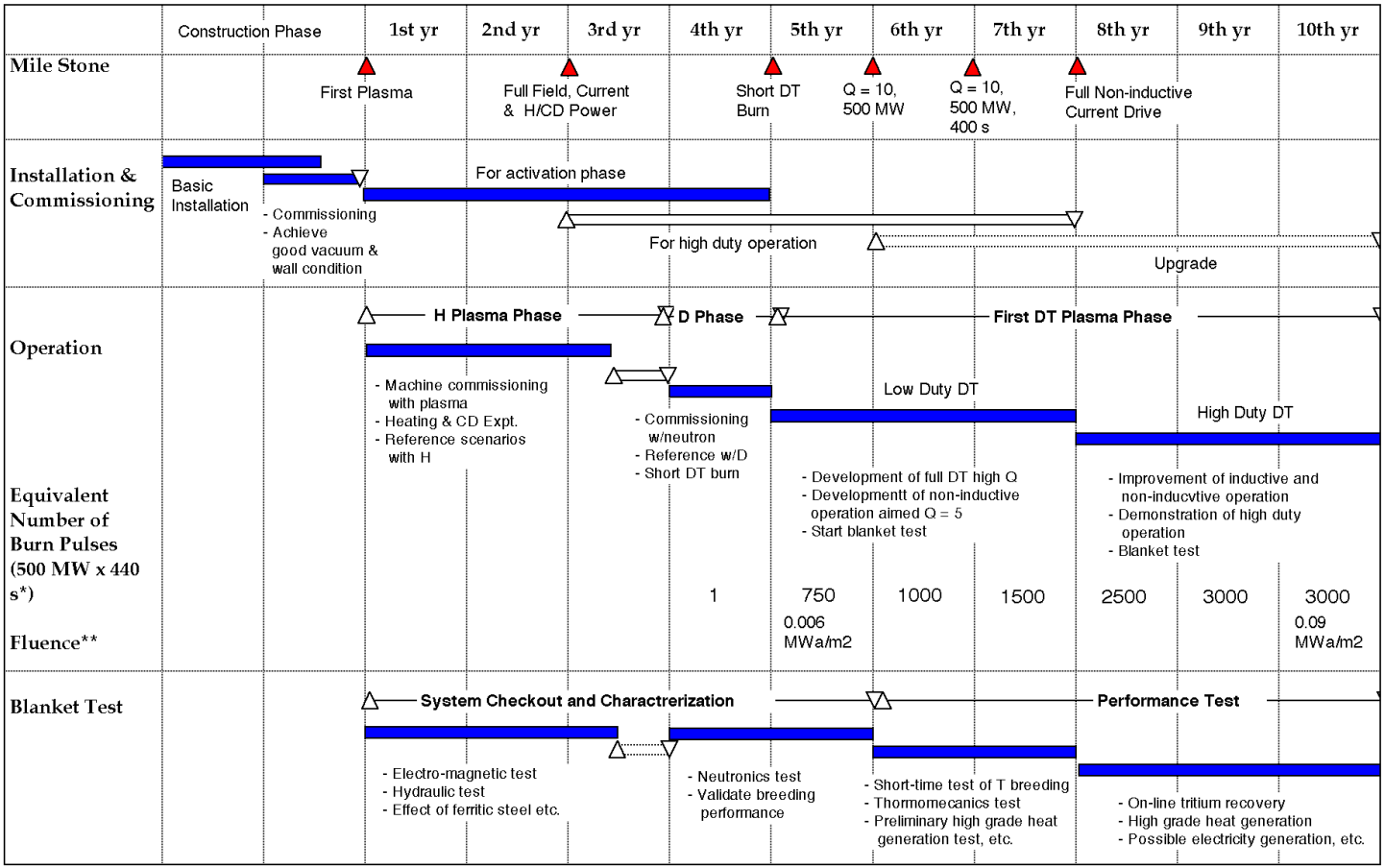

* The burn time of 440 s includes 400 s flat top and equivalent time which additional flux is counted during ramp-up and ramp-down.
** Average Fluence at First Wall (Neutron wall load is 0.56 MW/m2 in average and 0.77MW/m2 at outboard midplane.)

Figure 6.2.3-1 Initial Operation Plan

6.2.3.2 Pre-Conditioning Phase for First Plasma

After about one year of integrated commissioning including vacuum pumping of a few months and discharge cleaning of a few weeks, all of the ITER plant except some subsystems such as the tritium plant, hot cells and radioactive material storage will have been completed and be ready to operate with hydrogen plasmas with conservative coil currents (50%) and low heating power per system available (~ 10 MW) with a short pulse, and with the necessary diagnostics for hydrogen plasmas (see Table 2.6-1).

6.2.3.3 Hydrogen Phase

In this phase, lasting 2.5 years, no fusion reactions occur, and the ITER in-vessel components are not activated and not contaminated by tritium. However, ITER will be commissioned with tokamak discharges with the same electromagnetic characteristics as for D and DT operation.

In this H phase, a reference operational scenario is developed, i.e. plasma current initiation, current ramp-up, formation of divertor configuration, further current ramp-up, plasma density build up and ramp-down. By the end of the H phase, the nominal plasma current will have been achieved at the maximum toroidal magnetic field of 5.3 T at the plasma centre and about 70 MW of external heating power with a flat top duration of about one hundred seconds. The heat flux to the limiter and the peak heat flux to the divertor target will be in the same range of average values as for the reference operation during the DT phase. Therefore control of both the main plasma and the divertor plasma can be studied with a detached or partially detached plasma and compared with numerical predictions.

Adequacy of heating power for the L-H transition, $P_{L\text{-}H}$ should be confirmed as soon as possible. However, the L to H-mode transition may not be obtained in H plasma operation unless working with a low toroidal magnetic field, low density plasma, and high heating power. In order to use the RF H&CD system applicable for the second harmonic radio frequency, about 50% of the toroidal field would be needed. Due to the high divertor heat load and the high neutral beam shine-through with low density plasma, the operation space will be limited. Nevertheless, extrapolation to full power operation with DT plasma should be possible.

If the energy confinement of hydrogen plasma is as good as predicted by the scaling[1] of IPB98(y,1), the following operation would be possible at about 50% of the maximum toroidal field.

- Operation at high enough normalised beta (β_N = ~2) near the Greenwald density limit to test the stability and confinement property for the full DT operation. In this operation, the fusion figure of merit defined by $n\tau T$ will be at least one order of magnitude larger than the values achieved in present day tokamaks with $T_i \sim T_e$ conditions.
- Discharges with similar dimensionless parameter values to the reference DT discharges with the full additional heating power. Under this condition, stabilisation of neoclassical tearing modes and profile controllability can also be studied.
- Various schemes of non-inductive operations at plasma densities compatible with the divertor, with the full current drive heating power. Advanced scenarios will be tested.

[1] ITER Physics Basis, Nucl. Fus. 39, 2137 (1999)

However, many tokamak experiments have poorer confinement characteristics of H plasmas than D plasmas, except in JET. Even in JET, H plasmas have lower confinement than D plasmas unless the heating power is much higher than P_{L-H} (more than 30%). Therefore, it is not clear whether these operations are possible or not. If not, only limited studies will be done for the preparation of DT operation. For steady-state operation, only a preliminary experiment will be performed with a small bootstrap current due to the low power achieved in these H plasmas. Only fundamental tests of non-inductive current drive will be carried out.

Concerning transient phenomena, electromagnetic loads due to disruptions or vertical displacement events, and heat loads due to runaway electrons, have the same characteristics as in the DT phase. The confined plasma thermal energy of H plasma is much less than that of a full DT plasma. Thus, the very short pulsed thermal load due to the thermal quench preceding the current quench during disruption is much less than that of a full DT plasma. Therefore, three effects, i.e., the effect of this thermal quench (mainly evaporation of the surface of the divertor target), the effect of neutrons, and the effect of alpha particle plasma heating and material bombardment, can not be tested in this H-phase, but almost all other transient plasma effects can be investigated. This reduces uncertainty significantly and allows optimization of plasma control to prevent and/or mitigate severe disruptions and vertical displacement events (VDEs) in later phases.

Therefore, in conclusion, the H phase of operation is a useful and necessary step in the preparation for DT operation. Nevertheless, its duration will in fact be a reflection of how good is the confinement with hydrogen. In the case of good results, this phase will probably be extended a further year to explore further confinement studies.

The major steps of hydrogen operation are as follows:

First Year

- >10 MA, >100 s (flat top), > 4 T
- Commissioning of divertor, NB (H injection), RF, diagnostics

Remarks

(a) The most efficient combination of cleaning methods of the first wall and the divertor with EC/IC H&CD will be developed during this period. Good wall conditions will be achieved in the first few months.

(b) With relatively undemanding plasma operation, e.g. $q_{95} \geq 4$, all plasma control systems, pumping/fuelling systems, the initial set of diagnostics and most of NB/RF heating systems will be tested. On-line analysis and display of results are essential.

(c) In order to have careful and useful operation, pulse repetition time will be relatively long, typically one hour except for standard pulses for wall-conditioning shots or machine test shots.

(d) In parallel with plasma discharges, commissioning of the magnet system including AC loss measurements and increase of coil currents will continue.

(e) Heat load to the limiter is the same as in full DT operations.

(f) A major aim will be to reduce uncertainties of plasma transient and divertor operation.

Second Year

- 15 MA, 100 s, 5.3 T, NB/RF ~70 MW/ 50 s
  - Reference plasma current wave forms with full heating and current drive
  - Medium density (> ($0.7x10^{20}$ m^{-3}) and clean plasma (Z_{eff} ~ 2) with a detached/partially detached divertor
- Test the mitigation of VDEs and disruptions
- Start of remote experimental sites if required

Remarks

(a) Demonstrate the full engineering performance of ITER except systems relating to tritium.
(b) Focuses on reference scenarios at full current.
(c) Tests the heating power necessary for the L-H transition.
(d) Electromagnetic loads due to VDEs and disruptions are almost the same as in full DT operations.
(e) Peak heat flux on the divertor target is almost the same as in full DT operation.

Third Year, First Period

- Full non-inductive current drive
- Test of stabilization of neoclassical tearing and resistive wall modes, if present

Remarks

(a) If confinement of H plasma is sufficiently good, plasma operation simulating DT plasmas will be possible at about 50% of the maximum toroidal field.

Third Year, Second Period

This period is reserved for the maintenance of plasma-facing components with possible personnel access, and further installation/commissioning. Removal of hydrogen or replacement of hydrogen by deuterium will also be started by using baking, glow discharges and rf discharge cleaning during commissioning.

6.2.3.4 Preparation Phase for DT Operation

In parallel with the H phase, commissioning of the remote maintenance system, tritium system and other additional systems is to be completed. The final test of safety function such as interlock systems is also carried out. By the end of the phase, ITER is ready to go to the deuterium plasma phase, which in its later stages involves limited tritium use.

6.2.3.5 Deuterium Phase

By using limited amounts of tritium in a deuterium plasma, the integrated ITER system is commissioned, especially with regard to shielding performance, including:

- "nuclear commissioning" of the machine with D(T) plasma, including the check and calibration of nuclear diagnostics, shielding tests and radiation monitoring;
- plasma physics experiments with minority T plasma.

Characteristics of deuterium plasma behavior are expected to be very similar to that of deuterium tritium plasma even if the alpha heating power is much less than the external heating power. Therefore, the reference plasma operational scenario including L to H mode transition, very short burn, demonstration of ELMy H mode for a long period and plasma termination, may be confirmed in this phase. The tritium balance is studied. In this period, no vacuum vent is planned. The major steps are as follows:

DD Experiment with Limited T (Fourth Year)

- Replacement of H by D, clean D plasma
- Reference plasma (full current, heating power, density, detached/partially detached divertor, ELMy H mode)
- Finalize nuclear commissioning with a limited T including confirmation of neutron shield
- Obtain full operating license if required

6.2.3.6 First DT Phase

Development of a reference DT scenario will be intensively carried out by optimising and increasing tritium fuelling, the fusion power and burn pulse length. The reference operation with fusion power of ~ 0.5 GW and flat-top duration of ~ 400 s is planned to be achieved within the first two years of this phase. In this process, the key physics issues will be investigated, and development of a reliable reference operation without severe disruptions and vertical displacement events will be finalized. It is an important issue to develop a long burn operation scenario fitting to high fluence engineering tests and compatible with an appropriate long life time of the high heat flux components. In parallel, additional scenarios will be studied for future operation.

After developing a reliable operation scenario, series of experiments including repeated operation for a few days are planned mainly as an engineering test including tests for the breeding blanket modules.

The major steps are as follows:

DT-1 Experiment (5th - 6th year)

- Burn control with $P_{fus} \approx 0.5$GW and $t_{burn} \approx 400$ s
- Study of non-inductive operation
- Test of advanced modes
- Beta limit investigation

DT-2 Experiment (7 th year)

- 0.5 GW, 400 s, reliable operation
- Full non-inductive operation with a few hundred MW
- Fusion power and pulse length increase with advanced modes

DT-3 Experiment (8 th - 10th year)

- High repetition of the reference scenario
  - Development of improved modes
  - Reactor plasma basis
- Achievement of a fluence by the end of the phase of about 0.1 MWa/m^2 on the first wall at the outboard equator.

6.2.3.7 Operation after the First 10 Years – Second DT Phase

A detailed operational plan has not been developed because it will depend on the plasma performance and operating experience obtained during the first ten years. However, it is foreseen that there will be more emphasis on optimization of performance and reliable operation to produce high neutron fluxes and fluences, particularly for blanket testing, using the most promising operational modes developed during the first ten years. Conditions for DEMO operation will be defined, and as much understanding as possible of such operation and hardware performance will be obtained. The total average neutron fluence at the first wall will reach 0.3 MWa/m^2 (0.43 MWa/m^2 at the outboard mid-plane).

6.2.4 Maintenance

In the hydrogen plasma phase, 2-3 months will be needed for maintenance and small additional installation and commissioning every half a year. After the H phase, half a year is reserved for maintenance, installation and commissioning. After starting DD operation, maintenance will be remote. A few months regular maintenance will probably be needed every year.

6.2.5 Tritium Supply

The ITER plant must be operated, taking into account the available tritium externally supplied. A reasonable estimate of the available tritium from Canada, for example, is as follows:

- 22 kg by 2009 in storage,
- 1.5 kg/year from 2009.

The net tritium consumption is 0.4 g/plasma pulse at 500 MW burn with a flat top of 400 s. During the first 10 years of ITER operation, the total burn duration at 500 MW is planned to be about 0.15 years. The total consumption during the first 10 years is 4.7 kg. The typical tritium receipt, consumption, and site inventory during the first ten years are given in Table 6.2.5-1. During ITER operation, all tritium will be supplied by external sources.

For commissioning the tritium plant, several tens of grams of tritium will be needed. This will be carried out in parallel with hydrogen plasma operation. A small amount of tritium (< 0.01 g) will be burned during the deuterium plasma operation.

The maximum total tritium transportation per year will be about 1.2 kg/year in the first 10 years. Assuming a 50 g transport tritium container, there will be two shipments every month.

Table 6.2.5-1 Receipt, Consumption and Site Inventory of Tritium

Year	Receipt (kg)	Consumed (kg)	Site Inventory (kg)
1	0.0	0.0	0.0
2	0.0	0.0	0.0
3	0.1	0.0	0.1
4	0.8	< 0.01	~ 0.9
5	0.8	0.3	~ 1.4
6	0.8	0.4	~ 1.8
7	0.8	0.6	~ 2.0
8	1.0	1.0	~ 2.0
9	1.2	1.2	~ 2.0
10	1.2	1.2	~ 2.0

The total net tritium consumption over the plant life will be 16 kg with 500 MW x 0.55 year burn which gives 0.43 MWa/m^2 at the outboard equator or an average fluence of 0.3 MWa/m^2 on the first wall. This is well within the available Canadian reserves.

6.3 Decommissioning Plan

6.3.1 Introduction and Summary

It is assumed that the ITER organization at the end of operation will be responsible for starting the machine decommissioning through a de-activation period after which the facility will be handed over to a new organization inside the ITER host country. It is therefore necessary to provide a feasible and flexible plan for the decommissioning of the ITER machine and associated activated/contaminated components. The plan is based on a rationale of resources and equipment usage optimization, and takes into account the statutory occupational radiological exposure (ORE) limits. The plan provides a framework to help the organisation to decide when and how to implement the ITER facility dismantling, depending on priorities applicable at the time. Flexibility is provided by the use of two separate phases. Each phase duration and activity can be modified (to a certain extent) to accommodate the organisational requirements and constraints.

The proposed decommissioning plan takes into account the impact of essential drivers such as the availability of equipment, facilities, staff, etc., and basic constraints like activation decay time. The proposed plan:

a) allows the maximisation of the use of existing facilities and equipment while taking advantage of the experience and knowledge of the site personnel and equipment availability at the end of ITER operation;
b) reduces capital investment required for new equipment and facilities procurement required in the later stages of the decommissioning;
c) allows the choice between two decommissioning strategies by offering the following options for dismantling of most ex-vessel components:
   - option 1 = early dismantling most ex-vessel components during the de-activation phase;
   - option 2 = postponement of the expenditure required for the dismantling of ex-vessel components until after the decay period.

During the first phase, the machine will be de-activated and cleaned by removing tritium from the in-vessel components and any removable dust. Also, any liquid used in the ITER machine systems will be removed (no component cooling will be further required) and processed to remove activation products prior to their disposal. De-activation will include the removal and safe disposal of all the in-vessel components and, as an option, the ex-vessel components. The main vacuum vessel may be prepared for dismantling by cutting the inner vessel wall. The ITER de-activation will also provide corrosion protection, for components which are vulnerable to corrosion during the storage and dismantling period, if such corrosion would lead to a spread of contamination, or present unacceptable hazards to the public or workers. These activities will be carried out by the ITER organization using the remote handling facilities and staff existing at the end of the project. At the end of phase 1, the ITER facility will be handed over to the organization inside the host country that will be responsible for the subsequent phase of decommissioning after a dormant period for radioactive decay.

The plan does not include the dismantling of the buildings and of the non-activated/contaminated components (except, when applicable, for the ex-vessel components), or the removal of wastes from decommissioning. Outside of the pit, the re-use or scrap value of components is higher than the cost of their dismantling.

6.3.2 ITER Decommissioning Schedule

The proposed decommissioning scenario is broken down into its two main phases as shown in Table 6.3.2-1.

6.3.3 Overall Schedule

The estimated decommissioning schedule is summarized in Figures 6.3.3-1, -2 and -3.

Table 6.3.2-1 Summary of the ITER Decommissioning Plan

PHASE	ACTIVITY	DESCRIPTION	DURATION
1	De-activation	a) Removal of mobilizable* tritium and dust from the machine using available techniques and equipment. Removal and de-activation of coolants. b) Classification and packaging of active, contaminated and toxic material. c) Removal of all the in-vessel components. OPTION 1: removal of ex-vessel components (if not done in phase 2).	~ 5 years
	The ITER facility is handed over to a new organization within the host country, responsible for the completion of the decommissioning		
Radioactivity decay period		a) The vacuum vessel radioactivity is left to decay to a level which allows the extraction of vessel sectors into the tokamak building (during phase 2) for size reduction and removal. b) No site activities are required except security and monitoring.	
PHASE	**ACTIVITY**	**DESCRIPTION**	**DURATION**
2	Final Dismantling and Disposal	a) Removal of vacuum vessel sectors and their size reduction by remote/semi-remote operations. OPTION 2: removal of ex-vessel components (if not done in phase 1). b) Classification and packaging of active, contaminated and toxic material.	~ 6 years

* Mobilizable tritium is the tritium removable by the methods envisaged in Phase 1

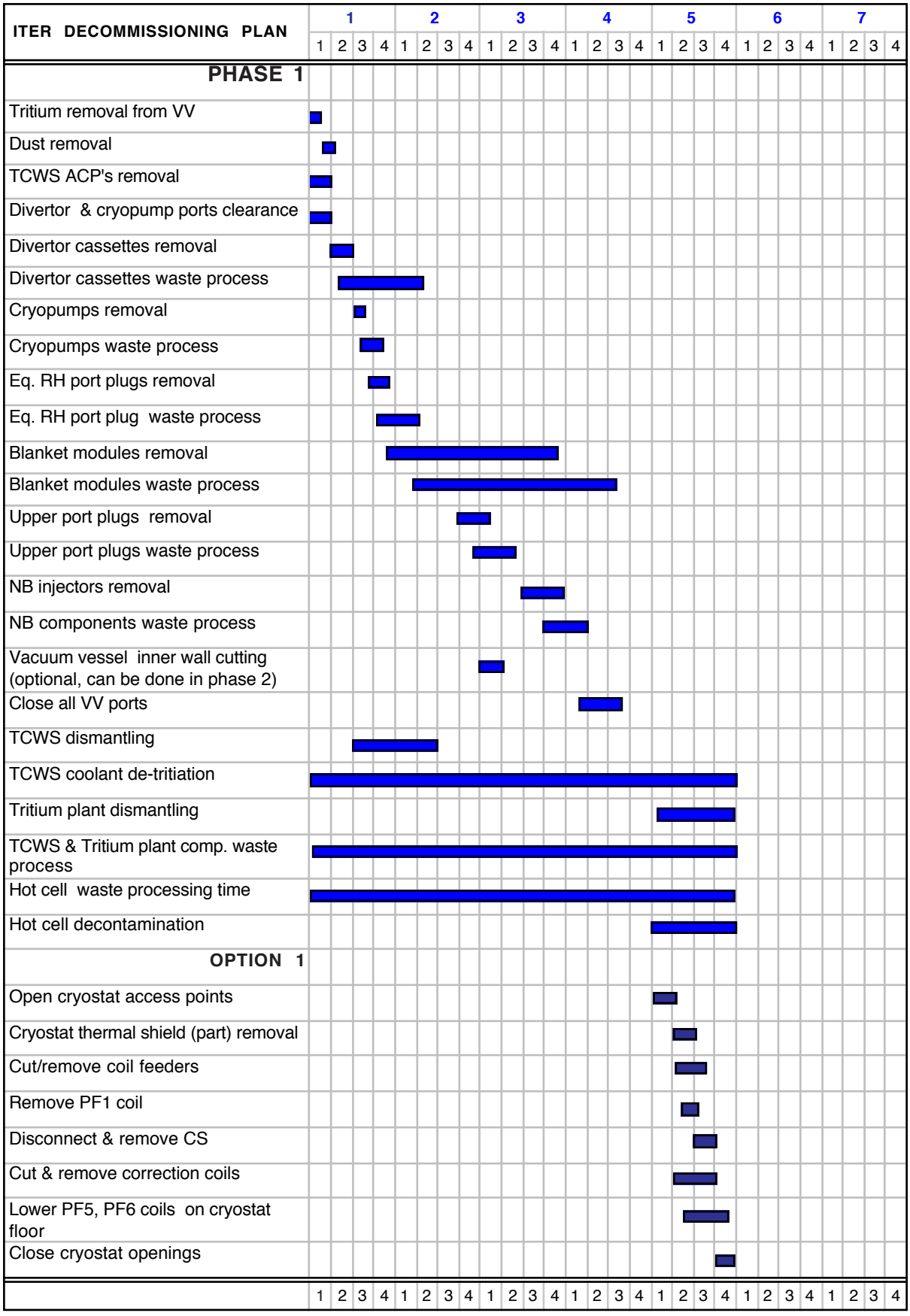

Figure 6.3.3-1 Decommissioning Schedule Phase 1

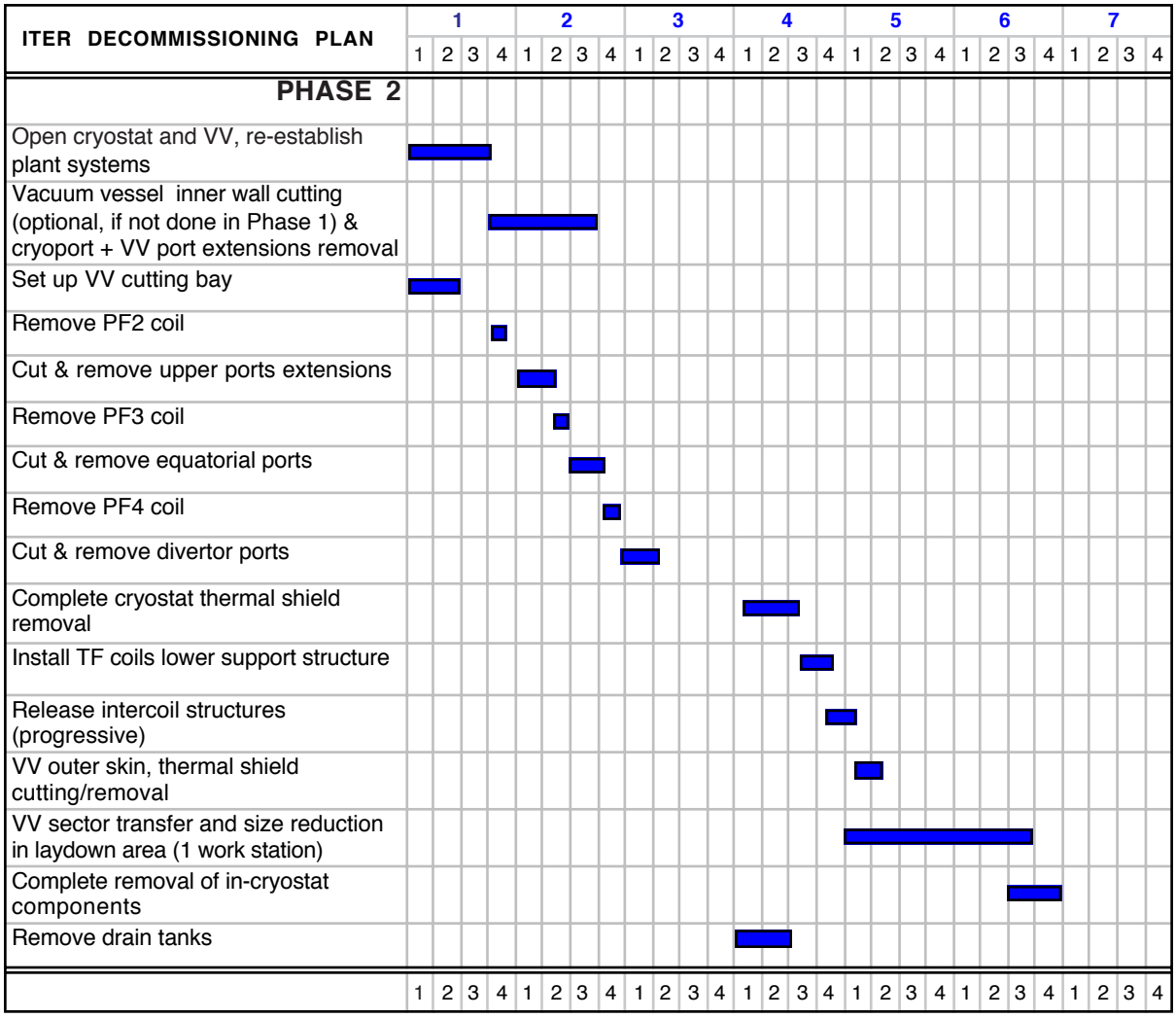

Figure 6.3.3-2 Decommissioning Schedule Phase 2

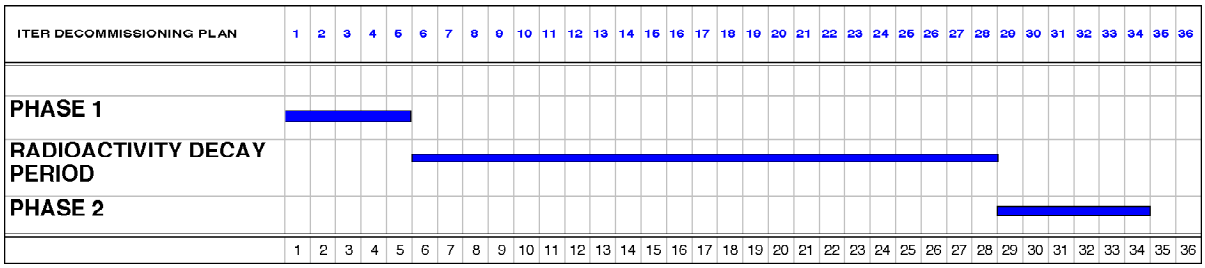

Figure 6.3.3-3 Decommissioning Schedule Overall

7 Resources

Article 2 of the ITER EDA Agreement states, inter alia, that the Parties shall conduct jointly the following EDA:

> "(a) to establish the engineering design of ITER including
>
> (iii) a planning schedule for various stages of supply, construction assembly, tests, and commissioning of ITER together with a corresponding plan for human and financial resources requirements;
>
> (c) to establish both the proposed program and the cost, manpower and schedule estimates for the operation, exploitation and decommissioning of ITER."

This report addresses the estimated human and financial resources requirements for the construction of ITER (Part I) and for its subsequent operations including integrated commissioning and exploitation (Part 2) and decommissioning (Part 3). The estimates follow from and are consistent with the plans for construction, operation and decommissioning as set out in "ITER Construction and Commissioning Plan" (Chapter 6).

7.1 Resources Required for ITER Construction

7.1.1 Cost Estimating Approach for ITER Construction

The approach to cost estimating for the construction of ITER is based on the presumption that ITER will be constructed as an international joint project in which the participants' (Parties') contributions will mainly be specific systems or components contributed directly to the project ("in kind").

The main objective of ITER cost estimates is to provide a realistic and sufficient basis for ITER Parties to make their decisions on the scope of their involvement and to select the desirable systems for them to manufacture. The estimates have been developed from the engineering designs following a "bottom-up" approach which emphasises physical estimates (such as labour hours, material quantities, physical processes, etc.) so as to ensure that the data are comprehensive and coherent and provide a basis for evaluating results from different Parties.

In considering the ITER cost estimate, it is important to recognize that:

- economic conditions in the Parties vary widely over time and these changes are not necessarily or adequately reflected in relative monetary exchange rates;
- domestic industrial practices, contracting policies and labour costs for manufacturing prototypes depend on Parties and are not reflected in relative currency exchanges (only valid for goods for which a worldwide market exists);
- the overall ITER management approach and specific procurement and contracting practices have not been determined and the host party has not been selected;
- the aggregate costs that will be incurred in constructing ITER will depend greatly on how the responsibilities for specific components are distributed between the different participants, and on the procurement policies pursued by each.

Given these uncertainties, the approach adopted focuses on establishing an "evaluated cost estimate" which normalizes the industry estimates from the Parties. The full scope of ITER is cost using itemized material and component pricing. This approach provides for consistent comparison of estimates. Manufacturing/installation costs are arrived at from estimated industry productivity and typical labour costs within the Parties' industries.

This approach allows the Parties, jointly, to appreciate the full cost of ITER and the relative contributions that each might make to building ITER and, individually, to estimate from underlying physical data the absolute costs (in their own currency) that each might expect to incur in providing a given overall percentage contribution.

7.1.2 Basic Data — Procurement Packages for Cost Estimation

In order to elicit the basic data for ITER cost estimates, about 85 "procurement packages" have been developed for the elements of the project work break down structure (WBS), each defined at a level consistent with a plausible procurement contract. Each package comprises comprehensive information, including the functional requirements, detailed designs, specifications, interfaces and other relevant data that would be needed by potential suppliers in order to prepare for contract quotations, e.g. the proposed split of responsibilities between supplier and customer and the necessary QA arrangements.

In some areas the packages provide for the possibility of splitting contracts between several suppliers in case more than one Party might wish to participate in a specific area. In some others, this splitting between suppliers in more than one Party is necessary in order to produce the volume required because of the limited capacity of each supplier (e.g. superconductor strand, shield/blanket modules, divertor targets).

The main categories of procurement type referred to in the procurement packages are defined below. The distribution of responsibility between supplier and customer (and hence the engineering resources required) vary significantly by procurement type; this is reflected in the cost estimates.

A. "Build-to-print": The design is fully specified and the performance responsibility lies with ITER. Suppliers use the design exactly as it is provided to develop fabrication/shop drawings. Suppliers can request changes to the design, if necessary during fabrication, but those changes have to be analysed, and approved by ITER.

B. "Detailed design": ITER specifies a design that a supplier must follow. ITER is responsible for the analyses leading to the main design. From this design, the supplier develops a detailed design to be approved by ITER prior to manufacture. Shop drawings are then generated from that detailed design. Analysis to verify adequacy of the detailed design are performed by the supplier. The supplier is responsible for those analyses, and therefore shares performance responsibility with ITER.

C. "Functional specifications": ITER provides functional specifications and accompanying explanatory drawings. The design and performance responsibility lie with the supplier.

Industrial companies or large laboratories with relevant experience were invited, through the Home Teams, to generate, from the procurement packages, their best estimates of the likely current costs of supply, assuming that all data necessary to support procurement would be available on schedule. To allow review and comparative evaluation of the estimates, the participants were requested to provide detailed supporting data and detailed descriptions of the potential deliverables and processes, in the format of standard ITER Cost Estimation Workbooks.

The information thus generated offers a comprehensive database for cost analysis, comparison and evaluation.

However, the cost estimates provided by each Party are not intended to be the lowest values which could be obtained in this Party, keeping the same technical specifications, since they were not the result of competitive estimation and tendering.

7.1.3 Evaluation of Cost Estimates

The JCT has analysed the results of the procurement package studies in consultation with Home Teams concerned, with the objective of deriving “evaluated estimates” which distill the database to a consistent set of project cost estimates. The main steps in this process for each package are:

(1) expression of input data in common terms;
(2) comparison and reconciliation of estimates from different Parties;
(3) “evaluated cost estimate” by JCT.

The final result is a complete set of "evaluated cost estimates" for building ITER, expressed in IUA, which is robust to currency fluctuations and domestic escalation rates and which can be used by the Parties jointly and individually in reviewing their options and the possible budgetary effects of participating in ITER construction [1 IUA = $ 1000 (Jan 1989 value)].

(1) Expression in common terms

Data expressed in terms of physical quantities can be readily compared directly, after confirming the definition of the terms. Data expressed in money values needs to be converted into common terms for the purposes of comparison and analysis.

Financial data have first been converted from current costs to the established reference date for ITER cost estimates of Jan 1989, using standard inflation factors for each Party. Where basic data for estimates from the EU were expressed in one of the European national currencies, the figures were first converted to Euro using the established fixed exchange rates and then converted through the Euro (ECU) inflation factors to Jan 1989 values. Because of the shortage of reliable price indices for the RF, basic data in 2000 roubles were converted to US dollars at current exchange rates and then converted to Jan 1989 dollars using, arbitrarily, the inflation factors for the US. The deflated figures were then converted to IUA using the prevailing exchange rates at Jan 1989. Table 7.1.3-1 shows the exchange rates and deflation factors used.

This methodology has already been applied for the ITER 1998 design cost estimates.

Table 7.1.3-1 Conversion Rates[1] from National Currencies and IUA

Currency	Conv. Rates to US$ 2000 (for comparison only)	Conversion Rates to Euro (Fixed)	Conversion Rates to US$, (January 1989)	Escalation Factors for Reference Years					Conversion Factor 2000 to IUA (x 10^{-3})
				1989	1997	1998	1999*	2000*	
US $	1.000		1.000	1.00	1.32	1.35	1.37	1.39	1.392
Can $	1.507		1.207	1.00	1.21	1.22	1.24	1.25	1.509
Euro	1.036	1.0000	0.876	1.00	1.37	1.41	1.44	1.46	1.279
DM		1.9558							
FF		6.5596							
Lira		1936.3							
UK Pound	0.634		0.585	1.00	1.42	1.47	1.51	1.55	0.906
Yen	107		128	1.00	1.13	1.14	1.15	1.16	0.148
Rouble	28.34		39.45	1.00	1.00	1.00	1.00	1.00	39.45

* Extrapolated data

It is not assumed that the 1989 exchange rates between currencies is better than those at any other date. Even, exchange rates between two currencies and inflation rates in their two countries do not sometimes vary in a coherent way (examples are Canadian and US Dollars, Sterling and Euro).

[1] International Financial Statistics Yearbook, International Monetary Fund, 1999; Eurostat Yearbook, Edition 98/99.

Nevertheless, looking backwards in time, using this approach the Parties have their own appreciation of these old rates and can apply at once the correction factor they feel appropriate (because of labour cost, industrial practices or any other reason) to quantify directly their potential contribution in their current money.

Moreover, a constant reference unit is the most appropriate tool to cost a project which extends in time over many decades in an international framework.

(2) Comparison and reconciliation of estimates

In consultation with the Home Teams concerned, the data were subjected to detailed analysis and comparison to check for consistency and completeness and, as far as possible, to identify and eliminate anomalies.

A distinct advantage of the ITER Project is the ability to obtain multiple estimates from industries in the different Parties. These multiple estimates were evaluated in detail and compared to identify missing items, possible misunderstandings, and opportunities from design or process improvements to achieve cost reductions. When possible, the estimates were discussed with industrial staff concerned to gain a thorough understanding of cost considerations. In some cases, industries suggested changes to reduce costs; these were considered and, where feasible, the cost saving changes were made.

(3) Evaluated cost estimate by the JCT

In order to emphasise the relative costs of the different systems/components, the following method has been used to derive from the basic data a JCT cost estimate, consistent across the whole ITER plant:

- world market prices have been used where they exist, for instance for standard materials or items of equipment;
- unified standard labour costs have been established which reflect (see Table 7.1.3-2):
  - rates in IUA/khour established for the main categories of labour, averaged across skill levels and Parties;
  - the different levels of manufacturing support costs, including facility, equipment, overhead and profit, for different types of industrial works and working conditions (e.g. staff in their existing home facilities, on site, or in a facility charged as an itemised cost).

After analysis of the proposals from the different Parties for amounts of tooling, material quantities and labour hours to manufacture each identified item, the JCT has established its own assessed numbers for these cost driving elements and, using the above-mentioned lists of standard materials prices and labour costs, has derived an “evaluated cost estimate” for each identified item.

Table 7.1.3-2 ITER Labour Rates

The cost estimates prepared for the EDA Final Design Report include a number of parameters which need to be normalised. A large table was established to provide a set of labour rates for both field construction and shop manufacturing operations. These rates were used for all estimates for both home and field manufacturing operations as well as site installations. Established in IUA /khours, these rates are assumed constant in time (which means that, converted in any Party's currency, they will follow the inflation rate of that Party).

Labour costs are composed of labour wage rates and support costs:

- *The Labour Wage rates are the Hourly Wages each worker earns plus fringe benefit packages including employer's contribution to taxes, health benefits, vacation benefits if any, and related employer-paid labour cost items.*

- *Support costs, also presented as an hourly rate, include the cost of use of the manufacturing facility and equipments, ship supervision, management, consumables, other overheads, and profit.*

For some commodities, such as for the TF or PF coils, in which Facilities, Special Tooling and Equipment are estimated separately, the support costs have been decreased accordingly. For those items to be fabricated on site (in the same Country as Home), it is assumed that the support costs will be the same as at Home, but that a premium (0.005 IUA) is added to the hourly wage.

The Wage Rates were determined by using an average of wage rate cost data from the U.S. ("R.S. Means, 30 City Average, January 1997"), Japan ("Chingin Jijyo", Factory labour direct cost and "Seskisan Shiryo", construction labour rate), and EU (Eurostat). All rates include 5% casual overtime. Manufacturing labour cost is based on a composite of Highly Skilled, Skilled, and Semi-Skilled Labour. Site Installation Labour is based on a composite of Craft Labour.

From these values of 1997 using conversion factors to IUA (according to inflation rate in each Party), one can note that in average:
- *the normalised labour wages are 20% above the European values and 20% below the Japanese ones;*
- *the normalised support cost per hour is equal to the European value and 10% below the Japanese one; it amounts to a value between about 2 (for welding) and 3 (for machining) times the normalised labour wage, and only about 1.25 (for welding) and 1.80 (for machining) if the special equipment is estimated separately.*

A few global values for Labour rates are mostly used in the ITER "estimated cost" (in IUA/khour):
- *for Engineering, a mix of professional designers (90), professional engineers (67), CAD and procurement technicians (38), in average 67-73;*
- *for machining including full support (67) or limited support (48);*
- *for welding including full support (55) or limited support (40);*
- *for QA and testing, (45);*
- *for assembly/installation, (35 to 45, depending on the amount of professional support).*
-

For civil work, the costing is done through the use of a table of commodity rates for all activities referred to the "unit measurement" of the quantity of the commodity used (m^3, m^2, t,etc..). They include material and labour amounts as well as specific support per unit.

Summing all items per procurement package, the JCT provides through this methodology a normalised cost for each package, the most credible given the present uncertainties on ITER construction management and procurement. For reasons described above, when applying to each package the conversion factor from IUA to the present value of currency in one Party, the result should not be expected to match the cost incurred by this Party to provide the given component.

7.1.4 Conclusions on the Approach to the ITER Construction Cost

The approach to develop a JCT evaluated cost estimate for ITER construction, expressed in IUA tries, to the extent possible, to remove variations in costs that are due to differences in estimating practices by the different Parties, and to exchange rate fluctuations. This means that although ITER costs for each item reflect the same "value" in two Parties, they will not, when expressed in these Parties' currencies, necessarily correspond to each other through exchange rates at any date.

The approach provides fair and consistent relative costs for the different ITER systems and components. The Parties can, jointly, appreciate in advance the relative contributions (in percentage) that each might make to building ITER and, individually, estimate from the underlying physical data the absolute costs (in their own currency) that each might expect to incur in providing specific components, inside their contribution "in kind", by applying their own appropriate conversion factor to IUA.

This detailed "evaluated cost estimate" aids the "design to cost" and, later, the "manufacture to cost" approaches by which design/process changes are made to maintain costs within the budgeted amount because itemized quantities and manufacturing man-hours are clearly defined.

7.1.5 Cost Estimates Summary

7.1.5.1 Component/system "Evaluated Cost Estimate"

The evaluated cost estimates for ITER construction in kIUA, summarised by procurement packages, are presented in Table 7.1.5-1. A much larger "Business Confidential" document provides for each procurement package the JCT detailed evaluation. The table also indicates, for each package, which of the Parties provided data, what is its direct capital cost, its percentage of the total capital investment, the cost of spares and of deferred items to be supported by operation funds, and their comparison with the relevant numbers for the ITER 1998 design.

For a few items (and a small total cost $\simeq$ 30 kIUA) no detailed cost estimate is yet possible following the described method, because their design has not yet reached the level of detail needed to make a cost estimate "bottom up". They are included in a cost element defined as "allowance for indeterminates (AFI)" and part of the deferred investment. The costs of transportation, being unknowable, are also excluded from the estimates, but each procurement package includes the cost of packaging for transoceanic crossing and transport to the closest port of embarkation (Free On Board - FOB).

As recognised by Experts from the four Parties, who have reviewed the details of the component/systems costing which support these estimates, they are not intended to be the

Table 7.1.5-1 ITER Cost Estimate Summary

WBS No.	Procurement Package	No.		HT Cost Estimate O : full estimate P : partial estimate X : no estimate E U	JA	R F	Direct Capital Cost (1) (kIUA)	Percentage / Total	Spares deferred Investment (2) (kIUA)	Ratio of (1) / (3) %	Direct capital cost (3) (kIUA)	Deferred Investment (4) (kIUA)
1.1	**Magnet Systems**	1	Toroidal Field Coils Windings	O	O	O	117.0		4.0			
		2	Magnet Structures	O	O	O	168.3		5.4			
		3	Poloidal Field Coil & Correction Coils	O	O	O	49.7		0.0			
		4	Central Solenoid Coil	O	O	O	31.1		3.4			
		5	Feeders	X	O	X	41.0		3.2			
		6	Conductor	O	O	O	355.0		24.2			
			Subtotal				**762.1**	27.7	**40.2**	42.3	1800.0	
1.5	**Vacuum Vessel**	1	Main Vessel	O	O	X	155.0		0.0			
		2	Port Assemblies	O	O	O	75.0		0.0			
			Subtotal				**230.0**	8.4	**0.0**	113.0	203.0	
1.6	**Blanket System**	1	Blanket Manifolds, Filler Shields	O	O	O	6.0		0.0			
		2-1	FW/Blanket Shield Modules	O	O	P	142.6		7.3			
		2-2	Port Limiters	O	O	O	6.1		1.3			
		3	Blanket Module Connections	P	O	O	10.5		0.0			
			Subtotal				**165.2**	6.0	**8.6**	38.6	428.5	
1.7	**Divertor**	1	Cassette Integration & Testing	O	P	X	10.7		0.5			
		2	Plasma Facing Components	O	O	O	65.3		6.4			
			Subtotal				**76.0**	2.8	**6.9**	34.5	220.6	
2.2	**Machine Assembly**	1	Assembly Operations	O	O	O	50.3		0.0			
		2	Assembly Tooling	O	O	O	42.4		0.0			
			Subtotal				**92.7**	3.4	**0.0**	71.0	130.5	
2.4	**Cryostat**	1	Cryostat & VV Pressure Suppr. System	O	O	X	**75.8**	2.8	**0.0**	70.6	107.4	
2.7	**Thermal Shields**	1	Thermal Shield System	O	O	O	**28.8**	1.0	**0.0**	75.2	38.3	
3.1	**Vacuum Pumping & Fueling System**	1	Non-standard Cryopumps & Related Equipment	O	O	X	8.9		2.3			
		2	Roughing Pump Sets & Change-over Boxes	O	O	X	6.7		0.0			
		3	Leak Detection Stations	X	X	X	5.0		0.0			
		4	Standard Components	X	X	X	5.3		0.0			
		5	Pellet Injector	X	X	X	2.5		2.5			
		6	Gas Injector Valve Boxes	X	X	X	4.3		1.3			
		7	GDC Conditioning System	O	O	X	1.5		0.6			
			Subtotal				**34.2**	**1.2**	**6.8**	36.7	93.3	
	Machine Core		*Subtotal*				*1464.8*	*53.2*	*62.5*	*48.5*	*3021.6*	*0*

Table 7.1.5-1 ITER Cost Estimate Summary

WBS No.	Procurement Package	No.		HT Cost Estimate O : full estimate P : partial estimate X : no estimate			Direct Capital Cost (1) (kIUA)	Percentage / Total	Spares deferred Investment (2) (kIUA)	Ratio of (1) / (3) %	Direct capital cost (3) (kIUA)	Deferred Investment (4) (kIUA)
				E U	JA	R F						
2.3	**R/H Equipment**		Blanket RH Equipment	O	O	X	27.1		0.8			
			In-Vessel Div. Maintenance Equipment	O	O	X	11.7		0.3			
			Transfer Cask System	O	O	X	10.0		6.4			
			Viewing/Metrology Systems	O	P	X	6.0		0.8			
			Neutral Beam RH Equipment	O	O	X	0.6		5.4			
			Hot Cell Repair/Maintenance Equipment	O	O	X	5.7		38.6			
			Subtotal				**61.1**	**2.2**	**52.3**	34.0	180.0	87.4
2.6	Cooling water	1	PHTS and CVCS	O	O	X	71.0		2.6			
		2	Heat Rejection System	O	O	X	37.4		10.8			
		3	Component Cooling & CW Systems	O	O	X	23.1		3.4			
			Subtotal				**131.5**	**4.8**	**16.8**	38.7	339.4	10
3.2	**Tritium Plant**	1	Tokamak Exhaust Processing System	O	O	X	6.1		6.9			
		2	Storage & Delivery, Long Term Storage System	O	O	X	11.9		2.6			
		3	HTD Isotope Separation	O	O	X	0.0		6.2			
		4	Atmosphere Detritiation	O	O	X	12.8		17.4			
		5	Water Detritiation	O	O	X	3.7		10.8			
		6	Tritium Plant Analytical System	O	O	X	1.0		0.6			
		7	Tritium Plant Automatic Control System	O	O	X	1.1		0.8			
			Subtotal				**36.6**	**1.3**	**45.2**	47.2	77.6	98
3.4	**Cryodistribution**		Cryoplant	O	O	X	60.5		2.5			
			Cryolines	O	O	X	12.2		4.0			
			Cryodistribution Components	O	O	X	16.2		1.4			
			Subtotal				**88.9**	**3.2**	**7.9**	61.7	144.2	24.2
4.1	**Power Supplies & Distribution**	1	High Voltage Substation and AC Distribution System	O	O	X	26.6		0.4			
		2	AC/DC Converters, Reactive Power Compensators and Harmonic Filters	O	O	X	81.2		1.0			
		3	Switching Networks, Discharge Circuits, DC Distribution and Instrumentation	O	O	O	67.2		1.8			
			Subtotal				**175.0**	**6.4**	**3.2**	54.2	323.0	0
4.1		8	Steady State Electrical Power Network	O	O	O						
			Subtotal				**39.7**	**1.4**	**0.3**	53.1	74.7	0

Table 7.1.5-1 ITER Cost Estimate Summary

WBS	Procurement Package			HT Cost Estimate			Direct Capital Cost (1)	Percentage / Total	Spares deferred Investment (2)	Ratio of (1) / (3) %	Direct capital cost (3)	Deferred Investment (4)
No.				O : full estimate								
				P : partial estimate								
				X : no estimate			(kIUA)		(kIUA)		(kIUA)	(kIUA)
		No.		E U	JA	R F						
6.2	**Buildings**	1	Reinforced Concrete and Site Infrastructure Elements	O	O	X	311.5		0.0			
		2	Steel Frame Buildings	O	O	X	68.8		0.0			
			Subtotal				**380.3**	**13.8**	**12.0**	46.5	818.1	11.4
6.3	**Waste Treatment and Storage**	1	Waste Treatment and Storage	O	X	X	**2.1**		**7.0**		87.4	0
6.4	**Radiological Protection**	1	Radiological Protection	O	O	X	**1.0**		**3.2**		7.4	0
	Auxiliaries		*Subtotal*				*916.2*	*33.3*	*148.0*	44.7	*2051.8*	*231*
5.1	**IC H&CD**	1	Antenna Arrays and Vacuum Transm. Lines	O	X	X	4.5		0.0			
		2	Main Transm. Line and Matching System	O	X	X	4.8		0.0			
		3	RF Power Sources & RF Monitoring Control	O	X	X	16.0		2.0			
		4	Power Supply	O	X	X	6.9		0.0			
			Subtotal				**32.2**	**1.2**	**2.0**	0.0	0.0	0
5.2	**EC H&CD**	1A	Equatorial Launcher	X	O	O	7.3		0.0			
		1B	Upper Launcher	X	O	O	8.9		0.0			
		2	Transmission Line	O	O	O	17.9		0.0			
		3	RF Power Sources and Controls	O	O	O	29.5		3.0			
		4	Power Supply	O	O	X	13.9		0.0			
			Subtotal				**77.5**	**2.8**	**3.0**	45.8	169.2	0
5.3	**NB H&CD**	1	Assembly and Testing	O	O	X	3.8		0.0			
		2	Beam Source and High voltage Bushing	O	O	O	9.5		0.0			
		3	Beamline Components	O	O	O	3.9		0.0			
		4	Pressure/Vacuum Vessels, Drift Duct and Passive Magnetic Shielding	O	O	X	11.9		0.0			
		5a	Active Corr./Compensation Coils	O	O	X	4.4		0.0			
		6	Power Supply	O	O	X	62.5		0.0			
			Subtotal				**96.0**	**3.5**	**0.2**	60.0	160.0	0
	H and CD		*73MW (100MW in 1998)*				*205.7*	*7.4*	*5.2*	*62.5*	*329.2*	*0*

Table 7.1.5-1 ITER Cost Estimate Summary

WBS	Procurement Package			HT Cost Estimate			Direct Capital Cost (1)	Percentage / Total	Spares deferred Investment (2)	Ratio of (1) / (3) %	Direct capital cost (3)	Deferred Investment (4)
No.				O : full estimate								
				P : partial estimate								
				X : no estimate			(kIUA)		(kIUA)		(kIUA)	(kIUA)
		No.		E U	JA	R F						
5.5	Diagnostics	A	Diagnostics. Magnetics	X	X	P	3.3		0.0			
		B	Neutron Systems	X	P	P	3.9		6.2			
		C	Optical Systems	X	X	P	16.9		8.8			
		D	Bolometry	O	X	X	6.7		0.0			
		E	Spectroscopic Systems	X	P	P	8.9		13.6			
		F	Microwave Systems	X	X	X	8.3		9.4			
		G	Operational Systems	X	X	X	11.0		0.0			
		N	Standard Diagnostics	O	X	X	36.3		4.2			
			Diagnostic Neutral Beam:Line	O	O	X	13.0		0.1			
			Diagnostic Neutral Beam:Power Supply	O	O	X	9.7		0.0			
			Subtotal				**118.0**	**4.3**	**42.3**	78.2	150.8	71
	CODAC		Hardware and Software (rough estimate)				**50**	**1.8**	**0.0**		50.0	0
			Grand Total				**2754.7**	**99.9**	**258.0**	**49.2**	**5603.4**	**302**

lowest values which could be obtained, keeping the same technical specifications, since they were not the result of competitive estimation and tendering within each Party.

Globally for ITER construction they represent the most credible cost estimates, given the present uncertainties on ITER Construction Management, Siting and Cost sharing: a global value inside which one can be confident to be able to build ITER.

In addition, there is room to achieve substantial savings in some areas already identified, and more might be found through the needed and expected industry feedback on design to optimise manufacturing processes.

7.1.5.2 Siting and Construction Costs

The present ITER design, and its "evaluated cost estimate", follows the "ITER Site Requirements and Site Design Assumptions", which have been approved by the ITER Council[1]. Site specific adaptations of the design may induce changes in the cost of some systems; they will be analysed during the Coordinated Technical Activities (CTA), when potential sites are characterised.

Similarly, the present design is consistent with codes, and standards which have been defined inside the project. These rules are coherent but are not identical to those of any specific Party, even if they do not contradict them. Regulatory bodies from a potential host country may request the application of different and specific design rules or quality assurance measures. This can induce cost variations to be analysed again during the CTA.

The "ITER Site Requirements and Site Design Assumptions" describe a list of Host responsibilities, for which the project bears no cost, and which include in summary:

- infrastructure for industrial support of ITER and socio-economic provisions;
- land for the ITER site;
- high quality (potable), and raw water, treatment for sanitary and industrial sewage;
- supply to steady state electrical power network and a tie line capable of large pulse power for magnet and plasma heating;
- off site fire protection equipment and personnel;
- receipt of waste of all types, generated from ITER operation and decommissioning.

7.1.5.3 Procurement Scheme

Each procurement package relies on a single dominant technology, and therefore mainly leads to a single industrial contract and avoids the need for a large amount of subcontracts. On the other hand, the possibility of sharing the work to be done for a package between more than one industry was always considered, even if this splitting leads to an increase in cost. This method provides for the ITER Parties the possibility, if they wish, to contribute in all fusion specific technologies. For example, the following list offers a possible splitting of procurement orders:

- the Nb_3Sn and NbTi conductors (355 kIUA in total) should be provided by contributions from all Parties; even more, industries in the Parties should be encouraged to prepare for a larger production capability, in particular in Russia for niobium of the required quality;

[1] Plant Design Specification G A0 SP 2 01-06-01 R2.0, Chapter 4

- two suppliers are proposed to share equally the manufacturing of the TF coils windings (117 kIUA in total);
- one or two equal suppliers for the procurement of TF coil mechanical structures (168 kIUA in total).

In these cases, it is thought appropriate that one contractor will have the responsibility to develop the design for the special toolings, which will be duplicated for use by the second contractor. The two sets of tools are anyway necessary to meet an acceptable manufacturing schedule. Therefore, this sharing possibility between two Parties' industries leads to only a small increase of cost due to a small loss of labour efficiency.

- one manufacturer for the central solenoid (31 kIUA);
- one manufacturer for the PF coils, (50 kIUA), assumed to work on the ITER site and thus from the Host;
- one manufacturer for coil Feeders (41 kIUA): a complex area of superconductor and cryogenic technologies and instrumentation;
- at most, three equal industrial partners for the vacuum vessel manufacture (155 kIUA in total), and one or two more to produce the port structures (75 kIUA in total), if they agree on cooperation in the engineering of the specific process toolings;
- no difficulty should be met to share between different industries the delivery of more than 420 blanket modules (143 kIUA in total);
- the high flux components for the divertor are assumed to be provided by three, or more industries (65 kIUA in total);
- a few of the packages require only one responsible supplier per package (joined by industrial subcontractors): assembly of the machine, (50 kIUA), reinforced concrete buildings (312 kIUA), the steel frame buildings (69 kIUA) – all activities on the ITER site and thus for the Host industries – the cryostat manufacturing (76 kIUA), the cooling water piping (60 kIUA), and the steady state electrical power network (40 kIUA) which all require also a large amount of work on site;
- all other packages should be procured through more than one supplier; particular ones provide for heating and current drive systems and diagnostics, and are discussed below.

In summary, the procurement of the machine core (1465 kIUA) could be possibly split into about 40 different contracts of 40 kIUA in average. The procurement of Auxiliaries and Heating and CD systems, except the Concrete Building (800 kIUA) could be split into 40 different contracts of 20 kIUA on average.

7.1.5.3.1 Heating and Current Drive Systems

The ITER requirements for plasma heating and current drive cannot be satisfied by a single method. Four have been envisaged (NB, IC, EC and LH), which could provide ITER with flexibility of operation. The machine design makes possible the installation of three NB lines, each assumed to provide 16.5 MW of neutral deuterium atoms at 1 MeV. All RF heating systems have been designed to provide 20 MW to the plasma per port. All these systems costs have been estimated per port of injection.

Provisions in the layout of equipments are such that heating and current drive systems procurement can be staged, to reach a maximum of 50 MW of NB (three lines), and 40 MW for any of the three RF methods: in all possible scenario, installed power cannot provide more than $\simeq$ 130 MW and more than 110 MW available at the same time.

The present status of R&D results in any of those heating methods has not achieved the level required to be confident in their assumed performance and therefore in their availability at the start up of ITER operation. An R&D effort in all Parties, more extended and more efficient, is absolutely needed with the highest priority.

For the time being, it is assumed that the start up scenario will use two NB lines (33 MW, 96 kIUA), one equatorial port equipped with an IC launcher (20 MW, 32 kIUA)) and 20 MW of EC power (77.5 kIUA) which can be delivered either through one equatorial port or through 3 upper ports (for NTM stabilisation).

7.1.5.3.2 Diagnostic System

ITER requires a comprehensive diagnostic system for monitoring in real time the conditions of the different machine components and for measuring the value of the key plasma parameters, in order either to control ITER operations or to increase the understanding in physical phenomena.

The diagnostic system comprises about forty individual measurement systems. The responsibility for design and procurement of these specific systems should be shared by the Laboratories of the Parties which aim at participating in ITER operations through their physicists. The central ITER Team cannot bear alone this responsibility, even if it should specify all interfaces with the machine and in particular the responsibility of all "generic" packages.

The cost of the diagnostic system has been estimated through:

- seven diagnostic specific procurement packages: A: Magnetic diagnostics – B: Neutron systems – C: Optical systems – D: Bolometry – E: Spectroscopic systems – F: Microwave systems – G: Operational systems;
- six "generic" packages: N01: In-vessel services - N03: Diagnostic port plugs and first closure flanges - N04: Port inter-space structures and second closure flanges - N05: Divertor diagnostic components - N06: Ex vessel services - N07: Windows assemblies.

In addition, the cost of the Diagnostic Neutral Beam has been obtained together with the Heating Neutral Beam cost. Other related costs are for Blanket Shield Modules for Diagnostics Ports and the Test Stand in the Hot Cell, which are included in other packages.

Costs of providing the diagnostic system are divided into several components (see Table 7.1.5-2.). The cost of diagnostics required for initial operation (startup) is determined separately from the cost of those that are not required until the DT operation (deferred). Included in the startup costs is the cost of the in-vessel and inter-space equipment, and interfaces, for the deferred systems which would otherwise be expensive and time consuming to install later. Further, the diagnostic costing identifies items which would have to be provided during construction under control of the central ITER Team (in-machine items) and those which could be provided by the ITER Parties directly (ex-machine items). Examples of the former could be in-vessel services and wiring, while examples of the latter could be specialised lasers and spectrometers. As in previous costing exercises, the cost of the specialist diagnostic effort to support the design, procurement and implementation of the

diagnostic systems is costed separately in PPY: part of this effort will be required early to prepare for consistent plans and interfaces with the central ITER Team.

Table 7.1.5-2 Diagnostic System – Procurement Scheme and Cost

Diagnostic category	Startup			Deferred	
		kIUA	Laboratories PPY	kIUA	Laboratories PPY
	Total	In-machine			
A	3.25	3.25	5.6	0	0
B	3.9	1.4	6.0	6.2	14.0
C	16.9	0.6	33.0	8.8	17.3
D	6.7	0	8.5	0	0
E	8.9	0.3	26.6	13.6	43.2
F	8.3	2.2	23.8	9.4	31.5
G	11.0	5.4	17.7	0	0
N01	8.0	8.0	0	0	0
N03	13.4	13.4	0	0	0
N04	5.7	5.7	0	0	0
N05	0.8	0.8	0	0	0
N06	4.4	4.4	0	1.8	0
N07	4.0	4.0	0	2.4	0
DNB	22.7	22.7	0	0	0
TOTAL	118.0	72.2	121	42.3	106

7.1.5.4 ITER Direct Capital Cost

Taking account of the previous assumptions, the total "JCT estimated capital investment" for ITER amounts to 2,755 kIUA; in addition the cost of spares and items needed only a few years after start of operation (full DT operation) amounts to 258 kIUA and is deferred to be supported by operating funds. The present investment cost is only 49.2% of the previous estimate for the ITER 1998 design, which amounted to 5603 kIUA and 302 kIUA deferred.

7.1.6 Construction Management and Engineering Support

An estimate of the cost of construction management and support cannot be done without assumptions on the future organisation to execute the construction and the manner of contracting and managing contracts for procurement.

7.1.6.1 Assumptions

For this purpose, it is assumed that the ITER Legal Entity (ILE), which will be responsible for the management of ITER during its whole life time, will provide a direct and effective line of accountability by incorporating all actors in a single management entity, including:

- an International Team at the ITER site which will have the overall responsibility to meet the project objectives and to ensure the design continuity and coherence.
  For this goal, it will:
  - define the technical specifications for procurement packages, the general QA rules and contracting rules;
  - control, analyse and decide upon design changes or deviations;
  - maintain databases on R&D and manufacturing results;
  - integrate all aspects of ITER: technology and physics - safety and licensing - assembly - CODAC and diagnostics - cost and schedule.
- a National Team, as part of the ILE in each Party, which will manage and follow up the technical content of the procurement contributed by the Party, when the financial and legal contents of the relevant contracts are being taken care of by a Domestic Agency.
  For this goal, each National Team will:
  - adapt technical specifications to its national usages and ensure engineering at detailed level;
  - implement QA;
  - assure technical control of each domestic supplier contract by a permanent presence in suppliers' premises, and a schedule control by accepting contractual payments according only to work progress.

With these assumptions it is clear that the size of the International Team can be deduced approximately from its functions, but the size of each Party National Team will depend on the level of the Party's contribution to ITER construction, on these specific packages in its contribution, and on the specific national practices in contract management.

Presently, when the respective choices of the ITER Partners in matters of procurement packages are unknown, a global approximation can only be given of the manpower necessary to follow up all the procurement packages, expressed in professional and technical man-years, integrating all National Teams, and taking no account of the possible splitting of procurement contracts between Parties and its relevant increase in manpower for their follow-up.

7.1.6.2 Estimated Personnel Cost during Construction

To exercise its responsibilities, the International Team will probably include a core management group and a few technical groups, in charge of physics, safety, engineering, assembly, etc.. These groups should be able to ensure technical continuity with the EDA and CTA, and, as construction approaches its end, these groups, suitably increased by personnel from the National Teams who have followed procurements, will eventually be involved in the integrated commissioning and start up of operation of the facilities. The number of professionals of this International Team can thus range from about 80 at the beginning of construction, to about 200 towards the end.

The support personnel for the core management (mostly administrative) and for the technical groups (mostly CAD) is expected to be in number equal to the number of professionals.

Following the assumed schedule (seven years of construction beginning two years after establishment of the ILE – the one year of integrated commissioning is assumed to be the

first year of operation) the global man-years for the International Team during construction amounts to 840 PPY and a similar number for support personnel.

The global estimate of professionals and support personnel (clerical, technicians and CAD) for the different National Teams to follow up all procurement contracts in all Parties amounts to about 960 PPY and twice this number for support personnel. The number of professionals is assumed to be about 120-140 in average for six years and decreasing during the last three years of construction, probably being transferred to the site to participate in the components installation and commissioning.

Assuming the annual cost of one professional and one support staff to be 150 IUA and 75 IUA respectively, the cost estimate for the International Team during construction until the start of ITER operation (integrated commissioning of the whole machine) amounts to 189 kIUA and the global estimate for all the National Teams during the same period amounts about 288 kIUA. Again, these costs are normalised and global, including all Parties; they might not be representative for the specific conditions of each Party. Excluded from the previous numbers are those relevant to diagnostic procurement referred in 7.1.5.3.2 above.

7.1.6.3 Possible R&D Cost during Construction

In addition to personnel costs, a certain amount of R&D during construction should always be considered. As already mentioned, R&D for all heating and current drive methods is required with high priority.

The EDA has provided the principle qualification of design solutions to be implemented in ITER. Nevertheless, during the manufacturing of components, proposed process improvements and design changes or unexpected difficulties could require new tests.

Moreover, to achieve in industrial production reliable results and good efficiency in the manufacturing of a large amount of high technology components (e.g. superconductor strands, high heat flux components, etc…), it is probably more efficient to launch, at the chosen industrial firm, a manufacturing R&D before contracting the global procurement. Along a similar line, it is conceivable that some Nb_3Sn coils (TF and CS) should be tested at their operational cryogenic temperature to confirm quality, even if presently the cost/ benefit ratio of technical results to be expected from these tests does not appear high enough.

It is therefore prudent to expect a spending in R&D of 60-80 kIUA during ITER construction.

7.1.7 Cash Flow for the Direct Capital Cost

The ITER construction plan discussed in section 6 requires a specific schedule for the procurement of each system and therefore appropriate profiles of commitments and payments, the total of which will amount to the JCT estimated capital investment. The most important to consider is the profile of payments, which when combined with the construction schedule, establishes the necessary cash flow over time for the project as a whole.

7.1.7.1 Payment Schemes for each Procurement

For each procurement package, the following simplified scheme is assumed for payment according to the planning of manufacturing until delivery after the ordering contract is signed:

- 10% of the whole contract value is paid when the contract is awarded;
- 80% of cost of professionals is distributed evenly, and paid accordingly, from the vendor's design phase to delivery of the components or acceptance of the system (as appropriate);
- 80% of labour cost is distributed evenly, and paid accordingly, during fabrication, installation and test if appropriate;
- 80% of tooling cost is paid when the tools become operational;
- 80% of materials or subcontracted equipment costs is paid when the materials or equipment are accepted by the main contractor and checked by the ILE QA representative if appropriate;
- the last 10% of their contractual value is paid when a component or a modular part is accepted by the ILE after the results of contractual acceptance tests, or when a system delivered on site, has satisfied the contractual performance test.

7.1.7.2 Cash Flow

Table 7.1.7-1 and Figure 7.1.7-1 show a yearly distribution of payments of the direct capital cost (including spares and deferred items) based on the above assumptions. Before the grant of license and the defined start of construction on site (T = 0), contracts for the conductor, TF coil fabrication, buildings and the water cooling pipes should be awarded and 10% of these contracts paid, i.e. about 180 kIUA in total. Annual payment reaches about 350 kIUA in the second year after T = 0 and continues at this level until the seventh year so that most of the direct capital cost is paid in nine years. The integrated commissioning activities are then started in the eighth year when the whole operation staff is fully on site, and this is the start of the operation phase of ITER.

Table 7.1.7-1 Cash Flow of Direct Capital Cost including Some Spares and Deferred Items

WBS/Year	-2	-1	1	2	3	4	5	6	7	8	9	10	11	Total
10: Magnets, VV and In-vessel Components	41	56	166	262	256	213	175	85	28	6	0	0	0	1289
20: Assembly, RH Equipment, Water Cooling	0	13	9	31	35	58	56	81	81	22	13	20	38	459
30: Cryoplant, Pumping and Tritium Plant	0	0	0	1	10	6	5	25	59	36	25	29	25	220
40: Coil and Heating System Power Supplies	0	4	1	10	9	25	64	89	79	24	0	0	0	305
50: Heating Systems, Diagnostics, CODAC	0	0	0	0	13	5	35	48	105	62	28	28	14	338
60: Buildings and Site Facility	37	27	61	47	38	41	26	57	20	13	6	7	5	385
Total	78	101	237	350	362	349	361	385	372	163	73	84	82	2996

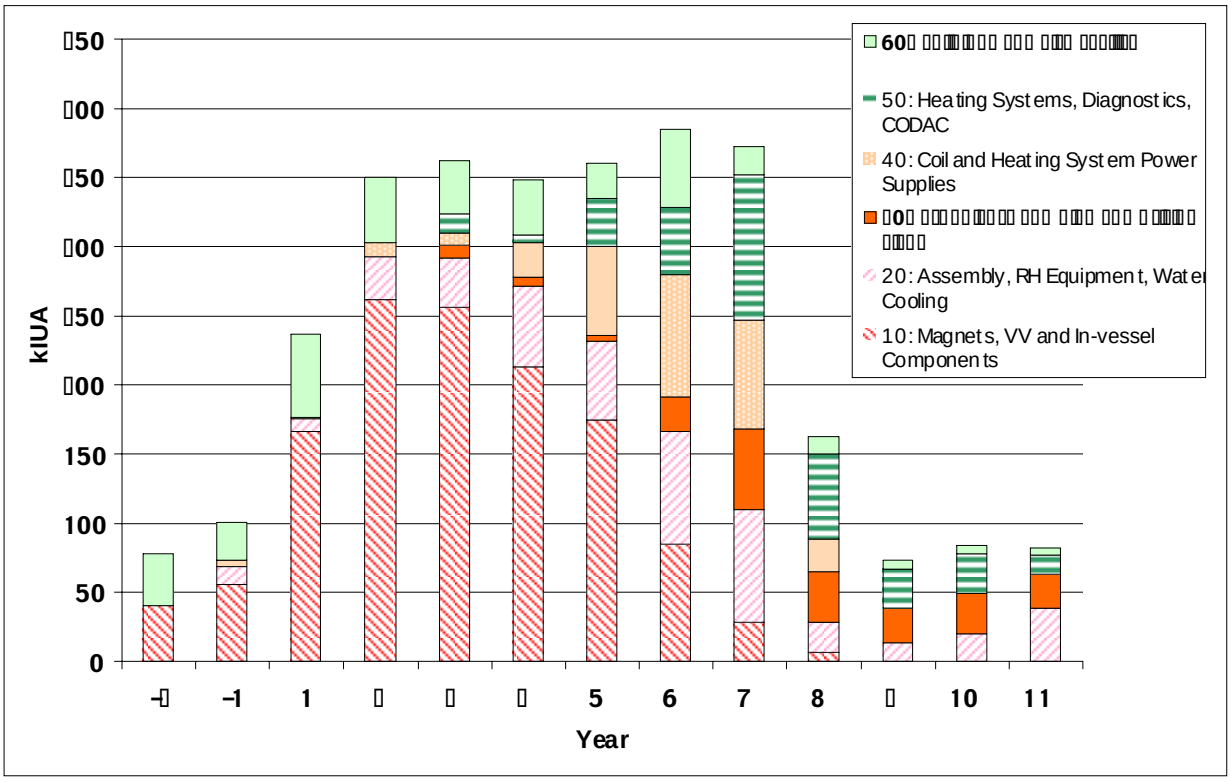

Figure 7.1.7-1 Cash Flow Diagram for Direct Capital Cost including Spares and Deferred Items

This example offers an illustrative first approximation and is capable of further refinement and modification, in particular by splitting the procurement of large packages into smaller ones in content or in successive time steps and by adjusting the assumptions on payments profiles.

7.2 Resources for ITER Operation

Operation costs for ITER include the following items:

- project personnel,
- energy costs during operation,
- fuel costs (largely hypothetical),
- spare parts, maintenance and material/capital improvements.

Some of the above costs are related directly to the usage the machine receives, whereas others depend directly on the project duration. An estimate of the above costs therefore is based on the operation scenario for the device described in Chapter 6.

7.2.1 Project Manpower Costs

Manpower costs of permanent staff on site and cost of extra manpower brought in from time to time to aid in maintenance of the device are costed assuming an average level of 200 professionals and 400 support staff (clerical, technicians and CAD), at 150 IUA and 75 IUA respectively per year; thus the annual personnel cost is about 60 kIUA.

The permanent professional and support staff above are expected to operate and maintain the facility, and support the experimental programme, for example diagnostics, or installation and testing of the blanket modules. However, visitors to the site to conduct experiments (experimentalists or theoreticians) are not included in the manpower cost: their costs are assumed borne by the Parties. This is consistent with including the cost of diagnostics in the construction or operating costs, but not the Laboratories staff having the responsibility of their procurement.

7.2.2 Energy Costs

Electric power costs, which not only include the power required for pulse operation, but also must cover energy consumption during various levels of standby/maintenance of the machine, depend on aspects of the load time profile and on the characteristics of the national electricity network of the host site. Whereas electric peak power to be delivered, and the average power to be made available over a certain time period, place a premium on the cost of energy consumed, the consumption dominates the cost in any well-provisioned site. Thus the electricity costs can be estimated knowing the steady state power levels required in the various operating states, and the fraction of time spent in those states, superimposing the integral of the pulsed power demand when in the plasma operating state.

A typical scenario is shown in Table 7.2.2-1. The steady state power loads are representative values over the whole life of the plant, but are somewhat uncertain. Similarly the time devoted to maintenance (or conversely to burn/dwell) as also difficult to specify at this stage. For this reason ranges are given, with the implications noted. A unit cost of 0.05 IUA/MWh is used.

Table 7.2.2-1 Key Features of Electricity Cost Calculation

	Low	Nominal	High
Steady state power loads			
Plasma operating state (POS)	100	100	100
Short-term standby (STS)	70	80	90
Short-term maintenance (STM)	50	60	70
Long-term maintenance (LTM)	30	35	40
Time usage (lifetime average)			
In LTM	0.25	0.375	0.5
In STM	0.5	0.375	0.25
Average annual cost over 20 year life (kIUA)	24.7	29.1	34.0

The most sensitive parameters of this calculation are shown above. The results are not sensitive to the average burn time, or to the details of the operation stages over the years, since the integral burn time is constrained to deliver the nominal fluence. Typical yearly cost variations from the average, at various operation stages, are below 5 kIUA.

7.2.3 Fuel Costs

Fuel costs include deuterium and tritium burnt during operation, plus that lost by decay of the inventory (taken as 2 kg) during plant operation. The deuterium cost is negligible at 2 IUA/kg. There is no market for tritium for the quantities required, and thus tritium may have little or no monetary value. Nevertheless a largely hypothetical 10 kIUA/kg for tritium

purchase is used. The total tritium received on site during the first 10 years of operation, according to Table 6.2.5.1, amounts to 6.7 kg. The total consumption of tritium during the plant life time may be 16 kg to provide a fluence of 0.3 MWa/m^2 in average on the first wall; this corresponds, due to tritium decay, to a purchase of about 17.5 kg of tritium.

Therefore the fuel costs are in average 6.7 kIUA per year during the first ten years, and probably 11.5 kIUA per year after.

7.2.4 Capital Improvement, Spare Parts, Maintenance Costs

Analysis of the expected capital costs to keep the ITER facility in the required effective state has shown that very different ratios (annual cost against the initial investment) should be considered for the different systems, going from almost 0% (e.g. magnets) to 10% (for RF power generators and diagnostics), up to 15% (e.g. computers).

Considering all systems, the required maintenance cost amounts to 2.5% of the initial investment, about 70kIUA per year. To this cost should be added investments deferred initially to operation costs and the cost of replacement of the divertor high heat flux components (possibly five times during the plant life time). This leads to a total of 90 kIUA per year in average during operation.

7.2.5 Conclusion: Average Annual Operation Costs

In summary, the ITER average annual operation costs amount to about 60 kIUA for the personnel permanently on site, 30 kIUA for the energy consumption, 8 kIUA for the tritium purchase and 90 kIUA for spare parts, maintenance and improvements, i.e. a total average per year of 188 kIUA. Again this value will depend on the ITER site, mostly through the electricity cost (assumed to be 0.05 IUA/MWh), and on the specific arrangement between the Parties on how to support the personnel cost.

7.3 ITER Decommissioning Costs

The policy proposed for the ITER decommissioning has been described in Chapters 2.11 and 6.3. The technical implementation and schedule have been detailed according to a credible option. Even if the Host Party may consider other options, the global cost to be borne should not change drastically as long as a full dismantling of the machine is not required before the vacuum vessel activity has decayed substantially.

The ITER facility, because of the remote maintenance implemented during operation, offers initially most of the tools, procedures, and even trained staff, to accomplish the decommissioning operations. This capacity is an essential element in keeping their cost down.

The manpower estimate is based on the requirements for the dismantling of the main active parts of the ITER facility only. The non-active parts are not considered, because their residual values are probably higher than their dismantling costs.

For the technical operations and their schedule in two active phases described in Chapter 6.3, the estimated integrated work force over 11 years amounts to about 2,800 man-years. The average cost per man-year is rated at 90 IUA as a mix of different staff categories. In

addition, it is assumed that new hardware may be required to replace a few aging tools, or to enhance the hot cell, and radwaste processing efficiency. For this purpose, one third of the manpower cost is put as an AFI, as observed in previous experience.

Other costs (dependent on the Host country) are not included in the present estimate:
- radwaste disposal;
- components and facilities salvage value after dismantling where applicable (e.g. materials below "clearance");
- non-active parts dismantling and salvage value;
- site restoration;
- financing-related costs, if spending is made at a later stage.

Under the assumptions and limitations listed above, the estimated cost for decommissioning amounts to 250 kIUA for manpower costs and 85 kIUA for possible hardware costs.

7.4 Summary

For reference, a summary of the cost estimates for all phases of ITER plant lifetime is set out in Table 7.4-1 and compared with estimates for the 1998 design. This summary is subject to all the qualifications and considerations outlined above.

In particular the construction cost estimates:
- assume the agreed Site Requirements and Site Design Assumptions, and are thus valid for a generic site;
- include the policy for additional heating and diagnostics procurement set out in 7.1.5.3.1 and 7.1.5.3.2;
- exclude costs associated with site hosting, notably, the provision of land, off-site facilities and all service supplies up to the boundary fence;
- exclude items deferred beyond the start of operation.

The average yearly operation cost estimates include permanent staff costs on site to operate and maintain the facility, but exclude the cost of visitors (physicists) to conduct the experimental programme of ITER.

Table 7.4-1 Overall Project Cost Summary

	ITER kIUA	Ratio 1/2 %	ITER 1998 Design kIUA
Construction costs			
A) Direct capital cost	2755	49.2	5603
B) Management and support	477	61.2	780
C) R&D during construction	60-80	$\simeq$ 50	150
Operation costs (average/year)			
A) Permanent personnel	60	66	90
B) Energy	$\simeq$ 30	50	$\simeq$ 60
C) Fuel	$\simeq$ 8	40	$\simeq$ 20
D) Maintenance/improvements	~ 90	50	$\simeq$ 180
Total	188	54	350
Decommissioning cost (total)	335	110	$\simeq$ 300